VNiVERSiDAD DE SALAMANCA

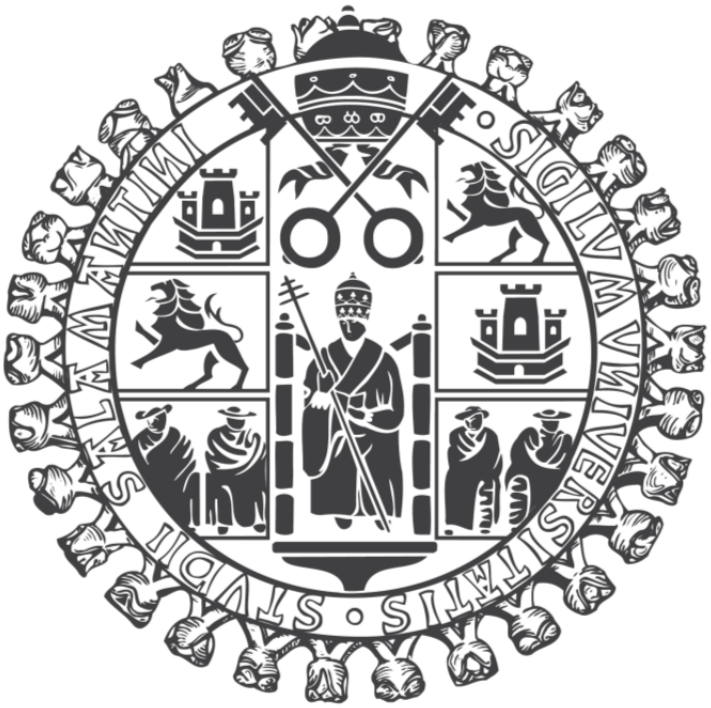

Macromoleculas y Ligandos: Péptido-Nucleótidos y β-Aminoácidos morfánicos. Síntesis, Modelización Molecular y Evaluación Biológica.

Carlos Tomás Nieto García

Departamento de Química Orgánica.

Noviembre 2013

Macromoleculas y Ligandos: Péptido-Nucleótidos y β-Aminoácidos morfánicos. Síntesis, Modelización Molecular y Evaluación Biológica.

Trabajo presentado para optar al
Título de Doctor Europeo por:

Carlos Tomás Nieto García

Visado en Salamanca

Noviembre de 2013

Narciso Martín Garrido

Prof. Titular de Química Orgánica

David Díez Martín

Catedrático de Química Orgánica

Este trabajo ha sido realizado en el Departamento de Química Orgánica de la Facultad de Ciencias Químicas de la Universidad de Salamanca, bajo la dirección de los Dres. D. NARCISO MARTÍN GARRIDO y D. DAVID DÍEZ MARTÍN, a los que quiero agradecer su apoyo, esfuerzo e interés mostrado hasta la conclusión del mismo.

Así mismo, agradezco la ayuda prestada por los Dres Dña. Pilar Basabe Barcala, D. Julio González Urones, Dña. Rosalina Fernández Moro, Dña. Mª José Sexmero y D. Isidro Sánchez Marcos.

A la Junta de Castilla y León por la concesión de una beca de formación de personal investigador en el período 2009-2013 y a la Universidad de Salamanca por la concesión de una ayuda para realizar estancias investigadoras en el año 2012.

Del mismo modo, expresar mi agradecimiento a los Dres Dña. Anna Lithgow del servicio de RMN, a la Dra. Dña. Francisca Sanz del servicio de Difracción de Rayos-X al Dr. D. César Raposo del servicio de Espectrometría de masas, a Dña. María José Pérez técnico de laboratorio y a Dña. Marisa Maldonado secretaria del departamento de Química Orgánica.

I would like to express my gratitude to those people who have made possible my research internships abroad in UK and Denmark.

Me gustaría agradecer a todos mis compañeros de laboratorio, tanto a los que continúan en el Departamento como a los que ya no están, por compartir conmigo estos años de duro trabajo y esfuerzo, dentro y fuera de los laboratorios. En especial, quiero agradecer a: Aitor, por ser un trabajador innato; Ana Belen, por esa alegría contagiosa; Ana Gil, por estar siempre ahí (aunque te tome el pelo a menudo); Carmen, por tu honestidad y tu particular visión del mundo; Isabel, por lo buenaza que eres y por compartir nuestro gusto por Zelda; Javier Peña, por esas discusiones tan entretenidas en el laboratorio; Juan, por tu manera de ver la música; Magda, por tu amistad incondicional; Mateo, por esa chispa indomable. De vosotros he aprendido tantas cosas que podría llenar otro libro como este.

Son muchas las aventuras y desventuras que hemos compartido juntos y que, sin duda, continuaremos: estemos donde estemos.

A mis Padres, por su amor, esfuerzo y sacrificio en todos estos años.

A Nae, por su cariño, paciencia y comprensión durante todo este tiempo.

A mis amigos (Bea, Emma, Luis, Marta, Sandra) por estar siempre ahí y haber compartido tanto.

“El juego de ponerse límites a sí mismo es uno de los placeres secretos de la vida”.

Gilbert Keith Chesterton

Indice/Index

How To Read this Thesis...

Several aspects should be pointed before reading this work, related with nomenclature, drawings and reaction schemes.

All chemicals used in the experimental section, commercial or synthetized in the lab, are referred as bold numbers (**23**). Compounds at the background chapter are referred as underlined numbers (5).

Reaction schemes come with a footnote legend, describing reagents and conditions. Immediately before a described condition, a reaction reference is displayed (M24 or P69). This reference guides to a more detailed description of that in the experimental chapter. For instance, M24 is referred to Morphan chapter reaction number 24, while P69 is referred to PNA chapter reaction number 69.

Stereochemistries of compounds are displayed using wedged () or straight bonds (). When the stereocenter has a defined asymmetry, wedged bonds are displayed. In case of epimeric centers, straight bonds are chosen.

Structure-based designed prototypes are referred as **DX** candidates (**X** is a number).

Abbreviations

$[\alpha]^{T}_{D}$	Optical Rotation at temperature T using sodium D line (589,29 nm)
9-BBN	9-BoraBicyclo[3.3.1]Nonane
AA	All Atom
AB	AB system
ABX	ABX system
AcOEt	Ethyl Acetate
ADT	AutoDock Tools
aegPNA	Aminoethylglycine PNA
AIBN	AzobisIsoButyroNitrile
B3LYP	Becke, three-parameter, Lee-Yang-Parr Fucntional
Boc	*tert*-butoxycarbonyl
calcd	calculated
CAN	Cerium (IV) Ammonium Nitrate
CAS	Chemical Abstracts Service
d	Doublet
d	days
DAMGO	H-Tyr-*D*-Ala-Gly-N-MePhe-Gly-OH
DBU	1,8-DiazaBicyclo[5.4.0]Undec-7-ene
DCE	1,2-DiChloroEthane
DCM	DiChloroMethane
dd	double-doublet
DFT	Density Functional Theory
DIAD	DiIsopropyl AzaDicarboxylate
DIBAL-H	DiIsoButylALuminium Hydride
DIPEA	DiIsopropylEthylAmine
DMAP	4-(*N*,*N*-DiMethylAmino)Pyridine
DMF	DiMethylFormamide
DMSO	DiMethylSulfoxyde
DNA	DesoxyrriboNucleic Ncid
DPN	[^{3}H]-DiPreNorphine
dt	doublet-triplet
EDCI	1-Ethyl-3-(3-Dimethylaminopropyl)CarbodiImide

equiv	Equivalents
Fmoc	9-Fluorenylmethoxycarbonyl
FTIR	Fourier Transform Infrared Spectroscopy
g	grames
GAFF	Generalized Amber Force Field
GBSA	Generalized Born Surface Area
GPCR	G-Protein Coupled Receptor
h	hours
HF	Hartree-Fock
HMBC	Heteronuclear Multiple Bond Correlation
HMPA	HexaMethylPhosphorAmide
HMQC	Heteronuclear Multiple Quantum Correlation
HOMO	Highest Occupied Molecular Orbital
J	Coupling constant
Ki	Inhibition Constant
LDA	Lithium DiisopropylAmide
LUMO	Lowest Unoccupied Molecular Orbital
M	Molar
m	multiplet
m/z	mass/charge ratio
M05-2X	Minnesota 2005 Functional, Type 2X
M06-2X	Minnesota 2006 Functional, Type 2X
MC	Monte Carlo
MD	Molecular Dynamics
mg	miligrames
MHz	MegaHerzs
min	minutes
mL	mililitres
MM	Molecular Mechanics
MMFF	Merck Molecular Force Field
mmol	milimoles
MMX	Molecular Mechanics type X
MP2	Møller-Plesset second-order perturbation theory
MsCl	MethaneSulfonyl Chloride
NAMD	Not (just) Another Molecular Dynamics program

nBuLi N-Butyllithium

nM nanoMolar

NMR Nucler Magnetic Resonance

NPT Moles-Pressure-Temperature ensemble

ns nanoseconds

NVT Moles-Volume-Temperature ensemble

Nx NaloXone

OPLS Optimized Potentials for Liquid Simulations

OPM Orientations of Proteins in Membranes

PBF Poisson Boltzmann Finite difference method

PBSA Poisson Boltzmann Surface Area

PME Particle Mesh Ewald method

PNA Peptide Nucleic Ncid

POPC Palmitoyl Oleoyl Phosphatidyl Choline

ps picoseconds

Py Pyridine

q Quartet

QM Quantum Mechanics

QRC Quick Reaction Coordinate

quant quantitative

R_f Ratio of Front

rfx reflux

RMSD Root Mean Square Deviation

RNA RiboNucleic Ncid

rt room temperature

s Singlet

s seconds

SASA Solvent Accessible Surface Area

t Triplet

TBAI TetraButylAmmonium Iodide

td triplet-doublet

TFA TriFluoroAcetic Acid

TFAA TriFluoroAcetic Anhydride

THF Tetrahydrofurane

TIP3P Transferable Intermolecular Potential 3P

TMEDA	N,N,N′,N′-TetraMethylEthyleneDiAmine
TMG	*N*,*N*,*N′*,*N′*-TetraMethylGuanidine
TMS	TriMethylSilyl
TPMA	Tris[(2-pyridyl)Methyl]Amine
TS	Transition State
uM	microMolar
W	Watts
δ	Chemical Shift
υ_{max}	Wavenumber absortion

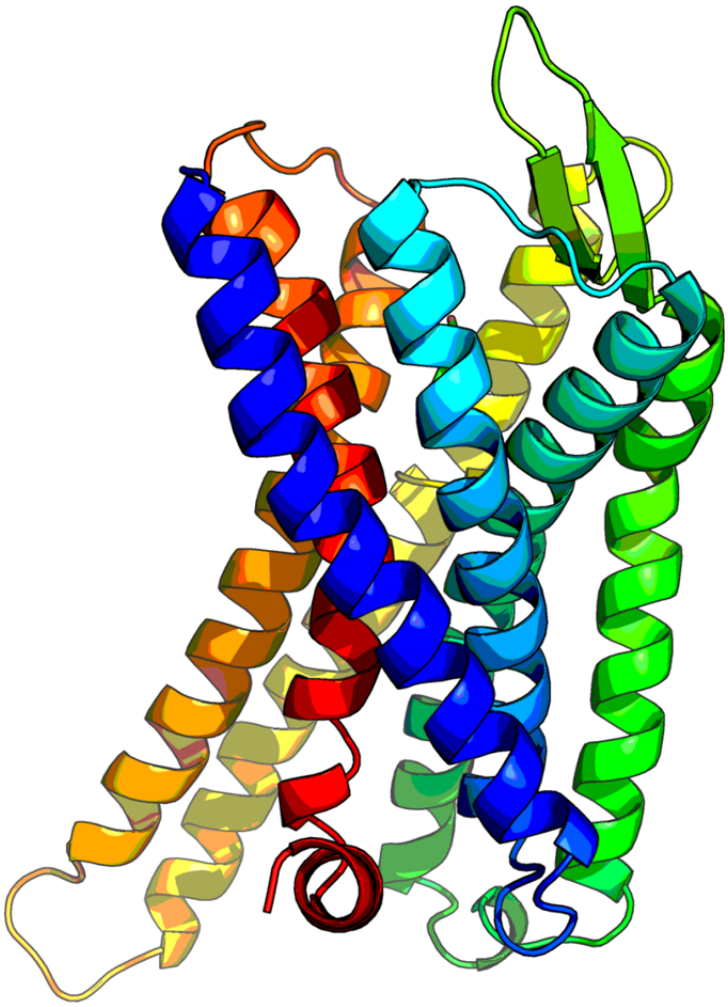

Introducción General

El Dolor: ¿Última Frontera?

El dolor es una de las principales razones para visitar a un médico de atención primaria, y es considerado un problema de salud pública. Entre 2009 y 2011, el promedio de población adulta en la Unión Europea con dolor crónico se estima en un 27%.[1] El dolor crónico está asociado con otras dolencias, como dolor muscular, migrañas, artritis, herpes zoster, diabetes, SIDA, cáncer, etc.[2] La búsqueda de nuevos analgésicos, es decir, principios que mitiguen o incluso eliminen la sensación del dolor ha sido constante en la historia de la Medicina, transformándose en un tema de actualidad en Química Médica. Muchos esfuerzos se han realizado para comprender las bases moleculares de la percepción de dolor, la estructura y función de macromoléculas relevantes y los efectos analgésicos de algunos compuestos químicos.

El dolor es mediado y modulado por los receptores acoplados a la proteína G (G-protein coupled receptors, GPCR). Estas proteínas constituyen la superfamilia más extensa de receptores transmembranosos y su función es la de transducir estímulos extracelulares en respuestas intercelulares. Estos estímulos pueden ser de índole físico (fotones, calor) o químicos (iones, neurotransmisores, péptidos, hormonas, lípidos).[3] Todos los receptores de esta índole poseen una estructura común: siete hélices transmembranosas con el extremo *N*-terminal extracelular y el *C*-terminal intracelular, tres bucles extracelulares y tres bucles intracelulares (**Fig. 1A**). Las proteínas G son heterotrimeros compuestos por tres subunidades: G_α, G_β y G_γ. Si un ligando se une al receptor, se induce un cambio conformacional[4] que promueve el intercambio de GDP (Guanosin difosfato) por GTP (Guanosin trifosfato) en la proteína G, causando la división de la proteína en la subunidad α con el GTP por un lado y las subunidades β-γ por otro (**Fig. 1B**). Ambos fragmentos pueden interferir con efectores, modulando diversas funciones biológicas.[5] La activación de los receptores opiáceos inhibe la actividad de la adenilil ciclasa, modulada por el fragmento GTP-subunidad α. Esta inhibición reduce la cantidad de cAMP (adenosin monofosfato cíclico) producido, disminuyendo la liberación de neurotransmisores. Además, la tensión/voltaje producido por los canales iónicos es más negativa, disminuyendo la amplitud de la señal de los impulsos nerviosos espontáneos, rebajando la excitabilidad.[6] Otra vía que poseen los receptores opiáceos de reducir la excitabilidad es la causada por la hiperpolarizacion de la membrana por activación

de los canales de potasio[7] e inhibición de los canales de calcio,[8] modulada por el fragmento β–γ.

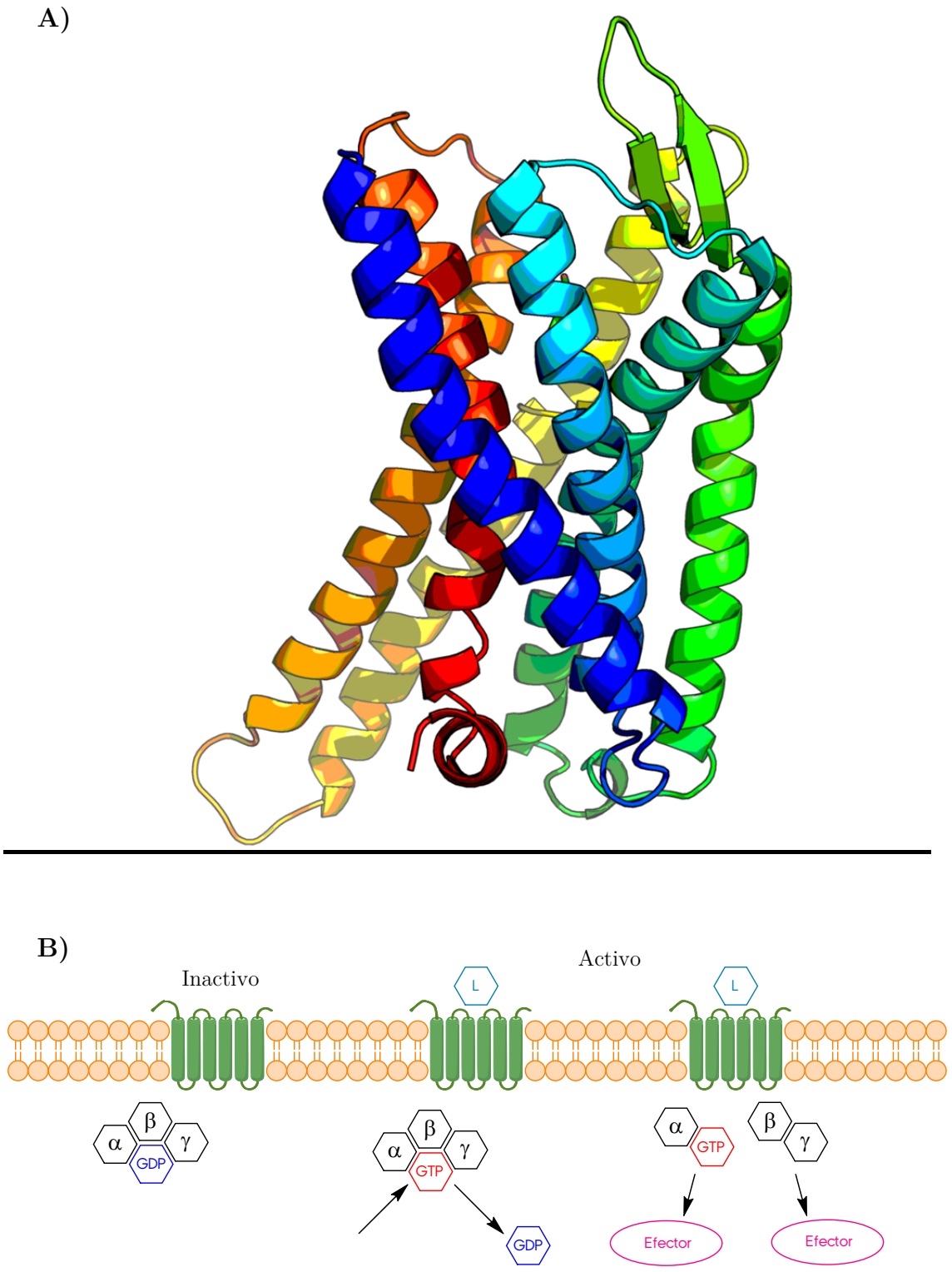

Figura 1. A) Estructura en cintas del receptor μ opioide de ratón (*Mus musculus*). B) Mecanismo de activación de un GPCR por un ligando.

La morfina es un analgésico narcótico usado ampliamente para tratar el dolor de intensidad fuerte. Se aisló por primera vez en 1803 de las amapolas del género *Papaver*, y más tarde, otros alcaloides del mismo tipo como codeina y tebaína. Actualmente, la morfina es considerada como estándar para el alivio del dolor, especialmente el de tipo crónico, a pesar de sus efectos secundarios como tolerancia, dependencia, trastornos respiratorios y constipación. En 1975, dos ligandos endógenos de los receptores opiáceos fueron descubiertos: Met-encefalina y Leu-encefalina.[9] Su origen deriva de la hidrólisis enzimática de sus precursores peptídicos y constituyen los inicios en el estudio de los opioides peptídicos endógenos.

Los ligandos opioides pueden clasificarse en dos tipos: agonistas y antagonistas. No existe una clara división estructural entre ambas clases de ligandos, de hecho, existen ligandos que actúan como agonistas para un receptor y antagonistas para otro. Los agonistas estabilizan el receptor opioide en su forma activa, mientras que los antagonistas lo estabilizan en su conformación inactiva, bloqueando además el acceso a los agonistas. Diversos estudios utilizando espectroscopia por resonancia de plasmones superficiales han revelado la diferencia estructural entre las conformaciones activa/inactiva en el receptor δ.[4]

Se están llevando a cabo muchos esfuerzos para desarrollar nuevos analgésicos que no contengan los efectos secundarios de la morfina; sin embargo, todos los candidatos que se han revisado hasta ahora no han sido capaces de sustituir a la morfina como principio activo de elección. Las principales vías de diseño de nuevos fármacos que actúen como ligandos opioides son dos: 1) la modificación de morfina o análogos y 2) la modificación de ligandos endógenos. Todas estas modificaciones pueden conllevar la adición, sustitución o eliminación de ciertos elementos estructurales y apertura o cierre de ciclos.

En 1975[9] se descubrieron los primeros ligandos endógenos, las encefalinas, y desde entonces se han detectado tanto oligopéptidos opiáceos como sus precursores. La sencillez en la modificación de la secuencia peptídica por síntesis en fase sólida, junto a la posibilidad de insertar aminoácidos no naturales,[10] hace que el diseño de fármacos basados en oligopéptidos sea popular hoy en día.

La modificación de morfina es, probablemente, la vía más explorada en la búsqueda de nuevos fármacos opiáceos. Las modificaciones de la morfina pueden clasificarse en tres tipos (**Fig. 2**):

- *Modificaciones modulativas*: donde la complejidad estructural es semejante.
- *Modificaciones conjuntivas*: en las que nuevos elementos estructurales son añadidos.
- *Modificaciones disyuntivas*: simplificando la diversidad estructural, pero conservando el fragmento esencial para la actividad.

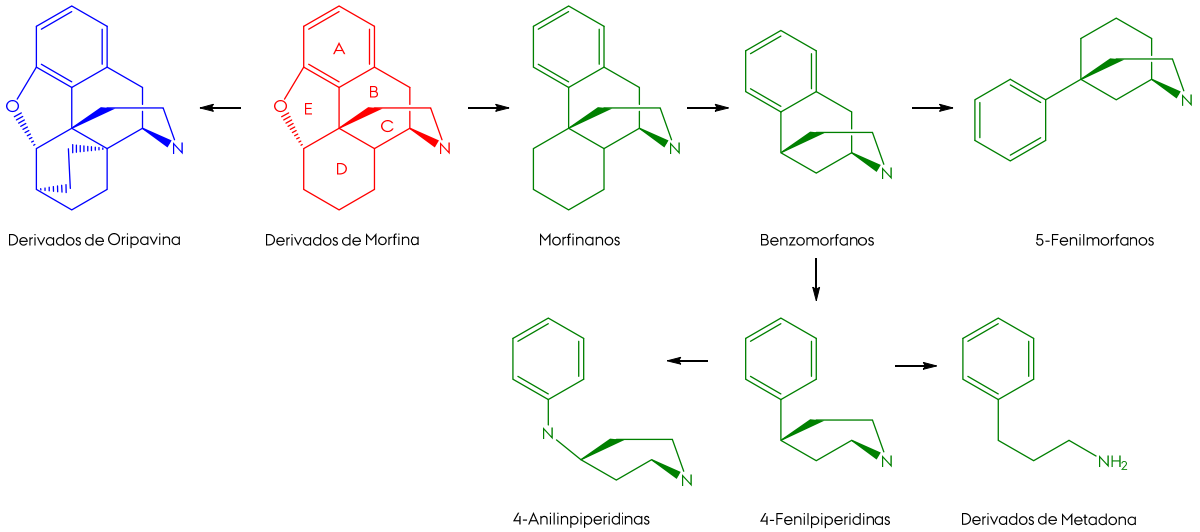

Figura 2. Modificaciones estructurales de la morfina. Azul, conjuntivas; rojo, modulativas; verde, disyuntivas.

Una modificación conjuntiva de morfina constituye la serie de derivados de oripavina. En 1967, Bentley *et al*[11] exploraron la reactividad de tebaína hacia las cicloadiciones de Diels-Alder. Esta nueva gama de productos poseen actividades similares e incluso superiores a la morfina. De entre los miembros de esta clase, cabe destacar Etorfina y Buprenorfina (**Fig. 3**). Etorfina es un agonista fuerte, solamente indicado para la anestesia e inmovilización de grandes animales. Buprenorfina es un ejemplo de agonista parcial, esto es, actúa con una eficacia inferior a la de un agonista puro.[12]

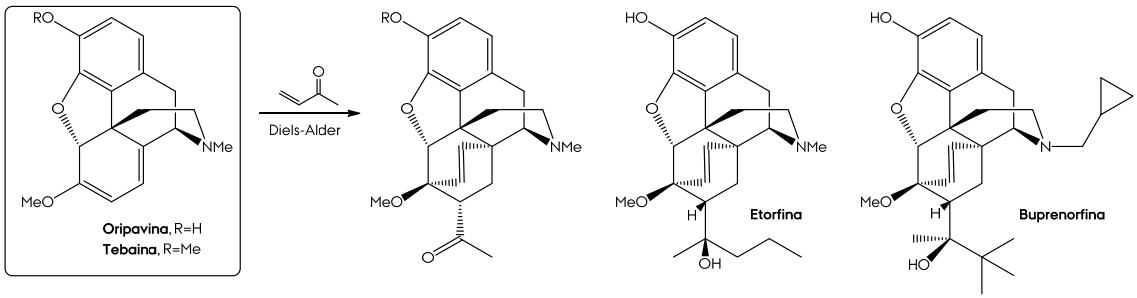

Figura 3. Derivados de oripavina.

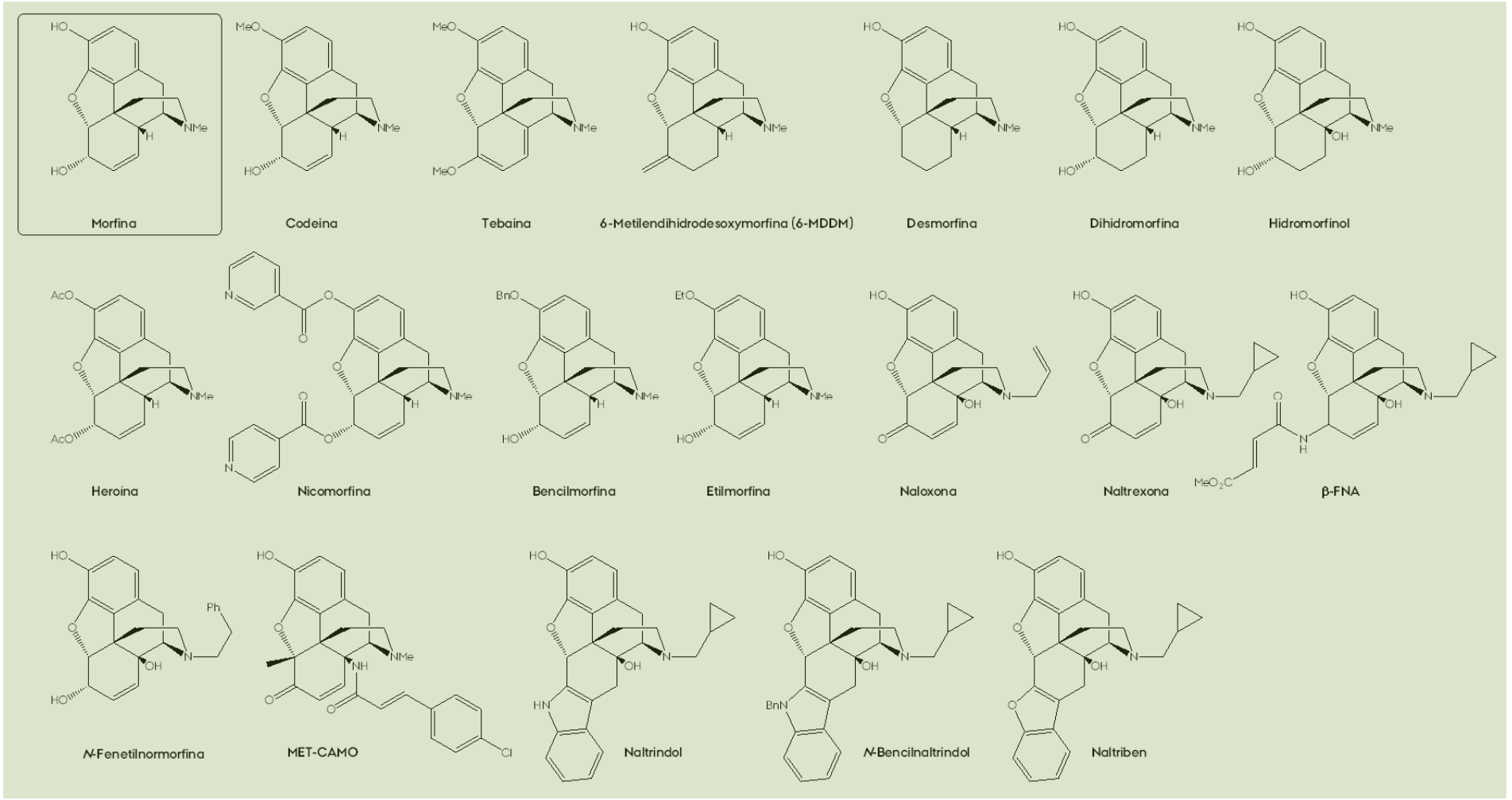

Figura 4. Diversos ejemplos de derivados de morfina.

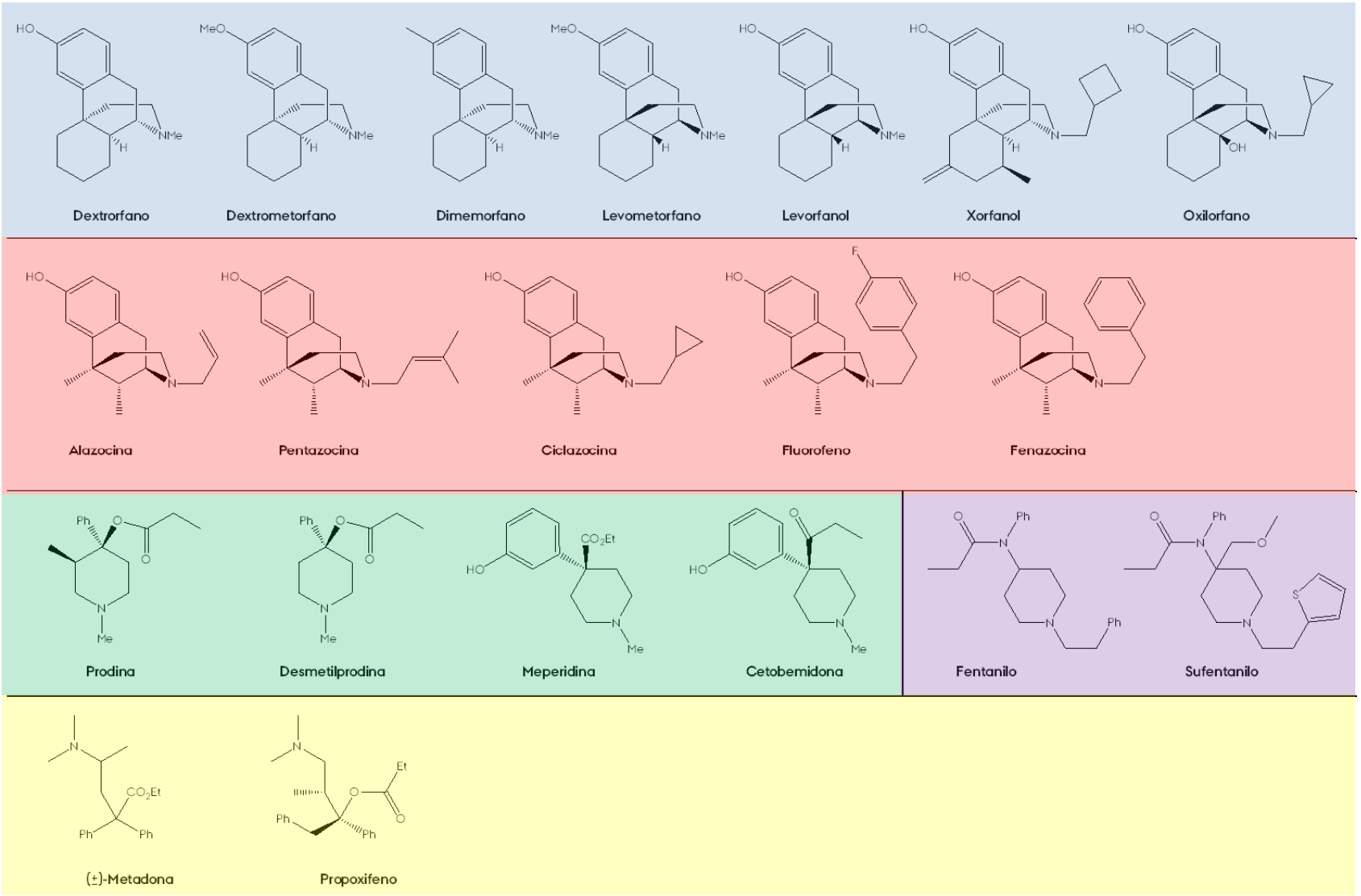

Figura 5. Estructuras de morfinanos, benzomorfanos, 4-fenilpiperidinas, 4-anilinilpiperidinas y metadonas.

Existen muchos compuestos estructuralmente similares a morfina, es decir, son farmacomodulaciones en las que los cinco anillos A-E se mantienen intactos (**Fig. 4**). Codeina es, por ejemplo, un agonista débil empleado como antitusivo. 6-MDDM actúa con mayor rapidez que la morfina, teniendo una actividad mayor.[13] Desmorfina (conocida como "krokodil") o la heroína son derivados conocidos por ser drogas de consumo. Naloxona[14] y naltrexona[15] son ejemplos de antagonistas puros de los receptores opiáceos. Los derivados de tipo indólico, como el naltrindol,[16] son antagonistas específicos del receptor delta.

La diversidad estructural de los fármacos opiáceos fue incrementada con las farmacomodulaciones disyuntivas, donde el esqueleto inicial es simplificado, conservando los fragmentos esenciales para la actividad. Surgen así, por ejemplo, los morfinanos, derivados de morfina en los que ha desaparecido el anillo E. Así, levometorfano y levorfanol son analgésicos ligeramente más activos que morfina. La incorporación en el nitrógeno de un anillo ciclopropánico transforma estos compuestos en antagonistas de los receptores (oxilorfano),[17] mientras que un anillo ciclobutánico les dota de una combinación agonista/antagonista (xorfanol).[18] La serie enantiomérica de los benzomorfanos es conocida por poseer características antitusivas: dextrorfano, dextrometorfano y dimemorfano. Además, estos compuestos actúan como agonistas de los receptores σ[19] y de los receptores NMDA (*N*-metil-*D*-aspartato).[20]

La siguiente modificación disyuntiva es aquella en la que se suprime el anillo D, dando lugar a los llamados morfinanos (**Fig. 5**). Compuestos como alazocina son agonistas opioides, mientras que ciclazocina,[21] pentazocina o fenazocina[22] son agonistas/antagonistas combinados. Fluorofeno,[23] a diferencia de los anteriores, es un agonista puro.

La supresión del anillo B da lugar a una serie de farmacomodulaciones sencillas con diversas propiedades, no solo como analgésicos. Las 4-fenilpiperidinas como prodina,[24] desmetilprodina,[25] meperidina[26] o cetobemidona[27] no solo actúan como ligandos opiáceos, sino que actúan también sobre otros receptores, como el ya comentado NMDA o las proteínas transportadoras de dopamina (DAT) o norepinefrina (NET). Las 4-anilinilpiperidinas tienen un efecto analgésico más corto, lo que hace que puedan emplearse también como anestésicos. Fentanil[28] o sufentanil[29] son así empleados en cirugía.

Finalmente, la supresión de todos los anillo salvo el anillo aromático A lleva a la obtención de las metadonas. Metadona[30] se ha utilizado para combatir la dependencia a otros fármacos opiáceos. Propoxifeno[31] posee propiedades como analgésico, anestésico y antitusivo.

Una farmacomodulación disyuntiva poco explorada es la constituida por los llamados 5-Fenilmorfanos, donde se conservan los anillos A, B y C; pero que se diferencia de las anteriores por no tener fusionados el anillo A-B. El origen de estas estructuras se debe a May *et al,*[32] que publicaron la primera elaboración de 5-fenilmorfano. Puede considerarse esta nueva familia de compuestos como una modificación de los benzomorfanos, donde el anillo A se encuentra reubicado en la posición 5 del sistema 2-azabiciclo[3.3.1]nonano (**Esq. 1**).

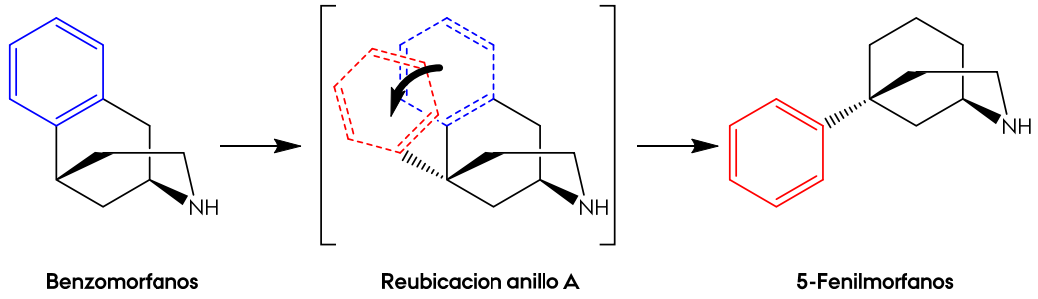

Esquema 1. Origen de los 5-fenilmorfanos.

Burke *et al*[33] continuaron la línea abierta por May, sintetizando nuevos derivados de 5-fenilmorfanos. Su investigación se centró en la preparación de diversos derivados y el chequeo de sus propiedades farmacológicas. Una de las conclusiones que obtuvieron fue que la disposición conformacional del anillo aromático con respecto al biciclo, es decir, su torsión, influye en la muestra o no de actividad. Froimowitz *et al*[34] estudiaron las propiedades conformacionales de este sistema mediante estudios de Mecánica Molecular y RMN, llegando a las mismas conclusiones. El número de derivados de 5-fenilmorfanos ha ido en aumento, en especial los que poseen un grupo hidroxilo en posición *meta* del anillo aromático, los llamados 5-*m*-hidroxifenil-morfanos, debido a su prominente actividad como agonistas/antagonistas de los receptores opiáceos.[35]

Con los conocimientos actuales, la frontera (¿ultima?) que resta en esta área se basa en dos claras ideas: 1) buscar nuevos opiáceos con menos efectos secundarios y 2) comprender las bases farmacológicas de la adicción.

Péptido-Nucleotidos (PNA): Retorno al Principio

El dogma central de la biología molecular[36] establece, como principio, que la información estructural y funcional fluye desde el DNA hacia las proteínas, pasando por el RNA. Es una transferencia de información codificada secuencialmente y refleja la importancia de los ácidos nucleicos y las proteínas para el desarrollo de la vida. Actualmente, esta tríada se completa con la unión de las pequeñas moléculas o metabolitos secundarios.

Debido a su importancia, los ácidos nucleicos también han sido objeto de estudio en la búsqueda de nuevos agentes terapéuticos (pequeñas moléculas, metabolitos o nuevas macromoléculas) capaces de controlar su funcionamiento, producción y/o expresión.

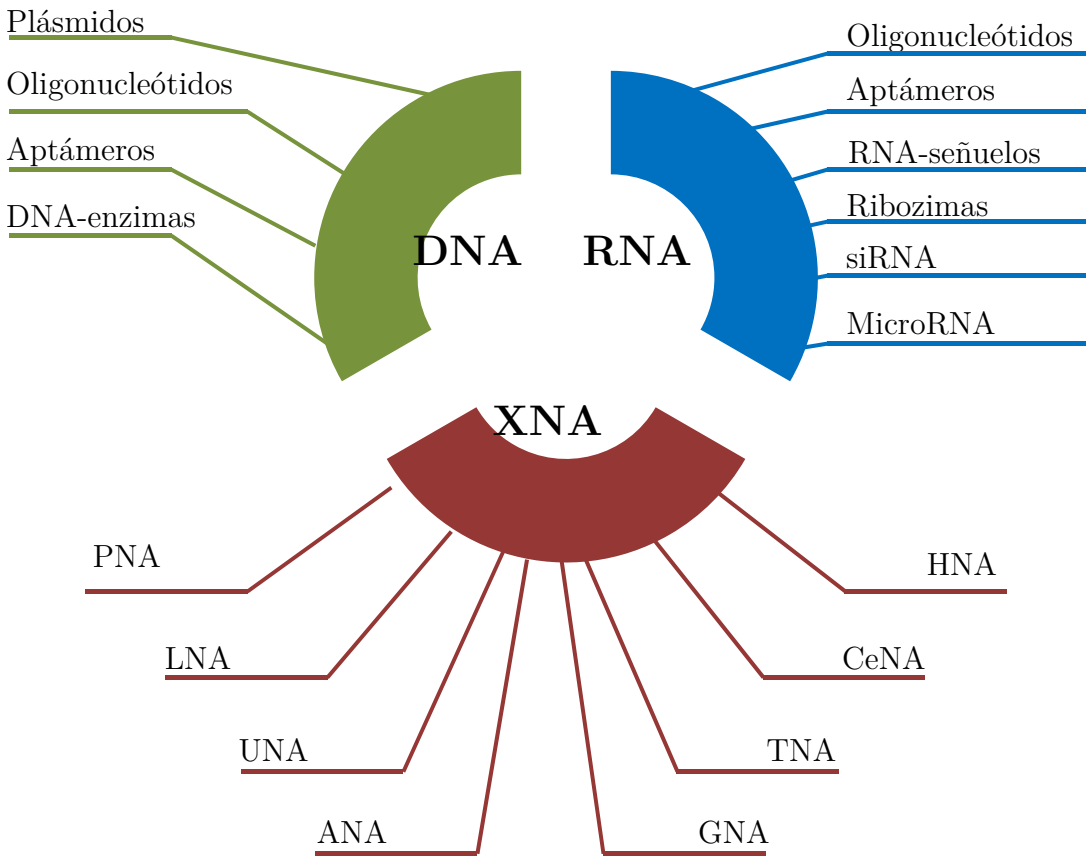

Figura 6. Áreas actuales de investigación terapeútica en ácidos nucleicos.

En la **Fig. 6** se encuentran recogidos los tres principales frentes de investigación en bioquímica de ácidos nucleicos: DNA, RNA y XNA. Los XNA (acidos *xeno*-nucleicos) son ácidos nucleicos no naturales, es decir, poseen alguna modificación

estructural. La esencia estructural es mantenida, es decir, se basa en obtener una serie de análogos similares a los ácidos nucleicos naturales (regresar a estructuras naturales), pero con ciertas modificaciones. Dichas modificaciones pueden efectuarse en el esqueleto del nucleótido (backbone), en el azúcar (sugar) o en la nucelobase (base). Así, obtenemos diversas familias *xeno*-nucleotidas (**Fig. 7**): PNA, ácidos péptido nucleótidos; LNA, ácidos nucleicos bloqueados; UNA, ácidos nucleicos no bloqueados; ANA, ácidos arabino-nucleicos (entre ellos, los populares FANA); GNA, ácidos glicero-nucleicos; TNA, ácidos α-*L*-treofuranosil nucleicos; CeNA, ácidos ciclohexenil-nucleicos; HNA, ácidos hexitol-nucleicos. La **figura 7** muestra una ordenación tridimensional de varias de estas familias de acuerdo con el origen de las modificaciones.

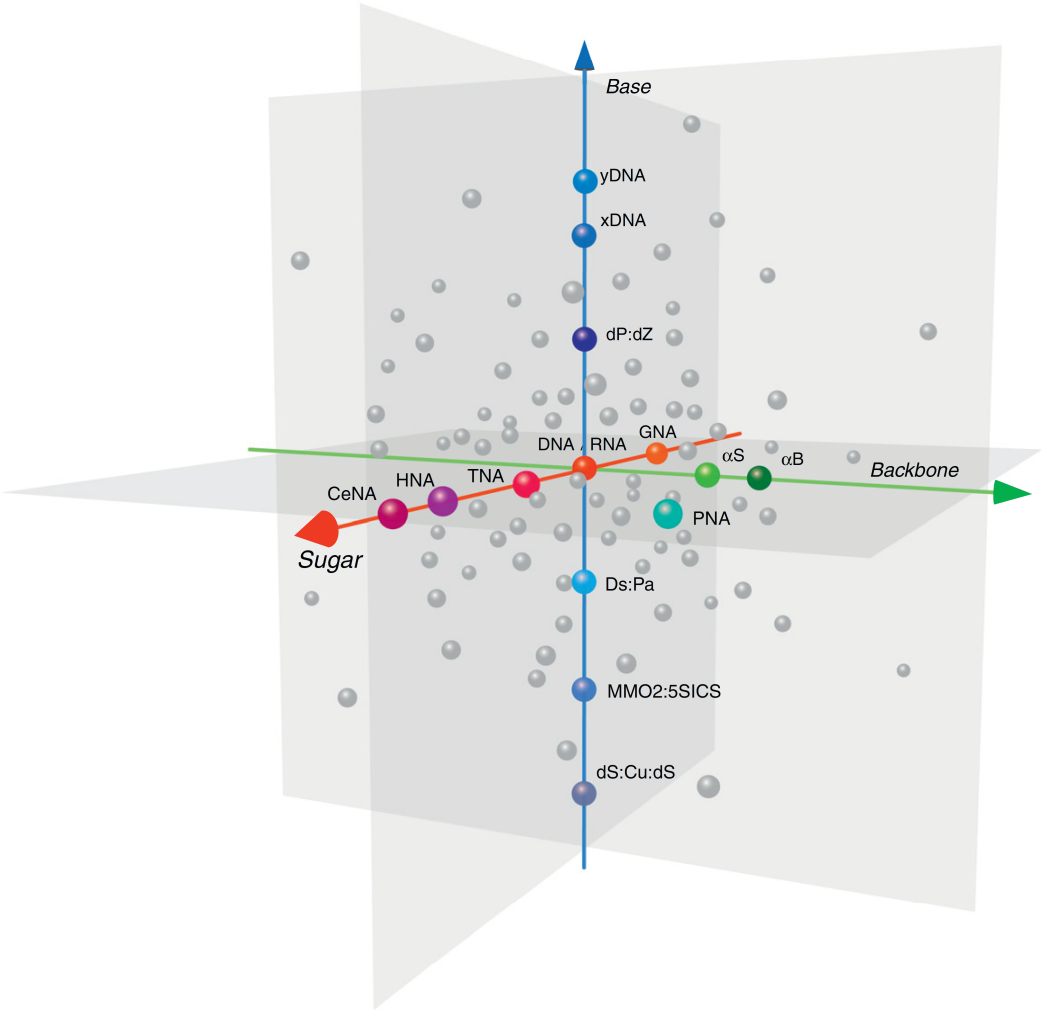

Figura 7. Ordenación tridimensional de varias familias de *xeno*-nucleótidos en función de su modificación estructural. Los PNA, por ejemplo, son el resultado de una modificación conjunta del esqueleto y del azúcar.

En 1991, Nielsen *et al* introdujeron uno de los primeros *xeno*-nucleotidos: los PNA o ácidos péptido-nucleicos. El esqueleto ribosa-fosfato es reemplazado (**Fig. 8**) por una cadena polipeptídica de longitud variable (x/y), pero discreta (6 átomos de longitud). Esto radica en la conservación de la longitud de la unidad monomérica: una unidad más larga o más corta no podría unirse adecuadamente con estructuras nativas.[37] La base nitrogenada se une a la cadena principal por medio de otra cadena.

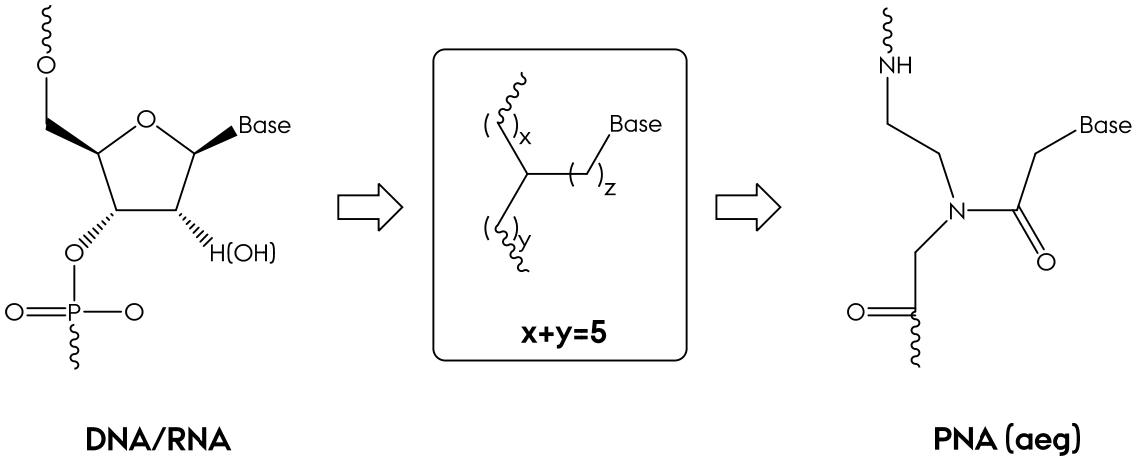

Figura 8. Analogía estructural entre DNA/RNA y PNA.

El primer PNA, desarrollado por Nielsen, fue el *aeg*PNA, el ácido aminoetilglicil nucleico y fue creado a partir de diseños teóricos asistidos por ordenador.[38] Este pseudopéptido pronto demostró una alta afinidad por secuencias complementarias de DNA/RNA, en diferentes concentraciones iónicas, obteniendo híbridos anticomplementarios.

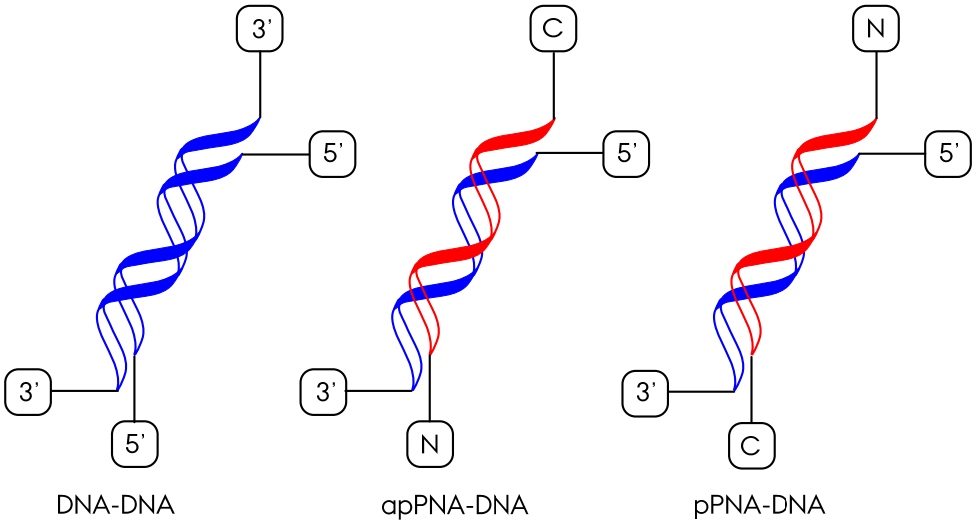

Figura 9. Esquemas de hibridación en los híbridos PNA:DNA.

Estos híbridos pueden ser paralelos o antiparalelos, en función de la orientación del extremo *N*-terminal de la hebra peptídica con respecto al extremo 5' de la hebra nucleótida. Se ha observado que los híbridos de naturaleza antiparalela son más estables que los de tipo paralelo (**Fig. 9**).

También, como consecuencia de su gran capacidad invasora, se han aislado trímeros $(PNA)_2$:DNA empleando péptido-nucleotido con elevada densidad de bases pirimidínicas. Este tipo de invasión requiere la formación de nuevos enlaces de hidrógeno mediante esquemas del tipo Hoogsten[39] (**Fig. 10**).

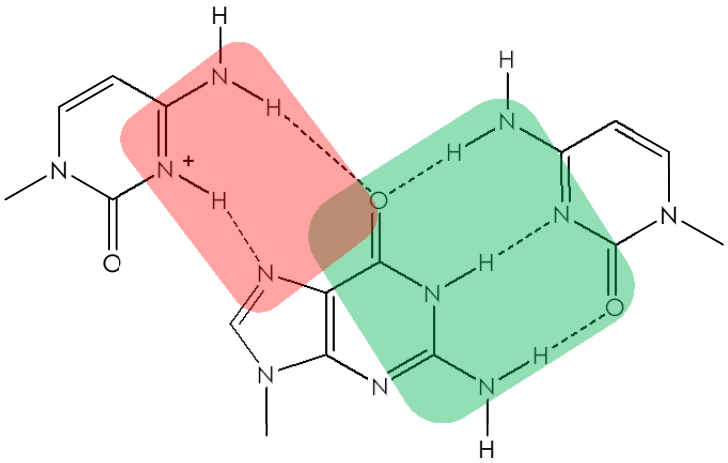

Figura 10. Emparejamiento Watson-Crick (verde) y Hoogsten (rojo).

Se han estudiado las propiedades de híbridos de *aeg*PNA mediante dicroísmo circular, mecánica molecular, RMN, medidas de punto de fusión y cristalografía:

- Dicroísmo circular: los espectros de dicroísmo circular de híbridos antiparalelos de PNA:DNA y PNA:RNA son similares a los espectros nativos de DNA:DNA, demostrando la formación de hélices a derechas no muy diferentes de las estructuras canónicas A y B del DNA. En cambio, los espectros de híbridos originados a partir de PNA paralelo se desvían de la forma nativa, indicando una estructura diferente.

- Mecánica molecular: el análisis conformacional de dobles y triples hélices de PNA:DNA mostró una libertad conformacional similar a la de las estructuras nativas de ADN.

- RMN: estudios de resonancia magnética en disolución probaron la existencia de dobles hélices de PNA:DNA del tipo B, con uniones del tipo Watson-Crick.

- Cristalografía: diversas estructuras cristalinas de dobles y triples hélices de *aeg*PNA:DNA han sido aisladas y sus topologías estudiadas.

Aunque el *aeg*PNA fue el primer péptido-nucleótido publicado y es el más extensamente estudiado, posee ciertos inconvenientes:

- Baja capacidad de absorción celular: estudios realizados *in vitro* han demostrado que las células eucariotas y procariotas no absorben estos análogos. Los *aeg*PNA son expulsados a través de los riñones en pruebas realizadas *in vivo*.

- Expulsión endosómica: uno de los mecanismos que poseen las células para eliminar grandes moléculas hidrofílicas es la expulsión mediante endosomas.

Por ello, se han desarrollado diversas estrategias para solventar estos problemas, basadas en la modificación estructural del esqueleto original de *aeg*PNA, la implantación de nuevas estructuras o la conjugación de otras estructuras.

Una de las primeras modificaciones fue la conjugación de cadenas polipeptídicas naturales para incrementar la captación celular. En 2002, Nielsen *et al*[40] incorporaron dos péptidos, pTAT y penetratin (CPPs, cell penetrating peptides o péptidos de penetración celular), obteniendo resultados interesantes en la absorción celular mediante la formación de endosomas. Otra alternativa utilizada por los mismos autores fue la de añadir colas oligopeptídicas de lisina, con resultados similares. Corey *et al*[41] y Gait *et al*[42] también emplearon oligolisinas conjugadas a cadenas de péptido-nucleótidos para aumentar la afinidad celular (**Fig. 11**). En 2003, Ly *et al*[43] elaboraron un homopolímero de timina-α-GPNA (aminoetilarginine-PNA) y probaron su capacidad de traspaso de membranas frente a varias líneas celulares. Constituye uno de los primeros ejemplos de modificación de la estructura original de *aeg*PNA. De igual manera, otros autores[44] han desarrollado péptido-nucleótidos catiónicos para facilitar la captación celular (**Fig. 11**).

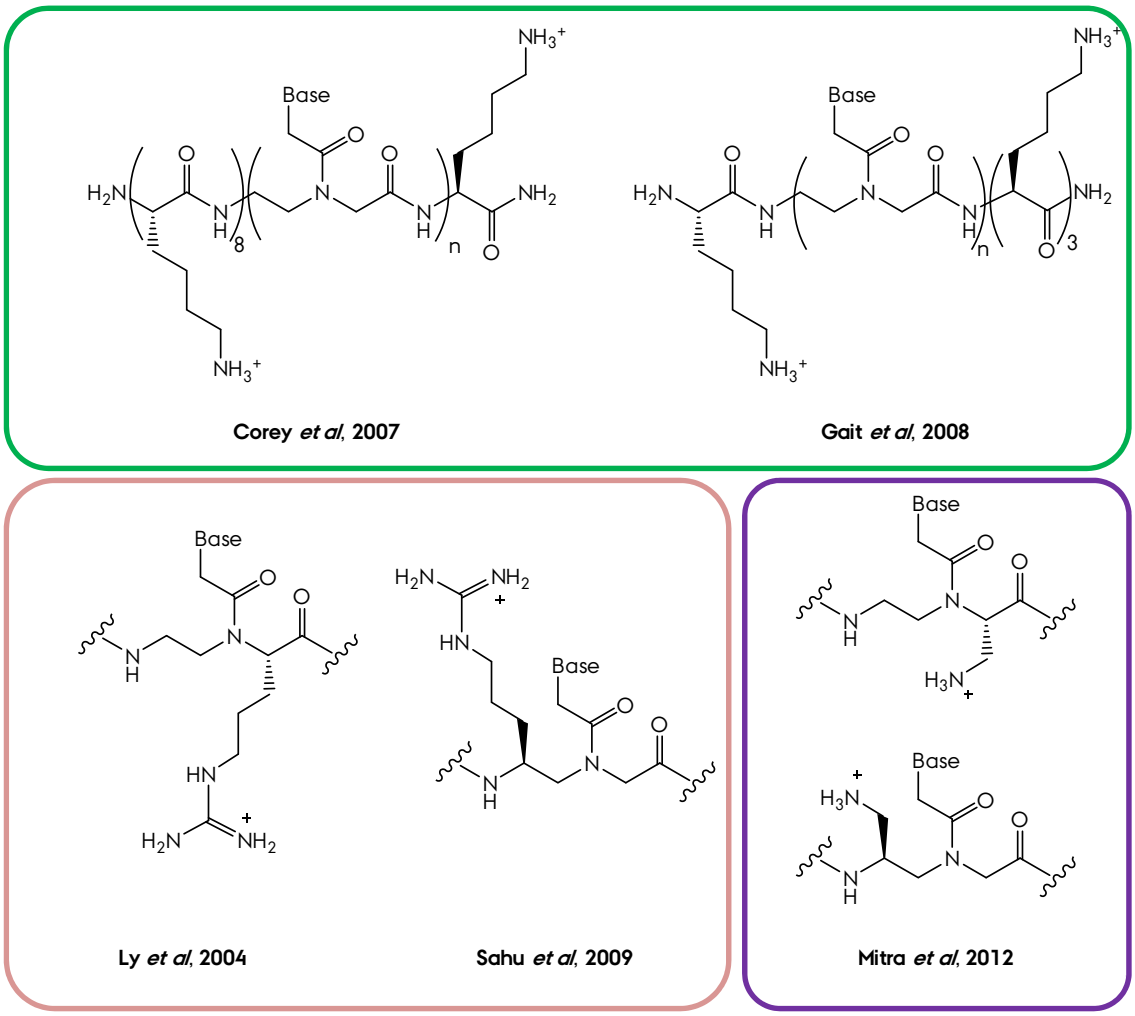

Figura 11. Modificaciones de péptido-nucleótidos para incrementar la captación celular.

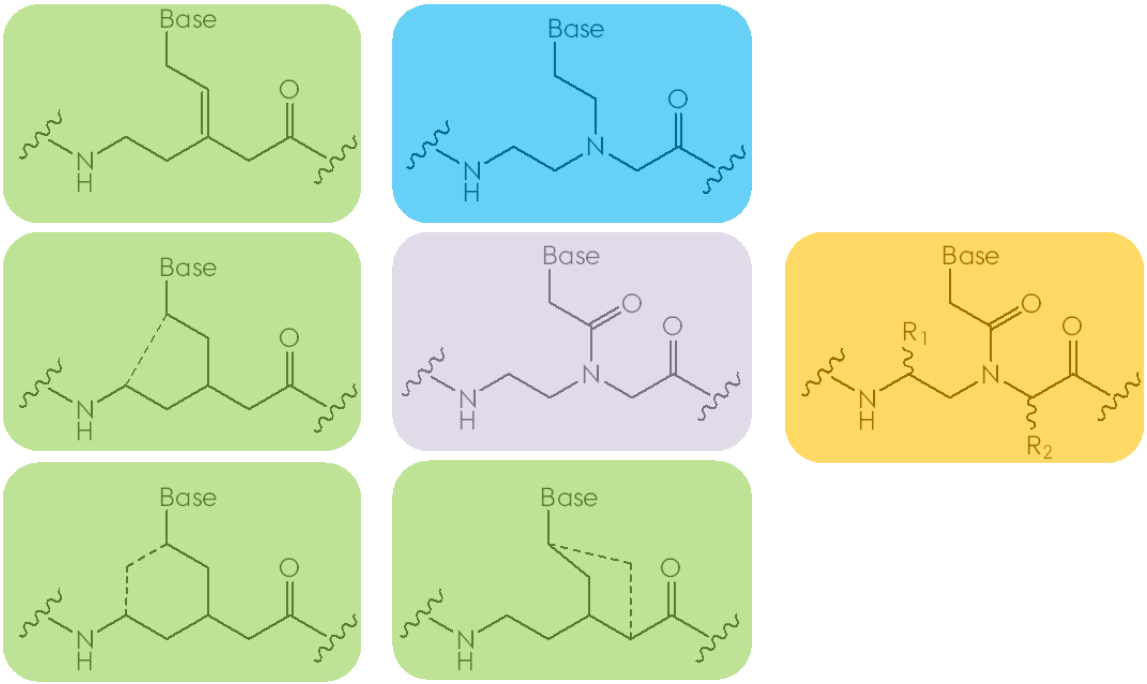

Figura 12. Modificaciones estructurales para el control topológico. Verde: restricción conformacional. Azul: liberación conformacional. Amarillo: inserción de estereocentros.

Otro tema importante en el diseño de péptido-nucleótidos es la preorganización de los oligopéptidos en función de sus estructuras monoméricas.[45] Para controlar su topología, existen diversas estrategias de modificación estructural sobre el esqueleto original de *aeg*PNA (**Fig. 12)**.

La libertad conformacional es clave para establecer una unión adecuada entre PNA y DNA/RNA. Una estructura demasiado rígida o demasiado flexible no se comporta tan bien como el original *aeg*PNA. Así, mediante el cierre de la estructura monomérica en ciclos o la inclusión de dobles enlaces permite restringir la libertad conformacional. Por otra parte, la activación de ciertas torsiones permite el aumento de la flexibilidad. La helicidad de las cadenas oligopeptídicas también puede controlarse estructuralmente. Así, la introducción de estereocentros en la molécula permite controlar el sentido helicoidal de los híbridos DNA-PNA, afectando a la estabilidad de los mismos.

Fig. 13 muestra una serie de péptido-nucleótidos de diversa índole. Una de las estructuras más empleadas es la basada en ciclos de 5 miembros. En verde se encuentran representadas una serie de monómeros cíclicos, muchos de los cuales son de naturaleza pirrolidínica. Esta clase de péptido-nuccelotidos son sintéticamente asequibles partiendo de hidroxiprolina homoquiral o derivados. Los estudios realizados con esta clase de compuestos son numerosos.[46] Otra serie de monómeros estudiados son aquellos con un ciclo de 6 miembros, piperidínicos o ciclohexánicos (**Fig. 13**, azul).[47] En rojo aparece un ejemplo sencillo de introducción de un estereocentro con drásticas consecuencias en la helicidad, como se ha demostrado mediante dicroísmo circular. La forma *S* contribuye a la formación de un híbrido DNA:PNA con helicidad a derechas, mientras que la forma *R* perjudica esta unión.[48] En amarillo se encuentra representado una unidad flexible y quiral de PNA, con un esqueleto puramente hidrocarbonado.[49] Finalmente, recuadrados en púrpura, se encuentran representados otra serie de monómeros de mayor polaridad, que facilitan la disolución de los mismos en disoluciones acuosas, reemplazando unidades metileno por oxígeno (oxyPNA)[50] o cambiando radicalmente la unión entre monómeros (de amida a triazol, T-PNA).[51]

En los últimos años, una variedad copolimérica de lo PNA, los llamados PNA-composites, han aparecido con fuerza, debido a la posibilidad de modular las propiedades de un monómero mediante la conjugación con una segunda unidad monomérica de naturaleza distinta.

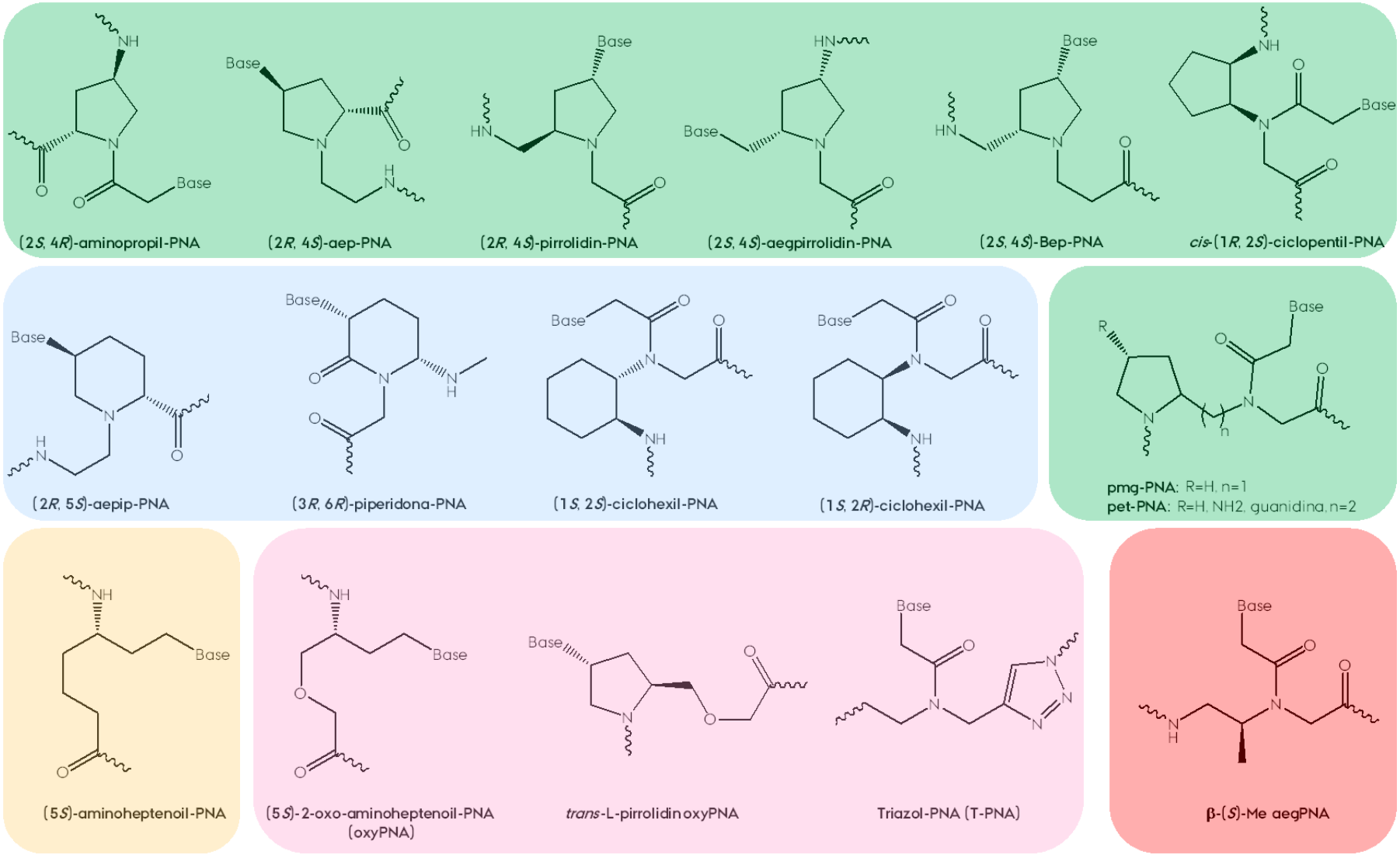

Figura 13. Modificaciones estructurales de péptido-nucleotidos.

Varios ejemplos están representados en la **Fig. 14**. Prolil-(ACPC)-PNA posee dos unidades monoméricas: una unidad de prolina que posee incorporada la base, y una unidad del ácido 2-amino-ciclopentanocarboxílico (ACPC). Se ha demostrado que este PNA-composite es capaz de unirse selectivamente al DNA con respecto al RNA. Por otra parte, reemplazando la unión amida por grupos fosfatos, como en el caso de (1*R*, 4*S*)-pHypPNA, incrementa la solubilidad en fase acuosa en los llamados fosfono-PNA.[52] Finalmente, las llamadas estructuras quimera-PNA permiten intercalar un residuo de PNA con otro de DNA, manteniendo ciertas características originales del DNA.[53]

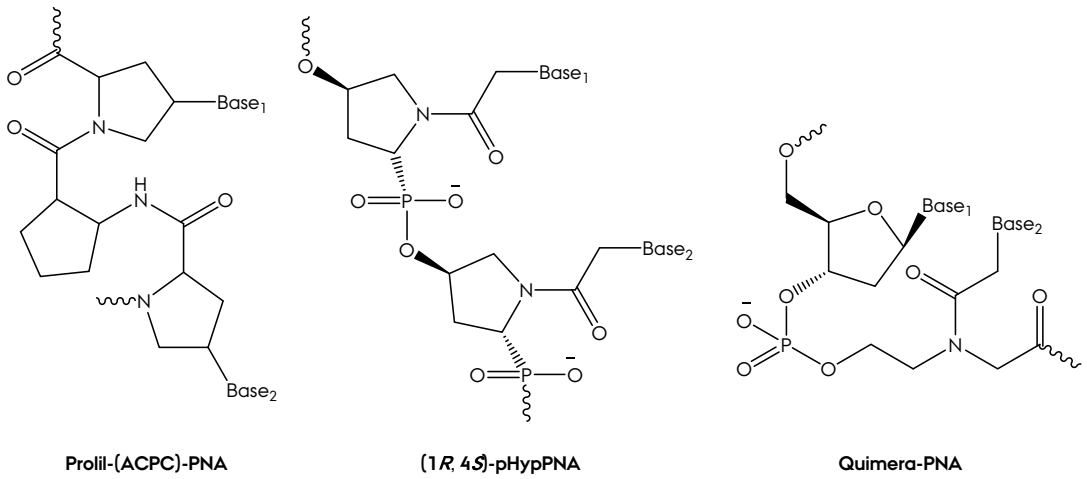

Figura 14. Ejemplos de PNA-composites.

En general, los péptido-nucleótidos (PNA) poseen las siguientes características:

- Gran afinidad por secuencias complementarias de DNA/RNA. La fuerza de unión es mayor, debido a la desaparición de la carga negativa en la hebra péptido-nucleica. Esta afinidad hace que los PNA posean una gran capacidad de invasión de otras estructuras nucleicas.

- Gran resistencia a endo/exonucleasas, permitiendo un mayor período de actuación.

- Facilidad de síntesis, recurriendo a los métodos de síntesis de proteínas, como la síntesis en fase sólida.

- Baja toxicidad en animales.

- Solubilidad variable, en función del esqueleto peptídico.

Una de las primeras aplicaciones de los PNAs se basa en la inhibición de la biosíntesis natural de proteínas. Los PNA pueden interferir en este proceso a través de dos vías (**Fig. 15**).

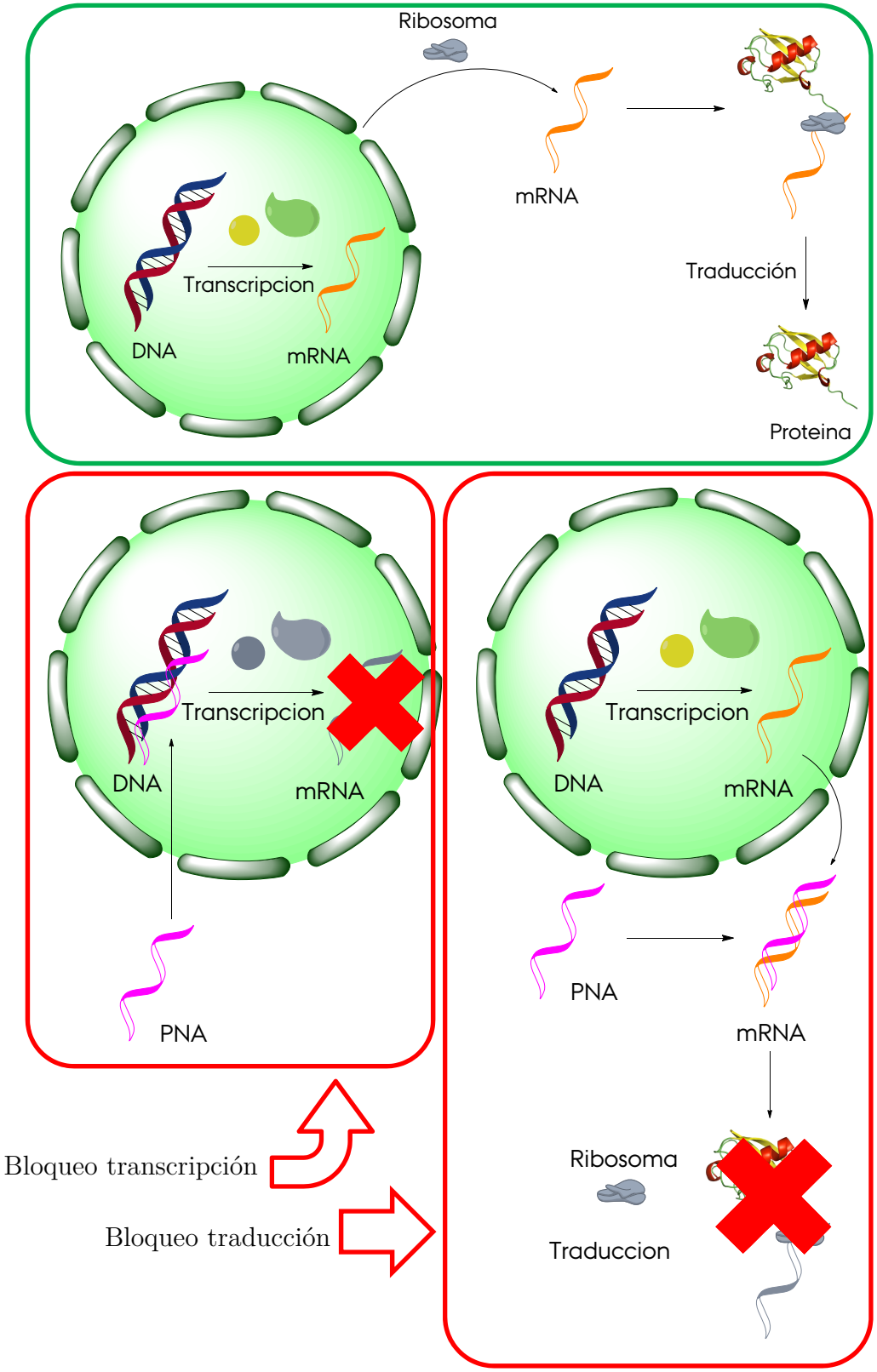

Figura 15. Rango de actuación de los PNA en la inhibición de biosíntesis de proteínas.

Mediante el bloqueo de un gen en particular de DNA con una hebra anticomplementaria de PNA, se suprime el proceso de transcripción del material genético, lo que es conocido como efecto antígeno. Por otra parte, el RNA mensajero citoplasmático también puede bloquearse con la acción de un PNA, de nuevo anticomplementario, bloqueando el proceso de traducción por parte de la batería de ribosomas citosólicos. Este efecto es conocido como efecto anti-sense. Así, una aplicación principal de los PNA es el control de la expresión genética. Otra aplicación relacionada es el bloqueo de la replicación. En este caso, se evita la proliferación celular al evitarse la duplicación del material genético.

Existen otras aplicaciones potenciales de los PNA, que pueden resumirse en el siguiente esquema:

- Biomedicina: a parte de la capacidad de inhibir la biosíntesis de proteínas, los PNA posee otras múltiples aplicaciones: amplificación PCR, medida de longitud de los telómeros, sistemas artificiales de enzimas de restricción, purificación de DNA, MRI, etc.[54]

- Biosensores: uno de las áreas más prometedoras de los PNA, especialmente en el área de análisis y control de alimentos.[55] La elaboración de biosensores basados en PNA permite la detección de organismos modificados genéticamente (GMO), determinación de organismos patógenos o la presencia de alérgenos.[56]

- Síntesis: un área poco explorada es la utilización de PNA para acelerar las reacciones químicas. Una hebra de DNA sirve de molde para una cadena anticomplementaria de PNA. Esta cadena es fragmentada en dos, uniendo a sus extremos dos sustratos. La hibridación de los fragmentos de PNA con el molde de DNA permite el rápido encuentro de los reactivos y su inmediata reacción.[57]

Modelización Molecular: Química Digital

Toda disciplina científica posee dos métodos de estudio:

- el método empírico, basado en el estudio experimental de los fenómenos que ocurren en la naturaleza: origen, desarrollo y consecuencias.

- el método teórico, el cual desarrolla ideas, hipótesis, modelos y fórmulas que tratan de describir los fenómenos que se suceden en la naturaleza.

El método científico es, así, dual, complementario y recíproco. La Química, como área científica, requiere de estos dos métodos para comprender los procesos implicados en la transformación de la materia. Desde sus inicios como ciencia experimental, la Química ha ido reuniendo conceptos teóricos propios, como por ejemplo los modelos atómicos o las teorías de enlace; pero además ha adquirido ideas y axiomas de otras áreas, como los principios de la termodinámica (Física), o los innumerables modelos matemáticos (Matemática). La Química teórica reúne siempre ideas y desarrollos propios de la Física y de las Matemáticas.

La complejidad de muchos problemas o situaciones reales requieren de complejos modelos que permitan describirlos teóricamente. Los computadores han permitido extender y acelerar el estudio de esta clase de modelos más allá de las capacidades humanas. Así, la Química Teórica y Computacional ha surgido como respuesta a la búsqueda de métodos capaces de gestionar grandes cantidades de información en poco tiempo. Esta rama incluye no solo los aspectos, teorías y modelos empleados en investigar los fenómenos químicos, sino que además se encarga de estudiar la implementación de dichos aspectos a un nuevo lenguaje: el lenguaje computacional.

Una de las áreas de la Química Teórica y Computacional es la Modelización Molecular, que recrea de manera teórica ("digital") el comportamiento real de las moléculas ("analógica"). La Modelización Molecular es un compendio de teorías, métodos matemáticos, algoritmos, implementaciones, etc., que constituyen una serie de herramientas para simular en un entorno *in silico* los procesos químicos reales.

Una de los criterios de clasificación de la Modelización Molecular es según el conjunto de leyes que describen las propiedades de un sistema, la llamada ecuación dinámica (**Fig. 16**). Toda partícula posee dos características identificativas: masa y

velocidad. En función de estas dos variables, los sistemas químicos (sistemas de partículas cargadas) pueden organizarse en cuatro grupos:

- Cuánticos: donde los sistemas están descritos de acuerdo con la ecuación de Schrödinger.

- Clásicos: en la que los sistemas se rigen por las leyes del movimiento de Newton.

- No relativistas: aquellas partículas cuyas velocidades son inferiores a las de la velocidad de la luz.

- Relativistas: cuando las partículas se mueven a velocidades próximas a las de la luz.

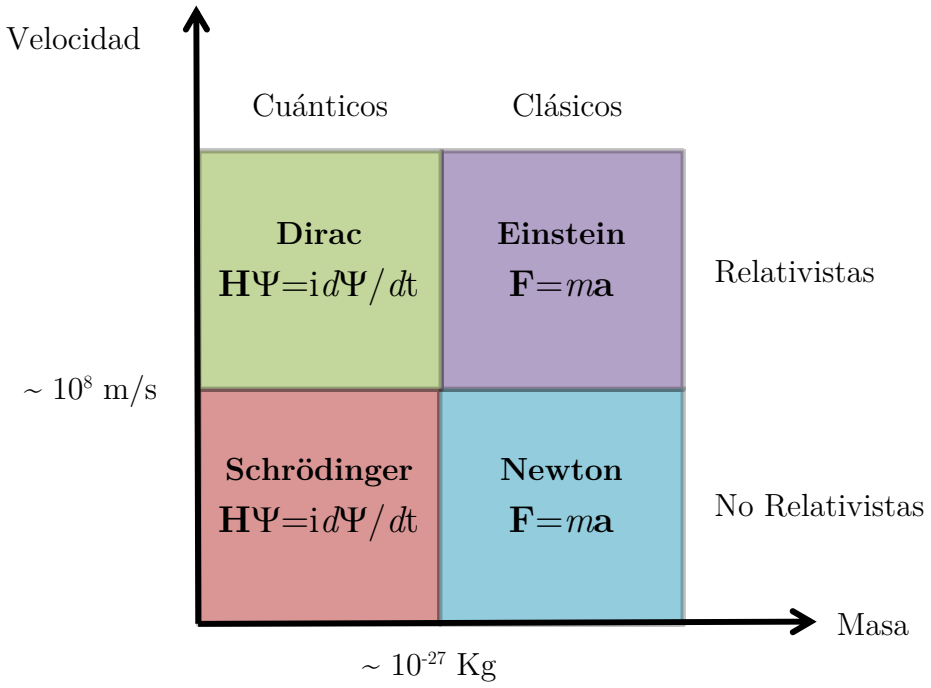

Figura 16. Dominios de las ecuaciones dinámicas.

Los métodos clásicos son *deterministas*, mientras que los métodos cuánticos son *probabilistas*. La división entre ambas concepciones es el átomo: los electrones solo pueden ser descritos por métodos cuánticos; los núcleos atómicos y sus conjuntos (moléculas) se comportan como partículas clásicas. La frontera de 1/3 de la

velocidad de la luz (~ 10^8 m/s) suele considerarse como límite en el tratamiento relativista de los sistemas.

Otro de los criterios generales de clasificación de la modelización molecular es la basada en las metodologías de estudio. Un criterio de organización personal, que describe los métodos recogidos en este trabajo, es el representado en la **Fig. 17**:

- *Mecánica Cuántica (QM)*: el estudio de los sistemas de acuerdo con el análisis de la ecuación de ondas y la resolución de la ecuación de Schrödinger por métodos aproximados. Es el método más general para estudiar mecanismos de reacción, estados de transición y propiedades moleculares con profundidad.

- *Mecánica Molecular (MM)*: aquí, los sistemas son estudiados de acuerdo con una concepción clásica, newtoniana, y el método se basa en resolver la ecuación de potenciales moleculares. Estos potenciales poseen una serie de parámetros, representativos de grupos locales atómicos, obtenidos por métodos cuánticos o empíricos. Unido a ciertos métodos adicionales, como el *Monte Carlo*, el *Metrópolis* o el algoritmo Genético, permite expandir sus aplicaciones más allá de simples cálculos de energías: Docking, análisis conformacional… Su rango de aplicabilidad se extiende a sistemas de cualquier tamaño.

- *Dinámica Molecular (MD)*: la evolución de los sistemas en el tiempo de acuerdo con el modelo clásico newtoniano. Los potenciales moleculares son aplicados conjuntamente con las ecuaciones del movimiento de Newton. Sus aplicaciones van desde los análisis conformacionales hasta el estudio dinámico de grandes sistemas moleculares, como proteínas o ácidos nucleicos.

La Modelización Molecular ha sido la base de muchos avances científicos en ciencia de los materiales, bioquímica y biomedicina, elucidación estructural, etc. Prueba de ello es el reconocimiento con el Premio Nobel de Química 2013 a Martin Karplus, Michael Levitt y Arieh Warshel, por su contribución al desarrollo de modelos multiescala para el estudio de sistemas químico complejos.

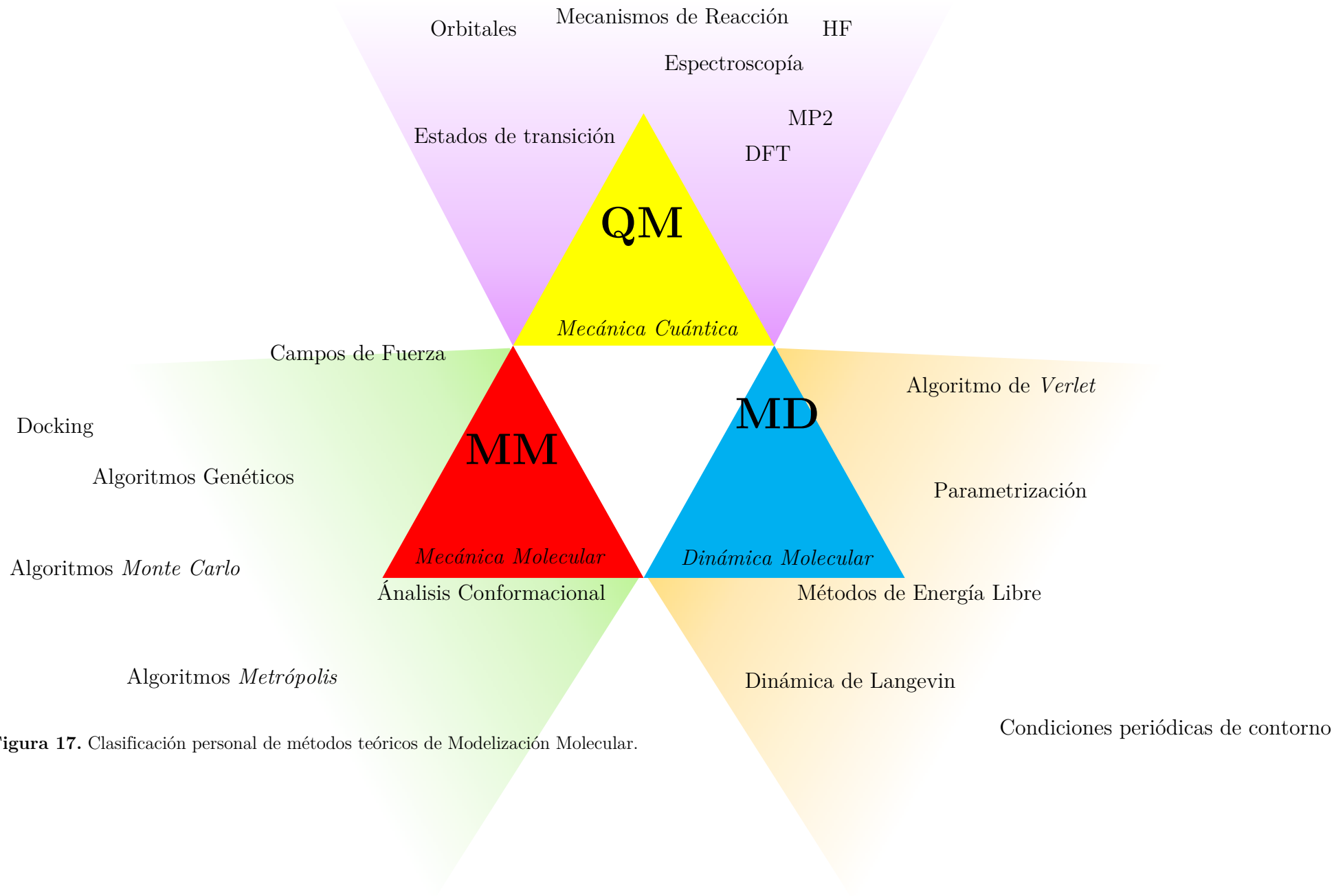

Figura 17. Clasificación personal de métodos teóricos de Modelización Molecular.

Amiduros de Litio Quirales: Un Camino Hacia los β–Aminoácidos

En 1973, Schlessinger *et al*[58] encontraron el primer caso de adición conjugada de amiduros de litio, mientras estudiaban la desprotonación en γ de *E*-crotonato de etilo con LDA. Hasta entonces, la utilización de los amiduros de litio había estado limitada a su uso como bases fuertes no nucleófilas, como es el caso de LDA, que puede producir desprotonación estequiométrica de carbonilos enolizables sin problemas de adición-1,2 (**Esq. 2**).

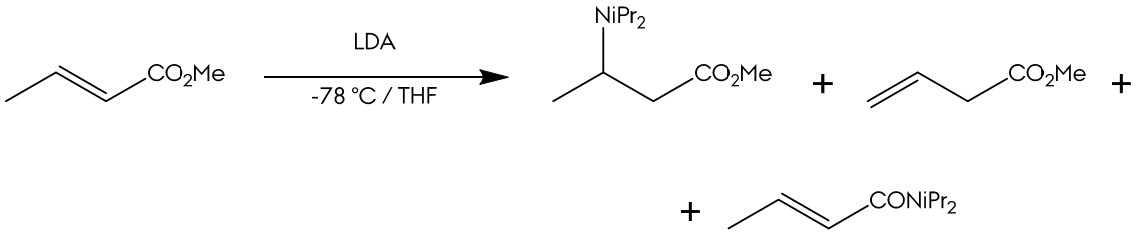

Esquema 2. Reacción de LDA con *E*-crotonato de metilo.

Sin embargo, el tema no fue estudiado con más detalle hasta 1987 por Yamamoto *et al*,[59] observando que amiduros de litio derivados de *N*-benciltrimetilsililamina experimentan limpiamente adición 1,4 (**Esq. 3**).

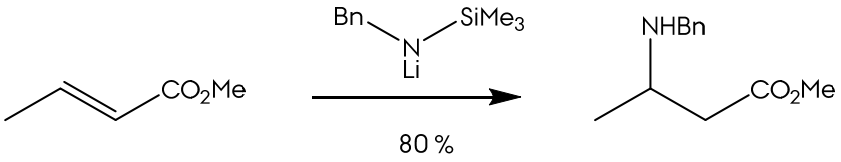

Esquema 3. Reacción de *N*-benciltrimetilsililamina con *E*-crotonato de metilo.

Hawkins *et al*[60] comunicaron la primera reacción de adición conjugada asimétrica por control del reactivo utilizando un amiduro de litio como nucleófilo. La adición de binaftil amiduro de litio quiral (**Esq. 4**) a ésteres *E*-crotónicos conduce a excesos diastereoisoméricos de hasta un 97 %. Este amiduro tiene el inconveniente de que además de ser caro, especialmente en su forma quiral, se elimina con dificultad una vez realizada la adición.[61]

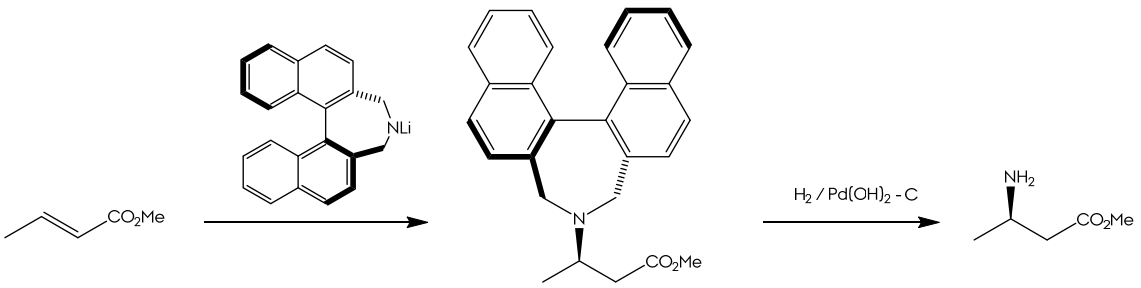

Esquema 4. Adición conjugada de Hawkins.

Enders *et al* ha descrito la adición de Michael nucleófila de *N*-silil amidas quirales a ésteres α,β-insaturados con elevada diastereoselectividad, aunque se requieren condiciones extremas para la posterior ruptura del enlace N–N (**Esq. 5**).

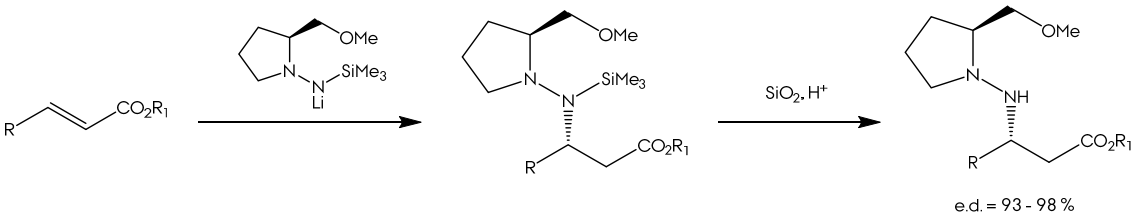

Esquema 5. Adición conjugada de Enders.

Davies *et al*[62] han publicado una revisión exhaustiva en esta área química explicando el alcance, limitaciones y aplicaciones sintéticas del uso de amiduros de litio quirales como equivalentes de amonio homoquiral en reacciones de adición conjugada. Especialmente, se han centrado en amiduros con el grupo *N*-α-metilbencilo como nucleófilos a ésteres *E*-α,β -insaturados y amidas, produciéndose la adición con elevado grado de selectividad π-facial (**Esq. 6**).

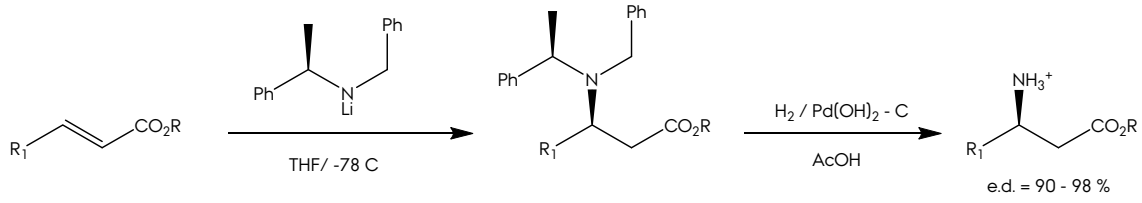

Esquema 6. Adición conjugada de Davies

Los grupos bencilos de la amina se pueden eliminar fácilmente por hidrogenolisis, lo que la convierte en una metodología general para la síntesis enantioselectiva de β-aminoácidos y β-aminoésteres. Además del elevado exceso enantiomérico que se consigue, atractivo adicional para esta metodología es el poder disponer de ambos enantiómeros de la α-metilbencilamina económicamente accesibles.

En los últimos años la síntesis de β-aminoácidos está teniendo especial relevancia, ya que aunque menos abundantes que sus análogos α, también se encuentran presentes en la naturaleza. Se han aislado β -aminoácidos en forma libre con importantes propiedades farmacológicas. Sus productos de ciclación, las β-lactamas, suponen la familia más numerosa de compuestos que poseen la unidad de β-aminoácido y durante mucho tiempo las más representativas han sido penicilina y cefalosporina (**Fig. 18**). Recientemente, se han descubierto nuevas clases de antibióticos β-lactámicos como son monobactamas, carbapenémicos y tribactamas, que combinan su gran rango de actividad con una elevada potencia y resistencia a β-lactamasas y elevada estabilidad frente a deshidropeptidasas.

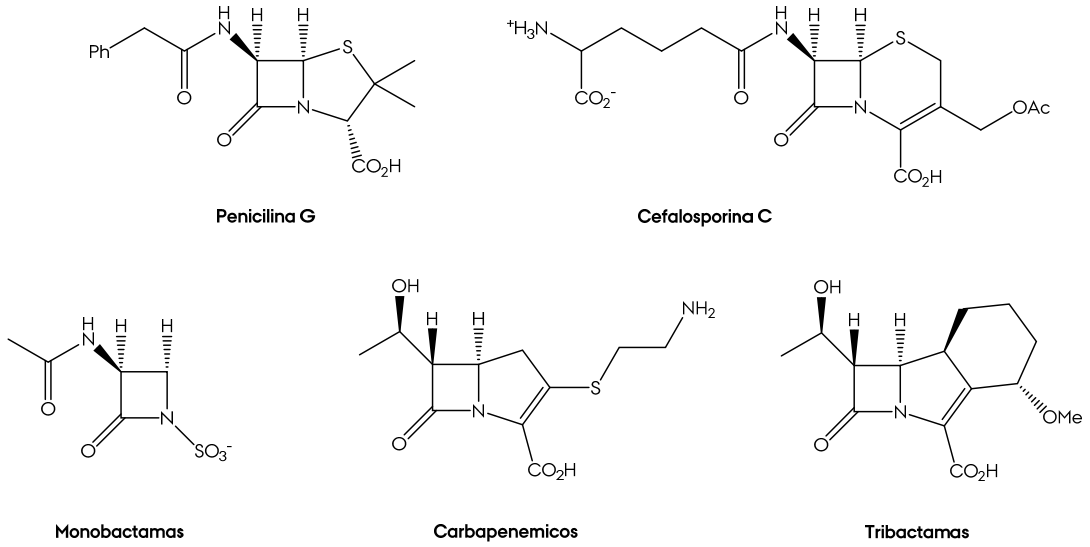

Figura 18. Ejemplos de varias β-lactamas con actividad antibacteriana.

En gran variedad de productos naturales se pueden encontrar β-aminoácidos más complejos. Así, lavandomicina aislada de *Streptomyces lavendulae*, es un antibiótico hexapeptídico que contiene la unidad de ácido (2*S*,3*S*)-2,3-diaminobutírico (Dab).

Uno de los productos naturales más interesantes y que ha sido objeto de extenso estudio es el taxol, complejo diterpénico polioxigenado aislado de *Taxus brevifolia* o *Taxus baccata* (tejo común), que contiene un α-hidroxi-β-aminoácido en su estructura, (–)-*N*-bencil-(2*R*,3*S*)-3-fenilisoserina (**Fig. 19**). Actualmente está considerado como el agente anticancerígeno más importante. Aunque las reservas naturales del taxol son limitadas, se ha encontrado un precursor del taxol, 10-deacetil baccatin, sin la cadena lateral de β-aminoácido y que no presenta actividad biológica.

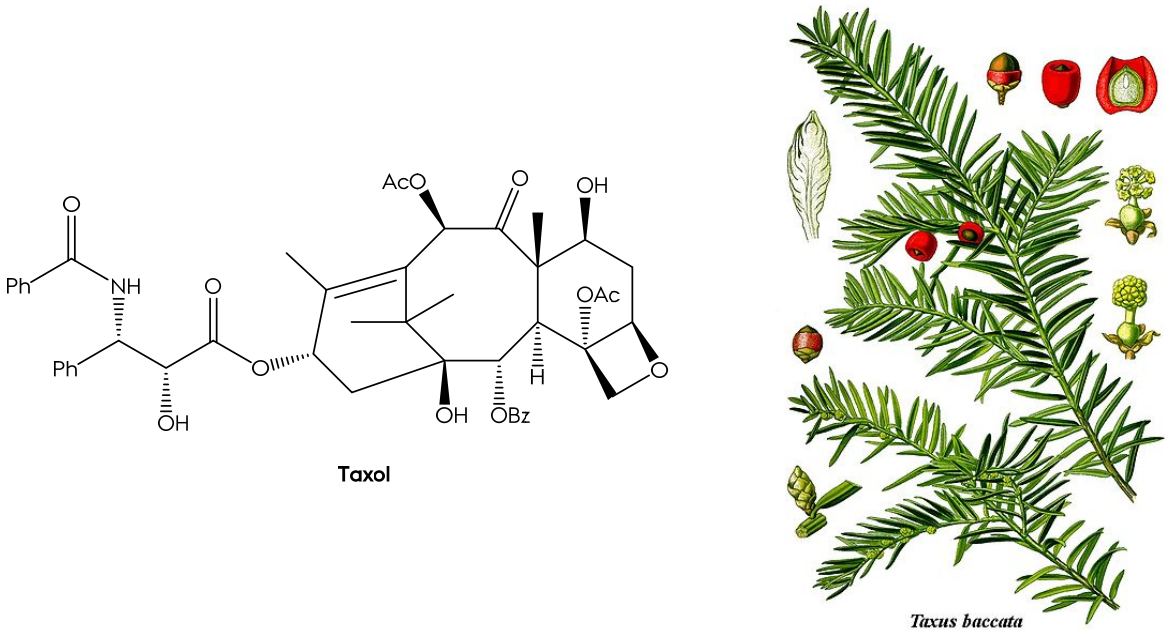

Figura 19. Estructura del taxol, de *Taxus baccata*.

Diferentes anillos de seis miembros aparecen en las estructuras de antibióticos producidos por las especies de *Streptomices* (**Fig. 20**). Así por ejemplo, Streptothricina F representa a una gran familia de los antibióticos streptothricinas que contienen el residuo de β-lisina y otro de aminoazúcar. Blasticidina S, un antibiótico aislado de *Streptomyces griseochromogenes*, tienen una cadena de β-arginina y un residuo de ACHC (ácido 2-amino-ciclohexanocarboxílico) y se usa en Japón contra *Pyricularia oryzae* (parásito del arroz).

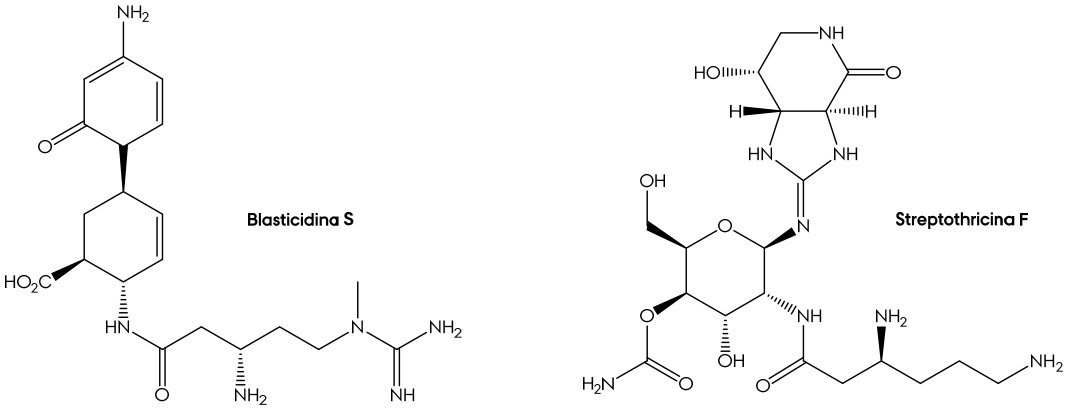

Figura 20. Estructuras de Blasticidina S y Streptothricina F.

En los últimos tiempos, el interés por estructuras cíclicas de β-aminoácidos ha aumentado exponencialmente, convirtiéndose en un área relevante en química sintética y medicinal. Algunos de ellos muestran actividad antibacteriana, como cispentacín, aislado de *Bacillus cereus* y *Streptomyces setonii* que forma parte del antibiótico amipurimicina, que es muy activo tanto *in vivo* como *in vitro* contra la

pilicularia del arroz. Otros ejemplos son BAY 9379 ó PLD-118, que constituyen bloques estructurales de péptidos, alcaloides y heterociclos (**Fig. 21**).

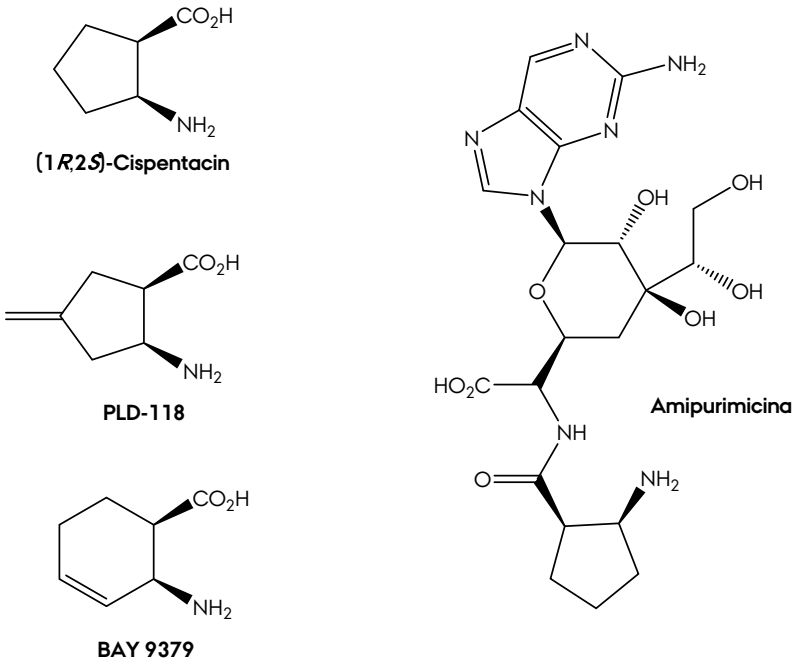

Figura 21. Estructuras de β-aminoácidos cíclicos.

Aunque existe un rango extenso de metodologías estereoselectivas para el acceso a estructuras monocíclicas, son pocos los estudios que se centran en esqueletos bicíclicos con interesantes perspectivas. De entre las distintas variedades de biciclos condensados con la funcionalidad comentada, aquellos con esqueleto biciclo[n.m.x]alcano (biciclos condensados tipo puente) representan un sector prometedor en el campo sintético y terapéutico. Así, la serie constituida por β-aminoácidos con construcción de norbornano/eno, poseen propiedades terapeúticas atractivas como analgésicos, al tanto que diversos derivados son prometedores agentes en el tratamiento del Alzheimer, artritis, esclerosis múltiple, fibrosis pulmonar, asma o rinoconjuntivitis (**Fig. 22**).

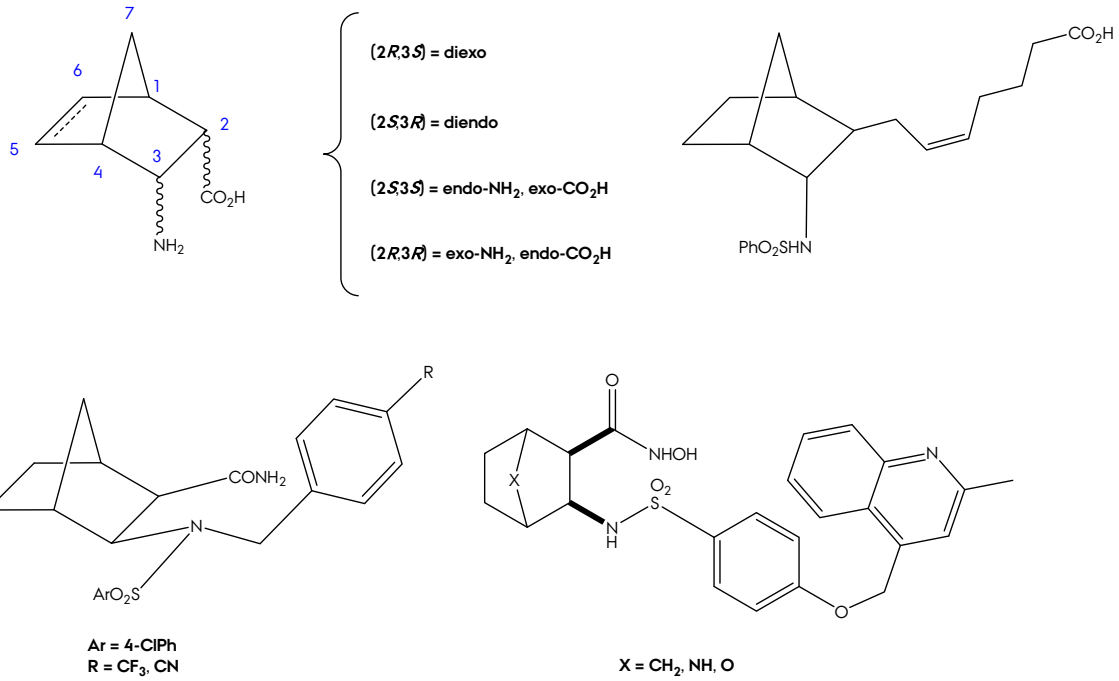

Figura 22. Estructuras de β-aminoácidos bicíclicos.

También han sido objeto de investigación los aminoácidos con el grupo amino integrado en la estructura mono/bicíclica. Así, los derivados del ácido nipecótico interactúan en la sinapsis GABAérgica: proceso de sinapsis neuronal en la que el ácido γ-aminobutírico inhibe la estimulación postsináptica, impidiendo la transmisión de impulsos nerviosos. El estudio del metabolismo del GABA y de la existencia de neuronas GABAérgicas, encargadas de la inhibición del impulso nervioso, determina un campo terapéutico prometedor en el estudio de desórdenes del sistema nervioso central como la epilepsia. Así, derivados como la isoguvacina son agonistas de la recepción de GABA, mientras que gabaculina, guvacina y el ácido nipecótico son antagonistas del metabolismo de este neurotransmisor. (**Fig. 23**).

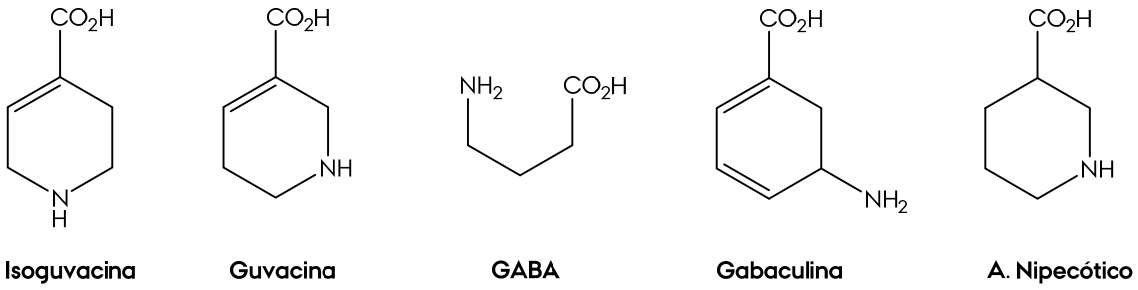

Figura 23. Estructuras de β-aminoácidos bicíclicos.

Referencias

[1] Leadley, R. M.; Armstrong, N.; Lee, Y. C.; Allen, A.; Kleijnen, J. *J. Pain Pall. Care Pharmacother.* **2012**, *26*, 310.

[2] Stucky, C. L.; Gold, M. S.; Zhang, X. *Proc. Natl. Acad. Sci. U. S. A.* **2001**, *98*, 11845.

[3] Stone, L. S.; Molliver, D. C. *Mol. Interventions* **2009**, *9*, 18.

[4] (a) Salamon, Z.; Cowell, S.; Varga, E.; Yamamura, H. I.; Hruby, V. J.; Tollin, G. *Biophys. J.* **2000**, *79*, 2463. (b) Salamon, Z.; Hruby, V. J.; Tollin, G.; Cowell, S. *J. Peptide Res.* **2002**, *60*, 322.

[5] Eguchi, M. *Med. Res. Rev.* **2004**, *24*, 182.

[6] Svoboda, K. R.; Lupica, C. R. *J. Neurosci.* **1998**, *18*, 7084.

[7] Jan, L. Y.; Jan, Y. N. *Curr. Opin. Cell Biol.* **1997**, *9*, 155.

[8] Wilding, T.; Womack, M.; McCleskey, E. *J. Neurosci.* **1995**, *15*, 4124.

[9] Hughes, J.; Smith, T. W.; Kosterlitz, H. W.; Fothergill, L. A.; Morgan, B. A.; Morris, H. R. *Nature* **1975**, *258*, 577.

[10] Liu, X.; Wang, Y.; Xing, Y.; Yu, J.; Ji, H.; Kai, M.; Wang, Z.; Wang, D.; Zhang, Y.; Zhao, D.; Wang, R. *J. Med. Chem.* **2013**, *56*, 3102.

[11] Bentley, K. W.; Hardy, D. G. *J. Am. Chem. Soc.* **1967**, *89*, 3267.

[12] Álvarez, Y.; Farré, M. *Adicciones* **2005**, *17*, 20.

[13] Abdel-Rahman, M. A.; Elliott, H. W.; Binks, R.; Küng, W.; Rapoport, H. *J. Med. Chem.* **1966**, *9*, 1.

[14] Blumberg, H.; Dayton, H. B.; Wolf, P. S. *Exp. Biol. Med.* **1966**, *123*, 755.

[15] Resnick, R. B.; Volavka, J.; Freedman, A. M.; Thomas, M. *Am. J. Psychiat.* **1974**, *131*, 5.

[16] Portoghese, P. S.; Sultana, M.; Takemori, A. E. *Eur. J. Pharmacol.* **1988**, *146*, 185.

[17] Pircio, A. W.; Gylys, J. A. *J. Pharmacol. Exp. Ther.* **1975**, *193*, 23.

[18] Howes, J. F.; Villarreal, J. E.; Harris, L. S.; Essigmann, E. M.; Cowan, A. *Drug Alcohol Depen.* **1985**, *14*, 373.

[19] Chou, Y.-C.; Liao, J.-F.; Chang, W.-Y.; Lin, M.-F.; Chen, C.-F. *Brain Res.* **1999**, *821*, 516.

[20] Church, J.; Jones, M. G.; Davies, S. N.; Lodge, D. *Can. J. Physiol. Pharmacol.* **1989**, *67*, 561.

[21] Archer, S.; Glick, S.; Bidlack, J. *Neurochem. Res.* **1996**, *21*, 1369.

[22] Clarke, E. G. C. *Nature* **1959**, *184*, 451.

[23] Rice, K. C.; Konicki, P. E.; Quirion, R.; Burke, T. R.; Pert, C. B. *J. Med. Chem.* **1983**, *26*, 1643.

[24] Fung, D. L.; Asling, J. H.; Eisele, J. H.; Martucci, R. *J. Clin. Pharmacol.* **1980**, *20*, 37.

[25] Ziering, A.; Lee, J. *J. Org. Chem.* **1947**, *12*, 911.

[26] Lomenzo, S. A.; Rhoden, J. B.; Izenwasser, S.; Wade, D.; Kopajtic, T.; Katz, J. L.; Trudell, M. L. *J. Med. Chem.* **2005**, *48*, 1336.

[27] Avison, A. W. D.; Morrison, A. L. *J. Chem. Soc.* **1950**, 1469.

[28] Stanley, T. H. *J. Pain Symptom Manage.* **1992**, *7*, S3.

[29] Monk, J.; Beresford, R.; Ward, A. *Drugs* **1988**, *36*, 286.

[30] Leppert, W. *Int. J. Clin. Pract.* **2009**, *63*, 1095.

[31] Slywka, G. W. A.; Melikian, A. P.; Whyatt, P. L.; Meyer, M. C. *J. Clin. Pharmacol.* **1975**, *15*, 598.

[32] (a) Murphy, J. G.; May, E. L. *J. Org. Chem.* **1954**, *19*, 615. (b) May, E. L.; Murphy, J. G. *J. Org. Chem.* **1954**, *19*, 618.

[33] (a) Burke, T. R.; Jacobson, A. E.; Rice, K. C.; Silverton, J. V. *J. Org. Chem.* **1984**, *49*, 1051. (b) Burke, T. R.; Jacobson, A. E.; Rice, K. C.; Silverton, J. V. *J. Org. Chem.* **1984**, *49*, 2508. (c) Burke, T. R.; Jacobson, A. E.; Rice, K. C.; Weissman, B. A.; Huang, H. C.; Silverton, J. V. *J. Med. Chem.* **1986**, *29*, 748.

[34] (a) Froimowitz, M.; Pangborn, W.; Cody, V. *Chirality* **1992**, *4*, 377. (b) DiMeglio, C.; Froimowitz, M.; Makriyannis, A. *Pharm. Res.* **1993**, *10*, 1200.

[35] (a) Bertha, C. M.; Mattson, M. V.; Flippen-Anderson, J. L.; Rothman, R. B.; Xu, H.; Cha, X.-Y.; Becketts, K.; Rice, K. C. *J. Med. Chem.* **1994**, *37*, 3163. (b) Bertha, C. M.; Vilner, B. J.; Mattson, M. V.; Bowen, W. D.; Becketts, K.; Xu, H.; Rothman, R. B.; Flippen-Anderson, J. L.; Rice, K. C. *J. Med. Chem.* **1995**, *38*, 4776. (c) Thomas, J. B.; Zheng, X.; Mascarella, S. W.; Rothman, R. B.; Dersch, C. M.; Partilla, J. S.; Flippen-Anderson, J. L.; George, C. F.; Cantrell, B. E.; Zimmerman, D. M.; Carroll, F. I. *J. Med. Chem.* **1998**, *41*, 4143. (d) Hofner, G.; Streicher, B.; Wunsch, B. *Arch. Pharm. (Weinheim)* **2001**, *334*, 284. (e) Hashimoto, A.; Jacobson, A. E.; Rothman, R. B.; Dersch, C. M.; George, C.; Flippen-Anderson, J. L.; Rice, K. C. *Biorg. Med. Chem.* **2002**, *10*, 3319. (f) Thomas, J. B.; Atkinson, R. N.; Namdev, N.; Rothman, R. B.; Gigstad, K. M.; Fix, S. E.; Mascarella, S. W.; Burgess, J. P.; Vinson, N. A.; Xu, H.; Dersch, C. M.; Cantrell, B. E.; Zimmerman, D. M.; Carroll, F. I. *J. Med. Chem.* **2002**, *45*, 3524. (g) Carroll, F. I.; Zhang, L.; Mascarella, S. W.; Navarro, H. A.; Rothman, R. B.; Cantrell, B. E.; Zimmerman, D. M.; Thomas, J. B. *J. Med. Chem.* **2003**, *47*, 281. (h) Thomas, J. B.; Zhang, L.; Navarro, H. A.; Carroll, F. I. *J. Med. Chem.* **2006**, *49*, 5597. (i) Carroll, F. I.; Melvin, M. S.; Nuckols, M. C.; Mascarella, S. W.; Navarro, H. A.; Thomas, J. B. *J. Med. Chem.* **2006**, *49*, 1781. (j) Cheng, K.; Kim, I. J.; Lee, M.-J.; Adah, S. A.; Raymond, T. J.; Bilsky, E. J.; Aceto, M. D.; May, E. L.; Harris, L. S.; Coop, A.; Dersch, C. M.; Rothman, R. B.; Jacobson, A. E.; Rice, K. C. *Org. Biomol. Chem.* **2007**, *5*, 1177. (k) Wiedemeyer, K.; Wünsch, B. *Carbohydr. Res.* **2012**, *359*, 24. (l) Iyer, M. R.;

Lee, Y. S.; Deschamps, J. R.; Dersch, C. M.; Rothman, R. B.; Jacobson, A. E.; Rice, K. C. *Eur. J. Med. Chem.* **2012**, *50*, 44. (m) Carroll, F. I.; Gichinga, M. G.; Williams, J. D.; Vardy, E.; Roth, B. L.; Mascarella, S. W.; Thomas, J. B.; Navarro, H. A. *J. Med. Chem.* **2013**.

[36] Crick, F. *Nature* **1970**, *227*, 561.

[37] Nielsen, P. E.; Haaima, G. *Chem. Soc. Rev.* **1997**, *26*, 73.

[38] Nielsen, P. E.; Egholm, M.; Buchardt, O. *Bioconjugate Chem.* **1994**, *5*, 3.

[39] Egholm, M.; Nielsen, P. E.; Buchardt, O.; Berg, R. H. *J. Am. Chem. Soc.* **1992**, *114*, 9677.

[40] Koppelhus, U.; Awasthi, S. K.; Zachar, V.; Holst, H. U.; Ebbesen, P.; Nielsen, P. E. *Antisense Nucleic Acid Drug Dev.* **2002**, *12*, 51.

[41] Hu, J.; Corey, D. R. *Biochemistry* **2007**, *46*, 7581.

[42] Fabani, M. M.; Gait, M. J. *RNA* **2008**, *14*, 336.

[43] (a) Zhou, P.; Wang, M.; Du, L.; Fisher, G. W.; Waggoner, A.; Ly, D. H. *J. Am. Chem. Soc.* **2003**, *125*, 6878. (b) Dragulescu-Andrasi, A.; Zhou, P.; He, G.; Ly, D. H. *Chem. Commun.* **2005**, 244.

[44] (a) Sahu, B.; Chenna, V.; Lathrop, K. L.; Thomas, S. M.; Zon, G.; Livak, K. J.; Ly, D. H. *J. Org. Chem.* **2009**, *74*, 1509. (b) Mitra, R.; Ganesh, K. N. *Chem. Commun. (Camb.)* **2011**, *47*, 1198. (c) Mitra, R.; Ganesh, K. N. *J. Org. Chem.* **2012**, *77*, 5696. (d) Manicardi, A.; Fabbri, E.; Tedeschi, T.; Sforza, S.; Bianchi, N.; Brognara, E.; Gambari, R.; Marchelli, R.; Corradini, R. *ChemBioChem* **2012**, *13*, 1327.

[45] Corradini, R.; Sforza, S.; Tedeschi, T.; Totsingan, F.; Manicardi, A.; Marchelli, R. *Curr. Top. Med. Chem.* **2011**, *11*, 1535.

[46] (a) Gangamani, B. P.; Kumar, V. A.; Ganesh, K. N. *Tetrahedron* **1996**, *52*, 15017. (b) Jordan, S.; Schwemler, C.; Kosch, W.; Kretschmer, A.; Stropp, U.; Schwenner, E.; Mielke, B. *Bioorg. Med. Chem. Lett.* **1997**, *7*, 687. (c) Gangamani, B. P.; Kumar, V. A.; Ganesh, K. N. *Tetrahedron* **1999**, *55*, 177. (d) Püschl, A.; Tedeschi, T.; Nielsen, P. E. *Org. Lett.* **2000**, *2*, 4161. (e) D'Costa, M.; Kumar, V.; Ganesh, K. N. *Org. Lett.* **2001**, *3*, 1281. (f) Kumar, V.; Pallan, P. S.; Meena, M.; Ganesh, K. N. *Org. Lett.* **2001**, *3*, 1269. (g) Slaitas, A.; Yeheskiely, E. *Eur. J. Org. Chem.* **2002**, *2002*, 2391. (h) Kumar, V. A.; Meena *Nucleos. Nucleot. Nucl.* **2003**, *22*, 1101. (i) Govindaraju, T.; Kumar, V. A.; Ganesh, K. N. *Chem. Commun.* **2004**, 860. (j) Kumar, V. A.; Ganesh, K. N. *Acc. Chem. Res.* **2005**, *38*, 404. (k) Govindaraju, T.; Kumar, V. A. *Tetrahedron* **2006**, *62*, 2321. (l) Gokhale, S. S.; Kumar, V. A. *Org. Biomol. Chem.* **2010**, *8*, 3742.

[47] (a) Lagriffoule, P.; Eriksson, M.; Jensen, K. K.; Nielsen, P. E.; Wittung, P.; Nordén, B.; Buchardt, O. *Chem. Eur. J.* **1997**, *3*, 912. (b) Puschl, A.; Boesen, T.; Tedeschi, T.; Dahl, O.; Nielsen, P. E. *J. Chem. Soc., Perkin Trans. 1* **2001**, 2757. (c) Shirude, P. S.; Kumar, V. A.; Ganesh, K. N.

Tetrahedron **2004**, *60*, 9485. (d) Sharma, S.; Sonavane, U. B.; Joshi, R. R. *J. Biomol. Struct. Dyn.* **2010**, *27*, 663. (e) Govindaraju, T.; Madhuri, V.; Kumar, V. A.; Ganesh, K. N. *J. Org. Chem.* **2005**, *71*, 14.

[48] Sugiyama, T.; Imamura, Y.; Demizu, Y.; Kurihara, M.; Takano, M.; Kittaka, A. *Bioorg. Med. Chem. Lett.* **2011**, *21*, 7317.

[49] Savithri, D.; Leumann, C.; Scheffold, R. *Helv. Chim. Acta* **1996**, *79*, 288.

[50] (a) Kuwahara, M.; Arimitsu, M.; Sisido, M. *J. Am. Chem. Soc.* **1998**, *121*, 256. (b) Kitamatsu, M.; Shigeyasu, M.; Okada, T.; Sisido, M. *Chem. Commun.* **2004**, 1208.

[51] Vergnaud, J.; Faugeras, P.-A.; Chaleix, V.; Champavier, Y.; Zerrouki, R. *Tetrahedron Lett.* **2011**, *52*, 6185.

[52] Efimov, V. A.; Klykov, V. N.; Chakhmakhcheva, O. G. *Nucleos. Nucleot. Nucl.* **2003**, *22*, 593.

[53] Hyrup, B.; Nielsen, P. E. *Biorg. Med. Chem.* **1996**, *4*, 5.

[54] Ray, A.; Norden, B. *FASEB J.* **2000**, *14*, 1041.

[55] Briones, C.; Moreno, M. *Anal. Bioanal. Chem.* **2012**, *402*, 3071.

[56] Sforza, S.; Corradini, R.; Tedeschi, T.; Marchelli, R. *Chem. Soc. Rev.* **2011**, *40*, 221.

[57] Rothlingshofer, M.; Gorska, K.; Winssinger, N. *Org. Lett.* **2012**, *14*, 482.

[58] Herrmann, J. L.; Kieczykowski, G. R.; Schlessinger, R. H. *Tetrahedron Lett.* **1973**, *14*, 2433.

[59] (a) Uyehara, T.; Asao, N.; Yamamoto, Y. *J. Chem. Soc., Chem. Commun.* **1987**, 1410. (b) Asao, N.; Uyehara, T.; Yamamoto, Y. *Tetrahedron* **1988**, *44*, 4173. (c) Uyehara, T.; Shida, N.; Yamamoto, Y. *J. Chem. Soc., Chem. Commun.* **1989**, 113. (d) Asao, N.; Uyehara, T.; Yamamoto, Y. *Tetrahedron* **1990**, *46*, 4563. (e) Uyehara, T.; Shida, N.; Yamamoto, Y. *J. Org. Chem.* **1992**, *57*, 3139.

[60] (a) Hawkins, J. M.; Fu, G. C. *J. Org. Chem.* **1986**, *51*, 2820. (b) Rudolf, K.; Hawkins, J. M.; Loncharich, R. J.; Houk, K. N. *J. Org. Chem.* **1988**, *53*, 3879.

[61] Hawkins, J. M.; Lewis, T. A. *J. Org. Chem.* **1992**, *57*, 2114.

[62] (a) Davies, S. G.; Smith, A. D.; Price, P. D. *Tetrahedron: Asymmetry* **2005**, *16*, 2833. (b) Davies, S. G.; Fletcher, A. M.; Roberts, P. M.; Thomson, J. E. *Tetrahedron: Asymmetry* **2012**, *23*, 1111.

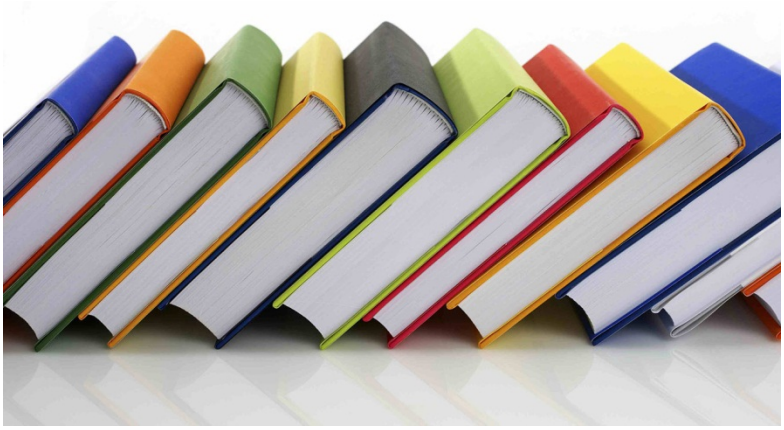

Antecedentes

Reacciones Dominó

En trabajos anteriores[1] se ha iniciado el estudio de la metodología y aplicación de la reactividad de di-ésteres di-insaturados con amiduros de litio quirales, empleando la ya comentada metodología de Davies *et al.*[2] Por adición de amiduros de litio (*R*)-1 y (*S*)-1 a ésteres di-insaturados (aceptores de Michael dobles) se ha conseguido obtener productos de monoadición, di-adición o productos cíclicos, dependiendo de las condiciones utilizadas o de los ésteres empleados.[3]

Por adición *dominó* inter/intramolecular de los amiduros de litio (*R*)-1 y (*S*)-1 a octa- y nonadiendioato de dimetilo, se obtienen los correspondientes derivados ciclopentánicos[4] y ciclohexánicos, respectivamente, (3) *trans,trans*-trisustituidos, con muy buen rendimiento y excelente estéreo y enantioselección. Además los productos cíclicos, con una secuencia estereoquímica diferente (*trans,cis*-trisustituidos), pueden obtenerse a partir del intermedio de monoadición con el doble enlace desconjugado al tratarlo con base.

En los productos cíclicos, las reacciones de eliminación del nucleófilo y nueva adición, permite conseguir todos los posibles diastereoisómeros en este sistema, como se indica a continuación. En esta línea se ha comunicado la síntesis asimétrica de los ocho diastereoisómeros del ácido 2-amino-5-carboximetil-ciclopentano-1-carboxílico (2),[5] utilizando la estrategia que se muestra en el esquema retrosintético (**Esq. 7**).

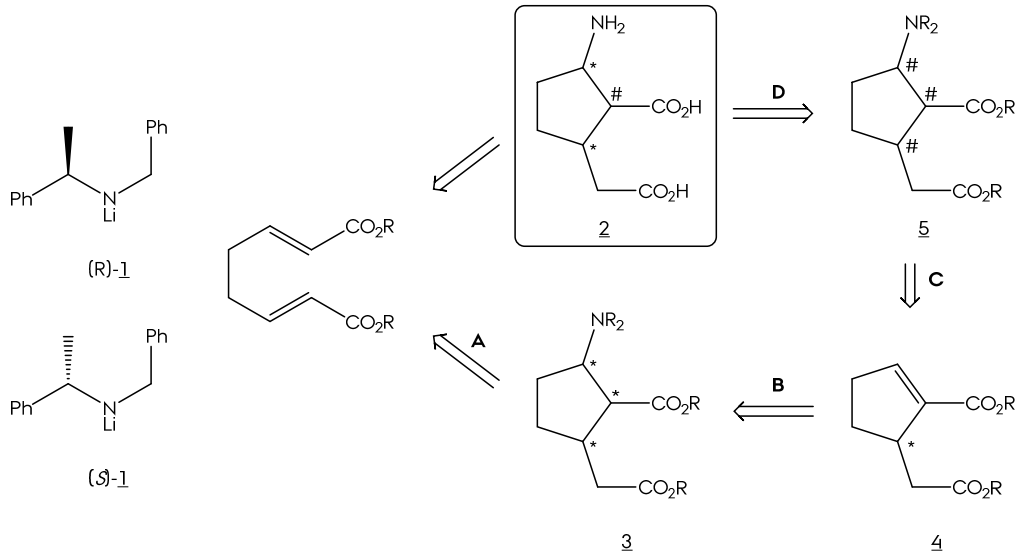

Esquema 7. A: Reacción dominó estereoselectiva de adición inter- e intramolecular. **B**: Eliminación estereoespecífica *syn*. **C**: Adición conjugada estereoselectiva. **D**: Desprotección.

Es de destacar que únicamente se ha utilizado (*E*,*E*)-octa-2,6-diendioato de dimetilo como precursor proquiral y las estrategias de adición para producir los intermedios cíclicos (3), eliminación de Cope (4) y re-adición (5) junto con la complementariedad de los amiduros (*R*)-1 y (*S*)-1 permite la síntesis de los ocho diastereoisómeros ópticamente puros.

Se ha iniciado también el estudio de las reacciones que permiten el control estereoquímico en los anillos ciclohexánicos.[6] Como se ha indicado, por adición de *N*-bencil-*N*-α-metilbencilamiduro de litio (*S*)-1 a (*E*,*E*)-nona-2,6-diendioato 6 se obtiene de manera estereoselectiva 7, con total control de los 3 nuevos centros estereogénicos formados (**Esq. 8**).

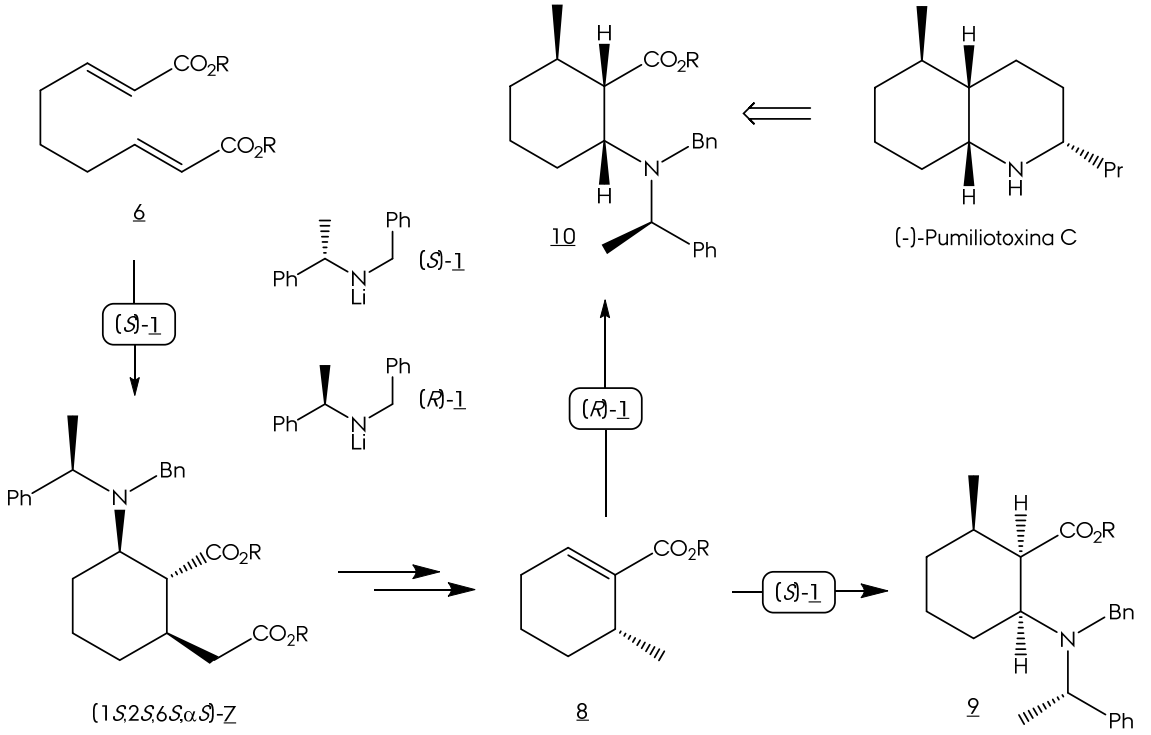

Esquema 8. Síntesis asimétrica del derivado homoquiral (1*S*,2*R*,6*R*,α*R*)-7 como intermedio en la síntesis de (-)-Pumiliotoxina-C.

En el esquema anterior se describe la metodología de síntesis asimétrica del sistema ciclohexánico *cis*,*cis*- y *cis*,*trans*-trisustituido por una estrategia combinada iniciada por la reacción dominó de adición asimétrica de Michael de (*S*)- y/o (*R*)-1 y posterior ciclación 6-*exo*-trigonal, eliminación de Cope y reacciones de hidrólisis selectiva y eliminación de Barton del ácido generado.[7] Una vez el metilo con la estereoquímica deseada en 8, la nueva adición de (*S*)- y (*R*)-1 es clave en el control estereoquímico para dar 9 ó 10. El compuesto 10 supone la síntesis formal de (-)-Pumiliotoxina C, al haber sido ya empleado en su síntesis total.[8]

Síntesis de Piperidinas

Recientemente se ha comunicado la síntesis de piperidinas y de derivados del ácido nipecótico (**Esq. 9**).[9] Así, cuando se trata 3-acetoxi-2-benciliden-propanoato con el amiduro de litio (*R*)-1 se obtiene de manera estereoselectiva el ácido (4*S*,5*S*,α*R*)-5-(*N*-bencil-*N*-α-metilbencilamino)-5-fenil-4-metoxicarbonil-pentanóico, siendo el resultado de una novedosa reacción dominó iniciada por un reordenamiento estereoespecífico de Ireland-Claisen seguida de una adición asimétrica de Michael del amiduro utilizado como único reactivo en la reacción. Esta reacción es generalizable para diferentes grupos y puede ser escalada. Se ha aplicado la metodología descrita a la síntesis asimétrica total de (+)-L-733.060,[10] un potente antagonista del receptor hNK1.

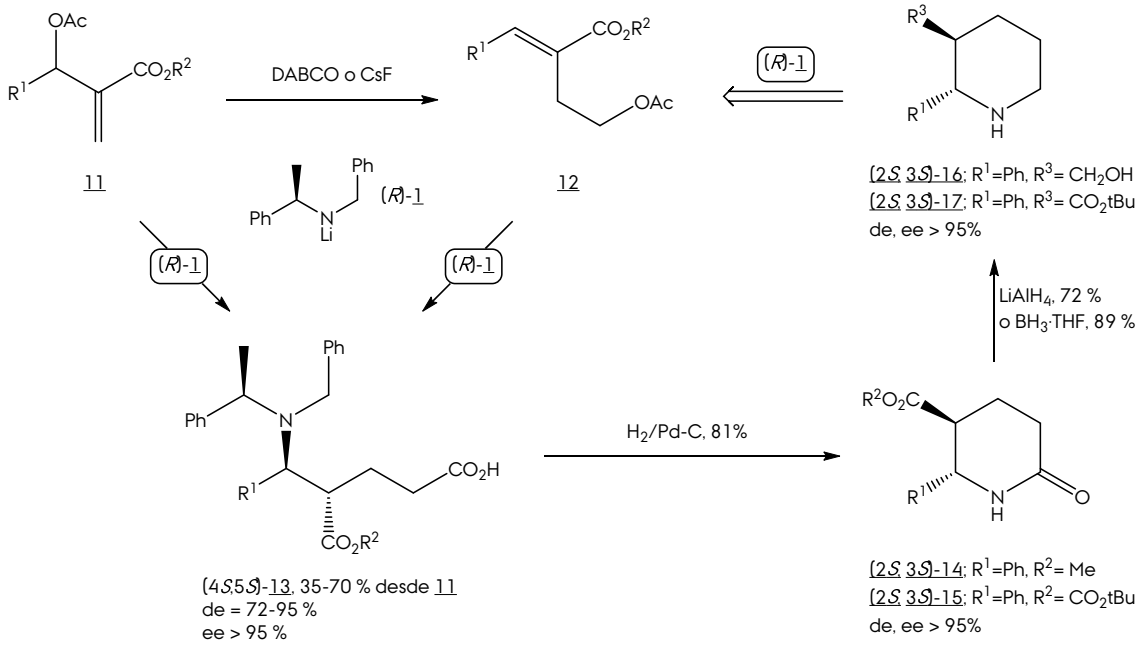

Esquema 9. Síntesis de piperidinas y derivados del ácido nipecótico.

Esto nos permite la obtención de β-aminoácidos cíclicos pero con el nitrógeno integrado en el anillo y ha sido aplicado recientemente a la síntesis asimétrica de los di-ácidos *cis*-(2*S*,3*R*)- y *trans*-(2*S*,3*S*)-piperidin-1,2-dicarboxílicos por medio de una reacción domino que involucra los reordenamientos del correspondiente acetato alílico y una reacción estereoselectiva de Ireland-Claisen además de una adición asimétrica de Michael como pasos claves en la obtención de δ-aminoácidos (**Esq. 10**).[11] Teniendo en cuenta la funcionalidad obtenida en uno de los precursores de estas dos síntesis asimétricas como lo son los respectivos derivados formilo, se está trabajando actualmente en el desarrollo de diferentes derivados piperidínicos.

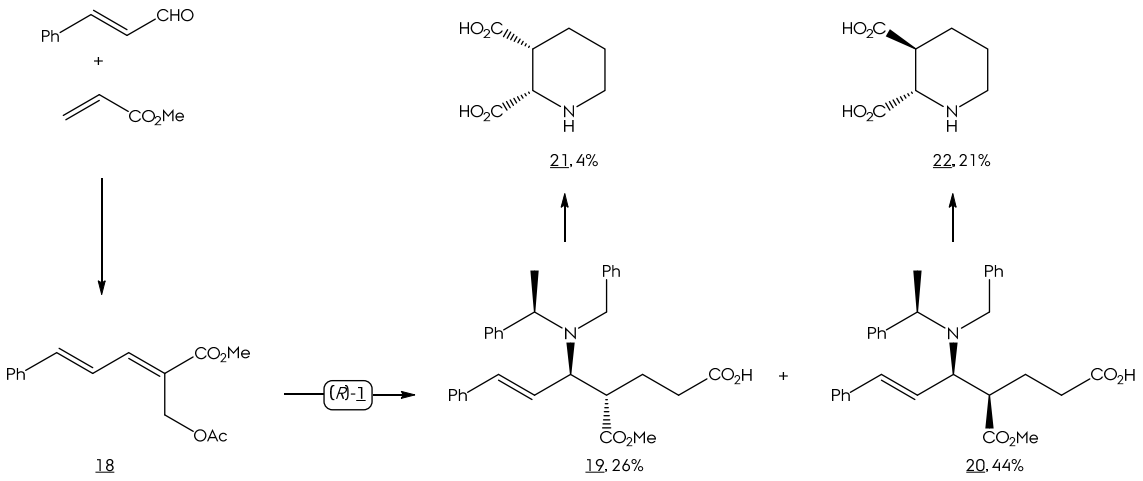

Esquema 10. Síntesis de ácidos piperidínicos.

Reactividad en Sistemas Ciclooctánicos

La reactividad de los amiduros de litio también ha sido estudiada en sistemas ciclooctánicos, especialmente en ciclooctadiencarboxilatos. Partiendo de los esteres diinsaturados 23 y 26, se ha efectuado la adición de (*R*)-*N*-bencil-*N*-α-metilbencilamiduro de litio obteniendo los productos de adición 26 y 29 con rendimientos diferentes (**Esq. 11**). Análisis conformacional de los sustrato 23 y 28 mostraron una predisposición conformacional diferente en ambos casos, la cual puede explicar el comportamiento diferenciado en la reacción.[12] Posterior desprotección de los grupos amina y ácido permitieron la obtención del ácido (1*S*,8*R*,*Z*)-8-aminociclooct-2-en-1-carboxilico 25.[13] Por otro lado, el intermedio 27 se modificó para efectuar una apertura de ciclo oxidativa empleando ozono en medio reductor. El compuesto 27 representa un atractivo intermedio para la síntesis de alcaloides, dada la posibilidad de realizar un cierre de ciclo entre las funcionalidades aldehído y la amina una vez liberada esta.

También han sido obtenidos una serie de β-aminoésteres de esqueleto ciclooctánico con diversa funcionalidad. Partiendo del éster 31, y efectuando una oxigenación en α con respecto al éster mediante la adición de (*R*)-1 con (−)-CSO ((−)-(8,8-diclorocamforilsulfonil)oxaziridina), se logra la familia de compuestos 32, la cual por desprotección lleva a los α-hidroxi-aminoésteres 33.

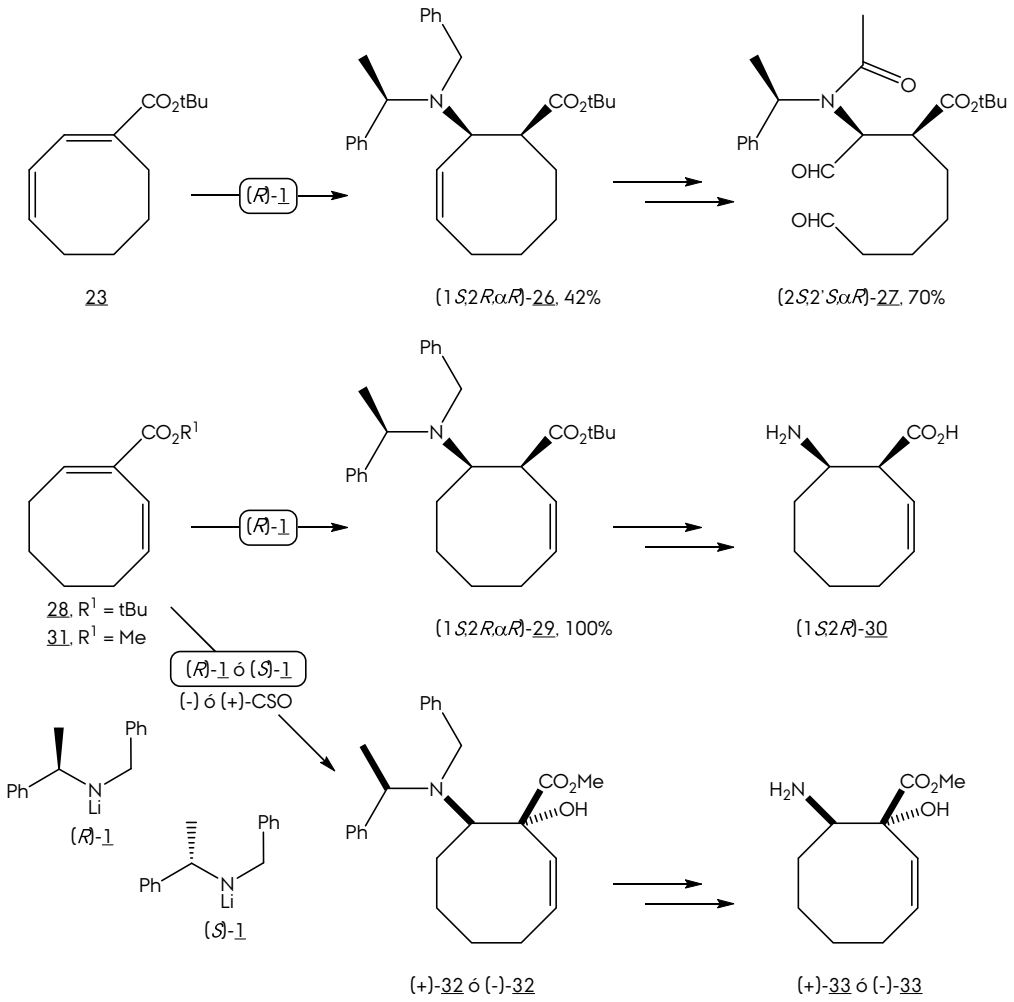

Esquema 11. Síntesis de ácidos β-amino-ciclooctanocarboxílicos

Referencias

[1] (a) Dominguez, S. H., Salamanca, 2001. (b) Garrido, N.; Díez, D.; Domínguez, S.; Sánchez, M.; García, M.; Urones, J. *Molecules* **2006**, *11*, 435.

[2] (a) Davies, S. G.; Smith, A. D.; Price, P. D. *Tetrahedron: Asymmetry* **2005**, *16*, 2833. (b) Davies, S. G.; Fletcher, A. M.; Roberts, P. M.; Thomson, J. E. *Tetrahedron: Asymmetry* **2012**, *23*, 1111.

[3] Urones, J. G.; Garrido, N. M.; Díez, D.; Dominguez, S. H.; Davies, S. G. *Tetrahedron: Asymmetry* **1999**, *10*, 1637.

[4] Urones, J. G.; Garrido, N. M.; Díez, D.; Dominguez, S. H.; Davies, S. G. *Tetrahedron: Asymmetry* **1997**, *8*, 2683.

[5] Urones, J. G.; Garrido, N. M.; Diez, D.; El Hammoumi, M. M.; Dominguez, S. H.; Antonio Casaseca, J.; Davies, S. G.; Smith, A. D. *Org. Biomol. Chem.* **2004**, *2*, 364.

[6] (a) Davies, S. G.; Diez, D.; Dominguez, S. H.; Garrido, N. M.; Kruchinin, D.; Price, P. D.; Smith, A. D. *Org. Biomol. Chem.* **2005**, *3*, 1284. (b) Garrido, N. M.; Díez, D.; Domínguez, S. H.; García, M.; Sánchez, M. R.; Davies, S. G. *Tetrahedron: Asymmetry* **2006**, *17*, 2183.

[7] Barton, D. H. R.; Samadi, M. *Tetrahedron* **1992**, *48*, 7083.

[8] Schultz, A. G.; McCloskey, P. J.; Court, J. J. *J. Am. Chem. Soc.* **1987**, *109*, 6493.

[9] (a) García, M. G., Salamanca, 2006. (b) Garrido, N. M.; García, M.; Díez, D.; Sánchez, M. R.; Sanz, F.; Urones, J. G. *Org. Lett.* **2008**, *10*, 1687.

[10] Garrido, N. M.; García, M.; Sánchez, M. R.; Díez, D.; Urones, J. G. *Synlett* **2010**, *2010*, 387.

[11] Garrido, N. M.; Rosa Sánchez, M.; Díez, D.; Sanz, F.; Urones, J. G. *Tetrahedron: Asymmetry* **2011**, *22*, 872.

[12] Zúñiga, M. C. B., Salamanca, 2012.

[13] Garrido, N. M.; Blanco, M.; Cascón, I. F.; Díez, D.; Vicente, V. M.; Sanz, F.; Urones, J. G. *Tetrahedron: Asymmetry* **2008**, *19*, 2895.

Objetivos (Objectives)

Introduction

Taking into account the progress that has been made in the study of the asymmetric Michael addition of chiral lithium amides and its different applications,[1] a combined experimental and theoretical project has been envisaged.

The mechanistic explanation of the observed high diastereomeric excess in the addition of lithium (*R*)-*N*-benzyl-*N*-(α-methylbenzyl)amide to α,β-unsaturated esters has remained without review since 1994.[2] Due to the advance of QM methods and computer resources, it will be attractive to revisit the mechanism, applying the most advanced techniques (**Fig. 24**).

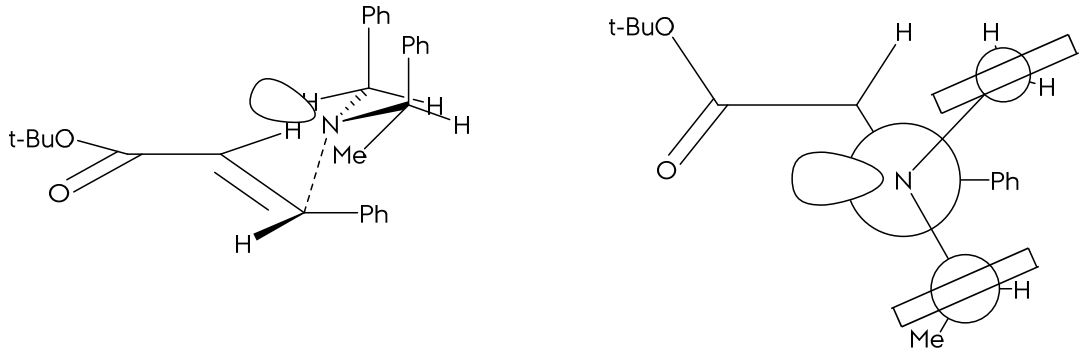

Figure 24. Proposed transition state in 1994 for the Michael addition of lithium *N*-benzyl-*N*-(α-methylbenzyl)amide to α,β-unsaturated esters.

Literature is plenty of synthetic methodologies of 2-azabiciclo[3.3.1]nonane production;[3] however, there is no many published results concerning asymmetric synthesis of aza-bridgeded structures, specially using chiral auxiliaries. Our group have a deep knowledge[4] in the synthesis of β-amino esters/acids through asymmetric Michael addition of lithium (*R*)-*N*-benzyl-*N*-α-methylbenzylamide to α,β-unsaturated esters. One of the studied areas is the synthesis of cyclopentane and cyclohexane derivatives through Michael asymmetric addition of the previous amide to *E*,*E*-diendioates, affording the cyclic products with control in the three new seterocenters.[4b,4d] The asymmetric synthesis of methyl (1*R*,5*R*,9*R*)-2-azabicyclo[3.3.1]nonane-9-carboxylate, a β-aminoester, is proposed as target molecule, taking an appropriate cyclized product (**Sch. 12**) as intermediate.

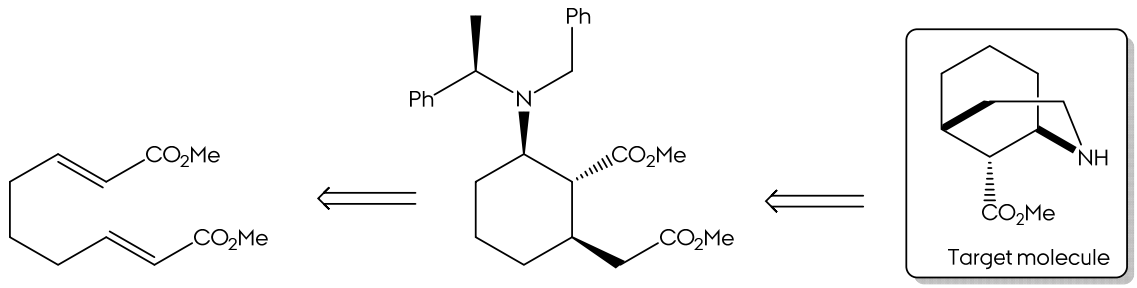

Scheme 12. Retrosynthetic plan in the synthesis of target molecule.

Although the morphan motif is a structural simplification of morphine, the resemblance leaded us to think in a promising new morphine derivatives as opioid agonists/antagonists. So, a combined biomodelling project and biological evaluation is envisaged to explore the potential activity of this kind of products. A series of morphan derivatives were designed, synthetized and submitted to biological trials. Exploration of the binding capabilities of these compounds was carried out through advanced computer simulations (Molecular Dynamics).

In 1996, Leumann *et al.*[5] synthetized a peptide nucleic acid monomer from Boc-Ser-OMe (**Sch. 13**). As the substrate incorporates the stereocenter, only chain homologation and functional group interconversions were required. This compound represents one of the first chiral, flexible PNA monomers with a structure substantially different from the original *aeg*PNA.[6] The synthesis of a variety of peptide-nucleotides is also discussed in this work.

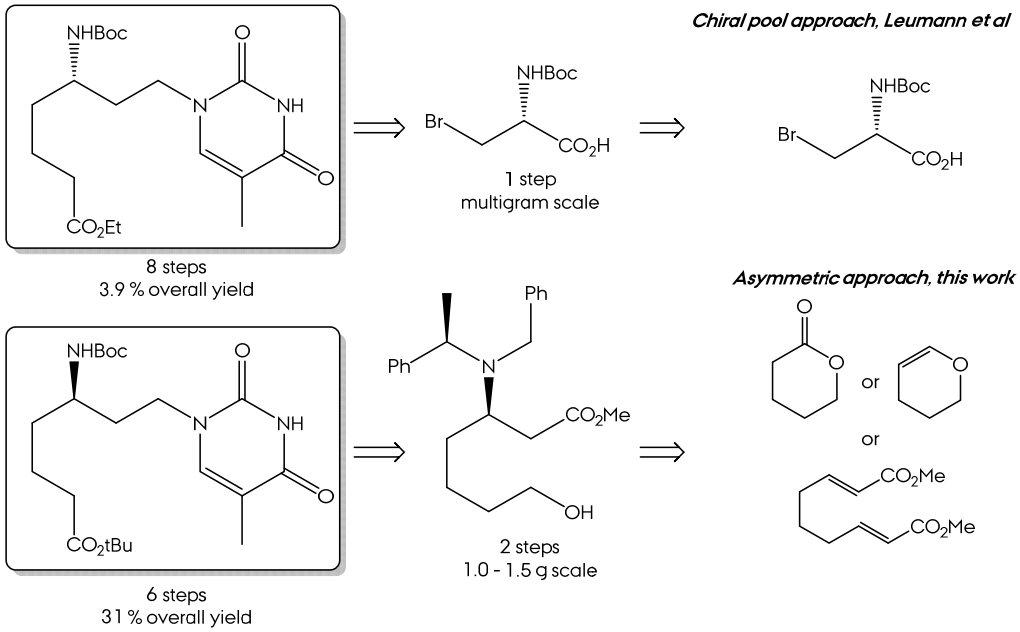

Scheme 13. Comparison between Leumann's approach of the PNA monomer synthesis and current approach.

Our approach is based on the asymmetric Michael addition of chiral amides as key step to obtain enantiomerically enriched intermediates and forward functional group interconversion. Among them, the enantiomer of Leumann's monomer has been elaborated with higher yield and productivity compared to Leumann's article.

The synthesis of novel peptide-nucleotide units requires a subsequent binding study of nucleic oligopeptides to natural oligonucleotides. Melting point titrations, circular dichroism or NMR are, among others, experimental techniques to evaluate the structure, binding strength and stability of nucleic acid hybrids.[7] Molecular modelling is also a routine tool to survey nucleic acid chemistry, natural and new synthetic structures. Locked and Peptide Nucleic acids have been extensively studied through Quantum Mechanics and Molecular Dynamics,[8] in order to check hybrids stability, topological information and thermodynamic properties. In this work, MD simulations studies of the hybridization properties of nucleic oligopeptides to natural DNA are envisaged. A thymine homopolymer was modelled, and hybridized with a complementary adenine DNA. Topological, solvation and thermodynamic properties were surveyed.

Specific Objectives

1.- Develop a new mechanistical study of the asymmetric Michael addition of lithium (*R*)-*N*-benzyl-*N*-α-methylbenzylamide to α,β-unsaturated esters using state of the art QM/DFT methods.

2.- Asymmetric synthesis of morphan type β-amino acids through the methodology of asymmetric Michael addition of chiral lithium amides, with special emphasis in the preparation of methyl (1*R*,5*R*,9*R*)-2-azabicyclo[3.3.1]nonane-9-carboxylate.

3.- Structure-based design and synthesis of novel μ-opioid receptor ligands based in the synthetized morphan type β-amino acids.

4.- Biological evaluation of synthetized novel μ-opioid receptor ligands.

5.- Asymmetric synthesis of flexible peptide-nucleotides (PNA) through the asymmetric Michael addition of chiral lithium amides. Special dedication to Leumann's type PNA.

6.- MD simulations and hybridization properties of flexible peptide-nucleotides based on the Leumann's type PNA.

References

[1] (a) Davies, S. G.; Smith, A. D.; Price, P. D. *Tetrahedron: Asymmetry* **2005**, *16*, 2833. (b) Davies, S. G.; Fletcher, A. M.; Roberts, P. M.; Thomson, J. E. *Tetrahedron: Asymmetry* **2012**, *23*, 1111.

[2] Costello, J. F.; Davies, S. G.; Ichihara, O. *Tetrahedron: Asymmetry* **1994**, *5*, 1999.

[3] (a) Aurrecoechea, J. M.; Gorgojo, J. M.; Saornil, C. *J. Org. Chem.* **2005**, *70*, 9640. (b) Diaba, F.; Bonjoch, J. *Org. Biomol. Chem.* **2009**, *7*, 2517. (c) Wang, Y.-F.; Chiba, S. *J. Am. Chem. Soc.* **2009**, *131*, 12570. (d) Diaba, F.; Martinez-Laporta, A.; Bonjoch, J.; Pereira, A.; Munoz-Molina, J. M.; Perez, P. J.; Belderrain, T. R. *Chem. Commun.* **2012**, *48*, 8799.

[4] (a) Urones, J. G.; Garrido, N. M.; Díez, D.; Dominguez, S. H.; Davies, S. G. *Tetrahedron: Asymmetry* **1997**, *8*, 2683. (b) Urones, J. G.; Garrido, N. M.; Díez, D.; Dominguez, S. H.; Davies, S. G. *Tetrahedron: Asymmetry* **1999**, *10*, 1637. (c) Urones, J. G.; Garrido, N. M.; Diez, D.; El Hammoumi, M. M.; Dominguez, S. H.; Antonio Casaseca, J.; Davies, S. G.; Smith, A. D. *Org. Biomol. Chem.* **2004**, *2*, 364. (d) Davies, S. G.; Diez, D.; Dominguez, S. H.; Garrido, N. M.; Kruchinin, D.; Price, P. D.; Smith, A. D. *Org. Biomol. Chem.* **2005**, *3*, 1284. (e) Garrido, N. M.; Díez, D.; Domínguez, S. H.; García, M.; Sánchez, M. R.; Davies, S. G. *Tetrahedron: Asymmetry* **2006**, *17*, 2183. (f) Garrido, N. M.; Blanco, M.; Cascón, I. F.; Díez, D.; Vicente, V. M.; Sanz, F.; Urones, J. G. *Tetrahedron: Asymmetry* **2008**, *19*, 2895. (g) Garrido, N. M.; Rubia, A. G.; Nieto, C.; Díez, D. *Synlett* **2010**, *2010*, 587. (h) Garrido, N. M.; Rosa Sánchez, M.; Díez, D.; Sanz, F.; Urones, J. G. *Tetrahedron: Asymmetry* **2011**, *22*, 872. (i) Garrido, N. M.; Nieto, C. T.; Díez, D. *Synlett* **2013**, *24*, 169.

[5] Savithri, D.; Leumann, C.; Scheffold, R. *Helv. Chim. Acta* **1996**, *79*, 288.

[6] Nielsen, P.; Egholm, M.; Berg, R.; Buchardt, O. *Science* **1991**, *254*, 1497.

[7] Hyrup, B.; Nielsen, P. E. *Biorg. Med. Chem.* **1996**, *4*, 5.

[8] (a) Natsume, T.; Ishikawa, Y.; Dedachi, K.; Tsukamoto, T.; Kurita, N. *Chem. Phys. Lett.* **2007**, *446*, 151. (b) Siriwong, K.; Chuichay, P.; Saen-oon, S.; Suparpprom, C.; Vilaivan, T.; Hannongbua, S. *Biochem. Biophys. Res. Commun.* **2008**, *372*, 765. (c) Sharma, S.; Sonavane, U. B.; Joshi, R. R. *J. Biomol. Struct. Dyn.* **2010**, *27*, 663. (d) Uppuladinne, M. V. N.; Jani, V.; Sonavane, U. B.; Joshi, R. R. *Int. J. Quantum Chem* **2013**, n/a.

Resultados y Discusión

(Results and Discussion)

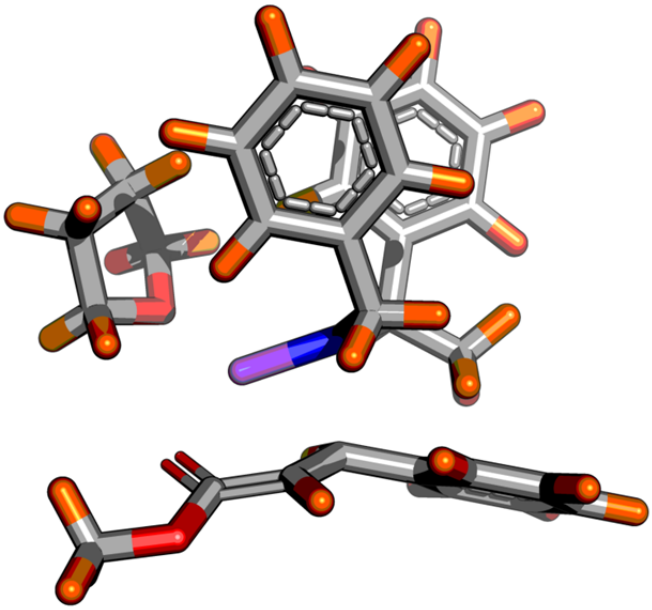

1 New Mechanistical Insights in the Asymmetric Michael Addition of Chiral Lithium Amides.

Introduction

In 1991, Davies *et al*[1] reported the first asymmetric Michael addition of lithium (*R*)-*N*-benzyl-*N*-(α-methylbenzyl)amide to α,β-unsaturated esters to afford chiral β-amino esters with high diastereomeric excess. Since then, this methodology has been extensively used is the elaboration of a wide variety of chiral β-amino esters, β-amino acids, alkaloids, etc.[2]

The mechanistic explanation of the high diastereoselectivity observed was published by Davies *et al*[3] in 1994. In this article, molecular mechanics calculations were performed to find the lowest energy transition state, evaluating a hierarchical analysis: (1) $N \cdots C_\beta$ distance, (2) σ_{lp}-N-C_β-C_α dihedral, (3) *R*/*S* stereocenter. Several approximations were also taken:

- Tetrahedral approach of the chiral amide to the beta center (N-C_β-C_α = 109º). s-*cis* disposition of the Michael acceptor (experimentally required). *Si*-face was only studied.

- Antiperiplanar disposition of the *tert*-butyl moiety.

- Lithium chelation was assumed.

From the different levels of confomational analysis, some conclusions were extracted:

- Level 1: at 2.0 Å the disposition of both aromatic rings were almost parallel, in a "butterfly" orientation. This bond length was kept in forward levels.

- Level 2: a minimum was found where the lone pair of the nitrogen is oriented towards the carbonyl group. This was also kept in the next level.

- Level 3: substitution of the model by *R*/*S* type amides revealed four lowest energy conformations: 2 energy minima in each one diastereomeric case. The predominant *R*-conformer (**Fig. 25**) was proposed as transition state of the reaction. Other conformational structures were found to have greater relative energies, due to steric clashes between groups.

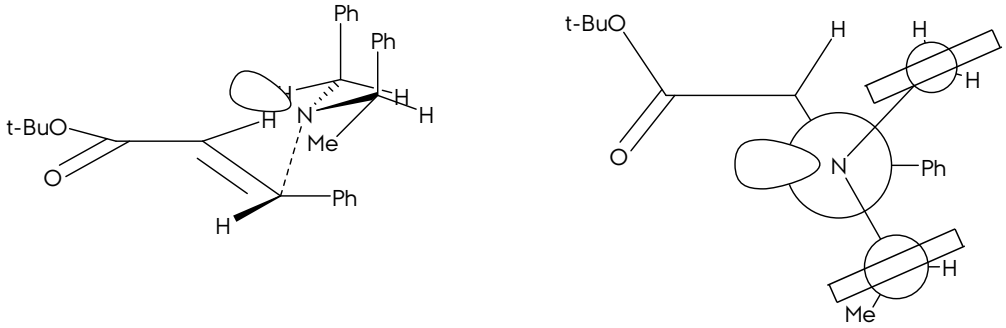

Figure 25. Proposed transition state in 1994 for the Michael addition of lithium *N*-benzyl-*N*-(α-methylbenzyl)amide to α,β-unsaturated esters.

These proposed mechanism/mnemotecnic rule have been assumed along this years. The stereochemical outcome of the reaction was found reproducible in a wide variety of reactions, and it has successfully tested in asymmetric double-induced transformations.[4]

With the increase of the computational capacity and the development of new theoretical areas, a revision of this mechanism is necessary, considering the conditions and the theories used then. To tackle this update, a series of ideas must be taken into account before starts the design of the theoretical work.

Solution structure of lithium amides is a complex matter. Their organometallic nature makes them organize in dimers, trimers, and even more complex structures, with the cooperation of solvent molecules in coordination. The earliest structural and electronic insights of lithium amides were published by Hinchliffe *et al*[5] in 1977.

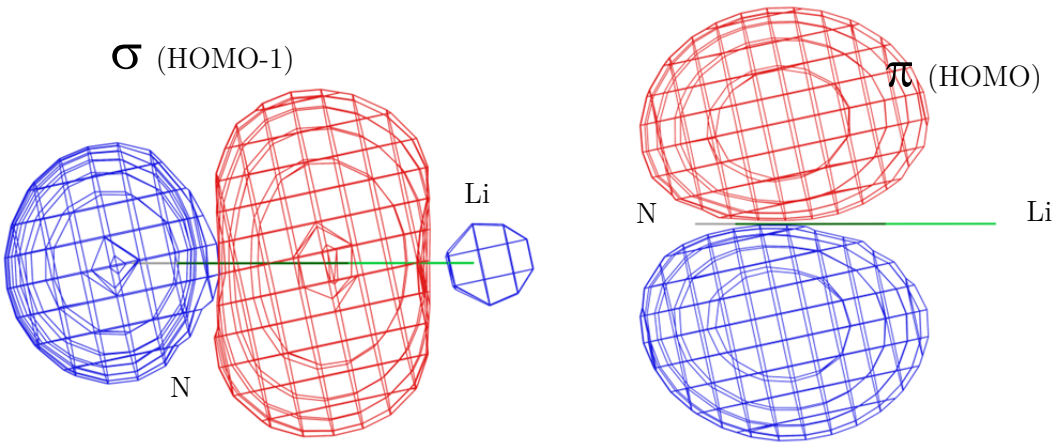

Figure 26. Representative molecular orbitals of $LiNH_2$ (Kohn-Sham type, M06-2X/6-31G(d)).

These authors evidenced the p-π character of the Li-N bond (**Fig. 26**), and hence the lower ionic character of these compounds. Wurthwein *et al*[6] completed the

studied extending the number of lithiated amines analysed. In this work, $LiNH_2$, Li_2NH and LiN_3 were found planar, effect that confirms the character π found at Hinchliffe's work. The hardness of lithium cation, the following after proton, polarizes the electron density of the nitrogen, accepting it from the lone pair orbital. This electronic phenomenon is the origin of aggregation in these species (**Fig. 27**). First theoretical study[7] of lithium amides aggregation used *ab initio* methods to calculate solution phase energies of optimized structures. Since then, many works have been published covering solution and solid-phase structural studies, being Collum who most efforts have done to study them, especially the well-known lithium diisopropylamide (LDA). In general, lithium alkyl amides or disilazydes[8] form aggregates in ethereal solutions. It was common to crystalize such aggregates with solvent molecules or esters, which supported the existence of them.[8-9] The aggregation pattern may be changed by adding salts like LiCl[10] or LiBr,[11] and the presence of cosolvents, as HMPA[12] or TMEDA.[13]

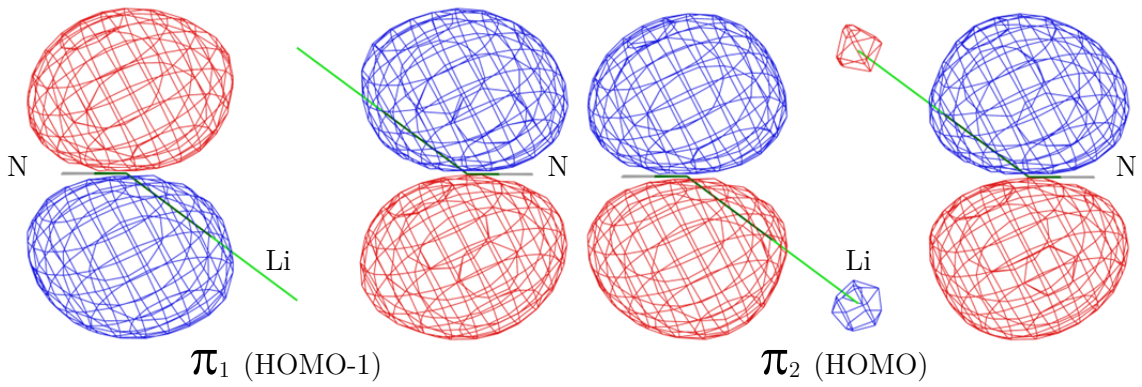

Figure 17. Representative molecular orbitals of $LiNH_2$ dimer (Kohn-Sham type, M06-2X/6-31G(d)).

^{6}Li and ^{15}N NMR spectroscopy have been used to detect lithium amide aggregates in solution.[14] Collum *et al* demonstrated[14a] via NMR that the only structure of LDA in low concentrated THF solutions was the dimer.

Deaggregation processes are fundamental to allow the reactivity of lithium amides. Collum *et al* have deeply studied the deaggregation processes of LDA via molecular modelling[15] and kinetic measurements over ketone and imine deprotonations[16] or eliminations.[17] Their studies concluded that close dimer species may evolve to open dimers, which are as stables as LDA monomers, where up to three THF molecules

are implied. Reaction kinetic studies, together with molecular modelling supports that certain dimer-based reaction pathways are faster than monomer-based ones.[17]

Collum *et al*[18] also studied Michael-type additions of LDA to α,β-unsaturated esters. From their kinetic studies and DFT calculations, a grid of the main participating species was created (**Sch. 14**). Deaggregative, autocatalystic and LiCl mediated pathways transforms LDA dimer into a three THF-solvated amide. 1,4-addition was proposed to be 1:1 substrate-lithium amide. Other additional dimers were also advanced: homodimers between lithium enolates and heterodimers between lithium enolates and lithium amides.

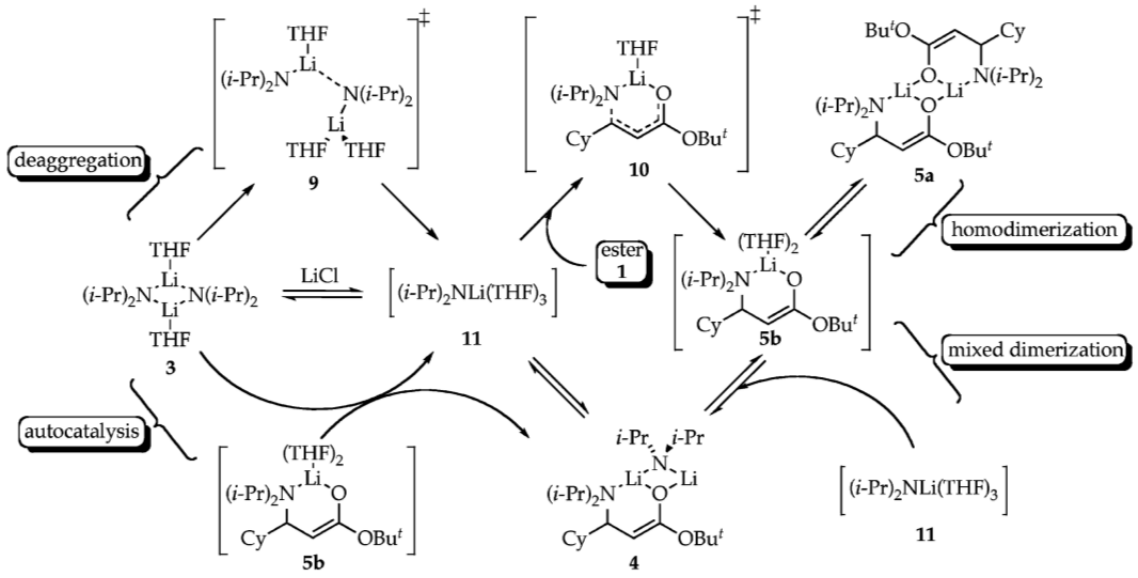

Scheme 14. Grid of species proposed by Collum et al in the explanation of the 1,4-addition of LDA to α,β-unsaturated esters.

The structure of chiral *N*-benzyl-*N*-(α-methylbenzyl)amide have also been studied both in solution and solid phase. Snaith *et al*[9,19] have cristalized $[(PhCH_2)_2NLi \cdot Et_2O]_2$ and homochiral (*R*)-$[PhCH_2(PhC(H)Me)NLi \cdot THF]_2$ from solutions of dibenzylamine with nBuLi in hexanes-ether and (*R*)-*N*-benzyl-*N*-(α-methylbenzyl)amide with nBuLi in hexanes-THF, respectively. Andrews *et al,*[20] published at the same time the crystallization of (*S*)-$[PhCH_2(PhC(H)Me)NLi \cdot THF]_2$ in the same conditions. Both crystals were crystallizazed from hexanes solution of equimolecular quantities of chiral amine, THF and nBuLi.

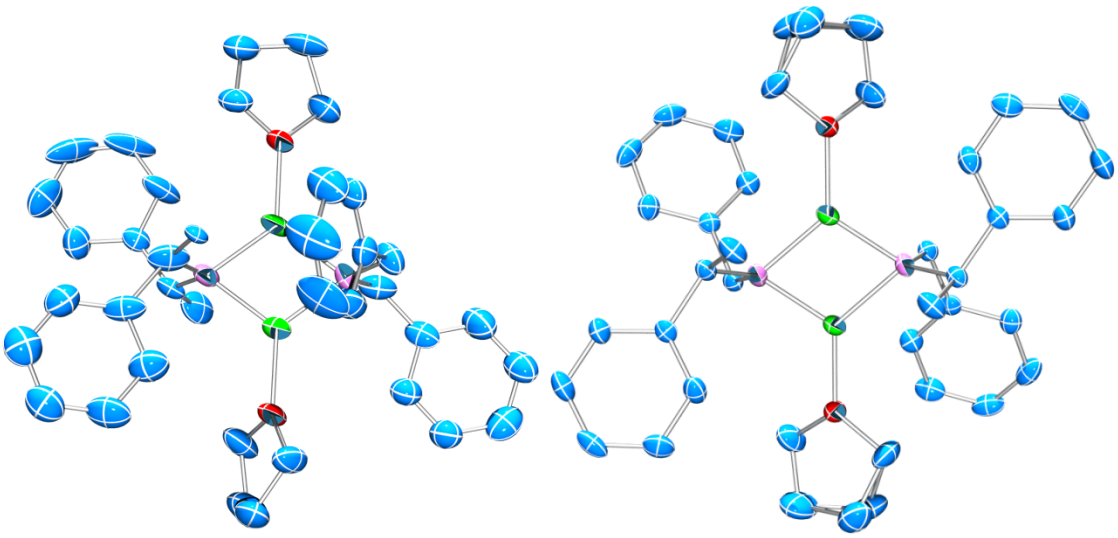

(*R*)-Crystal (*S*)-Crystal

	***R*-crystal**	***S*-crystal**
Reference	Snaith *et al*	Andrews *et al*
Description	colourless crystals	colourless crystals
m.p.	83-86 ºC	83-84 ºC
Space group	$P2_12_12_1$	$P4_32_12$
Analysis	$C_{38}H_{48}Li_2N_2O_2$	$C_{38}H_{48}Li_2N_2O_3$
Conformation	cisoid/transoid 44:56	exclusively cisoid

Table 1. Parameters of crystallized enantiomeric compounds $[PhCH_2(PhC(H)Me)NLi \cdot THF]_2$.

The enantiomeric crystals were expected to have the same space group, however, they were different (**Tab. 1**). Dimeric units were found in the crystal; however, the arrangement of the phenyl groups was different: in Snaith's crystals, one amide moiety has the phenyl groups in a parallel disposition, but the other has one of the phenyl rings orthogonal from the $(Li\text{-}N)_2$ plane. On the other hand, Andrew´s crystals have their phenyl groups in a parallel disposition. Other interesting feature is the conformation of the methyl groups: a 44:56 *cisoid/transoid* conformations were found at Snaith's crystals; nevertheless, exclusively the *cisoid* disposition was presented at Andrew's ones. These two polymorphic forms are two examples of how conformation influences crystal growth. Torsion energies, contrary to angle and bond stretching, are energetic comparable to weak hydrogen bonds (up to 4 Kcal/mol) or Van der Waals interactions (up to 1.0 Kcal/mol at room temperature), which determine crystal packaging.[21]

Despite of the colourless aspect of these crystals, THF or benzene solutions have an intense colour. Snaith *et al*[19b] recorded UV-Vis spectra of benzene solutions of $[(PhCH_2)_2Li \cdot Et_2O]$ of known concentrations. They showed a weak absortion at 525 nm, which are increased on dilution and proposed a forbidden charge-transfer of low-associated species. From molecular orbital calculations, it was concluded that the bathochromic shift into the visible region has its origin in a HOMO→LUMO charge transfer in monomeric species. Later in 1999,[9] *ab initio* molecular orbital calculations in (*S*,*S*)-bis(1-phenylethyl)amide[22] structures showed an orientation of both phenyl groups to the metal, which was also argued to be the lowest energy conformers and hence the responsible of the observed charge transfer from benzyls HOMO orbital to metal LOMO one.

In the same article, ^{6}Li NMR studies of d_8-toluene solutions of lithium (*S*,*S*)-bis(1-phenylethyl)amide probed the existence of a monomer/trimer equilibria. On the other hand, Sugasawa *et al*[23] recorded ^{6}Li and ^{15}N NMR of (*R*,*R*)-bis(1-phenylethyl)amide solutions in d_8-THF, demonstrating the existence of dimer structures in absence of lithium salts. Solution colours of (*S*,*S*)-bis(1-phenylethyl)amide were found red in THF,[24] but colourless in benzene/toluene,[9] contrary to enantiopure *N*-benzyl-*N*-(α-methylbenzyl)amide, which are red in benzene/toluene and pink in THF. This curious effect shows solvent is not only solvating, it also acts as ligand. Recently, Claridge *et al*[14c] have studied solution properties of ^{6}lithium (*S*)-^{15}*N*-benzyl-^{15}*N*-(α-methylbenzyl)amide, as well as racemic ^{6}lithium ^{15}*N*-benzyl-^{15}*N*-(α-methylbenzyl)amide by means of ^{6}Li and ^{15}N NMR. Enantiomeric solution of the amide in THF revealed the dimer structure as the only aggregate identifiable. A *cisoid*/*transoid* equilibria was also found between dimers, finding a 5.5/1.0 equilibria at 173 K. From this collection of experimental/theoretical research, it is clear to see that solution colours of these amides are connected with the aggregation and solvation level, which can be explored through NMR and UV-Vis experiments in junction with *ab initio* molecular orbital calculations.

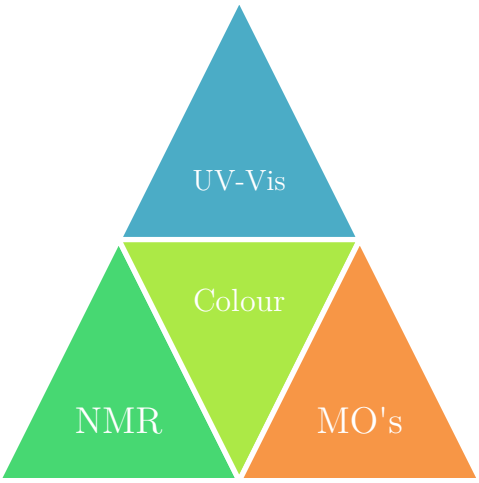

This background makes the study of reaction mechanisms of 1,4-addition of lithium amides a challenging task, due to the three levels of complexity required to study: solution structure, deaggregation process and reaction transition states. Due to this complexity, only the transition state level was covered. However, a complete study of all the stages will allow a global idea of the overall process.

Design of the Study

Taking into account the described background and especially the published work related with asymmetric Michael addition of enantiopure lithium *N*-benzyl-*N*-(α-methylbenzyl)amide, a QM mechanistic study have been done.

In brief, since Davies *et al*[3] 1994 article, no molecular modelling studies were performed in this king of reactions. Experimental reproducibility of the reaction was found since them, especially tested in asymmetric double-induced transformations.[4] Claridge *et al*[14c] also investigated through ^{6}Li and ^{15}N NMR monitoring the outcome of adding *tert*-butyl cinammate in a solution of homochiral (*S*)-*N*-benzyl-*N*-(α-methylbenzyl)amide. It was found a 1:1 mixture of *Z*-lithium enolate/lithium amide, together with the lithium amide dimer signals. This set of experimental work warrant the reproducibility of the reaction, but did not advanced forward. Thereby, the initial mechanism proposed in the 1994's paper is currently valid.

One relevant question concerning the nature of solution structure of lithium *N*-benzyl-*N*-(α-methylbenzyl)amide has to be proposed: as solution structure is undoubtedly dimeric, is it equal to transition state? It was previously described that the colour of related species comes from charge transfer between frontier orbitals in monomeric species. Nevertheless, *ab initio* molecular orbital calculations only covered crystalized geometries or a discrete conformational search, without considering solvent molecules. So the colour origin of these amides remains unclear, at least in THF solutions.

In their mechanistic study, Davies *et al* proposed a monomeric transition state in the studied Michael addition, but they did not neglect a dimeric one. In the present study, monomeric transition states were studied, while dimeric-type are being developed at the moment.

The beginning of this mechanistic study started with the design of the appropriate methodology. First, *E*-methyl cinnamate was used as Michael acceptor, and *R*-amine was chosen as reagent. Secondly, a monomeric type transition state was selected (**Sch. 15**).

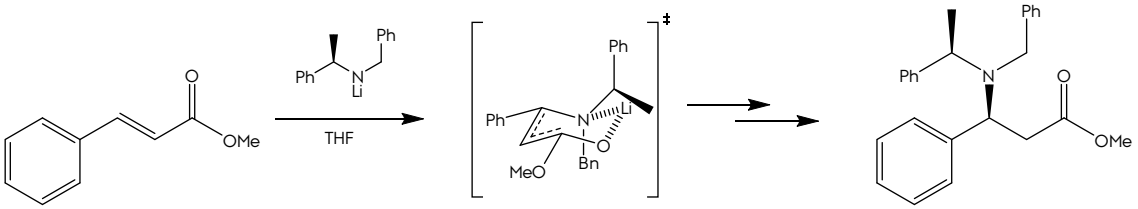

Scheme 15. Brief description of the nature of the transition state studied.

A six-membered transition state was proposed by Davies *et al* in their article. Initially, a quick check of the transition state geometry was performed, employing lithium dimethyl amide as model amide and *E*-methyl crotonate as model α,β-unsaturated ester. Employing DFT-B3LYP/6-31G(d), the transition state was quickly found (**Fig. 28**), and its nature was checked by vibrational normal mode analysis and QRC[25] scan.

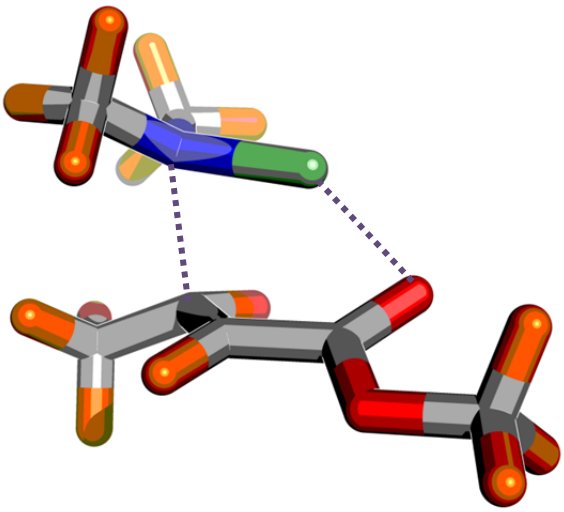

N-Cβ / Å	2.13
Li-O / Å	2.07
Li-N / Å	1.95
Cβ-Cα / Å	1.4
Cα-C / Å	1.46
C-O / Å	1.26
Cβ-Cα-C-O / º	22
ν / cm^{-1}	239i

Figure 28. Transition state geometry in Michael addition of lithium dimethylamide to *E*-methyl crotonate. Geometrical parameters were displayed with vibrational analysis.

The six-membered transition state has several features:

- The approximation angles of the amide moiety are 93º (N-Cβ-O), 106º (N-Cβ-C) and 110º (N-Cβ-Cα). QRC also confirmed the slight shift from the orthogonal proposed approximation by Davies *et al.*

- Bond lengths are slightly increased for Cβ-Cα and C-O, while Cα-C is lower. The animation of the reaction coordinate allows to inspect the dynamic behaviour of them.

- The Michael acceptor system is not planar anymore. A 22 º torsion is adopted in the system.

- QRC confirmed the nature of the stationary point, and no other intermediates apart from products or starting materials were detected.

Once confirmed the transition state model of the Michael addition, the model was modified adding the appropriate substituents to obtain the transition state of the reaction between *E*-methyl cinnamate and *R*-amine. As the transition state geometry was calculated, i.e. the atomic centers involved in the reaction, only a conformational search is required to optimize the disposition of the substituents. In their published work, Davies *et al* employed Molecular Mechanics calculations following a hierarchical level of search. First, the distance between amide's nitrogen and Cβ of the substrate was optimized. Later, the approximation angle together with the Lp-N-Cβ-Cα dihedral were minimized, locating the transition state. Finally, rotational conformations were generated in the benzyl arms of the amide moiety in order to find the most appropriate conformation that minimizes interactions.

At this point, several ideas must be introduced. The main drawback in modelling these systems is to properly account long-range dispersion forces, especially where aromatic rings are implied. Molecular Mechanics force fields incorporate *Lennard-Jones* or *Hill* type potentials to account Van der Waals interactions. Several force fields, like MMX series, MMFF, OPLS or AMBER accounts properly for dispersion interactions. However, their use in dealing with transition states is limited. DFT methods have become popular nowadays, due to accuracy, speed and agreement with experiments, as the result of including the correlation energy with a computational effort similar to HF theories. Nevertheless, the most important handicap in using DFT is the poor description of dispersion forces. In such sense, the improvements of DFT methods are focused on predict weak interactions. One of the

general ideas of the present mechanism, proposed by Davies *et al*, was the butterfly type disposition of the benzyl rings as the most favourable conformation, due to a predicted π-stacking interaction by MM. It is reasonable to think crystal structures may present this type of disposition as well. However, inspection of molecule packaging at Snaith's crystal or Andrew's one did not showed stacking interactions, but it showed T-shaped C-H $\cdot\cdot\cdot$ Ar interactions. Catak *et al*[26] have published the asymmetric nucleophilic ring-opening of *N*,*N*-dibenzylaziridinium ions. In this work, an asymmetric aziridinium intermediate, consisting of the derived (*R*)-*N*-benzyl-*N*-(α-methylbenzyl)amine was theoretically analysed by means of conformational search. MP2 based calculations revealed three transition states: a butterfly type π-π interaction (highest energy), and two T-stacking ones (lowest energies). Thereby, the stability of butterfly type conformations needs to be revisited.

Gas-phase transition states does not always match with solvated ones. Back to the 1994 mechanism, no allusion of solvent was done. Solvating step always stabilizes molecules and intermediates, but conformation plays an important role, due to the cavity modeling. In this case, there is an additional point: explicit solvent molecules are required. THF coordinates to the metal, as it is noted in crystal structures and in theoretical projects.

Considering these ideas, the methodology of the mechanism study has to follow certain points:

- As the molecules are modelled in the QM context, conventional DFT methods are not recommended. Corrected functionals, which deals properly weak interactions, should be used.

- A thorough benchmark of density functional methods will be interesting, in order to check the most suitable for these systems.

- Explicit solvation molecules are required, due to their ligand role.

- Implicit solvation scheme allows accounting non-polar and polar interactions between solute and a continuous solvent model.

- Accuracy/speed commitment is required, to obtain a valuable methodology for deal this kind of systems.

With all this considerations, the next theoretical methodology was designed:

Q1 - Systems set up (Maestro)

- Lithium (*R*)-*N*-benzyl-*N*-(α-methylbenzyl)amide → amide
- *E*-methyl cinnamate → substrate
- Geometry → Transition state (atomic centers implied)
- Substituentes have a random geometry (benzyl arms of amide, phenyl and methoxy moieties of cinnamate)
- One THF molecules coordinated to lithium.

The starting geometry was the previously described in the transition state (figure gg). Manually, the systems were modified in Maestro v9.1[27] to add the substituents: the amide was transformed into lithium (*R*)-*N*-benzyl-*N*-(α-methylbenzyl)amide and the substrate was modelled into *E*-methyl cinnamate. The geometry of the six centers implied in the transition state (N, Li, Cα, Cβ, C, O) was frozen, and remains unaltered along the entire protocol. The initial geometry of the additional substituents was random.

Two initial systems were created: the *Re* attack and the *Si* attack, as a function of the face where the amide is approximating. As the atomic centers were constrained, the interchange between amide's benzyl arms was no longer allowed. For this reason, each system was split into two homologues: 1 and 2, as a function of the methyl group placing in a benzyl arm or the other one. A total of four systems, ***Si*-1**, ***Si*-2**, ***Re*-1** and ***Re*-2** were created (**Fig. 29**).

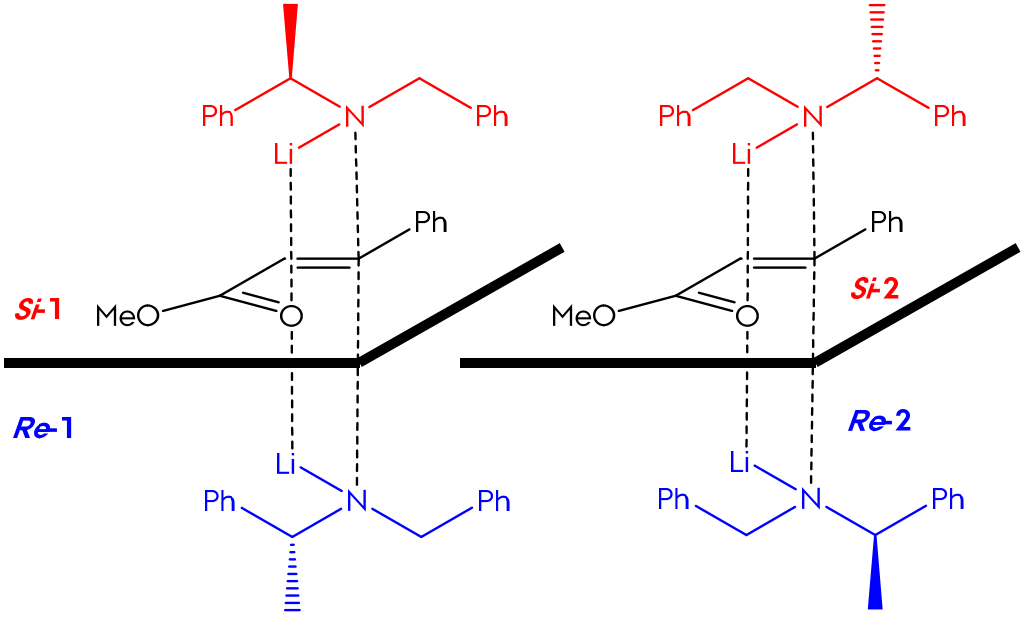

Figure 29. 2D- representation of the four initial transition state models.

Finally, a THF molecule, coordinated with lithium, was placed. It was tested; using this protocol, the energy of the transition states is lower when one molecules of THF is coordinated to the metal center. If two molecules were placed, the energy rises, and sometimes one of the THF molecules was expelled from the coordination sphere along the protocol progress. Consequently, only one molecule of THF was added, with a random distance from the metal center.

Q2 - Minimization (Tinker)

- The four systems were minimized by means of MM/OPLS.

Once modelled, the four systems were subjected to minimization through molecular mechanics, using OPLS[28] as force field invoking the MINIMIZE command of Tinker.[29] The atomic centers implied in the transition state were frozen.

Q3 - Coordinate Scan (Tinker)

- In each system, a coordinate scan of dihedrals φ_1 and φ_2 was performed.
- Each coordinate was divided in steps of 20 º, from 0→360 º.
- 324 conformers were taken in each system.
- Each conformer was minimized, extending the constraint level from atomic centers implied in the TS to atomic centers implied in the scanned torsions.

A rigorous conformational search was done following step Q3 and forward. A simple conformational search might not properly search the entire conformational space, and the neglect of representative conformers is possible. As one of the targets was identify parallel and T-type stacked conformers, a thorough sample was required.

First, a coordinate scan was performed only allowing dihedrals φ_1 and φ_2 to move. The purpose of these scan is generate a collective of conformers with all possible torsions between benzyl arms of the amide molecule. The scan was executed taking torsions with 20º of increment (**Fig. 30**). Each one of the 324 structures was modelled manually in Maestro v9.1, and each one was minimized by means of the command MINIMIZE of TINKER. The constraining level was extended to also cover scanned torsion atomic centers.

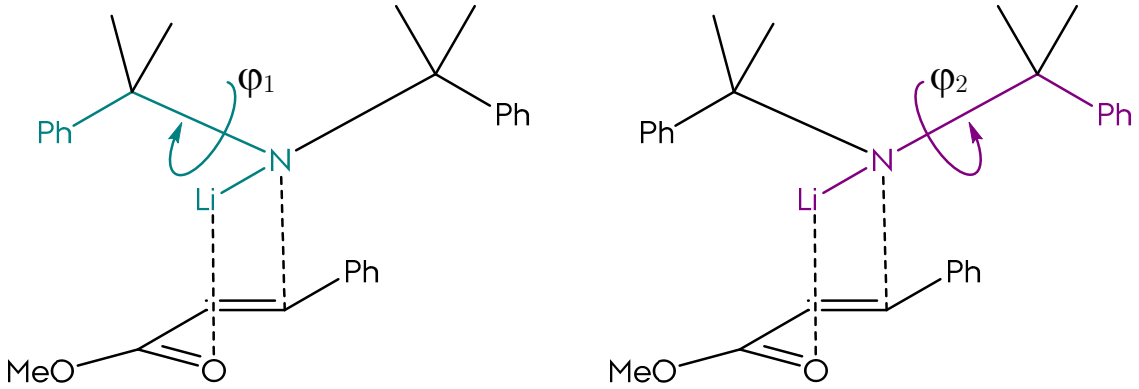

Figure 30. Selected torsions to perform the conformational scan.

Q4 - Conformational search 1 (Tinker)

- Each one of the previosuly obtained conformers was the starting point to perform a restrected conformational search.
- TS atomic centers, benzylic carbons and C_{ipso} centers were frozen.
- At this stage, dihedrals θ_1 and θ_2, and distance THF $\cdot\cdot\cdot$ Li were optimized.

To properly optimize the disposition of the aromatic rings in each rotamer, a restricted conformational search was done. It was restricted, because TS atomic centers, benzylic atoms and C_{ipso} centers were also frozen. The importance of this stage lies on the optimization of dihedrals θ_1 and θ_2, together with the optimization of the distance **d** between THF-Li and the relative conformation of this ligand (**Fig. 31**). The lowest conformer in each search was recorded.

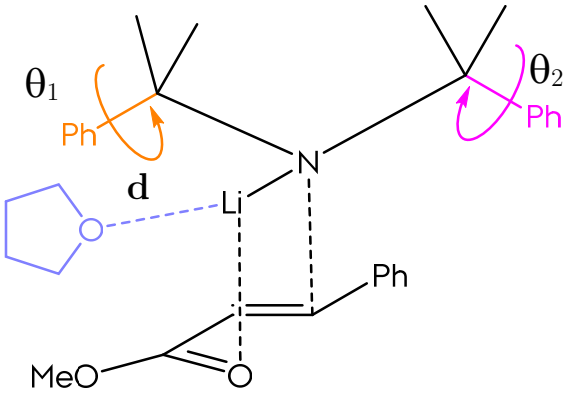

Figure 31. Selected coordinates to optimize in the conformational search of each rotamer.

Q5 - Conformational search 2 (Jaguar)

- Each one of the previosuly obtained conformers was evaluated by means of a QM single-point energy.
- A potential surface map was obtained (energy vs 2D map of torsions)
- All the minima in the potential surface was taken.

Each one of the rotamers was subjected to a QM single-point calculation, invoking Jaguar v7.9.[30] With this, a potential surface map was obtained, where two variables were the torsions φ_1 and φ_2. In this topological map, all the structures which has a local minima where extracted. These set of candidates where the representative starting conformers of the next stage.

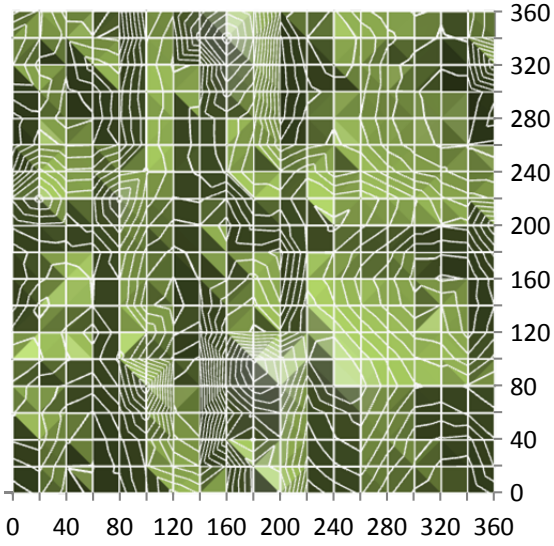

Q6 - Optimization (Jaguar)

- Each one of the previosuly obtained candidates was optimized through QM.
- Here, the constraining level was limited to TS centers.

Taking each one of the candidates, a QM optimization was performed, constraining only TS atomic centers. Benzyl arms disposition, together with THF ligand were relaxed.

Q7 - Solvation (Jaguar)

- Each one of the optimized structures was soaked into a continous solvent, by means of PBF model. Single-point energies were calculated.

Finally, each one of the structures was subjected to a solvated single-point energy, in the PBF context. The output structures were taken as definitive results.

DFT benchmark

Once designed the protocol, the next stage is the selection of the QM theories that will be used in the methodology. For this reason, a thorough benchmark study of DFT methods was developed with the next points:

- First, post Hartree-Fock method MP2 (second-order Møller-Plesset perturbation theory) was considered. It is well-known MP2 reproduces well geometries of stacked complexes, but overestimates interaction energies. Although MP2 has a refinement level (SCS, Spin-Component-Scaled treatment), pure MP2 theory was used.

- B3LYP,[31] the popular DFT standard, started the list of DFT explored methods. Despite of the popularity, it has several drawbacks: poorly described long-range interactions, homolytic bond breaking or isodesmic reactions.

- Truhlar *et al*[32] have designed a family of new hybrid meta exchange-correlation functionals, also referred as Minnesota functionals, which were parameterized on high-quality benchmark databases. M05-2X and M06-2X represent an improvement in accounting medium-range dispersion forces (up to 5 Å).[33] These two functional were also selected.

- Add-on dispersion corrections to standard DFT theories, i.e. DFT-D3 methods developed by Grimme *et al,*[34] have grown importance in the last times, as a low-cost substantial improving of the basic DFT functionals. B3LYP-D3, M05-2X-D3 and M06-2X-D3 completed the set of chosen functionals.

- 6-31G(d) basis set was selected at the Q5-6 steps. The basis set was augmented to 6-31G(d,p)++ in Q7.

The benchmarking was done in just one of the four systems modelled. ***Re*-2** was arbitrary selected as the system of choice. The protocol was followed for each one of the 6 DFT functionals, as well as the MP2. The results are described below.

The purpose of the protocol is not to find a real TS, because it was already defined, but this TS requires a conformational search to define what is the real conformation of the benzyl arms of the amide, which will define the stereochemical outcome of the reaction. Q4-5 generated a representative ensemble of conformers, minimized, with all the available torsions of φ_1 and φ_2. This topology map (**Fig. 32**) has several local minima, which are structures with lower energy, computed through single-point DFT 6-31G(d). It is reasonable to think, whatever structure of the PES will evolve to minimize its energy, in other words, will tend to locate its closest energy "well" and go to him (**Fig. 33**).

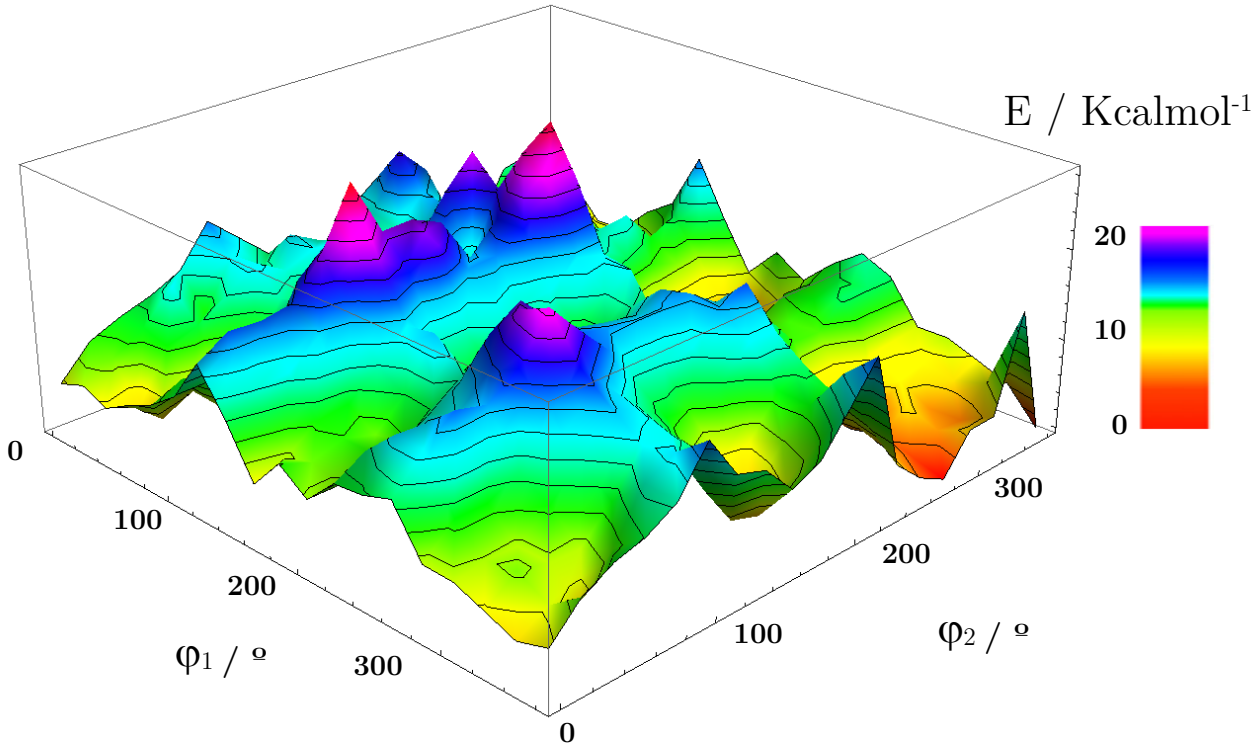

Figure 32. 3D-PES of the MP2 conformational search at the Q5 stage.

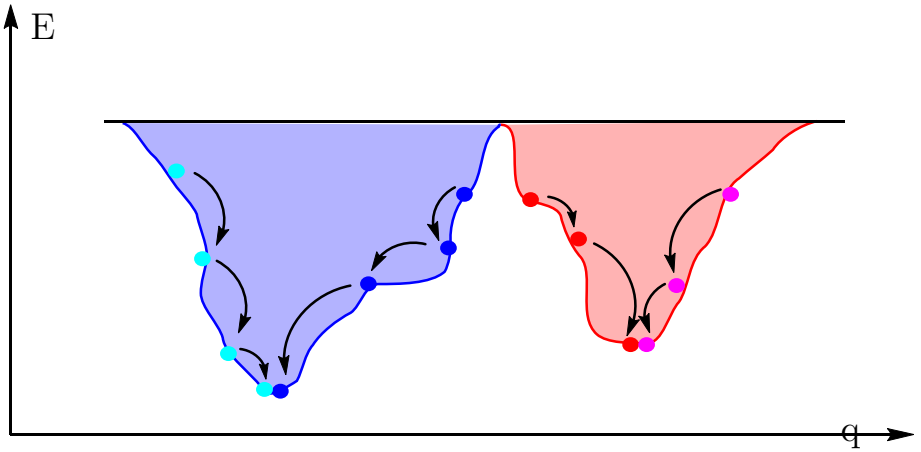

Figure 33. Prediction of the conformational evolution of the structures located at the PES (q, generalized coordinate; E, energy). Each one of the local minima is representative structures of the ensemble of geometries contained in each hole (faded region).

These local minima were selected as the representative conformers in this space: each one of the minimums represents all the structures contained in the associated "hole". As other internal coordinates were restrained at the Q5 stage, Q6 has the aim of relax the overall structure, just blocking the TS centers. Q6 results are presented as the final most populated conformers of each one of the systems. At the Q5 stage, around 15-30 low energy conformers per theory were obtained, being submitted to the Q6 stage.

Theory	Conformer	Class	RGPE (Kcal/mol)	RSPE (Kcal/mol)	SE (Kcal/mol)
M06-2X-D3	1	A	3.90	2.65	-11.24
	2	B	2.56	1.94	-10.62
	3	C	3.18	2.71	-10.46
	4	D	0.00	0.00	-10.00
	5	F	3.66	2.37	-11.28
M06-2X	1	A	1.92	0.35	-11.21
	2	B	0.85	0.59	-10.49
	3	C	3.28	2.17	-10.75
	4	D	0.00	0.00	-9.05
	5	F	1.73	0.66	-11.45
M05-2X-D3	1	A	2.27	1.73	-11.54
	2	B	2.59	2.05	-11.54
	3	D	0.00	0.00	-11.00
	4	E	3.07	2.00	-12.07
M05-2X	1	A	1.15	1.08	-11.27
	2	B	1.40	1.27	-11.33
	3	C	1.47	1.69	-10.99
	4	D	0.00	0.00	-11.20
	5	E	1.74	0.85	-12.09
B3LYP-D3	1	A	0.33	0.52	-9.06
	2	B	0.73	0.99	-8.99
	3	C	2.94	2.04	-10.14
	4	D	0.00	0.00	-9.25
	5	E	2.23	1.01	-10.47
B3LYP	1	A	1.88	2.01	-9.07
	2	B	1.45	2.04	-8.62
	3	C	2.60	2.25	-9.56
	4	D	0.23	0.00	-9.44
	5	E	0.00	0.17	-9.04
MP2	1	D	0.00	0.00	-9.26

Table 2. Q7 values of the validation stage. RGPE (relative gas-phase energy), RSPE (relative solution phase energy), SE (solvation energy).

It was found remarkable that in the progress of Q6, several optimizations converged in the same relaxed structure. That means the number of optimized geometries at Q6 is lower than the number of local minimums at Q5. In other words, the global minimums cover several local ones, and the complexity of the conformational space was simplified. A conformational window of 4 Kcal/mol from the minimum was selected to save conformers. Besides, the remaining structures were clustered as a function of the RMSD. The lowest energy member of each cluster was retained. **Table 2** summarizes the final geometries obtained with each theory. The geometries were classified as **A**-**E** as a function of the relative disposition of the benzyl arms, ignoring the THF disposition. Next figures show the classified geometries.

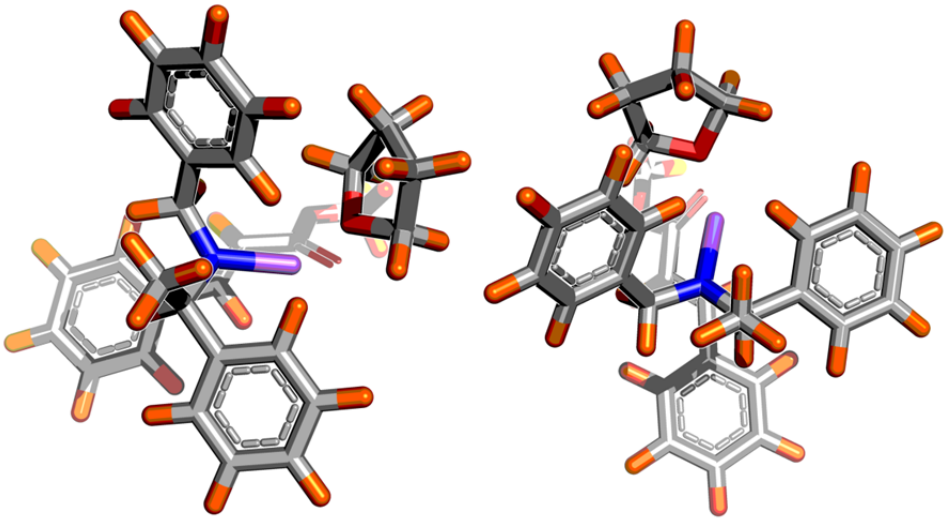

Class A (Semi-folded-1). One of the phenyl rings is extended, while the other one is vertically-folded. No π-stacking or CH · · · Ar interactions.

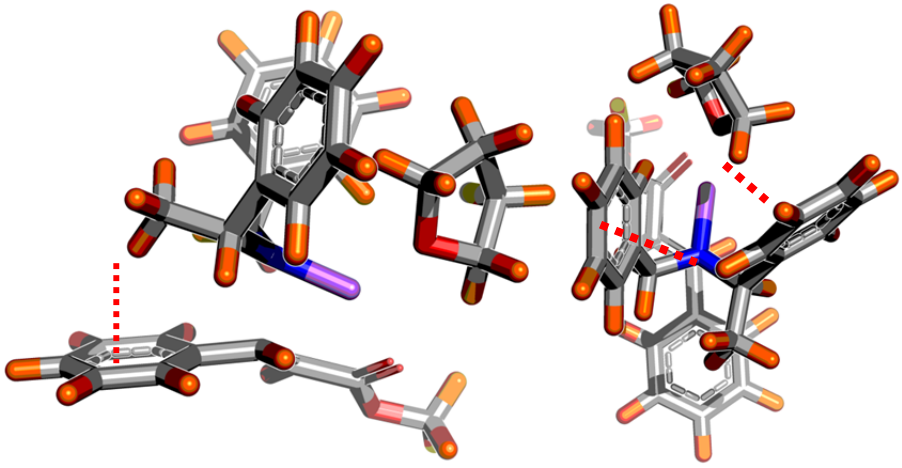

Class B (V-stacked). Both phenyl rings are vertically-folded, like the butterfly-type, but the disposition is not parallel: both rings form a V. Two CH · · · Ar interactions were detected (red).

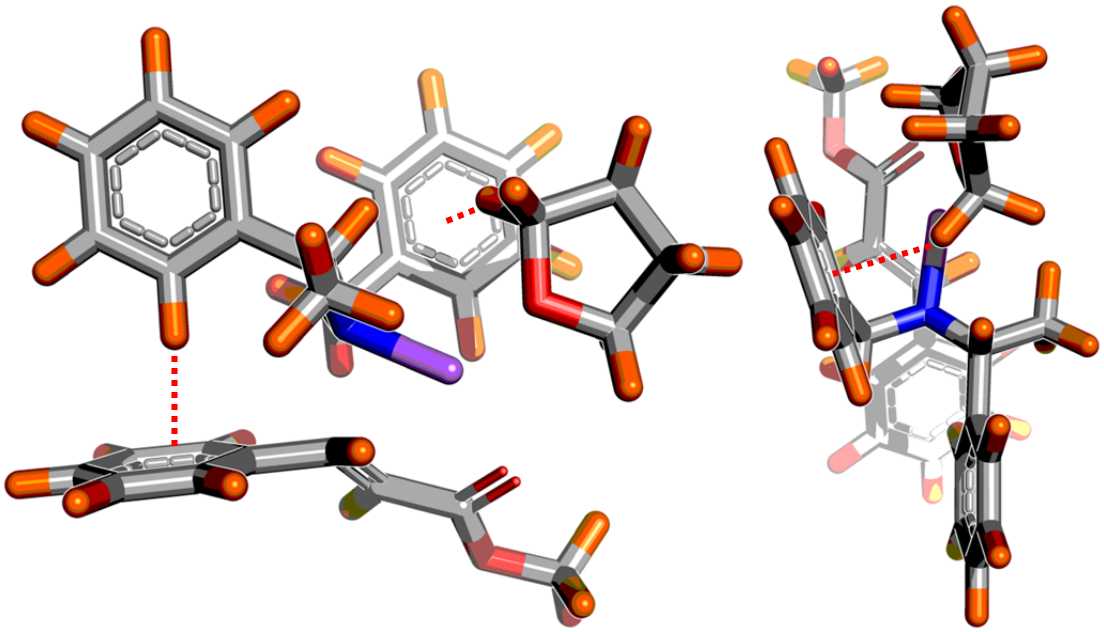

Class C (Back-T-stacked). Both phenyl rings have a vertical disposition. One of them is moved towards the THF molecule, establishing a CH · · · Ar interaction. The other phenyl group has a T-stacked conformation with native phenyl ring of the cinnamate moiety, with a CH · · · Ar interaction (red).

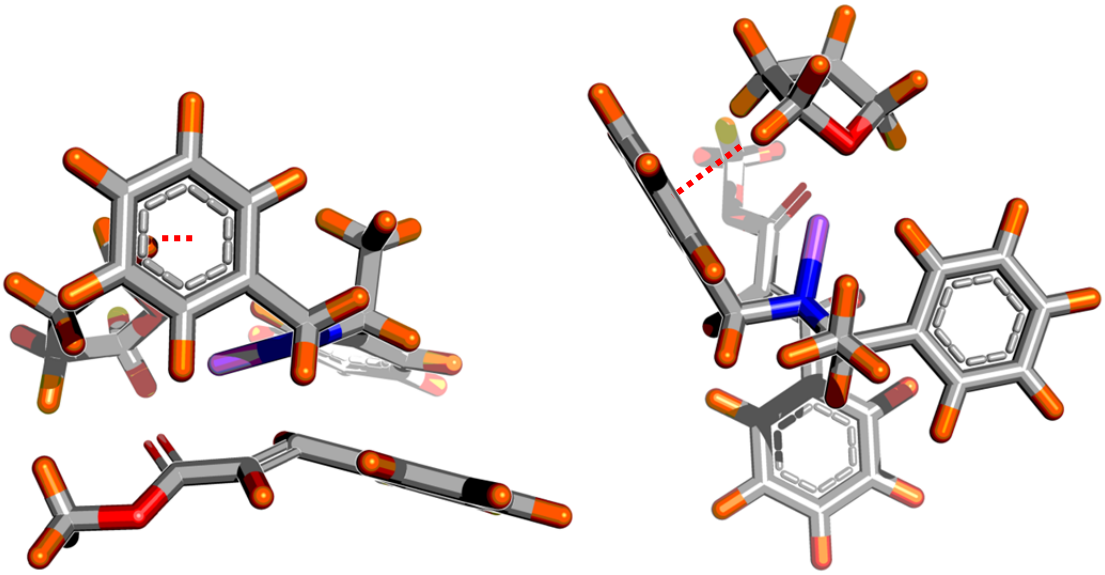

Class D (Semi-folded-2). Again, one of the phenyl rings is extended, while the other one is vertically-folded. Difference with type 1 lies in the θ torsion of the folded ring, which faces the THF molecule, resulting in a CH · · · Ar interaction (red).

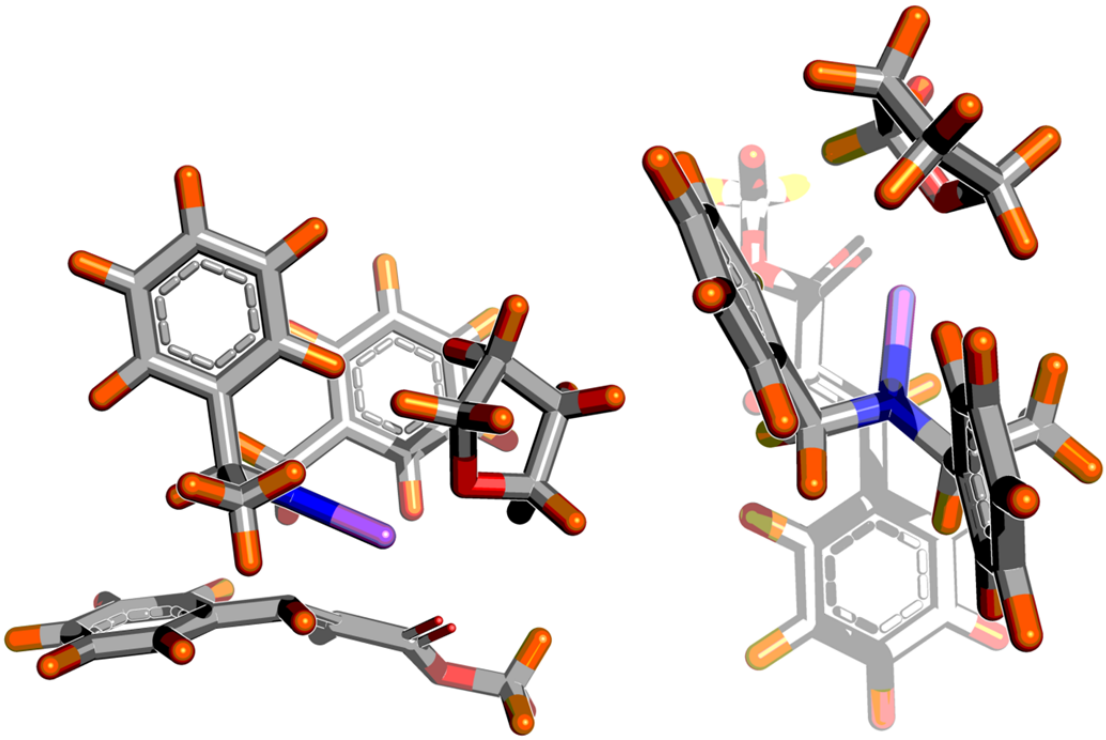

Class E (Distorted Butterfly). Both phenyl rings are vertically-folded, like class C, but here the phenyl groups are shifted. CH · · · Ar interaction can established between the THF and the more advanced phenyl ring (red).

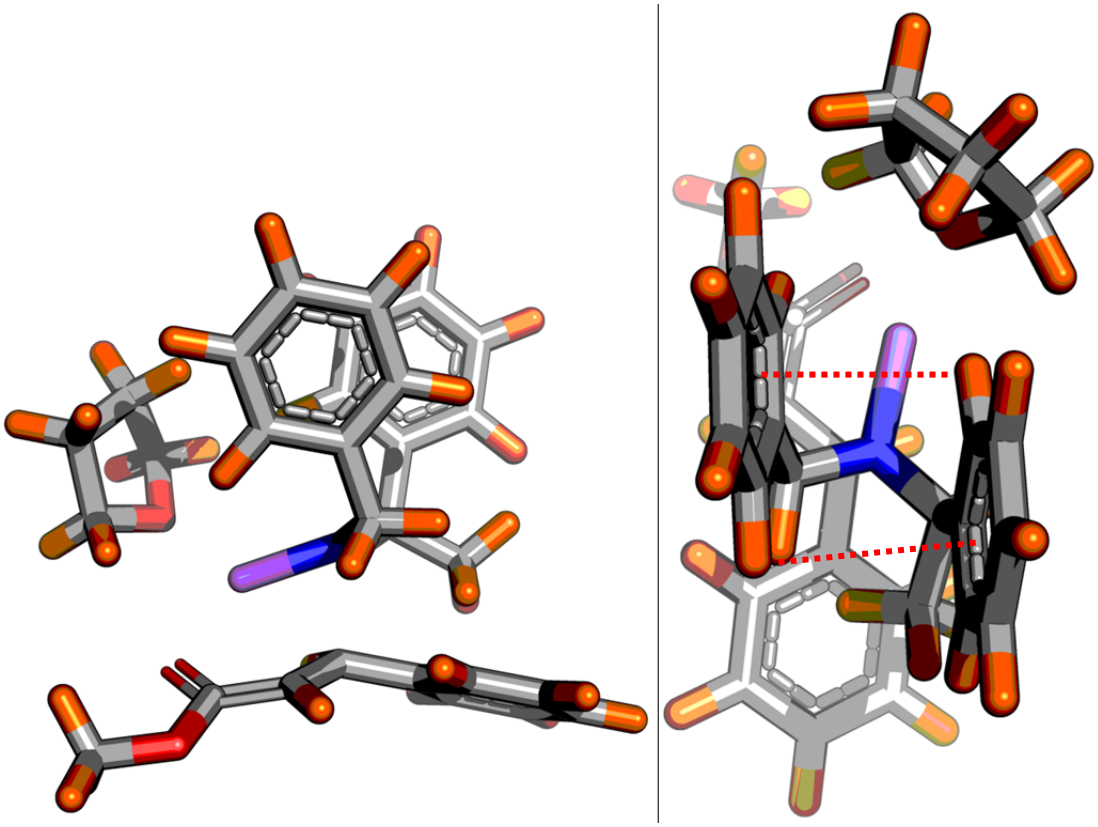

Class F (Butterfly). Both phenyl rings are vertically-folded, like class C-E, but here the phenyl groups have a π stacking interaction.

Figure 34 shows a 2D plot of the optimized structures as a function of dihedrals φ_1 and φ_2, together with the clustering of them in classes **A-F**.

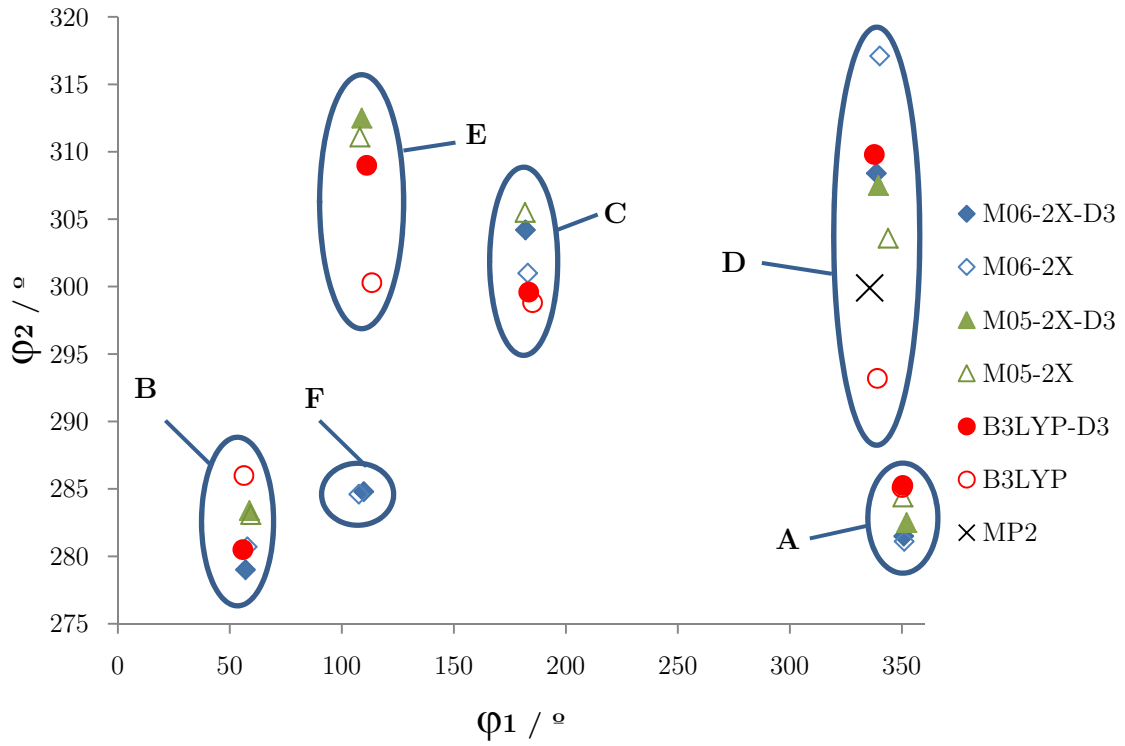

Figure 34. 2D plot of the optimized geometries as a function of dihedrals φ_1 and φ_2. Geometries belonging to the same class are inside the same ellipse.

From this figure and **table 2** we can extract some conclusions:

- Classes **A-D** appeared in all DFT theories. Class F (butterfly) only appears in the M06-2X and M06-2X-D3 theories, while its distorted counterpart (class E), is described in M05-2X, M05-2X-D3, B3lYP and B3LYP-D3.
- Regarding gas phase structures, all the theories predicted a class **D** as structure as the lowest energy conformer, excluding B3LYP, which predicted a class **E** conformer.
- Regarding the solution-phase structures, all the theories predicted a class **D** as structure as the lowest energy conformer.
- RMSD was measured to compare similarity between structures of different theories that belong to the same class. All geometries are practically the same (RMSD $<$ 1.5 Å), with minor changes due to THF arrangement. B3LYP conformers were found to have less structural relationships with other theories, so it is excluded for now on forward.

- B3LYP-D3 conformational results are similar to Truhlar-type functionals, so the D3 correction represented an improvement of accuracy.
- Regarding the geometrical outcome, no especial differences were found between basic Truhlar-type functionals and extended D3 ones (RMSD < 1.0 Å). Truhlar D3-type functionals was discarded.
- Post Hartree-Fock MP2 theory has only one conformer, despite of its trend to overestimate non-bonded interactions.
- All the solvated structures are more stable than non-solvated ones.
- From the energetic point of view, M06-2X, and B3LYP-D3 have more low energy conformers. Between the similar DFT functionals M05-2X and M06-2X, is better selecting a theory that retains more number of conformers. M05-2X was discarded.
- M06-2X, due to properly covered medium-range dispersion interactions have been successfully tested for non-covalent interactions.[32c] This is the selected functional to continue the mechanistic study.

The importance of this study not also is reflected in the selection of the most appropriate DFT functional, but additional ideas may be extracted from the outcome of the measurements.

DFT theories, which cover medium-range dispersion forces, are ideal for study this kind of systems, as the different classes are made of conformers with π-stacking and CH/π interactions. However, when the predicted diversity of conformers will be larger, an exhaustive conformational search is required. The search developed in the present protocol has the aim of explore in the best way the conformational space, but saving time due to the computational resources used. Thus, an accuracy/time commitment was made, and a dual hierarchical QM/MM conformational search was designed. Conformational sampling is prime to have a initial set of representative structures to apply the commented DFT theories, otherwise more computational time will be required if a pure QM search is desired.

A wider geometrical diversity was obtained, comparing with Davies *et al* work. Structural similar motifs were clustered into classes, among them, the butterfly-type (class **F**) predicted by Davies *et al*. However, geometries tend to maximize side chain interactions, and phenyl rings are displaced between them (class **C**) or their disposition is stacked but not utterly parallel (classes **B** or **E**).

The idea of the influence of the conformation in the stereochemical outcome of this reaction is fundamental.

It is necessary to note these results may be substrate-dependent. Although the reproducibility of the reactions was demonstrated, the diversity is wide. Thus, a robustness test would be necessary, to check if the mechanism is conservative upon changing the substrate.

Reaction Mechanism Study

Once selected the M06-2X DFT functional as the functional of choice, the same protocol was repeated with this theory, but extending to systems ***Si*-1**, ***Si*-2** and ***Re*-1**. Again, the results were clustered as a function of the RMSD and the lowest energy member of each cluster was retained. A conformational window of 3 Kcal/mol from the minimum was selected as well to save conformers.

At this point, the same classification profile of the optimized geometries was applied. However, new geometries have appeared in the extension of the study, which are schematized below.

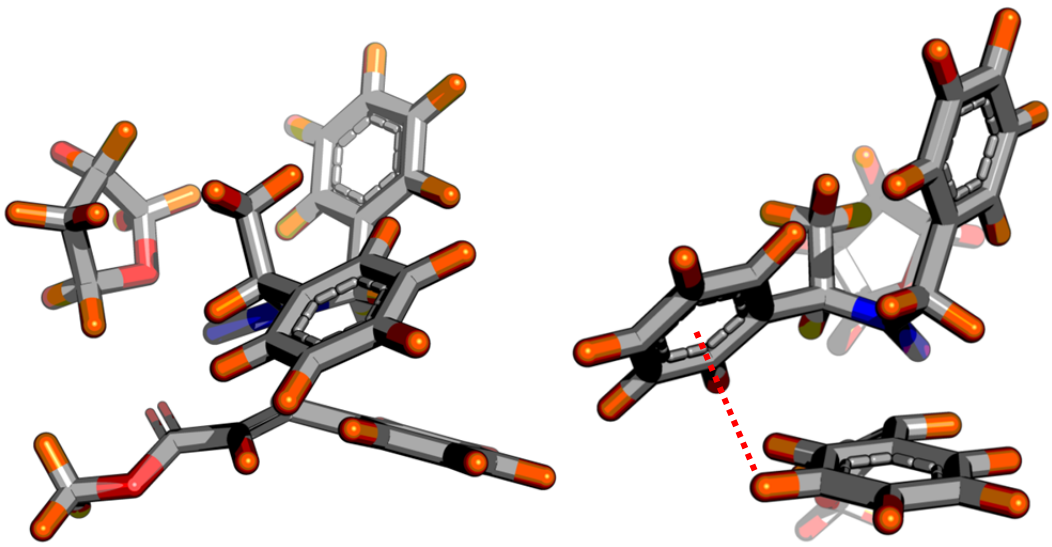

Class G (Semi-folded-3). Similar to classes **A** and **E**, one of the phenyl rings is vertically-folded, but the other one is extended to the back of the Michael acceptor, towards the third phenyl group. A CH · · · Ar interaction is established between them (red).

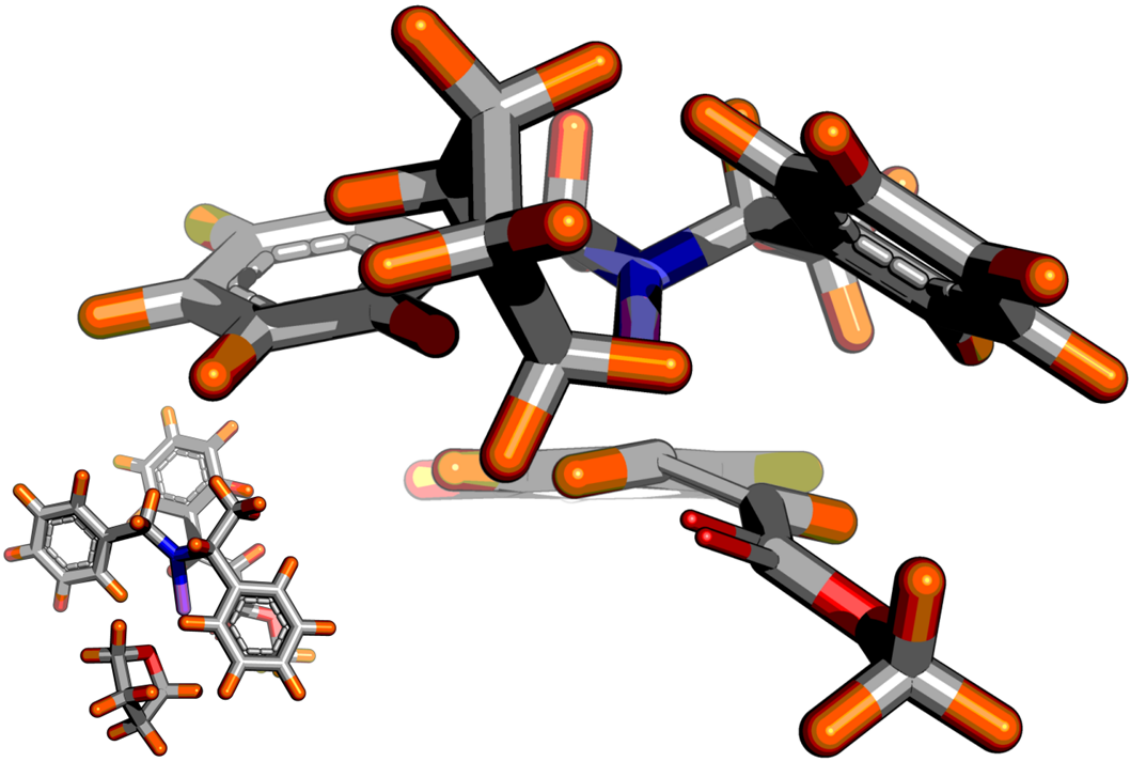

Class H (Seagull). In this class, the benzyl arms are completely extended, remembering a flying seagull. Frequent at high energy conformers.

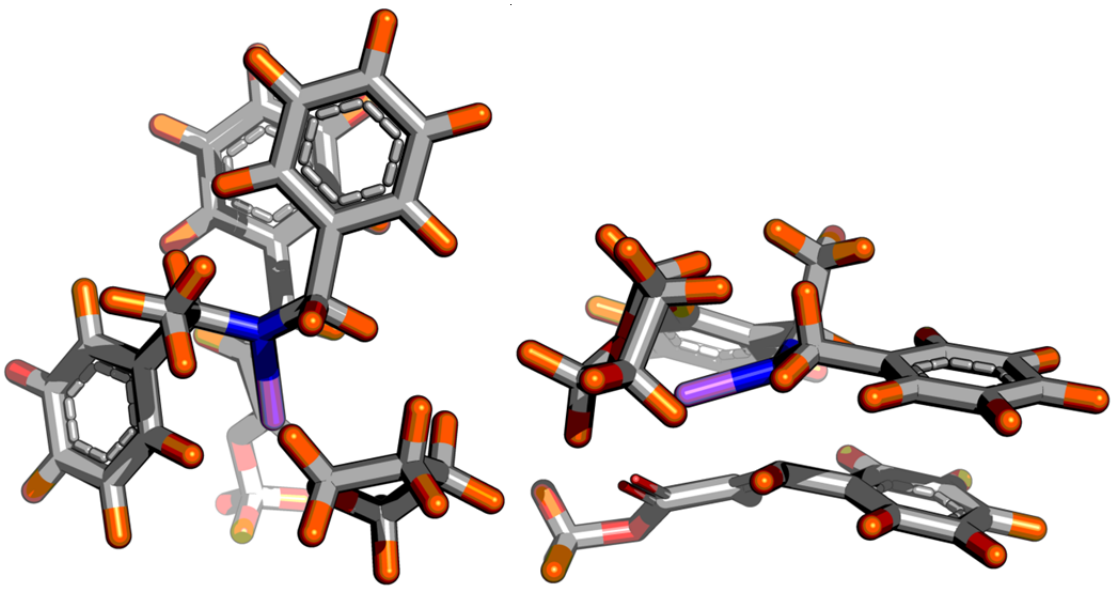

Class I (Back-π-stacked). In this class, one of the benzyl arms is completely extended, while the other one is back-folded to the native phenyl ring of the cinnamate. The disposition is parallel, thus interacting overlapping their pi orbitals (π-stacking).

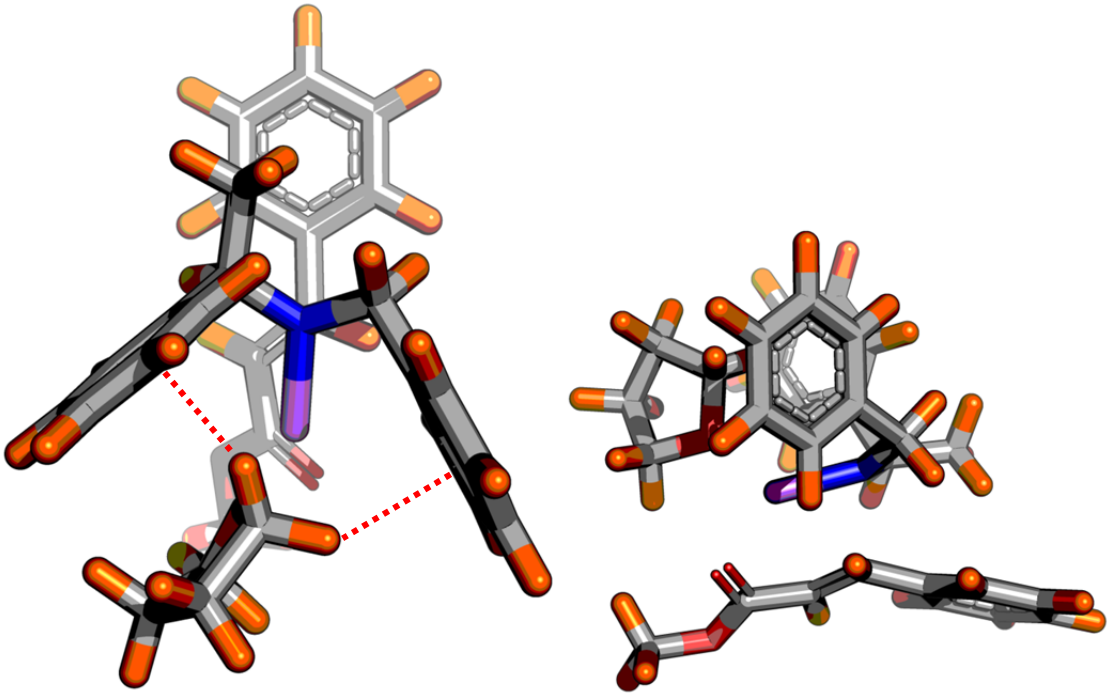

Class J (L-type). In this class, both benzyl arms are completely extended, covering the THF molecule and interacting with if through CH/π interactions.

Table 3 summarizes the final geometries obtained en each system. The geometries were classified as **A**-**J** as a function of the relative disposition of the benzyl arms, ignoring the THF disposition.

Having a look to **table 3**, it is easy to extract some conclusions:

- In each system, relative gas phase energies are not in agreement with solvated ones. This means the solute geometry itself is not governing the solvation energy. The Poisson-Boltzmann equation requires of the charge assignation of the atoms, which are topology-dependent. It also depends of the surface of the solvent cavity created to allocate the solute, and the dispersion interaction between solute and continuous solvent. Again, solvation energies are negative, indicating a stabilization of the solution upon solvation.
- New topological classes have appeared. This is due to the small conformational change of the methyl position of amides moiety and the two sides of the Michael acceptor system. That influences the conformational disposition of the system.
- The most stable classes are **B** and **D**. It is logic, as intramolecular interactions lower the global energy of the molecule.

System	Conformer	Class	RGPE (Kcal/mol)	RSPE (Kcal/mol)	SE (kcal/mol)	ASPE (Hartrees)	GRSPE (Kcal/mol)	CRP	SRP	DRP
	1	F	1.21	1.58	-9.89	-1413.011755	6.48	0.00%		
	2	G	5.11	1.80	-13.57	-1413.011403	6.70	0.00%		
	3	F	2.37	0.77	-11.85	-1413.013037	5.68	0.00%		
	4	A	0.69	0.00	-10.95	-1413.014266	4.90	0.00%		
***Re*-1**	5	F	2.86	1.71	-11.41	-1413.011539	6.62	0.00%		
	6	G	1.44	0.96	-10.73	-1413.012732	5.87	0.00%		
	7	A	0.63	0.02	-10.87	-1413.014231	4.93	0.00%		
	8	H	1.47	1.78	-9.95	-1413.011423	6.69	0.00%		
	9	G	2.83	1.37	-11.72	-1413.01208	6.28	0.00%	-	
	1	A	1.92	0.35	-11.21	-1413.019046	1.84	0.41%		
	2	B	0.85	0.59	-10.49	-1413.018214	2.43	0.09%		
***Re*-2**	3	C	3.28	2.17	-10.75	-1413.015696	4.01	0.00%		
	4	D	0.00	0.00	-9.05	-1413.019154	1.59	0.77%		
	5	F	1.73	0.66	-11.45	-1413.018102	2.50	0.07%	1.35%	1.35%
	1	D	0.07	0.65	-10.18	-1413.008658	8.42	0.00%		
	2	H	1.89	2.67	-9.97	-1413.010344	7.37	0.00%		
	3	I	1.79	2.67	-9.88	-1413.020176	1.20	2.14%		
***Si*-1**	4	H	0.00	0.13	-10.62	-1413.016952	3.22	0.01%		
	5	J	1.25	1.48	-10.52	-1413.018853	2.03	0.25%		
	6	B	0.06	0.63	-10.19	-1413.02021	1.17	2.26%		
	7	D	0.06	0.00	-10.82	-1413.021208	0.55	11.33%	15.99%	
***Si*-2**	1	B	0.00	0.10	-10.19	-1413.021926	0.10	36.15%		
	2	B	0.91	0.00	-11.20	-1413.022082	0.00	46.51%	82.66%	98.65%

Table 3. Low-energy conformers in each system. RGPE/RSPE, relative gas/solution phase energy (in the system). SE, Solvation energy. ASPE, absolute solution phase energy. GRSPE, global relative sol. phase energy (all conformers). CRP/SRP/DRP, conformational/system/diastereotopic population at -78 ºC.

- Taking all the conformers, the *Si* face is preferentially selected in the amide approaching. The ratio ***Re*-1**/***Re*-2**/***Si*-1**/***Si*-2** is 0/1/16/82. In other words, the predicted diastereotopic ratio *Re*/*Si* is 1/99, in good agreement with the experimental[3] result (95 % de).

To further analyze the diastereotopic preference of the amide moiety, topological analysis of the structures was developed. ***Si*-2** type attack accumulates almost the 83 % of the amide population in the asymmetric Michael mechanism. This approach led to two conformers, in a 4/6 relationship, both belonging to class **B** (V-stacked). Detailed inspection revealed that both conformers are identically the same, with varying only the THF arrangement (**Fig. 35**).

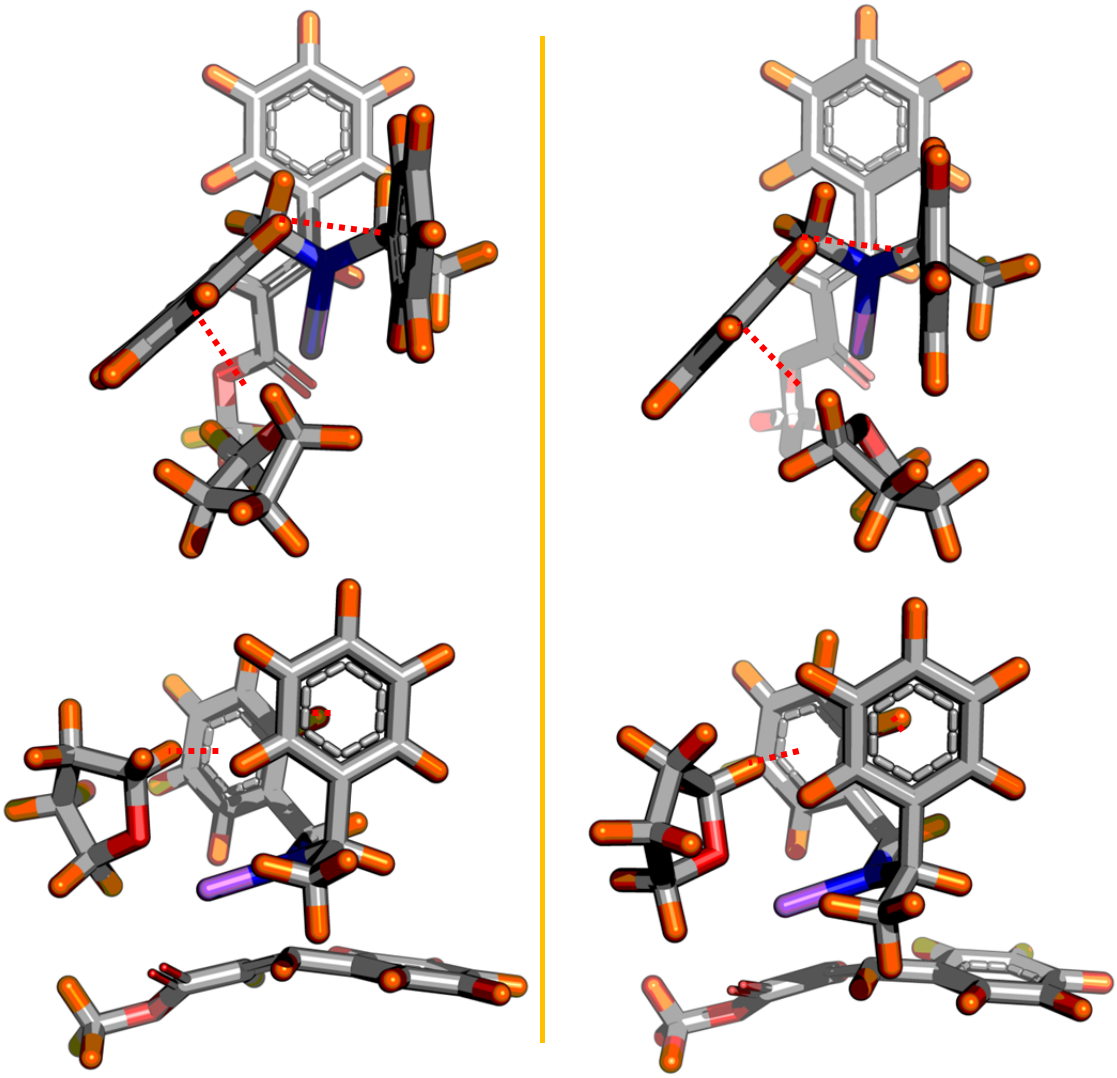

Figure 35. 3D-structure of the twin conformers ***Si*-2(1)**, right; and ***Si*-1(2)**, left. CH · · Ar interaction are depicted as red dashed lines.

These twins structures have the benzyl arms of the amide folded, but not parallel: one of the rings is slightly advanced and the disposition is V-type. The methyl moiety is placed outside the Michael acceptor region, avoiding sterical clashes. The no-parallel disposition of benzyl arms is not casual: a pure butterfly conformation only has the interanular interaction, but this king of V-stacked disposition has a partial interanular one, with additional CH $\cdot\cdot\cdot$ Ar interactions. The presence of the THF molecule not only stabilizes the metal center, it also stabilizes the phenyl rings in this kind of conformations through CH/π interactions.

Almost 16% of the lithium amides attack the *Si*-face of the substrate in a fashion different from the twins conformers: the methyl group is placed in the other benzyl arm, which are the family of ***Si*-1** conformers. **Figure 36** depicts the TS structures of ***Si*-1(7)**, which participates in an 11 % (class **D**).

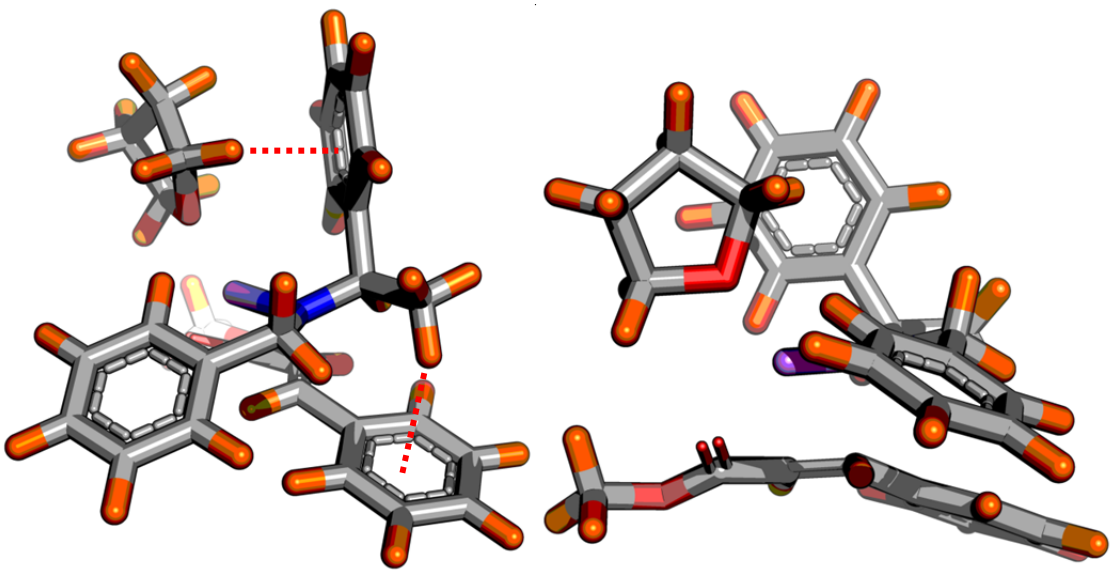

Figure 36. 3D-structures of TS conformer ***Si*-1(7).** CH/π interactions are depicted as red dashed lines.

This class **D** transition state structure has one of the benzyl arms extended equatorial from the plane of the unsaturated system. The other chain is axially placed, interacting with the THF again through a CH/π interaction. An additional similar interaction may be found between the methyl group and the phenyl ring of the cinnamate. This disposition is almost 0.55 Kcal/mol higher than the twins' structures. In this case, the benzyl ring torsion to the equatorial disposition breaks the transannular interaction. The two CH/π interactions block the conformation of the α-methylphenyl group.

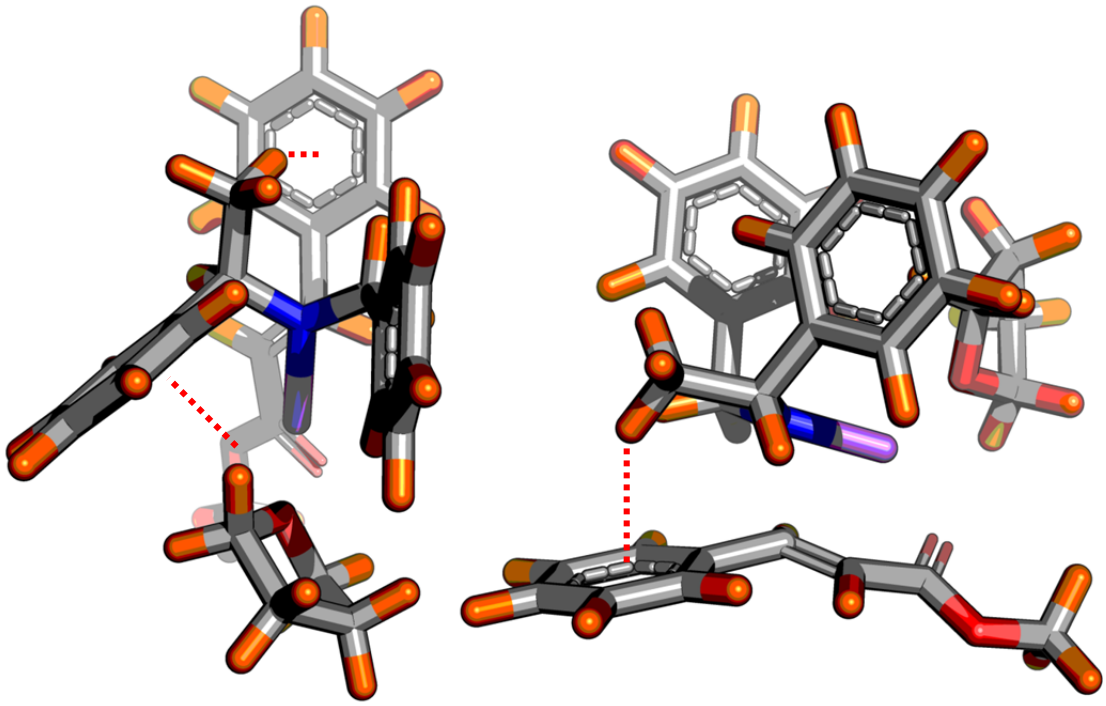

Figure 37. 3D-structures of TS conformer *Si*-1(6). CH/π interactions are depicted as red dashed lines.

Class **B** structure ***Si*-1(6)** contributes only a 2.1 %, but the study of it has interesting features (**Fig. 37**). It almost equal to one twin structure *Si*-2; however, only vary in the placing of the methyl group, which was in the other benzyl group. This methyl group is placed in the same manner as the previous case ***Si*-1(7)**, interacting with the native phenyl ring of cinnamate. The question is, Why has a higher energy (around 1.17 Kcal/mol) being almost equal to the twins' TS motifs? Obviously, the difference lies in the methyl group placing. So in this case, the methyl group placing has a negative consequence: behind the CH/π interaction there is also a sterical hindrance. The presence of the methyl group in this benzyl arm limits the movement, as it can see superimposing the structures of the seven ***Si*-1** conformers (**Fig. 38**). Only two available positions are allowed: an axial disposition (varying the other benzyl arm, leads to classes **B**, **I** and **J**) or an equatorial one (class **H**). Thus, behind the CH_3/Ph (cinnamate) there is also a soft sterical clash (soft, because is compensated by the CH/π interaction): the THF molecule blocks also the movement of this phenyl arm.

Class **I** structure ***Si*-1(3)** contributes only a 2.0 %, and represents an attractive example of the influence of substrate in the TS. It is logic to think, there is also a possibility to obtain a stacked conformation between a phenyl ring of the amide and the native phenyl ring of the cinamate.

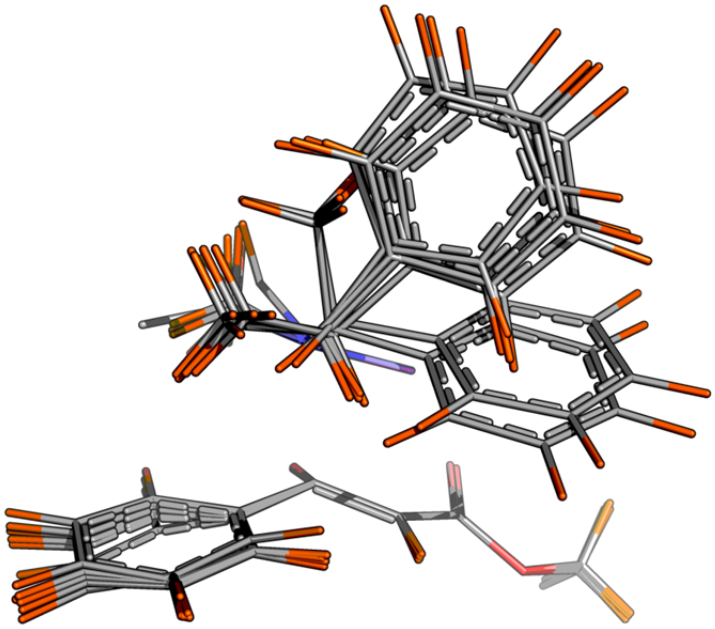

Figure 39. Superimposed structures of TS ***Si*-1** conformers. THF molecule and opposite benzyl arm were removed.

In this case, the benzyl branch is moved to the cinamate's aromatic ring, in a slightly displaced stacked conformation. This force the α-methylphenyl group to change the conformation to the other allowed one: in an extended equatorial placing (**Fig. 39**).

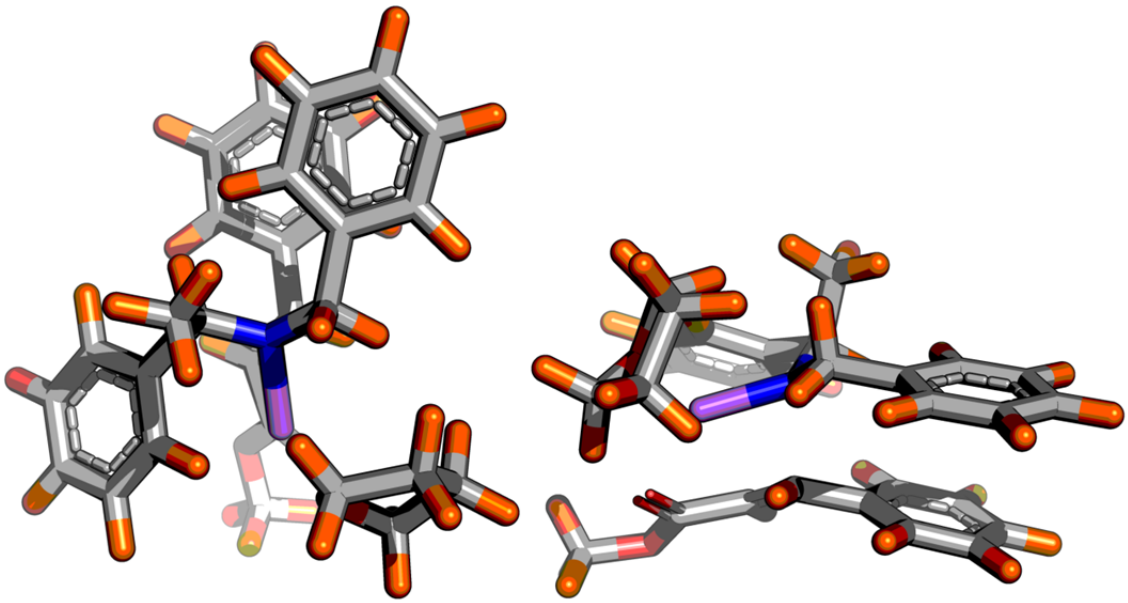

Figure 39. 3D-structures of TS conformer ***Si*-1(3)**. A π-stacking interaction is established between the phenyl groups.

Finally, the main contributor of the diastereotopic *Re*-face attack is ***Re*-2(4)**, with a participation of 0.77 % (**Fig. 40**). A class **D** motif is adopted here, with one extended phenyl ring and the other one interacting with THF ligand.

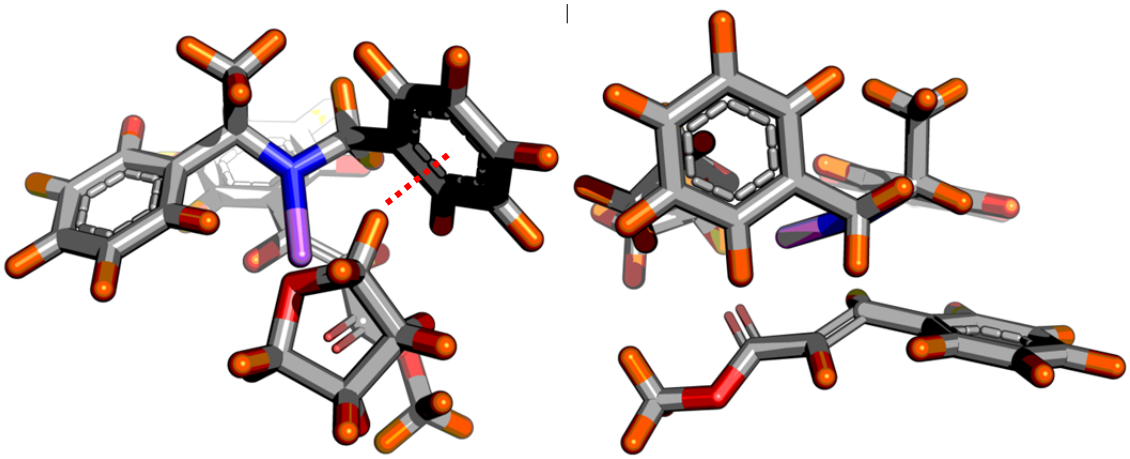

Figure 40. 3D-structures of TS conformer ***Re*-2(4)**. CH/π interactions are depicted as red dashed lines.

Re*-1** optimized TS had high energy values, so were not taking into account. To resume the outcome of the molecular modelling, figure 23 shows a clear and easy mechanistic explanation. One of the benzyl rings has a larger volume, the α-methylphenyl one, due to the methyl additional group, with a fixed stereochemistry. When considering only systems **1** or **2** (Re*-1**/***Re*-2** and ***Si*-1**/***Si*-2**), the favourable disposition is the one which minimizes sterical clashes due to rotation of the α-methylphenyl moiety (top view of **Fig. 41**). Thus, type 2 TS systems are the most favourable under this consideration. On the other hand, focusing only in the ***Re*/*Si*** preference of type 2 TS systems, it easy to observe the α-methylphenyl group is always placed in an axial disposition (bottom view of **Fig. 41**). With this conformation, the ***Si*-**type TS allocates the methyl group outside the TS atomic centers and substrate phenyl group. However, the ***Re*-**type TS placing of the methyl group, although the most appropriate, lead to a sterical hindrance with the phenyl group of the cinnamate. In this case, the sterical clash may be partially damped by CH/π interactions with the THF molecule.

In conclusion, the preferential *Si*-attack is due to a favourable allocation of the methyl moiety in a less hindered region. Although this is clearly the main driving force in the diastereotopic outcome, the TS conformation is modulated by CH/π interactions, not only between phenyl rings, but also with the THF ligand.

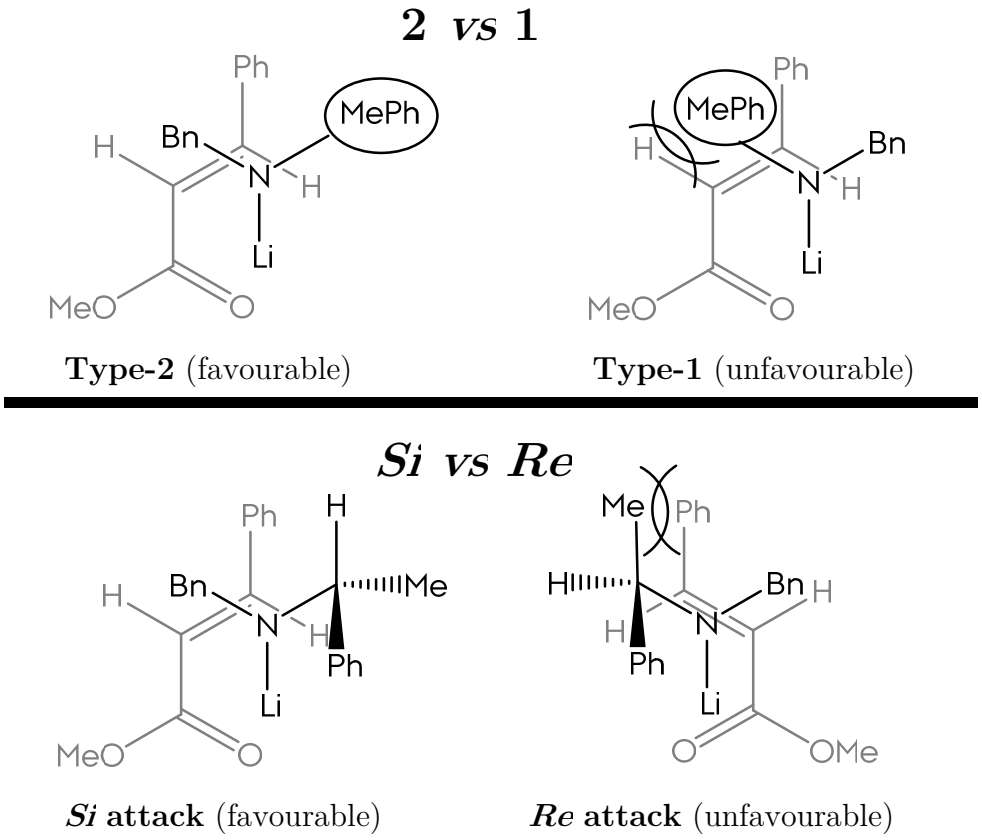

Figure 41. Brief summary of the mechanistic results of the molecular modeling study. Top: preference between type-1 and type-2 systems. Bottom: preference between *Re*/*Si* attacks.

This study ratifies the experimental stereochemical outcome of the reaction; nevertheless, is necessary to note a trimolecular TS modelling study is required, to check either a hypothetical dimeric lithium amide complex with a α,β-unsaturated ester is more/less favourable.

Conclusions

In this chapter, a QM molecular study was envisaged to bring new mechanistical insights in the addition of (*R*)-*N*-benzyl-*N*-(α-methylbenzyl)amide to α,β-unsaturated esters. The conclusions may be resumed in the next points:

- TS studies where lithium amides structures are involved are challenging tasks, due to the complexity of the solution state aggregation pattern, the dissociative processes to react with chemical species and finally the TS geometries. Extremely caution has to be taken upon treating these systems

- Although it is clear the aggregation state of (*R*)-*N*-benzyl-*N*-(α-methylbenzyl)amide in THF solutions, the origin of the coloured solutions remains uncertain.

- DFT theories with well-covered medium-range dispersion forces, like the family M05/M06 and the Grimme's D3 corrections are the most appropriate theories to cover the system, even better than MP2. To increase the representativity of the structures, a initial MM screening was performed considering benzylic arms dihedrals.

- THF-Li coordination is key to explain several of the interactions observed in the curse of the modelling work.

- Si-attacked are clearly the most favourable attack at -78 ºC, explaining the observed diastereoselectivity. The TS is mainly conformed by two twins structures, with both phenyl rings disposed axially respect to the olefin plane. CH/π interactions are detected. THF molecule can be arranged in two fashions. The predicted energies are in good agreement with experimental outcome.

- Although satisfied the experimental results, a dimeric amide-substrate TS is required to further study either a trimolecular TS is more favourable.

- Truhlar's type functionals are the recommended choices for study these kind of systems, where medium-range interactions modulate the conformation. At the moment, the molecular modelling studies keep using the M06-2X theory.

References

[1] Davies, S. G.; Ichihara, O. *Tetrahedron: Asymmetry* **1991**, *2*, 183.

[2] (a) Davies, S. G.; Smith, A. D.; Price, P. D. *Tetrahedron: Asymmetry* **2005**, *16*, 2833. (b) Davies, S. G.; Fletcher, A. M.; Roberts, P. M.; Thomson, J. E. *Tetrahedron: Asymmetry* **2012**, *23*, 1111.

[3] Costello, J. F.; Davies, S. G.; Ichihara, O. *Tetrahedron: Asymmetry* **1994**, *5*, 1999.

[4] (a) Davies, S. G.; Fletcher, A. M.; Hermann, G. J.; Poce, G.; Roberts, P. M.; Smith, A. D.; Sweet, M. J.; Thomson, J. E. *Tetrahedron: Asymmetry* **2010**, *21*, 1635. (b) Davies, S. G.; Lee, J. A.; Roberts, P. M.; Thomson, J. E.; Yin, J. *Tetrahedron* **2011**, *67*, 6382. (c) Davies, S. G.; Foster, E. M.; Frost, A. B.; Lee, J. A.; Roberts, P. M.; Thomson, J. E. *Org. Biomol. Chem.* **2012**, *10*, 6186.

[5] Hinchliffe, A. *Chem. Phys. Lett.* **1977**, *45*, 88.

[6] Wuerthwein, E. U.; Sen, K. D.; Pople, J. A.; Schleyer, P. v. R. *Inorg. Chem.* **1983**, *22*, 496.

[7] Sapse, A. M.; Kaufmann, E.; Schleyer, P. v. R.; Gleiter, R. *Inorg. Chem.* **1984**, *23*, 1569.

[8] Williard, P. G.; Liu, Q. Y.; Lochmann, L. *J. Am. Chem. Soc.* **1992**, *114*, 348.

[9] R. Armstrong, D.; W. Henderson, K.; R. Kennedy, A.; J. Kerr, W.; S. Mair, F.; H. Moir, J.; H. Moran, P.; Snaith, R. *J. Chem. Soc., Dalton Trans.* **1999**, 4063.

[10] Romesberg, F. E.; Collum, D. B. *J. Am. Chem. Soc.* **1994**, *116*, 9187.

[11] DePue, J. S.; Collum, D. B. *J. Am. Chem. Soc.* **1988**, *110*, 5518.

[12] Romesberg, F. E.; Collum, D. B. *J. Am. Chem. Soc.* **1992**, *114*, 2112.

[13] Bernstein, M. P.; Romesberg, F. E.; Fuller, D. J.; Harrison, A. T.; Collum, D. B.; Liu, Q. Y.; Williard, P. G. *J. Am. Chem. Soc.* **1992**, *114*, 5100.

[14] (a) Galiano-Roth, A. S.; Collum, D. B. *J. Am. Chem. Soc.* **1989**, *111*, 6772. (b) Koizumi, T.; Morihashi, K.; Kikuchi, O. *Bull. Chem. Soc. Jpn.* **1996**, *69*, 305. (c) Claridge, T. D. W.; Davies, S. G.; Kruchinin, D.; Odell, B.; Roberts, P. M.; Russell, A. J.; Thomson, J. E.; Toms, S. M. *Tetrahedron: Asymmetry* **2013**, *24*, 947.

[15] Hoepker, A. C.; Collum, D. B. *J. Org. Chem.* **2011**, *76*, 7985.

[16] Romesberg, F. E.; Collum, D. B. *J. Am. Chem. Soc.* **1995**, *117*, 2166.

[17] Collum, D. B.; McNeil, A. J.; Ramirez, A. *Angew. Chem. Int. Ed.* **2007**, *46*, 3002.

[18] Ma, Y.; Hoepker, A. C.; Gupta, L.; Faggin, M. F.; Collum, D. B. *J. Am. Chem. Soc.* **2010**, *132*, 15610.

[19] (a) Barr, D.; Clegg, W.; Mulvey, R. E.; Snaith, R. *J. Chem. Soc., Chem. Commun.* **1984**, 285. (b) Armstrong, D. R.; Mulvey, R. E.; Walker, G. T.; Barr, D.; Snaith, R.; Clegg, W.; Reed, D. *J. Chem. Soc., Dalton Trans.* **1988**, 617.

[20] Andrews, P. C.; Duggan, P. J.; Fallon, G. D.; McCarthy, T. D.; Peatt, A. C. *J. Chem. Soc., Dalton Trans.* **2000**, 1937.

[21] Boeyens, J. C. A.; Ogilvie, J. F. *Models, Mysteries, and Magic of Molecules*; Springer, 2008.

[22] Edwards, A. J.; Hockey, S.; Mair, F. S.; Raithby, P. R.; Snaith, R.; Simpkins, N. S. *J. Org. Chem.* **1993**, *58*, 6942.

[23] Sugasawa, K.; Shindo, M.; Noguchi, H.; Koga, K. *Tetrahedron Lett.* **1996**, *37*, 7377.

[24] Alvaro, G.; Savoia, D.; Valentinetti, M. R. *Tetrahedron* **1996**, *52*, 12571.

[25] Goodman, J. M.; Silva, M. a. A. *Tetrahedron Lett.* **2003**, *44*, 8233.

[26] Catak, S.; D'hooghe, M.; De Kimpe, N.; Waroquier, M.; Van Speybroeck, V. *J. Org. Chem.* **2009**, *75*, 885.

[27] *Maestro 9.3,* Schrödinger, L., New York, NY, 2012.

[28] Jorgensen, W. L.; Maxwell, D. S.; Tirado-Rives, J. *J. Am. Chem. Soc.* **1996**, *118*, 11225.

[29] Ren, P.; Wu, C.; Ponder, J. W. *J. Chem. Theory Comput.* **2011**, *7*, 3143.

[30] *Jaguar 7.9,* Schrödinger, L., New York , NY,

[31] (a) Lee, C.; Yang, W.; Parr, R. G. *Phys. Rev. B* **1988**, *37*, 785. (b) Becke, A. D. *Phys. Rev. A* **1988**, *38*, 3098.

[32] (a) Zhao, Y.; Schultz, N. E.; Truhlar, D. G. *J. Chem. Phys.* **2005**, *123*. (b) Zhao, Y.; Schultz, N. E.; Truhlar, D. G. *J. Chem. Theory Comput.* **2006**, *2*, 364. (c) Zhao, Y.; Truhlar, D. *Theor. Chem. Acc.* **2008**, *120*, 215.

[33] Zhao, Y.; Truhlar, D. G. *J. Chem. Theory Comput.* **2006**, *3*, 289.

[34] Grimme, S.; Antony, J.; Ehrlich, S.; Krieg, H. *J. Chem. Phys.* **2010**, *132*.

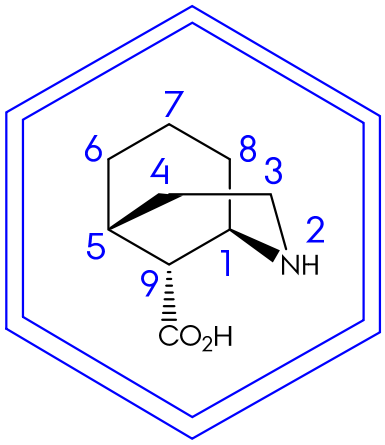

morphan

2 Asymmetric Synthesis of Morphan type β-Amino Acids.

Introduction

Morphan structure, 2-azabicyclo[3.3.1]nonane, may be found in nature as substructure of several well-known alkaloids (**Sch. 16**): morphine[1] (*Papaver somniferum*); dasicarpidone[2] (*Aspidosperma dasycarpon*) and uleine[3] (*Aspidosperma ulei*), or madangamines A-E[4] (*Xestospongia ingens*). Regarding the morphine, several structural simplifications of the morphine include the morphan bicyclic rings, like morphinans (levorphanol) or benzomorphans (phenazocine). High-order morphine structures also contain this system, like oripavin derivatives (buprenorphine).[5]

Papaver somniferum

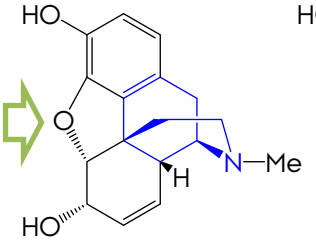

morphine

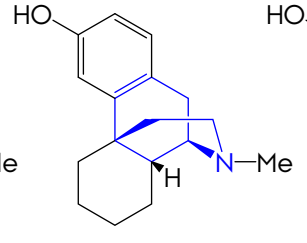

levorphanol

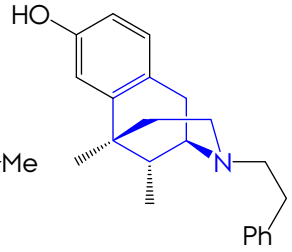

phenazocine

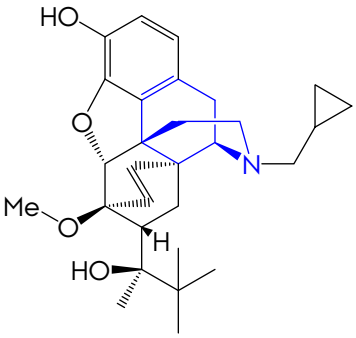

buprenorphine

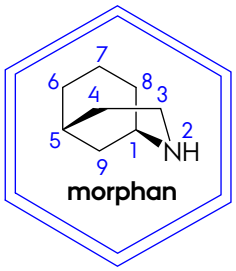

morphan

Aspidosperma dasycarpon

Xestospongia ingens

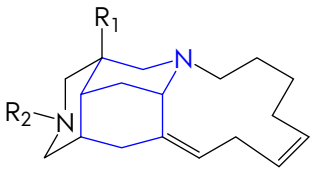

madangamines A-E

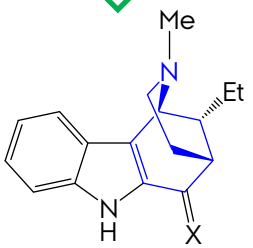

X=O, **dasicarpidone**
X=CH_2, **uleine**

Scheme 16. Synthetic and natural structures where the morphan scaffold is embedded.

First reported morphan synthesis dates from 1952. The elaboration of two morphan structures were reported by means of condensation methods of cyclohexane amides (Cronyn *et al.*)[6] or cyclization of ethyl *m*-nitrophenylacetate in reductive atmosphere (Ginsburg).[7]

Bonjoch and Bosch have published a complete series of synthetic procedures to obtain 2-azabicyclo[3.3.1]nonane compounds with different substitutions. One of these protocols is based on the cyclization of piperidylpropanones with mercuric acetate in acetic acid (**Sch. 17**).[8] The mercuric salt oxidizes the amine to an iminium salt, which was attacked by the enolic form of the ketone.

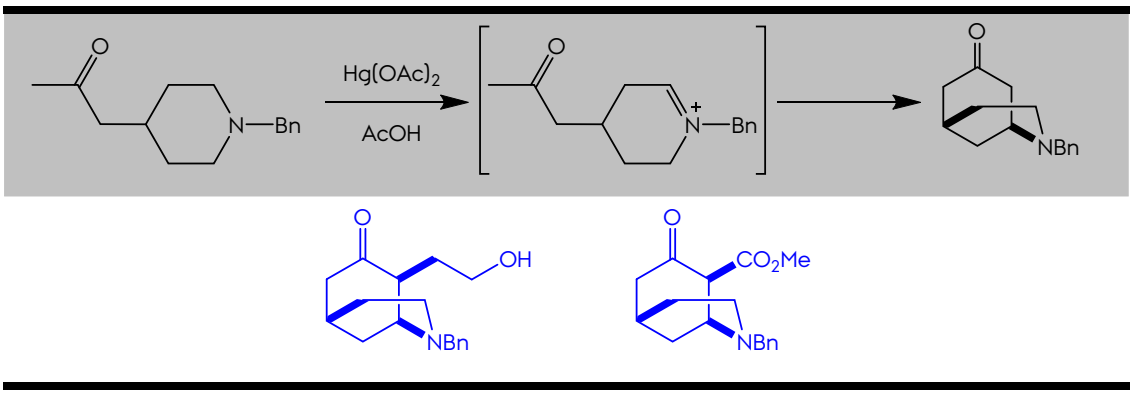

Scheme 17. Reaction and examples in the cyclization of piperidylpropanones with mercuric acetate in acetic acid.

Lately, acid-promoted cyclizations of 4-acetonyl-2-cyanopiperidines were reported to afford morphan bicyclic scaffolds (**Sch. 18**).[9]

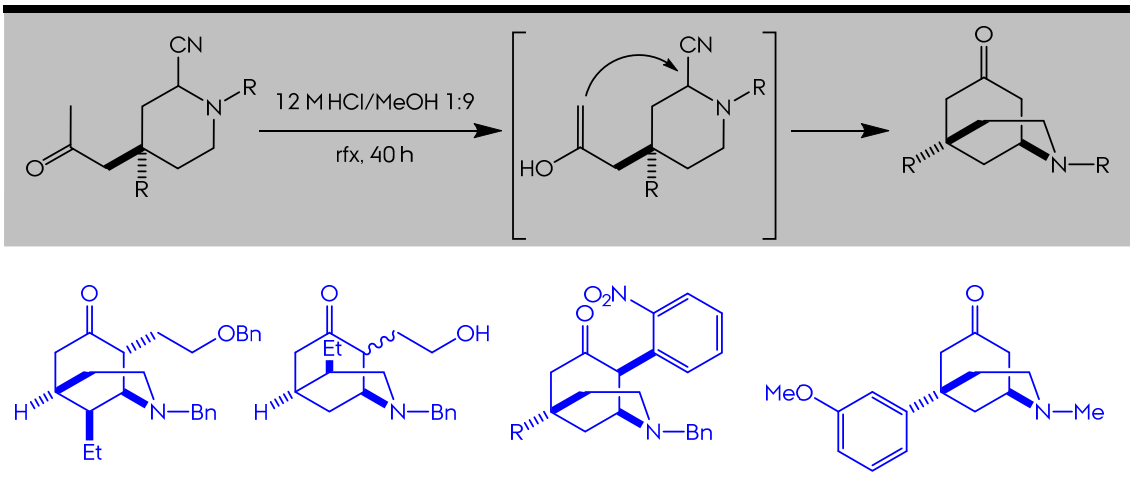

Scheme 18. Reaction and examples of acid-promoted cyclization of 4-acetonyl-2-piperidinecarbonitriles to morphan structures.

Other similar cyclizations which implies ring-opening/closing have been reported, like acid-promoted ring-opening of oxazolidines[10] or reductive rearrangement hexahydro-2-oxopyrano[3,2-*b*]pyridines (**Sch. 19**).[11]

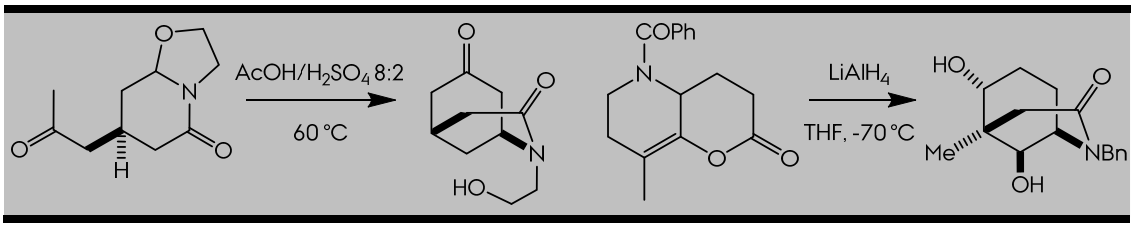

Scheme 19. Ring-opening/closing reaction of several bicyclics in the synthesis of morphan scaffolds.

Intramolecular coupling between amino-tethered allylic nitro moieties and vinyl halides in the presence of a palladium catalyst and base also leaded to bridged nitrogen compounds (**Sch. 20**).[12]

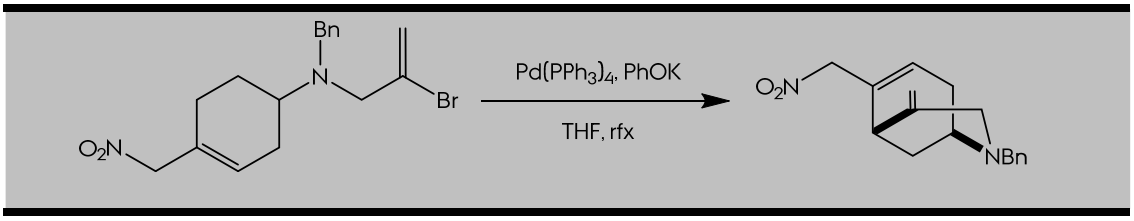

Scheme 20. Intramolecular coupling between amino-tethered allylic nitro moieties and vinyl halides.

Radical ring-closing have also successfully achieved morphan structures, using 3-aza-6-heptenyl radicals, generated from trichloroacetamido groups as carboradical precursors, in different reaction conditions (**Sch. 21**).[13]

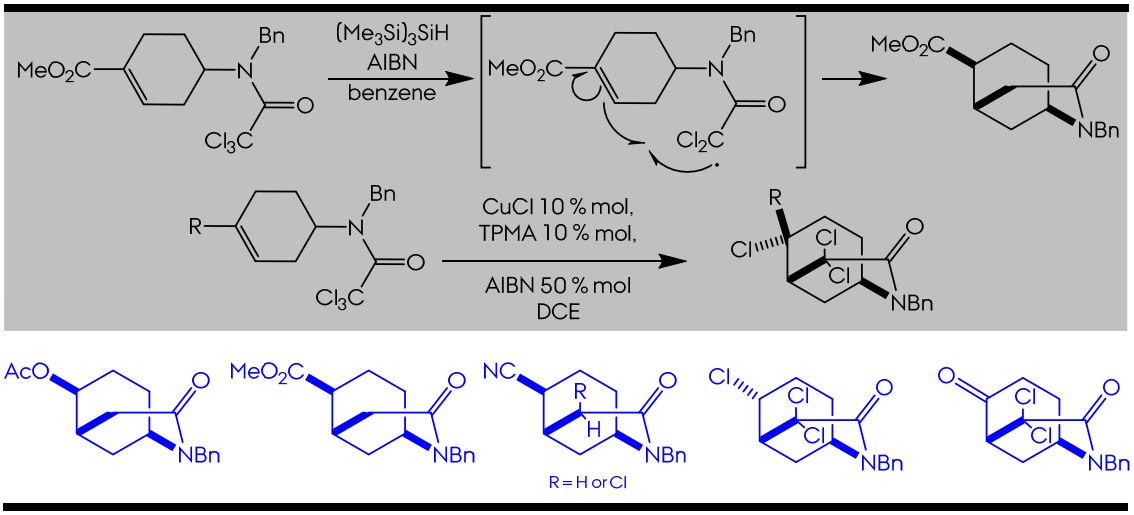

Scheme 21. Reaction and examples of acid-promoted cyclization of 4-acetonyl-2-piperidinecarbonitriles to morphan structures.

Aurreocoechea *et al.* have obtained a morphan skeleton from enamines by means of an intramolecular Mannich reaction (**Sch. 22**).[14]

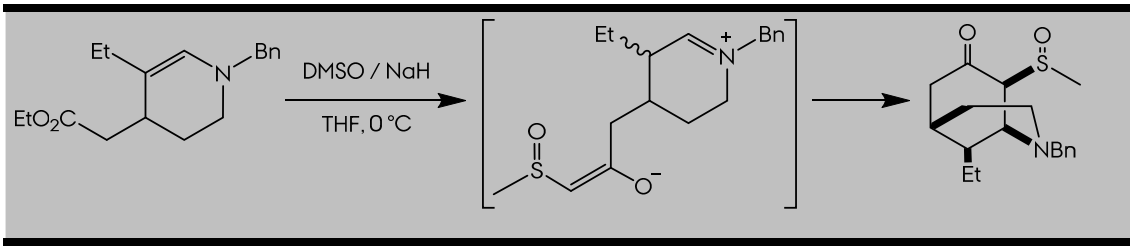

Scheme 22. Reaction of morphan assembly through intramolecular Mannich reaction.

Wang *et al.* also optimized a protocol to obtain 2-azabicylo[3.3.1]non-2-en-1-ol structures, through Mn(III) mediated cyclizations (**Sch. 23**).[15]

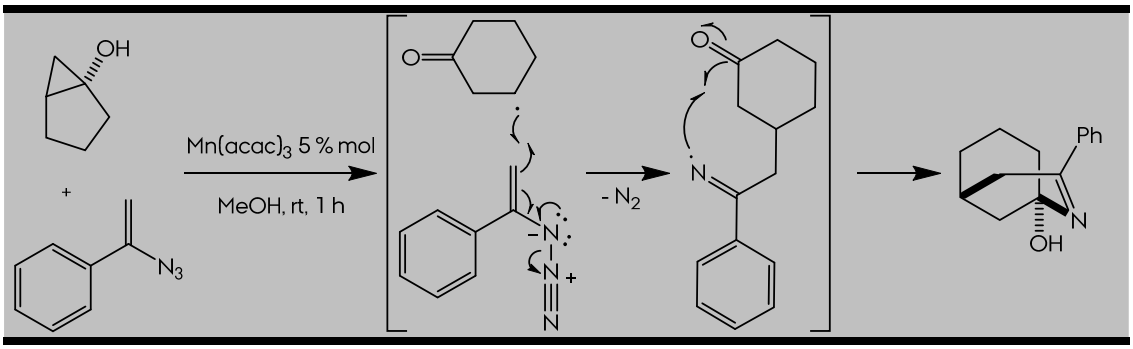

Scheme 23. Reaction of morphan assembly through Mn(III) mediated cyclization.

Although these protocols neglect the sterochemical issue, asymmetric methodologies have been optimized to tackle it. Bonjoch *et al.* have developed asymmetric ring closing reactions using chiral auxiliaries[16] or organocatalysis[17] (**Sch. 24**).

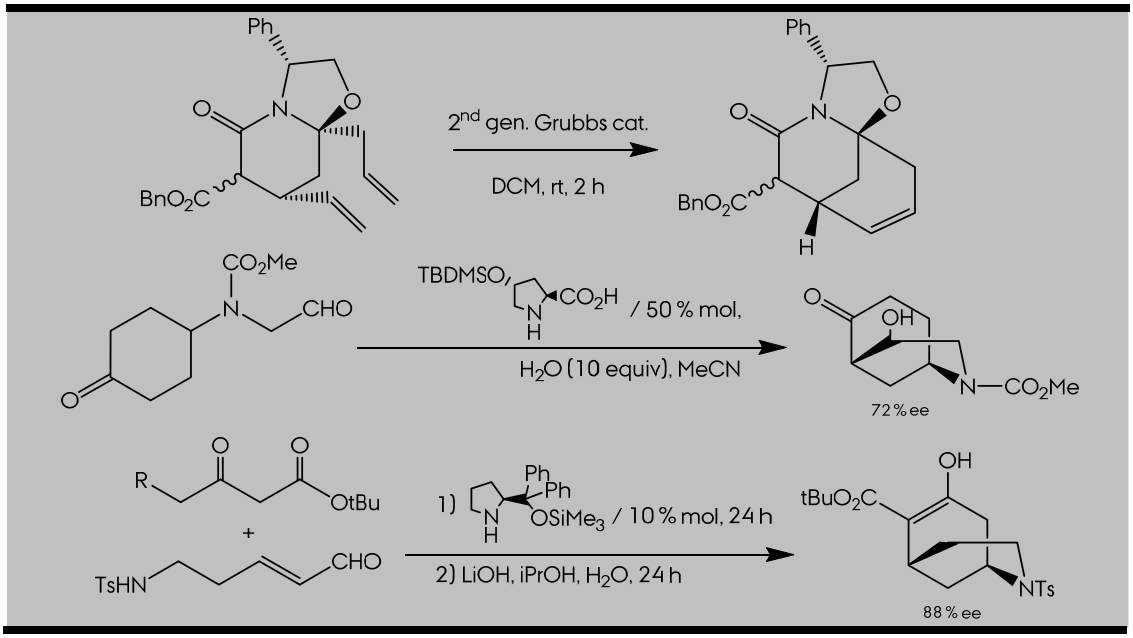

Scheme 24. Examples of asymmetric reactions of morphan core assembly.

In summary, literature is plenty of synthetic methodologies of 2-azabiciclo[3.3.1]nonane production; however, there is no many published results concerning asymmetric synthesis of aza-bridgeded structures, specially using chiral auxiliaries. Our group have a deep knowledge[18] in the synthesis of β-amino esters/acids through asymmetric Michael addition of (*R*)-*N*-benzyl-*N*-α-methylbenzylamide to (α,β)-unsaturated esters. In this chapter, the asymmetric synthesis of methyl (1*R*,5*R*,9*R*)-2-azabicyclo[3.3.1]nonane-9-carboxylate, a β-aminoester, is demonstrated (**Sch. 25**).

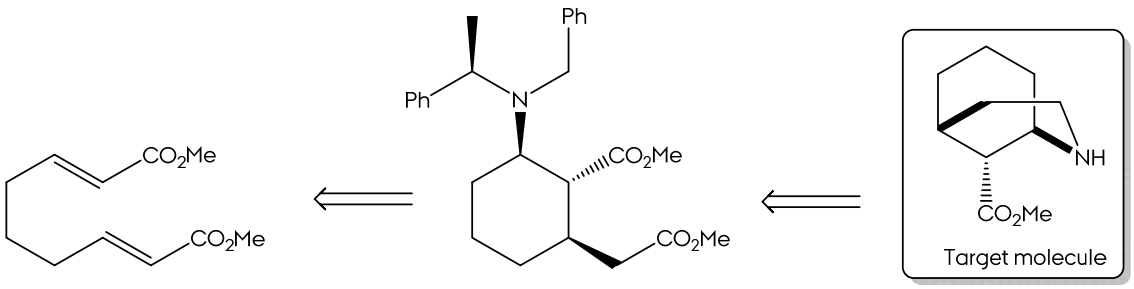

Scheme 25. Retrosynthetic plan in the synthesis of target molecule.

Michael Acceptors Preparation. Synthesis of Cyclic Intermediate 5.

The route towards the synthesis of the 2-azabicyclo[3.3.1]nonane core starts with the preparation of the Michael acceptor **3** as starting material. This is easily prepared in 2 steps from commercially available azelaic acid, following literature procedures (**Sch. 26**).[19] First, a combined esterification and Hell-Volhard-Zelinsky type reaction was achieved with high yield (98 %) and no further purification was required. In a second step, a double elimination was carried out with DMF at reflux temperature, obtaining a 1:1 mixture of **3**-**4** after workup.

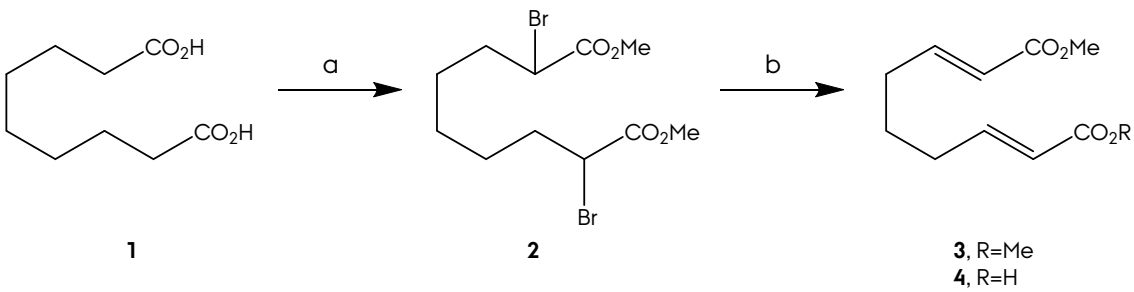

Scheme 26. *Reagents and conditions*: (a) i. $SOCl_2$, reflux 75 ºC, 90 min, ii. Br_2, hν, reflux 75 ºC, overnight, iii. MeOH, rt, 90 min, 98 % overall yield (M1). (b) DMF, reflux 153ºC, overnight, 46% (**3**) and 50 % (**4**) yield (M2).

Despite of following literature procedure, it was remarkable the obtaining of monoester **4** as byproduct, together with the expected diester **3**. A proposed hypothesis was the moisture condensation with DMF, resulting in an additional hydrolysis. As **4** was one of the starting materials in the PNA monomers line, the reaction was not further modified. Saturated $NaHCO_3$ washing allowed the separation of the two products. Separated flash chromatography column afforded both esters in a multigram scale.

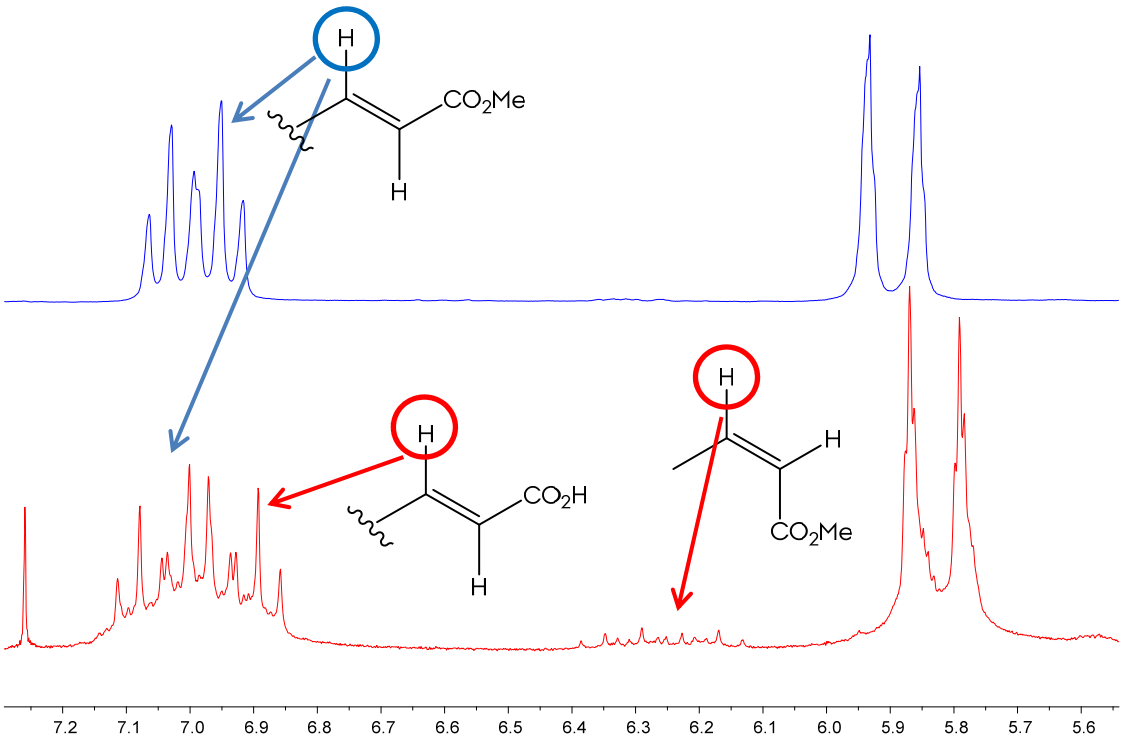

Figure 42. ^{1}H NMR spectra of compounds **3** (blue) and **4** (red), with relevant resonances at the 7.2-5.6 range.

2 and **3** have only half of NMR resonances, due to the C_2 symmetry of these systems.[20] Michael acceptors **3** and **4** are almost equal at ^{1}H NMR level: only a small displacement of the H3 signal of **4** is observed, due to the different electronic density profile between β center in α,β-unsaturated esters and acids (**Fig. 42**). In some chromatographic fractions, a small resonance around 6.2 ppm also reported the presence of traces of (*Z*,*E*) compounds.

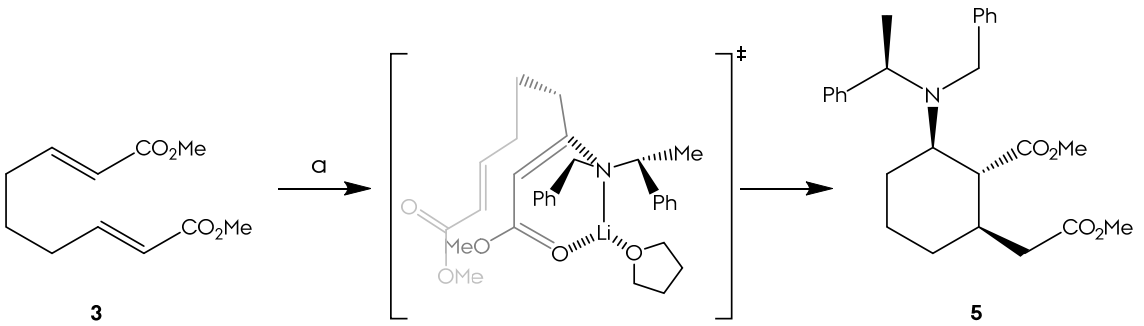

Scheme 27. *Reagents and conditions*: (a) (*R*)-*N*-benzyl-*N*-α-methylbenzylamine, nBuLi, THF, -78 ºC, 3 h, 91 % (M3).

The route continuous with the reaction between the lithium (*R*)-*N*-benzyl-*N*-α-methylbenzylamine and substrate **3** that furnished **5** in 91% yield (de > 95%) via a domino sequence comprising an asymmetric Michael addition and a 6-*exo*-trig cyclization that generated one ring and three contiguous stereocenters[18b,18d,18e] in a fully controlled fashion (**Sch. 27**). ^{1}H NMR spectra shows the complete disappearance of the olefinic systems, detachment of the ester resonances and the incorporation of chiral unit signals: a quartet at 4.00 ppm (C<u>H</u>CH$_3$), an AB system between 3.92-3.64 (NC<u>H$_2$</u>Ph) and a doublet at 1.39 (CHC<u>H$_3$</u>).

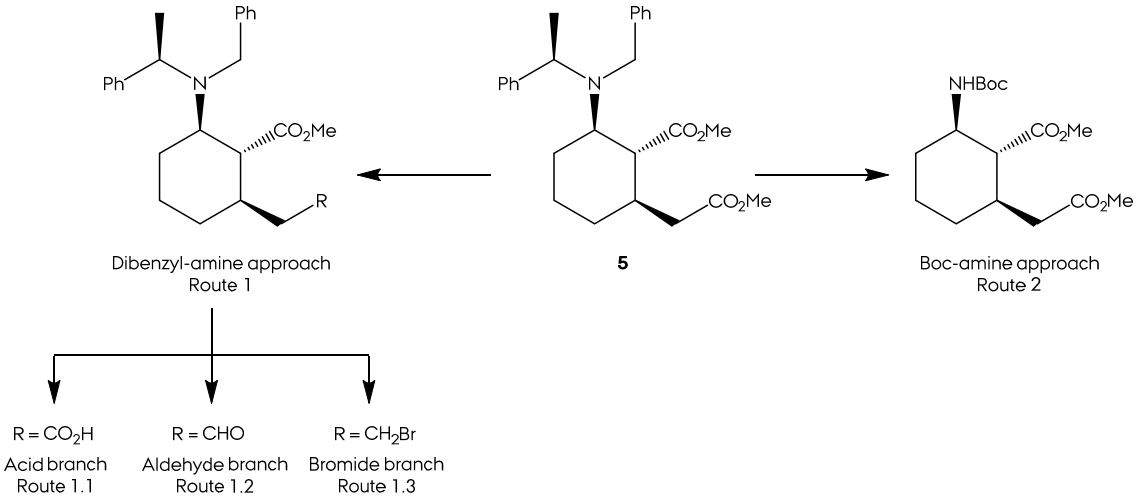

Scheme 28. General scheme of the routes developed in the search of the morphan core.

From **5**, three different approaches towards the morphan core target were taken, as a consequence of the singular reactivity of these systems (**Sch. 28**).

As a function of the protecting group nature of the amine group, a first division was created: the dibenzyl path (route 1) or the Boc-amine approach (route 2). Within the dibenzyl route, three different subdivisions were created accordingly to the lateral chain modification: acid, aldehyde or bromide alternatives (routes 1.1 to 1.3).

Route 1 (Dibenzyl-amine Approach)

The first route exploited was the approach where the dibenzyl protection of the amine was kept (route 1). This route is subdivided in three different paths, characterized by the functional group which would be responsible of the forward cyclization:

- Route 1.1: this route is characterized by the cyclization of a carboxylic acid with the released amine from the dibenzyl protection.
- Route 1.2: the cyclization between an aldehyde and the amine encompasses this derivation.
- Route 1.3: finally, the approach where a bromide is prepared to work as leaving group when the amine will be deprotected.

Route 1.1 (Acid Branch)

The diester **5** was selectively hydrolysed by lithium hydroxide in a mixture of methanol, tetrahydrofurane and water (3:3:1). The purpose of using lithium hydroxide instead of sodium or potassium homologue is control the chemoselectively of the saponification, avoiding harsh reactants, which may hydrolize both esters groups. The dibenzylamine also acts as shell, diminishing the exposure of the ester in position 1 to the reactants (**Fig. 43**). Acid **6** has the same ^{13}C resonances from **5**, with the exception of one the methyl groups.

Next step was the deprotection of the amine group, following a total cleavage protocol or a selective monodeprotective strategy. Long-time exposure of a solution of **6** in acetic acid to a 3.5 atm hydrogen atmosphere leaded to the acetic salt of compound **7**.[21] Conversion of the acetic salt to the amino acid **7** was carried out by ionic exchange through a sulfonic acid type resin (Dowex 50x8-200) and forward removal of the aqueous solution via freeze-drying.

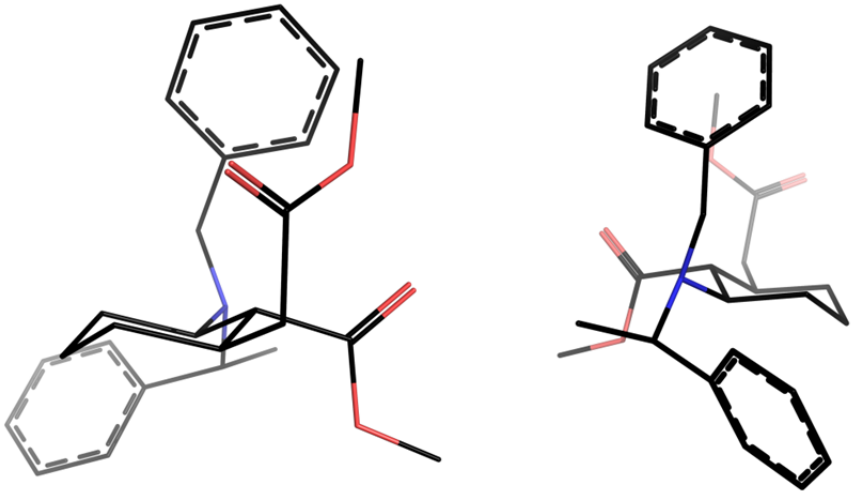

Figure 43. Two pictures of the most stable conformer of **6** (MMFFs, performed with TINKER-SCAN). It´s easy to observe the equatorial disposition of the three main exocyclic bonds and the spacial extension of the two benzyl arms of the amine group.

On the other hand, an oxidative exposure of the substrate **6** with ammonium cerium (IV) nitrate (CAN) in 5:1 mixture of acetonitrile-water deprotected selectively the amine, which remained as (*R*)-*N*-α-methylbenzylamine derivative **13** (**Sch. 29**).[22]

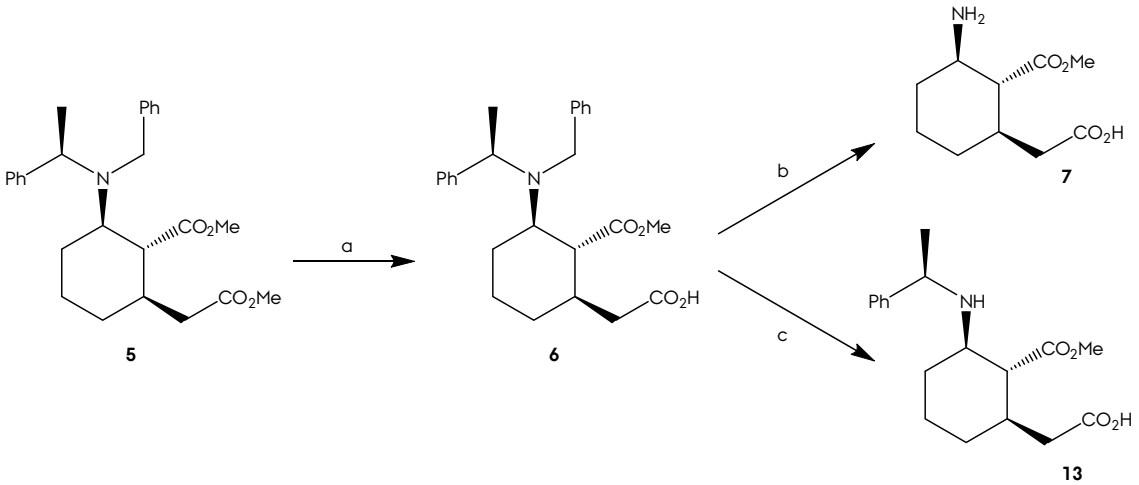

Scheme 29. *Reagents and conditions*: (a) LiOH, MeOH/THF/H_2O 3:1:1, h, 61 % (M4). (b) i. H_2 - $Pd(OH)_2$/C, AcOH, 3 d. ii. Dowex 50x8-200, 38 % (M5). (d) CAN, MeCN/H_2O 5:1, 4 h, 38 % (M18).

Once obtained the amino acids, the following step is the intramolecular cyclization to obtain the amides. This is conducted by a peptide coupling using *N*-(3-dimethylaminopropyl)-*N'*-ethylcarbodiimide hydrochloride (EDCI) together with 1-hydroxybenzotriazole hydrate as carboxyl activating agents. The intramolecular peptide couplings leaded to the morphan core, as 2-azabicyclo[3.3.1]non-3-one (**Sch. 30**).

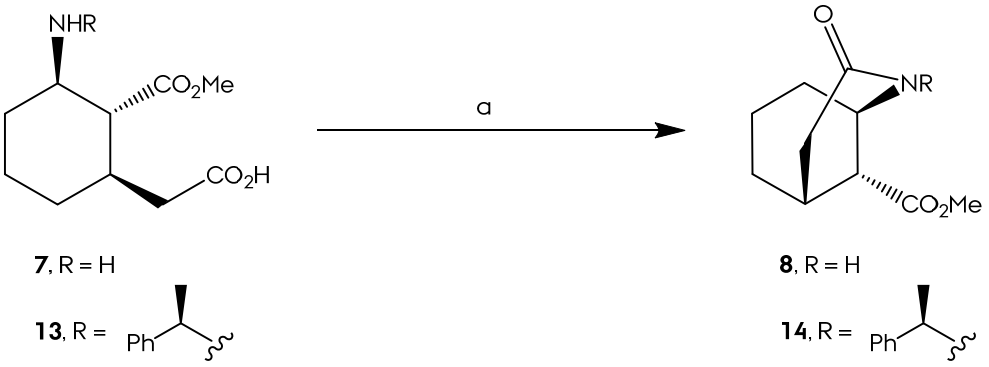

Scheme 30. *Reagents and conditions*: (a) EDCI, HOBt, DIPEA, DMF, 24 h. Yields: **8**, 46 % (M6); **14**, 16 % (M19).

8 was crystallized in hexanes/ethyl acetate 1:1, and the X-ray diffraction analysis allowed the corroboration of the structure and specially the stereochemistry of the stereocenters previously created in **5**. The 2-azabicylo[3.3.1]non-9-one scaffold has a cup motif, created by the two fused rings (**Fig. 44**).

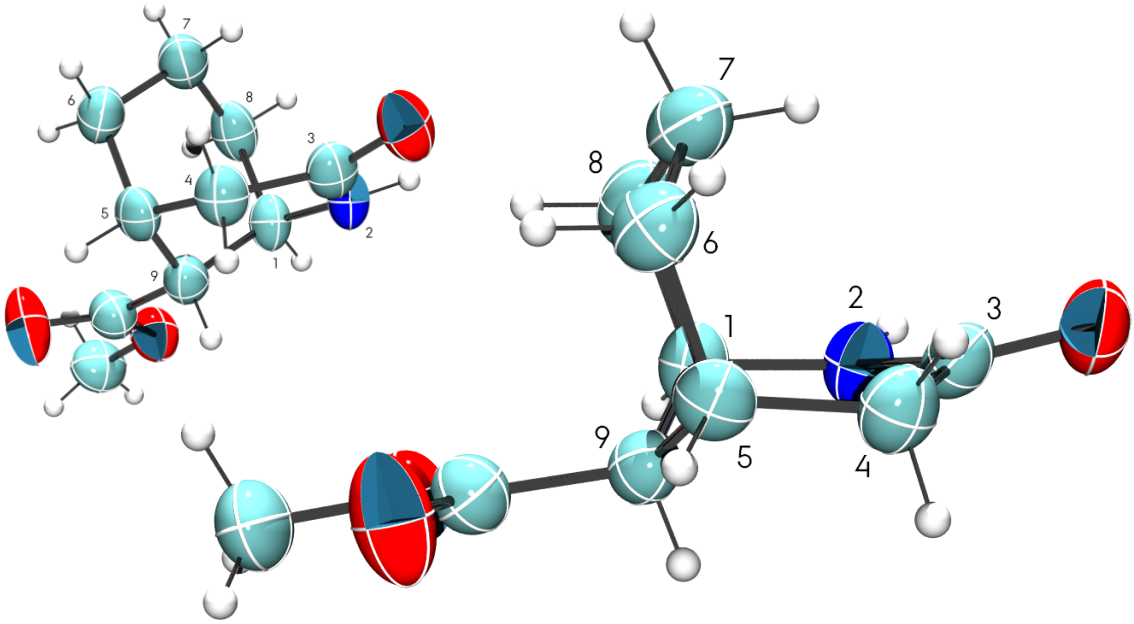

Figure 44. Two Ortep views (50 % probability) of the crystallized structure of **8**.

Derivatives **8** and **14** were the first synthetized morphans of this project, and the ^{1}H NMR study revealed three main characteristic signals: one singlet around 4.00 ppm (H1) and two additional ones between 3.0 – 2.0 ppm (H5 and H9). Once obtained the morphan structure, the last step is the reduction of the amide group to amine. We tested the reactivity of **8** and **14**, which is summarized in **schemes 31** and **32**.

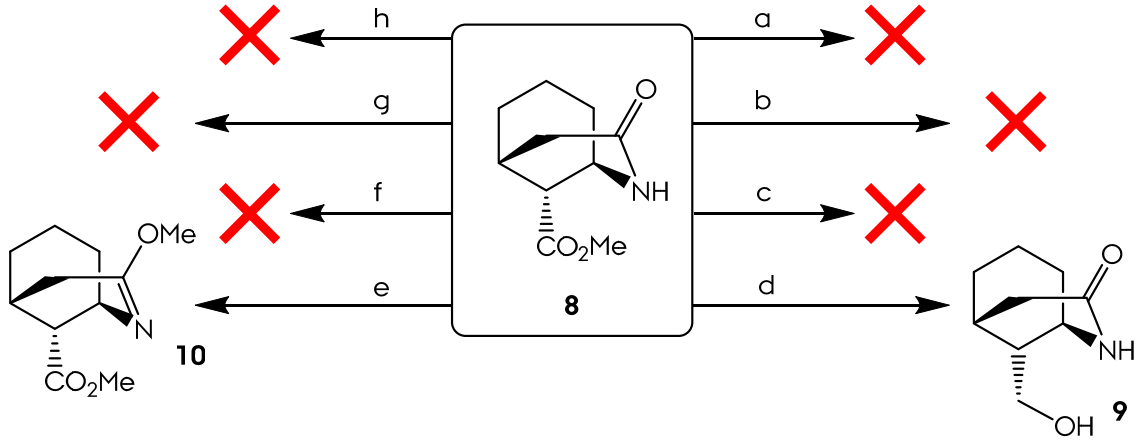

Scheme 31. *Reagents and conditions*: (a) $BH_3 \cdot Me_2S$, THF, rt, (M8). (b) $BH_3 \cdot THF$, THF, rt, (M7). (c) $BH_3 \cdot THF$, THF, 75ºC, (M9). (d) i. $BH_3 \cdot THF$, THF, 75ºC. ii. HCl 6 M (M10). (e) i. Me_3BOF_4, DCM, ii. $NaBH_4$, EtOH (M14). (f) $LiAlH_4$, THF, 75ºC (M11). (g) $LiAlH_4$, Dioxane, 101ºC (M12). (h) 9-BBN, THF, 75ºC (M13).

General reduction strategies like borane with different carriers[23] and lithium aluminium hydride[24] were tested, together with other selective procedures like Meerwin type alkylation followed by reduction.[25] All these transformations are presented in **table 4**.

Entry	Reaction conditions	Temp (ºC)	Time (h)	Product	Yield
1	$BH_3 \cdot Me_2S$	20	12	nr	
2	$BH_3 \cdot THF$	20	12	nr	
3	$BH_3 \cdot THF$	75	12	ni	
4	i. $BH_3 \cdot THF$ ii. HCl 6 M	75	1.5	**9**	17
5	9-BBN, THF	75	2	ni	
6	$LiAlH_4$, THF	75	20	ni	
7	$LiAlH_4$, Dioxane	105	20	ni	
8	i. Me_3BOF_4, DCM ii. $NaBH_4$, EtOH	20	24	**10**	18

Table 4. Reaction chart in the reduction of **8** (nr: no reaction, ni: no identifiable after column chromatography).

Borane or lithium Aluminium Hydride type reductions failed in the reduction of amide group of **8** in all cases. Nevertheless, the ester group is reduced to alcohol **9** when borane reduction was quenched with 6 M HCl. Reaction crudes were sometimes difficult to interpret and no identifiable products were eluated from

column chromatographies of some cases. One possibility is the borane-chelate complex formed in the course of the reduction. Sometimes these borates are water-soluble and have to be cleavage with acid quenching to avoid product lost during workup. Meerwin type reaction only produced the alkylation product **10**, which didn´t undergo further reduction with sodium or lithium borohydride (see Reaction Inventory, M13-14). This reveals the accessibility difficulties of reagents to morphan core centers, which structure is a steric shell avoiding that accessibility. However, Meerwin type alkylation product was isolated from the reaction conditions showed in entry 8. The reaction proceeds with the nucleophile attack of the carbonyl's group oxygen of the amide (more nucleophile than the ester) to one of the methyl groups of the oxonium cation. As the oxygen is "one bond" far away from the morphan core, the steric shell might be no longer a problem in reactivity.

Similarly to **8**, **14** were tested through similar reduction conditions (**table 5**). Again, the resistance of the amide to be reduced was observed, and only ester reduction product **15** was isolated with moderate yields, using borane in tetrahydrofurane complex with later acid quench.

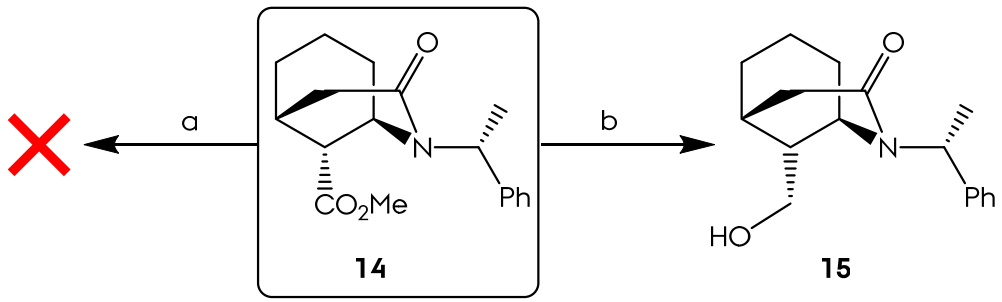

Scheme 32. *Reagents and conditions*: (a) $LiAlH_4$, THF, 75ºC (M23). (b) i. $BH_3 \cdot THF$, THF, 75ºC. ii. HCl 6 M (M22).

Entry	Reaction Conditions	Temp (ºC)	Time (h)	Product	Yield
1	$LiAlH_4$	75	3.5	nr	
2	$BH_3 \cdot THF$	75	3.5	**15**	50

Table 5. Reaction chart in the reduction of **14** (nr: no reaction).

As a consequence of the amide resistance to reduction, activation of the amide group was explored through a Boc-amide protection and again a series of reduction trials

were conducted (**Sch. 33**). It was reported,[26] the Boc group activate the amide group, enhancing the electrophile character of the carbon of the CO group.

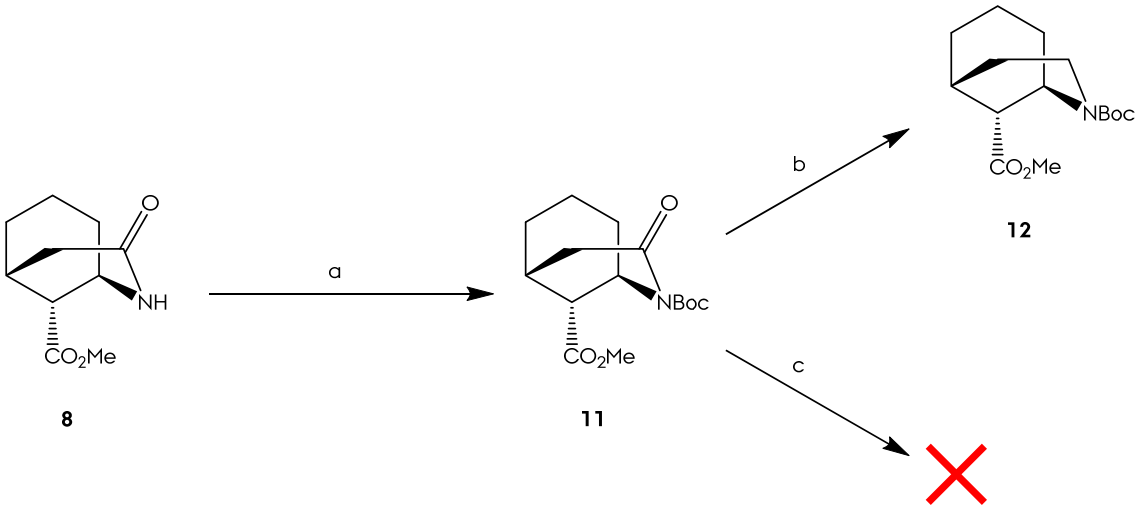

Scheme 33. *Reagents and conditions*: (a) Boc_2O, DMAP, DCM, 69 % (M17). (b) $BH_3 \cdot THF$, THF, 11 % (M22). (c) $BH_3 \cdot THF$, THF, 75 ºC (M23).

Reaction of amidoester **8** with Boc-anhydride and DMAP afforded the protected amide in moderate yield (69 %). ^1H NMR spectra of compound **11** (**Fig. 45**) evinced a slight displacement of amide group vicinal protons signals (H3 and H1), keeping the characteristic resonance of H5 and H9 almost unaltered. Reduction of protected amide with borane-tetrahydrofurane complex at room temperature achieved reduction morphan **12**, in 11 % yield, with recovery of the starting material (50 %). Attempts to reduce at higher temperature the amide moiety resulted in no product isolation (M19). Further optimization of the reaction at room temperature did not improve the yields.

Morphan protected amino-acid **12** ^1H NMR spectra keep the three characteristic resonances of H1, H5 and H9, with the difference of a splitting of the H1 resonances in two signals, due to rotameric forms. The presence of rotamers is intensively manifested in the ^{13}C NMR, where some resonances are duplicated. It is very common *tert*-butoxycarbamates like **12** exhibit this feature; however, compound **11**, does not show rotamers in its ^{13}C NMR spectra.

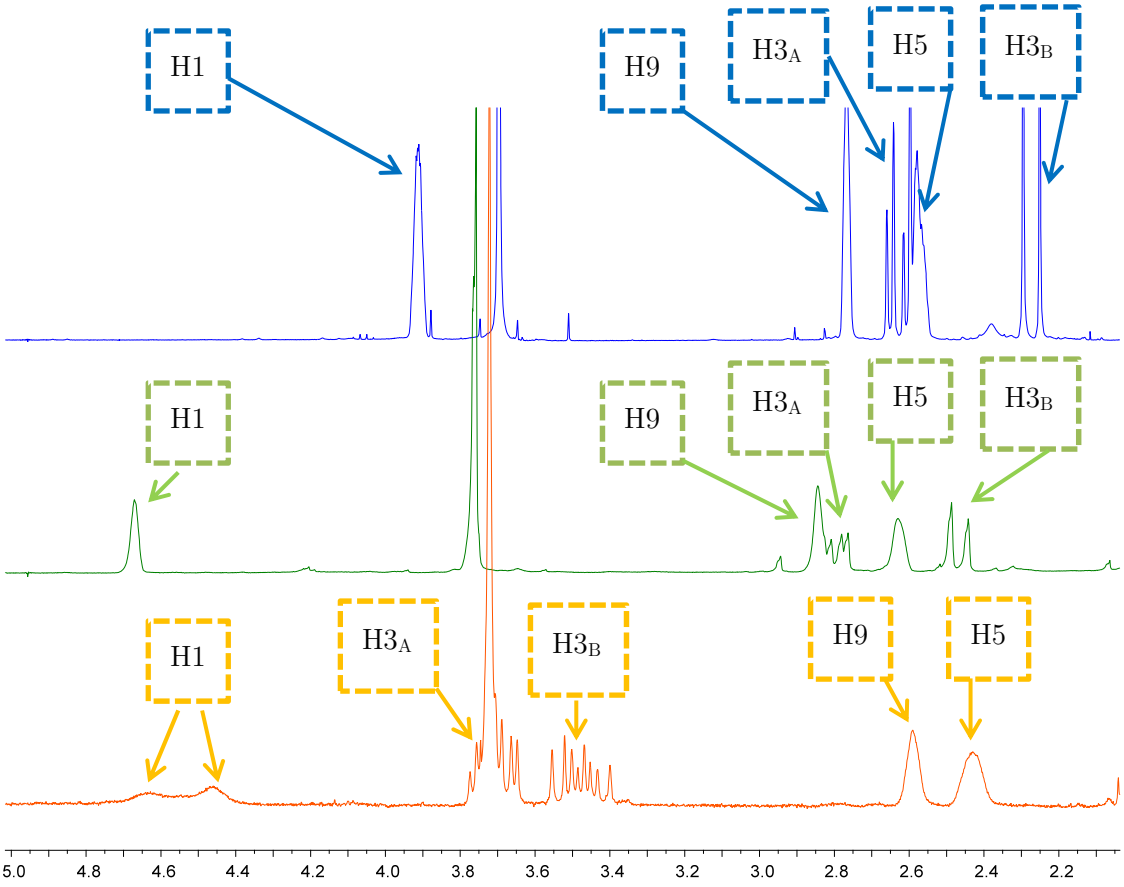

Figure 45. Comparison of ^{1}H NMR spectra of morphans **8** (blue) and **11** (green) and **12** (orange) at the 5.0-2.2 ppm range.

To explain these different results, a conformational analysis of both compounds **11** and **12** was carried out. First, both structures were subjected to conformational search invoking the SCAN module of Tinker,[27] in a MMFF[28] parametrization context. Each one of the conformers were further optimized in the QM context through Jaguar[29] and the DFT/B3LYP[30] theory, using 6-31G(d) as basis set.[31] PBF solvation model[32] was used together with $CHCl_3$ parameters.

Conformational analysis results are displayed in **figure 46**. Two rotamers were found in each compound: A and B. It was observed, the presence of the carbonyl group of **11** in position 3 results in a steric clash with the carbamate's carbonyl group, an invasion of the electronic cloud of each system to the other one. The outcome is an energy gap of 0.98 Kcal/mol, which resulted in a 8:2 distribution : only one rotamer is observed at room temperature. On the other hand, the energy gap between conformers 12A-B is only 0.004 Kcal/mol, due to the absence of the carbonyl group. Distribution in this case is 1:1, leading to detect both rotamers at room temperature. In conclusion, all related compounds to **12** will have detectable rotamers.

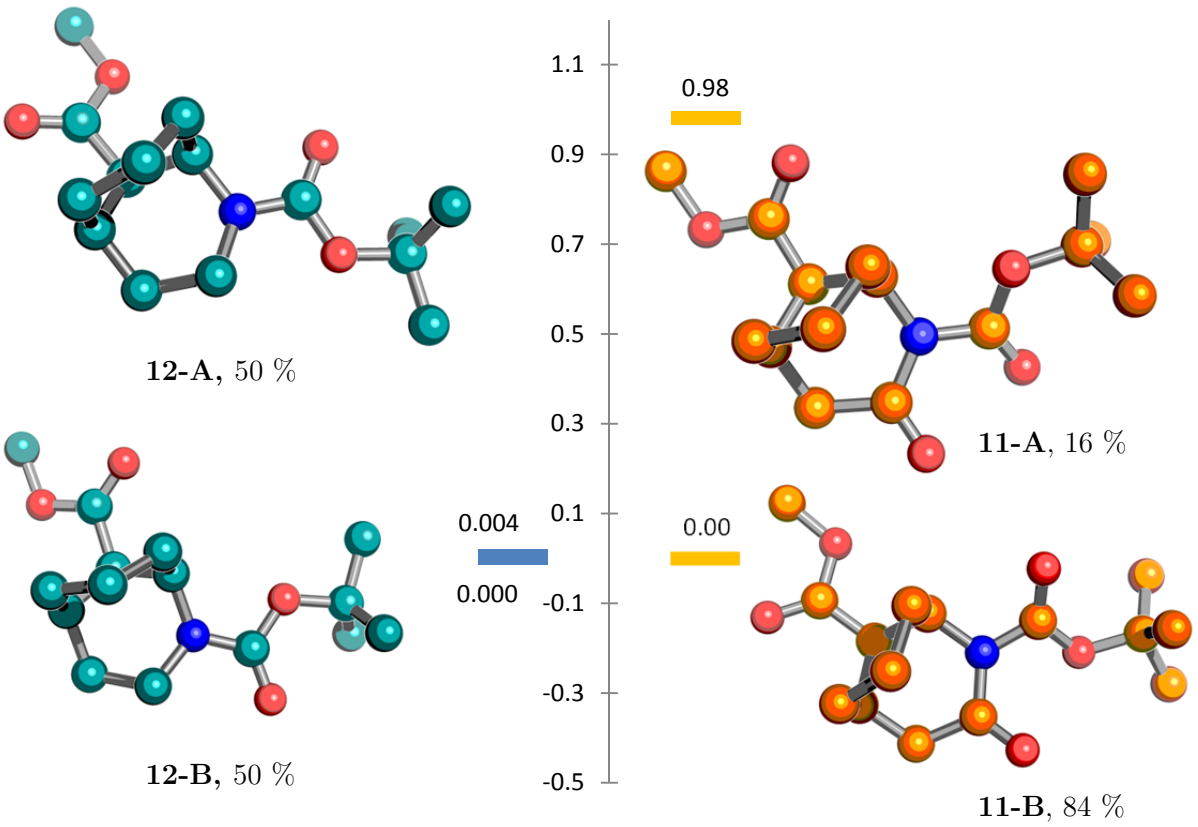

Figure 46. Relative energy plot of rotamers **12A-B** and **11A-B**.

Route 1.2 (Aldehyde Branch)

The previous route concluded in the morphan amine **12** isolation, but in a low yield and scale. With the purpose of increase yields and productivity, the transformation of the ester in lateral chain 6 is envisaged. The aim is to close the second ring of the morphan system as an amine, avoiding the troubles related to the amide reduction. The closing procedure in this route is an intramolecular reductive amination (**Sch. 34**).

Reduction of **4** with 2.2 equiv of diisobutylaluminum hydride afforded the aldehyde **16** with good yields. Time control is critic in order to obtain the maximum aldehyde yield. Reaction times further than 30 min finished in mixtures of aldehyde **16** and alcohol **17**.

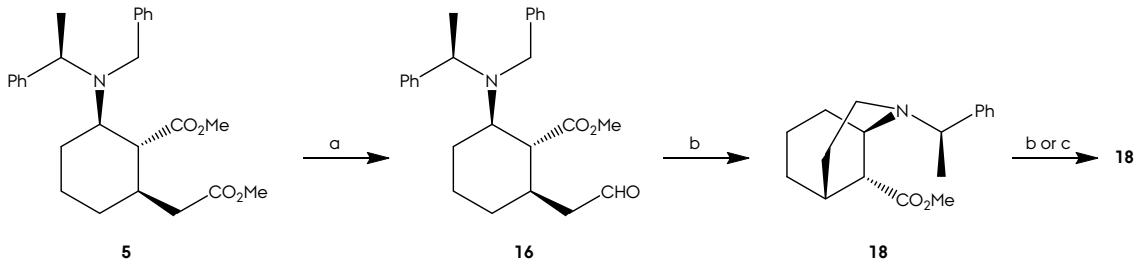

Scheme 34. *Reagents and conditions*: (a) DIBAL-H, DCM, -78ºC, 92 % (M24-25). (b) H_2 - $Pd(OH)_2/C$, AcOEt, 3 d, 6 % (M28-29). (c) H_2 - Pd/C 30 %, AcOEt, 3 d (M30).

Aldehyde **16** showed the aldehyde carbon resonance at 201.4 ppm (^{13}C NMR), as well as the aldehyde proton resonance at 9.5 ppm (^{1}H NMR).

Next step was the total deprotection of the amine group under hydrogen high pressure conditions together with palladium hydroxide. Morphan core with the tertiary amine **18** was obtained in low yields, no observing total deprotection. Repetition of the reaction in the same conditions afforded again the product **18** and changing the catalyst nature did not provoke reaction (M30). As the benzyl group is preferentially deprotected first over the α-methylbenzylamine, the partially released amine attacks immediately the aldehyde, condensing into the imine, and further reduced to the amine. However, the α-methylbenzylamine, was not further released. Again, the 2-azabicyclo[3.3.1]nonane acts as a steric shell, avoiding the adsorption of the substrate to the catalyst surface (hypothesis).

Route 1.3 (Bromide Branch)

Continuing to the strategy of transforming the ester in lateral chain 6, a route where the ester if converted into a bromide was developed (**Sch. 35**).

Alcohol **17** might be prepared taken different substrates and performing reductions with boron based reductive agents: from acid **6** via $BH_3 \cdot THF$ (M26), from ester **5** via DIBAL-H (M24), or from aldehyde **16** via $NaBH_4$ (M27). All reactions were chemoselective and alcohol **17** was obtained from moderate to good yields. Finally, functional group interconversion was achieved with CBr_4/PPh_3 in a 46 % yield (**19**).

Attempts to make the cyclization in reductive hydrogen atmosphere where unsuccessful: several attempts were tried and the reaction workup did not achieve any identifiable product.

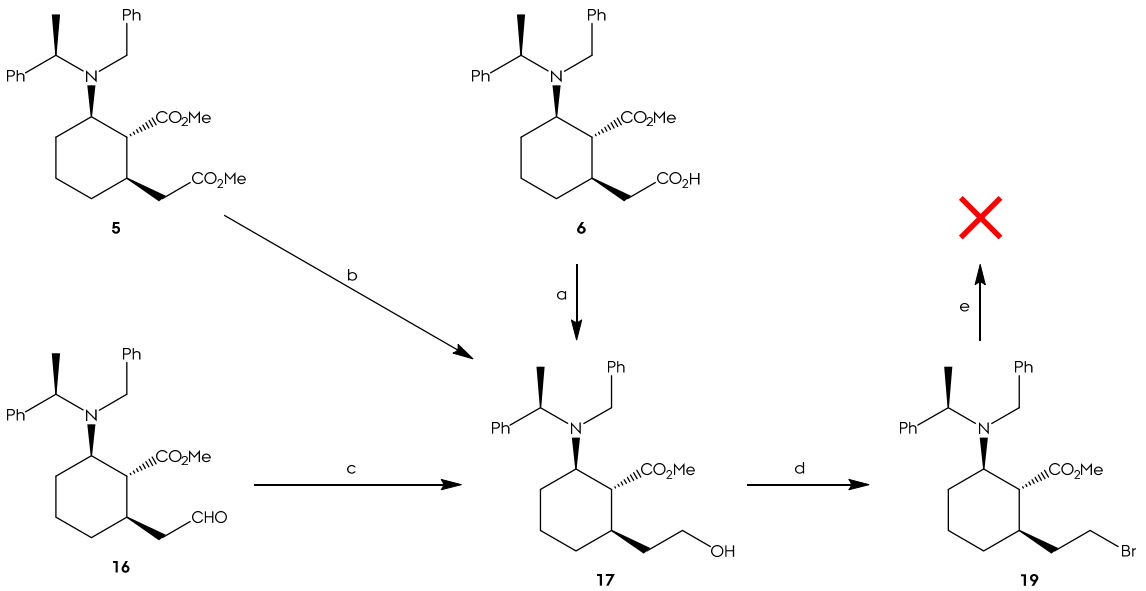

Scheme 35. *Reagents and conditions*: (a) $BH_3 \cdot THF$, THF, rt, 98 % (M26). (b) DIBAL-H, DCM, -78ºC, 20 % (M24). (c) $NaBH_4$, MeOH, 78 % (M27). (d) CBr_4, PPh_3, DCM, 46 % (M31). (e) H_2 - $Pd(OH)_2/C$, AcOEt, 3 d, (M32).

From the ^1H NMR point of view, the family of compounds **5-6** and **16-17**, **19** have identificative signals of these cyclohexene systems: a triplet-doublet around 3.05 ppm (H2), resonances of ring protons between 2.30-1.40 and the $H5_B$ high field peak around 0.8 ppm.

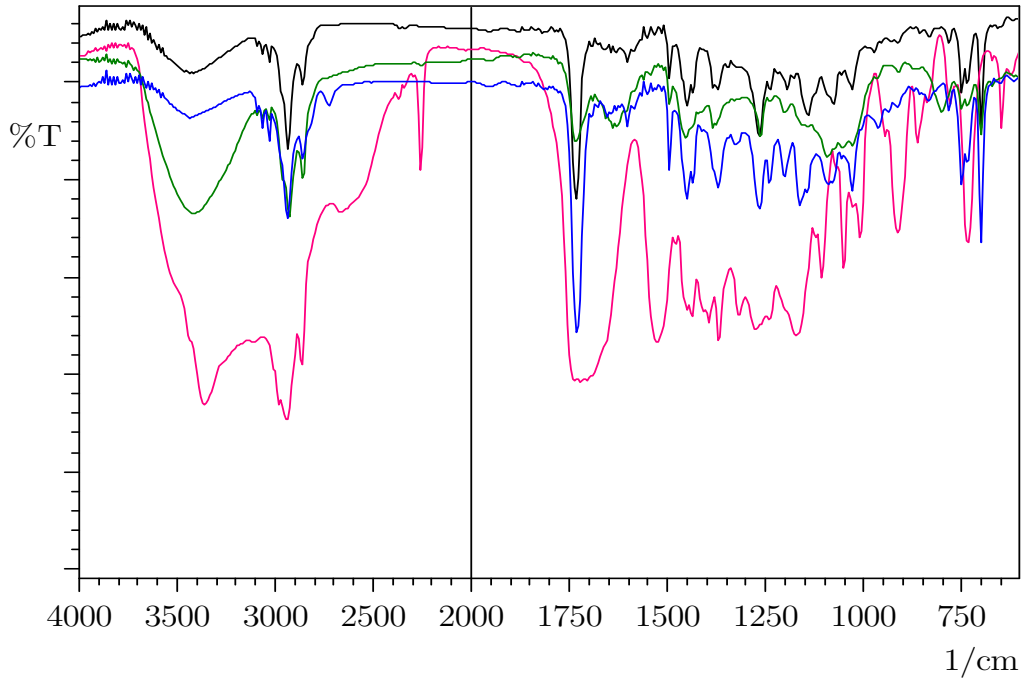

Figure 47. Stacked FTIR spectra of aldehyde **16** (blue), acid **6** (pink), alcohol **17** (green) and bromide **19** (black).

Regarding FTIR absorbances, all the compounds have the same dactylogram region, and the differences between functional groups are evidenced (**Fig. 47**).

Next chart summarizes the advantages and disadvantages of the reactions belong to route 1. In brief, this route allows accessing the morphan motif easily and fast, but further releasing/reduction of the amine/amide group is difficult, and the outcome is sometimes the reduction product in low yield.

Advantages	**Disadvantages**
2 - 3 steps to make the morphan system	Morphan amides no easy reductibles, required amide activation (low yields)
High chemoselectivity between both ester groups	Morphan amines no easily deprotected (**15**)
In route 1.2, one pot deprotection and cyclization	Pd/C mediated cyclizations are low yielding

Table 6. Summary of advantages/disadvantages of the route 1.

Route 2 (Boc-amine Approach)

Route 1 concluded with the synthesis of some structures with the morphan scaffold. However, several of these compounds are endpoints or the reactions gave low yields, due to the difficult of obtain a fully reactive amine. The strategy of route 2, in order to get better yields, lies in a protecting group interconversion: from the dibenzyl amine to the Boc amine. As in Route 1.2 and 1.3 the main problem was the protecting group, the use of *tert*-butoxycarbamate as amine's substituent is explored through reactivity. Boc group, compared to benzyl moieties has the next advantages:

- Easily preparation: taking the amine and combining with Boc_2O and DMAP, the protected amine is obtained, in goo yields. When the amine is protected with benzyl groups (this case) a one pot benzyl cleavage and reprotection with Boc_2O under high-pressure hydrogen atmosphere is enough.
- Less bulky group: depending on the case, accessibility to closer regions is allowed.
- Reaction monitoring: the *tert*-butyl resonance in ^1H NMR is very useful following reaction evolution.

- Deprotection strategies: milder than dibenzyl substituents, avoiding the use of harsh conditions.

First, a protecting group interconversion of substrate **5** was successfully achieved in one stage with Boc_2O and Pearlman's catalyst under high-pressure hydrogen atmosphere (**Sch. 36**). The spectroscopic outcome of the reaction is a simplification of the ^1H NMR spectra: dibenzyl resonances of substrate **5** dissapeared, diester signals get closer and overlap H2 resonance, and the signals of H1 and H3 are slightly displaced (**Fig. 48**). $^1H/^{13}C$ HMQC correlation experiments helped to identify correctly these signals.

Once performed this transformation, the lateral chain was modified in the same way of route 1.3, starting with the chemoselective hydrolysis of ester in position 6 with $LiOH \cdot H_2O$ (84 %). Using $LiBH_4$ instead of LiOH provoked the reduction of both esters (M34). Afterwards, BH_3 type reduction of acid **21** leaded to alcohol **22** in a 92 % yield. Finally, mesylation of **22** leaded to mesylate **23** in a 96 % yield.

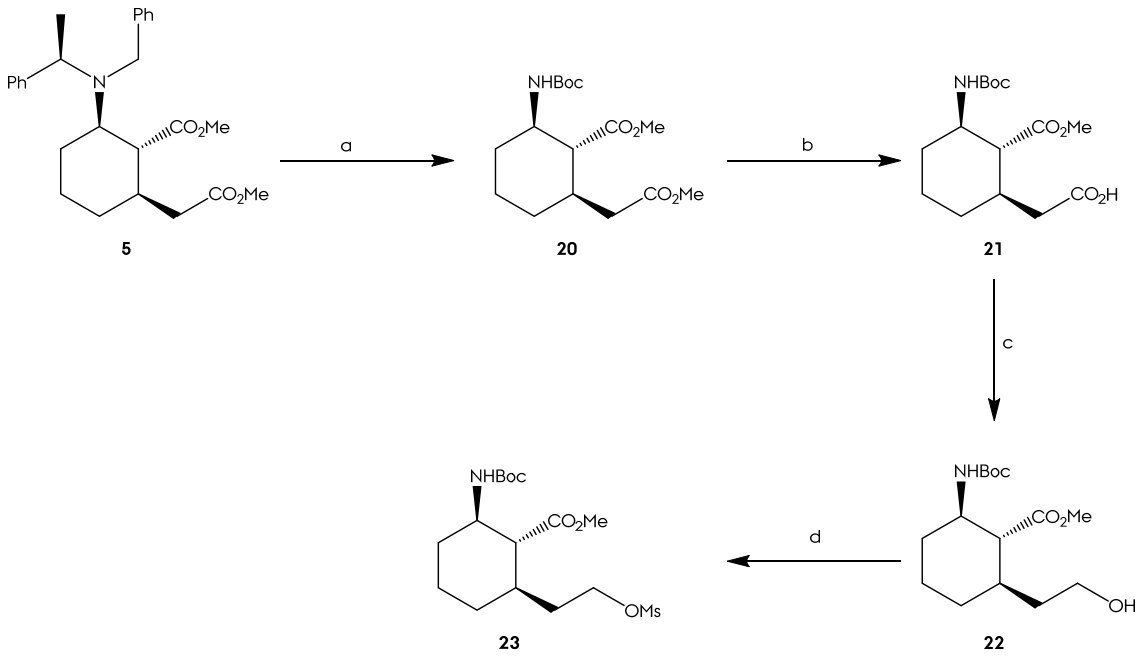

Scheme 36. *Reagents and conditions*: (a) H_2 - $Pd(OH)_2/C$, Boc_2O, AcOEt, 3 d, 81 % (M33). (b) $LiOH \cdot H_2O$, MeOH/THF/H_2O 3:1:1, 6 h, 84 % (M35). (c) $BH_3 \cdot THF$, THF, rt, 92 % (M36). (d) MsCl, DMAP, Py, DCM, rt, 12h, 96 % (M37).

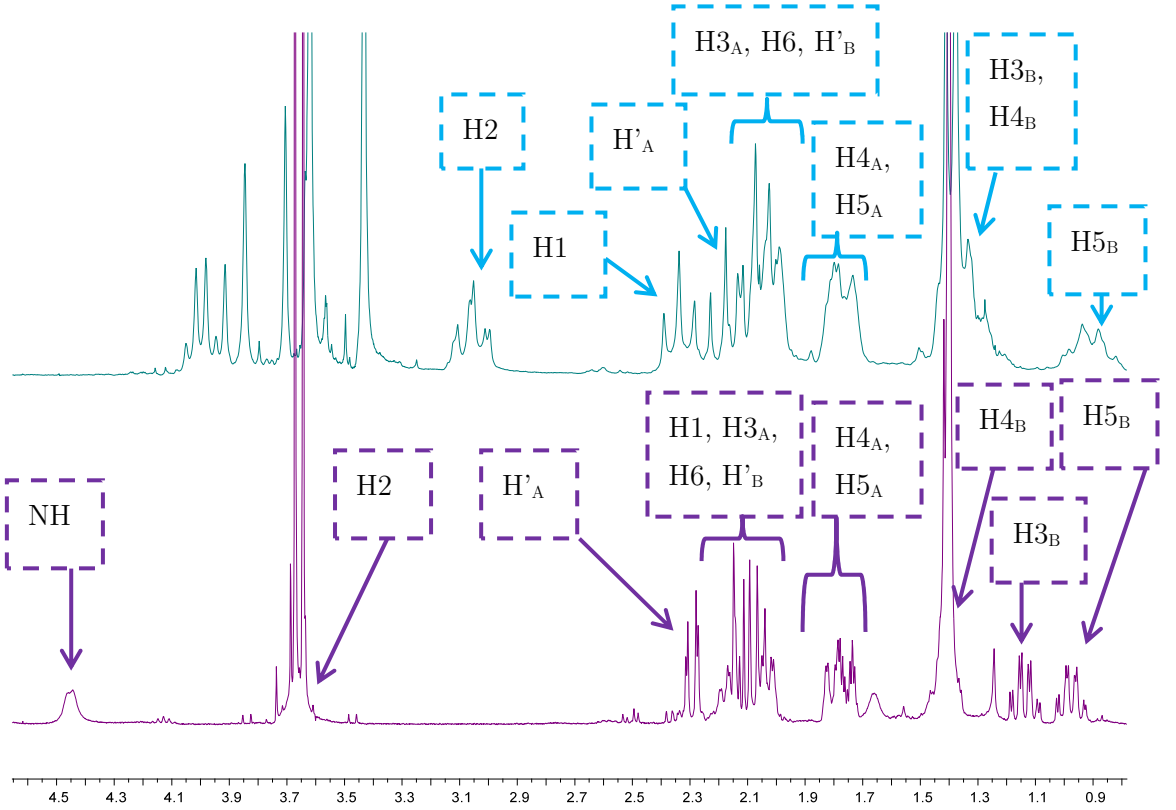

Figure 48. ^{1}H NMR stacked spectra of **5** (blue) and **20** (purple). H' resonances refer to C$\underline{H_2}$CO$_2$Me protons.

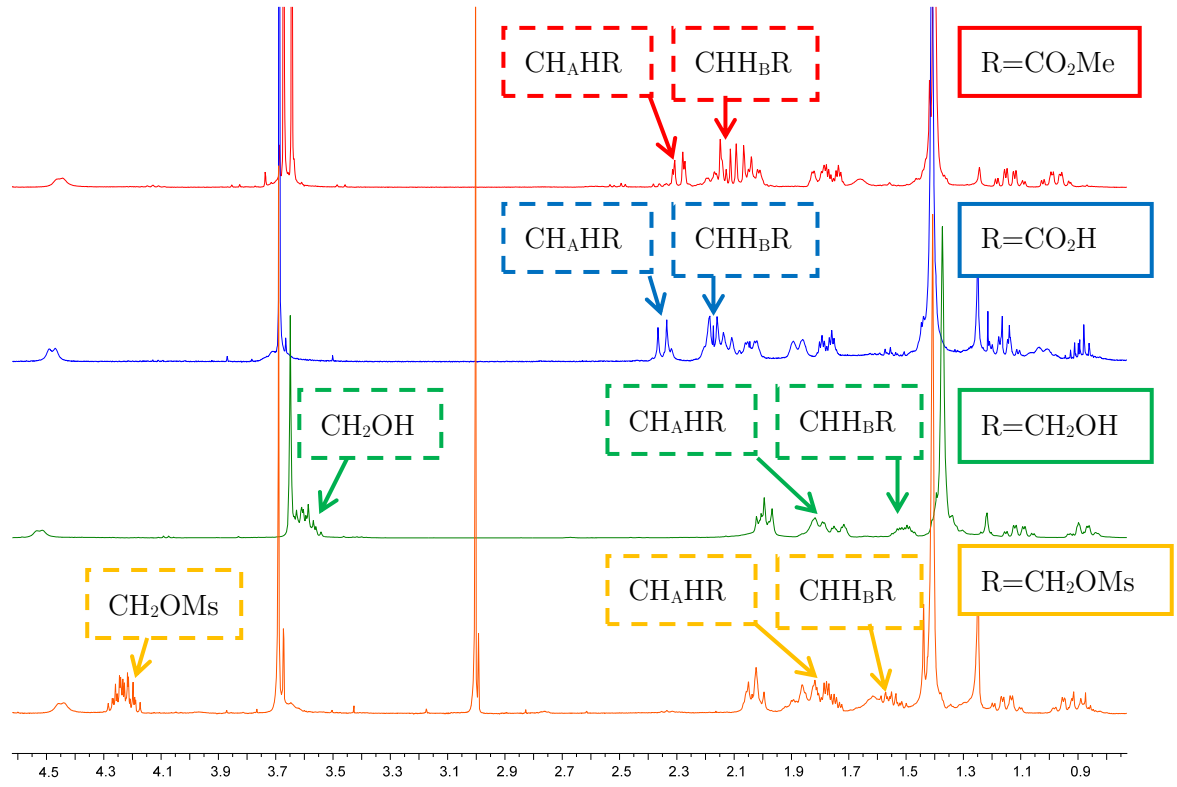

Figure 49. ^{1}H NMR stacked spectra of **20** (red), **21** (blue), **22** (green) and **23** (orange). Lateral chain resonances are highlighted.

Figure 49 shows the ^{1}H NMR spectra evolution along the route **20**-**23**. The main displacements are related with the new alpha protons of OH and OMs at **22**-**23** and the displacement of the protons of the lateral chain to high field.

Once transformed the lateral chain into a good leaving group (mesylate), several cyclization conditions were explored, which are depicted in **scheme 37**. *N*,*N*,*N'*,*N'*-tetramethylguanidine has been used in synthesis as a mild base in cyclization reactions of this type.[33] Treatment of TMG in DCM at room temperature did not provoke any reaction. Reaction took place increasing the temperature until boiling point of the solvent. After workup and posterior flash chromatography, a small quantity of protected morphan **12** was obtained, together with a 44 % yield of the substitution product **24** with TMG over substrate. In this case, TMG acted as nucleophile preferentially over base. When $CHCl_3$ was used instead of DCM, the chloride **25** was obtained in a 31 %.

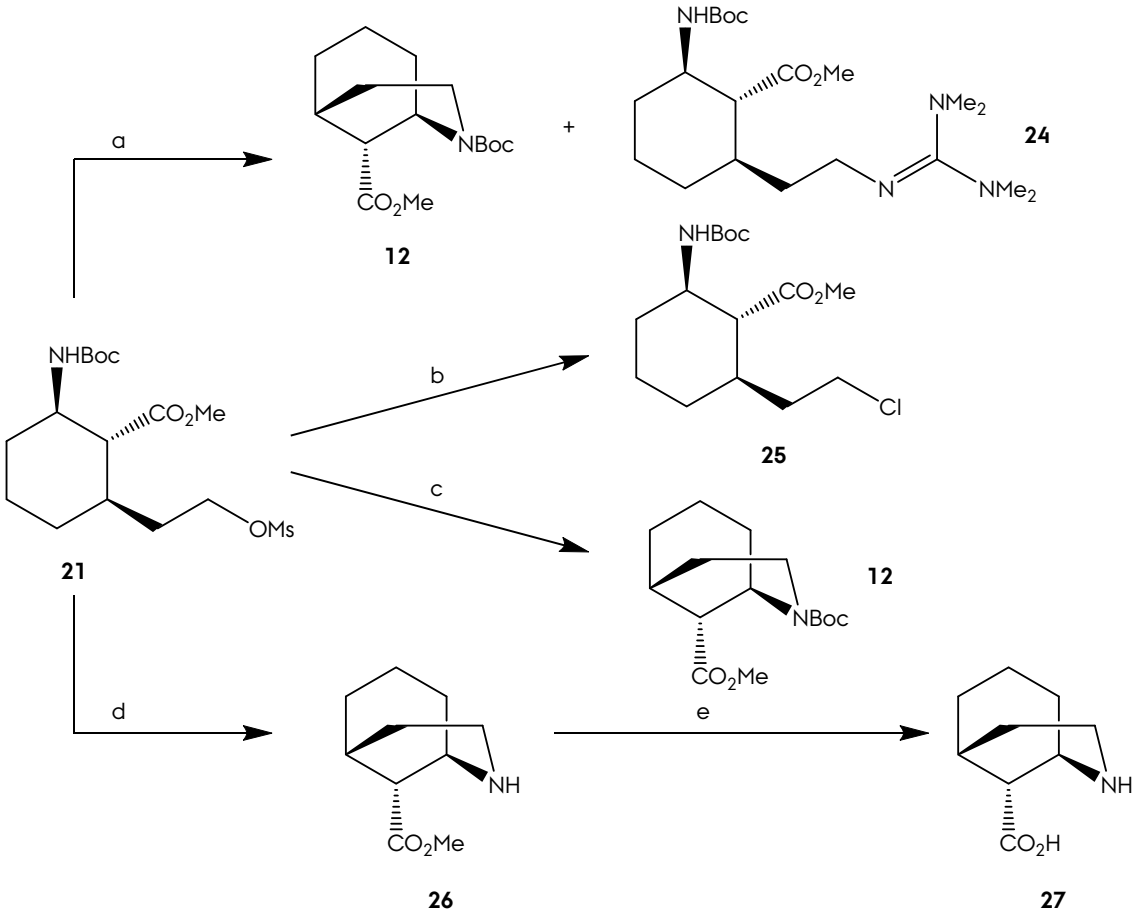

Scheme 37. *Reagents and conditions*: (a) TMG, DCM, 40 ºC, 5 h, 14 % (**12**) and 44 % (**24**) (M38). (b) TMG, $CHCl_3$, 60 ºC, 36 h, 31 % (M39). (c) DBU, DCM, 24 h, 23 % (M40). (d) i. TFA/DCM 1:1, 3 h. ii. Et_3N, EtOH 1:5, 12 h, 90 % (M41). (e) $LiOH \cdot H_2O$, MeOH/THF/H_2O 3:1:1, 12 h, quant yield (M42).

The source of the chlorine atom comes undoubtedly from the solvent. Although the solvent was properly prepared (see Methodologies and Materials section), it was purified and stored some time before its using.

When DBU was used instead of TMG, protected morphan **12** was successfully obtained, but in a 23 % yield. As the cyclizations where the Boc moiety is kept did not give good results, a total deprotective protocol was selected and carried out. Initial treatment of mesylate **21** with TFA:DCM 1:1 leaded to the total deprotection of the amine. Subsequent solvent removal and dissolving the crude in Et_3N/EtOH 5:1 at boiling temperature afforded the morphan **26** in excellent yields. Finally, amino acid **27** was obtained via hydrolysis of the ester **26** and isolation by means of freeze-drying, in a quantitative yield. Both morphans exhibits typical morphan scaffold resonances of protons H1, H5 and H9 (**Fig. 50**). As well as protected morphan **12**, H3 resonances are in the range 3.0-4.0 ppm.

To the best of our knowledge, the optimized route from diester **5** to morphan **26** is the best path to obtain morphan scaffolds with both amino and ester groups fully reactive.

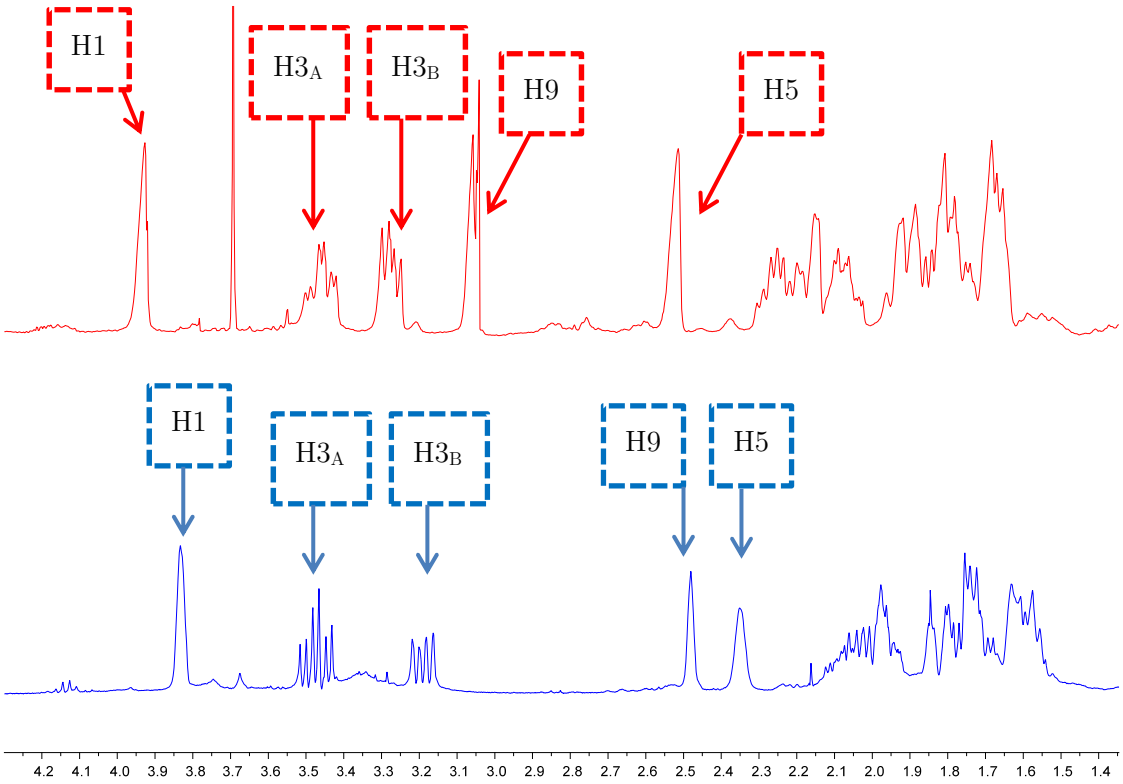

Figure 50. ^{1}H NMR stacked spectra of **26** (red, $CDCl_3$) and **27** (blue, D_2O).

The route is not only relevant in terms of yield (overall yield of 54 % in 5 steps), but in productivity as well: up to 100 mg of morphan **26** may be obtained with this procedure.

Synthesis of an Ala-26-Gly Tripeptide

Once obtained the morphan aminoester **26** and optimized the synthetic strategy, additional reactions were carried out to check either the two functional groups were plenipotentiary. As the compound **26** is an amino acid, the coupling of two residues on both sides of the amino acid would justify the reactivity or not of the carbon and nitrogen terminals.[18i] For this, a tripeptide was synthetized accordingly to **scheme 38**.

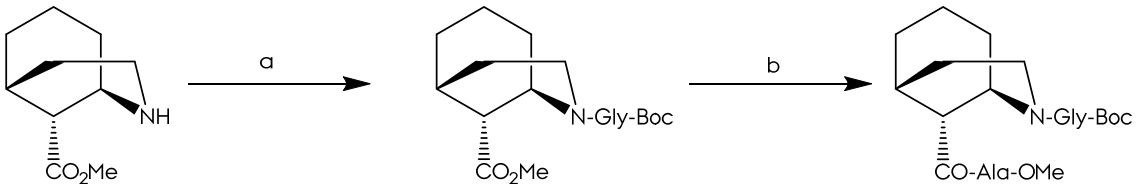

Scheme 38. *Reagents and conditions*: (a) Boc-Gly-OH, EDCI, HOBt, DIPEA, DMF, 24 h, 86 % (M43). (b) i. LiOH · H_2O, MeOH/THF/H_2O 3:1:1, 6 h. ii. [H_2-Ala-OMe]Cl, EDCI, HOBt, DIPEA, DMF, 24 h, 53 % (M44).

First, coupling reaction between morphan **26** and glycine yielded dipeptide **28** in 86 %. Forward chemoselective hydrolysis of the ester group followed by alanine copling resulted in the tripeptide **29** in a 53 % yield. As both functionalities reacted well (this also was evidenced in the synthesis of morphan derivatives, see chapter 3), we conclude this morphan residue have fully armed their amino and acid/ester group.

Interpretation of the ^{1}H and ^{13}C NMR is complex, due to the rotameric forms of the Boc and reaction scaling (10 mg). Glycine and alanine proton resonances are characteristic and may be found at 4.09 - 3.77 ppm (Gly), 4.62 (Ala) and 1.37 (Ala).

Conclusions

In this chapter, a total of 12 morphan type compounds were synthetized (**Fig. 51**), starting from chiral intermediate 5, reachable from azelaic acid in three steps.

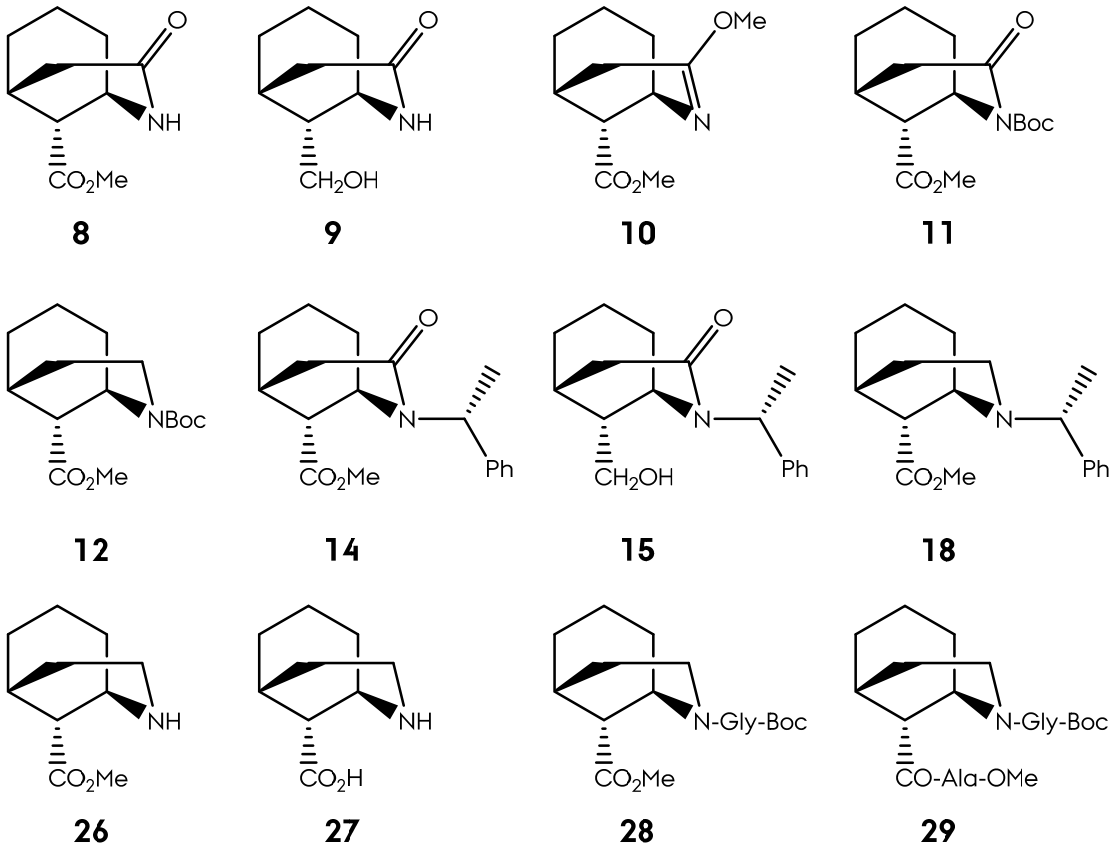

Figure 51. The 12 morphan compounds synthetized in this chapter.

Key step is the addition of chiral (*R*)-*N*-benzyl-*N*-α-methylbenzylamine, a domino conjugate addition followed by an intramolecular cyclization, where the stereochemistries of the three sterocenters are fixed. These stereochemistries are perfectly known due to knowledge of these asymmetric additions, as well as the isolation of **8** as crystal and further X-Ray analysis.

Several routes were explored in order to obtain a morphan structure with three requisites: (1) moderate to good overall yields, (2) good productivity and (3) with the amino and ester functionalities fully armored. Route 2 accomplished that, yielding a 54 % of **26** from intermediate **5**, obtaining up to 100 mg of production. Other routes failed to accomplished all the three targets, however, a series of morphan structures were obtained and allowed a better understanding of this systems: at reactivity and spectroscopic level.

References

[1] (a) Gates, M.; Tschudi, G. *J. Am. Chem. Soc.* **1952**, *74*, 1109. (b) Toth, J. E.; Fuchs, P. L. *J. Org. Chem.* **1987**, *52*, 473. (c) Taber, D. F.; Neubert, T. D.; Rheingold, A. L. *J. Am. Chem. Soc.* **2002**, *124*, 12416. (d) Uchida, K.; Yokoshima, S.; Kan, T.; Fukuyama, T. *Org. Lett.* **2006**, *8*, 5311.

[2] Dolby, L. J.; Biere, H. *J. Am. Chem. Soc.* **1968**, *90*, 2699.

[3] (a) Patir, S.; Uludag, N. *Tetrahedron* **2009**, *65*, 115. (b) Reekie, T. A.; Banwell, M. G.; Willis, A. C. *J. Org. Chem.* **2012**, *77*, 10773.

[4] (a) Kong, F.; Andersen, R. J.; Allen, T. M. *J. Am. Chem. Soc.* **1994**, *116*, 6007. (b) Yamazaki, N.; Kusanagi, T.; Kibayashi, C. *Tetrahedron Lett.* **2004**, *45*, 6509. (c) Yoshimura, Y.; Inoue, J.; Yamazaki, N.; Aoyagi, S.; Kibayashi, C. *Tetrahedron Lett.* **2006**, *47*, 3489.

[5] Eguchi, M. *Med. Res. Rev.* **2004**, *24*, 182.

[6] Cronyn, M. W.; Riesser, G. H. *J. Am. Chem. Soc.* **1953**, *75*, 1664.

[7] Ginsburg, D. *J. Org. Chem.* **1950**, *15*, 1003.

[8] (a) Bonjoch, J.; Casamitjana, N.; Bosch, J. *Tetrahedron* **1982**, *38*, 2883. (b) Bonjoch, J.; Casamitjana, N.; Quirante, J.; Rodriguez, M.; Bosch, J. *J. Org. Chem.* **1987**, *52*, 267. (c) Bonjoch, J.; Casamitjana, N.; Quirante, J.; Torrens, A.; Paniello, A.; Bosch, J. *Tetrahedron* **1987**, *43*, 377.

[9] (a) Bonjoch, J.; Casamitjana, N.; Bosch, J. *Tetrahedron* **1988**, *44*, 1735. (b) Bonjoch, J.; Quirante, J.; Rodriguez, M.; Bosch, J. *Tetrahedron* **1988**, *44*, 2087. (c) Bonjoch, J.; Casamitjana, N.; Gràcia, J.; Bosch, J. *Tetrahedron Lett.* **1989**, *30*, 5655. (d) Bonjoch, J.; Quirante, J.; Solé, D.; Castells, J.; Galceran, M.; Bosch, J. *Tetrahedron* **1991**, *47*, 4417. (e) Bonjoch, J.; Casamitjana, N.; Quirante, J.; Garriga, C.; Bosch, J. *Tetrahedron* **1992**, *48*, 3131. (f) Casamitjana, N.; Gràcia, J.; Bonjoch, J.; Bosch, J. *Tetrahedron Lett.* **1992**, *33*, 2055.

[10] Amat, M.; Sanfeliu, E.; Bonjoch, J.; Bosch, J. *Tetrahedron Lett.* **1989**, *30*, 3841.

[11] Bosch, J.; Bonjoch, J.; Serret, I. *Tetrahedron Lett.* **1982**, *23*, 1297.

[12] Solé, D.; Urbaneja, X.; Bonjoch, J. *Tetrahedron Lett.* **2004**, *45*, 3131.

[13] (a) Quirante, J.; Escolano, C.; Costejà, L.; Bonjoch, J. *Tetrahedron Lett.* **1997**, *38*, 6901. (b) Quirante, J.; Escolano, C.; Massot, M.; Bonjoch, J. *Tetrahedron* **1997**, *53*, 1391. (c) Diaba, F.; Martinez-Laporta, A.; Bonjoch, J.; Pereira, A.; Munoz-Molina, J. M.; Perez, P. J.; Belderrain, T. R. *Chem. Commun.* **2012**, *48*, 8799.

[14] Aurrecoechea, J. M.; Gorgojo, J. M.; Saornil, C. *J. Org. Chem.* **2005**, *70*, 9640.

[15] Wang, Y.-F.; Chiba, S. *J. Am. Chem. Soc.* **2009**, *131*, 12570.

[16] Amat, M.; Pérez, M.; Minaglia, A. T.; Bosch, J. *J. Org. Chem.* **2008**, *73*, 6920.

[17] (a) Diaba, F.; Bonjoch, J. *Org. Biomol. Chem.* **2009**, *7*, 2517. (b) Bradshaw, B.; Parra, C.; Bonjoch, J. *Org. Lett.* **2013**, *15*, 2458.

[18] (a) Urones, J. G.; Garrido, N. M.; Díez, D.; Dominguez, S. H.; Davies, S. G. *Tetrahedron: Asymmetry* **1997**, *8*, 2683. (b) Urones, J. G.; Garrido, N. M.; Díez, D.; Dominguez, S. H.; Davies, S. G. *Tetrahedron: Asymmetry* **1999**, *10*, 1637. (c) Urones, J. G.; Garrido, N. M.; Diez, D.; El Hammoumi, M. M.; Dominguez, S. H.; Antonio Casaseca, J.; Davies, S. G.; Smith, A. D. *Org. Biomol. Chem.* **2004**, *2*, 364. (d) Davies, S. G.; Diez, D.; Dominguez, S. H.; Garrido, N. M.; Kruchinin, D.; Price, P. D.; Smith, A. D. *Org. Biomol. Chem.* **2005**, *3*, 1284. (e) Garrido, N. M.; Díez, D.; Domínguez, S. H.; García, M.; Sánchez, M. R.; Davies, S. G. *Tetrahedron: Asymmetry* **2006**, *17*, 2183. (f) Garrido, N. M.; Blanco, M.; Cascón, I. F.; Díez, D.; Vicente, V. M.; Sanz, F.; Urones, J. G. *Tetrahedron: Asymmetry* **2008**, *19*, 2895. (g) Garrido, N. M.; Rubia, A. G.; Nieto, C.; Díez, D. *Synlett* **2010**, *2010*, 587. (h) Garrido, N. M.; Rosa Sánchez, M.; Díez, D.; Sanz, F.; Urones, J. G. *Tetrahedron: Asymmetry* **2011**, *22*, 872. (i) Garrido, N. M.; Nieto, C. T.; Díez, D. *Synlett* **2013**, *24*, 169.

[19] Scheffer, J. R.; Wostradowski, R. A. *J. Org. Chem.* **1972**, *37*, 4317.

[20] Gaudener, A. *Determination of Configuration by NMR Spectroscopy*; Thieme, 1997.

[21] Davies, S. G.; Ichihara, O. *Tetrahedron: Asymmetry* **1991**, *2*, 183.

[22] Bull, S. D.; Davies, S. G.; Fenton, G.; Mulvaney, A. W.; Prasad, R. S.; Smith, A. D. *J. Chem. Soc., Perkin Trans. 1* **2000**, 3765.

[23] Brown, H. C.; Heim, P. *J. Org. Chem.* **1973**, *38*, 912.

[24] Brown, W. G. In *Organic Reactions*; John Wiley & Sons, Inc.: 2004.

[25] Borch, R. F. *Tetrahedron Lett.* **1968**, *9*, 61.

[26] Pedregal, C.; Ezquerra, J.; Escribano, A.; Carreño, M. C.; García Ruano, J. L. *Tetrahedron Lett.* **1994**, *35*, 2053.

[27] Ren, P.; Wu, C.; Ponder, J. W. *J. Chem. Theory Comput.* **2011**, *7*, 3143.

[28] (a) Halgren, T. A. *J. Comput. Chem.* **1996**, *17*, 490. (b) Halgren, T. A. *J. Comput. Chem.* **1996**, *17*, 520. (c) Halgren, T. A. *J. Comput. Chem.* **1996**, *17*, 553. (d) Halgren, T. A.; Nachbar, R. B. *J. Comput. Chem.* **1996**, *17*, 587. (e) Halgren, T. A. *J. Comput. Chem.* **1996**, *17*, 616.

[29] *Jaguar 7.9,* Schrödinger, L., New York , NY,

[30] (a) Becke, A. D. *Phys. Rev. A* **1988**, *38*, 3098. (b) Lee, C.; Yang, W.; Parr, R. G. *Phys. Rev. B* **1988**, *37*, 785.

[31] Hehre, W. J.; Radom, L.; Schleyer, P. v. R.; Pople, J. *Ab Initio Molecular Orbital Theory*; Wiley-VCH, 1986.

[32] Marten, B.; Kim, K.; Cortis, C.; Friesner, R. A.; Murphy, R. B.; Ringnalda, M. N.; Sitkoff, D.; Honig, B. *J. Phys. Chem.* **1996**, *100*, 11775.

[33] Barco, A.; Baricordi, N.; Benetti, S.; De Risi, C.; Pollini, G. P.; Zanirato, V. *Tetrahedron* **2007**, *63*, 4278.

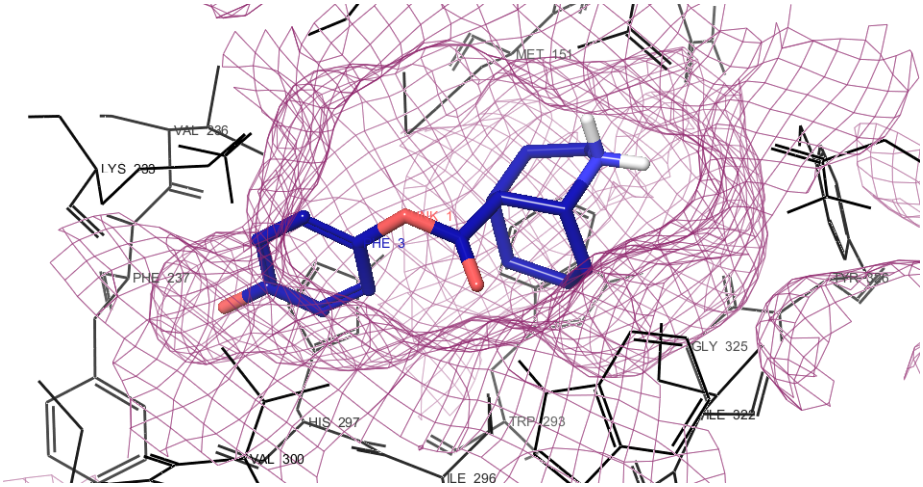

3 Structure-based Design and Synthesis of Novel Opioid Receptor Ligands.

Introduction

Opioid receptors were first identified 40 years ago,[1] and since then, they have been studied over the last decades, not only with the purpose of discover new therapeutic agents, but to elucidate the mechanism of in/activation of the opioid receptor. Opioid receptors biomodelling is primary to understand which compounds works and which not. In drug design, the knowledge of the system under study is essential to choose, project and organize the best theoretical methodology to explore new therapeutic agents.

In the last decade, several attractive theoretical studies about binding properties of new opiate drugs have been published. Oligopeptides[2] and morphine-derived analogs[3] have been tested both *in silico* and *in vivo* in different opioid receptors: μ,[4] κ,[5] δ.[6]

In chapter 2, we obtained the 2-azabicyclo[3.3.1]nonane scaffold, as the aminoester **26** as main target. Although this motif is a structural simplification of morphine, the resemblance leaded us to think in a promising new morphine derivatives as opioid agonists/antagonists. So, a combined biomodelling project and biological evaluation is envisaged to explore the potential activity of this kind of products. In this chapter, a complete biomodelling study is carried out with the aim of a series of software tools. Chapter 4 focus on the biological tests to evaluate the activity of these compounds and validate the theoretical study.

As the structure is well known, a theoretical structure based design project was initiated to explore potential modifications of our structure that could acts as opioid agonists. Antagonist studies are carried out at the moment.

The structure based design project followed the next workflow:

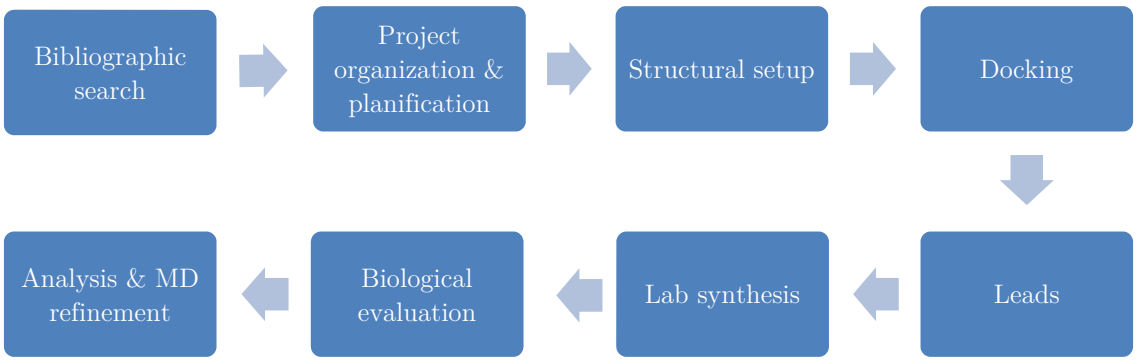

Receptor Selection

In a structure based design, the receptor structure choice is critical to the next steps, being fundamental a well validated 3D target[7] to perform the docking studies. Attending to the nature of the methodological technique to obtain the three dimensional structure, receptors fall into two classes:

- Experimental techniques: as X-Ray diffraction and NMR analysis. Although they are routine techniques, several difficulties like sample preparation and data collection and interpretation are still drawbacks in define high-throughput methods.
- Homology models: usually, many proteins do not have experimental data available. Homology modelling may be used to predict 3D structures from a closely related protein homolog. Although not as good as experimental techniques, can be used as docking targets.

Apart from this classification, receptors may be grouped in:

- Holoenzymes: ligand bounded receptors. The best models for docking, due to the conformational disposition of the target (specially the binding pocket).
- Apoenzymes: unligated protein. Usually inadequate structures due to the lack of conformational data related to the bounded state.

Opioid receptors structures elucidations have being a challenging task from their beginnings. They belong to the field of G protein-coupled receptors, a family of proteins that controls signaling pathways,[8] which are membrane-spanned. This fact makes them notoriously difficult to crystallize.

In 2000,[9] the three-dimensional (3D) structure of bovine rhodopsin at the 2.8 Å resolution has served as basic model for all opioid receptors. Since them, a large number of homology models have been built starting from it.[10]

In 2004, Mosberg *et al*,[11] communicate a homology study of a μ opid receptor complex with JOM6, a cyclic peptide agonist, which were modelled combining experimental constraints and theoretical methods. Such model has been used in many biomodelling studies, and was proved to be suitable for peptide agonist binding.[12]

We took the Mosberg´s rat mu opioid receptor (active state) bonded with morphine as the most appropriate target structure to our study. The main reasons are:

- Why μ-opioid receptor? Is the most well-known as it mediates the important physiological states of analgesia and addiction.
- Why "active" (agonist)? Regarding the structure of the ligands, the line between agonist and antagonist is thin. Agonist response was first assumed as hypothesis, which will be validated or rejected at the biological stage.
- Why Mosberg´s μ type? As it was previously commented, this 3D structure was probed to be suitable for peptide agonist binding. As the ligand core is a morphan type β-aminoacid, the receptor structure is recommended for our purposes.

The Docking Protocol. Design and Validation.

Once selected the receptor structure, the next step is design a docking protocol and validate it. The purpose of the validation is check how reliable the docking results could be.

First, the docking protocol must be created. The protocol should follow some points:

- Input ligand structures: prior to the docking stage, a geometric optimization stage is highly recommended. A low-energy relaxed structure will have a better behaviour than a high energy one. As the docking procedure usually involves a Monte Carlo algorithm, the search is highly dependent of the input structure.
- Input receptor structure: depending on the nature of the receptor (homology protein, apoenzyme, etc…), a structure refinement could be necessary. Again, the most reliable receptor structure is desired.
- Binding pocket: the position/geometry of the binding pocket must be found! Holoenzymes are the best, as the binding information is stored as a shape. This topology is ideal to perform docking simulations. Nevertheless, modern techniques to find hypothetical binding pockets at apoenzymes are being designed, although the level of confidence is still low.

- Search algorithm: the docking procedure must include an appropriate search algorithm, usually a modified Monte Carlo approach, to position molecules in various locations, orientations and conformations.
- Scoring algorithm: following the searching method, a quantification of each one of the poses is required. The stored positions are evaluated, and a list of hits (or leads) is defined. This allows studying how ligands fit better in the active site of the receptor.

Taking into account these requisites, the docking protocol summarized below is defined:

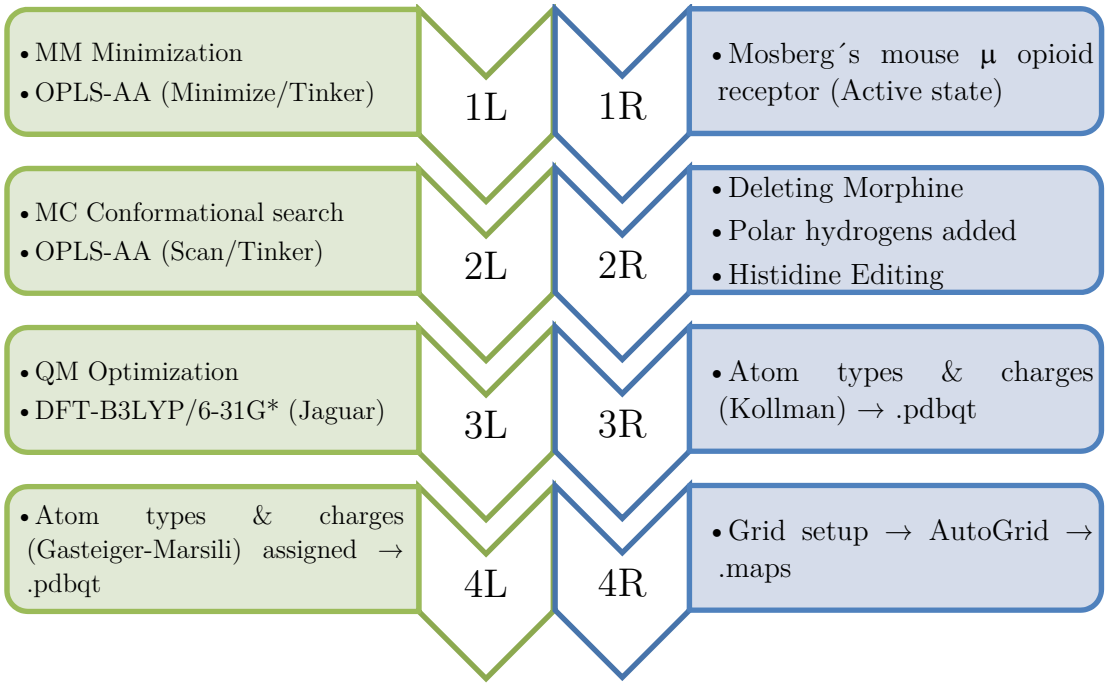

1C

- Docking setup: Genetic algorithm → AutoDock → .dlg
- 200 docking runs, 500 population in the genetic algorithm, 5000000 energy evaluations, 1000000 maximum number of iterations

2C

- 2.0 Å RMSD clustering
- Histogram analysis

First, the ligand structures were prepared using Maestro v.9.3.[13] Next, OPLS-AA[14] (Optimized Potentials for Liquid Simulations, all-atom type force field) atoms types

were assigned to the structures and a quasi-Newton minimization (MINIMIZE command, Tinker)[15] were performed. For each one of the minimized structures, a Monte Carlo conformational search was applied (SCAN command, tinker) and the set of low energy conformers were optimized through Jaguar v.7.9[16] and QM Density Funtional Theory (DFT), using the general hybrid B3LYP functional[17] together with the 6-31G(d) basis set.[18] Autodock atom types were assigned to the QM refined structures, together with Gasteiger–Marsili[19] partial charges using AutoDock tools (ADT).[20] Nonpolar hydrogen atoms were merged.

On the other hand, Mosberg´s mouse μ opioid receptor (active state) was opened with Maestro. Morphine ligand was deleted and polar hydrogens were added. Next stage was the edition of protein histidines. It is well known that histidines have several protonation states at physiological pH (**Sch. 39**), playing an important role in enzyme reactivity.

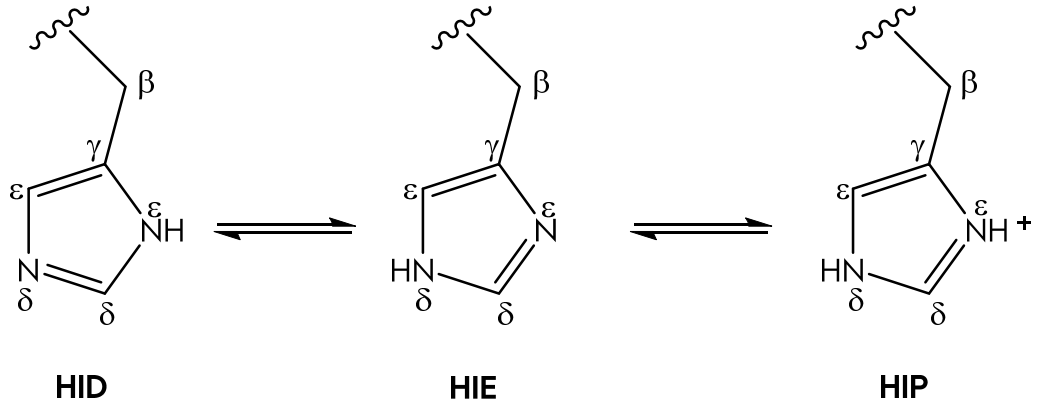

Scheme 39. Common protonation states of histidine inside proteins.

To edit histidines properly, is necessary to explore the 3D structure and check hydrogen bonding hypothesis. For this receptor, the protonation state assignation was the following: HID171, HID223, HIE297, HID319. Polar hydrogen atoms were added and Kollman charges,[21] atomic solvation parameters and fragmental volumes were assigned to the protein using AutoDock tools (ADT).

The auxiliary program AutoGrid generated the grid maps. Each grid was centered at the active site of the receptor. The grid dimensions were 60x60x60 $Å^3$ with points separated by 0.375 Å. This grid dimensions were large enough to cover the receptor binding site and the ligands. Lennard–Jones parameters 12–10 and 12–6, supplied with the program, were used for modeling H-bonds and van der Waals interactions, respectively. The distance-dependent dielectric permittivity of Mehler and Solmajer[22]

was used for the calculation of the electrostatic grid maps. For all ligands, random starting positions, random orientations, and torsions were used. The translation, quaternion, and torsion steps were taken from default values in AutoDock. All non-cyclic ligand torsions were allowed to rotate during docking. The Lamarckian genetic algorithm and the pseudo-Solis and Wets methods were applied for minimization, using default parameters. The number of docking runs was 200. The population in the genetic algorithm was 500, the energy evaluations were 5.000.000, and the maximum number of iterations 1.000.000.

Morphine was the first ligand subjected to docking, in order to validate the proposed method. Clustering analysis reveals two clusters at 2.0 Å of RMSD (**Fig. 52**), being the lowest energy cluster the most populated (2 clusters with a relative population of 199:1)

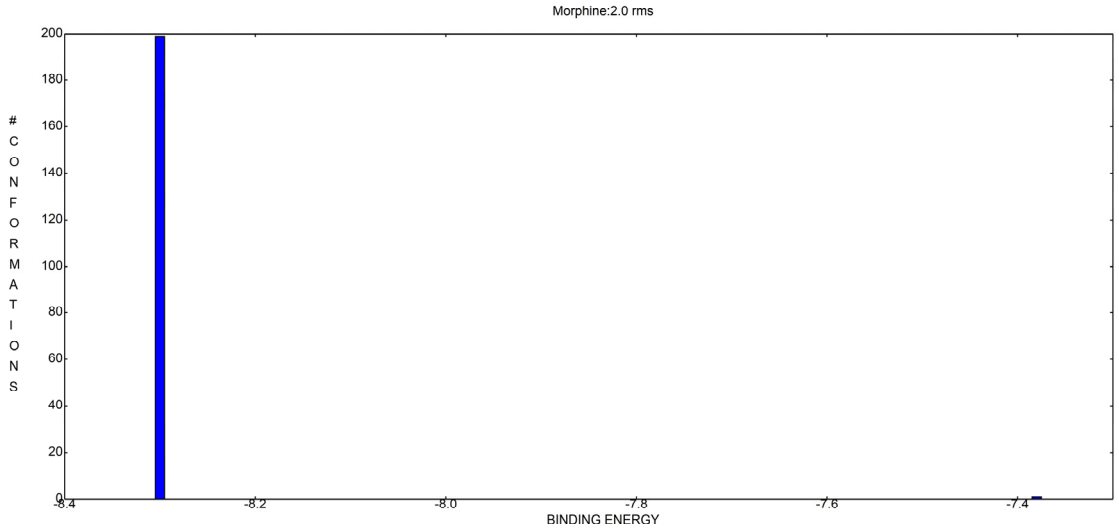

Figure 52. Clustering histogram of the validation stage at 2.0 Å level.

The mean binding energy of the most populated cluster was -8.26 Kcal/mol, while the lowest binding energy was -8.30 Kcal/mol. Here, the value of the binding energy is not relevant, being more important the comparison between docked and original structures. **Figure 53** shows a superposition between ligands at original state and docked state. This comparison reveals a good agreement between input (orange) and output (green) structures. Position of the docked morphine is slightly displaced to Asp147, strengthening the effect of the ionic bridge. Orientation and conformation is almost the same, and the RMSD between structures is 0.9628 Å. Concluding, as the structural differences are minimum and the RMSD is lower than 2.0 Å, the docking protocol was successfully validated.

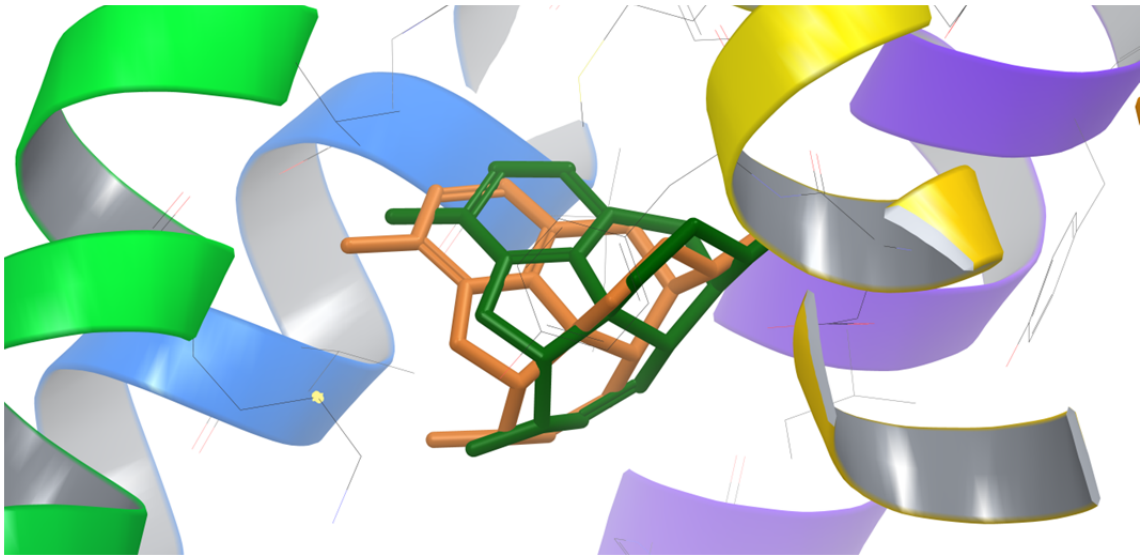

Figure 53. Structural superposition between original ligand (orange) and docked (green). Only heavy atoms are displayed.

Structure-Based Design.

Once validated the docking protocol, the next step was design a series of morphan derivatives and docked them. In this case, the process to design drug candidates depends of the knowledge of the system, and the choice of a central motif, our morphan core.

The pharmacophore model of morphine is well known,[23] as a result not only of molecular modelling studies, but skeletal simplifications to obtain the representative active centers. In **Figure 54**, a model of the interaction of morphine with the binding pocket of μ opioid receptor is depicted. The ionic bridge between protonated nitrogen of morphine and Asp147 is one of the intermolecular anchors. The A ring is important as well, interacting with residues Ile234, Trp293, Ile296 and Val300. Besides, the phenolic hydroxy group is placed close to the imidazole group of His297, establishing a hydrogen bond. This two sector of morphine are the most relevant, as may be notice in the different structural simplifications which always keep the A-ring and the basic amine group.

Figure 55 shows, together with morphine, some μ opioid receptor drugs. Phenazocine and Phenomorphan are structural simplifications of morphine: benzomorphan and morphinane, respectively. Phenazocine is a dual

agonist/antagonist, while Phenomorphan is a strong agonist. In both of them, the introduction of the *N*-phenetyl group increasing the affinity; around 60 fold more potent than morphine in case of Phenomorphan.[24]

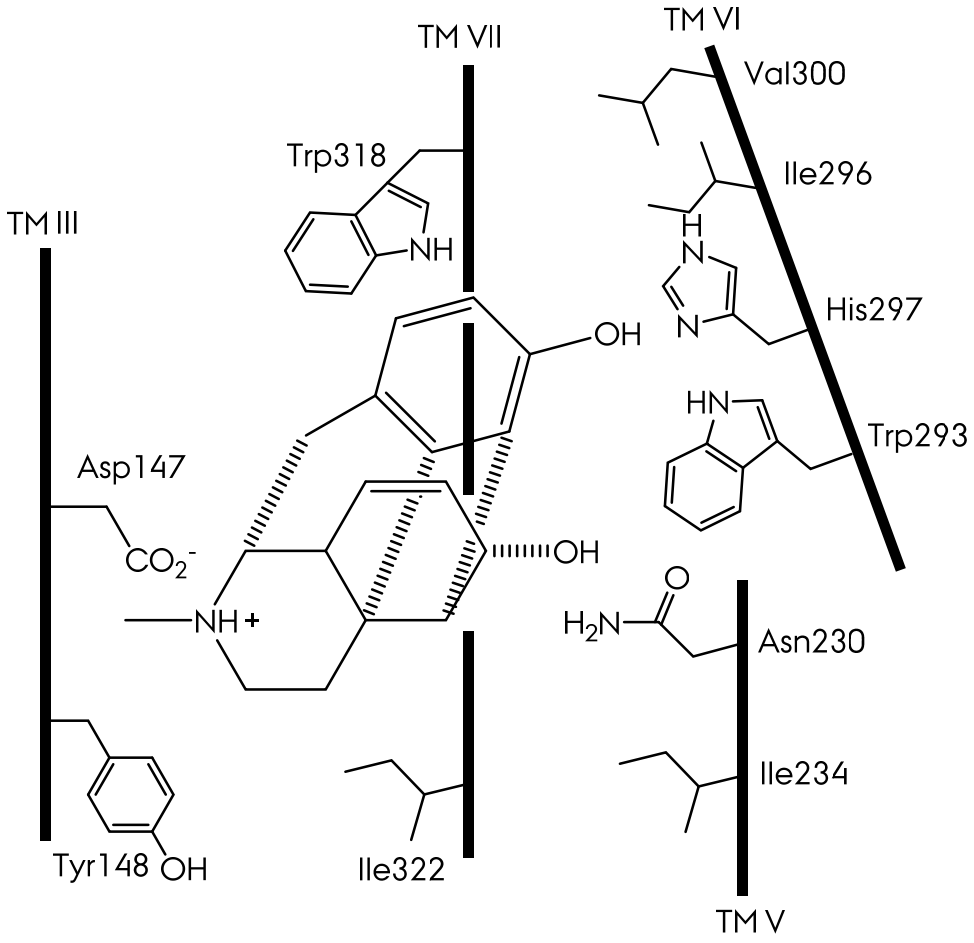

Figure 54. Pharmacophore model of morphine with the μ opioid receptor.

DAMGO and Endomorphin 1 are two examples of oligopeptide μ opioid receptor agonists. In both cases, the presence of the Tyr and Phe residues is required to manifest the activity.

In summary, it is important to keep the aromatic ring and the basic amine in the search of novel mu opioid agonists/antagonists. Additional aromatic groups may boost the affinity.

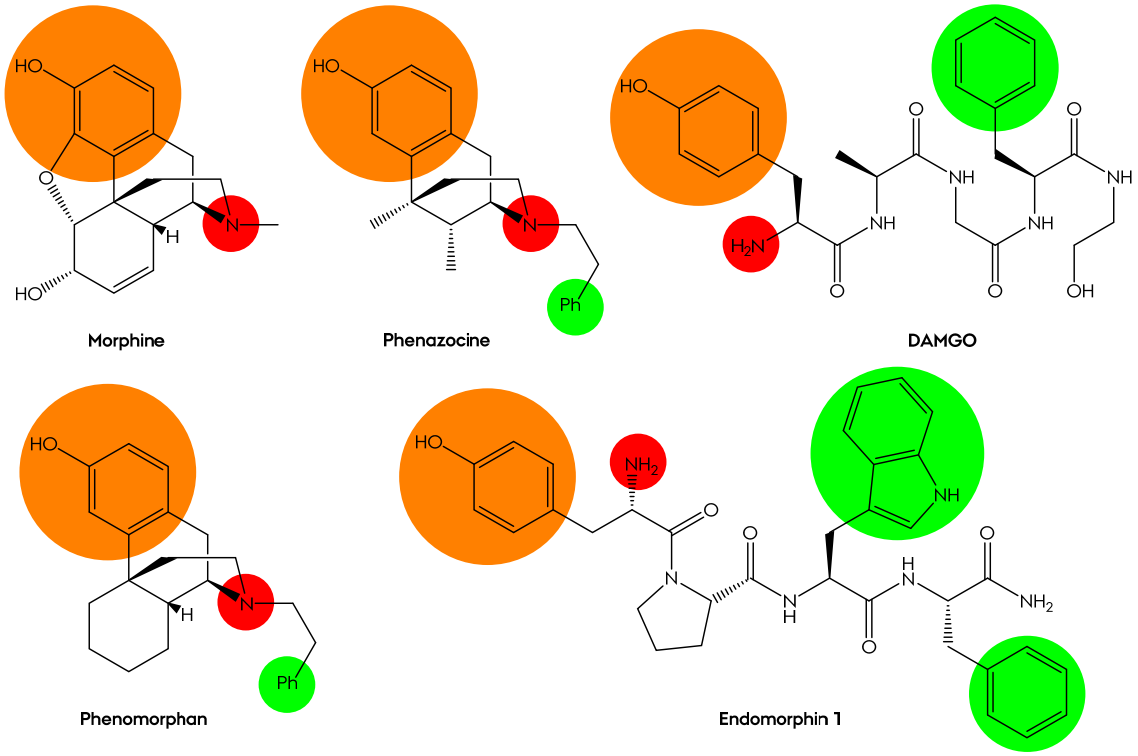

Figure 55. Morphine derivatives and oligopeptides with agonist character towards m receptors.

Our parent structure, the morphan aminoacid **26**, represents a promising building block in the design of novel μ opioid receptor small interacting molecules. The advantages are:

- Morphan scaffold: although rings B-C of morphine are not as relevant as ring A, the similarity to morphine is evident. The closer to morphine, the better affinity to the receptor. The conformational restriction of these systems also helps to increment the selectivity of the binding pose.
- Amino acid functionality: as many opioid agonists/antagonists are oligopeptides, the amino acid functionality, combined to the morphan motif, represents a unique core with dual possibilities: as a structural simplified morphine, and as a residue with the basic amine key region which may couple with other residues.
- In fact, is a β-amino acid: the majory of opioid oligopeptides undergo rapid enzymatic degradation by exo/endonucleases. The insertion of a β type amino acid increases the enzymatic resistance and, consequently, the persistence of the drug in the receptor.

26 has the basic amine functionality incorporated, however, the lack of an aromatic group lead us to reintroduce it in different fashions, which are schematized in **scheme 40**.

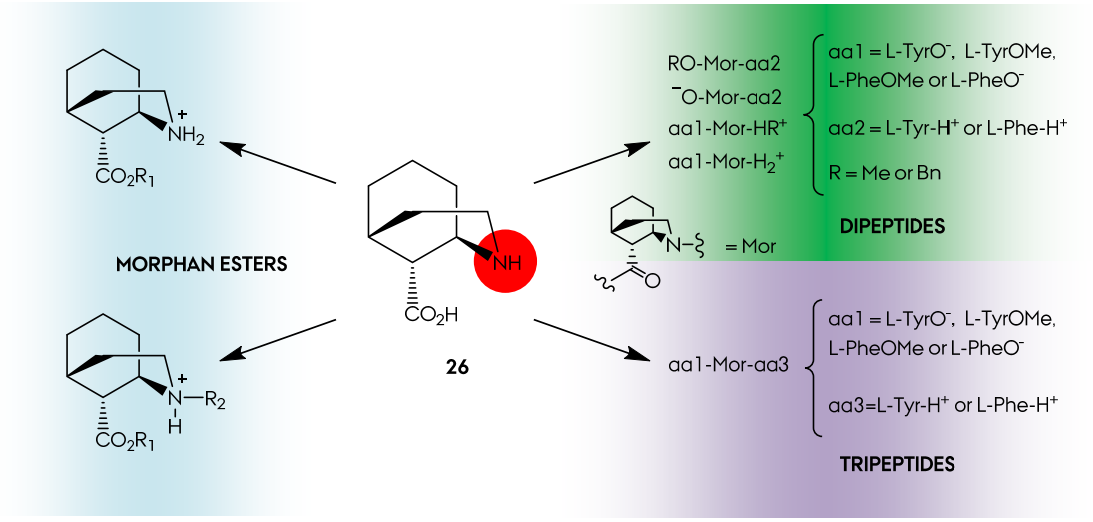

Scheme 40. Proposed modifications of the parent compound **26** in the design stage.

Three main derivative classes were designed:

- Morphan esters: different aromatic esters, with or without *N*-substitution, were proposed. This series of compounds was considered as morphan derivatives.
- Dipeptides: *L*-Phe and *L*-Tyr were taken as candidates in the coupling with morphan **26** to create different dipeptides, with the return of the phenyl group.
- Tripeptides: upgrading the previous group, tripeptides were obtained, with the Mor residue as central amino acid. These two groups were considered as morphan oligopeptides.

Table 7 shows a list of the candidates, created accordingly with the requisites explained earlier and classified as morphan esters, di- or tripeptides. All this candidates were subjected to the designed docking protocol. Average time was 1.5 days per candidate.

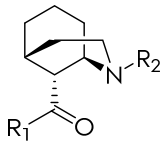

MORPHAN ESTERS

Name	R_1	R_2	Name	R_1	R_2
D1	$-O^-$	$-H_2^+$	**D12**	-OPh	$-H^+CH_2CH_2Ph$
D2	-OMe	$-H_2^+$	**D13**	-OPh	$-H^+Bn$
D3	-OMe	$-H^+Bn$	**D14**	$-O^-$	$-H^+CH_2CH_2Ph$
D4	$-O^-$	$-H^+Bn$	**D15**	-OMe	$-H^+CH_2CH_2Ph$
D5	-OBn	$-H_2^+$	**D16**	-OPhmOH	$-H_2^+$
D6	-OBn	$-H^+Bn$	**D17**	-OPhoOH	$-H_2^+$
D7	$-OCH_2C_6H_4OH$	$-H_2^+$	**D18**	-OPhmOH	$-H^+CH_2CH_2Ph$
D8	-OPh	$-H_2^+$	**D19**	-OPhoOH	$-H^+CH_2CH_2Ph$
D9	$-OC_6H_4F$	$-H_2^+$	**D20**	-OPhpOH	$-H_2^+$
D10	$-OCH_2C_6H_4OH$	$-H^+Bn$	**D21**	-OPhpOH	$-H^+CH_2CH_2Ph$
D11	$-OCH_2C_6H_4OH$	$-H^+CH_2CH_2Ph$	**D22**	-OPhpOH	$-H^+Bn$

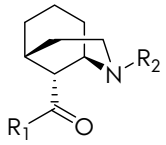

MORPHAN DIPEPTIDES

Name	R_1	R_2	Name	R_1	R_2
D23	-Phe-OMe	$-H_2^+$	**D30**	$-O^-$	$-Tyr-NH_3^+$
D24	$-Phe-O^-$	$-H_2^+$	**D31**	-Phe-OMe	$-H^+Bn$
D25	$-O^-$	$-Phe-NH_3^+$	**D32**	$-Phe-O^-$	$-H^+Bn$
D26	-OMe	$-Phe-NH_3^+$	**D33**	-Tyr-OMe	$-H^+Bn$
D27	-Tyr-OMe	$-H_2^+$	**D34**	$-Tyr-O^-$	$-H^+Bn$
D28	$-Tyr-O^-$	$-H_2^+$	**D35**	-OBn	$-Phe-NH_3^+$
D29	-OMe	$-Tyr-NH_3^+$	**D36**	-OBn	$-Tyr-NH_3^+$

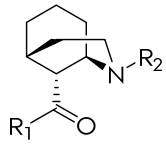

MORPHAN TRIPEPTIDES

Name	R_1	R_2	Name	R_1	R_2
D37	-Phe-OMe	$-Phe-NH_3^+$	**D39**	-Tyr-OMe	$-Tyr-NH_3^+$
D38	$-Phe-O^-$	$-Phe-NH_3^+$	**D40**	$-Tyr-O^-$	$-Tyr-NH_3^+$

Table 7. Designed candidates to the docking stage.

Docking Screening.

Table 8 summarizes the docking results in terms of inhibition constants and the parameter $\boldsymbol{\sigma}$, what we called "cluster selectivity".

Name	Ki / nM	σ	Name	Ki / nM	σ	Name	Ki / nM	σ
D1	30500	1.56	**D15**	296.7	1.81	**D28**	617.5	1.66
D2	11300	1.21	**D16**	275.9	1.12	**D29**	105.3	2.04
D3	686.5	1.21	**D17**	476.1	1.94	**D30**	74.1	2.89
D4	812.6	1	**D18**	3.8	1.58	**D31**	27.6	3.92
D5	508.13	1.04	**D19**	16.1	1.14	**D32**	17.9	2.73
D6	24.7	1.69	**D20**	454.2	1.07	**D33**	25.1	> 5
D7	159.6	1.24	**D21**	9.1	1.73	**D34**	27.8	> 5
D8	416.9	1.01	**D22**	64.5	2.32	**D35**	56.9	> 5
D9	407.7	1	**D23**	171.7	2.1	**D36**	26.4	> 5
D10	34.5	> 5	**D24**	177.9	3.33	**D37**	8.6	> 5
D11	5.2	4.04	**D25**	418.7	1.8	**D38**	6.1	> 5
D12	5.74	1.25	**D26**	205.7	2.85	**D39**	130.3	> 5
D13	38.6	2.32	**D27**	122.1	2.26	**D40**	418.7	> 5
D14	442.7	1.14						

Table 8. Tabulated docked compounds, inhibition constants and selectivity parameters.

In a routine clustering analysis, the histograms may reveal different binding poses: the more number of clusters, the larger number of binding poses. This is easily observed in **Figures 56** and **57**. In **Figure 56**, **D18** has one main cluster (125 population), four secondary sets (32, 27, 11 and 5) and six minor binding poses. This means that almost the 63 % of the ligands adopts the same topology in the binding. On the other hand, **D38** has a large number of clusters, with a range of populations between 5 – 40, without a clear excel cluster (**Fig. 57**). The more number of binding poses, the lower efficacy in provoke the conformational response of the receptor due to the binding.

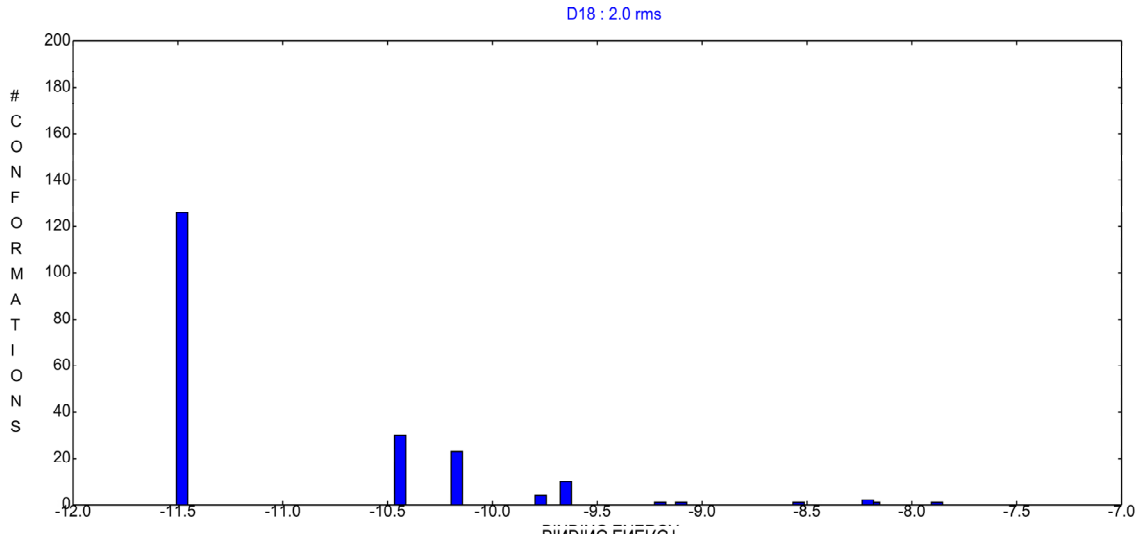

Figure 56. Histogram of the clustering pattern of docked **D18** at 2.0 Å level.

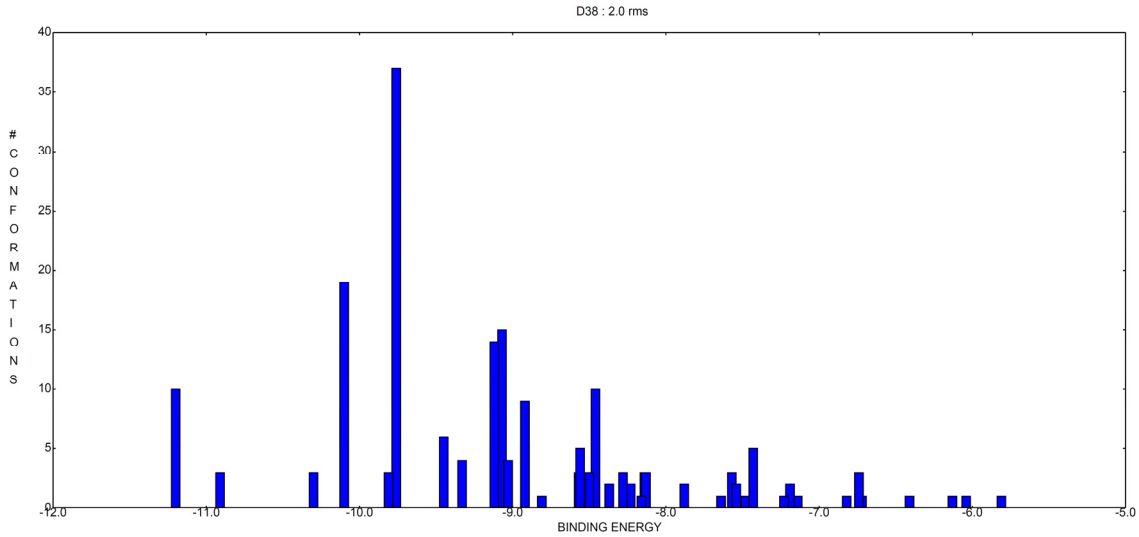

Figure 57. Histogram of the clustering pattern of docked **D38** at 2.0 Å level.

The correct pose will be capable to induce the appropriate conformational change and the other possibilities may not induce this conformational evolution, but they also means that a low percentage of the ligands are "useful". Obviously, the ideal situation is take ligands with just a few cluster, with a high-populated main cluster, where a high percentage of ligands complex with the receptor properly. To scan quickly among the results how many ligands are more or less selective, we introduced the parameter $\boldsymbol{\sigma}$, which is:

$$\sigma = \sum_i \frac{n_i}{n_l} \qquad [1]$$

where the summation is along all the i clusters, n_i is the population of cluster i and n_l is the population of the larger cluster. This parameter takes values from 1 to infinite and the lower value (closer to 1), the greater selectivity the ligand has. So, the best ligands will be those with low inhibition constants (nM) and low cluster selectivity.

Analysing **Table 8**, it is observed tripeptides are poor candidates, due to the low selectivity and the great range of clusters. Dipeptides are better, showing medium selectivities and inhibition constants at nanomolar range. There are no special differences between Phenylalanine and Tyrosine: inhibition constants may vary around between 100 - 130 nM in ester containing compounds.

Docking binding pose analysis shows always an ionic bridge as main anchor between the basic amine of the ligands and Asp147 of receptor. Visual inspection was realized to check reasonable poses and no strange effects like steric clashes.

As the docking studies were performed with a fixed receptor (no freely moving groups), a refinement of the complex structure between ligand and receptor is required. However, the docking study serves as initial screening of compounds, selecting the best hits. Our purpose was take a discrete number of leads, accordingly with the docking results, synthetize them, and perform biological test to demonstrate whether or not they were truly μ opioid receptor agonists. Once justified their biological potential, a molecular dynamics refinement was performed to explore in deep the nature of the binding and the differences between candidates.

In this work, we take candidates **D1**, **D2**, **D3**, **D8**, **D15**, **D16**, **D20**, **D23** and **D26**, to prepare them in laboratory (**Fig. 58**). The selection criteria were these:

- Parent compounds (group 1): despite of having inhibition constants in the micromolar range, **D1** and **D2** were submitted to the biological trials. They were already synthetized and served as "negative controls".
- Monosubstitutions was preferable than multisubstitutions. This leaded to a better understanding of the effects of the substitutions.
- Quaternary amines (group 2): due to the boosting properties of incorporating phenyl substituents at the amine position, **D3** and **D15** are attractive agents in testing this effect.
- Phenyl esters (group 3): the structural simplicity of **D8**, **D16** and **D20** and the good values of σ and inhibition make these ligands as promising μ opioid receptor inhibitor prototypes.
- *L*-Phenylalanine based dipeptides (group 4): as several dipeptides shown good docking characteristics, the positional isomers **D23** and **D26** were also included in the elaboration scheme. And besides, the coupling scheme between amino acids is simple, no requiring protecting groups (contrary to *L*-Tyrosine, which hydrody group might interfere in the coupling reaction).

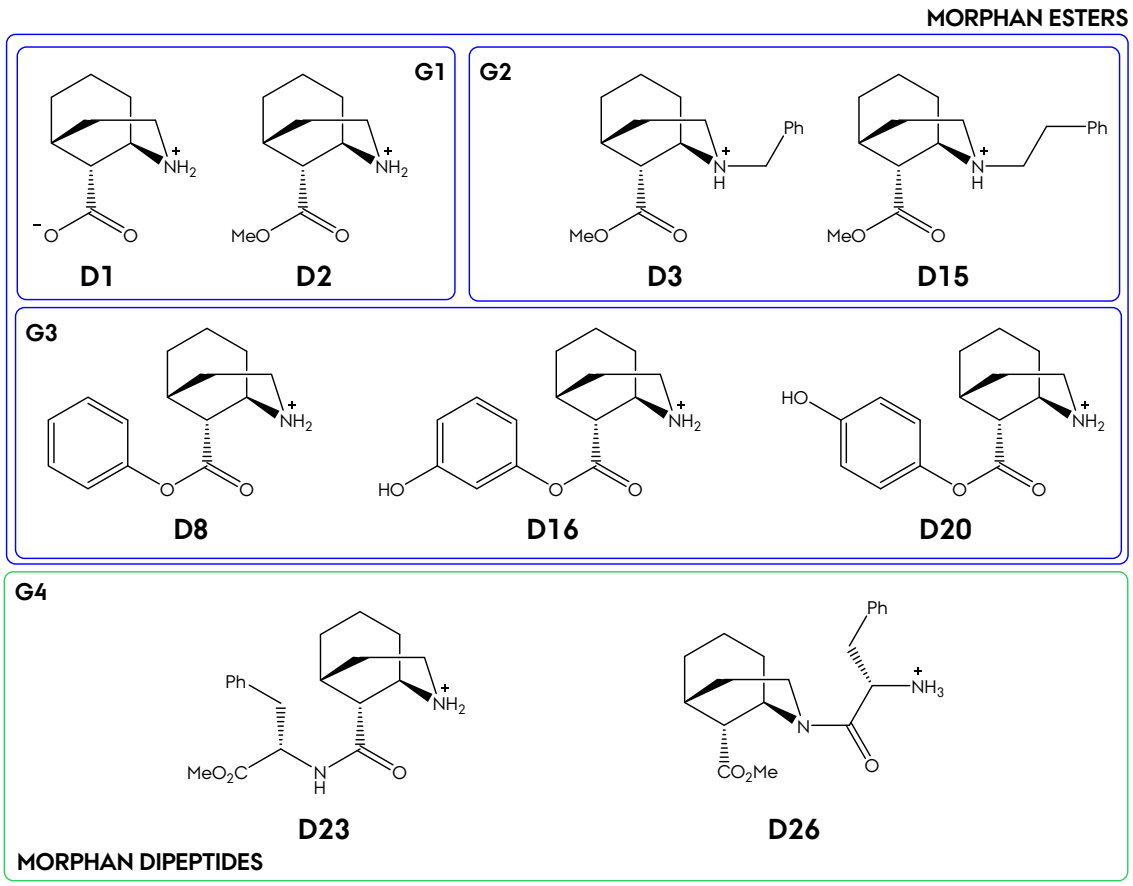

Figure 58. Selected hits to the laboratory synthesis.

Lead Compounds Synthesis.

In this section, lead compounds elaboration obtained from the docking analysis is explained. Starting from parent compound **26**, the ligands were obtained in few steps employing routinely procedures.

Group 2 compounds (quaternary amines) were easily synthetized from aminoester **26** in one step with a controlled *N*-alkylation[25] (**Sch. 41**).

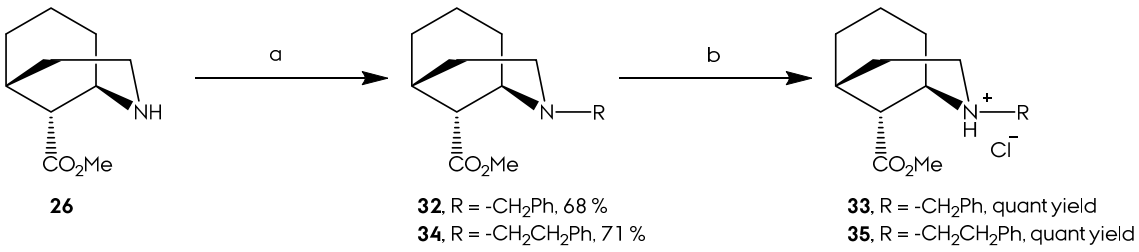

Scheme 41. *Reagents and conditions*: (a) RBr, DIPEA, MeCN, rt, (M47 and M49). (b) HCl (g), EtOH, (M48 and M50).

This procedure avoids the polyalkylation of the amine, obtaining in moderate/good yields the corresponding tertiary amines. Dissolving the alkylated compounds in ethanol and bubbling hydrogen chloride resulted in forming the chlorhydrates **33** and **35**, which were yielded through solvent removal at reduced pressure. The identities of the salts were confirmed by mass spectrometry, and the alkylated structures were checked by ^{1}H NMR as well (**Fig. 59**).

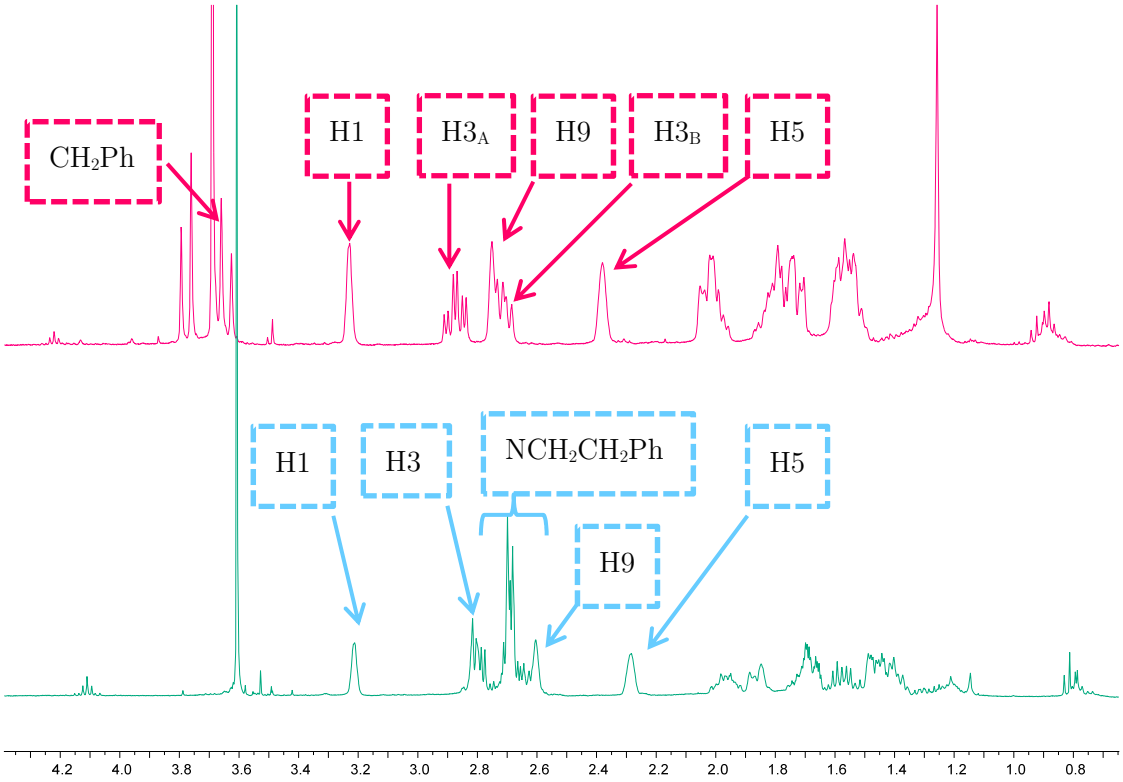

Figure 59. Comparison of ^{1}H NMR spectra of morphans **32** (pink) and **34** (blue) at the 1.0-4.2 ppm range.

Group 3 compounds (phenyl esters) synthesis is also affordable from **26**; nevertheless, requires additional protection of the amine group to avoid handling problems due to solubility issues of amino acid **27**. Consequently, the first step is the protection of the aminoester **26** as the *tert*-butoxycarbamate **12** with Boc_2O and DIPEA (**Sch. 42**).

Chemoselective hydrolysis of the ester with LiOH afforded the acid in 94 % yield. Finally esterification with the phenols was carried out using typical amide coupling reagents, HOBt and EDCI, in a mild way. Phenyl esters were obtained in good yields.

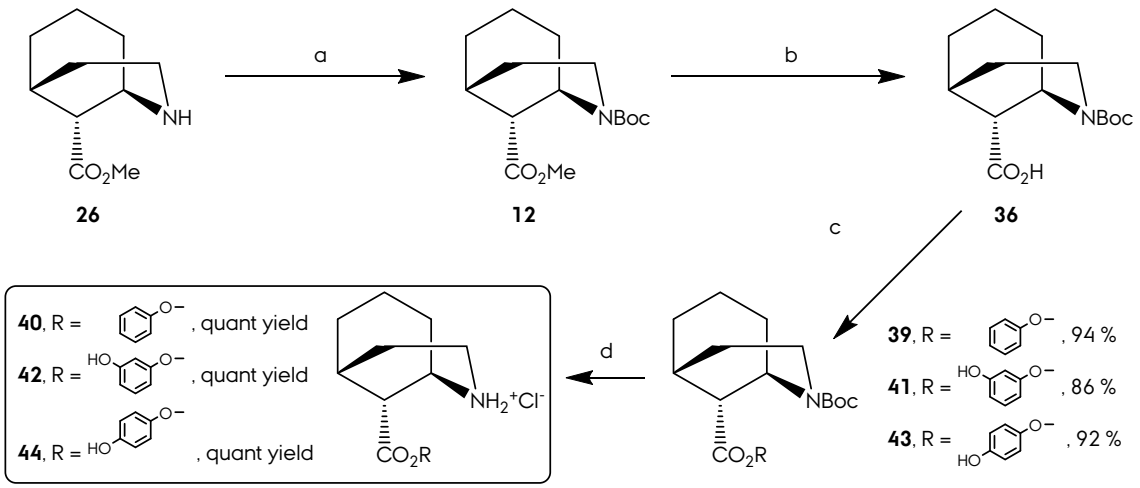

Scheme 42. *Reagents and conditions*: (a) Boc_2O, DMAP, DCM, rt, 97 % (M51). (b) LiOH, MeOH/THF/H_2O 3:1:1, h, 94 % (M52). (c) ROH, EDCI, HOBt, DIPEA, DMF, 24 h (M55, M57 and M59). (d) HCl (g), EtOH, (M56 , M58 and M60).

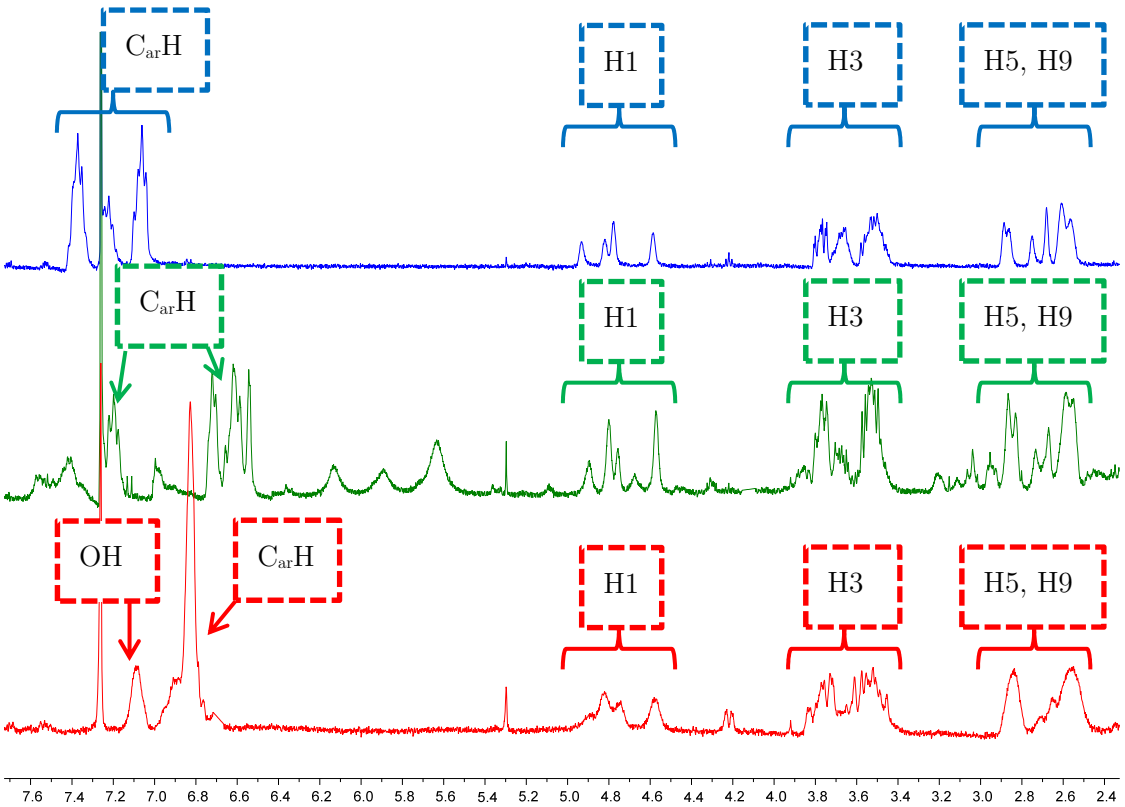

Figure 60. Comparison of ^{1}H NMR spectra of morphans **39** (blue), **41** (green) and **43** (red) at the 2.4-7.6 ppm range.

Boc protected morphans **36**, **39**, **41** and **43** showed also rotamers at room temperature in ^{13}C and ^{1}H NMR spectra (**Fig. 60**), which was predicted by conformational analysis in the previous chapter. Heteronuclear correlation

spectroscopy (HMQC/HMBC) was fundamental to identify correctly these compounds, together with mass spectrometry (see 2D NMR Experiments).

Chlorhydrates were obtained employing previously described conditions (bubbling hydrogen chloride in an ethanol solution where compounds were dissolved). Mass spectrometry confirmed the presence of the chloride salts.

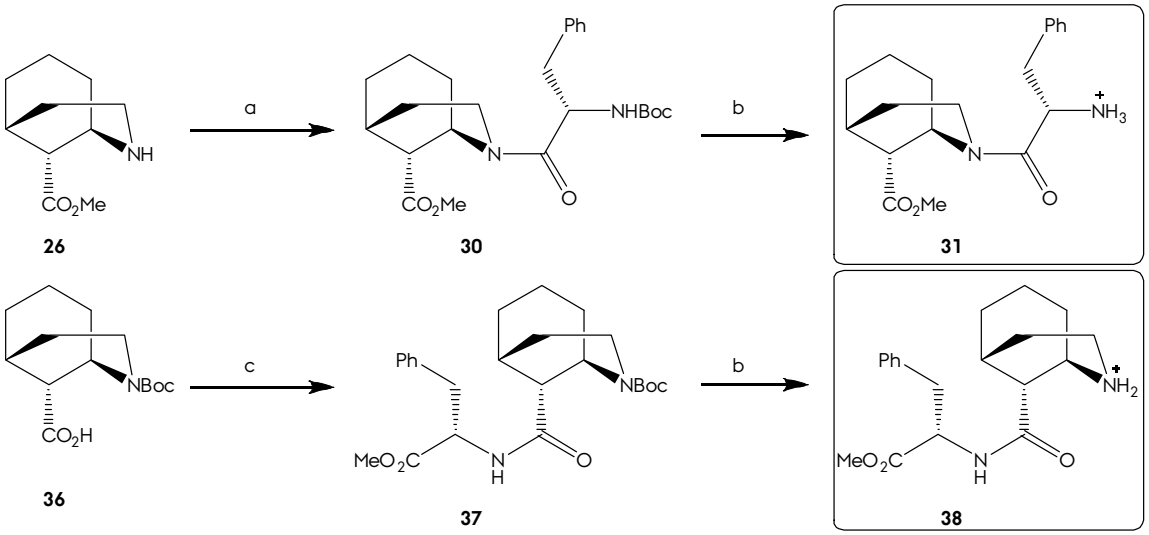

Scheme 43. *Reagents and conditions*: (a) Boc-Phe-OH, EDCI, HOBt, DIPEA, DMF, 24 h, 30 % (M45). (b) HCl (g), EtOH, quant yields both reactions (M46, M54). (c) [H_2-Phe-OMe]Cl, EDCI, HOBt, DIPEA, DMF, 24 h, 62 % (M53).

Last synthetic scheme corresponds to group 4 of lead compounds: the morphan dipeptides (**Sch. 43**). Both dipetides **30** and **37** were easily prepared by peptide coupling of the appropriate protected amino acids in one pot with EDCI and HOBt as activating agents. Forward acid deprotection of the amines afforded the salts **31** and **38** with quantitative yields. Again, protected compounds exhibits rotamers at ^{1}H and ^{13}C NMR spectra (**Fig. 61**).

Once synthetized the docking predicted leads, competition binding assays were carried out. The purpose was verify that the designed compounds are truly opioid ligands. The methodologies are described in the Methodologies and Materials section while the results are presented in chapter 4.

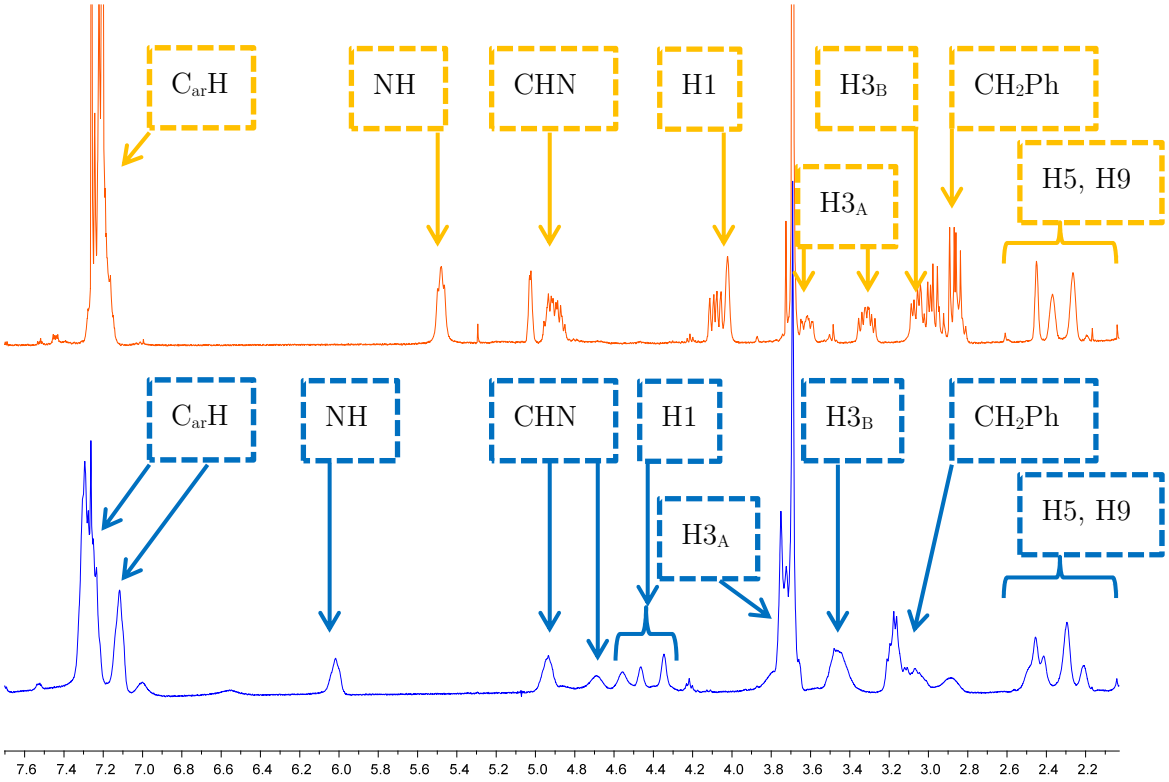

Figure 61. Comparison of ^{1}H NMR spectra of morphans **30** (orange) and **37** (blue) at the 2.4-7.6 ppm range.

Molecular Dynamics of Ligand-Receptor Complexes I: Design of the Simulations.

Biological tests of the submitted compounds shows that phenyl esters **40**, **42**, **44** (**D8**, **D16**, **D20**) and aminoester **35** (**D15**) have good affinities in the binding displacement assays.

Once experimentally confirmed, is necessary to take again the docked results of these compounds and refine the structure by MD simulations. The target of a MD refinement is:

- Recover receptor flexibility: although many docking programs have sidechain flexibility incorporated, start with a flexible-ligand rigid-receptor docking and continue with an MD simulation with a fully flexible complex is now commonplace.

- Environmental effects: docking procedures only consider receptors and ligand, neglecting solvent, ions, membranes … MD simulation allows incorporating all enzyme environments explicitly. The closer the simulation system to a real one, the more similar results will be obtained.

- Magnitudes measure: accordingly with statistical mechanics, the value of a macroscopic magnitude is the result of the average value of the microscopic one over a large set of systems, the ensemble. Ergodic hypothesis states that the average value of a magnitude measured over the ensemble trends to equalize to a time average magnitude measured in just one system:

$$\langle \theta \rangle_{ensemble} = \langle \theta \rangle_{time}$$

  Consequently, a MD simulation over certain period of time will capable of supply a magnitude value that corresponds with the experimental value.

- Conformational changes: MD simulations may predict the conformational change upon complexetion. However, it depends of the nature of the input docking receptor structure. If the receptor have already adopted the change, i.e. is an active state, the changes at the MD simulation level may not be relevant.

In this study, a MD refinement simulation in explicit water and membrane was carried out, in order to recover protein flexibility and adequate the protein to its normal environment. As opioid receptors are membrane bound proteins, this situation added an extra complexity level. First, as in the case of the docking stage, a MD simulation protocol is required. This protocol must follow some advices:

- Input structure: in a docking type refinement, this is usually the docked complex structure.

- Force field selection: the choice of the force field is sensitive, as a high quality set of parameters is required to describe molecular interactions properly. Among the most used distinguish AMBER[26] and CHARMM[27] sets of force fields.

- Parametrization and charge method: non-parametrized residues in the force fields like ligands need to be correctly parametrized. AMBER has a parametrization module (Antechamber) which assigns atom types and charges from a generalized force field for organic molecules.

- Solvent and ions: the system needs to be soaked in a box of the solvent of choice. Ions need also to be added till neutralization or certain concentration.

- Membranes: if the receptor is membrane bound, a pre-equilibrated lipid bilayer is also required. Several packages or web based services allows to add a lipid bilayer of a certain geometry and composition.

- Minimization stages: once the MD simulation system is assembled, a series of minimization steps helps to relax the system and avoids the appearance of artefacts like bubbles or solvent discontinuities. A constraint tree is created to minimize the system at different levels.

- Heating stages: one or two heating steps warm the system till the production temperature. Constraints are also used to control the process evolution.

- Equilibration steps: before the production step, the constraints are gradually retired to prepare the system to the final stage.

- Production stage: once heated and equilibrated, the system is subjected to the simulation for a certain period of time (depending on the study, the system and the results required).

Taking into account these considerations, the system setup up protocol is defined:

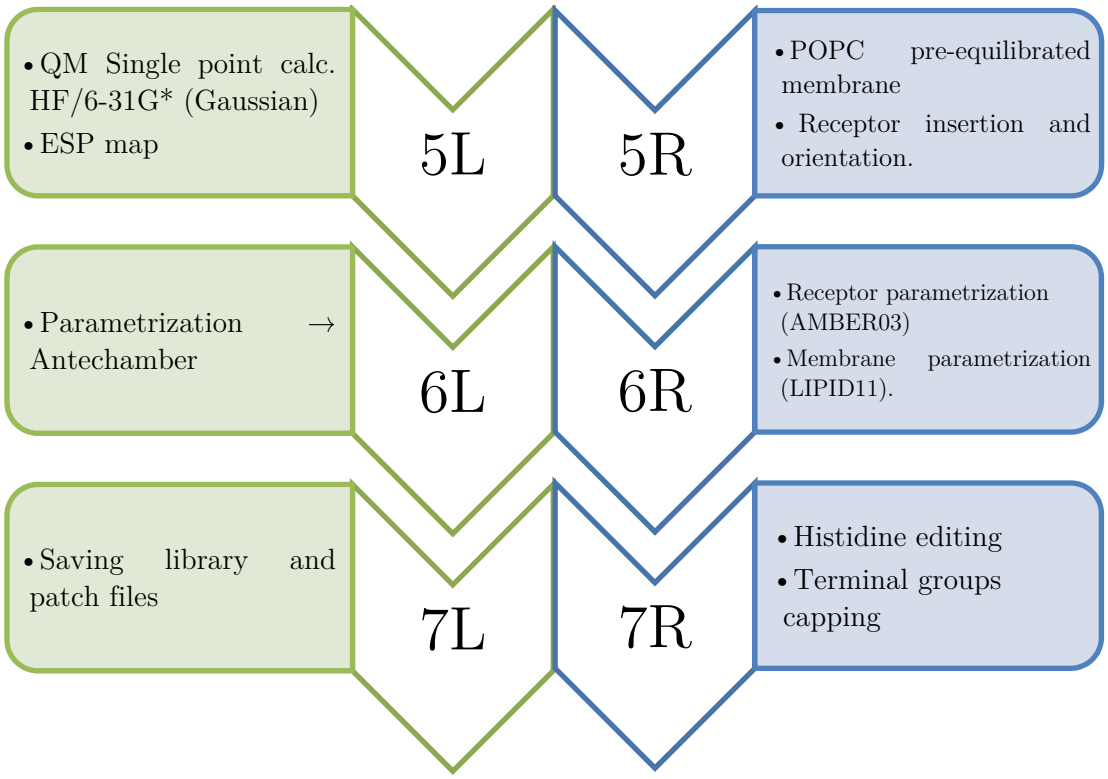

3C

- System assembly
- 10Å solvent shell (z direction): TIP3P
- NaCl added till 150 mM

On the other hand, a POPC pre-equilibrated bilayer of 75x75 Å was taken and combined with the receptor. Orientation of the protein was achieved by the OPM server.[28] Lipid molecules that clash with protein atoms were removed. Xleap module of AMBER was used for the last assembly stages. Membrane bounded protein was loaded and parametrized with AMBER03[29] (protein) and LIPID11[30] (POPC bilayer). Renaming of histidines and terminal group capping were last receptor steps.

Finally, ligand and membrane bounded protein were merged. A 10 Å TIP3P[31] water shell was added in the z direction. Sodium and chlorine ions were added, neutralizing the system till a final 150 mM concentration (**Fig. 62**).

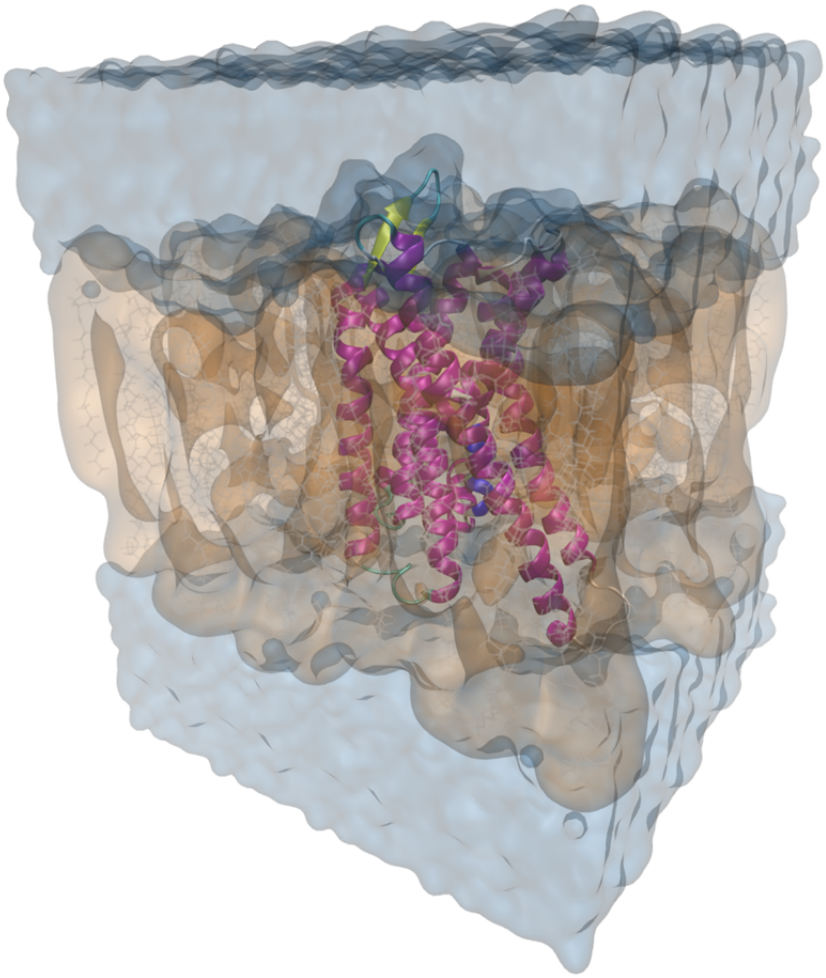

Figure 62. Assembled simulation system.

Once assembled the system, it was submitted to the MD simulation protocol:

All the MD simulations were performed with NAMD.[32] First, the system was minimized by stages, using five constraining levels (water/ions, POPC bilayer, protein backbone, alpha protein carbons and all unrestrained). In each one of the relaxing levels, 2000 steps of conjugate gradient were performed.

Secondly, the minimized system was heated by stages again, repeating a constraining hierarchy. First, the overall system was frozen except the membrane slab, which was heated at 150 K along 200 ps at the NVT ensemble, followed by a second heating step from 150 to 300 K along 200 ps at the NPT ensemble. In this step, all the atoms were allowed to move, excluding alpha carbon of the protein, which were subjected to a positional harmonic constraint of 1 Kcal/(mol $\cdot$ Å^2). Once heated, the constraining scheme continued for an extra 200 ps.

Finally, the harmonic constraints were retired and the system was subjected to a 5 ns constant pressure molecular dynamics simulation. Langevin Dynamics were applied at 1 atm and 300 K, with a Langevin damping coefficient of 2. Non-bonded interactions were calculated with the specified force fields (AMBER03 for protein, waters and ions; LIPID11 for POPC, GAFF for ligands) and applying Particle Mesh Ewald method[33] (PME) for long-range electrostatic forces in a periodic boundary condition context. A 10 Å cutoff was used together with a switching function between 9 - 10 Å. SHAKE algorithm was applied to freeze all bonds involving hydrogens, so a time step of 2 fs was applied.

Molecular Dynamics of Ligand-Receptor Complexes II: Topological Results.

In this chapter, the topological analysis of the MD simulation systems is discussed. The morphine-μ opioid receptor complex, as the validation system, is the first to be analysed.

Figure 63 shows the root mean square displacemet (RMSD) plot of unconstrained protein atoms along the simulation. It´s clearly to see that the system stabilizes at 1.5 ns and the average of the RMSD at the 1.5 - 5 ns range is 2.3 ± 0.1 Å.

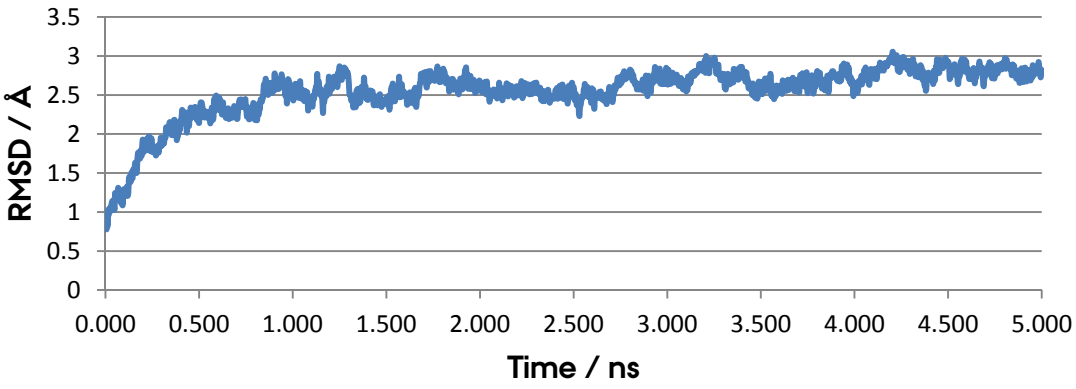

Figure 63. Plot of the RMSD of the morphine-μ opioid receptor complex along 5 ns.

Figure 64 shows the binding pose of morphine in the μ opioid receptor binding pocket after 5 ns of simulation time. The predicted binding mode is similar to the interaction model described afterwards, and also other molecular modelling studies have predicted a closer pose.

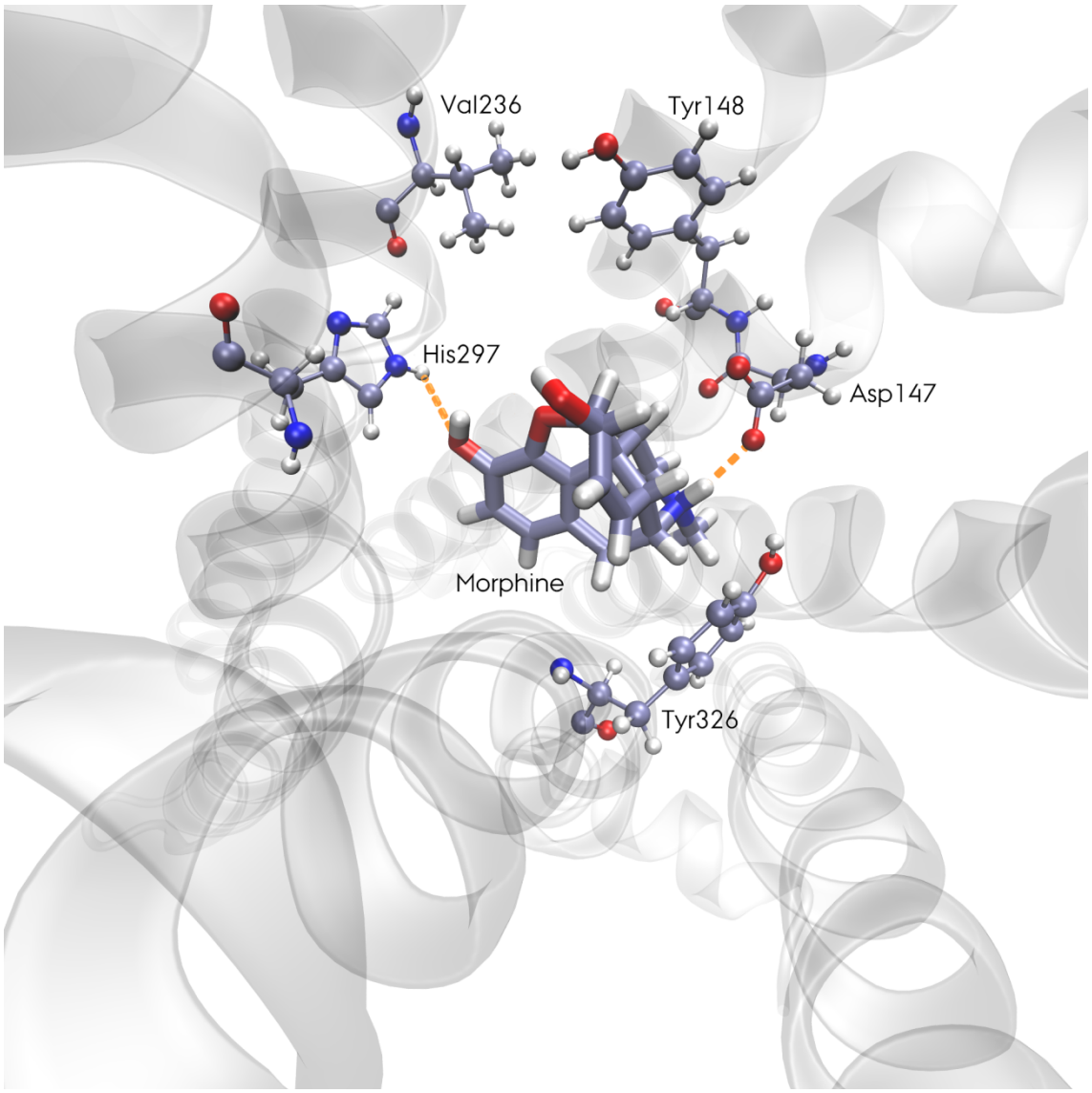

Figure 64. Binding pose of morphine after 5 ns. Relevant residues are depicted and protein ribbons are ghosted.

The main interaction is the salt bridge between the basic amine and carboxylic group of Asp147. The binding pocket have hydrophobic residues, like Val236, Ile322, Ile234, Val300, etc. A second anchor is the dipolar type interaction between Morphine and His297, establishing a hydrogen bond between the phenolic oxygen of the ligand and the amine hydrogen of the imidazole. Nevertheless, the acceptor/donor scheme of the ligand remains unclear, due to the flip of the imidazolic ring, which may reverse the electron density flow. A plot of both distances is depicted in **Figure 65** (last 500 ps). The salt bridge between the carboxylic group of Asp147 and the protonated amine was kept below 2.0 Å, with an average of 1.8 ± 0.1 Å. On the other hand, the hydrogen bond between His 297 and

the phenolic group of morphine is a little more fluctuating, with an average of 3.0 ± 0.5 Å.

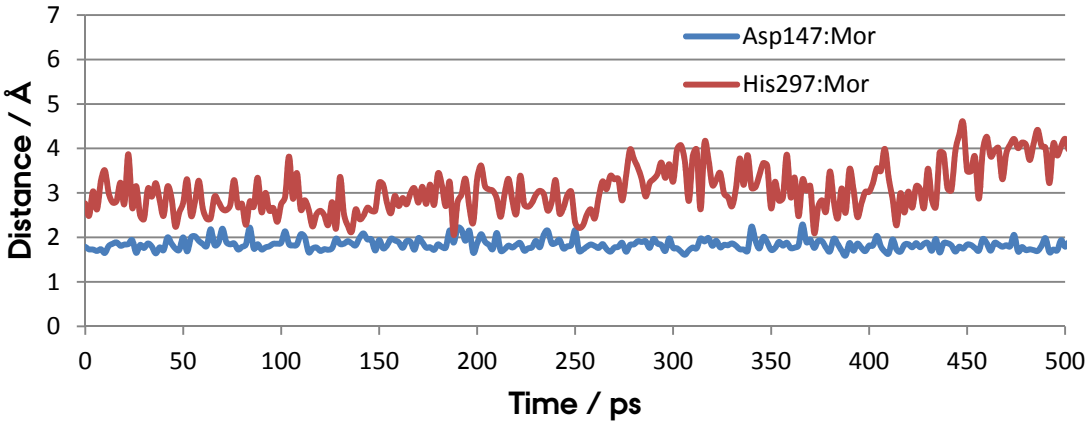

Figure 65. Graphical evolution of the interactions between morphine and Asp147 and His297.

Tyr326, Tyr148 and Trp318 complete the binding pocket residues list, closing the hydrophobic area for the ligand.

In summary, the binding pose of morphine matches the predicted mode in other studies. This served as reference to study the morphan ligands.

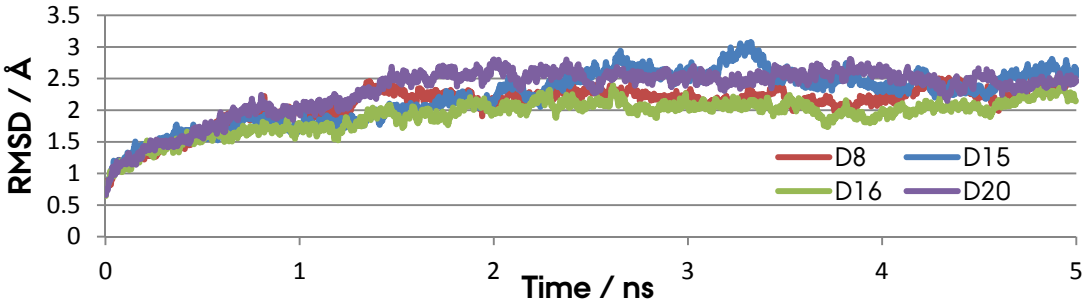

Figure 66. Plot of the RMSD of the mu opioid complexes between **D8**, **D15**, **D16** and **D20** with MOP.

Before starting the discussion about binding topologies of the lead compounds, the quality of the simulations is checked. RMSD plot of the four simulations are schematized in **Figure 66**. The four systems reached stabilization after 2 ns, ignoring **D15**, which took more time to stabilize, at 3.5 ns. The average of the RMSD at the 3.5 - 5 ns range was: **D8**, 2.2 ± 0.1 Å; **D15**, 2.4 ± 0.1 Å; **D16**, 2.0 ± 0.1 Å; **D20**, 2.5 ± 0.1 Å. As the systems were correctly stabilized, we conclude that the systems are ideal to study.

Ligand **D15** shows a binding mode different from morphine (**Fig. 67-68**). The more simplified the structure, the less conservative binding mode is found. Observing the complex, an ionic bridge between the protonated amine and the Asp 147 is established between ligand and receptor, in a similar way of morphine (**Fig. 69**).

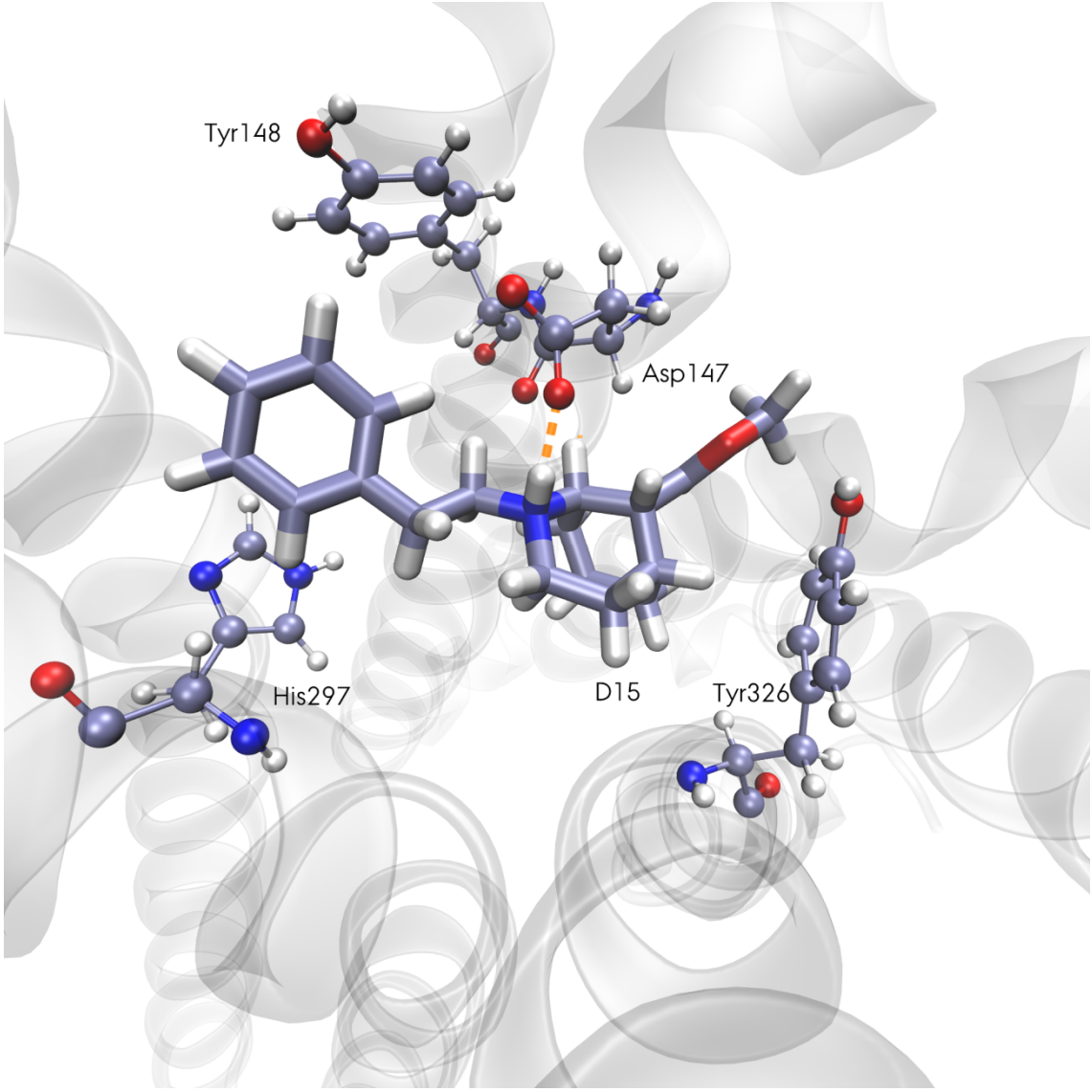

Figure 67. 3D binding pose of **D15** after 5 ns. Relevant residues are depicted and protein ribbons are ghosted.

Flip between oxygens of the carboxylic group is observed, due to a jump in the distance trend (**Fig. 69**, 2.5 ± 0.3 Å average). Nevertheless, the orientation of the 2-azabicyclo[3.3.1] is turned, around 120º around a hypothetical orthogonal axis to the C-ring of morphine (**Fig. 70**).

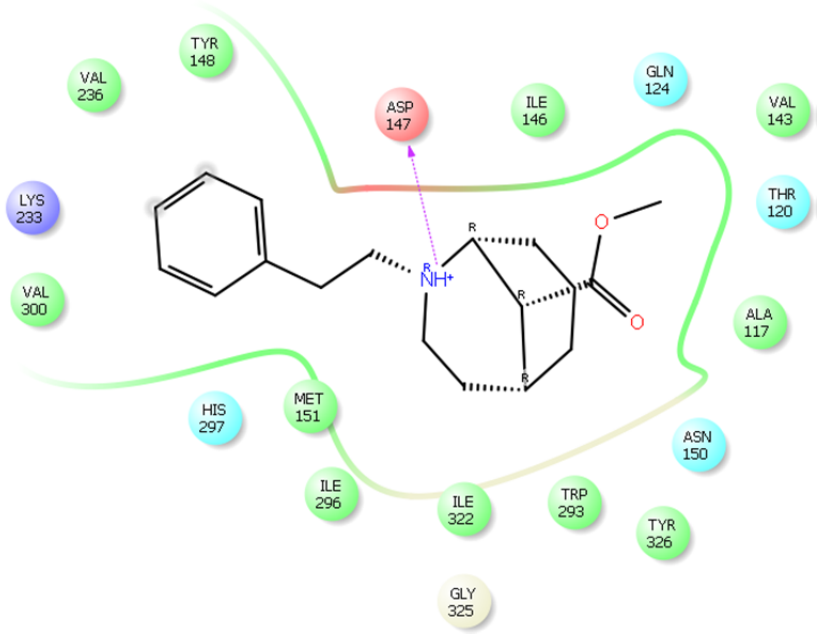

Figure 68. 2D binding pose of **D15** after 5 ns.

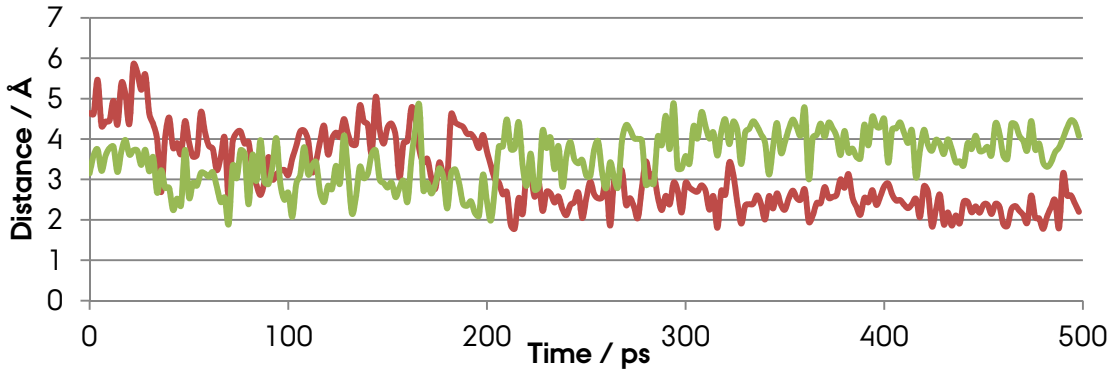

Figure 69. Distance plot of the ionic bridge between Asp147 and **D15**. Red line is distance NH · · · OaCO and green line is distance NH · · · ObCO.

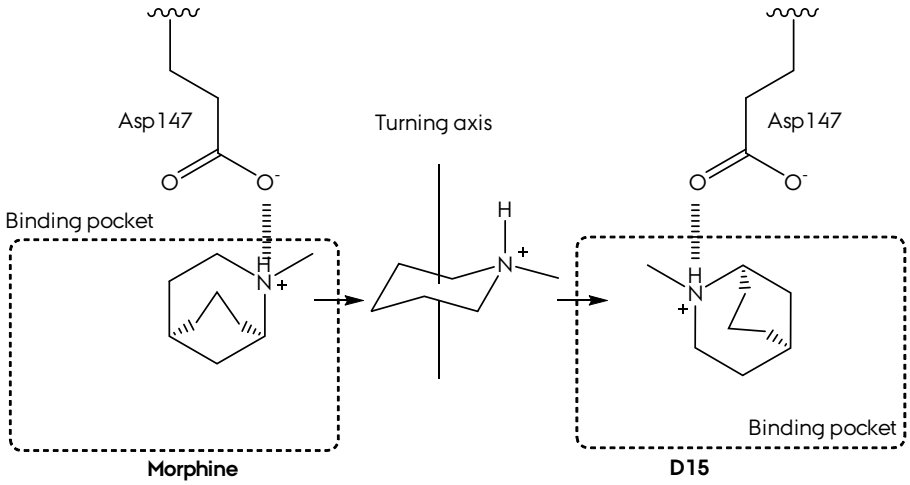

Figure 70. Drawing of the turn of the morphan core between morphine and hit **D15**. Only 2-azabicyclo[3.3.1] is depicted. The turn is made around an orthogonal axis to the morphine C-ring.

The ester group of **D15** is oriented towards a small pocket made by Ile146 and Ala117. Considering the phenylethyl moiety, this chain is placed in the large hydrophobic site of the pocket, between residues Ile296, His297, Val236, Tyr148 and Met151. Special interactions take place between aromatic ring of the ligand and Tyr148 and His297. Along the simulation, the phenyl ring was found slightly bent to the imidazolic ring of His297, in a typical CH/π stacking interaction. Aromatic ring of Tyr 148 also interacts punctually, with the consequently weak solapation of the aromatic rings. These two long-range dispersion interactions are likely responsible of keeping the phenyl moiety in this area of the binding pocket along the simulation.

Phenyl esters topological study showed a similar behaviour to **D15**. **D8** binding poses is mainly maintained by the typical ionic bridge between the protonated amine of the morphan core and the bidentate anionic group of Asp147. However, an additional anchoring point is set between the other hydrogen of the protonated amine and the carbonyl group of Asn150, a hydrogen bond (**Fig. 71-73**). Again, the bicyclic core has been turned, but in this occasion the turning axis belongs to the plane of the C-ring of morphine. Turning 180º resulted in the new placing of the morphan core (**Fig. 74**).

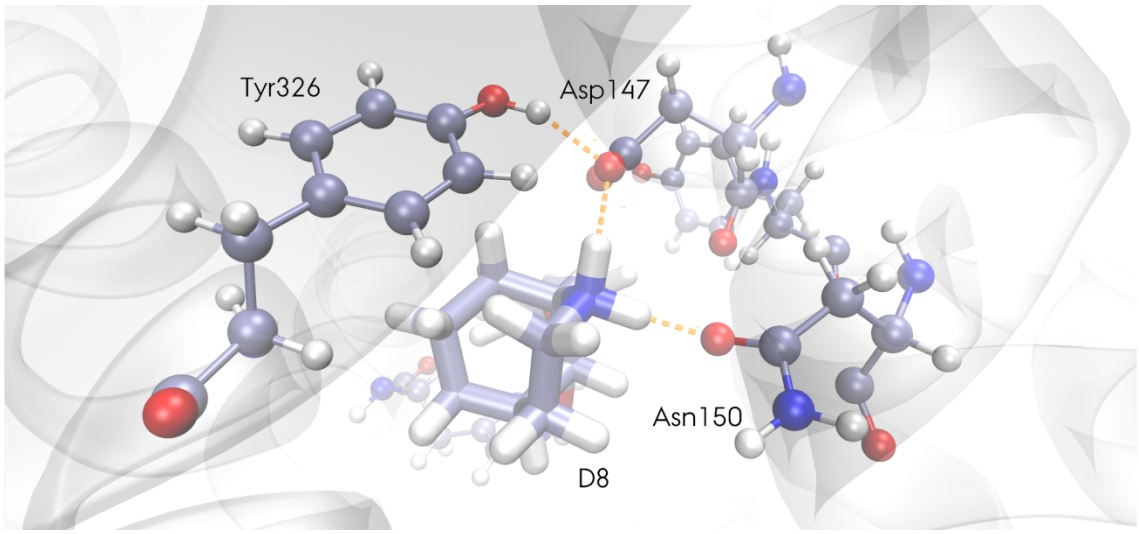

Figure 71. 3D back binding pose of **D8** after 5 ns.

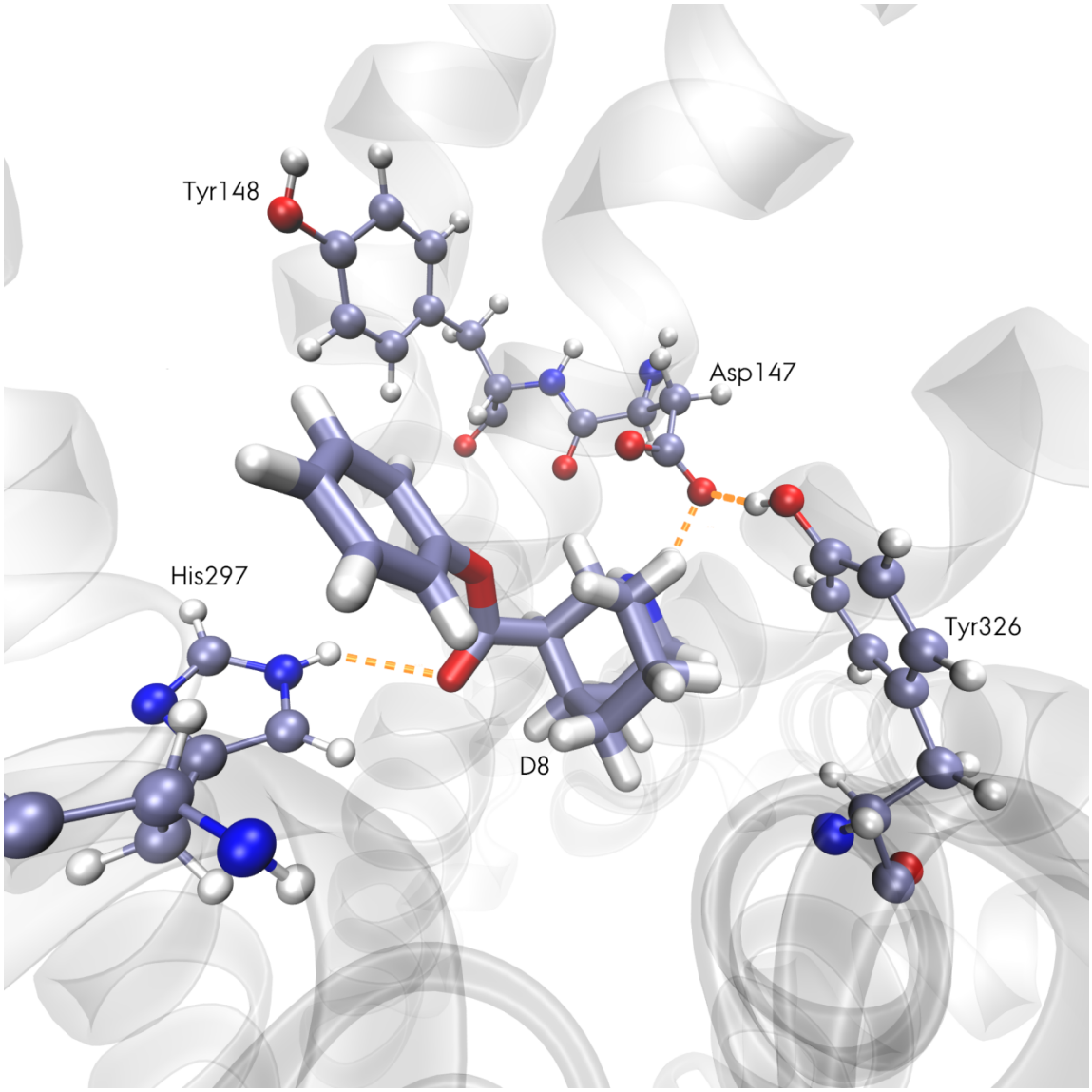

Figure 72. 3D binding pose of **D8** after 5 ns. Relevant residues are depicted and protein ribbons are ghosted.

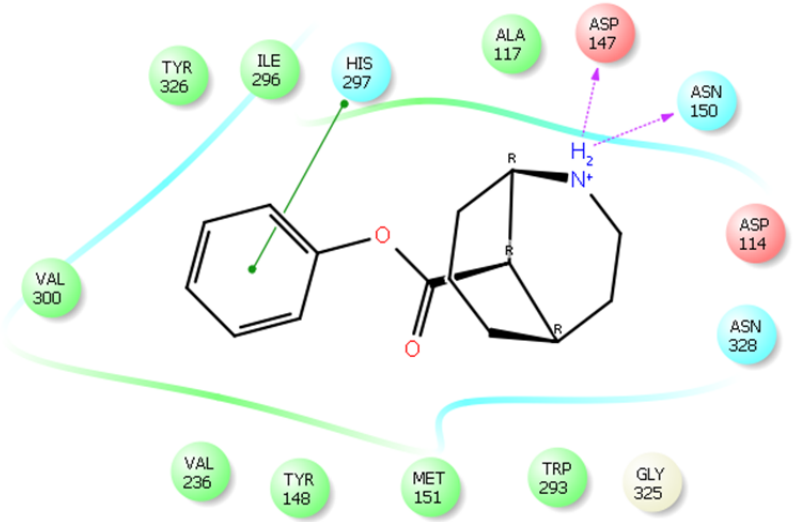

Figure 73. 2D binding pose of **D8** after 5 ns.

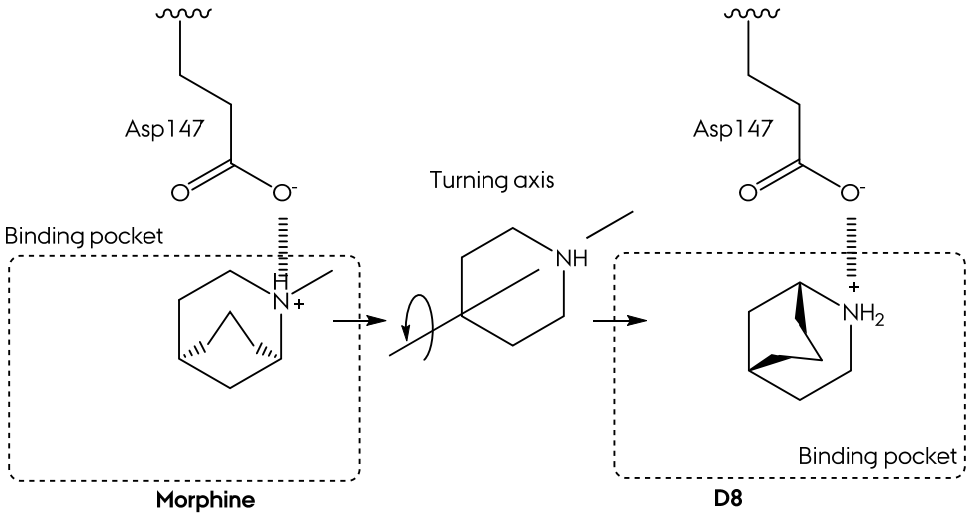

Figure 74. Drawing of the turn of the morphan core between morphine and hit **D8**. Only 2-azabicyclo[3.3.1] is depicted. The turn is made around a coplanar axis to the morphine C-ring.

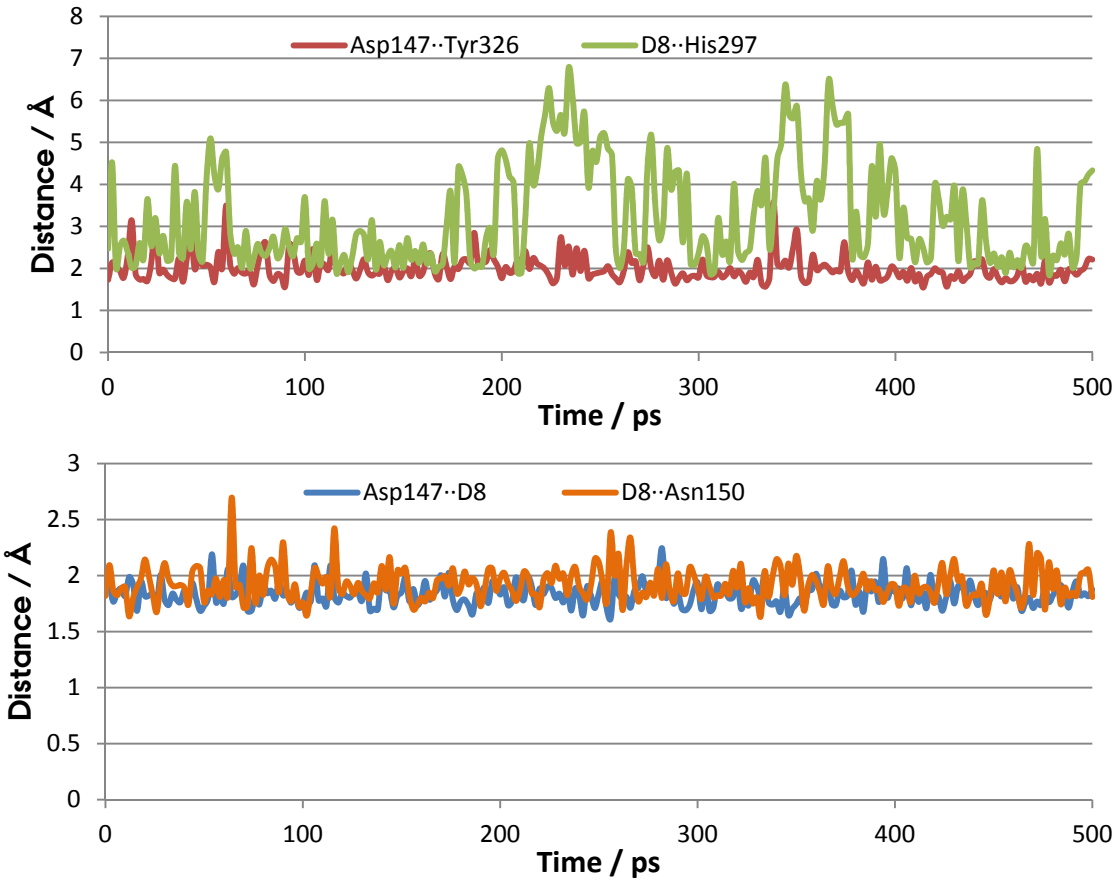

Figure 75. Graphical representation of interactions between **D8** and selected residues.

Regarding the ester group, the phenyl moiety is oriented towards the large hydrophobic cavity, in a similar fashion as **D15**. In this case, the aromatic ring of the ligand is closer to the imidazolic ring of His297. This proximity leads to a π – π

stacking interaction between the rings. This interaction could be checked through distance plotting between intermolecular distance of atoms of both rings. The achievement was made measuring three distances and comparing between them: if the three distances are equally kept, then the relative disposition of both rings is almost parallel, allowing the aromatic interaction (**Fig. 76**). Additionally, a hydrogen bond is frequently established between the NH group of His297 and the carbonyl group of ligand's ester.

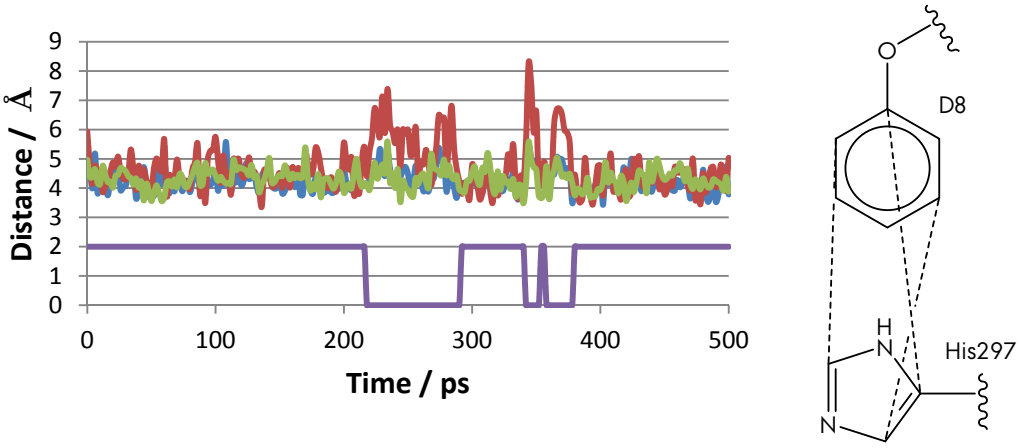

Figure 76. Left: Plot of three interannular distances. The purple value divide interaction regions (value = 2) and no interacting areas (value = 0). Right: sketch of the three taken distances.

D16 binding pose (**Fig. 77-78**) is almost similar to **D8**: a main ionic bridge interaction between the protonated amine of the ligand and the carboxylic functional group of Asp147, with a turned morphan core. This ionic interaction is shared between the two protons of the amine and the two oxygens of the carboxylate group of Asp147.

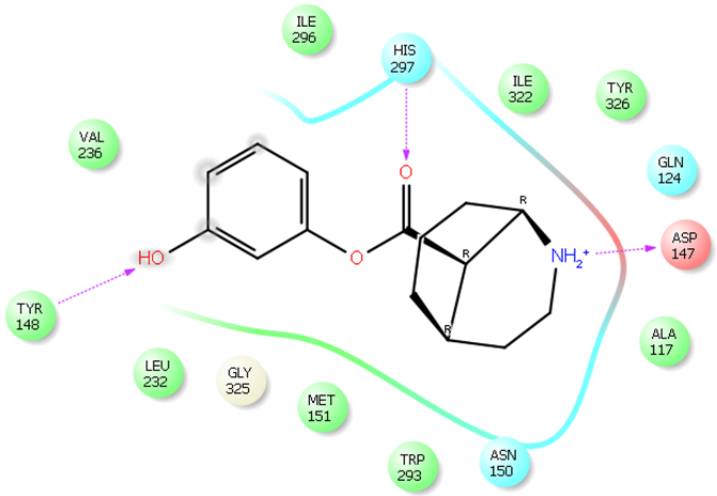

Figure 77. 2D binding pose of **D15** after 5 ns.

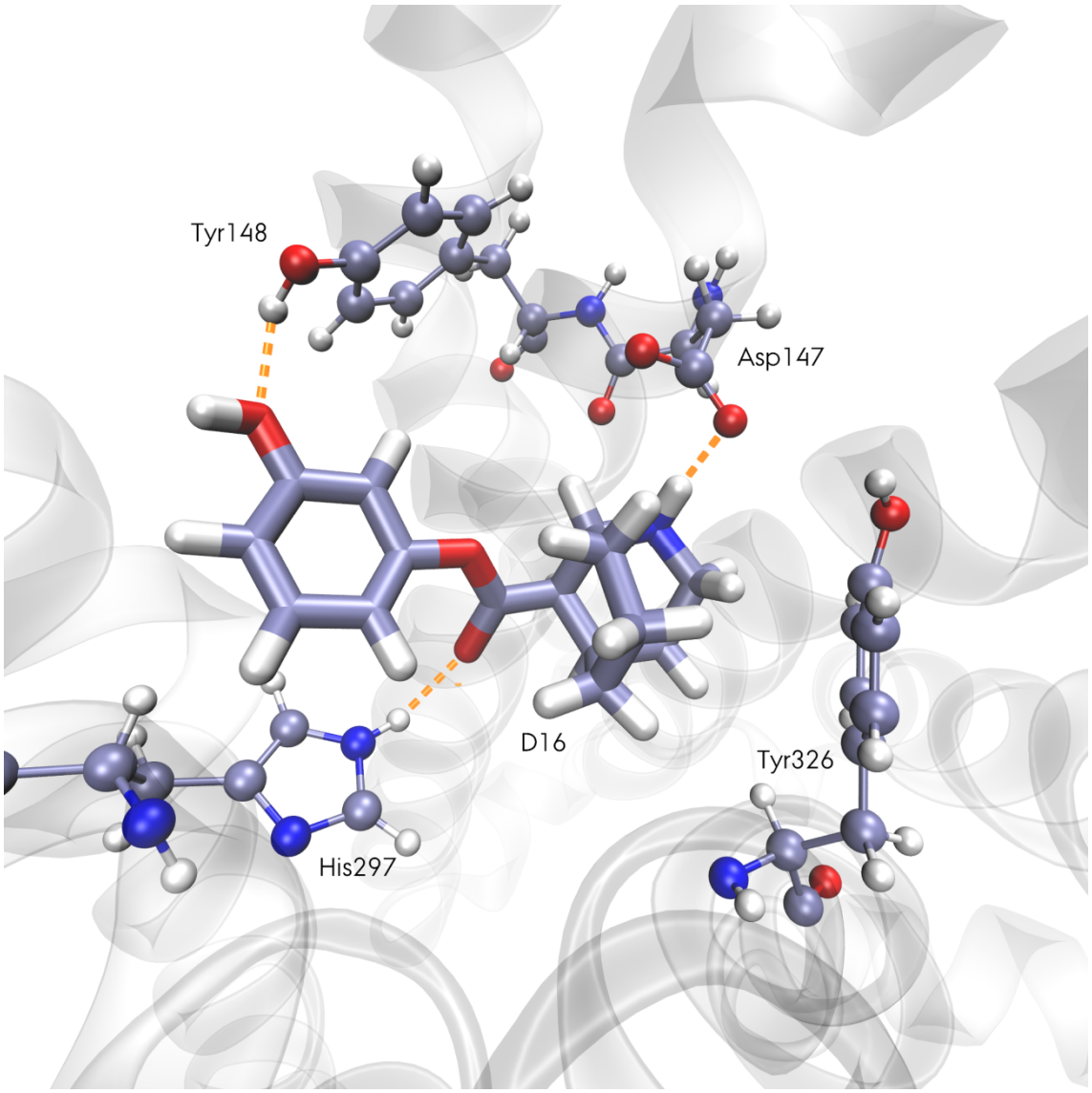

Figure 78. 3D binding pose of **D16** after 5 ns. Relevant residues are depicted and protein ribbons are ghosted.

Figure 79 shows a combined plot. On the right, a plot of three distances: NH1-O1 distance, NH1-O2 distance, and, NH2-O1 distance. It´s is clear to see this sharing is a consequence of the dynamics behaviour of the system, and this fluctuation is typical in the study of interactions between polydentate groups. In these cases, is easy to study the radial distribution of the distance between the two sets of atoms: basic amine hydrogens and carboxylate's oxygens (left-side plot). There are two maxima: at 1.85 Å (the shorter distance between groups, sharp), and at 2.75 Å (the larger one, broad). The turning scheme is similar to **D8**, with the turning axis placed in the C-ring plane, and a 180º turn.

Talking about the side aromatic chain (the 3-hydroxyphenyl ester group), the presence of the hydroxyl in position 3 has the consequence of interacting with Tyr148 phenolic group through a hydrogen bond (2.0 ± 0.3 Å average), in such a way that the π – π stacking interaction between imidalozic ring of His297 and the phenolic ring of **D16** is weaker than **D8** (**Fig. 80**).

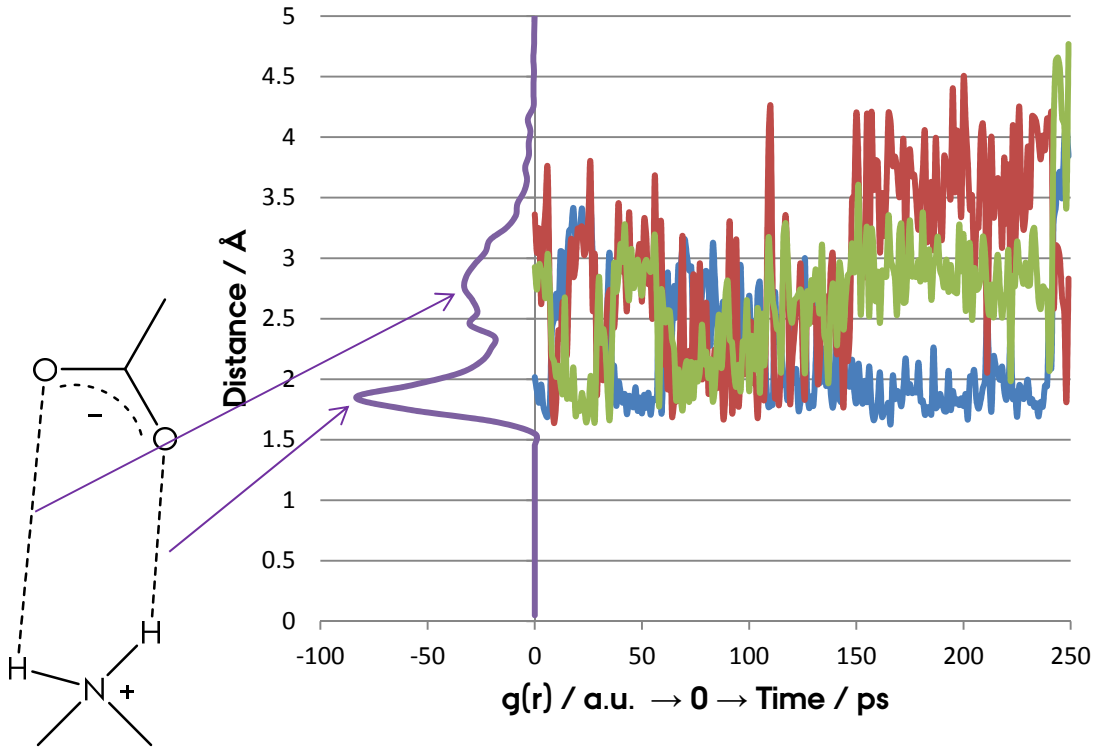

Figure 79. Rigth: plot of the three shorter NH · · · O distances in the **D15-μ** opioid receptor complex in the last 250 ps. Left: Radial distribution function of the distance NH · · · O.

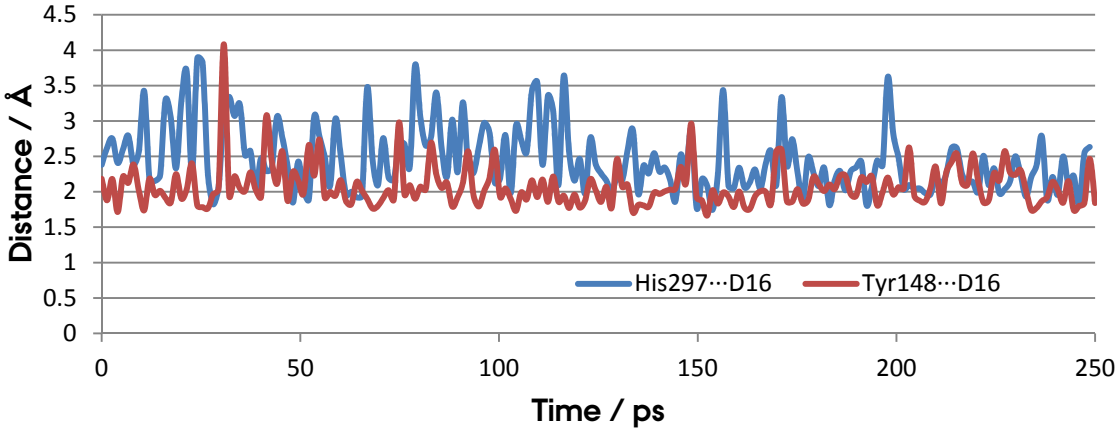

Figure 80. Graphical representations of the interactions between **D16** and His294 and Tyr446.

However, interaction between His297 and **D16** elapses by a hydrogen bond between the carbonyl group of the ester of **D16** and the hydrogen of the imidazolic amine.

The distance average is 2.4 ± 0.5 Å. It´s remarkable to note the hydrogen bonding between phenolic groups has the consequence of turning aside the carboxylic group of Asp147 from the proximity of Tyr326, avoiding the formation of a hydrogen bond between this two residues, as in the previous case.

Finally, **D20** is last ligand analysed (**Fig. 81-82**). Figure cc shows the binding pattern of this morphan phenyl ester, isomer of **D16**. The binding profile is similar to both **D8** and **D16**: a turned morphan backbone with an ionic anchor between protonated amine and acid group of Asp147. In this case, the residue acts in a polydentate fashion, with the carboxylic acid group interacting with one of the amine´s hydrogen and the carbonyl of the peptide bond interacting with the other one (**Fig. 83**).

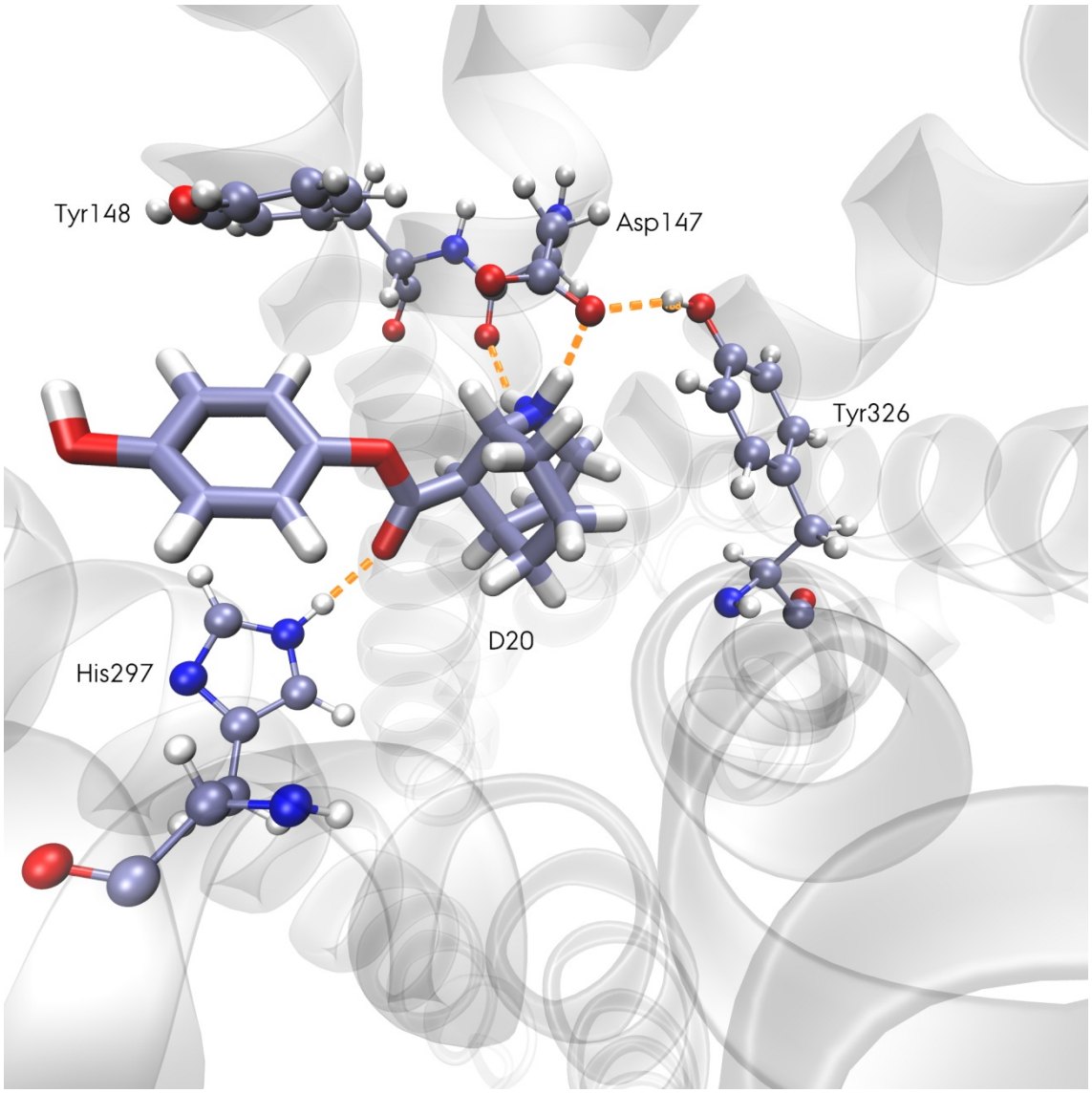

Figure 81. 3D binding pose of **D20** after 5 ns. Relevant residues are depicted and protein ribbons are ghosted.

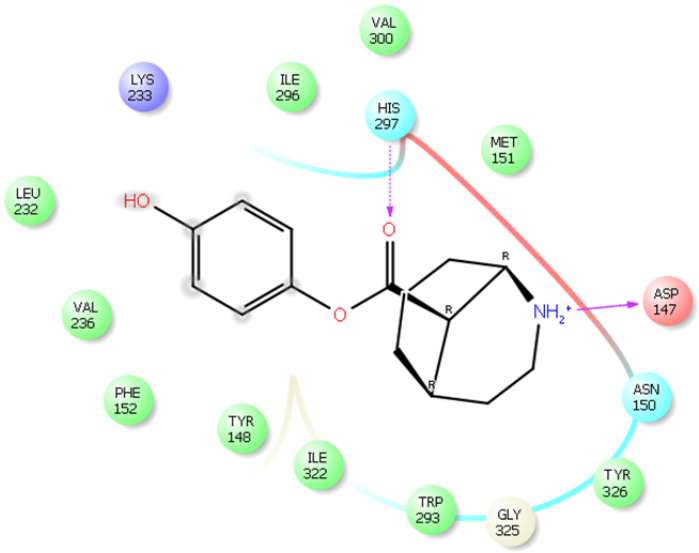

Figure 82. 2D binding pose of **D20** after 5 ns.

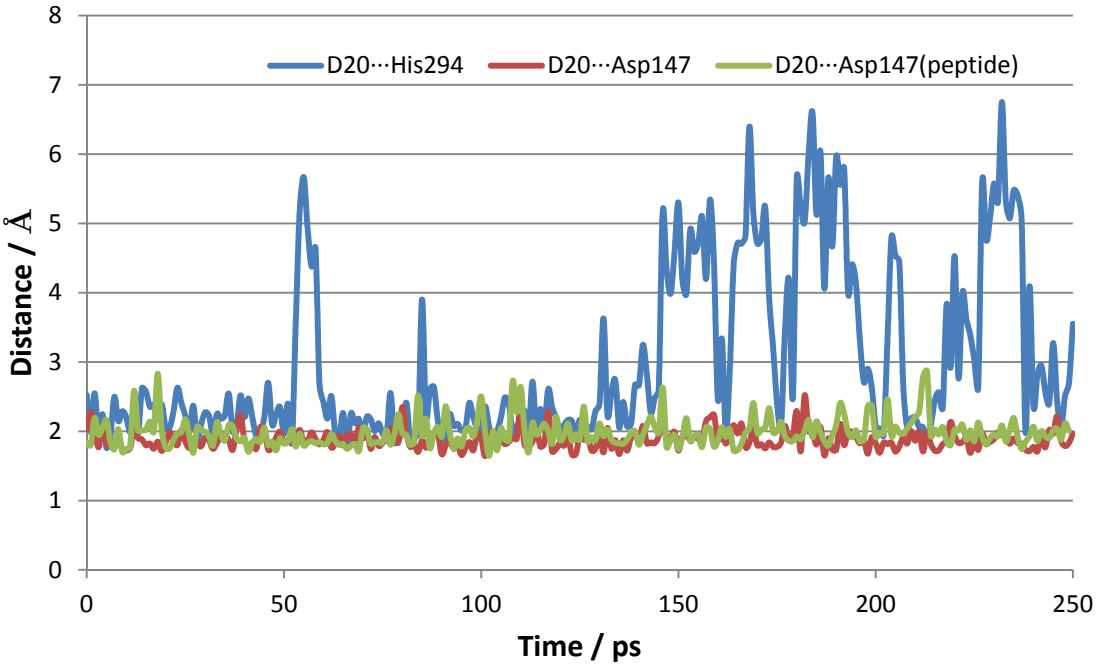

Figure 83. Plot of the main interactions between **D20** and selected residues.

Phenolic lateral chain (the 4-hydroxyphenyl ester group) is, again, placed at the large hydrophobic area. A frequent interaction between the carbonyl group of the ester and imidazolic amine of His294 is also found, in a similar way as **D16**. However, there is no π – π stacking interaction between rings, due to the deviation of the aromatic ring of the ligand. The position of the hydroxyl group in 4 also difficults the interaction with the phenolic group of Tyr148 as well. However, the analysis of trajectories shows a long range interaction between both phenolic groups: the hydroxyls are dipoles and the extension of their force field is larger than induced

dipoles. In this way, the hydrogen of the ligand´s focused towards the oxygen of tyrosine´s phenolic oxygen. So, the interaction of the ligand with Tyr148 may be more intense than His294. This orientation also deviates the aromatic ring of the ligand from the previously described stacking disposition.

Molecular Dynamics of Ligand-Receptor Complexes III: Thermodynamic Results.

Once studied the binding topologies of the complexes, a thermodynamic study of the binding process was performed as a complementary analysis tool.

Free energy calculations are particularly useful tools in biomodelling: they provide energy balances and levels of biomolecular systems, binding processes, preorganization paths or solvation phenomena. Several methodologies may be found in literature, covering methods theoretically rigorous or simplified schemes, from the more computationally demanding to the less. Thermodynamic Integration, Free Energy Perturbation or Replica Exchange Free Energy Perturbation, MMPBSA, MMGBSA, or Linear Interaction Energy are some of these thermodynamic methodologies.

Nowadays, those methodologies that combines molecular mechanics calculations and continuum solvation models are a standard in biomolecular simulation studies. MM/PBSA and MM/GBSA are computationally efficient methods, widely exploited in biomodelling. They serve not only to estimate absolute binding affinities of ligands to proteins, but to rank a set of ligands from the weaker to the stronger one.

In the MM/PBSA approach, Molecular Mechanics/Poisson Boltzmann Surface Area, the binding free energy is defined by the equation below:

$$\Delta G_{bind} = G_{complex} - G_{free\ protein} - G_{free\ ligand} \quad [1]$$

Each free energy term is decomposed in the next scheme:

$$G = H_{gas} - TS_{conformational} + G_{solvation} \quad [2]$$

$$H_{gas} = U_{gas} + E_{vdw} + E_{el} \quad [3]$$

$$G_{solvation} = G_{PB} + G_{SA} \quad [4]$$

$$G_{SA} = \gamma \cdot SASA + \beta \quad [5]$$

The free energy term is divided into the gas enthalpy of the system, the conformational entropy of the solute and the solvation free energy (**Eq. 2**). The gas enthalpy is subdivided into the internal gas energy of the system, which is the sum of the bonded energy terms according with Molecular Mechanics, and the non-bonded terms: the Van der Waals and the electrostatic (Coulombic) interactions (**Eq. 3**). Regarding the Solvation Gibbs energy, this is composed of the electrostatic contribution to the free energy (G_{PB}), calculated through a continuum solvent approximation by means of the linear Poisson-Boltzmann equation, and the non-polar contribution to the free energy (**Eq. 4**). This last contribution is calculated using Eq. 5, where the SASA is the Solvent Surface Accessible Area, and the parameters γ and β are empirically calculated. Finally, TS_{conf} is the conformational entropic contribution of the solute to the free energy at temperature T.

In this project, binding energies were estimated using the MMPBSA.py routine of the AmberTools suite of software. This routine evaluates the binding free energy (**Eq. 1**) through a thermodynamic cycle, summarized in **Figure 84**.

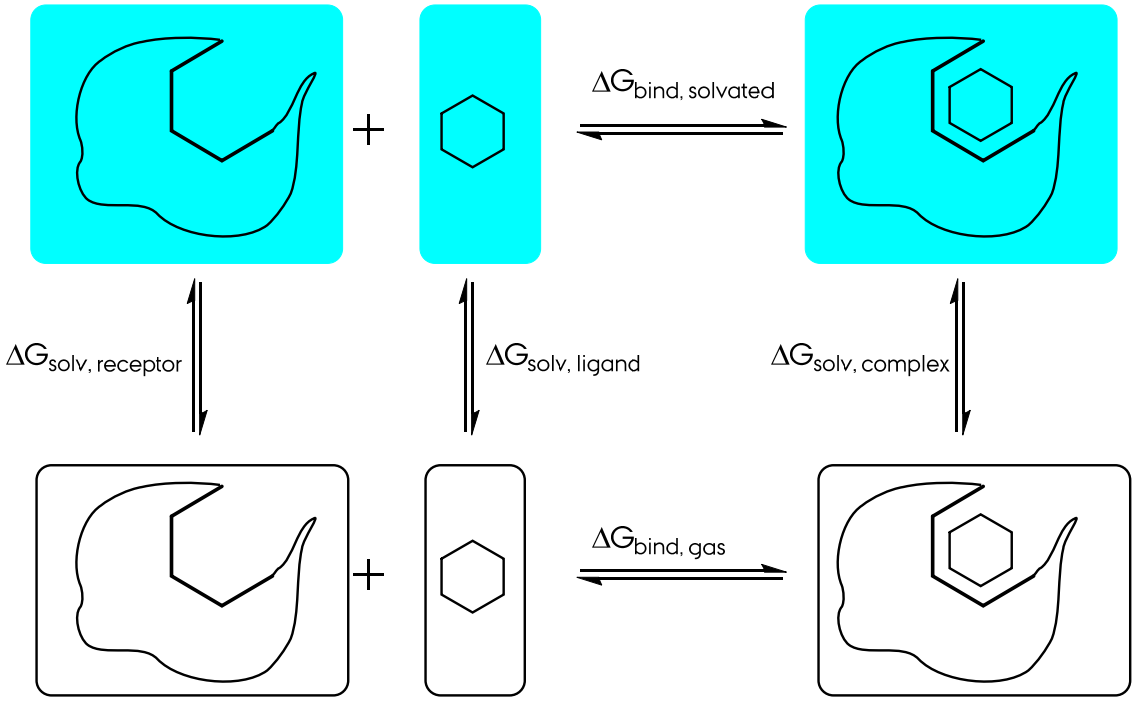

Figure 84. Thermodynamic cycle to calculate binding energies by means of MMPBSA.

For the four systems studied through MD simulations, MMPBSA free energies were calculated taking the last 500 picoseconds. As the simulation time is not enough to account for entropy lost upon binding, entropic terms were not calculated this time. The single trajectory approach was also used: the trajectories of the six required systems to the previously describe cycle were obtained using only the trajectory of the solvated complex system. Stripping the solvent, ions, membrane and ligand/receptor in case, it was easy to obtain the six simulated systems. In this approach, as the bonded terms are absolutely equal, the internal energy of the systems (bonded terms) was neglected.

The next set of parameters were used: external dielectric constant, 80.0; internal electric constant, 2.0; grid spacing of the cubic lattice, 4.0 Å; ionic strength, 150 mM; surface tension (γ), 0.0378 Kcal $\cdot$ mol^{-1} $\cdot$ Å^{-2}; solvent probe radius, 1.4 Å. Table 9 shows the results of the computed contributions to the free energy as well as the final value of the binding free energy. The internal dielectric constant has not a defined value: depend of the protein nature, the measuring point and its environment (charged/non-charged/polar/non-polar residues), the exposure to solvent, etc. In this case, the binding pocket has a dual character, due to the presence of the charged Asp147 and the hydrophobic site. It is also slightly exposure to water. Concluding, the definition of the internal dielectric constant is not an easy task. Although in literature is possible to find values of $\varepsilon = 1$ of related opioid systems, we take $\varepsilon = 2$, in order to account the charged environment of Asp147.

	ΔE_{vdw}	ΔE_{el}	$\Delta G_{s,\ polar}$	$\Delta G_{s,\ npolar}$	ΔG_{gas}	ΔG_{solv}	ΔG_{total}	$\Delta\Delta G_{total}$
D8	-35.67	12.52	-6.92	20.97	-23.15	14.04	-9.11	1.00
D15	-46.15	25.40	-13.88	21.56	-20.75	7.68	-13.07	1.43
D16	-33.53	1.65	0.65	19.95	-31.88	20.59	-11.28	1.24
D20	-34.28	8.69	-4.54	20.17	-25.59	15.63	-9.95	1.09

Table 9. Thermodynamic binding magnitudes calculated of the four complexes, accordingly to MMPBSA theory.

Analysing the table we may extract some information. First, the total free energy is negative, meaning a stabilizing effect of the binding of the ligands to the receptor. As this binding is not covering the entropic lost, this energy is overestimated (depending on the system, from 1 to 5 Kcal/mol). As the structural similarity and the binding pose between ligands were close, a relative binding energy is calculated. The relative ranking of the binding energies is **D15** < **D16** < **D20** < **D8**. Checking

the biological trials, the ranking matches with the *Danio rerio* μ opioid receptor tests. It´s noteworthy the tests with rat brains failed in the correct ranking of the ligands: this is logic as the response is a combination of the three classes of opioid receptors (μ, δ, κ). On the other hand, the percentage of identity between *Mus musculus* mu opioid receptor and *Danio rerio* is 100 % at the binding pocket. The highly conservative sequence at the binding site enables the comparison of the simulated results. Checking the non-bonded interactions, it is found the Van der Waals energy is the main stabilizing contribution upon binding. Electrostatic contribution was found positive: although the main anchoring point is the ionic bridge, the interaction field is larger, and is centred in a hydrophobic site, which interaction destabilizes the complex. Gas free energy is negative in all cases: molecules at vacuum are stabilized if they join together. Solvation free energy was positive: the non-polar contribution is positive, around 20 Kcal/mol, In balance, the Van der Waals contribution interaction upon binding is the key to the complexation of the ligands with the receptor.

D15 is clearly the most stabilizing: checking the binding pose, the aromatic side chain is placed at the bottom of the hydrophobic area of the pocket, interacting with the apolar lateral chains (**Fig. 85**). That is likely the reason of having the lowest Van der Waals interaction energy. **D16** is the next one in the rank: the hydroxyl of the aromatic chain is interacting through a hydrogen bond with Tyr148. This interaction lowered the electrostatic interaction (positive in all cases due to the hydrophobic surrounding area to the ionic bridge). This interaction deviates the aromatic ring from the hydrophobic site and from possible π – π stacking interactions. **D20** and **D8** have similar energetic behaviour: the lateral chain is placed in the hydrophobic site. Nevertheless, **D20** interacts with Tyr148 through a long range dipole-dipole mechanism, deviating the aromatic ring from stacked dispositions, and lowering the electrostatic contribution to the free energy. Finally, **D8** shows an aromatic ring stacked with the imidazolic ring of His294. The absence of polar groups in the aromatic group rises the electrostatic part of the Gibbs energy.

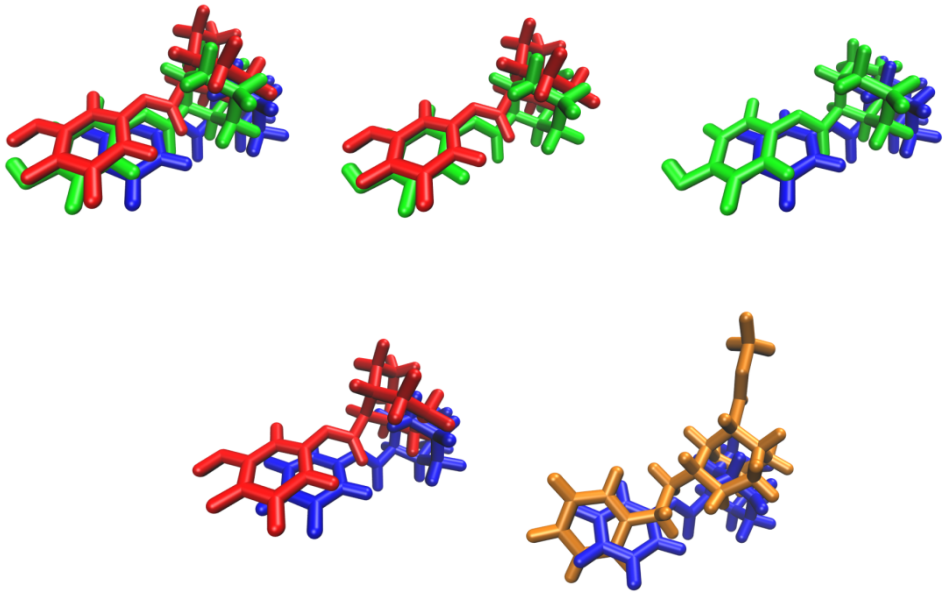

Figure 85. Superimposed structures of **D15** (orange), **D8** (blue), **D16** (red) and **D20** (green) at the binding site.

Which is the origin of the differences upon binding between **D8**, **D16** and **D20**? **Figure 86** shows the histogram of the interactions of **D8**, **D16** and **D20** with Tyr148 and His294, as well as the decomposition between electrostatic and Van der Waals terms.

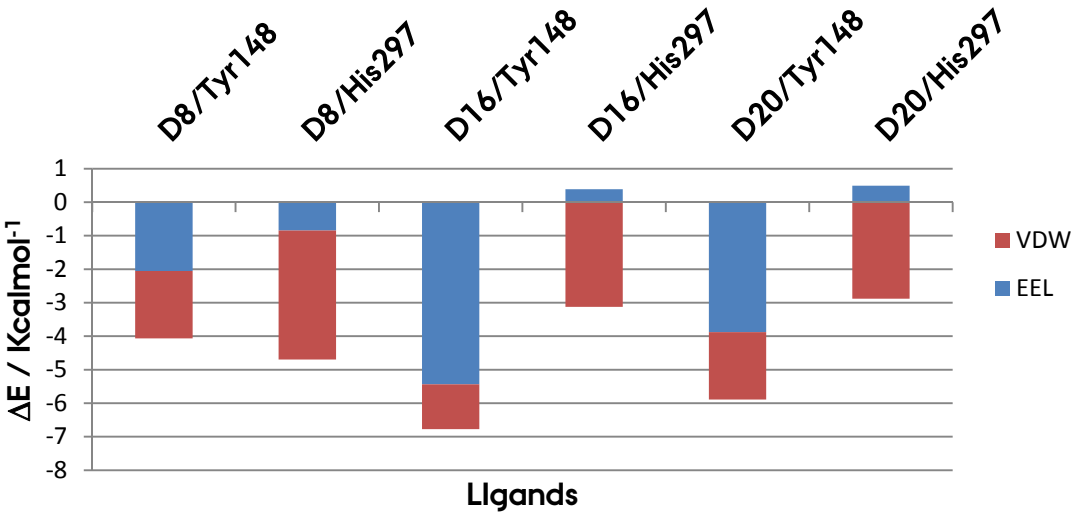

Figure 86. Energy contributions of residues Tyr148 and His297 upon binding of **D8**, **D16** and **D20** ligands.

D16 have a strong interaction with Tyr148, mainly electrostatic, due to the hydrogen bond established. **D20** also have a strong interaction, although the

electrostatic term is lower than **D16**. The distance between hydroxyl groups in wider in this case, and the Van der Waals term also increases. **D8** has a equipartition of the non-bonded terms, and a global interaction with the Tyrosine minor. Apart from Tyr148, His297 also interacts with D8: a moderate interaction, dipersion type mainly, due to the stacking of the aromatic rings. **D16** and **D20** also interacts with His294; however, the long-range dispersion forces are not as intense as in **D16**, since the aromatic rings of the ligands are not stacked with the aromatic five-membered ring of the Histidine. Electrostatic forces are even destabilizing, probably due to the polarization of the imidazolic ring and the facing of apolar sections of the phenolic ring of the ligands.

Conclusions

In summary, a complete design, testing, synthesis, biological evaluation feedback and Biomodelling resolution has been performed to study the activity of this series of morphan derived structures. In this chapter, the next conclusions are summarized:

- A structure-based design was envisaged taking the morphan structure **26** as parent/core compound. Design was carried out taking into account the double nature of our morphan structure: morphine simplification motif and β-aminoacid. Incorporation of aromatic side chains are presented as attractive and affordable modifications, as the docking studies revealed. A homology model of rat mu opioid receptor at the active state, frequently used and cited in literature, was taken as receptor structure.

- Dipeptides based on morphan aminoacid **26** coupled to Phenylalanine or Tyrosine showed lower inhibition constants. Morphan phenyl esters also exhibit good binding properties with receptors. A limited number of compounds, the hits of the docking stage, were synthetized in laboratory in few steps and submitted to biological trials.

- From the biological testing feedback, four MD simulations (corresponding to compounds **D8**, **D15**, **D16**, and **D20**) were carried out to refine the

docked structure, fit the receptor in a membrane slab, and analyse binding topologies and energies were simulated.

- Analysis of the binding topologies shows similar behaviour of the four ligands: an ionic bridge between protonated amines and Asp147 as main anchoring point and the lateral aromatic chains placed towards the hydrophobic area. **D15** lateral chain was placed at the bottom of the hydrophobic site, while **D8** aromatic ring is interacting through a $\pi - \pi$ interplay with His294. A hydrogen bond is made between phenolic groups of **D16** and Tyr148, while a weaker similar interaction occur in **D20**. Additional hydrogen bonds between carbonyl group of the esters ligands and the imidazolic amine of His294 are also frequent.

- Analysis of the relative binding energies allowed to rank the ligands from the stronger to the weaker in binding: **D15** > **D16** > **D20** > **D8**. Energy decomposition in non-bonded and relevant residues contributions showed the placing and the polar group introduction at the aromatic ring as key modifications to explain the differences. Best interactions occur when the aromatic rings are placed in the bottom of the hydrophobic area (**D15**), or 3-hydroxyphenyl ester interacts with Tyr148 through a hydrogen bond (**D16**).

References

[1] (a) Pert, C. B.; Snyder, S. H. *Science* **1973**, *179*, 4. (b) Simon, E. J.; Hiller, J. M.; Edelman, I. *Proc. Natl. Acad. Sci. U. S. A.* **1973**, *70*, 1947.

[2] (a) De Wachter, R.; de Graaf, C.; Keresztes, A.; Vandormael, B.; Ballet, S.; Toth, G.; Rognan, D.; Tourwe, D. *J. Med. Chem.* **2011**, *54*, 6538. (b) Liu, X.; Wang, Y.; Xing, Y.; Yu, J.; Ji, H.; Kai, M.; Wang, Z.; Wang, D.; Zhang, Y.; Zhao, D.; Wang, R. *J. Med. Chem.* **2013**, *56*, 3102.

[3] Manglik, A.; Kruse, A. C.; Kobilka, T. S.; Thian, F. S.; Mathiesen, J. M.; Sunahara, R. K.; Pardo, L.; Weis, W. I.; Kobilka, B. K.; Granier, S. *Nature* **2012**, *485*, 321.

[4] Kolinski, M.; Filipek, S. *Open Struct. Biol. J.* **2008**, *2*, 13.

[5] Sravanthi, N.; Renuka, S.; Krishna, K. R. *Int. J. Drug Des. Discovery* **2012**, *3*, 683.

[6] Collu, F.; Ceccarelli, M.; Ruggerone, P. *PLoS One* **2012**, *7*, e52633.

[7] Young, D. C. *Computational Drug Design*; Wiley-VCH, 2009.

[8] Katritch, V.; Cherezov, V.; Stevens, R. C. *Trends Pharmacol. Sci.* **2012**, *33*, 17.

[9] Palczewski, K.; Kumasaka, T.; Hori, T.; Behnke, C. A.; Motoshima, H.; Fox, B. A.; Trong, I. L.; Teller, D. C.; Okada, T.; Stenkamp, R. E.; Yamamoto, M.; Miyano, M. *Science* **2000**, *289*, 739.

[10] (a) Bera, I.; Laskar, A.; Ghoshal, N. *J Mol Model* **2011**, *17*, 1207. (b) Zhang, Y.; Sham, Y. Y.; Rajamani, R.; Gao, J.; Portoghese, P. S. *ChemBioChem* **2005**, *6*, 853.

[11] (a) Mosberg, H. I.; Fowler, C. B. *J. Pept. Res.* **2002**, *60*, 329. (b) Fowler, C. B.; Pogozheva, I. D.; Lomize, A. L.; LeVine, H.; Mosberg, H. I. *Biochemistry* **2004**, *43*, 15796.

[12] Liu, X.; Kai, M.; Jin, L.; Wang, R. *J. Comput. Aided Mol. Des.* **2009**, *23*, 321.

[13] *Maestro 9.3,* Schrödinger, L., New York, NY, 2012.

[14] Jorgensen, W. L.; Maxwell, D. S.; Tirado-Rives, J. *J. Am. Chem. Soc.* **1996**, *118*, 11225.

[15] Ren, P.; Wu, C.; Ponder, J. W. *J. Chem. Theory Comput.* **2011**, *7*, 3143.

[16] *Jaguar 7.9,* Schrödinger, L., New York , NY,

[17] (a) Becke, A. D. *Phys. Rev. A* **1988**, *38*, 3098. (b) Lee, C.; Yang, W.; Parr, R. G. *Phys. Rev. B* **1988**, *37*, 785.

[18] Hehre, W. J.; Radom, L.; Schleyer, P. v. R.; Pople, J. *Ab Initio Molecular Orbital Theory*; Wiley-VCH, 1986.

[19] Gasteiger, J.; Marsili, M. *Tetrahedron* **1980**, *36*, 3219.

[20] Morris, G. M.; Huey, R.; Lindstrom, W.; Sanner, M. F.; Belew, R. K.; Goodsell, D. S.; Olson, A. J. *J. Comput. Chem.* **2009**, *30*, 2785.

[21] Weiner, S. J.; Kollman, P. A.; Case, D. A.; Singh, U. C.; Ghio, C.; Alagona, G.; Profeta, S.; Weiner, P. *J. Am. Chem. Soc.* **1984**, *106*, 765.

[22] Mehler, E. L.; Solmajer, T. *Protein Eng.* **1991**, *4*, 903.

[23] Pogozheva, I. D.; Lomize, A. L.; Mosberg, H. I. *Biophys. J.* **1998**, *75*, 612.

[24] Pasternak, G. W. *The Opiate Receptors*; 2 ed.; Humana Press, 2011; Vol. 23.

[25] Moore, J. L.; Taylor, S. M.; Soloshonok, V. A. *Arkivoc* **2005**, *6*, 287.

[26] Ponder, J. W.; Case, D. A. In *Advances in Protein Chemistry*; Valerie, D., Ed.; Academic Press: 2003; Vol. Volume 66, p 27.

[27] Vanommeslaeghe, K.; Hatcher, E.; Acharya, C.; Kundu, S.; Zhong, S.; Shim, J.; Darian, E.; Guvench, O.; Lopes, P.; Vorobyov, I.; Mackerell, A. D. *J. Comput. Chem.* **2010**, *31*, 671.

[28] Lomize, M. A.; Lomize, A. L.; Pogozheva, I. D.; Mosberg, H. I. *Bioinformatics* **2006**, *22*, 623.

[29] Duan, Y.; Wu, C.; Chowdhury, S.; Lee, M. C.; Xiong, G.; Zhang, W.; Yang, R.; Cieplak, P.; Luo, R.; Lee, T.; Caldwell, J.; Wang, J.; Kollman, P. *J. Comput. Chem.* **2003**, *24*, 1999.

[30] Skjevik, Å. A.; Madej, B. D.; Walker, R. C.; Teigen, K. *J. Phys. Chem. B* **2012**, *116*, 11124.

[31] Mahoney, M. W.; Jorgensen, W. L. *J. Chem. Phys.* **2000**, *112*, 8910.

[32] Phillips, J. C.; Braun, R.; Wang, W.; Gumbart, J.; Tajkhorshid, E.; Villa, E.; Chipot, C.; Skeel, R. D.; Kalé, L.; Schulten, K. *J. Comput. Chem.* **2005**, *26*, 1781.

[33] Darden, T.; York, D.; Pedersen, L. *J. Chem. Phys.* **1993**, *98*, 10089.

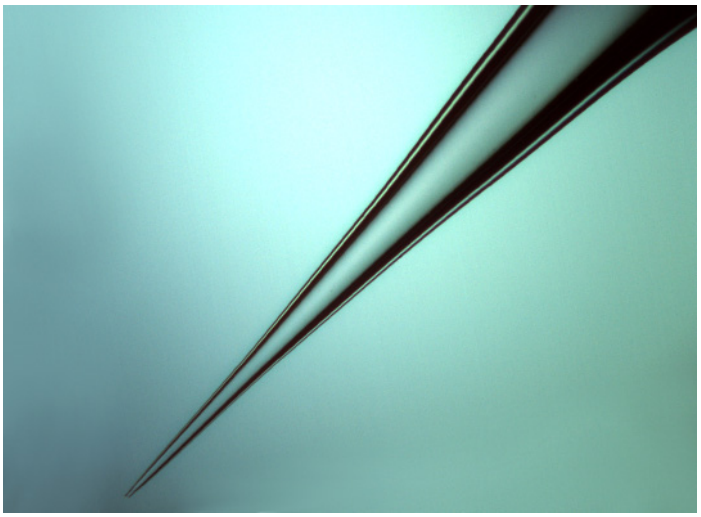

4 Biological Evaluation of Novel Opioid Receptor Ligands.

Introduction

Morphan derivatives previously synthetized in chapter 3 (**Fig. 87**) were submitted for a biological evaluation test, in order to explore their binding properties to morphan opioid receptors. Competition binding assays were conducted using rat brain membrane homogenates, known to contain μ, δ and κ binding sites.

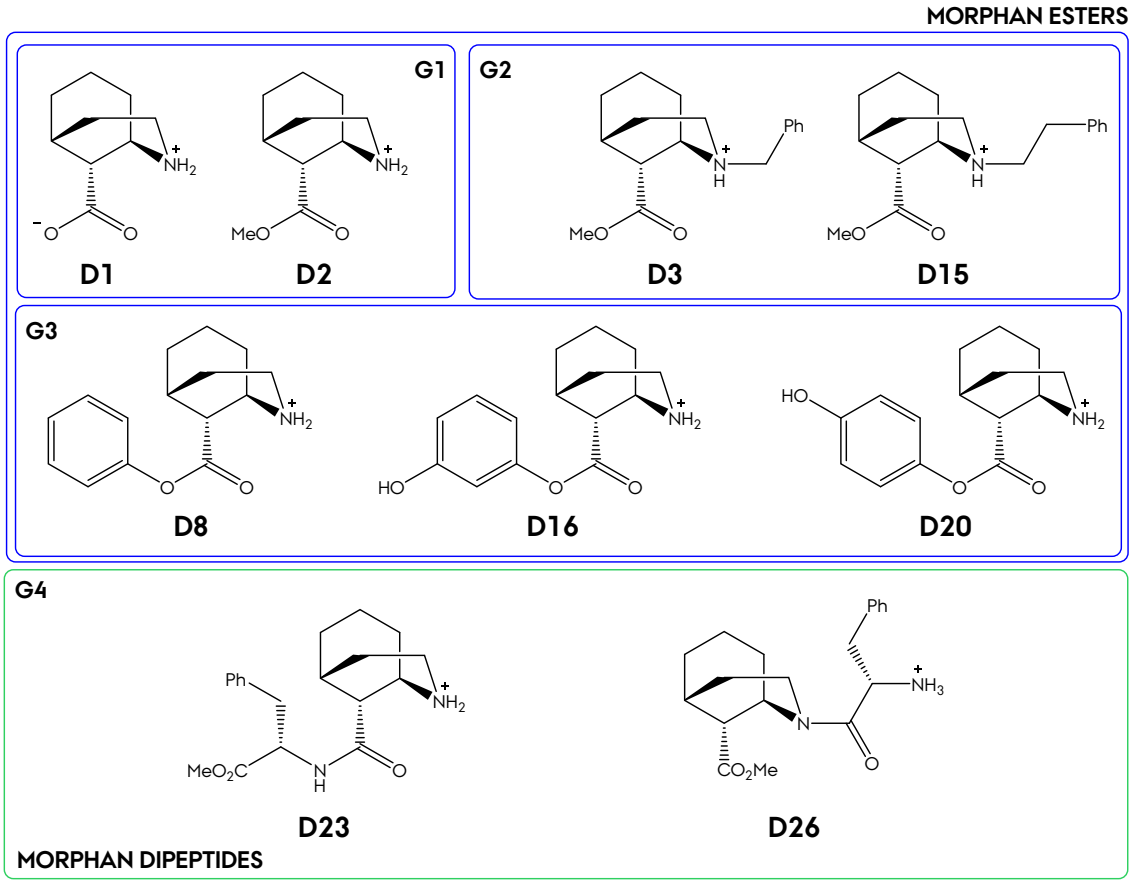

Figure 87. Selected hits to the biological evaluation survey.

Competition Binding Assays

The lead compounds that were synthesized (**D1**, **D2**, **D3**, **D8**, **D15**, **D16**, **D20**, **D23** and **D26**) were tested for their ability to displace [^{3}H]-diprenorphine (DPN) binding; morphine was used as positive control and 10 μM naloxone (Nx), the non-specific antagonist, was employed to determine non-specific binding (see Methodologies and Materials section). As predicted, **D1** could not displace [^{3}H]-DPN binding even at the highest concentration used, so that it was discarded for

subsequent analysis. The remaining eight ligands were able to displace the specific [^{3}H]-DPN binding (**Fig. 88** and **Tab. 10**), yet with different affinities, and in all cases data fitted better to the one-site displacement model. The rank order of affinity, which inversely correlates with the obtained Ki-values, was as follows: **D20** > **D15** ~ **D16** > **D8** > **D3** ~ **D23** > **D2** >> **D26**.

The pharmacological profile of these eight ligands was further characterized on the μ opioid receptor, so they were promoted for further competition binding analysis using membrane homogenates from HEK293 cell line stably transfected with the μ opioid receptor from zebrafish. In this case, the specific binding is only due to the interaction with the μ receptor. The rank order of affinity was **D15** ~ **D16** > **D20** > **D8** > **D2** ~ **D3** >> **D26** ~ **D23**. **D26** and **D16** showed almost the exact behaviour on brain homogenates as when tested on isolated μ receptors: competition curves were nearly superimposable for both conditions, indicating that μ receptor might be the major target of these ligands. In the case of **D2**, **D3**, **D8** and **D15**, slight differences were observed between ligand binding to brain homogenates and to the μ receptor.

Ligand	Ki Rat Brain	Ki μ	Ki δ
Morphine	K_{i1} 2.57 ± 0.70 nM K_{i2} 135.00 ± 18.71 nM	187.4 ± 94.07 nM[a]	1.43 ± 0.302 μM
D1	> 10^{-4} M	-	-
D2	17.10 ± 0.43 μM	35.28 ± 3.05 μM	-
D3	14.80 ± 1.10 μM	36.98 ± 2.45 μM	-
D8	10.94 ± 0.78 μM	32.00 ± 3.26 μM	-
D15	2.69 ± 0.36 μM	8.24 ± 0.72 μM	21.35 ± 0.82 μM
D16	4.04 ± 0.42 μM	9.52 ± 1.61 μM	23.60 ± 1.33 μM
D20	1.92 ± 0.1 μM	12.66 ± 0.80 μM	635.9 ± 113.2 nM
D23	14.81 ± 0.42 μM	78.02 ± 2.35 μM	-
D26	32.86 ± 2.76 μM	75.78 ± 2.27 μM	-

Table 10. Opioid receptor binding affinities (expressed as mean ± SEM) of the different morphan-derivatives for the opioid binding sites present in rat brain and for μ and δ opioid receptors. [a]Value taken from[1]

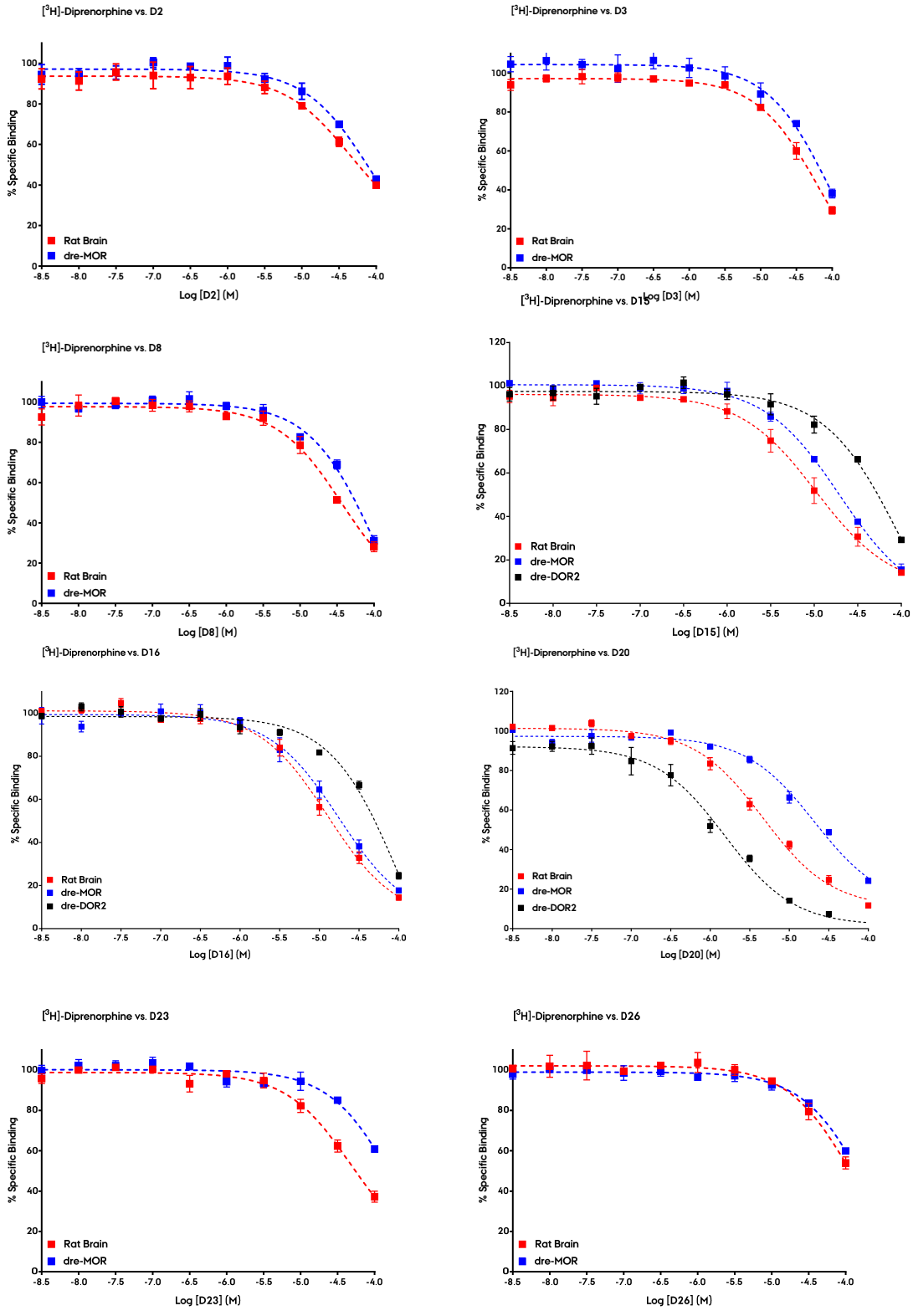

Figure 88. Competition binding assays of the morphan derivatives on rat brain and μ receptor membrane homogenates. Data were fit to the one-site competition model, and each point represents the mean ± standard error of the mean (SEM) (capped bars) of three independent experiments performed in triplicate. Legend: Rat brain, μ receptor, δ receptor.

Greater differences were seen for **D20** and **D23**, and in both cases higher affinity was obtained when brain homogenates were used, thus indicating that **D20** and **D23** might be also binding to other opioid receptor than the μ receptor that is present in the rat brain, such as the δ receptor.

Even though the two dipeptide derivatives **D23** and **D26** (group 4) contained a phenyl group, they did not behave as good competitors, while the phenyl esters **D8**, **D16**, and **D20** (group 3) seemed to be good candidates. Interestingly, these three compounds only differ in the position of a hydroxyl group: the m-position is preferred to the p-position, whereas lower binding affinity is seen when hydroxyl is absent. The two quaternary amines **D3** (*N*-benzyl) and **D15** (*N*-phenylethyl) (group 2) displayed very different behaviours: while **D15** exhibited a similar affinity than **D16**, being both of them the most promising candidates, **D3** was a poor competitor. As it has been previously shown,[2] *N*-phenylethyl substituents play a key role in binding to the μ receptor.

D15, **D16** and **D20** yielded the best results, so that they were also tested in membrane homogenates from HEK293 cell line stably transfected with the 1b opioid receptor from zebrafish.[3] **D15** and **D16** showed better affinities for the sites, whereas **D20** displayed a lower Ki-value for the receptor, about one rank order lower than morphine. In fact, **D20** displays a δ:μ selectivity of 20:1, thus implying that **D20** is the most promising candidate on the delta receptor.

Conclusions

The fourth best candidates were **D8**, **D15**, **D16** and **D20**. Structure-based design has successfully predicted these ligands to bind to μ opioid receptor with a selective pose, as it has been demonstrated through these biological tests. Group 3 phenyl esters are able to displace [^{3}H]-DPN with good affinity, as well as *N*-phenylethyl derivative **D15**. The aromatic ring boosts the affinity of these compounds, and hence the original placing of the aromatic ring in morphine is likely not to be mandatory. Dipeptides were found to have low affinities, probably due to the larger binding pose diversity, as predicted by docking analysis.

D15, **D16** and **D20** were also tested on the δ opioid receptor as well. Competition binding curves showed a remarkable behavior of **D20**, which displayed the lowest Ki-value, in the nanomolar range, and showed a 20-fold selectivity for the δ over the μ receptor.

To further study the nature of the binding pose, and the differences between these four ligands, a complete MD simulation was carried out in explicit solvent and membrane. The details are explained in chapter 3.

References

[1] Gonzalez-Nunez, V.; Jimenez Gonzalez, A.; Barreto-Valer, K.; Rodriguez, R. E. *Mol. Med.* **2013**, *19*, 7.

[2] Subramanian, G.; Paterlini, M. G.; Portoghese, P. S.; Ferguson, D. M. *J. Med. Chem.* **2000**, *43*, 381.

[3] Pinal-Seoane, N.; Martin, I. R.; Gonzalez-Nuñez, V.; de Velasco, E. M. F.; Alvarez, F. A.; Sarmiento, R. G.; Rodriguez, R. E. *J. Mol. Endocrinol.* **2006**, *37*, 391.

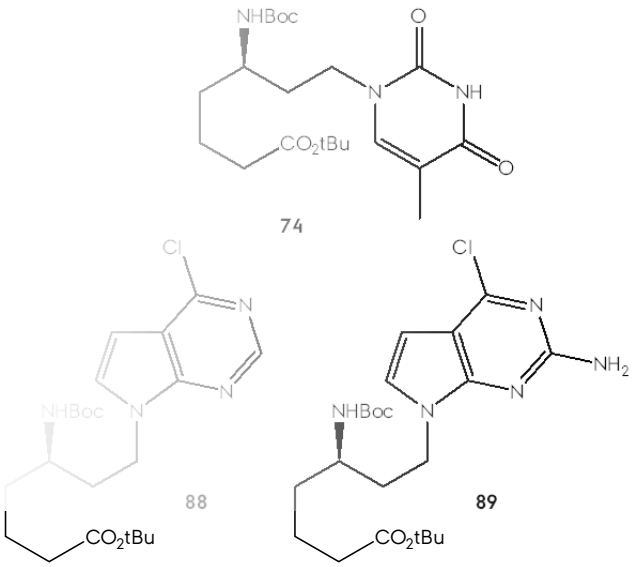

5 Asymmetric Synthesis of Flexible Peptide-Nucleotides (PNA)

Introduction

In 1996, Leumann *et al.*[1] synthetized a peptide nucleic acid monomer from Boc-Ser-OMe (**Sch. 44**). As the substrate incorporates the stereocenter, only chain homologation and functional group interconversions are required. This compound represents one of the first chiral, flexible PNA monomers with a structure substantially different from the original *aeg*PNA.

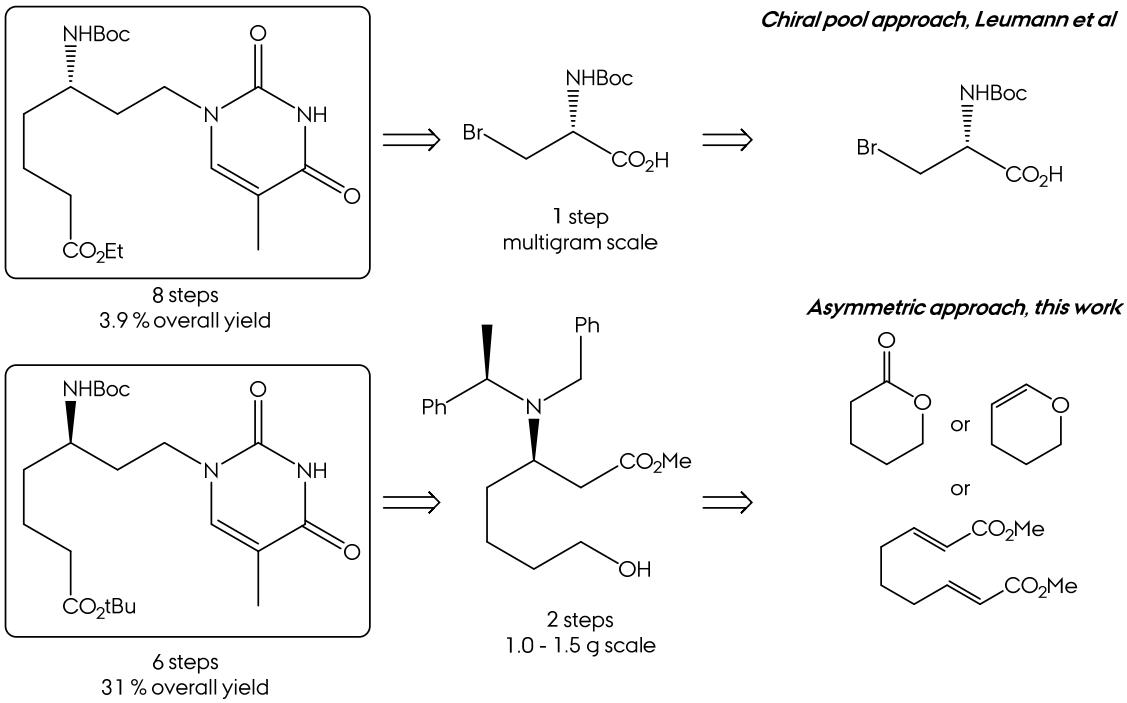

Scheme 44. Comparison between Leumann's approach of the PNA monomer synthesis and current approach.

On the next section, the synthesis of a variety of peptide-nucleotides is discussed. Our approach is based on the asymmetric Michael addition of chiral amides as key step to obtain enantiomerically enriched intermediate and forward functional group interconversion. Among them, the enantiomer of Leumann's monomer has been elaborated with higher yield and productivity compared to Leumann's article. The path to a series of peptide nucleic acid monomers with a hydrocarbonated scaffold takes, on the one hand monoacid **4**, and on the other hand δ-valerolactone or 3,4-dihydro-2*H*-pyran, as prime materials. Modifying the transformations and the chemoselectivity was possible to obtain three stereochemically controlled amino acid nucleotides, displayed in **Scheme 45**.

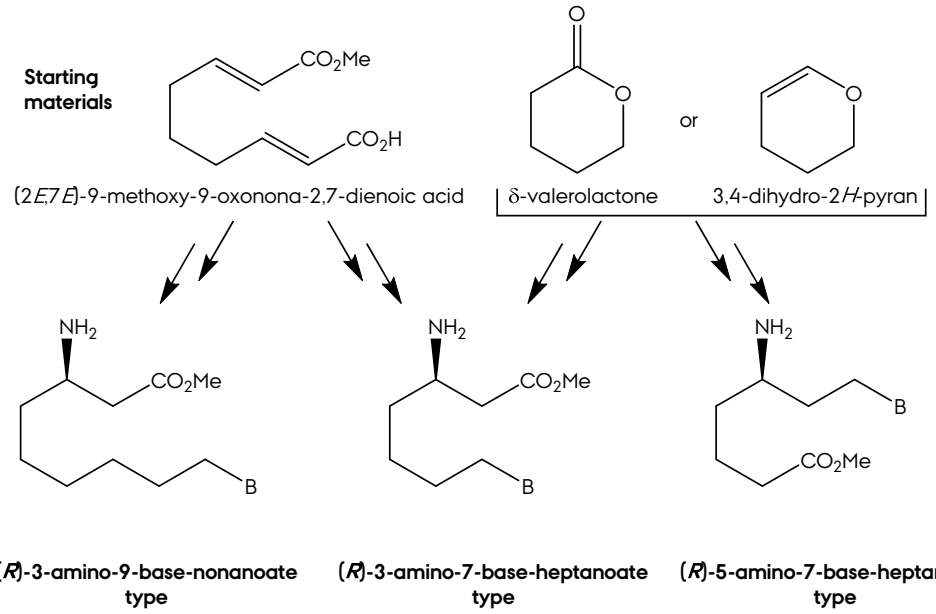

Scheme 45. General synthetic scheme of peptide nucleic acid synthesis. Starting materials selection and forward chemoselective treatment leads to the three different PNA families.

(*R*)-3-amino-9-base-nonanoate Type PNA Synthesis

Substrate **4**, obtained as a byproduct in the workup of the dehydrobrominative procedure with DMF, is the initial point in the elaboration of PNA monomers based on a (*R*)-3-amino-9-base-nonanoate type scaffold.[2] The reaction path is schematized in **Scheme 46**.

First step was asymmetric Michael monoaddition of the lithium (*R*)-*N*-benzyl-*N*-α-methylbenzylamide to **4** (**Sch. 46**). Unlike the diester **3**, the orthogonal substitution of the monoester **4** prevented the double-Michael addition, i.e. monoaddition followed by the 6-*exo*-trigonal cyclization, previously described in chapter 2. An equimolecular quantity of the lithium amide is consumed in the quick acid-base reaction with substrate's acid group. The negative charge created blocks the fluctuation of the electron density from the olefin to the carbonyl group, preventing the second attack (**Fig. 89**).

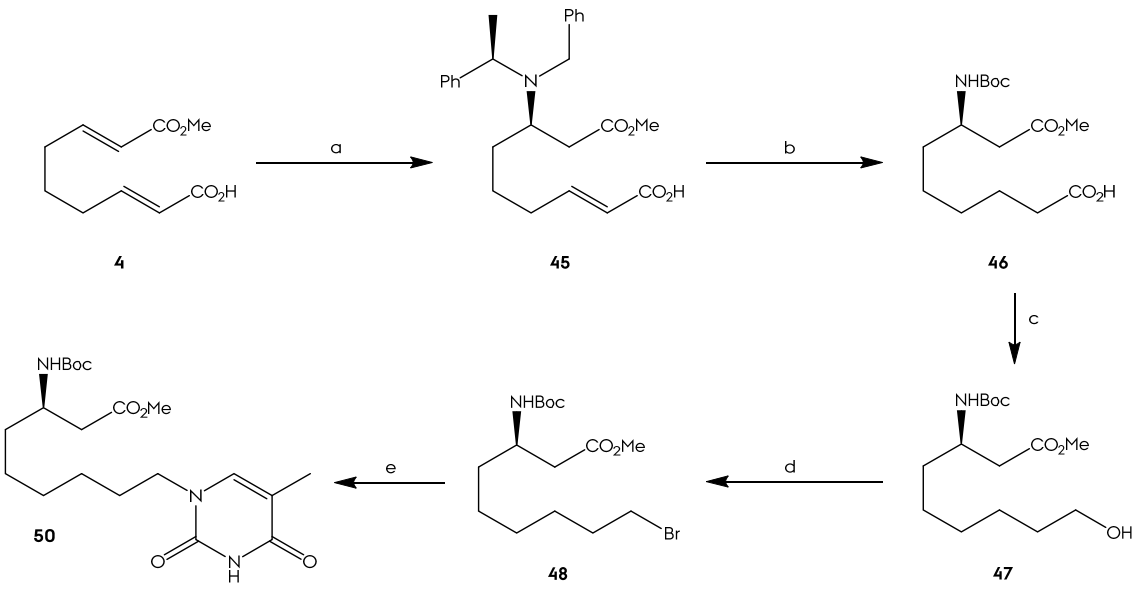

Scheme 46. *Reagents and conditions*: (a) (*R*)-*N*-benzyl-*N*-α-methylbenzylamine, nBuLi, THF, -78 ºC, 3 h, 84% (P1). (b) H_2/Pd(OH)$_2$ – C, Boc_2O, AcOEt, 3 d, 62 % (P2). (c) $BH_3 \cdot$ THF, THF, 20 ºC, 60 min, 77 % (P3). (d) CBr_4, PPh_3, DCM, 45 min, 81 % (P4). (e) Thymine, TBAI, K_2CO_3, DMF, 70 ºC 6 h, 38 % (P5).

^{1}H NMR spectra incorporates chiral unity signals, an AB system: 3.81 (1H, AB, *J* 13.6 Hz, NCH_AHPh), 3.87 (1H, AB, *J* 13.6 Hz, $NCHH_BPh$). Double-bond signal also appears: 5.80 (1H, d, *J* 15.6 Hz, H2), 7.10 (1H, dt, *J* 15.6 y 6.8 Hz, H3). Finally, the methyl doublet at 1.30 (3H, d, *J* 7.0 Hz, C(α)Me) and the coupled quartet of the CH at 4.1 (1H, q, C(α)H) completes the set of amine signals.

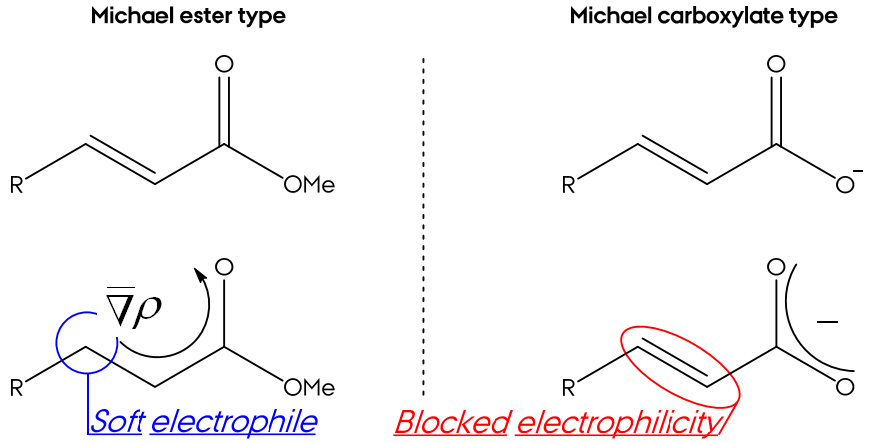

Figure 89. Sketch of the qualitative comparison of the electronic density profile between Michael acceptors ester and carboxylate.

Once obtained the homochiral aminoester **45**, next stage is a one pot multiple transformation: reduction of the olefin to alkane, complete debenzylation of the amine group and reprotection of the released amine as *tert*-butoxy carbonyl carbamate (Boc-amine). This straightforward stage was carried out in a reductive atmosphere, high-pressure hydrogen, with Pearlman's catalyst (palladium hydroxide on carbon, $Pd(OH)_2/C$) and Boc_2O. 3-days exposure of the reaction mixture to a hydrogen atmosphere of 3.5 atm leaded to product **46** in 62 % yield.

Last three reactions are functional group interconversions to allow the thymine attaching at position 9. Chemoselective reduction of the acid to alcohol by means of borane-tetrahydrofurane complex in tetrahydrofurane solution afforded the reduction product **47** in good yield (77 %). Triphenylphosphine mediated interchange between hydroxyl and bromine conducted to bromine **48** an excellent 81 % yield. These transformations are easily checked by ^{1}H NMR signal evolution of the functional group's alpha protons (**Fig. 90**).

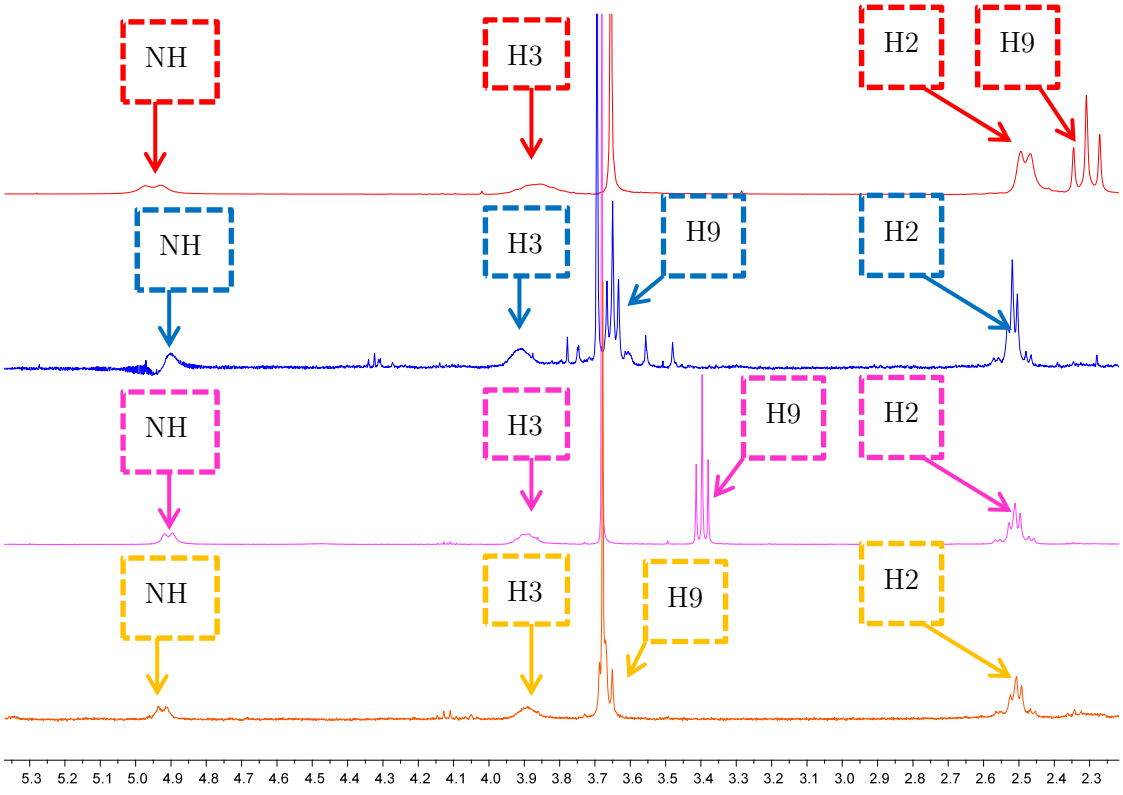

Figure 90. ^{1}H NMR spectra (200 MHz) of **46**, **47**, **48** and **49** at the 2.2 - 5.3 ppm range.

FTIR spectrum also validates the reaction sequence, due to the unchanged profiles at the dactilogram region of the spectra.

Isocyanate **49** was obtained as byproduct after column chromatography of a small crude quantity. Isocyanate mechanism formation might be explain due to the oxofilic capacity of triphenylphosphine, competing carbonile's oxygen of the carbamate with the hydroxyl one, as a consequence of their high electron density (**Sch. 47**). Evidence of this compound was demonstrated by means of FTIR checking, which shows a strong absorption at 2265 cm^{-1}, as well as the disappearance of 1171 and 1712 cm^{-1} absorptions, carbamate type signals (**Fig. 91**). ^{1}H NMR spectra did not show the *tert*-butyl peak, neither NH resonance, carbamate group characteristic resonances.

Additional information is supplied by mass spectrometry: molecular ion at 346.0621 (M + Na) revealed the presence of methyl carbamate, obtained in the reaction between isocyanate **49** and methanol. As compound **49** was dissolved in methanol and further injected in the chromatographic system, methanol reacted with the solvent.

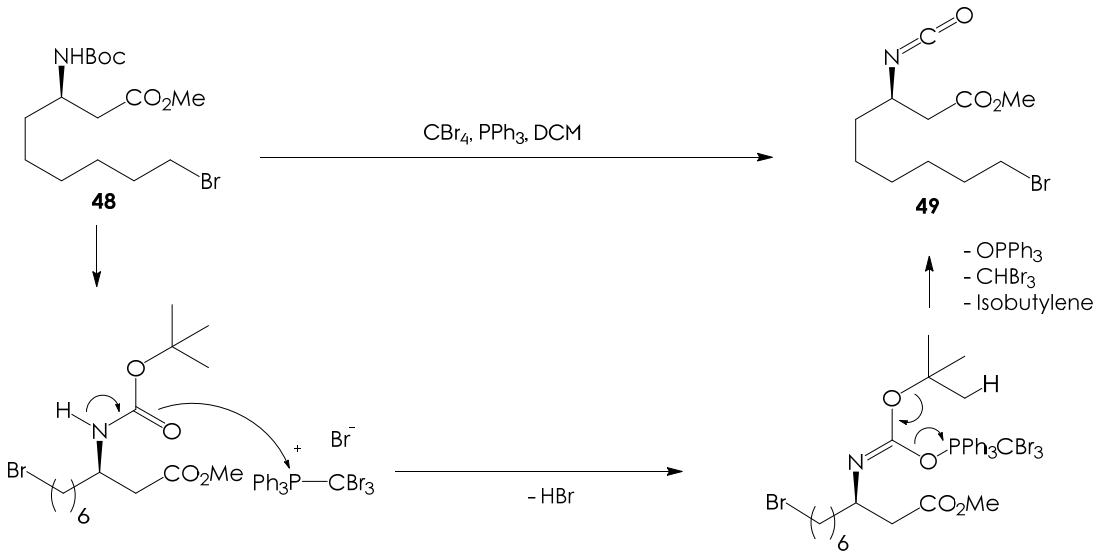

Scheme 47. Mechanistic hypothesis of isocyanate **49** formation.

At last, following the reaction conditions described in literature by Tadei *et al*,[3] bromine **49** was transformed into the thymine derivative **50** combining substrate with potassium carbonate, thymine and tetrabutylammonium iodide as catalyst, at 60 ºC along 6 hours. Column chromatography yielded target molecule **50**. This compound has combined resonances of **49** together with the incorporated heterocycle: 1.20 - 1.57 (10H, m, H4, H5, H6, H7, H8), 1.42 (9H, s, $C(CH_3)_3$), 1.92 (3H, s, Me-C5'), 2.50 (2H, m, H2), 3.65 – 3.70 (2H,m, H9), 3.67 (3H, s, OMe), 3.89 (1H, m, H3), 4.93 (1H, d, *J* 8.7 Hz, NH), 6.97 (1H, s, H6'), 8.22 (1H, s, H3').

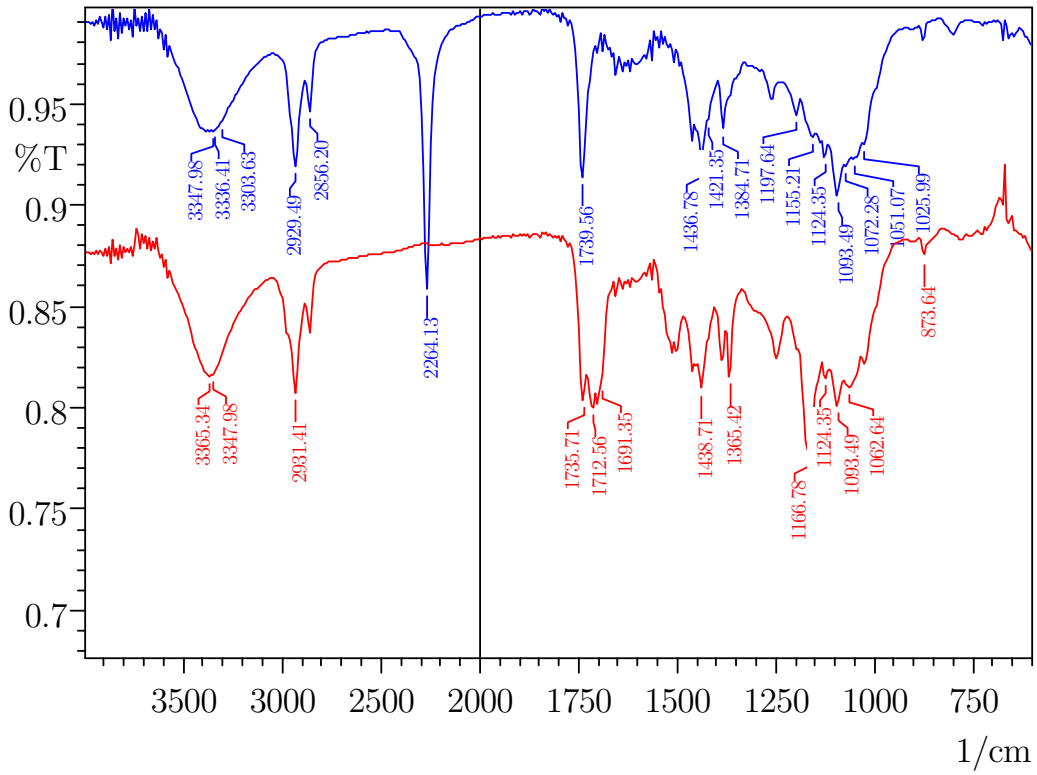

Figure 91. FTIR spectra of compounds **48** (red) and **49** (blue).

(*R*)-5-amino-7-base-heptanoate Type PNA Synthesis

Scheme 48 shows Leumann´s type peptide-nucleotide synthetic route summarized. As a function of the starting material selected, two different approaches may be used: the nonanoate branch and the heptanoate one. The reaction sequence is basic: starting materials provide a linear chain with a Michael system in one terminal and another oxidated functional group at the other one. The amine is properly incorporated through asymmetric Michael protocol described along this work.

Nonanoate route converge with the heptanoate by means of a fragmentation of the main chain, an ozonolysis. Chemoselective transformations leaded to the final PNA monomer.

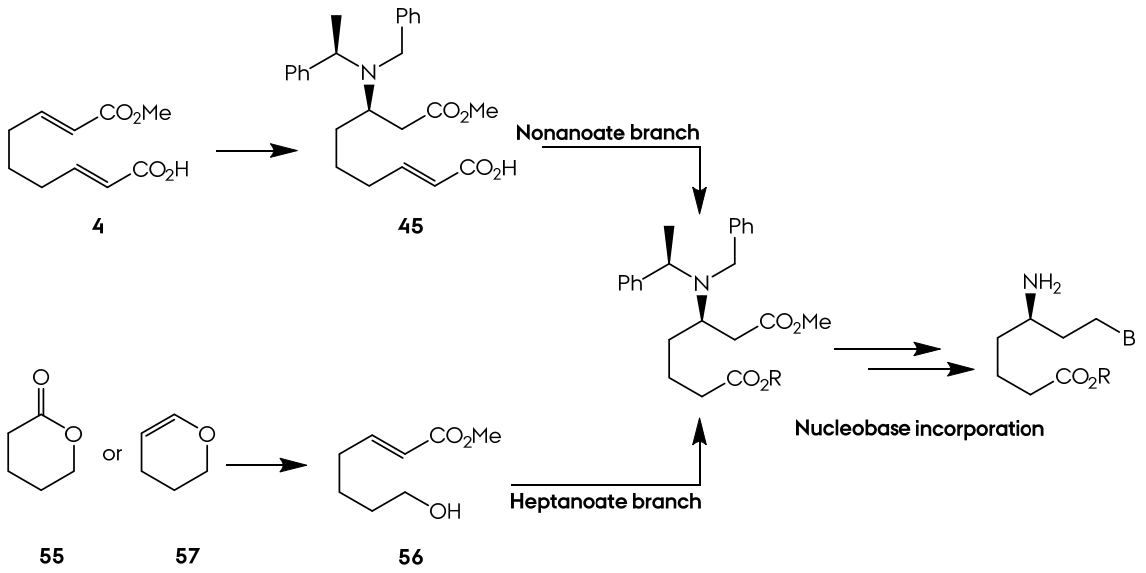

Scheme 48. Summary of the two synthetic routes towards Leumman´s PNA monomer.

Nonanoate branch

The path to key intermediate **54** takes advantage of compound **45**, which synthesis was discussed earlier (**Sch. 49**). Initially, the acid was transformed into the methyl ester, as was demonstrated in literature as requisite to overcome ozonolysis problems.[4] The procedure consisted in mix the acid with trimethylsilyl-diazomethane in a toluene/methanol 1:1 mixture. Excellent yield was obtained in the esterification (93 %).

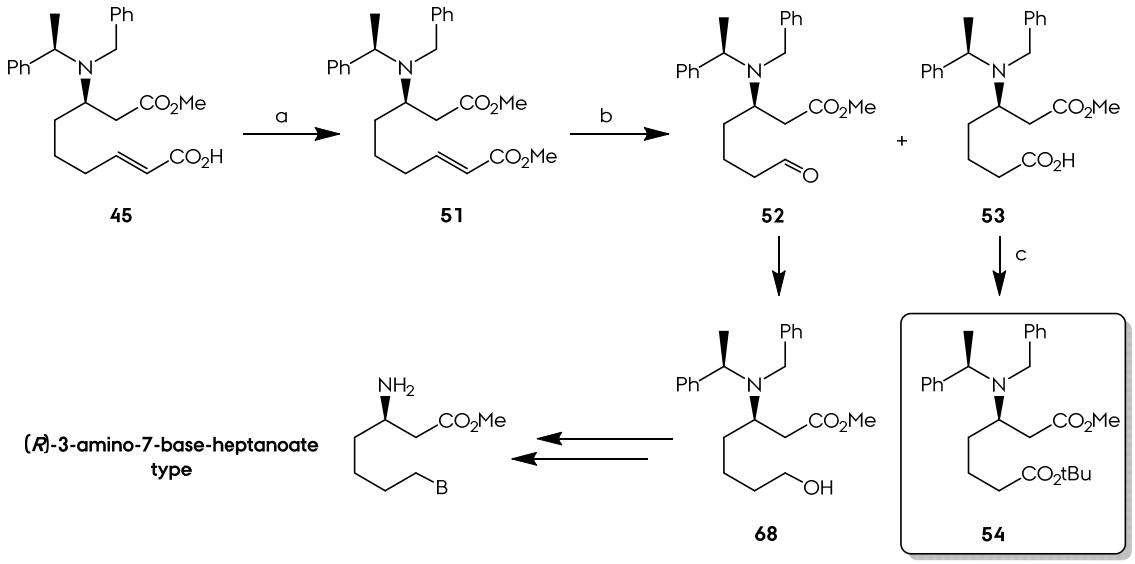

Scheme 49. *Reagents and conditions:* (a) $TMSCHN_2$, Toluene/MeOH 1:1, 30 min, 93 % (P6). (b) i. HCl (g), 10 min. ii. O_3 (g), 10 min. iii H_2O_2/DCM, (29 % of **52**, 31 % of **53** ,P7). (c) Boc_2O, DMAP, t-BuOH, 2 d, 62 % (P10).

Ozonolysis procedure was then performed. Substrate was dissolved into dichloromethane and cooled in a CO_2 - acetone bath till -78 ºC. A hydrogen chloride gas flow was bubbled in the solution, to avoid the formation of the *N*-oxide and prevent a Cope type elimination.[5] Forward hydrogen peroxide solution addition afforded a mixture 1:1 of the acid **53** and aldehyde **52**, as H^1 NMR revealed.

The ozonolysis cleavage had two main disadvantages:

- Attempts to obtain the fully oxidized acid as only product were unsuccessful. Although easily isolated through column chromatography, a mixture of the acid and aldehyde got in all cases.
- Scaling up the reaction lowered the reaction yield. The amount of crude obtained after reaction workup was less of the expected. Up to 200 mg the reaction yields were assumable, but beyond 200 mg, the material lost is remarkable. A propounded hypothesis was the not properly protonation of the amine by hydrogen chloride at high solution concentrations. Forward ozone bubbling yielded a considerable amount of *N*-oxide. This oxidized amine form is water-soluble, and difficult to isolate with acid-base extraction procedures.

Going on with the route, acid **53** was further esterificated to the *tert*-butyl ester **52**, as protecting group. Several reaction approaches were employed (**Tab. 11**). The fact that an ester derived from a tertiary alcohol is desired and, possibly, the steric effect of the benzyl arms of the amine, made almost all of them non-viable.

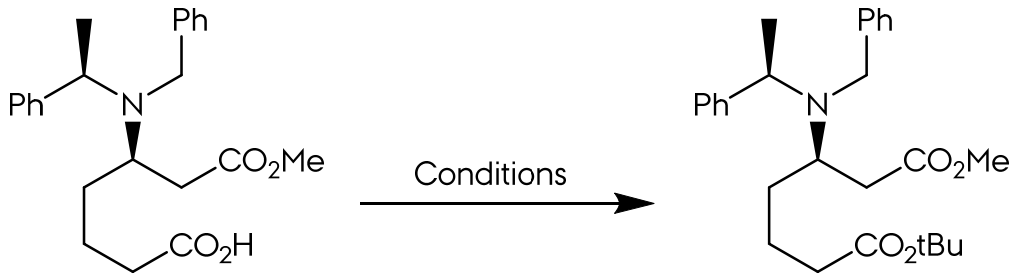

53 **54**

Entry	Reaction	Conditions	Time	53 (%)	54 (%)
1	**P8**	Isobutylene (g), H_2SO_4, DCM	21 h	25	46
2	**P9**	TFAA, tBuOH	13 h	79	20
3	**P10**	Boc_2O, DMAP, tBuOH	2 d	-	62

Table 11. Reaction conditions in the transformation of acid **53** into ester **54**.

However, using Boc_2O as activating, together with DMAP catalyst, in tBuOH as solvent, leaded to the ester in moderate yields (62 %). This reaction might be scaled up, getting quantities up to 1-1.2 g.

^{1}H NMR spectral properties of compounds 52-54 are almost the same, with backbone resonances well identified (**Fig. 92**).

Aldehyde **52** is an interesting intermediate which was used to obtain the (*R*)-3-amino-7-base heptanoate family of PNA monomers. This route will be discussed later.

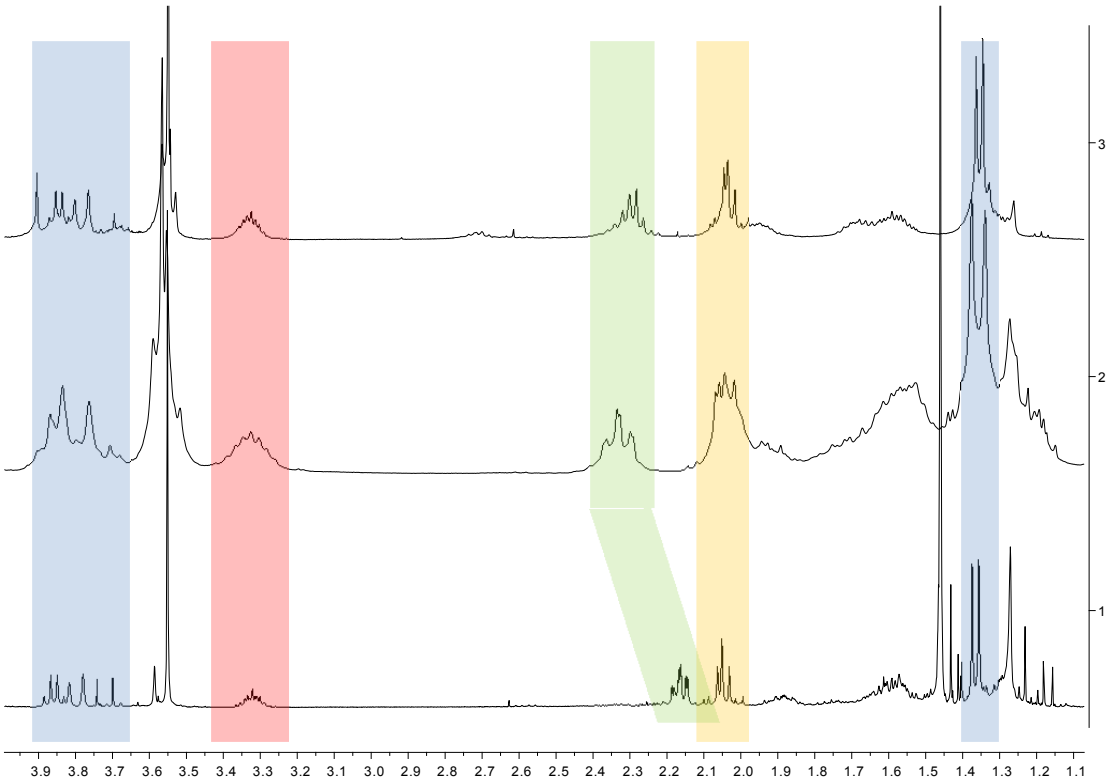

Figure 92. ^{1}H NMR spectra of compounds **52** (2), **53** (3) and **54** (1) at the 1.0-4.0 ppm range. Characteristic signals are highlighted in blue (chiral amine unit), red (C<u>H</u>N), green (C<u>H$_2$</u>COR) and yellow (C<u>H$_2$</u>CO_2Me).

Heptanoate branch

Two affordable products were the prime materials of this branch: δ-valerolactone and 3,4-dihydro-2*H*-pyran. This reaction branch, contrary to the nonanoate one, didn´t requires a fragmentation step, but a two-carbon homologation is needed to

obtain the correct number of carbons of the main chain. First reaction was, precisely, the homologation of the starting material, as **Scheme 50** states.

When δ-valerolactone **55** was selected,[6] an initial reduction of the lactone to lactol was carried out with DIBAL-H, at -78 ºC and inert atmosphere. Afterwards, a Horner-Wadsworth-Emmons protocol was used, employing methyl diethylphosphonoacetate. On the other hand, when 3,4-dihydro-2*H*-pyran was chosen,[7] only the Horner homologation was necessary, due to the appropriate oxidation state of the substrate. Both procedures required column chromatography to get rid of the phosphonate excess. Reaction yields were moderate, although the scaling level was at the 1-2 g scale (**Sch. 50**).

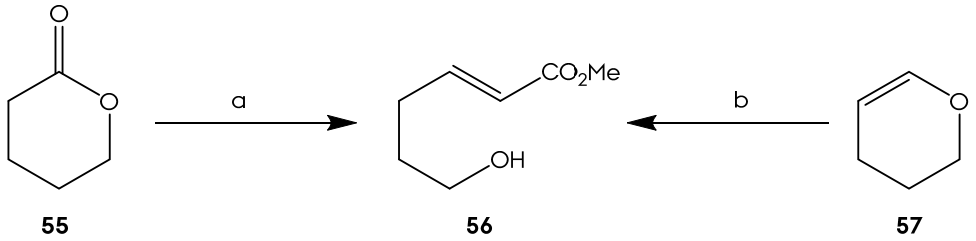

Scheme 50. *Reagents and conditions.* (a) i. DIBAL-H, THF, -78 ºC, 90 min. ii. $(EtO)_2POCH_2CO_2Me$, nBuLi, 17 h, 64 % (P11). (b) $(EtO)_2POCH_2CO_2Me$, K_2CO_3, LiCl, DMSO, 68 % (P12).

Once obtained the α,β-unsaturated ester, functional group interconversion of the other terminal was tackled (**Sch. 51**). Treatment of the alcohol **56** with *Jones reagent* (CrO_3, H_2SO_4, acetone) leaded to acid **58** in 85 % yield. Forward protection of the acid as *tert*-butyl ester was carried out employing earlier discussed conditions (Boc_2O, DMAP in tBuOH, 88 % yield). Once obtained the protected ester, next step was the asymmetric Michael addition of the chiral amine to afford the β-aminoester **54**. Employing routine conditions, the reaction yield was lower than expected, yielding 23 %. Reaction repetition did not improve the results. Literature search[8] revealed these kind of systems (long chain α,β-unsaturated ester) yielded low to moderate results. As one of the handicaps of the conjugate addition of lithium amides is competition with 1, 2-addition, the methyl ester was changed by *iso*-propyl ester and 3-pentyl ester. To obtain these derivatives, the same reaction sequence was developed; just changing the phosphonate's ester was enough. Conjugate addition of the lithium amide to the *iso*-propyl and 3-pentyl derivatives did not enhance the yields.

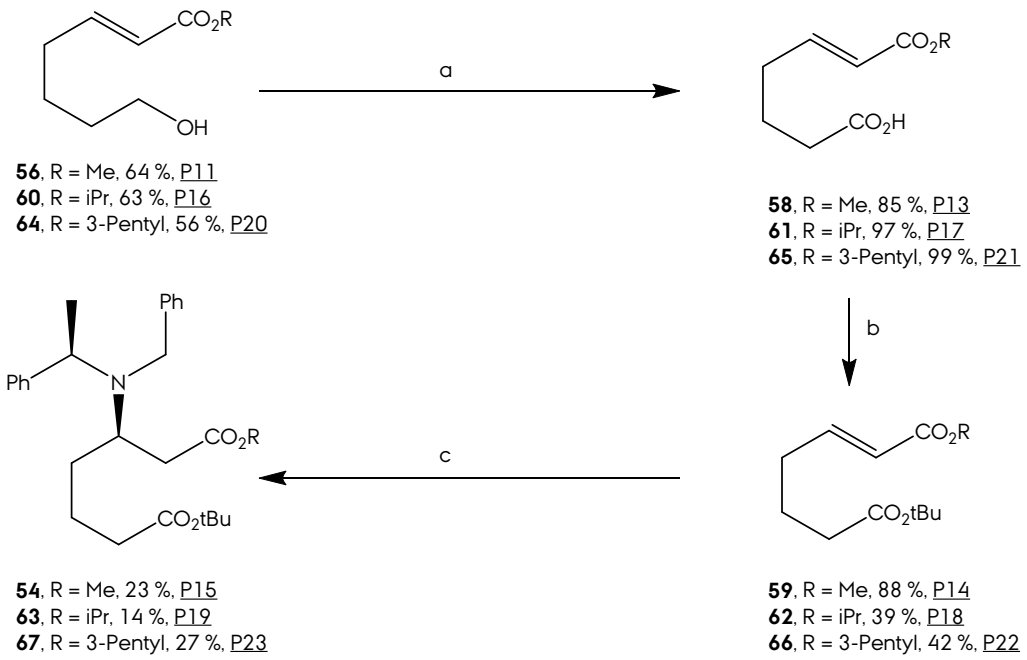

Scheme 51. *Reagents and Conditions:* (a) Jones reagent, acetone, 30 min. (b) Boc_2O, DMAP, tBuOH, 2 d, 30 ºC. (c) (*R*)-*N*-benzyl-*N*-*α*-methylbenzylamine, nBuLi, THF, -78 ºC, 3 h.

Spectroscopic characterization of each one of the ester series was easy, due to the small changes in the ^{1}H NMR profile.

Considering the drawbacks of realizing the addition in this point of the route, it was decided to make the addition to substrate **56**, the alcohol, which product was described in literature[6] with moderate to good yields. The inversion of the reaction sequence is depicted in **Scheme 52**.

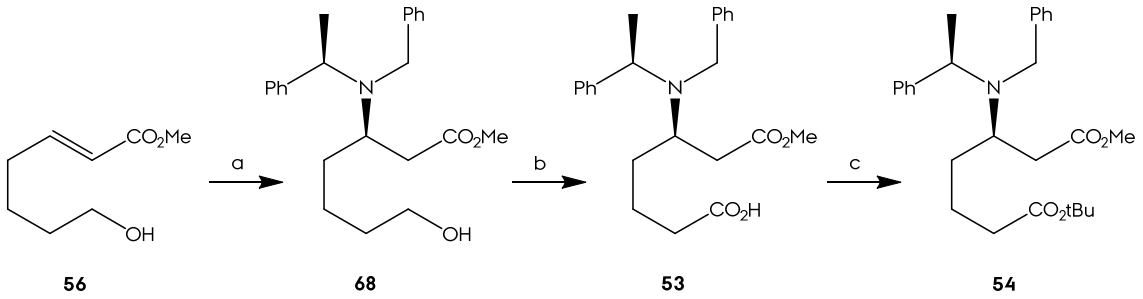

Scheme 52. *Reagents and Conditions:* (a) (*R*)-*N*-benzyl-*N*-*α*-methylbenzylamine, nBuLi, THF, -78 ºC, 3 h, 77 % (P24). (b) Jones reagent, acetone, 30 min, 91 % (P25). (c) Boc_2O, DMAP, tBuOH, 2 d, 30 ºC, 2 d, 62 % (P10).

Conjugate addition of the enantiomerically pure lithium amide give the adduct **68** in a 77 % yield. Column chromatography also yielded a mixture of 1, 2-addition and diaddition product (^{1}H NMR observed) which was not further purified. However, up to 1 g scale of **68** was obtained in this reaction after chromatography purification.

Treatment of this compound with *Jones reagent* afforded the acid **53**, without losing the enantiomerical purity (91 % yield). Final esterification of the acid with the combined Boc_2O-tBuOH mixture yielded the intermediate **54** with 62 % yield.

Nucleobase Incorporation

Once obtained the key intermediate **54**, last stage was the nucleobase introduction to the protected amino ester. Before proceeding to the nucleobase substitution, a few steps are required to change the protecting group of the amine and activate the position where the substitution will take place. From **54**, a protecting group interconversion was carried out, from dibenzyl amine to *tert*-butoxy carbonile amine, which is more appropriate in the amino acid context. A mixture of the substrate **54**, Boc_2O and $Pd(OH)_2$ over carbon was subjected to a hydrogen atmosphere of 3.5 atm. Short reaction times afforded a mixture of monoprotected amine **69** together with target product **70**. Increasing reaction time afforded only Boc protected amine **70** (**Tab. 12**).

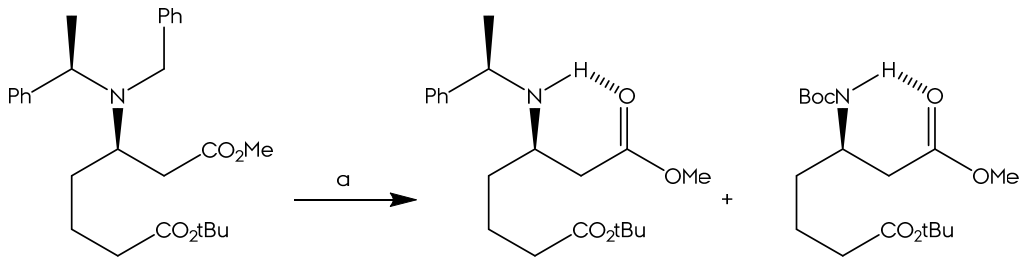

54 **69** **70**

Entry	Reaction	Conditions	Time	69 (%)	70 (%)
1	**P26**	H_2-$Pd(OH)_2$/C, Boc_2O, AcOEt	2d	13	50
2	**P27**		3d	-	83

Table 12. Reaction conditions in the transformation of **54** into **70**.

At first sight, the protecting groups of the amino and the ester group may be similar (*tert*-butyl ester and *tert*-butoxy carbamate); however, nowadays there is a number of articles describing orthogonal deprotection of one group in the presence of the other, being absolutely orthogonal.[9] Having a look at the ^{1}H NMR spectra (**Fig. 93**) of compounds **54**, **69** and **70**, the shift of H2 signals in the successive compounds represents an interesting feature. In **69**, this signal is an ABX system, while in **70** is a doublet. The reason is the intramolecular hydrogen bonding between amine group

and carbonyl in both compounds, which locks the conformation of the molecule (figure at the top of **Tab. 12**).

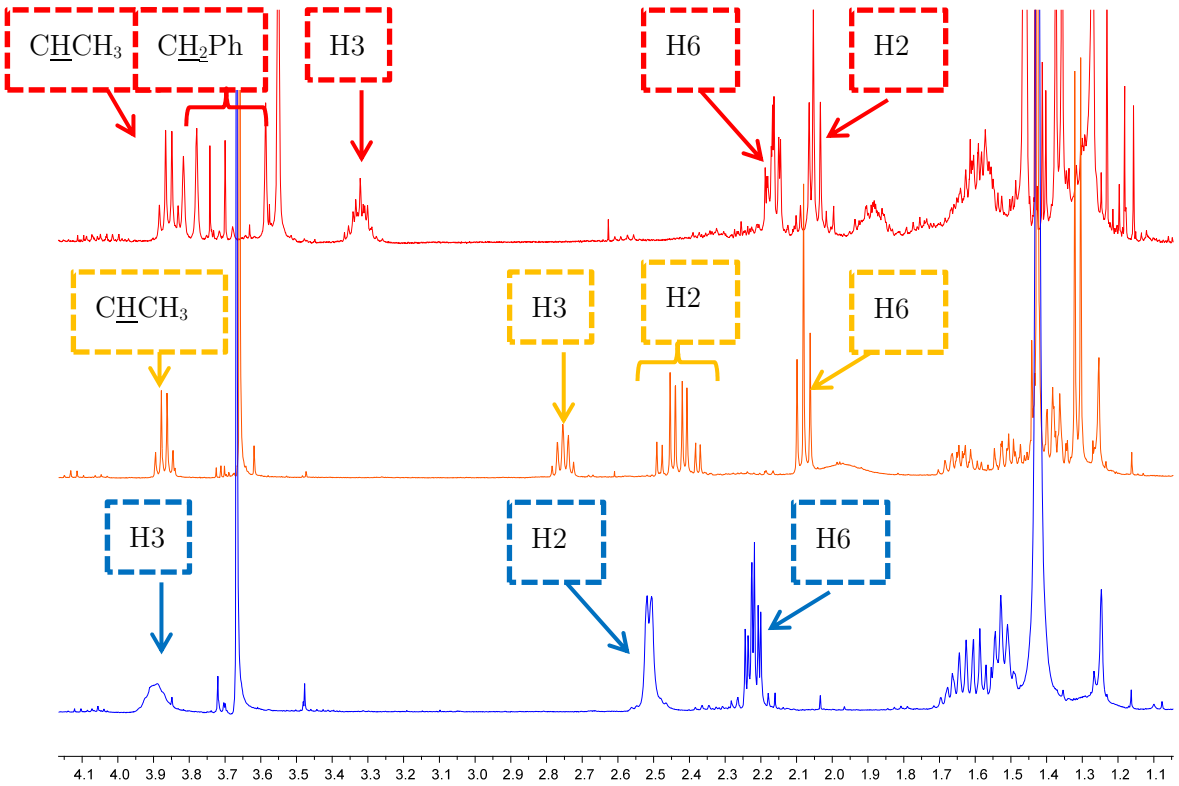

Figure 93. ^{1}H NMR spectra of **54 (red)**, **69** (orange) and **70** (blue) at the 1.0 – 4.2 ppm range.

Chemoselective reduction of the methyl ester to hydroxyl was achieved by lithium borohydride, in a 90 % yield. This hydroxyl compound **71** was one of the candidates to perform the substitution. To activate the hydroxyl group as leaving group, mesylation of the hydroxyl was carried out using methanesulfonyl chloride with pyridine, DMAP in DCM, obtaining the mesylate **72** with 96 % yield (**Sch. 53**).

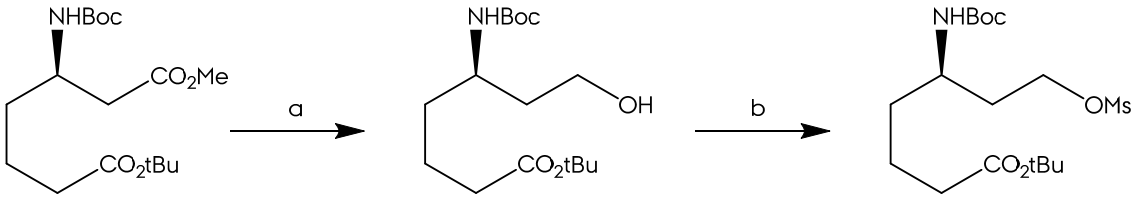

70 **71** **72**

Scheme 53. *Reagents and Conditions:* (a) $LiBH_4$, THF, 6 h, 90 % (P28). (b) MsCl, DMAP, Pyridine, DCM, 12 h, 96 % (P29).

Once prepared compound **72**, the last stage is the introduction of thymine, following described conditions of Tadei *et al.*[3] Reaction workup afforded a complex mixture of

products, which were clarified after flash chromatography: cyclization product **73** was obtained in a 37 % yield, together with an inseparable mixture of isomers **74** and **75** (**Sch. 54**). Carbamate **73** was correctly identified by means of ^{1}H NMR spectroscopy (cleavage of the *tert*-butyl ester).

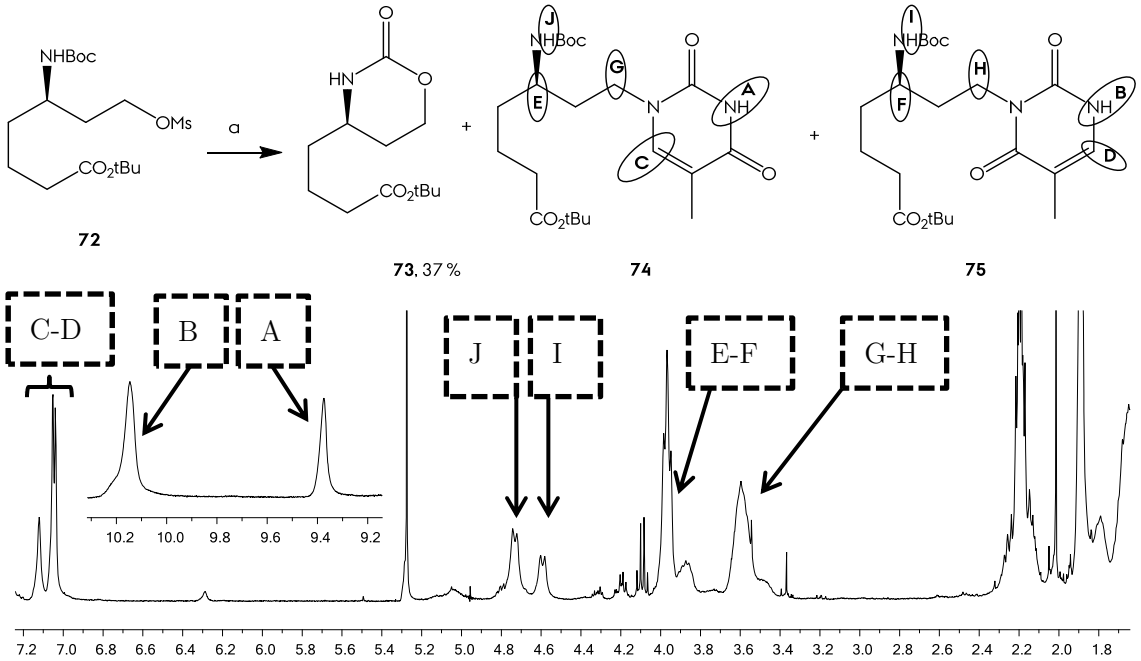

Scheme 54. *Reagents and Conditions:* (a) Thymine, TBAI, K_2CO_3, DMF, 70 ^{o}C, 6 h (P30). ^{1}H NMR spectra of mixture **74**:**75** at the 1.8-7.2 range. Bottom: ^{1}H NMR spectra of chromatographic fraction **74**+**75**.

Formation of **73** is explained in **Scheme 55**. Thermolysis of the *tert*-butoxycarbamate and forward cyclization has been observed in literature,[10] as a reason of the intermolecular attack via leaving group displacement.

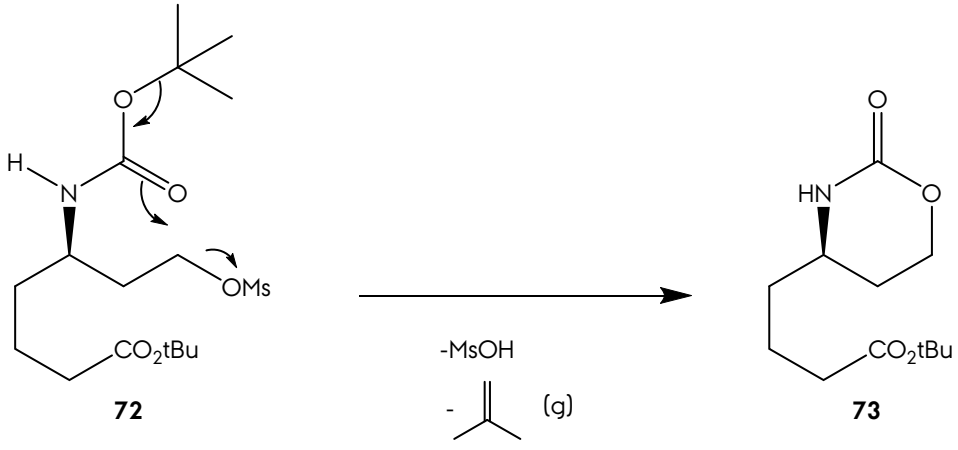

Scheme 55. Possible reaction mechanism in the cyclization of **72** to **73**.

The driving force of this cleavage is the stability of the *tert*-butyl cation, transformed later into isobutylene. This cyclization was also reported in our group.[11]

As the products were difficult to separate through column chromatography, a reaction protocol where there is no competition between *N*1 and *N*3 alkylation is required. The procedure developed by Rad *et al.* was taken to tackle this issue, as they justified that the method is regioselective in the case of thymine.[12] The procedure uses 1-(*p*-toluenesulfonyl)imidazole as activating agent, together with the substrate's alcohol, a 1:1 mixture of K_2CO_3/Et_3N in refluxing DMF.

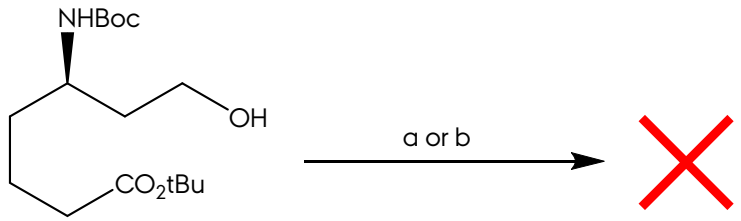

71

Scheme 56. *Reagents and Conditions:* (a) Thymine, 1-(*p*-toluenesulfonyl)imidazole, Et_3N, K_2CO_3, DMF, 70 ºC, 12 h (P31). (b) Thymine, 1-(*p*-toluenesulfonyl)imidazole, Et_3N, K_2CO_3, DMF, 150 ºC, 12 h (P32).

Reaction workup (**Sch. 56**) afforded a recovery of the starting material and the 1-(*p*-toluenesulfonyl)imidazole, both at 70 ºC and under reflux temperature. No cyclization product was observed, so an activation of the hydroxyl group is required. We envisaged to study which are the best conditions to avoid thermolysis and obtained the substitution product in good yields. To make this, we have to test some reactions with the following conditions:

- Thermolysis is a common problem in these systems, so a room temperature or not refluxing system is required.
- Basic conditions also cooperates in the cyclization.
- Thymine solubility may be a problem, and more soluble thymine based compounds are required.
- Thymine also may react with different regioselectivities, so a protecting group scheme is needed.

- To avoid wasting high valuable material, a simplified model would be an advantage.

Taking these considerations, a series of different nucleobase reaction tests were carried out over a simplified model of our substrate. We take 3-amino-1-propanol as starting material, and prepared a model compound in two steps (**Sch. 57**) by means of: (1) protecting the amine group and (2) activating the alcohol.

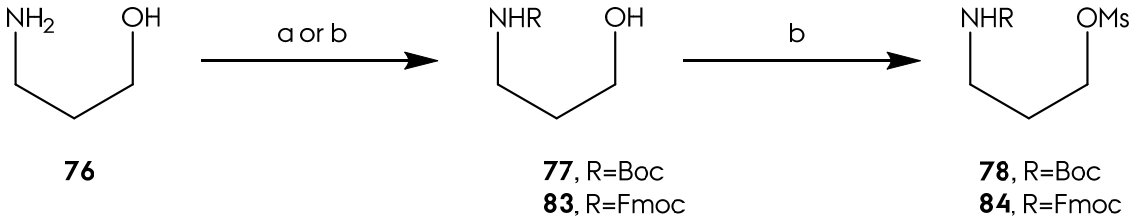

Scheme 57. *Reagents and Conditions:* (a) Boc_2O, DCM, 91 % (P32). (b) Fmoc-OSu, $NaHCO_3$, acetone:H_2O 6:4, 99 % (P42). (b) MsCl, DMAP, Py, DCM (75%, P33; 99 %, P43).

Two protected alcohol were synthetized, the Boc and the Fmoc protected amines, in good yields. Forward activation through mesylation leaded to compounds **78** and **84**. These two products are analogues of our parent structure **71**, without the lateral chain. Once synthetized these compounds, reaction trials were carried out at different conditions (**Tab. 13**).

Tadei type reaction conditions were tested first. When the reaction temperature was 70 ºC (entry 1), substitution product were obtained in a low yield (27 %). No regioisomer alkylation product was observed (easily identifiable by the duplication of the signals of the thymine and the alpha methylene group to thymine), but cyclization product **80** were detected at the reaction workup (**Fig. 94**). If the reaction was carried out at reflux temperature (entry 3), the reaction yield lowered drastically. Both reactions were repeated changing the base (from potassium carbonate to DBU), with the purpose of study base strength influence.

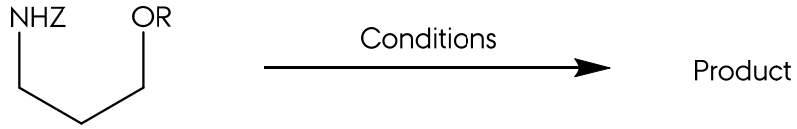

77, Z=Boc, R=H
78, Z=Boc, R=Ms
84, Z=Fmoc, R=Ms

Entry	R	S	Conditions	T	Product	Yield
1	P35	**78**	thymine, K_2CO_3, TBAI	70 ºC	**79, 80** (1:1)	27 % (**79**)
2	P36	**78**	thymine, K_2CO_3, TBAI	150 ºC	**79**	↓ 12 %
3	P37	**78**	thymine, DBU, TBAI	70 ºC	**79, 80** (1:1)	↓ 33 % (**79**)
4	P38	**78**	thymine, DBU, TBAI	150 ºC	**79**	↓ 6 %
5	P39	**78**	K_2CO_3, TBAI	70 ºC	**78, 80** (1:1)	
6	P40	**78**	6-chloropurine, K_2CO_3, TBAI	rt	**81, 78** (4:6)	
7	P41	**78**	6-chloropurine, K_2CO_3, TBAI	70 ºC	**81, 80** (3:1)	
8	P42	**77**	1-(*p*-toluenesulfonyl)imidazole, thymine, K_2CO_3, Et_3N	150 ºC	**77**	
9	P43	**77**	6-chloropurine, PBu_3, DIAD, THF	rt	**81**	68%
10	P47	**84**	thymine, K_2CO_3, TBAI	70 ºC	**85**	
11	P48	**84**	6-chloropurine, K_2CO_3, TBAI	70 ºC	**85**	
12	P49	**84**	K_2CO_3, TBAI	70 ºC	**85**	

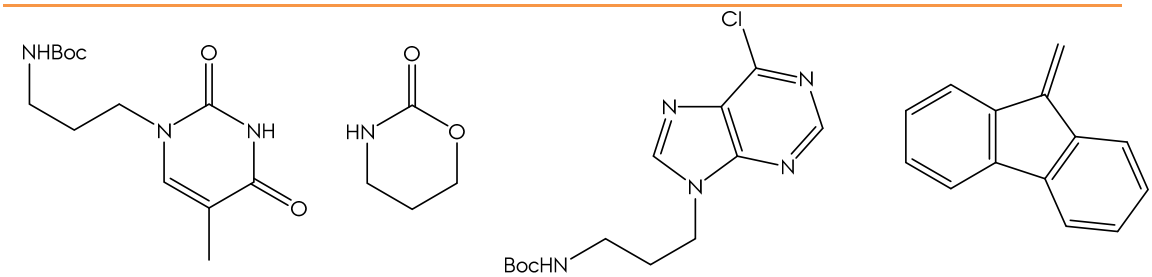

79 80 81 85

Table 13. Reaction conditions in the nucleobase introduction trials. Chromatographic yields.

The results were also the same, indicating several conclusions:

- Compared with substrate **72**, these reactions did not afford alkylated thymine regioisomer. As the conditions were the same, the structure of substrate is critical in the appearance of the parallel reaction. It was

postulated that substrate **72**, due to the presence of the lateral chain, may offer sterical hindrance to the attack of the nucleobase. This sterical obstacle, may retard the main reaction, allowing to deprotonated thymine to equilibrates and deprotonate the *N*3 position (base is limitant respect to thymine). This deprotonation is likely to be kinetically slower than the nucleophilic substitution, otherwise this effect would be observed always. On the other hand, products **50** and **92** did not show regioisomeric mixtures, ensuring the theory of the substrate-dependence of the reaction outcome.

- Compared with substrate **72**, these reactions also afforded cyclization product. Although product **80** were not isolated, comparison of crude workup with literature data[13] was enough to identify it (**Fig. 94**). Deprotonated thymine or the base also participates in the cleavage of the Boc-amine group.
- Refluxing conditions harmed the reaction outcome. Low temperature reactions are required.

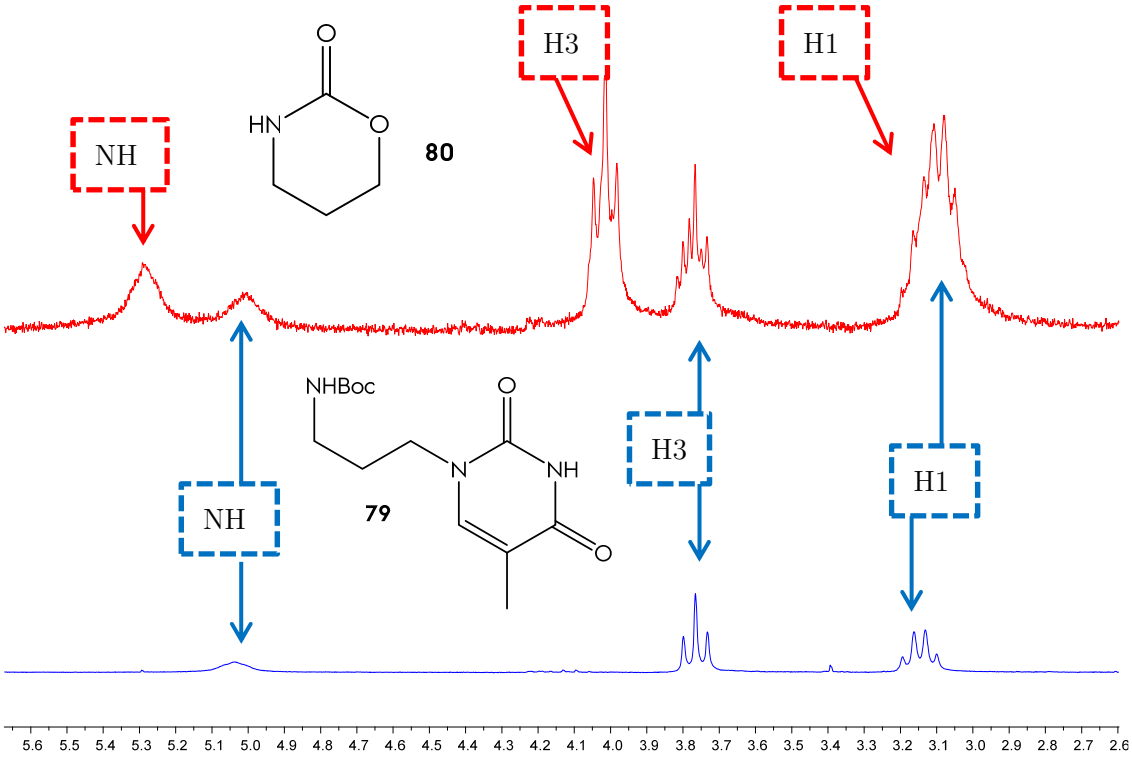

Figure 94. ^{1}H NMR spectra of **80**:**79** mixture (red) and **79** (blue) at the 2.6-5.6 ppm range. **80** signals are highlighted in red, while **79** ones are highlighted in blue.

As cyclization was one of the main disadvantages, reaction of substrate **78** with just base and TBAI in absence of thymine was carried out. A 1:1 mixture of mesylate **78** and cyclization product **80** were obtained, so it was confirmed the conditions were responsible of the parallel reaction.

The influence of the nucleobase was also checked. If the reaction were carried out with 6-chloropurine instead of thymine, cyclization product was also obtained, but in less quantity. When the reaction was carried out at room temperature, the reaction was not completed.

As the activated alcohol is also a handicap in the cyclization, 1-(*p*-toluenesulfonyl)imidazole method was tested. However, no reaction was manifested and the starting material was recovered. Next step was use Mitsunobu type nucleobase substitution. There are several examples in literature where this reaction has been successfully carried out.[14] We tested this reaction with 6-chloropurine and PBu_3 instead of PPh_3 to avoid isolation problems of the products. The reaction was successfully carried out, yielding a 68 % of the substitution product **81**. No cyclization product was detected. As the nucleobase was not adenine, it was proceeded to nucleobase transformation. Dissolving the substrate **81** in a 2 M solution of NH_3 in EtOH in a pressure vessel afforded the nucleophilic aromatic substitution product **82** in excellent yields (**Sch. 58**).

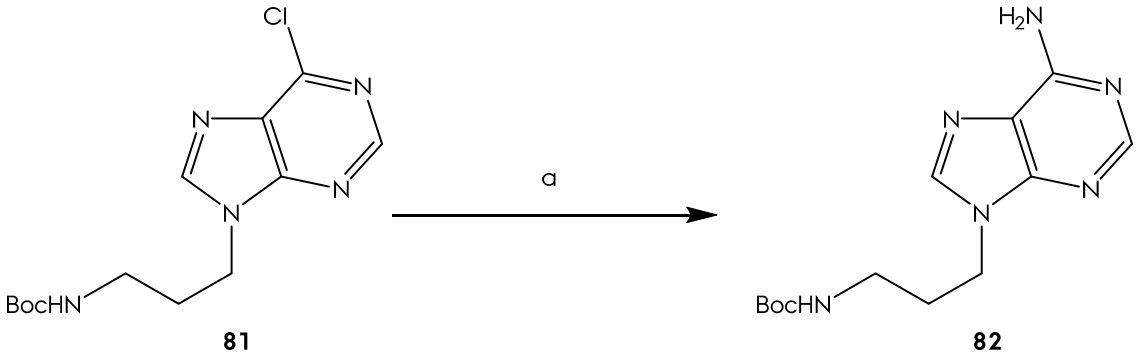

81 **82**

Scheme 58. *Reagents and Conditions:* (a) 2 M NH_3, EtOH, 120 ºC, 12 h, 94 % (P44).

Finally, the influence of the protecting group was checked through compound **84**, the Fmoc protected model. Tadei reaction conditions were used along with thymine and 6-choloropurine, however, the cleavage of the protecting group was observed, due to the identification in ^{1}H NMR crudes of the Fmoc degradation product **85**. If the reaction was carried out without nucleobase, the reaction outcome was the same.

From this reaction study, next conclusions may be extracted:

- Fmoc group protecting group doesn´t avoid protecting group cleavage.

- Tadei type conditions afford nucleobase substitution products in low yields, but cyclization products are obtained as well, as a consequence of the basic conditions and the activated substrate. Reflux conditions lowered drastically the yield.

- Regioisomeric thymine insertion product is a consequence of the structure of the substrate **72**. When 6-chloropurine was used, no regioisomeric product were obtained.

- Mitsunobu type reactions are the best in terms of yield and selectivity.

As Mitsunobu type reactions were the best conditions, this methodology was followed to introduce the nucleobase, avoiding the cyclization products. However, in the thymine case, protection of the *N*3 was carried out to avoid the reaction of this center.

The most common protection in thymine was the benzoylation of the *N*3 center. The N^3-Bz-thymine was synthetized accordingly with Reese *et al* procedure (see lab prepared reagents at the Methodologies and Materials section).[15] Apart from blocking the activity of the *N*3 center, the solubility of thymine in organic solvents was also increased.

If Tadei conditions were repeated with protected thymine, the substitution product **86** was obtained in a 23 % yield (entry 1, **Tab. 14**). No regioisomer was obtained, but cyclization secondary product was detected in small quantities. On the other hand, when Mitsunobu conditions was followed, the yield was increased significantly to 75 %, without detecting cyclization or regioisomer products. A possible O^2-alkylation product was also not observed, a competition product that appears in this kind of reactions.[16] The protocol was also used in the synthesis of the adenine and guanidine predecessors **88** and **89**, yielded in 61 % and 53 % (**Tab. 14** and **Fig. 95**).

71, Z = H
72, Z = Ms

Entry	R	S	Conditions	T	Product	Yield
1	P50	**72**	N^3-Bz-thymine, DBU, TBAI	70 °C	**86**	23%
2	P51	**71**	N^3-Bz-thymine, PBu_3, DIAD, THF	rt	**86**	75%
3	P54	**71**	6-chloropurine, PBu_3, DIAD, THF	rt	**88**	61%
4	P55	**71**	2-amino-6-chloropurine, PBu_3, DIAD, THF	rt	**89**	53%

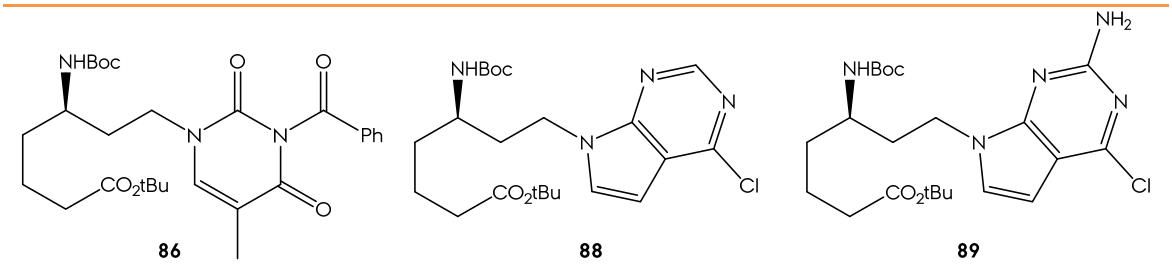

Table 14. Reaction conditions in the nucleobase introduction in **71** and **72**.

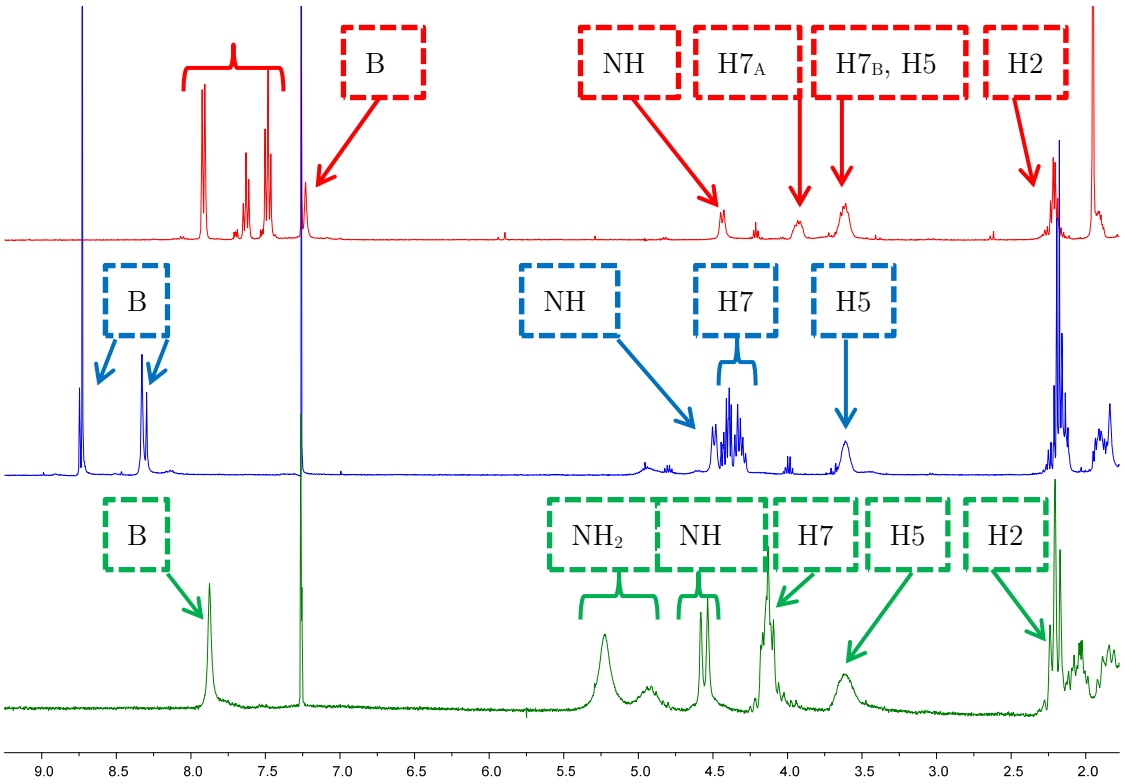

Figure 95. ^{1}H NMR spectra of **86** (red), **88** (blue) and **89** (green) at the 2.0-9.0 ppm range.

Finally, PNA monomer **86** was transformed into Leumann's enantiomer **87** (**Sch. 59**).

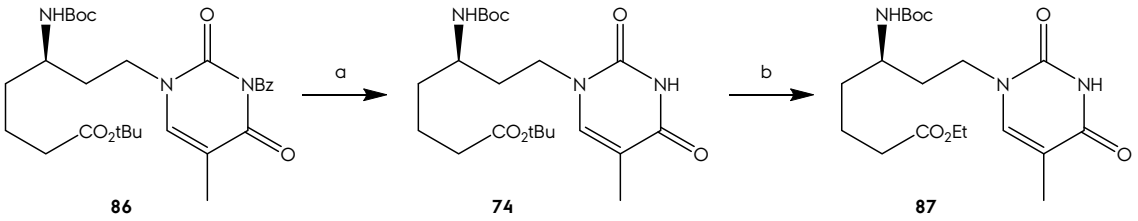

Scheme 59. *Reagents and Conditions:* (a) LiOH, MeOH/THF/H_2O 3:1:1, h, 97 % (P52). (b) i. HCl (g), EtOH. ii. Boc_2O, DMAP, DCM, rt, 54 % (P53).

First, lithium hydroxide based hydrolysis afforded free thymine derivative **87** in a 97 % yield. Next, a one pot complete cleavage of the *tert*-butyl protecting groups and esterification of the free acid as ethyl ester was carries out bubbling HCl gas in a solution of substrate **74** in EtOH. The crude was immediately dissolved in DCM and Boc_2O with DMAP was added. After carefully workup and flash chromatography, Leumann's PNA enantiomer **87** was obtained in a 54 % yield. 1H NMR resonances match with Leumann's published results: 8.03 (1H, s, CONHCO), 7.12 (1H, s, NCH), 4.41 (1H, d, *J* 7.4, NHCO), 4.12 (2H, q, *J* 7.1, OCH_2CH_3), 3.82 (1H, m, $H7_A$), 3.60 (2H, m, H5 and $H7_B$), 2.30 (2H, H2), 1.92 (3H, s, CCH_3), 1.69-1.45 (6H, H3, H4 and H6), 1.45 (9H, s, $C(CH_3)_3$), 1.25 (3H, t, *J* 7.1, OCH_2CH_3). Optical rotation was also measure. The value of compound **88** is $[\alpha]^{20}_D$ -9.2 (*c.* 0.24 in MeOH), while Leumann's PNA monomer is found to be $[\alpha]^{20}_D$ +12.1 (*c.* 0.01 in MeOH).[1]

(*R*)-3-amino-7-base-heptanoate Type PNA Synthesis

Last family of synthetized nucleopeptides corresponds to the (*R*)-3-amino-7-base-heptanoate type, a β-aminoester with the nucleobase at terminal 7. **Scheme 60** shows the path to this type of PNA monomer.

Intermediate **68**, obtained in the previous route, has the appropriate substitution: only the nucleobase is lacked. **68** might also be obtained from **52**, the aldehyde which was obtained with the acid **53** in the ozonolysis step in the first route of the section. Just a mild reduction with sodium borohydride is enough to achieve alcohol **68** in 98 % yield.

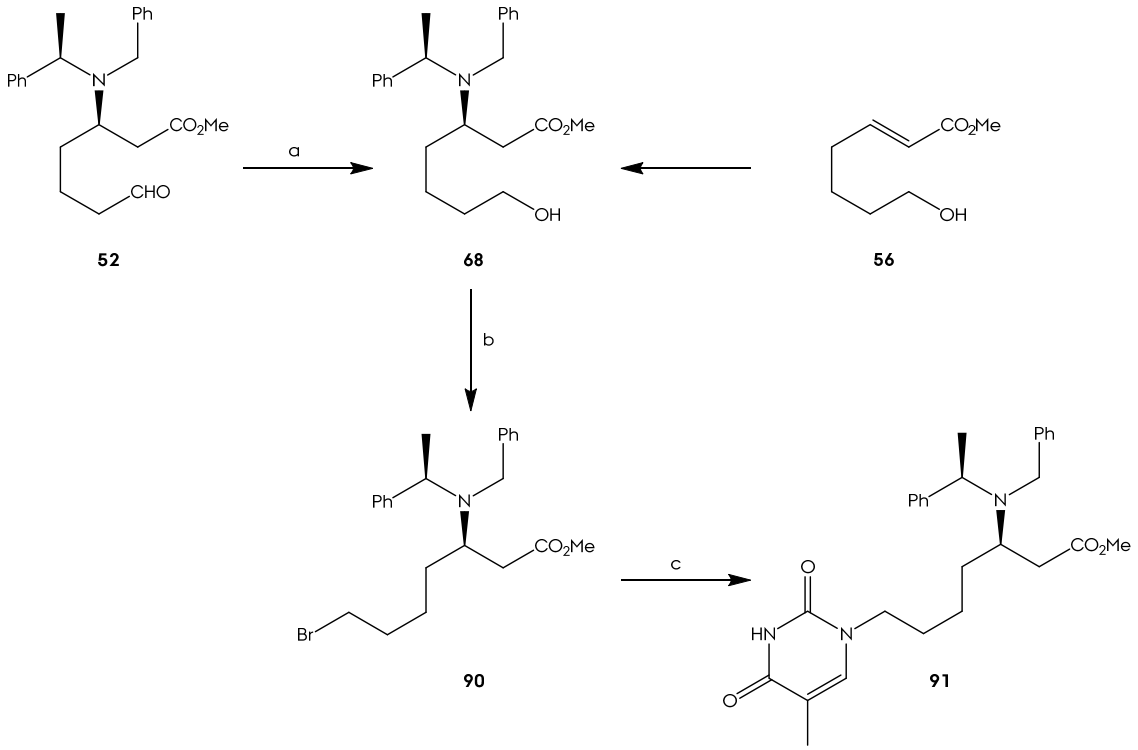

Scheme 60. *Reagents and conditions*: (a) $NaBH_4$, MeOH, rt, 98 % (P56). (b) CBr_4, PPh_3, DCM, 64 %, (P57). (c) Thymine, TBAI, K_2CO_3, DMF, 70 ºC, 34 % (P58).

Next reaction is the substitution of the hydroxyl by bromine, through carbon tetrabromide and triphenylphosphine as reagents in dichloromethane. Final substitution in the activated compound **90** leaded to PNA monomer **91**, in a 34 % yield. No regioisomeric product was detected. Although the protecting group of the amine is the debenzyl group, this compounds was reserved to check deprotection strategies in the presence of the heterocyclic ring.

Conclusions

In this chapter, 7 PNA monomers have been synthetized (**Fig. 96**): all in common have the same hydrophobic backbones. Key step was the asymmetric Michael addition of (*R*)-*N*-benzyl-*N*-α-methylbenzylamine to afford β-amino esters with total control of the stereochemistry. Using the *S* enantiomer, the other stereochemical family of compounds would be obtained.

The applied methodologies allowed preparing a diversity of PNA's only varying the positions of the functionalized groups in the main backbone. Mitsunobu type

nucleobase introduction has also proved to be a high valuable protocol to introduce nucleobases in high yield, one of the main disadvantages in nucleic acid synthetic chemistry. This was the first time this reaction was used in our group and allows to improve the results in obtaining future PNA monomers. It was, also, the first time of introducing different nucleobases than thymine, broadening the synthetic scopes.

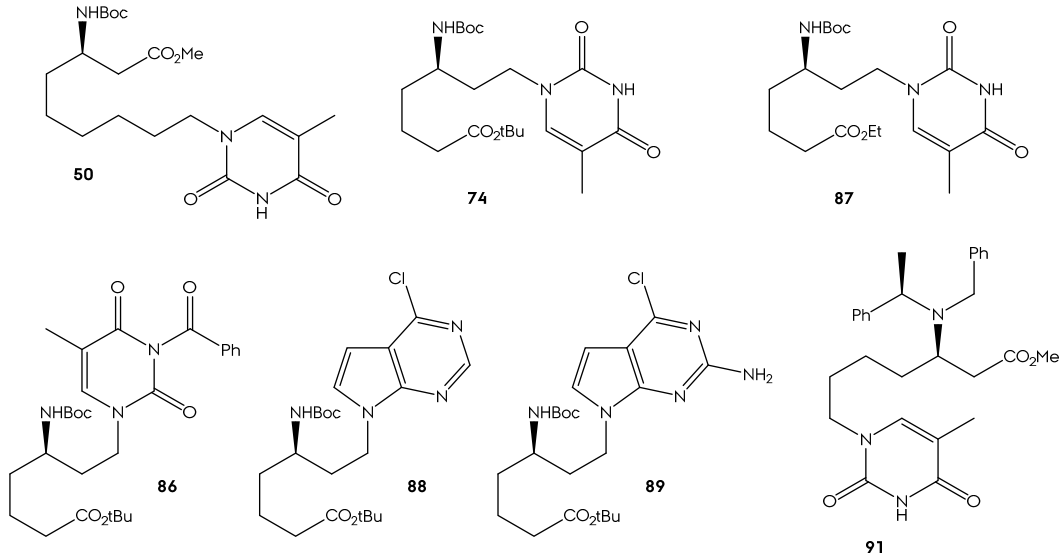

Figure 96. PNA monomers synthethized in this chapter.

Leumann's PNA enantiomer was obtained in moderate yields from PNA monomer **87**, and the spectroscopic information, as well as the optical rotation in coherence with data supplied by Leumann *et al.*

References

[1] Savithri, D.; Leumann, C.; Scheffold, R. *Helv. Chim. Acta* **1996**, *79*, 288.

[2] Garrido, N. M.; Rubia, A. G.; Nieto, C.; Díez, D. *Synlett* **2010**, *2010*, 587.

[3] Lenzi, A.; Reginato, G.; Taddai, M. *Tetrahedron Lett.* **1995**, *36*, 1713.

[4] (a) Pryor, W. A.; Giamalva, D.; Church, D. F. *J. Am. Chem. Soc.* **1983**, *105*, 6858. (b) Pryor, W. A.; Giamalva, D.; Church, D. F. *J. Am. Chem. Soc.* **1985**, *107*, 2793.

[5] Hanessian, S.; Sancéau, J.-Y.; Chemla, P. *Tetrahedron* **1995**, *51*, 6669.

[6] Davies, S. G.; Fletcher, A. M.; Hughes, D. G.; Lee, J. A.; Price, P. D.; Roberts, P. M.; Russell, A. J.; Smith, A. D.; Thomson, J. E.; Williams, O. M. H. *Tetrahedron* **2011**, *67*, 9975.

[7] Baenziger, M.; Gobbi, L.; Riss, B. P.; Schaefer, F.; Vaupel, A. *Tetrahedron: Asymmetry* **2000**, *11*, 2231.

[8] Davies, S. G.; Fletcher, A. M.; Roberts, P. M.; Thomson, J. E. *Tetrahedron: Asymmetry* **2012**, *23*, 1111.

[9] Marcantoni, E.; Massaccesi, M.; Torregiani, E.; Bartoli, G.; Bosco, M.; Sambri, L. *J. Org. Chem.* **2001**, *66*, 4430.

[10] Croucher, P. D.; Furneaux, R. H.; Lynch, G. P. *Tetrahedron* **1994**, *50*, 13299.

[11] Dominguez, S. H., Salamanca, 2001.

[12] Soltani Rad, M. N.; Khalafi-Nezhad, A.; Behrouz, S.; Faghihi, Mohammad A.; Zare, A.; Parhami, A. *Tetrahedron* **2008**, *64*, 1778.

[13] Inesi, A.; Mucciante, V.; Rossi, L. *J. Org. Chem.* **1998**, *63*, 1337.

[14] (a) Brückner, Arndt M.; Garcia, M.; Marsh, A.; Gellman, Samuel H.; Diederichsen, U. *Eur. J. Org. Chem.* **2003**, *2003*, 3555. (b) Paju, A.; Päri, M.; Selyutina, A.; Žusinaite, E.; Merits, A.; Pehk, T.; Siirde, K.; Müürisepp, A. M.; Kailas, T.; Lopp, M. *Nucleos. Nucleot. Nucl.* **2010**, *29*, 707. (c) Dreier, I.; Kumar, S.; Søndergaard, H.; Rasmussen, M. L.; Hansen, L. H.; List, N. H.; Kongsted, J.; Vester, B.; Nielsen, P. *J. Med. Chem.* **2012**, *55*, 2067. (d) Seth, P. P.; Yu, J.; Jazayeri, A.; Pallan, P. S.; Allerson, C. R.; Østergaard, M. E.; Liu, F.; Herdewijn, P.; Egli, M.; Swayze, E. E. *J. Org. Chem.* **2012**, *77*, 5074. (e) Eid, A. A.; Koubeissi, A.; Bou-Mjahed, R.; Khalil, N. A.; Farah, M.; Maalouf, R.; Nasser, N.; Bouhadir, K. H. *Bioorg. Med. Chem. Lett.* **2013**, *23*, 174.

[15] Cruickshank, K. A.; Jiricny, J.; Reese, C. B. *Tetrahedron Lett.* **1984**, *25*, 681.

[16] Ludek, O. R.; Meier, C. *Eur. J. Org. Chem.* **2006**, *2006*, 941.

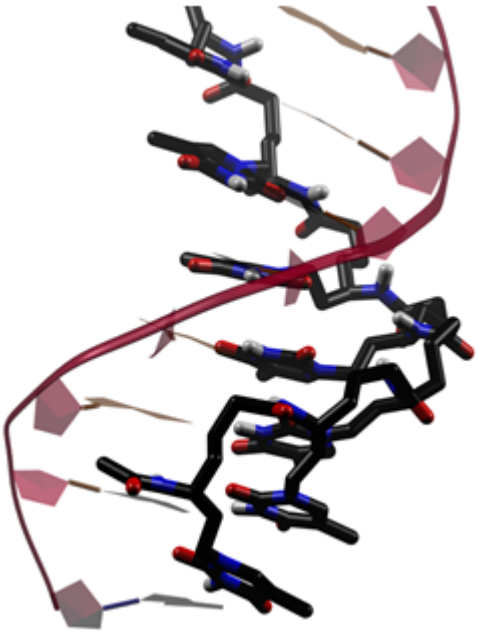

6 Molecular Dynamics Simulations of Flexible Peptide-Nucleotides (PNA)

Introduction

The synthesis of novel peptide-nucleic units requires a subsequent binding study of nucleic oligopeptides to natural oligonucleotides. Melting point titrations, circular dichroism or NMR are, among others, experimental techniques to evaluate the structure, binding strength and stability of nucleic acid hybrids.[1]

Molecular modelling is also a routine tool to survey nucleic acid chemistry, natural and new synthetic structures. Locked and Peptide Nucleic acids have been extensively studied through Quantum Mechanics[2] and Molecular Dynamics,[3] in order to check hybrids stability, topological information and thermodynamic properties. Quantum mechanics studies of peptide nucleic systems, due to its computationally demanding nature, is only relegated to single point calculations, electrostatic potential mapping, and frontier orbital estimation. Besides, the system size is often made by the nucleobases, rarely extensively to the entire strand. On the other hand, the more extended Molecular Dynamics simulations allows to study complete soaked systems, evaluating solvent accessibility, global and local topological features, ionic distribution, and even interaction with peptides, ligands or proteins.

In this chapter, an MD simulation study of the hybridization properties of nucleic oligopeptides to natural DNA is envisaged. Our peptide nucleic acid motif, **74**, has been used as monomer in modelling a hypothetical PNA-DNA hybrid. A just-thymine homopolymer was modelled, and hybridized with a complementary adenine DNA. Topological, solvation and thermodynamic properties were surveyed.

Systems modelling and MD protocol

The MD simulations of PNA-DNA hybrids required an initial set up of the systems which would be simulated. It is well known[4] peptide nucleic acids may hybridize in a parallel fashion, i.e. the C-terminal of the peptide is faced towards the 3' end of the complementary DNA, and in an antiparallel way, with the *N*-terminal of the peptide oriented to the 3' terminal of the natural oligonucleotide. It has demonstrated the antiparallel scheme is more stable than the parallel one.[5] Due to this double complementarity, three simulation systems were prepared (**Fig. 97**): DNA(A)-DNA(T); DNA(A)-pPNA(T), and DNA(A)-apPNA(T).

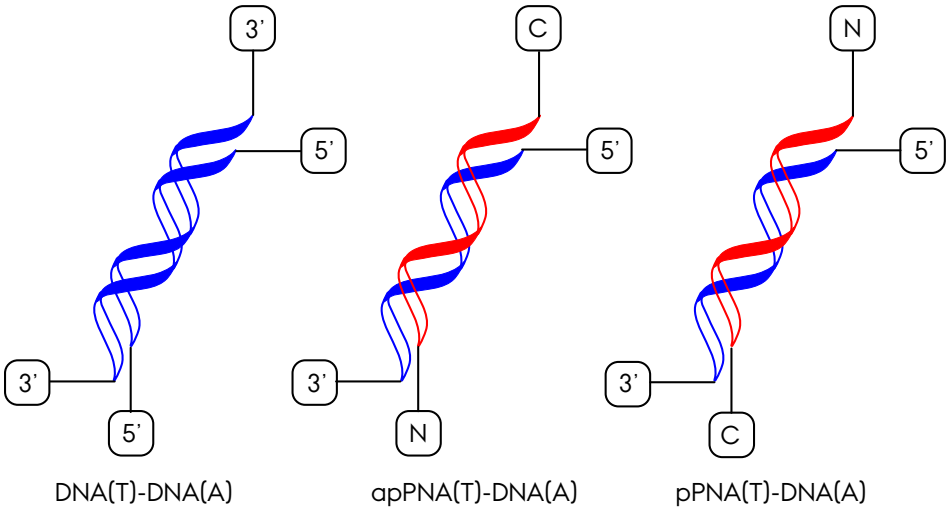

Figure 97 Image of the three simulated systems. Each strand is a homopolimer of 10 units.

To build the systems, Nugen module of AmberTools[6] was used. An anticomplementary B-type DNA-DNA duplex was generated and atoms were modified one-to-one to transform it in the PNA-DNA hybrids.

As the PNA is a novel structure, parametrization was required. The building block of the peptide strand was parametrized as novel residue using standardized procedure. HF/6-31G(d) single point energy and electrostatic potential mapping was achieved through Gaussian.[7] RESP fitting method was applied invoking Antechamber module of AmberTools and Generalized Amber Force Field[8] atoms types were assigned. Parmchk was also used to check for missing parameters and the set of ligand parameters was saved as library.

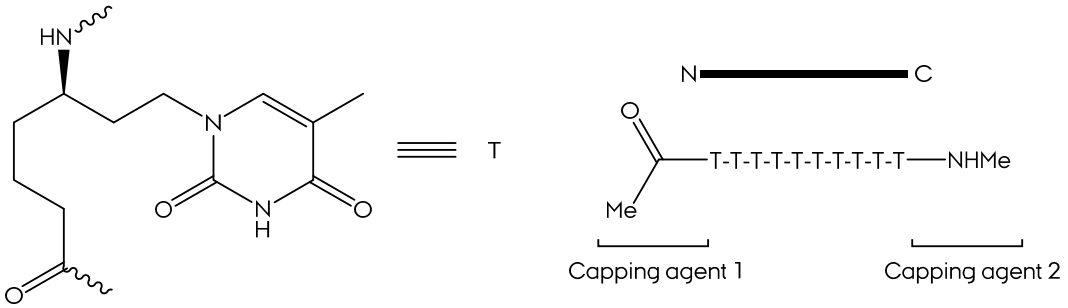

Figure 98. Residue unit and capping definition of PNA strands.

Xleap module of AmberTools 13 was used to assembly the systems. DNA structures were parametrized through Amber 99 force field with the bsc0 modification. Sodium cations were added to neutralize the system and the systems were surrounded by a 10 Å TIP3P water shell.

Once assembled the systems, the following MD simulation protocol was used (**Fig. 99**):

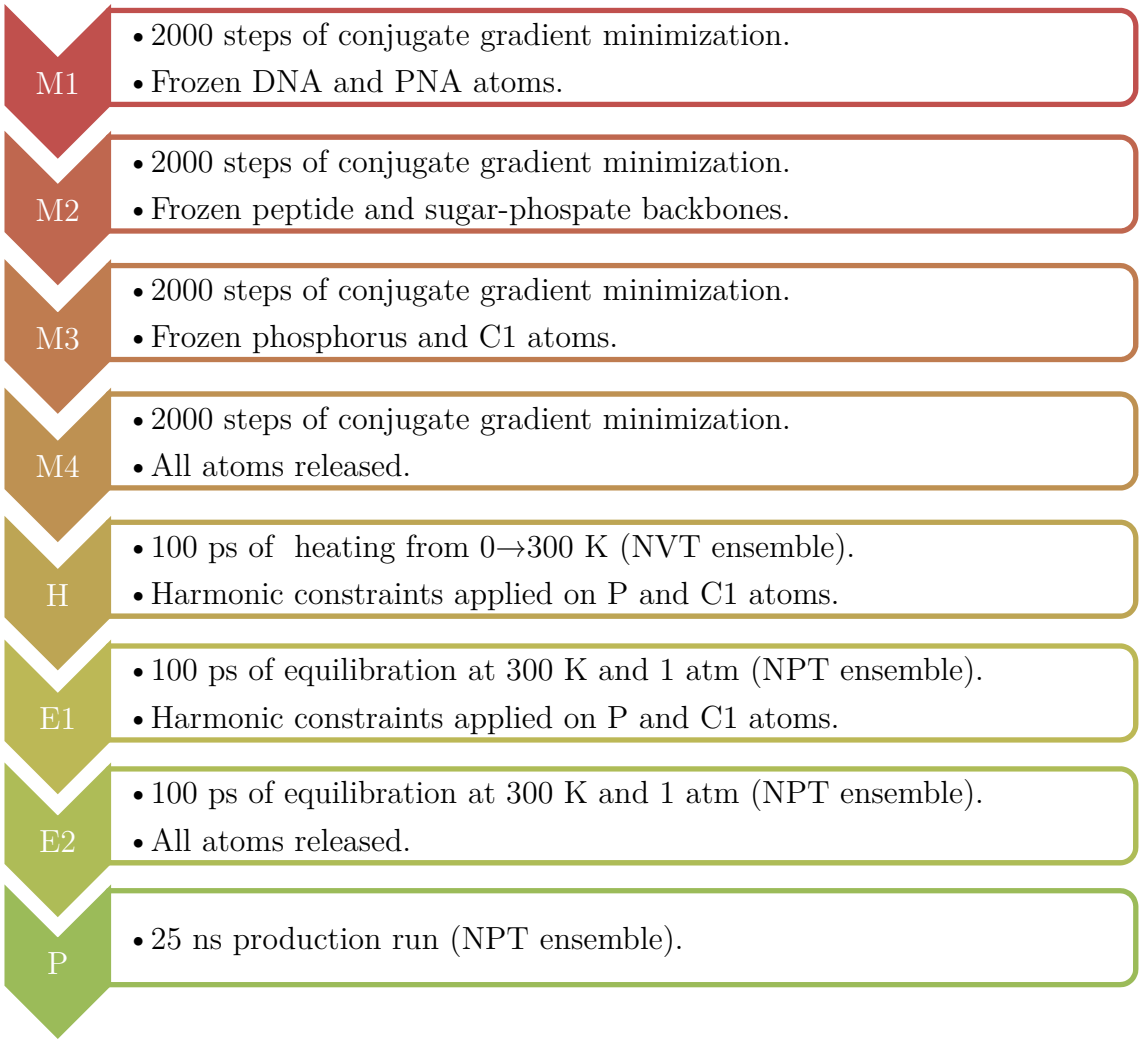

Figure 99. MD simulation protocol followed in modelling peptide nucleic acid systems.

All the MD simulations were performed with NAMD.[9] First, the system was minimized by stages, using four constraining levels (water/ions, peptide/sugar-phosphate backbone, P/C1 atoms and all unrestrained). In each one of the relaxing levels, 2000 steps of conjugate gradient were performed. Secondly, the minimized system was heated to 300 K along 100 ps at the NVT ensemble. In this step, all the atoms were allowed to move, excluding P and C1 atoms, which were subjected to a positional harmonic constraint of 1 Kcal/(mol · Å^2). Once heated, the constraining scheme continued for an extra 100 ps. Finally, the harmonic constraints were retired and the system was subjected to a 25 ns constant pressure molecular dynamics

simulation. Langevin Dynamics were applied at 1 atm and 300 K, with a Langevin damping coefficient of 2. Non-bonded interactions were calculated with the specified force fields (AMBER 99/bsc0 for DNA, waters and ions; GAFF for PNA) and applying Particle Mesh Ewald method[10] (PME) for long-range electrostatic forces in a periodic boundary condition context. A 10 Å cutoff was used together with a switching function between 9 – 10 Å. SHAKE algorithm was applied to freeze all bonds involving hydrogens, so a time step of 2 fs was applied.

Trajectories and Topological Analysis

Figure 100 shows a plot of the root mean square deviation (RMSD) of the three duplex systems along the 25 ns of simulation. Natural DNA has a RMSD average of 1.6 ± 0.2 Å, in other words, the RMSD value is low and the fluctuation of the structure is small. On the other hand, DNA-PNA hybrids have a RMSD average of 1.8 ± 0.3 Å (antiparallel) and 2.5 ± 0.5 Å (parallel), respectively. The value in the parallel case is a little higher than the antiparallel, which is almost equal to the natural system. Slightly higher is also the fluctuation in the parallel system. As the RMSD average value is lower than 3 Å and the systems were stable from approximately 13 ns, we might proceed to further study these simulations.

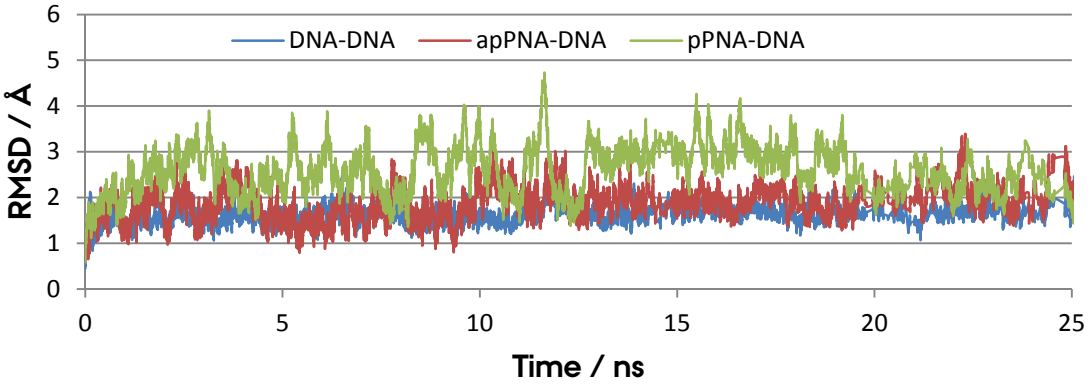

Figure 100. Plot of the RMSD of the three simulated duplexes.

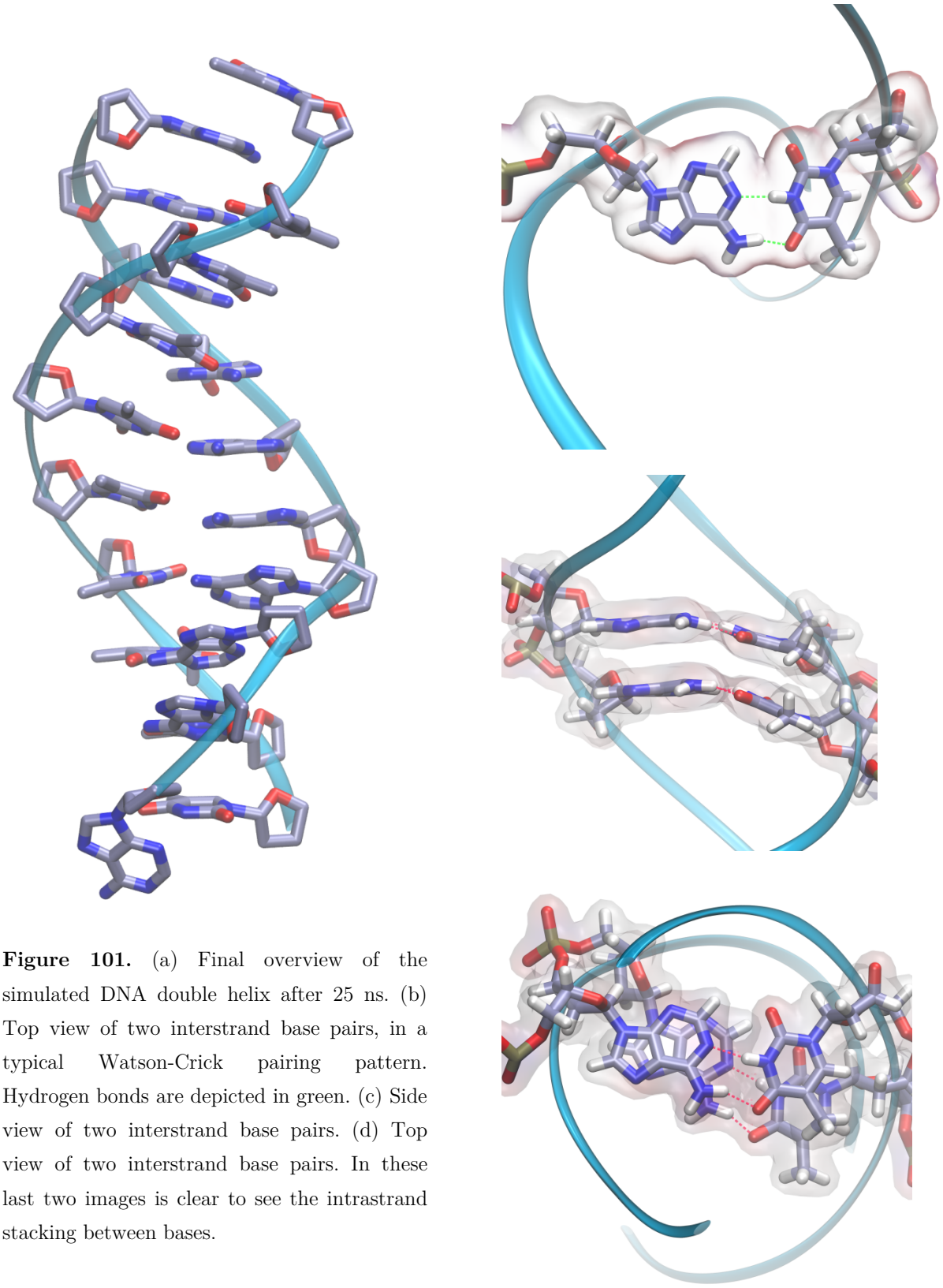

Figure 101. (a) Final overview of the simulated DNA double helix after 25 ns. (b) Top view of two interstrand base pairs, in a typical Watson-Crick pairing pattern. Hydrogen bonds are depicted in green. (c) Side view of two interstrand base pairs. (d) Top view of two interstrand base pairs. In these last two images is clear to see the intrastrand stacking between bases.

DNA natural duplex simulated structure is depicted in **Figure 101a**. The double helix motif was kept along the 25 ns of simulation, and the nucleobases of each strand are oriented towards their anticomplementary counterparts. As it could be observed, terminal nucleotides had a different behaviour than their inner

homologues. As the nucleobases placed in terminal positions just have one intrastrand base, solvent acceded to the surrounding area, interacting with them and interrupting the Watson-Crick pairing. Fluctuation of these terminal residues is a natural behaviour of double-stranded nucleic acids. Top view of one of the Watson-Crick base pairs is presented in **Figure 101b**. Excluding terminal units (due to the fluctuation described above), pairing scheme was kept along the simulation time. One of the stabilizing effects in a nucleic acid double strand is the stacking forces between intrastrand nucleobases.[11] **Figures 101c** and **101d** display two views of inner pairs of the double helix, showing the stacking orientation of the bases which belongs to the same strand.

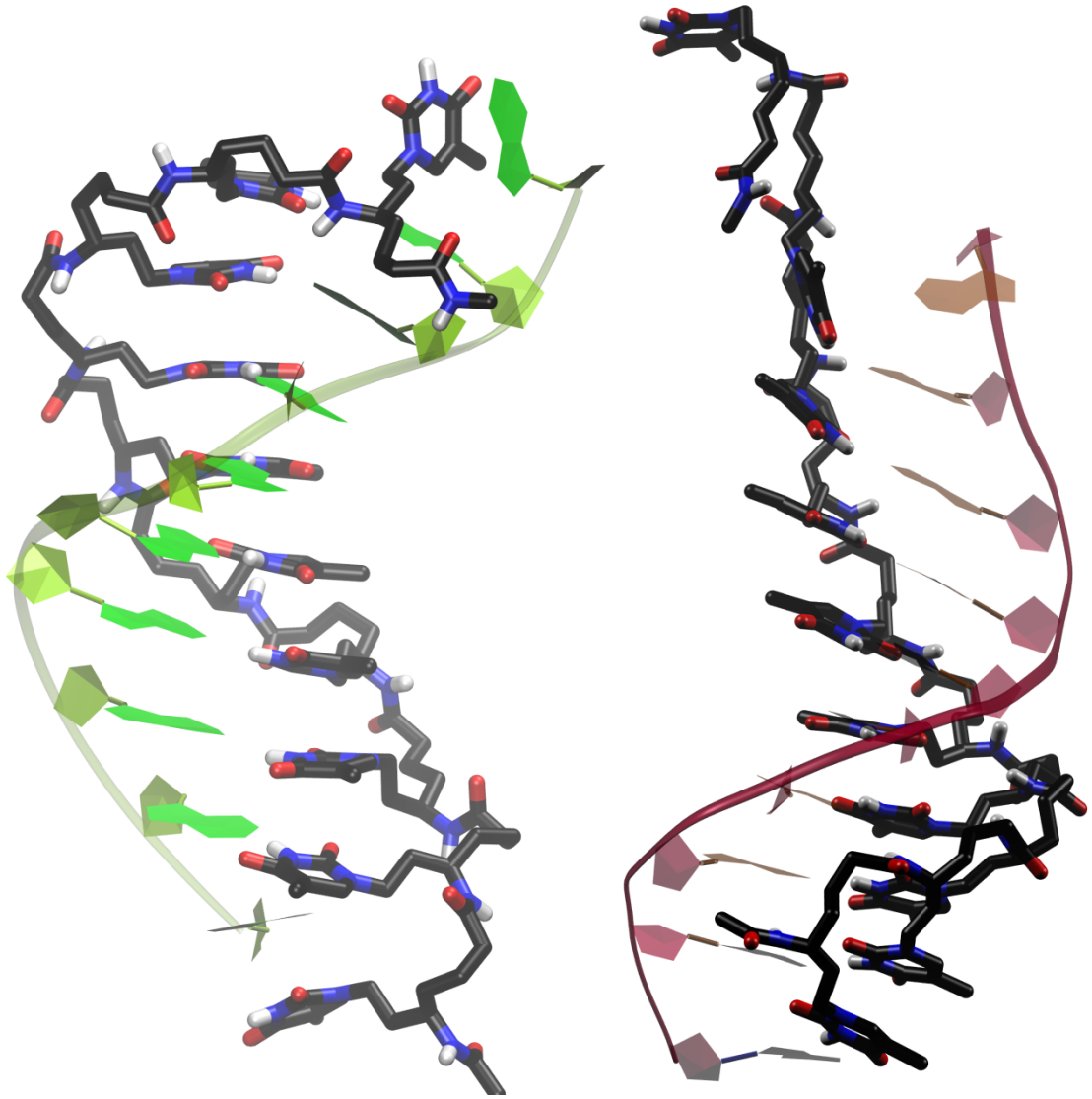

Figure 102. Final overview of the simulated PNA:DNA hybrids after 25 ns. DNA strands is depicted with coloured polygons, while PNA is displayed in tubestyle. Right: antiparallel hybrid. Left: parallel hybrid.

PNA:DNA simulated hybrids have a similar organization like natural DNA:DNA duplex. **Figure 102** shows both parallel and antiparallel hybrids after 25 ns. The right-handed helicity was kept along the overall simulation time; however, unpairing of terminal bases was observed like natural double-stranded DNA. Again, the invasion of water molecules in the surrounding area, together with the absence of additional stacking bases leaded them to break the Watson-Crick pairing scheme. Additionally, quick inspection of hybrids structure led to the next fact: parallel hybrid coiling is less than antiparallel coiling.

To further study the behaviour of nucleic acid double strands, a set of descriptors (local and global) were calculated. The target was to establish whether or not the initial B-motif have been kept along the complete simulation time. Topology of the double helix had been studied at three levels: helical, global and local.

Helical descriptors report about helical characteristics of motifs with helicity. There are four helical parameters (**Fig. 103**): x-displacement (**dx**), y-displacement (**dy**), inclination (η) and tip (θ).

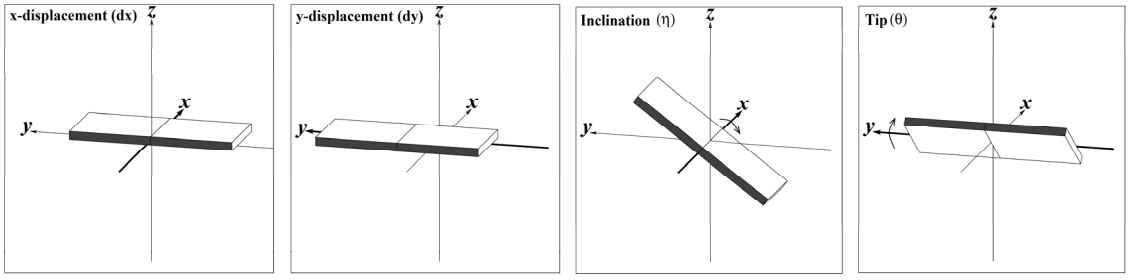

Figure 103. Definition of helical parameters.

Global descriptors (**Fig. 104**) informs about main characteristics of double-stranded nucleic acids: major (**M**) and minor grooves (**m**), hydrogen bond distance between bases (**d1** and **d2**).

Local descriptors (**Fig. 105**) notify about deformability of the structure at base level. This set comprises up to 12 parameters: shear ($\mathbf{S}_x$), stretch ($\mathbf{S}_y$), stagger ($\mathbf{S}_z$), buckle (κ), propeller (ω), opening (σ), shift ($\mathbf{D}_x$), slide ($\mathbf{D}_y$), rise ($\mathbf{D}_z$), tilt (τ), roll (ρ) and twist (Ω).

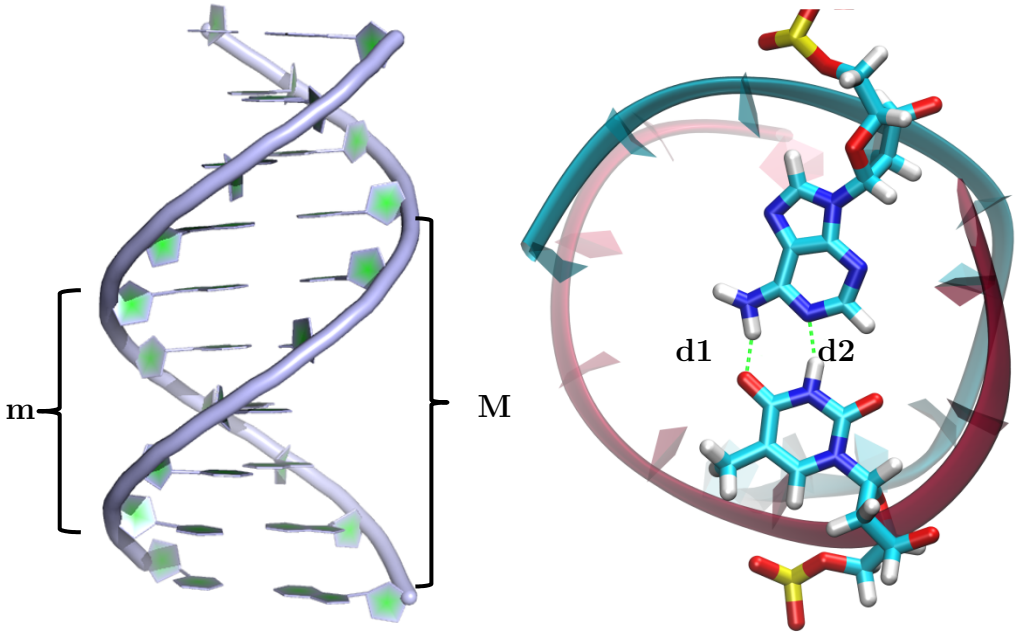

Figure 104. Definition of global parameters.

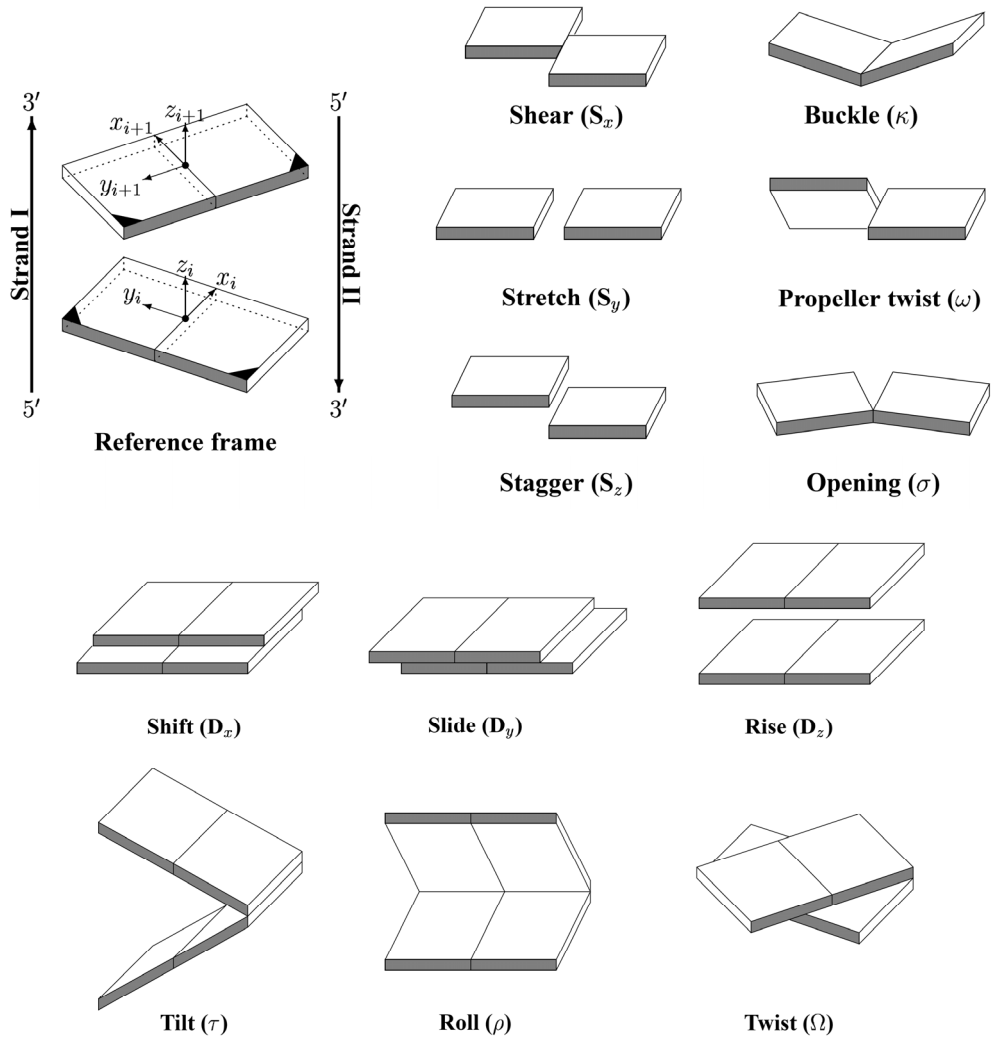

Figure 105. Definition of local parameters.

	APPNA		PPNA		DNA(MD)		B-DNA*		A-DNA*		Units
	Mean	RMSD	Mean	RMSD	Mean	RMSD	Mean	RMSD	Mean	RMSD	
Inclination	3.80	11.00	3.90	16.20	0.82	9.76	2.10	9.20	14.70	7.30	º
Tip	-0.52	10.10	-2.21	13.70	2.56	8.47	0.00	4.30	-0.10	5.20	º
Displacement-x	-6.91	1.75	-1.60	3.64	-1.22	1.29	0.05	1.28	-4.17	1.22	Å
Displacement-y	-0.01	1.36	-0.60	1.99	-0.18	1.30	0.02	0.87	0.01	0.89	Å
Minor groove	11.40	1.60	10.40	2.38	14.00	1.00	12.00				Å
Major groove	24.60	2.30	27.60	1.70	21.00	2.00	22.00				Å
HB/d1	2.00	0.03	2.02	0.05	1.98	0.05	1.80				Å
HB/d2	1.97	0.01	1.98	0.02	2.03	0.08	2.00				Å
Shear	-0.04	0.29	-0.09	0.27	0.09	0.27	0.00	0.21	0.01	0.23	Å
Stretch	-0.02	0.17	0.02	0.14	-0.01	0.15	-0.15	0.12	-0.18	0.10	Å
Stagger	-0.24	0.48	0.14	0.49	-0.16	0.50	0.09	0.19	0.02	0.25	Å
Buckle	-5.07	14.16	-13.60	17.60	4.64	11.63	0.50	6.70	-0.10	7.80	º
Propeller twist	-13.34	9.84	-16.10	14.30	-15.13	8.82	-11.40	5.30	-11.80	4.10	º
Opening	3.30	5.85	2.31	7.12	1.14	5.47	0.60	3.10	0.60	2.80	º
Shift	0.04	0.77	0.33	0.76	-0.05	0.51	-0.02	0.45	0.00	0.54	Å
Slide	-0.13	0.70	-0.41	1.23	-0.61	0.56	0.23	0.81	-1.53	0.34	Å
Rise	3.33	0.38	3.46	0.47	3.31	0.33	3.32	0.19	3.32	0.20	Å
Tilt	0.10	5.48	1.07	6.90	-1.38	4.44	-0.10	2.50	0.10	2.80	º
Roll	1.75	5.78	0.80	8.38	0.33	5.37	0.60	5.20	8.00	3.90	º
Twist	33.50	6.70	30.00	9.70	32.90	5.40	36.00	6.80	31.10	3.70	º

Table 15. summary of the calculated parameters of the simulated systems. Units and reference values[12] (*) of canonical A-DNA and B-DNA are also depicted.

Table 15 summarizes the calculated values of the helical, global and local parameters, which were obtained by means of X3DNA.[13]

First, helical parameter results are discussed. Hybrid systems values of inclination are close to the B-type reference value, as well as inclination value of simulated DNA. Tip angle are also slightly deviated in all cases. This means that the general disposition of anticomplementary pairs is slightly tilted from the orthogonal theoretical disposition respect z-axis. X-displacement of the nucleobases pairs is negative, and pronounced at the antiparallel hybrid, overpassing the A-type value. On the other hand, y-displacement is almost negligible in the three systems. In conclusion, comparing the helical parameters of the simulated systems with the tabulated ones, parallel PNA and natural DNA simulated structures are close to a B-type form, while antiparallel PNA one is a transition between B and A-type.

Next, the global parameters are analysed. The values for the minor groove are close to the referenced B-type ones. Nevertheless, major groove distance is slightly increased in the antiparallel hybrid, even more pronounced in the parallel hybrid. This increase is due to three features:

- PNA backbone flexibility, which number of degrees of freedom is larger than the sugar-phosphate backbone, allow to reach microconformers not possible with ring constrained structures.

- Short simulated duplexes. As terminal nucleobases interact with solvent and do not have Watson-Crick type pairing, this effect is slightly transferred to vicinal residues. This is enlarger when the oligonucleotide sequence is short.

- Negative charge disappearance of the PNA strand. The torque associated with negative repulsion between strands has decreased drastically, allowing a helical relaxation of the structure.

Hydrogen bonding distances are very close to referenced values, and all the base pairing schemes were identified as Watson-Crick types.

Finally, the local parameters were evaluated. Regarding the one-pair parameters, distance-based descriptors are close to zero in all systems. Angle-based parameters

have marked deviations in all systems, especially important in the propeller twist. The explanation is again related with the peptide nucleic nature: the flexibility of the backbone is transferred to the base pairing, allowing a range of interactions larger than in the natural case. Double-pair distance-based values are again close to zero, as well as angle-based tils and roll parameters. Twist value of the three systems was found closer to A-type DNA.

Having a look to these set of descriptors, x-displacement and slide are the best parameters to assign structural similarity. Although inclination and twist have different values in A and B-type duplexes, their RMSD is larger and overlap between structural motifs. Thereby, considering slide and x-displacement, hybrids and natural DNA have a B-type structural motif, although the antiparallel is slightly distorted.

One of the effects of replacing the sugar-phosphate backbone by a polypeptide is the modification in the solvation shell. In this case, the insertion of a hydrophobic shell increases the distance between solvent molecules and backbone, as it is depicted by radial distribution functions of thymine-based strands in **Figure 106**.

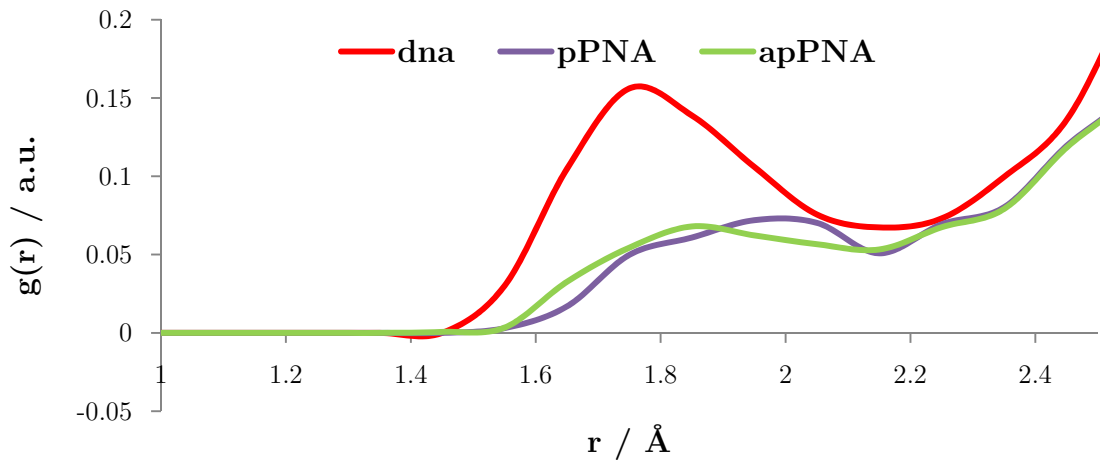

Figure 106. Radial distribution functions of thymine-based strands in the natural DNA (red), antiparallel PNA (green) and parallel PNA (purple).

In the natural double-strand, a maximum appears at 1.75 Å, meaning that the first solvation shell of water molecules has an average distance of 1.75 Å. However, in the hybrid systems, this range is enlarged up to 1.85 Å in the antiparallel case and 1.95 Å in the parallel scenario. The interaction is less favourable between solvent and peptide backbone, consisting of methylene units.

The radial functions have a minimum around 2.18 Å, due to the complementary strand, which avoids water molecules come closer.

Thermodynamic Analysis

To account for the energetic cost of hybridization between natural DNA strands and synthetic PNA oligopeptides, MM/GBSA energies (Molecular Mechanics/Generalized Born Surface Area) were calculated. The MM/GBSA approach has a similar mathematical formalism to MM/PBSA (see chapter 3):

$$\Delta G_{bind} = G_{complex} - G_{free\ protein} - G_{free\ ligand} \quad [1]$$

$$G = H_{gas} - TS_{conformational} + G_{solvation} \quad [2]$$

$$H_{gas} = U_{gas} + E_{vdw} + E_{el} \quad [3]$$

$$G_{solvation} = G_{GB} + G_{SA} \quad [4]$$

$$G_{SA} = \gamma \cdot SASA + \beta \quad [5]$$

The only difference is the calculation of the polar/electrostatic contribution by means of the generalized Born model[14] instead of the Poisson-Boltzmann theory.[15] The MM/GBSA method has been applied in several studies with nucleic acids involved, predicting relative binding energies.[16]

The MMPBSA.py routine of the AmberTools suite where invoked to calculate the energetic terms of the separated strands, the duplexes and the difference between them. As the main interest is the study of the relative energies between natural DNA duplex and the DNA:PNA hybrids, the single-trajectory approach was only considered.[17] Thereby, entropic terms were not considered as well. The next set of parameters were used: external dielectric constant, 80.0; internal electric constant, 1.0; ionic strength, 150 mM; surface tension (γ), 0.0072 Kcal $\cdot$ mol^{-1} $\cdot$ Å^{-2}; solvent probe radius, 1.4 Å. **Table 16** shows the results of the computed contributions to the free energy in the last 5 ns as well as the final values of the binding free energy calculated through the MMPBSA.py script.

	H	G_s	ΔG
DNA-A	-107.67	-1484.95	
DNA-T	-324.52	-1447.55	
A-T	976.76	-4399.91	
Δ	1408.95	-1467.41	-58.46
DNA-A	-108.39	-1487.80	
PNA-T	907.88	-177.37	
ap(A-T)	611.40	-1563.54	
Δ	-188.09	101.63	-86.46
DNA-A	-92.09	-1496.55	
PNA-T	853.36	-191.81	
p(A-T)	592.56	-1603.80	
Δ	-168.71	84.56	-84.15

Table 16. Thermodynamic parameters of the three calculated simulations in the last 5 ns.

From the table we can extract interesting results. In the natural double-stranded DNA, the binding enthalpy is highly positive: the union of the strands is highly destabilizing, as a consequence of the repulsion between the negatively charged sugar-phosphate backbones. However, the solvation free energy is very negative, due to the stabilizing effect of water molecules in the solvation. The results is a predominance of the solvation free energy, leading to a favourable pairing, thus the double strand is stable in water (as the structure was kept long the simulation). Substitution of one of the strands by the modelled PNA oligopeptide has a striking effect. Now, the unfavourable enthalpic contribution has turned into negative: the removal of the overall negative charge of one of the strands has strengthen the interaction between the strands. Nevertheless, the insertion of a non-charged backbone decreases the degree of interaction with solvent. As the monomers backbone is hydrophobic, the solvation free energy turned into positive. The outcome is a predominance now of the enthapic term, obtaining binding energies lower than in the case of natural DNA:DNA duplexes. Compairing the antiparallel and the parallel hybrids, the antiparallel scenario is slightly more favourable than the parallel one, of about 2.31 Kcal/mol.

Thermodynamic data have proven one of the main characteristics of peptide nucleic acids: the PNA based double helixes are more stable than natural ones, due to a stronger binding energy.

Conclusions

In this chapter, MD simulations of double stranded PNA:DNA systems were carried out. The PNA units were based in the synthetized nucleic acid **87**, Leumann´s enantiomer. The outcome of the simulations are schematized as it follows:

- 25 ns simulated systems revealed conservative double helixes motif, both natural DNA:DNA, as well as antiparallel and parallel hybrids.

- Topological analysis based on helical, local and global descriptors confirmed the B-type nature of these systems, with minimal deviations from the canonical structure.

- Radial distribution function revealed an increased distance of the first water molecules shell, due to the less favourable interaction between solvent and methylene units of the backbone.

- MM/GBSA calculations revealed the effect of replacing the backbone in each one of the energetic contributions. DNA natural duplexes are mainly stabilized by means of solvation interaction, dominating the free energy in contrast to the unfavourable enthalpic term, which records the energetic cost of combining to negatively charge moieties. On the other hand, PNA hybrids have a favourable enthalpic interaction, due to the neglecting of the associated charge of the backbone, but with the cost of increasing the free energy value up to the positive region. The dominance of the enthalpic terms results in a stronger free binding energy of PNA:DNA hybrids in contrast to DNA:DNA duplexes.

References

[1] (a) Nielsen, C. B.; Singh, S. K.; Wengel, J.; Jacobsen, J. P. *J. Biomol. Struct. Dyn.* **1999**, *17*, 175. (b) Ng, P.-S.; Bergstrom, D. E. *Nano Lett.* **2004**, *5*, 107. (c) Nielsen, J. T.; Arar, K.; Petersen, M. *Nucleic Acids Res.* **2006**, *34*, 2006. (d) Vokáčová, Z.; Trantírek, L. s.; Sychrovský, V. r. *J. Phys. Chem. A* **2010**, *114*, 10202. (e) Banerjee, A.; Kumar, V. A. *Biorg. Med. Chem.* **2013**, *21*, 4092.

[2] (a) Natsume, T.; Ishikawa, Y.; Dedachi, K.; Tsukamoto, T.; Kurita, N. *Chem. Phys. Lett.* **2007**, *446*, 151. (b) Paul, A.; Bezer, S.; Venkatramani, R.; Kocsis, L.; Wierzbinski, E.; Balaeff, A.; Keinan, S.; Beratan, D. N.; Achim, C.; Waldeck, D. H. *J. Am. Chem. Soc.* **2009**, *131*, 6498. (c) Wierzbinski, E.; de Leon, A.; Yin, X.; Balaeff, A.; Davis, K. L.; Reppireddy, S.; Venkatramani, R.; Keinan, S.; Ly, D. H.; Madrid, M.; Beratan, D. N.; Achim, C.; Waldeck, D. H. *J. Am. Chem. Soc.* **2012**, *134*, 9335. (d) Uppuladinne, M. V. N.; Jani, V.; Sonavane, U. B.; Joshi, R. R. *Int. J. Quantum Chem* **2013**, n/a.

[3] (a) Soliva, R.; Sherer, E.; Luque, F. J.; Laughton, C. A.; Orozco, M. *J. Am. Chem. Soc.* **2000**, *122*, 5997. (b) Sen, S.; Nilsson, L. *J. Am. Chem. Soc.* **2001**, *123*, 7414. (c) Norberg, J.; Nilsson, L. *Acc. Chem. Res.* **2002**, *35*, 465. (d) Sharma, S.; Sonavane, U. B.; Joshi, R. R. *J. Biomol. Struct. Dyn.* **2010**, *27*, 663. (e) Suresh, G.; Priyakumar, U. D. *J. Phys. Chem. B* **2013**, *117*, 5556.

[4] Egholm, M.; Buchardt, O.; Christensen, L.; Behrens, C.; Freier, S. M.; Driver, D. A.; Berg, R. H.; Kim, S. K.; Norden, B.; Nielsen, P. E. *Nature* **1993**, *365*, 566.

[5] Nielsen, P. E. *Chem. Biodiversity* **2010**, *7*, 786.

[6] *AmberTools 13* Case, D. A.; Darden, T. A.; III, T. E. C.; Simmerling, C. L.; Wang, J.; Duke, R. E.; Luo, R.; Walker, R. C.; Zhang, W.; Merz, K. M.; Roberts, B.; Hayik, S.; Roitberg, A.; Seabra, G.; Swails, J.; Goetz, A. W.; Kolossváry, I.; Wong, K. F.; Paesani, F.; Vanicek, J.; Wolf, R. M.; Liu, J.; Wu, X.; Brozell, S. R.; Steinbrecher, T.; Gohlke, H.; Cai, Q.; Ye, X.; Wang, J.; Hsieh, M.-J.; Cui, G.; Roe, D. R.; Mathews, D. H.; Seetin, M. G.; Salomon-Ferrer, R.; Sagui, C.; Babin, V.; Luchko, T.; Gusarov, S.; Kovalenko, A.; Kollman, P. A., University of California, San Francisco, 2012.

[7] *Gaussian 03 Revision E.01,* Frisch, M. J.; Trucks, G. W.; Schlegel, H. B.; G. E. Scuseria, M. A. R.; Cheeseman, J. R.; Montgomery, J. A.; Jr., T. V.; Kudin, K. N.; Burant, J. C.; Millam, J. M.; Iyengar, S. S.; Tomasi, J.; Barone, V.; Mennucci, B.; Cossi, M.; Scalmani, G.; Rega, N.; Petersson, G. A.; Nakatsuji, H.; Hada, M.; Ehara, M.; Toyota, K.; Fukuda, R.; Hasegawa, J.; Ishida, M.; Nakajima, T.; Honda, Y.; Kitao, O.; Nakai, H.; Klene, M.; Li, X.; Knox, J.

E.; Hratchian, H. P.; Cross, J. B.; Bakken, V.; Adamo, C.; Jaramillo, J.; Gomperts, R.; Stratmann, R. E.; Yazyev, O.; Austin, A. J.; Cammi, R.; Pomelli, C.; Ochterski, J. W.; Ayala, P. Y.; Morokuma, K.; Voth, G. A.; Salvador, P.; Dannenberg, J. J.; Zakrzewski, V. G.; Dapprich, S.; Daniels, A. D.; Strain, M. C.; Farkas, O.; Malick, D. K.; Rabuck, A. D.; Raghavachari, K.; Foresman, J. B.; Ortiz, J. V.; Cui, Q.; Baboul, A. G.; Clifford, S.; Cioslowski, J.; Stefanov, B. B.; Liu, G.; Liashenko, A.; Piskorz, P.; Komaromi, I.; Martin, R. L.; Fox, D. J.; Keith, T.; Al-Laham, M. A.; Peng, C. Y.; Nanayakkara, A.; Challacombe, M.; Gill, P. M. W.; Johnson, B.; Chen, W.; Wong, M. W.; Gonzalez, C.; Pople, J. A., Wallingford CT, 2004.

[8] Wang, J.; Wolf, R. M.; Caldwell, J. W.; Kollman, P. A.; Case, D. A. *J. Comput. Chem.* **2004**, *25*, 1157.

[9] Phillips, J. C.; Braun, R.; Wang, W.; Gumbart, J.; Tajkhorshid, E.; Villa, E.; Chipot, C.; Skeel, R. D.; Kalé, L.; Schulten, K. *J. Comput. Chem.* **2005**, *26*, 1781.

[10] Darden, T.; York, D.; Pedersen, L. *J. Chem. Phys.* **1993**, *98*, 10089.

[11] (a) Yakovchuk, P.; Protozanova, E.; Frank-Kamenetskii, M. D. *Nucleic Acids Res.* **2006**, *34*, 564. (b) Sen, A.; Nielsen, P. E. *Nucleic Acids Res.* **2007**, *35*, 3367. (c) Dailidonis, V.; Danilov, V.; Früchtl, H.; Mourik, T. *Theor. Chem. Acc.* **2011**, *130*, 859. (d) Parker, T. M.; Hohenstein, E. G.; Parrish, R. M.; Hud, N. V.; Sherrill, C. D. *J. Am. Chem. Soc.* **2012**, *135*, 1306.

[12] Olson, W. K.; Bansal, M.; Burley, S. K.; Dickerson, R. E.; Gerstein, M.; Harvey, S. C.; Heinemann, U.; Lu, X.-J.; Neidle, S.; Shakked, Z.; Sklenar, H.; Suzuki, M.; Tung, C.-S.; Westhof, E.; Wolberger, C.; Berman, H. M. *J. Mol. Biol.* **2001**, *313*, 229.

[13] Lu, X.-J.; Olson, W. K. *Nat. Protocols* **2008**, *3*, 1213.

[14] Onufriev, A.; Bashford, D.; Case, D. A. *J. Phys. Chem. B* **2000**, *104*, 3712.

[15] Fogolari, F.; Brigo, A.; Molinari, H. *J. Mol. Recognit.* **2002**, *15*, 377.

[16] Siriwong, K.; Chuichay, P.; Saen-oon, S.; Suparpprom, C.; Vilaivan, T.; Hannongbua, S. *Biochem. Biophys. Res. Commun.* **2008**, *372*, 765.

[17] Reyes, C. M.; Kollman, P. A. *J. Mol. Biol.* **2000**, *297*, 1145.

Metodologías y Materiales 1: Metodologías Generales

(General Methodologies)

Metodologías Teóricas

Metodologías Biológicas

Metodologías Químico-Instrumentales

Metodologías de Análisis Instrumental

Metodologías de Separación Cromatográfica

Metodologías de Elaboración de Reactivos de Laboratorio

Metodologías Teóricas

Aunque las metodologías teóricas están descritas en cada uno de los capítulos de modelización molecular (debido a la estrecha relación entre diseño-naturaleza del estudio), aquí se resume las diversas técnicas empleadas en conjunción con el software utilizado.

Plateamiento y Diseño Metodológico

Construcción de Sistemas

- A través de interfaces gráficas de usuario (GUI).
- Xleap, AutoDock Tools, Maestro.

Simulación

- A través de software de simulación.
- Jaguar (QM), Tinker (MM), Namd (MD).

Análisis e Interpretación

- De nuevo, a través de GUI's.
- Maestro, AutoDock Tools, VMD.

Visualización

- Software especializado en renderizado (rendering) y trazado de rayos (ray tracing). Imágenes y video.
- PyMOL, VMD, Maestro, POV-Ray.

La instrumentación empleada para los estudios *in silico* fue un equipo estándar informático, equipado con una memoria RAM de 4 GB y un procesador tipo Intel i3 de 1.9GHz.

Metodologías Biológicas

Cultivos Celulares

La línea celular empleada en nuestro estudio es la línea adherente HEK293, línea celular obtenida a partir de células embrionarias de riñón humano transformadas con adenovirus tipo 5 (Human Embryonic Kidney: ATCC: CRL-1573, obsequio del Prof. J. R. Traynor, de la Universidad de Michigan, USA).

Condiciones de crecimiento de la línea celular HEK293. Las células transfectadas establemente con el receptor opioide μ (dre-*oprm1*, número de acceso UniProt Q98UH1_DANRE) ó con el receptor δ1b (dre-*oprd1b*, número de acceso UniProt B3DH72_DANRE) se crecieron en medio *Dulbecco's modified Eagle's médium* o *DMEM*, suplementado con 10% suero bovino fetal descomplementado, 2mM Glutamina, 100U/mL penicilina, 0.1mg/mL estreptomicina, 25μg/mL fungizona y 250 μg/mL geneticina (G-418) (GibCo-BRL, Life Technologies). El medio se preparó en un volumen final de 550ml, esterilizándolo mediante filtración con un filtro de 0.22μm de polietilensulfona (Corning Costar), para así asegurar la completa esterilidad del medio suplementado. Las células se incubaron en un incubador *Forma* bajo las siguientes condiciones: 37ºC, 5% CO_2 y 95% de humedad. El medio se cambió cada 2 ó 3 días y las células se crecieron hasta llegar a un 80% de confluencia, momento en el que se recogieron para realizar los experimentos, se expandieron a nuevas botellas o se resembraron.

Recogida y siembra de células. Para recoger las células, éstas se levantaron con PBS + 2mM EDTA pH 7.4, de manera que las células adheridas a la pared de la botella se levantan y permanecen en suspensión. La suspensión celular se recogió en tubos *Falcon* de 50mL y se centrifugó a 500g durante 10min a R.T. El botón celular congeló a -80C hasta su empleo.

Obtención de Membranas de Cerebro y de Células en Cultivo

El cerebro de una rata fue extraído *post-mortem*, el cerebelo fue separado para eliminar los sitios de baja afinidad por los agentes opioides, y el resto del cerebro fue congelado a -80C hasta su empleo. El cerebro fue homogenizado inicialmente con un *polytron* (Kinematika) en tampón de ensayo (Tris-HCl 50mM pH 7.4 con inhibidores de proteasas: 0.1mg/mL bacitracina, 3.33μM captopril y el cocktail de

inhibidores de proteasas de Sigma-Aldrich). A partir de este momento, todos los procesos se llevaron a cabo en hielo. Tanto la suspensión de cerebro de rata como los botones celulares fueron homogenizados mecánicamente mediante un mortero con pistilo *Potter-Elvehjem* en tampón de ensayo y se centrifugaron inicialmente a 500g durante 10min a 4ºC para separar la fracción nuclear del resto de las fracciones de membranas. El sobrenadante se guardó y la fracción celular se volvió a homogenizar y a centrifugar. Ambos sobrenadantes fueron combinados, se volvieron a homogenizar y se centrifugaron a 18000g durante 1h a 4ºC para precipitar la fracción de las membranas celulares. El sobrenadante se eliminó y el precipitado se resuspendió en tampón de ensayo en un volumen tal que la concentración final de proteína fuera de 0.5-1 mg/mL. La concentración proteica fue determinada por el método de Bradford (BioRad Laboratories), empleando albúmina sérica (Sigma) como patrón.

Farmacos Empleados

Los fármacos utilizados se obtuvieron de las siguientes industrias químicas y farmacéuticas: la morfina fue obtenida del Departamento de Salud del Ministerio de Sanidad y Consumo en Madrid; el radioligando [^{3}H]-diprenorfina (DPN) (58Ci/mmol) se obtuvo de Perkin-Elmer (Boston MA) y la naloxona se adquirió a Sigma Chemical Company.

Ensayos de Competición sobre receptores Opioides

Los ensayos de competición permiten conocer la afinidad que presentan ciertos ligandos por un receptor, técnica que es muy útil cuando se carece de la forma radiactiva del ligando. Para ello se emplea un radioligando de afinidad conocida y se intenta desplazar la unión de dicho radioligando con distintas concentraciones del compuesto problema no radiactivo, de manera que la capacidad de desplazamiento es un indicador de la afinidad del ligando frío por el receptor. Los parámetros obtenidos de estos experimentos son la concentración inhibitoria media -IC_{50}-, definida como la cantidad de ligando frío necesaria para desplazar el 50% de la unión específica del radioligando, y la K_i o constante de disociación. Estos dos parámetros están interrelacionados por medio de la ecuación de Cheng-Prusoff.[1] Mientras que la IC_{50} varía en función de la concentración de radioligando empleada, la K_i es una constante. Por ello, en los resultados de los ensayos de competición siempre se han calculado los valores de K_i.

Los ligandos fríos se disolvieron en agua bidestilada y se realizaron alícuotas de 10mM, que se conservaron a -20ºC. Todos los pasos previos a la incubación se realizaron en hielo para así prevenir la degradación, tanto de los péptidos como de los receptores. Los ensayos de competición se realizaron bajo las mismas condiciones descritas en (Gonzalez-Nunez et al., 2013). En nuestro caso, los ensayos se llevaron a cabo con 7-30 μg de proteína, que fueron incubados con diferentes concentraciones de ligando frío desde 3 nM hasta 100 μM (concentración final), utilizando [^{3}H]-DPN como radioligando. La concentración final de [^{3}H]-DPN fue similar a la constante de afinidad K_D: 0.22 nM para el homogenado de cerebro de rata,[2] 1 nM para el receptor μ[3] y 3.4 nM para el receptor 1b.[4] También se determinó la unión total (en ausencia de ligando frío) y la unión no específica (con 10 M de naloxona fría) para cada uno de los ligandos empleados.

Las reacciones fueron incubadas durante 1h (para cerebros de rata y para el receptor μ) ó durante 4h (para el receptor δ1b) a 25ºC en tampón de ensayo (500μL de volumen final para cerebro de rata ó 250μL para homogenados celulares). Una vez concluida la incubación, la reacción se paró añadiendo 4mL de Tris-HCl 50mM pH=7.4 a 4ºC y la mezcla fue rápidamente filtrada al vacío con un *Brandel Cell Harvester* a través de filtros GF/B (Schleicher & Schuell) tratados previamente con polietilenimina (Sigma) al 0.2% durante al menos 1 h. Los filtros se lavaron dos veces con Tris-HCl 50mM pH=7.4 a 4ºC, se depositaron en viales con 3.5ml de líquido de centelleo *EcoScint A* (National Diagnostics) y se incubaron durante al menos 16 h a R.T. La radiactividad se cuantificó con un contador de centelleo *Beckman Coulter LS6500*. Todos los experimentos fueron realizados por triplicado (para cerebro de rata) ó por duplicado (para las membranas de cultivos celulares) y repetidos tres veces.

Análisis de los Datos

Para cada ligando se determinó la unión total, que se define como cantidad total de radioligando unido, y la unión no específica, que se define como la cantidad de radioligando unido en presencia de una concentración saturante de ligando frío. Teniendo en cuenta que el ligando frío desplaza toda la unión del radioligando al receptor objeto de estudio, la unión no específica se debe a la interacción del radioligando con cualquier otra estructura distinta de dicho receptor. Por lo tanto, la unión específica se define como la diferencia entre la unión total y la no específica.

En el caso de los receptores opioides, la unión no específica se determina utilizando naloxona fría 10 μM (concentración final), de manera que la unión específica se halló restando la unión no específica (con radioligando y naloxona) de la unión total (en presencia exclusivamente del radioligando).

En todos los casos, la unión específica, que se definió como la diferencia entre la unión total y la no específica, se equiparó al 100% y el 0% de unión se asemejó a la unión no específica medida con naloxona 10 μM. El resto de los valores de unión específica, que se corresponden con las incubaciones en presencia de ligando desplazante, se expresaron como porcentajes de unión específica respecto del 100%. Los datos obtenidos se ajustaron también a modelos de regresión no lineal, tanto de un sitio como de dos sitios de competición, y se calculó la constante de inhibición K_i mediante la ecuación de Cheng-Prusoff, que corrige la concentración de radioligando utilizado en cada experimento y tiene en cuenta el valor de K_D (Cheng & Prusoff, 1973).

Metodologías Químico-Instrumentales

Liofilización

Para liofilizar ciertos productos (especialmente aminoácidos no ionizados aislados a través de resinas de intercambio iónico), se utilizó un liofilizador Telstar Cryodos (**Fig. hh**), equipado con un compresor frigorífico y una bomba de vacío y dotado con 8 puertos de conexión. La máxima presión manométrica requerida es de $5 \cdot 10^{-2}$ bares.

Figura hh. Liofilizador Telstar Cryodos.

Reacciones en atmósfera de hidrógeno.

Para hidrogenaciones o desprotecciones, se empleó un hidrogenador Parr en línea con una bombona de H_2. Los matraces de

reacción se conectaron a esta línea y se purgaron 8-10 veces antes de presurizar a 3.5 atm.

Metodologías de Análisis Instrumental

Rotaciones específicas

Se midieron en un polarímetro digital Perkin-Elmer 241, en cubetas de 1 dm de paso óptico y en disolución de cloroformo o agua. La concentración a la que se realizó la medida se especifica en cada caso (**Fig. jj**).

Figura 1. Perkin-Elmer 241.

Puntos de fusión

Se determinaron en un microscopio de platina caliente (Kofler) y están sin corregir (figura 2).

Figura 2. Kofler.

Espectroscopía FTIR

Las medidas se han realizado en dos espectrofotómetros de Transformada de Fourier: AVATAR 370 FT-IR (Thermo Nicolet), e IR-Affinity 1 (Shimadzu). Las muestras se prepararon en cristales de KCl (figura 3).

Figura 3. AVATAR 370 FT-IR, de Thermo Nicolet (izquierda) e IR-Affinity 1, de Shimadzu (derecha).

Espectroscopía de RMN. ^{1}H y ^{13}C

Se han realizado en un espectrómetro Buker Avance 400 MHz DRX (400 MHz ^{1}H y 100 MHz ^{13}C) (Figura C), equipado con una sonda de detección inversa con bobina de gradientes y una sonda $^{1}H/^{13}C$ y en un espectrómetro Varian Mercury 200 (200 MHz ^{1}H y 50 MHz ^{13}C) (**Fig. 4** y **5**).

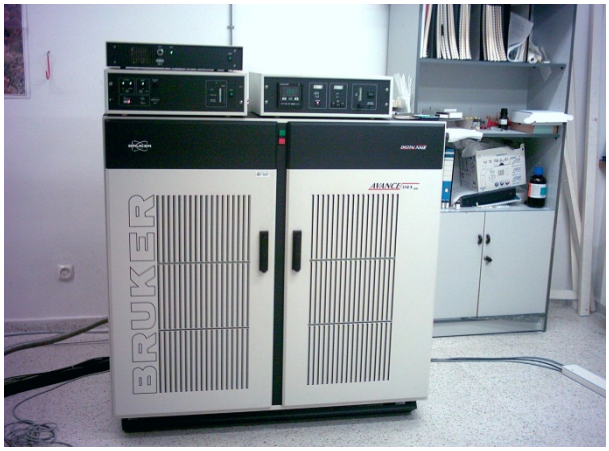

Figura 4. Bruker Avance 400 MHz DRX.

Figura 5. Varian Mercury 200 MHz.

Los espectros se realizaron en $CDCl_3$ como disolvente habitual (empleando otros disolventes deuterados alternativamente) y se referencian con respecto al disolvente residual $CHCl_3$ (7.26 ppm en ^1H y 77.0 ppm en ^{13}C). Los desplazamientos químicos (δ) se expresan en ppm y las constantes de acoplamiento (J) en Hz.

La multiplicidad de los carbonos se determina utilizando la secuencia de pulsos DEPT (Distorsionless Enhancement by Polarization Transfer). La secuencia distingue los carbonos protonados CH, CH_2 y CH_3 utilizando pulsos de protón a través del desacoplador a 90º y 135º.

Espectroscopía de RMN. Experimentos bidimensionales: HMQC (Heteronuclear Multiple Quantum Coherence)

Los experimentos de correlación heteronuclear $^1H/^{13}C$ a un enlace se adquieren utilizando la secuencia Bruker inv4gs, con selección de la secuencia de cero cuanto y doble cuanto con una serie de tres pulsos de gradientes sinusoidales. La longitud del pulso de gradiente es de 1.5 ms y los pulsos guardan una relación de 50:30:40 con respecto a la longitud total del pulso. El intervalo de recuperación del gradiente es de 100 ms.

Un experimento típico adquiere 256 series de uno o dos transientes c/u. El intervalo de reciclado es de tres segundos y la modulación se sintoniza para $^{1}J_{H,C} =$ 145 Hz, que corresponde a un intervalo de 3.45 ms, y desacoplando con una secuencia garp en ^{13}C en el momento de la adquisición.

La transformada de Fourier en ambas dimensiones se realiza después de aplicar una función exponencial de 0.3 Hz en F2 (^{1}H) y una función sinusoidal en F1 (^{13}C). Se obtiene un espectro de correlación en magnitud con 1024 puntos en F2 y 512 en F1, que corresponde a una resolución de 4.68 Hz/pt en F2 y 45.2 Hz/pt en F1.

Espectroscopía de RMN. Experimentos bidimensionales: HMBC (Heteronuclear Multiple Bond Conectivity).

Para las correlaciones a larga distancia, 2 ó 3 enlaces, se utiliza la secuencia inv4gslplrnd, que utiliza un filtro de paso largo para la eliminación de la correlación directa en función de la constante de acoplamiento $^{1}J_{H,C} = 145$ Hz. La secuencia de pulsos de gradientes para la selección de la coherencia es la misma que en el caso anterior y se aplica un nuevo intervalo de evolución (función $^{1}J_{H,C}$ cuyos valores pueden ser 50 ms (10 Hz), 83 ms (6 Hz) y 110 ms (4.5 Hz) antes de la selección de la coherencia y no se desacopla durante la adquisición. Un acoplamiento típico se adquiere con 256 series de 4 transientes c/u.

La transformada de Fourier (FT) en ambas dimensiones se realiza con las mismas funciones que en el caso anterior y se obtiene un espectro de correlación en magnitud con 1024 puntos en F2 y 512 en F1, que corresponde a una resolución de 4.8Hz/pt en ^{1}H y 45.2 Hz/pt en ^{13}C.

Espectroscopía de RMN. Experimentos bidimensionales: COSY (COrrelation SpectroscopY)

La secuencia básica del COSY tiene dos pulsos de 90º y un tiempo de evolución. Para el procesado se utilizan funciones sinusoidales en ambas direcciones, obteniendo así una matriz simétrica de 512 puntos en ambas dimensiones.

En general se utiliza se utiliza la secuencia con filtro de doble cuanto, que permite la eliminación o disminución de las señales intensas, ya sea de disolventes o singuletes en la diagonal y sus correspondientes artefactos.

Espectrometría de masas

Se realizaron en un espectrómetro VG-TS 250, 70 eV (**Fig. 6**), capaz de llevar a cabo experimentos de Impacto Electrónico (EI), FAB (Xenon, 10 KV), empleando como matriz alcohol m-nitrobencílico, y Ionización Química (CI), utilizando NH3 como gas ionizado.

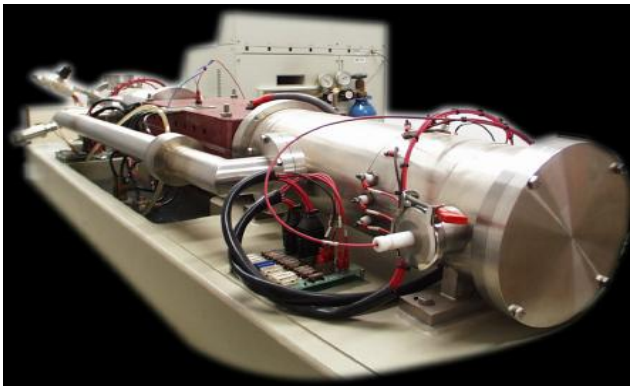

Figura 6. Espectrómetro VG TS-250.

Difracción de Rayos X

Las medidas de intensidades de las reflexiones de los monocristales presentados en este trabajo, se realizaron a temperatura ambiente con un difractómetro automático de cuatro círculos SEIFERT XRD 3003 SC (**Fig. 6**), usando radiación CuKa (λ =1.5418).

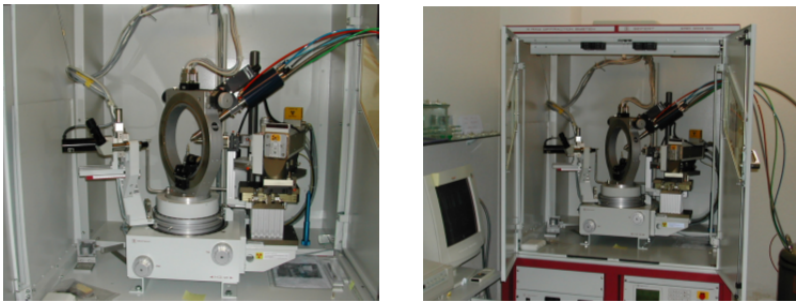

Figura 7. Rayos X de monocristal SEIFERT XRD 3003 SC

Metodologías de Separación Cromatográfica

Cromatografía en capa fina (CCF/TLC)

Se realizaron sobre placas de 0.2 mm de espesor de gel de sílice Merck (60 F254). Para su revelado se sumergían las placas bien en disoluciones de $KMnO_4$ en H_2O 0.1 g/mL y subsiguiente lavado en H_2O, bien en I2 sólido, bien en disoluciones de Ninhidrinaen nBuOH 1.0 g/L y subsiguiente revelado en caliente.

Las sustancias que presentan fluorescencia son visualizadas por iluminación con luz ultravioleta de λ = 254 nm antes de ser reveladas.

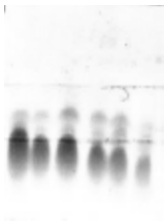

Cromatografía en columna (CC)

Se realizaron en columna de vidrio, llenándola con gel de sílice flash Merck–60 (0.063 – 0.040 mm) humedecida en hexano, agitando suavemente para eliminar el aire. La proporción que se emplea normalmente oscila entre 10 – 25 g de gel de sílice por gramo de sustancia a cromatografiar.

La elución se realiza con disolventes y combinaciones de disolventes de polaridad creciente (generalmente mezclas n–hexano/Acetato de Etilo, n–hexano/éter y cloroformo/metanol) y se sigue la composición de las fracciones eluidas por CCF.

Columnas de Intercambio Iónico

Se realizaron en columna de vidrio, llenándola con resina intercambiadora tipo Dowex 50X8-200 (Ácido fuerte, tipo catiónico), empleando una relación de unos 20g resina/g de producto. Para su acondicionamiento, se comienza empaquetando la resina en la columna con H_2O desionizada, lavando secuencialmente la columna con 200 mL de NaOH 1M, seguidos de 30 mL de H_2O y 200 mL de HCl 1M. Se

introduce la muestra disuelta en H_2O o en HCl 1M ó 0,5 M. Pasamos H_2O hasta pH neutro. A continuación, se eluye el aminoácido con NH_3 1M y se recogen las fracciones en tubos.

Se sigue el progreso de la columna mediante visualización en placa (revelando con ninhidrina). Aquellas placas donde se observe no color sino cercos, hay presente amina.

Purificación de Disolventes[5]

- Acetonitrilo (CH_3CN): Se destila y se almacena con P_2O_5.
- Cloroformo ($CHCl_3$): Se destila y se almacena con P_2O_5.
- Diclorometano (CH_2Cl_2): Se destila sobre CaH_2 bajo atmósfera de árgon.
- Eter (Et_2O): Se somete a ebullición sobre Na y benzofenona y se destila.
- n-Hexano (C_6H_{12}): Se destila y almacena con $CaCl_2$ o Na.
- Metanol (MeOH): Se destila.
- Piridina (C_5H_5N): Se destila y almacena con BaO.
- Tetrahidrofurano (C_4H_8O): Se somete a ebullición sobre Na y benzofenona y se destila.
- Tolueno (MeC_6H_5): Se destila y almacena con Na.

Metodologías de Elaboración de Reactivos de Laboratorio

Fosfonatos. Reacción de Arbuzov.[6]

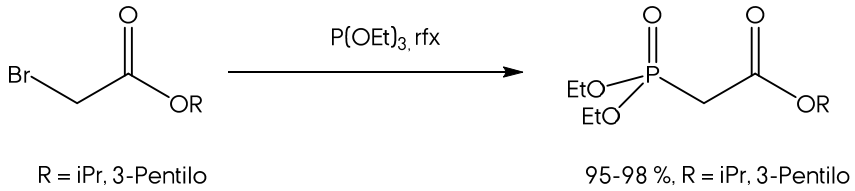

En un matraz de reflujo se colocan 2.0 g de bromoacetato (*iso*-propilo o 3-pentilo) junto con 1.0 equiv. de trietilfosfito (CAS: 122-52-1; liquido viscoso, 166.16 g/mol) en un sistema de reflujo. Se calienta a reflujo con agitación magnética durante 12 h. Tras enfriar el matraz, se obtiene un residuo, constituido exclusivamente por el fosfonato correspondiente.

N^3-Benzoil-Timina.

Preparada mediante el método descrito por Cruickshank *et al.*[7]

Referencias

[1] Cheng, Y.; Prusoff, W. H. *Biochem. Pharmacol.* **1973**, *22*, 3099.
[2] Gonzalez-Nunez, V.; Arsequell, G.; Szemenyei, E.; Toth, G.; Valencia, G.; Rodriguez, R. E. *J. Pharmacol. Exp. Ther.* **2005**, *314*, 862.
[3] Gonzalez-Nunez, V.; Jimenez Gonzalez, A.; Barreto-Valer, K.; Rodriguez, R. E. *Mol. Med.* **2013**, *19*, 7.
[4] Pinal-Seoane, N.; Martin, I. R.; Gonzalez-Nuñez, V.; de Velasco, E. M. F.; Alvarez, F. A.; Sarmiento, R. G.; Rodriguez, R. E. *J. Mol. Endocrinol.* **2006**, *37*, 391.
[5] Armarego, W. L. F. *Purification of Laboratory Chemicals*; Butterworth Heinemann, 2012.
[6] Bhattacharya, A. K.; Thyagarajan, G. *Chem. Rev.* **1981**, *81*, 415.
[7] Cruickshank, K. A.; Jiricny, J.; Reese, C. B. *Tetrahedron Lett.* **1984**, *25*, 681.

Metodogías y Materiales 2: Metodologías Químicas.

(Chemistry Methodology)

General Reaction Procedures (A-Z)

Reaction Inventory 1. Morphan Section (M)

Reaction Inventory 2. PNA Section (P)

General Reaction Procedures.

A. General Procedure for One Pot α-Bromination/Esterification of Acids.

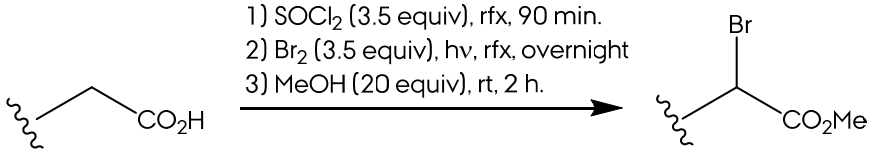

In a two-neckled round bottom flask provided with a condenser, a suitable amount of acid was placed together with 3.5 equiv of $SOCl_2$ (thionyl chloride, CAS: 7719-09-7, colourless liquid, 118.9 g/mol, commercial). The second neck was sealed and the suspension was magnetically stirred and heated at reflux temperature (75 ^{o}C) for 90 min. The solids were gradually dissolved.

After 90 min, the reaction was cooled to room temperature and a dropping funnel filled with Br_2 (bromine, CAS: 7726-95-6, dark red liquid, 159.8 g/mol, commercial) was place in the second neck. 3.5 equiv of bromine were added dropwise. The dark red mixture was irradiated with two 200 W incandescent light bulbs and stirring continued for 12 h.

The lamps were switched off and the mixture was cooled in an ice bath. 20 equiv of MeOH were carefully added dropwise, generating vapors vigorously. The orange mixture was allowed to stir for an additional 90 min. Finally, excess of sat. $NaHCO_3$ were added and stirred for other 30 min.

The reaction mixture was extracted with AcOEt 3 times. The organic extract was washed successively with water (3 times), a saturated solution of $NaHCO_3$ (3 times), a saturated solution of $Na_2S_2O_3$ (3 times) and brine (1 time). The result organic solution was dried with anhydrous Na_2SO_4, filtered and evaporated under reduced pressure, producing the crude product.

B. General Procedure for Debromination of α-Bromoesters in DMF.

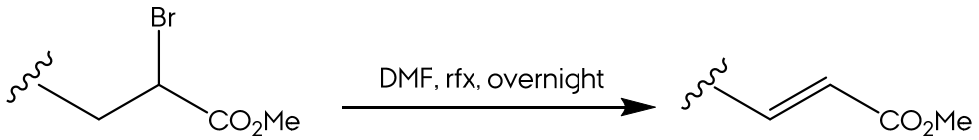

In a reflux system consisting in a round bottom flask with a condenser, a weighted amount of α-Bromo ester was dissolved in dry DMF. The organic solution was heated under reflux (153 ºC) for 12 h. Excess of water was added and the reaction mixture was allowed to cool to room temperature.

Excess of AcOEt were added to the reaction mixture. The organic extract was washed successively with water (5 times), a sat. solution of $NaHCO_3$ (3 times), a sat. solution of $Na_2S_2O_3$ (3 times) and brine (1 time). The dark organic solution was dried with anhydrous Na_2SO_4, filtrated and evaporated under reduced pressure, producing the crude product.

C. General Procedure for Lithium Amide Asymmetric Conjugate Addition.

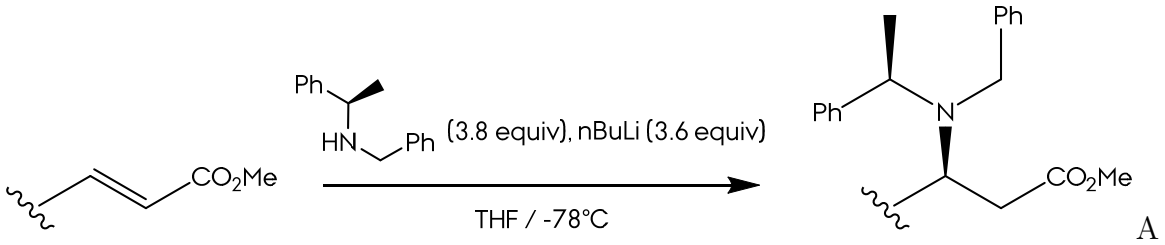

A suitable quantity of the α,β-unsaturated ester was dissolved in dry THF in a round bottom flask. The flask was sealed, purged with Ar, and cooled to -78 ºC in a CO_2 - acetone bath.

In a second pear-shaped flask, 3.8 equiv of (*R*)-(+)-*N*-benzyl- α -methylbenzylamine (CAS: 38235-77-7, viscous light yellow oil, 211.3 g/mol, commercial) were dissolved in dry THF. As the other flask, this one was also sealed, purged with Ar and cooled to -78 ºC. Once cooled, 3.6 equiv of nBuLi (n-buthyllithium, CAS: 109-72-8, 64.06 g/mol, 1.6 M commercial solution) were added dropwise, turning the solution from colourless to dark pink. The solution was stirred 15 min at -78 ºC, warmed to 0 ºC in an ice bath along 30 min and finally to -78 ºC again for other extra 15 min.

The pink solution was added dropwise over the substrate solution and the resulting mixture turned orange. Finished the addition, the resulting mixture was magnetically stirred for 3 h before quenching with an excess of sat. NH_4Cl. The solution turned from orange to yellow with precipitate.

60 min later, the yellow reaction mixture was extracted with AcOEt (3 times). The organic layers were combined and washed with water (3 times) and brine (1 time). The AcOEt washed solution was dried with anhydrous Na_2SO_4, filtered and the solvent was removed under reduced pressure affording a crude yellowish oil. This crude was redissolved in DCM, washed 3 times with a 10 % citric acid (3 times) and dried again with anhydrous Na_2SO_4. Final filtration and solvent removal leads to a viscous yellowish oil.

D. General Procedure for *N*-deprotection under Hydrogen High Pressure.

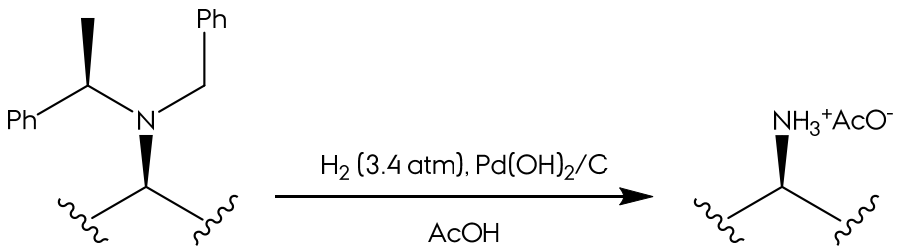

The protected substrate was dissolved in glacial AcOH. $Pd(OH)_2$ on carbon (palladium hydroxide on carbon 20 % wet, Perlman´s catalyst, CAS: 12135-22-7, black powder, 140.43 g/mol, commercial) were added in a mass ratio of 1:4 referred to the substrate, and the mixture was placed in a 5 mL pressure flask. The flask was connected to a H_2 gas line and the pressure was adjusted to 3.4 atm. The flask was mechanically stirred 3 days.

The flask was pressurized to atmospheric conditions and the mixture was filtered through a pad of Celite®, and generiously washed with glacial AcOH. The solvent was removed under reduced pressure, affording the quaternary ammonium salt.

E. General Procedure for *N*-benzyldeprotection and Boc-reprotection under Hydrogen High Pressure.

The protected substrate and 3 equiv of Boc_2O (di-*tert*-butyl dicarbonate, CAS: 24424-99-5, crystals, 218.25 g/mol, commercial) were dissolved in AcOEt. $Pd(OH)_2$ on carbon (palladium hydroxide on carbon 20 % wet, Perlman´s catalyst, CAS: 12135-22-7, black powder, 140.43 g/mol, commercial) were added in a mass ratio of 1:4 referred to the substrate, and the mixture was placed in a 5 mL pressure flask. The flask was connected to a H_2 gas line and the pressure was adjusted to 3.4 atm. The flask was mechanically stirred 3 days.

The flask was pressurized to atmospheric conditions and the mixture was filtered through a pad of Celite®, and generiously washed with AcOEt and DCM. The solvents were removed under reduced pressure, affording the carbamate.

F. General Procedure for selective *N*-benzyldeprotection with CAN (Cerium (IV) Ammonium Nitrate).

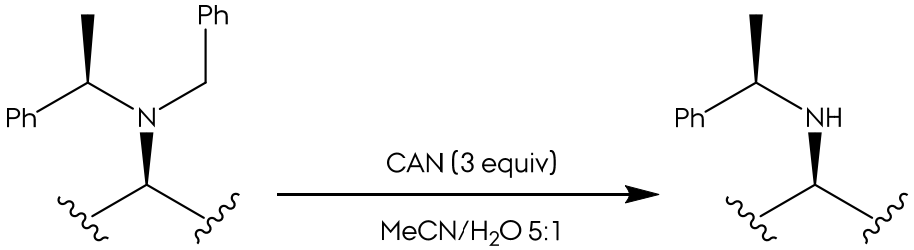

In a round bottom flask, a suitable amount of the protected amine was placed. A 5:1 $MeCN/H_2O$ mixture was added to dissolve the substrate. After that, 3 equiv of CAN (ammonium cerium (IV) nitrate, CAS: 16774-21-3, orange solid, 548.23 g/mol, commercial) were added, turning the solution from colourless to light yellow. Stirring was kept at room temperature for 4 h.

The reaction mixture was extracted 3 times with DCM. The organic layers were combined and dried with anhydrous Na_2SO_4, filtrated through a paper filter and the solvent was removed under reduced pressure, affording the monoprotected amine.

G. General Procedure for Amine Protection as *tert*-Butoxycarbonilcarbamate (-NHBoc)

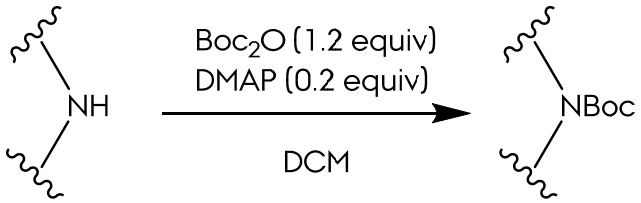

In a round bottom flask, a suitable amount of amine was dissolved together with 1.2 equiv of Boc_2O (di-*tert*-butyl dicarbonate, CAS: 24424-99-5, crystals, 218.25 g/mol, commercial) in dry DCM. 0.2 equiv of DMAP (4-(Dimethylamino)pyridine, CAS: 1122-58-3, white powder, 122.17 g/mol, commercial) were added, with forward gas generation. The mixture was stirred overnight at room temperature.

The reaction mixture was extracted with AcOEt, and the organic layer was washed with water (2 times), 1 M HCl (2 times) and brine (1 time). Drying the solution with anhydrous Na_2SO_4, filtration and forward solvent removal under reduced pressure, afforded the protected product.

H. General Procedure for Deprotection of tert-Butoxycarbonilcarbamates (-NHBoc).

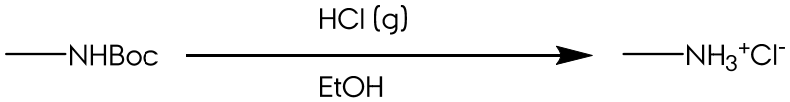

A suitable amount of protected amine was placed in a vial and dissolved in dry EtOH. HCl (hydrogen chloride, CAS: 7647-01-0, gas, 36.46 g/mol, commercial) was bubbled along 3 min. through a pipete, warming the vial. Solvent removal under reduced pressure afforded the amine chlorhydrate. This may be typically manipulated to convert it to the neutral amine.

I. General Procedure for Esterification of Acids to tert-butyl esters.

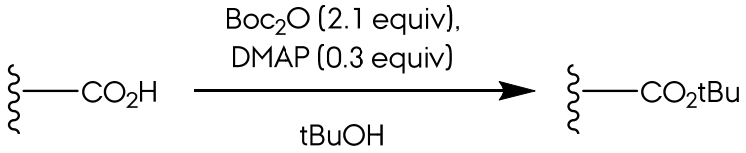

A suitable amount of acid was dissolved in tBuOH in a round bottom flask, together with 2.1 equiv of Boc_2O (di-*tert*-butyl dicarbonate, CAS: 24424-99-5, crystals, 218.25 g/mol, commercial). 0.3 equiv of DMAP (4-(dimethylamino)pyridine, CAS: 1122-58-3, white powder, 122.17 g/mol, commercial) were added and the reaction mixture was stirred at 30 ºC for 2 d, with a $CaCl_2$ tube as desiccant seal.

Solvent removal afforded the *tert*-butyl ester.

J. General Procedure for Esterification of Acids with Trimethylsilyldiazomethane.

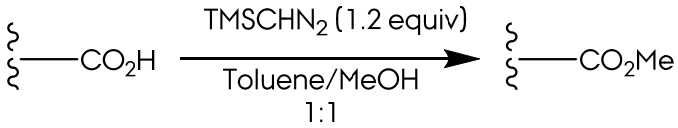

In a round bottom flask a suitable amount of acid was dissolved in toluene/MeOH 1:1. The flask was sealed and purged with Ar and cooled to 0ºC in an ice bath. 1.2 equiv of $TMSCHN_2$ ((trimethylsilyl)diazomethane solution, CAS: 18107-18-1, 114.22 g/mol, 2.0 M commercial solution) solution in were added through syringe and the light yellow reaction solution was magnetically stirred 5 min at 0 ºC, allowing warming to room temperature in the next 30 min.

The solvent was removed under reduced pressure, affording the methyl ester.

K. General Procedure for Solution Peptide Coupling.

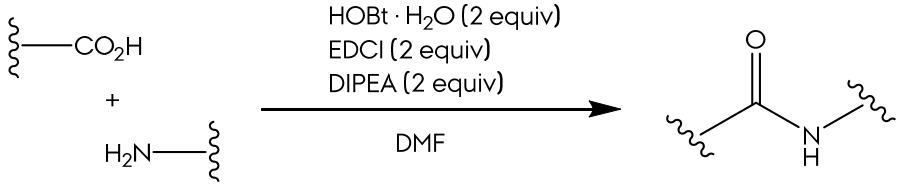

The selected acid and the amine were dissolved in dry DMF in a round bottom flask. 2 equiv of DIPEA (*N*,*N*-diisopropylethylamine, CAS: 7087-68-5, colourless liquid, 129.24 g/mol, commercial), 2 equiv of 1-hydroxybenzotriazole hydrate (HOBt · H_2O, CAS: 123333-53-9, white powder, 135.12 g/mol, commercial) and 2 equiv of EDCI (*N*-(3-dimethylaminopropyl)-*N′*-ethylcarbodiimide hydrochloride, CAS: 25952-53-8, hygroscopic white powder, 191.7 g/mol, commercial) were sequentially added and the final reaction solution was magnetically stirred for 24 h.

The reaction mixture was extracted with AcOEt (3 times), and the organic layer was washed with water (3 times), HCl 0.1 M (1 time), NaOH 0.1 M (1 time) and brine (1 time). The AcOEt solution was dried with anhydrous Na_2SO_4, filtrated through a paper filter and the solvent was removed under reduced pressure, affording the coupling product.

L. General Procedure for Esterification in Mild Conditions.

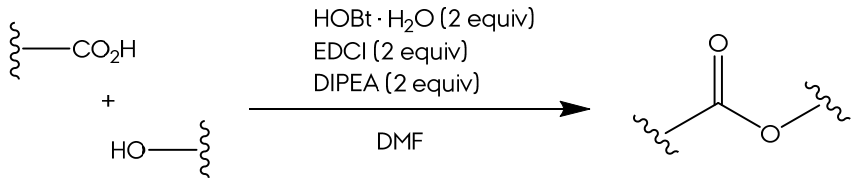

The selected acid and the alcohol were dissolved in dry DMF in a round bottom flask. 2 equiv of DIPEA (*N*,*N*-diisopropylethylamine, CAS: 7087-68-5, colourless liquid, 129.24 g/mol, commercial), 2 equiv of 1-hydroxybenzotriazole hydrate (HOBt · H_2O, CAS: 123333-53-9, white powder, 135.12 g/mol, commercial) and 2 equiv of EDCI (*N*-(3-dimethylaminopropyl)-*N′*-ethylcarbodiimide hydrochloride, CAS: 25952-53-8, hygroscopic white powder, 191.7 g/mol, commercial) were sequentially added and the final reaction solution was magnetically stirred for 24 h.

The reaction mixture was extracted with AcOEt (3 times), and the organic layer was washed with water (3 times), HCl 0.1 M (1 time), saturated $NaHCO_3$ (1 time)

and brine (1 time). The AcOEt solution was dried with anhydrous Na_2SO_4, filtrated through a paper filter and the solvent was removed under reduced pressure, affording the ester.

M. General Procedure for Mesylation of Alcohols with Mesyl Chloride.

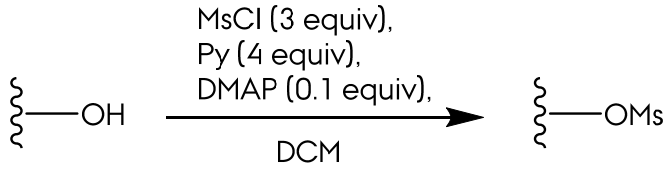

3 equiv of pyridine and 0.1 equiv of DMAP (4-(dimethylamino)pyridine, CAS: 1122-58-3, white powder, 122.17 g/mol, commercial) were added to a round bottom flask where a suitable amount of the alcohol in dry THF was previously prepared. The flask was sealed and the inner atmosphere was replaced with Ar. 3 equiv of MsCl (methanesulfonyl chloride, CAS: 124-63-0, light yellow liquid, 114.55 g/mol, commercial) were added through syringe and the reaction mixture was magnetically stirred at room temperature for 12 h. Excess of sat K_2CO_3 were dropwise added, with a vigorous bubbling, and stirring continued for an extra hour.

The reaction mixture was extracted with AcOEt (3 times) and the organic layers were combined and washed with water (3 times) and brine (1 time). Drying the solution with anhydrous Na_2SO_4, filtration and forward solvent removal under reduced pressure, afforded the alcohol.

N. General Procedure for the One Pot Reduction/Horner-Wadsworth-Emmons Homologation of Esters.

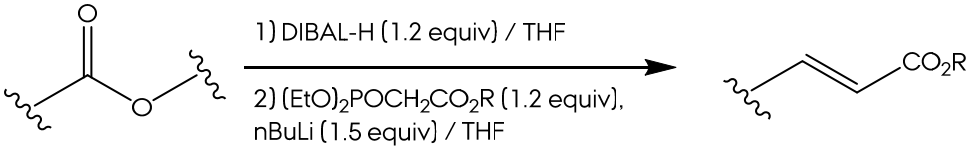

In a round bottom flask, an appropriate amount of substrate was dissolved in dry THF. The flask was sealed, urged with Ar and cooled at -78 ºC in an CO_2 - acetone bath. 1.2 equiv of DIBAL-H (diisobutylaluminum hydride, CAS: 1191-15-7, 142.22

g/mol, 1.5 M toluene commercial solution) were added and the reaction was magnetically stirred for 90 min.

In a pear-shaped flask, 1.2 equiv of alkyl diethylphosphonoacetate were dissolved in dry THF. This flask was sealed, purged with Ar and cooled at -78 ºC as well. 1.5 equiv of nBuLi (n-buthyllithium, CAS: 109-72-8, 64.06 g/mol, commercial solution) were added, turning the solution to yellowish. The solution was stirred 15 min at -78 ºC, warmed to 0 ºC in an ice bath along 30 min and finally to -78 ºC again for other extra 15 min.

The yellowish solution was added dropwise over the reaction mixture. Finished the addition, the resulting mixture was magnetically stirred for 4 h at -78 ºC. Then, the flask was allowed to warm to room temperature and stirred for 20 h more. Finally, the reaction was quenched with a saturated solution of sodium-potassium tartrate.

60 min later, the reaction mixture was extracted with AcOEt (3 times). The organic layers were combined and washed with sat. $NaHCO_3$ (3 times) and brine (1 time). The AcOEt washed solution was dried with anhydrous Na_2SO_4, filtered and the solvent was removed under reduced pressure affording the product.

O. General Procedure for the One Pot Cleavage of Vinyl Ethers/Horner-Wadsworth-Emmons Homologation.

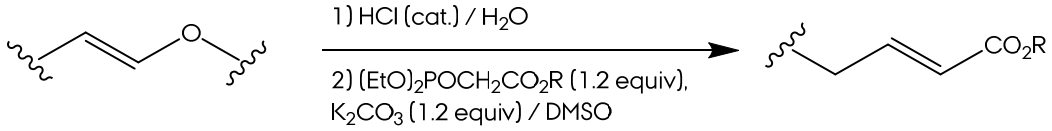

In a round bottom flask, a suitable amount of the vinyl ester was suspended in water. Catalytic amount of HCl 1 M was added and the reaction was stirred at room temperature for 3 h. After this, 1.2 equiv of K_2CO_3 (potassium carbonate, CAS: 584-08-7, white powder, 138.21 g/mol, commercial), 1.2 equiv of alkyl diethylphosphonoacetate and DMSO were added. The reaction mixture was sealed, the inner atmosphere were replaced by inert gas and stirred at 50 ºC overnight.

The reaction mixture was extracted with AcOEt (3 times) and the organic solution was dried with anhydrous Na_2SO_4 and filtrated through a paper filter. Solvent removal under reduced pressure, afforded the product.

P. General Procedure for Oxidative Ozonolysis.

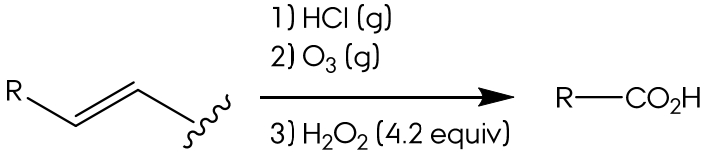

A suitable amount of olefin was dissolved in dry DCM in a round bottom flask. HCl gas (hydrogen chloride, CAS: 7647-01-0, gas, 36.46 g/mol, commercial) was bubbled through a pipette for 10 min, while the reaction solution was cooled at -78 ºC in a CO_2 - acetone bath. Next, ozone (O_3, gas, generated *in situ*) was bubbled for 15 min until the solution was light blue. Finally, 4.2 equiv of H_2O_2 (hydrogen peroxide, CAS: 7722-84-1, solution, 34.01 g/mol, 30 % commercial solution) was added and the reaction was allowed to warm to room temperature.

5 mL of 1 M NaOH was added, turning white the reaction mixture. After 15 min of stirring, the reaction was extracted with DCM (3 times). The organic solution was washed with brine 1 time. Drying the solution with anhydrous Na_2SO_4, filtration and forward solvent removal under reduced pressure, afforded the acid.

Q. General Procedure for Jones Oxidation of Alcohols to Acids.

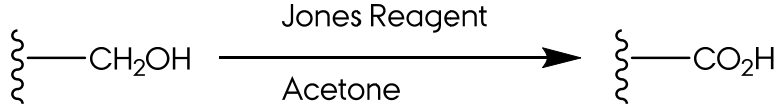

In a round bottom flask, a suitable amount of alcohol was dissolved in acetone. Jones reagent (prepared at lab, see laboratory prepared reagents) was added until the colour red persist in time. The reaction mixture was stirred for 30 min or until substrate was consumed (TLC). 10 mL of 2-propanol was added, turning the solution from dark red to dark green.

The reaction mixture was extracted with AcOEt (3 times) and the organic layers were combined and washed with water (6 times). Drying the ethyl acetate solution with anhydrous Na_2SO_4, filtration through a paper filter and solvent removal under reduced pressure afforded the product.

R. General Procedure for Ester Hydrolisis with Lithium Hydroxide.

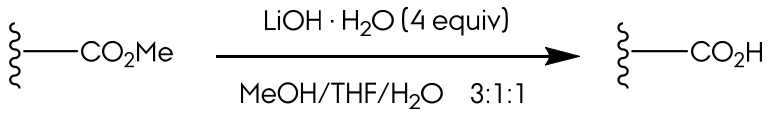

In a solution of the ester and MeOH/THF/H_2O 3:3:1 in a round bottom flask, 4 equiv of $LiOH \cdot H_2O$ (lithium hydroxide monohydrate, CAS: 1310-66-3, white solid, 41.96 g/mol, commercial) were added and the resulting solution was stirred at room temperature 5 h.

pH of the solution was checked (basic) and AcOEt was added. The mixture was partitioned between water and AcOEt and the aqueous solution was extracted again with AcOEt. The aqueous solution was acidified with HCl 1M and extracted three times with DCM. This organic solution was washed with brine, dried with anhydrous Na_2SO_4, filtrated and the solvent was evaporated to dryness, obtaining the acid.

S. General Procedure for Reduction of Carboxilic Acids to Alcohols with Borane in THF.

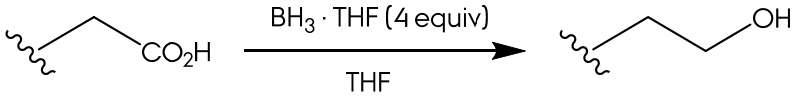

A solution of the acid in dry THF was prepared in a round bottom flask. The flask was sealed and purge with Ar. 4 equiv of $BH_3 \cdot THF$ (borane tetrahydrofuran complex solution, CAS: 14044-65-6, colourless solution, 85.94 g/mol, commercial) were added via syringe dropwise, and the colourless solution was magnetically stirred at room temperature for 7 h. Excess of sat. K_2CO_3 were dropwise added, with a vigorous bubbling, and stirring continued for an extra hour.

The reaction mixture was extracted with AcOEt (3 times) and the organic layers were combined and washed with water (3 times) and brine (1 time). Drying the solution with anhydrous Na_2SO_4, filtration and forward solvent removal under reduced pressure, afforded the alcohol.

T. General Procedure for Reduction of Esters to Aldehydes with Diisobutylaluminum Hydride.

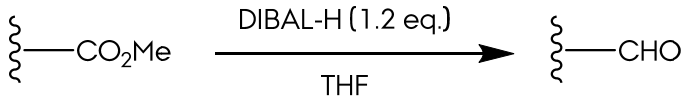

In a round bottom flask, a suitable amount of ester was placed and dissolved in dry DCM. The flask was sealed, purged with Ar and cooled to -78ºC in a CO_2 - acetone bath. Once cooled, 1.2 equiv of DIBAL-H (diisobutylaluminum hydride, CAS: 1191-15-7, 142.22 g/mol, 1.5 M toluene commercial solution) were added dropwise via syringe. Stirring continued until TLC monitoring showed consumption of starting material. Water excess was added and the reaction mixture was allowed to warm to room temperature.

The reaction solution was poured into an Erlenmeyer flask with 20 mL of AcOEt where 5 g of Na_2SO_4 and 5 g of $NaHCO_3$ were suspended. This mixture was stirred vigorously for 1 h. Finally, the solids were filtered through a pad of Celite® and the solvent were removed under reduced pressure, affording the aldehyde.

U. General Procedure for Reduction of Esters to Alcohols with Lithium Borohydride.

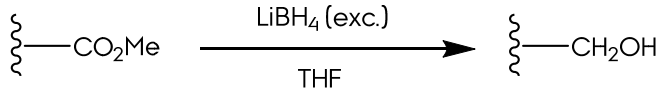

A 2 M solution of $LiBH_4$ was prepared in the next manner: 217.8 mg of $LiBH_4$ (lithium borohydride, CAS: 16949-15-8, white powder, 21.78 g/mol, commercial) were dissolved in 5 mL of dry THF in a 5 mL volumetric flask. The solution was shaken and sonicated 5 min, until the solids were dissolved.

A suitable amount of ester was dissolved in dry THF, sealed and the atmosphere was replaced by inert gas. An appropriate volume of 2 M lithium borohydride solution was added through a syringe, and the reaction mixture was stirred for 6 h.

1 mL of a saturated solution of NH_4Cl was added, and stirring was continued until gas generation ceased. Reaction mixture was extracted with AcOEt 3 times. The organic layer was washed with brine (1 time) and dried with anhydrous Na_2SO_4.

Filtration and forward solvent removal under reduced pressure, afforded the reduction product.

V. General Procedure for Bromination of Alcohols.

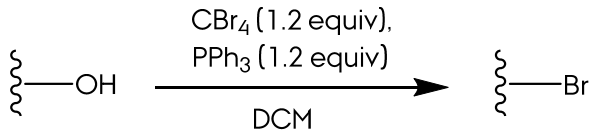

1.2 equiv of CBr_4 (tetrabromomethane, CAS: 558-13-4, white solid, 331.63 g/mol, commercial), 1.2 equiv of PPh_3 (triphenylphosphine, CAS: 603-35-0, white solid, 262.29 g/mol, commercial) and a suitable amount of alcohol were dissolved in dry DCM in a round bottom flask. The flask was sealed and the inner atmosphere was replaced with Ar. The solution was stirred 12 h.

The solvent was removed under reduced pressure and the crude was suspended in a Et_2O/hexanes 9:1 solution. This solution was filtrated through a chromatographic system consisting in 3 g of silica and 3 g of Celite®. Gradient elution with Et_2O/hexanes afforded the bromine product.

W. General Procedure for Substitution of Alcohols with Nucleobases via Mitsunobu Type Reaction.

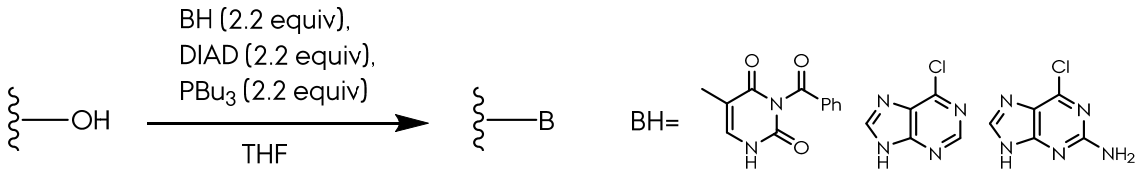

In a round bottom flask, a suitable amount of alcohol, 2.2 equiv of PBu_3 (tributylphosphine, CAS: 998-40-3, colorless liquid, 202.32 g/mol, commercial), 2.2 equiv of DIAD (diisopropyl azodicarboxylate, CAS: 2446-83-5, dark orange liquid, 202.21 g/mol, commercial) and 2.2 equiv of nucleobase were dissolved in dry THF. After sealing the flask and replacing the inner atmosphere with Ar, the reaction mixture was magnetically stirred at room temperature 48 h.

Water excess was added to the reaction mixture and later was extracted with AcOEt (3 times). The organic layers were combined and washed with water (3

times) and brine (1 time). Drying the solution with anhydrous Na_2SO_4, filtration and forward solvent removal under reduced pressure, afforded the substitution product.

X. General Procedure for Substitution of Mesylates with Thymine.

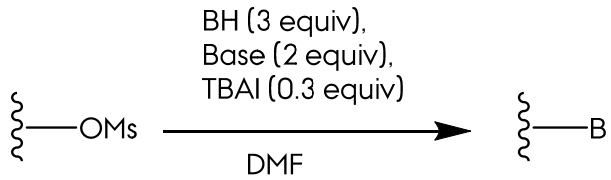

In a round bottom flask, 3 equiv of nucleobase and 2 equiv of base (K_2CO_3 or DBU) were suspended in dry DMF. This mixture was stirred 1 h at 60ºC.

Apart from this, a suitable amount of mesylate and 0.3 equiv of TBAI (tetrabutylammonium iodide, CAS: 311-28-4, white solid, 396.37 g/mol, commercial), were dissolved in dry DMF in round bottom flask. This mixture was added to the initial nucleobase mixture, and the reaction was stirred for 12 h at 70 ºC.

Water excess was added to the reaction mixture, which was later extracted with AcOEt (3 times). The organic extract was washed with water (5 times). Drying the AcOEt solution with anhydrous Na_2SO_4, filtration and forward solvent removal under reduced pressure, afforded the substitution product.

Y. General Procedure for One Pot Boc-amine Release and Intramolecular Mesylate Displacement.

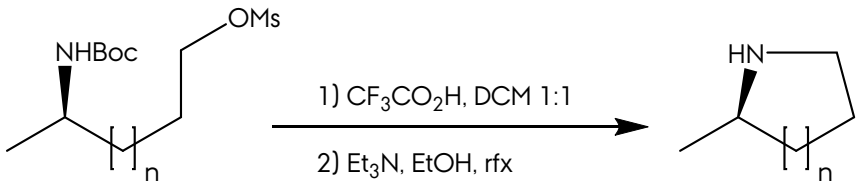

A 1:1 mixture of CF_3CO_2H/DCM (trifluoroacetic acid, CAS: 76-05-1, faint yellow liquid, 114.02 g/mol, commercial) was added to a round bottom flask where the substrate was previously placed. The flask was sealed, purged with Ar, stirred at room temperature and monitored by TLC.

When the reaction finished, the solvents were removed under reduced pressure and the brown oil was dissolved in EtOH. Et_3N was added in a ratio 1/5 referred to the EtOH volume, and the resulting mixture was stirred at reflux (78 ºC) for 12 h. The solvent was again evaporated and the crude dissolved in AcOEt and extracted with 0.5 M HCl 0.5 M. The aqueous phase was basified to pH 8 with NaOH (1 M) and extracted with AcOEt. The organic phase was dried over anhydrous Na_2SO_4, filtered, and the solvent was removed at reduced pressure, affording the cyclization product.

Z. General Procedure for Alkylation of Secondary Amines with Alkyl Bromides.

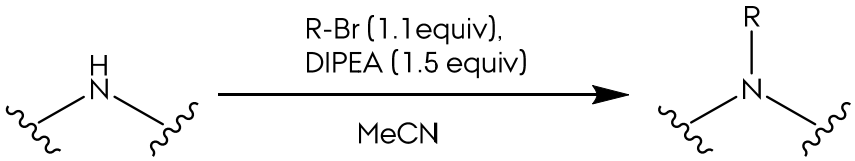

A suitable amount of the amine was dissolved in dry acetonitrile in a round bottom flask. 1.5 equiv of DIPEA (*N*,*N*-diisopropylethylamine, CAS: 7087-68-5, colourless liquid, 129.24 g/mol, commercial) were added and finally, 1.2 equiv of alkyl bromide were added. The flask was sealed, purged with Ar, stirred at room temperature and the reaction progress was monitored by TLC.

When the reaction finished, the solvents were removed under reduced pressure and the crude was dissolved in AcOEt. The organic solution was washed sequentially with water (3 times) and brine (1 time). Drying the AcOEt solution with anhydrous Na_2SO_4, filtration and forward solvent removal under reduced pressure, afforded the tertiary amine.

Reaction Inventory 1. Morphan Section

M1.- One Pot α-Bromination/Esterification of Azelaic Acid.

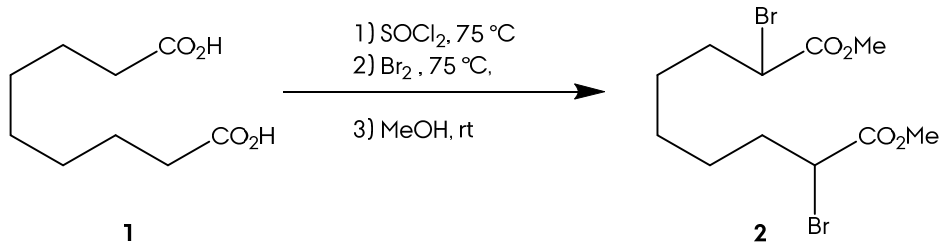

General procedure A was followed with the next quantities: 20 g of azelaic acid **1** (CAS: 123-99-9, white powder, 188.2 g/mol, 106 mmol, commercial); 27 mL of $SOCl_2$ (118.9 g/mol, 372 mmol); 19 mL of Br_2 (159.8 g/mol, 372 mmol); 86 ml of MeOH. Reaction workup afforded 38.77 g of product **2**, 98 % yield.

Dimethyl 2,8-dibromononanedioate (2).

δ_H (200 MHz, $CDCl_3$) 4.18 (2H, t, *J* 7.2, **H2** and **H8**), 3.74 (6H, s, **CO₂C<u>H</u>₃**), 2.08 - 1.91 (4H, **H3** and **H7**), 1.49 - 1.28 (6H, **H4**, **H5** and **H6**).

δ_C (50 MHz, $CDCl_3$) 170.4 (s, **C1** and **C9**), 53.1 (q, **CO<u>C</u>H₃**), 45.6 (d, **C2** and **C8**), 34.8 (d, **C3** and **C7**), 28.2 (t, **C5**), 27.1 (t, **C4** and **C6**).

M2.- Dehydrobromination of 2 to the (α,β)(α',β')-Unsaturated Systems.

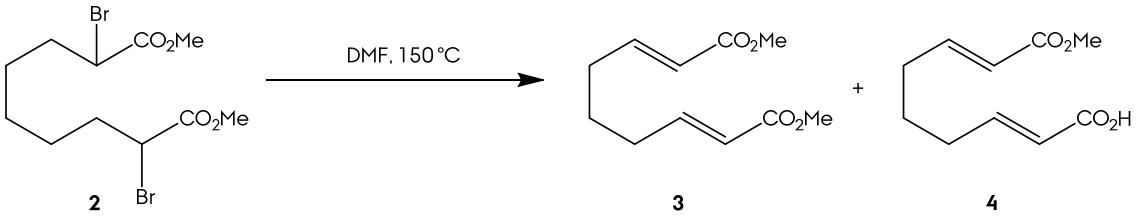

General procedure B were followed with the next quantities: 28 g of diester **2** (374.0 g/mol, 75 mmol); 1100 mL of dry DMF. Flash chromatography afforded 6.77 g of product **3** (Hexanes/AcOEt 9:1), 46 % yield. The $NaHCO_3$ washing fraction was coloured (orange), and were acidified with HCl 6M. This fraction was extracted with DCM (3 times) and washed with brine (1 time). Drying the DCM solution with anhydrous Na_2SO_4, filtration and forward solvent removal under reduced pressure,

afforded a dark viscous oil. Flash chromatography of this crude afforded 6.86 g of product **4** (Hexanes/AcOEt 8:2), 50 % yield.

Dimethyl (2*E*,7*E*)-nona-2,7-dienedioate (3)

$\mathbf{R}_f$ 0.58 (Hexanes/AcOEt, 9:1)

δ_H (200 MHz, $CDCl_3$) 6.99 (2H, dt, *J* 15.6 7.0, **H3** and **H7**), 5.90 (2H, d, *J* 15.7, **H2** and **H8**), 3.75 (6H, s, $\mathbf{CO_2C\underline{H}_3}$), 2.29 (4H, q, *J* 7.4, **H4** and **H6**), 1.70 (2H, quintet, *J* 7.4, **H5**).

δ_C (50 MHz, $CDCl_3$) 166.6 (**C1** and **C9**), 148.0 (**C3** and **C7**), 121.6 (**C2** and **C8**), 51.1 ($\mathbf{CO\underline{C}H_3}$), 31.3 (t, **C4** and **C6**), 26.3 (t, **C5**).

(2*E*,7*E*)-9-methoxy-9-oxonona-2,7-dienoic acid (4)

$\mathbf{R}_f$ 0.39 (Hexanes/AcOEt, 1:1)

δ_H (200 MHz, $CDCl_3$) 7.03 (1H, dt, *J* 15.6 6.9, **H3**), 6.93 (1H, dt, *J* 15.6 7.0, **H7**), 5.83 (2H, d, *J* 15.7, **H2** and **H8**), 3.72 (3H, s, $\mathbf{CO_2C\underline{H}_3}$), 2.25 (4H, **H4** and **H6**), 1.654 (2H, quintet, *J* 7.3, **H5**).

δ_C (50 MHz, $CDCl_3$) 171.3 (s, **C1**), 167.2 (s, **C9**), 150.9 (d, **C7**), 148.7 (d, **C3**), 121.6 (d, **C8**), 121.4 (d, **C2**), 51.6 (q, $\mathbf{CO\underline{C}H_3}$), 31.5 (d, **C6**), 31.5 (d, **C4**), 26.2 (d, **C5**).

m/z (M+Na) calcd for $\mathbf{C_{10}H_{14}O_4Na}$, 221.0784; found, 221.0786, $\mathbf{\Delta = 0.76\ ppm}$.

M3.- Asymmetric Michael Addition of Lithium (*R*)-*N*-benzyl-*N*-α-methylbenzylamide to 3.

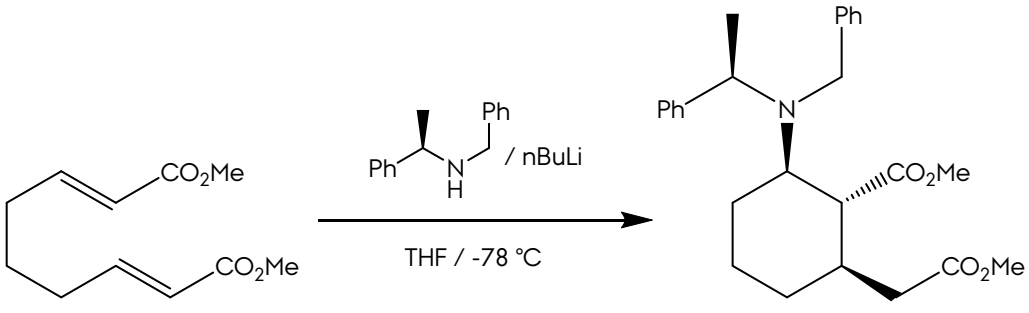

3 **5**

General procedure C was followed with the next quantities: 5.1 g of (*R*)-*N*-benzyl-*N*-α-methylbenzylamide (211.3 g/mol; 22.0 mmol) in 15 mL of THF; 12.4 mL of 1.6 M nBuLi in hexanes (64.06 g/mol; 19.9 mmol); 2.3 g of substrate **3** (198.2 g/mol; 11.6 mmol) in 8 mL of THF. Flash chromatography afforded 4.5 g of product **5** (Hexanes/AcOEt 9:1), 91 % yield.

Methyl (1*R*,2*R*,6*R*)-2-(benzyl((*R*)-1-phenylethyl)amino)-6-(2-methoxy-2-oxoethyl)cyclohexane-1-carboxylate (5)

$\mathbf{R}_f$ 0.63 (Hexanes/AcOEt, 8:2)

$[\alpha]^{26}_{D}$ +3.9 (c. 1.86 in $CHCl_3$)

υ_{max} (neat)/cm^{-1} 3459, 2947 (C-H), 1738 (C=O), 1435 (C-N), 1028 (C-O).

δ_H (200 MHz; $CDCl_3$) 7.38 - 7.20 (10H, $\mathbf{C_{ar}\underline{H}}$), 4.00 (1H, q, *J* 6.9, $\mathbf{C\underline{H}CH_3}$), 3.88 (1H, AB, *J* 13.6, $\mathbf{NC\underline{H}_AH}$), 3.67 (1H, AB, *J* 13.9, $\mathbf{NCH\underline{H}_B}$), 3.62 (3H, s, $\mathbf{CH_2CO_2C\underline{H}_3}$), 3.43 (3H, s, $\mathbf{CHCO_2C\underline{H}_3}$), 3.06 (1H, td, *J* 10.9 3.2, **H2**), 2.34 (1H, t, *J* 10.9, **H1**), 2.23 - 1.99 (4H, $\mathbf{H3_A}$, **H6** and $\mathbf{C\underline{H}_2CO_2CH_3}$), 1.83 - 1.71 (2H, $\mathbf{H4_A}$ and $\mathbf{H5_A}$), 1.43 - 1.27 (2H, $\mathbf{H3_B}$ and $\mathbf{H4_B}$), 1.39 (3H, d, *J* 7.0, $\mathbf{CHC\underline{H}_3}$), 0.91 (1H, q, *J* 11.1, $\mathbf{H5_B}$).

δ_C (50 MHz; $CDCl_3$) 174.4 (s, $\mathbf{CH_2\underline{C}O_2CH_3}$), 172.7 (s, $\mathbf{CH\underline{C}O_2CH_3}$), 144.3 (s, $\mathbf{C_{ipso}}$), 140.9 ($\mathbf{C_{ipso}}$), 129.4 (d, $\mathbf{C_{ar}}$), 128.4 (d, $\mathbf{C_{ar}}$), 128.2 (d, $\mathbf{C_{ar}}$), 128.0 (d, $\mathbf{C_{ar}}$), 127.0 (d, $\mathbf{C_{ar}}$), 126.6 (d, $\mathbf{C_{ar}}$), 58.9 (d, **C2**), 57.0 (d, $\mathbf{\underline{C}HCH_3}$), 54.7 (d, **C1**), 51.7 (q, $\mathbf{CH_2CO_2\underline{C}H_3}$), 51.4 (q, $\mathbf{CHCO_2\underline{C}H_3}$), 50.2 (t, $\mathbf{N\underline{C}H_2}$), 39.6 (t, $\mathbf{\underline{C}H_2CO_2CH_3}$), 37.5 (d, **C6**), 31.3 (t, **C3**), 28.8 (t, **C5**), 24.8 (t, **C4**), 16.3 (q, $\mathbf{CH\underline{C}H_3}$).

m/z (M+H) calcd for $\mathbf{C_{26}H_{34}NO_4}$, 424.2488; found, 424.2486, $\mathbf{\Delta = 0.47\ ppm}$.

M4.- Chemoselective Hydrolysis of 5 in Basic Conditions.

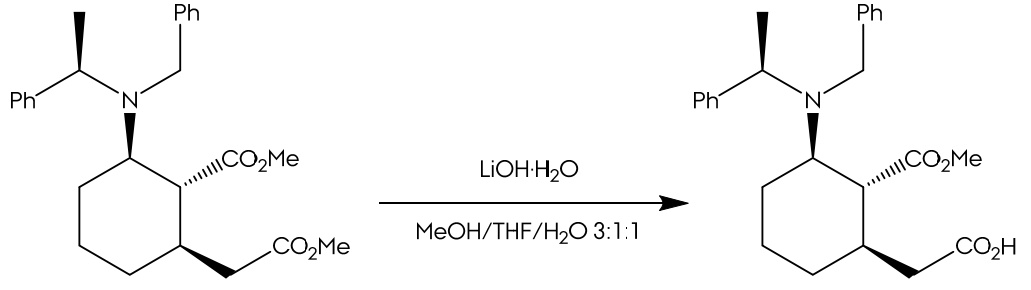

5 **6**

General procedure R was followed with the next quantities: 875.3 mg of **5** (423.5 g/mol; 2.0 mmol); 50 mL of MeOH/THF/H_2O 3:1:1 solution; 424 mg of $LiOH \cdot H_2O$ (41.9 g/mol; 10.0 mmol). Flash chromatography afforded 517 mg of product **6** (Hexanes/AcOEt 1:1), 61 % yield.

2-((1*R*,2*R*,3*R*)-3-(benzyl((*R*)-1-phenylethyl)amino)-2-(methoxycarbonyl)cyclohexyl)acetic acid (6)

R_f 0.58 (Hexanes/AcOEt, 1:1)

$[\alpha]^{26}_D$ +8.1 (c. 0.9 in $CHCl_3$)

υ_{max} (neat)/cm^{-1} 3367 (O-H), 2935 (C-H), 1718 (C=O), 1525, 1170 (C-O).

δ_H (200 MHz; $CDCl_3$) 8.28 (1H, br s, **COOH**), 7.39 - 7.18 (10H, **$C_{ar}H$**), 3.97 (1H, q, *J* 7.0, **CHCH$_3$**), 3.88 - 3.77 (1H, **NCH_AH**), 3.65 (1H, AB, *J* 13.9, **NCHH_B**), 3.41 (3H, s, **CO_2(CH_3)**), 3.04 (1H, td, *J* 10.8 2.6, **H3**), 2.37 - 1.96 (5H, **H1**, **H2**, **H4$_A$** and **CH_2CO$_2$H**), 1.83 - 1.71 (2H, **H5$_A$** and **H6$_A$**), 1.43 - 1.24 (2H, **H4$_B$** and **H5$_B$**), 1.37 (3H, d, *J* 7.1, **CHCH_3**), 0.90 (1H, **H6$_B$**).

δ_C (50 MHz; $CDCl_3$) 177.4 (s, **CO_2H**), 174.4 (s, **CO_2CH$_3$**), 144.1 (s, **C_{ipso}**), 141.1 (**C_{ipso}**), 129.5 (d, **C_{ar}**), 128.4 (d, **C_{ar}**), 128.0 (d, **C_{ar}**), 127.1 (d, **C_{ar}**), 126.8 (d, **C_{ar}**), 58.4 (d, **C3**), 56.6 (d, **CHCH$_3$**), 54.1 (d, **C2**), 51.0 (q, **CO_2CH_3**), 49.7 (t, **NCH_2**), 38.8 (t, **CH_2CO$_2$H**), 36.7 (d, **C1**), 30.6 (t, **C4**), 28.2 (t, **C6**), 24.2 (t, **C5**), 15.7 (q, **CHCH_3**).

m/z (M+Na) calcd for **$C_{26}H_{31}NO_4Na$**, 432.2145; found, 432.2150, **Δ = 1.08 ppm**.

M5.- Full Deprotection of Amine 6 under Hydrogen Atmosphere.

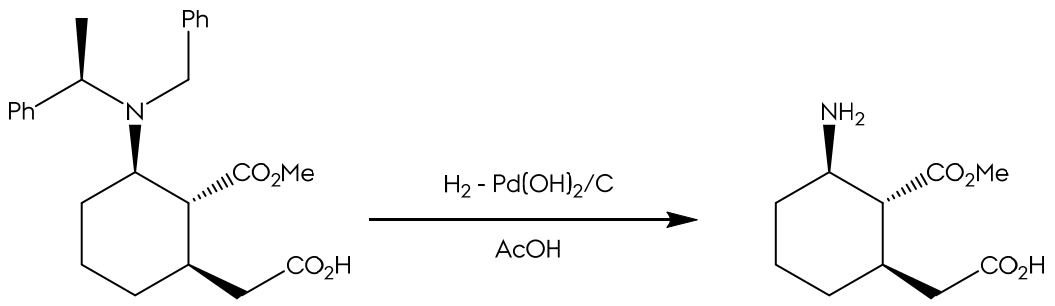

6 **7**

General procedure R was followed with the next quantities: 517 mg of **6** (409.2 g/mol; 1.2 mmol); 250 mg of $Pd(OH)_2$ 20% over carbon; 3 mL of AcOH. Product **7** was obtained as acetate salt. Ion-exchange resin (Dowex 50x8-200, NH_3 1 M) followed by freeze-drying afforded g of product **7**, 38 % yield.

2-((1*R*,2*R*,3*R*)-3-amino-2-(methoxycarbonyl)cyclohexyl)acetic acid (7)

$[\alpha]^{24}_D$ -4.73 (c. 1.0 in H_2O)

δ_H (200 MHz; D_2O) 3.58 (3H, s, $\mathbf{CO_2(C\underline{H_3})}$), 3.23 (1H, td, *J* 10.9 4.5, **H3**), 2.26 - (2H, **H2** and $\mathbf{C\underline{H_A}HCO_2H}$), 1.89 - 1.55 (5H, **H1**, $\mathbf{H4_A}$, $\mathbf{H5_A}$, $\mathbf{H6_A}$ and $\mathbf{CH\underline{H_B}COOH}$), 1.21 - 1.15 (2H, $\mathbf{H4_B}$, $\mathbf{H5_B}$), 0.90 (1H, q, *J* 10.9, $\mathbf{H6_B}$).

δ_C (50 MHz; D_2O) 180.7 (s, $\mathbf{\underline{C}O_2H}$), 174.8 (s, $\mathbf{\underline{C}O_2CH_3}$), 53.3 (d, **C3**), 52.8 (q, $\mathbf{CO_2\underline{C}H_3}$), 51.7 (d, **C2**), 42.7 (t, $\mathbf{\underline{C}H_2CO_2H}$), 37.3 (d, **C1**), 30.2 (t, **C4**), 29.8 (t, **C6**), 22.9 (t, **C5**).

m/z (M+Na) calcd for $\mathbf{C_{10}H_{27}NO_4Na}$, 216.1242; found, 216.1229, $\mathbf{\Delta = 6.01\ ppm}$.

M6.- Ring-closing/Lactamization of 7.

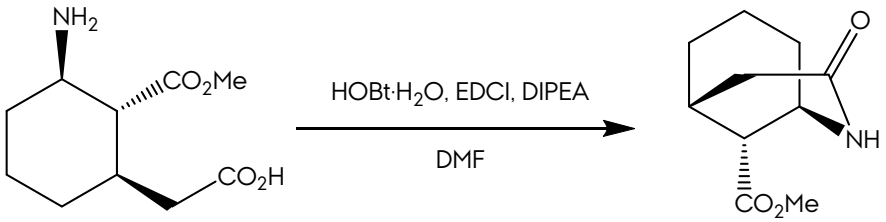

7 **8**

General procedure K was followed with the next quantities: 196 mg of **7** (215.1 g/mol; 0.9 mmol); 3 mL of DMF; 0.3 mL of DIPEA (129.2 g/mol; 1.8 mmol); 272 mg of HOBt · H_2O (135.1 g/mol; 2.0 mmol); 385 mg of EDCI (191.7 g/mol; 2.0 mmol). Flash chromatography afforded 82 mg of product **8** (Hexanes/AcOEt 1:1), 46 % yield.

Methyl (1*R*,5*R*,9*R*)-3-oxo-2-azabicyclo[3.3.1]nonane-9-carboxylate (8)

mp 106 °C;

$\mathbf{R}_f$ 0.45 (Hexanes/AcOEt, 1:1)

$[\alpha]^{24}_{D}$ -10.2 (*c.* 1.1 in $CHCl_3$);

υ_{max} (neat)/cm^{-1} 3214 (N-H), 2942 (C-H), 1731 (C=O, ester), 1664 (C=O, amide), 1222 (C-O).

δ_H (400 MHz; $CDCl_3$) 7.28 (1H, d, *J* 2.5, **H2**), 3.91 (1H, **H1**), 3.70 (3H, s, **$CO_2(C\underline{H}_3)$**), 2.77 (1H, **H9**), 2.63 (1H, ABX, *J* 17.7 6.9, **$H4_A$**), 2.58 (1H, **H5**), 2.27 (1H, AB, *J* 17.7, **$H4_B$**), 1.70 - 1.42 (6H, **H6**, **H7** and **H8**).

δ_C (50 MHz; $CDCl_3$) 173.8 (s, **$\underline{C}O_2(CH_3)$**), 171.6 (s, **$\underline{C}ONH$**), 52.2 (q, **$CO_2(\underline{C}H_3)$**), 48.3 (d, **C1**), 44.2 (d, **C9**), 37.7 (t, **C4**), 29.9 (t, **C6**), 28.5 (t, **C8**), 28.2 (d, **C5**), 15.5 (t, **C7**).

m/z (M+Na) calcd for **$C_{10}H_{15}NO_3Na$**, 220.0944; found, 220.0939, **Δ = -2.34 ppm**.

M7.- Reaction of 8 with $BH_3 \cdot THF$

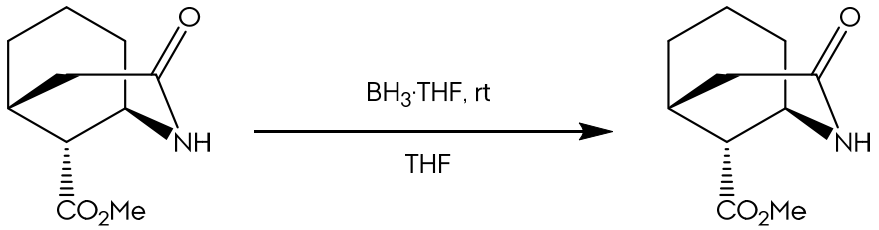

8 **8**

18 mg of of **8** (197.1 g/mol; 0.09 mmol) were dissolved in 1 mL of dry THF in a round bottom flask. The flask was sealed and purge with Ar. 0.91 mL (10 equiv) of $BH_3 \cdot THF$ (borane tetrahydrofuran complex solution, CAS: 14044-65-6, colourless solution, 85.9 g/mol, 1 M commercial solution) were added via syringe dropwise, and the colourless solution was magnetically stirred at room temperature for 12 h. Excess of sat. K_2CO_3 was added dropwise, with a vigorous bubbling, and stirring continued for an extra hour.

The reaction mixture was extracted with AcOEt (3 times) and the organic layers were combined and washed with water (3 times) and brine (1 time). Drying the solution with anhydrous Na_2SO_4, filtration and forward solvent removal afforded 23 mg of starting material **8**.

M8.- Reaction of 8 with $BH_3 \cdot Me_2S$.

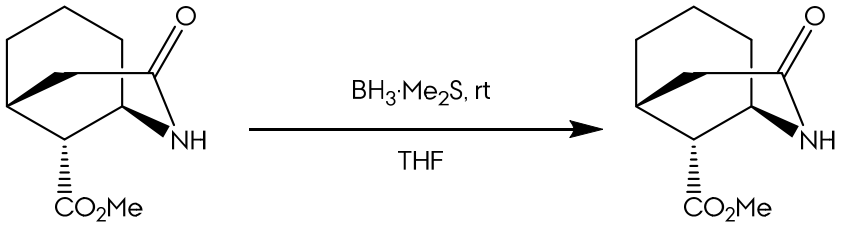

8 **8**

9 mg of of **8** (197.1 g/mol; 0.046 mmol) were dissolved in 1 mL of dry THF in a round bottom flask. The flask was sealed and purge with Ar. 0.23 mL (4 equiv) of $BH_3 \cdot Me_2S$ (borane dimethylsulfide complex solution, CAS: 13292-87-0, colourless solution, 75.9 g/mol, 5 M commercial solution) were added via syringe dropwise, and the colourless solution was magnetically stirred at room temperature for 12 h. Excess of sat. K_2CO_3 were dropwise added, with a vigorous bubbling, and stirring continued for an extra hour.

The reaction mixture was extracted with AcOEt (3 times) and the organic layers were combined and washed with water (3 times) and brine (1 time). Drying the solution with anhydrous Na_2SO_4, filtration and forward solvent removal afforded 13 mg of starting material **8**.

M9.- Reaction of 8 with $BH_3 \cdot THF$ at 75 ºC.

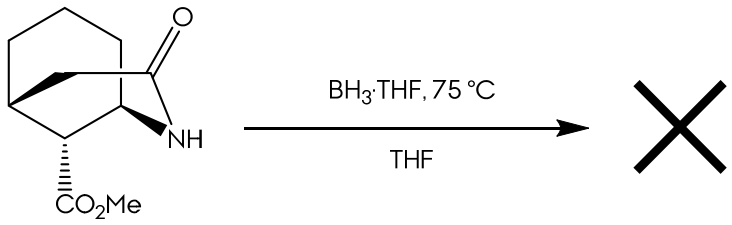

8

10 mg of of **8** (197.1 g/mol; 0.05 mmol) were dissolved in 1 mL of dry THF in a round bottom flask. The flask was sealed, purged with Ar and heated to 75 ºC. 0.51 mL (10 equiv) of $BH_3 \cdot THF$ (borane tetrahydrofuran complex solution, CAS: 14044-65-6, colourless solution, 85.94 g/mol, 1 M commercial solution) were added via syringe dropwise, and the colourless solution was magnetically stirred at 75 ºC for 12

h. Excess of sat. K_2CO_3 were dropwise added, with a vigorous bubbling, and stirring continued for an extra hour.

The reaction mixture was extracted with AcOEt (3 times) and the organic layers were combined and washed with water (3 times) and brine (1 time). Drying the solution with anhydrous Na_2SO_4, filtration and forward solvent removal afforded a crude oil. Flash chromatography did not elute any identifiable product.

M10.- Reaction of 8 with $BH_3 \cdot THF$ at 75 ºC with Acid Quenching.

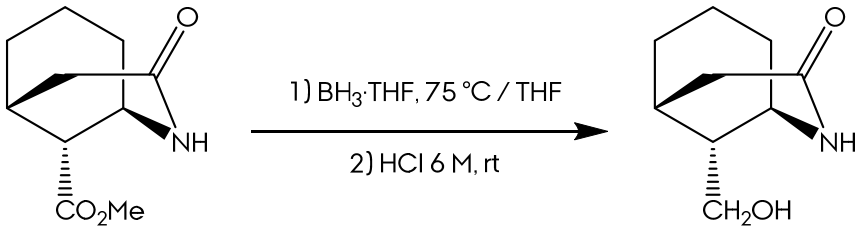

8 **9**

20 mg of of **8** (197.1 g/mol; 0.10 mmol) were dissolved in 1.5 mL of dry THF in a round bottom flask. The flask was sealed, purged with Ar and heated to 75 ºC. 0.41 mL (10 equiv) of $BH_3 \cdot THF$ (borane tetrahydrofuran complex solution, CAS: 14044-65-6, colourless solution, 85.9 g/mol, 1 M commercial solution) were added via syringe dropwise, and the colourless solution was magnetically stirred at 75 ºC for 1.5 h. Once cooled the reaction, 1 mL of 6 M HCl was added and stirring continued 10 min. Reaction mixture was neutralized with 1 M NaOH.

The reaction mixture was extracted with AcOEt (3 times) and the organic layers were combined and dried with anhydrous Na_2SO_4. Filtration and forward solvent removal afforded alcohol **9**, 17 % yield.

(1*R*,5*R*,9*R*)-9-(hydroxymethyl)-2-azabicyclo[3.3.1]nonan-3-one (9)

$\mathbf{R}_f$ 0.36 (Hexanes/AcOEt, 1:1)

$[\alpha]^{24}_D$ +24.0 (*c.* 0.5 in $CHCl_3$);

υ_{max} (film)/cm^{-1} 3292 (N-H), 2923 (C-H), 1637 (C=O), 1460 (C-N), 1037 (C-O).

δ_H (400 MHz; $CDCl_3$) 6.03 (1H, br s, **H2**), 3.83 (1H, dd, *J* 6.7 4.7, **C$\underline{H_A}$HOH**), 3.70 (1H, t, *J* 5.9, **C$\underline{H_A}$HOH**), 3.64 (1H, **H1**), 2.67 (1H, ABX, *J* 18.2 6.8, **$H4_A$**), 2.33 (1H, AB, *J* 18.2, **$H4_B$**), 2.13 (2H, **H5** and **H9**), 1.93 - 1.12 (6H, **H6**, **H7** and **H8**).

δ_C (50 MHz; $CDCl_3$) 174.3 (s, **$\underline{C}$ONH**), 62.5 (t, **$\underline{C}H_2OH$**), 48.3 (d, **C1**), 41.4 (d, **C9**), 38.8 (t, **C4**), 30.0 (t, **C6**), 27.8 (d, **C5**), 26.6 (t, **C8**), 15.8 (t, **C7**).

m/z (M+Na) calcd for **$C_9H_{15}NO_2Na$**, 192.1000; found, 192.1017, **Δ = -8.8 ppm**.

M11.- Reaction of 8 with $LiAlH_4$ at 75 ºC.

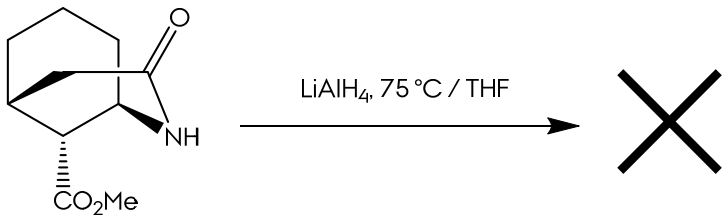

8

16 mg of of **8** (197.1 g/mol; 0.09 mmol) were dissolved in 1 mL of dry THF in a round bottom flask. 38.2 mg (7 equiv) of $LiAlH_4$ (lithium aluminium hydride, CAS: 16853-85-3, grey powder, 37.9 g/mol, commercial) were added and the flask was sealed, purged with Ar and heated to 75 ºC for 20 h. Reaction mixture were quenched with 5 mL of DCM and 2 mL of water. Drying the solution with anhydrous Na_2SO_4, filtration and forward solvent removal afforded a crude oil. Flash chromatography did not elute any identifiable product.

M12.- Reaction of 8 with $LiAlH_4$ at 105 ºC.

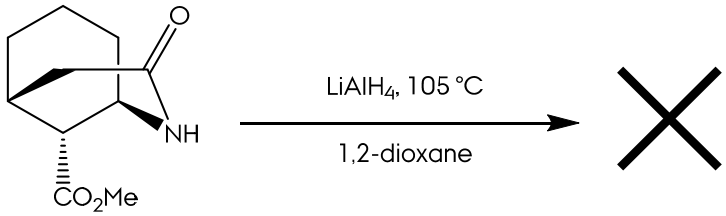

8

19 mg of of **8** (197.1 g/mol; 0.09 mmol) were dissolved in 2 mL of dry 1,2-dioxane in a round bottom flask. 37 mg (10 equiv) of $LiAlH_4$ (lithium aluminium hydride, CAS:

16853-85-3, grey powder, 37.9 g/mol, commercial) were added and the flask was sealed, purged with Ar and heated to 105 ºC for 20 h. Reaction mixture were quenched with 5 mL of DCM and 2 mL of water. Drying the solution with anhydrous Na_2SO_4, filtration and forward solvent removal afforded a crude oil. Flash chromatography did not elute any identifiable product.

M13.- Reaction of 8 with 9-BBN at 75 ºC.

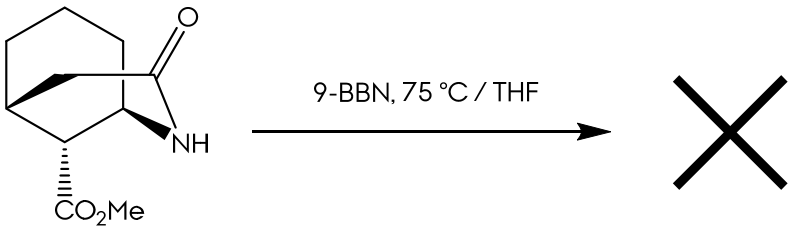

8

9.4 mg of of **8** (197.1 g/mol; 0.05 mmol) were dissolved in 2 mL of dry THF in a round bottom flask. The flask was sealed, purged with Ar and heated to 75 ºC. 1.27 mL (13 equiv) of 9-BBN · THF (9-borabicyclo[3.3.1]nonane solution, CAS: 280-64-8, colourless solution, 122.0 g/mol, 0.5 M commercial solution) were added via syringe dropwise, and the colourless solution was magnetically stirred at 75 ºC for 2 h. After that, 6.4 mg of ethanolamine where added, with emergence of a white precipitate. The reaction mixture was filtrated through a pad of Celite® and the solvent was removed under reduced pressure. Flash chromatography did not elute any identifiable product.

M14.- Reaction of 8 with Meerwin Type Salt and Forward $NaBH_4$ Reduction.

8 **10**

In a round bottom flask, 21.6 mg (211.1 g/mol; 0.11 mmol) of amide **8** were dissolved in 1 mL of dry DCM, together with 20 mg (1.2 equiv) of Me_3OBF_4 (trimethyloxonium tetrafluoroborate, CAS: 420-37-1, white powder, 147.91 g/mol, commercial). The flask was sealed, purged with Ar and magnetically stirred for 24 h.

The solvents were evaporated and the residue dissolved EtOH. 10.3 mg (2.5 equiv) of $NaBH_4$ (sodium borohydride, CAS: 16940-66-2, white solid, 37.83 g/mol, commercial) were added at 0ºC in an ice - water bath, and stirring continued at room temperature for extra 24 h.

pH was checked (basic) and the reaction mixture was neutralized with HCl 1 M. Later, the neutralized solution was extracted 3 times with AcOEt. The organic layers were combined, dried with anhydrous Na_2SO_4 and filtrated. Forward solvent removal under reduced pressure, afforded a crude product. Flash chromatography afforded 4.1 mg of intermediate **10** (Hexanes/AcOEt 8:2), 18 % yield.

Methyl (1*R*,5*R*,9*R*)-3-methoxy-2-azabicyclo[3.3.1]non-2-ene-9-carboxylate (10)

$\mathbf{R}_f$ 0.53 (Hexanes/AcOEt, 1:1)

$[\alpha]^{25}_D$ +15.8 (*c.* 0.4 in $CHCl_3$);

υ_{max} (neat)/cm^{-1} 2939 (C-H), 1735 (C=O), 1673 (C=N), 1436, 1209 (C-O).

δ_H (200 MHz, $CDCl_3$) 4.14 - 4.24 (1H, m, **H1**), 3.74 (3H, s, **$CO_2(C\underline{H}_3)$**), 3.66 (3H, s, **$CNO(C\underline{H}_3)$**), 2.60 - 2.50 (3H, **H4** and **H9**), 2.19 (1H, **H5**), 1.75 – 1.33 (6H, **H6**, **H7** and **H8**).

δ_C (50 MHz, $CDCl_3$) 173.2 (s, **$\underline{C}O_2(CH_3)$**), 165.4 (s, **C3**), 52.8 (q, **$CNO(\underline{C}H_3)$**), 51.9 (q, **$CO_2(\underline{C}H_3)$**), 51.0 (d, **C1**), 43.8 (d, **C9**), 33.9 (t, **C4**), 28.3 (t, **C6**), 27.2 (d, **C5**), 26.7 (t, **C8**), 15.4 (t, **C7**).

m/z (M+H) calcd for $\mathbf{C_{11}H_{18}NO_3}$, 212.1281; found, 212.1277, **Δ = -1.98 ppm**.

M15.- Reaction of 10 with $NaBH_4$.

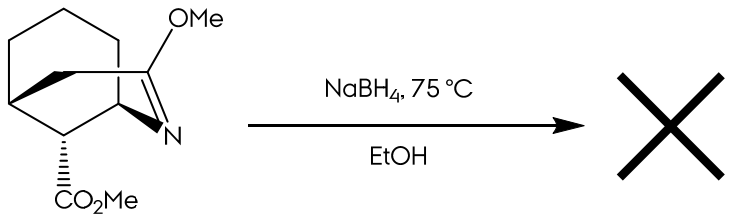

10

In a round bottom flask, 8.7 mg (211.1 g/mol; 0.04 mmol) of bifunctional compound **10** were dissolved in 1 mL of dry EtOH. The flask was sealed, purged with Ar and cooled to 0 ºC in an ice – water bath. 10.3 mg (6.5 equiv) of $NaBH_4$ (sodium borohydride, CAS: 16940-66-2, white solid, 37.8 g/mol, commercial) were added and stirring continued at 75 ºC for 24 h.

pH was checked (basic) and the reaction mixture was neutralized with HCl 1 M. Later, the neutralized solution was extracted 3 times with AcOEt. The organic layers were combined, dried with anhydrous Na_2SO_4 and filtrated. Forward solvent removal under reduced pressure, afforded a crude product. Flash chromatography did not elute any identifiable product.

M16.- Reaction of 10 with $LiBH_4$.

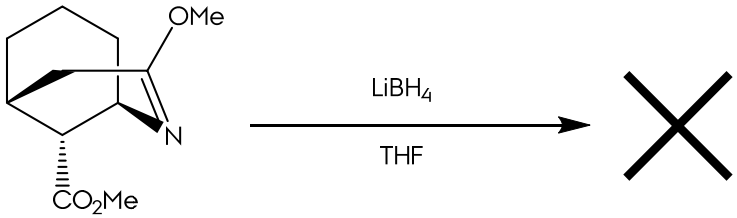

10

In a round bottom flask, 5.5 mg (211.1 g/mol; 0.03 mmol) of bifunctional compound **10** were dissolved in 1 mL of dry THF. The flask was sealed, purged with Ar and cooled to 0 ºC in an ice – water bath. 2 mg (3.1 equiv) of $LiBH_4$ (lithium borohydride, CAS: 16949-15-8, white powder, 21.7 g/mol, commercial) were added and stirring continued at room temperature for 20 h.

pH was checked (basic) and the reaction mixture was neutralized with HCl 1 M. Later, the neutralized solution was extracted 3 times with AcOEt. The organic

layers were combined, dried with anhydrous Na_2SO_4 and filtrated. Forward solvent removal under reduced pressure, afforded a crude product. Flash chromatography did not elute any identifiable product.

M17.- Protection of 8 as Boc-amide.

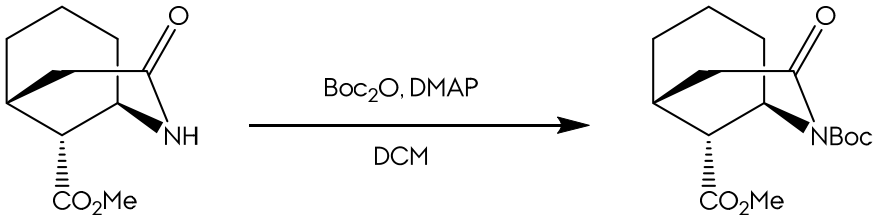

8 **11**

General procedure G was followed with the next quantities: 21.4 mg of 8 (197.1 g/mol; 0.11 mmol) in 3 mL of DCM; 48 mg of Boc_2O (218.2 g/mol; 0.22 mmol); 13.4 mg of DMAP (122.1 g/mol; 0.11 mmol). 22.4 mg of product **11** (69 % yield) were obtained.

2-(*tert*-butyl) 9-methyl (1*R*,5*R*,9*R*)-3-oxo-2-azabicyclo[3.3.1]nonane-2,9-dicarboxylate (11)

$\mathbf{R}_f$ 0.86 (Hexanes/AcOEt, 1:1)

$[\alpha]^{20}_D$ -21.1 (*c.* 1.3 in $CHCl_3$);

υ_{max} (neat)/cm^{-1} 2919 (C-H), 1735 (C=O, ester), 1718 (C=O, carbamate), 1222 (C-O), 1097.

δ_H (400 MHz; $CDCl_3$) 4.67 (1H, **H1**), 3.76 (3H, s, **$CO_2(C\underline{H}_3)$**), 2.84 (1H, **H9**), 2.80 (1H, ABX, *J* 18.1 7.0, **$H4_A$**), 2.63 (1H, **H5**), 2.47 (1H, AB, *J* 18.1, **$H4_B$**), 1.92 - 1.62 (6H, **H6**, **H7** and **H8**), 1.53 (9H, s, **$C(C\underline{H}_3)_3$**).

δ_C (50 MHz; $CDCl_3$) 171.6 (s, **$\underline{C}O_2(CH_3)$**), 171.4 (s, **$\underline{C}ON$**), 152.3 (s, **$N\underline{C}O$**), 83.2 (s, **$\underline{C}(CH_3)_3$**), 52.3 (q, **$CO_2(\underline{C}H_3)$**), 52.2 (d, **C1**), 44.7 (d, **C9**), 40.9 (t, **C4**), 28.7 (d, **C5**), 28.2 (q, **$C(\underline{C}H_3)_3$**), 27.9 (t, **C6**), 27.1 (d, **C8**), 15.5 (t, **C7**).

m/z (M+Na) calcd for **$C_{15}H_{23}NO_5Na$**, 320.1473; found, 320.1476, **Δ = -0.93 ppm**.

M18.- Reaction of 11 with $BH_3 \cdot THF$

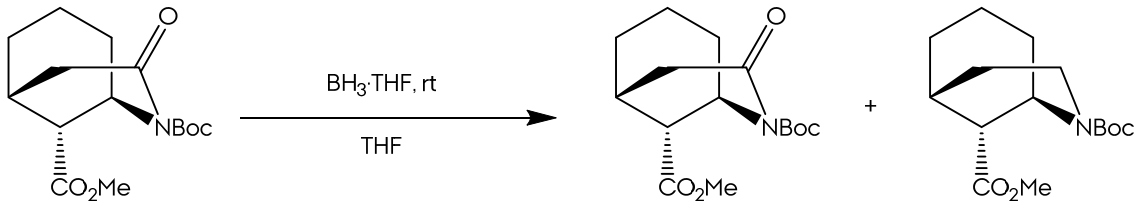

11 **11** **12**

22.4 mg of of **11** (297.1 g/mol; 0.075 mmol) were dissolved in 3 mL of dry THF in a round bottom flask. The flask was sealed and purge with Ar. 0.17 mL (2.2 equiv) of $BH_3 \cdot THF$ (borane tetrahydrofuran complex solution, CAS: 14044-65-6, colourless solution, 85.9 g/mol, 1 M commercial solution) were added via syringe dropwise, and the colourless solution was magnetically stirred at room temperature for 8 h, monitoring the reaction through TLC. 2 mL of MeOH were added and stirring continued for an extra hour. Solvent removal under reduced pressure leaded a crude product. Flash chromatography afforded 2.4 mg of intermediate **12** (Hexanes/AcOEt 95:5), 11 % yield; and 11 mg of starting material **11** (Hexanes/AcOEt 8:2, 50 %).

2-(*tert*-butyl) 9-methyl (1*R*,5*R*,9*R*)-2-azabicyclo[3.3.1]nonane-2,9-dicarboxylate (12)

$\mathbf{R}_f$ 0.76 (Hexanes/AcOEt, 1:1)

$[\alpha]^{20}_D$ -57.1 (c. 1.51 in $CHCl_3$)

υ_{max} (neat)/cm^{-1} 2931 (C-H), 1734 (C=O, ester), 1689 (C=O, carbamate), 1168 (C-O), 1105.

δ_H (200 MHz; $CDCl_3$; (*) minor rotamer) 4.63* (br s, **H1**), 4.46 (1H, br s, **H1**), 3.77 - 3.65 (1H, $\mathbf{H3_A}$), 3.72 (3H, s, $\mathbf{CO_2(C\underline{H}_3)}$), 3.49 (1H, dd, *J* 13.7 6.7, $\mathbf{H3_B}$), 3.44* (dd, *J* 13.7 6.7, $\mathbf{H3_B}$), 2.59 (1H, br s, **H9**), 2.43 (1H, br s, **H5**), 1.89 - 1.49 (8H, **H4, H6, H7** and **H8**), 1.46 (9H, s, $\mathbf{C(C\underline{H}_3)_3}$).

δ_C (50 MHz; $CDCl_3$; (*) minor rotamer) 173.0 (s, $\mathbf{\underline{C}O_2(CH_3)}$), 155.6 (s, $\mathbf{N\underline{C}OO}$), 79.7 (s, $\mathbf{\underline{C}(CH_3)_3}$), 51.9 (q, $\mathbf{CO_2(\underline{C}H_3)}$), 47.7 (d, **C1**), 46.6* (d, **C1**), 46.0* (d, **C9**), 45.8 (d, **C9**), 41.4 (t, **C3**), 40.6* (t, **C3**), 30.3* (t, **C4**), 29.7 (t, **C4**), 28.7 (q, $\mathbf{C(\underline{C}H_3)_3}$), 27.2 (d, **C5**), 26.9* (t, **C6**), 26.8 (t, **C6**), 26.5 (t, **C8**), 19.8* (t, **C7**), 19.4 (t, **C7**).

m/z (M+Na) calcd for $\mathbf{C_{15}H_{25}NO_4Na}$, 306.1675; found, 306.1680, $\mathbf{\Delta = 1.37\ ppm}$.

M19.- Reaction of 11 with $BH_3 \cdot THF$ at 75 ºC.

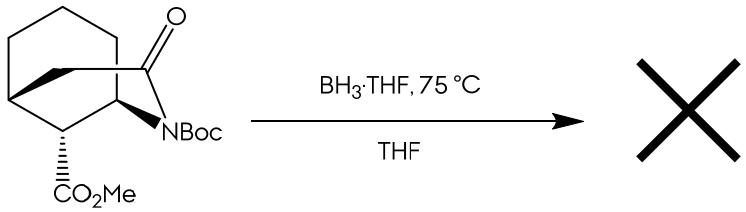

11

16.3 mg of of **11** (297.1 g/mol; 0.055 mmol) were dissolved in 3 mL of dry THF in a round bottom flask. The flask was sealed and purge with Ar. 0.17 mL (3.2 equiv) of $BH_3 \cdot THF$ (borane tetrahydrofuran complex solution, CAS: 14044-65-6, colourless solution, 85.9 g/mol, 1 M commercial solution) were added via syringe dropwise, and the colourless solution was magnetically stirred at 75 ºC for 8 h, monitoring the reaction through TLC. 2 mL of MeOH were added and stirring continued for an extra hour. Solvent removal under reduced pressure leaded a crude product. Flash chromatography did not elute any identifiable product.

M20.- Selective Deprotection of Amine 6 under Oxidative Conditions.

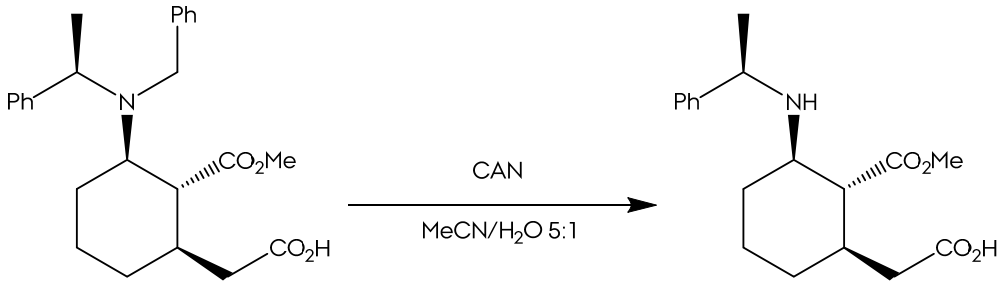

6 **13**

General procedure F was followed with the next quantities: 500 mg of **6** (409.2 g/mol; 1.16 mmol); 2.01 g of CAN (548.2 g/mol; 1.22 mmol); 240 mL of MeCN/H_2O 5:1. 351 mg of product **13** was obtained (90 % yield).

2-((1*R*,2*R*,3*R*)-2-(methoxycarbonyl)-3-(((*R*)-1-phenylethyl)amino)cyclohexyl)acetic acid (13)

R_f 0.25 (Hexanes/AcOEt, 1:1)

$[\alpha]^{24}_D$ +8.5 (c. 1.0 in $CHCl_3$)

υ_{max} (film)/cm^{-1} 3423 (N-H), 2929 (C-H), 1730 (C=O), 1614 (C=O), 1449 (C-N) y 1269 (C-O).

δ_H (200 MHz; $CHCl_3$) 7.29 - 7.23 (5H, **$C_{ar}\underline{H}$**), 6.46 (1H, br s, **N<u>H</u>**), 3.81 (1H, q, *J* 6.4, **C<u>H</u>CH$_3$**), 3.70 (3H, s, **$CO_2(C\underline{H}_3)$**), 2.78 (1H, t, *J* 9.6, **H3**), 2.32 - 2.01 (4H, **H2**, **H1** and **$C\underline{H}_2CO_2H$**), 1.85 - 1.59 (3H, **$H4_A$**, **$H5_A$**, **$H6_A$**), 1.30 - 1.15 (2H, **$H4_B$, $H5_B$**), 1.27 (3H, d, *J* 6.5, **CHC<u>H</u>$_3$**), 0.90 (1H, q, *J* 10.9, **$H6_B$**).

δ_C (50 MHz; $CHCl_3$) 177.3 (s, **<u>C</u>O_2H**), 175.3 (s, **<u>C</u>O_2CH_3**), 145.1 (s, **C_{ipso}**), 128.7 (d, **C_{ar}**), 127.5 (d, **C_{ar}**), 126.9 (d, **C_{ar}**), 56.9 (d, **<u>C</u>HCH$_3$**), 56.5 (d, **C3**), 56.4 (d, **C2**), 51.8 (q, **$CO_2\underline{C}H_3$**), 40.0 (t, **<u>C</u>H_2CO_2H**), 36.9 (d, **C1**), 32.7 (t, **C4**), 31.0 (t, **C6**), 24.3 (t, **C5**), 23.3 (**CH<u>C</u>H_3**).

m/z (M+Na) calcd for **$C_{18}H_{25}NO_4Na$**, 342.1681; found, 342.1695, **Δ = -4.09 ppm**.

M21.- Ring-closing/Lactamization of 13.

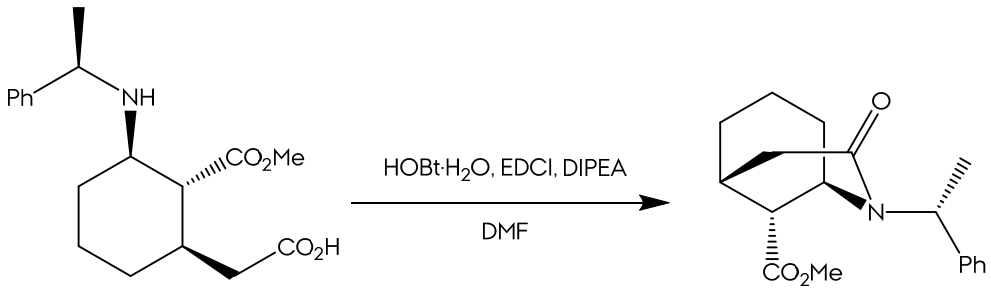

13 **14**

General procedure K was followed with the next quantities: 120 mg of **13** (319.4 g/mol; 0.37 mmol); 6 mL of DMF; 0.22 mL of DIPEA (129.2 g/mol; 0.82 mmol); 100 mg of HOBt · H_2O (135.1 g/mol; 0.74 mmol); 142 mg of EDCI (191.7 g/mol; 0.74 mmol). Flash chromatography afforded 18 mg of product **14** (Hexanes/AcOEt 8:2), 16 % yield.

Methyl (1*R*,5*R*,9*R*)-3-oxo-2-((*R*)-1-phenylethyl)-2-azabicyclo[3.3.1]nonane-9-carboxylate (14)

$\mathbf{R}_f$ 0.30 (Hexanes/AcOEt, 1:1)

$[\alpha]^{24}_D$ +24.0 (*c.* 0.8 in $CHCl_3$);

υ_{max} (film)/cm^{-1} 2927 (C-H), 1733 (C=O, ester), 1635 (C=O, amide), 1436 (C-N), 1207 (C-O).

δ_H (400 MHz; $CDCl_3$) 7.33 - 7.24 (5H, $\mathbf{C_{ar}\underline{H}}$), 6.07 (1H, q, *J* 7.3, $\mathbf{NC\underline{H}C_{ar}}$), 3.67 (1H, **H1**), 3.62 (3H, s, $\mathbf{CO_2(C\underline{H_3})}$), 2.81 (1H, ABX, *J* 18.3 7.4, $\mathbf{H4_A}$), 2.59 (1H, **H9**), 2.45 (1H, AB, *J* 18.3 $\mathbf{H4_B}$), 2.44 (1H, **H5**), 1.78 - 1.46 (6H, **H6**, **H7** and **H8**), 1.57 (3H, d, *J* 7.3 , $\mathbf{CHC\underline{H_3}}$),

δ_C (50 MHz; $CDCl_3$) 171.6 (s, $\mathbf{\underline{C}O_2(CH_3)}$), 171.4 (s, $\mathbf{\underline{C}ONH}$), 140.6 (s, $\mathbf{C_{ipso}}$), 128.7 (d, $\mathbf{C_{ar}}$), 127.7 (d, $\mathbf{C_{ar}}$), 127.3 (d, $\mathbf{C_{ar}}$), 52.1 (d, $\mathbf{\underline{C}H(CH_3)}$), 52.0 (q, $\mathbf{CO_2(\underline{C}H_3)}$), 48.7 (d, **C1**), 45.6 (d, **C9**), 38.5 (t, **C4**), 28.6 (d, **C5**), 28.5 (t, **C6**), 28.4 (t, **C8**), 17.2 (q, $\mathbf{CH(\underline{C}H_3)}$), 15.9 (t, **C7**).

m/z (M+Na) calcd for $\mathbf{C_{18}H_{23}NO_3Na}$, 324.1576; found, 324.1560, $\mathbf{\Delta = -4.9\ ppm}$.

M22.- Reaction of 14 with $BH_3 \cdot THF$ at 75 ºC with Acid Quenching.

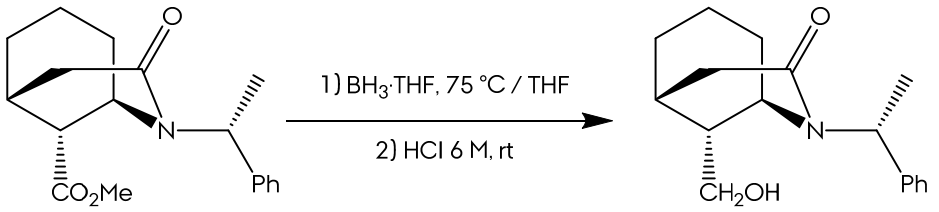

14 **15**

8 mg of of **14** (301.4 g/mol; 0.026 mmol) were dissolved in 1.5 mL of dry THF in a round bottom flask. The flask was sealed, purged with Ar and heated to 75 ºC. 0.12 mL (4.5 equiv) of $BH_3 \cdot THF$ (borane tetrahydrofuran complex solution, CAS: 14044-65-6, colourless solution, 85.9 g/mol, 1 M commercial solution) were added via syringe dropwise, and the colourless solution was magnetically stirred at 75 ºC for 3.5 h. 1 mL of 6 M HCl was added and stirring continued 10 min. Reaction mixture was neutralized with 1 M NaOH.

The reaction mixture was extracted with AcOEt (3 times) and the organic layers were combined and dried with anhydrous Na_2SO_4. Filtration and forward solvent removal resulted in obtain a reaction crude. Flash chromatography afforded 4 mg of product **15** (Hexanes/AcOEt 1:1), 50 % yield.

(1*R*,5*R*,9*R*)-9-(hydroxymethyl)-2-((*R*)-1-phenylethyl)-2-azabicyclo[3.3.1]nonan-3-one (15)

$\mathbf{R}_f$ 0.26 (Hexanes/AcOEt, 1:1)

$[\alpha]^{24}_D$ +47.7 (*c.* 0.81 in $CHCl_3$);

υ_{max} (film)/cm^{-1} 3577 (O-H), 2869 (C-H), 1610 (C=O, amide), 1453 (C-N) y 1075 (C-O).

δ_H (200 MHz; $CDCl_3$) 7.31 - 7.26 (5H, $\mathbf{C_{ar}H}$), 6.08 (1H, q, *J* 7.3, $\mathbf{NCHC_{ar}}$), 3.71 - 3.58 (2H, $\mathbf{CH_2OH}$), 3.30 (1H, **H1**), 2.77 (1H, ABX, *J* 18.2 7.2, $\mathbf{H4_A}$), 2.46 (1H, AB, *J* 18.2 $\mathbf{H4_B}$), 2.16 - 2.09 (2H, **H5** and **H9**), 1.76 - 1.42 (6H, **H6**, **H7** and **H8**), 1.57 (3H, d, *J* 7.3 , $\mathbf{CHCH_3}$).

δ_C (50 MHz; $CDCl_3$) 171.9 (s, $\mathbf{CONH}$), 140.9 (s, $\mathbf{C_{ipso}}$), 128.6 (d, $\mathbf{C_{ar}}$), 127.5 (d, $\mathbf{C_{ar}}$), 127.5 (d, $\mathbf{C_{ar}}$), 62.3 (t, $\mathbf{CH_2OH}$), 51.9 (d, $\mathbf{CH(CH_3)}$), 48.9 (d, **C1**), 43.1 (d, **C9**), 39.5 (t, **C4**), 27.9 (t, **C5**), 26.8 (d, **C6**), 26.5 (t, **C8**), 17.3 (q, $\mathbf{CH(CH_3)}$), 16.2 (t, **C7**).

m/z (M+Na) calcd for $\mathbf{C_{17}H_{23}NO_2Na}$, 296.1626; found, 296.1635, $\mathbf{\Delta = -3.0\ ppm}$.

M23.- Reaction of 14 with $LiAlH_4$ at 75 ºC.

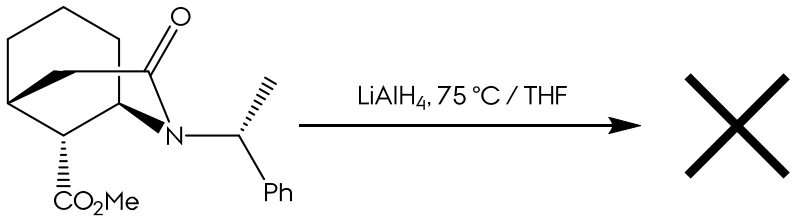

14

25 mg of of **8** (301.3 g/mol; 0.08 mmol) were dissolved in 2 mL of dry THF in a round bottom flask. 9.5 mg (3 equiv) of $LiAlH_4$ (lithium aluminium hydride, CAS: 16853-85-3, grey powder, 37.9 g/mol, commercial) were added and the flask was

sealed, purged with Ar and heated to 75 ºC for 20 h. Reaction mixture were quenched with 5 mL of DCM and 2 mL of water. Drying the solution with anhydrous Na_2SO_4, filtration and forward solvent removal afforded a crude oil. Flash chromatography did not elute any identifiable product.

M24.- Chemoselective Partial reduction of Acid 6 to Aldehyde 16 (1).

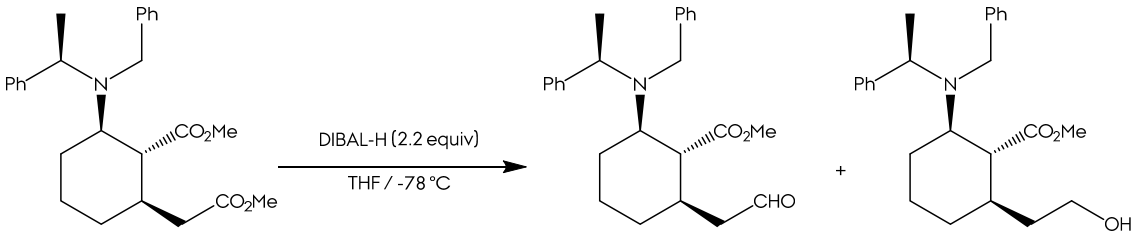

5 **16** **17**

General procedure T was followed with the next quantities: 142 mg of **5** (423.5 g/mol; 0.335 mmol); 0.5 mL of 1.5 M DIBAL-H in toluene (142.2 g/mol, 0.74 mmol); 10 mL of dry THF; 1.5 h of reaction time. Flash chromatography afforded 65 mg of aldehyde **16** (Hexanes/AcOEt 9:1, 49 % yield) and alcohol **17** (Hexanes/AcOEt 9:1, 20 % yield).

Methyl (1*R*,2*R*,6*R*)-2-(benzyl((*R*)-1-phenylethyl)amino)-6-(2-oxoethyl)cyclohexane-1-carboxylate (16)

$\mathbf{R}_f$ 0.83 (Hexanes/AcOEt, 1:1)

$[\alpha]_{25}^{D}$ -2.07 (c. 1.1 in $CHCl_3$)

υ_{max} (neat)/cm^{-1} 2933 (C-H), 1729 (C=O), 1494, 1263 (C-O), 700.

δ_H (400 MHz; $CDCl_3$) 9.58 (1H, t, *J* 1.6, **C<u>H</u>O**), 7.34 - 7.18 (10H, **C$_{ar}$<u>H</u>**), 3.97 (1H, q, *J* 7.2, **C<u>H</u>CH$_3$**), 3.85 (1H, AB, *J* 13.7, **NC<u>H$_A$</u>H**), 3.67 (1H, AB, *J* 13.7, **NCH<u>H$_B$</u>**), 3.42 (3H, s, **CO$_2$(C<u>H$_3$</u>)**), 3.04 (1H, td, *J* 11.1 3.1, **H2**), 2.32 (1H, t, *J* 10.6, **H1**), 2.21 - 1.98 (4H, **H3$_A$**, **H6** and **C<u>H$_2$</u>CHO**), 1.81 - 1.69 (2H, **H4$_A$** and **H5$_A$**), 1.43 - 1.27 (2H, **H3$_B$** and **H4$_B$**), 1.38 (3H, d, *J* 7.0, **CHC<u>H$_3$</u>**), 0.90 (1H, q, *J* 12.4, **H5$_B$**).

δ_C (50 MHz; $CDCl_3$) 201.4 (d, **<u>C</u>HO**), 174.4 (s, **<u>C</u>O$_2$CH$_3$**), 144.2 (s, **C$_{ipso}$**), 140.7 (**C$_{ipso}$**), 129.4 (d, **C$_{ar}$**), 128.2 (d, **C$_{ar}$**), 128.0 (d, **C$_{ar}$**), 127.0 (d, **C$_{ar}$**), 126.7 (d, **C$_{ar}$**), 58.9 (d, **C2**), 57.0 (d, **<u>C</u>HCH$_3$**), 54.7 (d, **C1**), 51.4 (q, **CO$_2$<u>C</u>H$_3$**), 50.2 (t, **N<u>C</u>H$_2$**),

49.1 (t, **C**H$_2$CHO), 35.6 (d, **C6**), 31.8 (t, **C3**), 28.7 (t, **C5**), 24.9 (t, **C4**), 16.3 (q, CH**C**H$_3$).

m/z (M+Na) calcd for **$C_{25}H_{31}NO_3Na$**, 416.2196; found, 416.2216, **Δ = 4.77 ppm**.

Methyl (1*R*,2*R*,6*R*)-2-(benzyl((*R*)-1-phenylethyl)amino)-6-(2-hydroxyethyl)cyclohexane-1-carboxylate (17)

R$_f$ 0.65 (Hexanes/AcOEt, 1:1)

υ_{max} (neat)/cm^{-1} 3398 (O-H), 2923 (C-H), 1735 (C=O), 1452, 1091 (C-O).

δ_H (200 MHz; $CDCl_3$) 7.31 - 7.18 (10H, **C$_{ar}$H**), 3.99 (1H, q, *J* 6.9, **CHCH$_3$**), 3.88 (1H, AB, *J* 14.0, **NCH$_A$H**), 3.66 (1H, AB, *J* 14.0, **NCHH$_B$**), 3.55 (2H, **CH$_2$OH**), 3.44 (3H, s, **CO$_2$(CH$_3$)**), 3.00 (1H, td, *J* 11.4 3.2, **H2**), 2.30 (1H, t, *J* 11.4, **H1**), 2.04 - 1.93 (1H, **H6**), 1.86 - 1.58 (5H, **CH$_2$CH$_2$OH, H3, H4**, **H5$_A$**), 1.38 (3H, d, *J* 6.9, **CHCH$_3$**), 0.83 (1H, **H5$_B$**).

δ_C (50 MHz; $CDCl_3$) 175.3 (s, **C**O$_2$CH$_3$), 144.5 (s, **C$_{ipso}$**), 140.9 (s, **C$_{ipso}$**), 129.4 (d, **C$_{ar}$**), 128.2 (d, **C$_{ar}$**), 127.9 (d, **C$_{ar}$**), 126.9 (d, **C$_{ar}$**), 126.6 (d, **C$_{ar}$**), 60.3 (t, **C**H$_2$OH), 59.0 (d, **C2**), 56.8 (d, **C**HCH$_3$), 55.4 (d, **C1**), 51.3 (q, CO$_2$**C**H$_3$), 50.2 (t, N**C**H$_2$), 37.9 (t, **C**H$_2$CH$_2$OH), 37.5 (d, **C6**), 31.0 (t, **C3**), 28.9 (t, **C5**), 25.1 (t, **C4**), 16.3 (q, CH**C**H$_3$).

m/z (M+Na) calcd for **$C_{25}H_{33}NO_3Na$**, 418.2352; found, 418.2365, **Δ = 2.95 ppm**.

M25.- Chemoselective Partial reduction of Acid 6 to Aldehyde 16 (2).

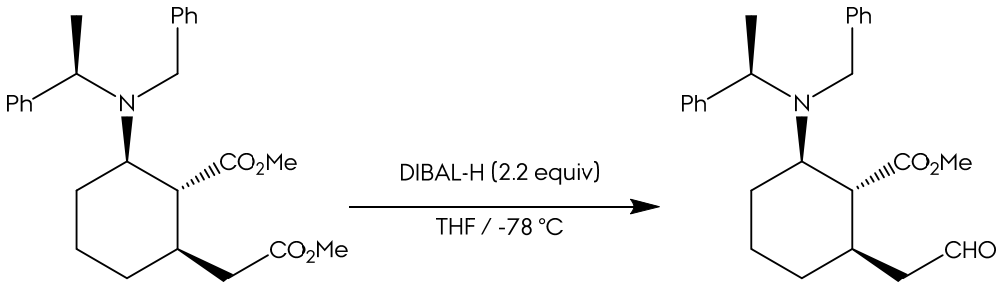

5 **16**

General procedure T was followed with the next quantities: 297 mg of **5** (423.5 g/mol; 0.701 mmol); 1.04 mL of 1.5 M DIBAL-H in toluene (142.2 g/mol, 1.54

mmol); 20 mL of dry THF; 30 min of reaction time. Reaction workup afforded 257 mg of aldehyde **16**, 92 % yield.

M26.- Chemoselective reduction of Acid 6 to Alcohol 17.

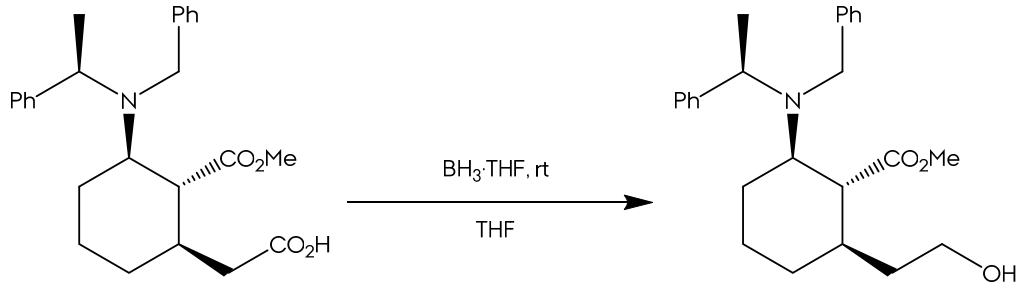

6 **16**

General procedure S was followed with the next quantities: 186 mg of **6** (409.2 g/mol; 0.45 mmol); 1.82 mL of $BH_3 \cdot THF$ (85.9 g/mol, 1.828 mmol); 15 mL of THF. 177 mg of product **17** were obtained, 98 % yield.

M27.- Chemoselective reduction of Aldehyde 16 to Alcohol 17.

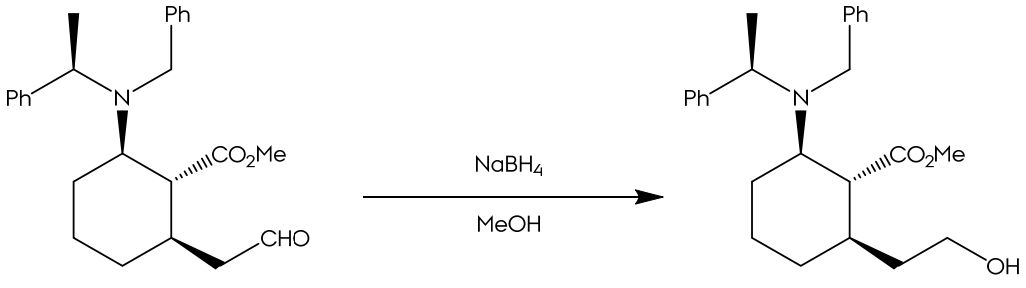

16 **17**

65.3 mg of aldehyde **16** were dissolved in 10 mL of dry MeOH. 13.8 mg (2.2 equiv) of $NaBH_4$ (sodium borohydride, CAS: 16940-66-2, white solid, 37.8 g/mol, commercial) were added, turning the solution from brown-coloured to yellowish. The flask was sealed and the atmosphere was replaced by inert gas. The solution was magnetically stirred for 45 min. 4 mL of water were added, and stirring was continued until gas generation ceased. Reaction mixture was extracted with AcOEt 3 times. The organic layer was washed with brine (1 time) and dried with anhydrous

Na_2SO_4. Filtration and forward solvent removal under reduced pressure, afforded the 49 mg of alcohol **17**, 78 % yield.

M28.- Deprotection of Amine 16 under Hydrogen Atmosphere.

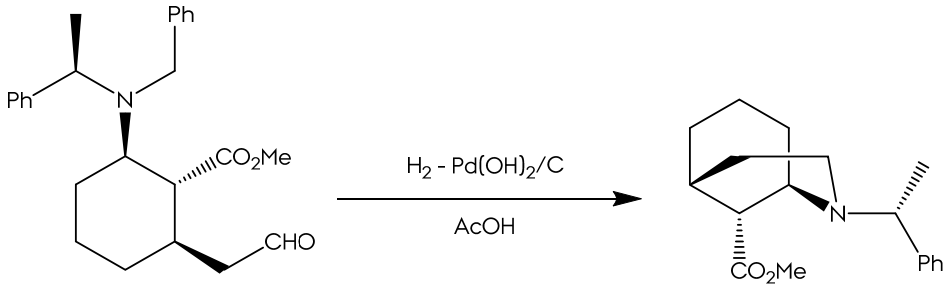

16 **18**

General procedure R was followed with the next quantities: 109 mg of **16** (393.23 g/mol; 0.278 mmol); 24 mg of $Pd(OH)_2$ 20% over carbon; 3 mL of AcOH; reaction time of 3 days. Product **18** was obtained as acetate salt. The salt was dissolved in 50 mL of DCM and washed 3 times with $NaHCO_3$ sat. Drying with anhydrous Na_2SO_4, filtration and forward solvent removal under reduced pressure resulted in a reaction crude. Flash chromatography afforded 5 mg of morphan **18** (Hexanes/AcOEt 95:5) in a 6 % yield.

Methyl (1*R*,5*R*,9*R*)-2-((*R*)-1-phenylethyl)-2-azabicyclo[3.3.1]nonane-9-carboxylate (18)

$\mathbf{R}_f$ 0.46 (Hexanes/AcOEt, 8:2)

$[\alpha]^{25}_D$ +0.39 (*c.* 0.5 in $CHCl_3$);

υ_{max} (neat)/cm^{-1} 3357, 2923 (C-H), 1731 (C=O), 1384, 1087 (C-O).

δ_H (400 MHz; $CDCl_3$) 7.37 - 7.23 (5H, $\mathbf{C_{ar}\underline{H}}$), 3.76 (3H, s, $\mathbf{CO_2(C\underline{H_3})}$), 3.67 (1H, **H1**), 3.64 (1H, q, *J* 6.4, $\mathbf{NC\underline{H}C_{ar}}$), 2.77 (1H, **H9**), 2.65 (1H, td, *J* 12.2 5.2, $\mathbf{H3_A}$), 2.52 (1H, $\mathbf{H3_B}$), 2.37 (1H, H5), 2.02 - 1.51 (8H, **H4, H6, H7** and **H8**) 1.35 (3H, d, *J* 6.4, $\mathbf{CH(\underline{C}H_3)}$).

δ_C (50 MHz; $CDCl_3$) 174.3 (s, $\mathbf{\underline{C}O_2(CH_3)}$), 147.2 (s, $\mathbf{C_{ipso}}$), 128.5 (d, $\mathbf{C_{ar}}$), 127.3 (d, $\mathbf{C_{ar}}$), 126.8 (d, $\mathbf{C_{ar}}$), 62.9 (d, $\mathbf{\underline{C}H(CH_3)}$), 51.7 (q, $\mathbf{CO_2(\underline{C}H_3)}$), 48.3 (d, **C1**), 47.7 (t,

C3), 31.8 (t, **C4**), 27.9 (d, **C5** and **C9**), 26.8 (t, **C6**), 21.8 (q, **CH(CH$_3$)**), 21.7 (t, **C8**), 21.3 (t, **C7**).

m/z (M+H) calcd for **$C_{18}H_{26}NO_2$**, 288.1958; found, 288.1966, **Δ = -2.8 ppm**.

M29.- Reaction of Morphan 18 under Hydrogen Atmosphere (1).

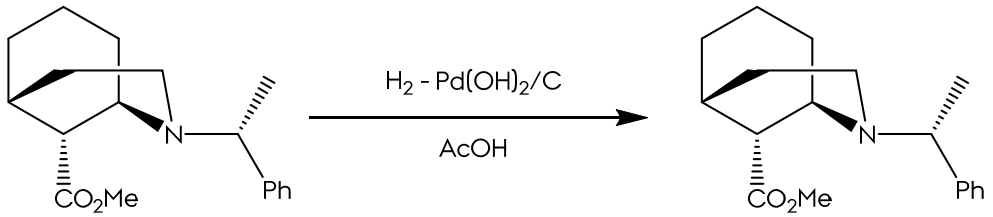

18 **18**

General procedure R was followed with the next quantities: 5 mg of **18** (393.2 g/mol; 0.017 mmol); 5 mg of $Pd(OH)_2$ 20% on carbon; 3 mL of AcOH; reaction time of 3 days. After solvent removal, the crude was dissolved in 10 ml of DCM and washed 3 times with $NaHCO_3$ sat. Drying with anhydrous Na_2SO_4, filtration and forward solvent removal under reduced pressure resulted in recovering 4 mg of starting material.

M30.- Reaction of Morphan 18 under Hydrogen Atmosphere (2).

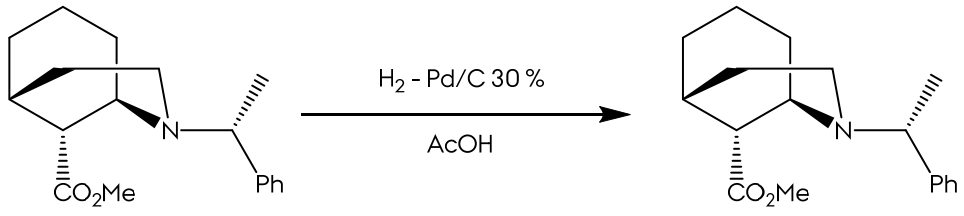

18 **18**

General procedure R was followed changing the catalyst with the next quantities: 4 mg of **18** (393.2 g/mol; 0.014 mmol); 5 mg of Pd/C 30%; 3 mL of AcOH; reaction time of 3 days. After solvent removal, the crude was dissolved in 10 ml of DCM and washed 3 times with $NaHCO_3$ sat. Drying with anhydrous Na_2SO_4, filtration and forward solvent removal under reduced pressure resulted in recovering 2 mg of starting material.

M31.- Funtional Group Interconversion of Alcohol 17 to Bromide 19

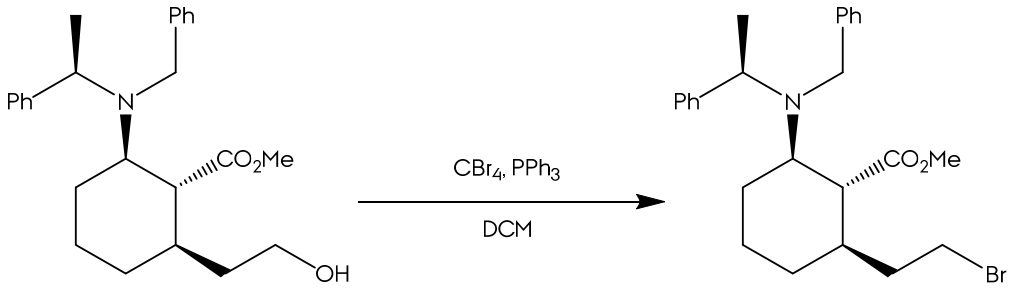

16 **19**

General procedure V was followed with the next quantities: 132 mg of 16 (395.2 g/mol, 0.336 mmol); 167 mg of CBr_4 (331.6 g/mol, 0.504 mmol); 132 mg of PPh_3 (262.2 g/mol, 0.504 mmol); 5 mL of dry DCM. After workup, 70.9 mg of bromide **19** were obtained, 46 % yield.

Methyl (1*R*,2*R*,6*R*)-2-(benzyl((*R*)-1-phenylethyl)amino)-6-(2-bromoethyl)cyclohexane-1-carboxylate (19)

$\mathbf{R}_f$ 0.94 (Hexanes/AcOEt, 8:2)

$[\alpha]_{20}^{D}$ +4.90 (c. 0.88 in $CHCl_3$)

υ_{max} (neat)/cm^{-1} 3400, 2931 (C-H), 1731 (C=O), 1450, 1265 (C-O).

δ_H (400 MHz; $CDCl_3$) 7.35 - 7.18 (10H, $\mathbf{C_{ar}\underline{H}}$), 3.97 (1H, q, *J* 6.8, $\mathbf{C\underline{H}CH_3}$), 3.85 (1H, AB, *J* 13.7, $\mathbf{NC\underline{H}_AH}$), 3.66 (1H, AB, *J* 13.7, $\mathbf{NCH\underline{H}_B}$), 3.44 (3H, s, $\mathbf{CO_2(C\underline{H_3})}$), 3.37 (1H, $\mathbf{C\underline{H}_AHBr}$), 3.24 (1H, q, *J* 8.3, $\mathbf{CH\underline{H}_BBr}$), 3.02 (1H, td, *J* 11.0 2.0, **H6**), 2.26 (1H, t, *J* 10.1, **H1**), 1.98 (1H, d, *J* 12.0, **H6**), 1.82 - 1.57 (5H, $\mathbf{C\underline{H_2}CH_2Br}$**, H3, H4**, $\mathbf{H5_A}$), 1.37 (3H, d, *J* 6.8, $\mathbf{CHC\underline{H_3}}$), 0.78 (1H, q, *J* 12.6, $\mathbf{H5_B}$).

δ_C (50 MHz; $CDCl_3$) 174.6 (s, $\mathbf{\underline{C}O_2CH_3}$), 144.3 (s, $\mathbf{C_{ipso}}$), 140.9 (s, $\mathbf{C_{ipso}}$), 129.4 (d, $\mathbf{C_{ar}}$), 128.2 (d, $\mathbf{C_{ar}}$), 128.0 (d, $\mathbf{C_{ar}}$), 126.9 (d, $\mathbf{C_{ar}}$), 126.6 (d, $\mathbf{C_{ar}}$), 58.8 (d, **C2**), 56.9 (d, $\mathbf{\underline{C}HCH_3}$), 55.1 (d, **C1**), 51.4 (q, $\mathbf{CO_2\underline{C}H_3}$), 50.2 (t, $\mathbf{N\underline{C}H_2}$), 39.4 (d, **C6**), 38.2 (t, $\mathbf{\underline{C}H_2CH_2Br}$), 30.9 (t, **C3**), 30.2 (t, $\mathbf{C\underline{H_2}Br}$), 28.9 (t, **C5**), 24.8 (t, **C4**), 16.3 (q, $\mathbf{CH\underline{C}H_3}$).

m/z (M+H) calcd for $\mathbf{C_{25}H_{33}NO_2}$, 458.1689; found, 458.1727, $\mathbf{\Delta = 8.26\ ppm}$.

M32.- Reaction of Bromide 19 under Hydrogen Atmosphere.

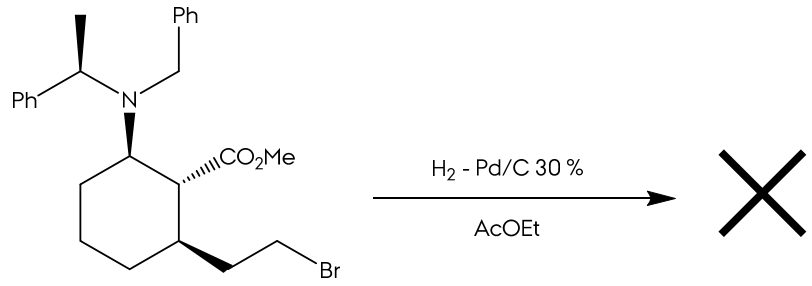

19

General procedure R was followed changing the catalyst and solvent with the next quantities: 30 mg of **19** (456.2 g/mol; 0.065 mmol); 30 mg of Pd/C 30%; 3 mL of AcOEt; reaction time of 4 days. Flash chromatography did not elute any identifiable product.

M33.- Protecting Group Interconversion from 5 to 20.

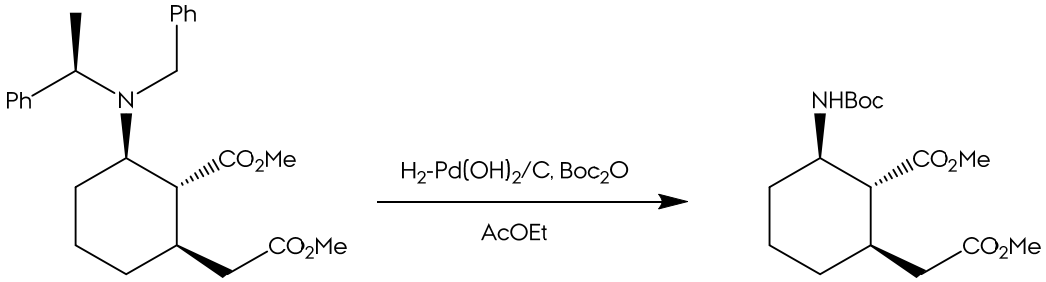

5 **20**

General procedure E was followed with the next quantities: 140 mg of **5** (423.5 g/mol, 0.331 mmol); 231 mg of Boc_2O (218.2 g/mol, 1.06 mmol); 60 mg of $Pd(OH)_2$ on carbon; 3 mL of AcOEt. Flash chromatography afforded 88 mg of product **20** (Hexanes/AcOEt 8:2) in a 81 % yield.

Methyl (1*R*,2*R*,6*R*)-2-((tert-butoxycarbonyl)amino)-6-(2-methoxy-2-oxoethyl)cyclohexane-1-carboxylate (20)

$\mathbf{R}_f$ 0.57 (Hexanes/AcOEt, 6:4)

$[\alpha]^{26}_D$ +10.6 (c. 1.0 in $CHCl_3$)

υ_{max} (neat)/cm^{-1} 3369 (N-H), 2950 (C-H), 1735 (C=O, ester), 1697 (C=O, carbamate), 1170 (C-O).

δ_H (400 MHz; $CHCl_3$) 4.45 (1H, d, *J* 6.1, **NH**), 3.67 - 3.64 (1H, **H2**), 3.67 (3H, s, **$CH_2CO_2(CH_3)$**), 3.64 (3H, s, **$CHCO_2(CH_3)$**), 2.29 (1H, ABX, *J* 14.1 2.8, **$CH_AHCO_2(CH_3)$**), 2.20 - 2.01 (3H, **H1, $H3_A$** and **H6**), 2.15 - 2.04 (1H, AB, *J* 14.1, **$CHH_BCO_2(CH_3)$**), 1.81 (1H, quintet-d, *J* 12.8 2.7, **$H5_A$**), 1.76 (1H, quintet-d, *J* 16.7 3.3, **$H4_A$**), 1.43 - 1.39 (1H, **$H4_B$**), 1.40 (9H, s, **$C(CH_3)_3$**), 1.14 (1H, qd, *J* 12.7 3.8, **$H3_B$**), 0.97 (1H, qd, *J* 12.9 3.6 , **$H5_B$**).

δ_C (50 MHz; $CHCl_3$) 173.7 (s, **$CH_2CO_2CH_3$**), 172.5 (s, **$CHCO_2CH_3$**), 155.0 (s, **NCOO**), 79.5 (s, **$C(CH_3)_3$**), 56.1 (d, **C1**), 52.1 (q, **$CH_2CO_2CH_3$**), 51.9 (d, **C2**), 51.8 (q, **$CHCO_2CH_3$**), 39.3 (t, **$CH_2CO_2CH_3$**), 36.2 (d, **C6**), 33.0 (t, **C3**), 30.6 (t, **C5**), 28.5 (q, **$C(CH_3)_3$**), 24.1 (t, **C4**).

m/z (M+Na) calcd for **$C_{16}H_{27}NO_6Na$**, 352.1730; found, 352.1750, **Δ = -6.0 ppm**.

M34.- Reaction of 20 with $LiBH_4$.

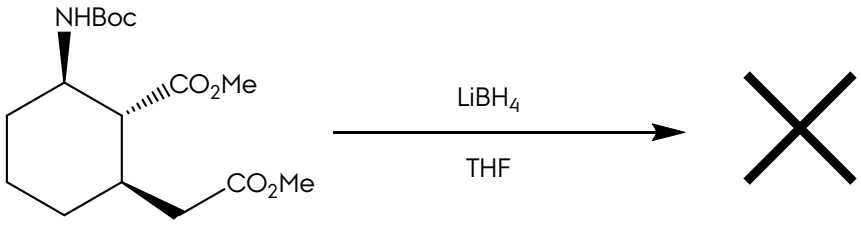

20

General procedure U was followed changing the amount of $LiBH_4$ added with the next quantities: 30 mg of **20** (329.2 g/mol, 0.093 mmol); 3 mg of $LiBH_4$ (21.7 g/mol, 0.137 mmol); 2 mL of THF. Reaction crude analysis showed a complex mixture of reduction products, which were complex to isolate through flash chromatography.

M35.- Chemoselective Hydrolysis of 20 in Basic Media.

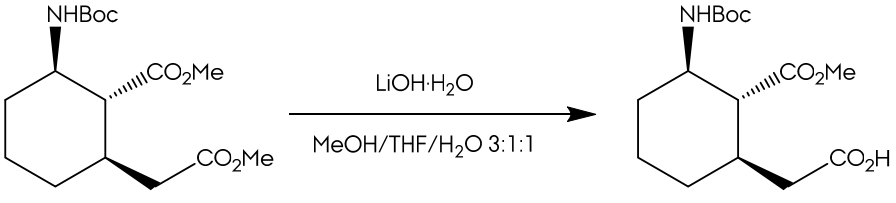

20 **21**

General procedure R were followed with the next quantities: 110 mg of **20** (329.2 g/mol; 0.34 mmol); 8 mL of MeOH/THF/H_2O 3:1:1 solution; 31 mg of $LiOH \cdot H_2O$ (41.9 g/mol; 0.74 mmol). Reaction workup afforded 89 mg of product **21**, 84 % yield.

2-((1*R*,2*R*,3*R*)-3-((tert-butoxycarbonyl)amino)-2-(methoxycarbonyl)cyclohexyl)acetic acid (21)

$\mathbf{R}_f$ 0.42 (Hexanes/AcOEt, 6:4)

$[\alpha]^{20}_D$ +2.14 (c. 1.0 in $CHCl_3$)

δ_H (400 MHz; $CHCl_3$) 4.48 (1H, d, *J* 8.5, **NH**), 3.75 - 3.66 (1H, **H3**), 3.69 (3H, s, **$CO_2(CH_3)$**), 2.35 (1H, AB, *J* 12.1, **CH_AHCO_2H**), 2.19 - 2.11 (1H, AB, *J* 12.1, **CHH_BCO_2H**), 2.20 - 2.00 (2H, **H1** and **H2**), 2.07 - 2.01 (1H, dd, *J* 12.9 3.2, **$H4_A$**), 1.90 - 1.85 (1H, d, *J* 12.8 3.1, **$H6_A$**), 1.88 (1H, d-quintet, *J* 13.7 3.2, **$H5_A$**), 1.44 - 1.39 (1H, **$H5_B$**), 1.41 (9H, s, **$C(CH_3)_3$**), 1.14 (1H, qd, *J* 12.5 3.9, **$H4_B$**), 1.02 (1H, q, *J* 11.6, **$H6_B$**).

δ_C (50 MHz; $CHCl_3$) 177.2 (s, **CO_2H_3**), 173.9 (s, **$CH_2CO_2CH_3$**), 155.1 (s, **NCOO**), 79.6 (s, **$C(CH_3)_3$**), 56.0 (d, **C2**), 52.2 (q, **$CH_2CO_2CH_3$**), 51.8 (d, **C3**), 39.2 (t, **CH_2CO_2H**), 36.0 (d, **C1**), 32.9 (t, **C4**), 30.5 (t, **C6**), 28.4 (q, **$C(CH_3)_3$**), 24.1 (t, **C5**).

m/z (M+Na) calcd for **$C_{15}H_{25}NO_6Na$**, 338.1574; found, 338.1592, **Δ = -5.3 ppm**.

M36.- Chemoselective Reduction of Acid 21 to Alcohol 22.

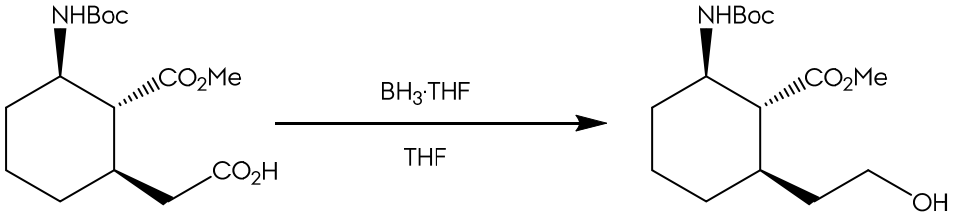

21 **22**

General procedure S was followed with the next quantities: 89 mg of **21** (315.2 g/mol; 0.282 mmol); 1.13 mL of $BH_3 \cdot THF$ (85.9 g/mol, 1.13 mmol); 5 mL of THF. Reaction workup afforded 78 mg of product **22**, 92 % yield.

Methyl (1R,2R,6R)-2-((tert-butoxycarbonyl)amino)-6-(2-hydroxyethyl)cyclohexane-1-carboxylate (22)

Mp 111 ºC

R_f 0.41 (Hexanes/AcOEt, 4:6)

$[\alpha]^{26}_D$ +2.39 (c. 1.1 in $CHCl_3$)

υ_{max} (neat)/cm^{-1} 3363 (N-H), 2915 (C-H), 1724 (C=O, ester), 1683 (C=O, carbamate), 1170 (C-Cl).

δ_H (400 MHz; $CHCl_3$) 4.52 (1H, d, *J* 7.4, **NH**), 3.65 - 3.56 (3H, **H2** and **CH_2OH**), 3.65 (3H, s, **$CHCO_2(CH_3)$**), 2.02 - 1.96 (3H, **H1, $H3_A$** and **H6**), 1.86 - 1.70 (3H, **$H4_A$**, **$H5_A$** and **CH_AHCH_2OH**), 1.54 - 1.47 (1H, m, **CHH_BCH_2OH**), 1.41 - 1.33 (1H, **$H4_B$**), 1.37 (9H, s, **$C(CH_3)_3$**), 1.10 (1H, qd, *J* 12.9 3.6, **$H3_B$**), 0.88 (1H, qd, *J* 12.5 3.2 , **$H5_B$**).

δ_C (50 MHz; $CHCl_3$) 174.7 (s, **$CHCO_2CH_3$**), 155.1 (s, **NCOO**), 79.4 (s, **$C(CH_3)_3$**), 60.2 (t, **CH_2OH**), 57.1 (d, **C1**), 52.1 (d, **C2**), 52.0 (q, **$CH_2CO_2CH_3$**), 37.7 (t, **CH_2CH_2OH**), 36.3 (d, **C6**), 33.2 (t, **C3**), 30.4 (t, **C5**), 28.5 (q, **$C(CH_3)_3$**), 24.3 (t, **C4**).

m/z (M+Na) calcd for **$C_{15}H_{26}NO_4Na$**, 342.1448; found, 324.1447, **Δ = 0.2 ppm**.

M37.- Mesylation of Alcohol 22 to Mesylate 23.

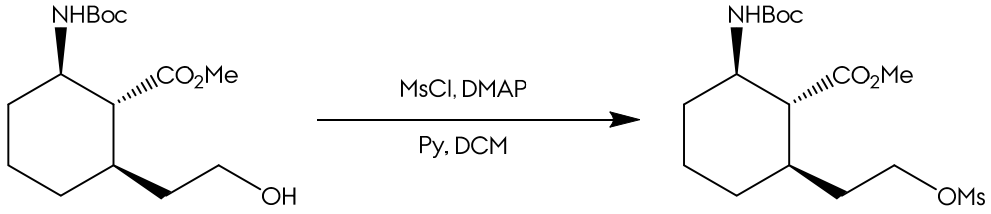

22 **23**

General procedure M was followed with the next quantities: 9 mg of **22** (301.2 g/mol; 0.03 mmol); 0.37 mg of DMAP (122.1 g/mol, 0.003); 8 µL of pyridine; 9.7 µL of MsCl (114.5 g/mol, 0.15 mmol); 2 mL of dry DCM. Reaction workup afforded 11 mg of mesylate **23**, 96 % yield.

Methyl (1*R*,2*R*,6*R*)-2-((tert-butoxycarbonyl)amino)-6-(2-((methylsulfonyl)oxy)ethyl)cyclohexane-1-carboxylate (23)

$\mathbf{R}_f$ 0.58 (Hexanes/AcOEt, 4:6)

$[\alpha]^{20}_D$ +9.94 (c. 0.7 in $CHCl_3$)

υ_{max} (neat)/cm^{-1} 3373 (N-H), 2927 (C-H), 1735 (C=O, ester), 1687 (C=O, carbamate), 1168 (S=O).

δ_H (400 MHz; $CHCl_3$) 4.45 (1H, d, *J* 7.9, **NH**), 4.23 (2H, m, **$CH_2OSO_2CH_3$**), 3.70 - 3.68 (1H, **H2**), 3.69 (3H, s, **$CHCO_2(CH_3)$**), 3.00 (3H, s, **OSO_2CH_3**), 2.07 - 2.00 (2H, **H1**, and **$H3_A$**), 1.92 - 1.72 (4H, **$H4_A$**, **$H5_A$**, **H6** and **$CH_AHCH_2OSO_2$**), 1.64 - 1.50 (1H, **CHH_BCH_2OH**), 1.44 - 1.39 (1H, **$H4_B$**), 1.41 (9H, s, **$C(CH_3)_3$**), 1.15 (1H, quartet-d, *J* 12.8 3.7, **$H3_B$**), 0.93 (1H, quartet-d, *J* 13.1 3.1, **$H5_B$**).

δ_C (50 MHz; $CHCl_3$) 173.9 (s, **$CHCO_2CH_3$**), 155.0 (s, **NCOO**), 79.4 (s, **$C(CH_3)_3$**), 67.5 (t, **$CH_2OSO_2CH_3$**), 56.6 (d, **C1**), 52.8 (q, **$CHCO_2CH_3$**), 52.0 (d, **C2**), 37.6 (q, **OSO_2CH_3**), 36.1 (d, **C6**), 33.9 (t, **C3**), 32.9 (t, **$CH_2CH_2OSO_2$**), 30.0 (t, **C5**), 28.4 (q, **$C(CH_3)_3$**), 24.3 (t, **C4**).

m/z (M+Na) calcd for **$C_{16}H_{29}NO_7SNa$**, 402.1556; found, 402.1573, **Δ = -4.2 ppm**.

M38.- Reaction of 23 with TMG (1).

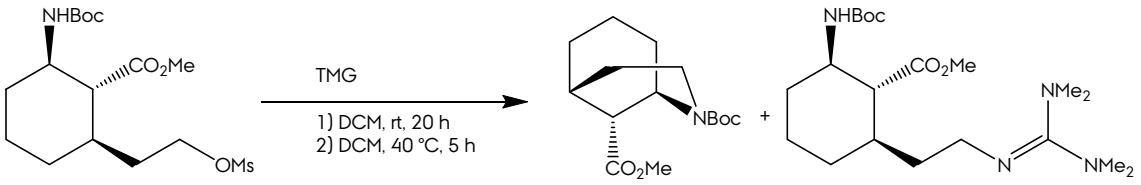

23 **12** **24**

29 mg of of **23** (379.3 g/mol; 0.079 mmol) were dissolved in 2 mL of dry DCM in a round bottom flask. 11 µL (1.2 equiv) of TMG (*N*,*N*,*N'*,*N'*-tetramethylguanidine, CAS: 80-70-6, liquid, 115.1 g/mol, commercial) were added and the flask was sealed, purged with Ar and magnetically stirred at room temperature for 20 h, monitoring the progress by means of TLC. After 20 h, no reaction product appeared, so the reaction was heated at reflux, 40 ºC. This time, TLC revealed reaction progress with substrate disappearance.

Reaction mixture was cooled and extracted with AcOEt (3 times). The organic layers were combined and washed with 0.5 M HCl (2 times), $NaHCO_3$ 10 % (2 times) and brine (1 time). Drying the solution with anhydrous Na_2SO_4, filtration and forward solvent removal resulted in a crude oil. Flash chromatography afforded 3 mg of morphan **12** (Hexanes/AcOEt 9:1, 14 % yield) and 13 mg of byproduct **24** (Hexanes/AcOEt 7:3, 44 % yield).

Methyl (1*R*,2*R*,6*R*)-2-(2-((bis(dimethylamino)methylene)amino)ethyl)-6-((*tert*-butoxycarbonyl)amino)cyclohexane-1-carboxylate (24)

$\mathbf{R}_f$ 0.32 (Hexanes/AcOEt, 6:4)

$[\alpha]^{20}_D$ +16.2 (c. 1.6 in $CHCl_3$)

υ_{max} (neat)/cm^{-1} 3367 (N-H), 2931 (C-H), 1729 (C=O), 1697 (C=O, carbamate), 1616 (C=N), 1170 (C-O).

δ_H (400 MHz; $CHCl_3$) 4.43 (1H, d, *J* 8.5, **NH**), 3.65 (3H, s, **CHCO$_2$(CH$_3$)**), 3.61 (1H, **H2**), 3.28 (1H, ddd, *J* 13.4 8.5 4.5, **CH$_A$HNC(N(CH$_3$CH$_3$)$_2$)**), 3.17 (1H, dd, *J* 13.4 7.4, **CH$_B$NC(N(CH$_3$CH$_3$)$_2$)**), 3.08 (6H, br s, **CH$_A$HNC(N(CH$_3$CH$_3$)$_2$)**), 2.90 (6H, br s, **CH$_A$HNC(N(CH$_3$CH$_3$)$_2$)**), 2.02 – 1.86 (4H, **H1**, **H3$_A$**, **H5$_A$** and **H6**), 1.78 (1H, d-quintet, *J* 12.8 3.7, **H4$_A$**), 1.70 - 1.49 (2H, **CH$_2$CH2OSO2**), 1.42 - 1.33 (1H, **H4$_B$**), 1.39 (9H, s, **C(CH$_3$)$_3$**), 1.11 (1H, quartet-d, *J* 12.7 3.7, **H3$_B$**), 0.93 (1H, quartet-d, *J* 13.2 3.5, **H5$_B$**).

δ_C (50 MHz; $CHCl_3$) 174.5 (s, **CHCO$_2$CH$_3$**), 161.4 (s. **NCN$_2$**), 155.0 (s, **NCOO**), 79.5 (s, **C(CH$_3$)$_3$**), 56.5 (d, **C1**), 52.2 (q, **CHCO$_2$CH$_3$**), 52.0 (d, **C2**), 42.4 (t, **CH$_2$NCN$_2$**), 40.8 (q, **C(NCH$_3$CH$_3$)$_2$**), 40.1 (q, **C(NCH$_3$CH$_3$)$_2$**), 36.9 (d, **C6**), 34.6 (t, **C3**), 33.1 (t, **CH$_2$CH$_2$N**), 30.0 (t, **C5**), 28.5 (q, **C(CH$_3$)$_3$**), 24.2 (t, **C4**).

m/z (M+H) calcd for $C_{20}H_{39}N_4O_4$, 399.2965; found, 399.2982, **Δ = -4.0 ppm**.

M39.- Reaction of 23 with TMG (2).

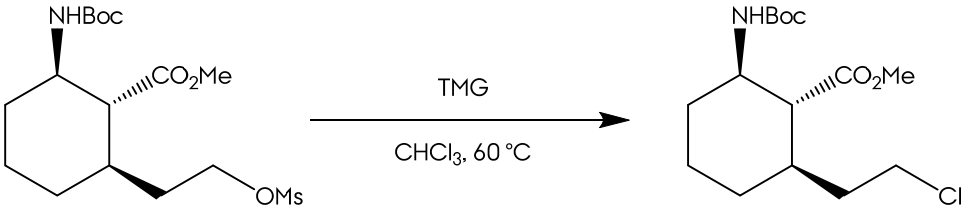

23 **25**

50 mg of of **23** (379.3 g/mol; 0.13 mmol) were dissolved in 5 mL of dry $CHCl_3$ in a round bottom flask. 37 μL (2.2 equiv) of TMG (*N*,*N*,*N'*,*N'*-tetramethylguanidine, CAS: 80-70-6, liquid, 115.1 g/mol, commercial) were added and the flask was sealed, purged with Ar and magnetically stirred at 60 ºC for 36 h. Reaction mixture was cooled and extracted with AcOEt (3 times). The organic layers were combined and washed with 0.5 M HCl (2 times), $NaHCO_3$ 10 % (2 times) and brine (1 time). Drying the solution with anhydrous Na_2SO_4, filtration and forward solvent removal resulted in a crude oil. Flash chromatography afforded 13 mg of chloride **25** (Hexanes/AcOEt 9:1, 31 % yield).

Methyl (1*R*,2*R*,6*R*)-2-((tert-butoxycarbonyl)amino)-6-(2-chloroethyl)cyclohexane-1-carboxylate (25)

$\mathbf{R}_f$ 0.71 (Hexanes/AcOEt, 6:4)

$[\alpha]^{20}_D$ +18.7 (c. 0.7 in $CHCl_3$)

υ_{max} (film)/cm^{-1} 3357, 2931 (C-H), 1710 (C=O, ester), 1691 (C=O, amide), 1170 (C-O).

δ_H (400 MHz; $CHCl_3$) 4.45 (1H, d, *J* 6.3, **NH**), 3.71 (3H, s, **CHCO$_2$(CH$_3$)**), 3.71 - 3.68 (1H, **H2**), 3.57 (1H, ddd, *J* 13.1 8.1 5.0, **CH$_A$HCl**), 3.48 (1H, **CHH_BCl**), 2.08 - 1.73 (3H, **H1, H3$_A$**, **H4$_A$**, **H5$_A$**, **H6** and **CH$_A$HCH$_2$Cl**), 1.64 - 1.56 (1H, m, **CHH_BCH$_2$Cl**), 1.47 - 1.33 (1H, **H4$_B$**), 1.42 (9H, s, **C(CH$_3$)$_3$**), 1.15 (1H, qd, *J* 12.8 3.8, **H3$_B$**), 0.89 (1H, qd, *J* 12.5 3.0, **H5$_B$**).

δ_C (50 MHz; $CHCl_3$) 174.0 (s, **CHCO$_2$CH$_3$**), 155.1 (s, **NCOO**), 79.4 (s, **C(CH$_3$)$_3$**), 56.7 (d, **C1**), 51.5 (d, **C2**), 51.4 (q, **CHCO$_2$CH$_3$**), 41.5 (t, **CH$_2$Cl**), 37.1 (t, **CH$_2$CH$_2$Cl**), 36.5 (d, **C6**), 32.7 (t, **C3**), 29.2 (t, **C5**), 27.5 (q, **C(CH$_3$)$_3$**), 23.4 (t, **C4**).

m/z (M+Na) calcd for **$C_{15}H_{27}NO_5ClNa$**, 324.1781; found, 324.1789, **Δ = -2.4 ppm**.

M40.- Reaction of 23 with DBU.

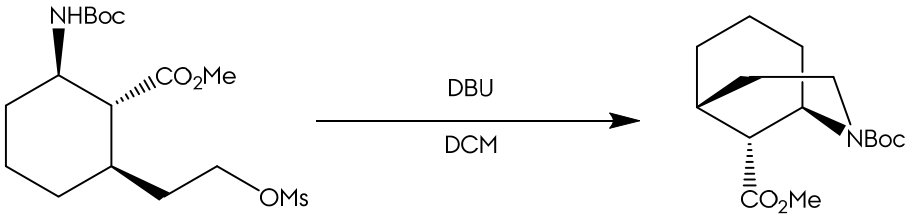

23 **12**

166 mg of of **23** (379.38 g/mol; 0.43 mmol) were dissolved in 25 mL of dry DCM in a round bottom flask. 37 μL (2.2 equiv) of DBU (1,8-diazabicyclo[5.4.0]undec-7-ene, CAS: 6674-22-2, commercial liquid, 152.2 g/mol, 0.946 mmol) were added and the flask was sealed, purged with Ar and magnetically stirred at room temperature for 24 h. Reaction mixture was extracted with AcOEt (3 times). The organic layers were combined and washed with water (3 times) and brine (1 time). Drying the solution with anhydrous Na_2SO_4, filtration and forward solvent removal resulted in a crude oil. Flash chromatography afforded 29 mg of morphan **12** (Hexanes/AcOEt 9:1, 23 % yield).

M41.- Ring-closing reaction of 23 with Acid-Base Sequence.

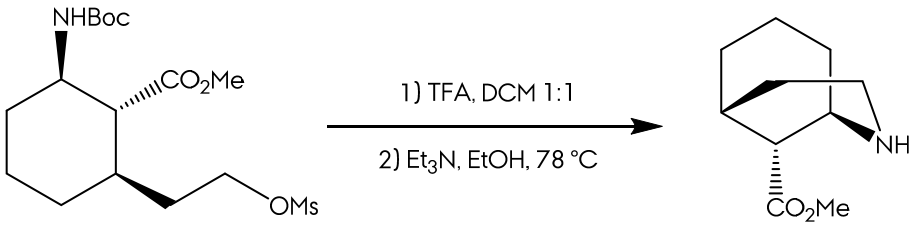

23 **26**

General procedure Y was followed with the next quantities: 370 mg of product **23** (379.3 g/mol, 0.97 mmol); 5 mL of TFA:DCM 1:1; 50 mL of Et_3N/EtOH 1:5; reaction time of 12 h. Flash chromatography afforded 161 mg of morphan **12** ($CHCl_3$/MeOH 9:1, 90 % yield).

Methyl (1*R*,5*R*,9*R*)-2-azabicyclo[3.3.1]nonane-9-carboxylate (26)

$\mathbf{R}_f$ 0.48 ($CHCl_3$/MeOH, 9:1)

$[\alpha]^{20}_D$ -4.01 (*c.* 0.71 in $CHCl_3$);

υ_{max} (neat)/cm^{-1} 3400, 2931 (C-H), 1729 (C=O), 1384, 1209 (C-O).

δ_H (400 MHz; $CDCl_3$) 5.78 (1H, **H2**), 3.92 (1H, s, **H1**), 3.68 (3H, s, **$CO_2(C\underline{H}_3)$**), 3.46 (1H, td, *J* 13.5 8.0, **$H3_A$**), 3.27 (1H, dd, *J* 13.5 7.3, **$H3_B$**), 3.05 (1H, **H9**), 2.51 (1H, **H5**), 2.25 (1H, m, **$H4_A$**), 2.17 (1H, m, **$H7_A$**), 2.08 (1H, m, **$H8_A$**), 1.94 - 1.65 (5H, m, **$H4_B$, $H8_B$, $H7_B$** and **H6**).

δ_C (50 MHz; $CDCl_3$) 171.3 (s, **$\underline{C}O_2(CH_3)$**), 52.3 (q, **$CO_2(\underline{C}H_3)$**), 47.7 (d, **C1**), 43.7 (d, **C9**), 40.1 (t, **C3**), 28.9 (t, **C4**), 26.9 (d, **C5**), 25.8 (t, **C6**), 23.5 (t, **C8**), 19.9 (t, **C7**).

m/z (M+H) calcd for **$C_{10}H_{18}NO_2$**, 184.1332; found, 184.1321, **Δ = -10.3 ppm**.

M42.- Hydrolysis of 26 in Basic Media.

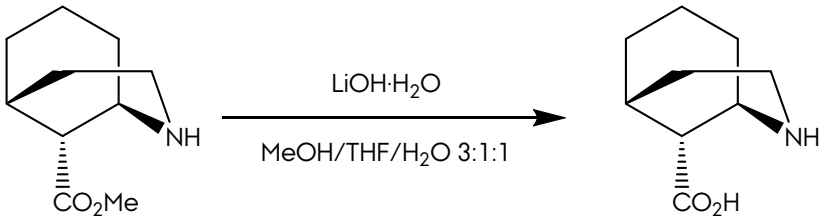

26 **27**

General procedure R was followed with the next quantities: 7 mg of **26** (183.2 g/mol; 0.038 mmol); 2 mL of MeOH/THF/H_2O 3:1:1 solution; 8 mg (5 equiv) of $LiOH \cdot H_2O$ (41.96 g/mol; 0.194 mmol). Ion-exchange resin (Dowex 50x8-200, NH_3 1 M) followed by freeze-drying afforded 7 mg of product **27**, quant yield.

(1*R*,5*R*,9*R*)-2-azabicyclo[3.3.1]nonane-9-carboxylic acid (27)

$[\alpha]^{20}_D$ -8.76 (*c.* 0.17 in H_2O);

δ_H (400 MHz; D_2O) 3.83 (1H, s, **H1**), 3.47 (1H, td, *J* 13.6 6.6, $\mathbf{H3_A}$), 3.19 (1H, dd, *J* 14.8 7.2, $\mathbf{H3_B}$), 2.48 (1H, **H9**), 2.35 (1H, **H5**), 2.12 - 1.92 (2H, m, $\mathbf{H4_A}$, $\mathbf{H7_A}$), 1.87 - 1.66 (4H, m, $\mathbf{H6_A}$, $\mathbf{H4_B}$ and **H8**), 1.65 - 1.54 (2H, m, $\mathbf{H6_B}$ and $\mathbf{H7_B}$).

δ_C (50 MHz; D_2O) 178.2 (s, $\mathbf{\underline{C}O_2H}$), 49.3 (d, **C1**), 44.9 (d, **C9**), 39.9 (t, **C3**), 28.1 (t, **C4**), 26.8 (d, **C5**), 24.7 (t, **C6**), 22.5 (t, **C8**), 18.8 (t, **C7**).

m/z (M+H) calcd for $\mathbf{C_9H_{16}NO_2}$, 170.1175; found, 170.1168, **Δ = -4.44 ppm**.

M43.- Peptide Coupling between Morphan 26 and Glycine.

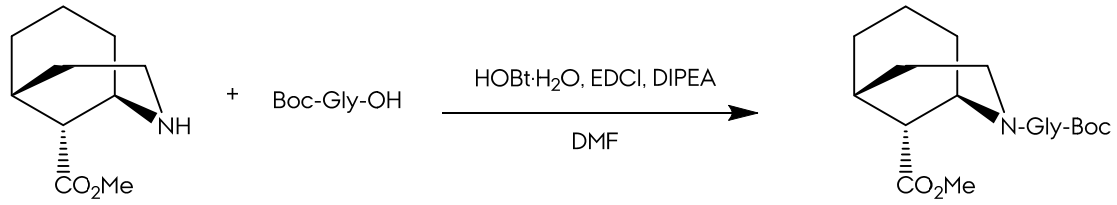

26 **28**

General procedure K was followed with the next quantities: 14 mg of **26** (183.2 g/mol; 0.077 mmol); 20 mg (1.5 equiv) of Boc-Gly-OH (*N*-(*tert*-Butoxycarbonyl)glycine, CAS: 4530-20-5, white powder, 175.1 g/mol, commercial); 3 mL of DMF; 26 μL of DIPEA (129.2 g/mol; 0.154 mmol); 22 mg of HOBt · H_2O (135.1 g/mol; 0.169 mmol); 32 mg of EDCI (191.7 g/mol; 0.169 mmol). Flash chromatography afforded 22 mg of dipeptide **28** (Hexanes/AcOEt 9:1), 86 % yield.

Methyl (1*R*,5*R*,9*R*)-2-((tert-butoxycarbonyl)glycyl)-2-azabicyclo[3.3.1]nonane-9-carboxylate (28)

$\mathbf{R}_f$ 0.81 (AcOEt)

$[\alpha]^{20}_D$ -32.4 (c. 1.54 in $CHCl_3$)

υ_{max} (neat)/cm^{-1} 2933 (C-H), 1718 (C=O, ester), 1637 (C=O, carbamate), 1458, 1168 (C-O).

δ_H (200 MHz; $CDCl_3$) 5.59 and 5.01 (1H, s rotamers, $\mathbf{N\underline{H}}$); 4.21 (1H, m, rotamers, **H1**); 3.95 (2H, m, $\mathbf{C\underline{H_2}NCOO}$); 3.74 and 3.73 (3H, s, rotamers, $\mathbf{CO_2(C\underline{H_3})}$); 3.56 (1H, m, $\mathbf{H3_A}$); 3.37 (1H, m, $\mathbf{H3_B}$); 2.55 (1H, br s, **H9**), 2.49 (1H, br s, **H5**), 1.93 - 1.52 (8H, **H4, H6, H7** and **H8**), 1.44 (9H, s, $\mathbf{C(C\underline{H_3})_3}$).

δ_C (50 MHz; $CDCl_3$; (*) minor rotamer) 172.4 (s, **<u>C</u>O₂(CH₃)**), 172.0* (s, **<u>C</u>O₂(CH₃)**), 168.0 (s, **<u>C</u>ON**), 156.1 (s, **N<u>C</u>OO**), 79.8 (s, **<u>C</u>(CH₃)₃**), 52.2 (q, **CO₂(C<u>H₃</u>)**), 52.0* (q, **CO₂(C<u>H₃</u>)**), 47.8 (d, **C1**), 46.3* (d, **C1**), 46.0 (d, **C9**), 45.2* (d, **C9**), 43.2 (t, **<u>C</u>H₂NCOO**), 42.7* (t, **<u>C</u>H₂NCOO**), 41.3 (t, **C3**), 40.3* (t, **C3**), 30.0 (t, **C4**), 29.8* (t, **C4**), 28.5 (q, **C(<u>C</u>H₃)₃**), 27.6 (t, **C6**), 27.4 (d, **C5**), 27.2* (d, **C5**), 26.3 (t, **C8**), 26.0* (t, **C8**), 20.0 (d, **C7**), 19.4* (d, **C7**).

m/z (M+Na) calcd for **$C_{17}H_{28}N_2O_5Na$**, 363.1890; found, 363.1889, **Δ = -0.39 ppm**.

M44.- Peptide Coupling between Dipeptide 28 and Alanine.

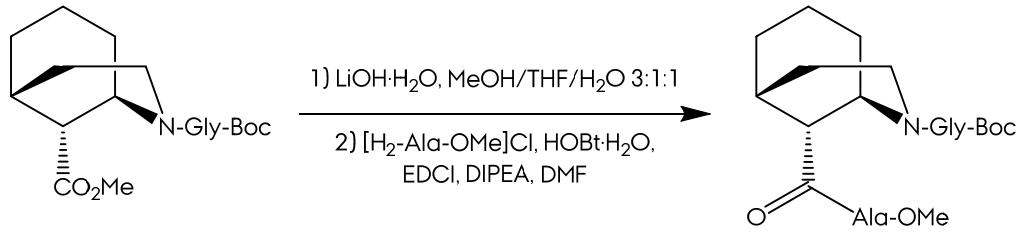

28 **29**

General procedure R was followed with the next quantities: 17 mg of **28** (340.1 g/mol; 0.051 mmol); 2 mL of MeOH/THF/H_2O 3:1:1 solution; 4 mg (2 equiv) of $LiOH \cdot H_2O$ (41.96 g/mol; 0.103 mmol). Reaction workup afforded 8 mg of carboxylic acid of **28** which was used *in situ*.

General procedure K was followed with the next quantities: 8 mg of **28**-acid (326.3 g/mol; 0.026 mmol); 5 mg (1.5 equiv) of [H_2-Ala-OMe]Cl (*L*-Alanine methyl ester hydrochloride, CAS: 2491-20-5, white powder, 139.5 g/mol, commercial); 3 mL of DMF; 9 μL of DIPEA (129.2 g/mol; 0.052 mmol); 8 mg of $HOBt \cdot H_2O$ (135.1 g/mol; 0.058 mmol); 11 mg of EDCI (191.7 g/mol; 0.058 mmol). Flash chromatography afforded 11 mg of dipeptide **29** (Hexanes/AcOEt 9:1), 53 % yield.

***<u>tert</u>*-<u>butyl 3-(((1*R*,5*R*,9*R*)-9-(((*S*)-1-methoxy-1-oxopropan-2-yl)carbamoyl)-2-azabicyclo[3.3.1]nonan-2-yl)amino)-2-oxopropanoate</u> (29)**

R_f 0.71 (AcOEt)

$[\alpha]^{20}_D$ -7.6 (c. 0.41 in $CHCl_3$).

δ_H (200 MHz; $CDCl_3$) 5.57 - 4.92 (2H, s rotamers, **NH**), 4.62 (1H, **CHCH$_3$**), 4.27 (1H, m, rotamers, **H1**), 4.09 - 3.77 (2H, m, **CH$_2$NCOO**); 3.76 and 3.68 (3H, s, rotamers, **CO$_2$(CH$_3$)**), 3.64 - 3.51 (2H, m, **H3**), 2.60 - 2.32 (2H, **H5** and **H9**), 2.11 - 1.49 (8H, **H4, H6, H7** and **H8**), 1.45 (9H, s, **C(CH$_3$)$_3$**), 1.37 (3H, **CHCH$_3$**).

m/z (M+Na) calcd for **$C_{20}H_{33}N_3O_6Na$**, 434.2261; found, 434.2263, **Δ = 0.33 ppm**.

M45.- Peptide Coupling between Morphan 26 and *L*-Phenylalanine.

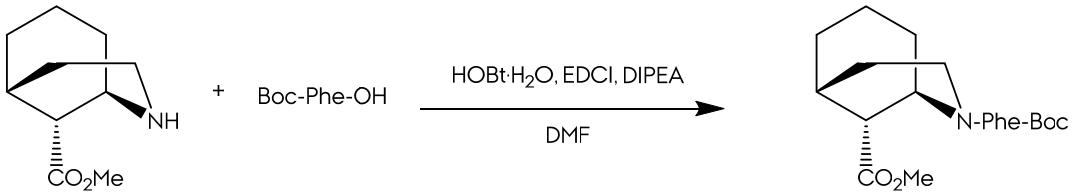

26 **30**

General procedure K was followed with the next quantities: 10 mg of **26** (183.2 g/mol; 0.054 mmol); 22 mg (1.5 equiv) of Boc-Phe-OH (*N*-(*tert*-butoxycarbonyl)-*L*-phenylalanine, CAS: 13734-34-4, white powder, 265.3 g/mol, commercial); 3 mL of DMF; 18 μL of DIPEA (129.2 g/mol; 0.108 mmol); 16 mg of HOBt · H_2O (135.1 g/mol; 0.119 mmol); 22 mg of EDCI (191.7 g/mol; 0.119 mmol). Flash chromatography afforded 7 mg of dipeptide **30** (Hexanes/AcOEt 9:1), 30 % yield.

Methyl (1*R*,5*R*,9*R*)-2-((tert-butoxycarbonyl)-L-phenylalanyl)-2-azabicyclo[3.3.1]nonane-9-carboxylate (30)

R_f 0.69 (Hexanes/AcOEt, 1:1)

$[\alpha]^{20}_D$ -30.9 (c. 1.97 in $CHCl_3$)

υ_{max} (neat)/cm^{-1} 2929 (C-H), 1701 (C=O, ester), 1629 (C=O, carbamate), 1431, 1168 (C-O).

δ_H (400 MHz; $CDCl_3$; (*) minor rotamer) 7.27 - 7.18 (5H, **C$_{ar}$H**), 5.50 - 5.46 (1H, m, **NH**), 4.96 - 4.85 (1H, m, **CHNH**), 4.02 (1H, br s, **H1**), 3.69 (3H, s, **CO$_2$(CH$_3$)**), 3.65 - 3.59* (m, **H3$_A$**), 3.31 (1H, td, *J* 12.8 6.8, **H3$_A$**), 3.05 (1H, td, *J* 12.8 5.9, **H3$_B$**), 2.98 (1H, dd, *J* 12.9 10.4, **CH$_A$HC$_{ar}$**), 2.86 (1H, dd, *J* 12.9 9.0, **CHH$_B$C$_{ar}$**), 2.45 (1H, br s, **H9**), 2.37* (br s, **H5**), 2.26 (1H, br s, **H5**), 1.80 - 1.48 (8H, **H4, H6, H7** and **H8**), 1.42 (9H, s, **C(CH$_3$)$_3$**).

δ_C (50 MHz; $CDCl_3$; (*) minor rotamer) 172.4 (s, **$\underline{C}O_2(CH_3)$**), 171.9* (s, **$\underline{C}O_2(CH_3)$**), 171.6 (s, **$\underline{C}ON$**), 171.3* (s, **$\underline{C}ON$**), 155.2 (s, **$N\underline{C}OO$**), 136.6 (d, **C_{ipso}**), 129.8 (d, **C_{ar}**), 129.7* (d, **C_{ar}**), 128.6 (d, **C_{ar}**), 128.5* (d, **C_{ar}**), 127.1 (d, **C_{ar}**), 126.9* (d, **C_{ar}**), 79.8 (s, **$\underline{C}(CH_3)_3$**), 51.8 (q, **$CO_2(C\underline{H_3})$**), 51.5 (d, **$\underline{C}HNH$**), 51.4* (d, **$\underline{C}HNH$**), 48.9 (d, **C1**), 45.3 (d, **C9**), 42.3 (t, **C3**), 40.2* (t, **C3**), 41.4 (t, **$\underline{C}H_2C_{ar}$**), 40.7* (t, **$\underline{C}H_2C_{ar}$**), 30.2 (t, **C4**), 29.7* (t, **C4**), 28.5 (q, **$C(\underline{C}H_3)_3$**), 27.9 (t, **C6**), 27.3 (d, **C5**), 27.1* (d, **C5**), 26.2 (t, **C8**), 25.8* (t, **C8**), 20.0 (t, **C7**), 19.2* (t, **C7**).

m/z (M+Na) calcd for **$C_{24}H_{34}N_2O_5Na$**, 453.2359; found, 453.2360, **Δ = 0.01 ppm**.

M46.- Acid Deprotection of 30.

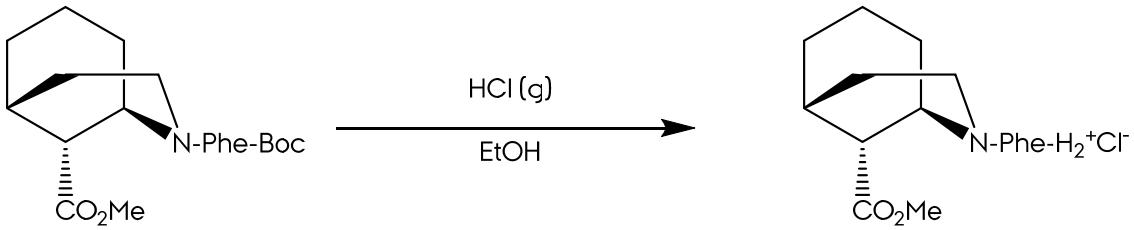

30 **31**

General procedure H was followed with the next quantities: 9 mg of **30** (430.6 g/mol; 0.021 mmol). Reaction workup afforded 7 mg of **31**, quant yield.

m/z (M-Cl)+ calcd for **$C_{19}H_{27}N_2O_3$**, 331.2016; found, 331.2023, **Δ = -2.11 ppm**.

M47.- Alkylation of Amine 26 with Benzyl Bromide.

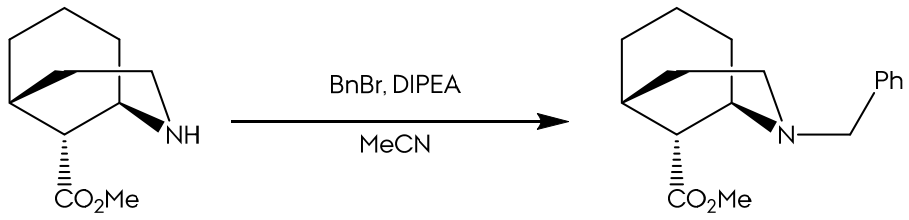

26 **32**

General procedure Z was followed with the next quantities: 17 mg of **26** (183.2 g/mol; 0.093 mmol); 13 µL (1.1 equiv) of BnBr (benzyl bromide, CAS: 100-39-0, liquid, 171.0 g/mol, commercial); 2 mL of MeCN; 18 mg of DIPEA (129.2 g/mol;

0.141 mmol). Flash chromatography afforded 17 mg of morphan **32** (Hexanes/AcOEt 9:1), 68 % yield.

Methyl (1*R*,5*R*,9*R*)-2-benzyl-2-azabicyclo[3.3.1]nonane-9-carboxylate (32)

$\mathbf{R}_f$ 0.76 (Hexanes/AcOEt, 1:1)

$[\alpha]^{20}_D$ -14.5 (c. 0.71 in $CHCl_3$)

υ_{max} (neat)/cm^{-1} 2922 (C-H), 1734 (C=O, ester), 1654, 1201 (C-O), 1120.

δ_H (400 MHz; $CDCl_3$) 7.34 - 7.22 (5H, $\mathbf{C_{ar}\underline{H}}$), 3.78 (1H, AB, *J* 13.4, $\mathbf{C\underline{H}_AHC_{ar}}$), 3.69 (3H, s, $\mathbf{CO_2(C\underline{H}_3)}$), 3.64 (1H, AB, *J* 13.4, $\mathbf{CH\underline{H}_BC_{ar}}$), 3.23 (1H, s, **H1**), 2.87 (1H, td, *J* 11.9 5.4, $\mathbf{H3_A}$), 2.75 (1H, s, **H9**), 2.75 - 2.68 (1H, $\mathbf{H3_B}$), 2.38 (1H, **H5**), 2.01 (2H, m, $\mathbf{H4_A}$, $\mathbf{H7_A}$), 1.85 - 1.70 (3H, m, $\mathbf{H6_A}$, $\mathbf{H8_A}$ and $\mathbf{H4_B}$), 1.61 - 1.51 (3H, m, $\mathbf{H6_B}$, $\mathbf{H8_B}$ and $\mathbf{H7_B}$).

δ_C (50 MHz; $CDCl_3$) 174.1 (s, $\mathbf{\underline{C}O_2(CH_3)}$), 139.8 (s, $\mathbf{C_{ipso}}$), 128.8 (d, $\mathbf{C_{ar}}$), 128.4 (d, $\mathbf{C_{ar}}$), 126.9 (d, $\mathbf{C_{ar}}$), 60.4 (t, $\mathbf{C\underline{H}_2C_{ar}}$), 52.6 (d, **C1**), 51.6 (q, $\mathbf{CO_2(\underline{C}H_3)}$), 48.7 (t, **C3**), 48.2 (d, **C9**), 31.7 (t, **C4**), 28.1 (d, **C5**), 26.8 (t, **C6**), 21.7 (t, **C8**), 21.3 (t, **C7**).

m/z (M+H) calcd for $\mathbf{C_{17}H_{24}NO_2}$, 274.1801; found, 274.1799, $\mathbf{\Delta = -0.93\ ppm}$.

M48.- Acid Deprotection of 30.

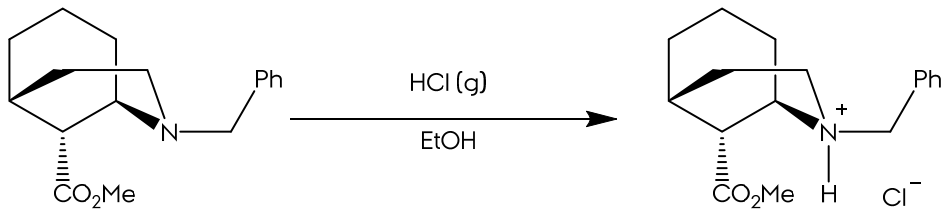

32 **33**

General procedure H was followed with the next quantities: 8 mg of **32** (273.2 g/mol; 0.029 mmol). Reaction workup afforded 6 mg of **33**, quant yield.

M49.- Alkylation of Amine 26 with Benzyl Bromide.

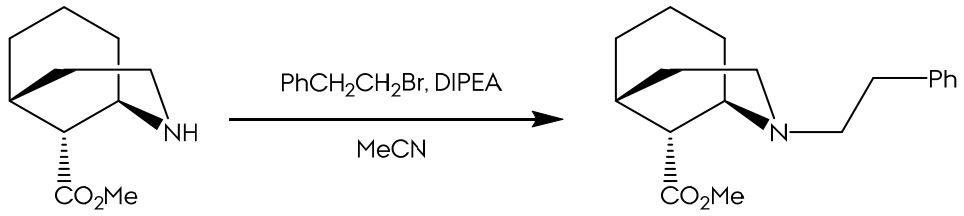

26 **34**

General procedure Z was followed with the next quantities: 24 mg of **26** (183.2 g/mol; 0.135 mmol); 26.7 mg (1.1 equiv) of $PhCH_2CH_2Br$ (2-phenylethyl bromide, CAS: 103-63-9, liquid, 185.0 g/mol, commercial); 2 mL of MeCN; 26 mg of DIPEA (129.2 g/mol; 0.203 mmol). Flash chromatography afforded 53 mg of morphan **34** (Hexanes/AcOEt 9:1), 71 % yield.

Methyl (1*R*,5*R*,9*R*)-2-phenethyl-2-azabicyclo[3.3.1]nonane-9-carboxylate (34)

$\mathbf{R}_f$ 0.41 (Hexanes/AcOEt, 1:1)

$[\alpha]^{20}_D$ +3.38 (c. 0.77 in $CHCl_3$)

υ_{max} (neat)/cm^{-1} 2626 (C-H), 1730 (C=O), 1286 (C-O), 1195, 1132.

δ_H (400 MHz; $CDCl_3$) 7.19 - 7.08 (5H, m, $\mathbf{C_{ar}\underline{H}}$), 3.61 (3H, s, $\mathbf{CO_2(C\underline{H_3})}$), 3.21 (1H, br s, **H1**), 2.82 - 2.77 (2H, m, **H3**), 2.70 - 2.62 (4H, $\mathbf{NC\underline{H_2}CH_2C_{ar}}$, and $\mathbf{NCH_2C\underline{H_2}C_{ar}}$), 2.60 (1H, br s, **C9**), 2.28 (1H, s, **C5**), 2.01 - 1.92 (1H, m, $\mathbf{H4_A}$), 1.89 - 1.84 (1H, m, $\mathbf{H7_A}$), 1.73 - 1.65 (3H, m, $\mathbf{H4_B}$, $\mathbf{H6_A}$ and $\mathbf{H8_A}$), 1.61 - 1.37 (3H, m, $\mathbf{H6_B}$, $\mathbf{H7_B}$ and $\mathbf{H8_B}$).

δ_C (50 MHz; $CDCl_3$) 173.9 (s, $\mathbf{\underline{C}O_2(CH_3)}$), 140.8 (s, $\mathbf{C_{ipso}}$), 128.9 (d, $\mathbf{C_{ar}}$), 128.5 (d, $\mathbf{C_{ar}}$), 126.2 (d, $\mathbf{C_{ar}}$), 58.0 (t, $\mathbf{N\underline{C}H_2CH_2C_{ar}}$), 52.1 (d, **C1**), 51.7 (q, $\mathbf{CO_2(\underline{C}H_3)}$), 49.3 (t, **C3**), 48.0 (d, **C9**), 34.7 (t, $\mathbf{NCH_2\underline{C}H_2C_{ar}}$), 31.7 (t, **C4**), 28.0 (d, **C5**), 26.7 (t, **C6**), 21.6 (t, **C8**), 21.0 (t, **C7**).

m/z (M+H) calcd for $\mathbf{C_{18}H_{26}NO_2}$, 288.1958; found, 288.1952, $\mathbf{\Delta = -2.10\ ppm}$.

M50.- Acid Deprotection of 34.

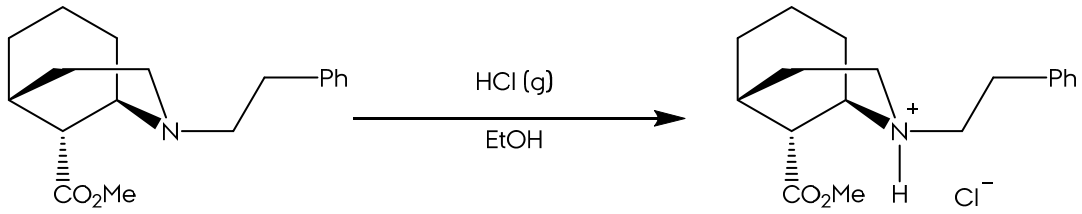

34 **35**

General procedure H was followed with the next quantities: 8 mg of **34** (273.6 g/mol; 0.028 mmol). Reaction workup afforded 6 mg of **35**, quant yield.

m/z (M-Cl)+ calcd for $\mathbf{C_{18}H_{26}NO_2}$, 288.1958; found, 288.1957, $\mathbf{\Delta = 0.34\ ppm}$.

M51.- Protection of Morphan 26 as Boc-amine.

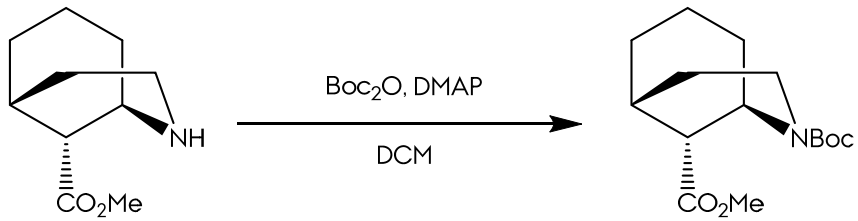

26 **12**

General procedure G was followed with the next quantities: 21 mg of **26** (183.2 g/mol, 0.11 mmol); 30 mg of Boc_2O (218.2 g/mol, 0.139 mmol); 2.85 mg of DMAP (122.1 g/mol, 0.023); 5 mL of DCM. Reaction workup afforded 31 mg of protected morphan **12**, 97 % yield.

M52.- Hydrolysis of 12 in Basic Media.

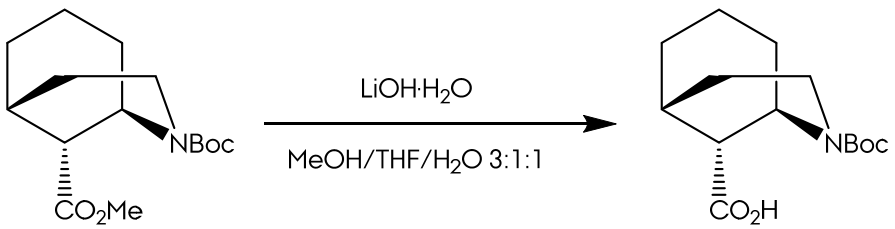

12 **36**

General procedure R were followed with the next quantities: 19 mg of **12** (283.2 g/mol; 0.067 36mmol); 5 mL of MeOH/THF/H_2O 3:1:1 solution; 6 mg (2.2 equiv) of

$LiOH \cdot H_2O$ (41.96 g/mol; 0.147 mmol): reaction time of 12 h. Reaction workup afforded 17 mg of product **36**, 94 %.

(1*R*,5*R*,9*R*)-2-(tert-butoxycarbonyl)-2-azabicyclo[3.3.1]nonane-9-carboxylic acid (36)

$\mathbf{R}_f$ 0.89 ($CHCl_3$/MeOH, 4:1)

υ_{max} (neat)/cm^{-1} 3186 (O-H, acid), 2931 (C-H), 1701 (C=O), 1629 (C=O, carbamate), 1406, 1170 (C-O).

δ_H (400 MHz; $CDCl_3$; (*) minor rotamer) 4.63 (1H, br s, **H1**), 4.46* (br s, **H1**), 3.71* (td, *J* 8.5 3.7, $\mathbf{H3_A}$), 3.59 (1H, td, *J* 8.5 3.7, $\mathbf{H3_A}$), 3.45 (1H, dd, *J* 9.9 6.8, $\mathbf{H3_B}$), 3.43* (dd, *J* 9.9 6.8, $\mathbf{H3_B}$), 2.65 - 2.60* (m, **H5**), 2.47 (2H, **H5** and **H9**), 2.16 - 2.07 (1H, m, $\mathbf{H4_A}$), 2.05 - 2.00 (1H, $\mathbf{H7_A}$), 1.83 - 1.66 (4H, $\mathbf{H6_A}$, $\mathbf{H8_A}$, $\mathbf{H4_B}$ and $\mathbf{H6_B}$), 1.83 - 1.66 (2H, $\mathbf{H8_B}$ and $\mathbf{H7_B}$), 1.45 (9H, s, $\mathbf{C(C\underline{H}_3)_3}$).

δ_C (50 MHz; $CDCl_3$; (*) minor rotamer) 178.5 (s, $\mathbf{\underline{C}O_2H}$), 178.0* (s, $\mathbf{\underline{C}O_2H}$), 155.9* (s, $\mathbf{N\underline{C}OO}$), 155.6 (s, $\mathbf{N\underline{C}OO}$), 79.9 (s, $\mathbf{\underline{C}(CH_3)_3}$), 79.7* (s, $\mathbf{\underline{C}(CH_3)_3}$), 47.5* (d, **C1**), 46.5 (d, **C1**), 45.9* (d, **C9**), 45.7 (d, **C9**), 41.4* (t, **C3**), 40.5 (t, **C3**), 32.1 (t, **C4**), 29.7* (t, **C4**), 28.7 (q, $\mathbf{C(\underline{C}H_3)_3}$), 27.3 (d, **C5**), 26.9 (t, **C6**), 26.7* (t, **C6**), 25.4 (t, **C8**), 19.4 (t, **C7**).

m/z (M+Na) calcd for $\mathbf{C_{14}H_{23}NO_4Na}$, 292.1519; found, 292.1528, $\mathbf{\Delta = 2.97\ ppm}$.

M53.- Peptide Coupling between Morphan 36 and *L*-Phenylalanine.

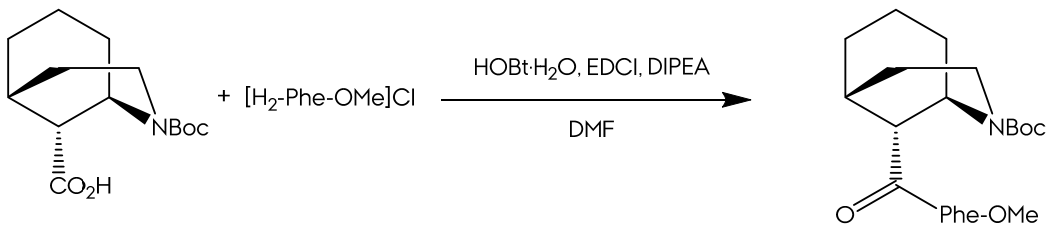

36 **37**

General procedure K was followed with the next quantities: 14 mg of **36** (269.4 g/mol; 0.053 mmol); 17 mg (1.5 equiv) of [H_2-Phe-OMe]Cl (*L*-Phenylalanine methyl ester hydrochloride, CAS: 7524-50-7, white powder, 215.6 g/mol, commercial); 4 mL of DMF; 18 μL of DIPEA (129.2 g/mol; 0.106 mmol); 16 mg of $HOBt \cdot H_2O$ (135.1

g/mol; 0.117 mmol); 22 mg of EDCI (191.7 g/mol; 0.117 mmol). Flash chromatography afforded 14 mg of dipeptide **37** (Hexanes/AcOEt 8:2), 62 % yield.

<u>*tert*-butyl (1*R*,5*R*,9*R*)-9-(((*S*)-1-methoxy-1-oxo-3-phenylpropan-2-yl)carbamoyl)-2-azabicyclo[3.3.1]nonane-2-carboxylate (37)</u>

$\mathbf{R}_f$ 0.53 (Hexanes/AcOEt, 1:1)

$[\alpha]^{20}_{D}$ +9.6 (c. 1.5 in $CHCl_3$)

υ_{max} (neat)/cm^{-1} 3346 (N-H), 2931 (C-H), 1743 (C=O, ester), 1685 (C=O, amide), 1654 (C=O, carbamate), 1363, 1172 (C-O).

δ_H (400 MHz; $CDCl_3$; (*) minor rotamer) 7.32 - 7.21 (4H, ***o*-C$_{ar}$<u>H</u>** and ***m*-C$_{ar}$<u>H</u>**), 7.12 (1H, ***p*-C$_{ar}$<u>H</u>**), 6.02 (1H, br s, **N<u>H</u>**), 4.93 (1H, br s, **C<u>H</u>NH**), 4.69* (br s, **C<u>H</u>NH**), 4.56* (br s, **H1**), 4.46* (br s, **H1**), 4.35 (1H, br s, **H1**), 3.76* (3H, s, **CO$_2$(C<u>H$_3$</u>)**), 3.69 (3H, s, **CO$_2$(C<u>H$_3$</u>)**), 3.74 - 3.68 (1H, **H3$_A$**), 3.48 (1H, **H3$_B$**), 3.21 - 2.88 (2H, **C<u>H$_2$</u>C$_{ar}$**), 2.46 (1H, **H9**), 2.41* (**H9**), 2.30* (**H9**), 2.30 (1H, **H5**), 2.21* (br s, **H5**), 2.00 - 1.49 (8H, **H4, H6, H7** and **H8**), 1.47 (9H, s, **CO$_2$C(C<u>*H*$_3$</u>)$_3$**).

δ_C (50 MHz; $CDCl_3$; (*) minor rotamer) 173.3 (s, **<u>C</u>O$_2$(CH$_3$)**), 172.4* (s, **<u>C</u>ON**), 171.7 (s, **<u>C</u>ON**), 156.7 (s, **N<u>C</u>OO**), 155.6* (s, **N<u>C</u>OO**), 136.6* (d, **C$_{ipso}$**), 136.1 (d, **C$_{ipso}$**), 129.3* (d, **C$_{ar}$**), 128.8 (d, **C$_{ar}$**), 127.4* (d, **C$_{ar}$**), 127.2 (d, **C$_{ar}$**), 80.2* (s, **<u>C</u>(CH$_3$)$_3$**), 79.7 (s, **<u>C</u>(CH$_3$)$_3$**), 53.0 (d, **<u>C</u>HNH**), 52.5 (q, **CO$_2$(C<u>H$_3$</u>)**), 52.3* (q, **CO$_2$(C<u>H$_3$</u>)**), 48.2 (d, **C1**), 47.2 (d, **C9**), 46.4* (d, **C3**), 46.1 (d, **C3**), 38.0 (t, **<u>C</u>H$_2$C$_{ar}$**), 37.7* (t, **<u>C</u>H$_2$C$_{ar}$**), 31.7 (t, **C4**), 30.1* (t, **C4**), 28.6 (q, **C(<u>C</u>H$_3$)$_3$**), 28.5 (d, **C5**), 27.8* (t, **C8**), 27.5 (t, **C8**), 26.6 (t, **C6**), 26.3* (t, **C6**), 20.6 (t, **C7**), 19.3* (t, **C7**).

m/z (M+H) calcd for **$C_{24}H_{35}N_2O_5$**, 431.2540; found, 453.2270, **Δ = 4.52 ppm**.

M54.- Acid Deprotection of 37.

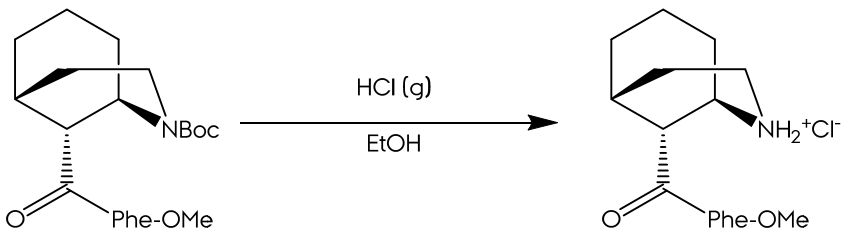

37 **38**

General procedure H was followed with the next quantities: 9 mg of **30** (430.5 g/mol; 0.021 mmol). Reaction workup afforded 7 mg of **31**, quant yield.

m/z (M-Cl) calcd for $\mathbf{C_{19}H_{27}N_2O_3}$, 331.2016; found, 331.2029, **Δ = -3.92 ppm**.

M55.- Esterification of Morphan 36 with Phenol.

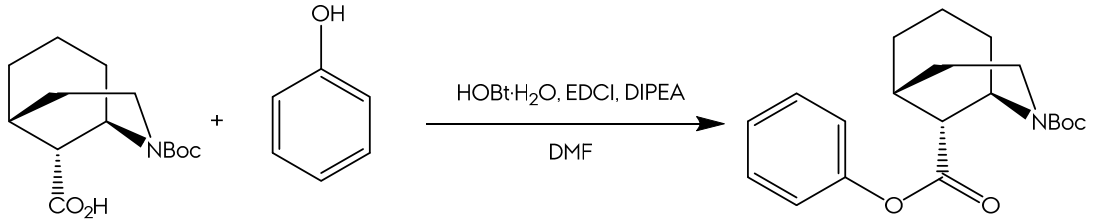

36 **39**

General procedure L was followed with the next quantities: 9 mg of **36** (269.8 g/mol; 0.033 mmol); 17 mg (1.5 equiv) of phenol (CAS: 108-95-2, crystals, 94.1 g/mol, commercial); 3 mL of DMF; 8 μL of DIPEA (129.2 g/mol; 0.066 mmol); 10 mg of HOBt · H_2O (135.1 g/mol; 0.073 mmol); 14 mg of EDCI (191.7 g/mol; 0.073 mmol): reaction time of 16 h. Flash chromatography afforded 11 mg of ester **39** (Hexanes/AcOEt 9:1), 94 % yield.

2-(*tert*-butyl) 9-phenyl (1*R*,5*R*,9*R*)-2-azabicyclo[3.3.1]nonane-2,9-dicarboxylate (39)

$\mathbf{R}_f$ 0.92 (Hexanes/AcOEt, 1:1)

$[\alpha]^{20}_D$ -10.3 (c. 0.71 in $CHCl_3$)

υ_{max} (neat)/cm^{-1} 2927 (C-H), 1751 (C=O, phenolic ester), 1689 (C=O, carbamate), 1363, 1165.

δ_H (400 MHz; $CDCl_3$; (*) minor rotamer) 7.38 (2H, m, **m-C_{ar}H**), 7.23 (1H, m, **p-C_{ar}H**), 7.06 (2H, m, **o-C_{ar}H**), 4.93* (br s, **H1**), 4.82* (br s, **H1**), 4.77 (1H, br s, **H1**), 4.59* (br s, **H1**), 3.77 (1H, **$H3_A$**), 3.68 - 3.62* (m, **$H3_A$**), 3.50 (1H, **$H3_B$**), 2.89* (br s, **H9**), 2.86* (br s, **H9**), 2.75* (br s, **H9**), 2.68 (1H, br s, **H9**), 2.61 (1H, br s, **H5**), 2.56* (br s, **H5**), 2.28 - 2.20 (1H, m, **$H4_A$**), 2.09 - 2.01 (1H, m, **$H7_A$**), 1.91 - 1.73 (3H, **$H6_A$**, **$H8_A$** and **$H4_B$**), 1.72 - 1.52 (3H, **$H6_B$**, **$H8_B$** and **$H7_B$**), 1.48 (9H, s **C(C$\underline{H_3}$)$_3$**), 1.44* (s, **C(C$\underline{H_3}$)$_3$**).

δ_C (50 MHz; $CDCl_3$; (*) minor rotamer) 171.1 (s, **C**OO), 155.6 (s, **NC**OO), 150.9 (s, $\mathbf{C_{ipso}}$), 129.6 (d, $\mathbf{C_{ar}}$), 126.0 (d, $\mathbf{C_{ar}}$), 121.7 (d, $\mathbf{C_{ar}}$), 79.8 (s, **C**$\mathbf{(CH_3)_3}$), 48.0 (d, **C1**), 47.7* (d, **C1**), 47.1 (d, **C1**), 47.0 (d, **C9**), 46.9* (d, **C9**), 41.5* (t, **C3**), 40.9 (t, **C3**), 32.2* (t, **C4**), 32.1 (t, **C4**), 28.7 (q, **C**$\mathbf{(C H_3)_3}$), 27.7 (t, **C5**), 27.5* (t, **C5**), 27.1 (t, **C6**), 26.8* (t, **C6**), 25.3 (t, **C8**), 24.9* (t, **C8**), 19.7 (t, **C7**), 19.6* (t, **C7**).

m/z (M+Na) calcd for $\mathbf{C_{20}H_{27}NO_4Na}$, 368.1832; found, 368.1841, $\mathbf{\Delta = 2.36\ ppm}$.

M56.- Acid Deprotection of 37.

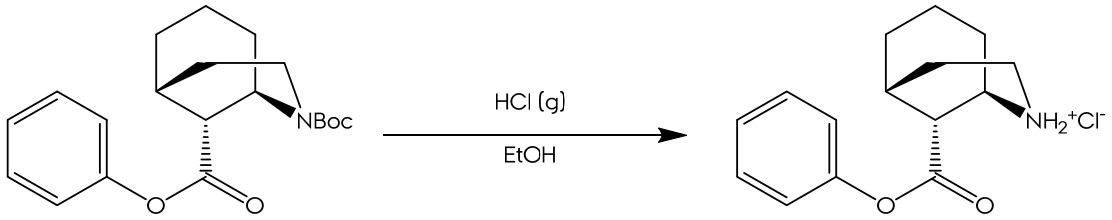

39 **40**

General procedure H was followed with the next quantities: 7 mg of **40** (345.5 g/mol; 0.020 mmol). Reaction workup afforded 5 mg of **40**, quant yield.

m/z (M-Cl) calcd for $\mathbf{C_{15}H_{20}NO_2}$, 246.1488; found, 246.1488, $\mathbf{\Delta = -0.22\ ppm}$.

M57.- Esterification of Morphan 36 with Resorcinol.

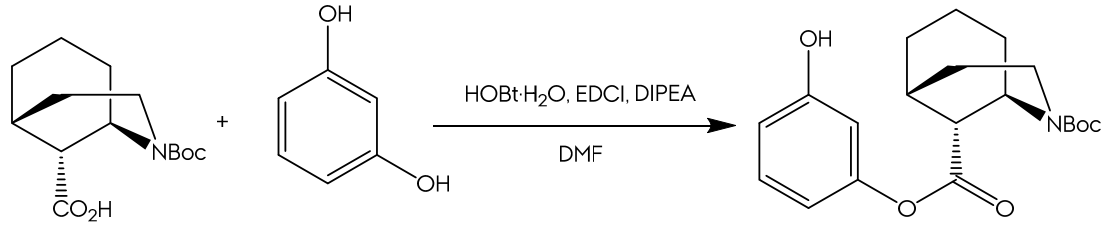

36 **41**

General procedure L was followed with the next quantities: 7 mg of **36** (269.5 g/mol; 0.028 mmol); 5 mg (1.5 equiv) of resorcinol (CAS: 108-46-3, white powder, 110.1 g/mol, commercial); 3 mL of DMF; 10 μL of DIPEA (129.2 g/mol; 0.056 mmol); 8 mg of HOBt · H_2O (135.1 g/mol; 0.062 mmol); 11 mg of EDCI (191.7 g/mol; 0.062 mmol): reaction time of 20 h. Flash chromatography afforded 9 mg of ester **41** (Hexanes/AcOEt 9:1), 86 % yield.

2-(*tert*-butyl) 9-(3-hydroxyphenyl) (1*R*,5*R*,9*R*)-2-azabicyclo[3.3.1]nonane-2,9-dicarboxylate (41)

$\mathbf{R}_f$ 0.58 (Hexanes/AcOEt, 1:1)

$[\alpha]^{20}_{D}$ -30.7 (c. 0.9 in $CHCl_3$)

υ_{max} (neat)/cm^{-1} 3346 (O-H), 2931 (C-H), 1757 (C=O, phenolic ester), 1654 (C=O, carbamate), 1406, 1165 (C-O).

δ_H (400 MHz; $CDCl_3$; (*) minor rotamer) 7.22 (1H, t, *J* 9.1, $\mathbf{C_{ar}5'\underline{H}}$), 6.72 (1H, d, *J* 7.1, $\mathbf{C_{ar}4'\underline{H}}$), 6.65 - 6.60 (2H, m, $\mathbf{C_{ar}2'\underline{H}}$ and $\mathbf{C_{ar}6'\underline{H}}$), 6.54 (1H, br s, $\mathbf{O\underline{H}}$), 4.89* (br s, **H1**), 4.80* (br s, **H1**), 4.76* (br s, **H1**), 4.57 (1H, br s, **H1**), 3.77 (1H, $\mathbf{H3_A}$), 3.70 - 3.65* (m, $\mathbf{H3_A}$), 3.58 - 3.49 (1H, m, $\mathbf{H3_B}$), 2.87 (1H, br s, **H9**), 2.83* (br s, **H9**), 2.73* (br s, **H9**), 2.67* (br s, **H9**), 2.59 (1H, br s, **H5**), 2.55* (br s, **H5**), 1.98 - 1.47 (8H, **H4, H6, H7** and **H8**), 1.49 (9H, s, $\mathbf{C(C\underline{H}_3)_3}$), 1.44* (s, $\mathbf{C(C\underline{H}_3)_3}$).

δ_C (50 MHz; $CDCl_3$; (*) minor rotamer) 171.1 (s, $\mathbf{\underline{C}OO}$), 157.3 (s, $\mathbf{C_{ipso}3'}$), 157.1 (s, $\mathbf{C_{ipso}3'}$), 155.7 (s, $\mathbf{N\underline{C}OO}$), 151.7 (s, $\mathbf{C_{ipso}1'}$), 130.5 (d, $\mathbf{C_{ar}5'}$), 130.2* (d, $\mathbf{C_{ar}5'}$), 113.6 (d, $\mathbf{C_{ar}6'}$), 113.3 (d, $\mathbf{C_{ar}4'}$), 109.3 (d, $\mathbf{C_{ar}2'}$), 80.1 (s, $\mathbf{\underline{C}(CH_3)_3}$), 47.8 (d, **C1**), 47.7* (d, **C1**), 46.5 (d, **C9**), 46.3* (d, **C9**), 41.4* (t, **C3**), 41.8 (t, **C3**), 32.1 (t, **C4**), 29.8* (t, **C4**), 28.7 (q, $\mathbf{C(\underline{C}H_3)_3}$), 27.4 (d, **C5**), 26.9 (t, **C6**), 26.5 (t, **C8**), 19.7 (t, **C7**), 19.4* (t, **C7**).

m/z (M+H) calcd for $\mathbf{C_{20}H_{28}NO_5}$, 369.1962; found, 362.1971, $\mathbf{\Delta = 2.49\ ppm}$.

M58.- Acid Deprotection of 41.

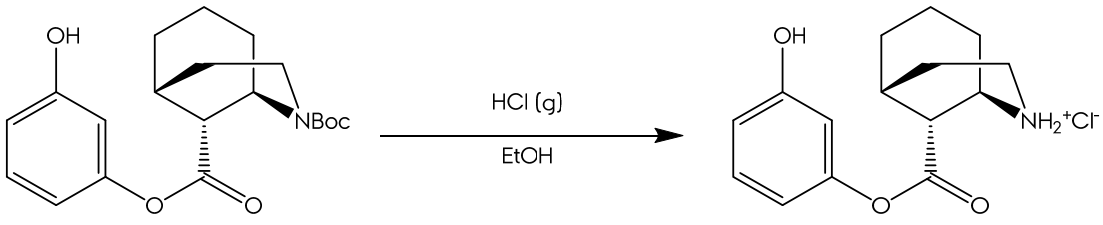

41 **42**

General procedure H was followed with the next quantities: 9 mg of **41** (361.7 g/mol; 0.025 mmol). Reaction workup afforded 7 mg of **42**, quant yield.

m/z (M-Cl) calcd for $\mathbf{C_{15}H_{20}NO_3}$, 262.1437; found, 262.1434, $\mathbf{\Delta = 1.14\ ppm}$.

M59.- Esterification of Morphan 36 with Hydroquinone.

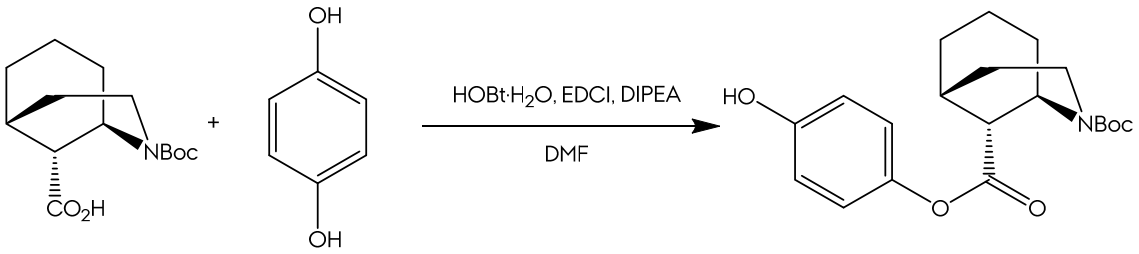

36 **43**

General procedure L was followed with the next quantities: 12 mg of **36** (269.2 g/mol; 0.046 mmol); 7 mg (1.5 equiv) of hydroquinone (CAS: 123-31-9, white powder, 110.1 g/mol, commercial); 3 mL of DMF; 16 μL of DIPEA (129.2 g/mol; 0.092 mmol); 14 mg of HOBt · H_2O (135.1 g/mol; 0.101 mmol); 19 mg of EDCI (191.7 g/mol; 0.101 mmol): reaction time of 24 h. Flash chromatography afforded 15 mg of ester **39** (Hexanes/AcOEt 9:1), 92 % yield.

2-(*tert*-butyl) 9-(4-hydroxyphenyl) (1*R*,5*R*,9*R*)-2-azabicyclo[3.3.1]nonane-2,9-dicarboxylate (43)

$\mathbf{R}_f$ 0.69 (Hexanes/AcOEt, 1:1)

$[\alpha]^{20}_D$ -21.8 (c. 0.93 in $CHCl_3$)

υ_{max} (neat)/cm^{-1} 3348 (O-H), 2931 (C-H), 1757 (C=O, phenolic ester), 1654 (C=O, carbamate), 1363, 1163 (C-O).

δ_H (200 MHz; $CDCl_3$; (*) minor rotamer) 7.09 (1H, br s, **OH**), 6.92 - 6.78 (4H, $\mathbf{C_{ar}H}$), 4.82 (1H, br s, **H1**), 4.74* (br s, **H1**), 4.58* (br s, **H1**), 3.84 - 3.69 (1H, m, $\mathbf{H3_A}$), 3.62 - 3.47 (1H, m, $\mathbf{H3_B}$), 2.84 (1H, br s, **H9**), 2.57 (1H, br s, **H5**), 2.16 - 1.46 (8H, **H4, H6, H7** and **H8**), 1.49 (9H, s, $\mathbf{C(CH_3)_3}$), 1.45* (s, $\mathbf{C(CH_3)_3}$).

δ_C (50 MHz; $CDCl_3$; (*) minor rotamer) 171.3 (s, **COO**), 155.8 (s, **NCOO**), 154.2 (s, $\mathbf{C_{ipso}4'}$), 153.9* (s, $\mathbf{C_{ipso}4'}$), 149.7 (s, $\mathbf{C_{ipso}1'}$), 122.6 (d, $\mathbf{C_{ar}2'}$ and $\mathbf{C_{ar}6'}$), 122.5* (d, $\mathbf{C_{ar}2'}$ and $\mathbf{C_{ar}6'}$), 116.3* (d, $\mathbf{C_{ar}3'}$ and $\mathbf{C_{ar}5'}$), 116.1 (d, $\mathbf{C_{ar}3'}$ and $\mathbf{C_{ar}5'}$), 80.1 (s, $\mathbf{C(CH_3)_3}$), 46.9 (d, **C1**), 46.1 (d, **C9**), 45.9* (d, **C9**), 41.6 (d, **C3**), 40.6* (d, **C3**), 32.1 (t, **C4**), 29.9* (t, **C4**), 28.7 (q, $\mathbf{C(CH_3)_3}$), 27.4 (d, **C5**), 27.0 (t, **C6**), 26.8 (t, **C8**), 19.7 (t, **C7**).

m/z (M+Na) calcd for $\mathbf{C_{20}H_{27}NO_5Na}$, 384.1781; found, 384.1784, $\mathbf{\Delta = 0.66\ ppm}$.

M60.- Acid Deprotection of 43.

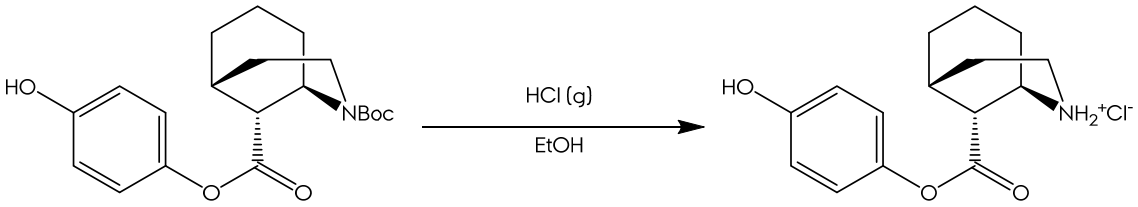

43 **44**

General procedure H was followed with the next quantities: 9 mg of **43** (361.5 g/mol; 0.025 mmol). Reaction workup afforded 7 mg of **44**, quant yield.

m/z (M-Cl) calcd for $\mathbf{C_{15}H_{20}NO_3}$, 262.1437; found, 262.1439, **Δ = -0.76 ppm**.

Reaction Inventory 2. PNA Section

P1.- Asymmetric Michael Addition of Lithium (*R*)-*N*-benzyl-*N*-α-methylbenzylamide to 4.

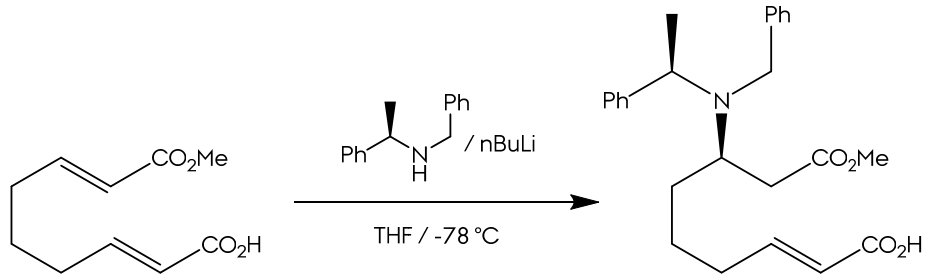

4 **45**

General procedure C was followed with the next quantities: 1.89 g of (*R*)-*N*-benzyl-*N*-α-methylbenzylamide (211.3 g/mol; 8.98 mmol) in 10 mL of THF; 5.3 mL of 1.6 M nBuLi in hexanes (64.0 g/mol; 8.51 mmol); 468 mg of substrate **4** (198.1 g/mol; 2.3 mmol) in 10 mL of THF. Flash chromatography afforded 814 mg of product **45** (Hexanes/AcOEt 9:1), 84 % yield.

(*R*,*E*)-7-(benzyl((*R*)-1-phenylethyl)amino)-9-methoxy-9-oxonon-2-enoic acid (45)

$\mathbf{R}_f$ 0.61 (Hexanes/AcOEt, 1:1)

$[\alpha]^{26}_D$ +4.6 (*c.* 1.6 in $CHCl_3$)

υ_{max} (film)/cm^{-1} 2926 (C-H), 1732 (C=O), 1688 (C=O, 1452 (C-N), 1299, 1145 (C-O).

δ_H (200 MHz, $CDCl_3$) 7.46 - 7.26 (10H, $\mathbf{C_{ar}\underline{H}}$), 7.05 (1H, dt, *J* 15.5 7.1, **H3**), 5.83 (1H, d, *J* 15.7, **H2**), 3.84 (1H, q, *J* 7.0, $\mathbf{C\underline{H}(CH_3)}$), 3.80 (1H, AB, *J* 15.0, $\mathbf{NC\underline{H_A}H}$), 3.57 - 3.50 (4H, $\mathbf{CO_2C\underline{H_3}}$ and $\mathbf{NCH\underline{H_B}}$), 3.35 - 3.25 (1H, m, **H7**), 2.20 - 2.01 (6H, **H4, H6** and **H8**), 1.63 - 1.48 (2H, **H5**), 1.35 (3H, d, *J* 7.0, $\mathbf{CHC\underline{H_3}}$).

δ_C (50 MHz, $CDCl_3$) 173.3 (s, **C9**), 172.0 (s, **C1**), 152.2 (d, **C3**), 143.2 (s, $\mathbf{C_{ipso}}$), 141.6 (s, $\mathbf{C_{ipso}}$), 128.5 (d, $\mathbf{C_{ar}}$), 128.4 (d, $\mathbf{C_{ar}}$), 128.1 (d, $\mathbf{C_{ar}}$), 127.3 (d, $\mathbf{C_{ar}}$), 126.9 (d, $\mathbf{C_{ar}}$), 121.0 (d, **C2**), 58.3 (d, $\mathbf{\underline{C}HCH_3}$), 53.8 (d, **C7**), 51.7 (s, $\mathbf{CO_2\underline{C}H_3}$), 50.2 (t, $\mathbf{\underline{C}H_2C_{ar}}$), 36.4 (t, **C8**), 33.2 (t, **C4**), 32.3 (t, **C6**), 25.4 (t, **C5**), 20.2 (q, $\mathbf{CH\underline{C}H_3}$).

m/z (M+H) calcd for $\mathbf{C_{27}H_{38}NO_4}$, 440.2795; found, 440.2805, $\mathbf{\Delta = 2.19\ ppm}$.

P2.- One Pot Protecting Group Interconversion and Regioselective Reduction of Acid 45.

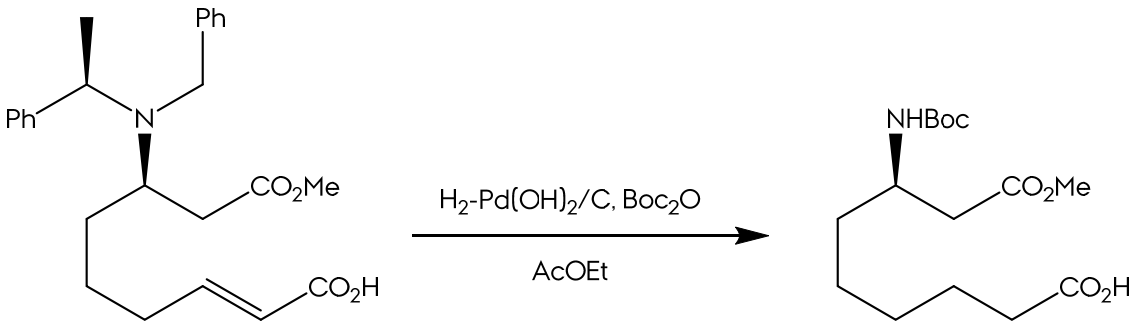

45 **46**

General procedure E was followed with the next quantities: 324 mg of 4**5** (423.7 g/mol, 0.766 mmol); 560 mg (3.3 equiv) of Boc_2O (218.2 g/mol, 2.56 mmol); 135 mg of $Pd(OH)_2$ on carbon; 3 mL of AcOEt. Flash chromatography afforded 88 mg of product **46** (Hexanes/AcOEt 7:3) in a 62 % yield.

(*R*)-7-((tert-butoxycarbonyl)amino)-9-methoxy-9-oxononanoic acid (46)

$\mathbf{R}_f$ 0.38 (Hexanes/AcOEt, 1:1)

$[\alpha]^{25}_D$ +15.7 (*c.* 0.81 in $CHCl_3$);

δ_H (200 MHz, $CDCl_3$) 8.98 (1H, **COOH**), 4.95 (1H, d, *J* 8.9, **NH**), 3.86 (1H, **H7**), 3.65 (3H, s, $\mathbf{CO_2CH_3}$), 2.48 (2H, d, *J* 5.4, **H8**), 2.31 (2H, t, *J* 7.4, **H2**), 1.64 - 1.34 (8H, **H3, H4, H5** and **H6**), 1.41 (9H, s, $\mathbf{C(CH_3)_3}$).

δ_C (50 MHz, $CDCl_3$) 179.2 (s, **C1**), 172.3 (s, **C9**), 155.6 (s, **NCOO**), 79.5 (s, $\mathbf{C(CH_3)_3}$), 51.8 (s, $\mathbf{CO_2CH_3}$), 47.7 (d, **C7**), 39.3 (t, **C8**), 34.6 (t, **C6**), 34.1 (t, **C2**), 28.9 (t, **C4**), 28.5 (q, $\mathbf{C(CH_3)_3}$), 25.9 (t, **C5**), 24.7 (t, **C3**).

m/z (M+Na) calcd for $\mathbf{C_{15}H_{27}NO_5Na}$, 340.1730; found, 340.1723, $\mathbf{\Delta = -2.23\ ppm}$.

P3.- Chemoselective Reduction of Acid 46.

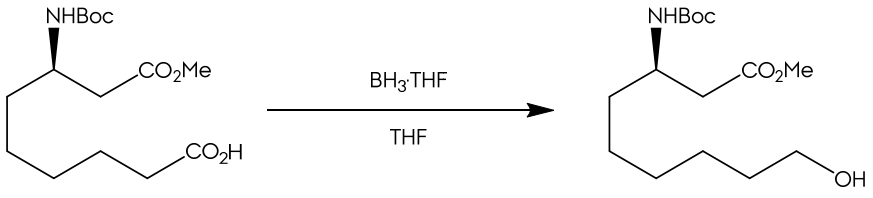

46 **47**

General procedure S was followed with the next quantities: 162 mg of 4**6** (317.1 g/mol; 0.511 mmol); 2.04 mL (4 equiv) of 1 M $BH_3 \cdot THF$ (85.9 g/mol, 2.04 mmol); 15 mL of THF. Reaction workup afforded 125 mg of alcohol **47**, 77 % yield.

Methyl (*R*)-3-((tert-butoxycarbonyl)amino)-9-hydroxynonanoate (47)

$[\alpha]^{25}_{D}$ +16.6 (*c.* 1.04 in $CHCl_3$);

υ_{max} (neat)/cm^{-1} 3369 (O-H), 2927 (C-H), 1735 (C=O, ester), 1691 (C=O, carbamate), 1162 (C-O).

δ_H (400 MHz, $CDCl_3$) 4.90 (1H, **NH**), 3.91 (1H, **H3**), 3.69 (3H, s, $\mathbf{CO_2C\underline{H_3}}$), 3.65 (2H, t, *J* 6.6, **H9**), 2.52 (2H, m, **H2**), 1.56 - 1.30 (10H, **H4**, **H5**, **H6**, **H7** and **H8**), 1.44 (9H, s, $\mathbf{C(C\underline{H_3})_3}$).

δ_C (50 MHz, $CDCl_3$) 172.3 (s, **C1**), 155.6 (s, $\mathbf{N\underline{C}OO}$), 79.4 (s, $\mathbf{\underline{C}(CH_3)_3}$), 62.8 (t, **C9**), 51.8 (s, $\mathbf{CO_2\underline{C}H_3}$), 47.7 (d, **C3**), 39.4 (t, **C2**), 34.6 (t, **C4**), 32.7 (t, **C8**), 29.1 (t, **C6**), 28.5 (q, $\mathbf{C(\underline{C}H_3)_3}$), 26.1 (t, **C7**), 25.7 (t, **C5**).

m/z (M+Na) calcd for $\mathbf{C_{15}H_{29}NO_5Na}$, 326.1937; found, 326.1942, $\mathbf{\Delta = 1.24\ ppm}$.

P4.- Chemoselective Reduction of Acid 46.

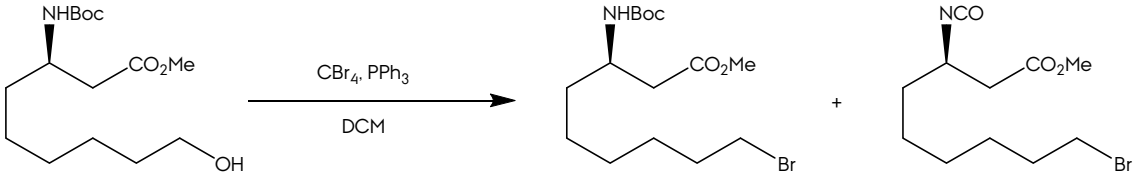

47 **48** **49**

General procedure V was followed with the next quantities: 125 mg of **47** (303.2 g/mol, 0.413 mmol); 164 mg of CBr_4 (331.6 g/mol, 0.495 mmol); 129 mg of PPh_3 (262.2 g/mol, 0.495 mmol); 3 mL of dry DCM. Flash chromatography afforded 122

mg of bromide **48** (Hexanes/AcOEt 9:1, 81 % yield), and 1 mg of isocyanate **49** (Hexanes/AcOEt 9:1, 4 % yield).

Methyl (*R*)-9-bromo-3-((tert-butoxycarbonyl)amino)nonanoate (48)

$\mathbf{R}_f$ 0.85 (Hexanes/AcOEt, 7:3)

$[\alpha]^{25}_D$ +5.24 (*c.* 0.91 in $CHCl_3$);

υ_{max} (neat)/cm^{-1} 3365 (N-H), 2931 (C-H), 1735 (C=O, ester), 1691 (C=O, carbamate), 873 (C-Br).

δ_H (400 MHz, $CDCl_3$) 4.91 (1H, d, *J* 8.8, **NH**), 3.89 (1H, **H3**), 3.68 (3H, s, **$CO_2C\underline{H}_3$**), 3.40 (2H, t, *J* 6.8, **H9**), 2.51 (2H, m, **H2**), 1.84 (2H, quintet, *J* 6.9, **H8**), 1.57 - 1.32 (8H, **H4**, **H5**, **H6** and **H7**), 1.43 (9H, s, **$C(C\underline{H}_3)_3$**).

δ_C (50 MHz, $CDCl_3$) 172.3 (s, **C1**), 155.6 (s, **$N\underline{C}OO$**), 79.5 (s, **$\underline{C}(CH_3)_3$**), 51.8 (s, **$CO_2\underline{C}H_3$**), 47.7 (d, **C3**), 39.3 (t, **C2**), 34.7 (t, **C4**), 34.0 (t, **C9**), 32.8 (t, **C8**), 29.9 (t, **C7**), 28.6 (q, **$C(\underline{C}H_3)_3$**), 28.2 (t, **C6**), 26.1 (t, **C5**).

m/z (M+Na) calcd for **$C_{15}H_{28}NO_4NaBr$**, 388.1093; found, 388.1085, **Δ = -2.29 ppm**.

Methyl (*R*)-9-bromo-3-isocyanatenonanoate (49)

$\mathbf{R}_f$ 0.75 (Hexanes/AcOEt, 7:3)

υ_{max} (neat)/cm^{-1} 3347, 2929 (C-H), 2264 (N=C=O), 1739 (C=O, ester), 1093 (C-O).

δ_H (200 MHz, $CDCl_3$) 3.94 (1H, quintet, *J* 6.4, **H3**), 3.73 (3H, s, **$CO_2C\underline{H}_3$**), 3.41 (2H, t, *J* 6.4, **H9**), 2.53 (2H, d, *J* 12.4, **H2**), 1.86 (2H, **H8**), 1.54 - 1.25 (8H, **H4**, **H5**, **H6** and **H7**).

m/z (M+MeOH+Na) calcd for **$C_{12}H_{22}NO_4NaBr$**, 346.0618; found, 346.0621, **Δ = -0.98 ppm**.

P5.- Thymine Introduction in Bromide 48.

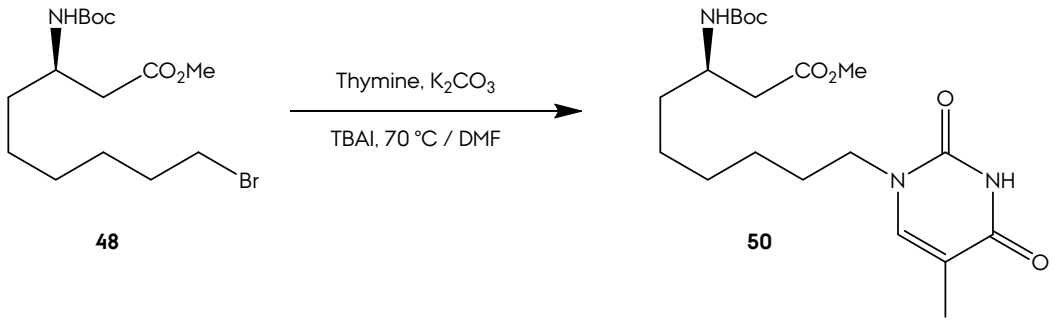

48 **50**

General procedure X was followed with the next quantities: 17 mg of bromide **48** (366.7 g/mol; 0.04 mmol); 108 mg of thymine (CAS: 65-71-4, white powder, 126.1 g/mol, 0.861 mmol, commercial); 34 mg of TBAI (396.3 g/mol, 0.086 mmol); 59 mg of K_2CO_3 (138.2 g/mol, 0.431 mmol); 5 mL of dry DMF. Flash chromatography afforded 122 mg of PNA monomer **50** (Hexanes/Ether 1:4), 38 % yield.

Methyl (R)-3-((tert-butoxycarbonyl)amino)-9-(thiminyl)nonanoate (50)

$\mathbf{R}_f$ 0.32 (Hexanes/AcOEt, 2:8)

$[\alpha]^{25}_{D}$ +7.23 (*c.* 0.94 in $CHCl_3$);

υ_{max} (neat)/cm^{-1} 3322 (N-H), 2925 (C-H), 1685 (C=O), 1384, 1093 (C-O).

δ_H (400 MHz, $CDCl_3$) 8.23 (1H, br s, **NH**), 6.97 (1H, s, **NCH**), 4.92 (1H, d, *J* 8.8, **OOCNH**), 3.89 (1H, **H3**), 3.68 (3H, s, **$CO_2C\underline{H}_3$**), 3.68 - 3.65 (2H, **H9**), 2.51 (2H, m, **H2**), 1.92 (3H, **$CC\underline{H}_3$**), 1.68 - 1.30 (10H, **H4**, **H5**, **H6**, **H7** and **H8**), 1.43 (9H, s, **$C(C\underline{H}_3)_3$**).

δ_C (50 MHz, $CDCl_3$) 172.3 (s, **C1**), 164.3 (s, **$\underline{C}ONH$**), 155.6 (s, **$N\underline{C}OO$**), 150.9 (s, **$HN\underline{C}ON$**), 140.6 (d, **$N\underline{C}H$**), 110.7 (s, **$\underline{C}CH_3$**), 79.5 (s, **$\underline{C}(CH_3)_3$**), 51.8 (t, **C9**), 48.7 (s, **$CO_2\underline{C}H_3$**), 47.5 (d, **C3**), 39.4 (t, **C2**), 34.7 (t, **C4**), 32.1 (t, **C8**), 29.9 (q, **$C(\underline{C}H_3)_3$**), 28.9 (t, **C7**), 28.6 (t, **C6**), 26.1 (t, **C5**), 12.5 (q, **$C\underline{C}H_3$**).

m/z (M+Na) calcd for **$C_{20}H_{33}N_3O_6Na$**, 434.2261; found, 434.2260, **Δ = -0.36 ppm**.

P6.- Esterification of Acid 45.

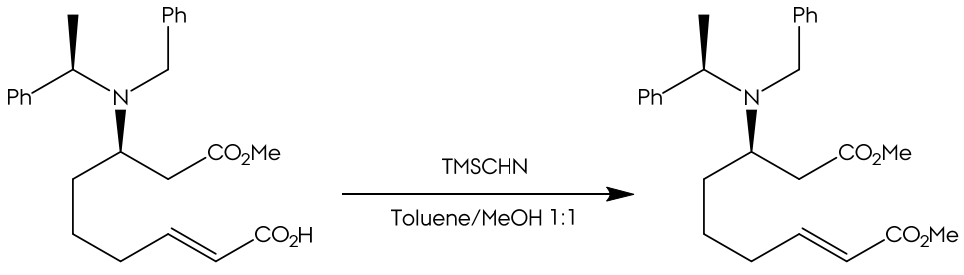

45 **51**

General procedure J was followed with the next quantities: 529 mg of **45** (410 g/mol; 1.29 mmol); 20 mL of tolune/MeOH 1:1; 0.97 mL (1.5 equiv) of $TMSCHN_2$ (114.22 g/mol, 1.935 mmol). Reaction workup afforded 508 mg of product **51**, 93 % yield.

Dimethyl (*R*,*E*)-7-(benzyl((*R*)-1-phenylethyl)amino)non-2-enedioate (51)

$\mathbf{R}_f$ 0.85 (Hexanes/AcOEt, 1:1)

$\boldsymbol{\delta}_{\mathbf{H}}$ (200 MHz, $CDCl_3$) 7.41 – 6.93 (10H, $\mathbf{C_{ar}\underline{H}}$), 6.97 (1H, dt, *J* 15.6 6.8, **H3**), 5.83 (1H, dt, *J* 15.6 1.4, **H2**), 3.89 - 3.81 (2H, $\mathbf{C\underline{H}CH_3}$ and $\mathbf{NC\underline{H_A}H}$), 3.76 - 3.72 (4H, $\mathbf{CHCO_2C\underline{H_3}}$ and $\mathbf{NCH\underline{H_B}}$), 3.56 (3H, s, $\mathbf{CH_2CO_2C\underline{H_3}}$), 3.33 (1H, m, **H7**), 2.17 - 2.00 (6H, **H4, H6** and **H8**), 1.53 (2H, **H5**), 1.34 (3H, d, *J* 7.1, $\mathbf{CHC\underline{H_3}}$).

m/z (M+H) calcd for $\mathbf{C_{26}H_{34}NO_4}$, 424.2487; found, 424.2475, $\boldsymbol{\Delta}$ **= 2.83 ppm**. (M+Na) calcd for $\mathbf{C_{26}H_{33}NO_4Na}$, 446.2307; found, 446.2287, $\boldsymbol{\Delta}$ **= 4.48 ppm**.

P7.- Oxidative Ozonolysis of 51.

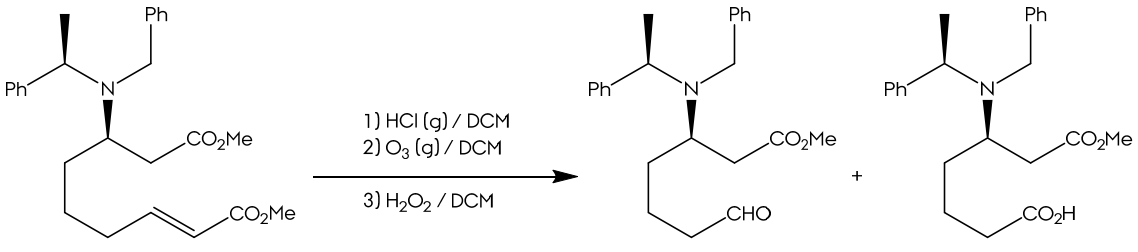

51 **52** **53**

General procedure P was followed with the next quantities: 287 mg of **51** (424.4 g/mol; 0.68 mmol); 1.5 mL (20 equiv) of H_2O_2 (34.0 g/mol, 13.6 mmol); 5 mL of

DCM. Flash chromatography afforded 72 mg of aldehyde **52** (Hexanes/AcOEt 9:1, 29 % yield), and 80 mg of acid **53** (Hexanes/AcOEt 7:3, 31 % yield).

Methyl (*R*)-3-(benzyl((*R*)-1-phenylethyl)amino)-7-oxoheptanoate (52)

$\mathbf{R}_f$ 0.83 (Hexanes/AcOEt, 1:1)

$[\alpha]^{26}_{D}$ +12.5 (*c.* 0.4 in $CHCl_3$);

υ_{max} (neat)/cm^{-1} 2933 (C-H), 1734 (C=O, ester), 1701 (C=O, acid), 1201 (C-O), 1155.

δ_H (200 MHz, $CDCl_3$) 9.73 (1H, t, *J* 1.6, **H7**), 7.46 - 7.26 (10H, $\mathbf{C_{ar}\underline{H}}$), 3.90 - 3.70 (2H, $\mathbf{C\underline{H}CH_3}$ and $\mathbf{NC\underline{H_A}H}$), 3.59 - 3.52 (4H, $\mathbf{NCH\underline{H_B}}$ and $\mathbf{CO_2C\underline{H_3}}$), 3.33 (1H, m, **H5**), 2.33 (2H, td, *J* 7.1 1.6, **H6**), 2.08 - 1.92 (2H, **H2**), 1.67 - 1.47 (4H, **H3** and **H4**), 1.36 (3H, d, *J* 6.9, $\mathbf{CHC\underline{H_3}}$).

m/z (M+Na) calcd for $\mathbf{C_{23}H_{29}NO_3Na}$, 390.2045; found, 390.2039, **Δ = 1.54 ppm**.

(*R*)-5-(benzyl((*R*)-1-phenylethyl)amino)-7-methoxy-7-oxoheptanoic acid (53)

$\mathbf{R}_f$ 0.54 (Hexanes/AcOEt, 1:1)

$[\alpha]^{20}_{D}$ +2.1 (*c.* 3.36 in $CHCl_3$);

υ_{max} (neat)/cm^{-1} 2933 (C-H), 1734 (C=O, ester), 1701 (C=O, acid), 1201 (C-O), 1155.

δ_H (400 MHz, $CDCl_3$) 7.44 - 7.22 (10H, $\mathbf{C_{ar}\underline{H}}$), 3.84 (1H, q, *J* 6.9, $\mathbf{C\underline{H}CH_3}$), 3.78 (1H, AB, *J* 14.6, $\mathbf{NC\underline{H_A}H}$), 3.57 - 3.53 (4H, $\mathbf{NCH\underline{H_B}}$ and $\mathbf{CO_2C\underline{H_3}}$), 3.33 (1H, m, **H5**), 2.29 (2H, m, **H6**), 2.08 - 1.92 (2H, **H2**), 1.74 - 1.53 (4H, **H3** and **H4**), 1.36 (3H, d, *J* 6.9, $\mathbf{CHC\underline{H_3}}$).

δ_C (100 MHz, $CDCl_3$) 179.3 (s, **COOH**), 173.1 (s, $\mathbf{\underline{C}O_2CH_3}$), 142.8 (s, $\mathbf{C_{ipso}}$), 141.3 (s, $\mathbf{C_{ipso}}$), 128.2 (d, $\mathbf{C_{ar}}$), 128.2 (d, $\mathbf{C_{ar}}$), 128.1 (d, $\mathbf{C_{ar}}$), 127.8 (d, $\mathbf{C_{ar}}$), 126.9 (d, $\mathbf{C_{ar}}$), 126.7 (d, $\mathbf{C_{ar}}$), 57.7 (d, $\mathbf{\underline{C}HCH_3}$), 53.5 (d, **C5**), 51.4 (q, $\mathbf{CO_2\underline{C}H_3}$), 49.9 (t, $\mathbf{N\underline{C}H_2}$), 36.3 (t, **C6**), 33.8 (t, **C2**), 32.8 (t, **C4**), 22.1 (t, **C3**), 19.6 (q, $\mathbf{CH\underline{C}H_3}$).

m/z (M+H) calcd for $\mathbf{C_{23}H_{30}NO_4}$, 384.2096; found, 384.2090, **Δ = 1.56 ppm**.

P8.- Esterification of Acid 53 to *tert*-Butyl Ester 54 (1).

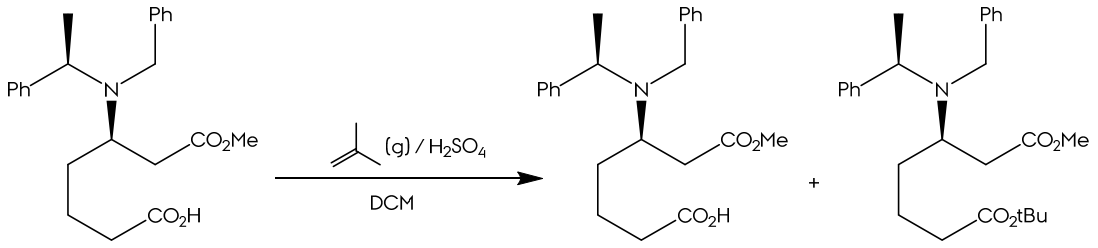

53 **53** **54**

In a Schlenk type flask, 24 mg of **53** (383.7 g/mol. 0.063 mmol) were dissolved in 5 mL of DCM. A few drops of conc. H_2SO_4 were added and the reaction was cooled to -78 ºC in an CO_2 - acetone bath. Isobutylene (2-methylpropene, CAS: 115-11-7, gas, 56.1 g/mol, commercial) was bubbled for 2 min and the reaction was magnetically stirred for 1 h at -78 ºC. Afterwards, the reaction was stirred at room temperature for 20 h.

20 mL of dry DCM were added and the organic solution was washed with sat $NaHCO_3$ (1 time) and brine (1 time). Drying the solution with anhydrous Na_2SO_4, filtration and forward solvent removal afforded 6 mg of starting acid **53**. The washing fractions were neutralized with 1 M HCl and extracted with AcOEt. Drying the ethyl acetate solution with anhydrous Na_2SO_4, filtration and forward solvent removal leaded to obtain 13 mg of ester **54**, 46% yield.

7-(*tert*-butyl) 1-methyl (*R*)-3-(benzyl((*R*)-1-phenylethyl)amino)heptanedioate (54)

$\mathbf{R}_f$ 0.83 (Hexanes/AcOEt, 1:1)

$[\alpha]^{20}_D$ +9.8 (*c.* 0.6 in $CHCl_3$);

υ_{max} (neat)/cm^{-1} 2974 (C-H), 1730 (C=O), 1450, 1367, 1151 (C-O).

δ_H (400 MHz, $CDCl_3$) 7.44 - 7.24 (10H, $\mathbf{C_{ar}\underline{H}}$), 3.86 (1H, q, *J* 7.0, $\mathbf{C\underline{H}CH_3}$), 3.80 (1H, AB, *J* 14.7, $\mathbf{NC\underline{H}_A H}$), 3.57 (1H, AB, *J* 14.7, $\mathbf{NCH\underline{H}_B}$), 3.55 (3H, s, $\mathbf{CO_2C\underline{H}_3}$), 3.36 – 3.30 (1H, m, **H3**), 2.17 (2H, td, *J* 7.0 and 1.9, **H2**), 2.05 (2H, t, *J* 7.9, **H6**), 1.69 - 1.51 (4H, **H4** and **H5**), 1.46 (9H, s, $\mathbf{CO_2C(C\underline{H}_3)_3}$), 1.37 (3H, d, *J* 7.0, $\mathbf{CHC\underline{H}_3}$).

δ_C (50 MHz, $CDCl_3$) 173.3 (s, **C7**), 173.2 (s, **C1**), 143.1 (s, **C_{ipso}**), 141.6 (s, **C_{ipso}**), 128.5 (d, **C_{ar}**), 128.3 (d, **C_{ar}**), 127.1 (d, **C_{ar}**), 126.9 (d, **C_{ar}**), 80.1 (s, **$\underline{C}(CH_3)_3$**), 57.8 (d, **$\underline{C}HCH_3$**), 53.8 (d, **C3**), 51.6 (q, **$CO_2\underline{C}H_3$**), 50.1 (t, **$N\underline{C}H_2$**), 36.7 (t, **C2**), 35.7 (t, **C6**), 33.0 (t, **C4**), 28.3 (q, **$C(\underline{C}H_3)_3$**), 22.9 (q, **$CH\underline{C}H_3$**), 19.6 (t, **C5**).

m/z (M+H) calcd for **$C_{27}H_{38}NO_4$**, 440.2795; found, 440.2805, **Δ = 2.19 ppm**.

P9.- Esterification of Acid 53 to *tert*-Butyl Ester 54 (2).

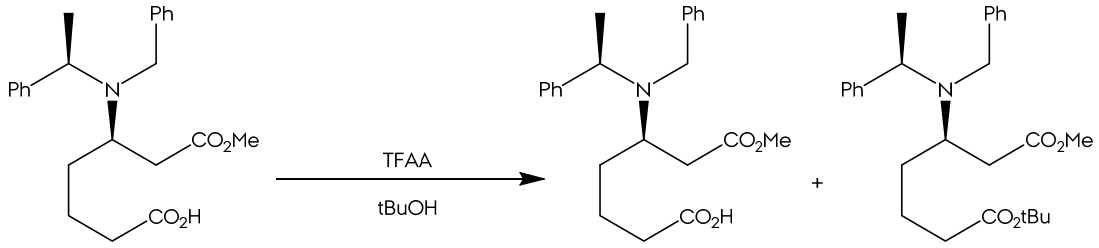

53 **53** **54**

In a round bottom flask, 47 mg of acid **53** (383.7 g/mol. 0.122 mmol) were dissolved in 1 mL of TFAA (trifluoroacetic anhydride, CAS: 407-25-0, liquid, 210.0 g/mol, commercial). The flask was sealed, purged with Ar and magnetically stirred for 1 h. 1 mL of tBuOH was added and stirring at room temperature for 12 h.

5 mL of water were added and reaction mixture was extracted with AcOEt (3 times). The organic layers were combined and washed with 10 % $NaHCO_3$ (3 times), water (3 times) and brine (1 time). Drying the solution with anhydrous Na_2SO_4, filtration and forward solvent removal afforded 37 mg of starting acid **53**. The washing fractions were netutralized with 1 M HCl and extracted with DCM. Drying the DCM solution with anhydrous Na_2SO_4, filtration and forward solvent removal leaded to obtain 10 mg of ester **54**, 20% yield.

P10.- Esterification of Acid 53 to *tert*-Butyl Ester 54 (3).

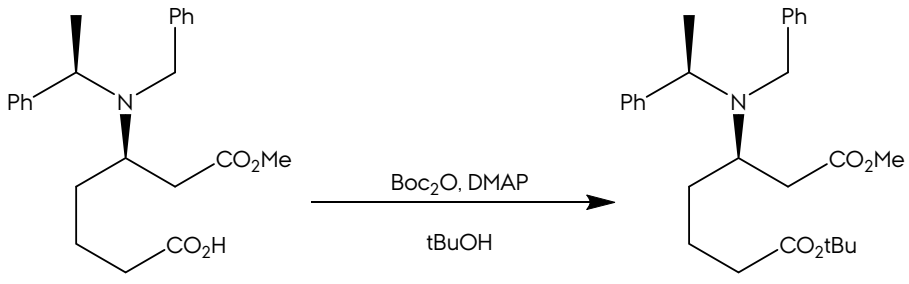

53 **54**

General procedure I was followed with the next quantities: 2.128 g of **51** (383.7 g/mol; 5.55 mmol); 2.6 g of Boc_2O (218.2 g/mol, 11.7 mmol); 204 mg of DMAP (122.1 g/mol, 1.665 mmol); 20 mL of tBuOH. Flash chromatography afforded 1.509 g of ester **54** (Hexanes/AcOEt 95:5, 62 % yield).

P11.- Synthesis of methyl (*E*)-7-hydroxyhept-2-enoate from δ-valerolactone.

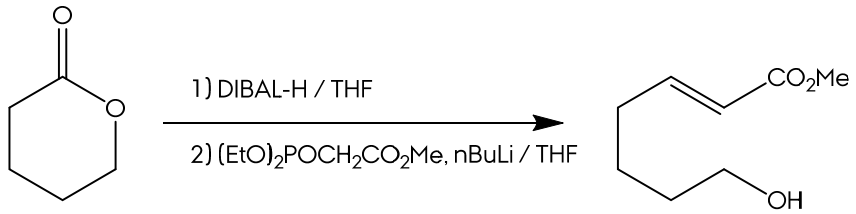

55 **56**

General procedure N was followed with the next quantities: 3.0 g of **55** (100.0 g/mol; 30 mmol) in 10 mL of dry THF; 24 mL of 1.5 M DIBAL-H in toluene (142.2 g/mol, 36 mmol); 7.56 g of methyl diethylphosphonoacetate (CAS: 1067-74-9, liquid, 210.1 g/mol, commercial solution, 0.036 mmol) in 24 mL of dry THF; 22.5 mL of 1.6 M nBuLi in hexanes (64.0 g/mol, 45 mmol). Flash chromatography afforded 1.509 g of ester **56** (Hexanes/AcOEt 98:2, 64 % yield).

Methyl (*E*)-7-hydroxyhept-2-enoate (56)

$\mathbf{R}_f$ 0.46 (Hexanes/AcOEt, 1:1)

υ_{max} (neat)/cm^{-1} 3367 (O-H), 2937 (C-H), 1718 (C=O), 1436, 1201 (C-O).

δ_H (200 MHz, $CDCl_3$) 6.95 (1H, dt, *J* 15.5 and 6.8, **H3**), 5.81 (1H, d, *J* 15.7, **H2**), 3.70 (1H, s, $\mathbf{CO_2C\underline{H}_3}$), 3.63 (2H, t, *J* 5.7, **H7**), 2.22 (2H, q, *J* 6.7, **H4**), 1.87 (1H, br s, **O<u>H</u>**), 1.60 - 1.52 (4H, **H5** and **H6**).

δ_C (50 MHz, $CDCl_3$) 167.3 (s, **C1**), 149.5 (d, **C3**), 121.2 (d, **C2**), 62.4 (t, **C7**), 51.6 (s, $\mathbf{CO_2\underline{C}H_3}$), 32.2 (t, **C6**), 32.0 (t, **C4**), 24.4 (t, **C5**).

m/z (M+Na) calcd for $\mathbf{C_{10}H_{14}O_3Na}$, 181.0835; found, 181.0845, $\mathbf{\Delta = 5.43\ ppm}$.

P12.- Synthesis of methyl (*E*)-7-hydroxyhept-2-enoate from 3,4-dihydro-2*H*-pyran.

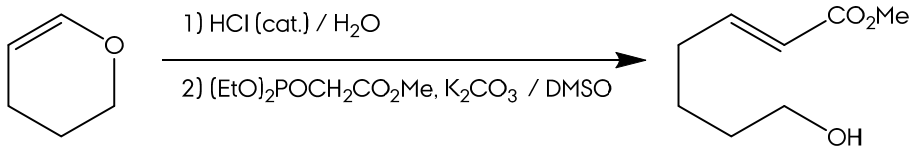

57 **56**

General procedure O was followed with the next quantities: 3.84 g of **57** (84.0 g/mol; 46 mmol) in 5 mL of water; 0.4 mL of 1 M HCl; 11.6 g of methyl diethylphosphonoacetate (CAS: 1067-74-9, liquid, 210.1 g/mol, commercial solution, 0.055 mmol); 7.62 g of K_2CO_3 (138.2 g/mol, 0.055 mmol); 16 mL of DMSO. Flash chromatography afforded 4.868 g of ester **56** (Hexanes/AcOEt 98:2, 68 % yield).

P13.- Oxidation of Alcohol 56 to Acid 58.

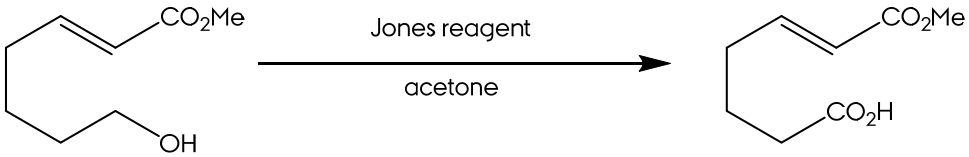

56 **58**

General procedure Q was followed with the next quantities: 29 mg of **56** (158.0 g/mol; 0.18 mmol) in 5 mL of acetone. Reaction workup afforded 26 mg of acid **58**, 85 % yield.

(*E*)-7-methoxy-7-oxohept-5-enoic acid (58)

R$_f$ 0.63 (Hexanes/AcOEt, 4:1)

δ$_H$ (200 MHz, $CDCl_3$) 11.1 (1H, br s, **COOH**), 6.85 (1H, dt, *J* 15.6 and 6.9, **H5**), 5.81 (1H, d, *J* 15.7, **H6**), 3.62 (1H, s, **CO_2CH_3**), 2.29 (2H, t, *J* 7.3, **H2**), 2.18 (2H, q, *J* 7.5, **H4**), 1.71 (2H, quintet, *J* 7.3, **H3**).

δ$_C$ (50 MHz, $CDCl_3$) 178.8 (s, **C1**), 167.1 (s, **C7**), 148.2 (d, **C5**), 121.8 (d, **C6**), 51.6 (s, **CO_2CH_3**), 33.2 (t, **C2**), 31.3 (t, **C4**), 23.0 (t, **C3**).

m/z (M+Na) calcd for **$C_{10}H_{14}O_3Na$**, 181.0835; found, 181.0845, **Δ = 5.43 ppm**.

P14.- Esterification of Acid 58 to *tert*-Butyl Ester.

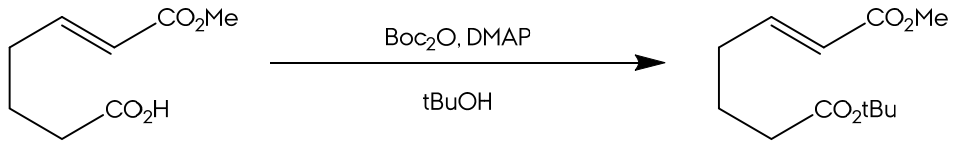

58 **59**

General procedure I was followed with the next quantities: 188 mg of **58** (172.0 g/mol; 1.09 mmol); 478 mg of Boc_2O (218.2 g/mol, 2.2 mmol); 40 mg of DMAP (122.1 g/mol, 0.33 mmol); 5 mL of tBuOH. Flash chromatography afforded 1.509 g of ester **54** (Hexanes/AcOEt 95:5, 88 % yield).

7-(*tert*-butyl) 1-methyl (*E*)-hept-2-enedioate (59)

R$_f$ 0.88 (Hexanes/AcOEt, 1:1)

υ$_{max}$ (neat)/cm^{-1} 2978 (C-H), 1716 (C=O), 1658, 1147 (C-O), 848.

δ$_H$ (400 MHz, $CDCl_3$) 6.85 (1H, dt, *J* 15.5 and 6.9, **H3**), 5.75 (1H, dt, *J* 15.5 and 1.6, **H2**), 3.63 (1H, s, **CO_2CH_3**), 2.15 (2H, m, **H4** and **H6**), 1.67 (2H, quintet, *J* 7.7, **H5**), 1.35 (9H, s, **$C(CH_3)_3$**).

δ$_C$ (50 MHz, $CDCl_3$) 172.4 (s, **C7**), 166.9 (s, **C1**), 148.4 (d, **C3**), 121.7 (d, **C2**), 80.3 (s, **$C(CH_3)_3$**) 51.4 (s, **CO_2CH_3**), 34.7 (t, **C6**), 31.5 (t, **C4**), 28.2 (q, **$C(CH_3)_3$**), 23.5 (t, **C5**).

m/z (M+Na) calcd for $\mathbf{C_{12}H_{20}O_4Na}$, 251.1253; found, 251.1246, **Δ = -3.11 ppm**.

P15.- Asymmetric Michael Addition of Lithium (*R*)-*N*-benzyl-*N*-α-methylbenzylamide to 59.

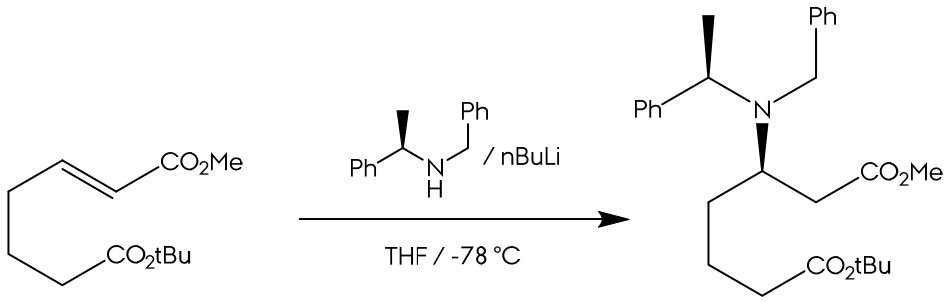

59 **54**

General procedure C was followed with the next quantities: 456 mg of (*R*)-*N*-benzyl-*N*-α-methylbenzylamide (211.3 g/mol; 2.16 mmol) in 4 mL of THF; 1.3 mL of 1.6 M nBuLi in hexanes (64.06 g/mol; 2.04 mmol); 137 mg of substrate **59** (228 g/mol; 0.6 mmol) in 4 mL of THF. Flash chromatography afforded 60 mg of product **54** (Hexanes/AcOEt 9:1), 23 % yield.

P16.- Synthesis of *iso*-propyl (*E*)-7-hydroxyhept-2-enoate from δ-valerolactone.

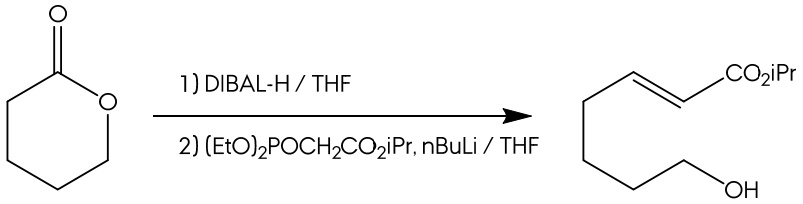

55 **60**

General procedure N was followed with the next quantities: 1.5 g of **55** (100.0 g/mol; 15 mmol) in 12 mL of dry THF; 12 mL of 1.5 M DIBAL-H in toluene (142.2 g/mol, 18 mmol); 4.29 g of *iso*-propyl diethylphosphonoacetate (prepared at lab, see laboratory prepared reagents, 238.1 g/mol, 18 mmol) in 5 mL of dry THF; 14 mL of 1.6 M nBuLi in hexanes (64.0 g/mol, 23 mmol). Flash chromatography afforded 1.762 g of ester **60** (Hexanes/AcOEt 95:5, 63 % yield).

Isopropyl (*E*)-7-hydroxyhept-2-enoate (60)

$\mathbf{R}_f$ 0.39 (Hexanes/AcOEt, 1:1)

υ_{max} (neat)/cm^{-1} 3412 (O-H), 2935 (C-H), 1716 (C=O), 1653, 1273.

δ_H (200 MHz, $CDCl_3$) 6.91 (1H, dt, *J* 15.6 and 6.9, **H3**), 5.77 (1H, d, *J* 15.6, **H2**), 5.02 (1H, septet, *J* 6.2, **C<u>H</u>(CH$_3$)$_2$**), 3.61 (2H, t, *J* 5.2, **H7**), 2.20 (2H, q, *J* 6.9, **H4**), 1.86 (1H, br s, **O<u>H</u>**), 1.51 - 1.56 (4H, **H5** and **H6**), 1.22 (6H, d, *J* 6.2, **CH(C<u>H</u>$_3$)$_2$**).

δ_C (50 MHz, $CDCl_3$) 166.5 (s, **C1**), 148.9 (d, **C3**), 122.0 (d, **C2**), 67.6 (d, **<u>C</u>H(CH$_3$)$_2$**), 62.1 (t, **C7**), 32.1 (t, **C6**), 31.9 (t, **C4**), 24.4 (t, **C5**), 21.9 (q, **CH(<u>C</u>H$_3$)$_2$**).

m/z (M+Na) calcd for **$C_{10}H_{18}O_3Na$**, 209.1148; found, 209.1158, **Δ = 4.70 ppm**.

P17.- Oxidation of Alcohol 60 to Acid 61.

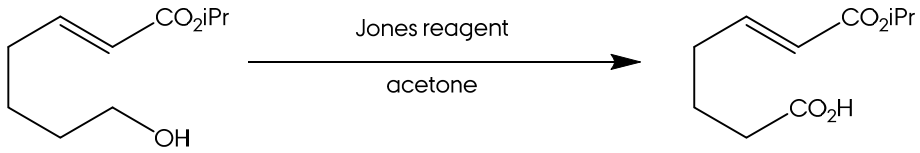

60 **61**

General procedure Q was followed with the next quantities: 1.762 g of **60** (186.0 g/mol; 9.4 mmol) in 10 mL of acetone. Reaction workup afforded 1.577 g of acid **61**, 97 % yield.

(*E*)-7-isopropoxy-7-oxohept-5-enoic acid (61)

$\mathbf{R}_f$ 0.76 (Hexanes/AcOEt, 1:1)

υ_{max} (neat)/cm^{-1} 3190 (O-H), 2981 (C-H), 1701 (C=O), 1647 (C=O), 1406, 1170 (C-O).

δ_H (200 MHz, $CDCl_3$) 6.87 (1H, dt, *J* 15.8 and 6.8, **H5**), 5.78 (1H, d, *J* 15.7, **H6**), 5.01 (1H, septet, *J* 6.4, **C<u>H</u>(CH$_3$)$_2$**), 2.35 (2H, t, *J* 7.5, **H2**), 2.23 (2H, q, *J* 7.0, **H4**), 1.77 (2H, quintet, *J* 7.3, **H3**), 1.22 (6H, d, *J* 6.4, **CH(C<u>H</u>$_3$)$_2$**).

δ_C (50 MHz, $CDCl_3$) 179.2 (s, **C1**), 166.3 (s, **C7**), 147.5 (d, **C5**), 122.8 (d, **C6**), 67.8 (d, **$\underline{C}H(CH_3)_2$**), 33.3 (t, **C2**), 31.3 (t, **C4**), 23.1 (t, **C3**), 22.0 (q, **$CH(\underline{C}H_3)_2$**).

m/z (M+Na) calcd for **$C_{10}H_{16}O_4Na$**, 223.0941; found, 223.0942, **Δ = 0.53 ppm**.

P18.- Esterification of Acid 61 to *tert*-Butyl Ester 62.

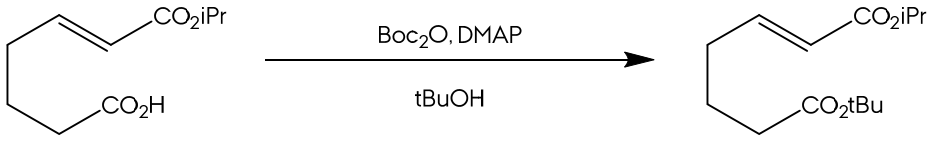

61 **62**

General procedure I was followed with the next quantities: 1.067 g of **61** (200.0 g/mol; 5.3 mmol); 2.4 g of Boc_2O (218.2 g/mol, 11 mmol); 195 mg of DMAP (122.1 g/mol, 1.6 mmol); 10 mL of tBuOH. Flash chromatography afforded 535 mg of ester **62** (Hexanes/AcOEt 99:1, 39 % yield).

7-(*tert*-butyl) 1-isopropyl (*E*)-hept-2-enedioate (62)

R_f 0.93 (Hexanes/AcOEt, 1:1)

υ_{max} (neat)/cm^{-1} 2980 (C-H), 1716 (C=O), 1654, 1145 (C-O), 1111.

δ_H (200 MHz, $CDCl_3$) 6.79 (1H, dt, *J* 15.7 and 7.0, **H3**), 5.69 (1H, dd, *J* 15.7 and 1.5, **H2**), 4.93 (1H, septet, *J* 6.3, **$C\underline{H}(CH_3)_2$**), 2.06-2.16 (4H, **H4** and **H6**), 1.60-1.71 (2H, **H5**), 1.33 (9H, s, **$C(C\underline{H}_3)_3$**), 1.14 (6H, d, *J* 6.3, **$CH(C\underline{H}_3)_2$**).

δ_C (50 MHz, $CDCl_3$) 172.3 (s, **C7**), 165.9 (s, **C1**), 147.6 (d, **C3**), 122.6 (d, **C2**), 80.2 (s, **$\underline{C}(CH_3)_3$**), 67.4 (d, **$\underline{C}H(CH_3)_2$**), 34.7 (t, **C6**), 31.4 (t, **C4**), 28.1 (q, **$C(\underline{C}H_3)_3$**), 23.5 (t, **C5**), 21.9 (q, **$CH(\underline{C}H_3)_2$**).

m/z (M+Na) calcd for **$C_{14}H_{24}O_4Na$**, 279.1566; found, 279.1566, **Δ = -0.28 ppm**.

P19.- Asymmetric Michael Addition of Lithium (*R*)-*N*-benzyl-*N*-α-methylbenzylamide to 62.

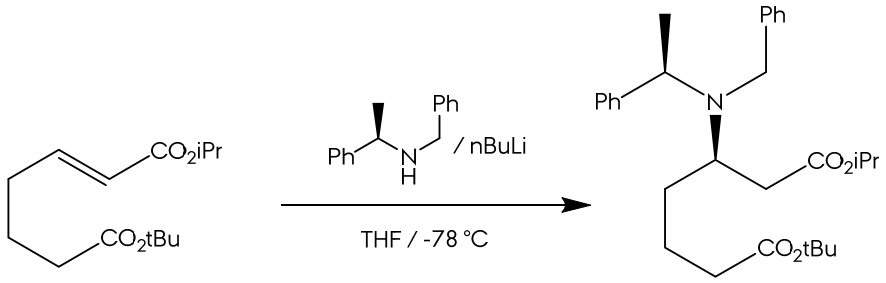

62 **63**

General procedure C was followed with the next quantities: 1.59 g of (*R*)-*N*-benzyl-*N*-α-methylbenzylamide (211.3 g/mol; 7.53 mmol) in 10 mL of THF; 4.4 mL of 1.6 M nBuLi in hexanes (64.0 g/mol; 7.11 mmol); 535 mg of substrate **62** (256.0 g/mol; 2.1 mmol) in 10 mL of THF. Flash chromatography afforded 138 mg of product **63** (Hexanes/AcOEt 99:1), 14 % yield. Diaddition products were also observed, but were difficult to separate.

7-(tert-butyl) 1-isopropyl (*R*)-3-(benzyl((*R*)-1-phenylethyl)amino)heptanedioate (63)

$\mathbf{R}_f$ 0.74 (Hexanes/AcOEt, 8:2)

$[\alpha]^{20}_D$ +6.37 (*c.* 1.24 in $CHCl_3$);

υ_{max} (neat)/cm^{-1} 2978 (C-H), 1724 (C=O), 1367, 1153 (C-O), 1109.

δ_H (400 MHz, $CDCl_3$) 7.45 - 7.20 (10H, $\mathbf{C_{ar}H}$), 4.91 (1H, septet, *J* 6.2, $\mathbf{CH(CH_3)_2}$), 3.83 (2H, q, *J* 7.0 , $\mathbf{CH(CH_3)}$), 3.80(1H, AB, *J* 14.8, $\mathbf{NCH_AH}$), 3.51 (1H, AB, *J* 14.8, $\mathbf{NCHH_B}$), 3.32 (1H, septet, *J* 4.3, **H3**), 2.13 (2H, td, *J* 7.6 and 2.9, **H2**), 2.03 - 1.89 (4H, **H5** and **H6**), 1.45 (9H, s, $\mathbf{C(CH_3)_3}$), 1.35 (3H, d, *J* 7.0, $\mathbf{CHCH_3}$), 1.31 - 1.21 (2H, **H4**), 1.17 (6H, d, *J* 6.2, $\mathbf{CH(CH_3)_2}$).

δ_C (50 MHz, $CDCl_3$) 173.2 (s, **C7**), 172.3 (s, **C1**), 143.0 (s, $\mathbf{C_{ipso}}$), 141.7 (s, $\mathbf{C_{ipso}}$), 128.4 (d, $\mathbf{C_{ar}}$), 128.0 (d, $\mathbf{C_{ar}}$), 127.2 (d, $\mathbf{C_{ar}}$), 126.8 (d, $\mathbf{C_{ar}}$), 80.1 (s, $\mathbf{C(CH_3)_3}$), 67.5 (d, $\mathbf{CH(CH_3)_2}$), 58.1 (d, $\mathbf{CHCH_3}$), 53.7 (d, **C3**), 50.1 (t, $\mathbf{NCH_2}$), 36.7 (t, **C2**), 35.5 (t, **C6**), 32.9 (t, **C4**), 28.2 (q, $\mathbf{C(CH_3)_3}$), 22.7 (t, **C5**), 21.8 (t, $\mathbf{CH(CH_3)_2}$), 20.3 (q, $\mathbf{CHCH_3}$).

m/z (M+H) calcd for $\mathbf{C_{29}H_{42}NO_4}$, 468.3108; found, 468.3100, **Δ = -1.78 ppm**.

P20.- Synthesis of 3-pentyl (*E*)-7-hydroxyhept-2-enoate from δ-valerolactone.

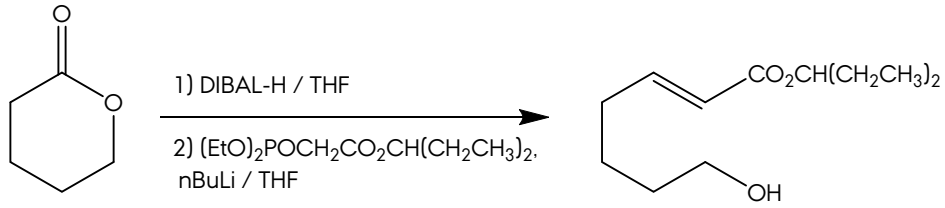

55 **64**

General procedure N was followed with the next quantities: 525 mg of **55** (100.0 g/mol; 5.25 mmol) in 12 mL of dry THF; 5.25 mL of 1.5 M DIBAL-H in toluene (142.2 g/mol, 6.30 mmol); 1.68 g of 3-pentyl diethylphosphonoacetate (prepared at lab, see laboratory prepared reagents, 266.1 g/mol, 6.30 mmol) in 5 mL of dry THF; 5.0 mL of 1.6 M nBuLi in hexanes (64.0 g/mol, 7.88 mmol). Flash chromatography afforded 629 mg of ester **64** (Hexanes/AcOEt 95:5, 56 % yield).

Pentan-3-yl (*E*)-7-hydroxyhept-2-enoate (64)

$\mathbf{R}_f$ 0.59 (Hexanes/AcOEt, 1:1)

υ_{max} (neat)/cm^{-1} 3412 (O-H), 2937 (C-H), 1716 (C=O), 1269 (C-O), 1031.

δ_H (200 MHz, $CDCl_3$) 6.87 (1H, dt, *J* 15.6 and 6.8, **H3**), 5.75 (1H, dt, *J* 15.6 and 1.5, **H2**), 4.72 (1H, quintet, *J* 6.3, $\mathbf{C\underline{H}(CH_2CH_3)_2}$), 3.55 (2H, t, *J* 5.9, **H7**), 2.66 (1H, **O<u>H</u>**), 2.15 (2H, q, *J* 7.1, **H4**), 1.57 - 1.43 (8H, **H5**, **H6** and $\mathbf{CH(C\underline{H_2}CH_3)_2}$), 0.80 (6H, t, *J* 7.0, $\mathbf{CH(CH_2C\underline{H_3})_2}$).

δ_C (50 MHz, $CDCl_3$) 166.8 (s, **<u>C</u>OO**), 148.8 (d, **C3**), 121.9 (d, **C2**), 76.6 (d, $\mathbf{\underline{C}H(CH_2CH_3)_2}$), 62.3 (t, **C7**), 32.2 (t, **C6**), 32.0 (t, **C4**), 26.6 (t, $\mathbf{CH(\underline{C}H_2CH_3)_2}$), 24.4 (t, **C5**), 9.7 (q, $\mathbf{CH(CH_2\underline{C}H_3)_2}$).

m/z (M+Na) calcd for $\mathbf{C_{12}H_{22}O_3Na}$, 279.1566; found, 279.1566, **Δ = -1.75 ppm**.

P21.- Oxidation of Alcohol 64 to Acid 65.

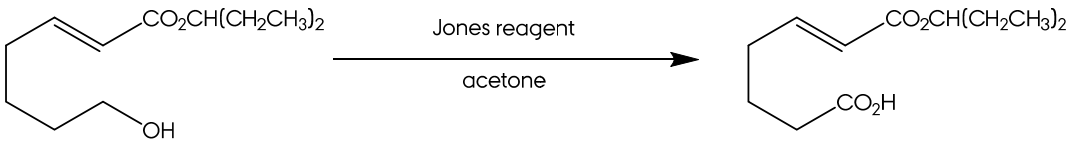

64 **65**

General procedure Q was followed with the next quantities: 969 mg of **64** (214.0 g/mol; 9.4 mmol) in 10 mL of acetone. Reaction workup afforded 1.04 g of acid **65**, 99 % yield.

(*E*)-7-oxo-7-(pentan-3-yloxy)hept-5-enoic acid (65)

R$_f$ 0.72 (Hexanes/AcOEt, 1:1)

δ$_H$ (200 MHz, $CDCl_3$) 6.92 (1H, dt, *J* 16.0 and 6.0, **H5**), 5.85 (1H, dt, *J* 15.6 and 2.0, **H6**), 4.14 (1H, quintet, *J* 7.1, **C<u>H</u>(CH$_2$CH$_3$)$_2$**), 2.39 (2H, t, *J* 7.3, **H2**), 2.25 (2H, q, *J* 7.5, **H4**), 1.82 (2H, quintet, *J* 6.8, **H3**), 1.58 (4H, m, **CH(C<u>H$_2$</u>CH$_3$)$_2$**), 0.80 (6H, t, *J* 7.3, **CH(CH$_2$C<u>H$_3$</u>)$_2$**).

δ$_C$ (50 MHz, $CDCl_3$) 177.7 (s, **C1**), 166.5 (s, **C7**), 147.5 (d, **C5**), 122.4 (d, **C6**), 76.5 (d, **<u>C</u>H(CH$_2$CH$_3$)$_2$**), 33.2 (t, **C2**), 31.3 (t, **C4**), 26.5 (t, **CH(<u>C</u>H$_2$CH$_3$)$_2$**), 23.1 (t, **C3**), 9.6 (q, **CH(CH$_2$<u>C</u>H$_3$)$_2$**).

m/z (M+Na) calcd for **$C_{12}H_{20}O_4Na$**, 251.1253; found, 251.1249, **Δ = -1.91 ppm**.

P22.- Esterification of Acid 65 to *tert*-Butyl Ester 66.

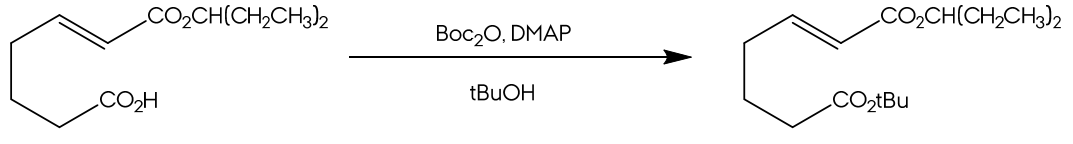

65 **66**

General procedure I was followed with the next quantities: 1.04 g of **65** (228.0 g/mol; 4.5 mmol); 2.0 g of Boc_2O (218.2 g/mol, 9.1 mmol); 167 mg of DMAP (122.1 g/mol, 1.4 mmol); 10 mL of tBuOH. Flash chromatography afforded 544 mg of ester **66** (Hexanes/AcOEt 99:1, 42 % yield).

7-(*tert*-butyl) 1-(pentan-3-yl) (*E*)-hept-2-enedioate (66)

$\mathbf{R}_f$ 0.93 (Hexanes/AcOEt, 1:1)

υ_{max} (neat)/cm^{-1} 2970 (C-H), 1718 (C=O), 1458, 1228, 1147 (C-O).

δ_H (200 MHz, $CDCl_3$) 6.84 (1H, dt, *J* 15.5 and 7.6, **H3**), 5.75 (1H, d, *J* 15.6, **H2**), 4.73 (1H, quintet, *J* 6.1, $\mathbf{C\underline{H}(CH_2CH_3)_2}$), 2.21 - 2.09 (4H, **H4** and **H6**), 1.68 (2H, quintet, *J* 7.5, **H4**), 1.50 (4H, $\mathbf{CH(C\underline{H_2}CH_3)_2}$), 1.36 (9H, s, $\mathbf{C(C\underline{H_3})_3}$), 0.80 (6H, t, *J* 7.3, $\mathbf{CH(CH_2C\underline{H_3})_2}$).

δ_C (50 MHz, $CDCl_3$) 172.5 (s, **C7**), 166.5 (s, **C1**), 147.7 (d, **C3**), 122.4 (d, **C2**), 80.3 (s, $\mathbf{\underline{C}(CH_3)_3}$), 76.5 (d, $\mathbf{\underline{C}H(CH_2CH_3)_2}$), 34.8 (t, **C6**), 31.5 (t, **C4**), 28.2 (q, $\mathbf{C(\underline{C}H_3)_3}$), 26.6 (t, $\mathbf{CH(\underline{C}H_2CH_3)_2}$), 23.5 (t, **C5**), 9.7 (q, $\mathbf{CH(CH_2\underline{C}H_3)_2}$).

m/z (M+Na) calcd for $\mathbf{C_{16}H_{28}O_4Na}$, 307.1879; found, 307.1883, $\mathbf{\Delta = 1.03\ ppm}$.

P23.- Asymmetric Michael Addition of Lithium (*R*)-*N*-benzyl-*N*-α-methylbenzylamide to 66.

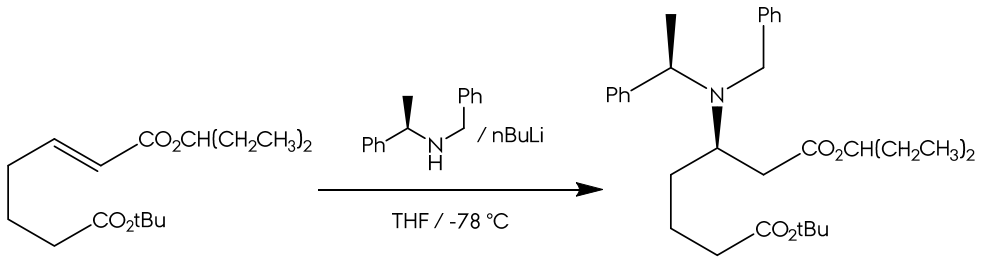

66 **67**

General procedure C was followed with the next quantities: 500 mg of (*R*)-*N*-benzyl-*N*-α-methylbenzylamide (211.3 g/mol; 2.37 mmol) in 4 mL of THF; 1.4 mL of 1.6 M nBuLi in hexanes (64.0 g/mol; 2.22 mmol); 210 mg of substrate **66** (284.3 g/mol; 0.74 mmol) in 4 mL of THF. Flash chromatography afforded 98 mg of product **67** (Hexanes/AcOEt 99:1), 27 % yield. Diaddition products were also observed, but were difficult to separate.

7-(*tert*-butyl) 1-(pentan-3-yl) (*R*)-3-(benzyl((*R*)-1-phenylethyl)amino)heptanedioate (67)

$\mathbf{R}_f$ 0.74 (Hexanes/AcOEt, 1:1)

$[\alpha]^{20}_{D}$ +10.1 (*c.* 1.0 in $CHCl_3$).

υ_{max} (neat)/cm^{-1} 2970 (C-H), 1728 (C=O), 1367, 1255, 1153 (C-O).

δ_H (400 MHz, $CDCl_3$) 7.46 - 7.20 (10H, $\mathbf{C_{ar}\underline{H}}$), 4.67 (1H, quintet, *J* 7.0, $\mathbf{C\underline{H}(CH_2CH_3)_2}$), 3.86 - 3.79 (3H, $\mathbf{C\underline{H}(CH_3)}$ and $\mathbf{NC\underline{H_A}H}$), 3.49 (1H, AB, *J* 14.7, $\mathbf{NCH\underline{H_B}}$), 3.36 (1H, m, **H3**), 2.14 (2H, m, **H2**), 1.94 - 2.00 (2H, **H6**), 1.54 – 1.47 (6H, $\mathbf{CH(C\underline{H_2}CH_3)_2}$ and **H5**), 1.45 (9H, s, $\mathbf{C(C\underline{H_3})_3}$), 1.35 (3H, d, *J* 7.0, $\mathbf{CHC\underline{H_3}}$), 1.33 - 1.25 (2H, **H4**), 0.84 (3H, t, *J* 7.4, $\mathbf{CH(CH_2C\underline{H_3})(CH_2CH_3)}$), 0.84 (3H, t, *J* 7.4, $\mathbf{CH(CH_2CH_3)(CH_2C\underline{H_3})}$).

δ_C (50 MHz, $CDCl_3$) 173.3 (s, **C7**), 172.8 (s, **C1**), 142.8 (s, $\mathbf{C_{ipso}}$), 141.8 (s, $\mathbf{C_{ipso}}$), 128.6 (d, $\mathbf{C_{ar}}$), 128.5 (d, $\mathbf{C_{ar}}$), 128.4 (d, $\mathbf{C_{ar}}$), 128.1 (d, $\mathbf{C_{ar}}$), 127.3 (d, $\mathbf{C_{ar}}$), 126.9 (d, $\mathbf{C_{ar}}$), 80.1 (s, $\mathbf{\underline{C}(CH_3)_3}$), 76.7 (d, $\mathbf{\underline{C}H(CH_3)_2}$), 58.2 (d, $\mathbf{\underline{C}HCH_3}$), 53.5 (d, **C3**), 50.3 (t, $\mathbf{N\underline{C}H_2}$), 36.8 (t, **C2**), 35.8 (t, **C6**), 33.2 (t, **C4**), 28.4 (q, $\mathbf{C(\underline{C}H_3)_3}$), 26.6 (t, $\mathbf{CH(\underline{C}H_2CH_3)(CH_2CH_3)}$), 22.9 (t, $\mathbf{CH(CH_2CH_3)(\underline{C}H_2CH_3)}$), 9.9 (q, $\mathbf{CH(CH_2\underline{C}H_3)(CH_2CH_3)}$), 9.8 (q, $\mathbf{CH(CH_2CH_3)(CH_2\underline{C}H_3)}$).

m/z (M+H) calcd for $\mathbf{C_{31}H_{46}NO_4}$, 496.3421; found, 496.3419, **Δ = -0.47 ppm**.

P24.- Asymmetric Michael Addition of Lithium (*R*)-*N*-benzyl-*N*-α-methylbenzylamide to 56.

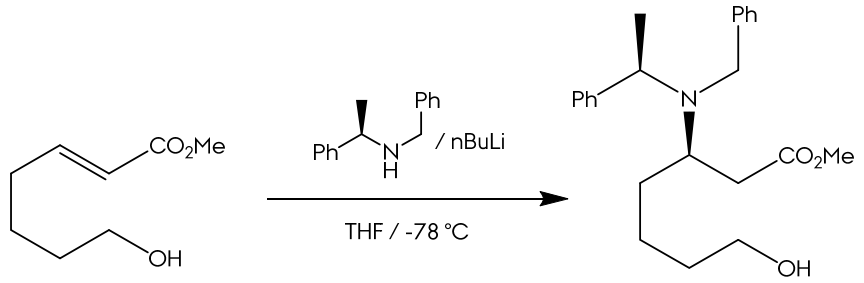

56 **68**

General procedure C were followed with the next quantities: 7.18 g of (*R*)-*N*-benzyl-*N*-α-methylbenzylamide (211.3 g/mol; 34 mmol) in 60 mL of THF; 16 mL of 1.6 M nBuLi in hexanes (64.0 g/mol; 32 mmol); 1.48 g of substrate **56** (158.0 g/mol; 9.37 mmol) in 06 mL of THF. Flash chromatography afforded 4.40 g of product **68** (Hexanes/AcOEt 9:1), 77 % yield. Diaddition products were also observed, but were difficult to separate.

Methyl (*R*)-3-(benzyl((*R*)-1-phenylethyl)amino)-7-hydroxyheptanoate (68)

$\mathbf{R}_f$ 0.55 (Hexanes/AcOEt, 1:1)

$[\alpha]^{20}_D$ +8.1 (*c.* 0.7 in $CHCl_3$);

υ_{max} (neat)/cm^{-1} 3431 (O-H), 2933 (C-H), 1730 (C=O), 1450, 1155 (C-O).

δ_H (400 MHz, $CDCl_3$) 7.43 - 7.22 (10H, $\mathbf{C_{ar}\underline{H}}$), 3.85 (1H, q, *J* 6.9, $\mathbf{C\underline{H}CH_3}$), 3.79 (1H, AB, *J* 14.9, $\mathbf{NC\underline{H_A}H}$), 3.62 (3H, t, *J* 6.3, **H7**), 3.59 - 3.55 (1H, $\mathbf{NCH\underline{H_B}}$), 3.55 (3H, s, $\mathbf{CO_2C\underline{H_3}}$), 3.31 (1H, m, **H3**), 2.09 (1H, ABX, *J* 14.7 4.6, $\mathbf{H2_A}$), 2.03 (1H, ABX, *J* 14.6 8.3, $\mathbf{H2_B}$), 1.64 - 1.37 (6H, **H4, H5** and **H6**), 1.35 (3H, d, *J* 7.0, $\mathbf{CHC\underline{H_3}}$).

δ_C (50 MHz, $CDCl_3$) 173.5 (s, $\mathbf{\underline{C}O_2CH_3}$), 143.3 (s, $\mathbf{C_{ipso}}$), 141.8 (s, $\mathbf{C_{ipso}}$), 128.5 (d, $\mathbf{C_{ar}}$), 128.4 (d, $\mathbf{C_{ar}}$), 128.3 (d, $\mathbf{C_{ar}}$), 128.1 (d, $\mathbf{C_{ar}}$), 127.1 (d, $\mathbf{C_{ar}}$), 126.9 (d, $\mathbf{C_{ar}}$), 63.1 (t, **C7**), 58.1 (d, $\mathbf{\underline{C}HCH_3}$), 54.0 (d, **C3**), 51.6 (q, $\mathbf{CO_2\underline{C}H_3}$), 50.1 (t, $\mathbf{N\underline{C}H_2}$), 36.6 (t, **C2**), 33.4 (t, **C6**), 32.8 (t, **C4**), 23.3 (t, **C5**), 19.8 (q, $\mathbf{CH\underline{C}H_3}$).

m/z (M+H) calcd for $\mathbf{C_{23}H_{32}NO_3}$, 370.2376; found, 370.2374, $\mathbf{\Delta = -0.73\ ppm}$.

P25.- Oxidation of Alcohol 68 to Acid 53.

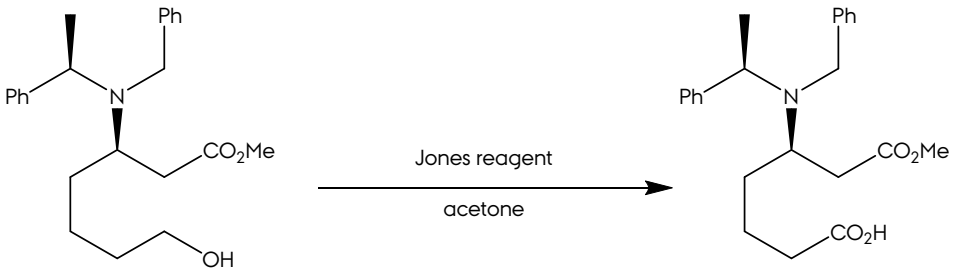

68 **53**

General procedure Q was followed with the next quantities: 1.0 g of **68** (369.3 g/mol; 2.7 mmol) in 10 mL of acetone. Reaction workup afforded 942 mg of acid **65**, 91 % yield.

P26.- Protecting Group Interconversion from 54 to 70 (1).

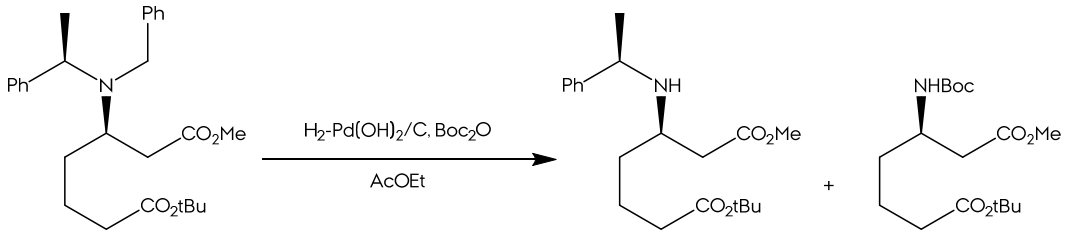

54 **69** **70**

General procedure E was followed with the next quantities: 457 mg of **54** (439.0 g/mol, 1.04 mmol); 729 mg of Boc_2O (218.2 g/mol, 3.33 mmol); 100 mg of $Pd(OH)_2$ on carbon; 3 mL of AcOEt; reaction time of 1 d. Flash chromatography afforded 51 mg of monprotected amine **69** (Hexanes/AcOEt 8:2, 13 % yield) and 181 mg of product **70** (Hexanes/AcOEt 98:2, 50 % yield).

7-(*tert*-butyl) 1-methyl (*R*)-3-(((*R*)-1-phenylethyl)amino)heptanedioate (69)

$\mathbf{R}_f$ 0.51 (Hexanes/AcOEt, 1:1)

$[\alpha]^{20}_D$ +6.9 (*c.* 1.64 in $CHCl_3$);

υ_{max} (neat)/cm^{-1} 2966 (C-H), 1734 (C=O), 1458, 1255, 1153 (C-O).

δ_H (400 MHz, $CDCl_3$) 7.31 - 7.22 (5H, $\mathbf{C_{ar}\underline{H}}$), 3.87 (1H, q, *J* 6.5, $\mathbf{C\underline{H}CH_3}$), 3.66 (3H, s, $\mathbf{CO_2C\underline{H}_3}$), 2.75 (1H, quintet, **H3**), 2.46 (1H, ABX, *J* 14.8 5.9, $\mathbf{H2_A}$), 2.39 (1H, ABX, *J* 14.8 5.2, $\mathbf{H2_B}$), (2H, td, *J* 7.0 and 1.9, **H2**), 2.08 (2H, t, *J* 7.4, **H6**), 1.70 - 1.36 (4H, **H4** and **H5**), 1.43 (9H, s, $\mathbf{CO_2C(C\underline{H}_3)_3}$), 1.31 (3H, d, *J* 6.5, $\mathbf{CHC\underline{H}_3}$).

δ_C (50 MHz, $CDCl_3$) 173.1 (s, **C7**), 172.9 (s, **C1**), 145.9 (s, $\mathbf{C_{ipso}}$), 128.4 (d, $\mathbf{C_{ar}}$), 127.1 (d, $\mathbf{C_{ar}}$), 126.8 (d, $\mathbf{C_{ar}}$), 80.1 (s, $\mathbf{\underline{C}(CH_3)_3}$), 55.2 (d, $\mathbf{\underline{C}HCH_3}$), 51.7 (d, **C3**), 51.4 (q, $\mathbf{CO_2\underline{C}H_3}$), 38.3 (t, **C2**), 35.4 (t, **C6**), 34.6 (t, **C4**), 28.0 (q, $\mathbf{C(\underline{C}H_3)_3}$), 24.9 (q, $\mathbf{CH\underline{C}H_3}$), 21.5 (t, **C5**).

m/z (M+H) calcd for $\mathbf{C_{20}H_{32}NO_4}$, 350.2325; found, 350.2335, $\mathbf{\Delta = 2.6\ ppm}$.

7-(*tert*-butyl) 1-methyl (*R*)-3-((tert-butoxycarbonyl)amino)heptanedioate (70)

$\mathbf{R}_f$ 0.90 (Hexanes/AcOEt, 1:1)

$[\alpha]^{20}_{D}$ +15.3 (*c.* 1.8 in $CHCl_3$);

υ_{max} (neat)/cm^{-1} 3367 (N-H), 2978 (C-H), 1734 (C=O), 1367, 1165 (C-O).

δ_H (400 MHz, $CDCl_3$) 4.91 (1H, d, *J* 7.9, **NH**), 3.89 (1H, **H3**), 3.67 (3H, s, **CO_2CH_3**), 2.51 (2H, d, *J* 5.1, **H2**), 2.22 (2H, td, *J* 7.1 and 2.7, **H6**), 1.70-1.49 (4H, **H4** and **H5**), 1.43 (9H, s, **$C(CH_3)_3$**).

δ_C (50 MHz, $CDCl_3$) 172.9 (s, **C7**), 172.2 (s, **C1**), 155.5 (s, **NCOO**), 80.4 (s, **$CO_2C(CH_3)_3$**), 79.5 (s, **$NCO_2C(CH_3)_3$**), 51.8 (q, **CO_2CH_3**), 47.5 (d, **C3**), 39.3 (t, **C2**), 35.2 (t, **C6**), 34.1 (t, **C4**), 28.5 (q, **$CO_2C(CH_3)_3$**), 28.3 (q, **$NCO_2C(CH_3)_3$**), 21.8 (t, **C5**).

m/z (M+Na) calcd for **$C_{17}H_{31}NO_6Na$**, 368.2043; found, 368.2025, **Δ = -5.0 ppm**.

P27.- Protecting Group Interconversion from 54 to 70 (2).

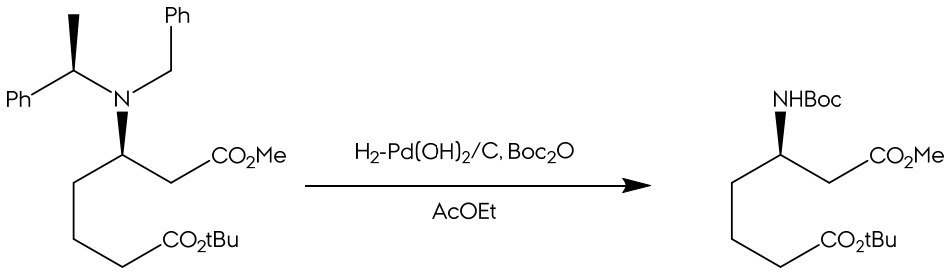

54 **70**

General procedure E was followed with the next quantities: 356 mg of **54** (439.0 g/mol, 0.812 mmol); 568 mg of Boc_2O (218.2 g/mol, 2.59 mmol); 120 mg of $Pd(OH)_2$ on carbon; 3 mL of AcOEt, reaction time of 2 d. Flash chromatography afforded 297 mg of product **70** (Hexanes/AcOEt 95:5) in 83 % yield.

P28.- Reaction of 70 with $LiBH_4$.

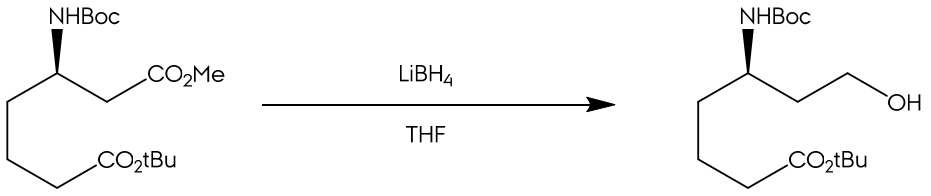

70 **71**

General procedure U was followed with the next quantities: 167 mg of **70** (345.0 g/mol, 0.48 mmol); 2 mL of 2 M $LiBH_4$ in THF (21.7 g/mol, 4 mmol); 2 mL of THF. Reaction workup afforded 138 mg of alcohol **71**, 90 % yield.

***tert*-butyl (*R*)-5-((tert-butoxycarbonyl)amino)-7-hydroxyheptanoate (71)**

$\mathbf{R}_f$ 0.64 (Hexanes/AcOEt, 4:1)

$[\alpha]^{20}_D$ +9.78 (*c.* 0.7 in $CHCl_3$).

υ_{max} (neat)/cm^{-1} 3367 (O-H), 2931 (C-H), 1707 (C=O), 1365, 1168 (C-O).

δ_H (400 MHz, $CDCl_3$) 4.42 (1H, d, *J* 9.1, **NH**), 3.81-3.69 (1H, **H5**), 3.68 - 3.58 (2H, **H7**), 2.23 (2H, td, *J* 7.5 and 4.8, **H2**), 1.87-1.47 (6H, **H3**, **H4** and **H6**), 1.44 (9H, s, **C(CH$_3$)$_3$**).

δ_C (50 MHz, $CDCl_3$) 173.0 (s, **C1**), 157.4 (s, **NCOO**), 80.5 (s, **CO$_2$C(CH$_3$)$_3$**), 80.1 (s, **NCO$_2$C(CH$_3$)$_3$**), 58.9 (t, **C7**), 47.3 (d, **C5**), 39.3 (t, **C6**), 35.3 (t, **C2**), 35.1 (t, **C4**), 28.6 (q, **CO$_2$C(CH$_3$)$_3$**), 28.3 (q, **NCO$_2$C(CH$_3$)$_3$**), 21.7 (t, **C3**).

m/z (M+Na) calcd for **$C_{16}H_{31}NO_5Na$**, 340.2094; found, 440.2102, **Δ = 2.22 ppm**.

P29.- Mesylation of Alcohol 71 to Mesylate 72.

71 **72**

General procedure M was followed with the next quantities: 89 mg of **71** (395.0 g/mol; 0.23 mmol); 2.82 mg of DMAP (122.1 g/mol, 0.023); 74 μL of pyridine; 44 μL of MsCl (114.5 g/mol, 0.68 mmol); 5 mL of dry DCM. Reaction workup afforded 102 mg of mesylate **72**, 96 % yield.

<u>*tert*-butyl (*R*)-5-((tert-butoxycarbonyl)amino)-7-((methylsulfonyl)oxy)heptanoate (72)</u>

$\mathbf{R}_f$ 0.69 (Hexanes/AcOEt, 1:1)

$[\alpha]^{20}_D$ -0.98 (*c.* 2.2 in $CHCl_3$);

υ_{max} (neat)/cm^{-1} 3375 (N-H), 2976 (C-H), 1701 (C=O), 1174 (S=O). 974.

δ_H (200 MHz, $CDCl_3$) 4.39 (1H, d, *J* 8.0, **N<u>H</u>**), 4.27 (2H, t, *J* 6.4, **H7**), 3.71 (1H, **H5**), 3.03 (3H, s, **$OSO_2C\underline{H}_3$**), 2.23 (2H, td, *J* 6.9 1.8, **H2**), 2.03-1.51 (6H, **H3**, **H4** and **H6**), 1.43 (18H, s, **$C(C\underline{H}_3)_3$**).

δ_C (50 MHz, $CDCl_3$) 172.8 (s, **C1**), 155.8 (s, **N<u>C</u>OO**), 80.5 (s, **$CO_2\underline{C}(CH_3)_3$**), 79.4 (s, **$NCO_2\underline{C}(CH_3)_3$**), 67.4 (t, **C7**), 47.5 (d, **C5**), 37.4 (q, **$OSO_2\underline{C}H_3$**), 35.2 (t, **C6**), 35.1 (t, **C2**), 35.0 (t, **C4**), 28.5 (q, **$CO_2C(C\underline{H}_3)_3$**), 28.3 (q, **$NCO_2C(C\underline{H}_3)_3$**), 21.5 (t, **C3**).

m/z (M+Na) calcd for **$C_{17}H_{33}NO_7NaS$**, 418.1869; found, 418.1865, **Δ = -1.18 ppm**.

P30.- Thymine Introduction in Mesylate 72.

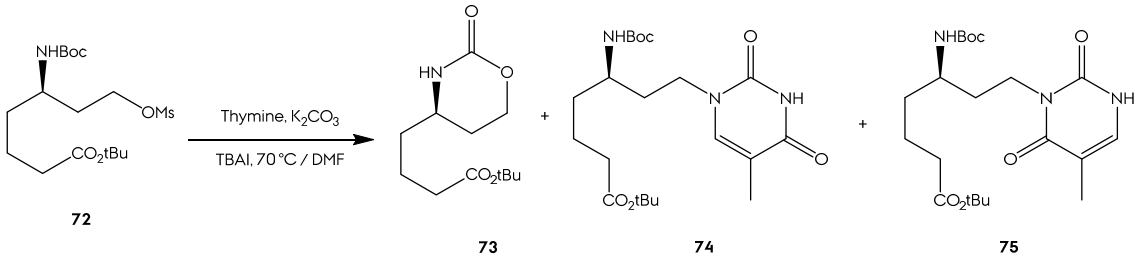

72 73 74 75

General procedure X was followed with the next quantities: 102 mg of ester **72** (395.0 g/mol; 0.26 mmol); 98 mg of thymine (CAS: 65-71-4, white powder, 126.1 g/mol, 0.77 mmol, commercial); 31 mg of TBAI (396.3 g/mol, 0.078 mmol); 72 mg of K_2CO_3 (138.2 g/mol, 0.518 mmol); 5 mL of dry DMF. Flash chromatography

afforded 23 mg of cyclic carbamate **73** (Hexanes/AcOEt 9:1, 37 %) and 38 mg of the PNA monomers mixture **74-75** (Hexanes/AcOEt 7:3, 35 %).

***tert*-butyl (*R*)-4-(2-oxo-1,3-oxazinan-4-yl)butanoate (73)**

$\mathbf{R}_f$ 0.90 (Hexanes/AcOEt, 1:1)

υ_{max} (neat)/cm^{-1} 3253 (N-H), 2927 (C-H), 1718 (C=O), 1363, 1153 (C-O).

δ_H (400 MHz, $CDCl_3$) 5.43 (1H, s, **NH**), 4.33 (1H, dt, *J* 11.2 4.3, **CH$_A$HO**), 4.33 (1H, td, *J* 11.2 2.7, **CHH$_B$O**), 3.47 (1H, quintet, *J* 5.6, **CHN**), 2.25 (2H, td, *J* 6.8 2.8, **H2**), 2.02 (1H, **CH$_A$HCH$_2$O**), 1.75-1.49 (5H, **H3**, **H4** and **CHH$_B$CH$_2$O**), 1.44 (9H, s, **C(CH$_3$)$_3$**).

δ_C (50 MHz, $CDCl_3$) 172.6 (**C1**), 154.2 (**NCOO**), 80.9 (**C(CH$_3$)$_3$**), 65.8 (**CH$_2$O**), 50.9 (**CHN**), 36.1 (**C2**), 35.2 (**C4**), 28.4 (**C(CH$_3$)$_3$**), 27.5 (t, **CH$_2$CH$_2$O**), 20.9 (**C3**).

m/z (M+Na) calcd for **$C_{12}H_{21}NO_4Na$**, 266.1362; found, 266.1356, **Δ = -2.55 ppm**.

P31.- Reaction of 71 with 1-(*p*-toluenesulfonyl)imidazole (1).

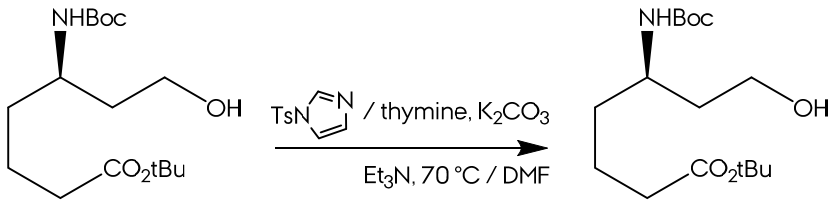

71 **71**

In a round bottom flask, 71 mg of **71** (379.3 g/mol; 0.187 mmol) and 62 mg of 1-(*p*-toluenesulfonyl)imidazole (CAS: 2232-08-8, white powder, 222.26 g/mol, 0.279 mmol, commercial) were dissolved in 2 mL of dry DMF. The flask was sealed, purged with Ar and magnetically stirred at room temperature for 1 h. In other round bottom flask, 113 mg of thymine (CAS: 65-71-4, white powder, 126.1 g/mol, 0.89 mmol, commercial), 45 mg of Et_3N (101.1 g/mol, 0.45 mmol), and 31 mg of K_2CO_3 (138.2 g/mol, 0.22 mmol) were dissolved in 3 mL of DMF. The flask was sealed, purged with Ar and magnetically stirred at 70 ºC for 1 h. The substrate solution was added via cannula to the other one, and stirred continued 12 h at 70 ºC.

The reaction mixture was filtrated through a pad of Celite® and washed with DCM. The organic solution was washed with water (3 times) and brine (1 time). Drying the solution with anhydrous Na_2SO_4, filtration and forward solvent removal resulted in recovery of the starting alcohol **71** and the 1-(*p*-toluenesulfonyl)imidazole.

P32.- Reaction of 71 with 1-(*p*-toluenesulfonyl)imidazole (2).

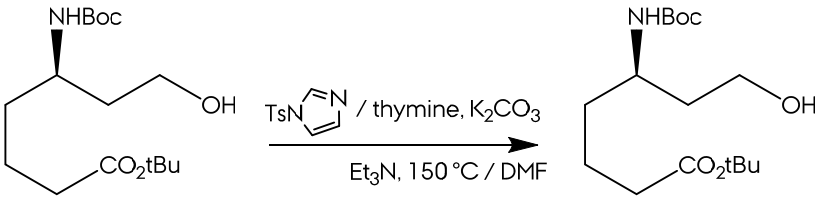

71 **71**

In a round bottom flask, 52 mg of **71** (379.3 g/mol; 0.165 mmol) and 44 mg of 1-(*p*-toluenesulfonyl)imidazole (CAS: 2232-08-8, white powder, 222.26 g/mol, 0.198 mmol, commercial) were dissolved in 3 mL of dry DMF. The flask was sealed, purged with Ar and magnetically stirred at room temperature for 1 h. In other round bottom flask, 25 mg of thymine (CAS: 65-71-4, white powder, 126.1 g/mol, 0.198 mmol, commercial), 33 mg of Et_3N (101.1 g/mol, 0.45 mmol), and 31 mg of K_2CO_3 (138.2 g/mol, 0.22 mmol) were dissolved in 3 mL of DMF. The flask was sealed, purged with Ar and magnetically stirred at 150 ºC for 1 h. The substrate solution was added via cannula to the other one, and stirred continued 12 h at 150 ºC.

The reaction mixture was filtrated through a pad of Celite® and washed with DCM. The organic solution was washed with water (3 times) and brine (1 time). Drying the solution with anhydrous Na_2SO_4, filtration and forward solvent removal resulted in recovery 58.6 mg of the starting alcohol **71** and the 1-(*p*-toluenesulfonyl)imidazole.

P33.- Protection of 76 as Boc-amine.

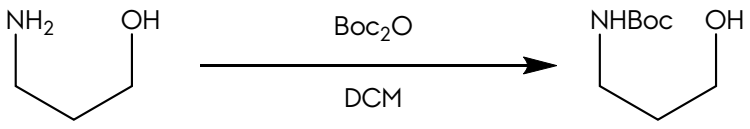

76 **77**

General procedure G was followed without using DMAP and with the next quantities: 1.00 g of **76** (3-amino-1-propanol, CAS: 156-87-6, commercial liquid, 75.1 g/mol, 13.3 mmol); 3.17 g of Boc_2O (218.2 g/mol, 13.3 mmol). Reaction workup afforded 2.12 g of protected amine **77**, 91 % yield.

***Tert*-butyl (3-hydroxypropyl)carbamate (77)**

δ_H (200 MHz; $CHCl_3$) 4.96 (1H, br s, **NH**), 3.62 (2H, t, *J* 5.6, **H3**), 3.23 (2H, q, *J* 6.2, **H1**), 3.06 (1H, br s, **OH**), 1.63 (2H, quintet, *J* 6.2, **H2**), 1.40 (9H, s, **C(CH$_3$)$_3$**).

δ_C (50 MHz; $CHCl_3$) 157.3 (s, **NCOO**), 79.7 (s, **C(CH$_3$)$_3$**), 59.4 (t, **C3**), 37.1 (t, **C1**), 32.9 (t, **C2**), 28.5 (q, **C(CH$_3$)$_3$**).

m/z (M+H) calcd for **$C_8H_{18}NO_3$**, 176.1281; found, 176.1288, **Δ = -1.0 ppm**.

P34.- Mesylation of Alcohol 76.

77 **78**

General procedure M was followed with the next quantities: 100 mg of **77** (175.0 g/mol; 0.57 mmol); 7 mg of DMAP (122.1 g/mol, 0.059); 186 mg of pyridine; 170 mg of MsCl (114.5 g/mol 1.77 mmol); 5 mL of dry DCM. Reaction workup afforded 110 mg of mesylate **78**, 75 % yield.

3-((*tert*-butoxycarbonyl)amino)propyl methanesulfonate (78)

δ_H (200 MHz; $CHCl_3$) 4.78 (1H, br s, **NH**), 4.28 (2H, t, *J* 6.0, **H1**), 3.23 (2H, **H3**), 3.02 (3H, s, **SO$_2$CH$_3$**), 1.92 (2H, quintet, *J* 6.2, **H2**), 1.42 (9H, s, **C(CH$_3$)$_3$**).

δ_C (50 MHz; $CHCl_3$) 156.2 (s, **NCOO**), 79.6 (s, **C(CH$_3$)$_3$**), 67.7 (t, **C1**), 37.5 (q, **SO$_2$CH$_3$**), 36.9 (t, **C3**), 29.8 (t, **C2**), 28.5 (q, **C(CH$_3$)$_3$**).

P35.- Reaction of Mesylate 78 with Thymine (1).

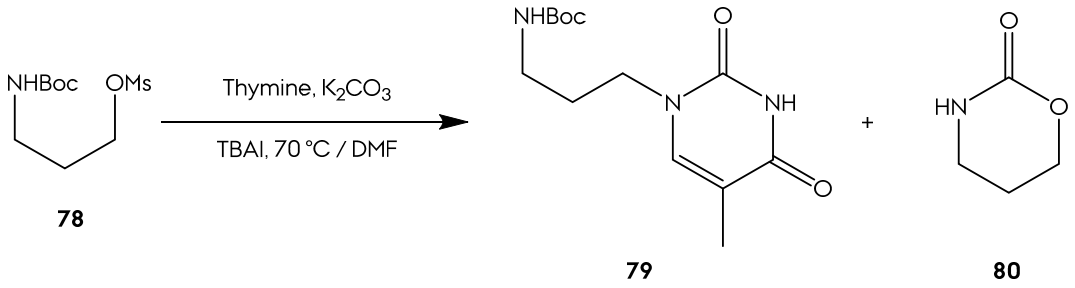

78 79 80

General procedure X was followed with the next quantities: 56 mg of mesylate **78** (253.0 g/mol; 0.22 mmol); 86 mg of thymine (CAS: 65-71-4, white powder, 126.1 g/mol, 0.68 mmol, commercial); 27 mg of TBAI (396.3 g/mol, 0.067 mmol); 63 mg of K_2CO_3 (138.2 g/mol, 0.456 mmol); 5 mL of dry DMF. Reaction workup resulted in 27 mg of crude. Flash chromatography afforded 17 mg of product **79** (Hexanes/AcOEt 9:1, 27 %).

***tert*-butyl (3-(5-methyl-2,4-dioxo-3,4-dihydropyrimidin-1(2*H*)-yl)propyl)carbamate (79)**

$\mathbf{R}_f$ 0.44 (Hexanes/AcOEt, 1:1)

$\boldsymbol{\delta}_H$ (200 MHz; $CHCl_3$) 9.15 (1H, br s, **CONHCO**), 7.04 (1H, br s, **NCH**), 5.04 (1H, br s, **NH**), 3.77 (2H, t, *J* 6.6, **H3**), 3.23 (2H, q, *J* 6.1, **H1**), 1.92 (3H, s, **CCH$_3$**), 1.84 (2H, quintet, *J* 6.4, **H2**), 1.43 (9H, s, **C(CH$_3$)$_3$**).

$\boldsymbol{\delta}_C$ (50 MHz; $CHCl_3$) 164.5 (s, **HNCOC**), 156.3 (s, **NCOO**), 151.4 (s, **NCON**), 140.6 (d, **CH**), 111.2 (s, **CCH$_3$**), 79.7 (s, **C(CH$_3$)$_3$**), 45.9 (t, **C3**), 37.2 (t, **C1**), 29.7 (t, **C2**), 28.6 (q, **C(CH$_3$)$_3$**), 12.5 (q, **CCH$_3$**).

m/z (M+Na) calcd for **$C_{13}H_{21}N_3O_4Na$**, 306.1424; found, 306.1429, **Δ = 1.5 ppm**.

P36.- Reaction of Mesylate 78 with Thymine (2).

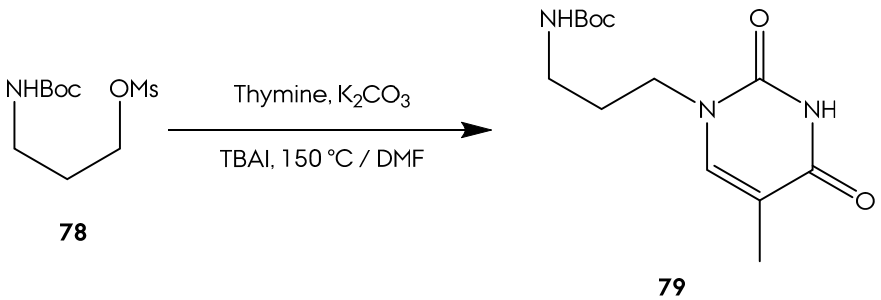

78 79

General procedure X was followed with the next quantities: 65 mg of mesylate **78** (253.0 g/mol; 0.25 mmol); 99 mg of thymine (CAS: 65-71-4, white powder, 126.1 g/mol, 0.79 mmol, commercial); 31 mg of TBAI (396.3 g/mol, 0.079 mmol); 72 mg of K_2CO_3 (138.2 g/mol, 0.524 mmol): 5 mL of dry DMF. Reaction workup afforded 9 mg of product **79** with impurities.

P37.- Reaction of Mesylate 78 with Thymine (3).

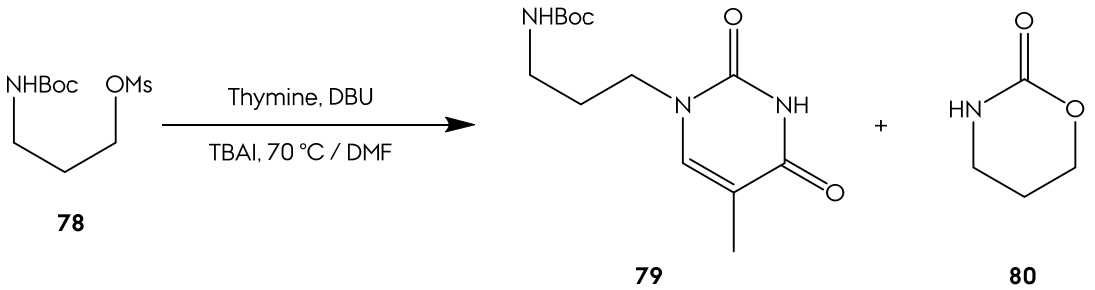

General procedure X was followed with the next quantities: 46 mg of mesylate **78** (253.0 g/mol; 0.18 mmol); 71 mg of thymine (CAS: 65-71-4, white powder, 126.1 g/mol, 0.56 mmol, commercial); 22 mg of TBAI (396.3 g/mol, 0.056 mmol); 52 mg of DBU (1,8-diazabicyclo[5.4.0]undec-7-ene, CAS: 6674-22-2, commercial liquid, 152.2 g/mol, 0.341 mmol); 5 mL of dry DMF. Reaction workup resulted in 51 mg of crude, which was mainly composed of a mixture product **79**:**80** 4:1.

P38.- Reaction of Mesylate 78 with Thymine (4).

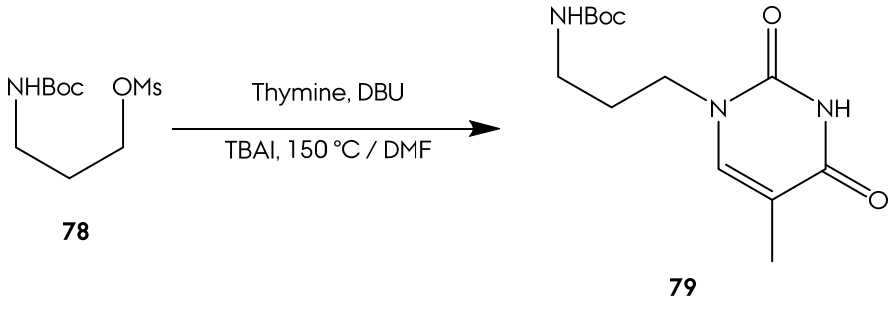

General procedure X was followed with the next quantities: 27 mg of mesylate **78** (253.0 g/mol; 0.11 mmol); 39 mg of thymine (CAS: 65-71-4, white powder, 126.1 g/mol, 0.312 mmol, commercial); 12 mg of TBAI (396.3 g/mol, 0.03 mmol); 28 mg of DBU (1,8-diazabicyclo[5.4.0]undec-7-ene, CAS: 6674-22-2, commercial liquid,

152.2 g/mol, 0.183 mmol); 5 mL of dry DMF. Reaction workup resulted in 2 mg of crude, which was mainly composed of product **79.**

P39.- Reaction of Mesylate 78 with Potassium Carbonate.

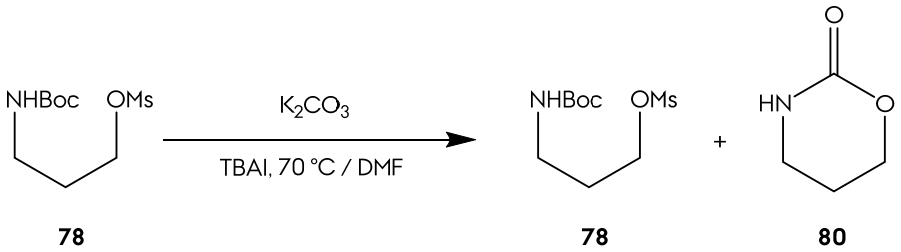

General procedure X was followed with the next quantities: 80 mg of mesylate **78** (253.0 g/mol; 0.32 mmol); 39 mg of TBAI (396.3 g/mol, 0.097 mmol); 90 mg of K_2CO_3 (138.2 g/mol, 0.652 mmol); 5 mL of dry DMF. Reaction workup afforded 28 mg of a 1:1 mixture of product **79** and **80**.

P40.- Reaction of Mesylate 78 with 6-Chloropurine (1).

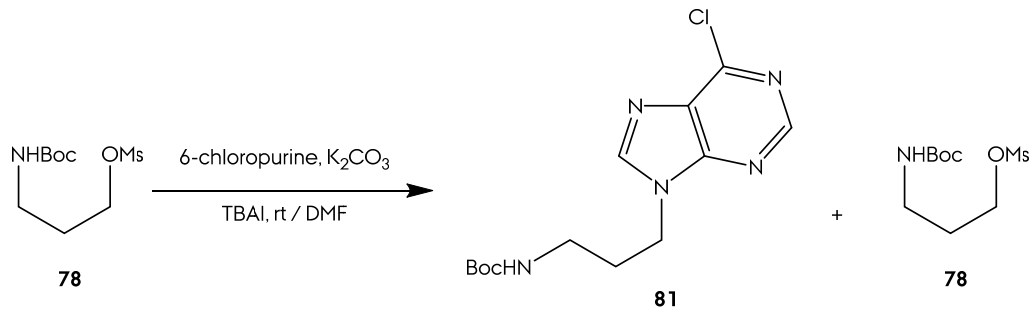

General procedure X was followed with the next quantities: 60 mg of mesylate **78** (253.0 g/mol; 0.24 mmol); 29 mg of TBAI (396.3 g/mol, 0.072 mmol); 40 mg of K_2CO_3 (138.2 g/mol, 0.292 mmol); 45 mg of 6-chloropurine (CAS: 87-42-3, orange powder, 154.5 g/mol, 0.292 mmol, commercial); 5 mL of dry DMF. Reaction workup afforded 28 mg of a 4:6 mixture of product **81** and **78**.

***tert*-butyl (3-(6-chloro-9H-purin-9-yl)propyl)carbamate (81)**

$\mathbf{R}_f$ 0.09 (Hexanes/AcOEt, 1:1)

υ_{max} (neat)/cm^{-1} 3329 (N-H), 2976 (C-H), 1695 (C=O), 1654, 1595, 1170 (C-O).

δ_H (200 MHz; $CHCl_3$) 8.77 (1H, s, **$CH_2NC\underline{H}N$**), 8.26 (1H, br s, **$NC\underline{H}NCCl$**), 5.00 (1H, br s, **$N\underline{H}$**), 4.37 (2H, t, *J* 6.7, **H3**), 3.13 (2H, q, *J* 6.0, **H1**), 2.10 (2H, quintet, *J* 6.4, **H2**), 1.45 (9H, s, **$C(C\underline{H}_3)_3$**).

δ_C (50 MHz; $CHCl_3$) 156.3 (**$N\underline{C}OO$**), 152.1 (**$\underline{C}Cl$**), 152.0 (**$N\underline{C}HNCCl$**), 151.3 (**$CH_2N\underline{C}N$**), 145.8 (**$CH_2N\underline{C}HN$**), 131.8 (**$N\underline{C}CCl$**), 79.9 (**$\underline{C}(CH_3)_3$**), 42.0 (**C3**), 37.4 (**C1**), 30.7 (**C2**), 28.5 (**$C(\underline{C}H_3)_3$**).

m/z (M+Na) calcd for **$C_{13}H_{18}N_5O_2ClNa$**, 334.1041; found, 334.1046, **Δ = 1.4 ppm**.

P41.- Reaction of Mesylate 78 with 6-Chloropurine (2).

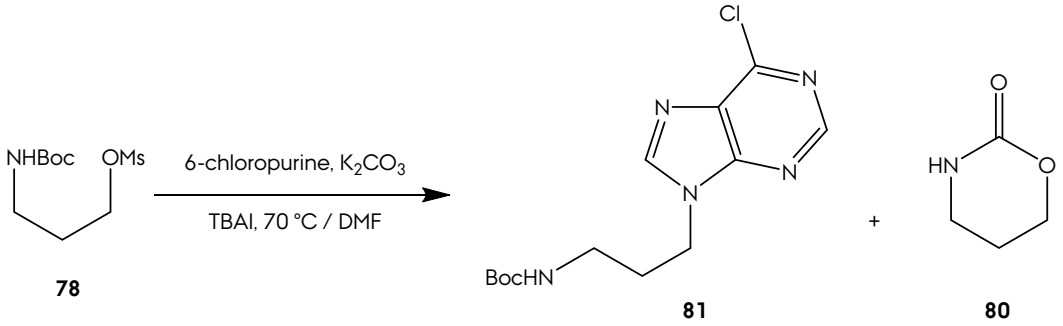

General procedure X was followed with the next quantities: 46 mg of mesylate **78** (253.0 g/mol; 0.18 mmol); 86 mg of 6-chloropurine (CAS: 87-42-3, orange powder, 154.5 g/mol, 0.558 mmol, commercial); 22 mg of TBAI (396.3 g/mol, 0.055 mmol); 51 mg of K_2CO_3 (138.2 g/mol, 0.372 mmol); 5 mL of dry DMF. Reaction workup afforded 14 mg of a 3:1 mixture of product **81** and **80**.

P42.- Reaction of 71 with 1-(*p*-toluenesulfonyl)imidazole.

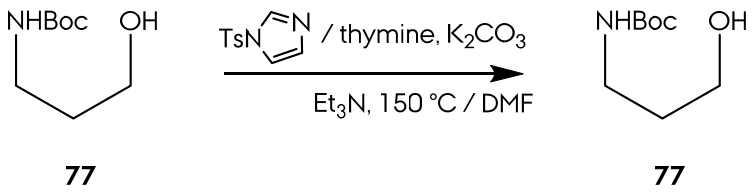

In a round bottom flask, 61 mg of **77** (169.0 g/mol; 0.364 mmol) and 97 mg of 1-(*p*-toluenesulfonyl)imidazole (CAS: 2232-08-8, white powder, 222.26 g/mol, 0.44 mmol, commercial) were dissolved in 3 mL of dry DMF. The flask was sealed, purged with

Ar and magnetically stirred at room temperature for 1 h. In other round bottom flask, 183 mg of thymine (CAS: 65-71-4, white powder, 126.1 g/mol, 1.45 mmol, commercial), 73 mg of Et_3N (101.1 g/mol, 0.72 mmol), and 50 mg of K_2CO_3 (138.2 g/mol, 0.22 mmol) were dissolved in 3 mL of DMF. The flask was sealed, purged with Ar and magnetically stirred at 150 ºC for 1 h. The substrate solution was added via cannula to the other one, and stirred continued 12 h at 150 ºC.

The reaction mixture was filtrated through a pad of Celite® and washed with DCM. The organic solution was washed with water (3 times) and brine (1 time). Drying the solution with anhydrous Na_2SO_4, filtration and forward solvent removal resulted in recovery 22.8 mg of the starting alcohol **77** and the 1-(*p*-toluenesulfonyl)imidazole.

P43.- Reaction of Alcohol 77 with 6-Chloropurine.

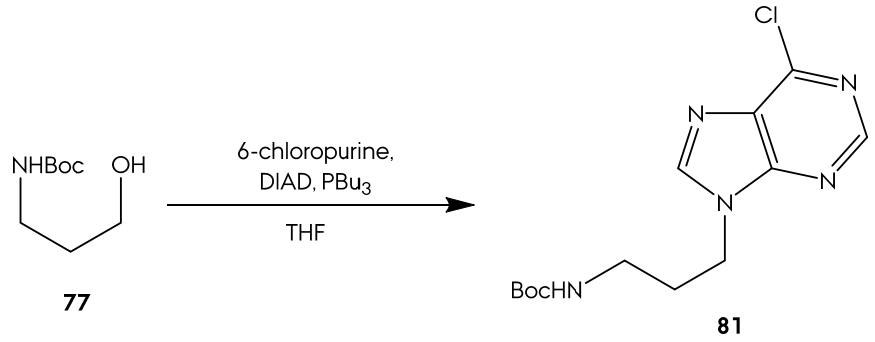

77 **81**

General procedure W was followed with the next quantities: 100 mg of alcohol **77** (175.0 g/mol; 0.57 mmol); 109 mg of 6-chloropurine (CAS: 87-42-3, orange powder, 154.5 g/mol, 0.71 mmol, commercial); 143 mg of PBu_3 (202.3 g/mol, 0.71 mmol); 143 mg of DIAD (202.2 g/mol, 0.71 mmol); 4 mL of dry THF. Flash chromatography afforded 101 mg of product **81** (Hexanes/AcOEt 7:3, 68 % yield).

P44.- Nucleofile Aromatic Substitution in 81.

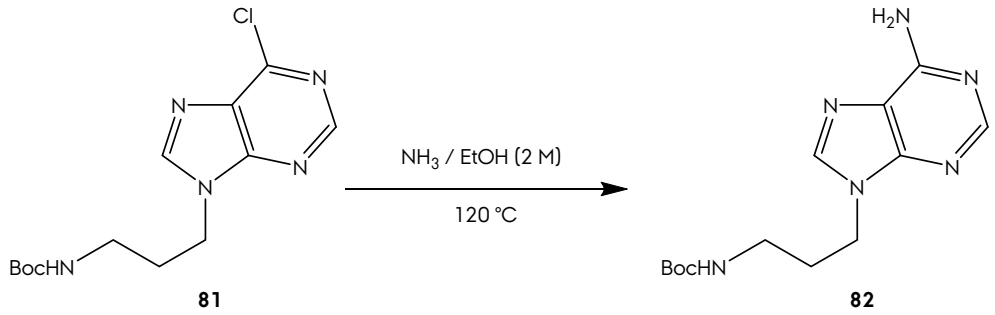

81 **82**

In a 20 mL pressure flask, 28 mg of amine **81** were dissolved in 5 mL of 2 M NH_3 in EtOH. The flask was sealed and heated at 120 ºC for 12h.

Solvent was removed under reduced pressure. The crude was dissolved in 10 mL of AcOEt and washed with sat $NaHCO_3$ (2 times) and brine (1 time). Drying with anhydrous Na_2SO_4, filtration and forward solvent removal under reduced pressure afforded 24 mg of adenine derivative **82**, 94 % yield.

***tert*-butyl (3-(6-amino-9*H*-purin-9-yl)propyl)carbamate (82)**

υ_{max} (neat)/cm^{-1} 3329 (N-H), 2974 (C-H), 1701 (C=O), 1593, 1560, 1170 (C-O).

δ_H (200 MHz; $CHCl_3$) 8.34 (1H, s, **$CH_2NC\underline{H}N$**), 7.85 (1H, br s, **$NC\underline{H}NCCl$**), 6.06 (2H, br s, **$N\underline{H_2}$**), 5.39 (1H, br s, **$N\underline{H}$**), 4.37 (2H, t, *J* 6.9, **H3**), 3.14 (2H, q, *J* 6.3, **H1**), 2.09 (2H, quintet, *J* 6.4, **H2**), 1.44 (9H, s, **$C(C\underline{H_3})_3$**).

P45.- Protection of 76 as Fmoc-amine.

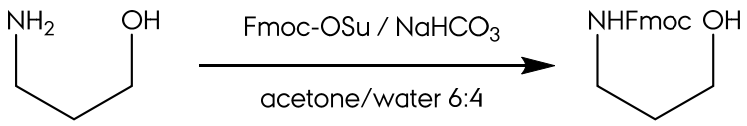

76 **83**

In a round bottom flask, 200 mg of **76** (3-amino-1-propanol, CAS: 156-87-6, commercial liquid, 75.1 g/mol, 2.67 mmol), 1.17 g of Fmoc-OSu (*N*-(9-fluorenylmethoxycarbonyloxy)succinimide, CAS: 82911-69-1, white powder, 337.3 g/mol, 3.48 mmol) and 485 mg of $NaHCO_3$ (84.0 g/mol, 5.78 mmol) were suspended in 5 mL of acetone/water 6:4. The suspension was magnetically stirred for 24 h. 30 mL of AcOEt/water 1:1 were added to the suspension and stirred. The organic layer

was separated and washed with brine (1 time). Drying with anhydrous Na_2SO_4, filtration and forward solvent removal under reduced pressure afforded 790 mg of protected amine **83**, 99 % yield.

(9*H*-fluoren-9-yl)methyl (3-hydroxypropyl)carbamate (83)

δ_H (200 MHz; $CHCl_3$) 7.77 (2H, d, *J* 7.3, **C4$_{ar}$H** and **C5$_{ar}$H**), 7.59 (2H, d, *J* 7.2, **C1$_{ar}$H** and **C8$_{ar}$H**), 7.40 (2H, t, *J* 7.0, **C3$_{ar}$H** and **C6$_{ar}$H**), 7.31 (2H, t, *J* 7.6, **C2$_{ar}$H** and **C7$_{ar}$H**), 5.20 (1H, **NH**), 4.43 (2H, d, *J* 6.6, **CHC$\underline{H_2}$O**), 4.19 (1H, t, *J* 6.6, **C9$_{ar}$H**), 3.63 (2H, t, *J* 5.7, **H3**), 3.32 (2H, q, *J* 6.0, **H1**), 1.68 (2H, quintet, *J* 5.9, **H2**).

δ_C (50 MHz; $CHCl_3$) 153.1 (s, **O$\underline{C}$ON**), 144.1 (s, **C10$_{ar}$** and **C13$_{ar}$**), 141.5 (s, **C11$_{ar}$** and **C12$_{ar}$**), 127.9 (d, **C2$_{ar}$** and **C7$_{ar}$**), 127.2 (d, **C3$_{ar}$** and **C6$_{ar}$**), 125.2 (d, **C1$_{ar}$** and **C8$_{ar}$**), 120.2 (d, **C4$_{ar}$** and **C5$_{ar}$**), 66.8 (t, **$\underline{C}$H$_2$OCON**), 59.7 (t, **C3**), 47.5 (d, **C9$_{ar}$**), 37.9 (t, **C1**), 32.7 (t, **C2**).

m/z (M+Na) calcd for **$C_{18}H_{19}NO_3Na$**, 320.1262; found, 320.1272, **Δ = -3.1 ppm**.

P46.- Mesylation of Alcohol 83.

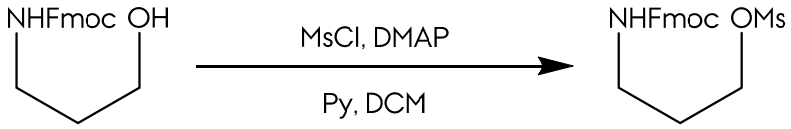

83 **84**

General procedure M was followed with the next quantities: 200 mg of alcohol **83** (297.0 g/mol; 0.67 mmol); 8 mg of DMAP (122.1 g/mol, 0.071); 226 mg of pyridine; 206 mg of MsCl (114.5 g/mol 2.15 mmol); 5 mL of dry DCM. Reaction workup afforded 250 mg of mesylate **84**, 99 % yield.

3-((((9*H*-fluoren-9-yl)methoxy)carbonyl)amino)propyl methanesulfonate (84)

υ_{max} (film)/cm^{-1} 2950-2840 (CH), 1028 (S=O);

δ_H (200 MHz; $CHCl_3$) 7.75 (2H, dd, *J* 7.1 1.3, **C4$_{ar}$H** and **C5$_{ar}$H**), 7.58 (2H, d, *J* 7.1, **C1$_{ar}$H** and **C8$_{ar}$H**), 7.39 (2H, td, *J* 7.3 1.1, **C3$_{ar}$H** and **C6$_{ar}$H**), 7.30 (2H, td, *J* 7.3 1.5, **C2$_{ar}$H** and **C7$_{ar}$H**), 5.2 (1H, **NH**), 4.39 (2H, d, *J* 6.6, **CHC$\underline{H_2}$O**), 4.27 - 4.19

(3H, **C9$_{ar}$H** and **H1**), 3.29 (2H, q, *J* 5.8, **H3**), 2.97 (3H, s, **SO$_2$C$\underline{\mathbf{H}}_3$**), 1.68 (2H, quintet, *J* 5.9, **H2**).

P47.- Reaction of Mesylate 84 with Thymine.

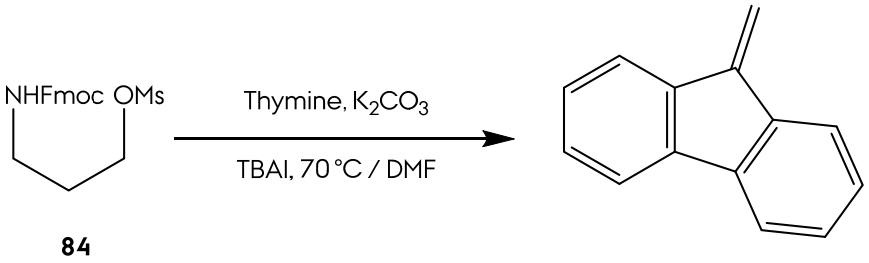

84 **85**

General procedure X was followed with the next quantities: 95 mg of mesylate **84** (375.0 g/mol; 0.25 mmol); 96 mg of thymine (CAS: 65-71-4, white powder, 126.1 g/mol, 0.76 mmol, commercial); 30 mg of TBAI (396.3 g/mol, 0.076 mmol); 70 mg of K_2CO_3 (138.2 g/mol, 0.508 mmol); 5 mL of dry DMF. Reaction workup resulted in 39 mg of crude mainly composed of 9-methylene-9*H*-fluorene, **85**.

P48.- Reaction of Mesylate 84 with 6-chloropurine.

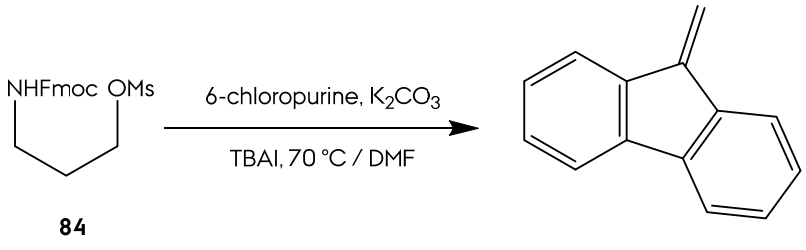

84 **85**

General procedure X was followed with the next quantities: 125 mg of mesylate **84** (375.0 g/mol; 0.335 mmol); 154 mg of 6-chloropurine (CAS: 87-42-3, orange powder, 154.5 g/mol, 1.00 mmol, commercial); 40 mg of TBAI (396.3 g/mol, 0.100 mmol); 92 mg of K_2CO_3 (138.2 g/mol, 0.67 mmol); 5 mL of dry DMF. Reaction workup resulted in 57 mg of crude mainly composed of 9-methylene-9*H*-fluorene, **85**.

P49.- Reaction of Mesylate 84 with Potassium Carbonate.

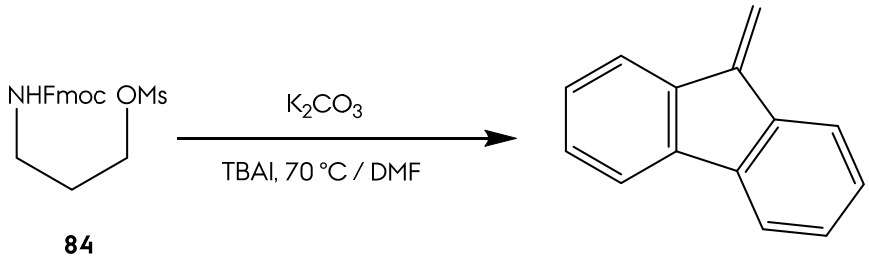

84 **85**

General procedure X was followed with the next quantities: 62 mg of mesylate **84** (375.0 g/mol; 0.167 mmol); 20 mg of TBAI (396.3 g/mol, 0.050 mmol); 46 mg of K_2CO_3 (138.2 g/mol, 0.334 mmol); 5 mL of dry DMF. Reaction workup resulted in 31 mg of crude composed of 9-methylene-9*H*-fluorene, **85**.

P50.- Reaction of Mesylate 72 with *N*³-benzoyl-thymine.

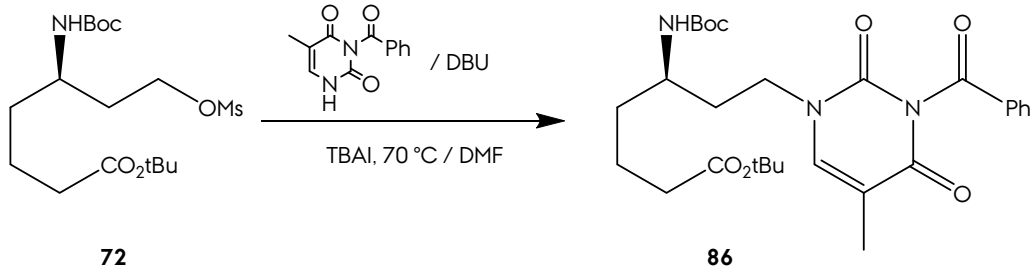

72 **86**

General procedure X was followed with the next quantities: 64 mg of mesylate **72** (395.0 g/mol; 0.164 mmol); 113 mg of *N*³-benzoyl-thymine (prepared at lab, see laboratory prepared reagents, 230.2 g/mol, 0.492 mmol); 19 mg of TBAI (396.3 g/mol, 0.049 mmol); 45 mg of DBU (1,8-diazabicyclo[5.4.0]undec-7-ene, CAS: 6674-22-2, commercial liquid, 152.2 g/mol, 0.328 mmol); 5 mL of dry DMF. Flash chromatography afforded 20 mg of product **86** (Hexanes/AcOEt 75:25, 23 %).

***tert*-butyl (*R*)-7-(3-benzoyl-5-methyl-2,4-dioxo-3,4-dihydropyrimidin-1(2*H*)-yl)-5-((tert-butoxycarbonyl)amino)heptanoate (86)**

$\mathbf{R}_f$ 0.55 (Hexanes/AcOEt, 1:1)

$[\alpha]^{20}_{D}$ -16.8 (*c.* 1.0 in MeOH)

υ_{max} (neat)/cm^{-1} 3354 (N-H), 2976 (C-H), 1701 (C=O), 1647, 1251 (C-O).

δ_H (400 MHz, $CDCl_3$) 7.91 (2H, dd, *J* 8.5 1.2, **o-C_{ar}H**), 7.63 (1H, tt, *J* 7.4 1.6, **p-C_{ar}H**), 7.63 (1H, t, *J* 7.4, **m-C_{ar}H**), 7.23 (1H, br s, **NC<u>H</u>**), 4.43 (1H, d, *J* 9.1, **N<u>H</u>**), 3.93 (1H, **$H7_A$**), 3.61 (2H, **H5** and **$H7_B$**), 2.21 (2H, q, *J* 6.3, **H2**), 1.95 (3H, s, **CC<u>H_3</u>**), 1.91 (1H, **$H4_A$**), 1.74 - 1.37 (5H, **H3**, **$H4_B$** and **H6**), 1.44 (18H, s, **C(C<u>H_3</u>)$_3$**).

δ_C (50 MHz, $CDCl_3$) 172.8 (s, **C1**), 169.3 (**N<u>C</u>OC$_{ar}$**), 163.4 (s, **N<u>C</u>O**), 156.0 (s, **N<u>C</u>OO**), 150.0 (s, **N<u>C</u>ON**), 141.0 (d, **N<u>C</u>H**), 135.1 (d, **p-C_{ar}**), 131.9 (s, **C_{ipso}**), 130.6 (d, **o-C_{ar}**), 129.3 (d, **m-C_{ar}**), 110.8 (s, **<u>C</u>CH$_3$**), 80.5 (s, **CO$_2$<u>C</u>(CH$_3$)$_3$**), 79.8 (s, **NCO$_2$<u>C</u>(CH$_3$)$_3$**), 48.4 (d, **C5**), 46.8 (t, **C7**), 35.2 (t, **C2**), 35.1 (t, **C4**), 34.9 (t, **C6**), 28.5 (q, **CO$_2$C(C<u>H_3</u>)$_3$**), 28.3 (q, **NCO$_2$C(C<u>H_3</u>)$_3$**), 21.5 (t, **C3**), 12.6 (q, **C<u>C</u>H$_3$**).

m/z (M+Na) calcd for **$C_{28}H_{39}N_3O_7Na$**, 552.2680; found, 552.2695, **Δ = 2.67 ppm**.

P51.- Reaction of Alcohol 71 with *N*^{3}-benzoyl-thymine.

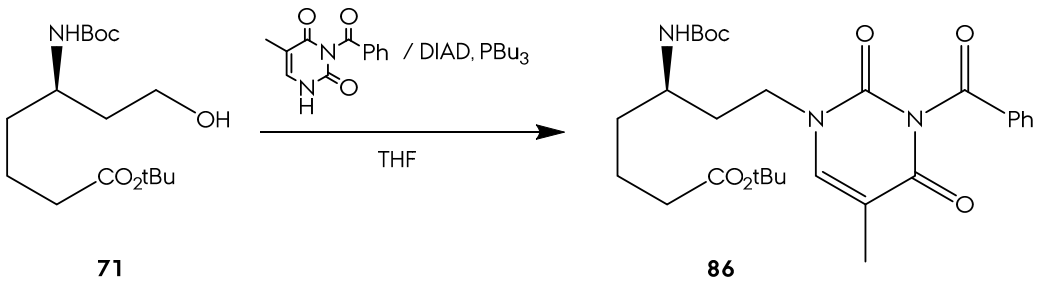

71 **86**

General procedure W was followed with the next quantities: 46 mg of alcohol **71** (395.0 g/mol; 0.118 mmol); 60 mg of *N*^{3}-benzoyl-thymine (prepared at lab, see laboratory prepared reagents, 230.2 g/mol, 0.261 mmol); 52 mg of PBu_3 (202.3 g/mol, 0.261 mmol); 52 mg of DIAD (202.2 g/mol, 0.261 mmol); 4 mL of dry THF. Flash chromatography afforded 47 mg of product **86** (Hexanes/AcOEt 75:25, 75 % yield).

P52.- Selective Deprotection of PNA monomer 86.

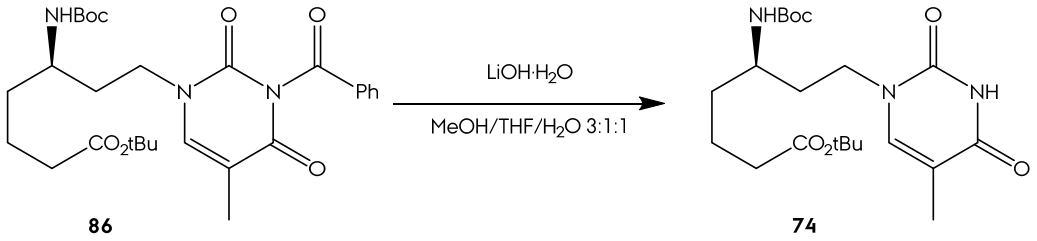

For this hydrolysis, general procedure R was followed with the next quantities: 9 mg of **86** (529.2 g/mol; 0.058 mmol); 2 mL of MeOH/THF/H_2O 3:1:1 solution; 5 mg (2.2 equiv) of $LiOH \cdot H_2O$ (41.9 g/mol; 0.13 mmol): reaction time of 4 h. Flash chromatography afforded 7 mg of product **74** (Hexanes/AcOEt 7:3, 97 % yield).

***tert*-butyl (*R*)-5-((tert-butoxycarbonyl)amino)-7-(5-methyl-2,4-dioxo-3,4-dihydropyrimidin-1(2*H*)-yl)heptanoate (74)**

$\mathbf{R}_f$ 0.40 (Hexanes/AcOEt, 1:1)

$[\alpha]^{20}_D$ -15.4 (*c.* 0.7 in MeOH);

υ_{max} (neat)/cm^{-1} 3327 (N-H), 2976 (C-H), 1701 (C=O), 1670, 1166 (C-O).

δ_H (400 MHz, $CDCl_3$) 8.49 (1H, s, **CONHCO**), 7.12 (1H, s, **NCH**), 4.47 (1H, d, *J* 9.2, **NHCO**), 3.88 (1H, quintet, *J* 6.6, $\mathbf{H7_A}$), 3.59 (2H, m, **H5** and $\mathbf{H7_B}$), 2.23 (2H, td, *J* 7.1 and 4.3, **H2**), 1.91 (3H, s, $\mathbf{CCH_3}$), 1.72 - 1.41 (6H, **H3**, **H4** and **H6**), 1.44 (18H, s, $\mathbf{C(CH_3)_3}$).

δ_C (50 MHz, $CDCl_3$) 172.9 (s, **C1**), 164.2 (s, **NCO**), 156.0 (s, **NCOO**), 150.9 (s, **NCON**), 141.3 (d, **NCH**), 110.7 (s, $\mathbf{CCH_3}$), 80.5 (s, $\mathbf{CO_2C(CH_3)_3}$), 79.8 (s, $\mathbf{NCO_2C(CH_3)_3}$), 48.3 (d, **C5**), 46.4 (t, **C7**), 35.3 (t, **C2**), 35.1 (t, **C4**), 34.9 (t, **C6**), 28.5 (q, $\mathbf{CO_2C(CH_3)_3}$), 28.3 (q, $\mathbf{NCO_2C(CH_3)_3}$), 21.4 (t, **C3**), 12.5 (q, $\mathbf{CCH_3}$).

m/z (M+Na) calcd for $\mathbf{C_{21}H_{35}N_3O_6Na}$, 448.2418; found, 448.2420, $\mathbf{\Delta = 0.42\ ppm}$.

P53.- Two Steps Transesterification of 74 to 87.

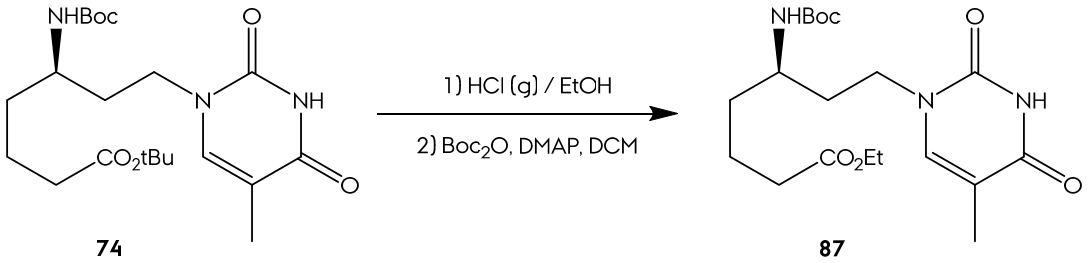

4.8 mg of **74** (425.2 g/mol, 0.073 mmol) were dissolved in 3 mL of dry EtOH. HCl gas (hydrogen chloride, CAS: 7647-01-0, gas, 36.4 g/mol, commercial) was bubbled for 5 min. Solvent was removed under reduced pressure and the crude was dissolved in 2 mL of dry DCM. 8 mg of Boc_2O (di-*tert*-butyl dicarbonate, CAS: 24424-99-5, crystals, 218.2 g/mol, 0.038 mmol, commercial) and 9 mg of DMAP (4-(dimethylamino)pyridine, CAS: 1122-58-3, white powder, 122.1 g/mol, 0.073 mmol, commercial). The solution was magnetically stirred at room temperature for 12 h.

10 mL of DCM were added and the mixture was washed with water (2 times), 1 M HCl (2 times) and brine (1 time). The solution was dried with anhydrous Na_2SO_4, filtrated and the solvent removed under reduced pressure. Flash chromatography afforded 2.4 mg of product **87** (Hexanes/AcOEt 7:3, 54 % yield).

Ethyl (*R*)-5-((tert-butoxycarbonyl)amino)-7-(5-methyl-2,4-dioxo-3,4-dihydropyrimidin-1(2*H*)-yl)heptanoate (87)

$\mathbf{R}_f$ 0.45 (Hexanes/AcOEt, 1:1)

$[\alpha]^{20}_D$ -9.2 (*c.* 0.24 in MeOH);

υ_{max} (film)/cm^{-1}

δ_H (400 MHz, $CDCl_3$) 8.03 (1H, s, **CONHCO**), 7.12 (1H, s, **NCH**), 4.41 (1H, d, *J* 7.4, **NHCO**), 4.12 (2H, q, *J* 7.1, **OCH_2CH_3**), 3.82 (1H, m, **$H7_A$**), 3.60 (2H, m, **H5** and **$H7_B$**), 2.30 (2H, **H2**), 1.92 (3H, s, **CCH_3**), 1.69-1.45 (6H, **H3**, **H4** and **H6**), 1.45 (9H, s, **$C(CH_3)_3$**), 1.25 (3H, t, *J* 7.1, **OCH_2CH_3**).

δ_C (50 MHz, $CDCl_3$) 173.1 (s, **C1**), 163.5 (s, **NCO**), 156.0 (s, **NCOO**), 150.2 (s, **NCON**), 140.9 (d, **NCH**), 110.2 (s, **CCH_3**), 79.2 (s, **$CO_2C(CH_3)_3$**), 60.6 (t, **OCH_2CH_3**), 48.8 (d, **C5**), 46.7 (t, **C7**), 33.9 (t, **C2**), 35.1 (t, **C4**), 33.8 (t, **C6**), 28.5 (q, **$C(CH_3)_3$**), 21.4 (t, **C3**), 14.3 (q, **OCH_2CH_3**), 12.4 (q, **CCH_3**).

m/z (M+H) calcd for $\mathbf{C_{19}H_{32}N_3O_6}$, 398.2285; found, 398.2287, $\mathbf{\Delta = 0.34\ ppm}$.

P54.- Reaction of Alcohol 71 with 6-chloropurine.

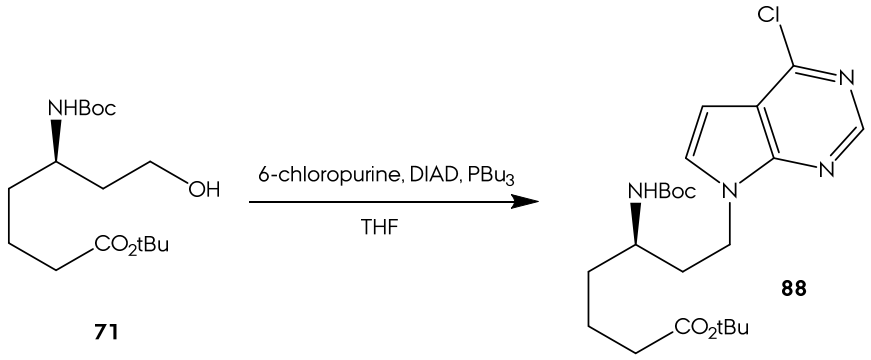

71 88

General procedure W was followed with the next quantities: 39 mg of alcohol **71** (395.0 g/mol; 0.099 mmol); 34 mg of 6-chloropurine (CAS: 87-42-3, orange powder, 154.5 g/mol, 0.22 mmol, commercial); 44 mg of PBu_3 (202.3 g/mol, 0.22 mmol); 44 mg of DIAD (202.2 g/mol, 0.22 mmol); 4 mL of dry THF. Flash chromatography afforded 26 mg of product **88** (Hexanes/AcOEt 75:25, 61 % yield).

***tert*-butyl (*R*)-5-((tert-butoxycarbonyl)amino)-7-(6-chloro-9*H*-purin-9-yl)heptanoate (88)**

$\mathbf{R}_f$ 0.47 (Hexanes/AcOEt, 1:1)

$[\alpha]^{20}_D$ -10.5 (*c.* 1.4 in MeOH);

υ_{max} (neat)/cm^{-1} 3329 (N-H), 2978 (C-H), 1701 (C=O, ester), 1593, 1251 (C-O).

δ_H (400 MHz, $CDCl_3$) 8.75 (1H, s, **NC<u>H</u>NCCl**), 8.73 (1H, s, rotamer, **NC<u>H</u>NCCl**), 8.33 (1H, s, **CH_2NC<u>H</u>N**), 8.30 (1H, s, rotamer, **CH_2NC<u>H</u>N**), 4.49 (1H, d, *J* 8.0, **N<u>H</u>**), 4.40 (1H, ABXY, *J* 14.1 7.2 5.2, **H7$_A$**), 4.33 (1H, quintet, *J* 7.2, **H7$_B$**), 3.61 (1H, **H5**), 2.18 (2H, m, **H2**), 1.91 - 1.84 (2H, **H6**), 166-1.40 (2H, **H3** and **H4**), 1.44 (9H, s, **$CO_2C(CH_3)_3$**), 1.40 (9H, s, **$NCO_2C(CH_3)_3$**).

δ_C (50 MHz, $CDCl_3$) 172.7 (s, **C1**), 156.1 (s, **N<u>C</u>OO**), 152.1 (d, **ClCN<u>C</u>H**), 152.0 (s, **<u>C</u>Cl**), 151.2 (s, **ClCC<u>C</u>**), 146.2 (d, **CN<u>C</u>HNC**), 131.9 (s, **ClC<u>C</u>**), 80.5 (s, **CO_2<u>C</u>$(CH_3)_3$**), 80.0 (s, **NCO_2<u>C</u>$(CH_3)_3$**), 48.3 (d, **C5**), 42.0 (t, **C7**), 36.1 (t, **C6**),

35.1 (t, **C2**), 35.0 (t, **C4**), 28.5 (q, $\mathbf{CO_2C(C\underline{H_3})_3}$), 28.3 (q, $\mathbf{NCO_2C(C\underline{H_3})_3}$), 21.4 (t, **C3**).

m/z (M+Na) calcd for $\mathbf{C_{21}H_{32}N_5O_4NaCl}$, 476.2035; found, 476.2040, **Δ = 1.04 ppm**.

P55.- Reaction of Alcohol 71 with 2-amino-6-chloropurine.

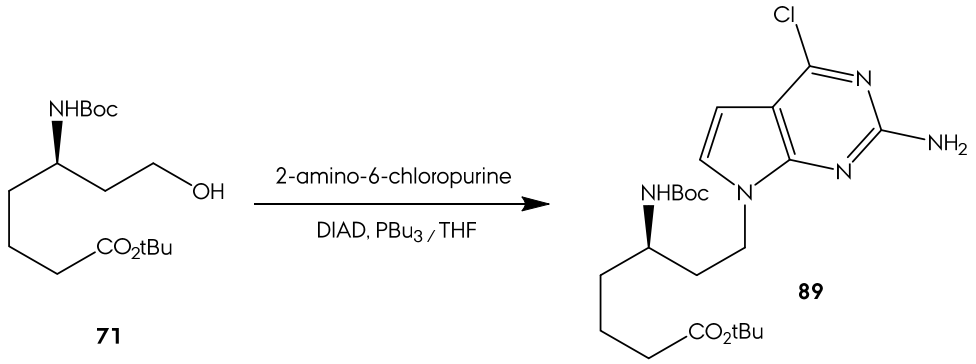

71 89

General procedure W was followed with the next quantities: 35 mg of alcohol **71** (395.0 g/mol; 0.103 mmol); 53 mg of 2-amino-6-chloropurine (CAS: 10310-21-1, white powder, 169.5 g/mol, 0.311 mmol, commercial); 63 mg of PBu_3 (202.3 g/mol, 0.311 mmol); 63 mg of DIAD (202.2 g/mol, 0.311 mmol); 4 mL of dry THF. Flash chromatography afforded 22 mg of product **89** (Hexanes/AcOEt 75:25, 53 % yield).

<u>*tert*-butyl (*R*)-7-(2-amino-6-chloro-9*H*-purin-9-yl)-5-((tert-butoxycarbonyl)amino)heptanoate (89)</u>

$\mathbf{R}_f$ 0.35 (Hexanes/AcOEt, 1:1)

$[\alpha]^{20}_D$ -15.7 (*c.* 1.2 in MeOH);

υ_{max} (neat)/cm^{-1} 3329 (N-H), 2976 (C-H), 1701 (C=O, ester), 1610 (C=O, carbamate), 1251 (C-O).

δ_H (200 MHz, $CDCl_3$) 7.88 (1H, s, $\mathbf{NC\underline{H}N}$), 5.23 (2H, br s, $\mathbf{N\underline{H_2}}$), 4.56 (1H, d, *J* 8, $\mathbf{N\underline{H}}$), 4.13 (2H, **H7**), 3.62 (1H, br s, **H5**), 2.21 (2H, t, *J* 7.0, **H2**), 2.03-1.46 (6H, **H3**, **H4** and **H6**), 1.44 (9H, s, $\mathbf{CO_2C(C\underline{H_3})_3}$), 1.42 (9H, s, $\mathbf{NCO_2C(C\underline{H_3})_3}$).

δ_C (50 MHz, $CDCl_3$) 172.9 (s, **C1**), 159.2 (s, $\mathbf{\underline{C}NH_2}$), 155.9 (s, $\mathbf{N\underline{C}OO}$), 153.9 (s, $\mathbf{\underline{C}Cl}$), 151.4 (s, $\mathbf{ClCC\underline{C}}$), 143.0 (d, $\mathbf{N\underline{C}H}$), 125.6 (s, $\mathbf{ClC\underline{C}}$), 80.5 (s,

$CO_2\underline{C}(CH_3)_3$), 79.8 (s, **$NCO_2\underline{C}(CH_3)_3$**), 48.5 (d, **C5**), 41.3 (t, **C7**), 35.7 (t, **C2**), 35.1 (t, **C4**), 35.0 (t, **C6**), 28.5 (q, **$CO_2C(C\underline{H}_3)_3$**), 28.3 (q, **$NCO_2C(C\underline{H}_3)_3$**), 21.4 (t, **C3**).

m/z (M+Na) calcd for **$C_{21}H_{33}N_6O_4NaCl$**, 491.2144; found, 491.2150, **Δ = 1.21 ppm**.

P56.- Chemoselective Reduction of Aldehyde 52 to Alcohol 68.

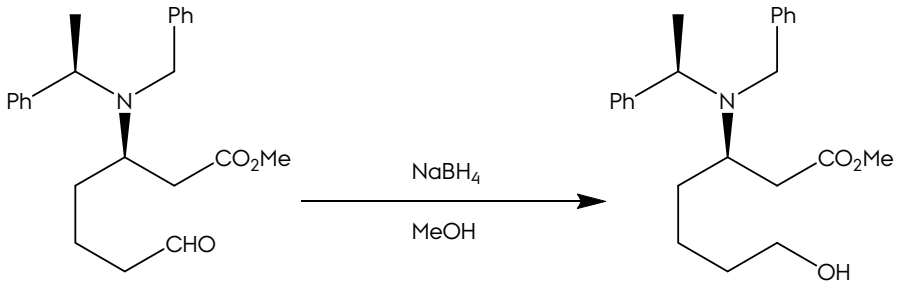

54 **68**

In a round bottom flask, 23 mg (368.0 g/mol; 0.063 mmol) of aldehyde **54** were dissolved in 5 mL of dry MeOH. The flask was sealed, purged with Ar and cooled to 0 ºC in an ice - water bath. 9.6 mg (4 equiv) of $NaBH_4$ (sodium borohydride, CAS: 16940-66-2, white solid, 37.8 g/mol, 0.253 mmol, commercial) were added and stirring continued at room temperature for 1 h.

3 mL of water were added and the solution was extracted 3 times with AcOEt. The organic layers were combined, washed with water (2 times) and brine (1 time). Drying the solution with anhydrous Na_2SO_4, filtration and forward solvent removal under reduced pressure, afforded 23 mg of alcohol **68**, 98 % yield.

P57.- Funtional Group Interconversion of Alcohol 54 to Bromide 90.

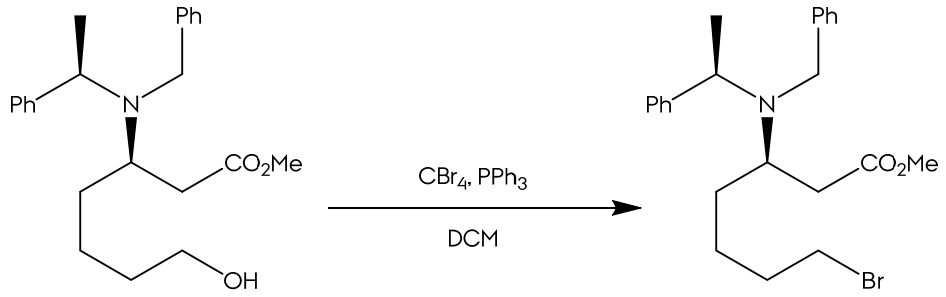

68 **90**

General procedure V was followed with the next quantities: 80 mg of alcohol **68** (370.0 g/mol, 0.217 mmol); 100 mg of CBr_4 (331.6 g/mol, 0.303 mmol); 79 mg of PPh_3 (262.2 g/mol, 0.303 mmol); 3 mL of dry DCM. After workup, 60 mg of bromide **90** were obtained, 64 % yield.

Methyl (*R*)-3-(benzyl((*R*)-1-phenylethyl)amino)-7-bromoheptanoate (90).

$\mathbf{R}_f$ 0.88 (Hexanes/AcOEt, 1:1)

$[\alpha]^{20}_{D}$ +9.26 (*c.* 0.88 in $CHCl_3$)

υ_{max} (neat)/cm^{-1} 2929 (C-H), 1734 (C=O), 1452, 1201 (C-O), 702 (C-Br).

δ_H (400 MHz, $CDCl_3$) 7.44 - 7.24 (10H, $\mathbf{C_{ar}\underline{H}}$), 3.84 (1H, q, *J* 7.0, $\mathbf{C\underline{H}CH_3}$), 3.79 (1H, AB, *J* 15.2, $\mathbf{NC\underline{H_A}H}$), 3.57 - 3.53 (1H, $\mathbf{NCH\underline{H_B}}$), 3.56 (3H, s, $\mathbf{CO_2C\underline{H_3}}$), 3.40 (3H, t, *J* 6.6, **H7**), 3.31 (1H, **H3**), 2.04 (2H, m, **H2**), 1.78 (2H, **H6**), 1.49 (2H, **H4**), 1.36 - 1.26 (2H, **H5**), 1.35 (3H, d, *J* 6.9, $\mathbf{CHC\underline{H_3}}$).

δ_C (50 MHz, $CDCl_3$) 173.4 (s, $\mathbf{\underline{C}O_2CH_3}$), 143.2 (s, $\mathbf{C_{ipso}}$), 141.7 (s, $\mathbf{C_{ipso}}$), 128.5 (d, $\mathbf{C_{ar}}$), 128.4 (d, $\mathbf{C_{ar}}$), 128.3 (d, $\mathbf{C_{ar}}$), 128.1 (d, $\mathbf{C_{ar}}$), 127.2 (d, $\mathbf{C_{ar}}$), 126.9 (d, $\mathbf{C_{ar}}$), 58.2 (d, $\mathbf{\underline{C}HCH_3}$), 53.9 (d, **C3**), 51.6 (q, $\mathbf{CO_2\underline{C}H_3}$), 50.1 (t, $\mathbf{N\underline{C}H_2}$), 36.5 (t, **C2**), 34.1 (t, **C4**), 32.8 (t, **C7**), 32.7 (t, **C6**), 25.8 (t, **C5**), 20.0 (q, $\mathbf{CH\underline{C}H_3}$).

m/z (M+H) calcd for $\mathbf{C_{23}H_{31}NO_2Br}$, 432.1532; found, 370.2374, $\mathbf{\Delta = 5.16\ ppm}$.

P58.- Thymine Introduction in Bromide 90.

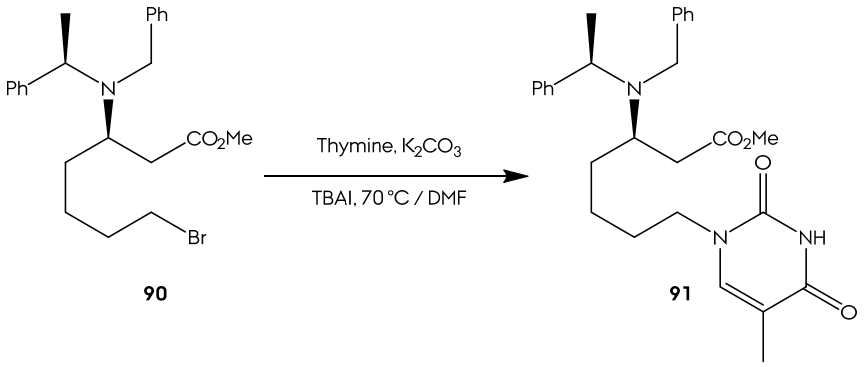

90 **91**

General procedure X was followed with the next quantities: 37 mg of bromide **91** (432.0 g/mol; 0.087 mmol); 33 mg of thymine (CAS: 65-71-4, white powder, 126.1 g/mol, 0.262 mmol, commercial); 10 mg of TBAI (396.3 g/mol, 0.0262 mmol); 18 mg of K_2CO_3 (138.2 g/mol, 0.131 mmol); 5 mL of dry DMF. Flash chromatography afforded 14 mg of PNA monomer **91** (Hexanes/AcOEt 6:4), 34 % yield.

Methyl (*R*)-3-(benzyl((*R*)-1-phenylethyl)amino)-7-thiminylheptanoate (91).

$\mathbf{R}_f$ 0.32 (Hexanes/AcOEt, 1:1).
$[\alpha]^{20}_D$ +4.36 (*c.* 1.66 in $CHCl_3$).
υ_{max} (neat)/cm^{-1} 3172 (N-H), 2927 (C-H), 1676 - 1627 (C=O), 1211 (C-O), 732.

δ_H (400 MHz, $CDCl_3$) 8.66 (1H, br s, **NH**), 7.41 - 7.23 (10H, $\mathbf{C_{ar}H}$), 6.96 (1H, q, *J* 1.2, **NCH**), 3.84 (1H, q, *J* 6.8, **CHCH₃**), 3.80 (1H, AB, *J* 15.2, $\mathbf{NCH_AH}$), 3.66 (2H, m, **H7**), 3.58 - 3.53 (1H, $\mathbf{NCHH_B}$), 3.58 (3H, s, $\mathbf{CO_2CH_3}$), 3.30 (1H, septet, *J* 4.3, **H3**), 2.08 (1H, ABX, *J* 14.9 3.9, $\mathbf{H2_A}$), 2.01 (1H, ABX, *J* 15.0 8.9, $\mathbf{H2_B}$), 1.94 (3H, d, *J* 1.1, **CCH₃**), 1.65 - 1.52 (2H, **H6**), 1.40 (4H, **H4**, **H5**), 1.34 (3H, d, *J* 7.0, **CHCH₃**).

δ_C (50 MHz, $CDCl_3$) 173.4 (s, $\mathbf{CO_2CH_3}$), 164.3 (s, **NCO**), 150.9 (s, **NCON**), 143.1 (s, $\mathbf{C_{ipso}}$), 141.6 (s, $\mathbf{C_{ipso}}$), 140.7 (d, **NCH**), 128.5 (d, $\mathbf{C_{ar}}$), 128.4 (d, $\mathbf{C_{ar}}$), 128.2 (d, $\mathbf{C_{ar}}$), 128.0 (d, $\mathbf{C_{ar}}$), 127.3 (d, $\mathbf{C_{ar}}$), 126.9 (d, $\mathbf{C_{ar}}$), 110.6 (s, **CCH₃**), 58.2 (d, **CHCH₃**), 53.8 (d, **C3**), 51.7 (q, $\mathbf{CO_2CH_3}$), 50.1 (t, $\mathbf{NCH_2}$), 48.5 (t, **C7**), 36.1 (t, **C2**), 33.0 (t, **C4**), 28.9 (t, **C6**), 23.9 (t, **C5**), 20.3 (q, **NCHCH₃**), 12.5 (q, **CCCH₃**).

m/z (M+H) calcd for $\mathbf{C_{28}H_{36}N_3O_4}$, 478.2700; found, 478.2710, **Δ = 2.02 ppm**.

Inventario Espectroscópico

(Spectroscopical Inventory)

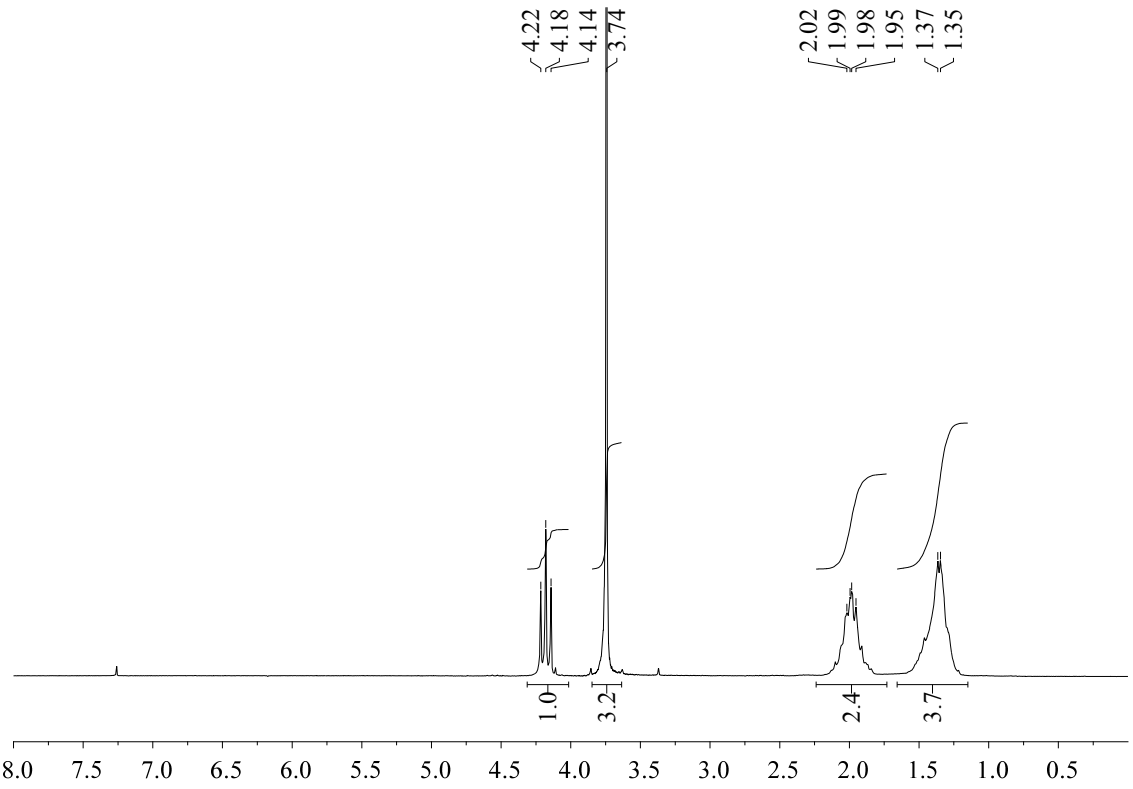
4.22
4.18
4.14
3.74
2.02
1.99
1.98
1.95
1.37
1.35
1.0
3.2
2.4
3.7
8.0 7.5 7.0 6.5 6.0 5.5 5.0 4.5 4.0 3.5 3.0 2.5 2.0 1.5 1.0 0.5

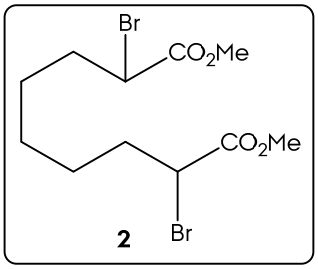
Br
CO2Me
CO2Me
Br
2

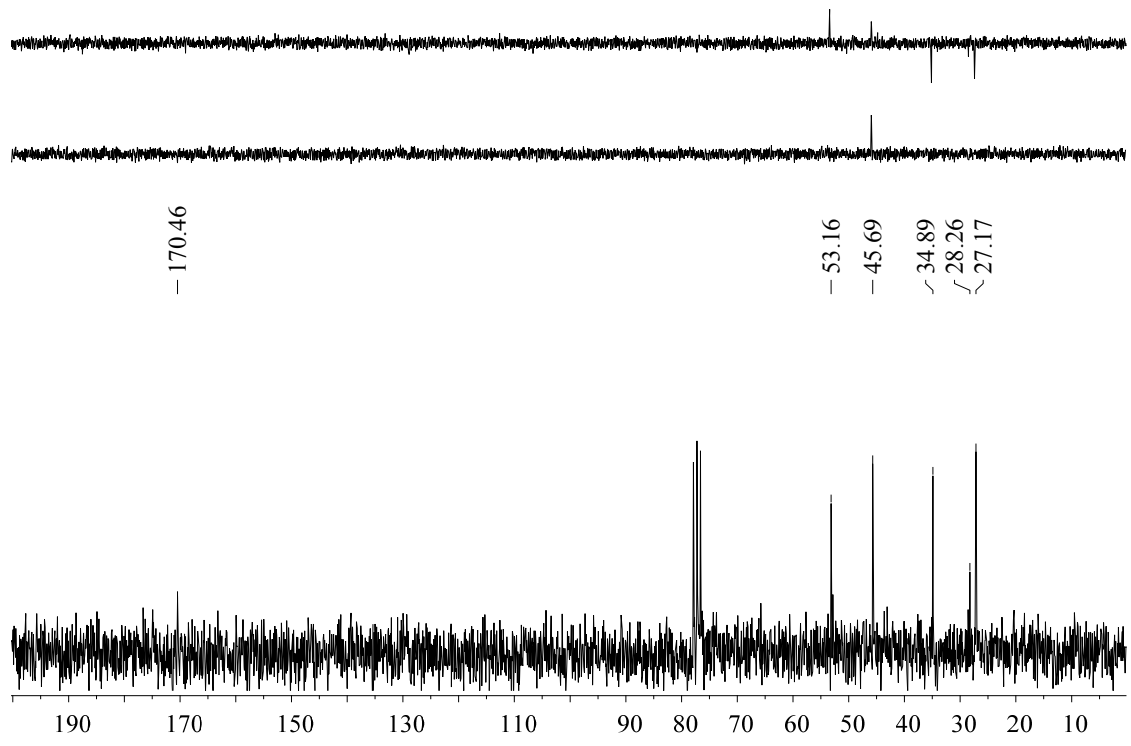
170.46
53.16
45.69
34.89
28.26
27.17
190 170 150 130 110 90 80 70 60 50 40 30 20 10

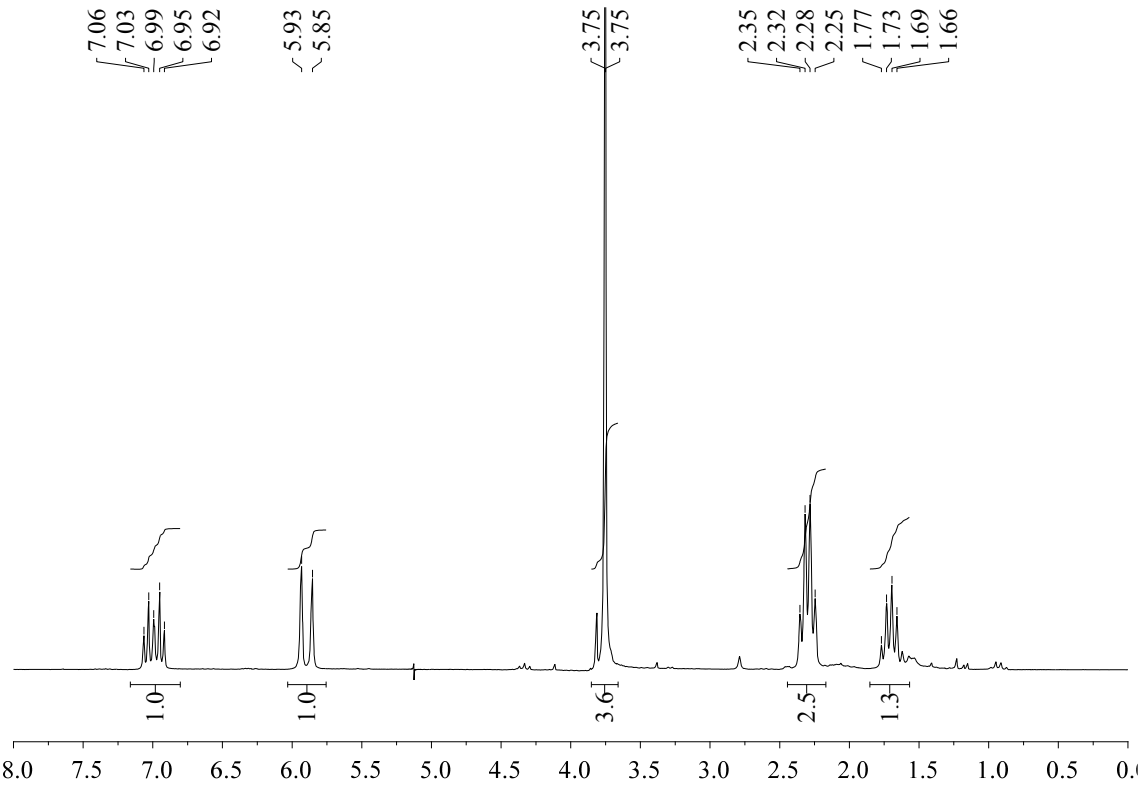
7.06
7.03
6.99
6.95
6.92
5.93
5.85
3.75
3.75
2.35
2.32
2.28
2.25
1.77
1.73
1.69
1.66
1.0
1.0
3.6
2.5
1.3
8.0
7.5
7.0
6.5
6.0
5.5
5.0
4.5
4.0
3.5
3.0
2.5
2.0
1.5
1.0
0.5

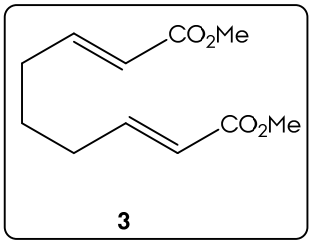
CO2Me
CO2Me

3

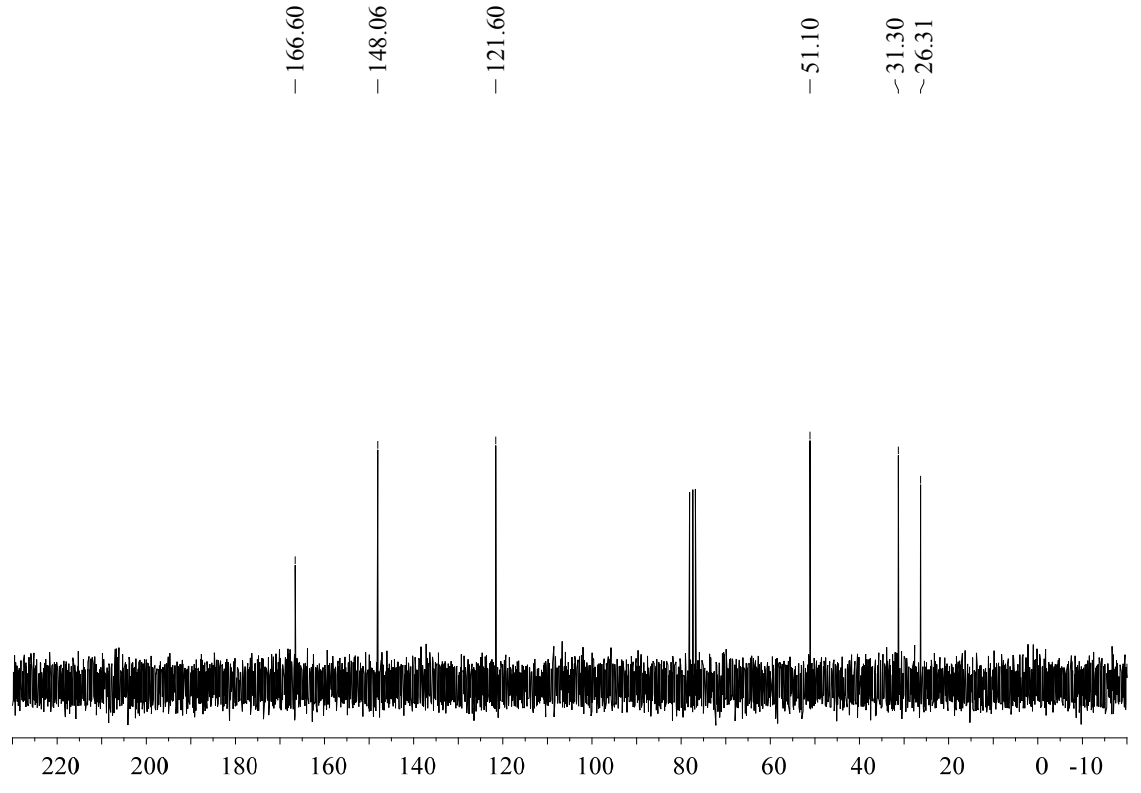
166.60
148.06
121.60
51.10
31.30
26.31
220
200
180
160
140
120
100
80
60
40
20
0
-10

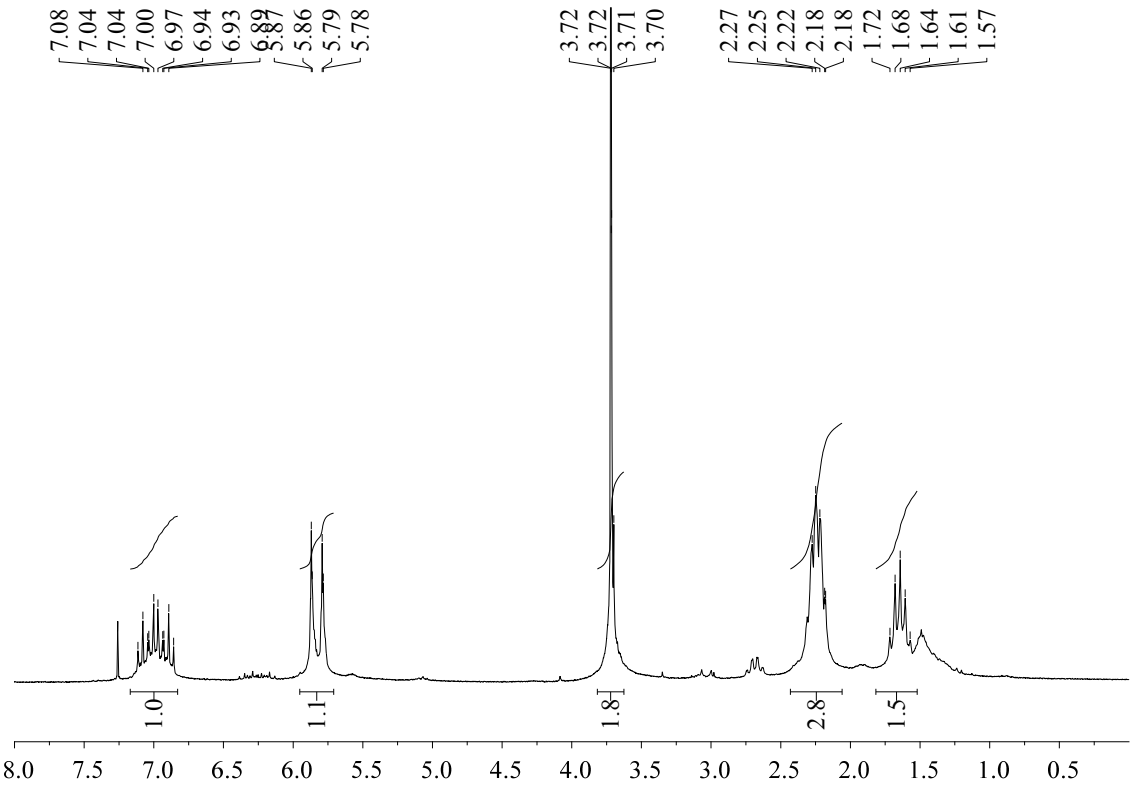
7.08
7.04
7.04
7.00
6.97
6.94
6.93
6.89
6.87
5.86
5.79
5.78
3.72
3.72
3.71
3.70
2.27
2.25
2.22
2.18
2.18
1.72
1.68
1.64
1.61
1.57
1.0
1.1
1.8
2.8
1.5
8.0 7.5 7.0 6.5 6.0 5.5 5.0 4.5 4.0 3.5 3.0 2.5 2.0 1.5 1.0 0.5

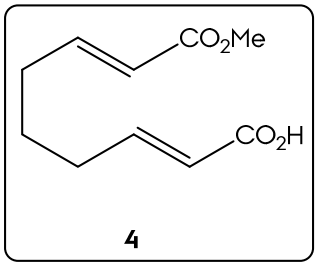
CO2Me
CO2H

4

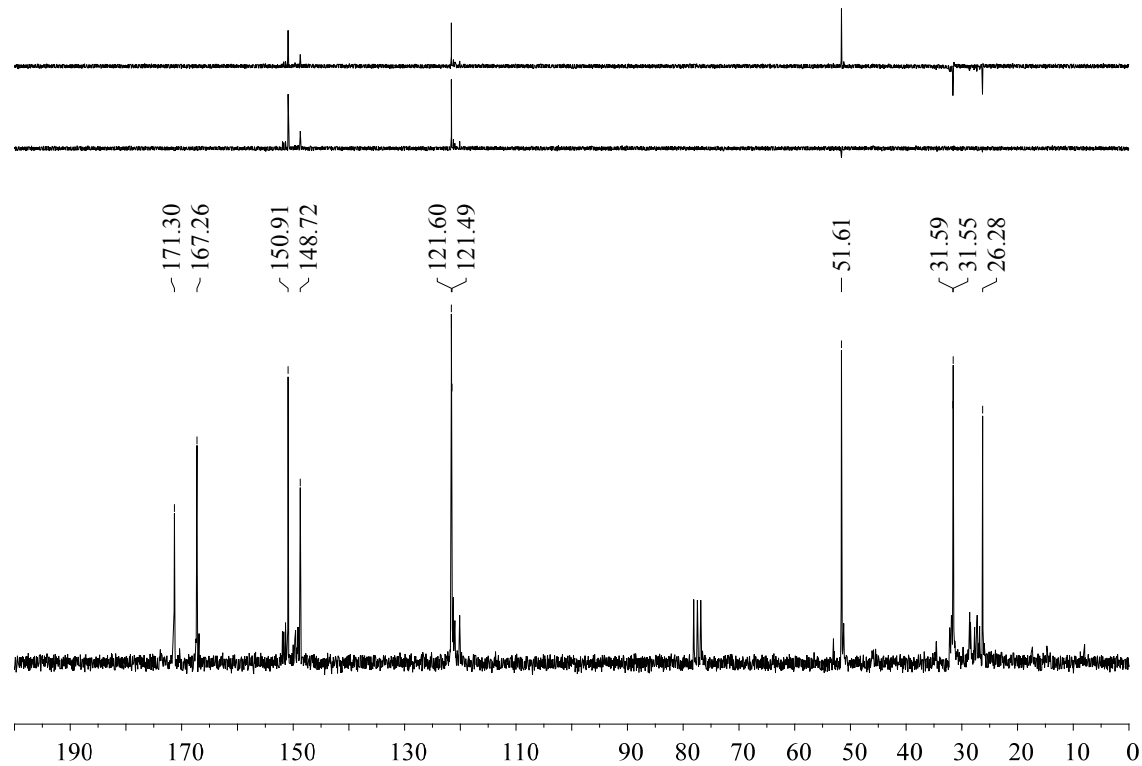
171.30
167.26
150.91
148.72
121.60
121.49
51.61
31.59
31.55
26.28
190 170 150 130 110 90 80 70 60 50 40 30 20 10 0

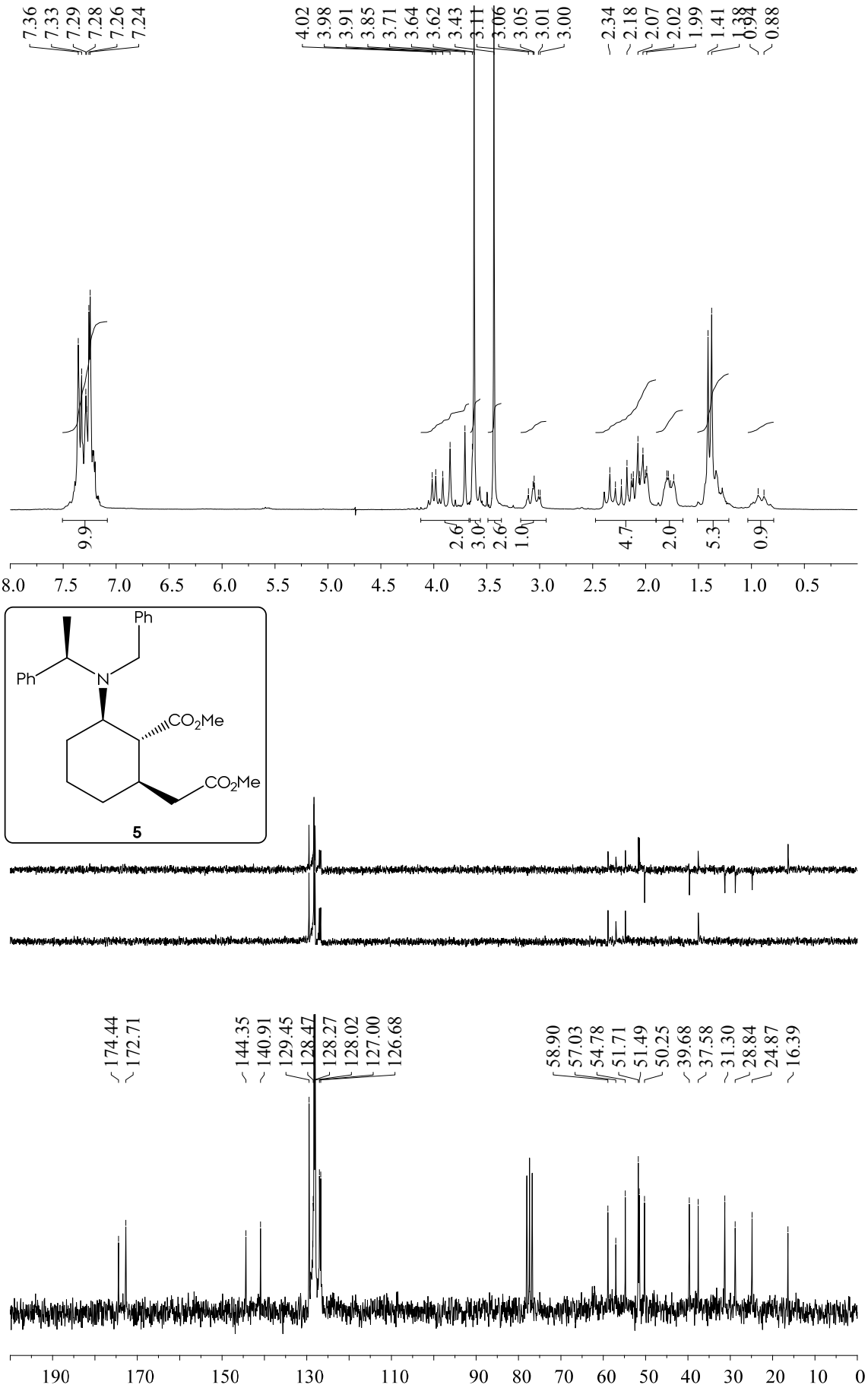
7.36
7.33
7.29
7.28
7.26
7.24
4.02
3.98
3.91
3.85
3.71
3.64
3.62
3.43
3.11
3.06
3.05
3.01
3.00
2.34
2.18
2.07
2.02
1.99
1.41
1.38
0.94
0.88
9.9
2.6
3.0
2.6
1.0
4.7
2.0
5.3
0.9
8.0 7.5 7.0 6.5 6.0 5.5 5.0 4.5 4.0 3.5 3.0 2.5 2.0 1.5 1.0 0.5
Ph
Ph
N
CO2Me
CO2Me
5
174.44
172.71
144.35
140.91
129.45
128.47
128.27
128.02
127.00
126.68
58.90
57.03
54.78
51.71
51.49
50.25
39.68
37.58
31.30
28.84
24.87
16.39
190 170 150 130 110 90 80 70 60 50 40 30 20 10 0

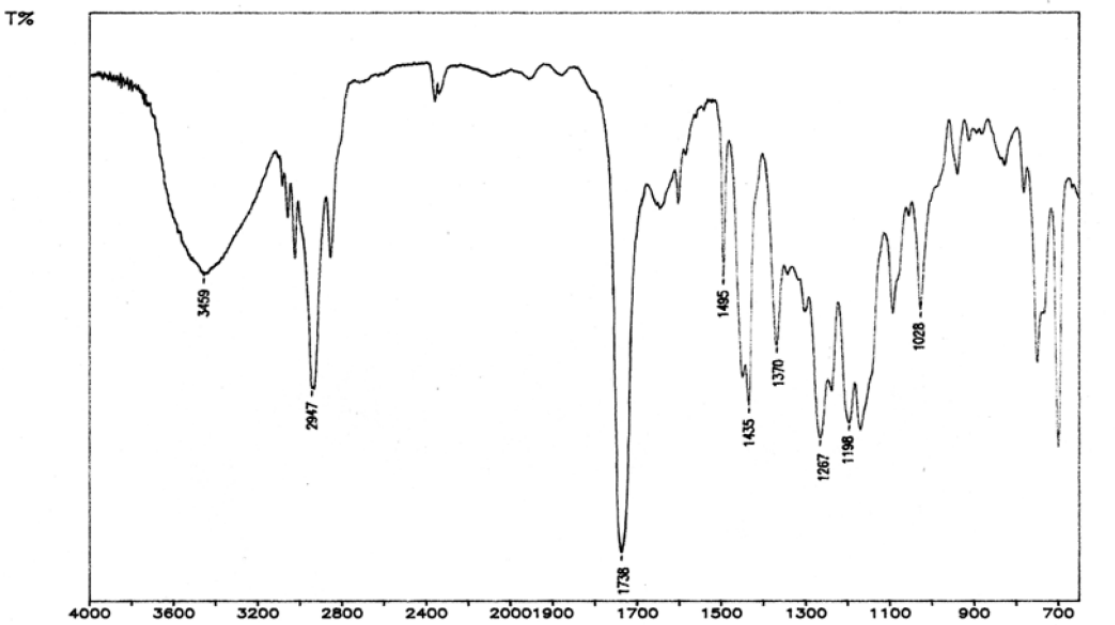
T%
3459
2947
1738
1495
1435
1370
1267
1198
1028
4000
3600
3200
2800
2400
2000
1900
1700
1500
1300
1100
900
700
cm⁻¹

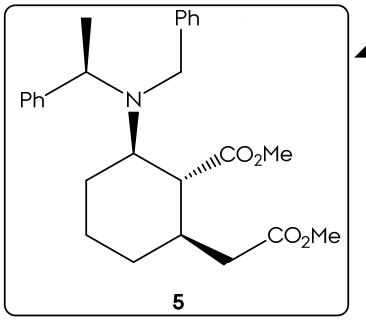
Ph
Ph
N
CO2Me
CO2Me
5

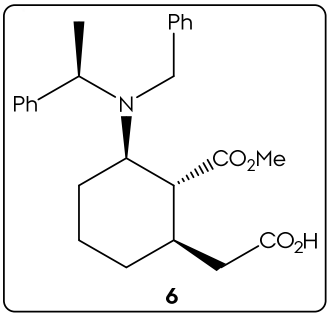
Ph
Ph
N
CO2Me
CO2H
6

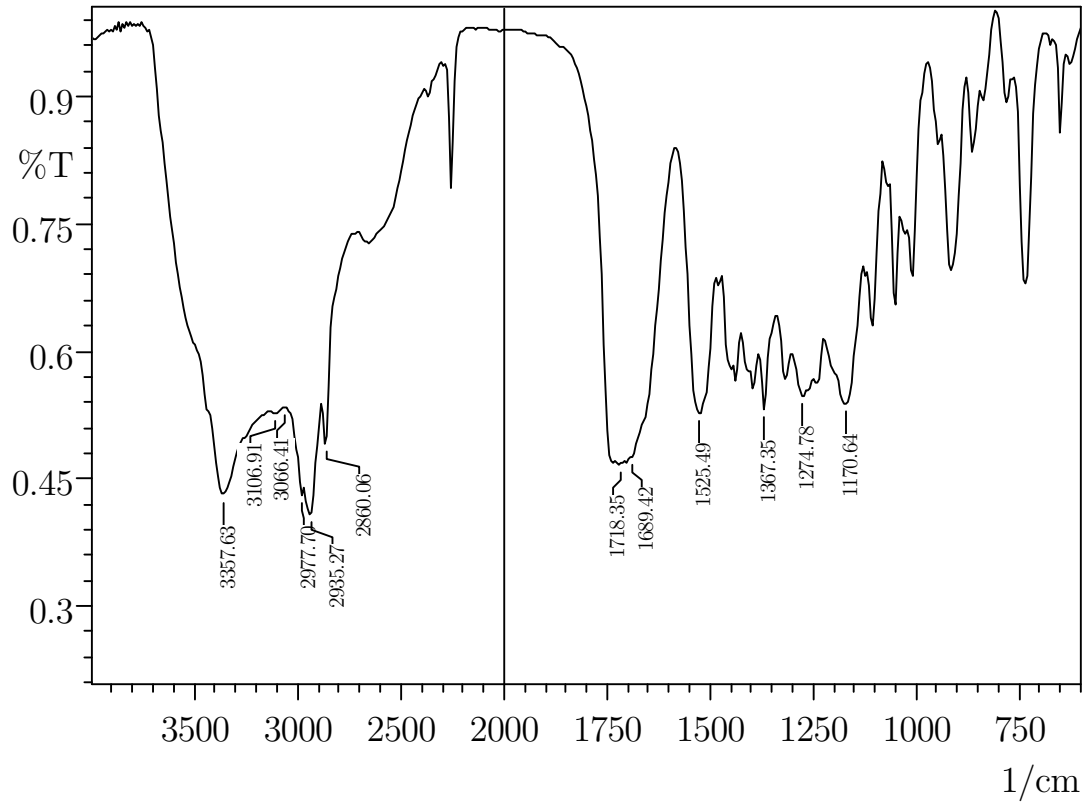
0.9
%T
0.75
0.6
0.45
0.3
3357.63
3106.91
3066.41
2977.70
2935.27
2860.06
1718.35
1689.42
1525.49
1367.35
1274.78
1170.64
3500
3000
2500
2000
1750
1500
1250
1000
750
1/cm

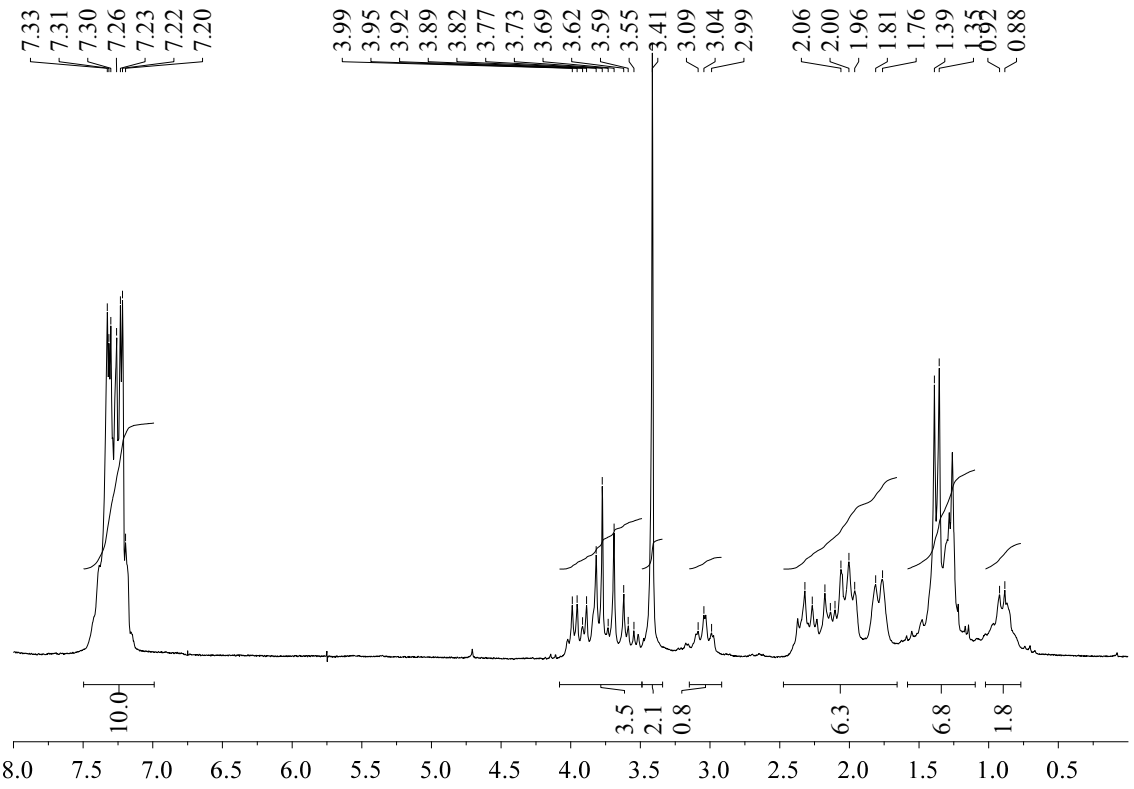
7.33
7.31
7.30
7.26
7.23
7.22
7.20
3.99
3.95
3.92
3.89
3.82
3.77
3.73
3.69
3.62
3.59
3.55
3.41
3.09
3.04
2.99
2.06
2.00
1.96
1.81
1.76
1.39
1.35
0.92
0.88
10.0
3.5
2.1
0.8
6.3
6.8
1.8
8.0 7.5 7.0 6.5 6.0 5.5 5.0 4.5 4.0 3.5 3.0 2.5 2.0 1.5 1.0 0.5

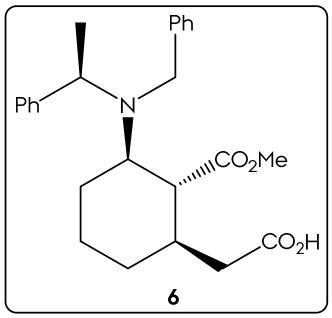
Ph
Ph
N
CO2Me
CO2H
6

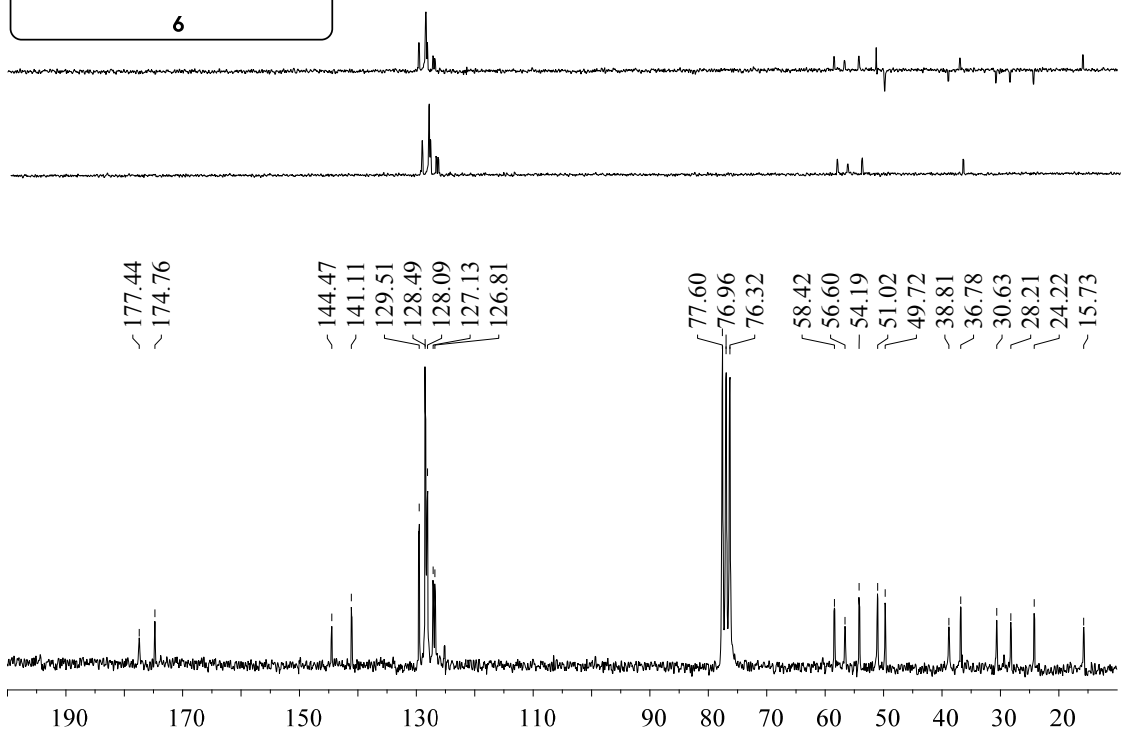
177.44
174.76
144.47
141.11
129.51
128.49
128.09
127.13
126.81
77.60
76.96
76.32
58.42
56.60
54.19
51.02
49.72
38.81
36.78
30.63
28.21
24.22
15.73
190 170 150 130 110 90 80 70 60 50 40 30 20

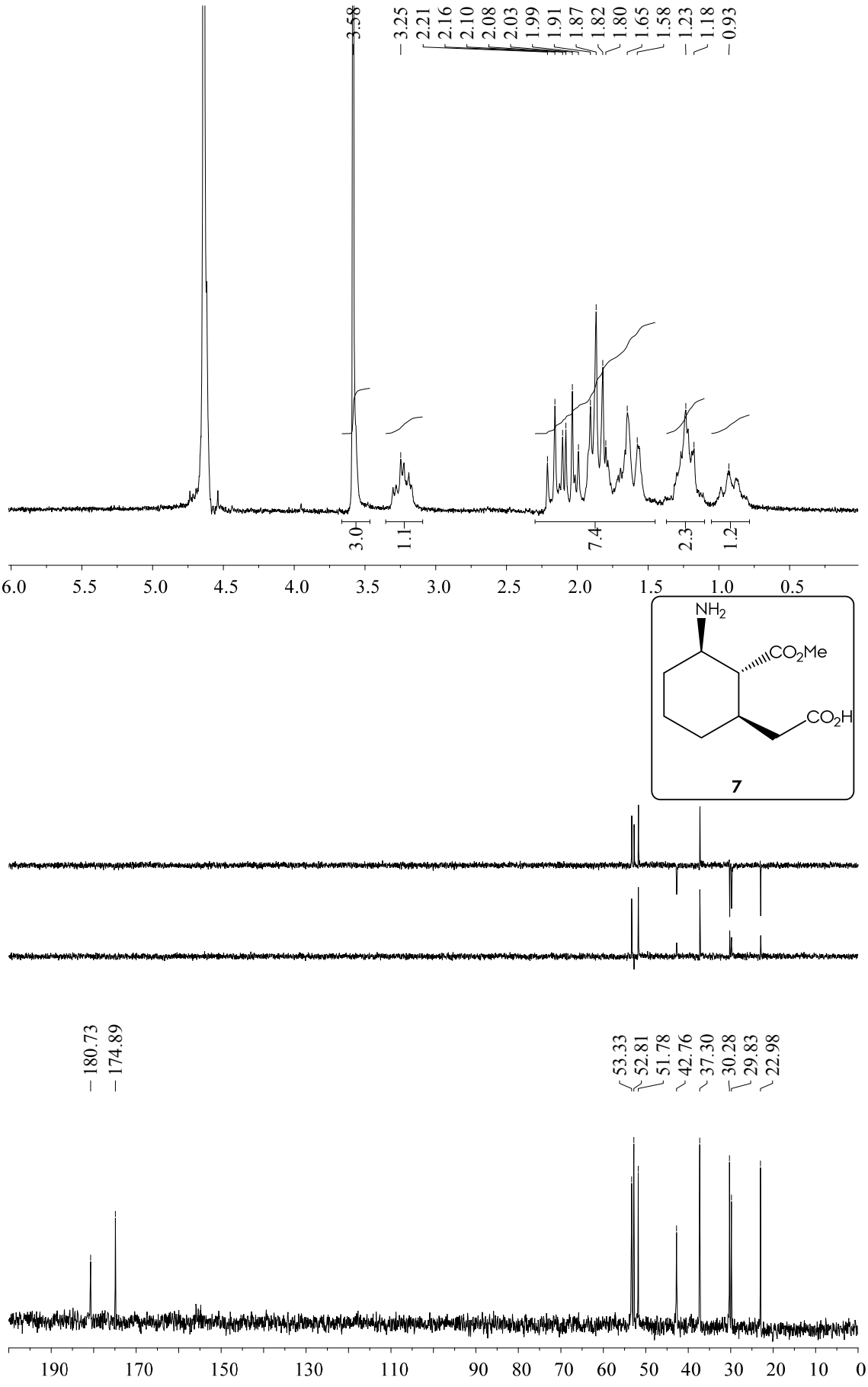
3.58
3.25
2.21
2.16
2.10
2.08
2.03
1.99
1.91
1.87
1.82
1.80
1.65
1.58
1.23
1.18
0.93
3.0
1.1
7.4
2.3
1.2
6.0
5.5
5.0
4.5
4.0
3.5
3.0
2.5
2.0
1.5
1.0
0.5
NH2
CO2Me
CO2H
7
180.73
174.89
53.33
52.81
51.78
42.76
37.30
30.28
29.83
22.98
190
170
150
130
110
90
80
70
60
50
40
30
20
10
0

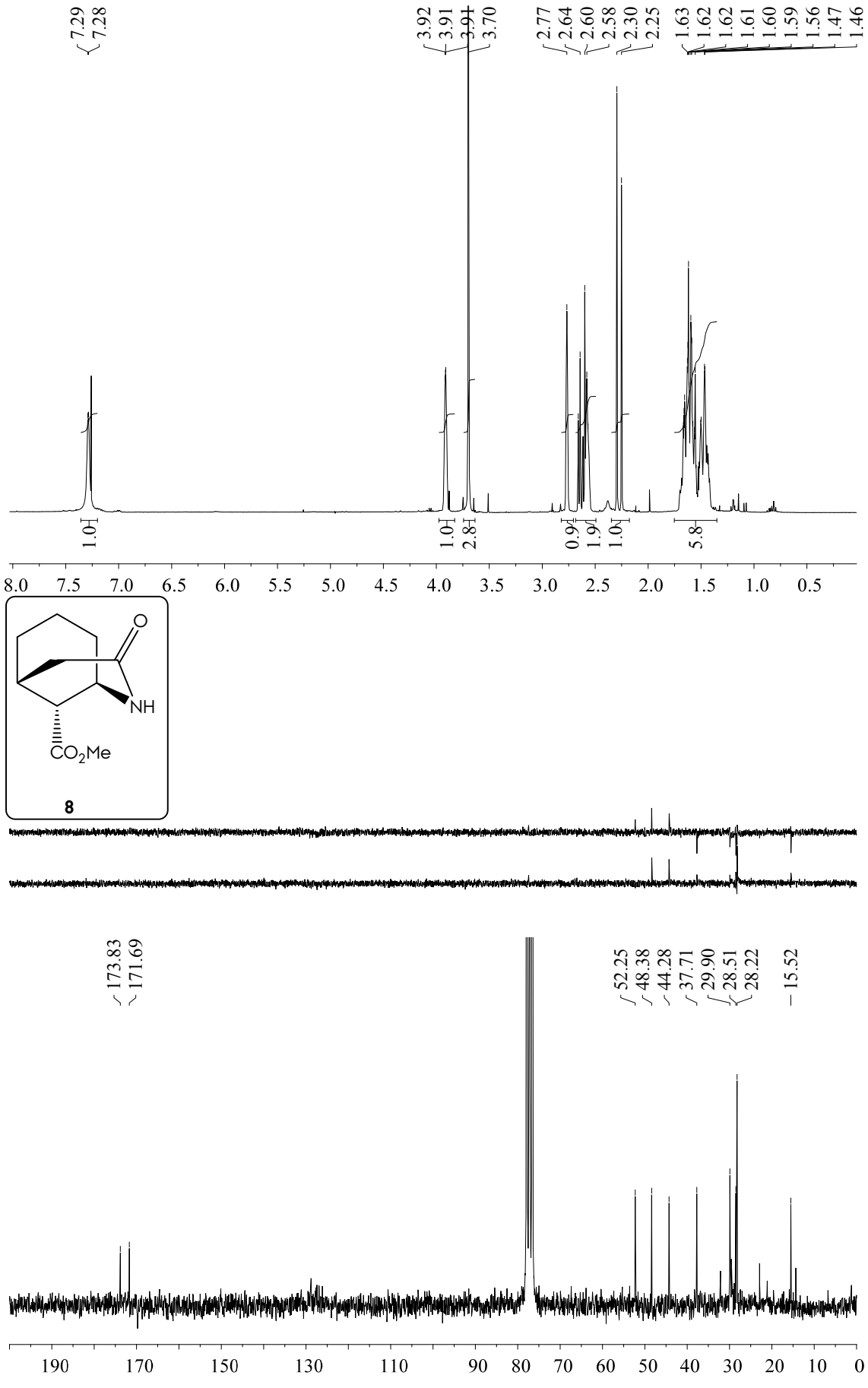
7.29
7.28
3.92
3.91
3.91
3.70
2.77
2.64
2.60
2.58
2.30
2.25
1.63
1.62
1.62
1.61
1.60
1.59
1.56
1.47
1.46
1.0
1.0
2.8
0.9
1.9
1.0
5.8
8.0 7.5 7.0 6.5 6.0 5.5 5.0 4.5 4.0 3.5 3.0 2.5 2.0 1.5 1.0 0.5
O
NH
CO2Me
8
173.83
171.69
52.25
48.38
44.28
37.71
29.90
28.51
28.22
15.52
190 170 150 130 110 90 80 70 60 50 40 30 20 10 0

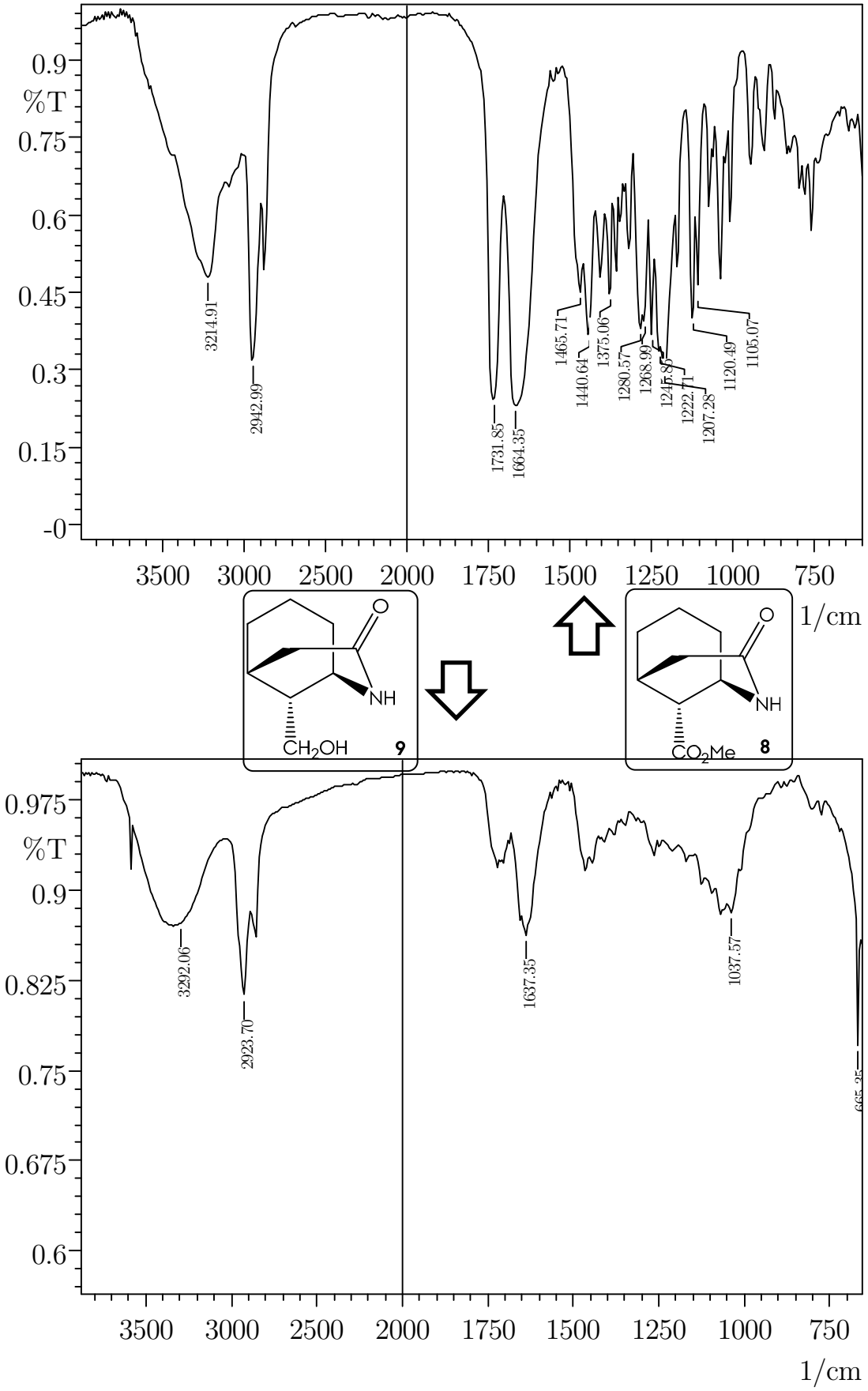
0.9
%T
0.75
0.6
0.45
0.3
0.15
-0
3214.91
2942.99
1731.85
1664.35
1465.71
1440.64
1375.06
1280.57
1268.99
1245.85
1222.71
1207.28
1120.49
1105.07
3500 3000 2500 2000 1750 1500 1250 1000 750
1/cm
NH
CH2OH
9
NH
CO2Me
8
0.975
%T
0.9
0.825
0.75
0.675
0.6
3292.06
2923.70
1637.35
1037.57
665.25
3500 3000 2500 2000 1750 1500 1250 1000 750
1/cm

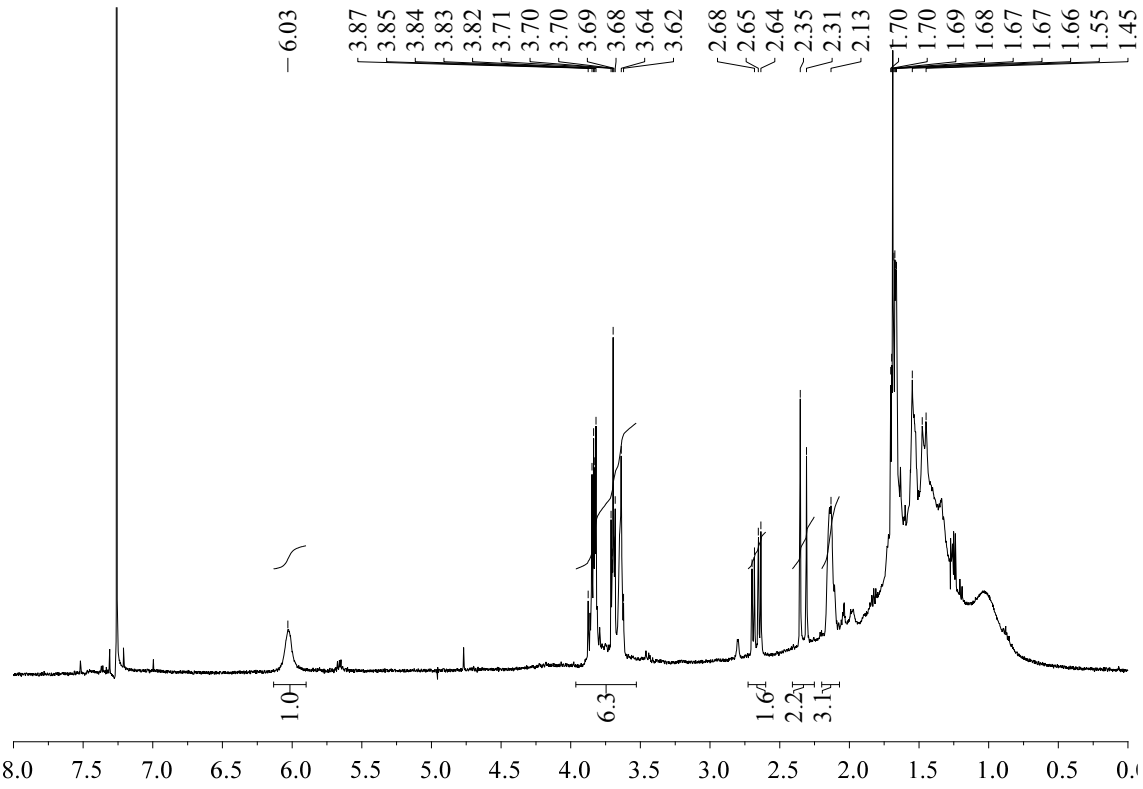
6.03
3.87
3.85
3.84
3.83
3.82
3.71
3.70
3.70
3.69
3.68
3.64
3.62
2.68
2.65
2.64
2.35
2.31
2.13
1.70
1.70
1.69
1.68
1.67
1.67
1.66
1.55
1.45
1.0
6.3
1.6
2.2
3.1
8.0 7.5 7.0 6.5 6.0 5.5 5.0 4.5 4.0 3.5 3.0 2.5 2.0 1.5 1.0 0.5

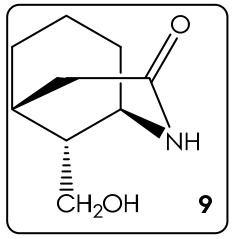
O
NH
CH2OH
9

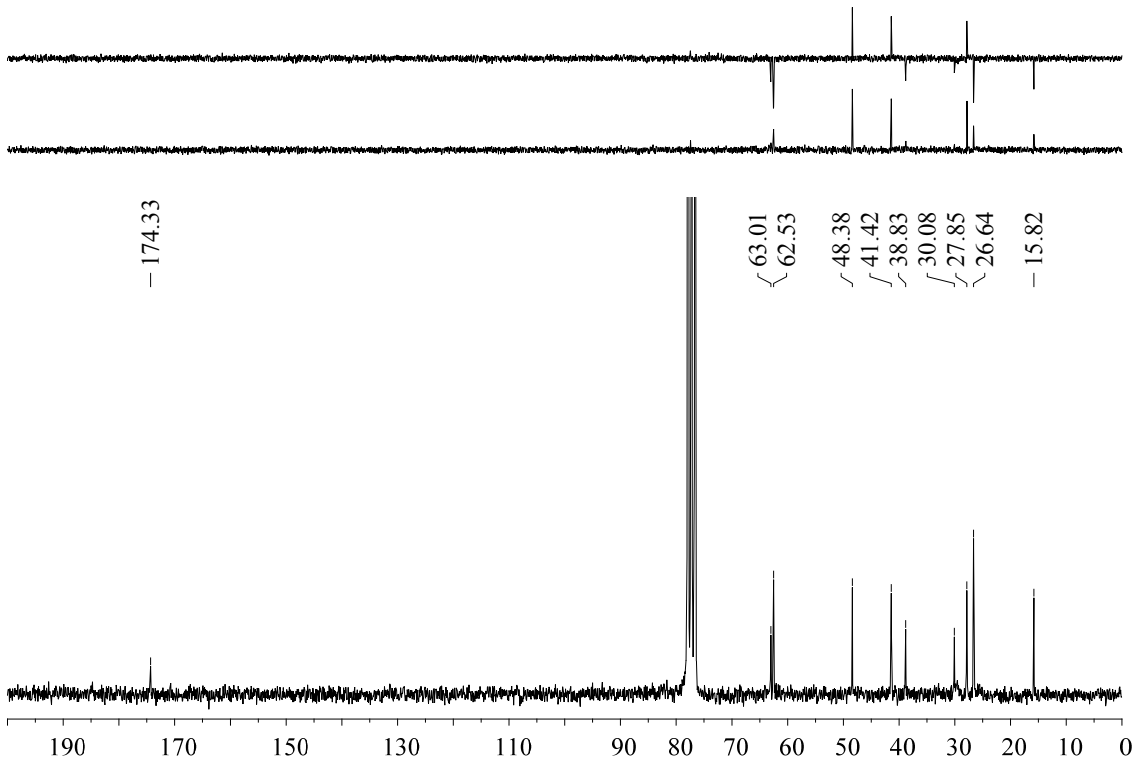
174.33
63.01
62.53
48.38
41.42
38.83
30.08
27.85
26.64
15.82
190 170 150 130 110 90 80 70 60 50 40 30 20 10 0

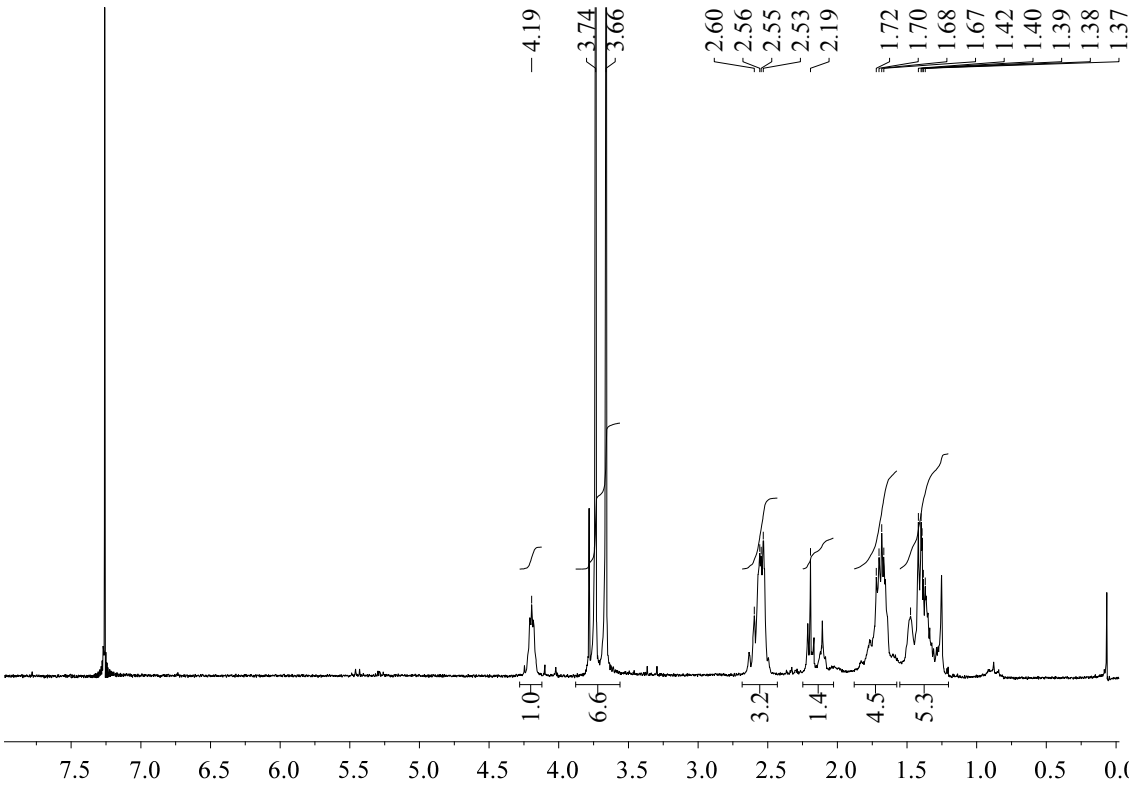
4.19
3.74
3.66
2.60
2.56
2.55
2.53
2.19
1.72
1.70
1.68
1.67
1.42
1.40
1.39
1.38
1.37
1.0
6.6
3.2
1.4
4.5
5.3
7.5 7.0 6.5 6.0 5.5 5.0 4.5 4.0 3.5 3.0 2.5 2.0 1.5 1.0 0.5

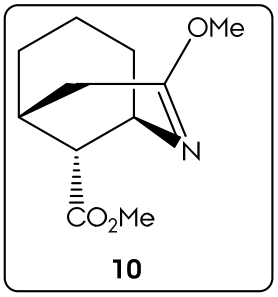
OMe
N
CO2Me

10

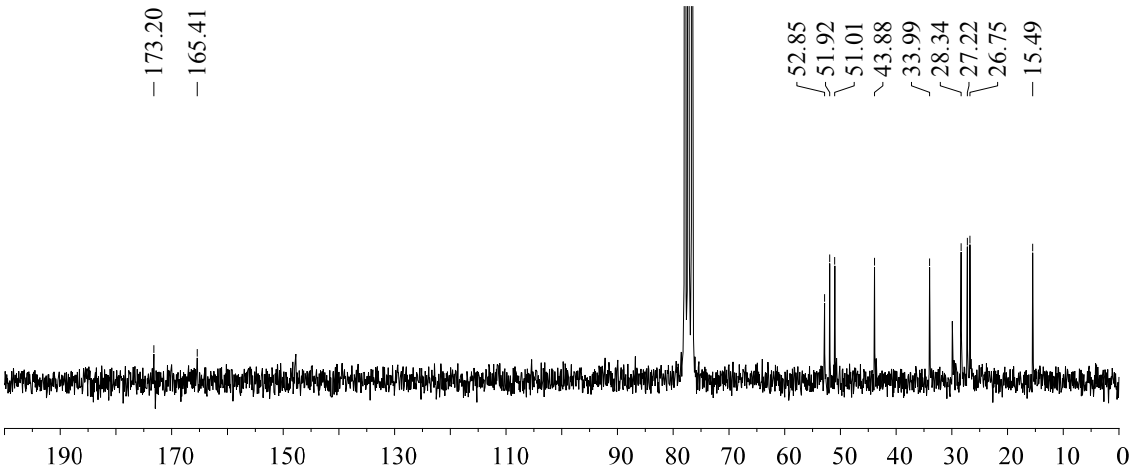
173.20
165.41
52.85
51.92
51.01
43.88
33.99
28.34
27.22
26.75
15.49
190 170 150 130 110 90 80 70 60 50 40 30 20 10 0

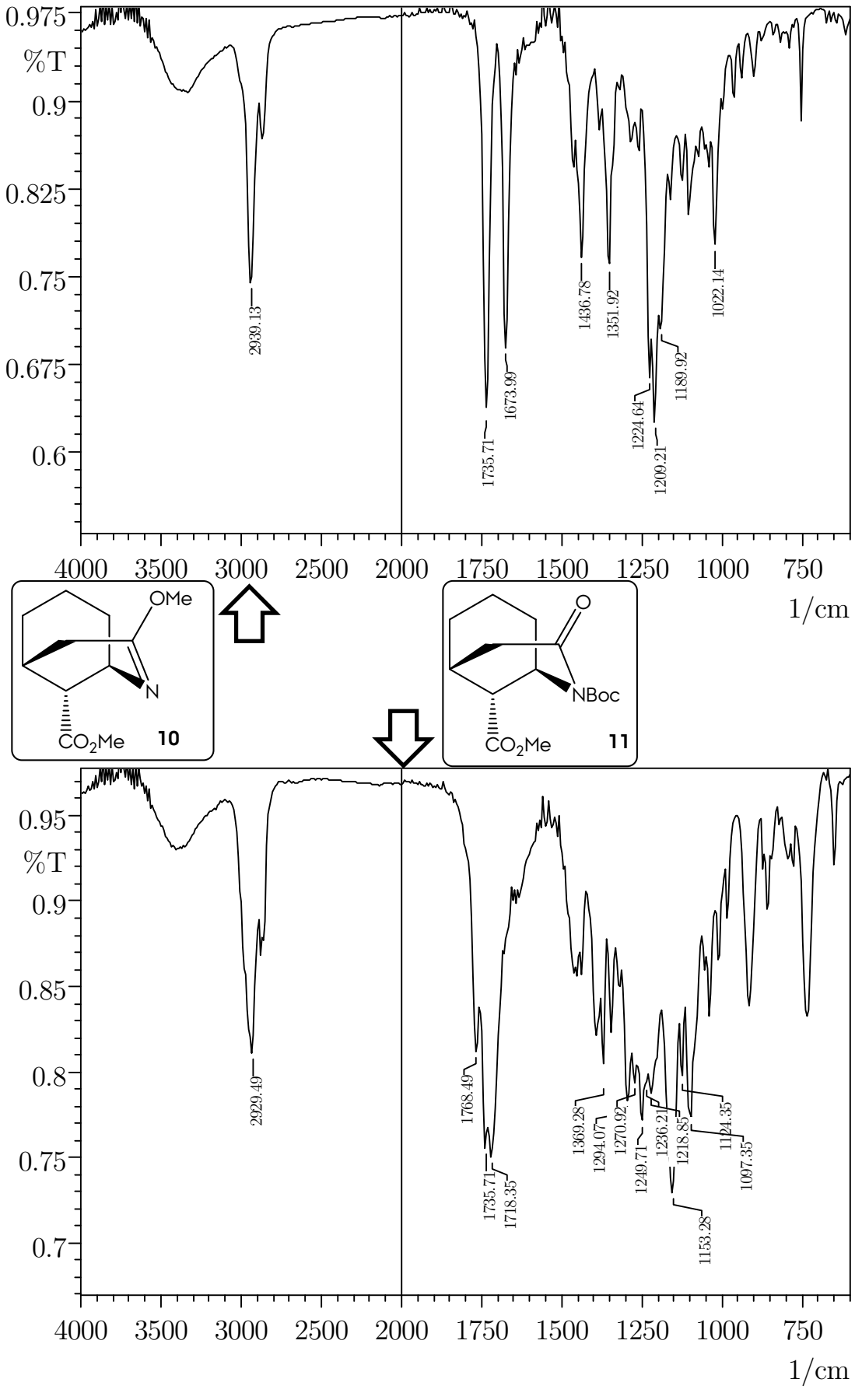
0.975
%T
0.9
0.825
0.75
0.675
0.6
2939.13
1735.71
1673.99
1436.78
1351.92
1224.64
1209.21
1189.92
1022.14
4000 3500 3000 2500 2000 1750 1500 1250 1000 750
1/cm
OMe
N
CO2Me
10
O
NBoc
CO2Me
11
0.95
%T
0.9
0.85
0.8
0.75
0.7
2929.49
1768.49
1735.71
1718.35
1369.28
1294.07
1270.92
1249.71
1236.21
1218.85
1153.28
1124.35
1097.35
4000 3500 3000 2500 2000 1750 1500 1250 1000 750
1/cm

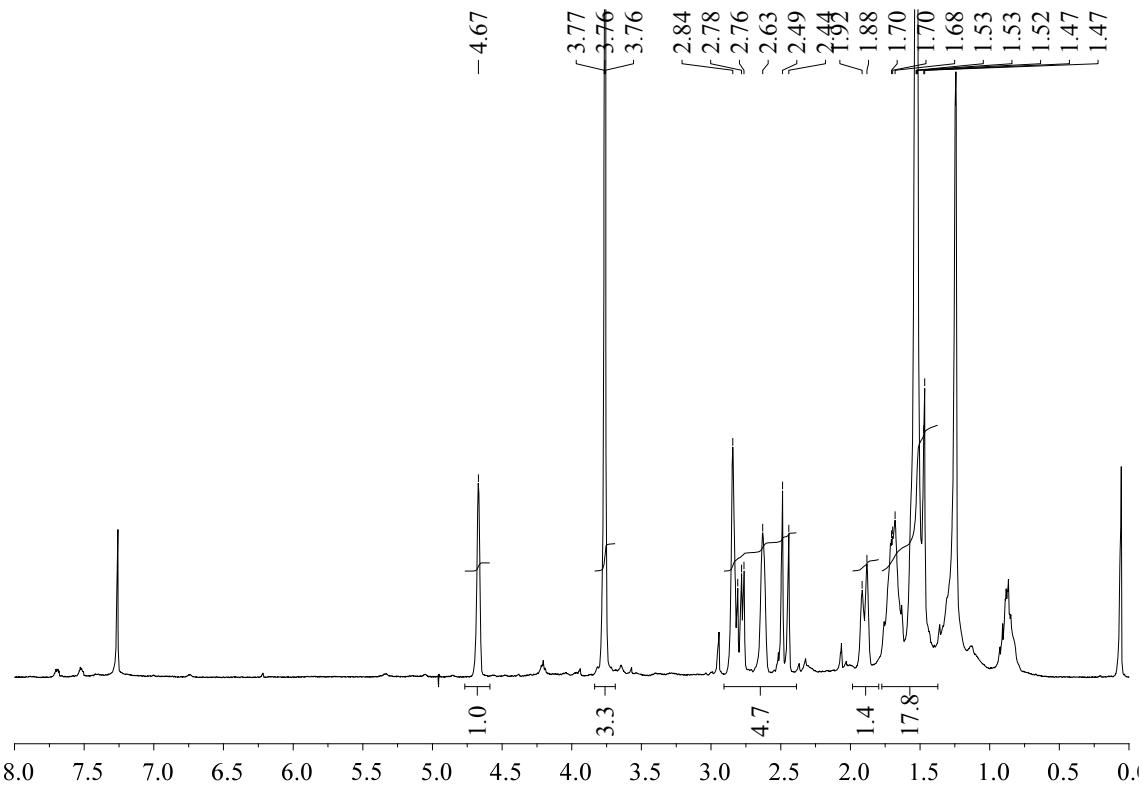
4.67
3.77
3.76
3.76
2.84
2.78
2.76
2.63
2.49
1.92
1.88
1.70
1.70
1.68
1.53
1.53
1.52
1.47
1.47
1.0
3.3
4.7
1.4
17.8
8.0
7.5
7.0
6.5
6.0
5.5
5.0
4.5
4.0
3.5
3.0
2.5
2.0
1.5
1.0
0.5

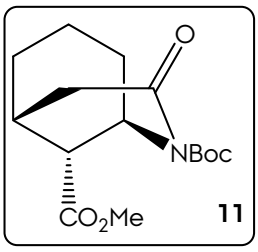
O
NBoc
CO2Me
11

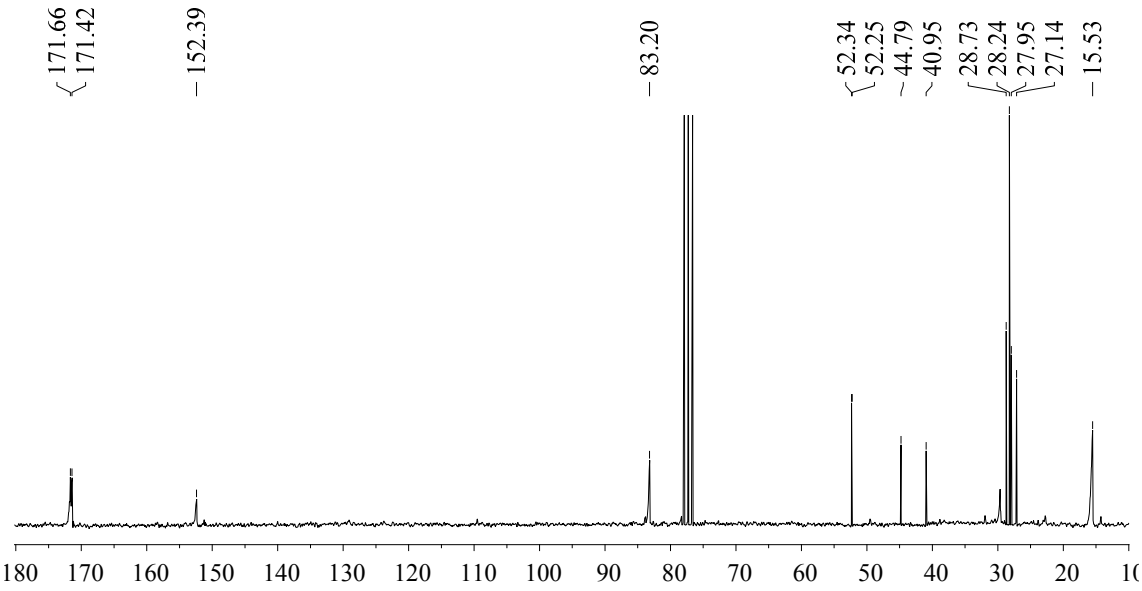
171.66
171.42
152.39
83.20
52.34
52.25
44.79
40.95
28.73
28.24
27.95
27.14
15.53
180
170
160
150
140
130
120
110
100
90
80
70
60
50
40
30
20

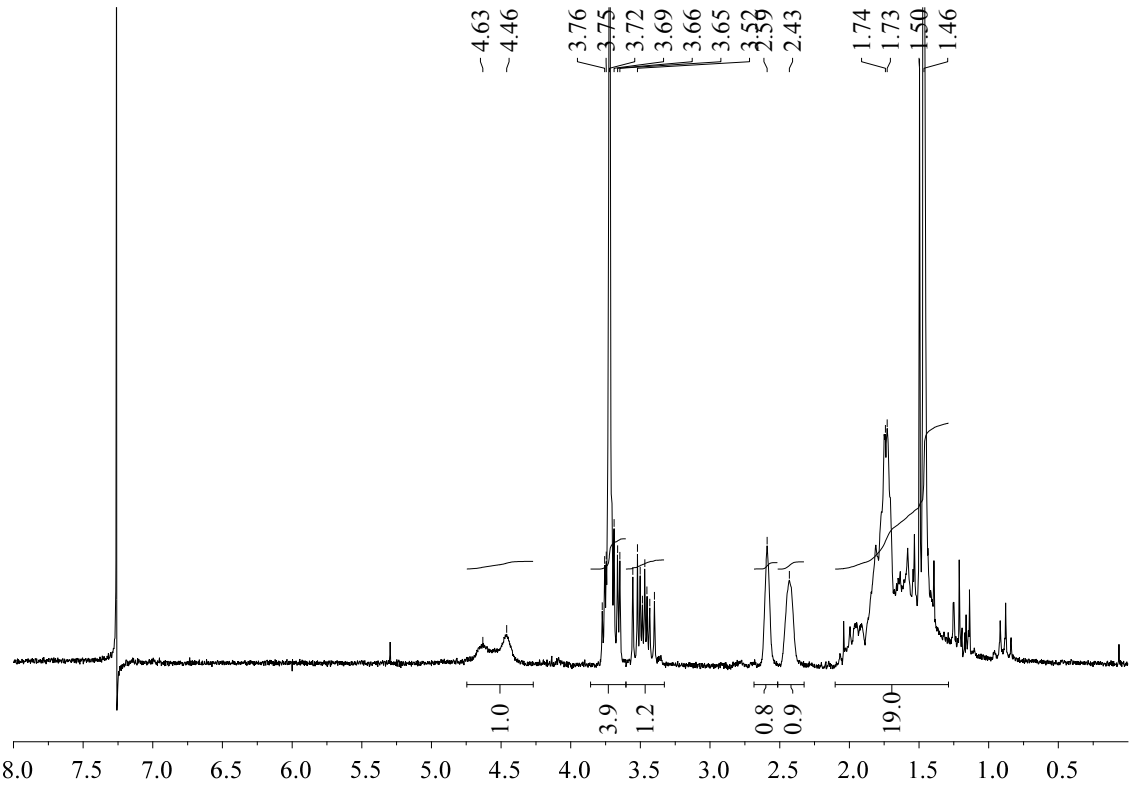
4.63
4.46
3.76
3.75
3.72
3.69
3.66
3.65
3.52
3.50
2.59
2.43
1.74
1.73
1.50
1.46
1.0
3.9
1.2
0.8
0.9
19.0
8.0
7.5
7.0
6.5
6.0
5.5
5.0
4.5
4.0
3.5
3.0
2.5
2.0
1.5
1.0
0.5

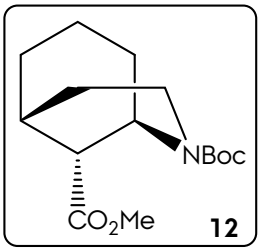
NBoc
CO2Me
12

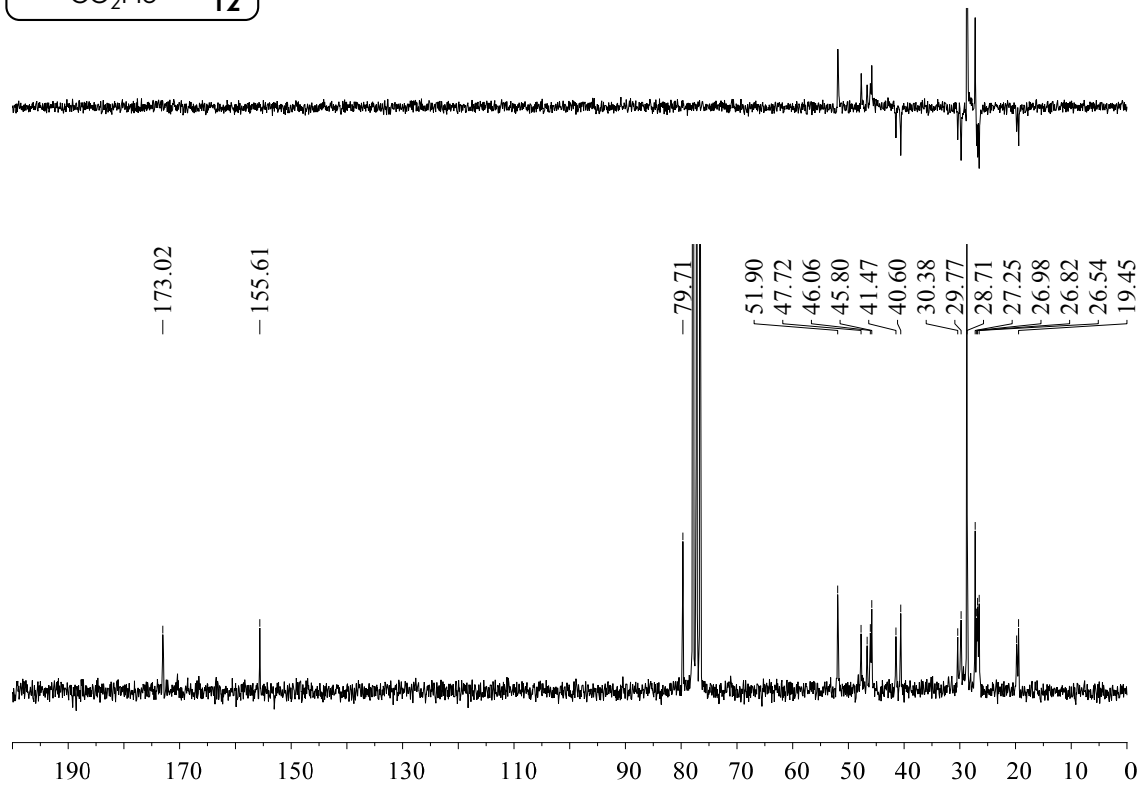
173.02
155.61
79.71
51.90
47.72
46.06
45.80
41.47
40.60
30.38
29.77
28.71
27.25
26.98
26.82
26.54
19.45
190
170
150
130
110
90
80
70
60
50
40
30
20
10
0

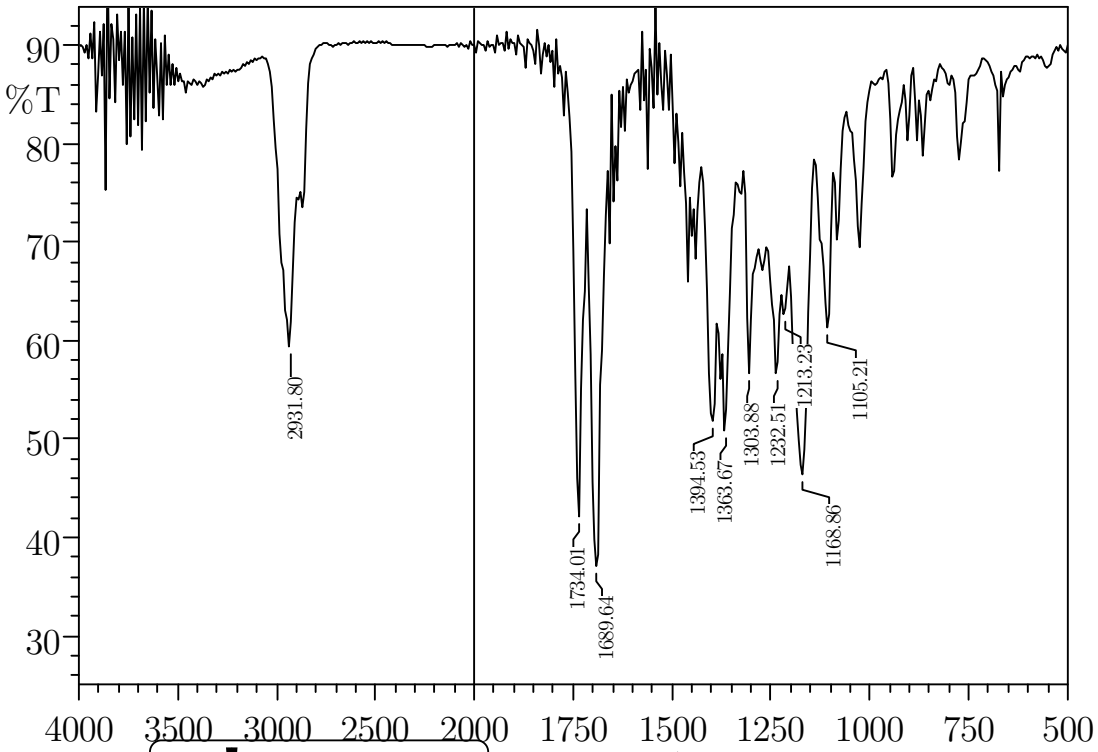
%T
90
80
70
60
50
40
30
2931.80
1734.01
1689.64
1394.53
1363.67
1303.88
1232.51
1213.23
1168.86
1105.21
4000
3500
3000
2500
2000
1750
1500
1250
1000
750
500
1/cm

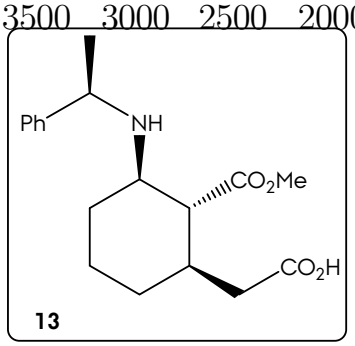
Ph
NH
CO2Me
CO2H
13

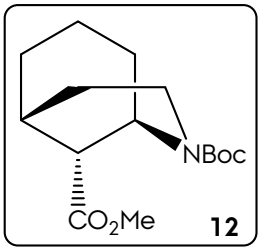
NBoc
CO2Me
12

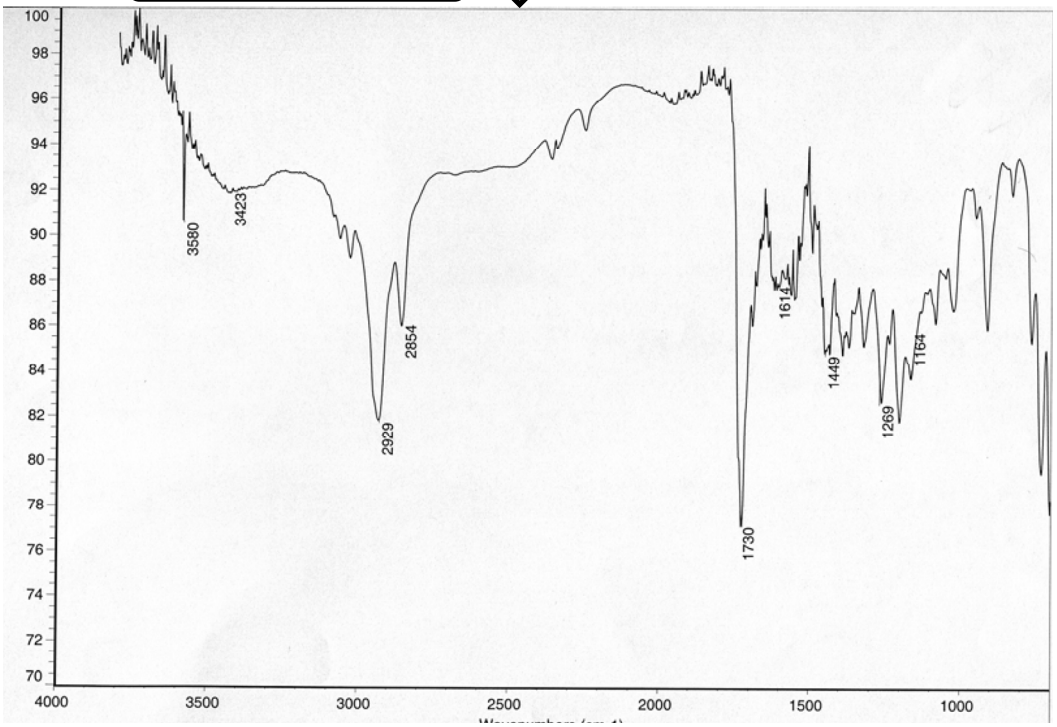
3580
3423
2929
2854
1730
1614
1449
1269
1164
4000
3500
3000
2500
2000
1500
1000

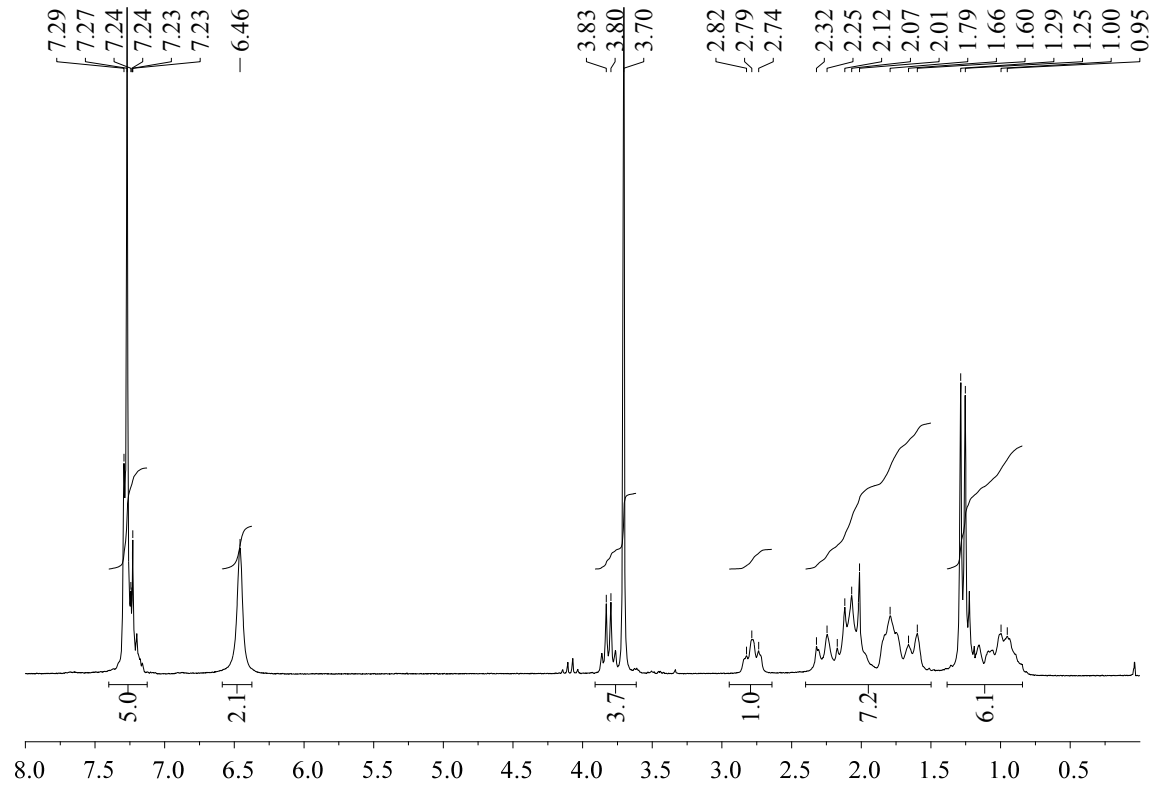
7.29
7.27
7.24
7.24
7.23
7.23
6.46
3.83
3.80
3.70
2.82
2.79
2.74
2.32
2.25
2.12
2.07
2.01
1.79
1.66
1.60
1.29
1.25
1.00
0.95
5.0
2.1
3.7
1.0
7.2
6.1
8.0 7.5 7.0 6.5 6.0 5.5 5.0 4.5 4.0 3.5 3.0 2.5 2.0 1.5 1.0 0.5

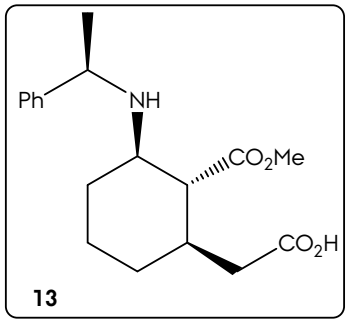
Ph
NH
CO2Me
CO2H
13

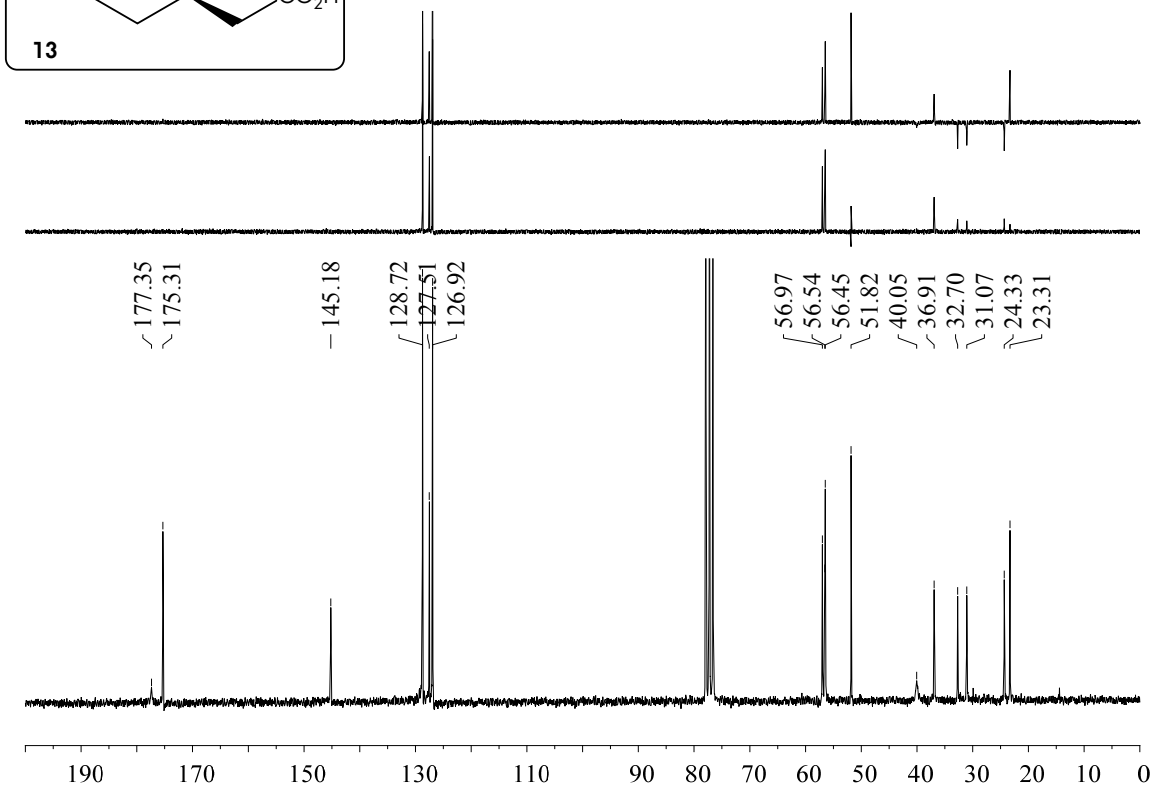
177.35
175.31
145.18
128.72
127.51
126.92
56.97
56.54
56.45
51.82
40.05
36.91
32.70
31.07
24.33
23.31
190 170 150 130 110 90 80 70 60 50 40 30 20 10 0

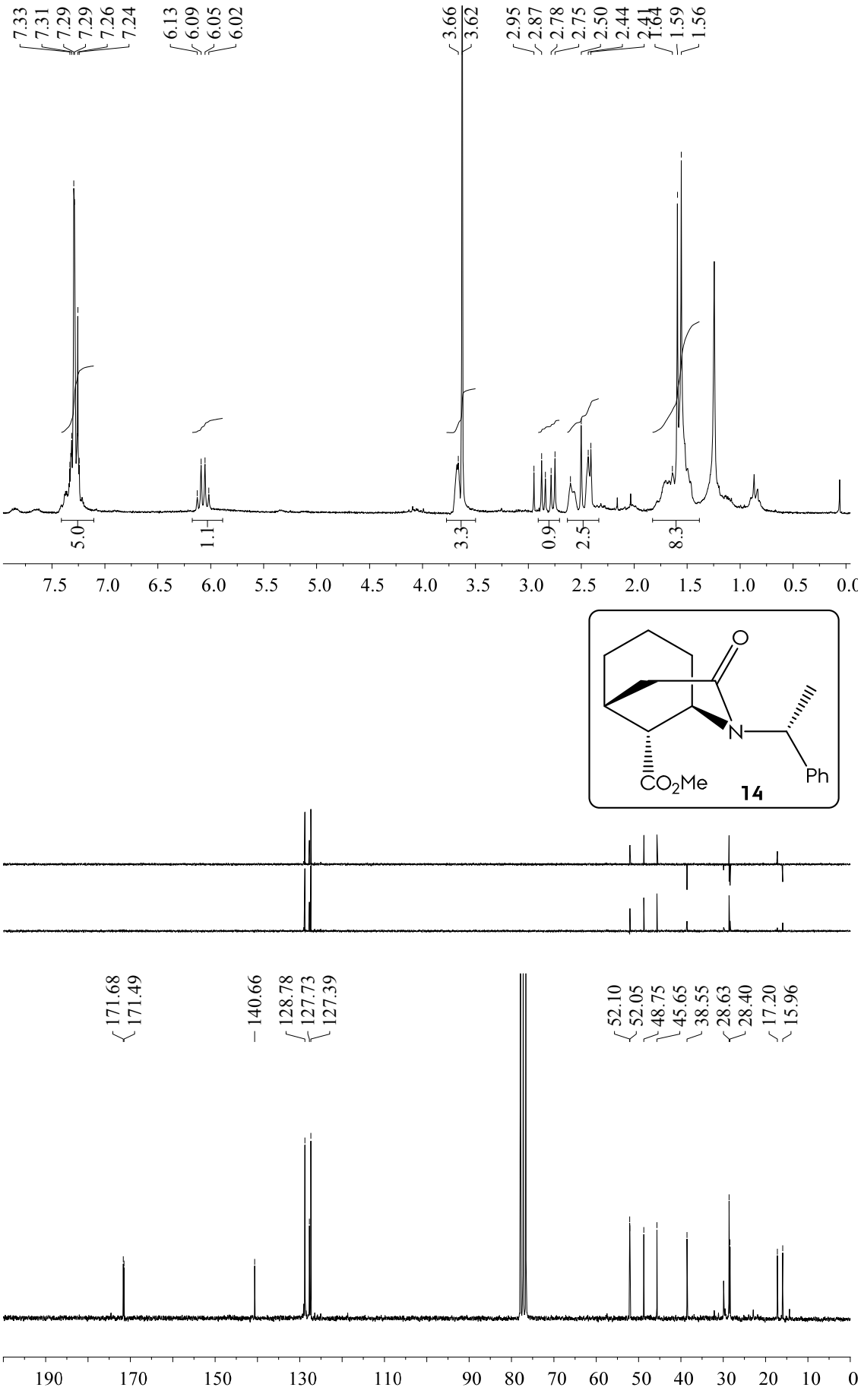
7.33
7.31
7.29
7.29
7.26
7.24
6.13
6.09
6.05
6.02
3.66
3.62
2.95
2.87
2.78
2.75
2.50
2.44
2.41
1.64
1.59
1.56
5.0
1.1
3.3
0.9
2.5
8.3
7.5 7.0 6.5 6.0 5.5 5.0 4.5 4.0 3.5 3.0 2.5 2.0 1.5 1.0 0.5 0.0
O
N
Ph
CO2Me
14
171.68
171.49
140.66
128.78
127.73
127.39
52.10
52.05
48.75
45.65
38.55
28.63
28.40
17.20
15.96
190 170 150 130 110 90 80 70 60 50 40 30 20 10 0

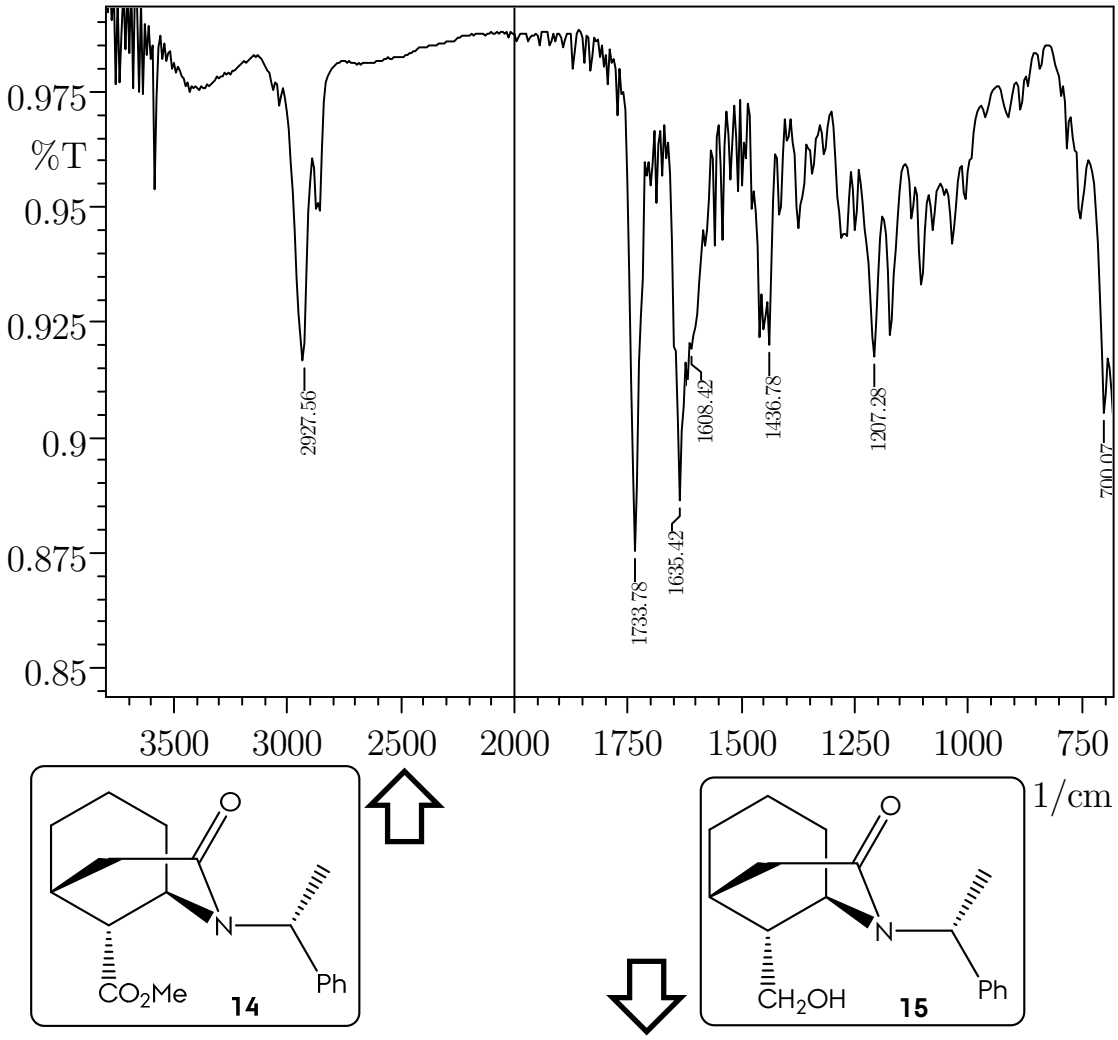
0.975
%T
0.95
0.925
0.9
0.875
0.85
2927.56
1733.78
1635.42
1608.42
1436.78
1207.28
700.07
3500
3000
2500
2000
1750
1500
1250
1000
750
1/cm
O
N
CO2Me
Ph
14
O
N
CH2OH
Ph
15

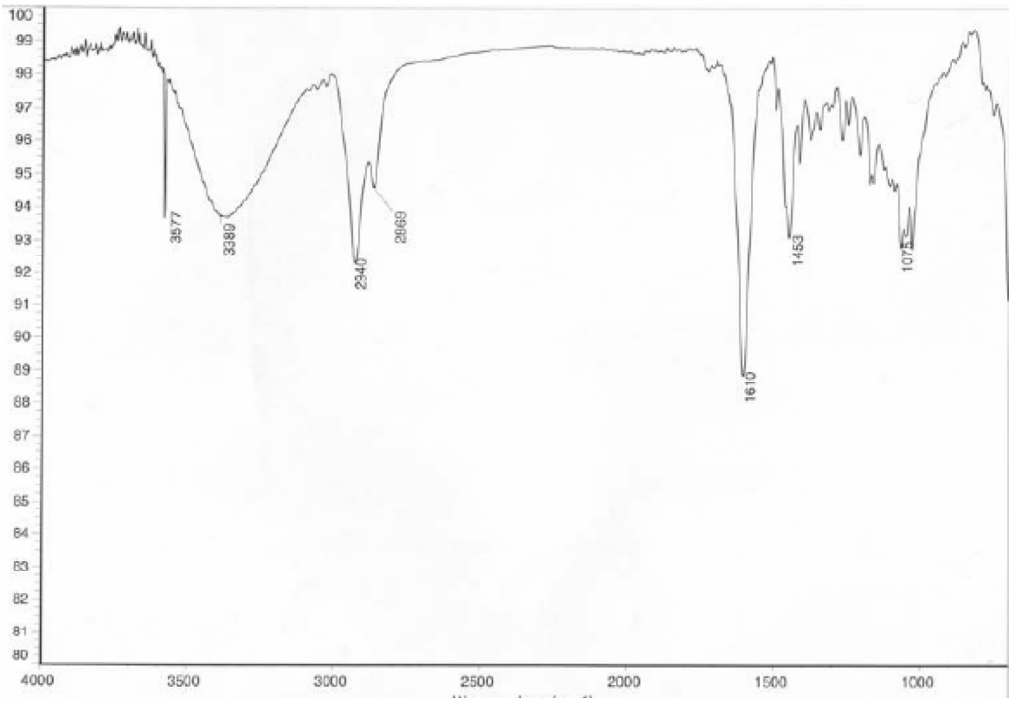
3577
3389
2940
2869
1610
1453
4000
3500
3000
2500
2000
1500
1000

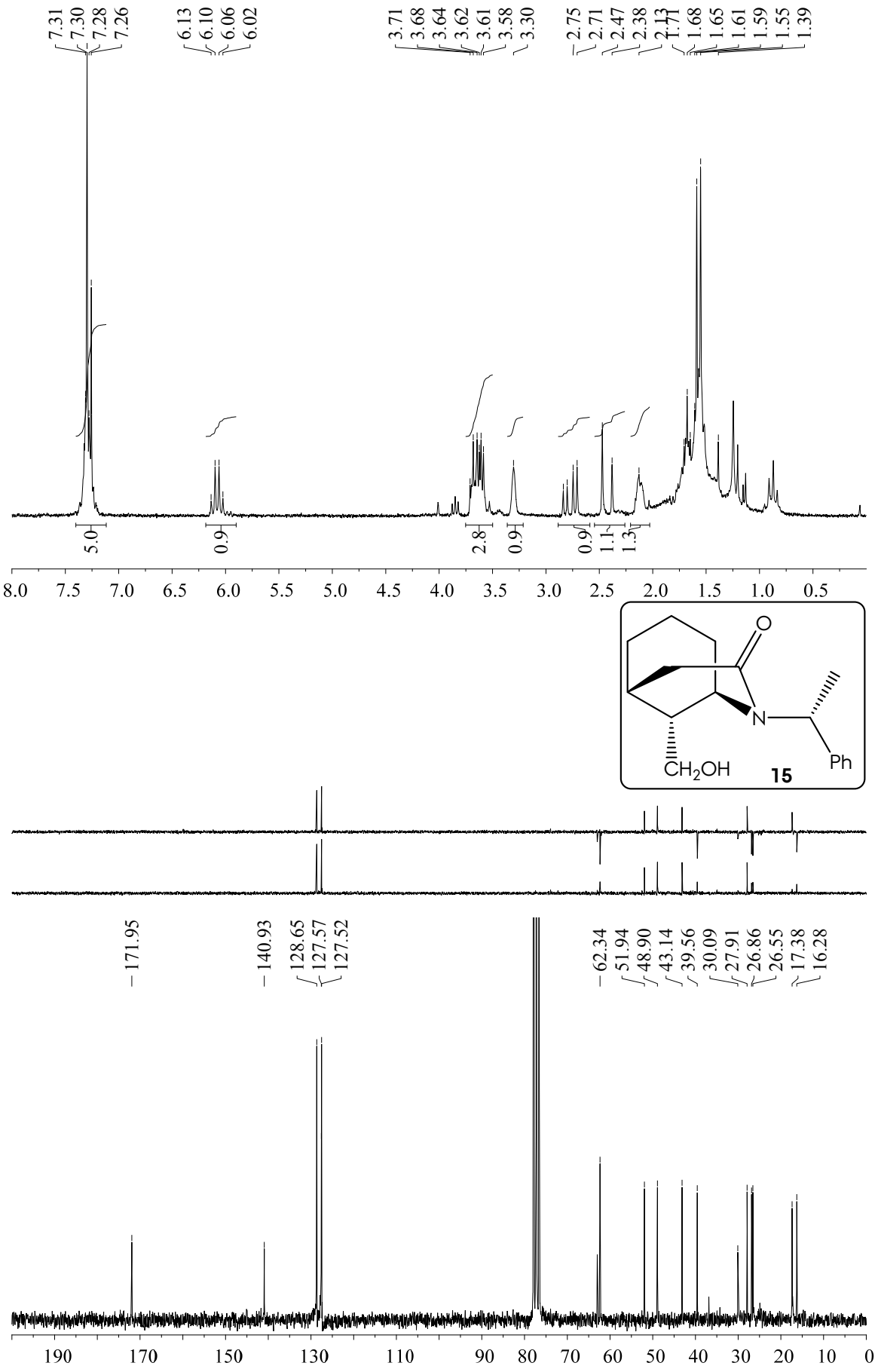
7.31
7.30
7.28
7.26
6.13
6.10
6.06
6.02
3.71
3.68
3.64
3.62
3.61
3.58
3.30
2.75
2.71
2.47
2.38
2.13
1.71
1.68
1.65
1.61
1.59
1.55
1.39
5.0
0.9
2.8
0.9
0.9
1.1
1.3
8.0 7.5 7.0 6.5 6.0 5.5 5.0 4.5 4.0 3.5 3.0 2.5 2.0 1.5 1.0 0.5
O
N
CH2OH
Ph
15
171.95
140.93
128.65
127.57
127.52
62.34
51.94
48.90
43.14
39.56
30.09
27.91
26.86
26.55
17.38
16.28
190 170 150 130 110 90 80 70 60 50 40 30 20 10 0

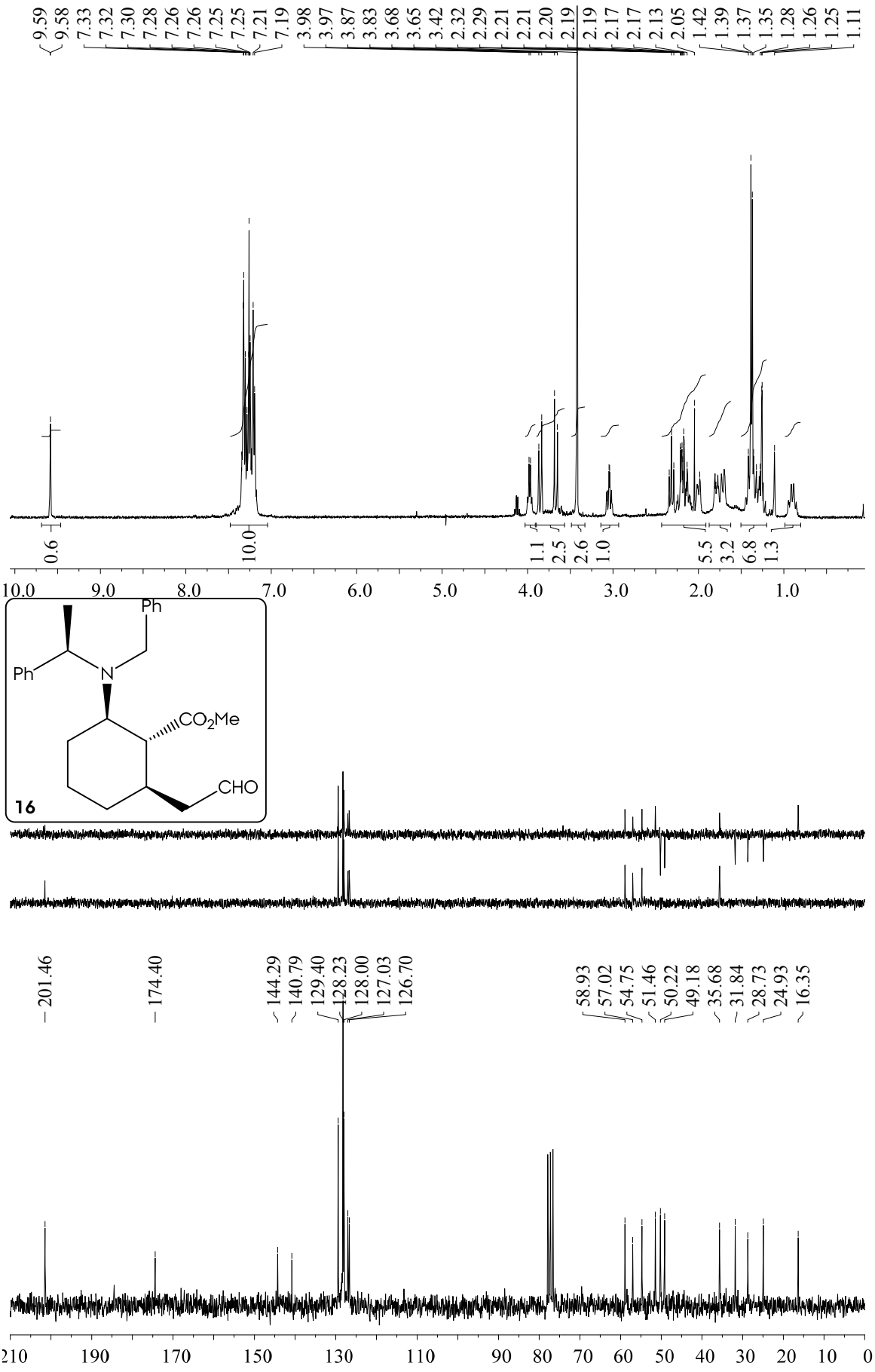
9.59
9.58
7.33
7.32
7.30
7.28
7.26
7.26
7.25
7.25
7.21
7.19
3.98
3.97
3.87
3.83
3.68
3.65
3.42
2.32
2.29
2.21
2.21
2.20
2.19
2.19
2.17
2.17
2.13
2.05
1.42
1.39
1.37
1.35
1.28
1.26
1.25
1.11
0.6
10.0
1.1
2.5
2.6
1.0
5.5
3.2
6.8
1.3
10.0
9.0
8.0
7.0
6.0
5.0
4.0
3.0
2.0
1.0
Ph
Ph
N
CO2Me
CHO
16
201.46
174.40
144.29
140.79
129.40
128.23
128.00
127.03
126.70
58.93
57.02
54.75
51.46
50.22
49.18
35.68
31.84
28.73
24.93
16.35
210
190
170
150
130
110
90
80
70
60
50
40
30
20
10
0

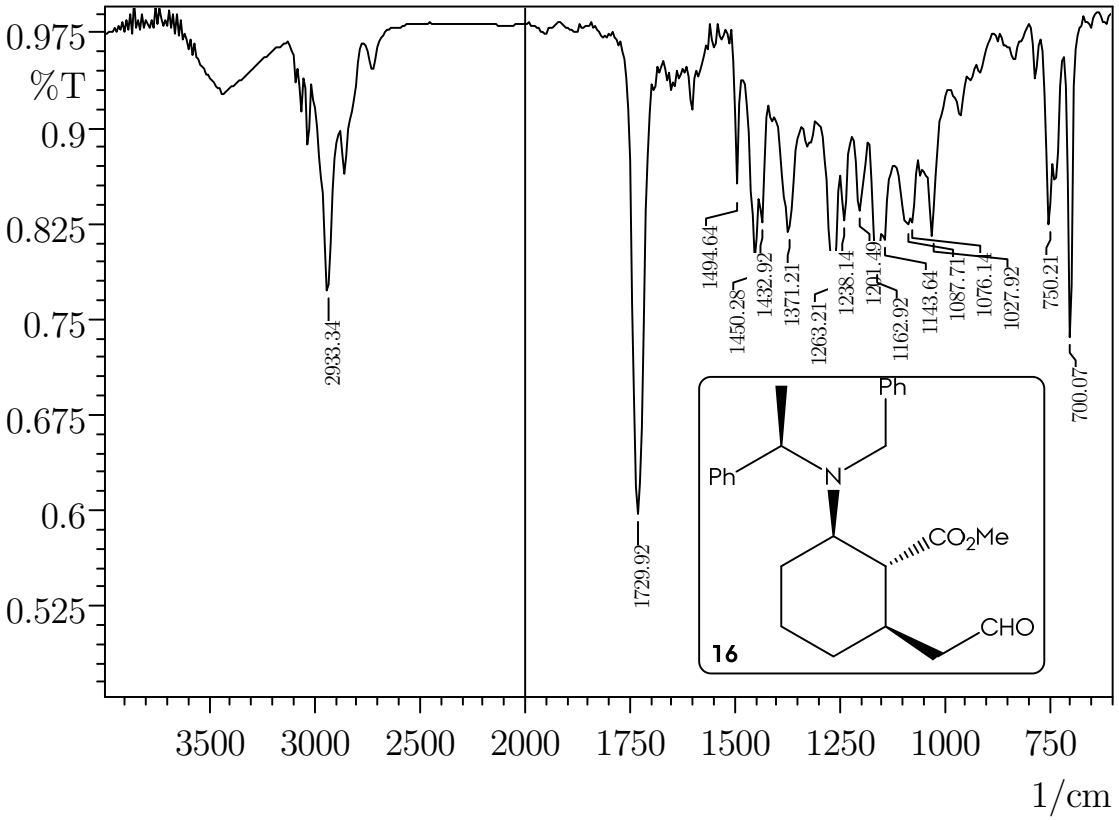
0.975
%T
0.9
0.825
0.75
0.675
0.6
0.525
2933.34
1729.92
1494.64
1450.28
1432.92
1371.21
1263.21
1238.14
1201.49
1162.92
1143.64
1087.71
1076.14
1027.92
750.21
700.07
Ph
Ph
N
CO2Me
CHO
16
3500
3000
2500
2000
1750
1500
1250
1000
750
1/cm

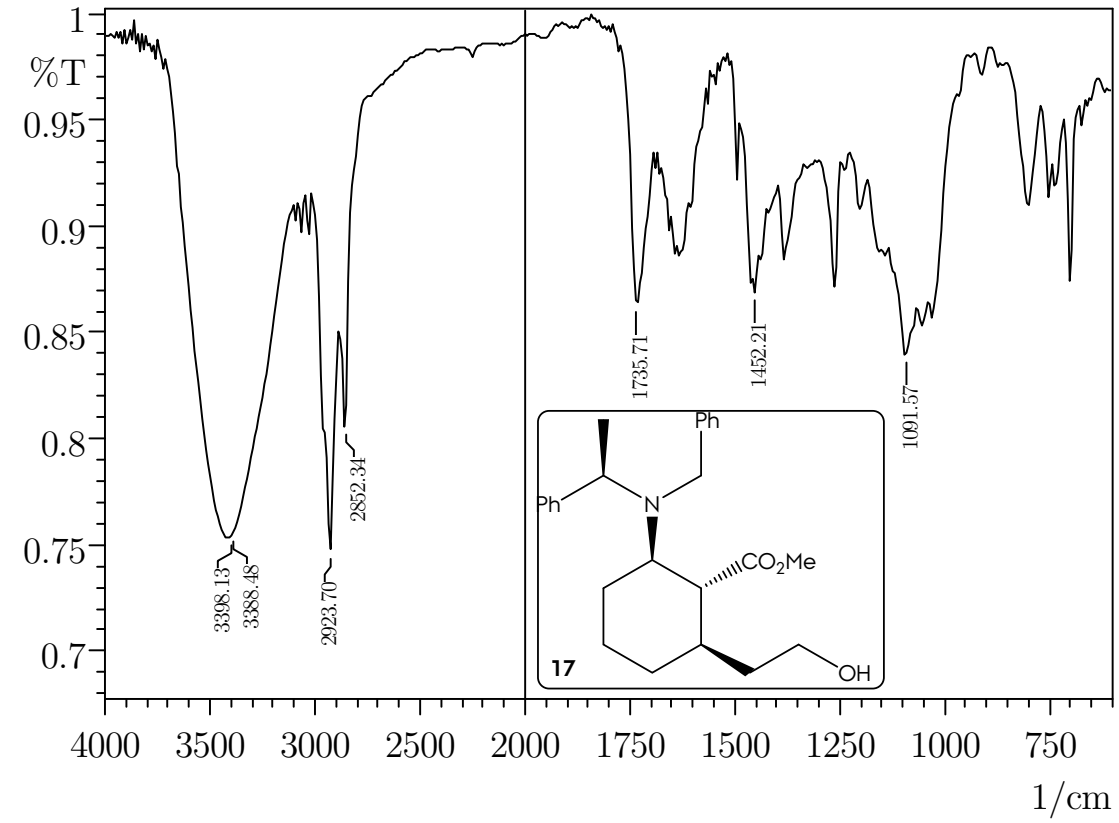
1
%T
0.95
0.9
0.85
0.8
0.75
0.7
3398.13
3388.48
2923.70
2852.34
1735.71
1452.21
1091.57
Ph
Ph
N
CO2Me
OH
17
4000
3500
3000
2500
2000
1750
1500
1250
1000
750
1/cm

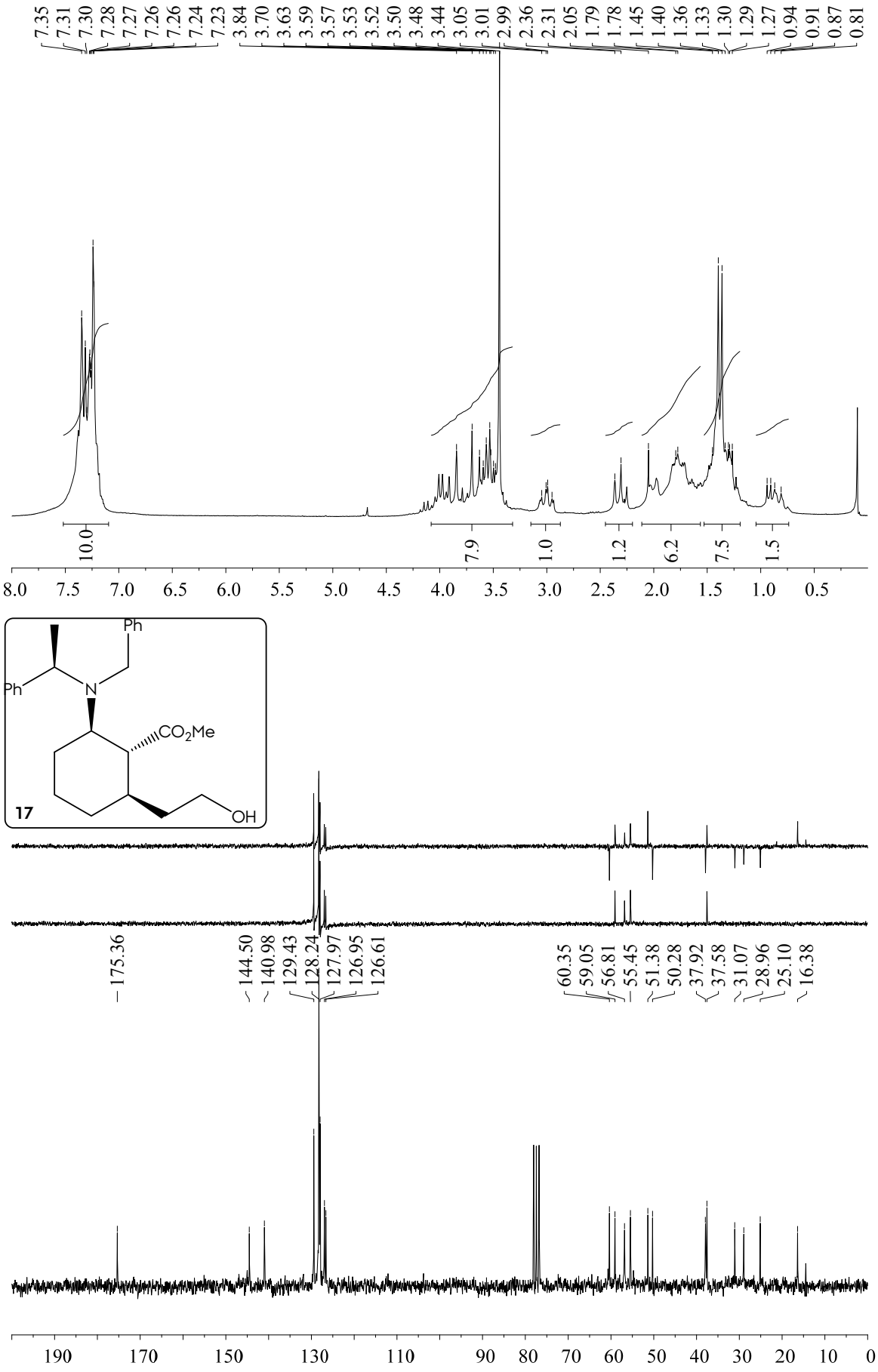
7.35
7.31
7.30
7.28
7.27
7.26
7.26
7.24
7.23
3.84
3.70
3.63
3.59
3.57
3.53
3.52
3.50
3.48
3.44
3.05
3.01
2.99
2.36
2.31
2.05
1.79
1.78
1.45
1.40
1.36
1.33
1.30
1.29
1.27
0.94
0.91
0.87
0.81
10.0
7.9
1.0
1.2
6.2
7.5
1.5
8.0 7.5 7.0 6.5 6.0 5.5 5.0 4.5 4.0 3.5 3.0 2.5 2.0 1.5 1.0 0.5
Ph
Ph
N
CO2Me
OH
17
175.36
144.50
140.98
129.43
128.24
127.97
126.95
126.61
60.35
59.05
56.81
55.45
51.38
50.28
37.92
37.58
31.07
28.96
25.10
16.38
190 170 150 130 110 90 80 70 60 50 40 30 20 10 0

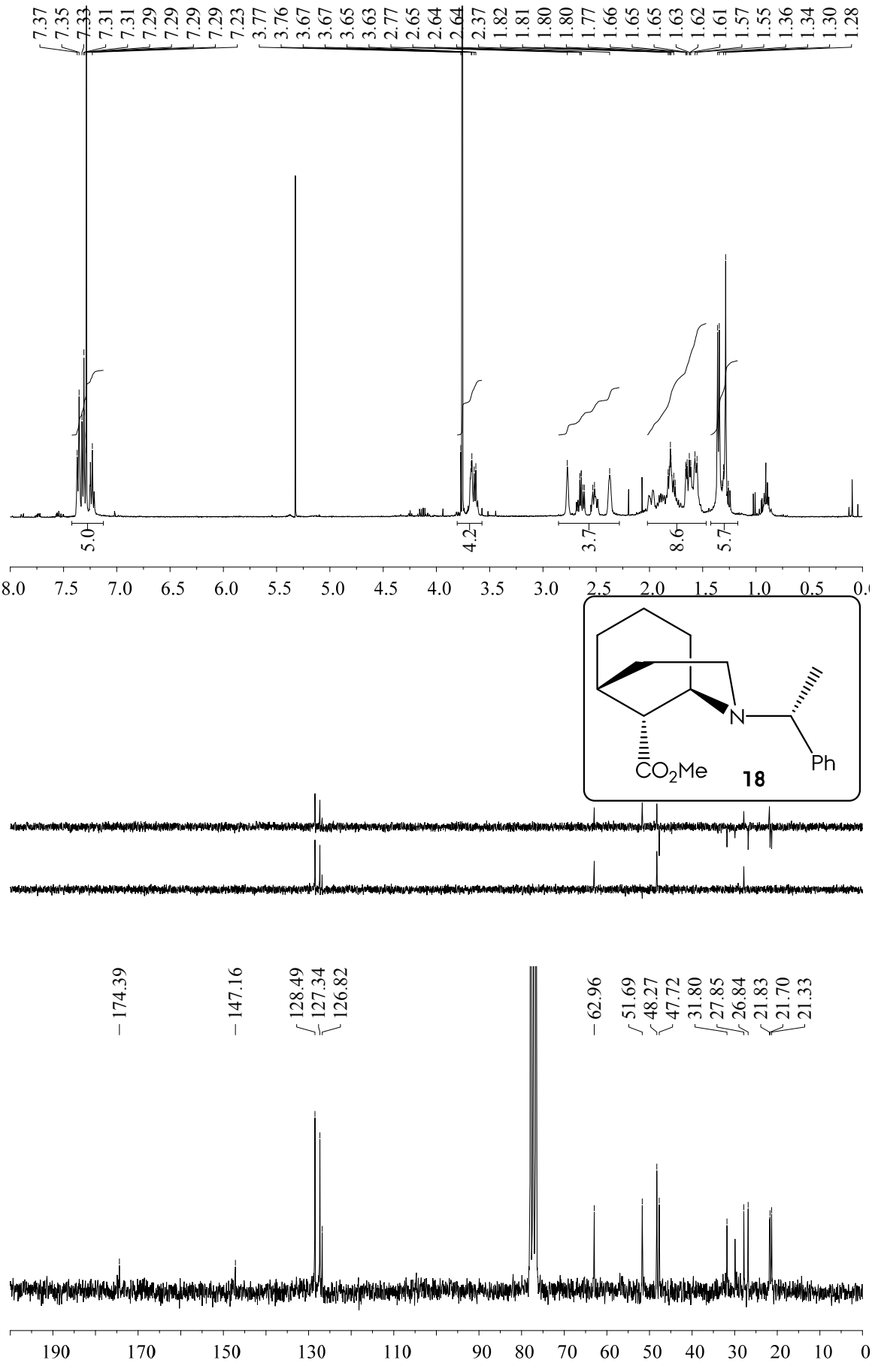
7.37
7.35
7.33
7.31
7.31
7.29
7.29
7.29
7.29
7.23
3.77
3.76
3.67
3.67
3.65
3.63
2.77
2.65
2.64
2.64
2.37
1.82
1.81
1.80
1.80
1.77
1.66
1.65
1.65
1.63
1.62
1.61
1.57
1.55
1.36
1.34
1.30
1.28
5.0
4.2
3.7
8.6
5.7
8.0 7.5 7.0 6.5 6.0 5.5 5.0 4.5 4.0 3.5 3.0 2.5 2.0 1.5 1.0 0.5
N
CO2Me
Ph
18
174.39
147.16
128.49
127.34
126.82
62.96
51.69
48.27
47.72
31.80
27.85
26.84
21.83
21.70
21.33
190 170 150 130 110 90 80 70 60 50 40 30 20 10 0

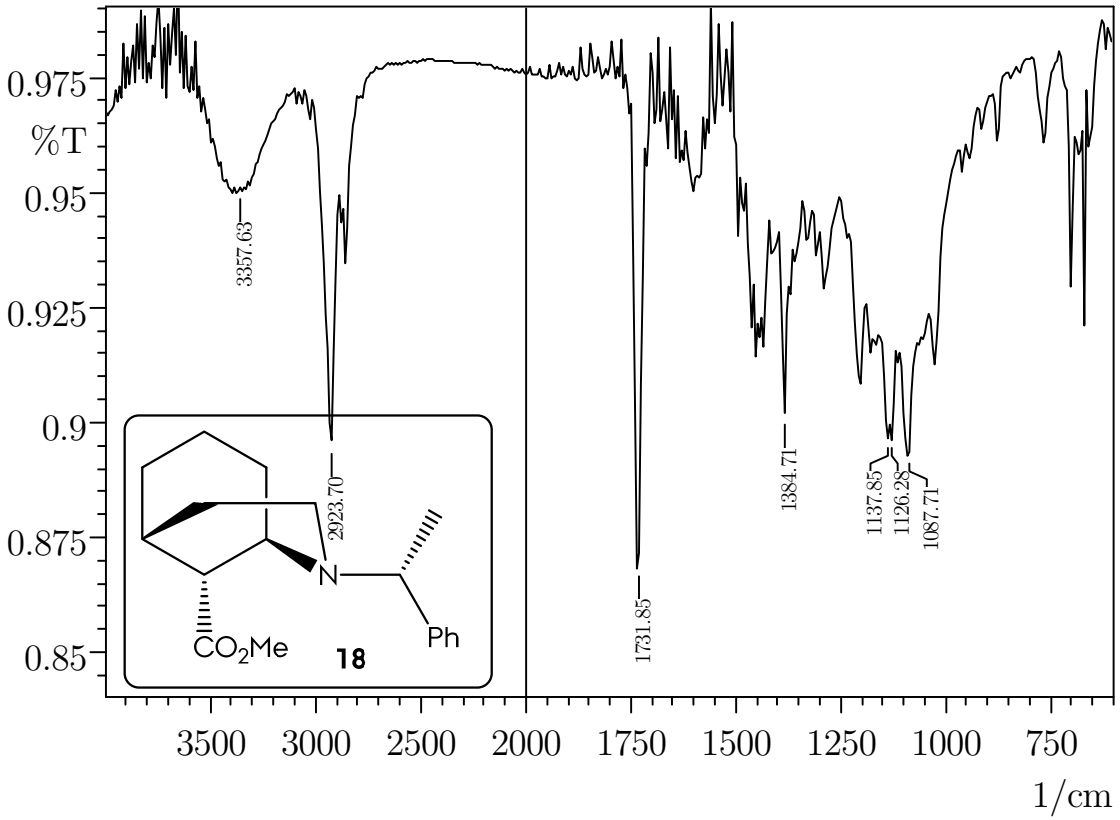
0.975
%T
0.95
0.925
0.9
0.875
0.85
3357.63
2923.70
1731.85
1384.71
1137.85
1126.28
1087.71
CO2Me
N
Ph
18
3500
3000
2500
2000
1750
1500
1250
1000
750
1/cm

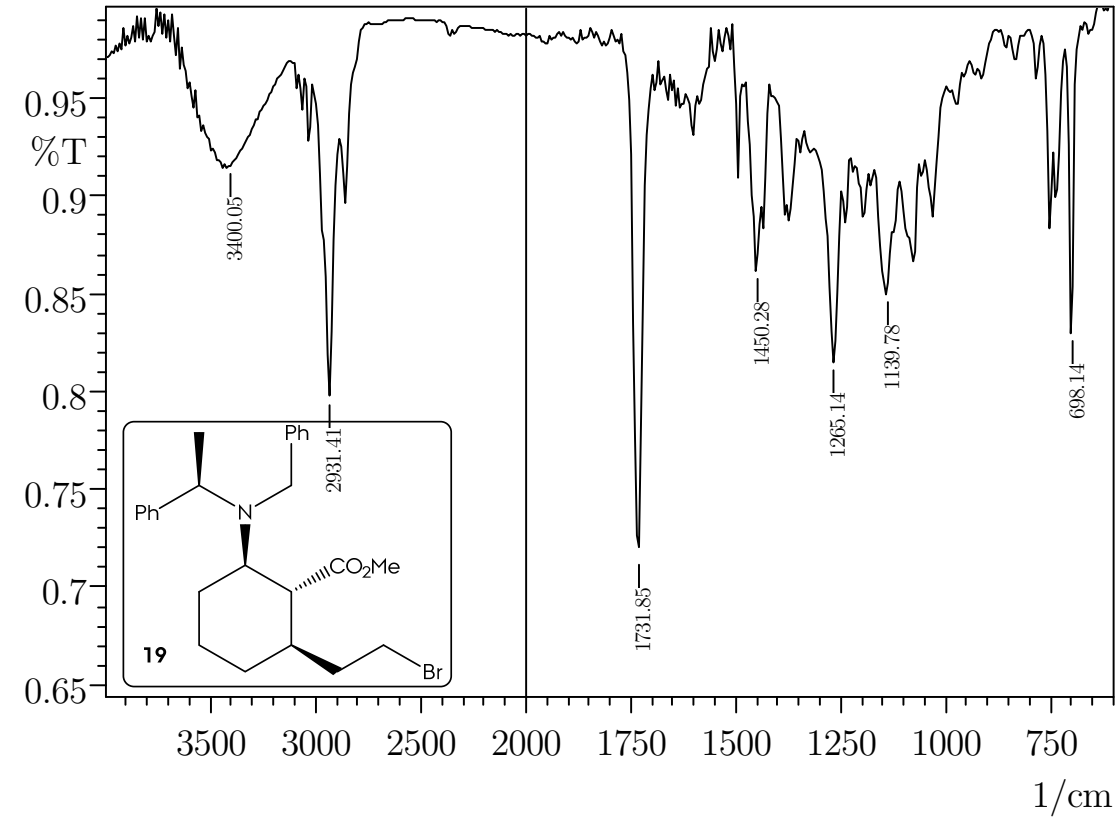
0.95
%T
0.9
0.85
0.8
0.75
0.7
0.65
3400.05
2931.41
1731.85
1450.28
1265.14
1139.78
698.14
Ph
Ph
N
CO2Me
19
Br
3500
3000
2500
2000
1750
1500
1250
1000
750
1/cm

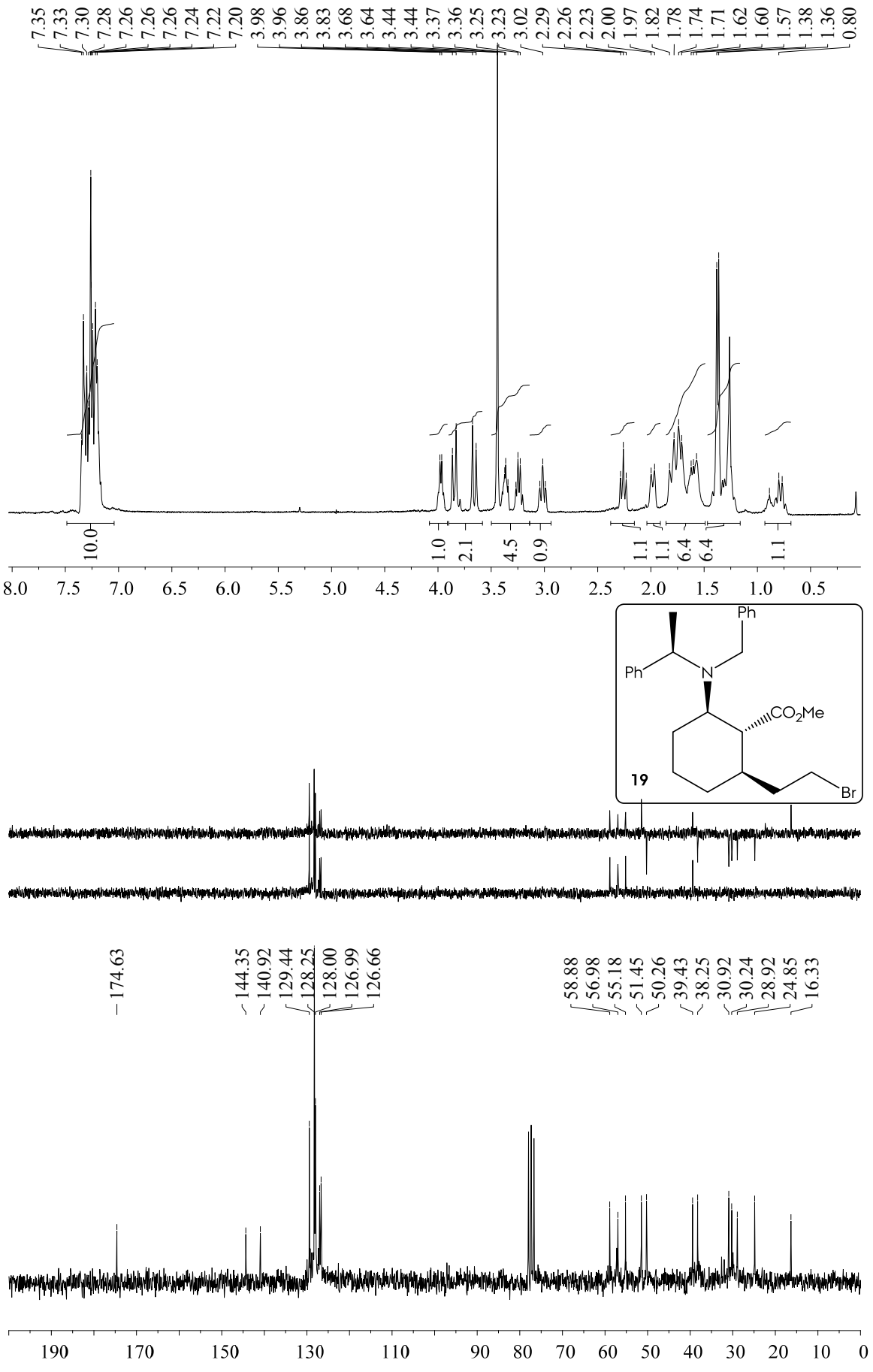
7.35
7.33
7.30
7.28
7.26
7.26
7.26
7.24
7.22
7.20
3.98
3.96
3.86
3.83
3.68
3.64
3.44
3.44
3.37
3.36
3.25
3.23
3.02
2.29
2.26
2.23
2.00
1.97
1.82
1.78
1.74
1.71
1.62
1.60
1.57
1.38
1.36
0.80
10.0
1.0
2.1
4.5
0.9
1.1
1.1
6.4
6.4
1.1
8.0 7.5 7.0 6.5 6.0 5.5 5.0 4.5 4.0 3.5 3.0 2.5 2.0 1.5 1.0 0.5
Ph
Ph
N
CO2Me
19
Br
174.63
144.35
140.92
129.44
128.25
128.00
126.99
126.66
58.88
56.98
55.18
51.45
50.26
39.43
38.25
30.92
30.24
28.92
24.85
16.33
190 170 150 130 110 90 80 70 60 50 40 30 20 10 0

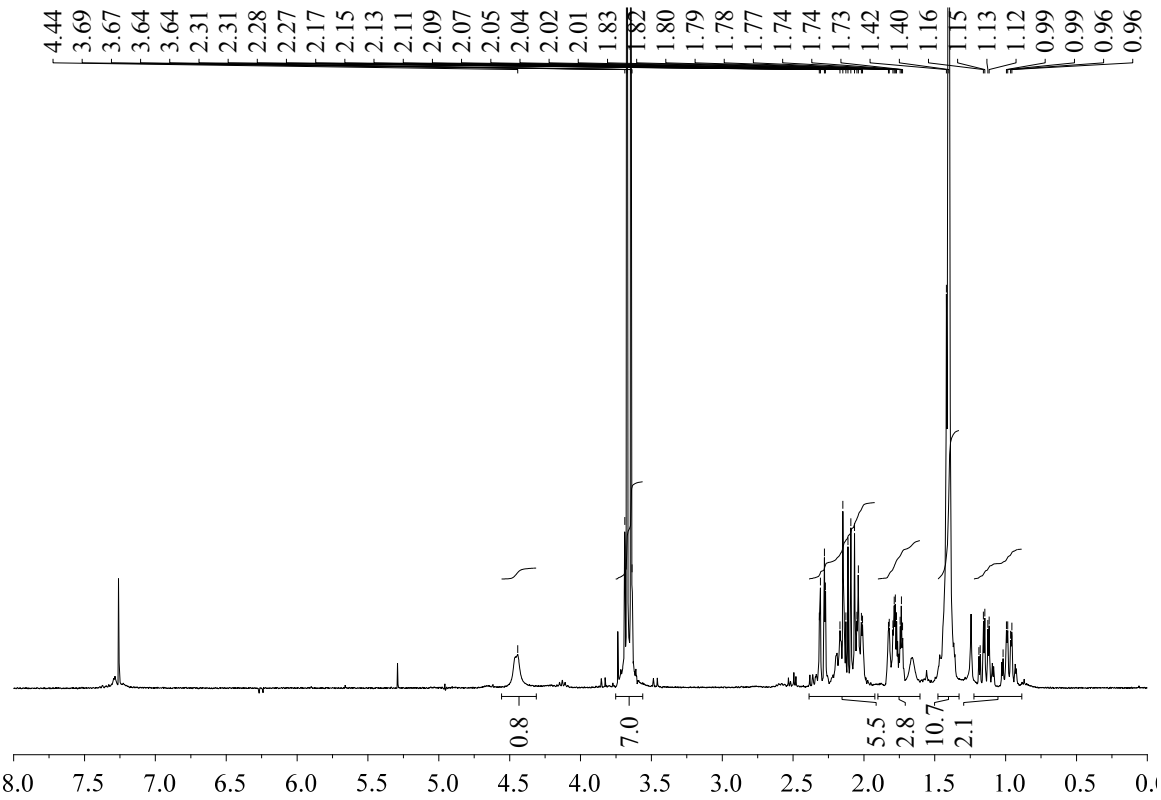
4.44
3.69
3.67
3.64
3.64
2.31
2.31
2.28
2.27
2.17
2.15
2.13
2.11
2.09
2.07
2.05
2.04
2.02
2.01
1.83
1.82
1.80
1.79
1.78
1.77
1.74
1.74
1.73
1.42
1.40
1.16
1.15
1.13
1.12
0.99
0.99
0.96
0.96
0.8
7.0
5.5
2.8
10.7
2.1
8.0
7.5
7.0
6.5
6.0
5.5
5.0
4.5
4.0
3.5
3.0
2.5
2.0
1.5
1.0
0.5

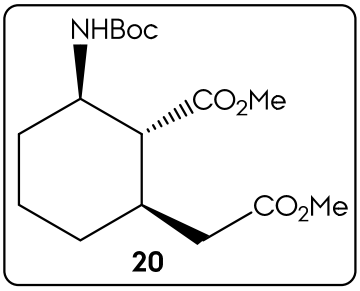
NHBoc
CO2Me
CO2Me
20

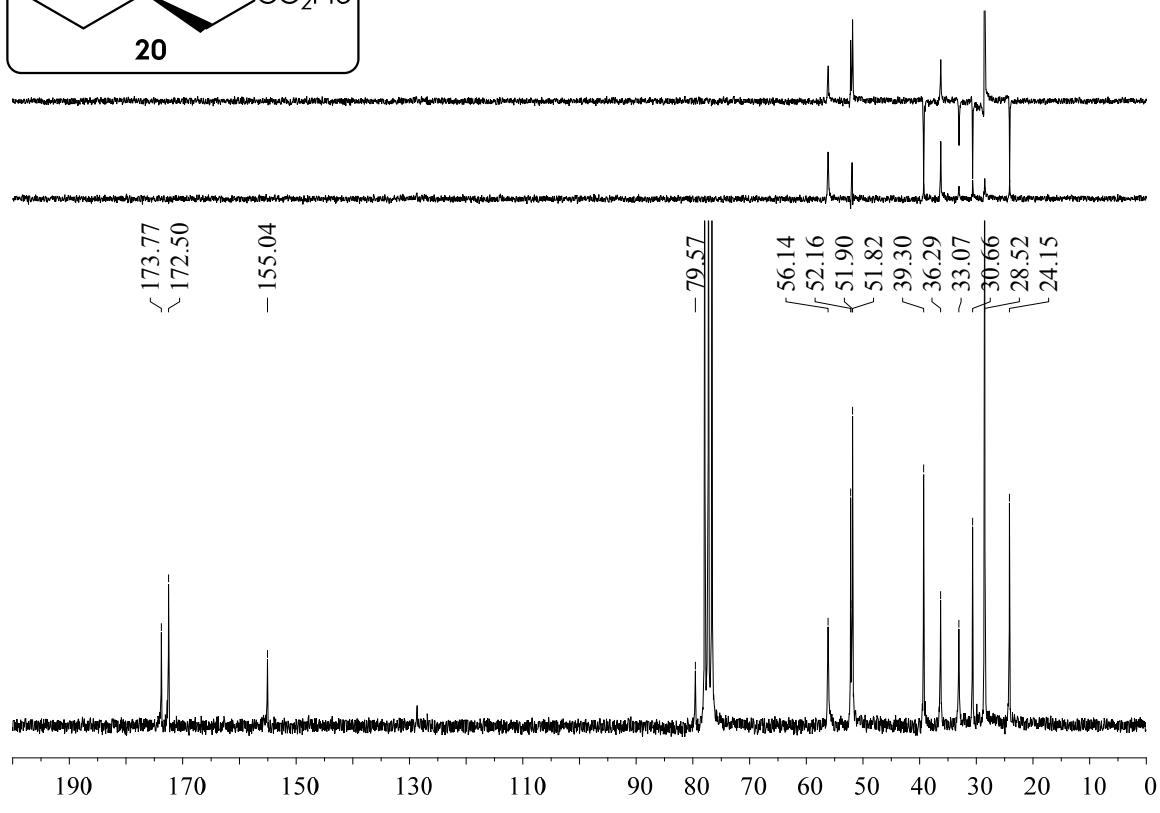
173.77
172.50
155.04
79.57
56.14
52.16
51.90
51.82
39.30
36.29
33.07
30.66
28.52
24.15
190
170
150
130
110
90
80
70
60
50
40
30
20
10
0

HMQC

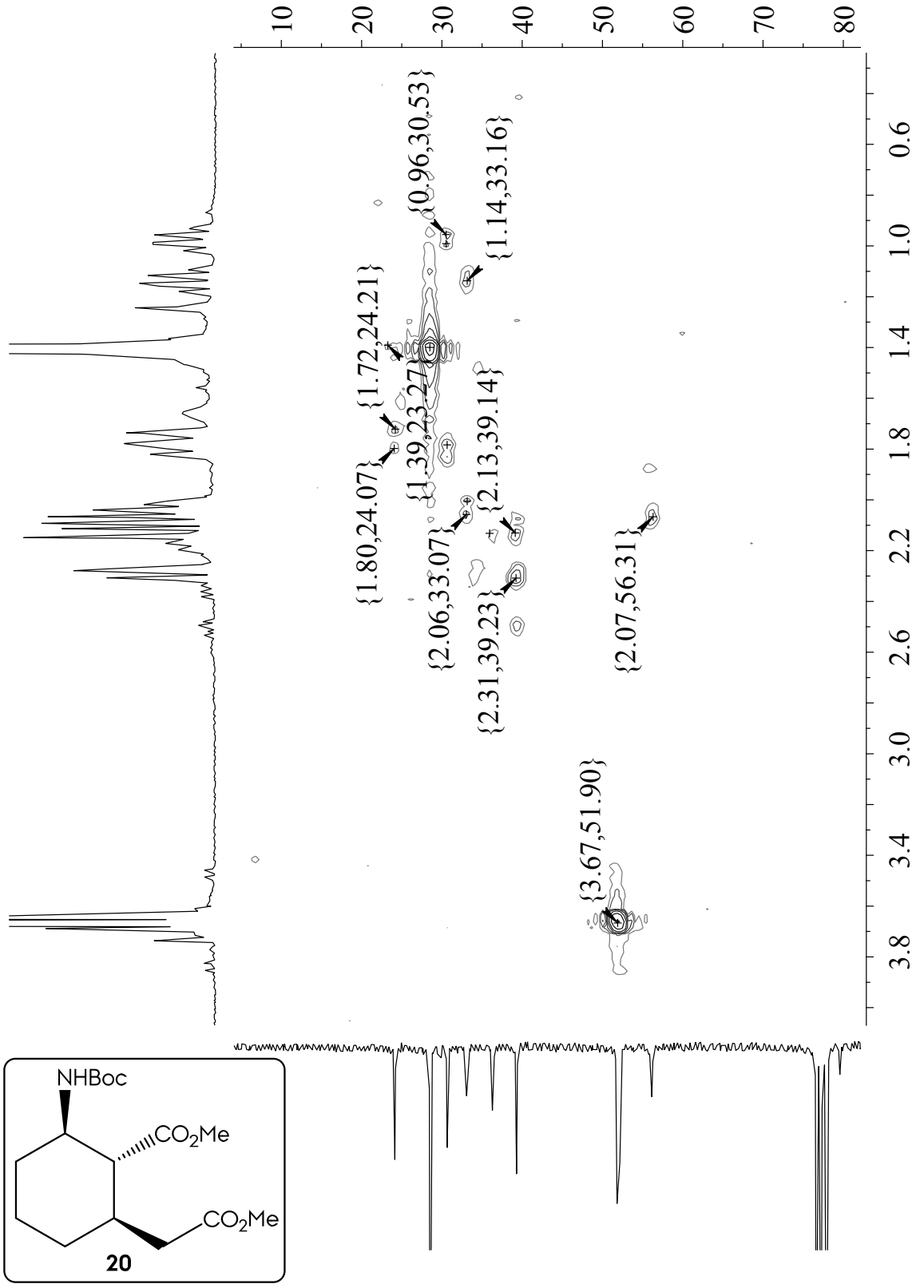
10
20
30
40
50
60
70
80
0.6
1.0
1.4
1.8
2.2
2.6
3.0
3.4
3.8
{0.96,30.53}
{1.14,33.16}
{1.72,24.21}
{1.39,23.27}
{1.80,24.07}
{2.13,39.14}
{2.06,33.07}
{2.31,39.23}
{2.07,56.31}
{3.67,51.90}
NHBoc
CO2Me
CO2Me
20

HMBC

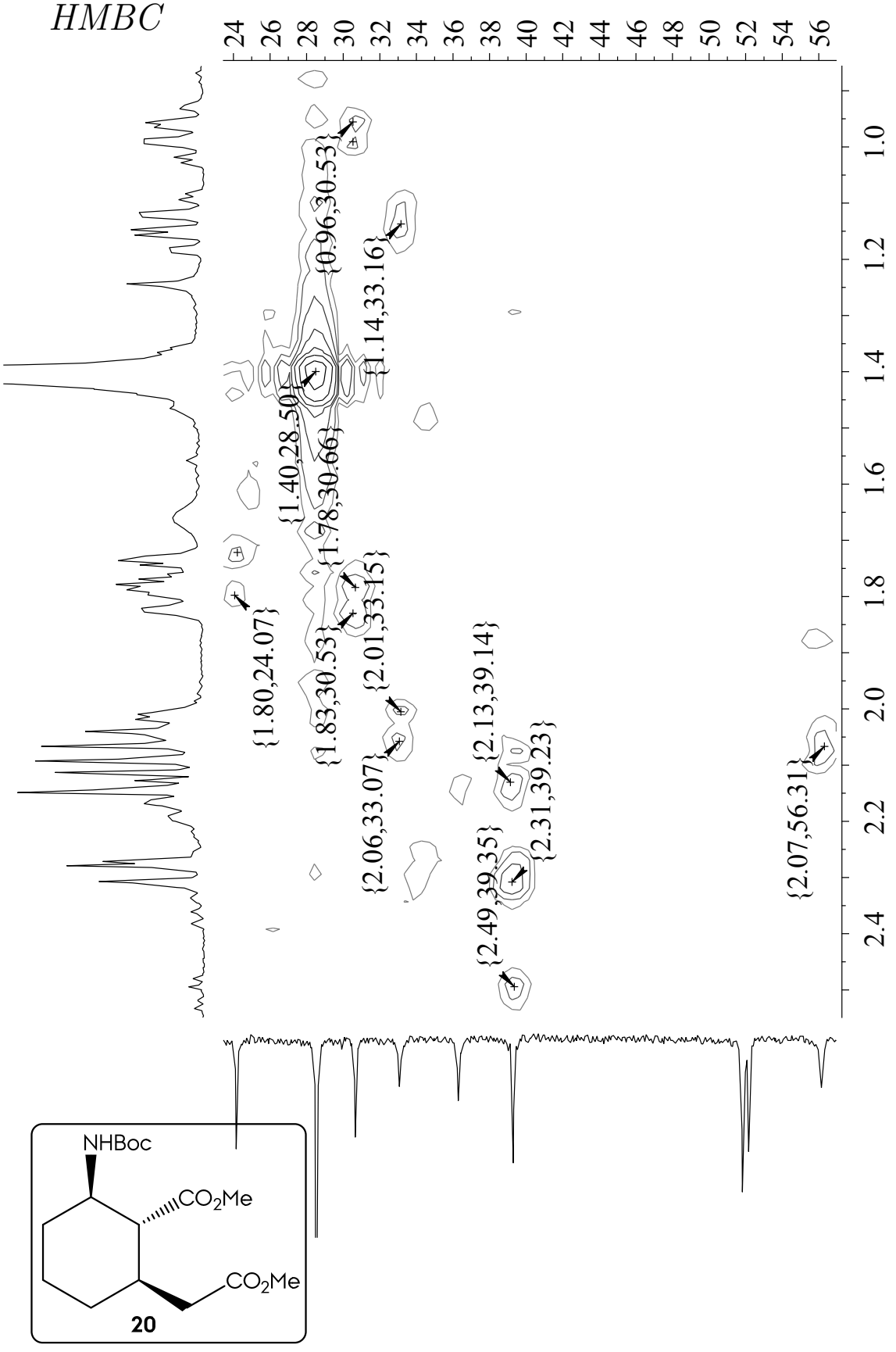
{1.80,24.07}
{1.83,30.53}
{1.40,28.50}
{1.78,30.66}
{2.01,33.15}
{0.96,30.53}
{1.14,33.16}
{2.06,33.07}
{2.13,39.14}
{2.31,39.23}
{2.49,39.35}
{2.07,56.31}
NHBoc
CO2Me
CO2Me
20

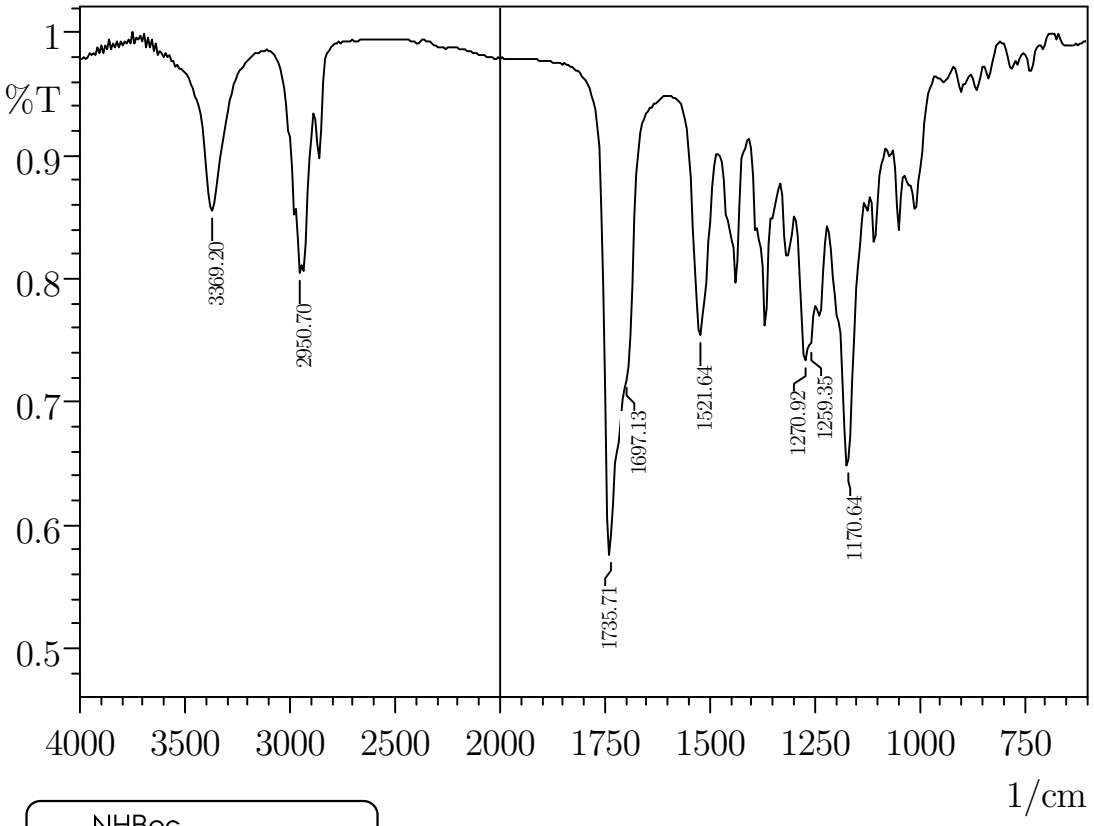
%T
1
0.9
0.8
0.7
0.6
0.5
3369.20
2950.70
1735.71
1697.13
1521.64
1270.92
1259.35
1170.64
4000
3500
3000
2500
2000
1750
1500
1250
1000
750
1/cm

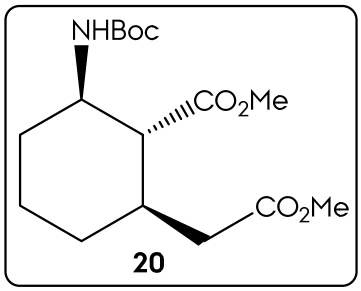
NHBoc
CO2Me
CO2Me

20

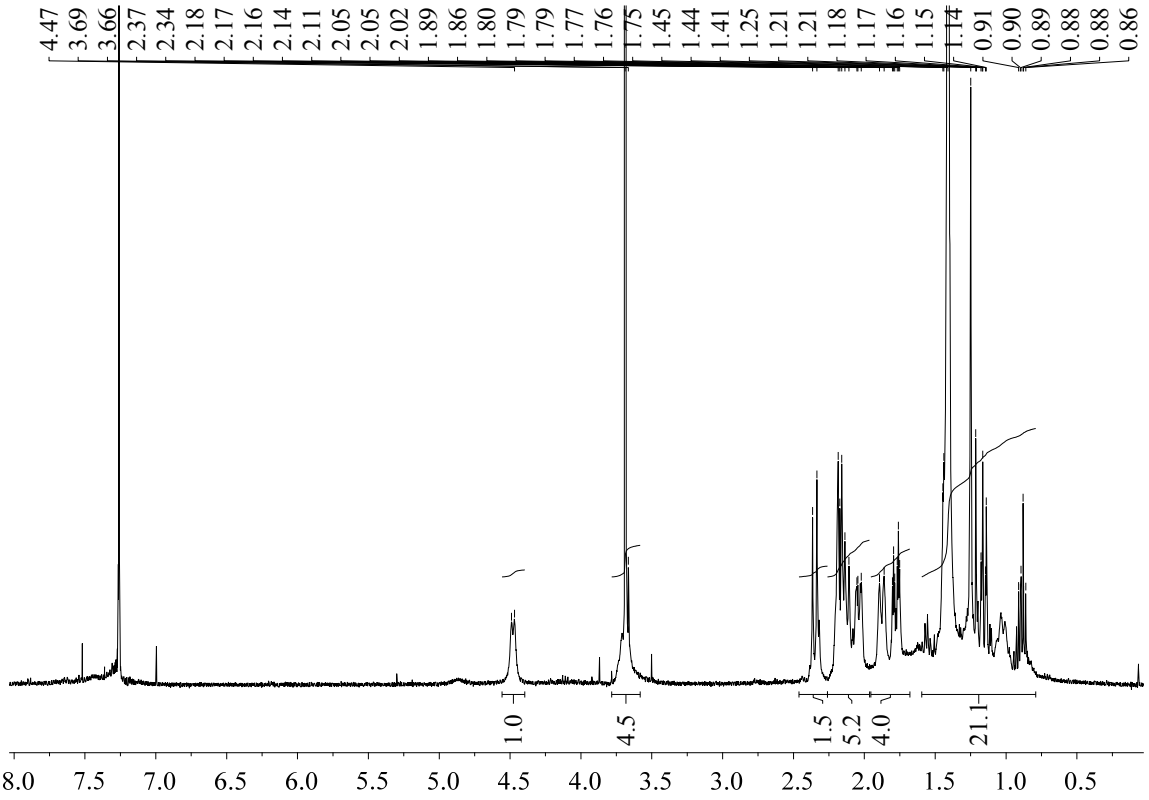
4.47
3.69
3.66
2.37
2.34
2.18
2.17
2.16
2.14
2.11
2.05
2.05
2.02
1.89
1.86
1.80
1.79
1.79
1.77
1.76
1.75
1.45
1.44
1.41
1.25
1.21
1.21
1.18
1.17
1.16
1.15
1.14
0.91
0.90
0.89
0.88
0.88
0.86
1.0
4.5
1.5
5.2
4.0
21.1
8.0
7.5
7.0
6.5
6.0
5.5
5.0
4.5
4.0
3.5
3.0
2.5
2.0
1.5
1.0
0.5

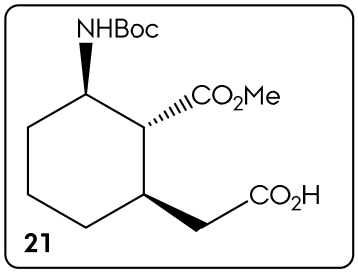
NHBoc
CO2Me
CO2H
21

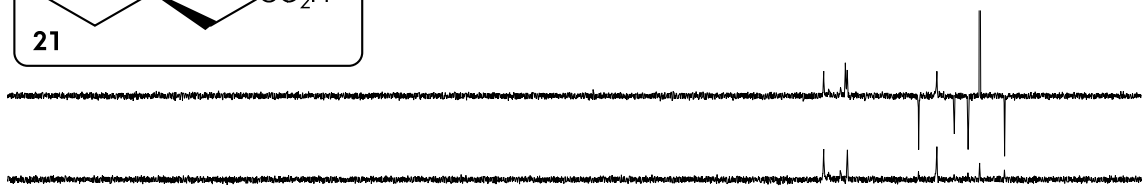

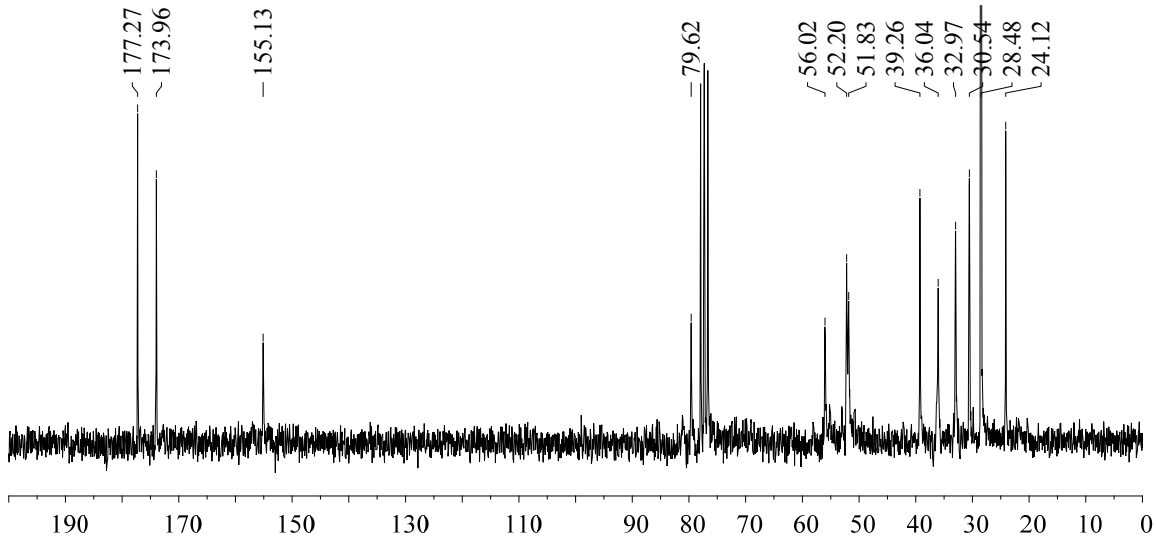
177.27
173.96
155.13
79.62
56.02
52.20
51.83
39.26
36.04
32.97
30.54
28.48
24.12
190
170
150
130
110
90
80
70
60
50
40
30
20
10
0

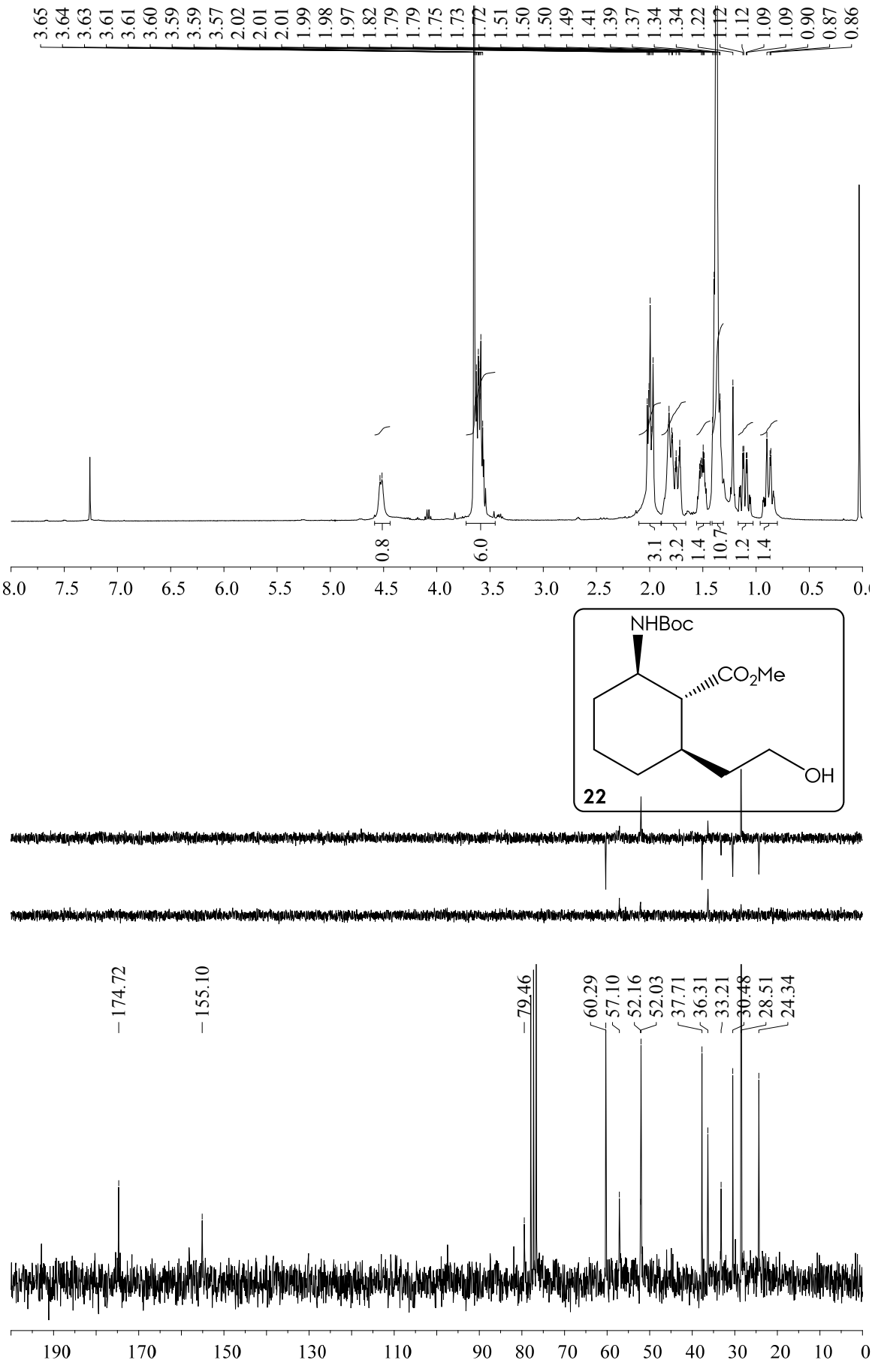
3.65 3.64 3.63 3.61 3.61 3.60 3.59 3.59 3.57 2.02 2.01 2.01 1.99 1.98 1.97 1.82 1.79 1.79 1.75 1.73 1.72 1.51 1.50 1.50 1.49 1.41 1.39 1.37 1.34 1.34 1.22 1.12 1.12 1.09 1.09 0.90 0.87 0.86
0.8 6.0 3.1 3.2 1.4 10.7 1.2 1.4
8.0 7.5 7.0 6.5 6.0 5.5 5.0 4.5 4.0 3.5 3.0 2.5 2.0 1.5 1.0 0.5
NHBoc
CO2Me
OH
22
174.72 155.10 79.46 60.29 57.10 52.16 52.03 37.71 36.31 33.21 30.48 28.51 24.34
190 170 150 130 110 90 80 70 60 50 40 30 20 10 0

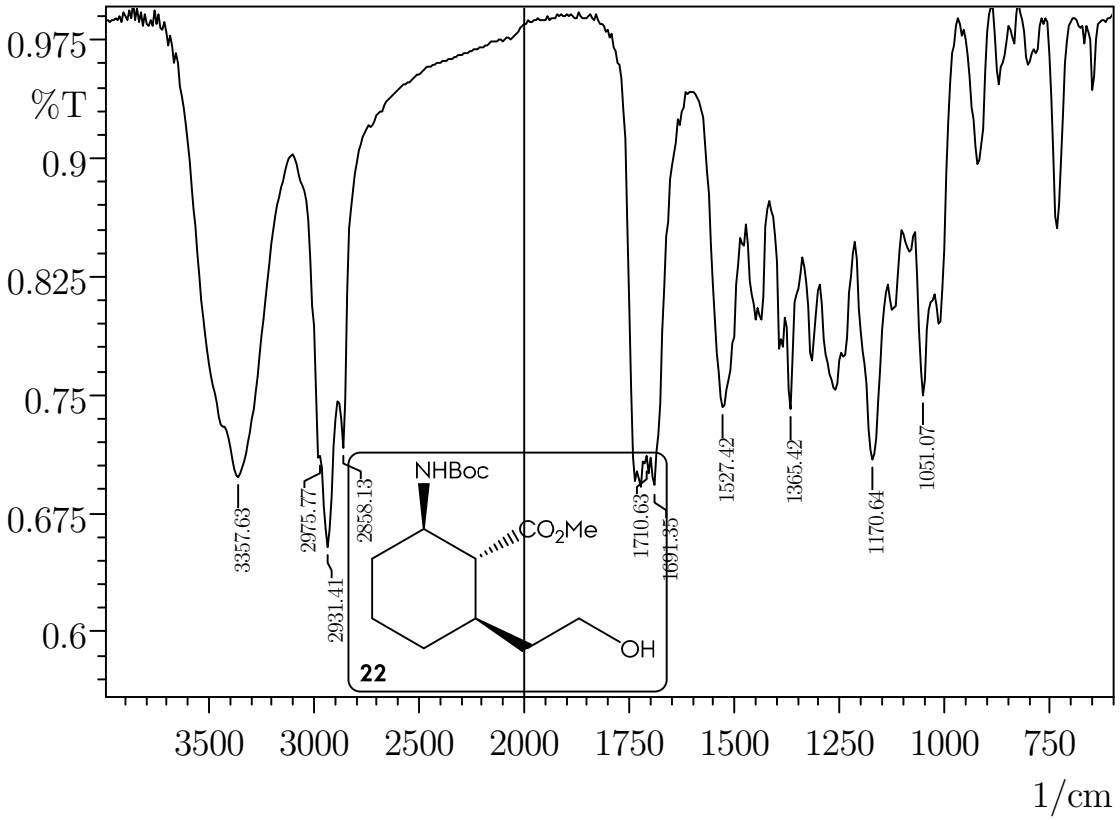
0.975
%T
0.9
0.825
0.75
0.675
0.6
3357.63
2975.77
2931.41
2858.13
1710.63
1691.35
1527.42
1365.42
1170.64
1051.07
NHBoc
CO2Me
OH
22
3500
3000
2500
2000
1750
1500
1250
1000
750
1/cm

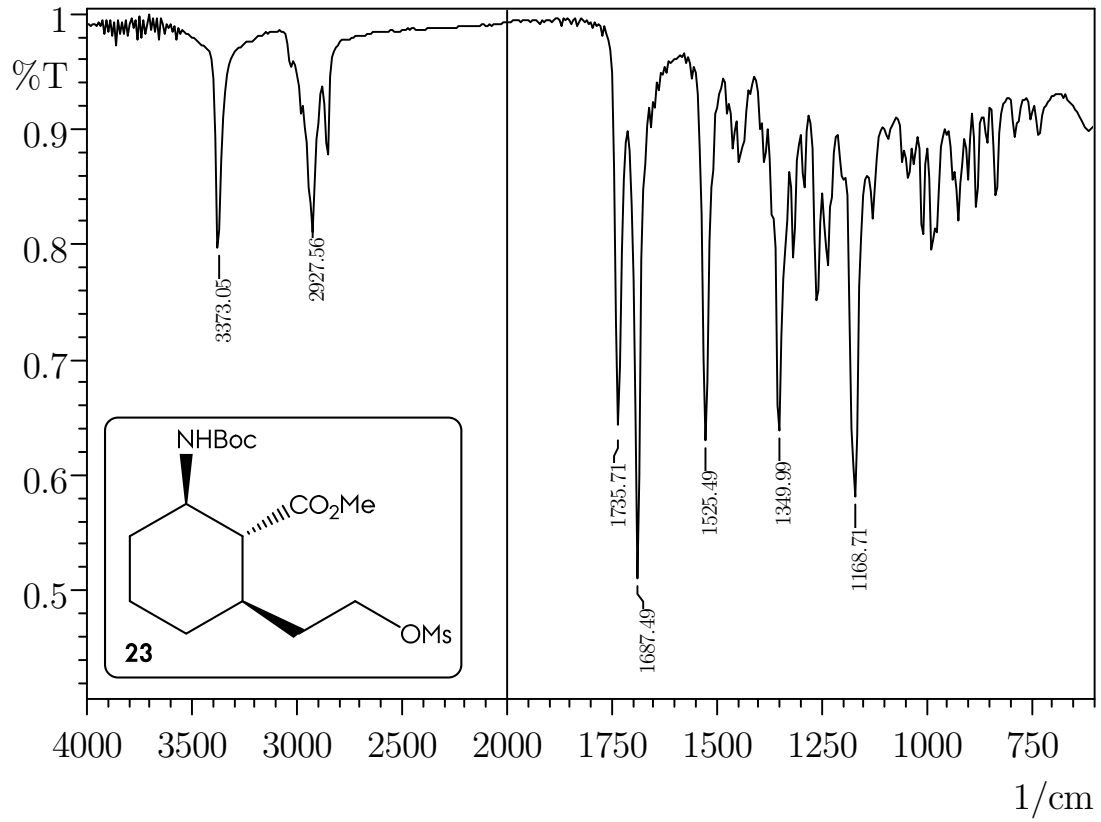
1
%T
0.9
0.8
0.7
0.6
0.5
3373.05
2927.56
1735.71
1687.49
1525.49
1349.99
1168.71
NHBoc
CO2Me
OMs
23
4000
3500
3000
2500
2000
1750
1500
1250
1000
750
1/cm

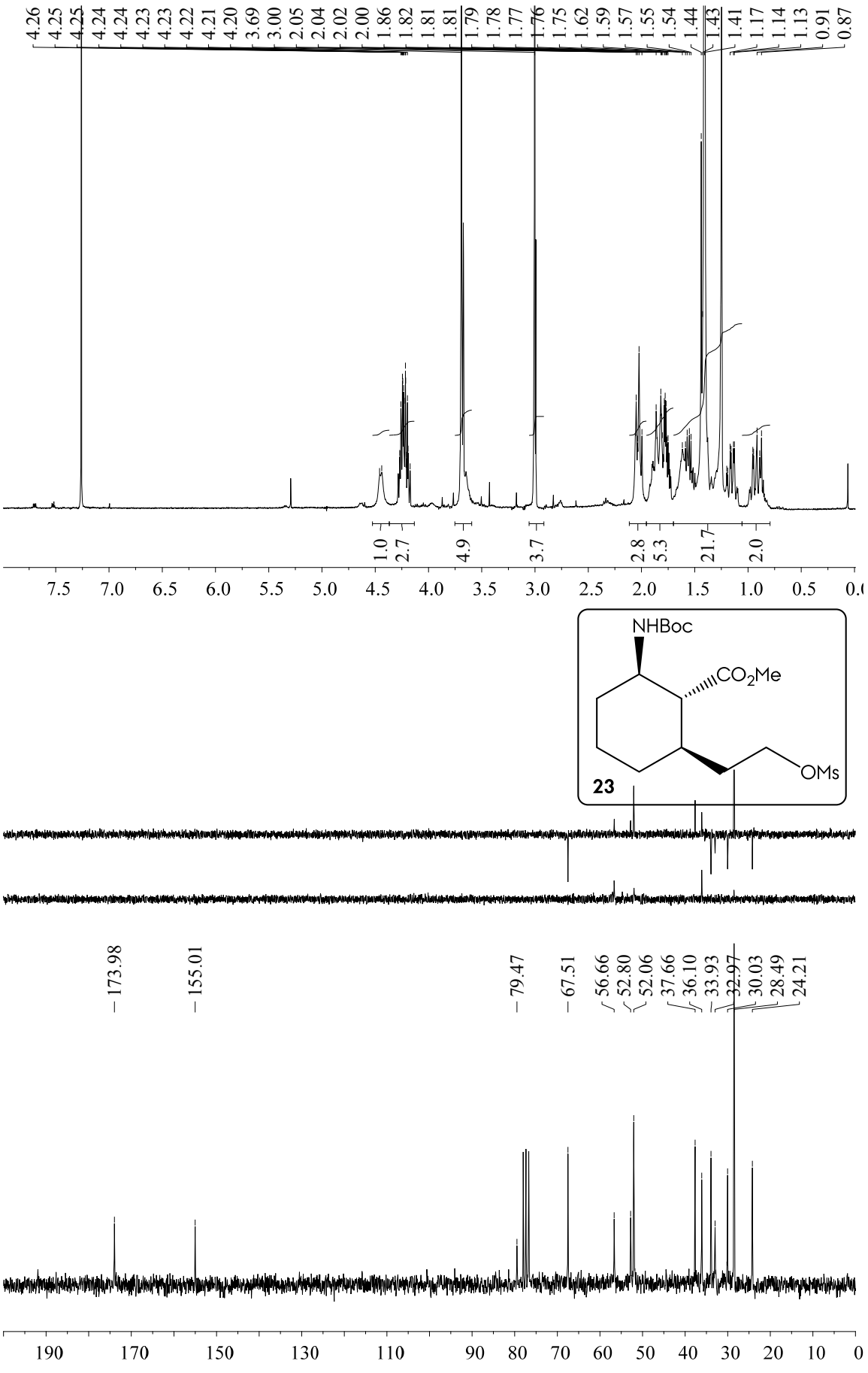
4.26
4.25
4.25
4.24
4.24
4.23
4.23
4.22
4.21
4.20
3.69
3.00
2.05
2.04
2.02
2.00
1.86
1.82
1.81
1.81
1.79
1.78
1.77
1.76
1.75
1.62
1.59
1.57
1.55
1.54
1.44
1.43
1.41
1.17
1.14
1.13
0.91
0.87
1.0
2.7
4.9
3.7
2.8
5.3
21.7
2.0
7.5 7.0 6.5 6.0 5.5 5.0 4.5 4.0 3.5 3.0 2.5 2.0 1.5 1.0 0.5
NHBoc
CO2Me
OMs
23
173.98
155.01
79.47
67.51
56.66
52.80
52.06
37.66
36.10
33.93
32.97
30.03
28.49
24.21
190 170 150 130 110 90 80 70 60 50 40 30 20 10 0

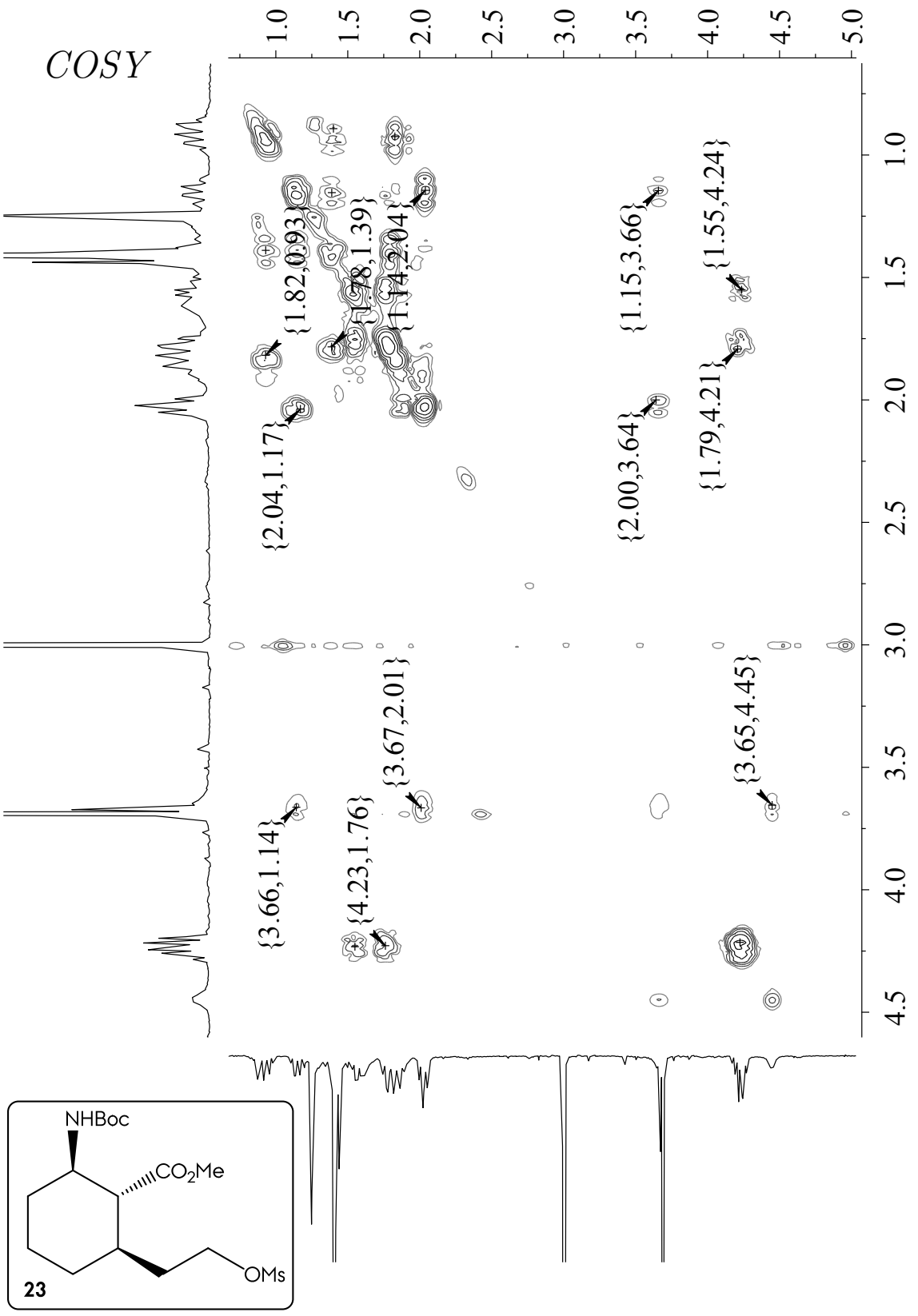
COSY
1.0
1.5
2.0
2.5
3.0
3.5
4.0
4.5
5.0
{1.82,0.93}
{1.78,1.39}
{1.14,2.04}
{2.04,1.17}
{1.15,3.66}
{1.55,4.24}
{2.00,3.64}
{1.79,4.21}
{3.66,1.14}
{4.23,1.76}
{3.67,2.01}
{3.65,4.45}
NHBoc
CO2Me
OMs
23

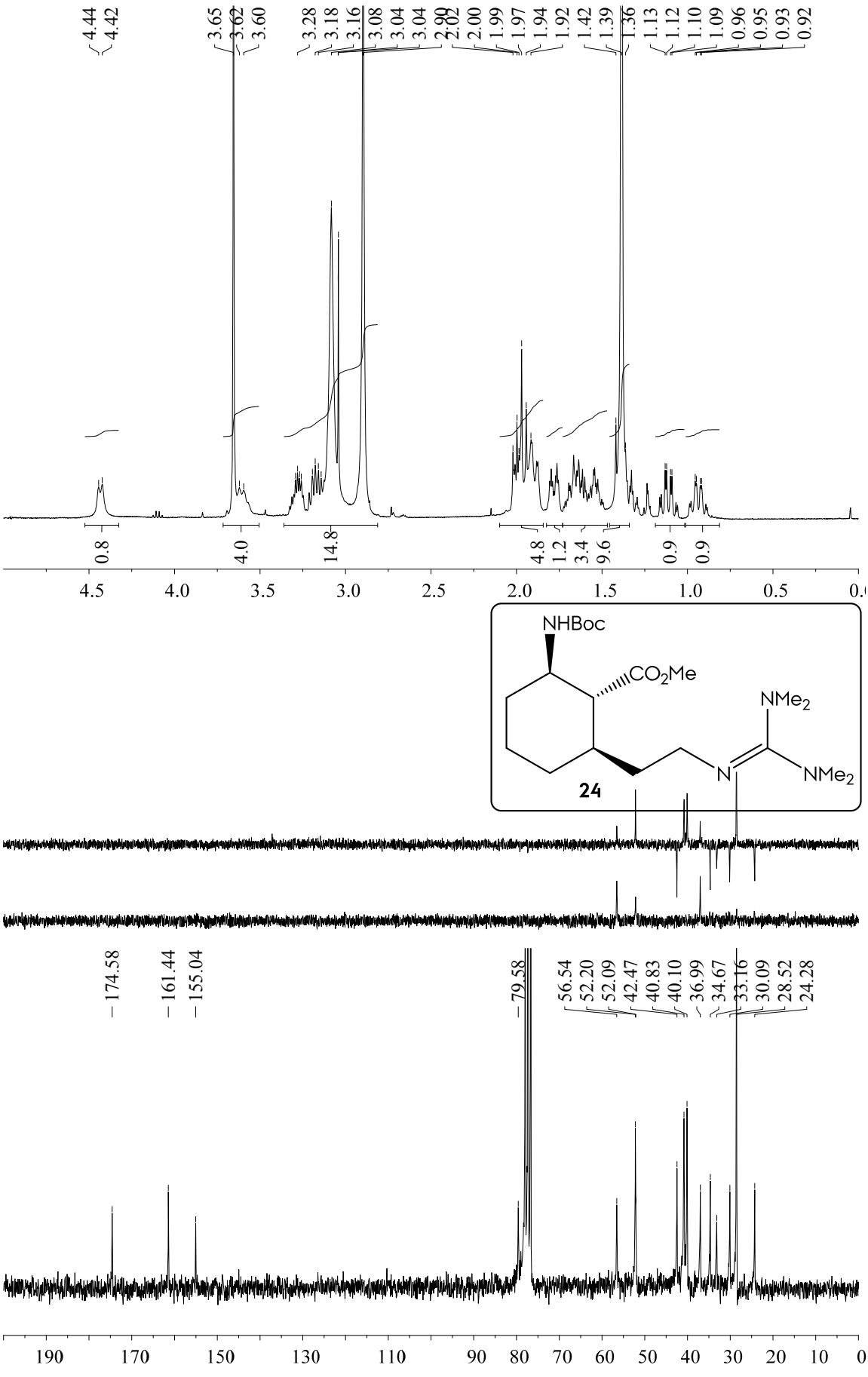
4.44
4.42
3.65
3.62
3.60
3.28
3.18
3.16
3.08
3.04
3.04
2.00
1.99
1.97
1.94
1.92
1.42
1.39
1.36
1.13
1.12
1.10
1.09
0.96
0.95
0.93
0.92
0.8
4.0
14.8
4.8
1.2
3.4
9.6
0.9
0.9
4.5
4.0
3.5
3.0
2.5
2.0
1.5
1.0
0.5
NHBoc
CO2Me
NMe2
N
NMe2
24
174.58
161.44
155.04
79.58
56.54
52.20
52.09
42.47
40.83
40.10
36.99
34.67
33.16
30.09
28.52
24.28
190
170
150
130
110
90
80
70
60
50
40
30
20
10
0

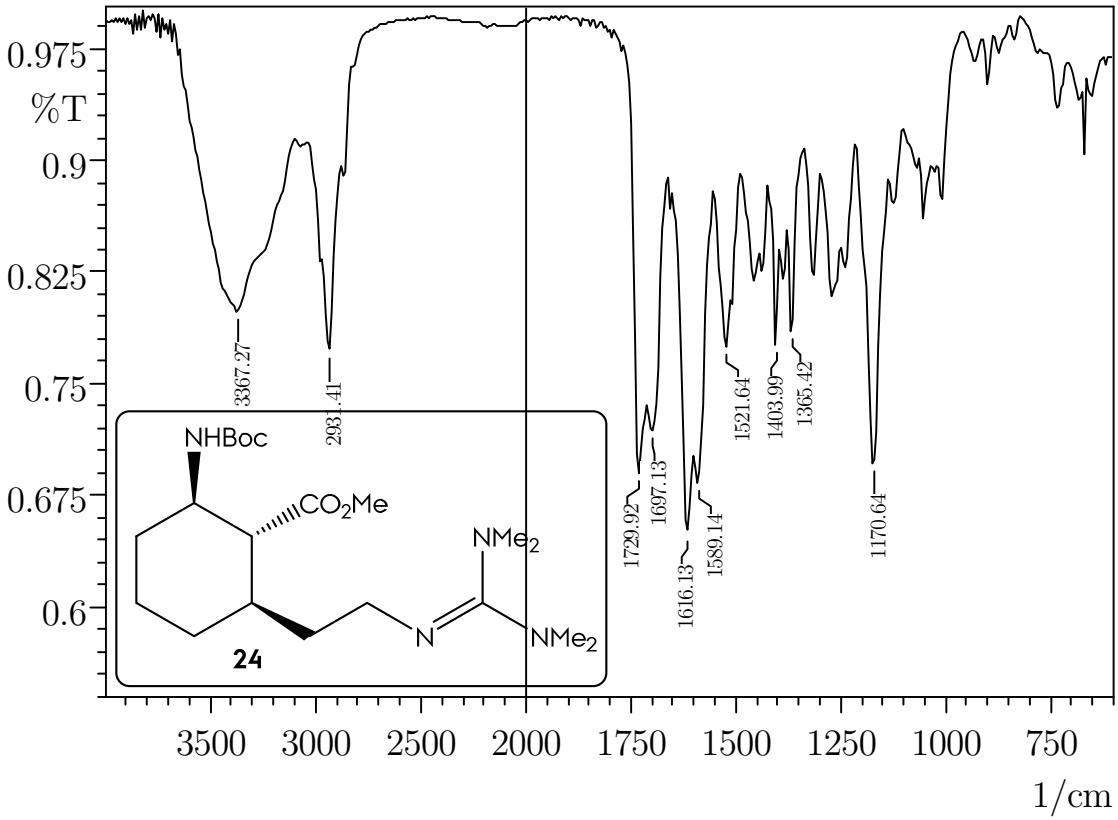
0.975
%T
0.9
0.825
0.75
0.675
0.6
3367.27
2931.41
1729.92
1697.13
1616.13
1589.14
1521.64
1403.99
1365.42
1170.64
NHBoc
CO2Me
NMe2
N
NMe2
24
3500
3000
2500
2000
1750
1500
1250
1000
750
1/cm

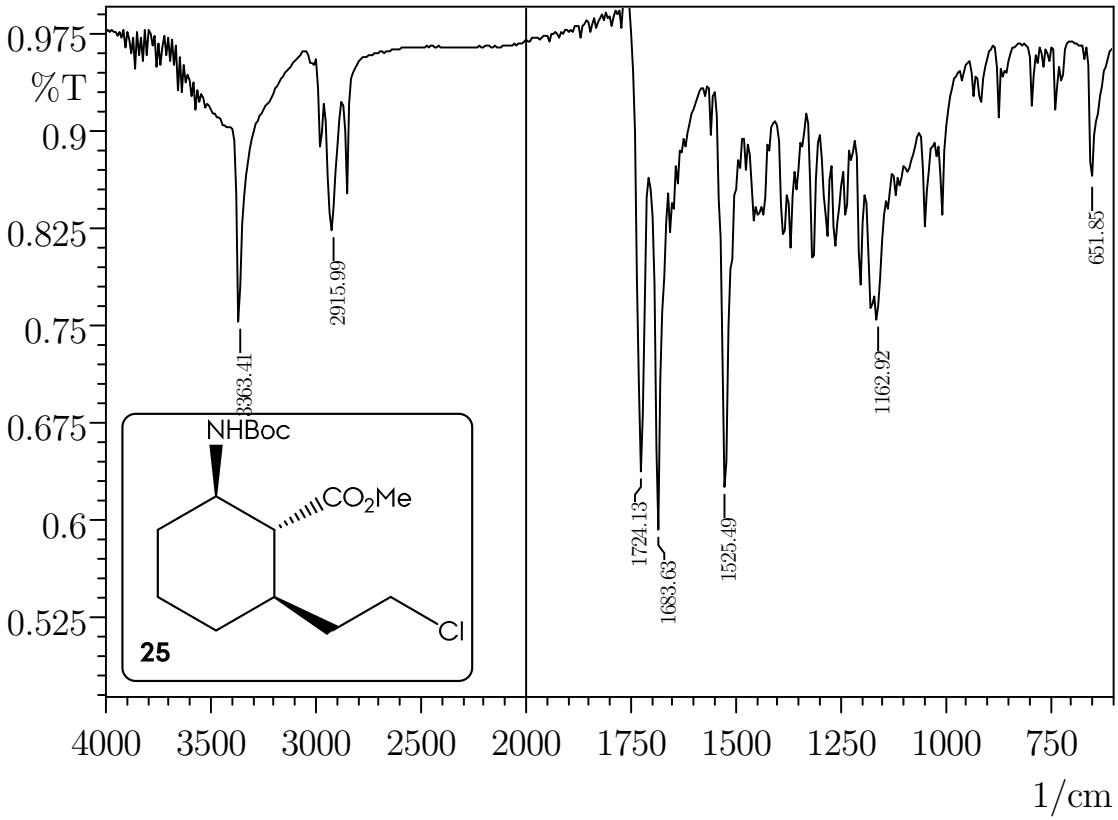
0.975
%T
0.9
0.825
0.75
0.675
0.6
0.525
3363.41
2915.99
1724.13
1683.63
1525.49
1162.92
651.85
NHBoc
CO2Me
Cl
25
4000
3500
3000
2500
2000
1750
1500
1250
1000
750
1/cm

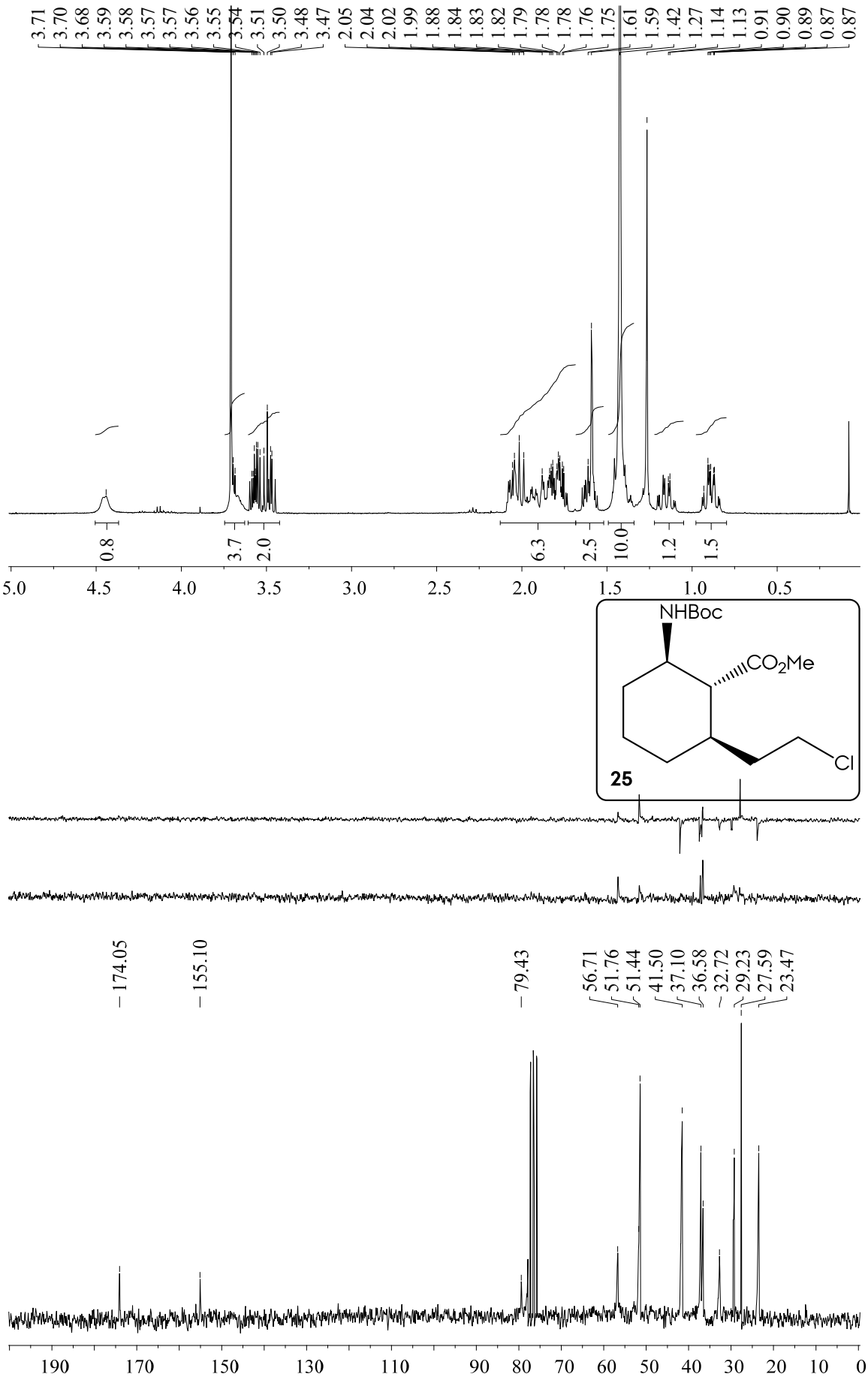
3.71
3.70
3.68
3.59
3.58
3.57
3.57
3.56
3.55
3.54
3.51
3.50
3.48
3.47
2.05
2.04
2.02
1.99
1.88
1.84
1.83
1.82
1.79
1.78
1.78
1.76
1.75
1.61
1.59
1.42
1.27
1.14
1.13
0.91
0.90
0.89
0.87
0.87
0.8
3.7
2.0
6.3
2.5
10.0
1.2
1.5
5.0
4.5
4.0
3.5
3.0
2.5
2.0
1.5
1.0
0.5
NHBoc
CO2Me
Cl
25
174.05
155.10
79.43
56.71
51.76
51.44
41.50
37.10
36.58
32.72
29.23
27.59
23.47
190
170
150
130
110
90
80
70
60
50
40
30
20
10
0

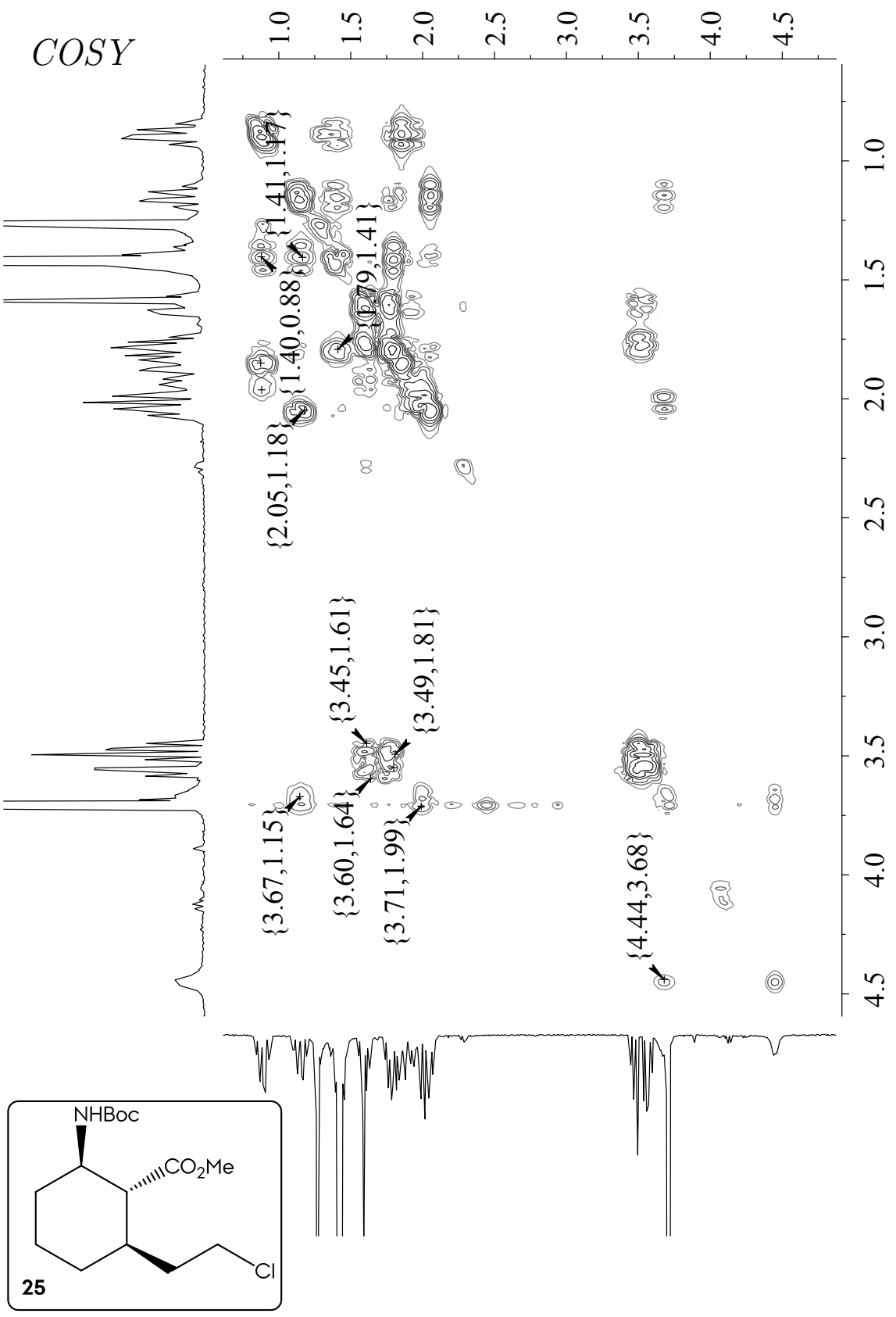
COSY
1.0
1.5
2.0
2.5
3.0
3.5
4.0
4.5
{2.05,1.18}
{1.40,0.88}
{1.41,1.14}
{1.79,1.41}
{3.67,1.15}
{3.60,1.64}
{3.45,1.61}
{3.71,1.99}
{3.49,1.81}
{4.44,3.68}
NHBoc
CO2Me
Cl
25

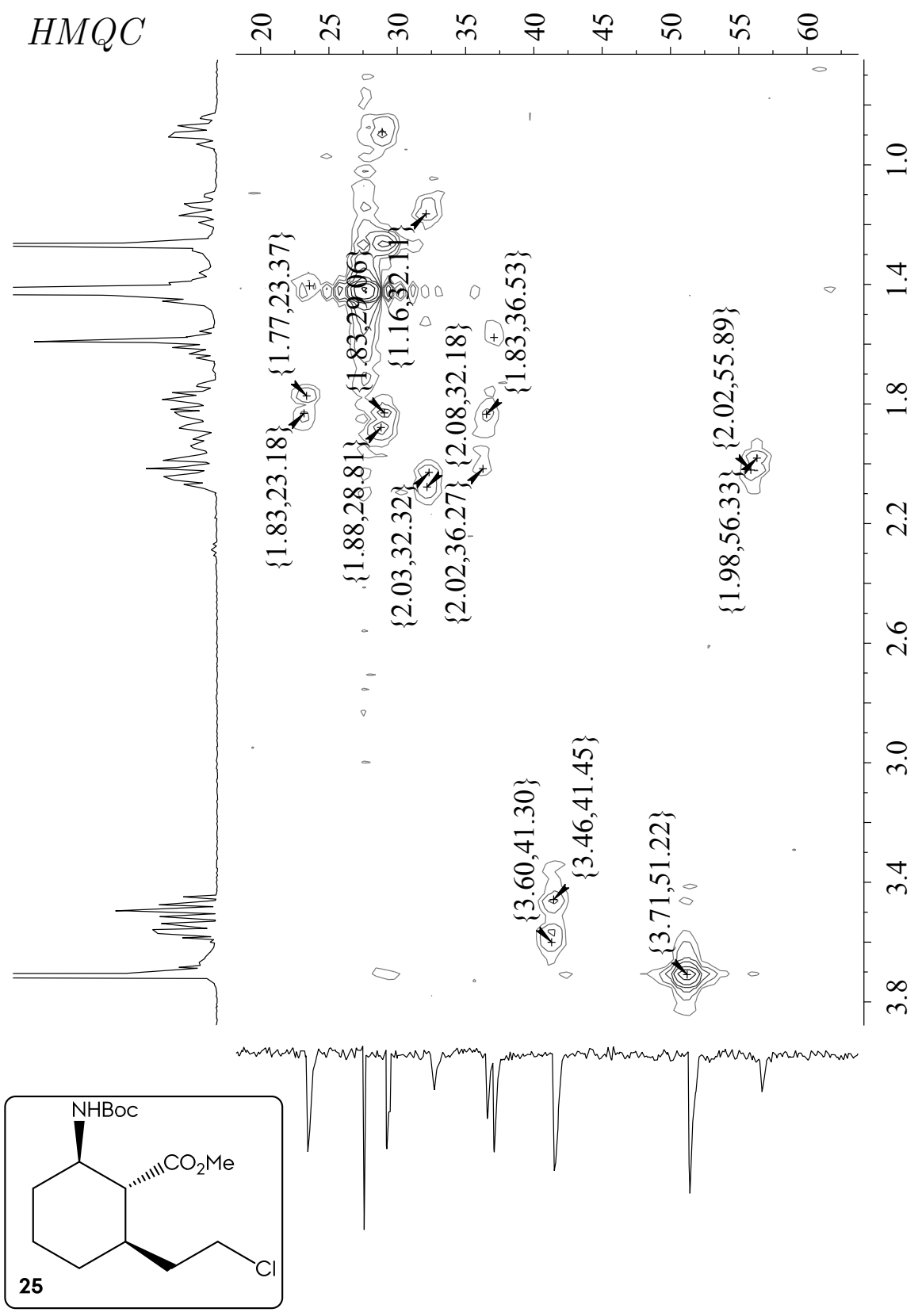
HMQC
20
25
30
35
40
45
50
55
60
1.0
1.4
1.8
2.2
2.6
3.0
3.4
3.8
{1.83,23.18}
{1.77,23.37}
{1.88,28.81}
{1.83,29.06}
{1.16,32.11}
{2.03,32.32}
{2.02,36.27}
{2.08,32.18}
{1.83,36.53}
{1.98,56.33}
{2.02,55.89}
{3.60,41.30}
{3.46,41.45}
{3.71,51.22}
NHBoc
CO2Me
Cl
25

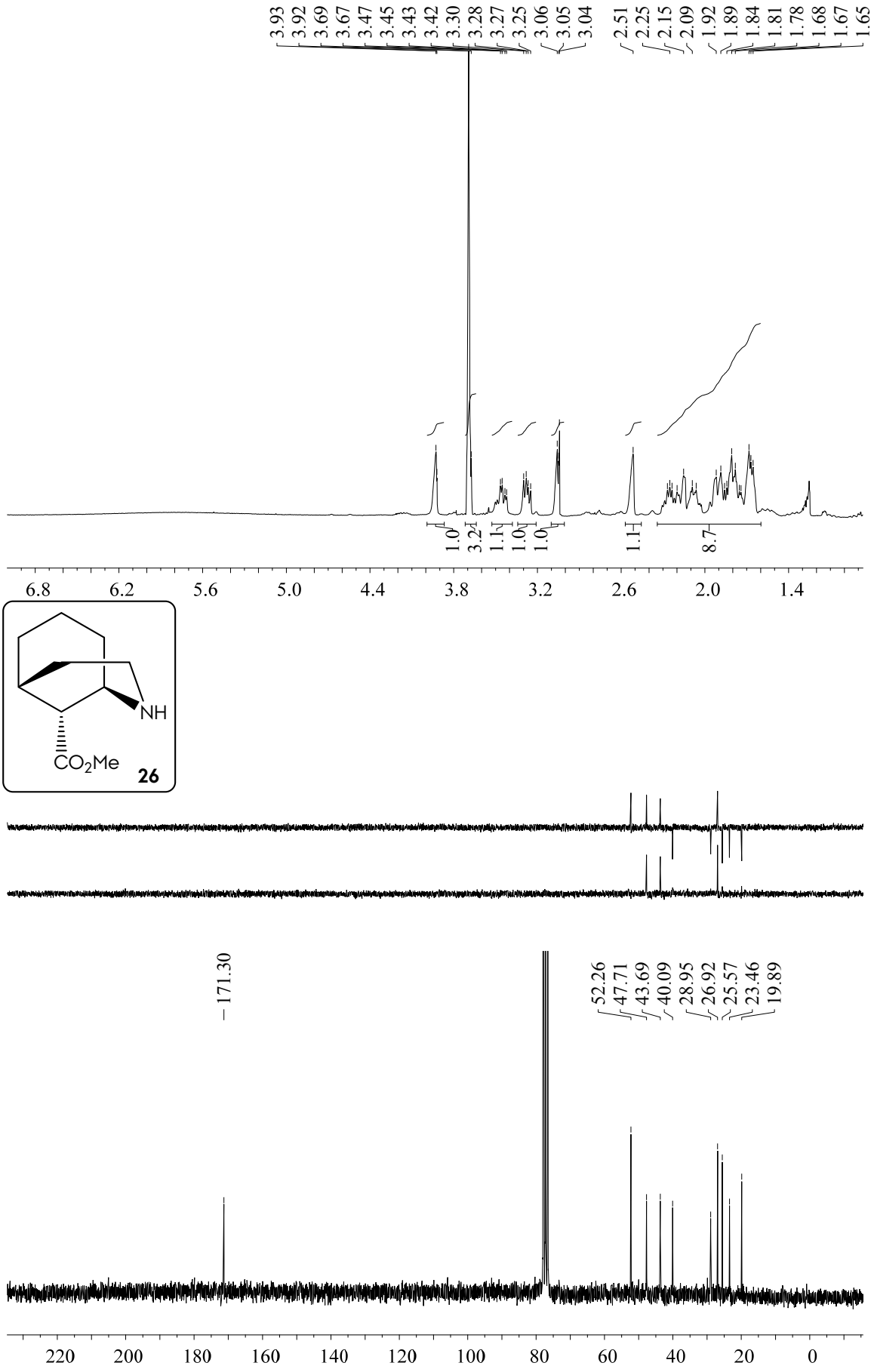
3.93
3.92
3.69
3.67
3.47
3.45
3.43
3.42
3.30
3.28
3.27
3.25
3.06
3.05
3.04
2.51
2.25
2.15
2.09
1.92
1.89
1.84
1.81
1.78
1.68
1.67
1.65
1.0
3.2
1.1
1.0
1.0
1.1
8.7
6.8
6.2
5.6
5.0
4.4
3.8
3.2
2.6
2.0
1.4
NH
CO2Me
26
171.30
52.26
47.71
43.69
40.09
28.95
26.92
25.57
23.46
19.89
220
200
180
160
140
120
100
80
60
40
20
0

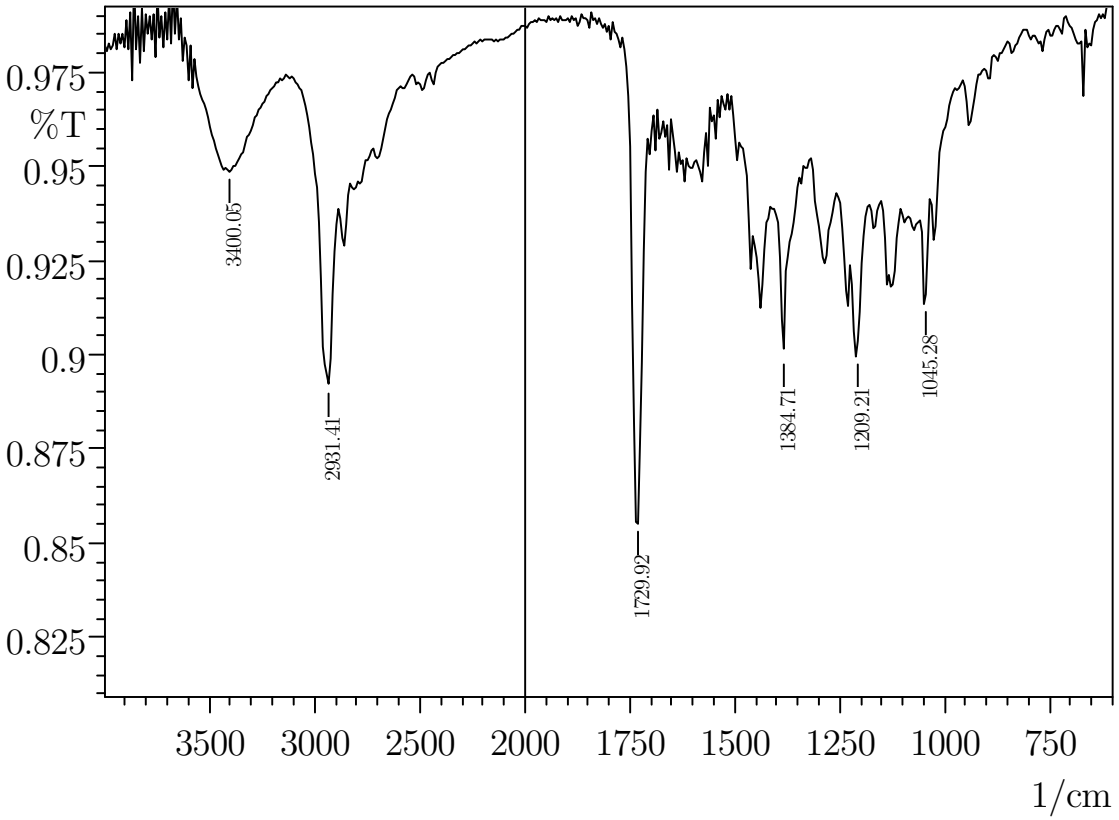
0.975
%T
0.95
0.925
0.9
0.875
0.85
0.825
3400.05
2931.41
1729.92
1384.71
1209.21
1045.28
3500
3000
2500
2000
1750
1500
1250
1000
750
1/cm

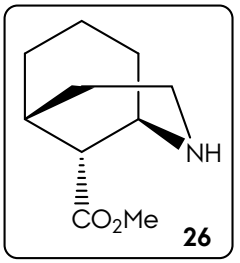
NH
CO2Me
26

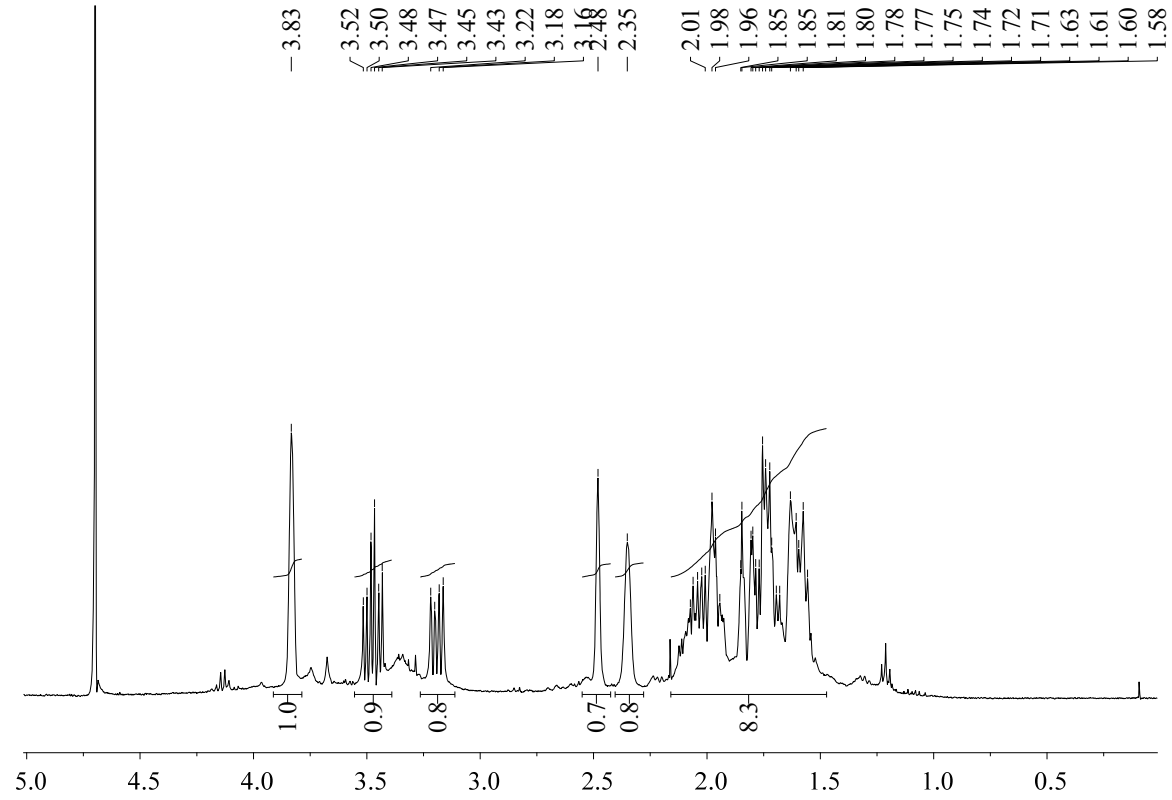
3.83
3.52
3.50
3.48
3.47
3.45
3.43
3.22
3.18
2.48
2.35
2.01
1.98
1.96
1.85
1.85
1.81
1.80
1.78
1.77
1.75
1.74
1.72
1.71
1.63
1.61
1.60
1.58
1.0
0.9
0.8
0.7
0.8
8.3
5.0
4.5
4.0
3.5
3.0
2.5
2.0
1.5
1.0
0.5

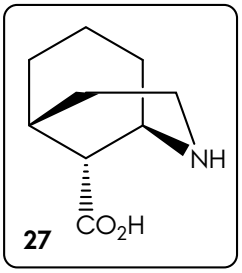
NH
CO2H
27

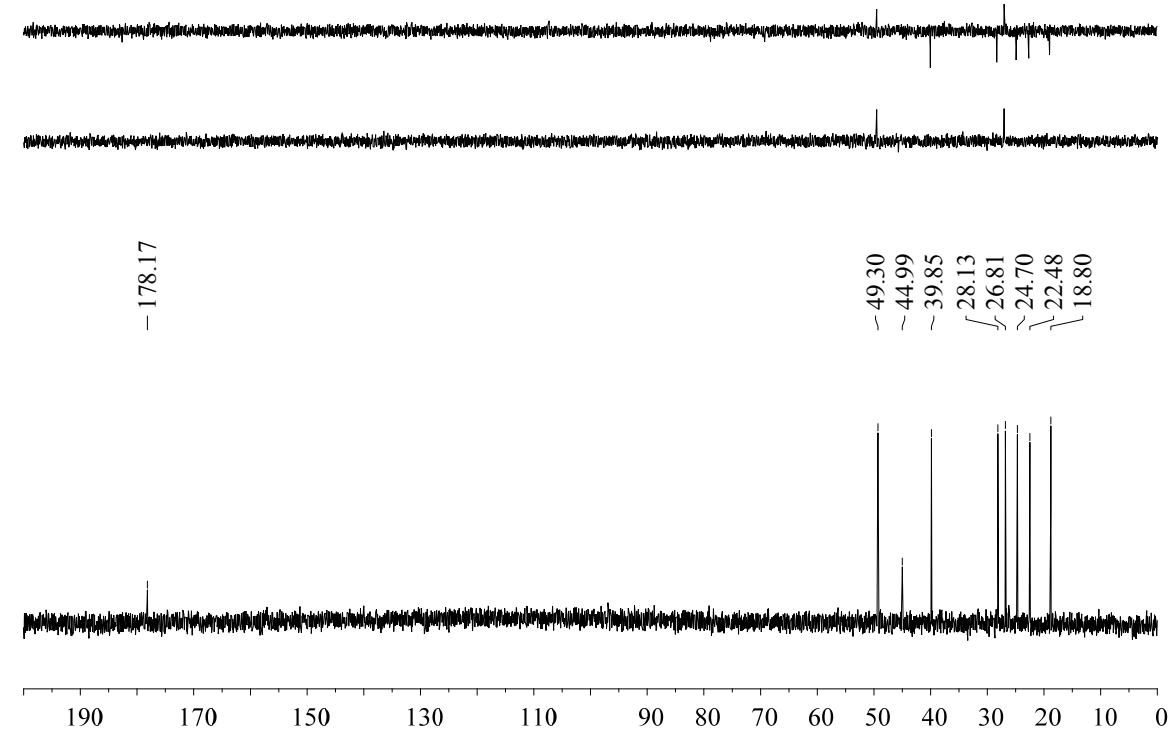
178.17
49.30
44.99
39.85
28.13
26.81
24.70
22.48
18.80
190
170
150
130
110
90
80
70
60
50
40
30
20
10
0

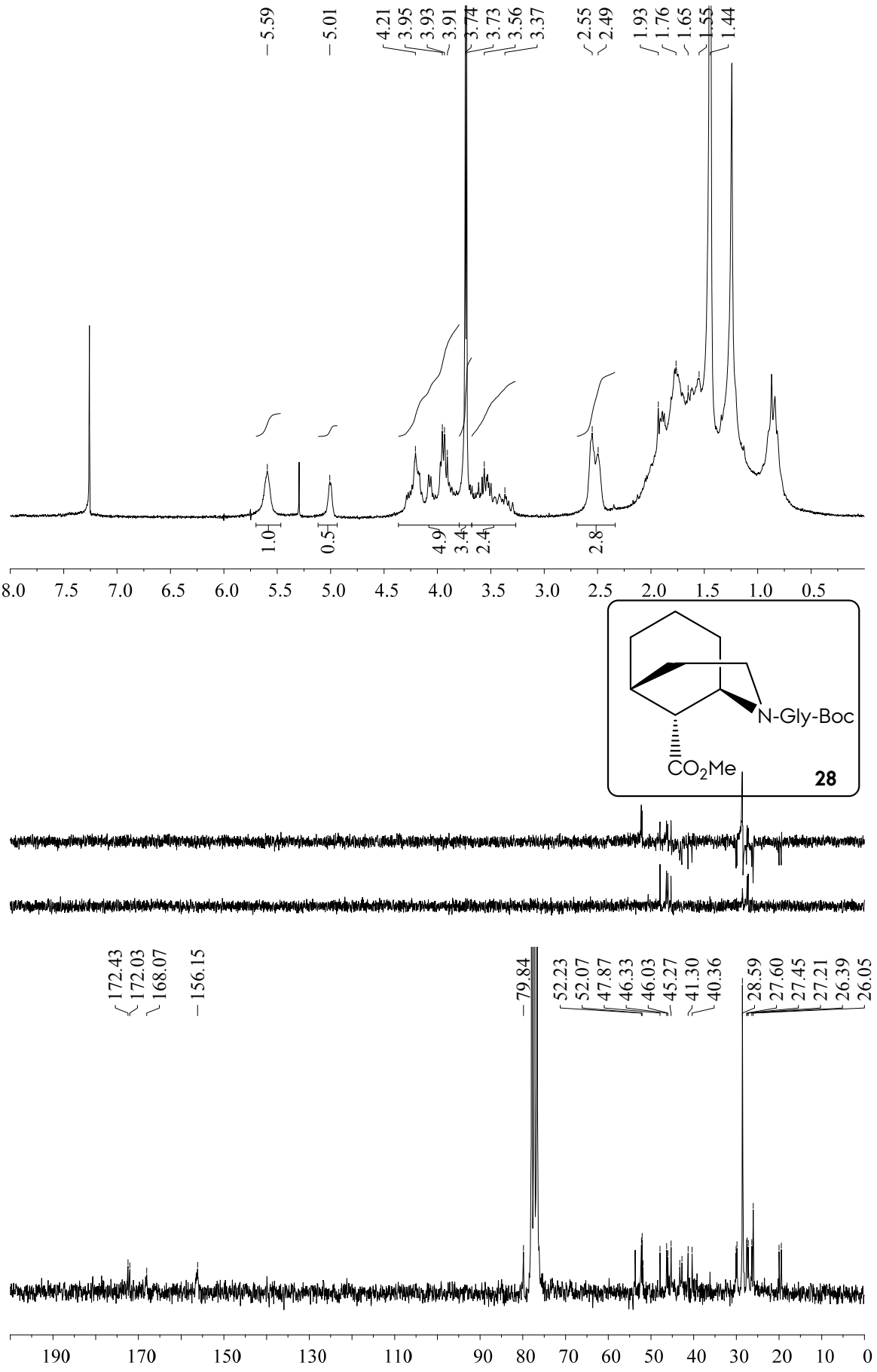
5.59
5.01
4.21
3.95
3.93
3.91
3.74
3.73
3.56
3.37
2.55
2.49
1.93
1.76
1.65
1.55
1.44
1.0
0.5
4.9
3.4
2.4
2.8
8.0 7.5 7.0 6.5 6.0 5.5 5.0 4.5 4.0 3.5 3.0 2.5 2.0 1.5 1.0 0.5
N-Gly-Boc
CO2Me
28
172.43
172.03
168.07
156.15
79.84
52.23
52.07
47.87
46.33
46.03
45.27
41.30
40.36
28.59
27.60
27.45
27.21
26.39
26.05
190 170 150 130 110 90 80 70 60 50 40 30 20 10 0

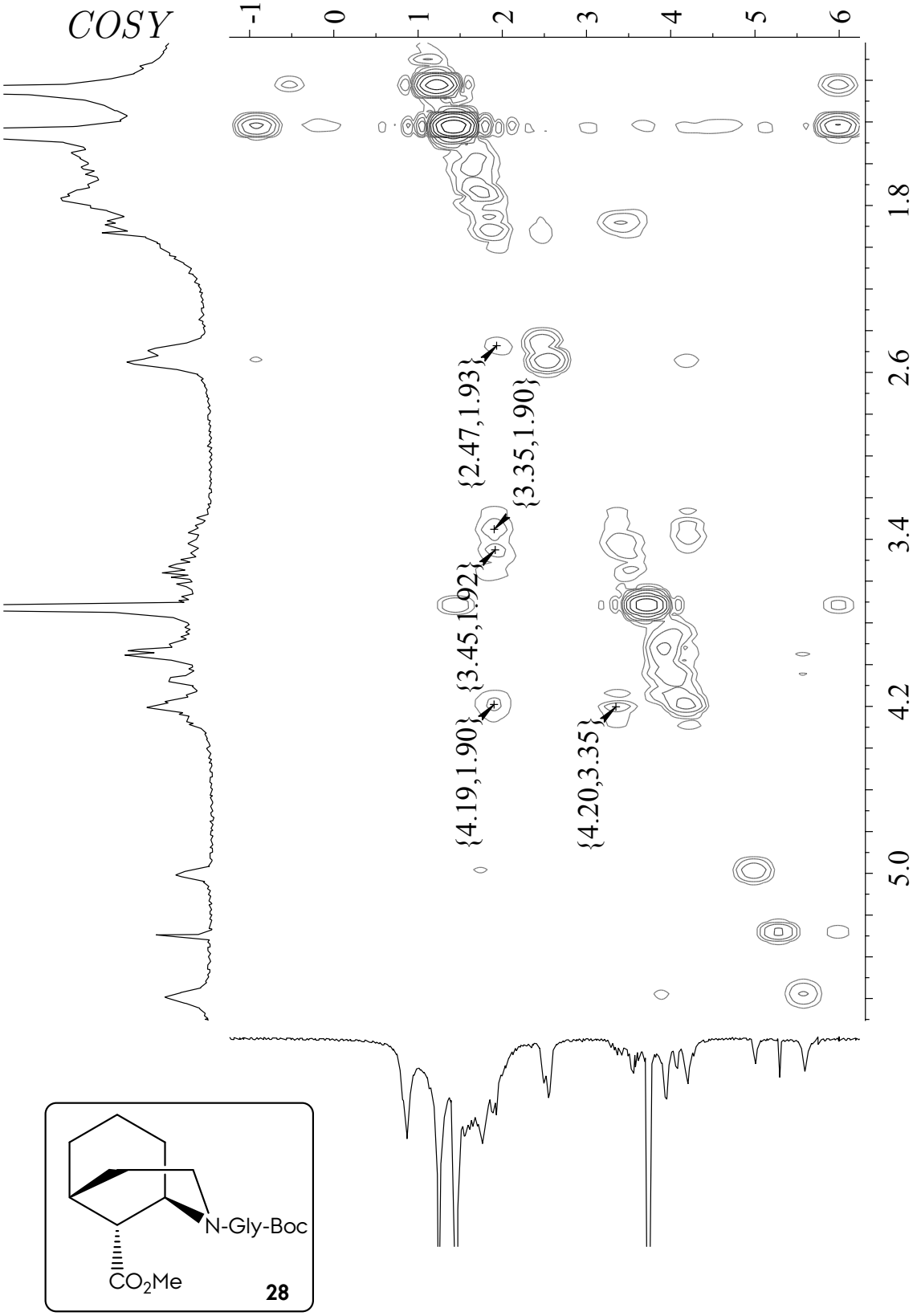
COSY
-1
0
1
2
3
4
5
6
1.8
2.6
3.4
4.2
5.0
{2.47,1.93}
{3.35,1.90}
{3.45,1.92}
{4.19,1.90}
{4.20,3.35}
N-Gly-Boc
CO2Me
28

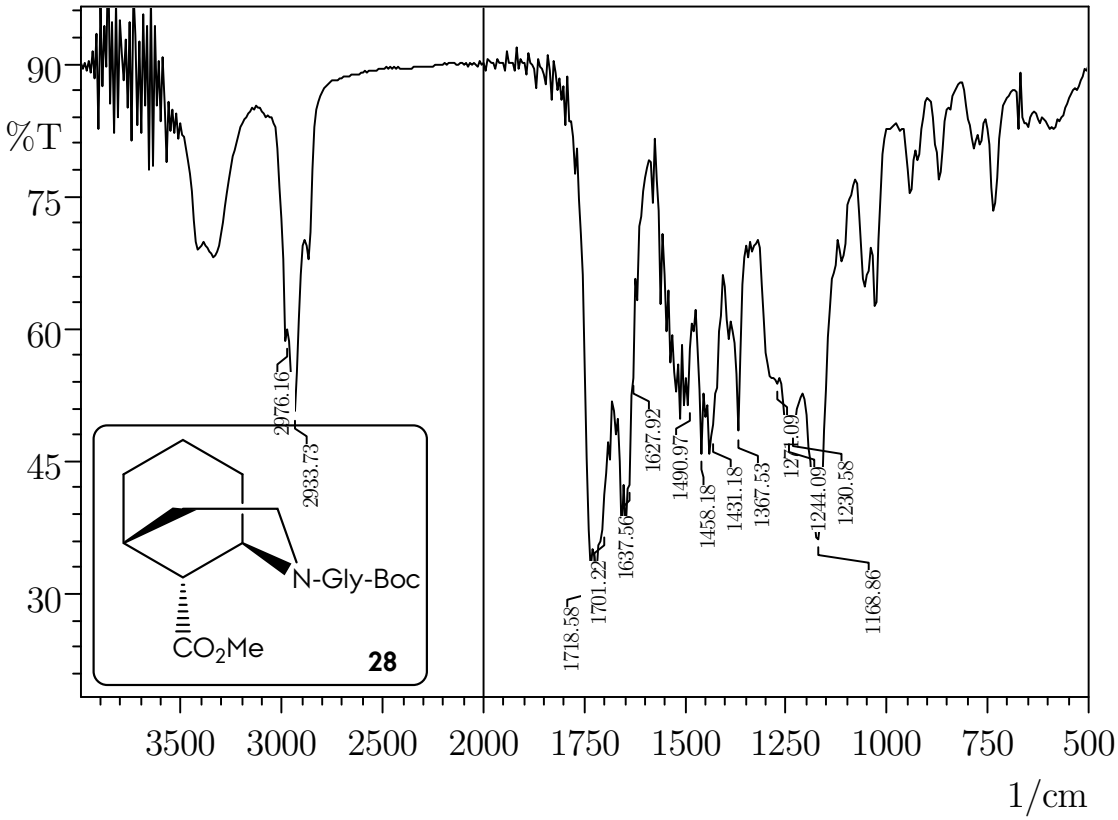
90
%T
75
60
45
30
2976.16
2933.73
1718.58
1701.22
1637.56
1627.92
1490.97
1458.18
1431.18
1367.53
1277.09
1244.09
1230.58
1168.86
N-Gly-Boc
CO2Me
28
3500 3000 2500 2000 1750 1500 1250 1000 750 500
1/cm

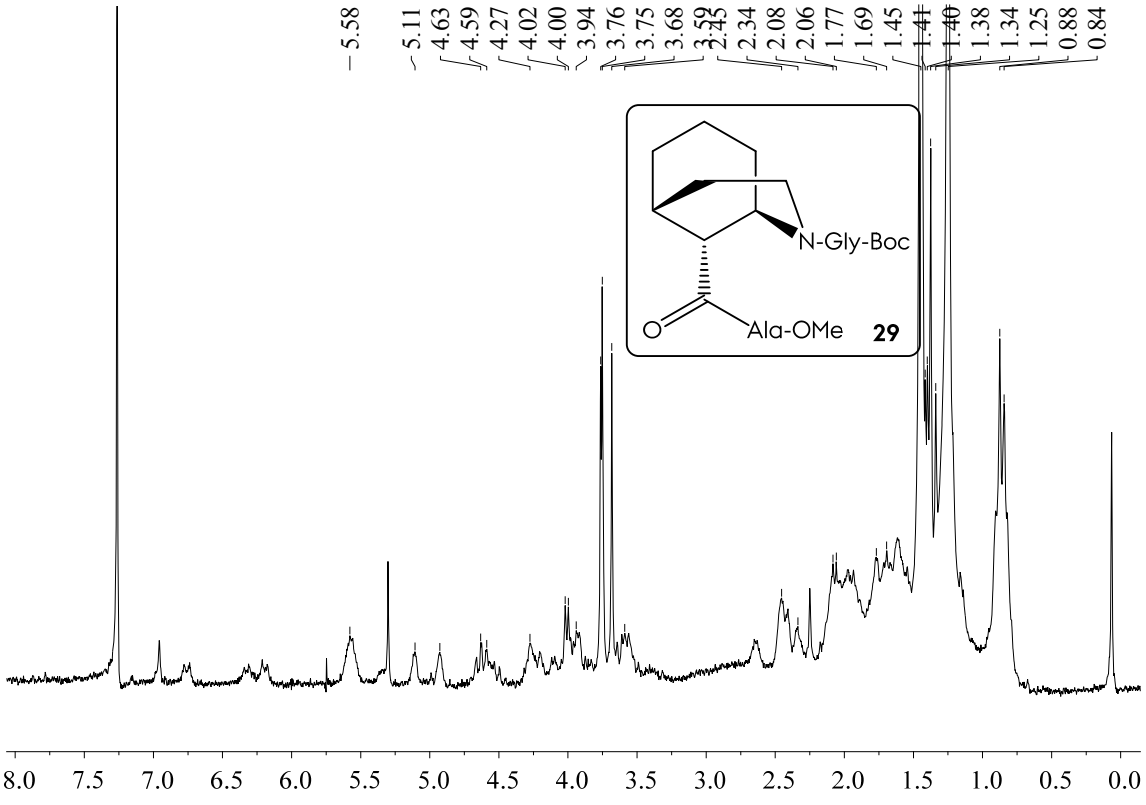
5.58
5.11
4.63
4.59
4.27
4.02
4.00
3.94
3.76
3.75
3.68
2.34
2.08
2.06
1.77
1.69
1.45
1.38
1.34
1.25
0.88
0.84
N-Gly-Boc
O
Ala-OMe
29
8.0 7.5 7.0 6.5 6.0 5.5 5.0 4.5 4.0 3.5 3.0 2.5 2.0 1.5 1.0 0.5 0.0

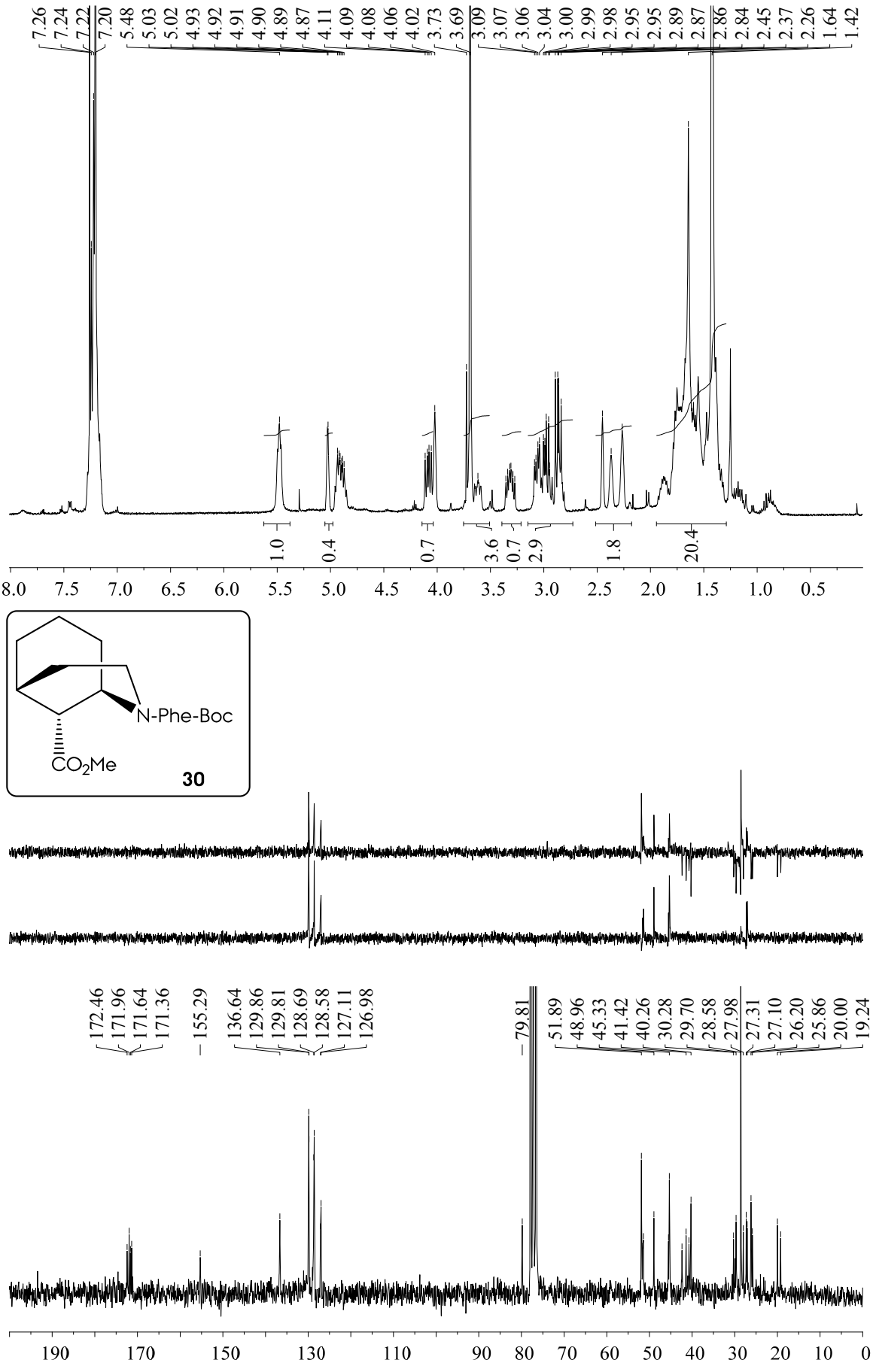
7.26
7.24
7.22
7.20
5.48
5.03
5.02
4.93
4.92
4.91
4.90
4.89
4.87
4.11
4.09
4.08
4.06
4.02
3.73
3.69
3.09
3.07
3.06
3.04
3.00
2.99
2.98
2.95
2.95
2.89
2.87
2.86
2.84
2.45
2.37
2.26
1.64
1.42
1.0
0.4
0.7
3.6
0.7
2.9
1.8
20.4
8.0 7.5 7.0 6.5 6.0 5.5 5.0 4.5 4.0 3.5 3.0 2.5 2.0 1.5 1.0 0.5
N-Phe-Boc
CO2Me
30
172.46
171.96
171.64
171.36
155.29
136.64
129.86
129.81
128.69
128.58
127.11
126.98
79.81
51.89
48.96
45.33
41.42
40.26
30.28
29.70
28.58
27.98
27.31
27.10
26.20
25.86
20.00
19.24
190 170 150 130 110 90 80 70 60 50 40 30 20 10 0

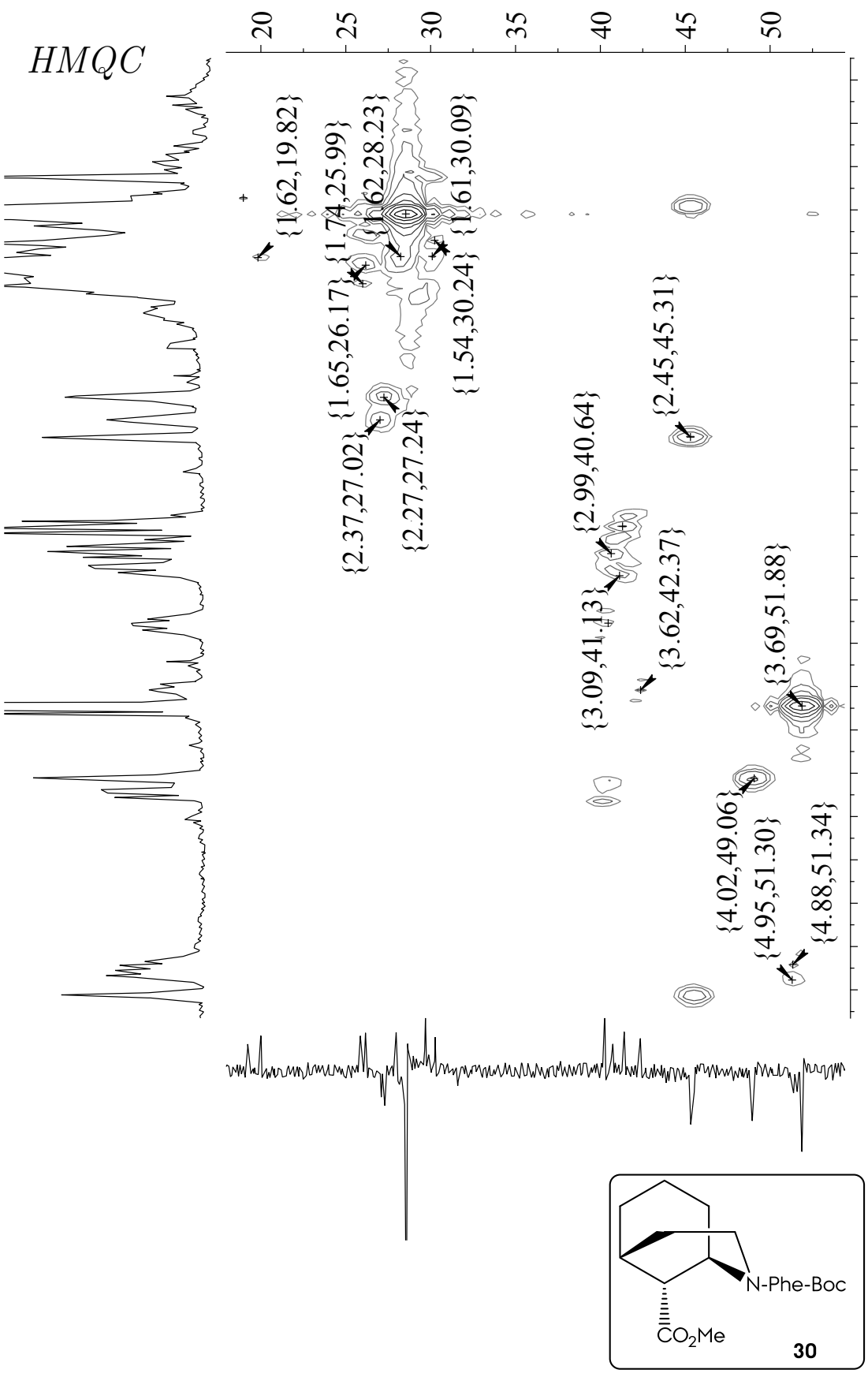
HMQC
20
25
30
35
40
45
50
1.2
1.8
2.4
3.0
3.6
4.2
4.8
{1.62,19.82}
{1.74,25.99}
{1.62,28.23}
{1.61,30.09}
{1.54,30.24}
{1.65,26.17}
{2.37,27.02}
{2.27,27.24}
{2.45,45.31}
{2.99,40.64}
{3.09,41.13}
{3.62,42.37}
{3.69,51.88}
{4.02,49.06}
{4.95,51.30}
{4.88,51.34}
N-Phe-Boc
CO2Me
30

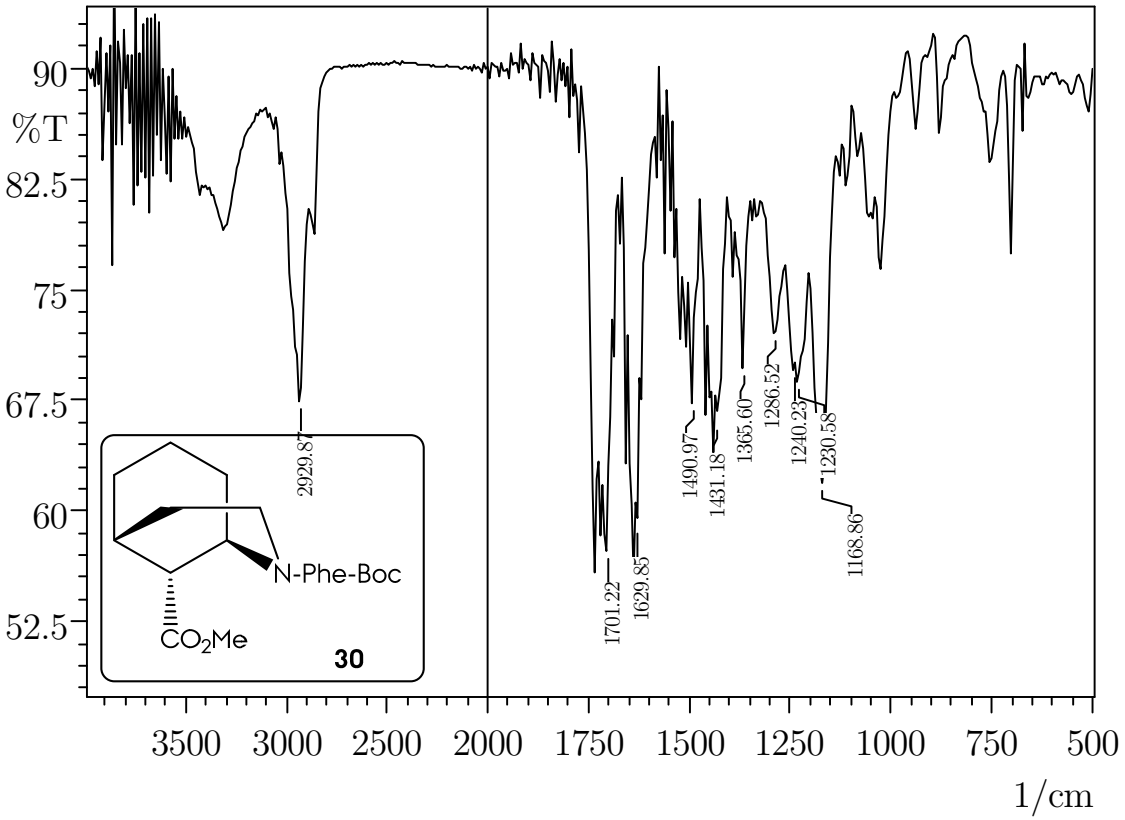
90
%T
82.5
75
67.5
60
52.5
2929.87
1701.22
1629.85
1490.97
1431.18
1365.60
1286.52
1240.23
1230.58
1168.86
N-Phe-Boc
CO2Me
30
3500 3000 2500 2000 1750 1500 1250 1000 750 500
1/cm

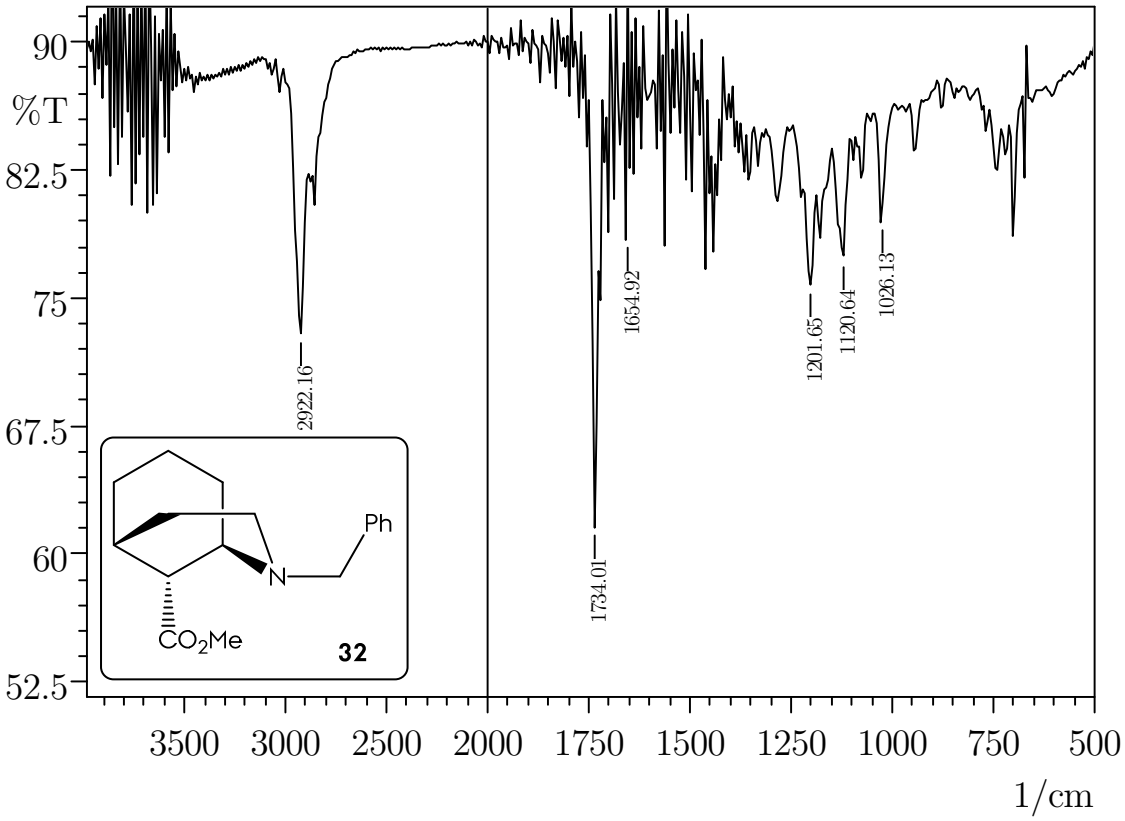
90
%T
82.5
75
67.5
60
52.5
2922.16
1734.01
1654.92
1201.65
1120.64
1026.13
Ph
N
CO2Me
32
3500 3000 2500 2000 1750 1500 1250 1000 750 500
1/cm

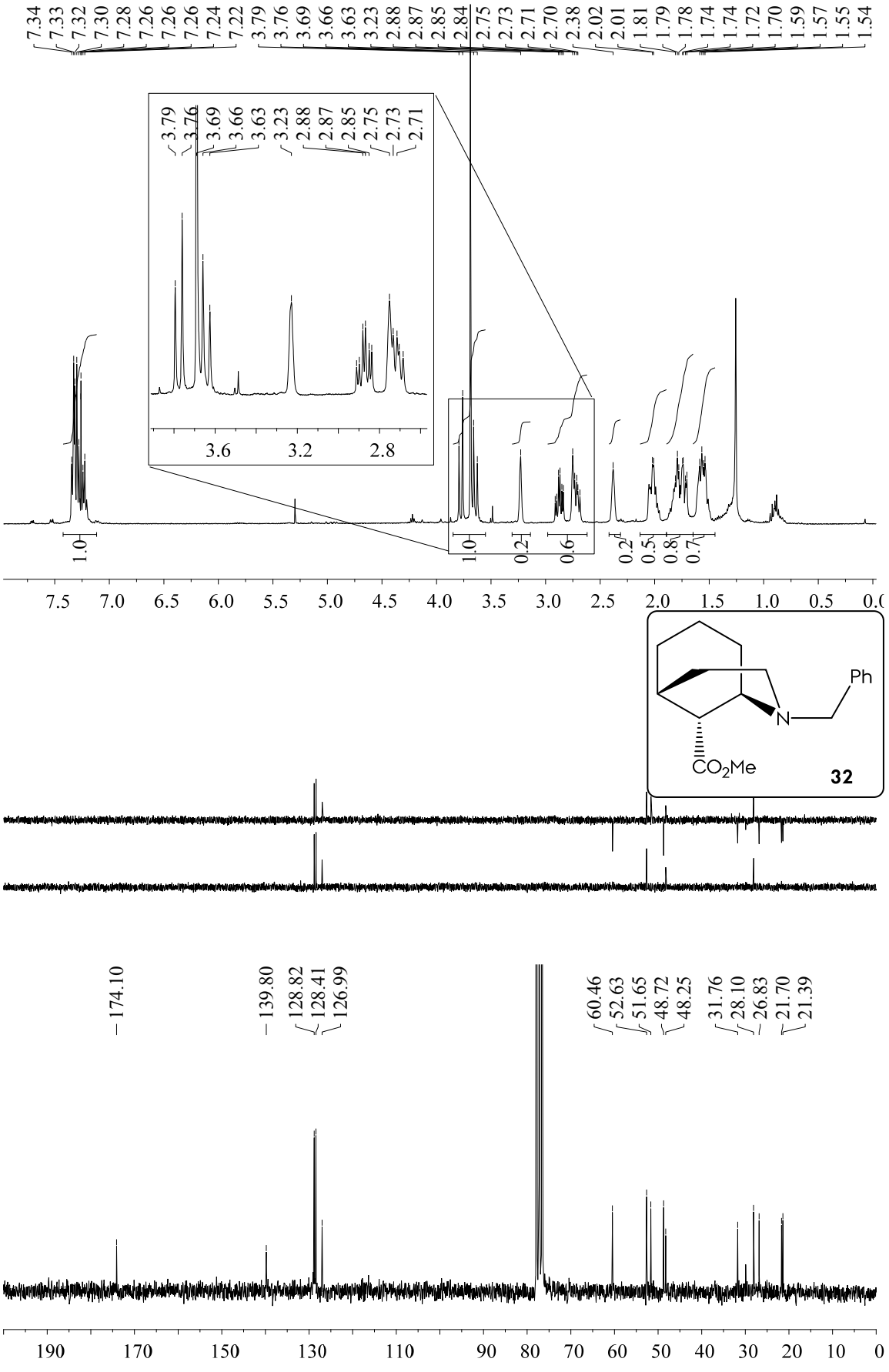
7.34
7.33
7.32
7.30
7.28
7.26
7.26
7.26
7.24
7.22
3.79
3.76
3.69
3.66
3.63
3.23
2.88
2.87
2.85
2.84
2.75
2.73
2.71
2.70
2.38
2.02
2.01
1.81
1.79
1.78
1.74
1.74
1.72
1.70
1.59
1.57
1.55
1.54
3.6
3.2
2.8
1.0
1.0
0.2
0.6
0.2
0.5
0.8
0.7
7.5 7.0 6.5 6.0 5.5 5.0 4.5 4.0 3.5 3.0 2.5 2.0 1.5 1.0 0.5
Ph
N
CO2Me
32
174.10
139.80
128.82
128.41
126.99
60.46
52.63
51.65
48.72
48.25
31.76
28.10
26.83
21.70
21.39
190 170 150 130 110 90 80 70 60 50 40 30 20 10 0

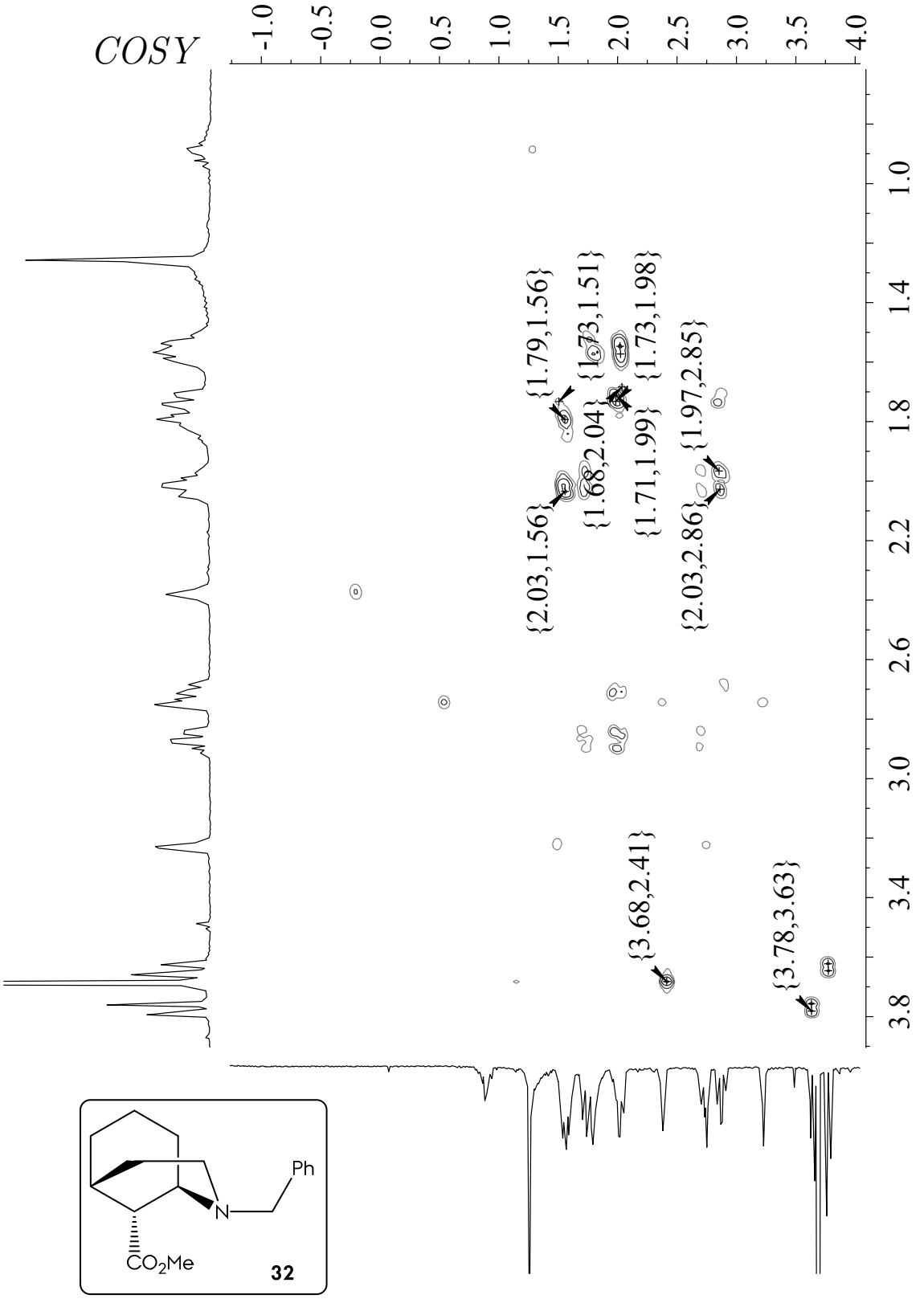
COSY
-1.0
-0.5
0.0
0.5
1.0
1.5
2.0
2.5
3.0
3.5
4.0
3.8
3.4
3.0
2.6
2.2
1.8
1.4
1.0
{1.79,1.56}
{1.73,1.51}
{1.68,2.04}
{1.71,1.99}
{1.73,1.98}
{1.97,2.85}
{2.03,1.56}
{2.03,2.86}
{3.68,2.41}
{3.78,3.63}
Ph
N
CO2Me
32

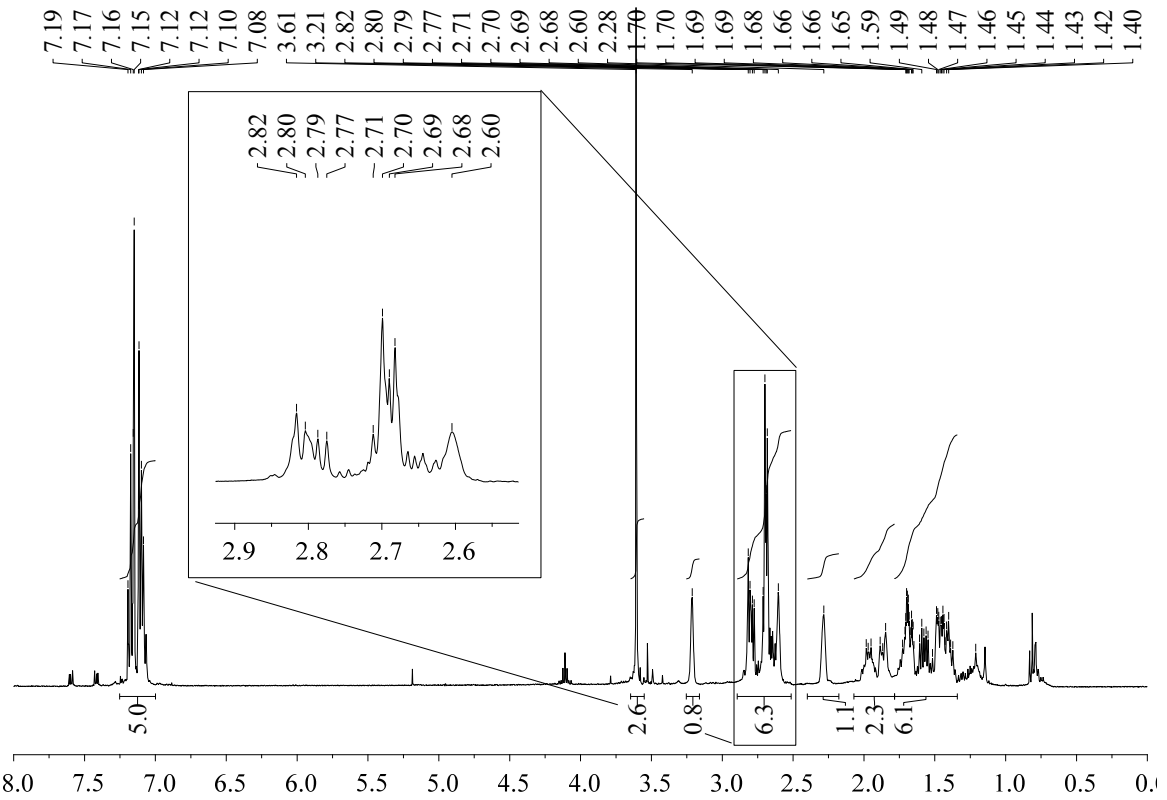
7.19 7.17 7.16 7.15 7.12 7.12 7.10 7.08
3.61 3.21 2.82 2.80 2.79 2.77 2.71 2.70 2.69 2.68 2.60 2.28 1.70 1.70 1.69 1.69 1.68 1.66 1.66 1.65 1.59 1.49 1.48 1.47 1.46 1.45 1.44 1.43 1.42 1.40
2.82 2.80 2.79 2.77 2.71 2.70 2.69 2.68 2.60
2.9 2.8 2.7 2.6
5.0 2.6 0.8 6.3 1.1 2.3 6.1
8.0 7.5 7.0 6.5 6.0 5.5 5.0 4.5 4.0 3.5 3.0 2.5 2.0 1.5 1.0 0.5

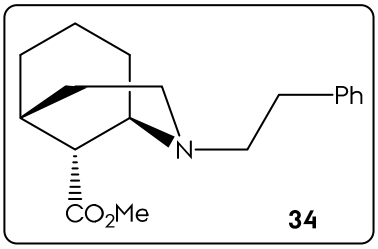
Ph
N
CO2Me
34

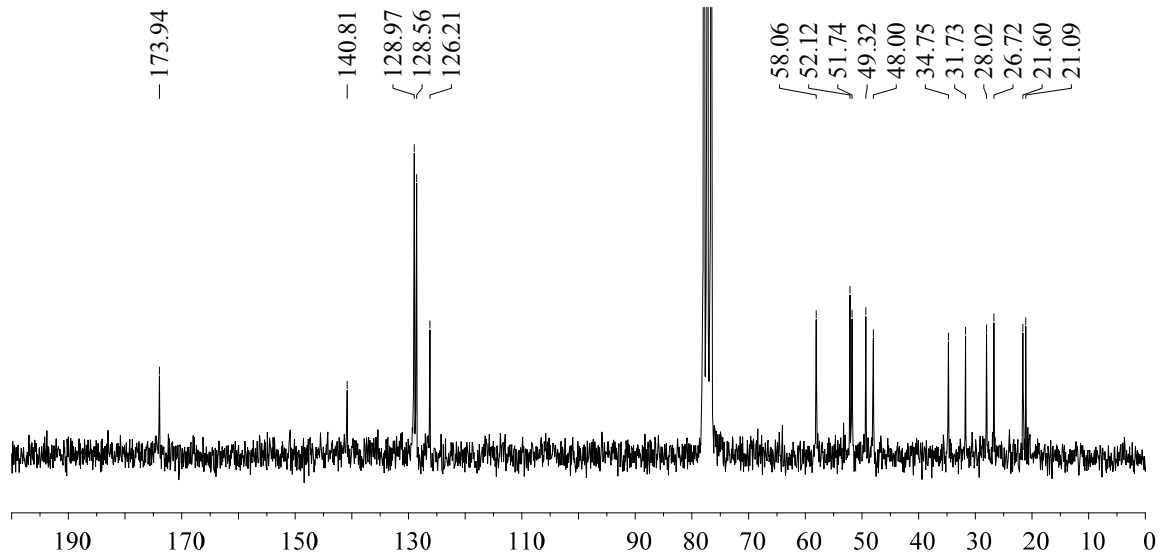
173.94
140.81
128.97
128.56
126.21
58.06
52.12
51.74
49.32
48.00
34.75
31.73
28.02
26.72
21.60
21.09
190 170 150 130 110 90 80 70 60 50 40 30 20 10 0

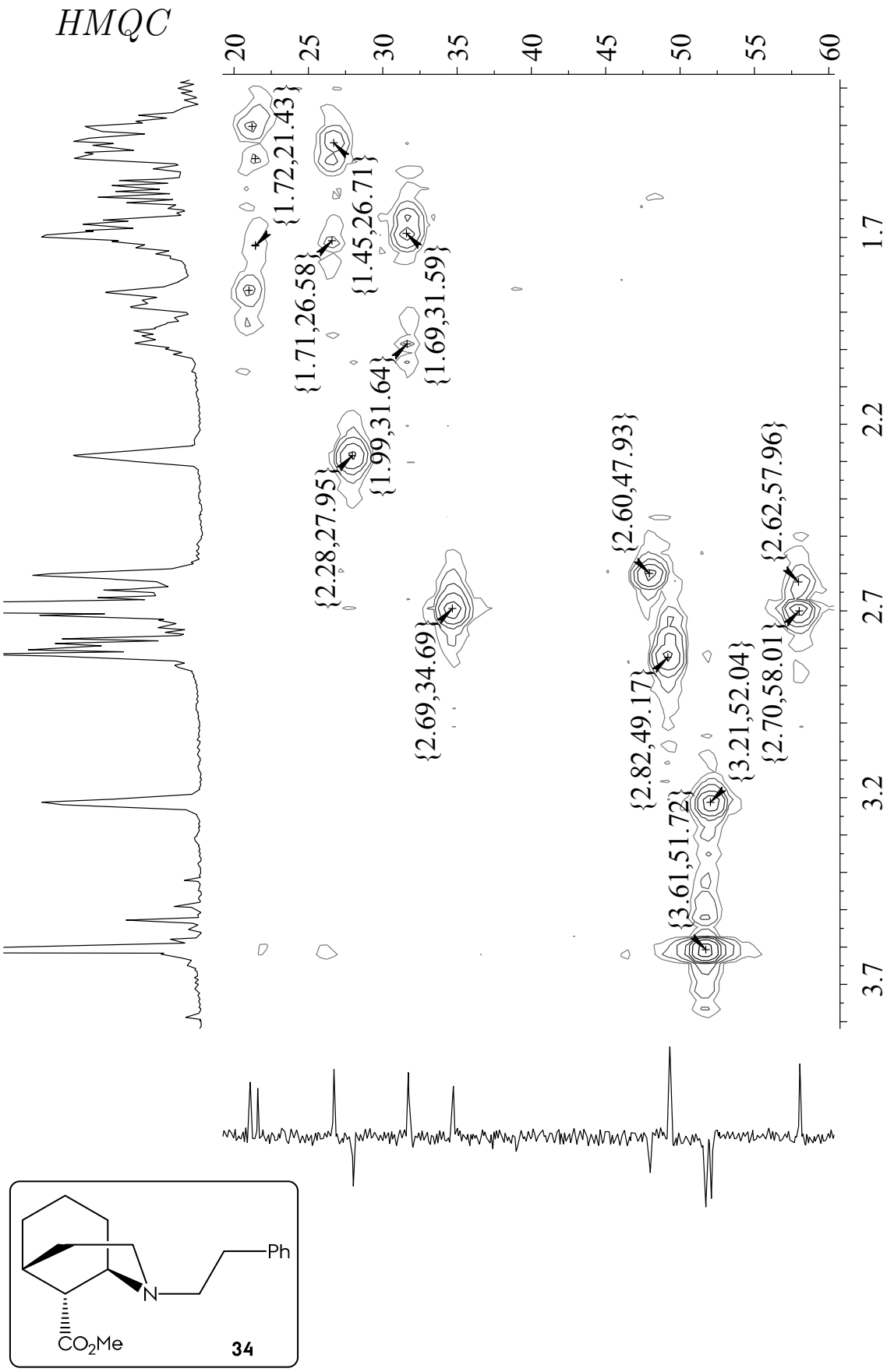
HMQC
20
25
30
35
40
45
50
55
60
1.7
2.2
2.7
3.2
3.7
{1.72,21.43}
{1.71,26.58}
{1.45,26.71}
{1.69,31.59}
{1.99,31.64}
{2.28,27.95}
{2.69,34.69}
{2.60,47.93}
{2.62,57.96}
{2.82,49.17}
{3.21,52.04}
{2.70,58.01}
{3.61,51.72}
Ph
N
CO2Me
34

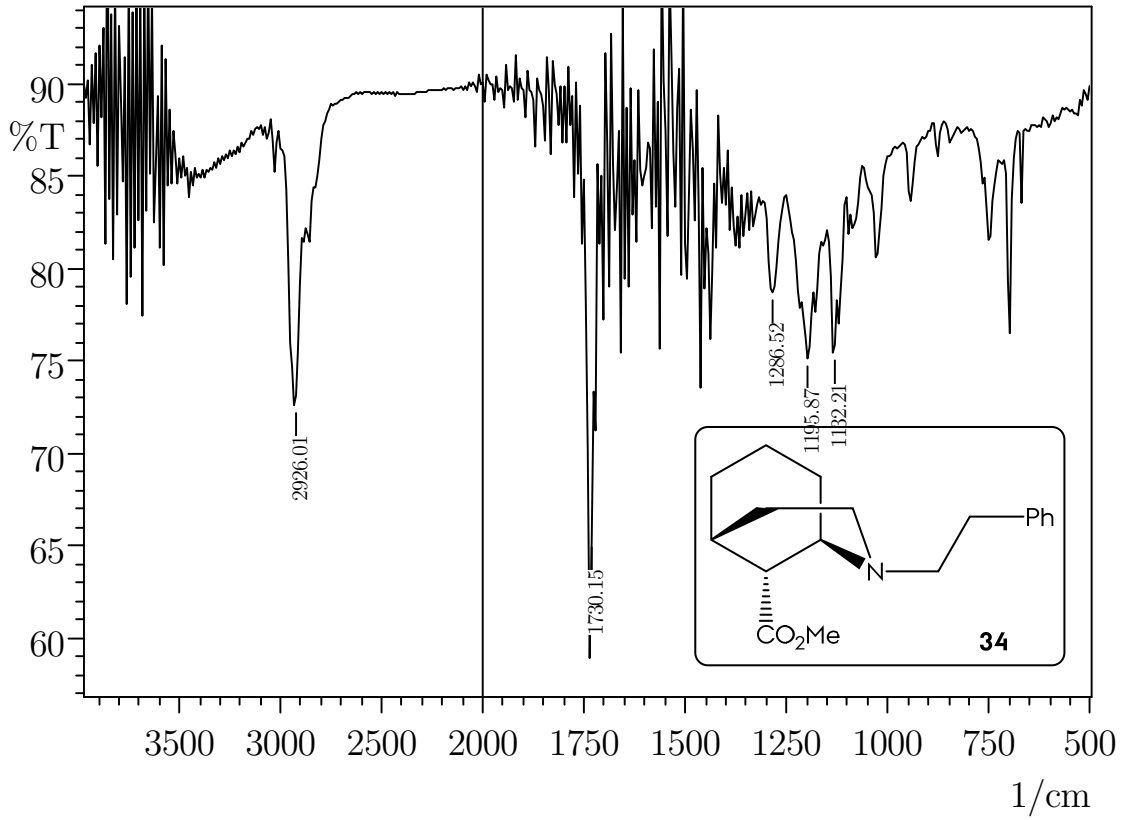
90
%T
85
80
75
70
65
60
2926.01
1730.15
1286.52
1195.87
1132.21
Ph
N
CO2Me
34
3500 3000 2500 2000 1750 1500 1250 1000 750 500
1/cm

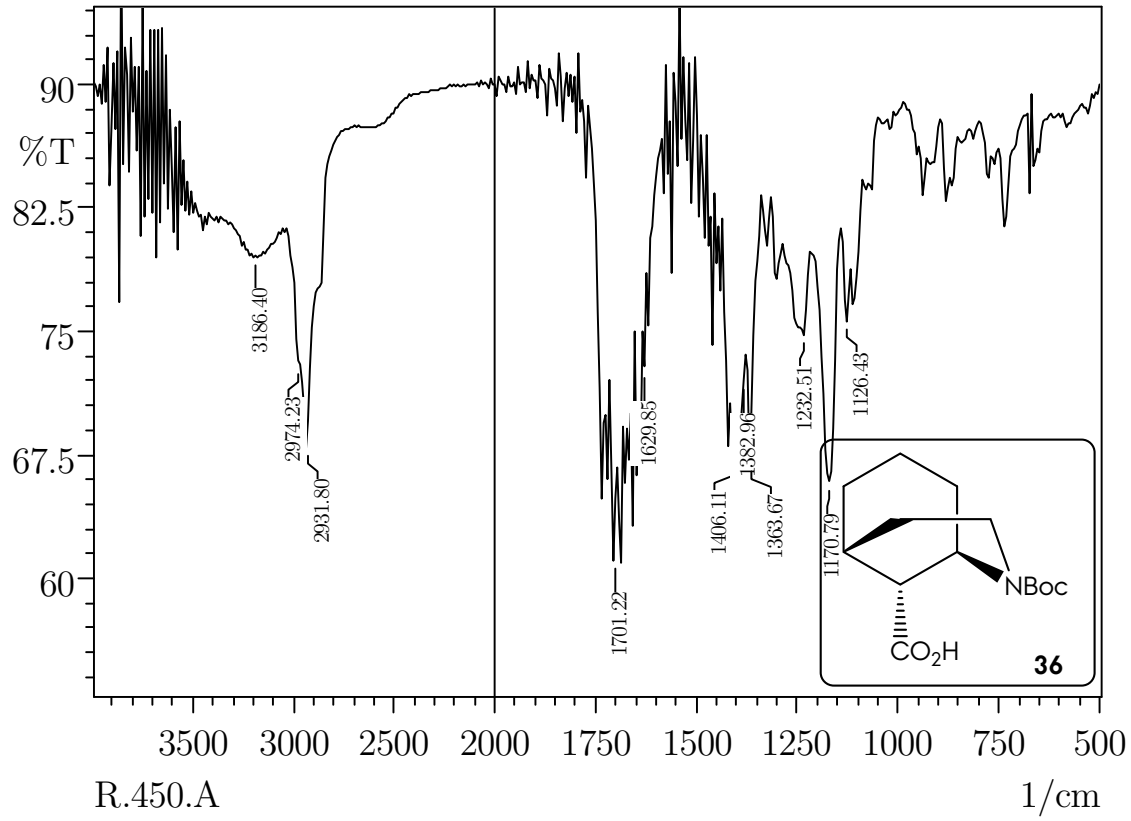
90
%T
82.5
75
67.5
60
3186.40
2974.25
2931.80
1701.22
1629.85
1406.11
1382.96
1363.67
1232.51
1170.79
1126.43
NBoc
CO2H
36
3500 3000 2500 2000 1750 1500 1250 1000 750 500
R.450.A
1/cm

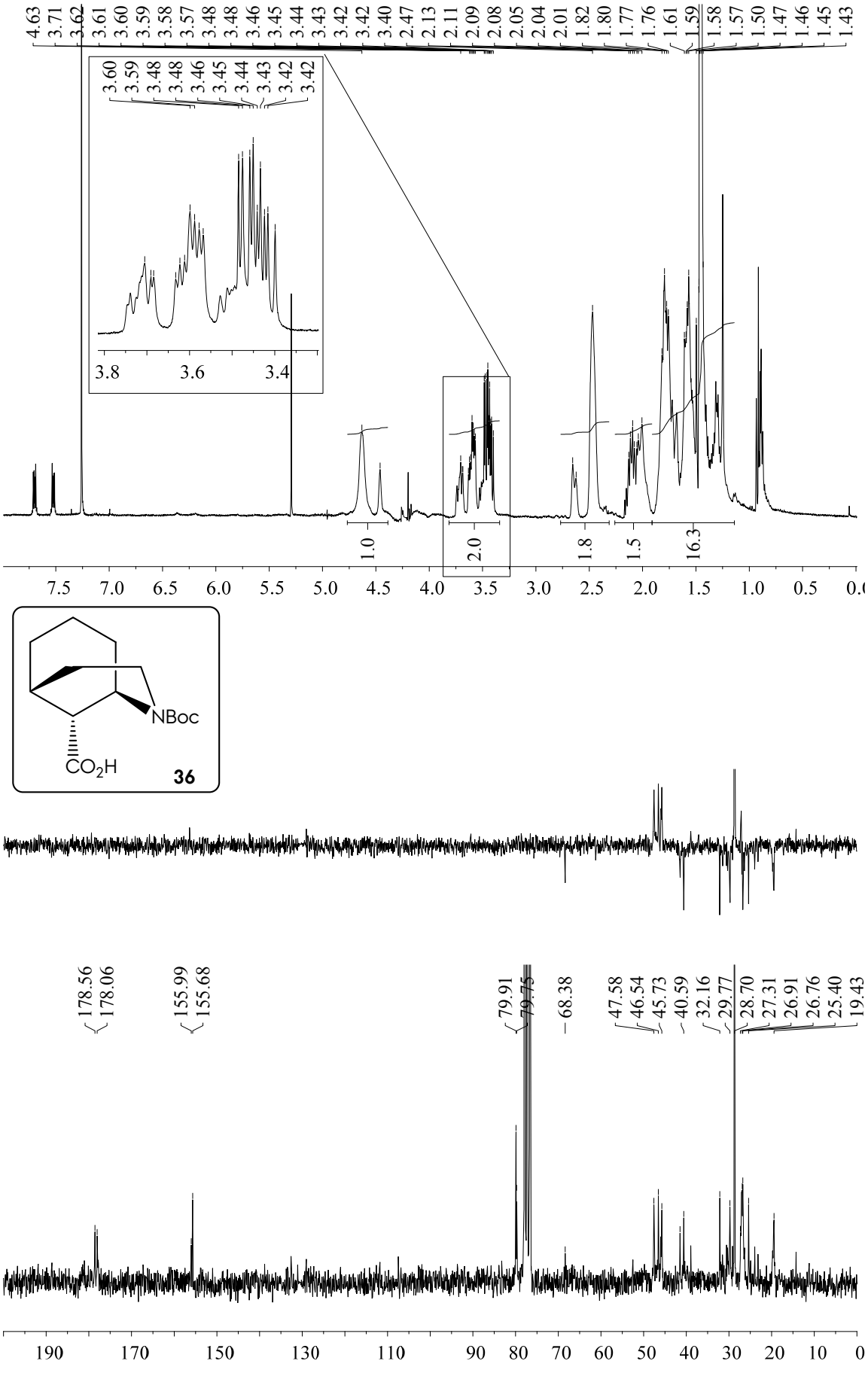
4.63 3.71 3.62 3.61 3.60 3.59 3.58 3.57 3.48 3.48 3.46 3.45 3.44 3.43 3.42 3.42 3.40 2.47 2.13 2.11 2.09 2.08 2.05 2.04 2.01 1.82 1.80 1.77 1.76 1.61 1.59 1.58 1.57 1.50 1.47 1.46 1.45 1.43
3.60 3.59 3.48 3.48 3.46 3.45 3.44 3.43 3.42 3.42
3.8 3.6 3.4
1.0 2.0 1.8 1.5 16.3
7.5 7.0 6.5 6.0 5.5 5.0 4.5 4.0 3.5 3.0 2.5 2.0 1.5 1.0 0.5
NBoc
CO_2H
36
178.56 178.06 155.99 155.68 79.91 79.75 68.38 47.58 46.54 45.73 40.59 32.16 29.77 28.70 27.31 26.91 26.76 25.40 19.43
190 170 150 130 110 90 80 70 60 50 40 30 20 10 0

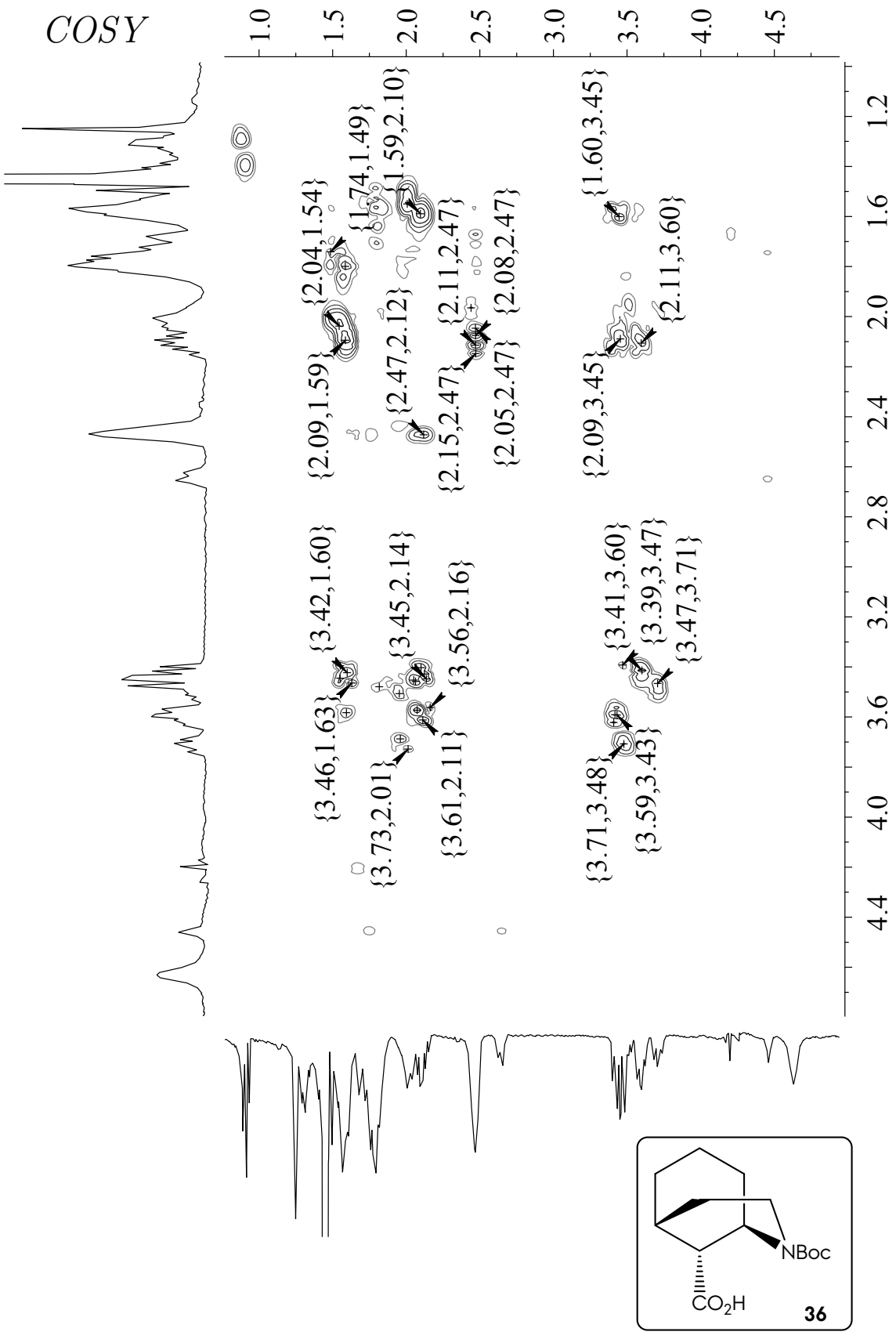
COSY
1.0
1.5
2.0
2.5
3.0
3.5
4.0
4.5
1.2
1.6
2.0
2.4
2.8
3.2
3.6
4.0
4.4
{2.09,1.59}
{2.04,1.54}
{1.74,1.49}
{1.59,2.10}
{2.47,2.12}
{2.11,2.47}
{2.15,2.47}
{2.05,2.47}
{2.08,2.47}
{1.60,3.45}
{2.09,3.45}
{2.11,3.60}
{3.46,1.63}
{3.42,1.60}
{3.45,2.14}
{3.73,2.01}
{3.61,2.11}
{3.56,2.16}
{3.71,3.48}
{3.41,3.60}
{3.39,3.47}
{3.59,3.43}
{3.47,3.71}
NBoc
CO_2H
36

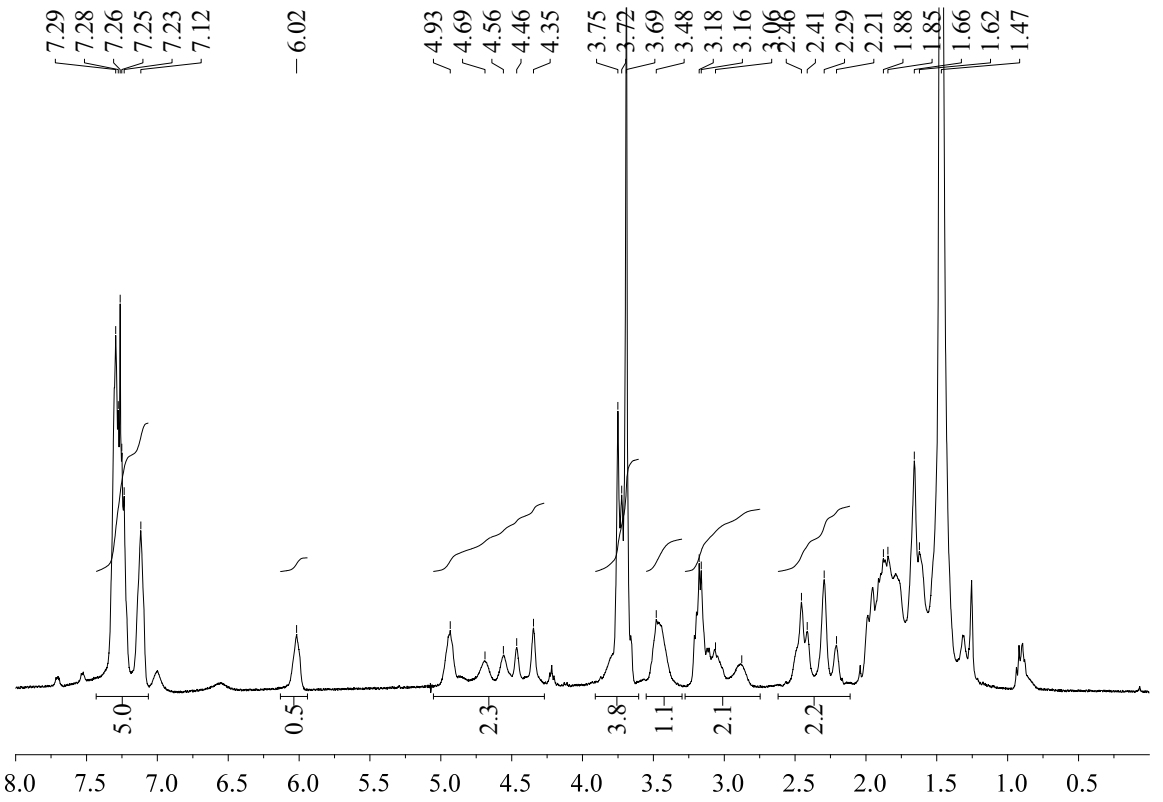
7.29
7.28
7.26
7.25
7.23
7.12
6.02
4.93
4.69
4.56
4.46
4.35
3.75
3.72
3.69
3.48
3.18
3.16
3.06
2.48
2.41
2.29
2.21
1.88
1.85
1.66
1.62
1.47
5.0
0.5
2.3
3.8
1.1
2.1
2.2
8.0
7.5
7.0
6.5
6.0
5.5
5.0
4.5
4.0
3.5
3.0
2.5
2.0
1.5
1.0
0.5

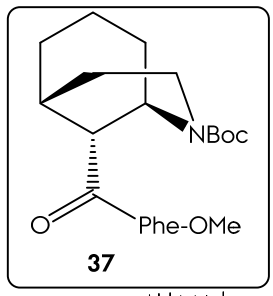
NBoc
O
Phe-OMe
37

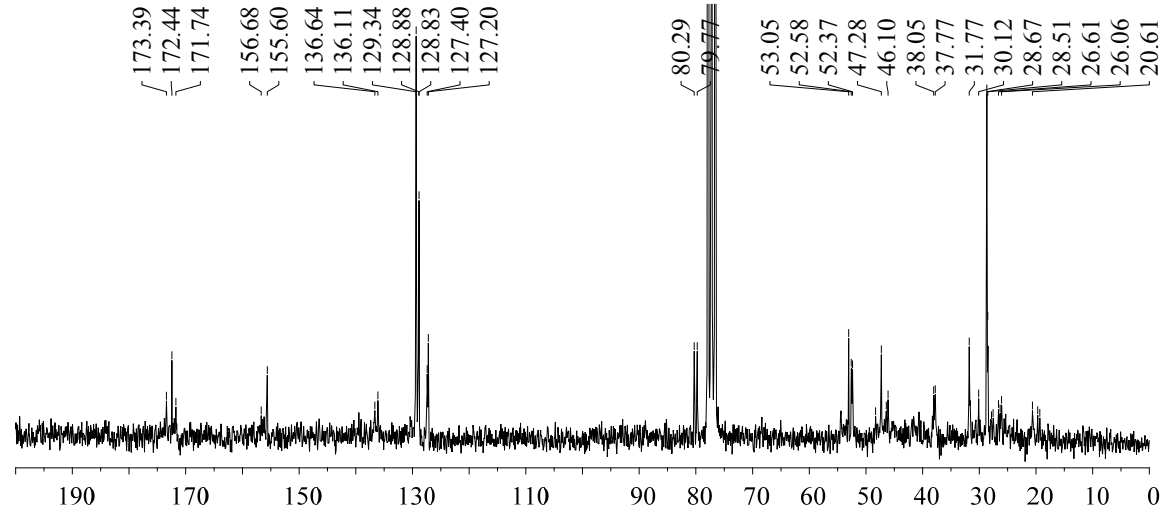
173.39
172.44
171.74
156.68
155.60
136.64
136.11
129.34
128.88
128.83
127.40
127.20
80.29
79.77
53.05
52.58
52.37
47.28
46.10
38.05
37.77
31.77
30.12
28.67
28.51
26.61
26.06
20.61
190
170
150
130
110
90
80
70
60
50
40
30
20
10
0

HMQC

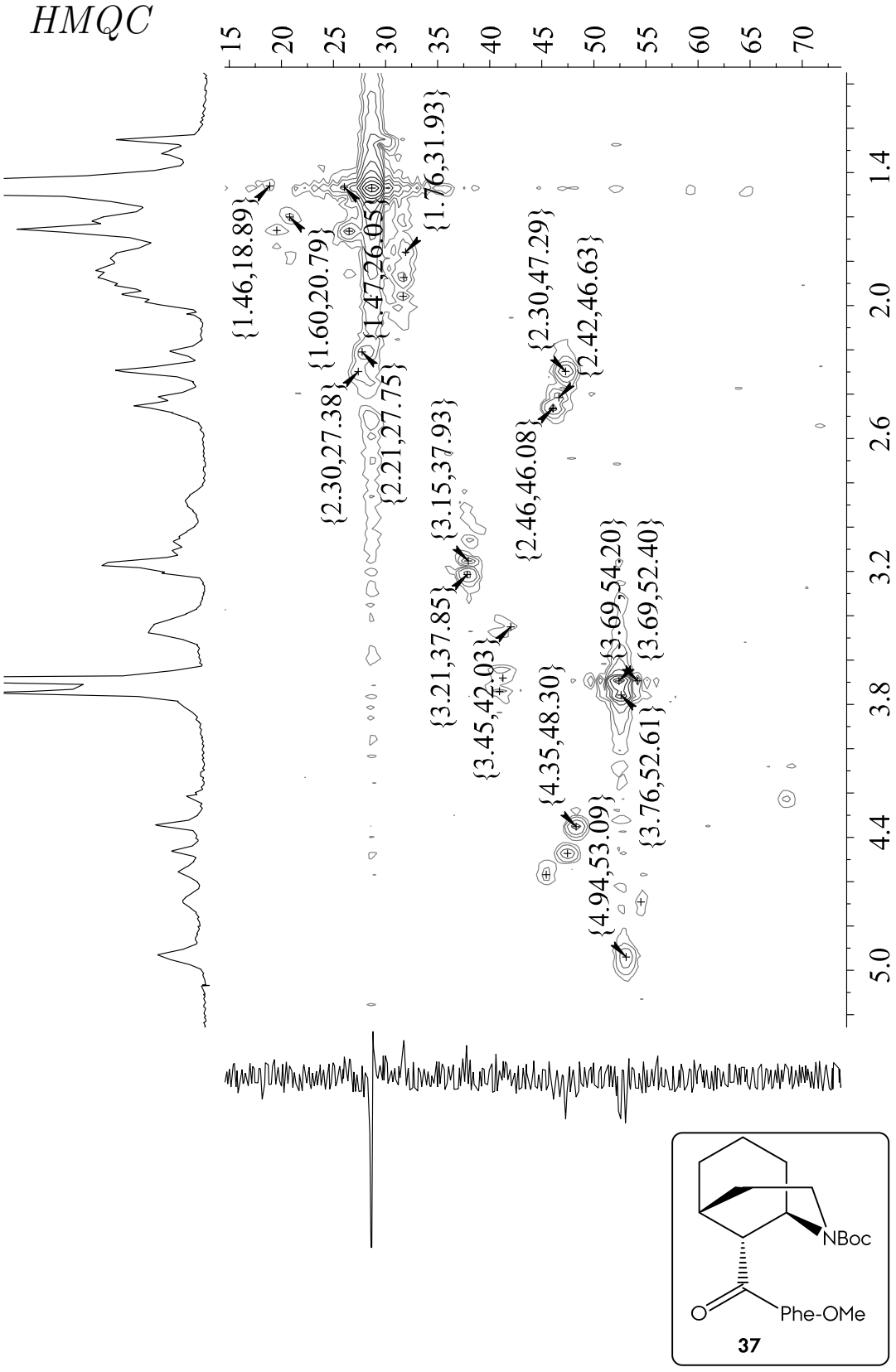
15
20
25
30
35
40
45
50
55
60
65
70
1.4
2.0
2.6
3.2
3.8
4.4
5.0
{1.46,18.89}
{1.60,20.79}
{1.47,26.05}
{1.76,31.93}
{2.30,27.38}
{2.21,27.75}
{3.15,37.93}
{2.30,47.29}
{2.42,46.63}
{2.46,46.08}
{3.21,37.85}
{3.45,42.03}
{3.69,54.20}
{3.69,52.40}
{4.35,48.30}
{3.76,52.61}
{4.94,53.09}
NBoc
O
Phe-OMe
37

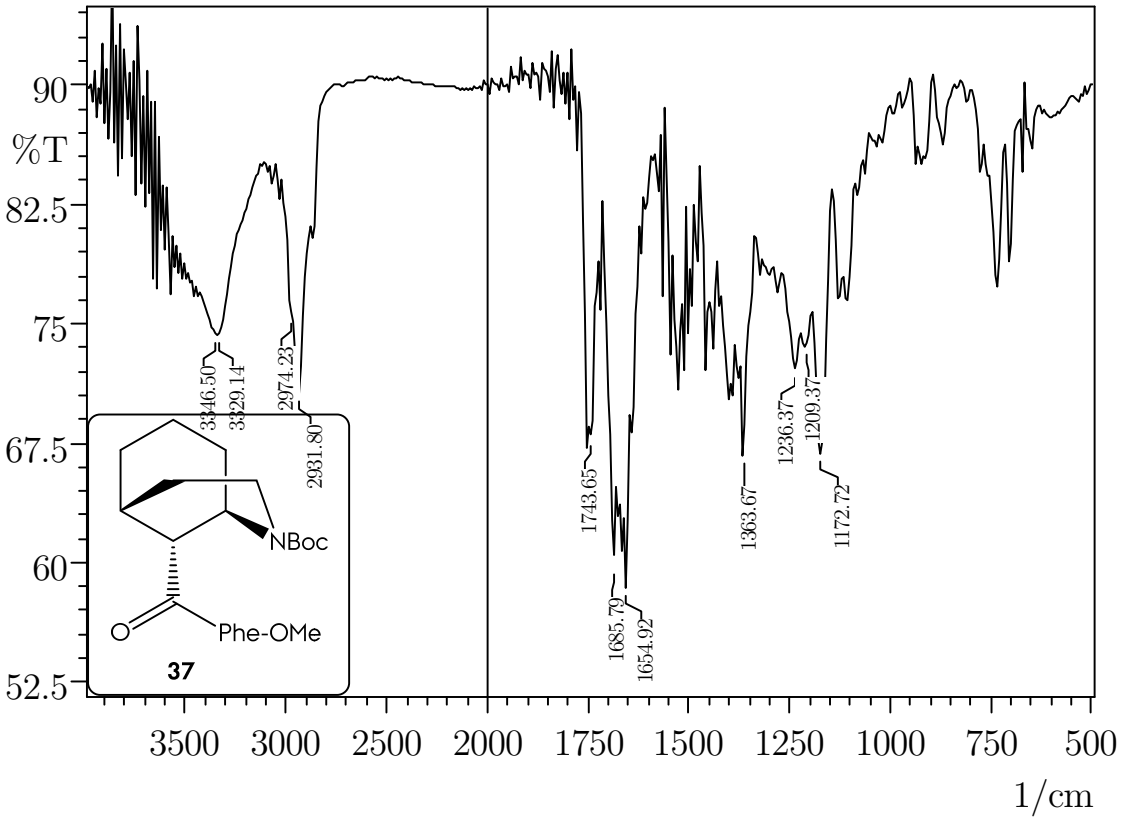
90
%T
82.5
75
67.5
60
52.5
3346.50
3329.14
2974.23
2931.80
1743.65
1685.79
1654.92
1363.67
1236.37
1209.37
1172.72
NBoc
Phe-OMe
37
3500 3000 2500 2000 1750 1500 1250 1000 750 500
1/cm

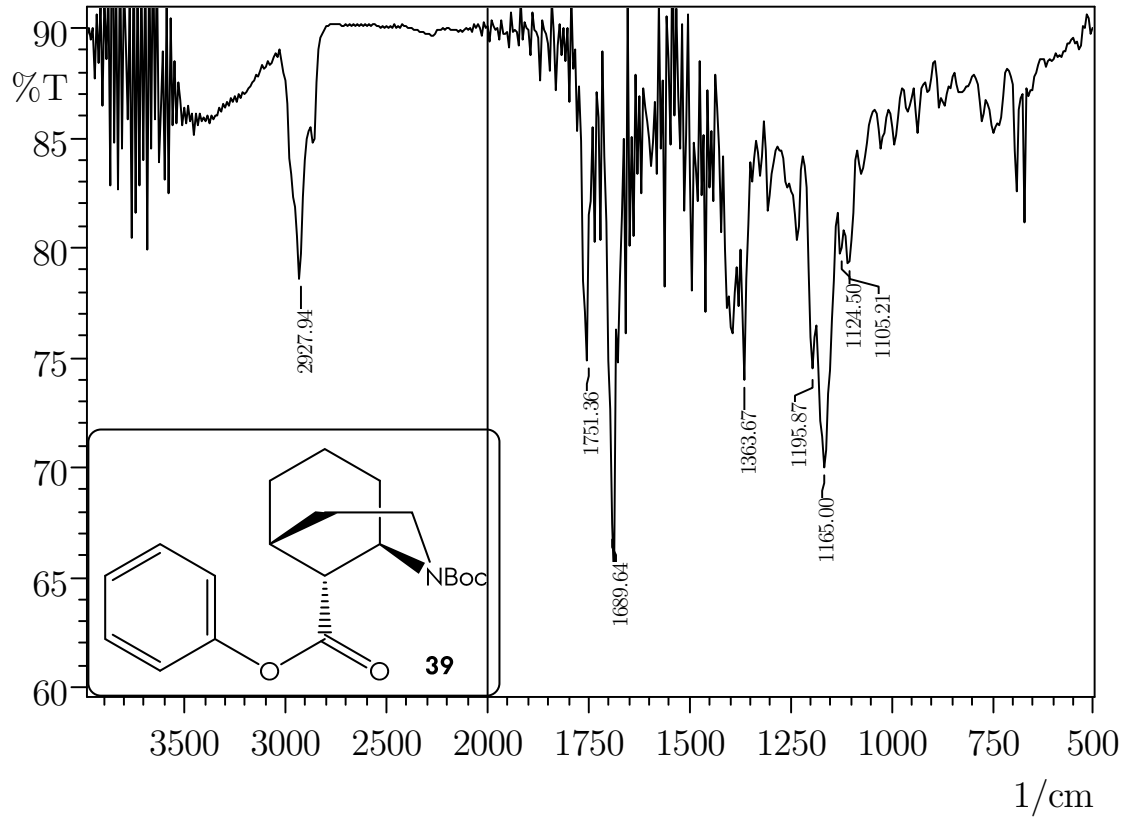
90
%T
85
80
75
70
65
60
2927.94
1751.36
1689.64
1363.67
1195.87
1165.00
1124.50
1105.21
NBoc
39
3500 3000 2500 2000 1750 1500 1250 1000 750 500
1/cm

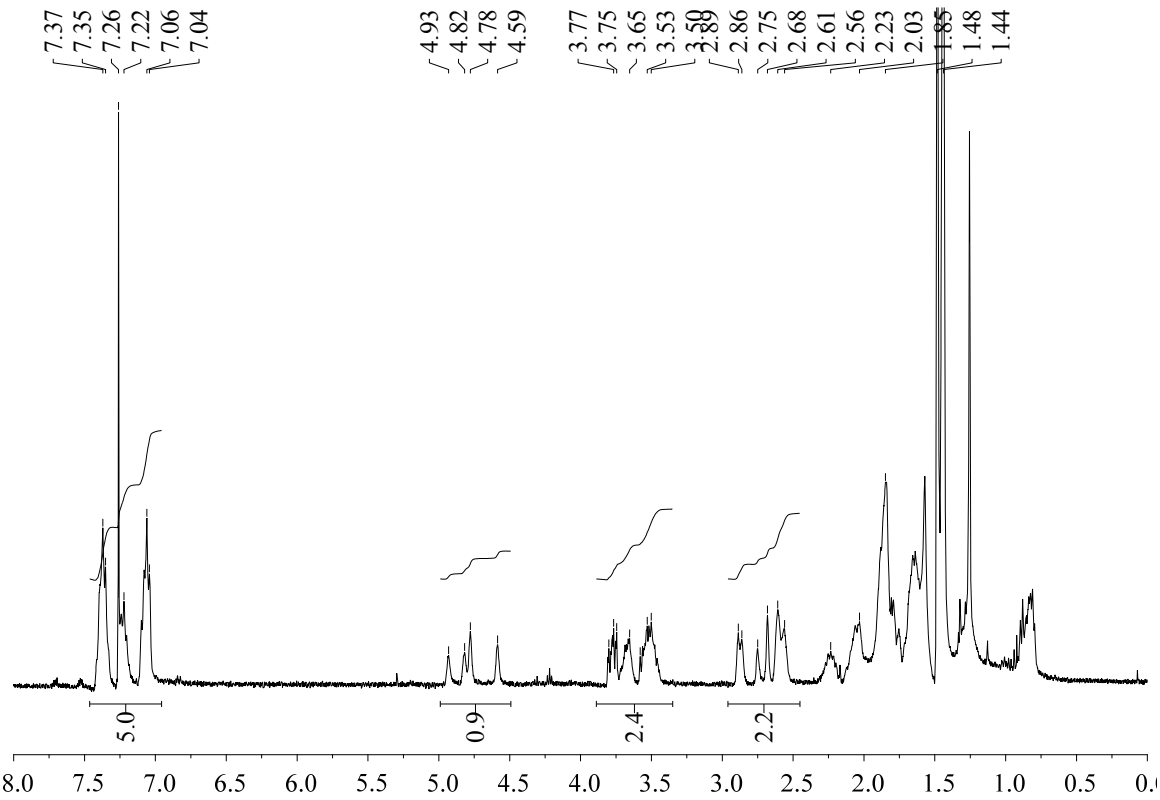
7.37
7.35
7.26
7.22
7.06
7.04
4.93
4.82
4.78
4.59
3.77
3.75
3.65
3.53
3.50
2.89
2.86
2.75
2.68
2.61
2.56
2.23
2.03
1.85
1.48
1.44
5.0
0.9
2.4
2.2
8.0
7.5
7.0
6.5
6.0
5.5
5.0
4.5
4.0
3.5
3.0
2.5
2.0
1.5
1.0
0.5

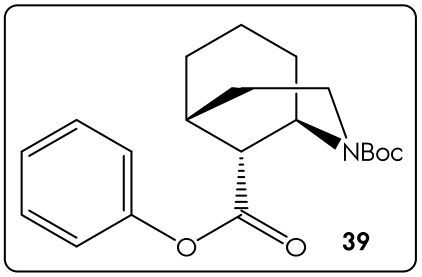
NBoc
39

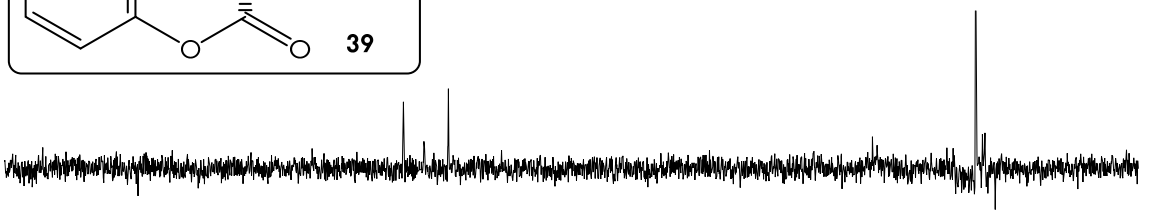

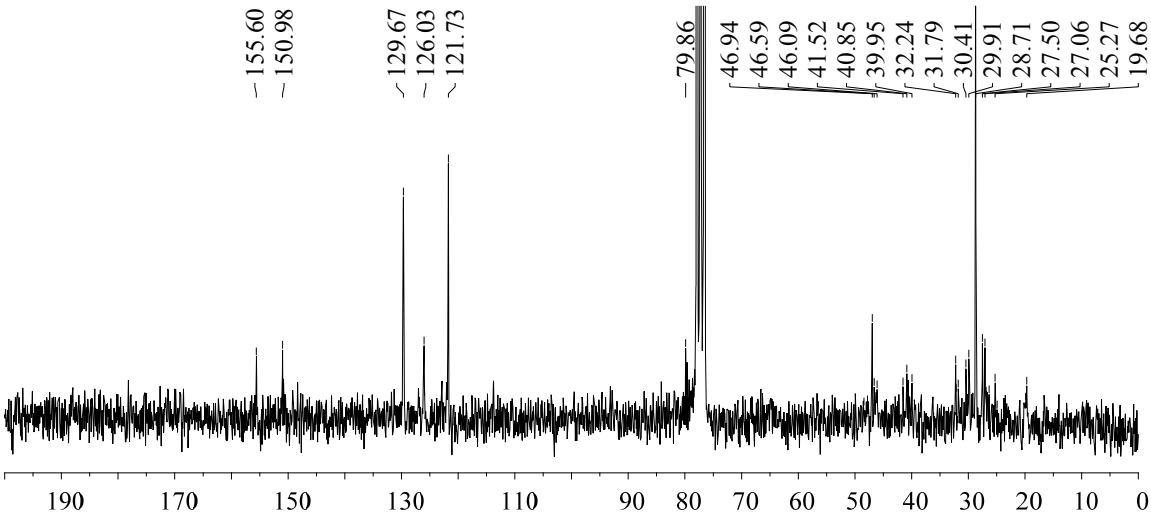
155.60
150.98
129.67
126.03
121.73
79.86
46.94
46.59
46.09
41.52
40.85
39.95
32.24
31.79
30.41
29.91
28.71
27.50
27.06
25.27
19.68
190
170
150
130
110
90
80
70
60
50
40
30
20
10
0

HMQC

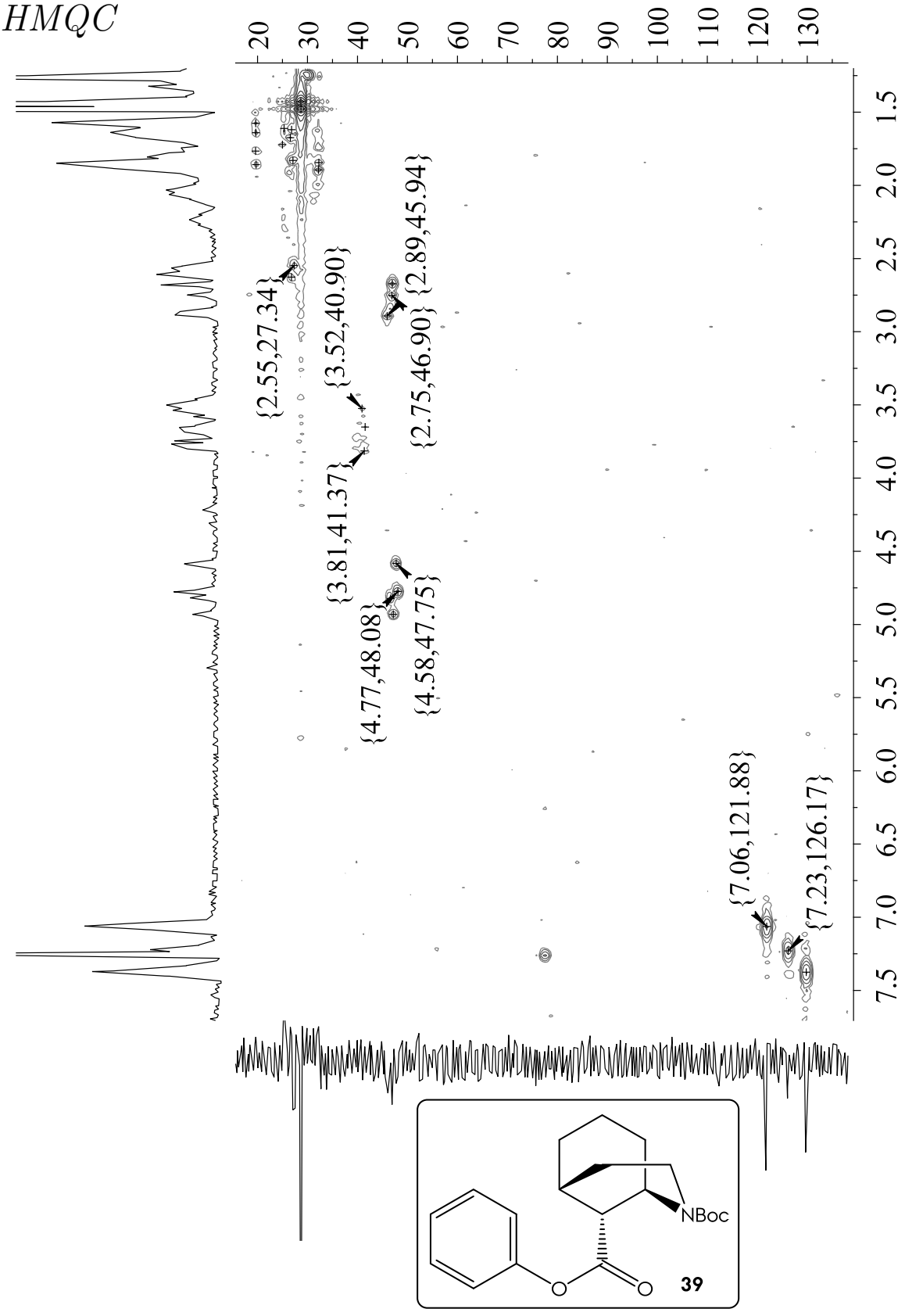
{2.55,27.34}
{3.52,40.90}
{2.89,45.94}
{2.75,46.90}
{3.81,41.37}
{4.77,48.08}
{4.58,47.75}
{7.06,121.88}
{7.23,126.17}
NBoc
39

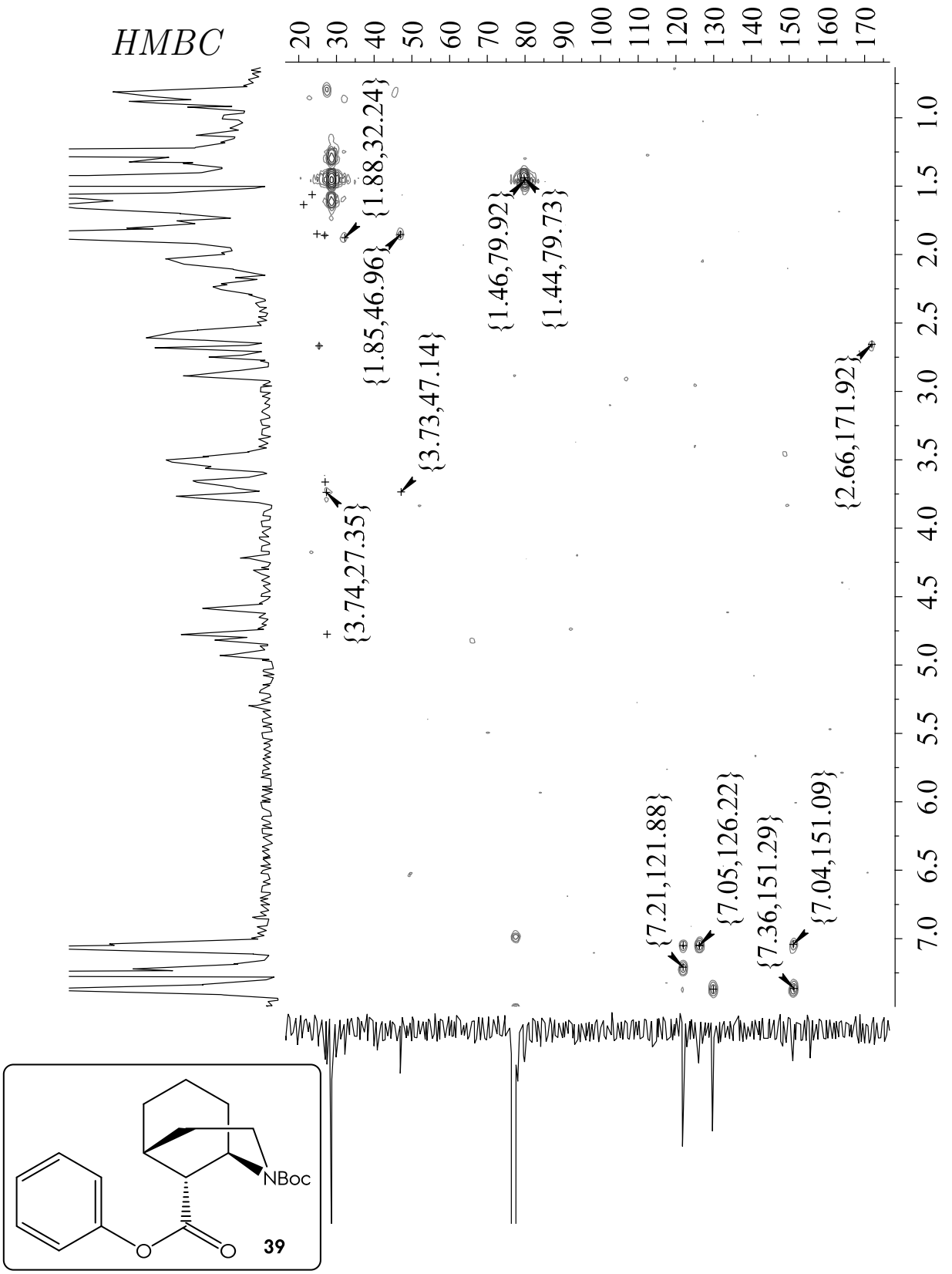
HMBC
{3.74,27.35}
{1.85,46.96}
{1.88,32.24}
{3.73,47.14}
{1.46,79.92}
{1.44,79.73}
{2.66,171.92}
{7.21,121.88}
{7.05,126.22}
{7.36,151.29}
{7.04,151.09}
NBoc
39

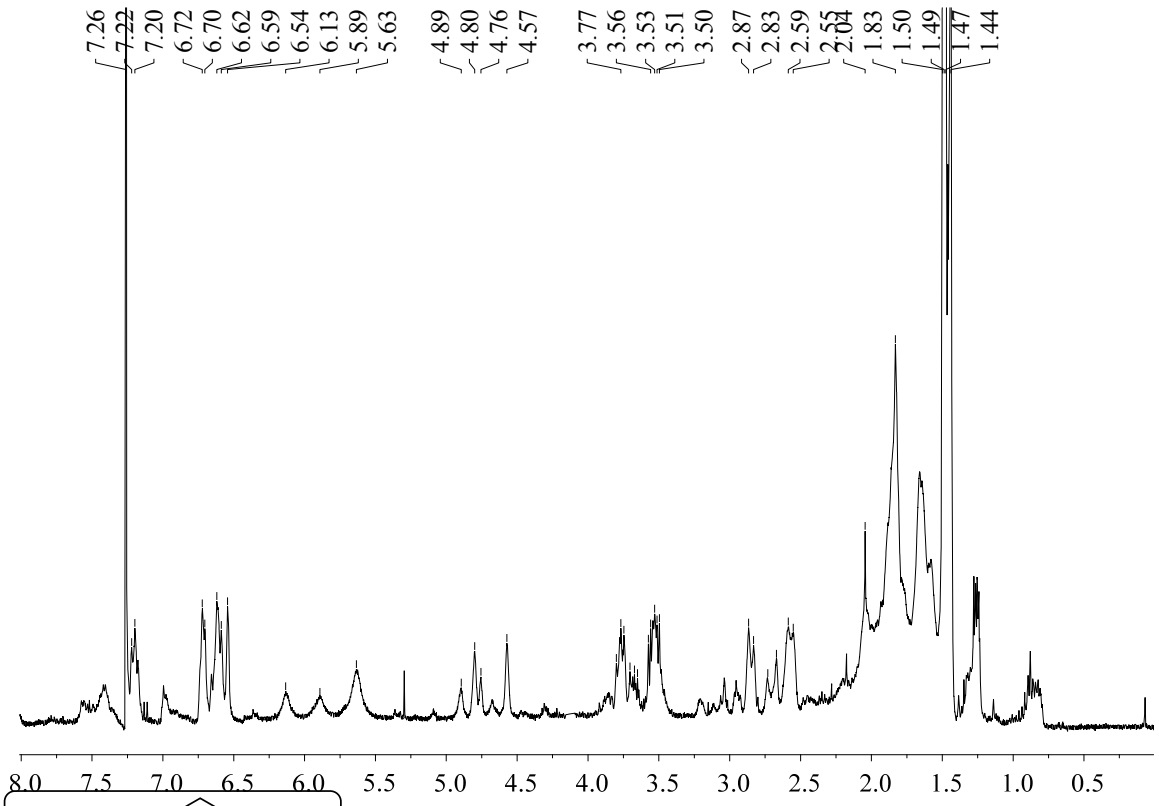
7.26
7.22
7.20
6.72
6.70
6.62
6.59
6.54
6.13
5.89
5.63
4.89
4.80
4.76
4.57
3.77
3.56
3.53
3.51
3.50
2.87
2.83
2.59
2.55
2.04
1.83
1.50
1.49
1.47
1.44
8.0
7.5
7.0
6.5
6.0
5.5
5.0
4.5
4.0
3.5
3.0
2.5
2.0
1.5
1.0
0.5

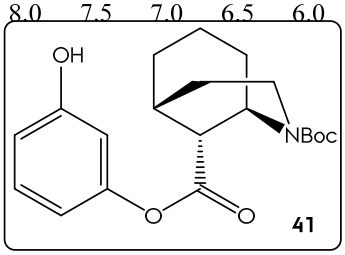
OH
NBoc
O
O
41

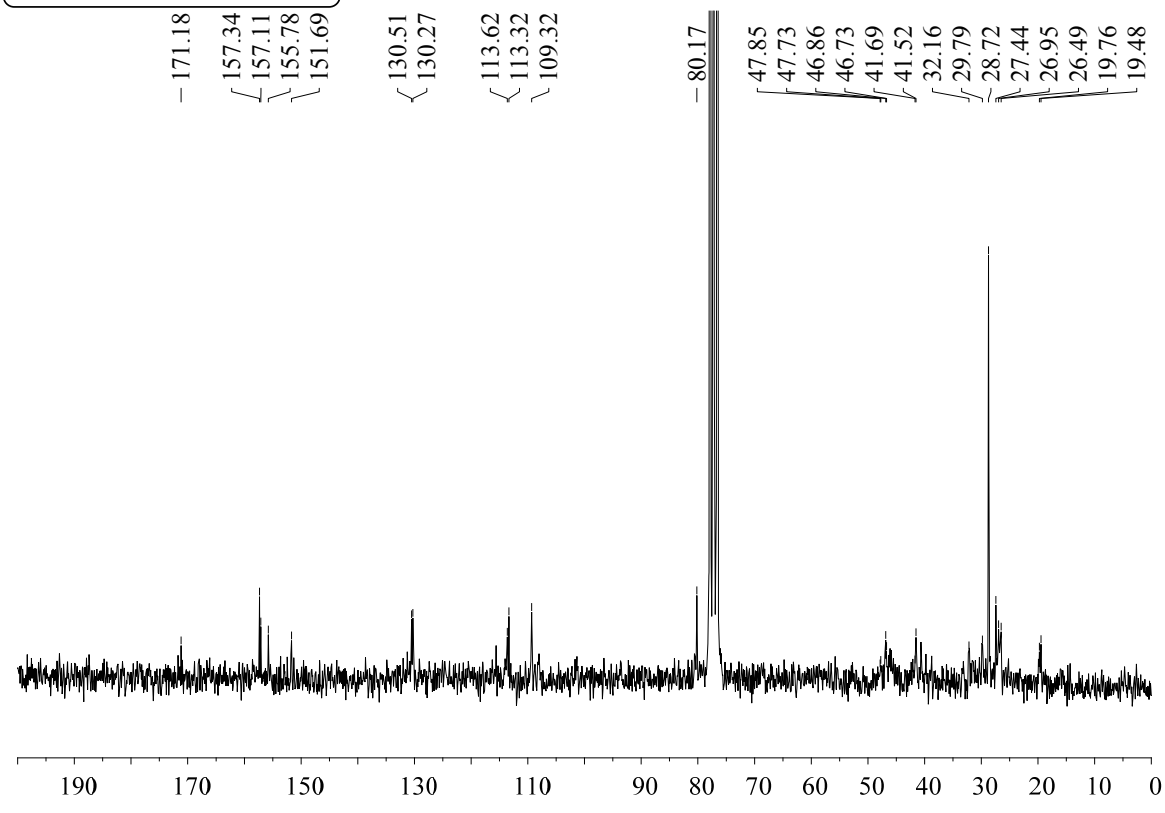
171.18
157.34
157.11
155.78
151.69
130.51
130.27
113.62
113.32
109.32
80.17
47.85
47.73
46.86
46.73
41.69
41.52
32.16
29.79
28.72
27.44
26.95
26.49
19.76
19.48
190
170
150
130
110
90
80
70
60
50
40
30
20
10
0

HMQC

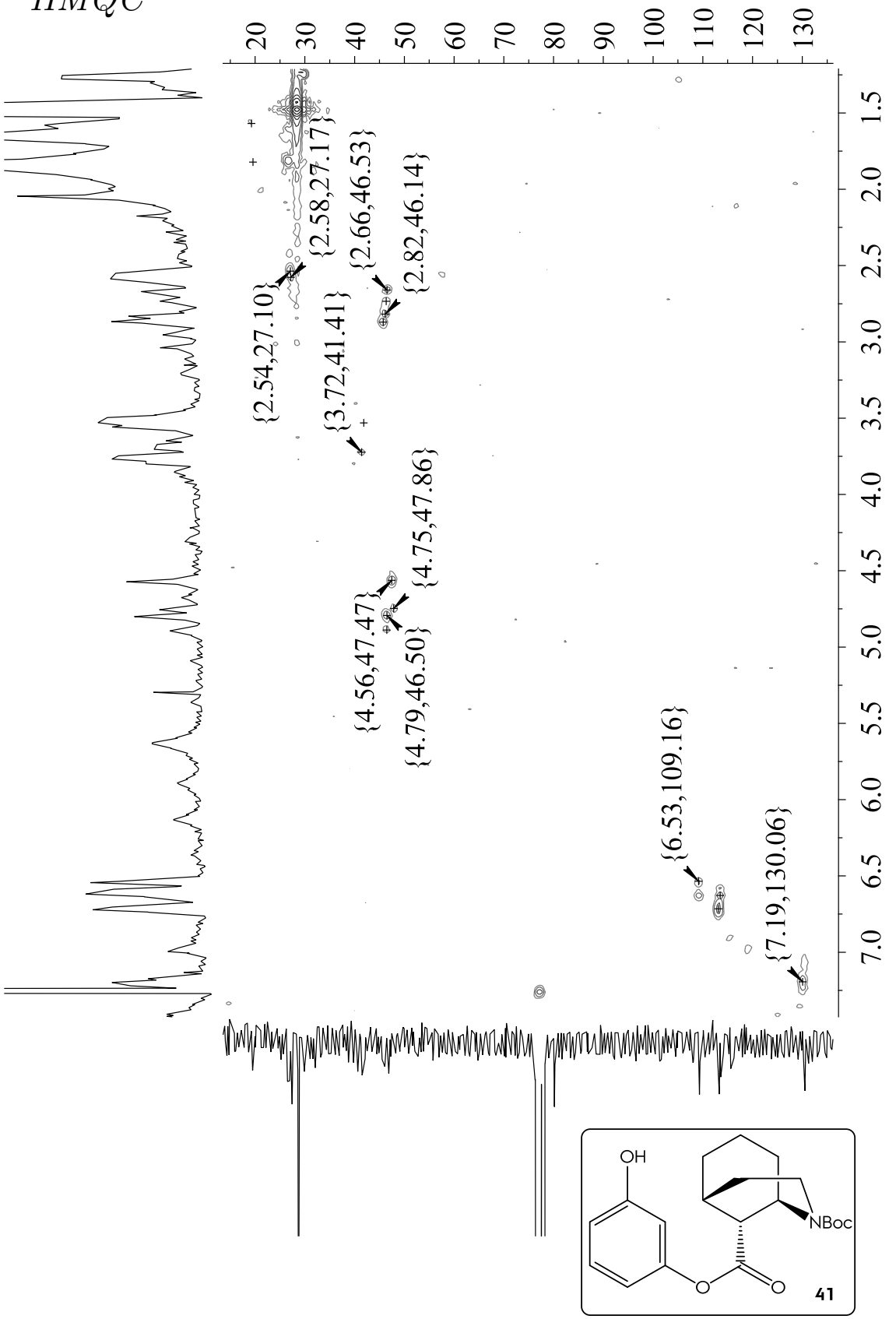
{2.54,27.10}
{2.58,27.17}
{2.66,46.53}
{2.82,46.14}
{3.72,41.41}
{4.56,47.47}
{4.75,47.86}
{4.79,46.50}
{6.53,109.16}
{7.19,130.06}
OH
NBoc
41

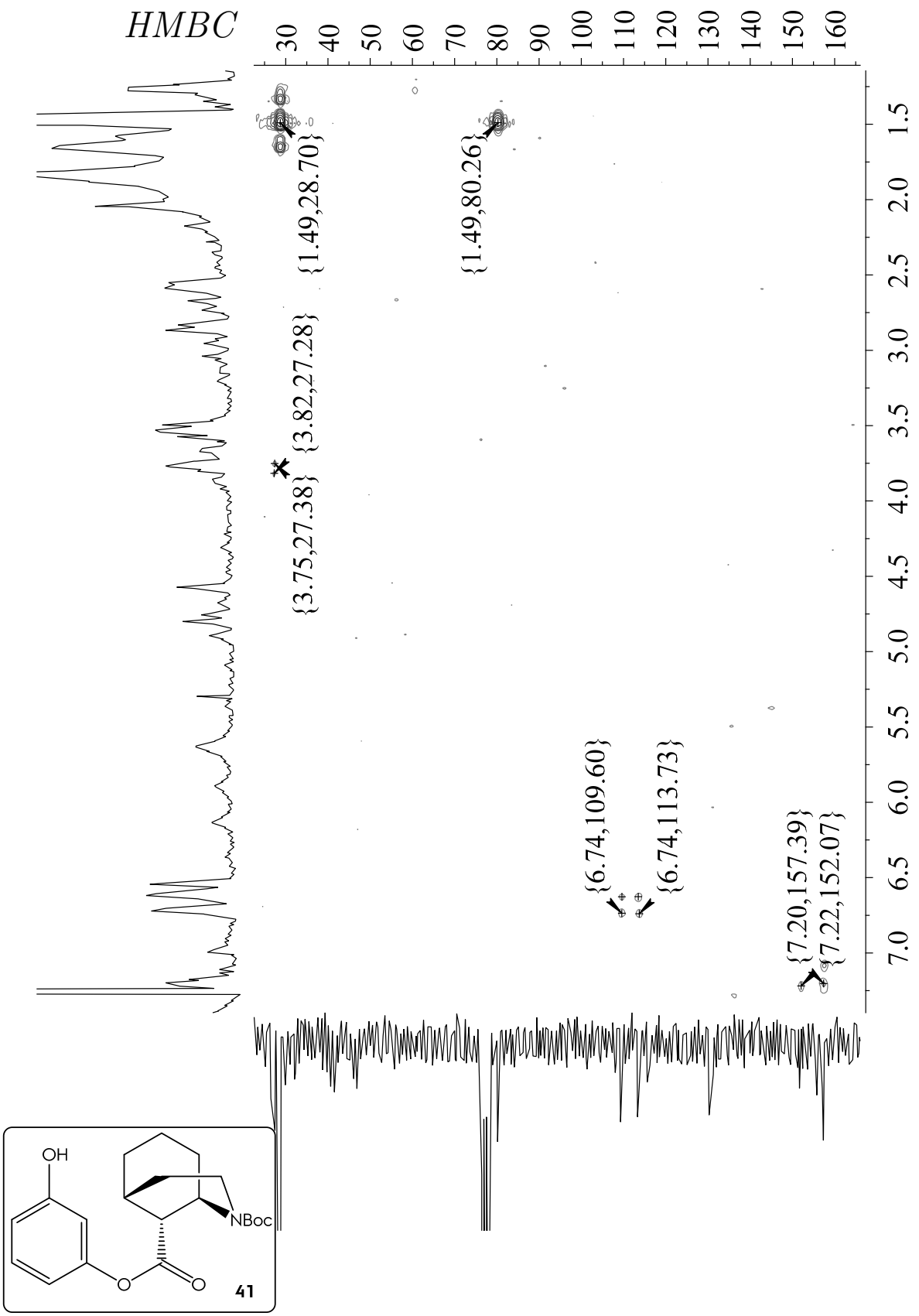
HMBC
{1.49,28.70}
{1.49,80.26}
{3.75,27.38}
{3.82,27.28}
{6.74,109.60}
{6.74,113.73}
{7.20,157.39}
{7.22,152.07}
OH
NBoc
O
O
41

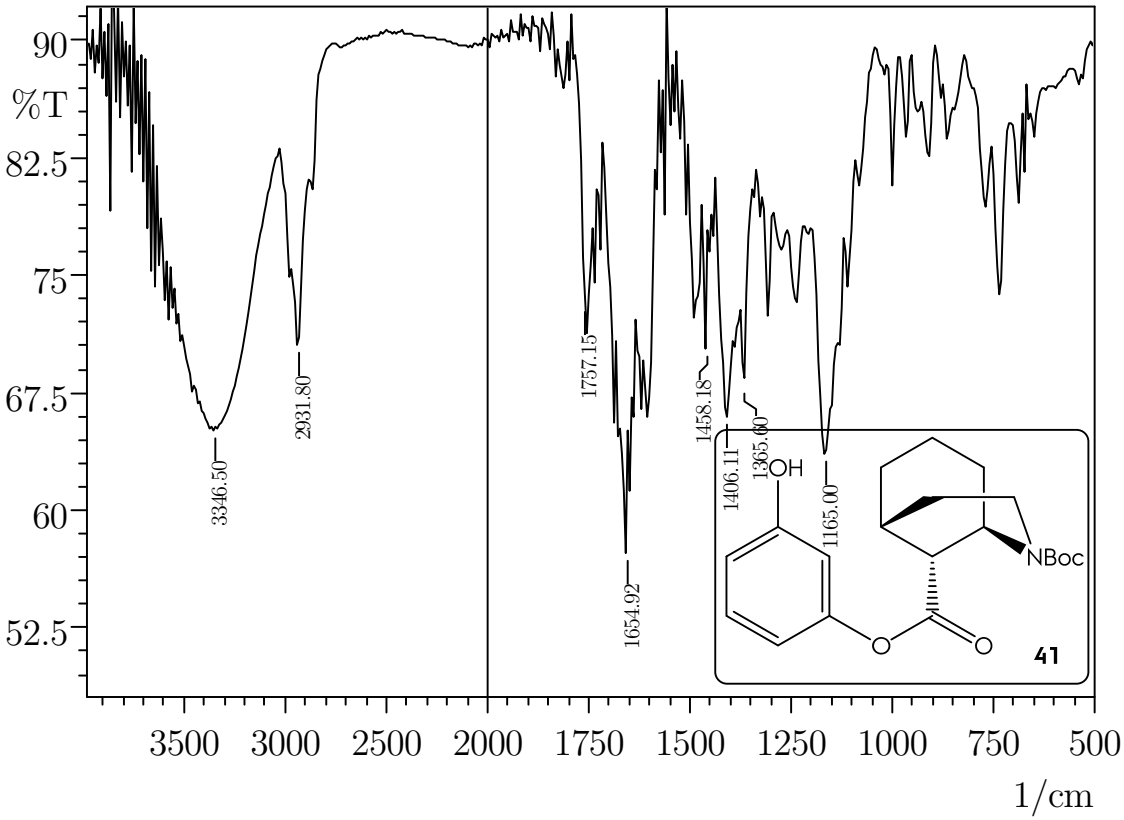
90
%T
82.5
75
67.5
60
52.5
3346.50
2931.80
1757.15
1654.92
1458.18
1406.11
1365.60
1165.00
OH
NBoc
O
O
41
3500 3000 2500 2000 1750 1500 1250 1000 750 500
1/cm

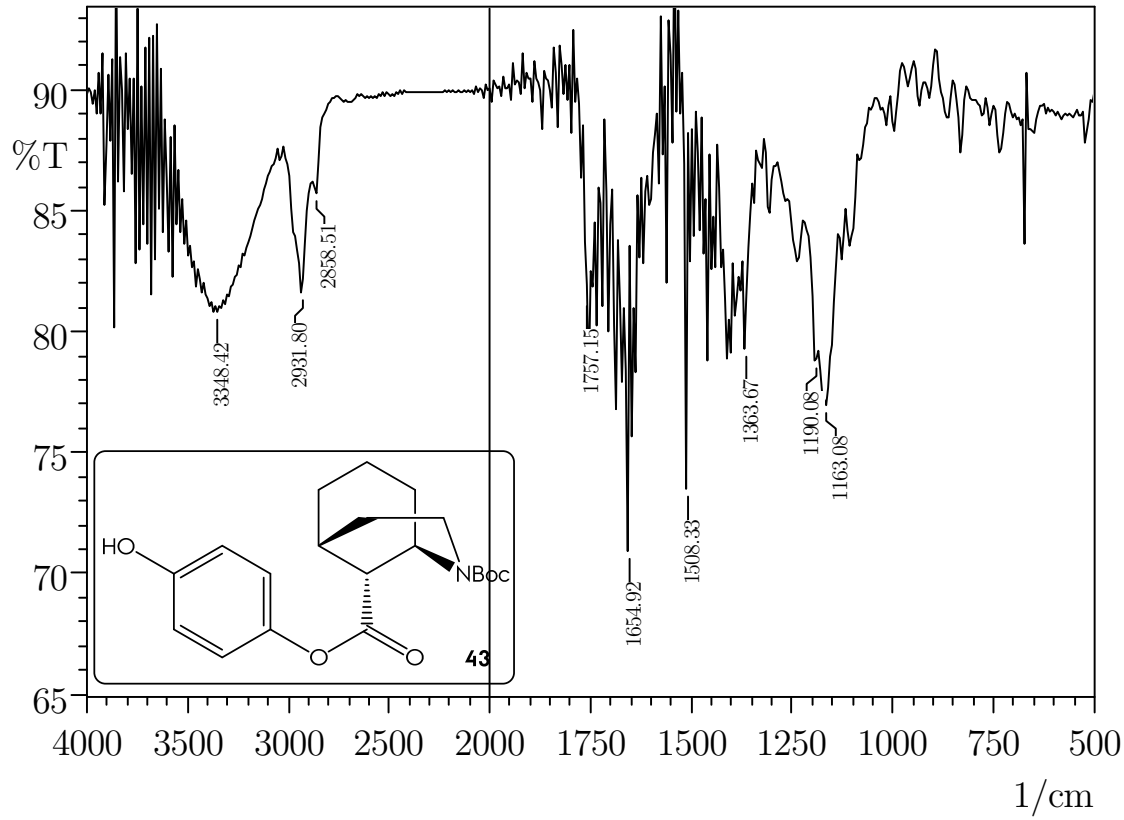
90
%T
85
80
75
70
65
3348.42
2931.80
2858.51
1757.15
1654.92
1508.33
1363.67
1190.08
1163.08
HO
NBoc
O
O
43
4000 3500 3000 2500 2000 1750 1500 1250 1000 750 500
1/cm

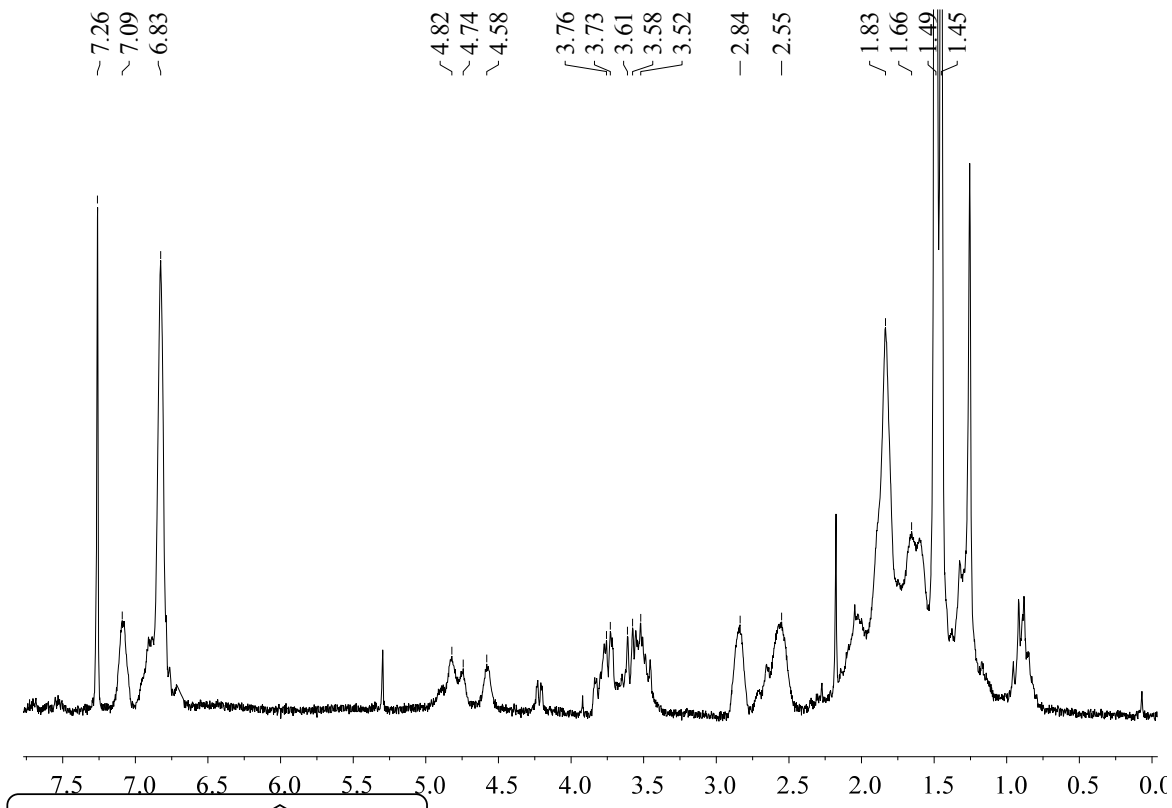
7.26
7.09
6.83
4.82
4.74
4.58
3.76
3.73
3.61
3.58
3.52
2.84
2.55
1.83
1.66
1.49
1.45
7.5 7.0 6.5 6.0 5.5 5.0 4.5 4.0 3.5 3.0 2.5 2.0 1.5 1.0 0.5 0.0

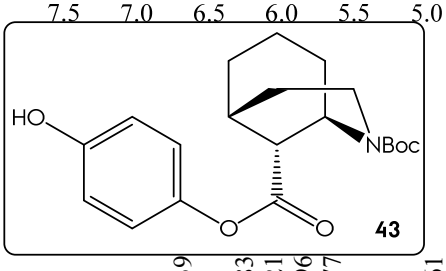
HO
NBoc
O
O
43

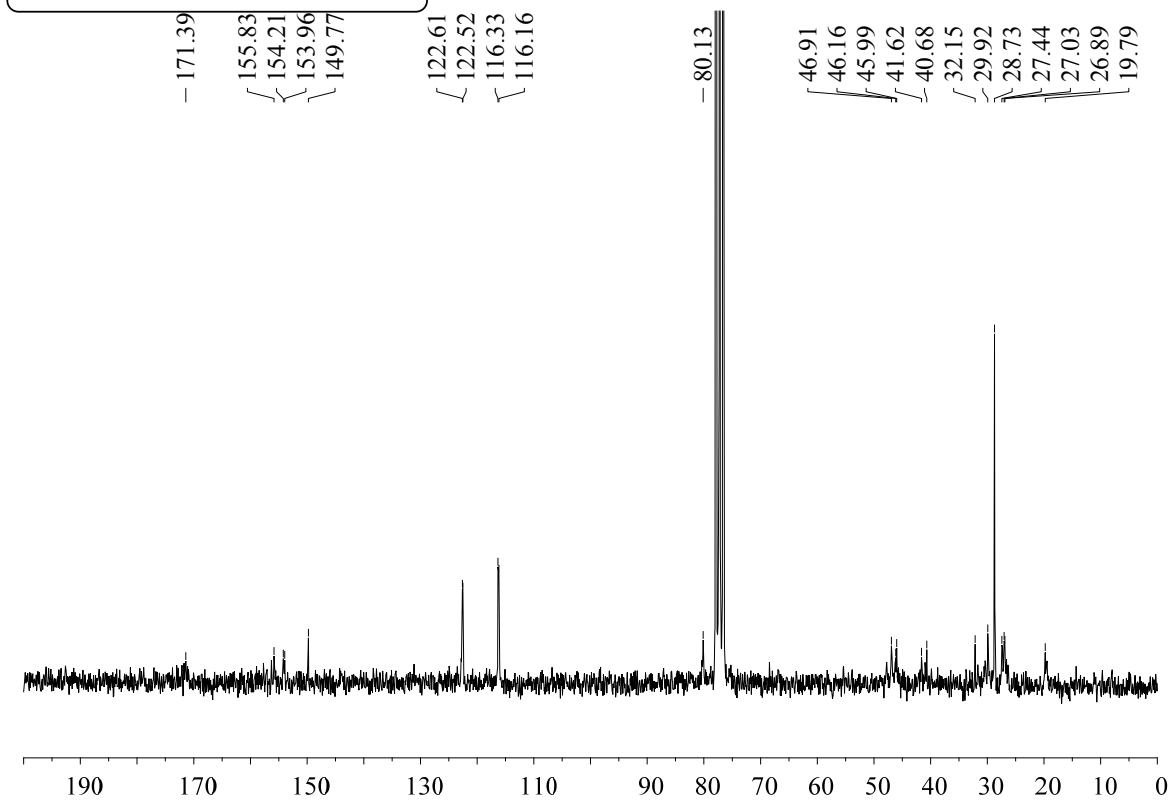
171.39
155.83
154.21
153.96
149.77
122.61
122.52
116.33
116.16
80.13
46.91
46.16
45.99
41.62
40.68
32.15
29.92
28.73
27.44
27.03
26.89
19.79
190 170 150 130 110 90 80 70 60 50 40 30 20 10 0

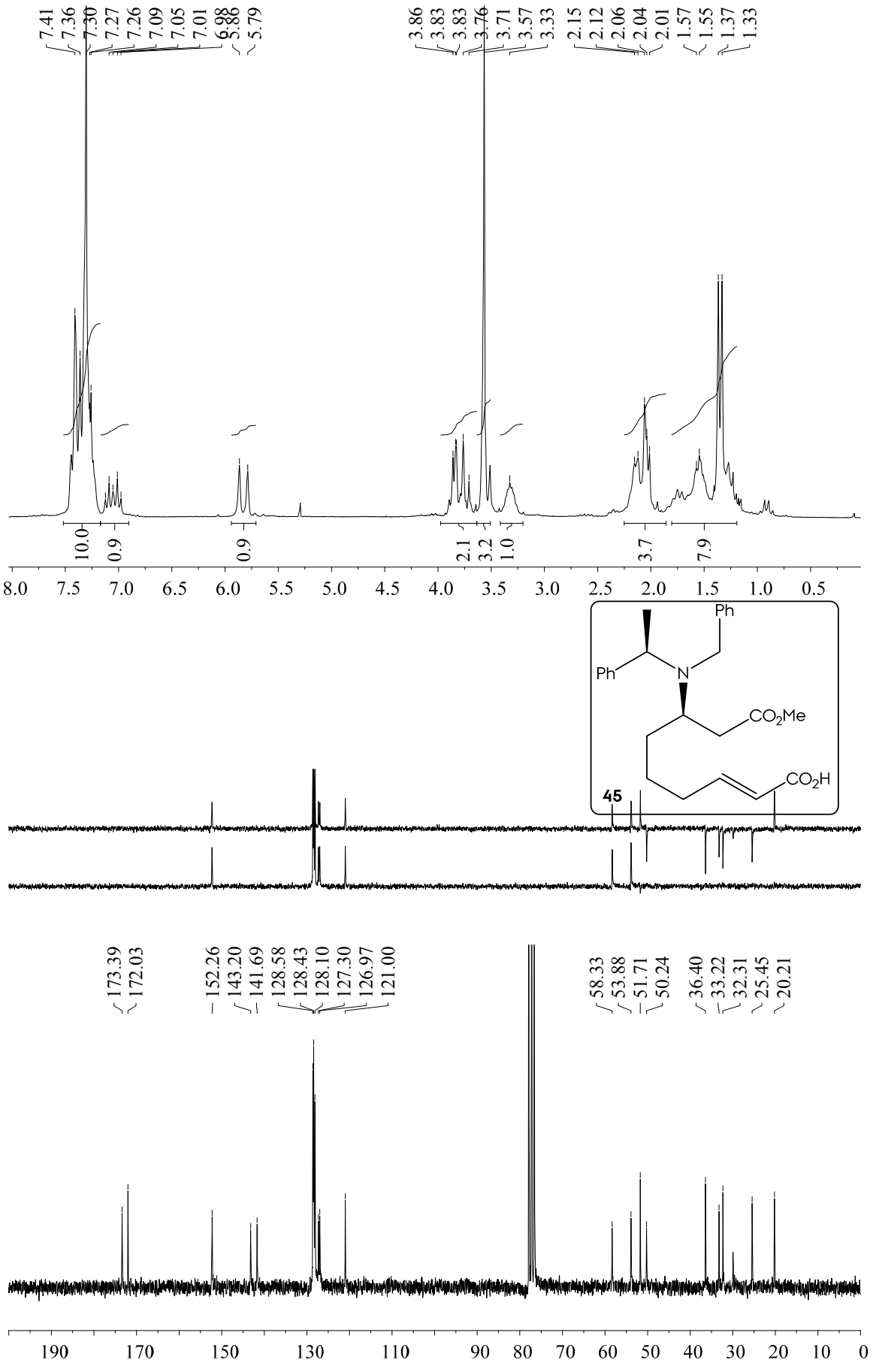
7.41
7.36
7.30
7.27
7.26
7.09
7.05
7.01
6.88
5.86
5.79
3.86
3.83
3.83
3.76
3.71
3.57
3.33
2.15
2.12
2.06
2.04
2.01
1.57
1.55
1.37
1.33
10.0
0.9
0.9
2.1
3.2
1.0
3.7
7.9
8.0 7.5 7.0 6.5 6.0 5.5 5.0 4.5 4.0 3.5 3.0 2.5 2.0 1.5 1.0 0.5
Ph
Ph
N
CO2Me
CO2H
45
173.39
172.03
152.26
143.20
141.69
128.58
128.43
128.10
127.30
126.97
121.00
58.33
53.88
51.71
50.24
36.40
33.22
32.31
25.45
20.21
190 170 150 130 110 90 80 70 60 50 40 30 20 10 0

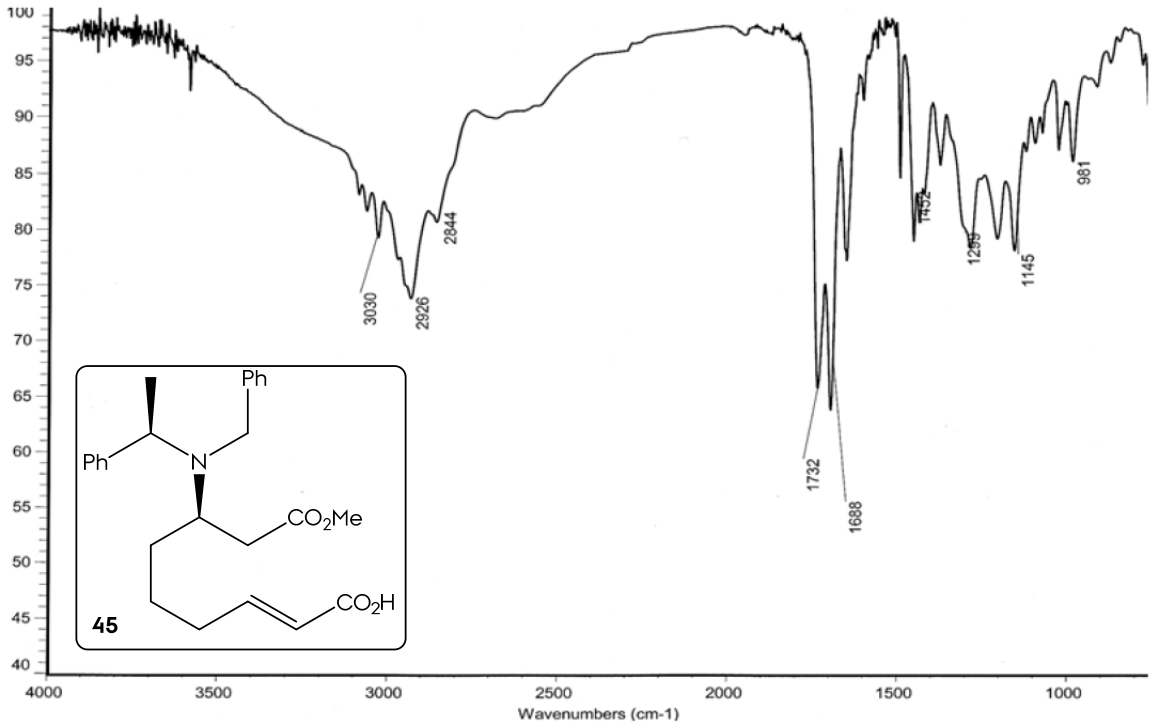
100
95
90
85
80
75
70
65
60
55
50
45
40
4000
3500
3000
2500
2000
1500
1000
Wavenumbers (cm-1)
3030
2926
2844
1732
1688
1452
1299
1145
981
Ph
N
Ph
CO2Me
CO2H
45

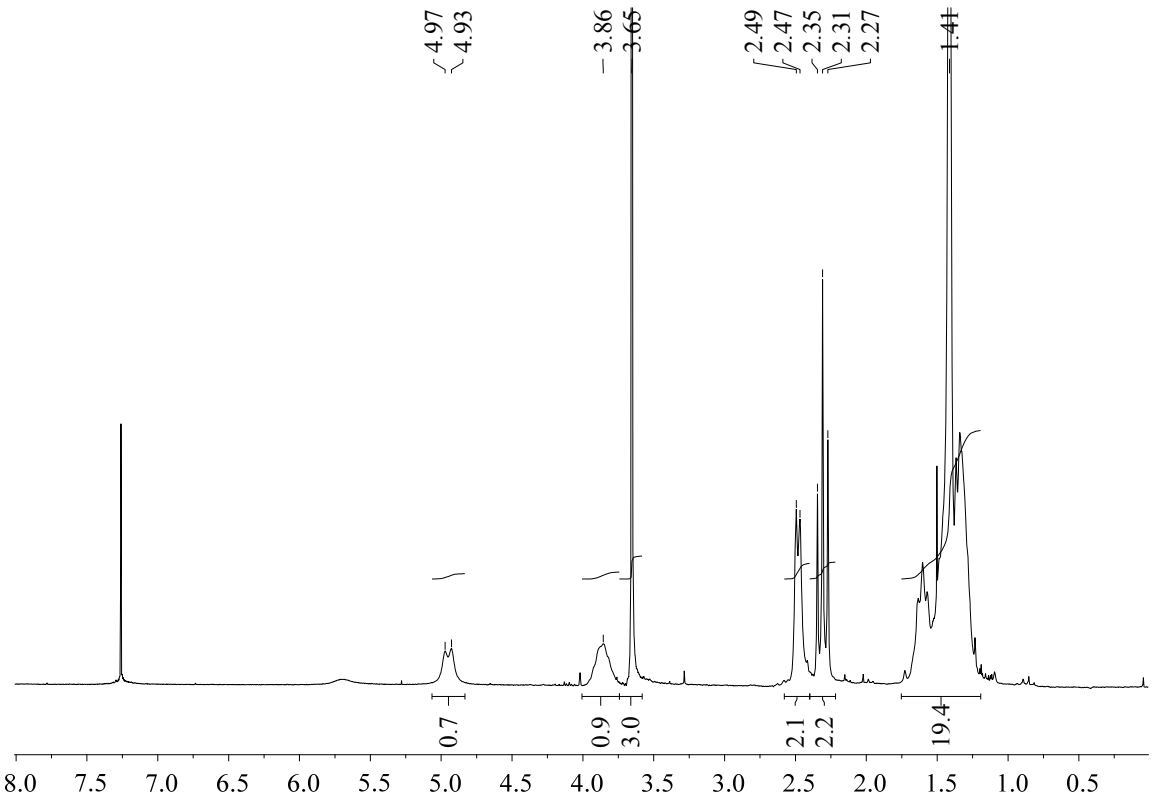
4.97
4.93
3.86
3.65
2.49
2.47
2.35
2.31
2.27
1.41
0.7
0.9
3.0
2.1
2.2
19.4
8.0
7.5
7.0
6.5
6.0
5.5
5.0
4.5
4.0
3.5
3.0
2.5
2.0
1.5
1.0
0.5

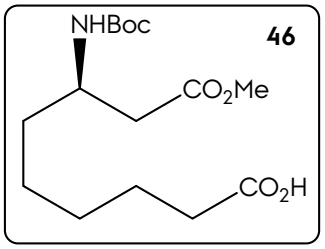
NHBoc
46
CO2Me
CO2H

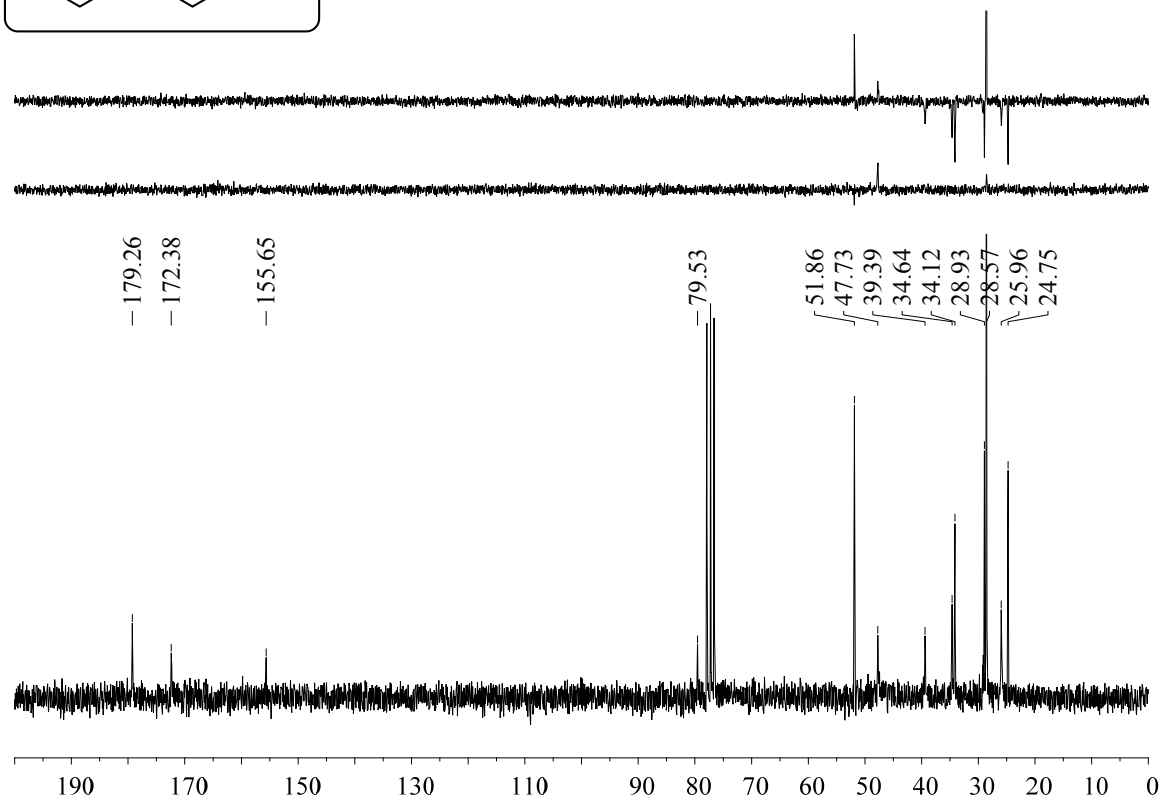
179.26
172.38
155.65
79.53
51.86
47.73
39.39
34.64
34.12
28.93
28.57
25.96
24.75
190
170
150
130
110
90
80
70
60
50
40
30
20
10
0

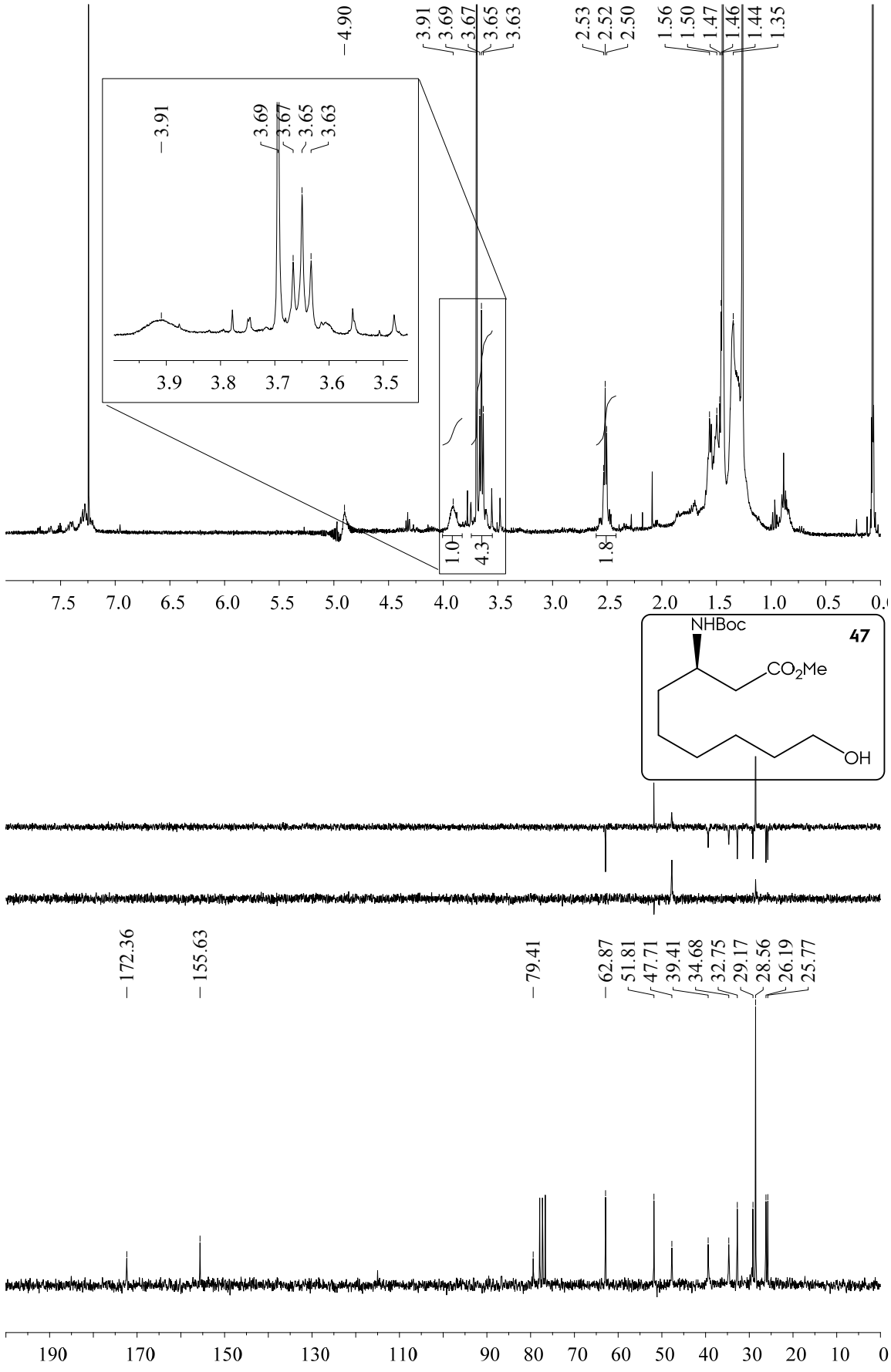
4.90
3.91
3.69
3.67
3.65
3.63
2.53
2.52
2.50
1.56
1.50
1.47
1.46
1.44
1.35
1.0
4.3
1.8
7.5 7.0 6.5 6.0 5.5 5.0 4.5 4.0 3.5 3.0 2.5 2.0 1.5 1.0 0.5
3.9 3.8 3.7 3.6 3.5
NHBoc
47
CO2Me
OH
172.36
155.63
79.41
62.87
51.81
47.71
39.41
34.68
32.75
29.17
28.56
26.19
25.77
190 170 150 130 110 90 80 70 60 50 40 30 20 10 0

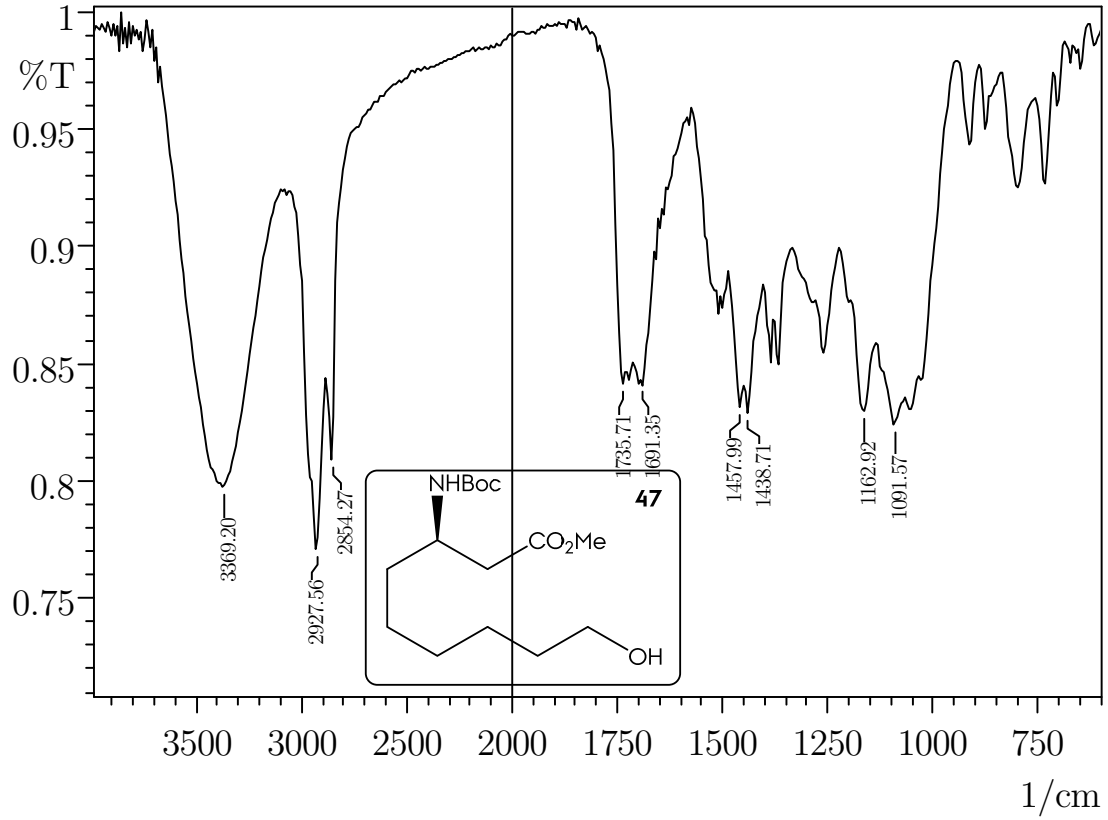
1
%T
0.95
0.9
0.85
0.8
0.75
3369.20
2927.56
2854.27
1735.71
1691.35
1457.99
1438.71
1162.92
1091.57
NHBoc
47
CO2Me
OH
3500
3000
2500
2000
1750
1500
1250
1000
750
1/cm

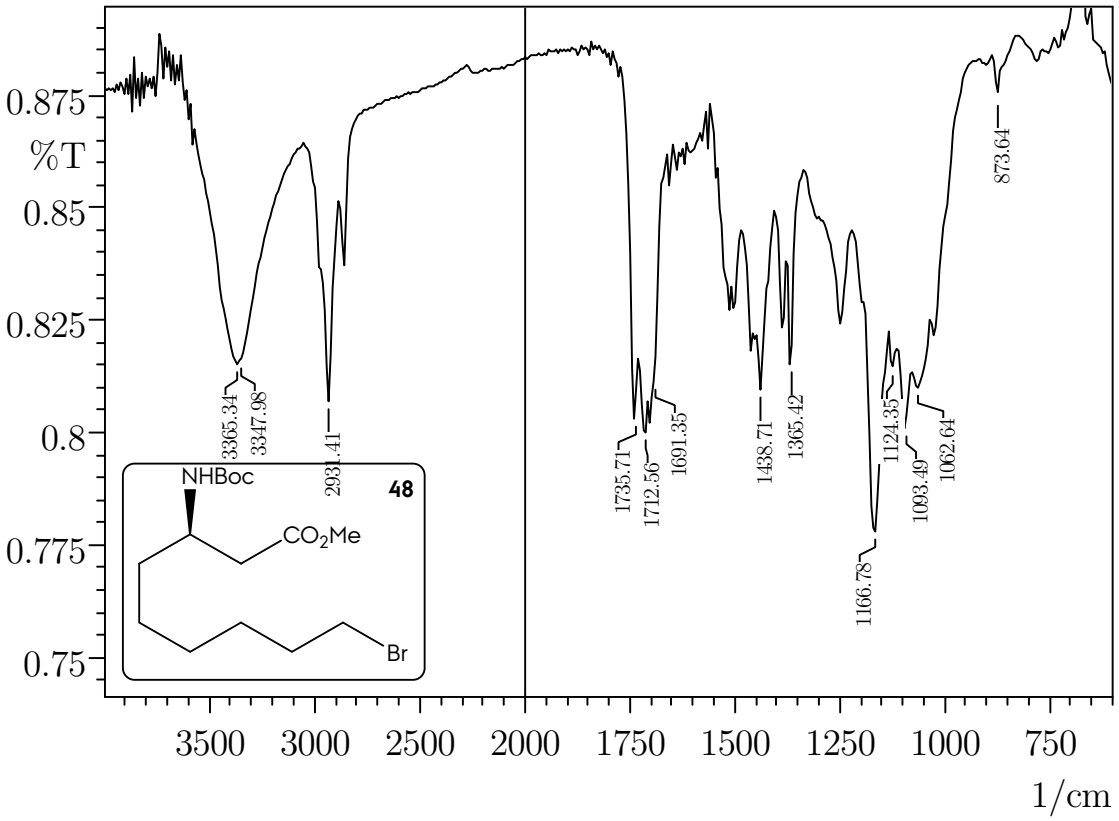
0.875
%T
0.85
0.825
0.8
0.775
0.75
3365.34
3347.98
2931.41
1735.71
1712.56
1691.35
1438.71
1365.42
1166.78
1124.35
1093.49
1062.64
873.64
NHBoc
48
CO2Me
Br
3500
3000
2500
2000
1750
1500
1250
1000
750
1/cm

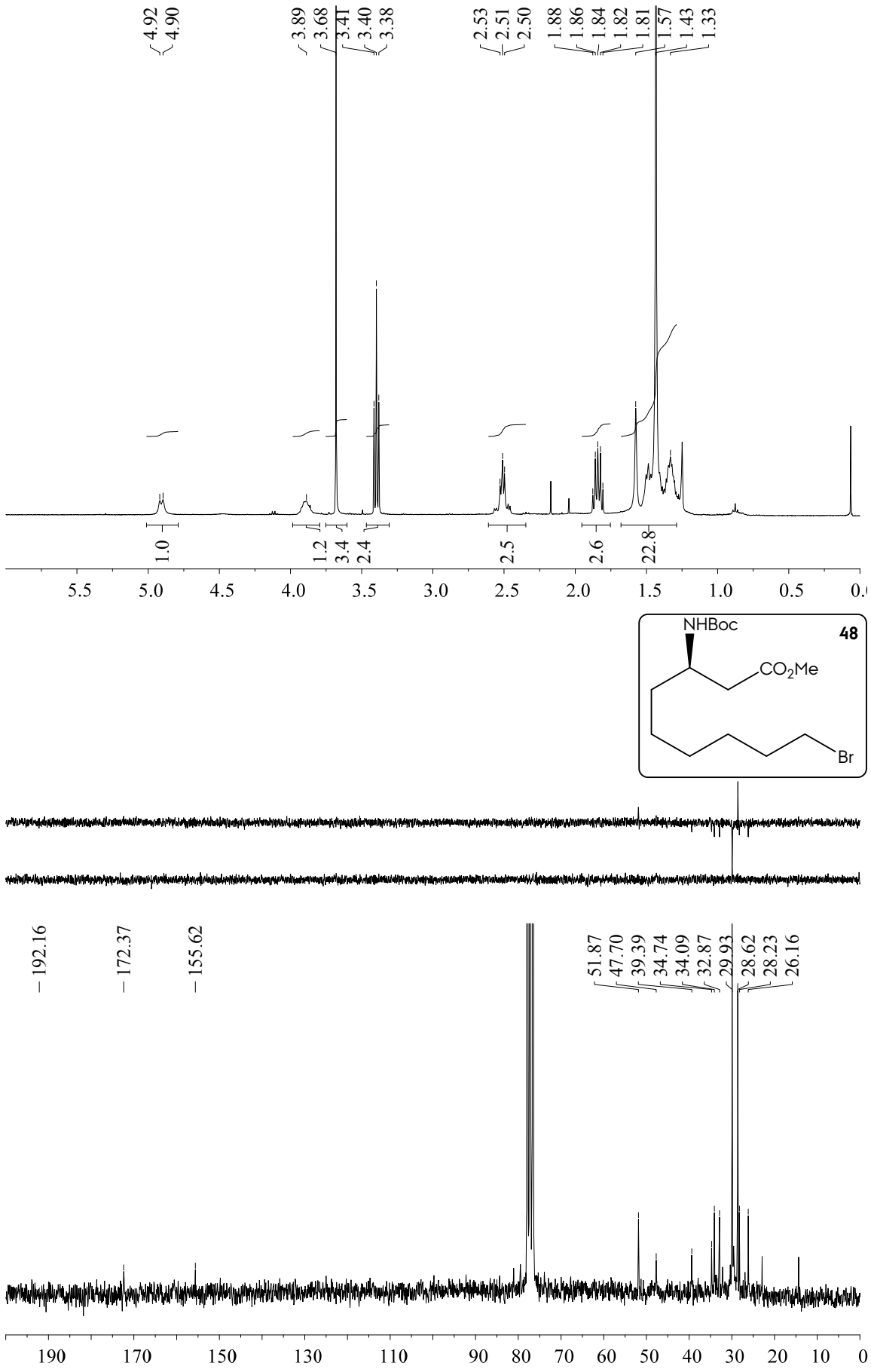
4.92
4.90
3.89
3.68
3.41
3.40
3.38
2.53
2.51
2.50
1.88
1.86
1.84
1.82
1.81
1.57
1.43
1.33
1.0
1.2
3.4
2.4
2.5
2.6
22.8
5.5
5.0
4.5
4.0
3.5
3.0
2.5
2.0
1.5
1.0
0.5
NHBoc
48
CO2Me
Br
192.16
172.37
155.62
51.87
47.70
39.39
34.74
34.09
32.87
29.93
28.62
28.23
26.16
190
170
150
130
110
90
80
70
60
50
40
30
20
10
0

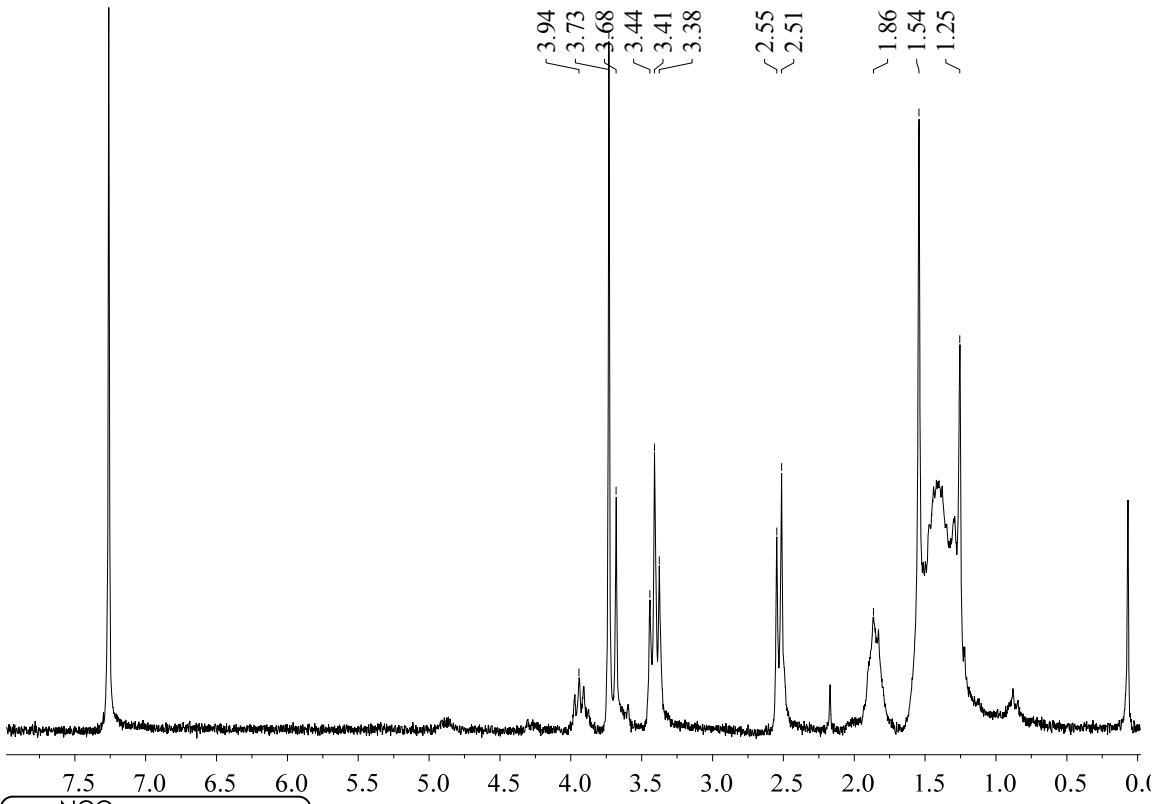
3.94
3.73
3.68
3.44
3.41
3.38
2.55
2.51
1.86
1.54
1.25
7.5 7.0 6.5 6.0 5.5 5.0 4.5 4.0 3.5 3.0 2.5 2.0 1.5 1.0 0.5 0.0

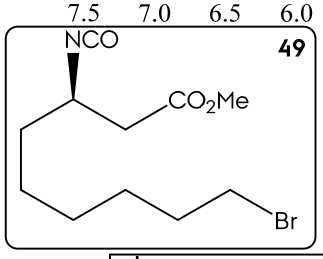
NCO
49
CO_2Me
Br

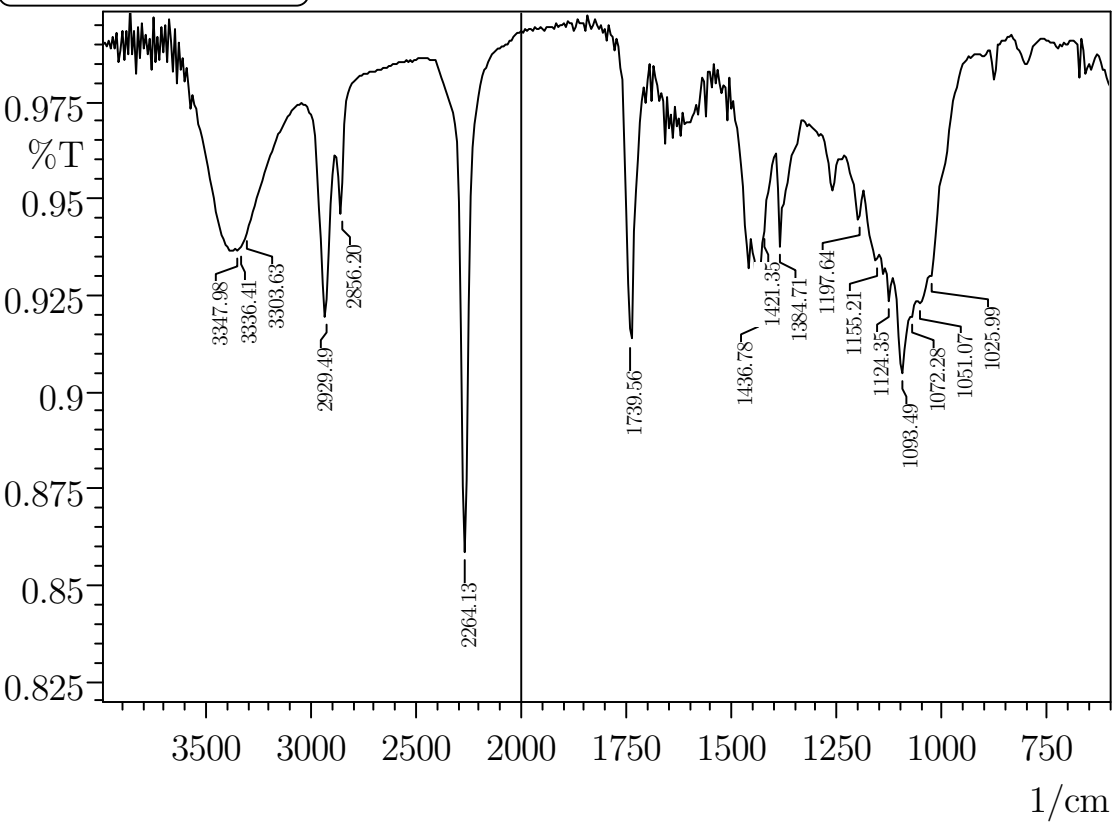
0.975
%T
0.95
0.925
0.9
0.875
0.85
0.825
3347.98
3336.41
3303.63
2929.49
2856.20
2264.13
1739.56
1436.78
1421.35
1384.71
1197.64
1155.21
1124.35
1093.49
1072.28
1051.07
1025.99
3500 3000 2500 2000 1750 1500 1250 1000 750
1/cm

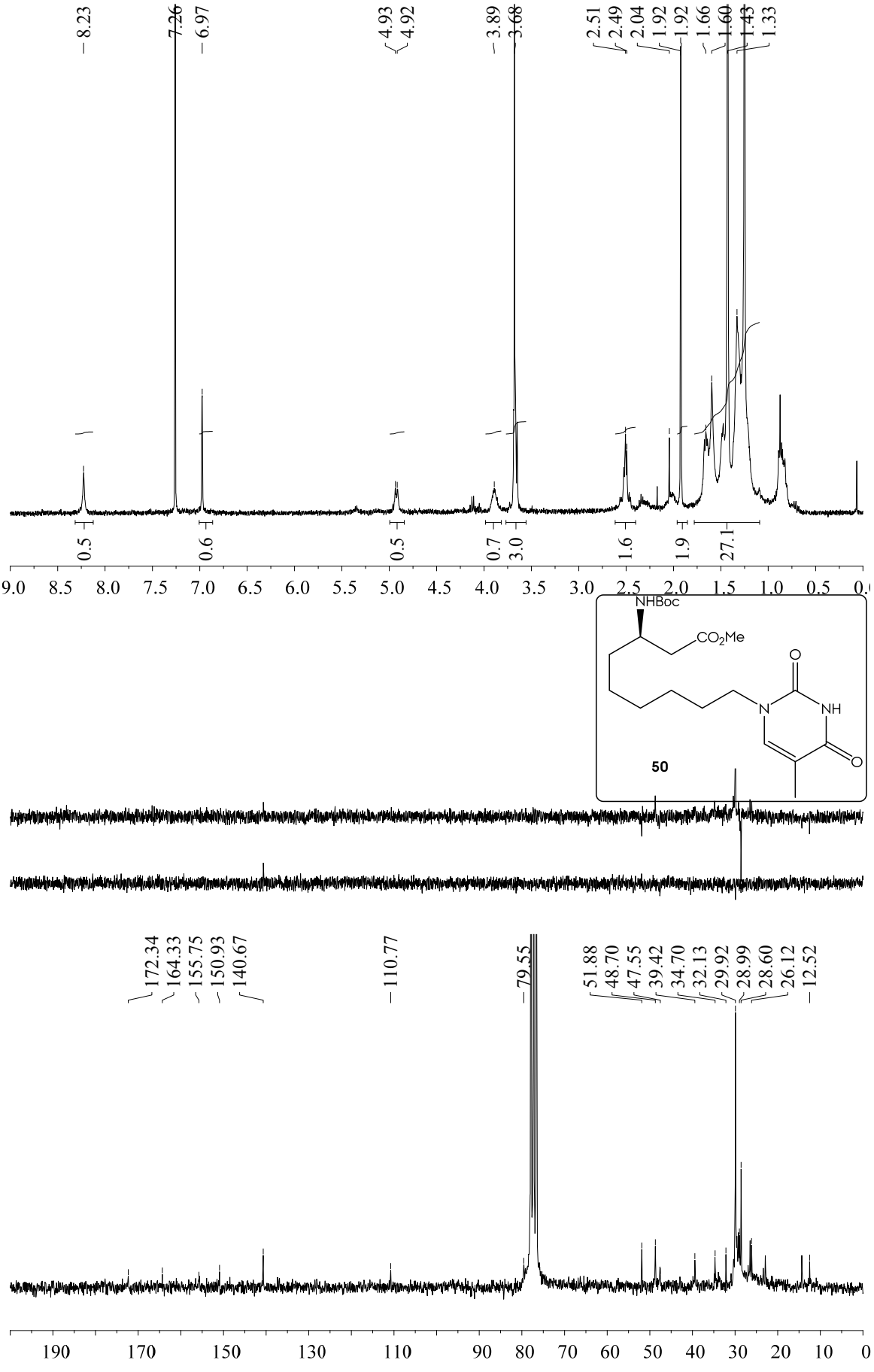
8.23
7.26
6.97
4.93
4.92
3.89
3.68
2.51
2.49
2.04
1.92
1.92
1.66
1.60
1.43
1.33
0.5
0.6
0.5
0.7
3.0
1.6
1.9
27.1
NHBoc
CO2Me
O
N
NH
O
50
172.34
164.33
155.75
150.93
140.67
110.77
79.55
51.88
48.70
47.55
39.42
34.70
32.13
29.92
28.99
28.60
26.12
12.52

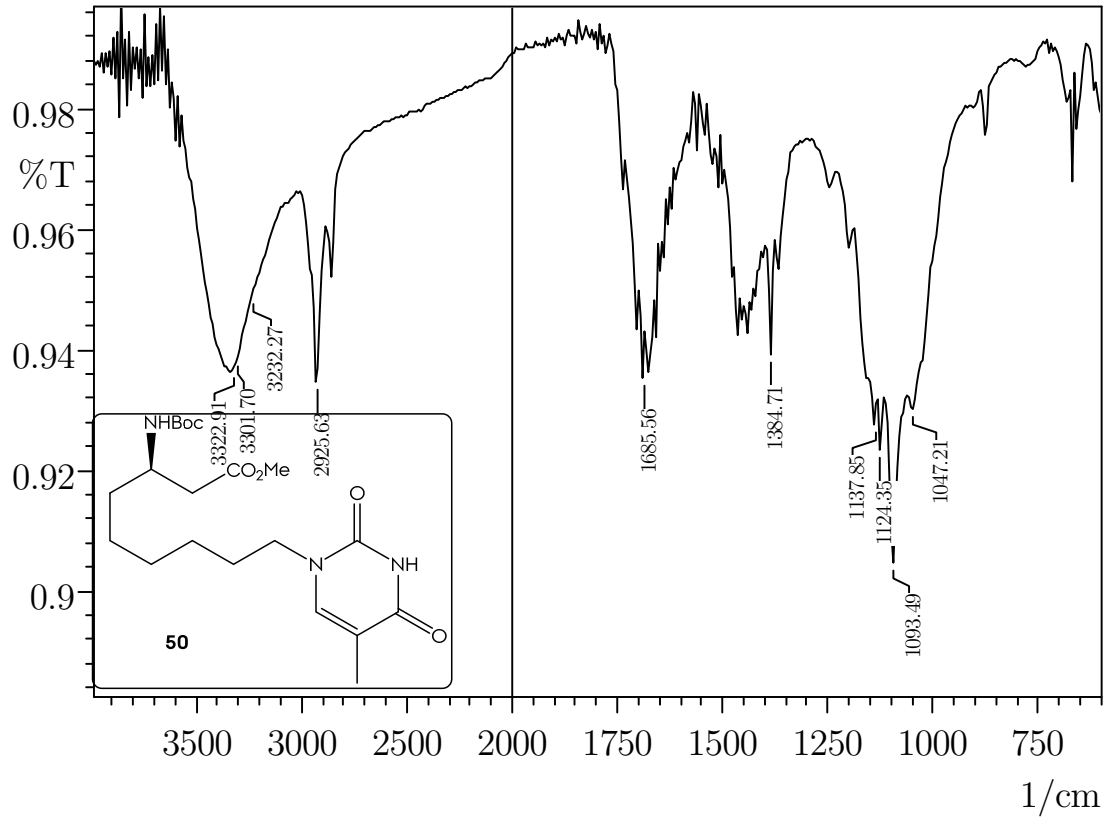
0.98
%T
0.96
0.94
0.92
0.9
3322.91
3301.70
3232.27
2925.63
1685.56
1384.71
1137.85
1124.35
1093.49
1047.21
NHBoc
CO2Me
N
NH
O
O
50
3500 3000 2500 2000 1750 1500 1250 1000 750
1/cm

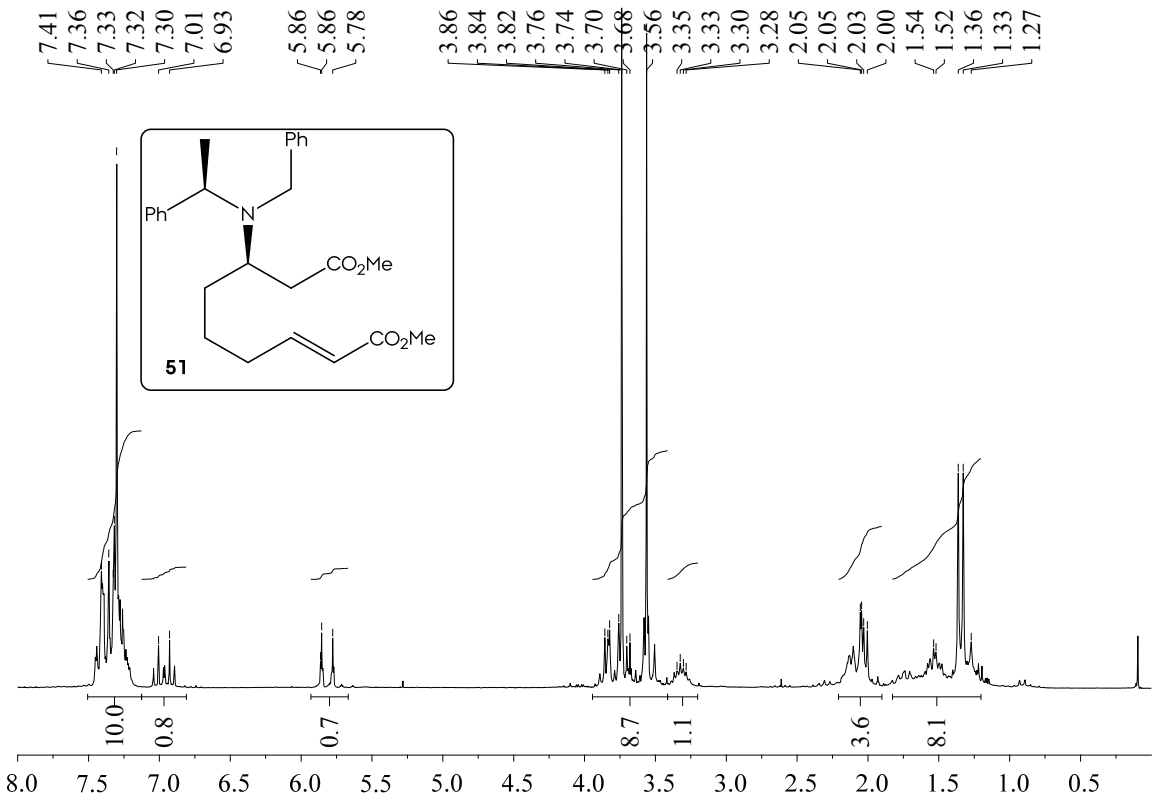
7.41 7.36 7.33 7.32 7.30 7.01 6.93
5.86 5.86 5.78
3.86 3.84 3.82 3.76 3.74 3.70 3.68 3.56 3.35 3.33 3.30 3.28
2.05 2.05 2.03 2.00
1.54 1.52 1.36 1.33 1.27
Ph
Ph
N
CO2Me
CO2Me
51
10.0 0.8 0.7 8.7 1.1 3.6 8.1
8.0 7.5 7.0 6.5 6.0 5.5 5.0 4.5 4.0 3.5 3.0 2.5 2.0 1.5 1.0 0.5

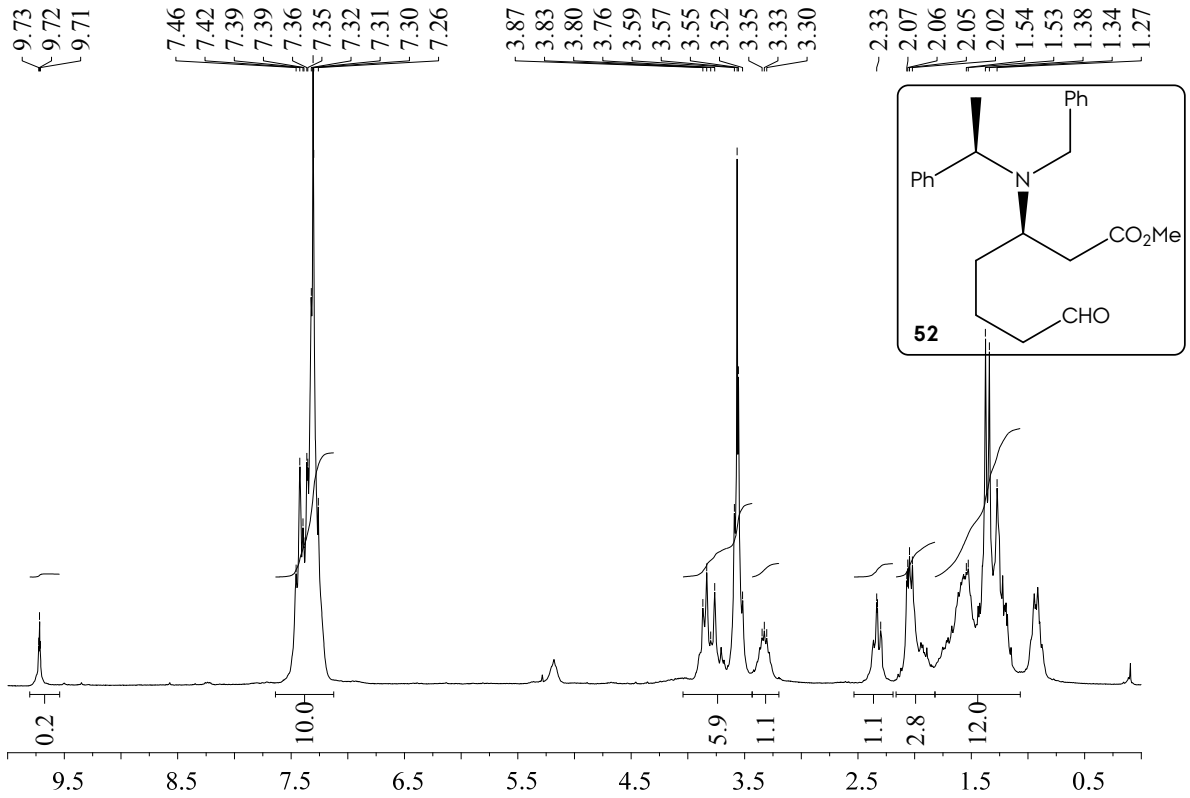
9.73
9.72
9.71
7.46
7.42
7.39
7.39
7.36
7.35
7.32
7.31
7.30
7.26
3.87
3.83
3.80
3.76
3.59
3.57
3.55
3.52
3.35
3.33
3.30
~2.33
2.07
2.06
2.05
2.02
1.54
1.53
1.38
1.34
1.27
Ph
Ph
N
CO2Me
CHO
52
0.2
10.0
5.9
1.1
1.1
2.8
12.0
9.5
8.5
7.5
6.5
5.5
4.5
3.5
2.5
1.5
0.5

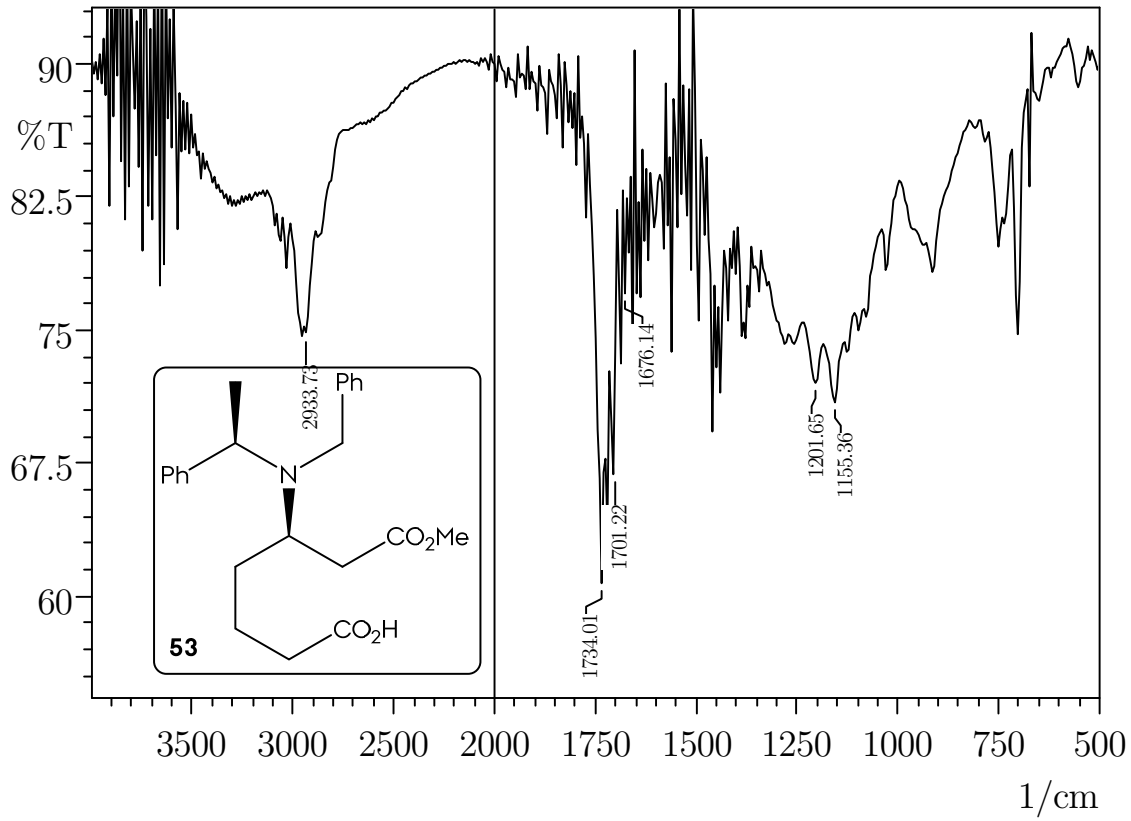
90
%T
82.5
75
67.5
60
2933.73
1734.01
1701.22
1676.14
1201.65
1155.36
Ph
Ph
N
CO2Me
CO2H
53
3500
3000
2500
2000
1750
1500
1250
1000
750
500
1/cm

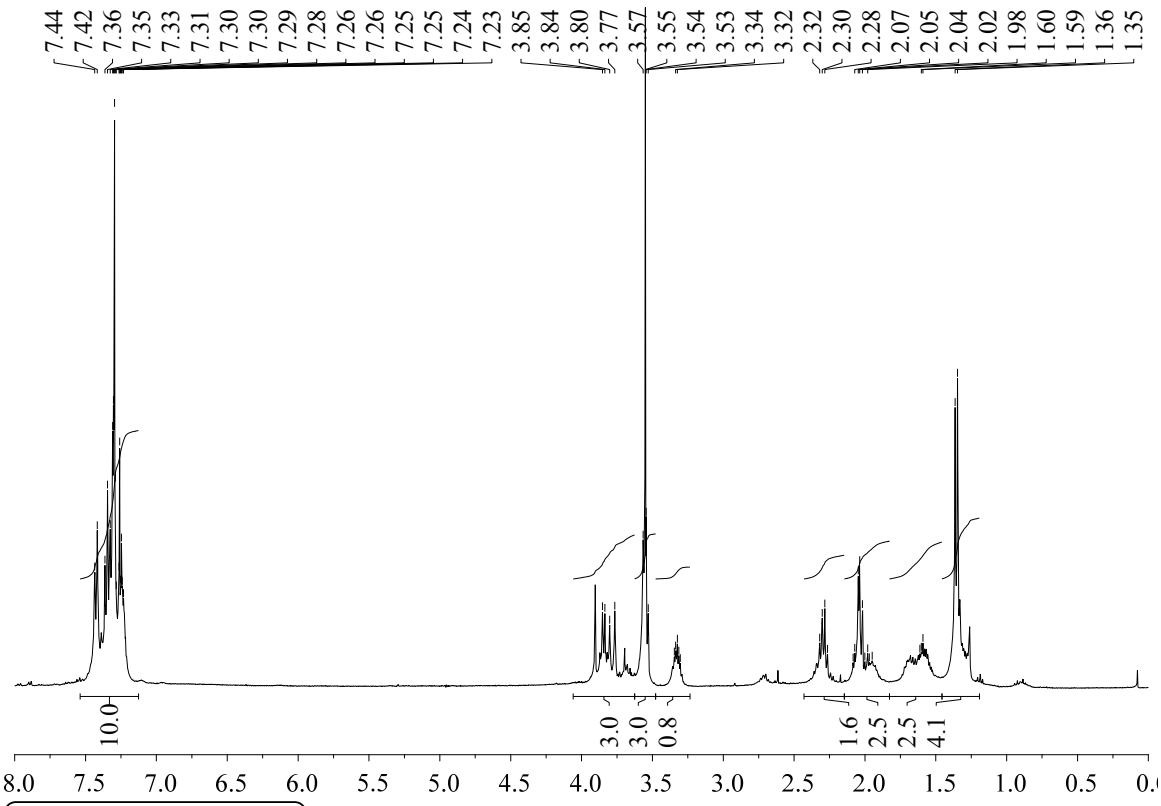
7.44
7.42
7.36
7.35
7.33
7.31
7.30
7.30
7.29
7.28
7.26
7.26
7.25
7.25
7.24
7.23
3.85
3.84
3.80
3.77
3.57
3.55
3.54
3.53
3.34
3.32
2.32
2.30
2.28
2.07
2.05
2.04
2.02
1.98
1.60
1.59
1.36
1.35
10.0
3.0
3.0
0.8
1.6
2.5
2.5
4.1
8.0
7.5
7.0
6.5
6.0
5.5
5.0
4.5
4.0
3.5
3.0
2.5
2.0
1.5
1.0
0.5

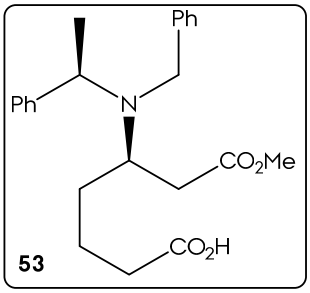
Ph
Ph
N
CO2Me
CO2H
53

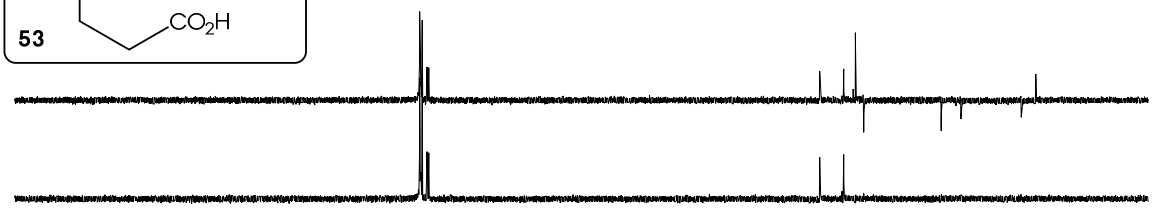

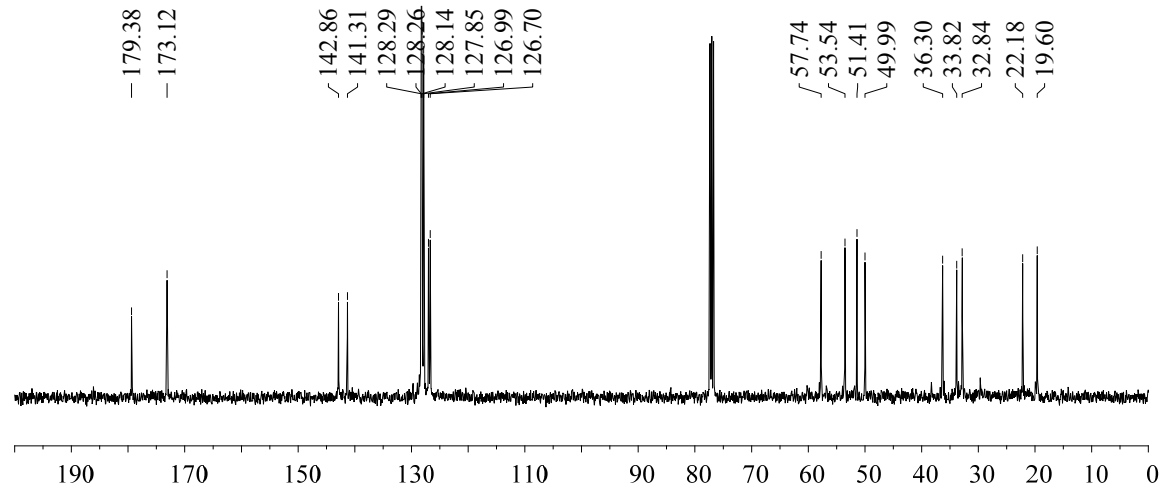
179.38
173.12
142.86
141.31
128.29
128.26
128.14
127.85
126.99
126.70
57.74
53.54
51.41
49.99
36.30
33.82
32.84
22.18
19.60
190
170
150
130
110
90
80
70
60
50
40
30
20
10
0

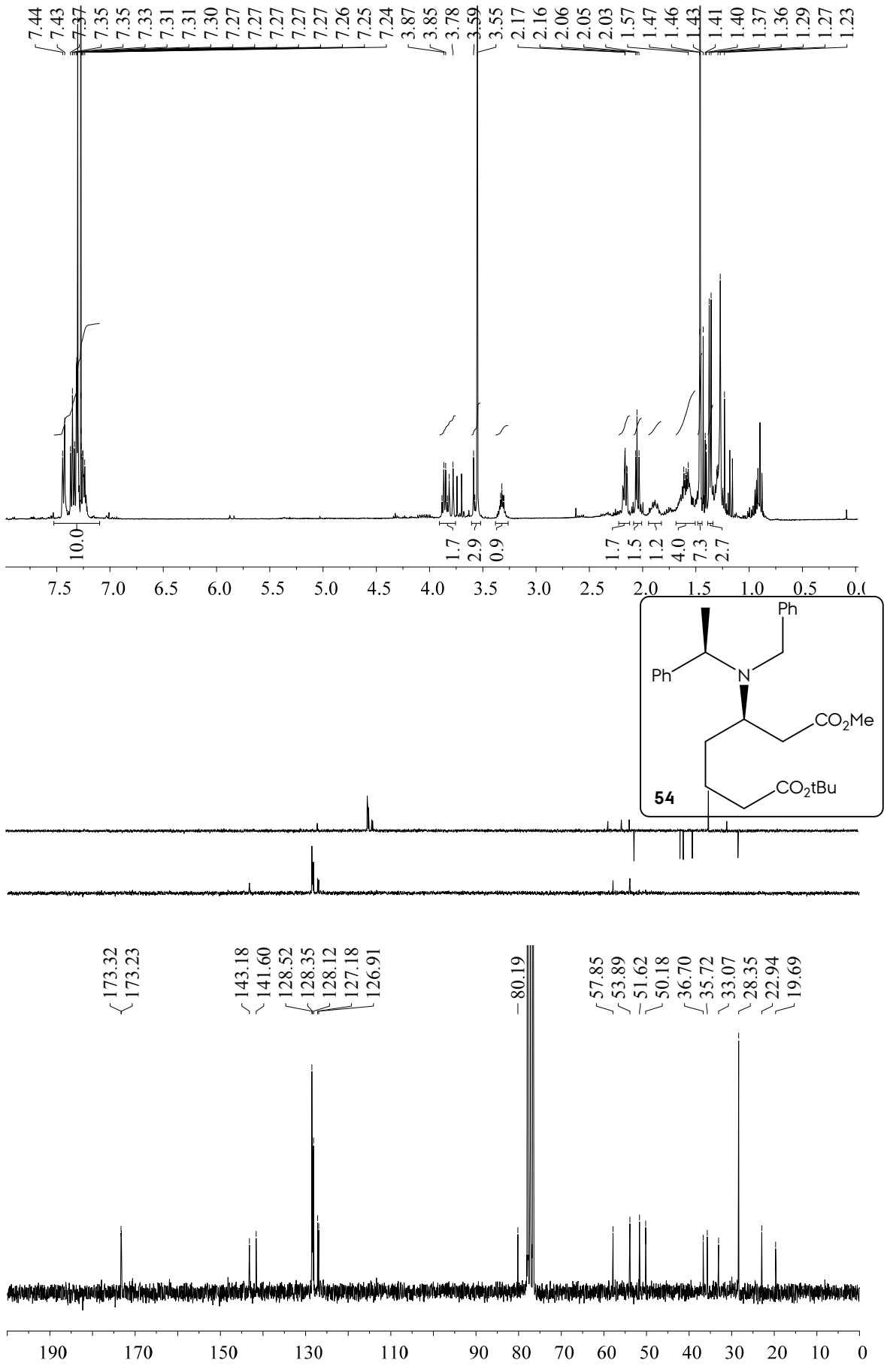
7.44
7.43
7.37
7.35
7.35
7.33
7.31
7.31
7.30
7.27
7.27
7.27
7.27
7.27
7.26
7.25
7.24
3.87
3.85
3.78
3.59
3.55
2.17
2.16
2.06
2.05
2.03
1.57
1.47
1.46
1.43
1.41
1.40
1.37
1.36
1.29
1.27
1.23
10.0
1.7
2.9
0.9
1.7
1.5
1.2
4.0
7.3
2.7
7.5 7.0 6.5 6.0 5.5 5.0 4.5 4.0 3.5 3.0 2.5 2.0 1.5 1.0 0.5
Ph
Ph
N
CO2Me
CO2tBu
54
173.32
173.23
143.18
141.60
128.52
128.35
128.12
127.18
126.91
80.19
57.85
53.89
51.62
50.18
36.70
35.72
33.07
28.35
22.94
19.69
190 170 150 130 110 90 80 70 60 50 40 30 20 10 0

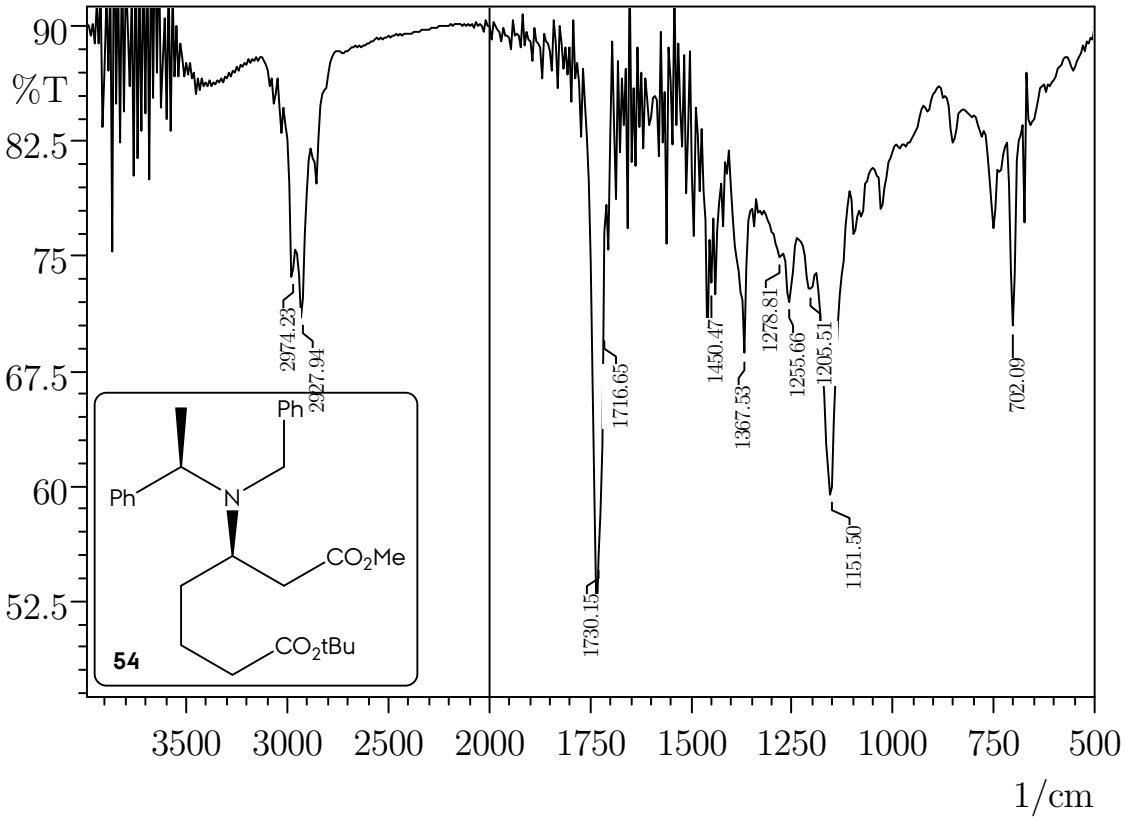
90
%T
82.5
75
67.5
60
52.5
2974.23
2927.94
1730.15
1716.65
1450.47
1367.53
1278.81
1255.66
1205.51
1151.50
702.09
Ph
N
Ph
CO2Me
CO2tBu
54
3500 3000 2500 2000 1750 1500 1250 1000 750 500
1/cm

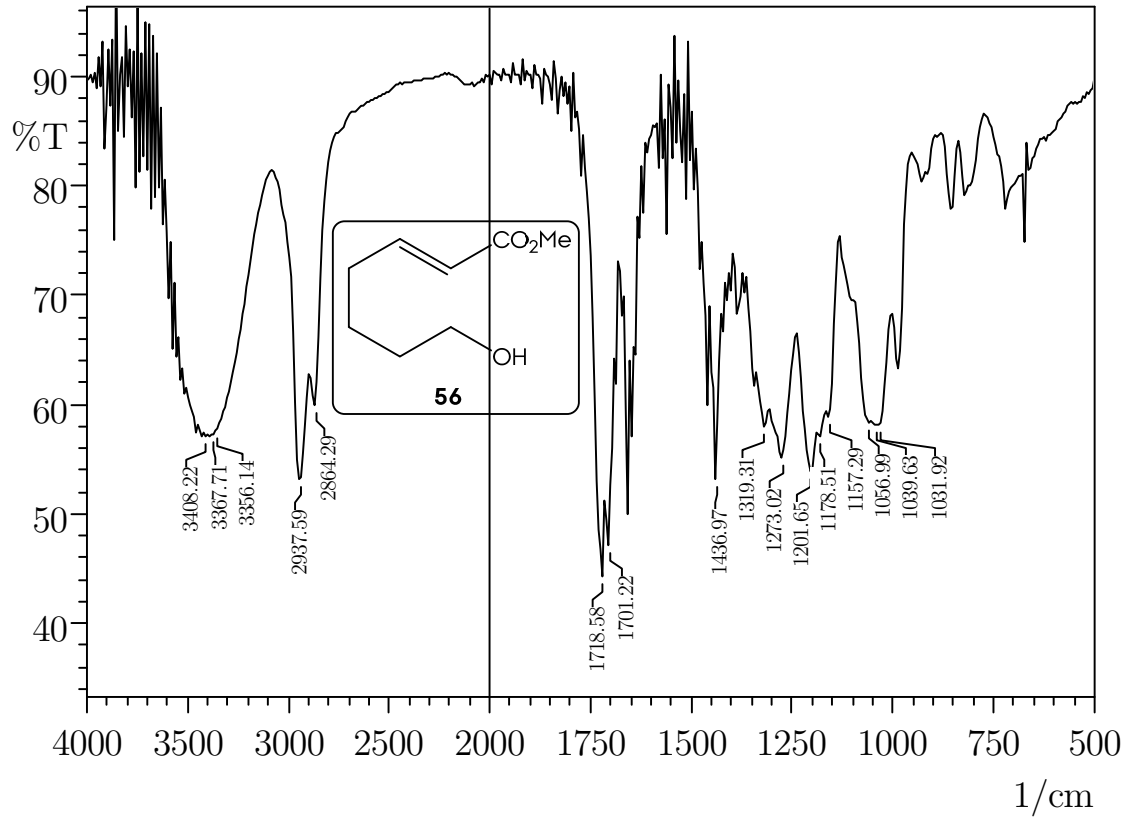
90
%T
80
70
60
50
40
3408.22
3367.71
3356.14
2937.59
2864.29
1718.58
1701.22
1436.97
1319.31
1273.02
1201.65
1178.51
1157.29
1056.99
1039.63
1031.92
CO2Me
OH
56
4000 3500 3000 2500 2000 1750 1500 1250 1000 750 500
1/cm

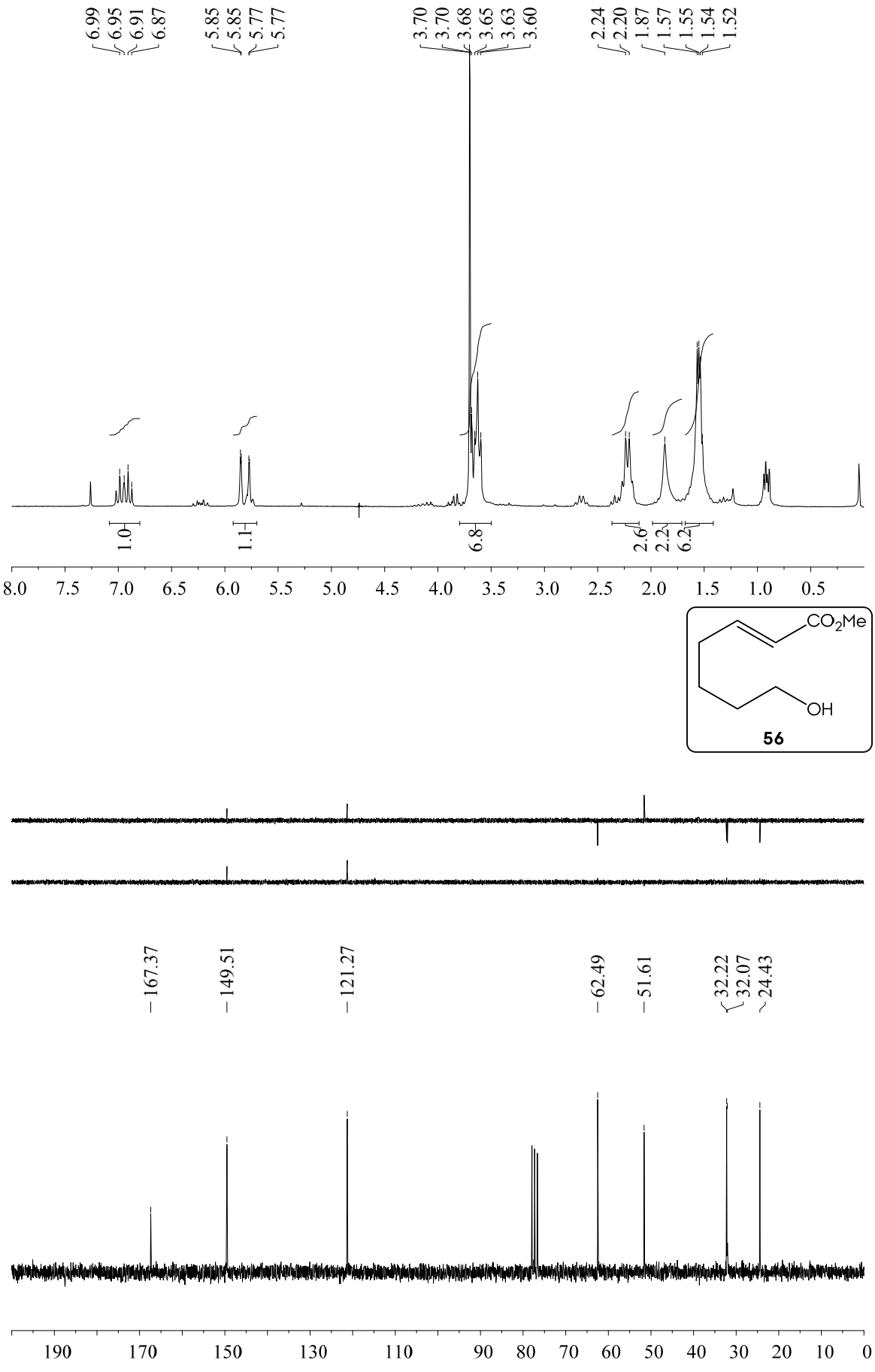
6.99
6.95
6.91
6.87
5.85
5.85
5.77
5.77
3.70
3.70
3.68
3.65
3.63
3.60
2.24
2.20
1.87
1.57
1.55
1.54
1.52
1.0
1.1
6.8
2.6
2.2
6.2
8.0
7.5
7.0
6.5
6.0
5.5
5.0
4.5
4.0
3.5
3.0
2.5
2.0
1.5
1.0
0.5
CO2Me
OH
56
167.37
149.51
121.27
62.49
51.61
32.22
32.07
24.43
190
170
150
130
110
90
80
70
60
50
40
30
20
10
0

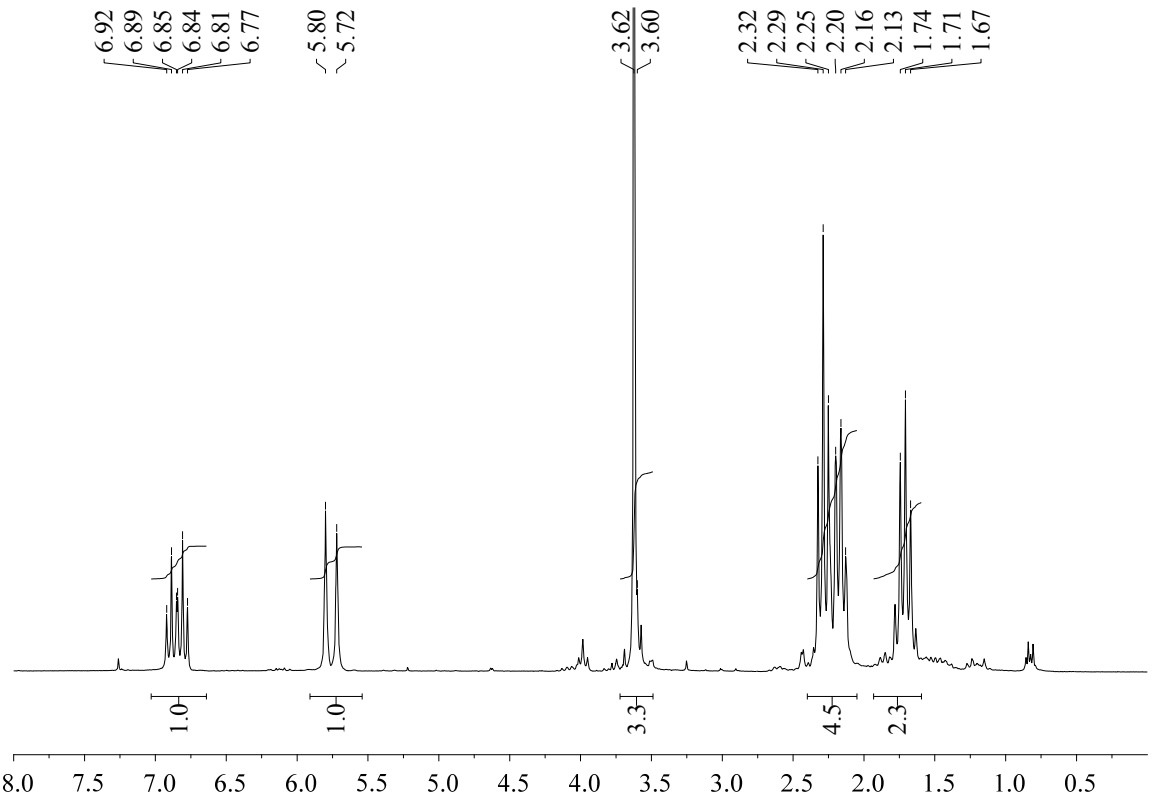
6.92
6.89
6.85
6.84
6.81
6.77
5.80
5.72
3.62
3.60
2.32
2.29
2.25
2.20
2.16
2.13
1.74
1.71
1.67
1.0
1.0
3.3
4.5
2.3
8.0 7.5 7.0 6.5 6.0 5.5 5.0 4.5 4.0 3.5 3.0 2.5 2.0 1.5 1.0 0.5

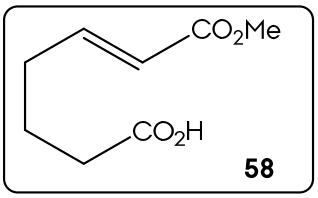
CO2Me
CO2H
58

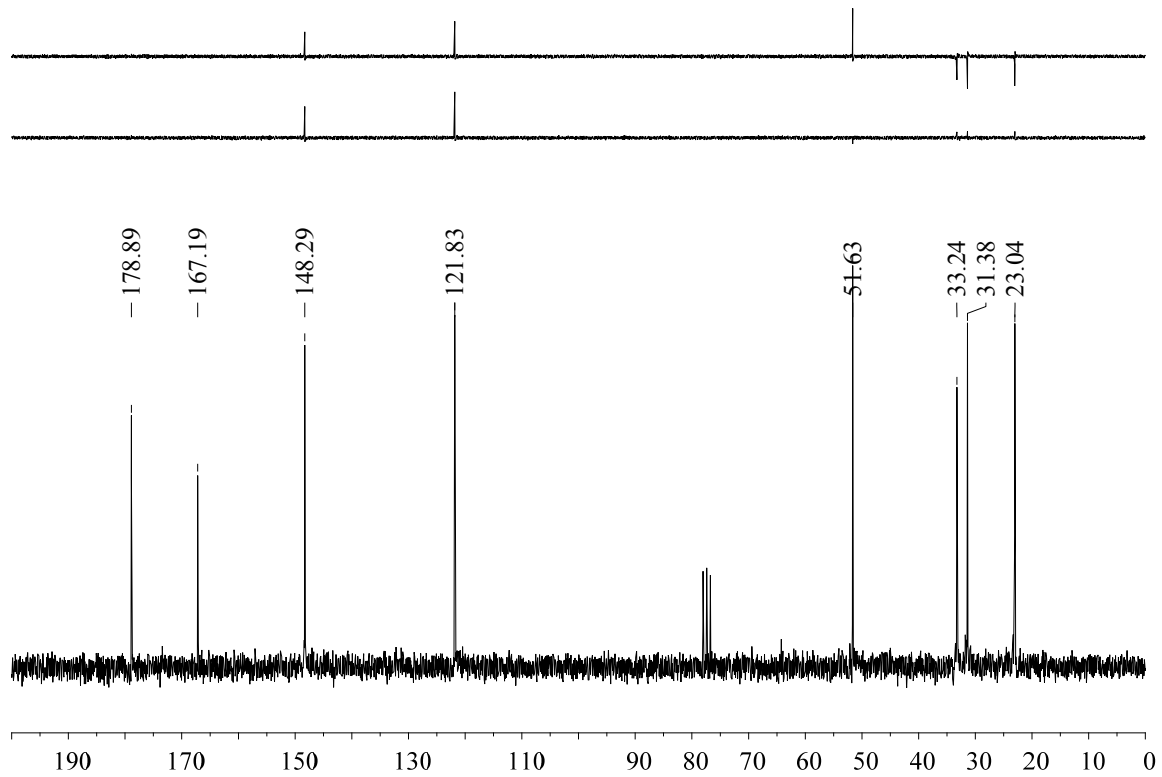
178.89
167.19
148.29
121.83
51.63
33.24
31.38
23.04
190 170 150 130 110 90 80 70 60 50 40 30 20 10 0

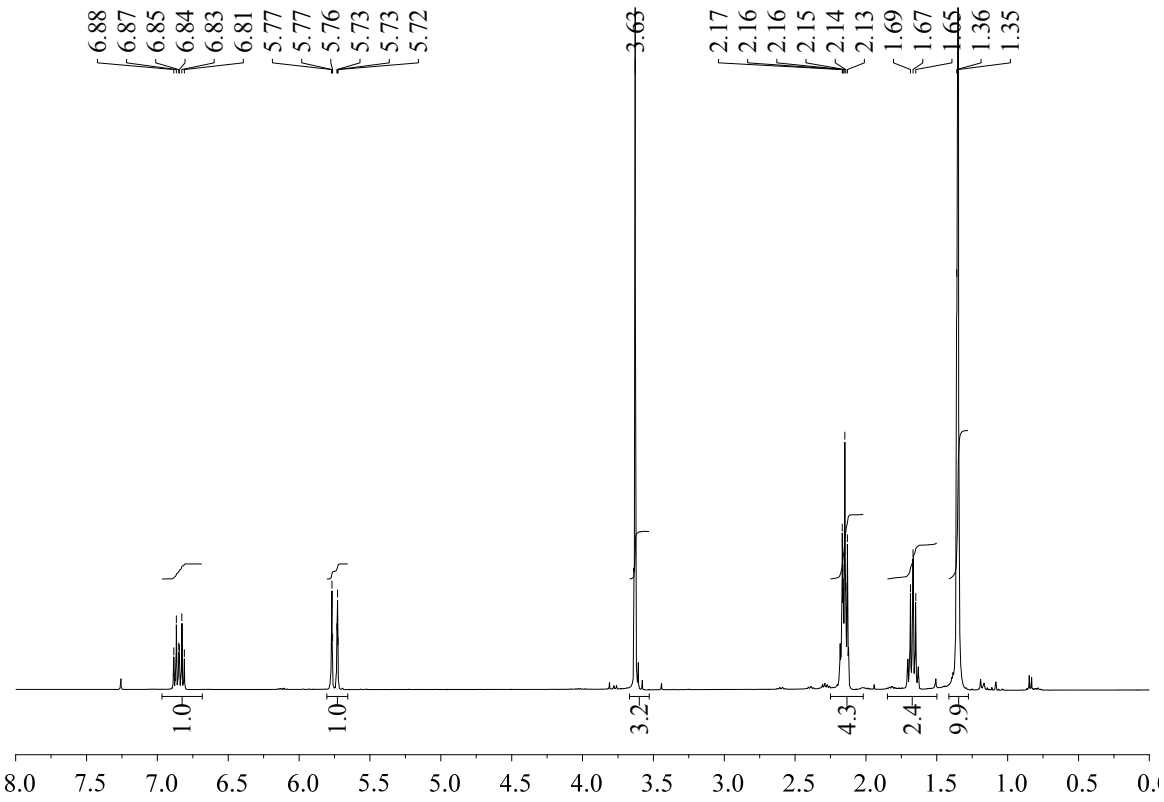
6.88
6.87
6.85
6.84
6.83
6.81
5.77
5.77
5.76
5.73
5.73
5.72
3.63
2.17
2.16
2.16
2.15
2.14
2.13
1.69
1.67
1.65
1.36
1.35
1.0
1.0
3.2
4.3
2.4
9.9
8.0 7.5 7.0 6.5 6.0 5.5 5.0 4.5 4.0 3.5 3.0 2.5 2.0 1.5 1.0 0.5

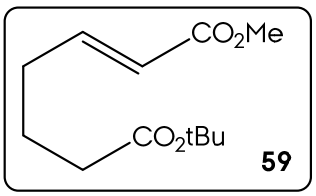
CO2Me
CO2tBu
59

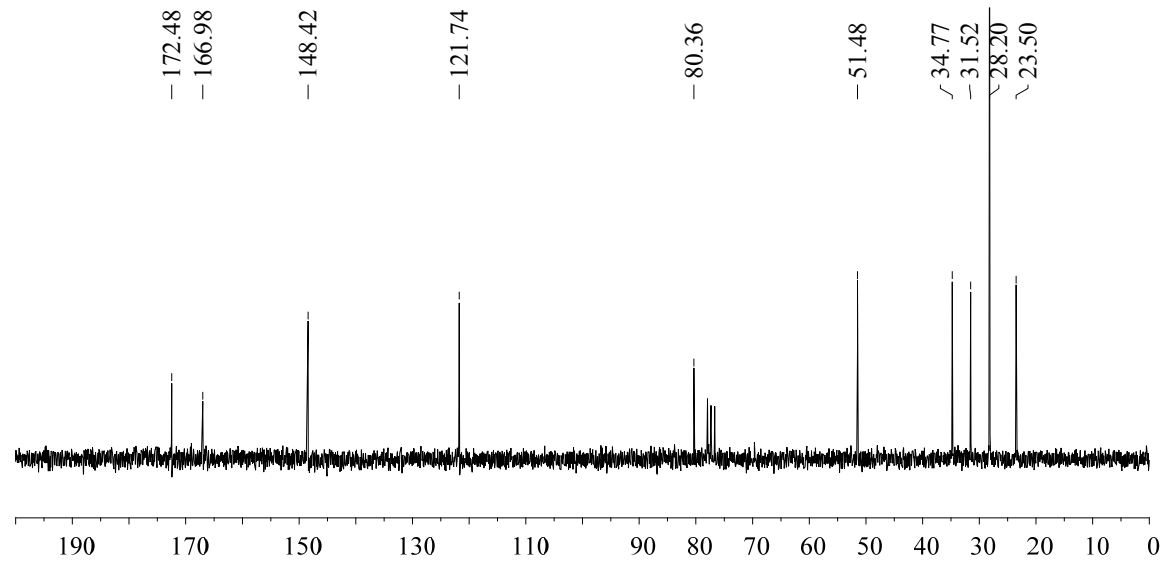
172.48
166.98
148.42
121.74
80.36
51.48
34.77
31.52
28.20
23.50
190 170 150 130 110 90 80 70 60 50 40 30 20 10 0

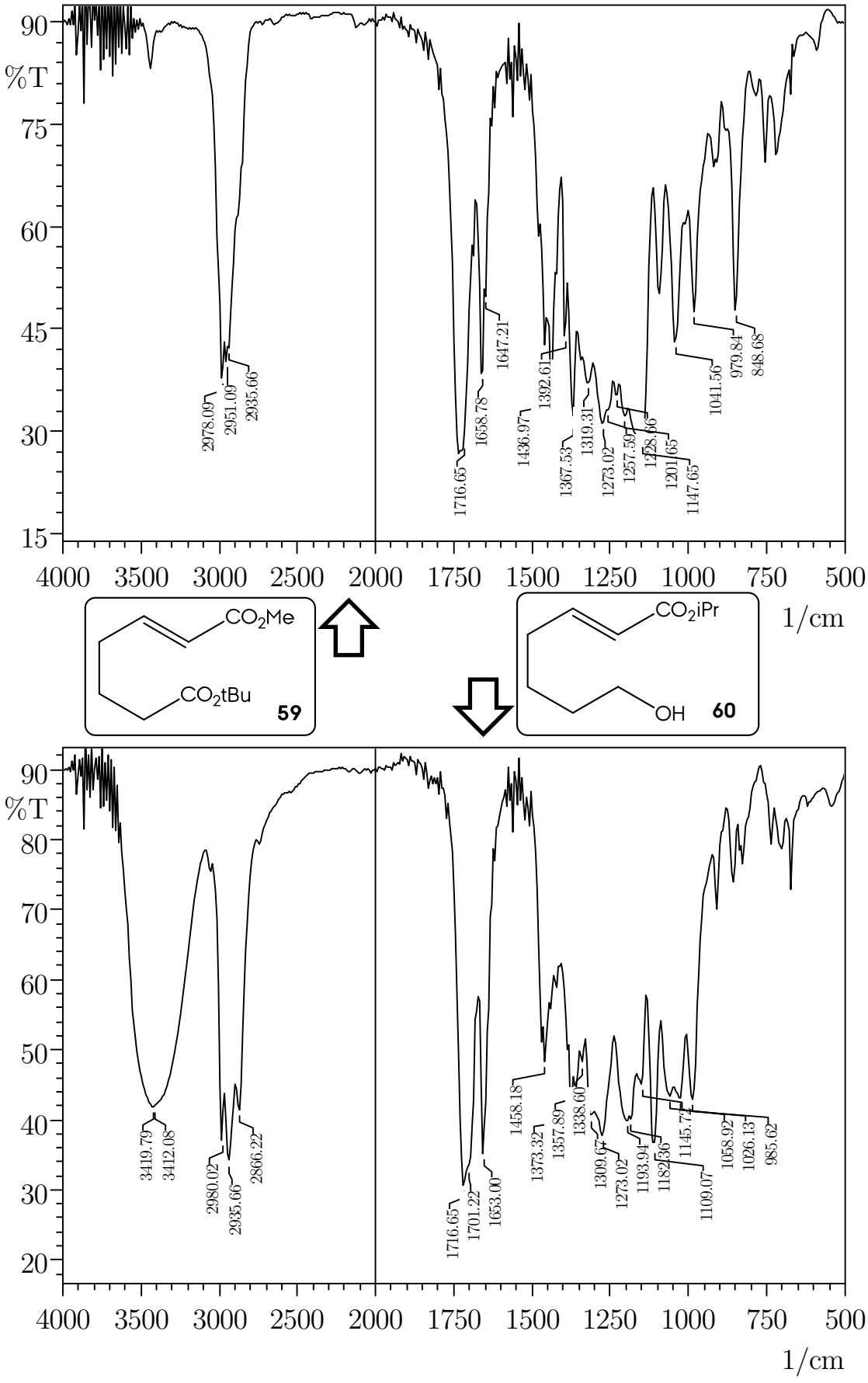
%T
1/cm
2978.09
2951.09
2935.66
1716.65
1658.78
1647.21
1436.97
1392.61
1367.53
1319.31
1273.02
1257.59
1041.56
979.84
848.68
1147.65
1201.65
CO2Me
CO2tBu
59
CO2iPr
OH
60
3419.79
3412.08
2980.02
2935.66
2866.22
1716.65
1701.22
1653.00
1458.18
1373.32
1357.89
1338.60
1309.67
1273.02
1193.94
1182.36
1145.72
1109.07
1058.92
1026.13
985.62

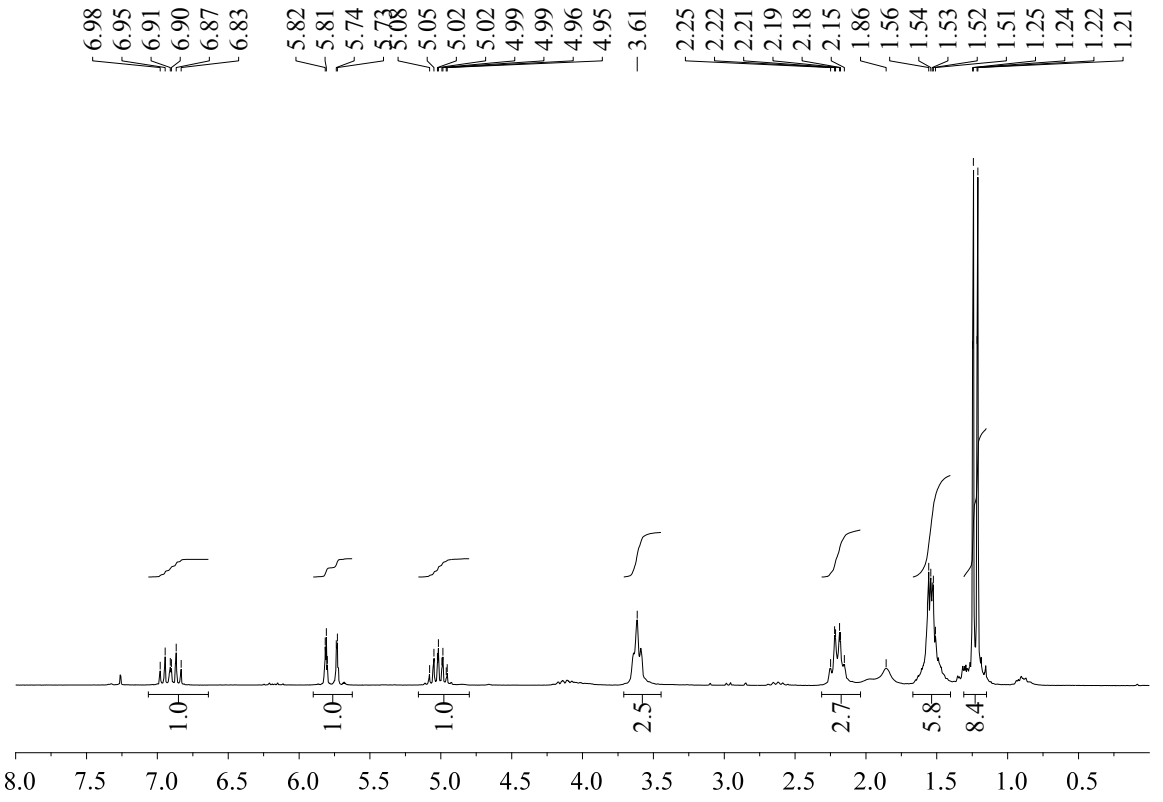
6.98
6.95
6.91
6.90
6.87
6.83
5.82
5.81
5.74
5.73
5.08
5.05
5.02
5.02
4.99
4.99
4.96
4.95
3.61
2.25
2.22
2.21
2.19
2.18
2.15
1.86
1.56
1.54
1.53
1.52
1.51
1.25
1.24
1.22
1.21
1.0
1.0
1.0
2.5
2.7
5.8
8.4
8.0 7.5 7.0 6.5 6.0 5.5 5.0 4.5 4.0 3.5 3.0 2.5 2.0 1.5 1.0 0.5

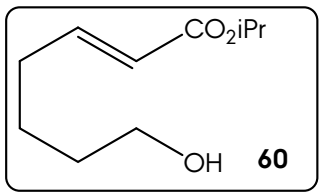
CO2iPr
OH
60

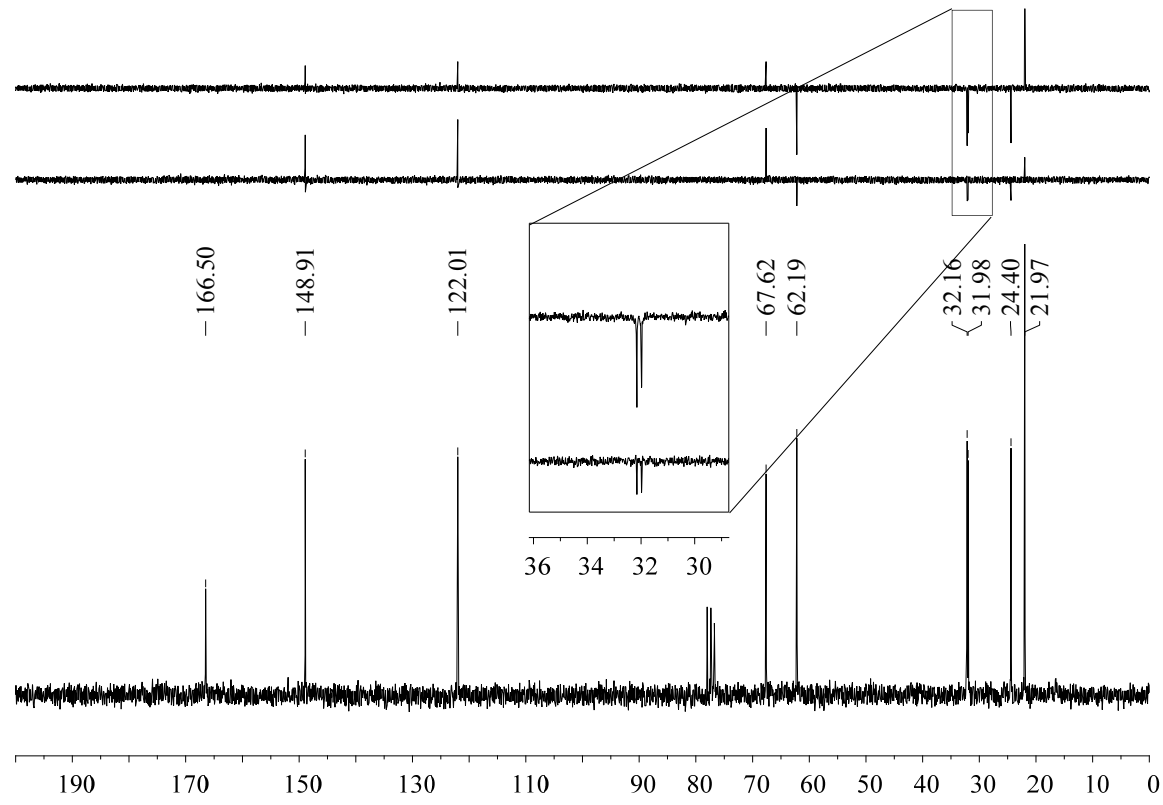
166.50
148.91
122.01
67.62
62.19
32.16
31.98
24.40
21.97
36 34 32 30
190 170 150 130 110 90 80 70 60 50 40 30 20 10 0

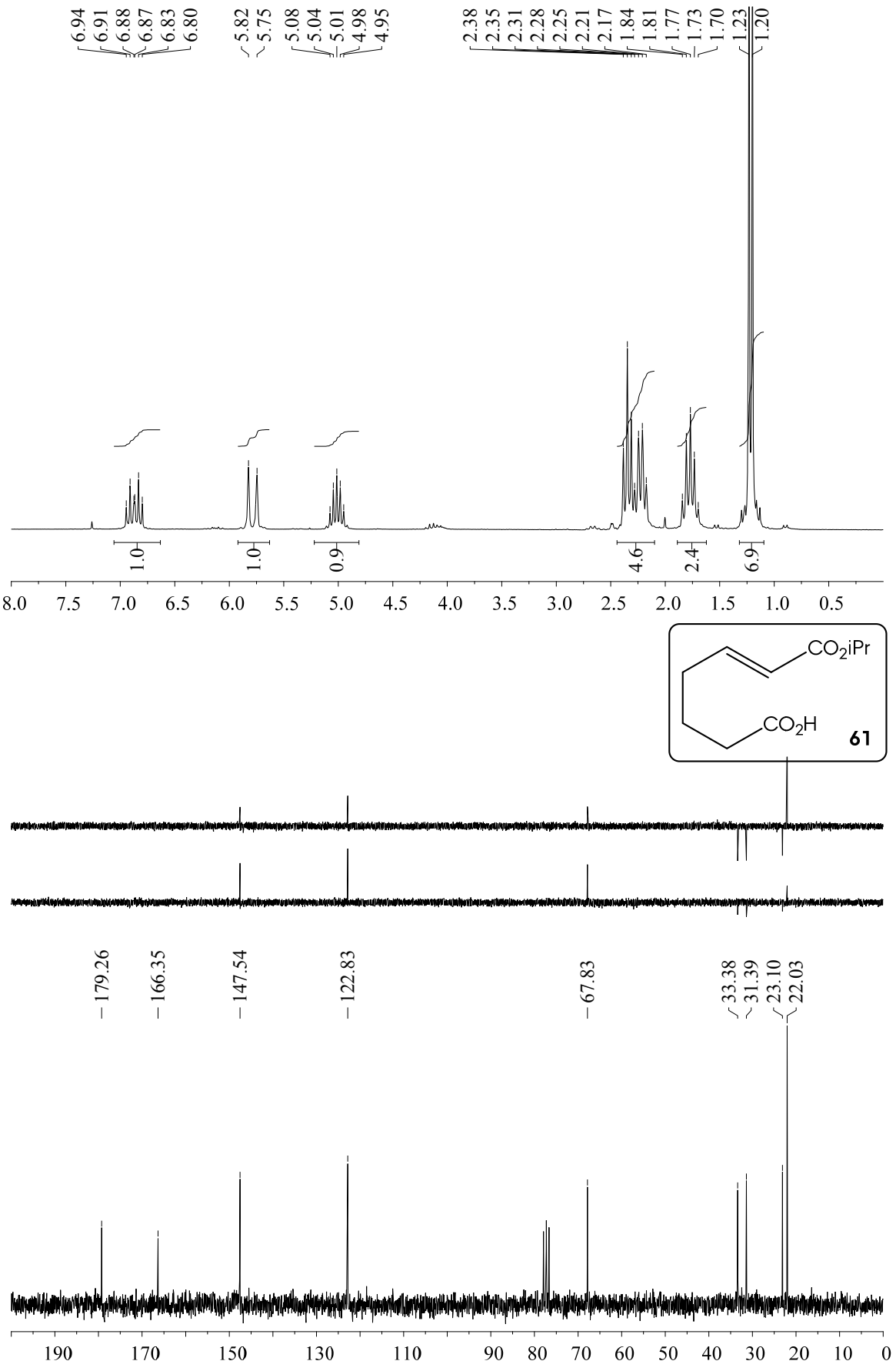
6.94
6.91
6.88
6.87
6.83
6.80
5.82
5.75
5.08
5.04
5.01
4.98
4.95
2.38
2.35
2.31
2.28
2.25
2.21
2.17
1.84
1.81
1.77
1.73
1.70
1.23
1.20
1.0
1.0
0.9
4.6
2.4
6.9
8.0 7.5 7.0 6.5 6.0 5.5 5.0 4.5 4.0 3.5 3.0 2.5 2.0 1.5 1.0 0.5
CO2iPr
CO2H
61
179.26
166.35
147.54
122.83
67.83
33.38
31.39
23.10
22.03
190 170 150 130 110 90 80 70 60 50 40 30 20 10 0

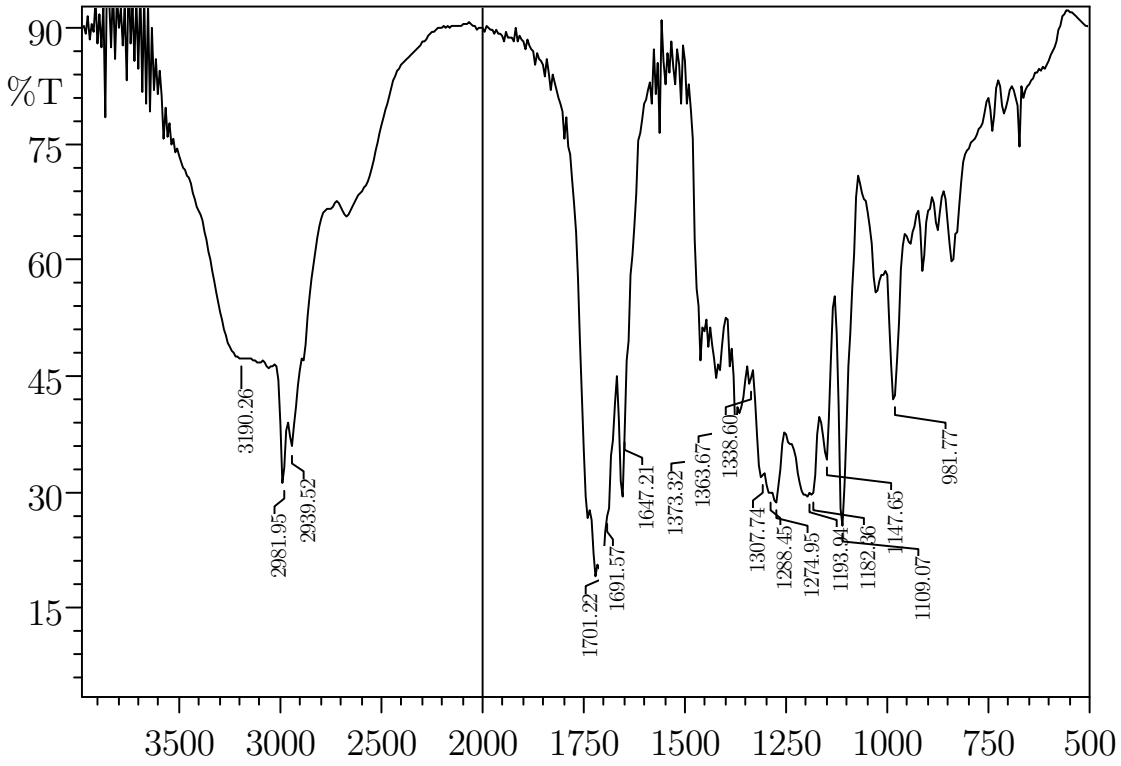
90
%T
75
60
45
30
15
3190.26
2981.95
2939.52
1701.22
1691.57
1647.21
1373.32
1363.67
1338.60
1307.74
1288.45
1274.95
1193.94
1182.36
1147.65
1109.07
981.77
3500 3000 2500 2000 1750 1500 1250 1000 750 500
1/cm

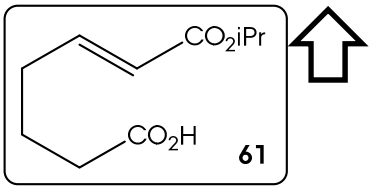
CO2iPr
CO2H
61

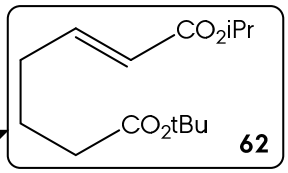
CO2iPr
CO2tBu
62

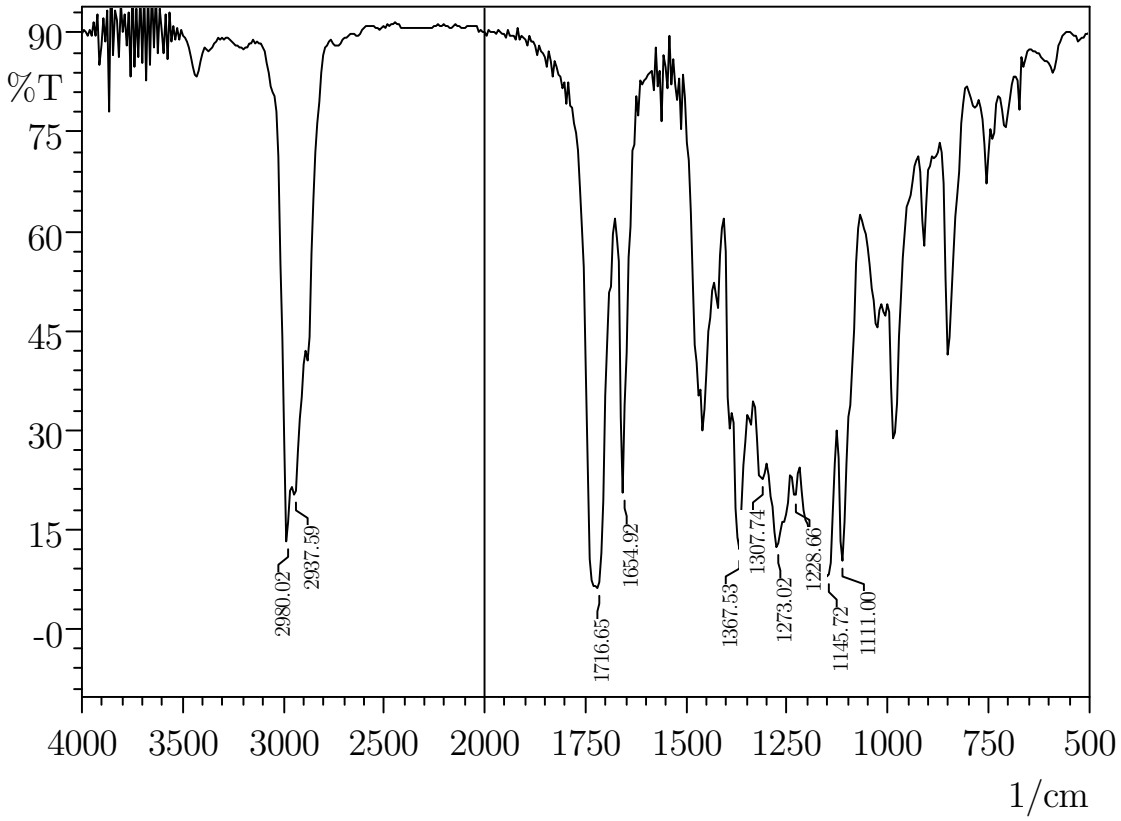
90
%T
75
60
45
30
15
-0
2980.02
2937.59
1716.65
1654.92
1367.53
1307.74
1273.02
1228.66
1145.72
1111.00
4000 3500 3000 2500 2000 1750 1500 1250 1000 750 500
1/cm

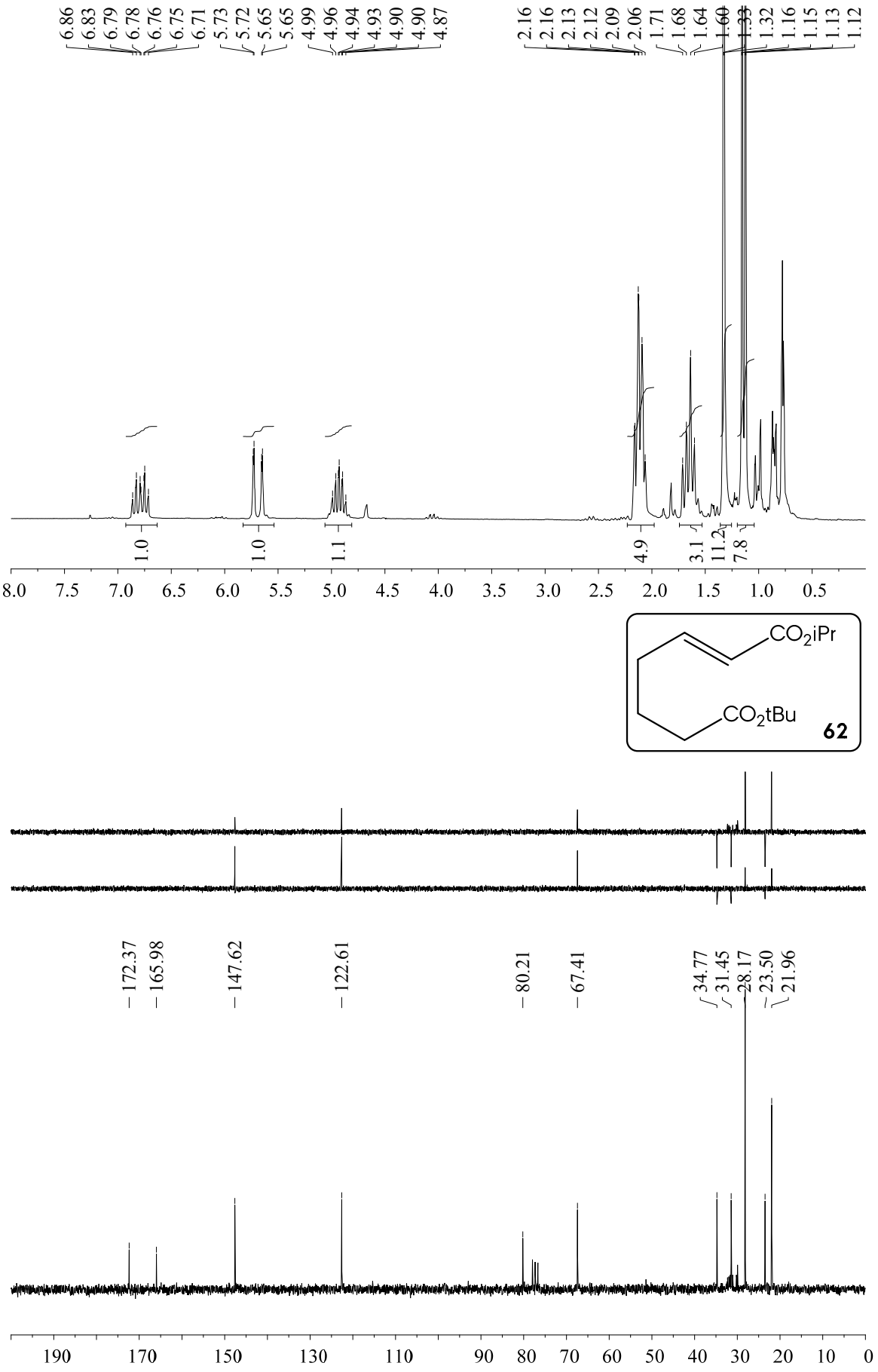
6.86
6.83
6.79
6.78
6.76
6.75
6.71
5.73
5.72
5.65
5.65
4.99
4.96
4.94
4.93
4.90
4.90
4.87
2.16
2.16
2.13
2.12
2.09
2.06
1.71
1.68
1.64
1.60
1.33
1.32
1.16
1.15
1.13
1.12
1.0
1.0
1.1
4.9
3.1
11.2
7.8
8.0 7.5 7.0 6.5 6.0 5.5 5.0 4.5 4.0 3.5 3.0 2.5 2.0 1.5 1.0 0.5
CO2iPr
CO2tBu
62
172.37
165.98
147.62
122.61
80.21
67.41
34.77
31.45
28.17
23.50
21.96
190 170 150 130 110 90 80 70 60 50 40 30 20 10 0

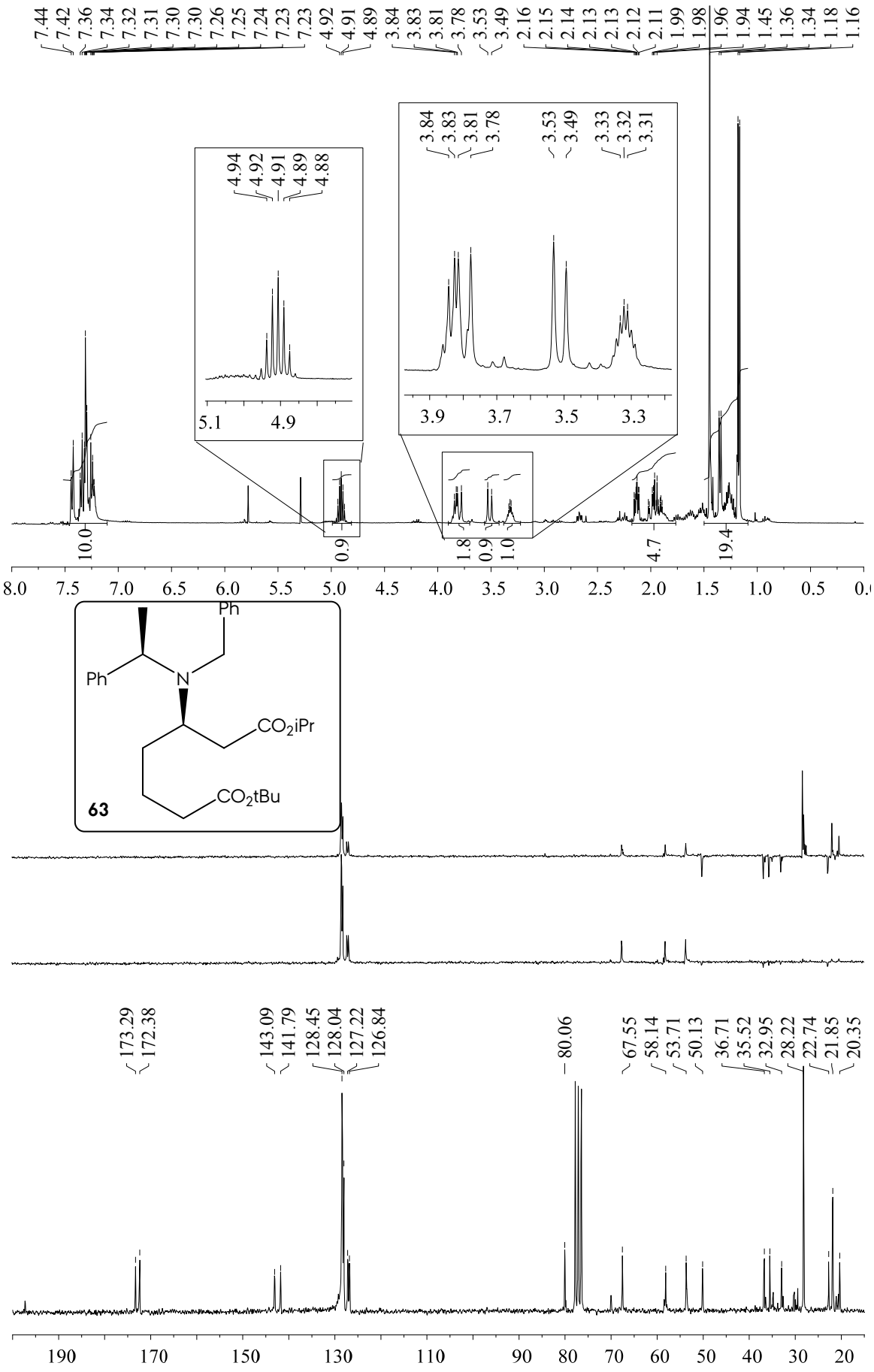
7.44 7.42 7.36 7.34 7.32 7.31 7.30 7.30 7.26 7.25 7.24 7.23 7.23 4.92 4.91 4.89 3.84 3.83 3.81 3.78 3.53 3.49 2.16 2.15 2.14 2.13 2.13 2.12 2.11 1.99 1.98 1.96 1.94 1.45 1.36 1.34 1.18 1.16
4.94 4.92 4.91 4.89 4.88
5.1 4.9
3.84 3.83 3.81 3.78 3.53 3.49 3.33 3.32 3.31
3.9 3.7 3.5 3.3
10.0 0.9 1.8 0.9 1.0 4.7 19.4
8.0 7.5 7.0 6.5 6.0 5.5 5.0 4.5 4.0 3.5 3.0 2.5 2.0 1.5 1.0 0.5
Ph
Ph
N
CO2iPr
CO2tBu
63
173.29 172.38 143.09 141.79 128.45 128.04 127.22 126.84 80.06 67.55 58.14 53.71 50.13 36.71 35.52 32.95 28.22 22.74 21.85 20.35
190 170 150 130 110 90 80 70 60 50 40 30 20

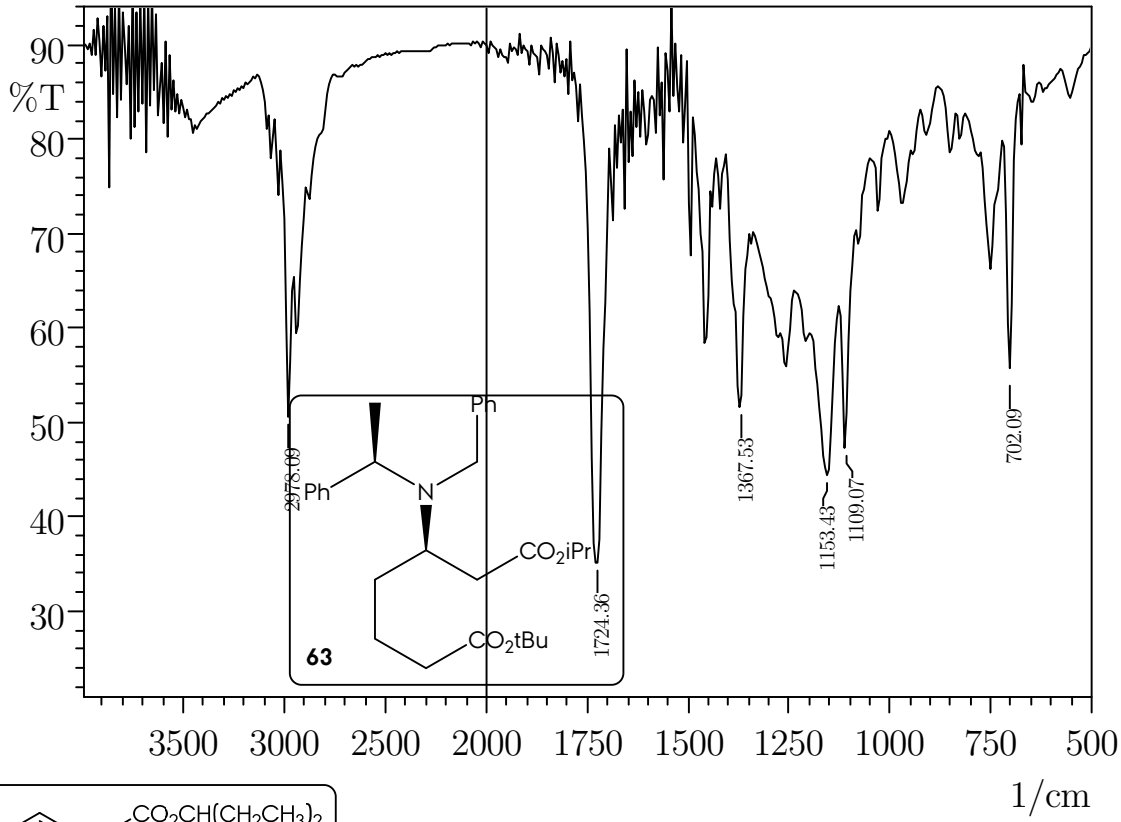
%T
90
80
70
60
50
40
30
3500 3000 2500 2000 1750 1500 1250 1000 750 500
1/cm
2978.09
1724.36
1367.53
1153.43
1109.07
702.09
Ph
Ph
N
CO2iPr
CO2tBu
63

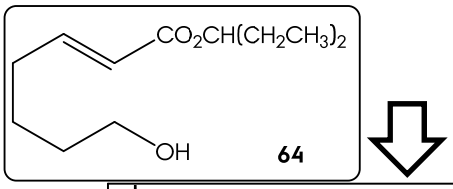
CO2CH(CH2CH3)2
OH
64

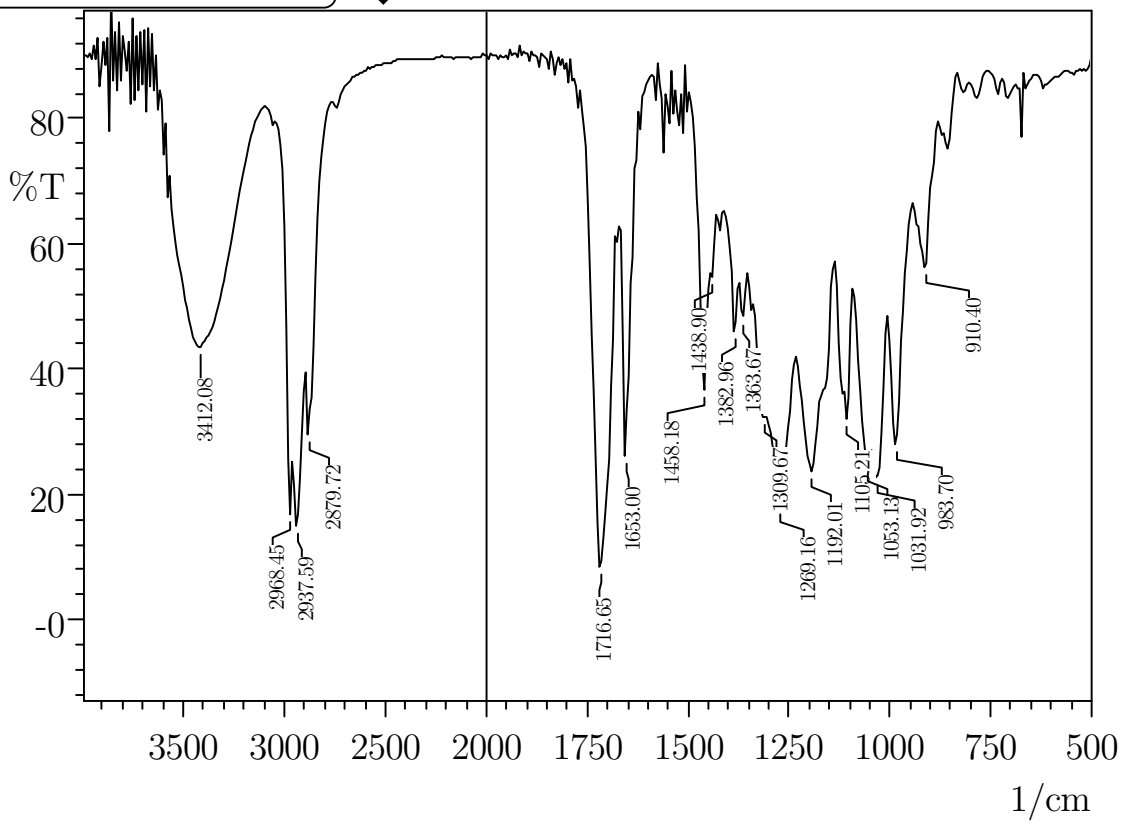
%T
80
60
40
20
-0
3500 3000 2500 2000 1750 1500 1250 1000 750 500
1/cm
3412.08
2968.45
2937.59
2879.72
1716.65
1653.00
1458.18
1438.90
1382.96
1363.67
1309.67
1269.16
1192.01
1105.21
1053.13
1031.92
983.70
910.40

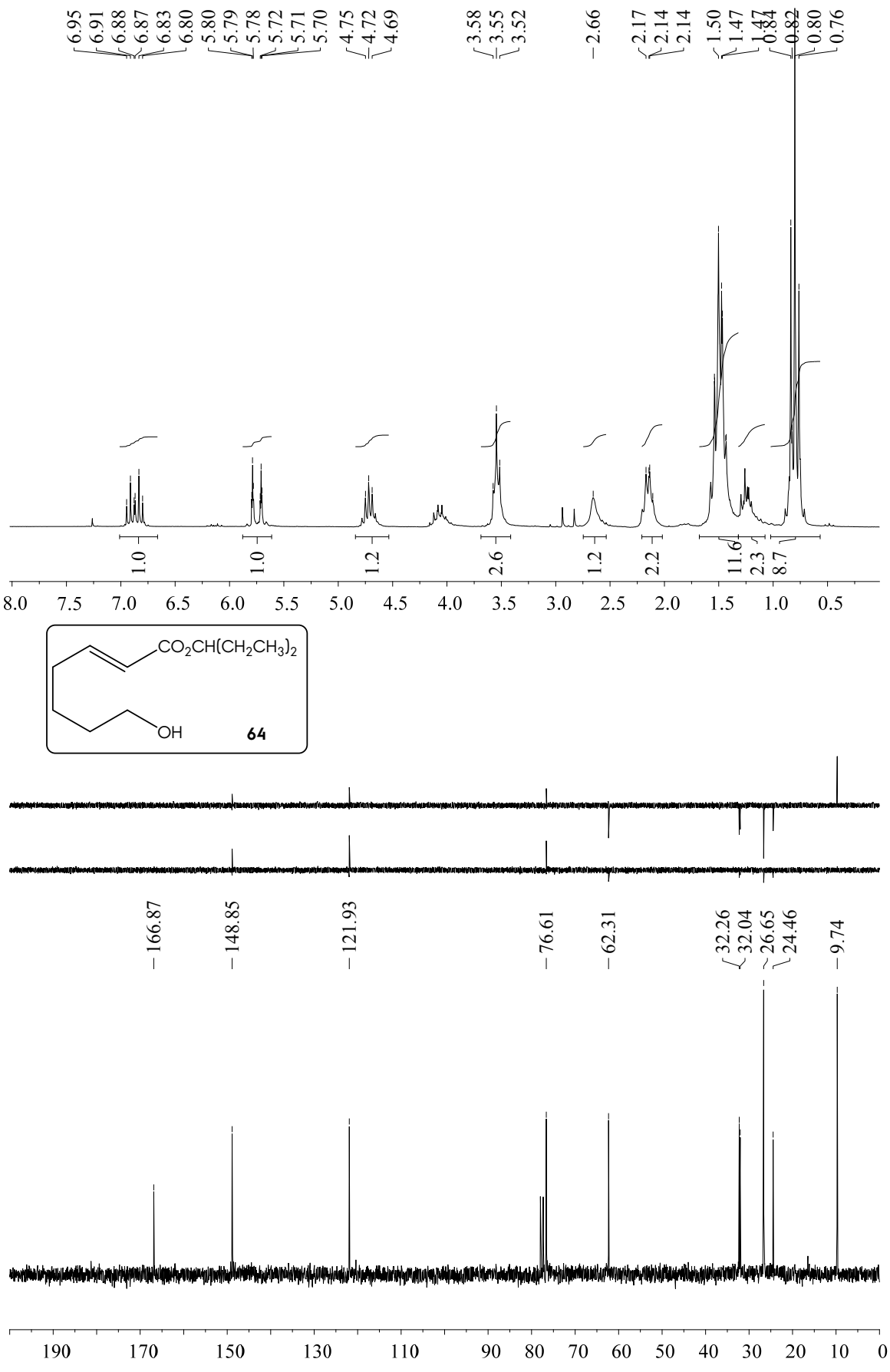
6.95
6.91
6.88
6.87
6.83
6.80
5.80
5.79
5.78
5.72
5.71
5.70
4.75
4.72
4.69
3.58
3.55
3.52
2.66
2.17
2.14
2.14
1.50
1.47
1.47
0.84
0.82
0.80
0.76
1.0
1.0
1.2
2.6
1.2
2.2
11.6
2.3
8.7
8.0 7.5 7.0 6.5 6.0 5.5 5.0 4.5 4.0 3.5 3.0 2.5 2.0 1.5 1.0 0.5
CO2CH(CH2CH3)2
OH
64
166.87
148.85
121.93
76.61
62.31
32.26
32.04
26.65
24.46
9.74
190 170 150 130 110 90 80 70 60 50 40 30 20 10 0

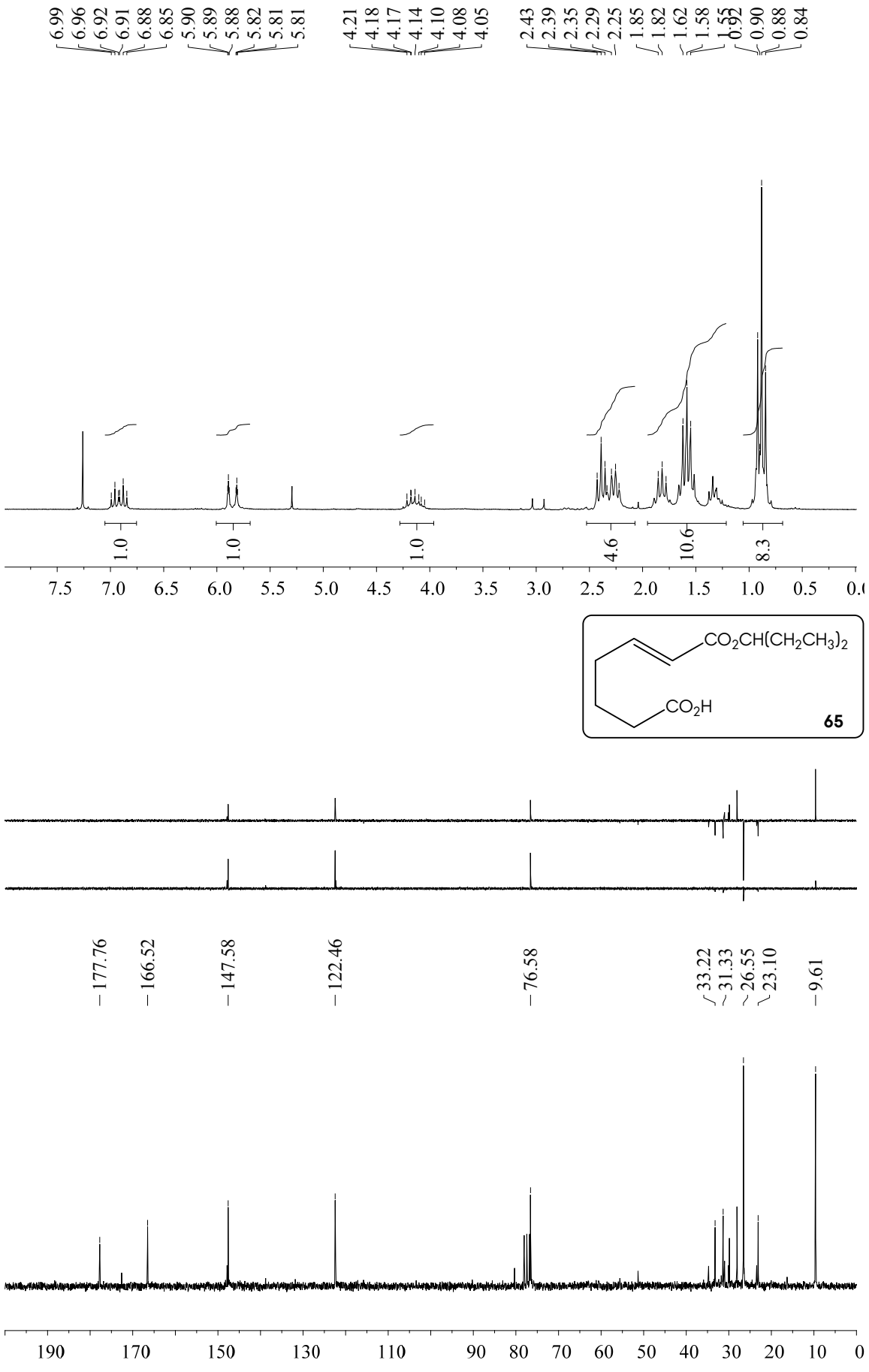
6.99
6.96
6.92
6.91
6.88
6.85
5.90
5.89
5.88
5.82
5.81
5.81
4.21
4.18
4.17
4.14
4.10
4.08
4.05
2.43
2.39
2.35
2.29
2.25
1.85
1.82
1.62
1.58
1.55
0.92
0.90
0.88
0.84
1.0
1.0
1.0
4.6
10.6
8.3
7.5
7.0
6.5
6.0
5.5
5.0
4.5
4.0
3.5
3.0
2.5
2.0
1.5
1.0
0.5
CO2CH(CH2CH3)2
CO2H
65
177.76
166.52
147.58
122.46
76.58
33.22
31.33
26.55
23.10
9.61
190
170
150
130
110
90
80
70
60
50
40
30
20
10
0

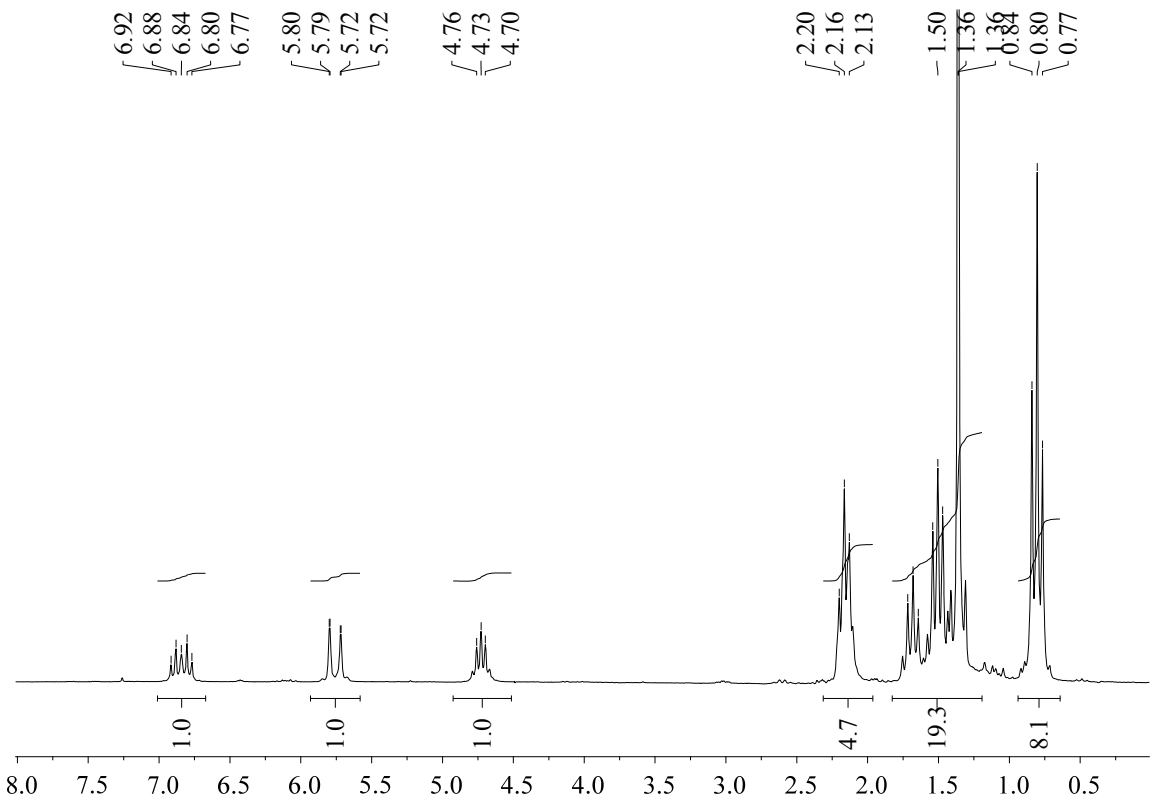
6.92
6.88
6.84
6.80
6.77
5.80
5.79
5.72
5.72
4.76
4.73
4.70
2.20
2.16
2.13
1.50
1.36
1.36
0.84
0.80
0.77
1.0
1.0
1.0
4.7
19.3
8.1
8.0 7.5 7.0 6.5 6.0 5.5 5.0 4.5 4.0 3.5 3.0 2.5 2.0 1.5 1.0 0.5

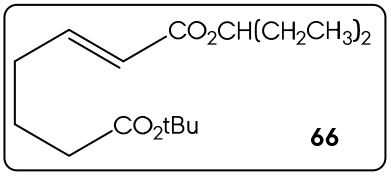
CO2CH(CH2CH3)2
CO2tBu
66

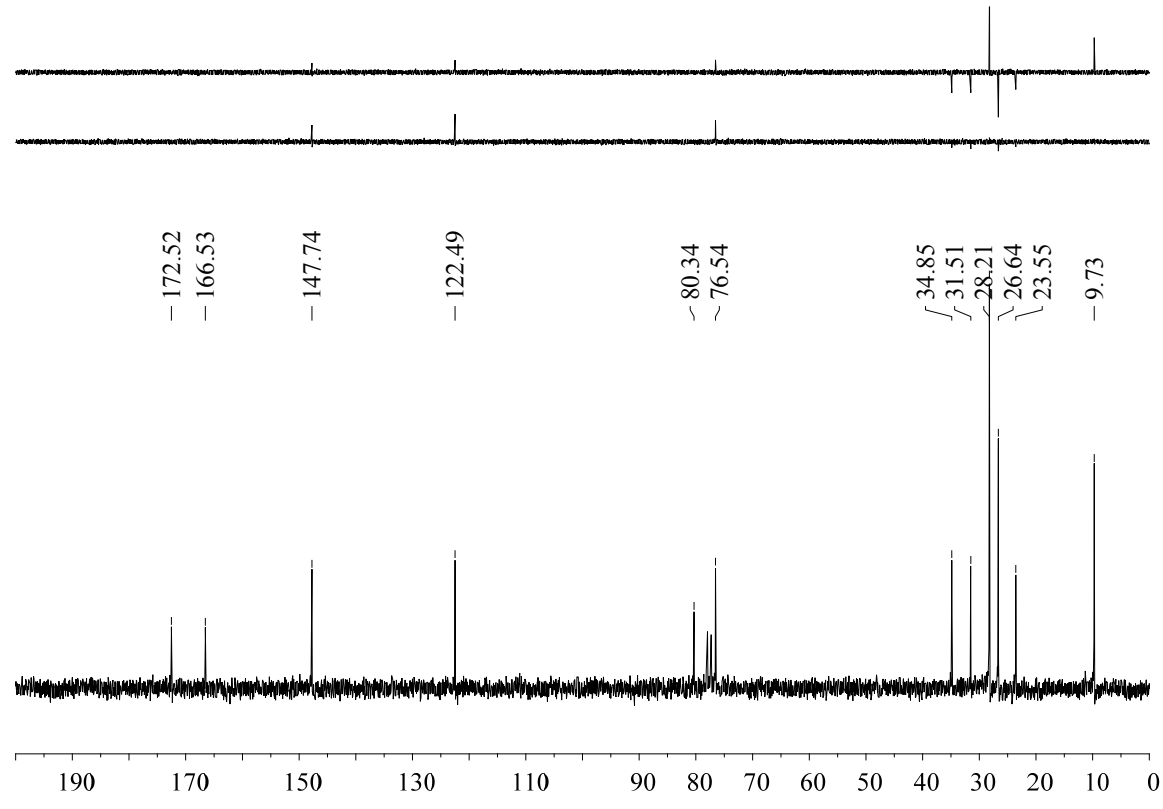
172.52
166.53
147.74
122.49
80.34
76.54
34.85
31.51
28.21
26.64
23.55
9.73
190 170 150 130 110 90 80 70 60 50 40 30 20 10 0

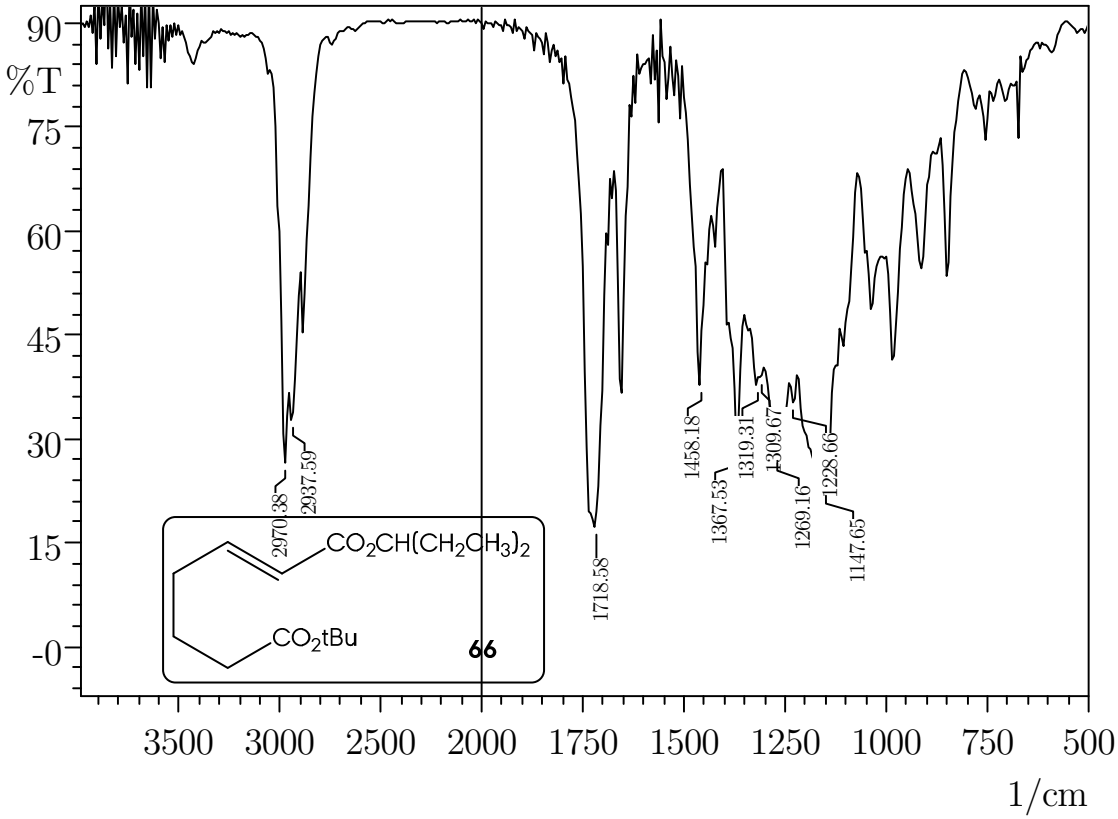
%T
90
75
60
45
30
15
-0
2970.38
2937.59
1718.58
1458.18
1367.53
1319.31
1309.67
1269.16
1228.66
1147.65
$CO_2CH(CH_2CH_3)_2$
CO_2tBu
66
3500 3000 2500 2000 1750 1500 1250 1000 750 500
1/cm

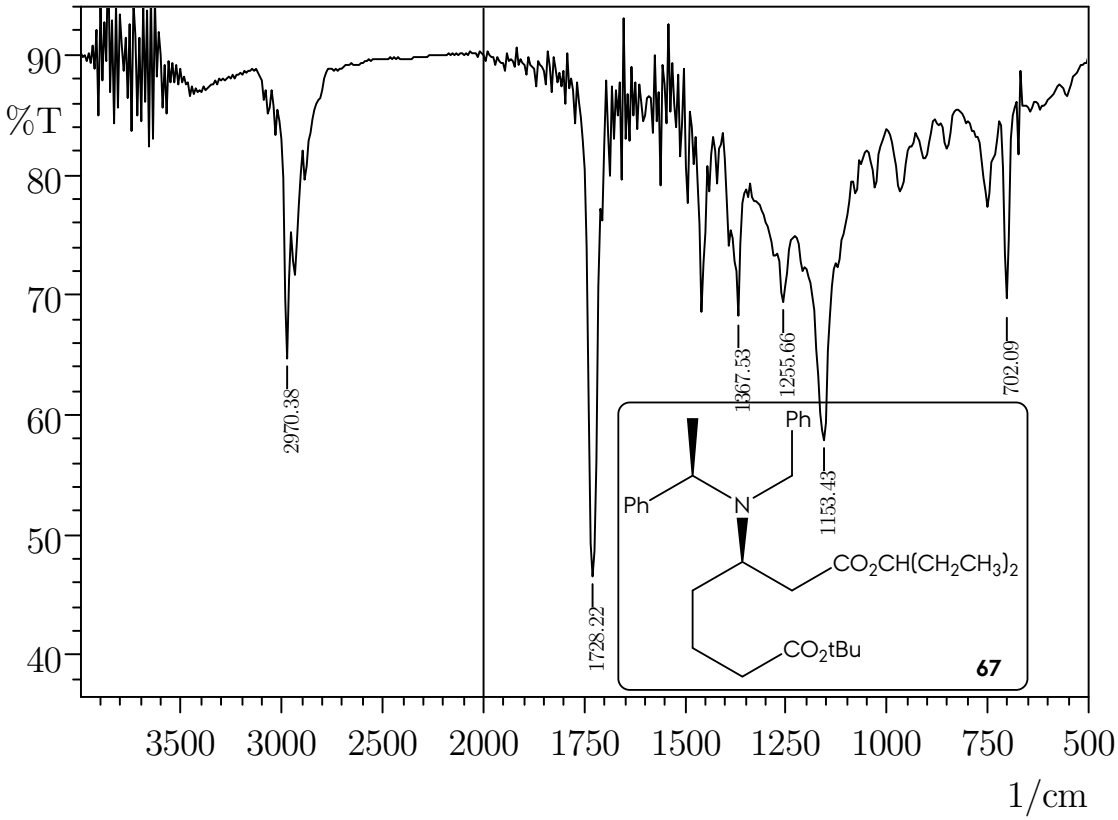
%T
90
80
70
60
50
40
2970.38
1728.22
1367.53
1255.66
1153.43
702.09
Ph
Ph
N
$CO_2CH(CH_2CH_3)_2$
CO_2tBu
67
3500 3000 2500 2000 1750 1500 1250 1000 750 500
1/cm

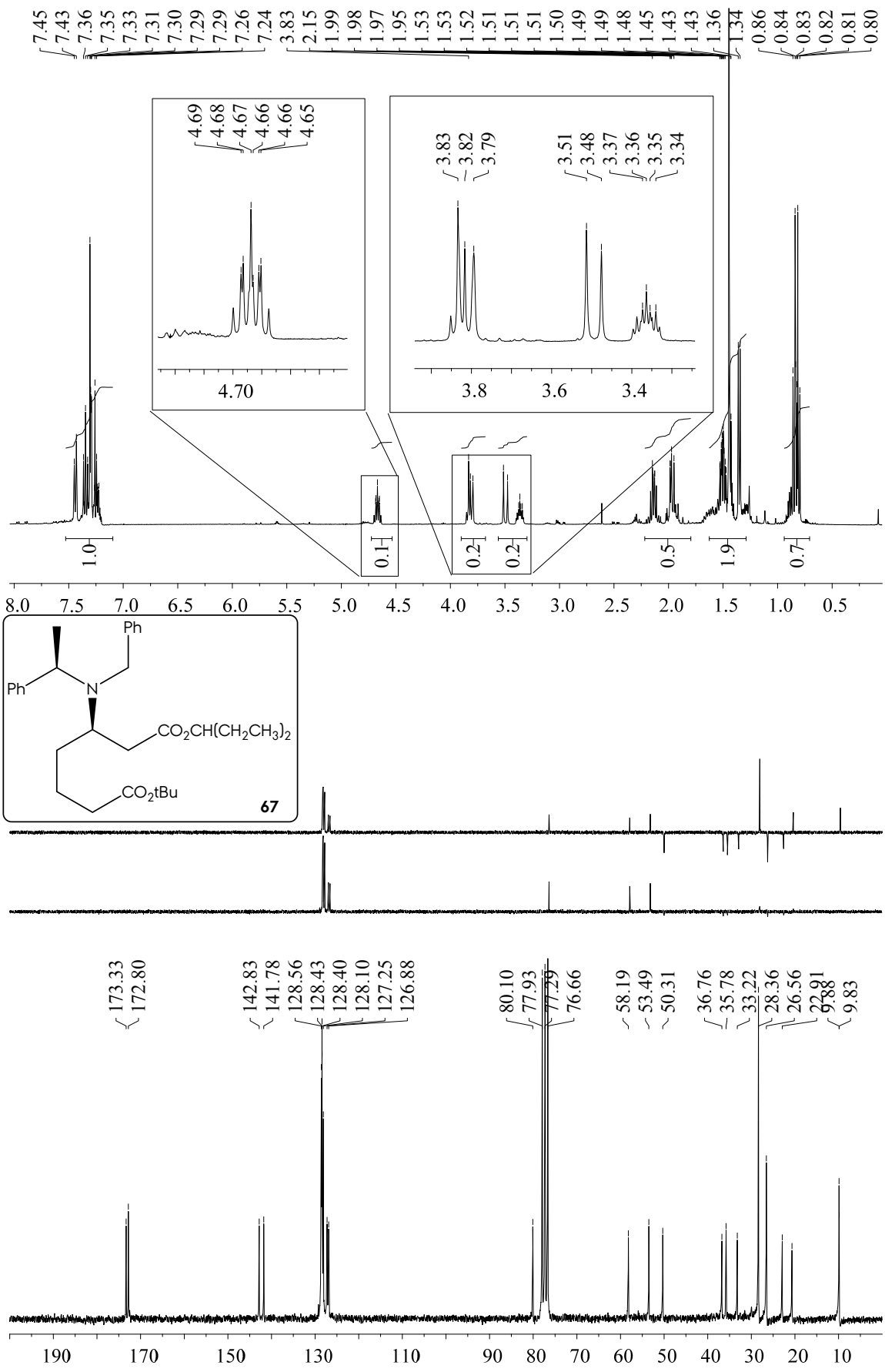
7.45 7.43 7.36 7.35 7.33 7.31 7.30 7.29 7.29 7.26 7.24
3.83 2.15 1.99 1.98 1.97 1.95 1.53 1.53 1.52 1.51 1.51 1.51 1.50 1.49 1.49 1.48 1.45 1.43 1.43 1.36 1.34 0.86 0.84 0.83 0.82 0.81 0.80
4.69 4.68 4.67 4.66 4.66 4.65
4.70
3.83 3.82 3.79 3.51 3.48 3.37 3.36 3.35 3.34
3.8 3.6 3.4
1.0 0.1 0.2 0.2 0.5 1.9 0.7
8.0 7.5 7.0 6.5 6.0 5.5 5.0 4.5 4.0 3.5 3.0 2.5 2.0 1.5 1.0 0.5
Ph
Ph
N
CO2CH(CH2CH3)2
CO2tBu
67
173.33 172.80 142.83 141.78 128.56 128.43 128.40 128.10 127.25 126.88 80.10 77.93 77.29 76.66 58.19 53.49 50.31 36.76 35.78 33.22 28.36 26.56 22.91 9.88 9.83
190 170 150 130 110 90 80 70 60 50 40 30 20 10

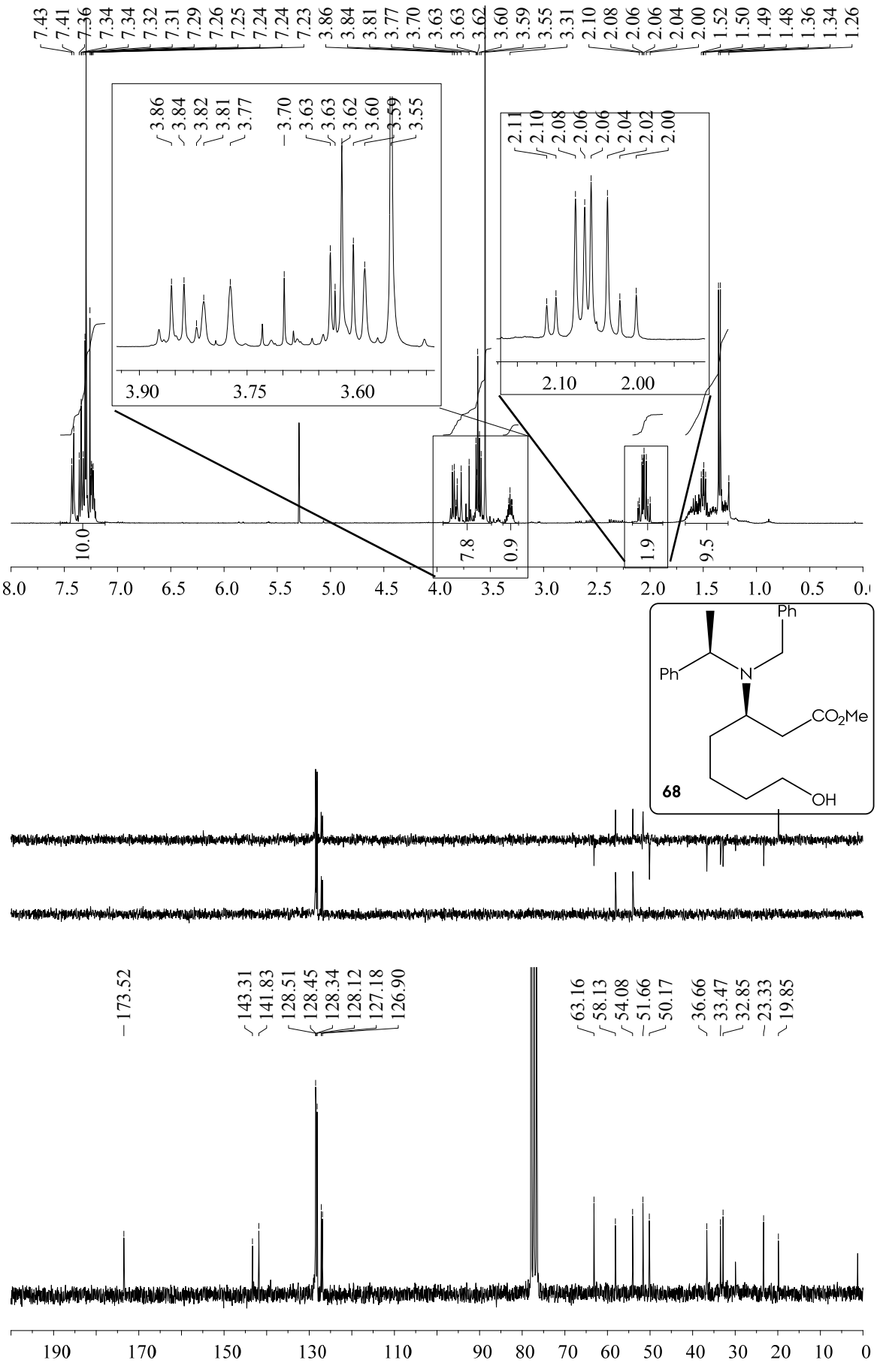
7.43 7.41 7.36 7.34 7.34 7.32 7.31 7.29 7.26 7.25 7.24 7.24 7.23
3.86 3.84 3.81 3.77 3.70 3.63 3.63 3.62 3.60 3.59 3.55 3.31
2.10 2.08 2.06 2.06 2.04 2.00 1.52 1.50 1.49 1.48 1.36 1.34 1.26
3.90 3.75 3.60
2.10 2.00
10.0 7.8 0.9 1.9 9.5
8.0 7.5 7.0 6.5 6.0 5.5 5.0 4.5 4.0 3.5 3.0 2.5 2.0 1.5 1.0 0.5
Ph
Ph
N
CO2Me
OH
68
173.52
143.31 141.83 128.51 128.45 128.34 128.12 127.18 126.90
63.16 58.13 54.08 51.66 50.17 36.66 33.47 32.85 23.33 19.85
190 170 150 130 110 90 80 70 60 50 40 30 20 10 0

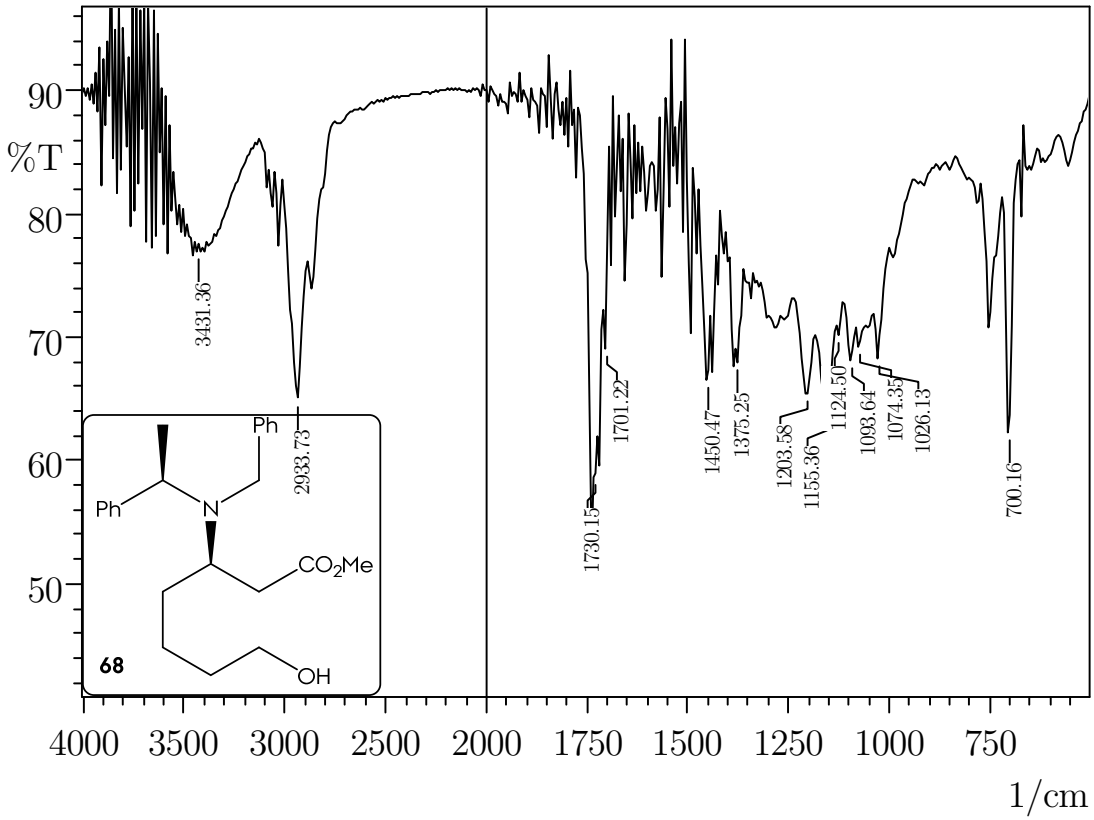
%T
90
80
70
60
50
4000 3500 3000 2500 2000 1750 1500 1250 1000 750
1/cm
3431.36
2933.73
1730.15
1701.22
1450.47
1375.25
1203.58
1155.36
1124.50
1093.64
1074.35
1026.13
700.16
Ph
N
Ph
CO2Me
OH
68

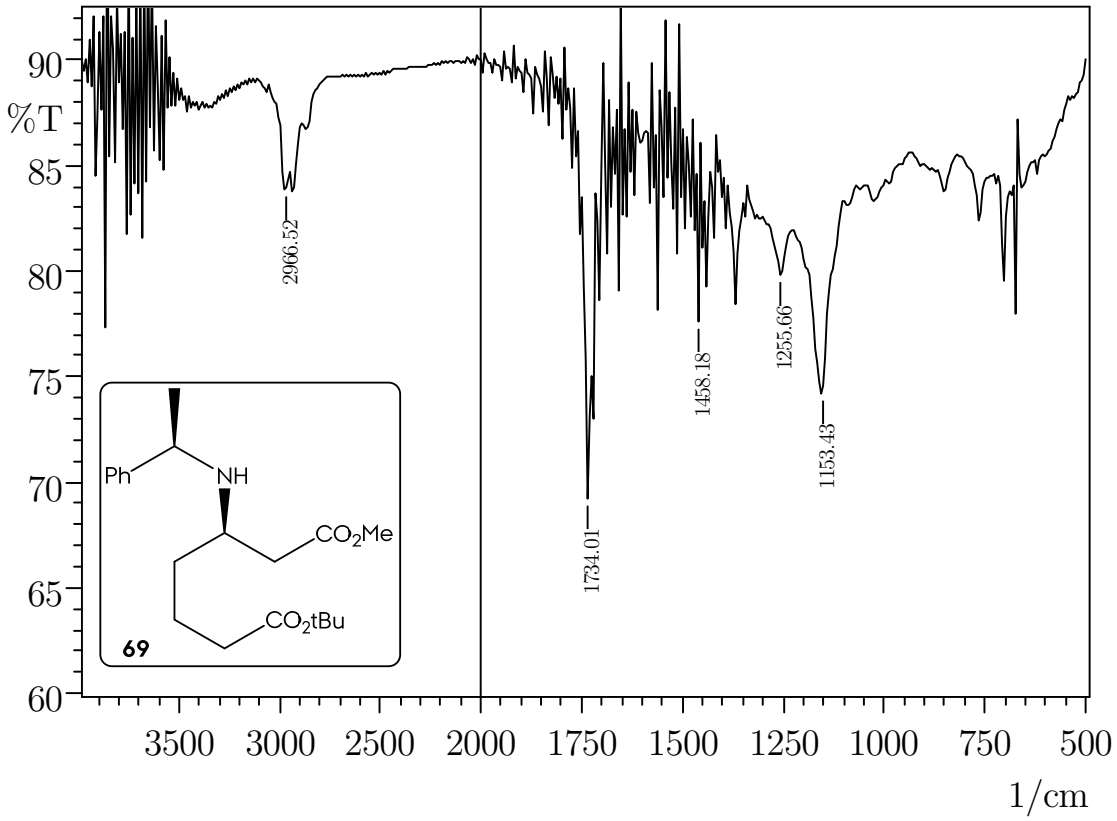
%T
90
85
80
75
70
65
60
3500 3000 2500 2000 1750 1500 1250 1000 750 500
1/cm
2966.52
1734.01
1458.18
1255.66
1153.43
Ph
NH
CO2Me
CO2tBu
69

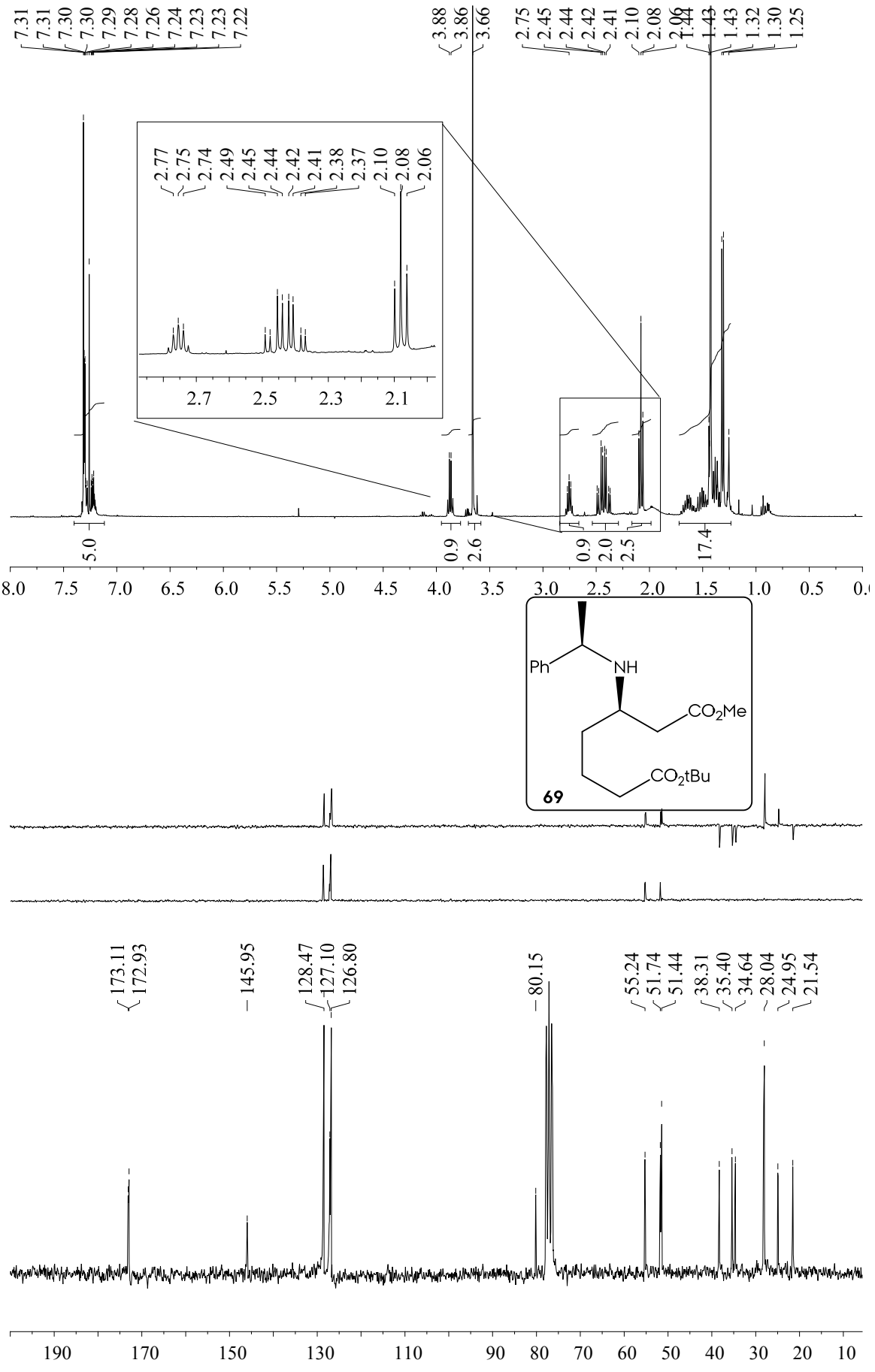
7.31
7.31
7.30
7.30
7.29
7.28
7.26
7.24
7.23
7.23
7.22
3.88
3.86
3.66
2.75
2.45
2.44
2.42
2.41
2.10
2.08
2.06
1.44
1.43
1.43
1.32
1.30
1.25
2.77
2.75
2.74
2.49
2.45
2.44
2.42
2.41
2.38
2.37
2.10
2.08
2.06
2.7
2.5
2.3
2.1
5.0
0.9
2.6
0.9
2.0
2.5
17.4
8.0
7.5
7.0
6.5
6.0
5.5
5.0
4.5
4.0
3.5
3.0
2.5
2.0
1.5
1.0
0.5
Ph
NH
CO2Me
CO2tBu
69
173.11
172.93
145.95
128.47
127.10
126.80
80.15
55.24
51.74
51.44
38.31
35.40
34.64
28.04
24.95
21.54
190
170
150
130
110
90
80
70
60
50
40
30
20
10

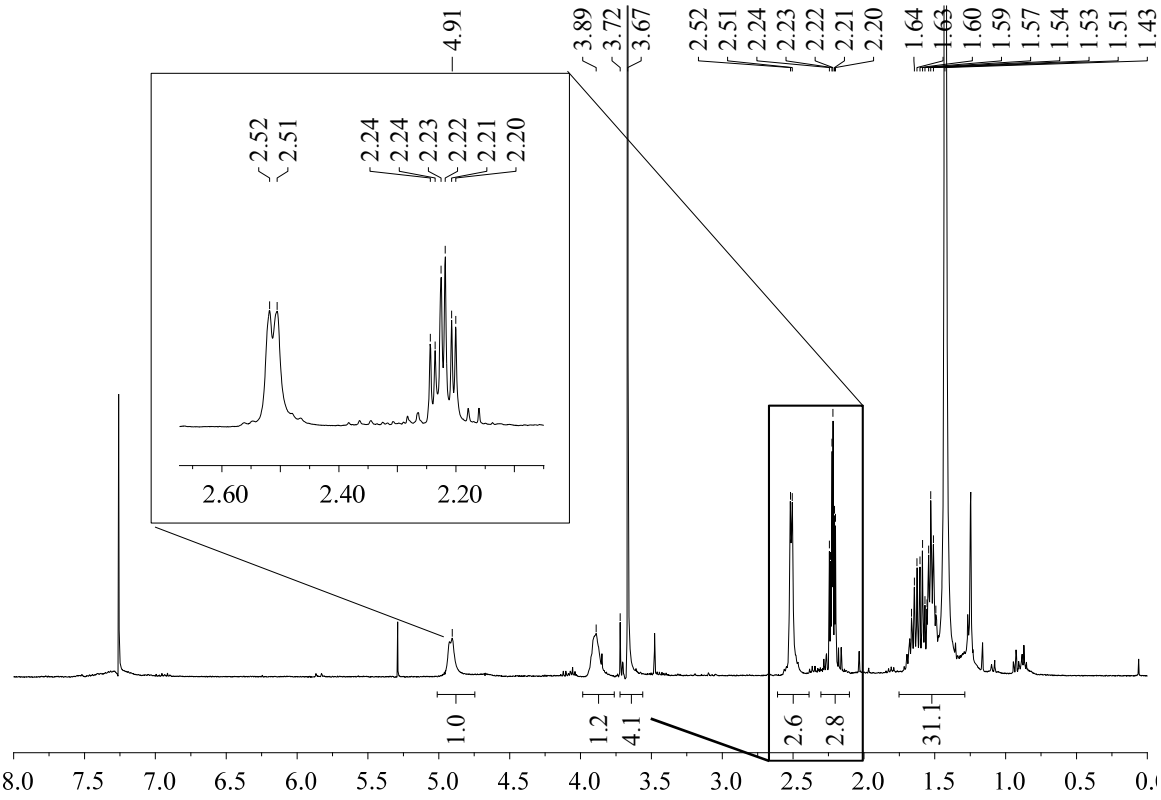
4.91
3.89
3.72
3.67
2.52
2.51
2.24
2.23
2.22
2.21
2.20
1.64
1.63
1.60
1.59
1.57
1.54
1.53
1.51
1.43
2.60
2.40
2.20
1.0
1.2
4.1
2.6
2.8
31.1
8.0
7.5
7.0
6.5
6.0
5.5
5.0
4.5
4.0
3.5
3.0
2.5
2.0
1.5
1.0
0.5

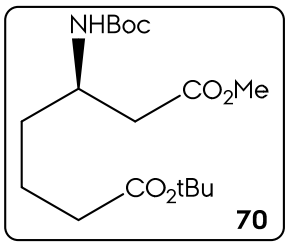
NHBoc
CO2Me
CO2tBu
70

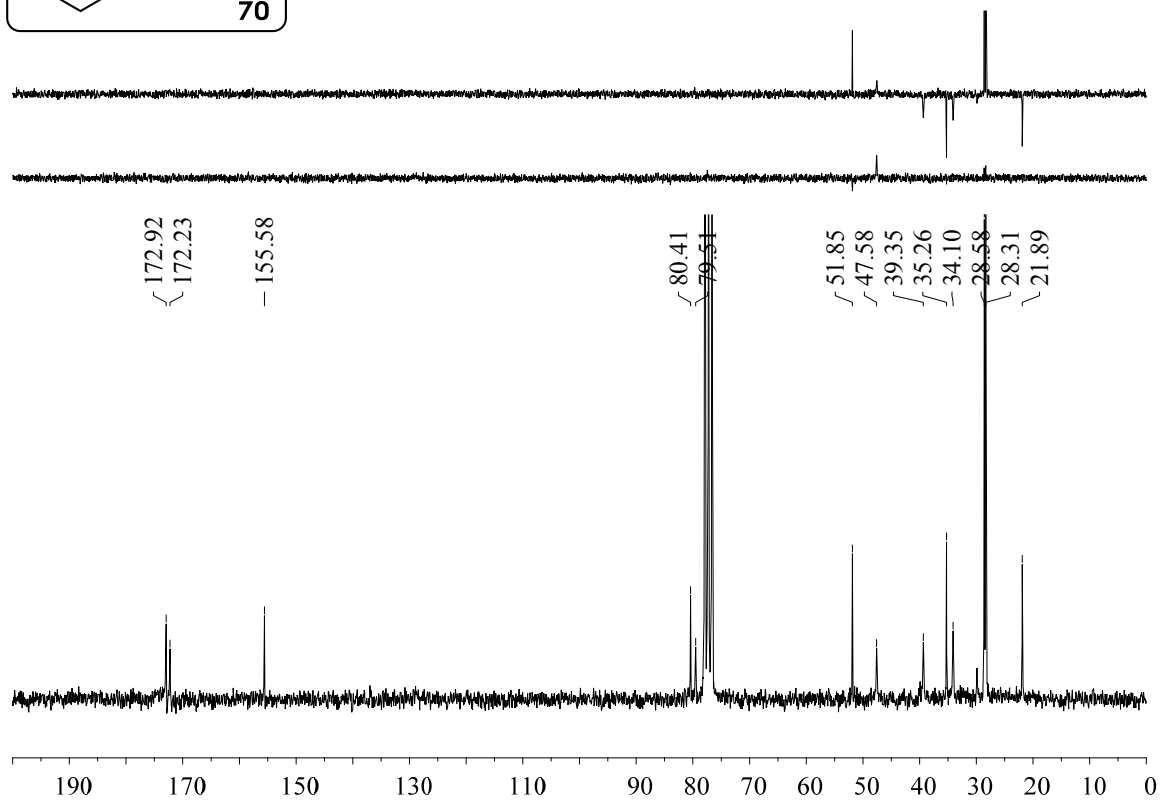
172.92
172.23
155.58
80.41
79.51
51.85
47.58
39.35
35.26
34.10
28.58
28.31
21.89
190
170
150
130
110
90
80
70
60
50
40
30
20
10
0

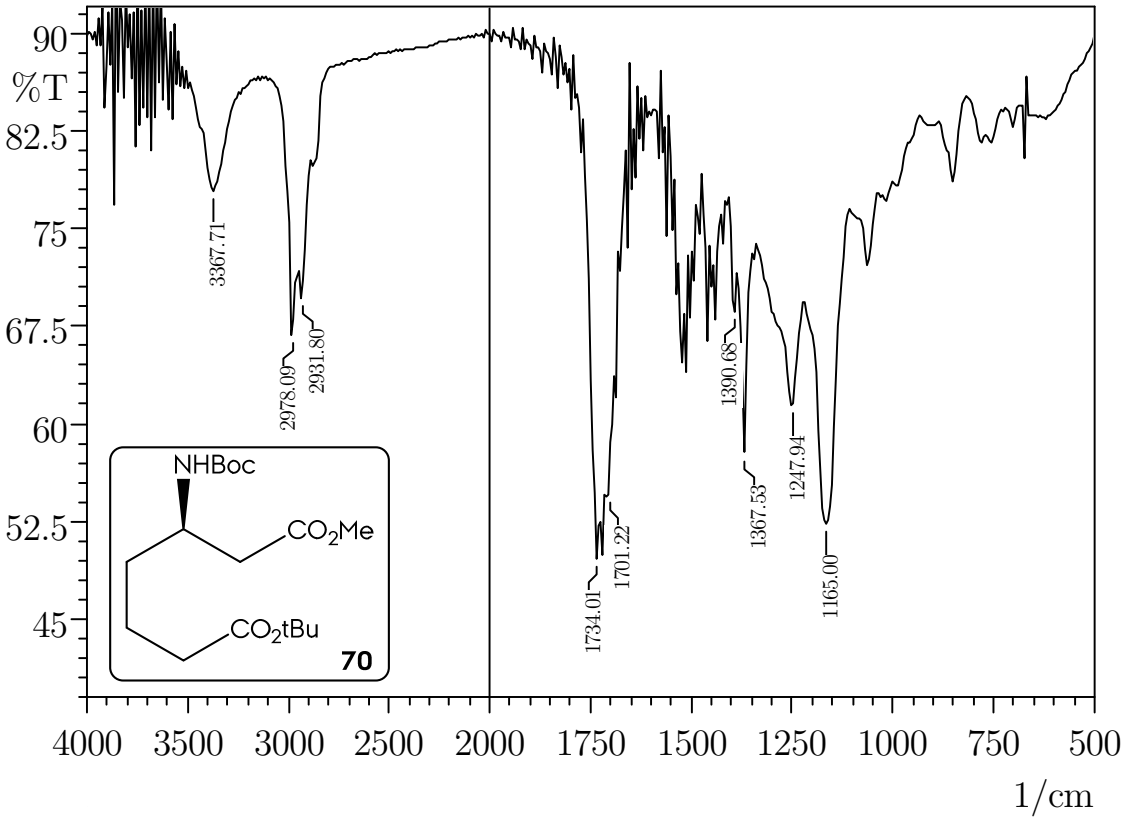
90
%T
82.5
75
67.5
60
52.5
45
3367.71
2978.09
2931.80
1734.01
1701.22
1390.68
1367.53
1247.94
1165.00
NHBoc
CO2Me
CO2tBu
70
4000 3500 3000 2500 2000 1750 1500 1250 1000 750 500
1/cm

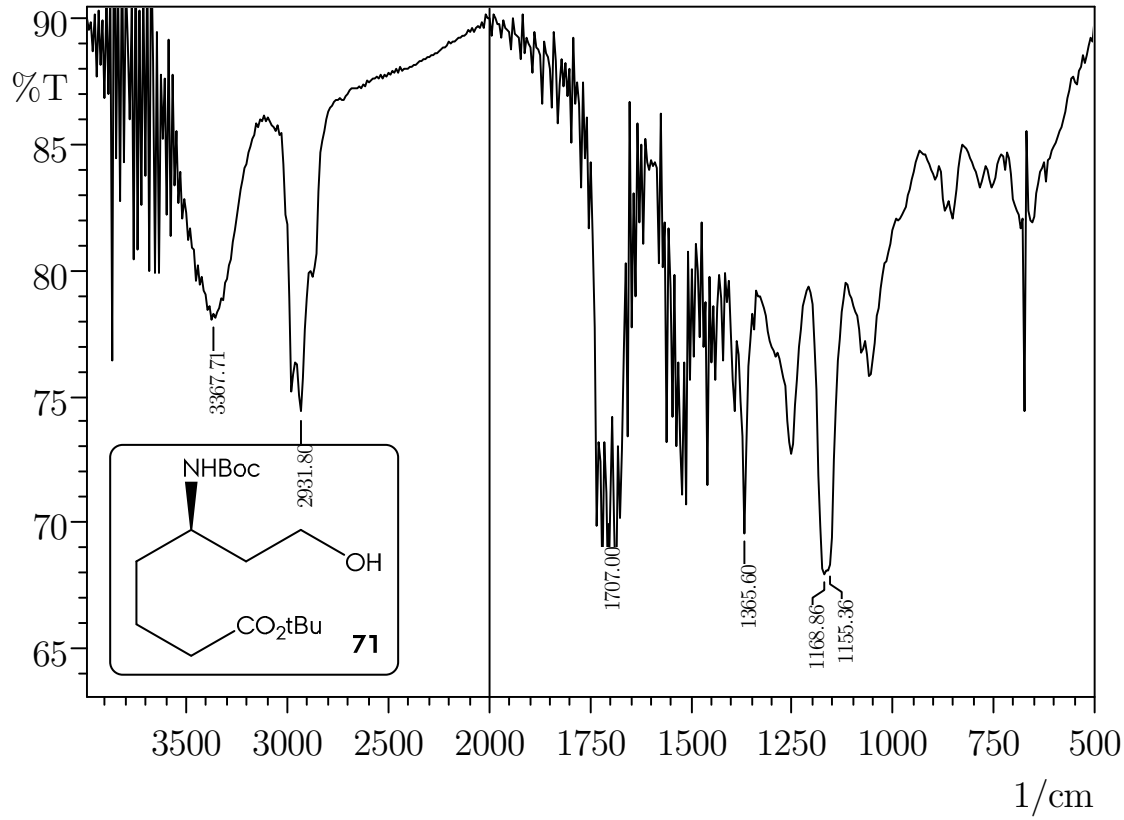
90
%T
85
80
75
70
65
3367.71
2931.80
1707.00
1365.60
1168.86
1155.36
NHBoc
OH
CO2tBu
71
3500 3000 2500 2000 1750 1500 1250 1000 750 500
1/cm

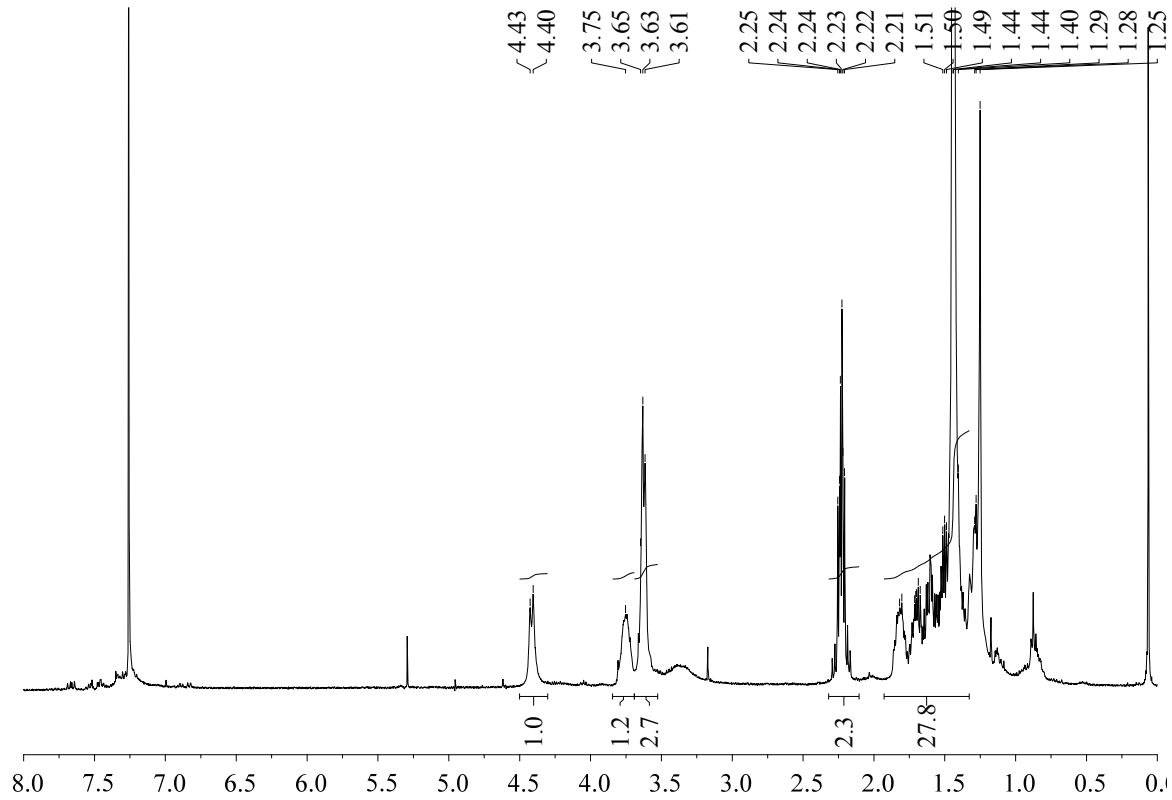
4.43
4.40
3.75
3.65
3.63
3.61
2.25
2.24
2.24
2.23
2.22
2.21
1.51
1.50
1.49
1.44
1.44
1.40
1.29
1.28
1.25
1.0
1.2
2.7
2.3
27.8
8.0
7.5
7.0
6.5
6.0
5.5
5.0
4.5
4.0
3.5
3.0
2.5
2.0
1.5
1.0
0.5

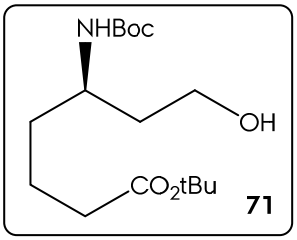
NHBoc
OH
CO2tBu
71

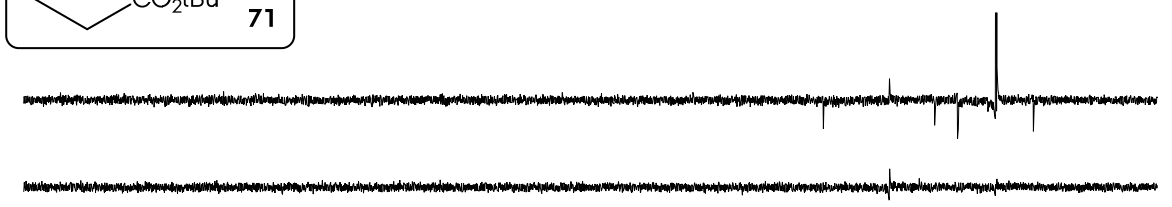

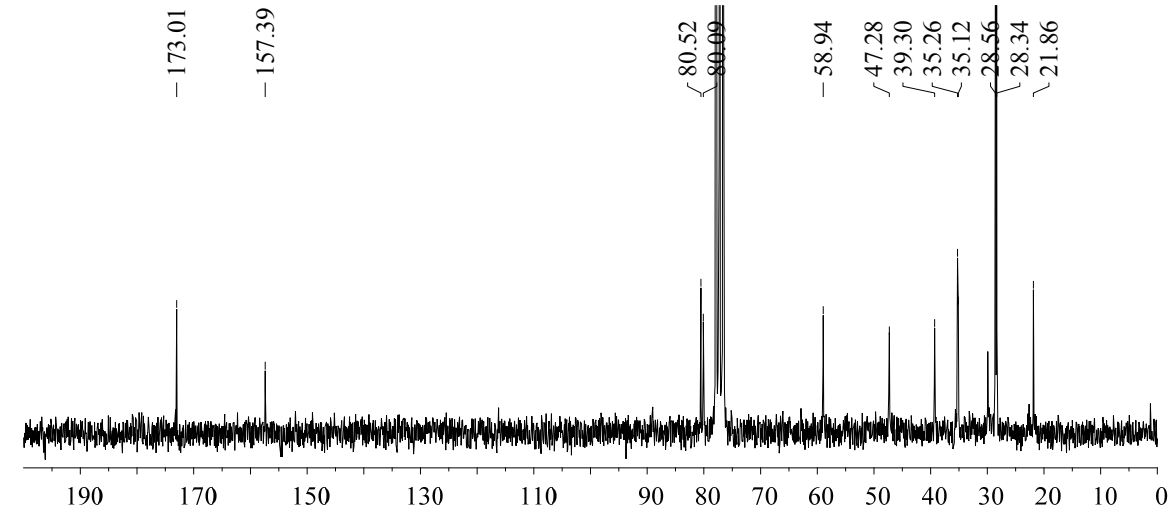
173.01
157.39
80.52
80.09
58.94
47.28
39.30
35.26
35.12
28.56
28.34
21.86
190
170
150
130
110
90
80
70
60
50
40
30
20
10
0

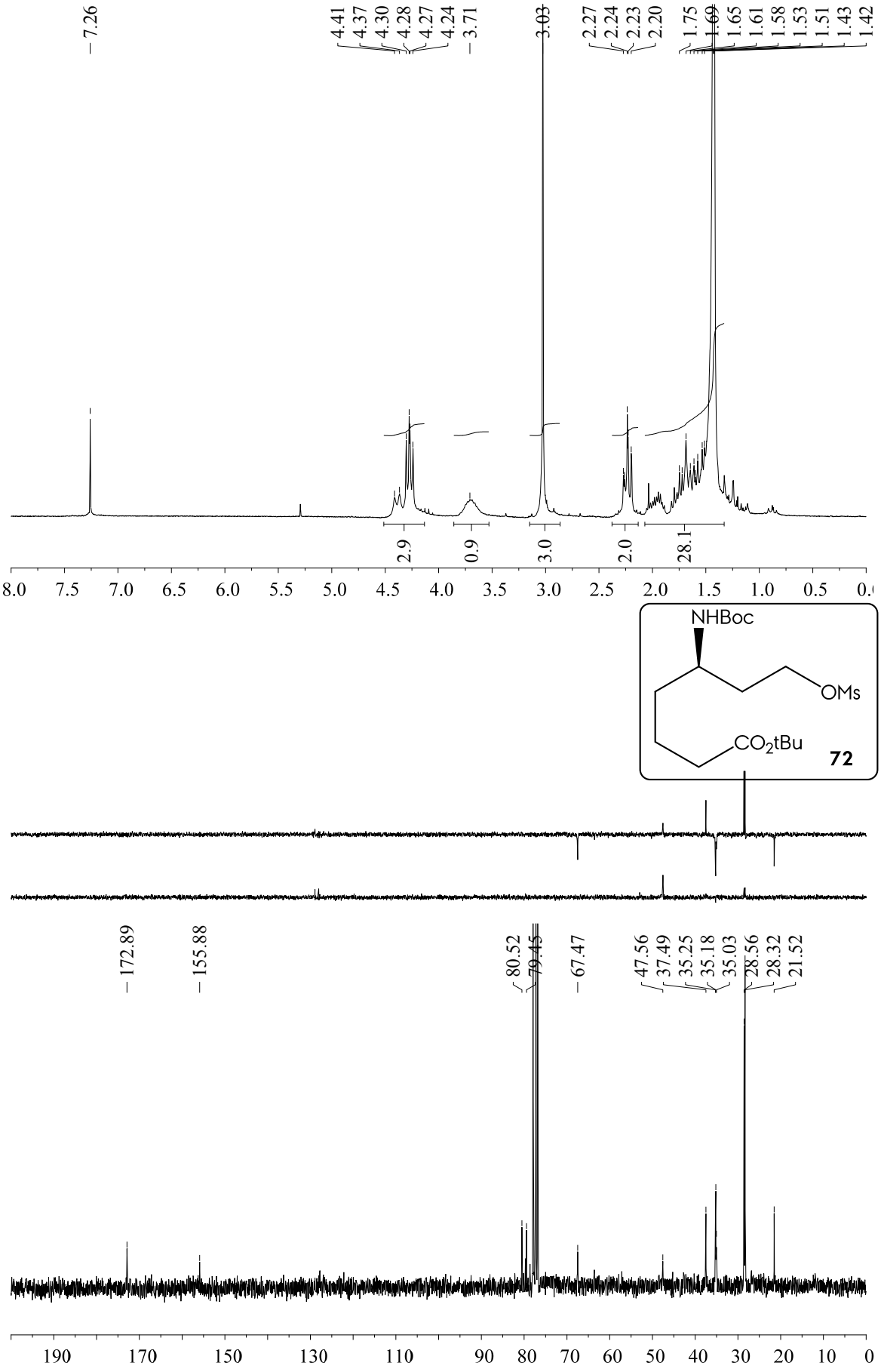
7.26
4.41
4.37
4.30
4.28
4.27
4.24
3.71
3.03
2.27
2.24
2.23
2.20
1.75
1.69
1.65
1.61
1.58
1.53
1.51
1.43
1.42
2.9
0.9
3.0
2.0
28.1
8.0 7.5 7.0 6.5 6.0 5.5 5.0 4.5 4.0 3.5 3.0 2.5 2.0 1.5 1.0 0.5
NHBoc
OMs
CO2tBu
72
172.89
155.88
80.52
79.45
67.47
47.56
37.49
35.25
35.18
35.03
28.56
28.32
21.52
190 170 150 130 110 90 80 70 60 50 40 30 20 10 0

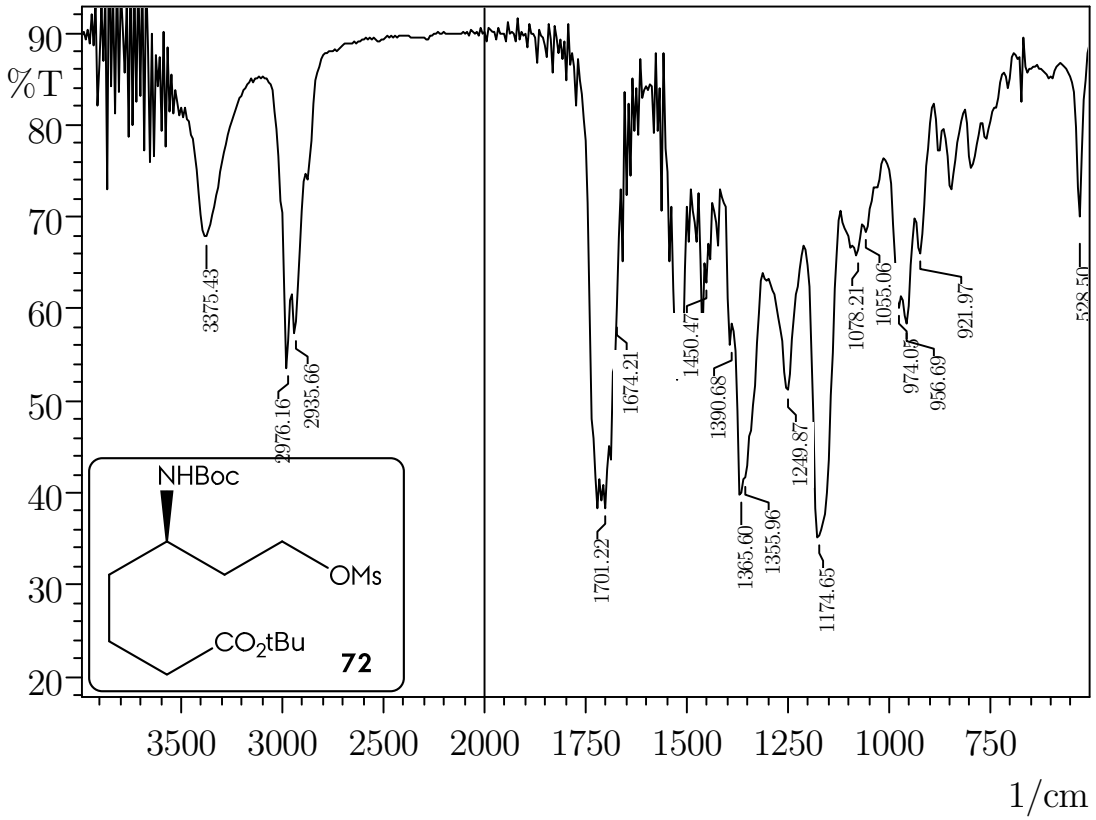
%T
90
80
70
60
50
40
30
20
3500
3000
2500
2000
1750
1500
1250
1000
750
1/cm
3375.43
2976.16
2935.66
1701.22
1674.21
1450.47
1390.68
1365.60
1355.96
1249.87
1174.65
1078.21
1055.06
974.05
956.69
921.97
528.50
NHBoc
OMs
CO2tBu
72

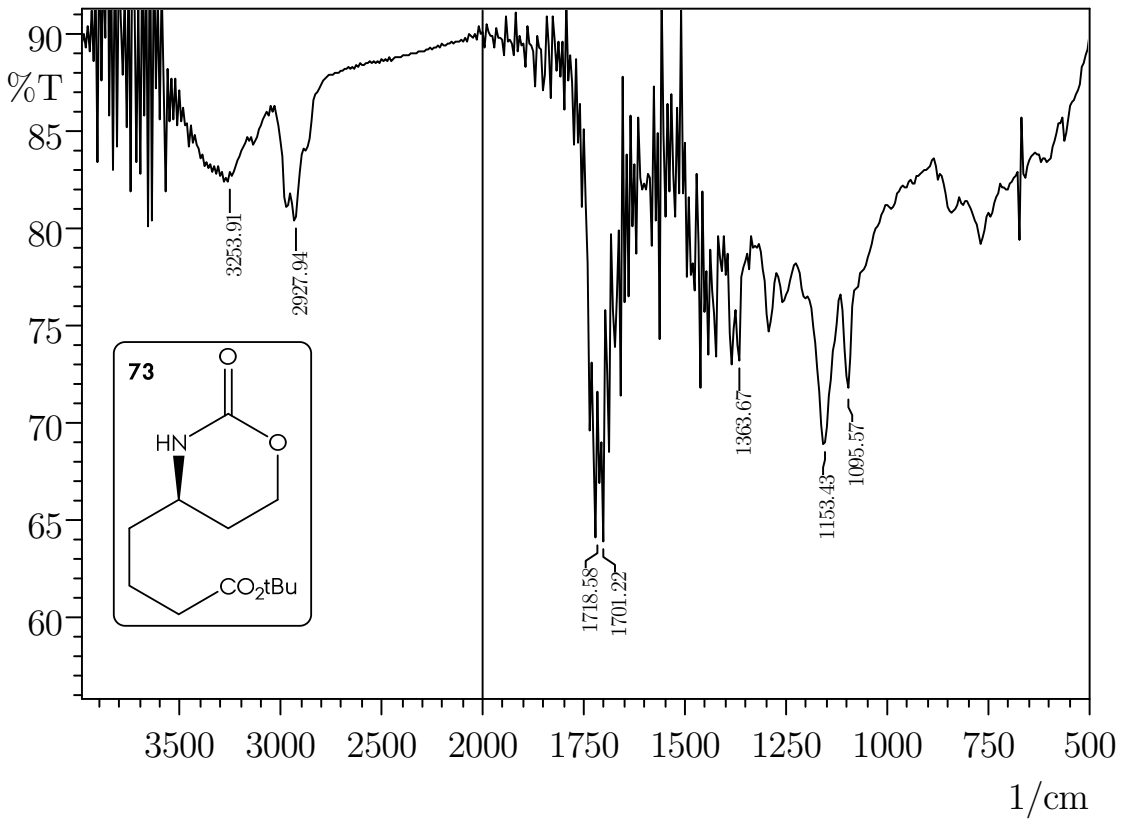
%T
90
85
80
75
70
65
60
3500
3000
2500
2000
1750
1500
1250
1000
750
500
1/cm
3253.91
2927.94
1718.58
1701.22
1363.67
1153.43
1095.57
73
HN
O
O
CO2tBu

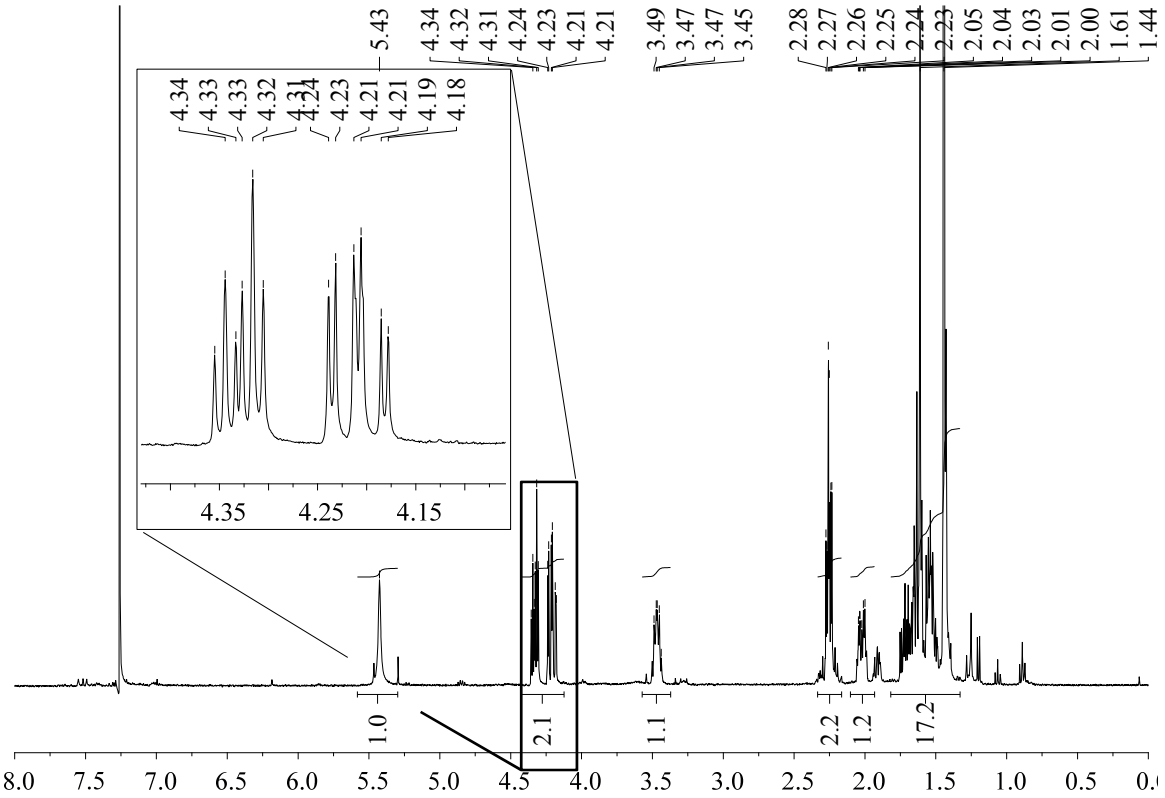
5.43
4.34
4.32
4.31
4.24
4.23
4.21
4.21
3.49
3.47
3.47
3.45
2.28
2.27
2.26
2.25
2.24
2.23
2.05
2.04
2.03
2.01
2.00
1.61
1.44
4.34
4.33
4.33
4.32
4.31
4.24
4.23
4.21
4.21
4.19
4.18
4.35
4.25
4.15
1.0
2.1
1.1
2.2
1.2
17.2
8.0
7.5
7.0
6.5
6.0
5.5
5.0
4.5
4.0
3.5
3.0
2.5
2.0
1.5
1.0
0.5

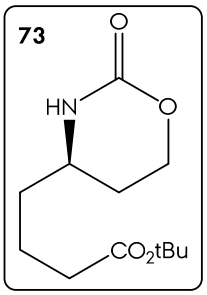
73
HN
O
O
CO2tBu

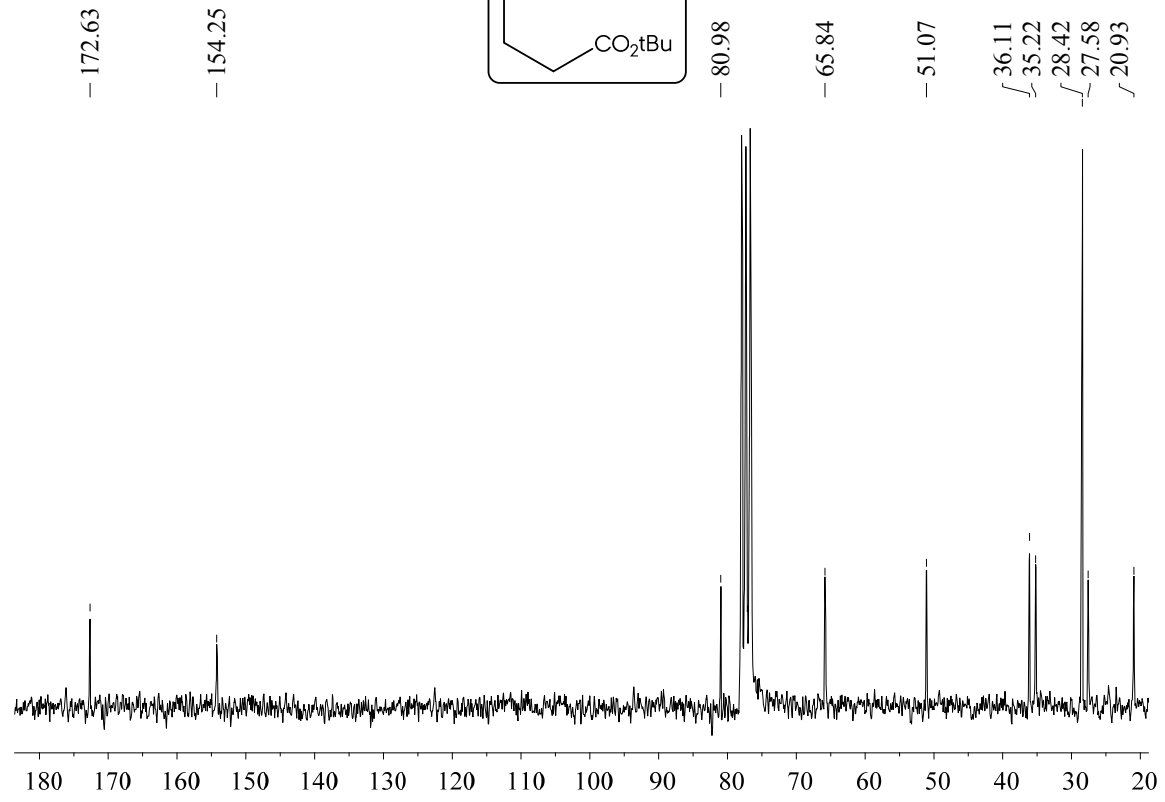
172.63
154.25
80.98
65.84
51.07
36.11
35.22
28.42
27.58
20.93
180
170
160
150
140
130
120
110
100
90
80
70
60
50
40
30
20

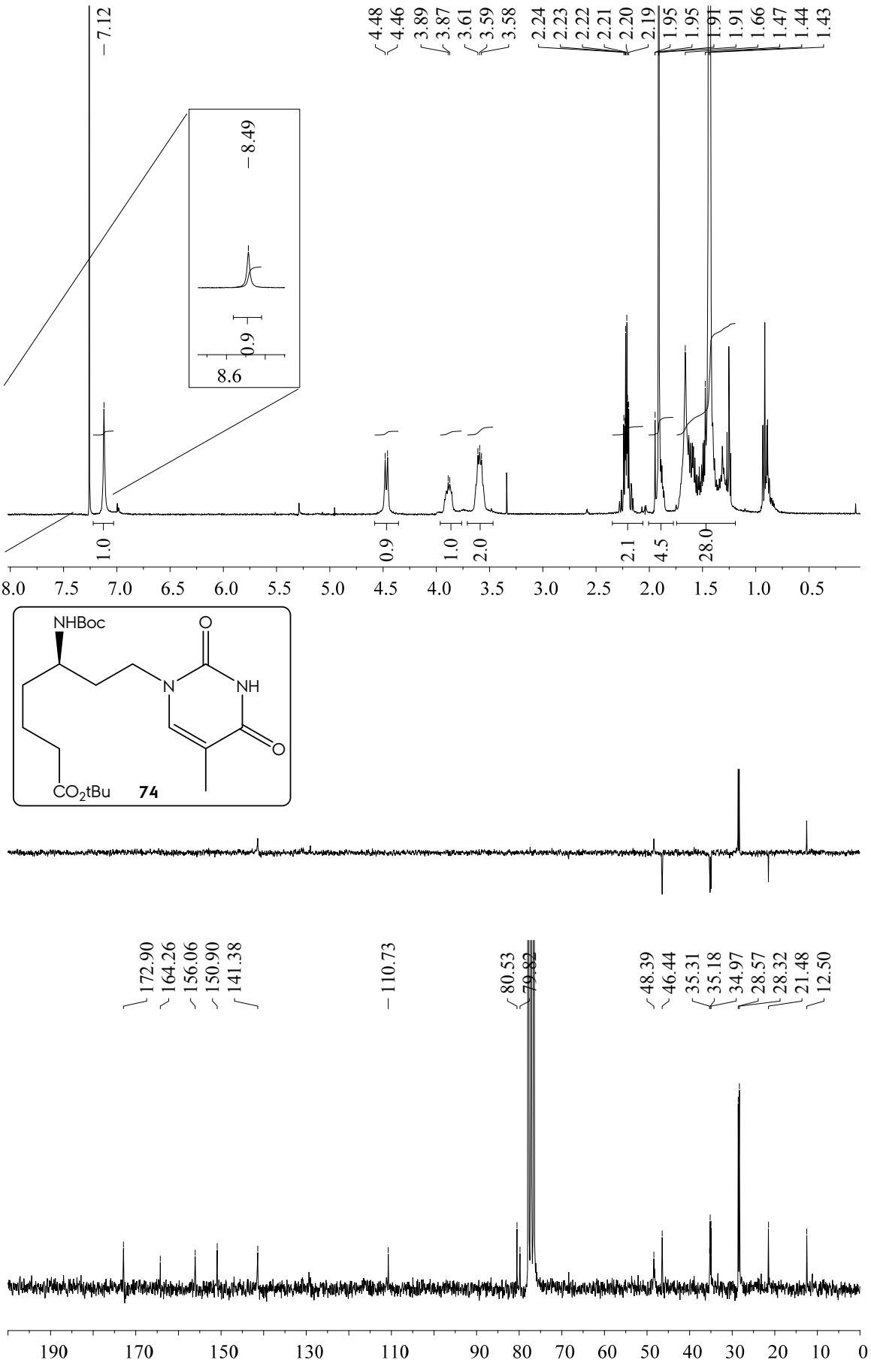
7.12
8.49
4.48
4.46
3.89
3.87
3.61
3.59
3.58
2.24
2.23
2.22
2.21
2.20
2.19
1.95
1.95
1.91
1.91
1.66
1.47
1.44
1.43
0.9
8.6
1.0
0.9
1.0
2.0
2.1
4.5
28.0
8.0 7.5 7.0 6.5 6.0 5.5 5.0 4.5 4.0 3.5 3.0 2.5 2.0 1.5 1.0 0.5
NHBoc
O
N
NH
O
CO2tBu
74
172.90
164.26
156.06
150.90
141.38
110.73
80.53
79.82
48.39
46.44
35.31
35.18
34.97
28.57
28.32
21.48
12.50
190 170 150 130 110 90 80 70 60 50 40 30 20 10 0

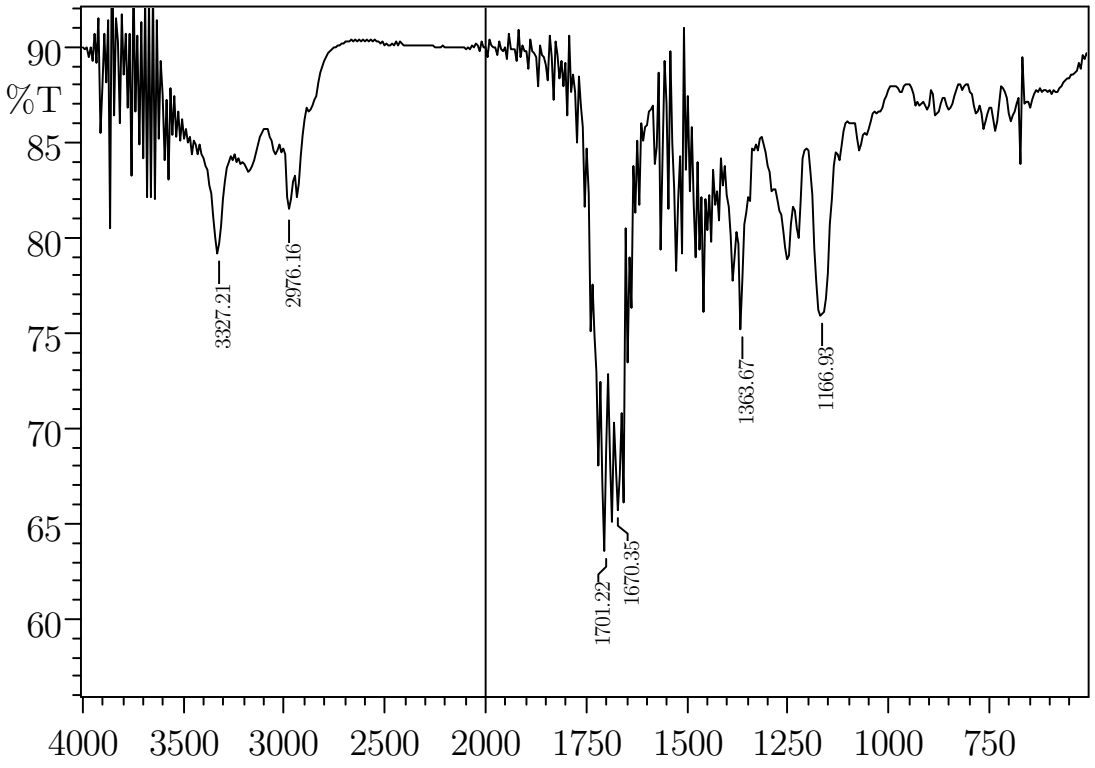
90
%T
85
80
75
70
65
60
3327.21
2976.16
1701.22
1670.35
1363.67
1166.93
4000 3500 3000 2500 2000 1750 1500 1250 1000 750
1/cm

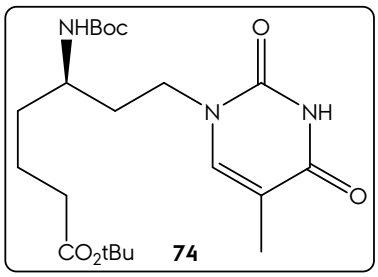
NHBoc
O
N
NH
O
CO2tBu
74

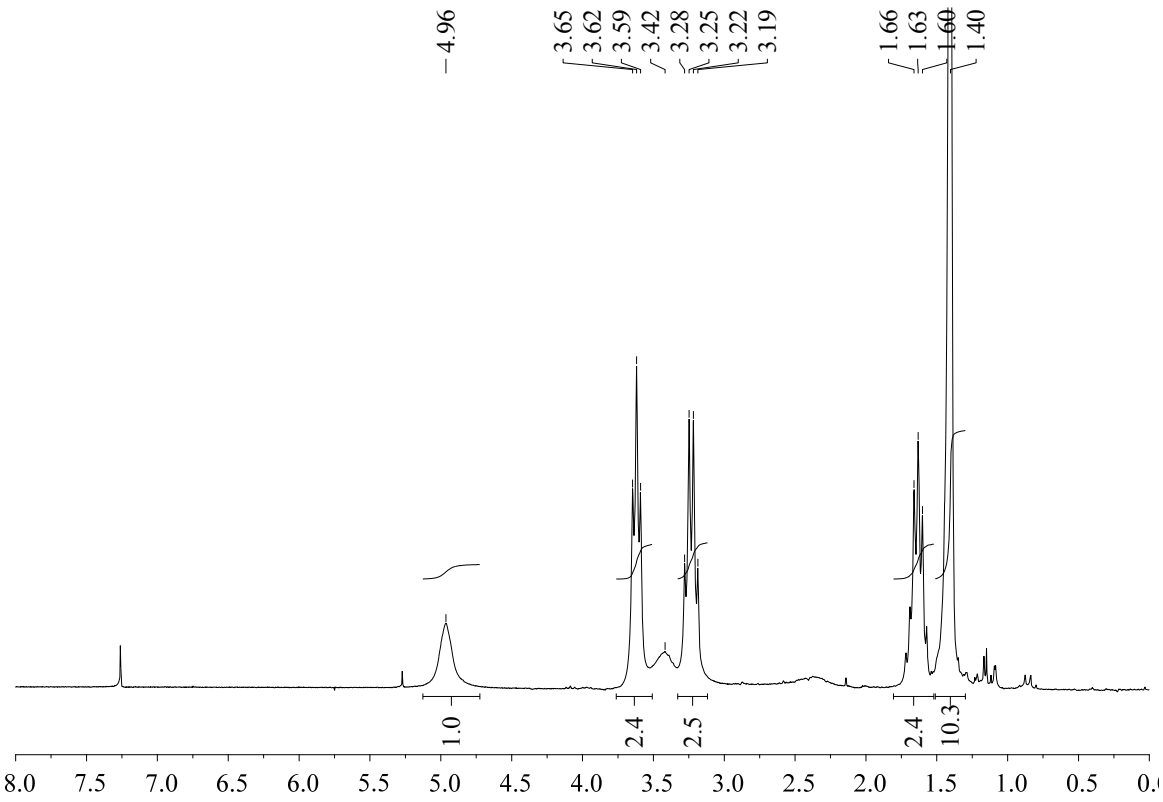
4.96
3.65
3.62
3.59
3.42
3.28
3.25
3.22
3.19
1.66
1.63
1.60
1.40
1.0
2.4
2.5
2.4
10.3
8.0
7.5
7.0
6.5
6.0
5.5
5.0
4.5
4.0
3.5
3.0
2.5
2.0
1.5
1.0
0.5

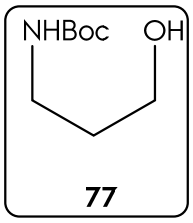
NHBoc
OH
77

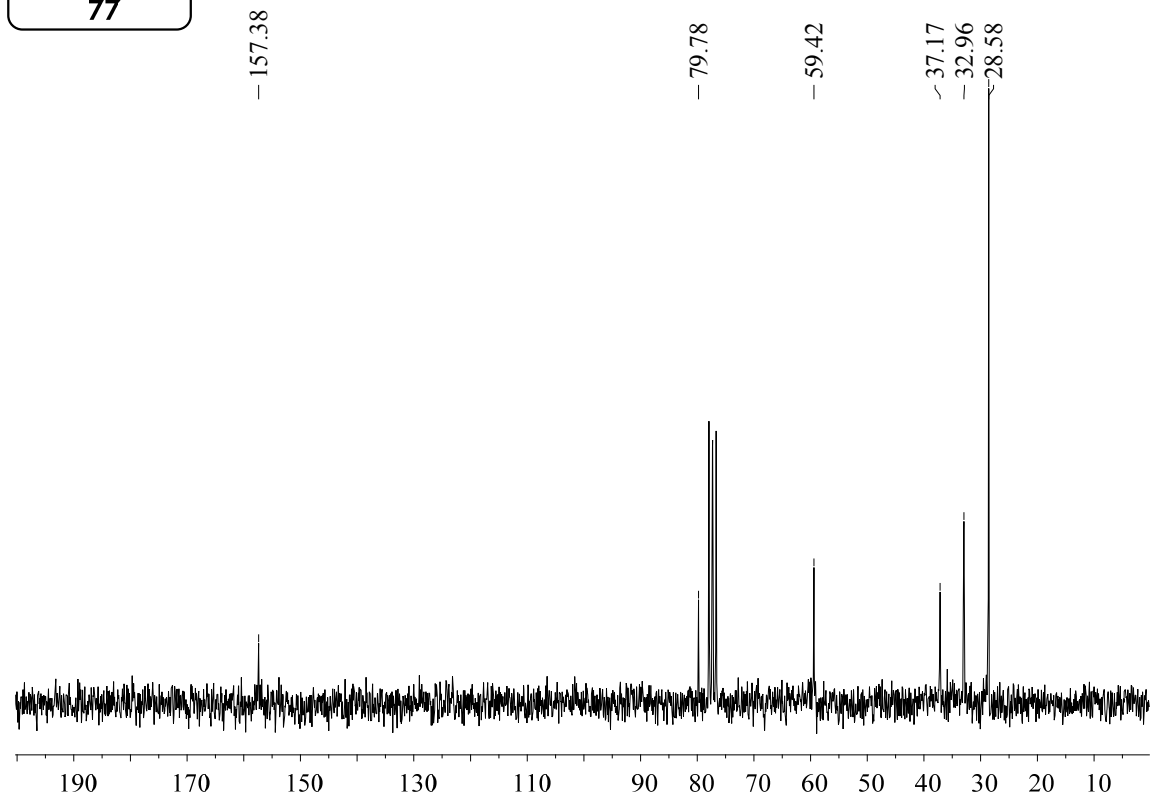
157.38
79.78
59.42
37.17
32.96
28.58
190
170
150
130
110
90
80
70
60
50
40
30
20
10

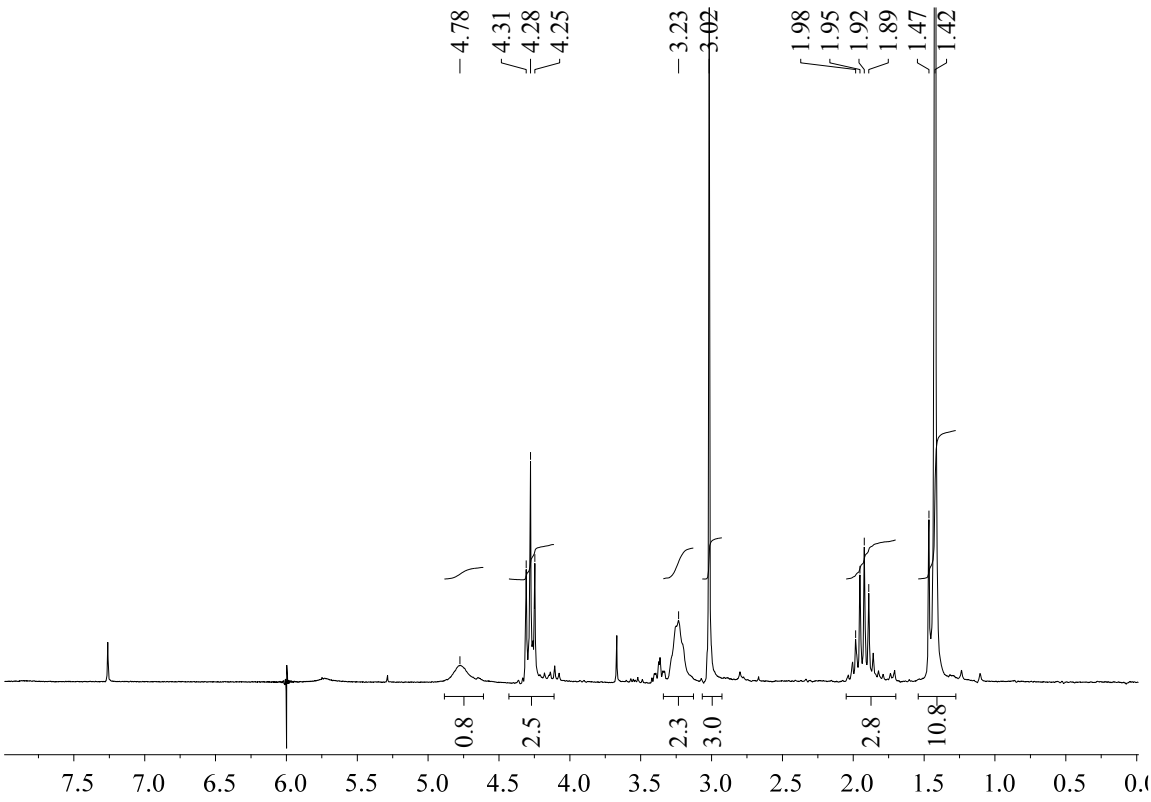
4.78
4.31
4.28
4.25
3.23
3.02
1.98
1.95
1.92
1.89
1.47
1.42
0.8
2.5
2.3
3.0
2.8
10.8
7.5 7.0 6.5 6.0 5.5 5.0 4.5 4.0 3.5 3.0 2.5 2.0 1.5 1.0 0.5

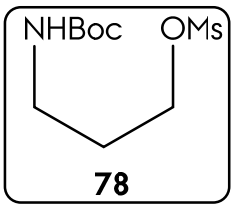
NHBoc
OMs
78

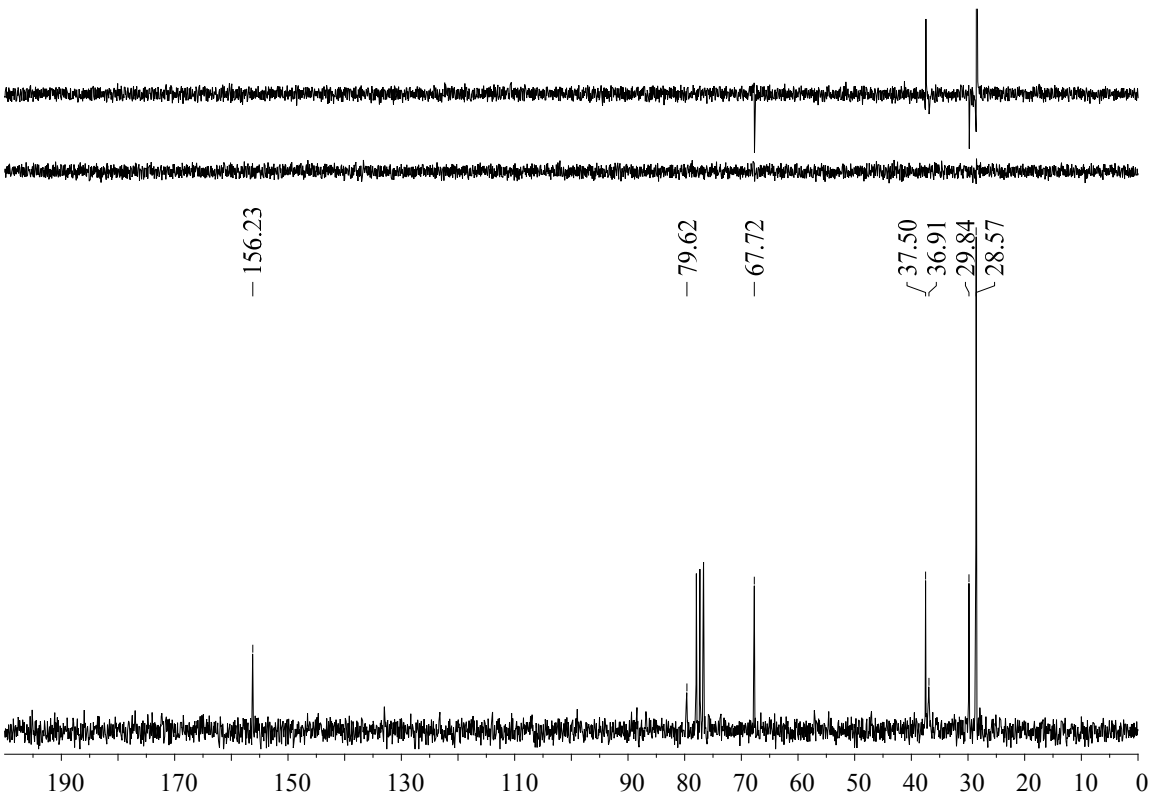
156.23
79.62
67.72
37.50
36.91
29.84
28.57
190 170 150 130 110 90 80 70 60 50 40 30 20 10 0

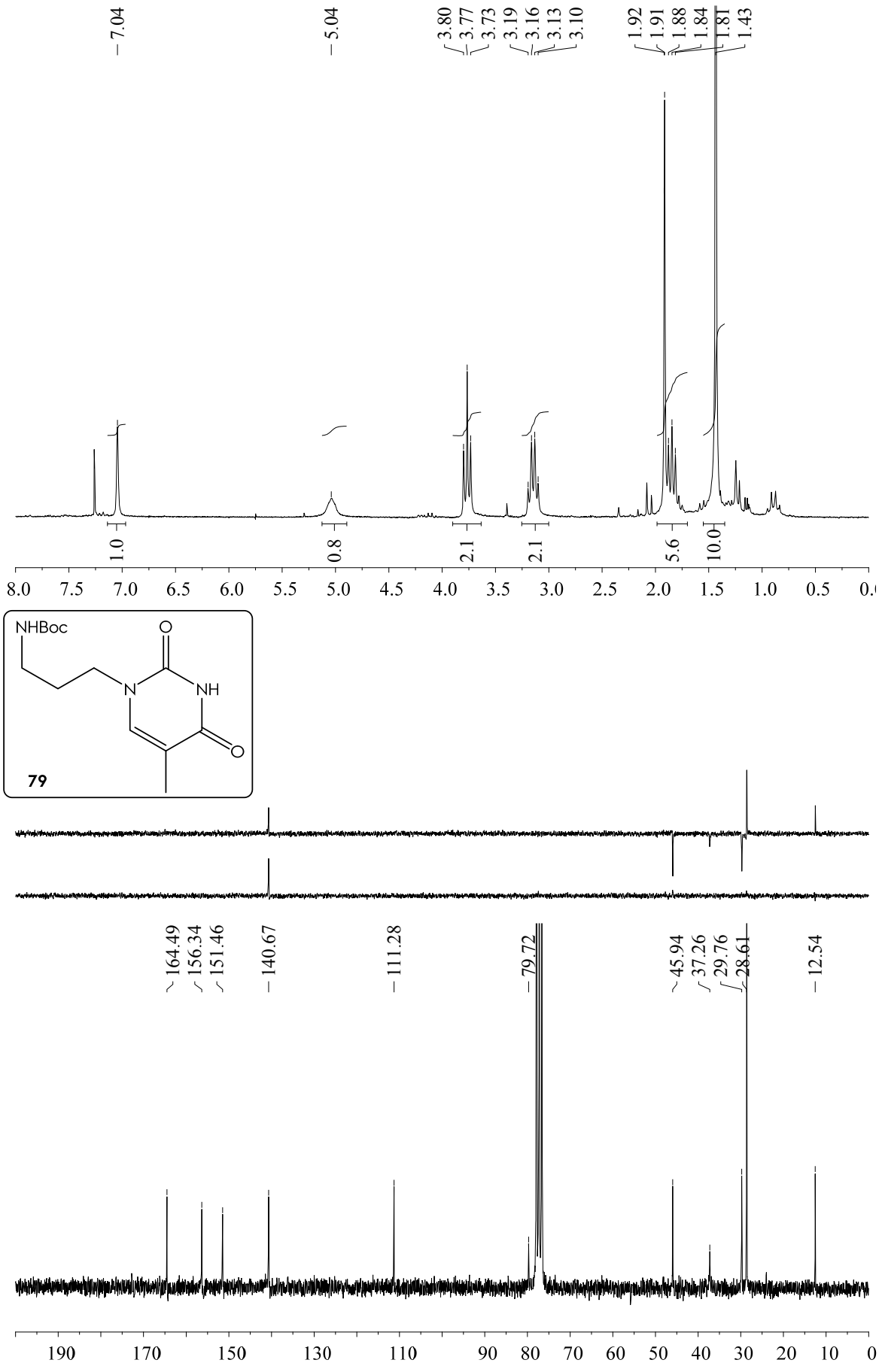
7.04
5.04
3.80
3.77
3.73
3.19
3.16
3.13
3.10
1.92
1.91
1.88
1.84
1.81
1.43
1.0
0.8
2.1
2.1
5.6
10.0
8.0 7.5 7.0 6.5 6.0 5.5 5.0 4.5 4.0 3.5 3.0 2.5 2.0 1.5 1.0 0.5
NHBoc
O
N
NH
O
79
164.49
156.34
151.46
140.67
111.28
79.72
45.94
37.26
29.76
28.61
12.54
190 170 150 130 110 90 80 70 60 50 40 30 20 10 0

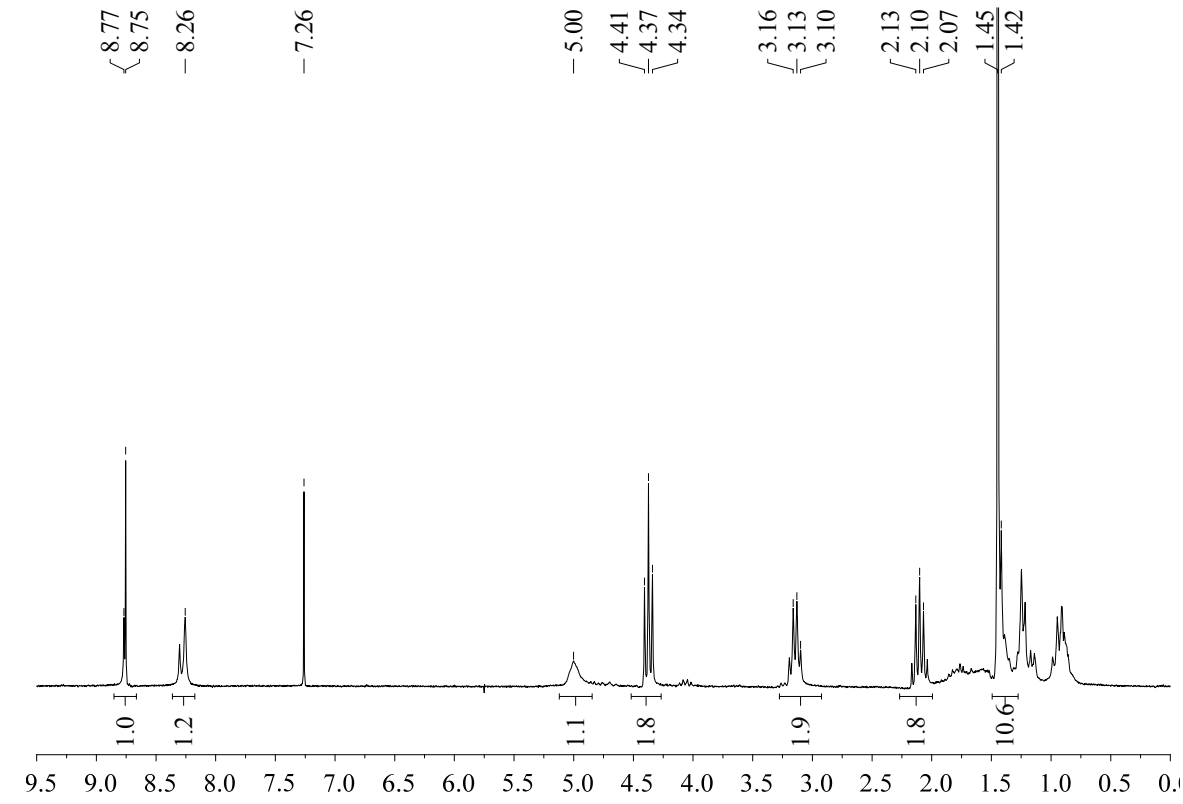
8.77
8.75
8.26
7.26
5.00
4.41
4.37
4.34
3.16
3.13
3.10
2.13
2.10
2.07
1.45
1.42
1.0
1.2
1.1
1.8
1.9
1.8
10.6
9.5 9.0 8.5 8.0 7.5 7.0 6.5 6.0 5.5 5.0 4.5 4.0 3.5 3.0 2.5 2.0 1.5 1.0 0.5

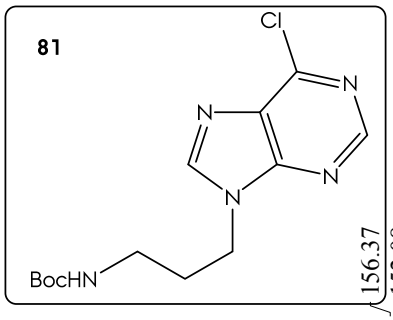
81
Cl
N
N
N
N
BocHN

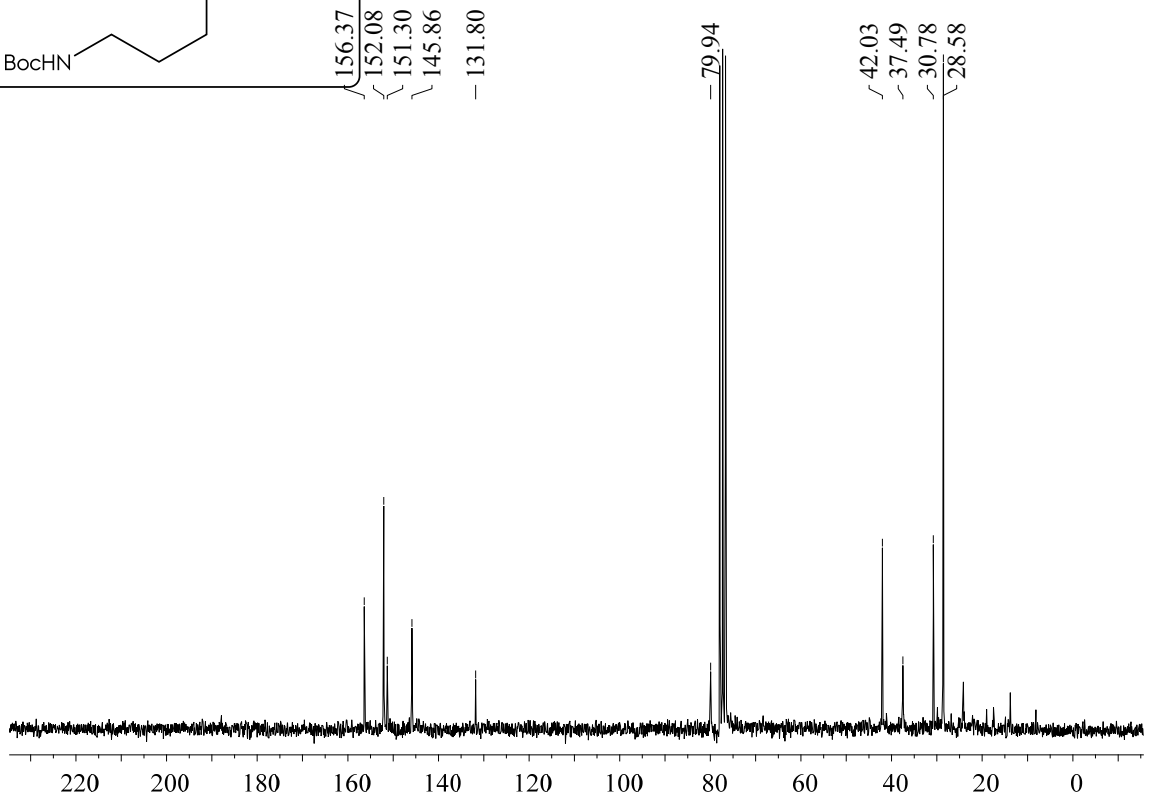
156.37
152.08
151.30
145.86
131.80
79.94
42.03
37.49
30.78
28.58
220 200 180 160 140 120 100 80 60 40 20 0

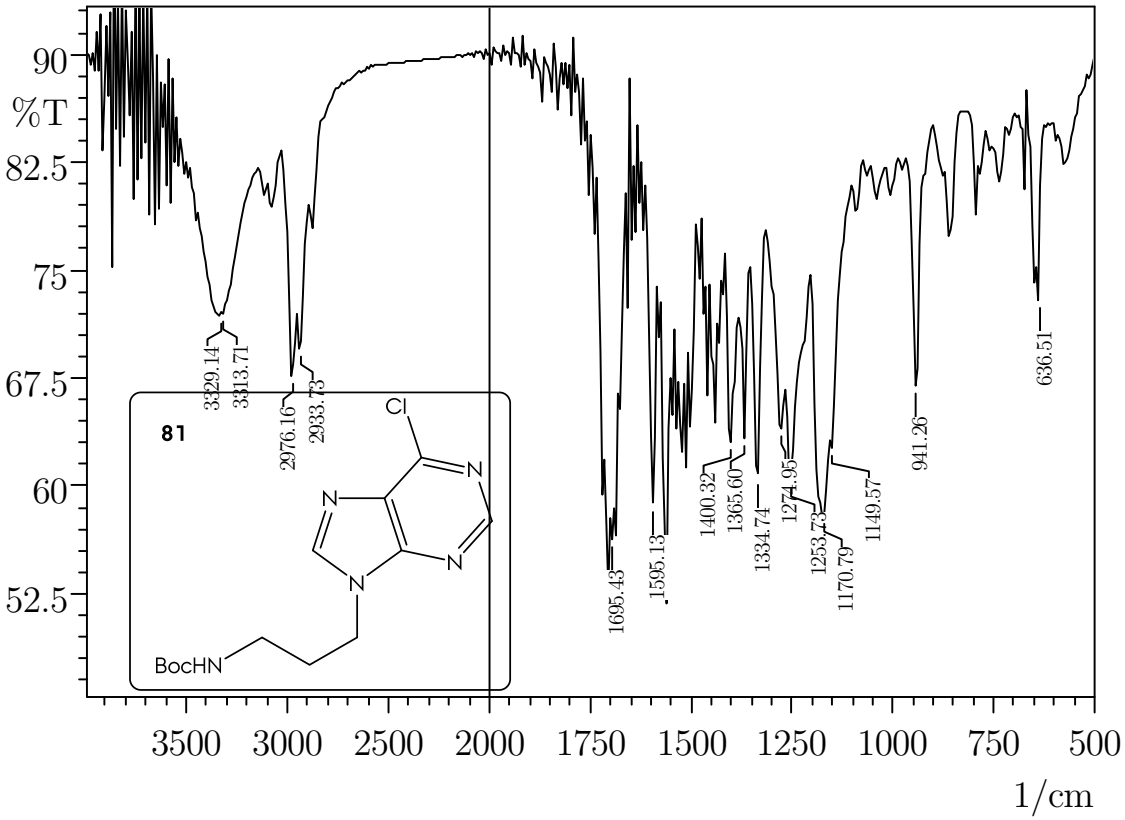
90
%T
82.5
75
67.5
60
52.5
3329.14
3313.71
2976.16
2933.73
1695.43
1595.13
1400.32
1365.60
1334.74
1274.95
1253.73
1170.79
1149.57
941.26
636.51
81
Cl
N
N
N
N
BocHN
3500 3000 2500 2000 1750 1500 1250 1000 750 500
1/cm

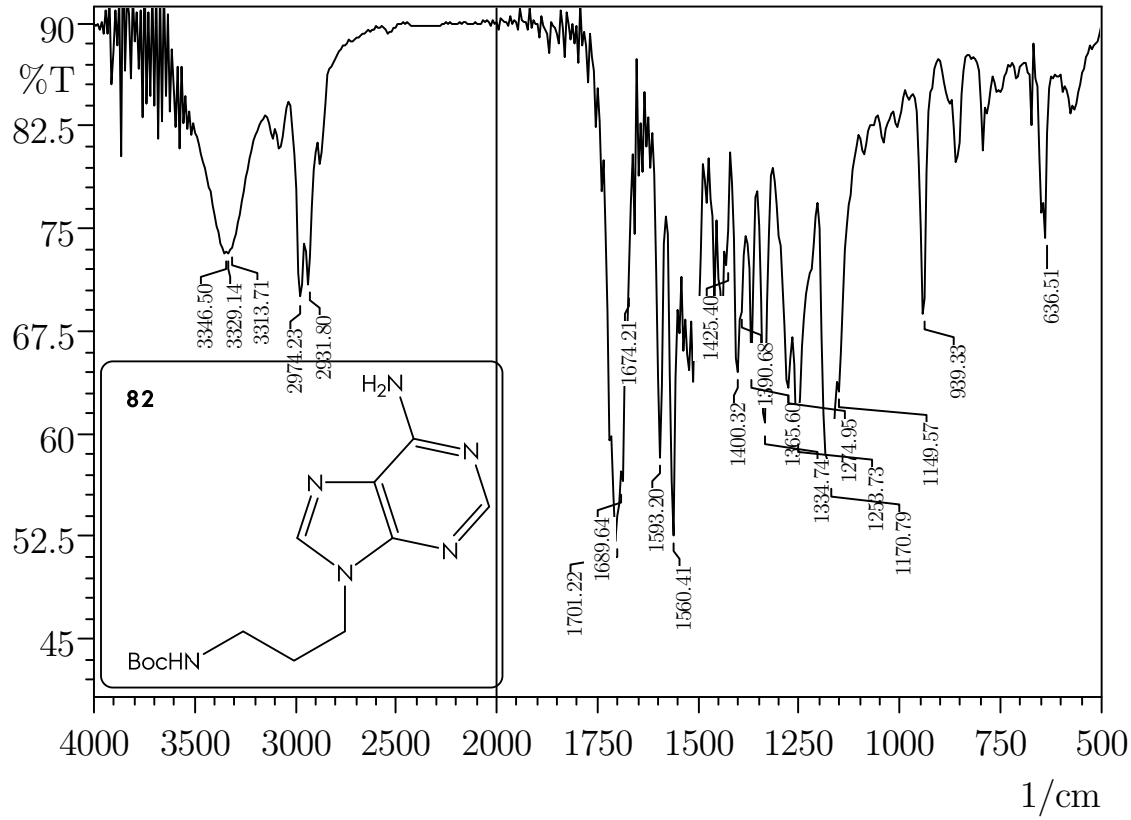
%T
90
82.5
75
67.5
60
52.5
45
4000 3500 3000 2500 2000 1750 1500 1250 1000 750 500
1/cm
3346.50
3329.14
3313.71
2974.25
2931.80
1701.22
1689.64
1674.21
1593.20
1560.41
1425.40
1400.32
1365.60
1334.74
1274.95
1253.73
1170.70
1149.57
939.33
636.51
82
H_2N
N
N
N
N
BocHN

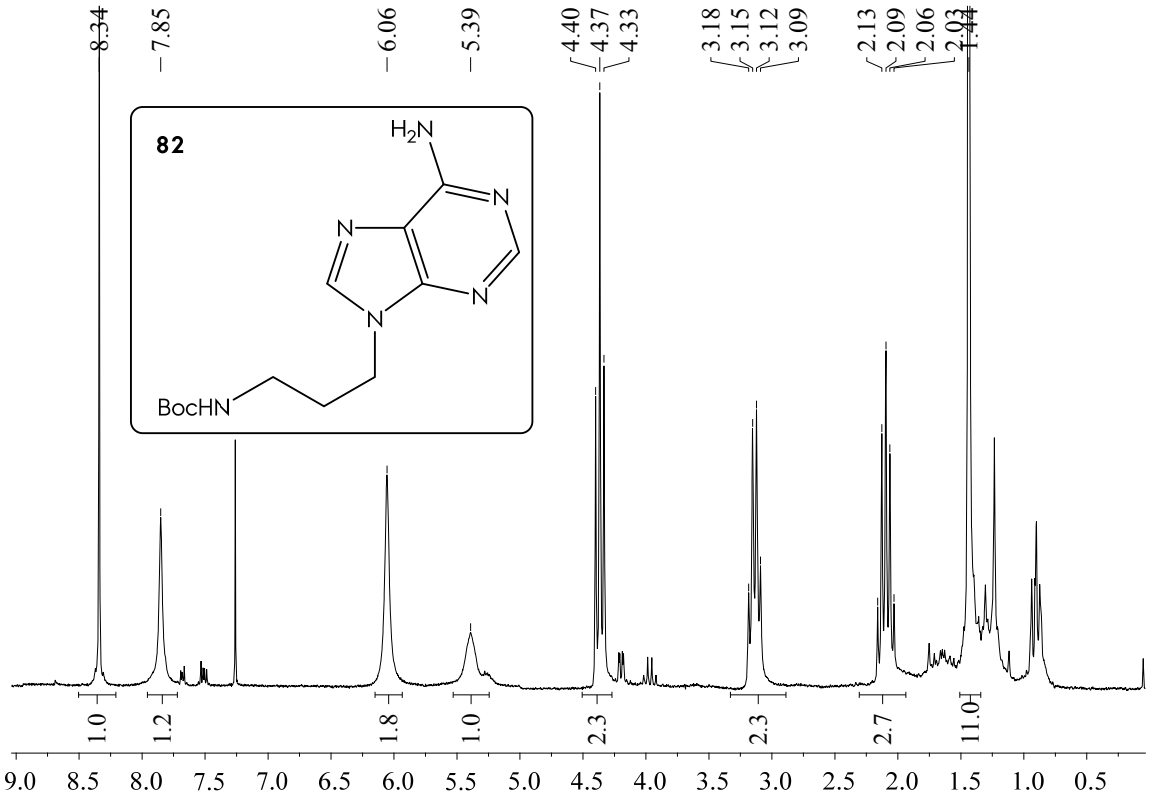
8.34
7.85
6.06
5.39
4.40
4.37
4.33
3.18
3.15
3.12
3.09
2.13
2.09
2.06
2.03
1.44
1.0
1.2
1.8
1.0
2.3
2.3
2.7
11.0
9.0 8.5 8.0 7.5 7.0 6.5 6.0 5.5 5.0 4.5 4.0 3.5 3.0 2.5 2.0 1.5 1.0 0.5
82
H_2N
N
N
N
N
BocHN

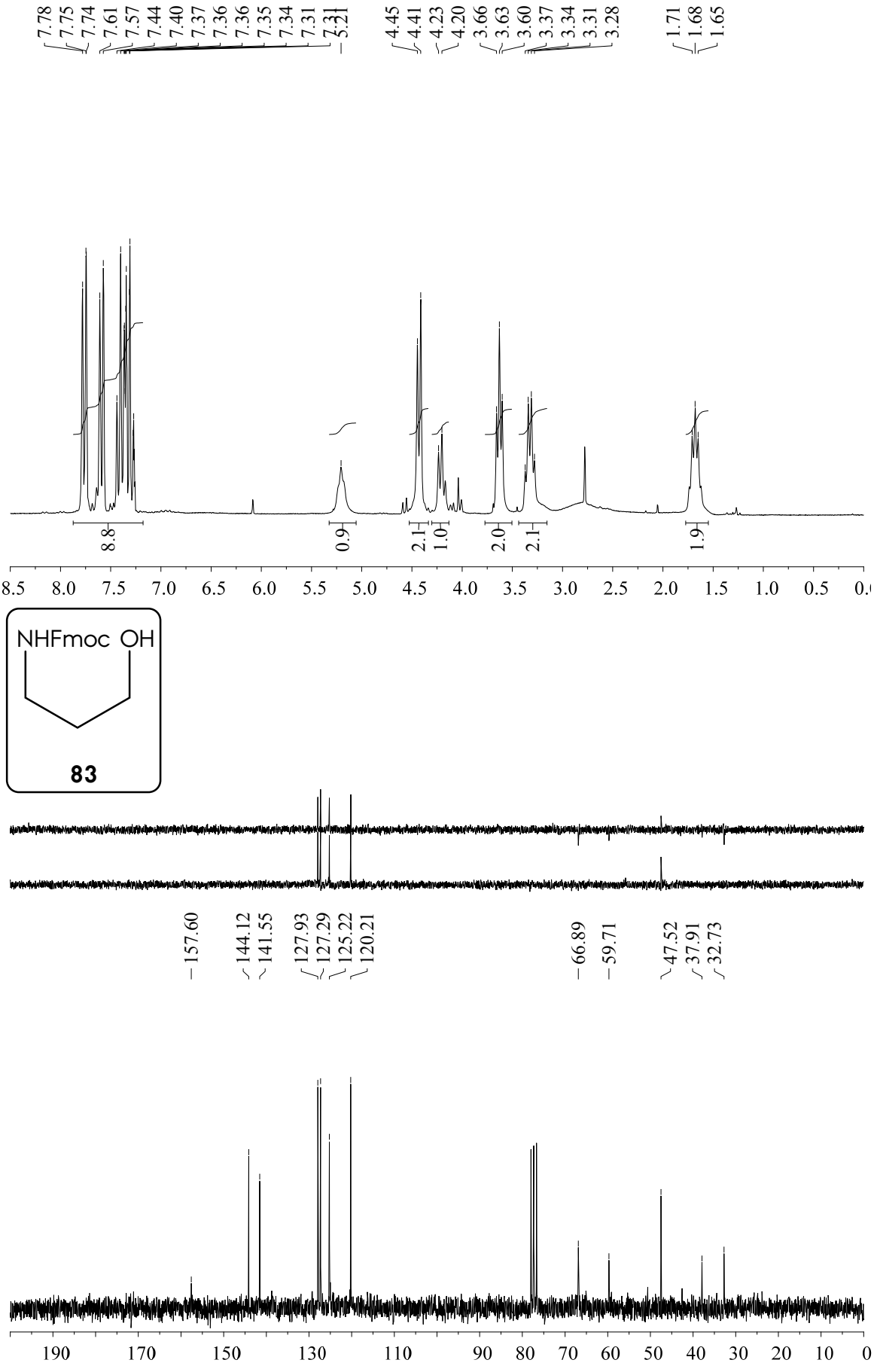
7.78
7.75
7.74
7.61
7.57
7.44
7.40
7.37
7.36
7.36
7.35
7.34
7.31
7.31
5.21
4.45
4.41
4.23
4.20
3.66
3.63
3.60
3.37
3.34
3.31
3.28
1.71
1.68
1.65
8.8
0.9
2.1
1.0
2.0
2.1
1.9
8.5 8.0 7.5 7.0 6.5 6.0 5.5 5.0 4.5 4.0 3.5 3.0 2.5 2.0 1.5 1.0 0.5
NHFmoc OH
83
157.60
144.12
141.55
127.93
127.29
125.22
120.21
66.89
59.71
47.52
37.91
32.73
190 170 150 130 110 90 80 70 60 50 40 30 20 10 0

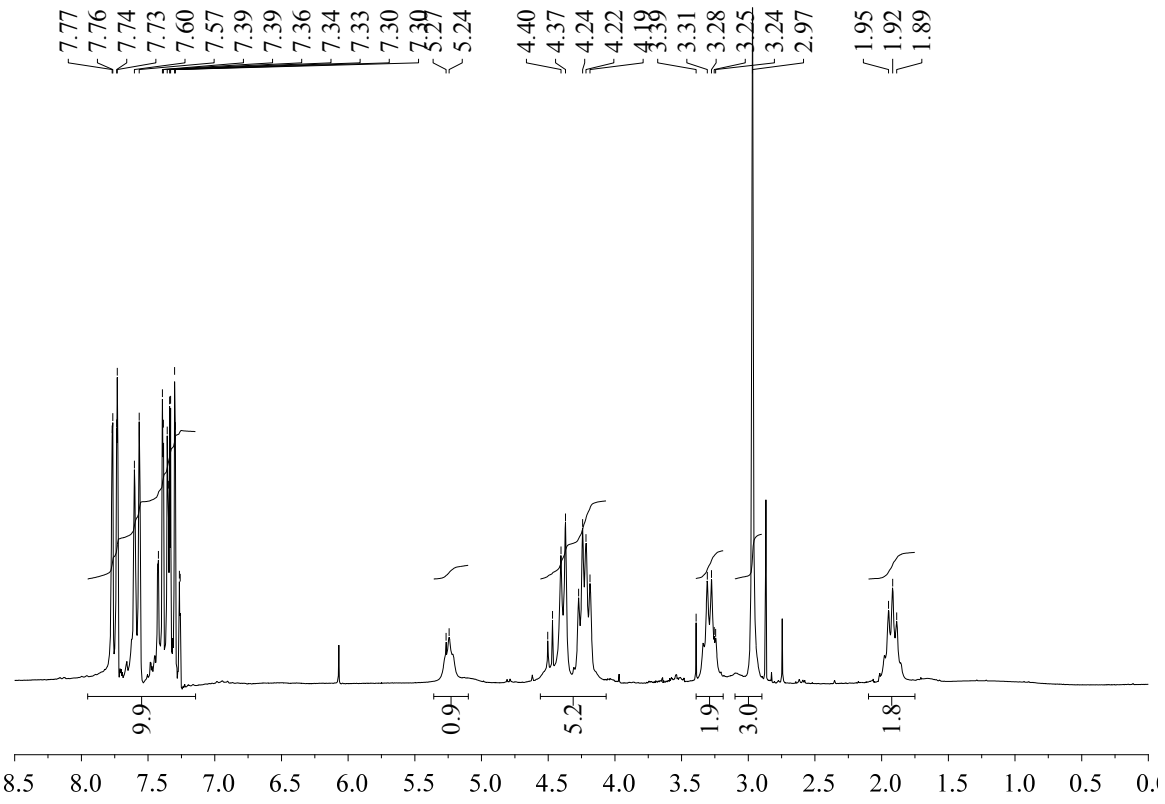
7.77
7.76
7.74
7.73
7.60
7.57
7.39
7.39
7.36
7.34
7.33
7.30
5.27
5.24
4.40
4.37
4.24
4.22
3.31
3.28
3.25
3.24
2.97
1.95
1.92
1.89
9.9
0.9
5.2
1.9
3.0
1.8
8.5
8.0
7.5
7.0
6.5
6.0
5.5
5.0
4.5
4.0
3.5
3.0
2.5
2.0
1.5
1.0
0.5

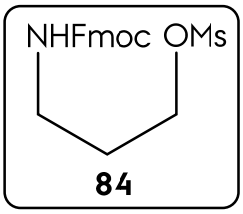
NHFmoc
OMs
84

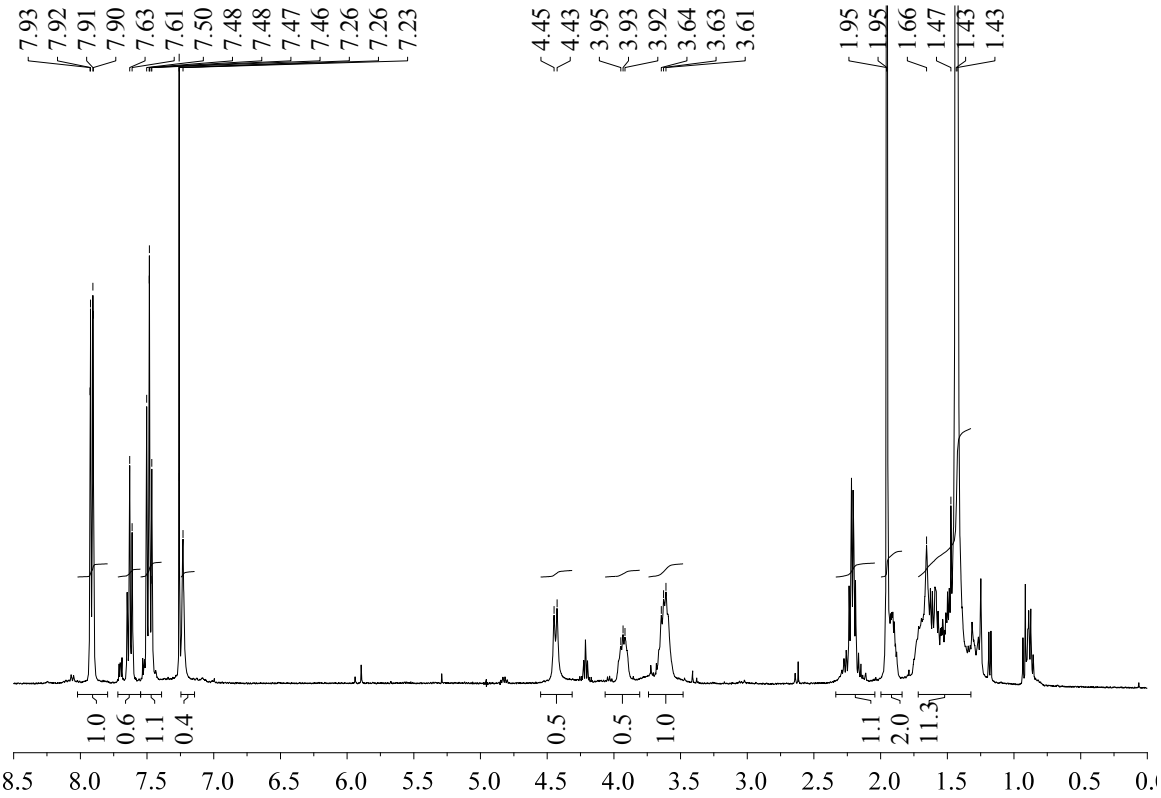
7.93
7.92
7.91
7.90
7.63
7.61
7.50
7.48
7.48
7.47
7.46
7.26
7.26
7.23
4.45
4.43
3.95
3.93
3.92
3.64
3.63
3.61
1.95
1.95
1.66
1.47
1.43
1.43
1.0
0.6
1.1
0.4
0.5
0.5
1.0
1.1
2.0
11.3
8.5
8.0
7.5
7.0
6.5
6.0
5.5
5.0
4.5
4.0
3.5
3.0
2.5
2.0
1.5
1.0
0.5

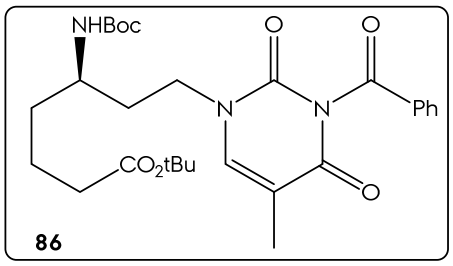
NHBoc
O
O
N
N
Ph
CO2tBu
O
86

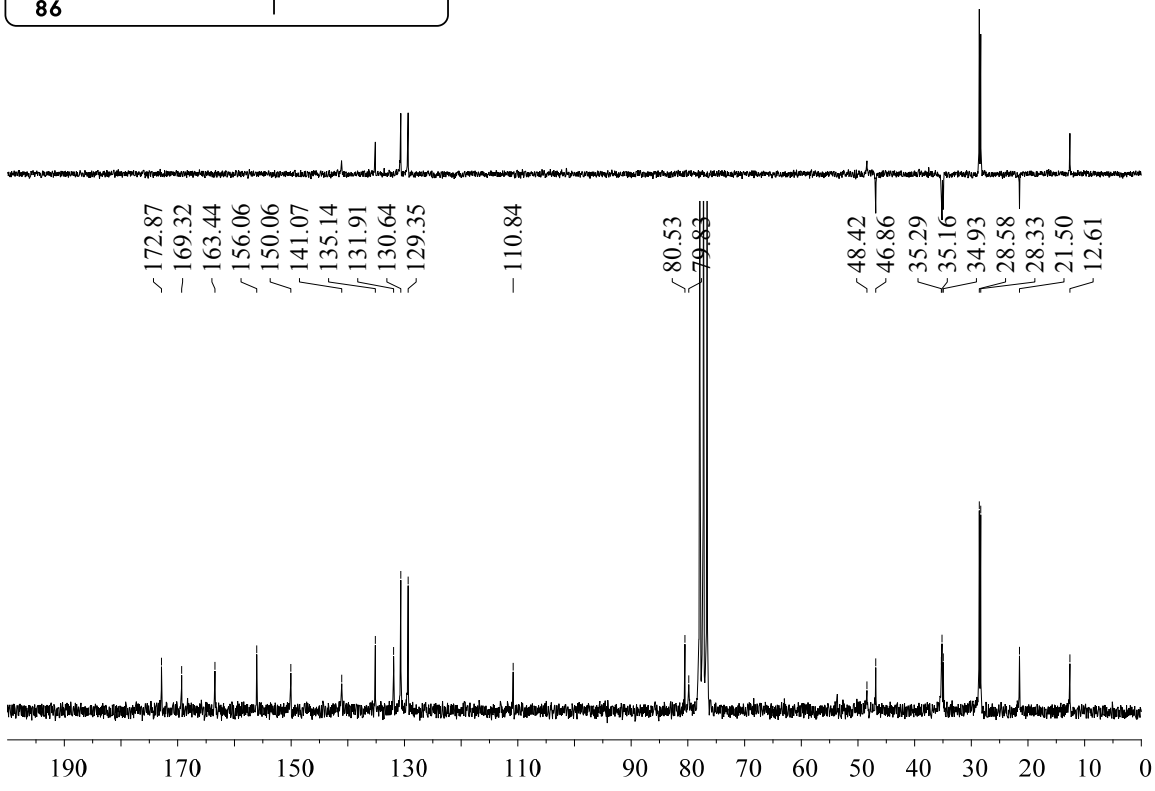
172.87
169.32
163.44
156.06
150.06
141.07
135.14
131.91
130.64
129.35
110.84
80.53
79.83
48.42
46.86
35.29
35.16
34.93
28.58
28.33
21.50
12.61
190
170
150
130
110
90
80
70
60
50
40
30
20
10
0

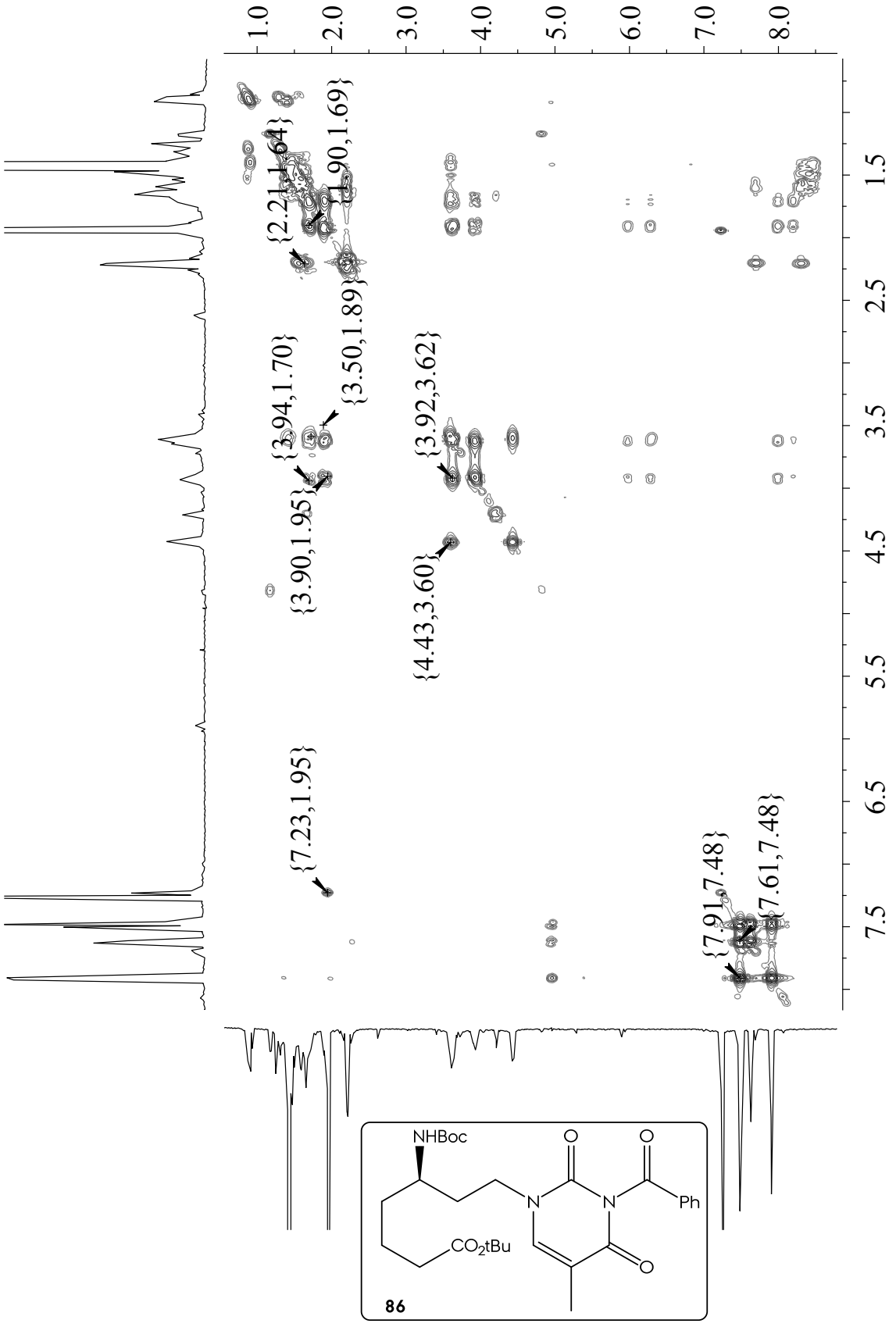
1.0
2.0
3.0
4.0
5.0
6.0
7.0
8.0
1.5
2.5
3.5
4.5
5.5
6.5
7.5
{2.21,1.64}
{1.90,1.69}
{3.50,1.89}
{3.94,1.70}
{3.90,1.95}
{3.92,3.62}
{4.43,3.60}
{7.23,1.95}
{7.91,7.48}
{7.61,7.48}
NHBoc
O
O
N
N
Ph
CO2tBu
O
86

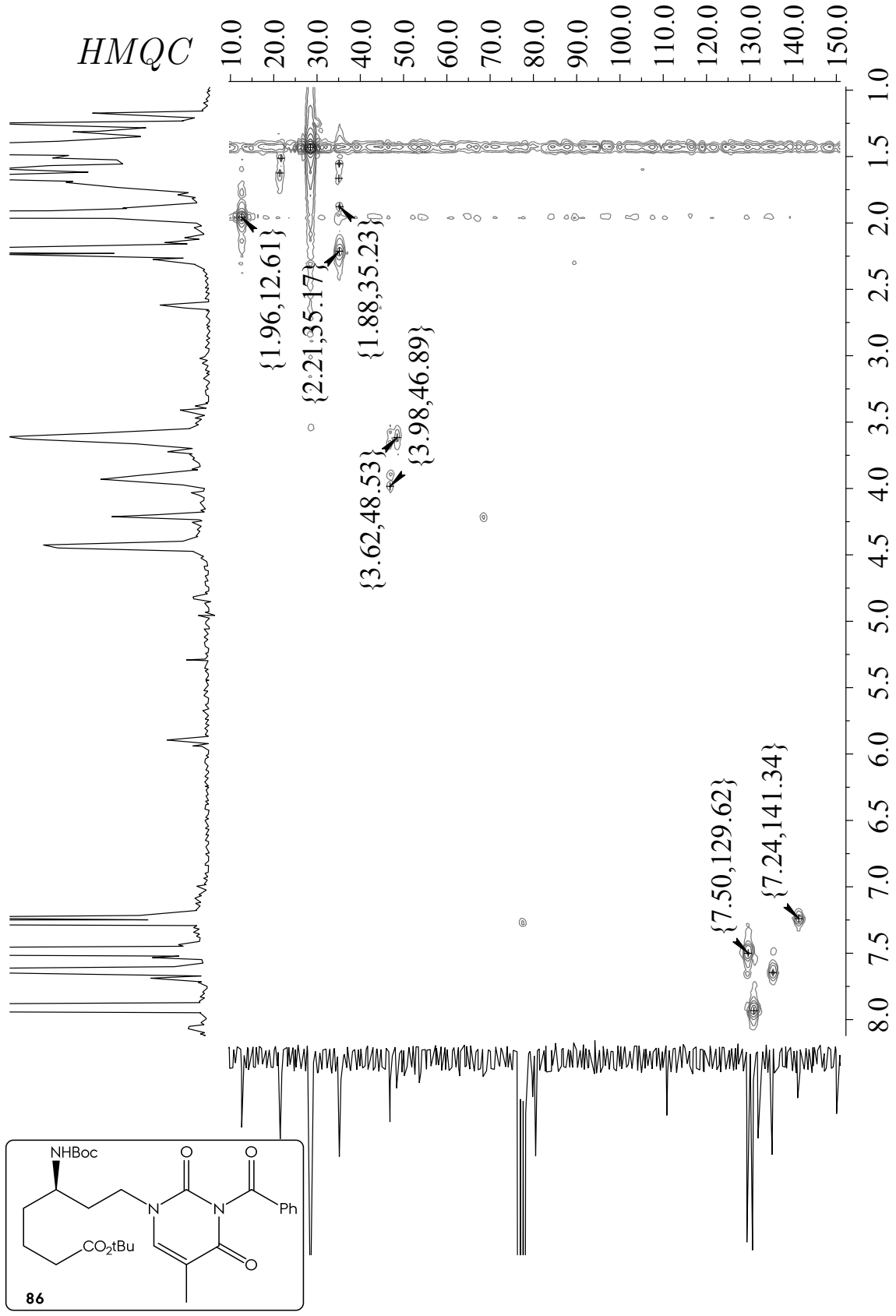
HMQC
10.0
20.0
30.0
40.0
50.0
60.0
70.0
80.0
90.0
100.0
110.0
120.0
130.0
140.0
150.0
1.0
1.5
2.0
2.5
3.0
3.5
4.0
4.5
5.0
5.5
6.0
6.5
7.0
7.5
8.0
{1.96,12.61}
{2.21,35.17}
{1.88,35.23}
{3.62,48.53}
{3.98,46.89}
{7.50,129.62}
{7.24,141.34}
NHBoc
O
O
N
N
Ph
CO2tBu
O
86

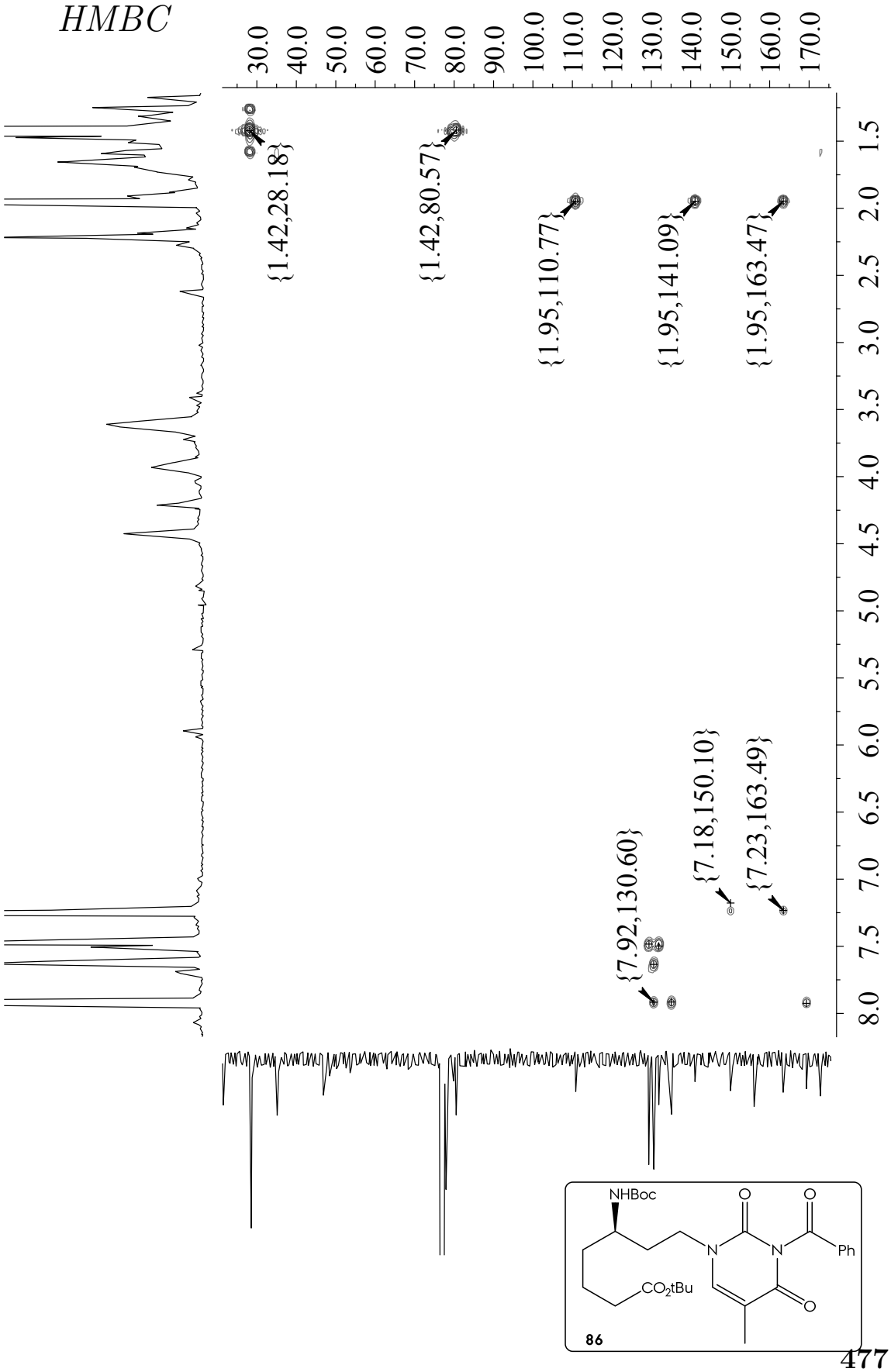
HMBC
{1.42,28.18}
{1.42,80.57}
{1.95,110.77}
{1.95,141.09}
{1.95,163.47}
{7.92,130.60}
{7.18,150.10}
{7.23,163.49}
NHBoc
CO2tBu
Ph
86

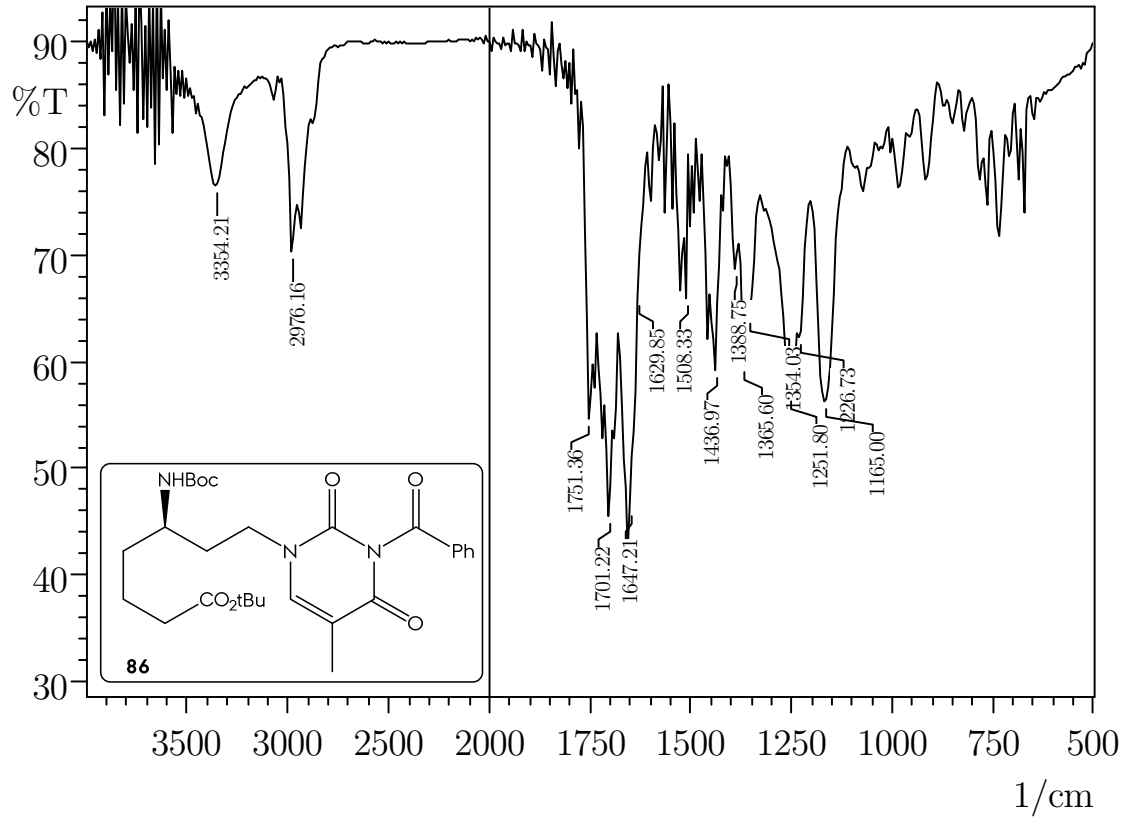
%T
1/cm
3354.21
2976.16
1751.36
1701.22
1647.21
1629.85
1508.33
1436.97
1388.75
1365.60
1354.03
1251.80
1226.73
1165.00
NHBoc
CO2tBu
Ph
86

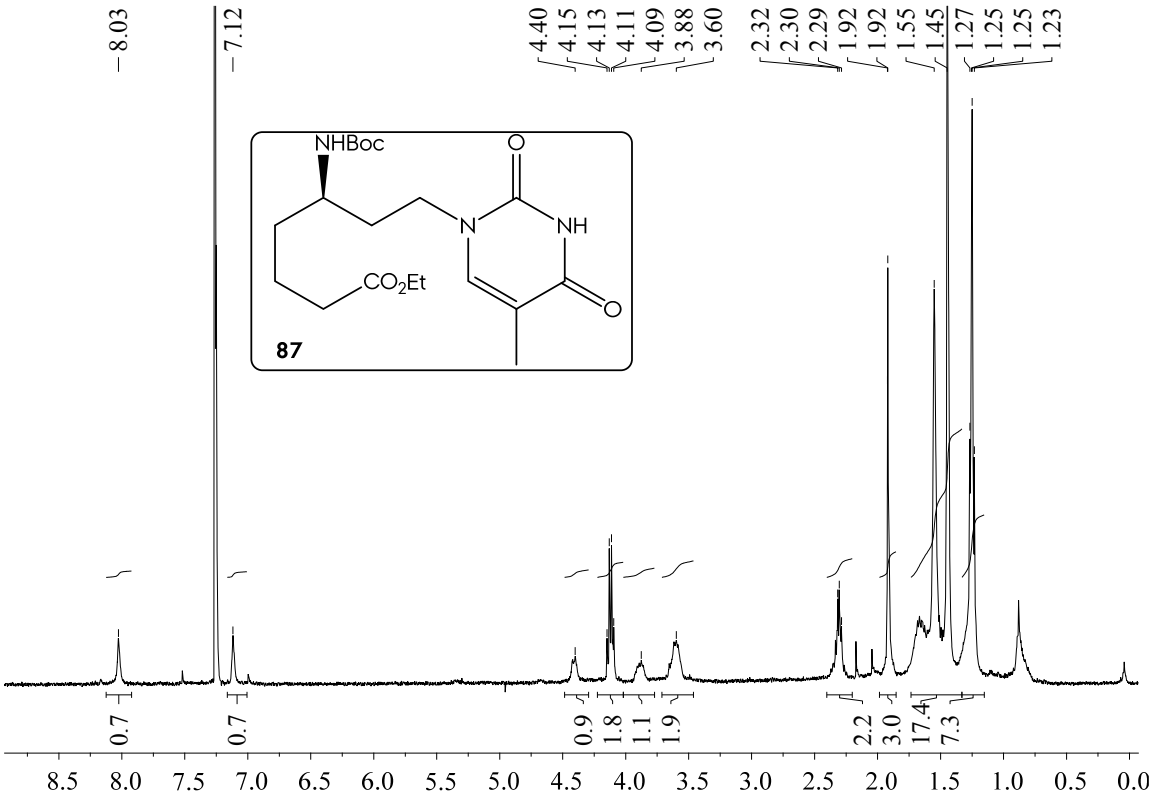
8.03
7.12
4.40
4.15
4.13
4.11
4.09
3.88
3.60
2.32
2.30
2.29
1.92
1.92
1.55
1.45
1.27
1.25
1.25
1.23
NHBoc
CO2Et
NH
87
0.7
0.7
0.9
1.8
1.1
1.9
2.2
3.0
17.4
7.3

COSY

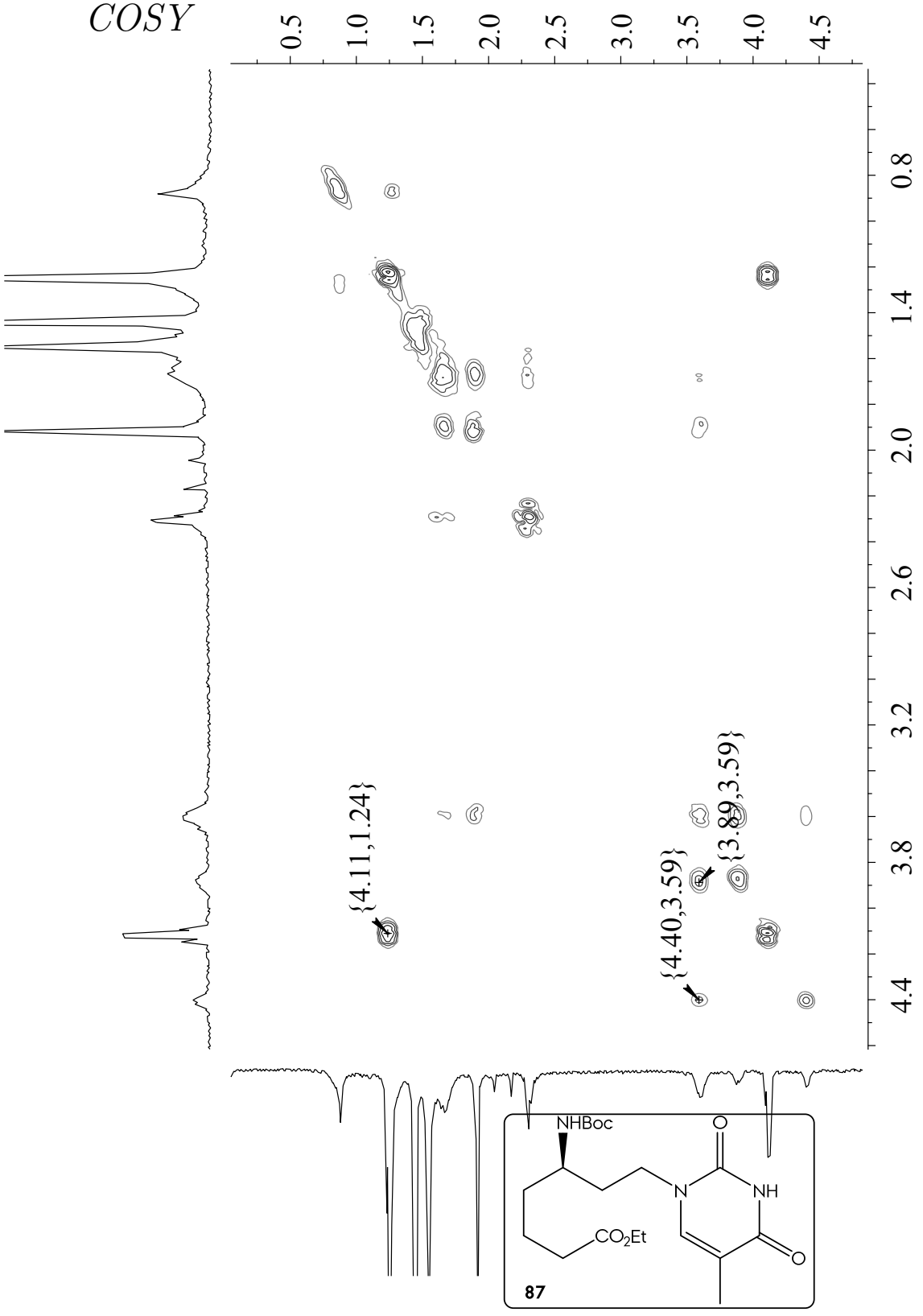
0.5
1.0
1.5
2.0
2.5
3.0
3.5
4.0
4.5
0.8
1.4
2.0
2.6
3.2
3.8
4.4
{4.11,1.24}
{4.40,3.59}
{3.89,3.59}
NHBoc
O
N
NH
CO2Et
O
87

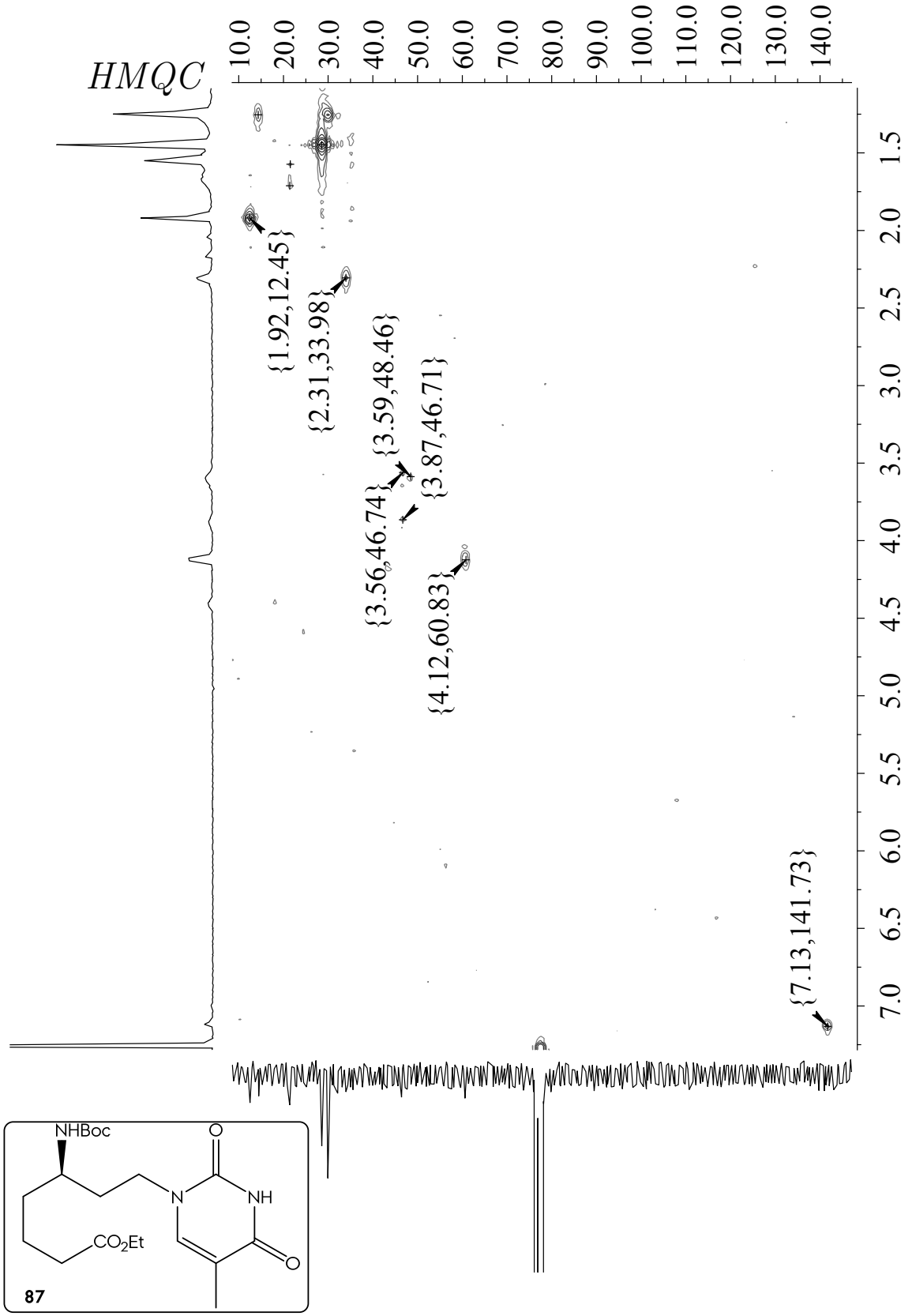
HMQC
10.0
20.0
30.0
40.0
50.0
60.0
70.0
80.0
90.0
100.0
110.0
120.0
130.0
140.0
1.5
2.0
2.5
3.0
3.5
4.0
4.5
5.0
5.5
6.0
6.5
7.0
{1.92,12.45}
{2.31,33.98}
{3.59,48.46}
{3.87,46.71}
{3.56,46.74}
{4.12,60.83}
{7.13,141.73}
NHBoc
O
N
NH
CO2Et
O

87

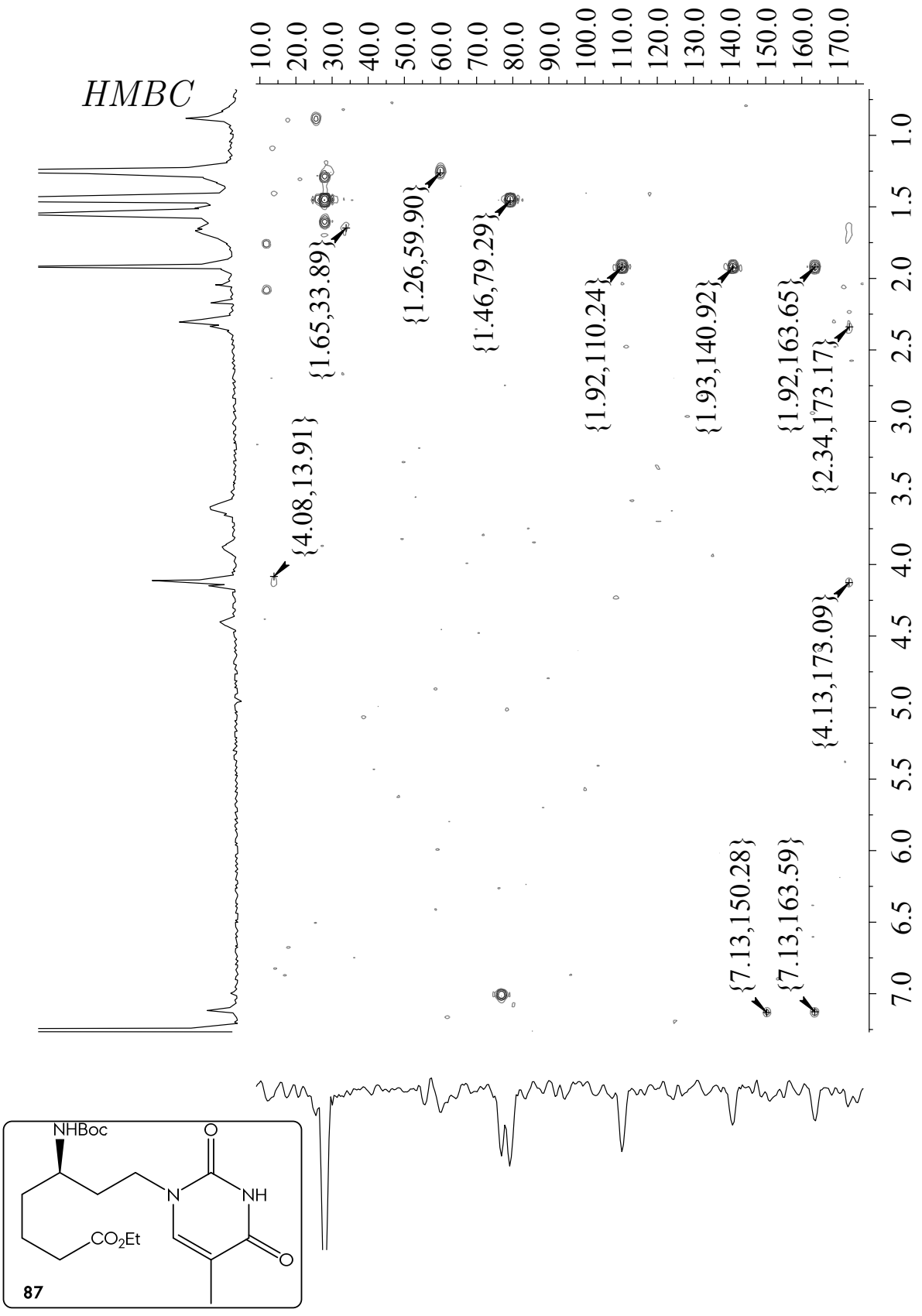
HMBC
{4.08,13.91}
{1.65,33.89}
{1.26,59.90}
{1.46,79.29}
{1.92,110.24}
{1.93,140.92}
{1.92,163.65}
{2.34,173.17}
{4.13,173.09}
{7.13,150.28}
{7.13,163.59}
NHBoc
O
N
NH
CO2Et
O
87

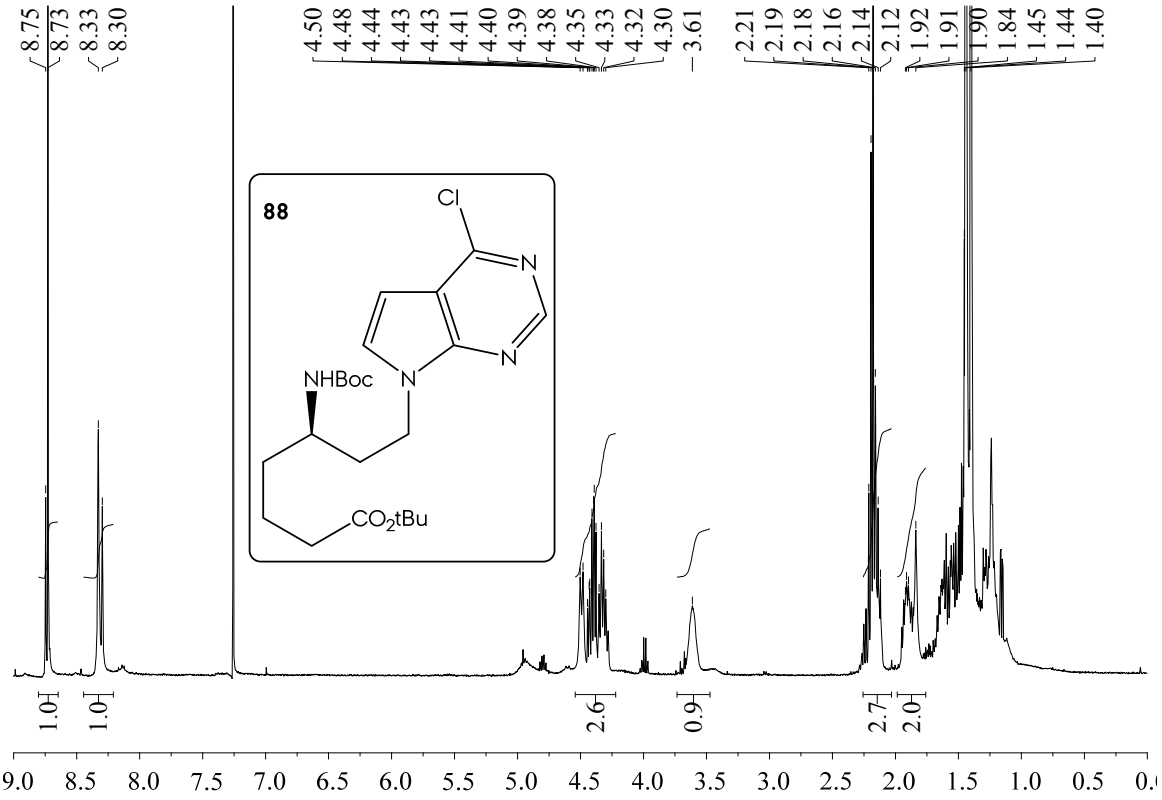
8.75
8.73
8.33
8.30
4.50
4.48
4.44
4.43
4.43
4.41
4.40
4.39
4.38
4.35
4.33
4.32
4.30
3.61
2.21
2.19
2.18
2.16
2.14
2.12
1.92
1.91
1.90
1.84
1.45
1.44
1.40
88
Cl
N
N
N
NHBoc
CO2tBu
1.0
1.0
2.6
0.9
2.7
2.0
9.0
8.5
8.0
7.5
7.0
6.5
6.0
5.5
5.0
4.5
4.0
3.5
3.0
2.5
2.0
1.5
1.0
0.5

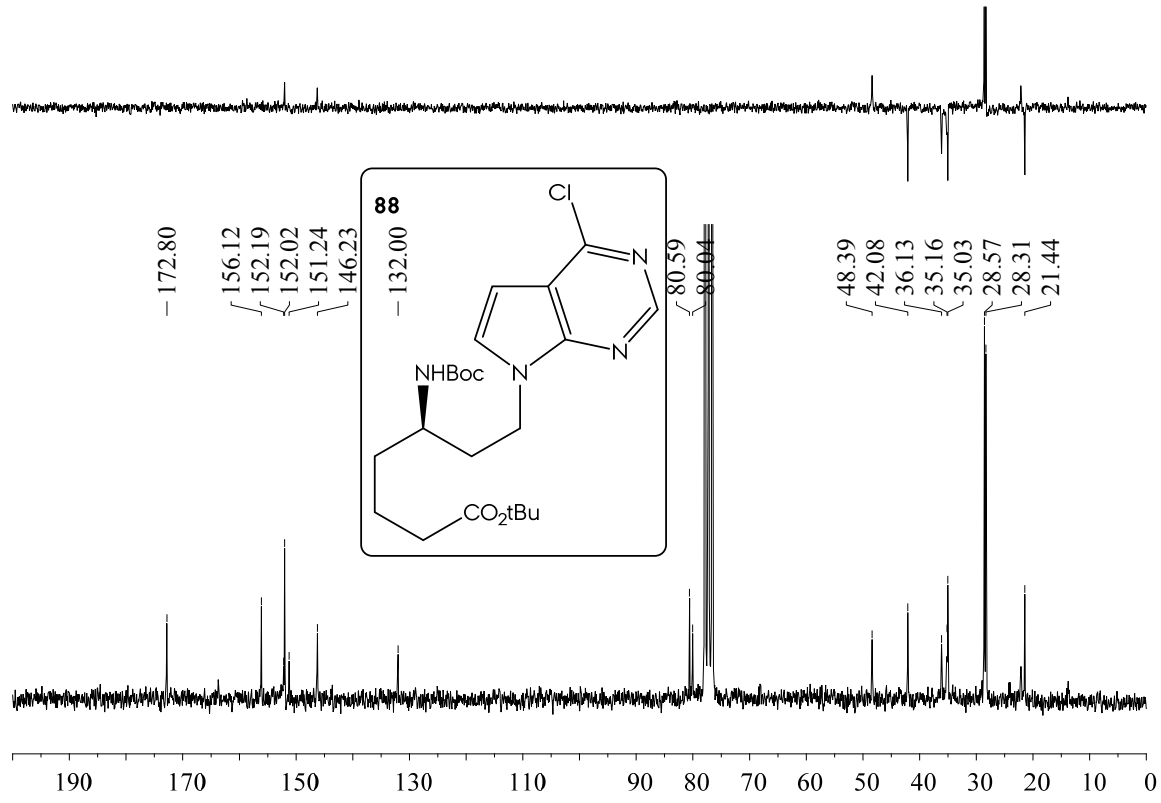
172.80
156.12
152.19
152.02
151.24
146.23
132.00
80.59
80.04
48.39
42.08
36.13
35.16
35.03
28.57
28.31
21.44
88
Cl
N
N
N
NHBoc
CO2tBu
190
170
150
130
110
90
80
70
60
50
40
30
20
10
0

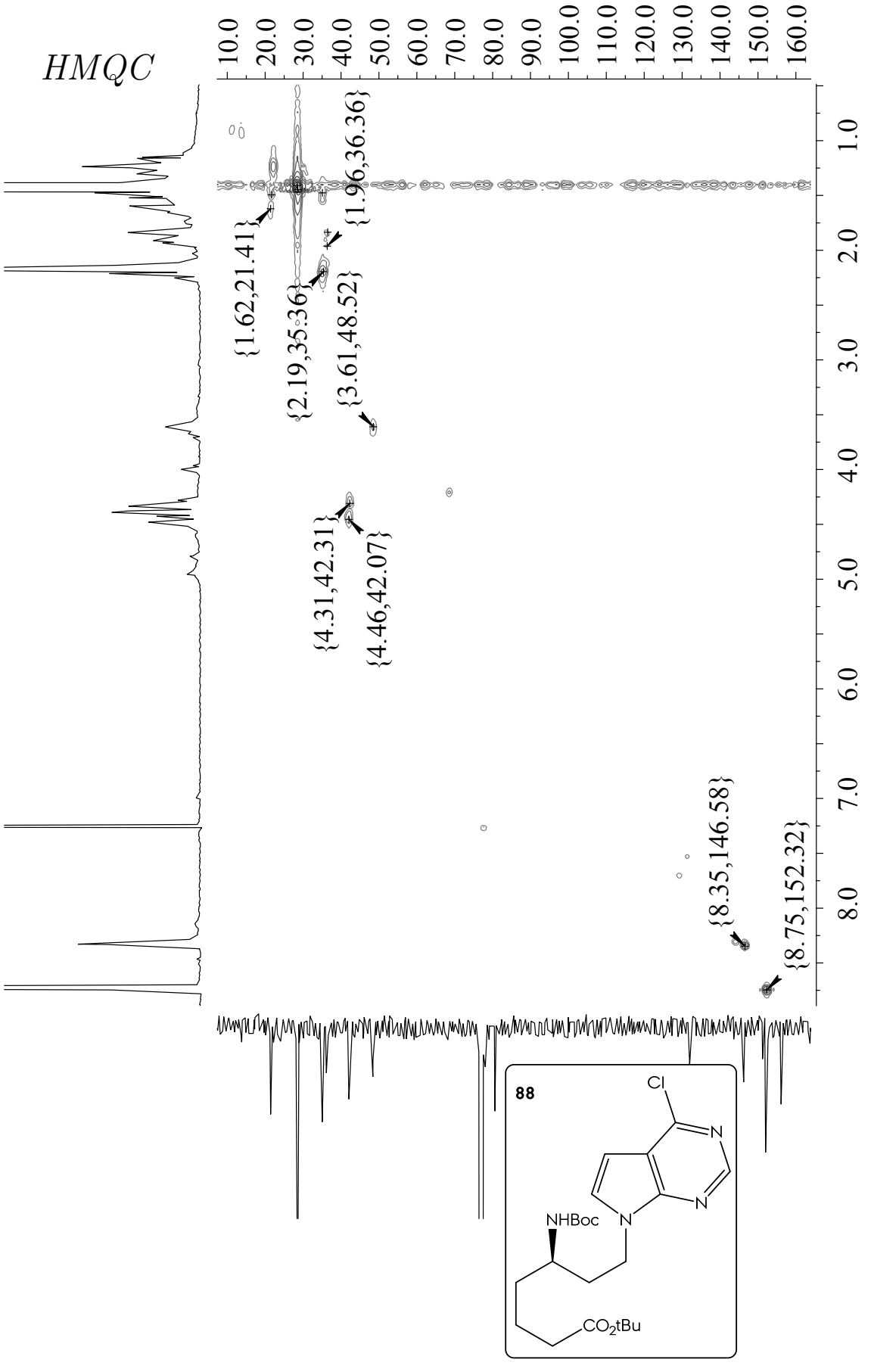
HMQC
10.0
20.0
30.0
40.0
50.0
60.0
70.0
80.0
90.0
100.0
110.0
120.0
130.0
140.0
150.0
160.0
1.0
2.0
3.0
4.0
5.0
6.0
7.0
8.0
{1.62,21.41}
{2.19,35.36}
{1.96,36.36}
{3.61,48.52}
{4.31,42.31}
{4.46,42.07}
{8.35,146.58}
{8.75,152.32}
88
Cl
N
N
NHBoc
N
CO2tBu

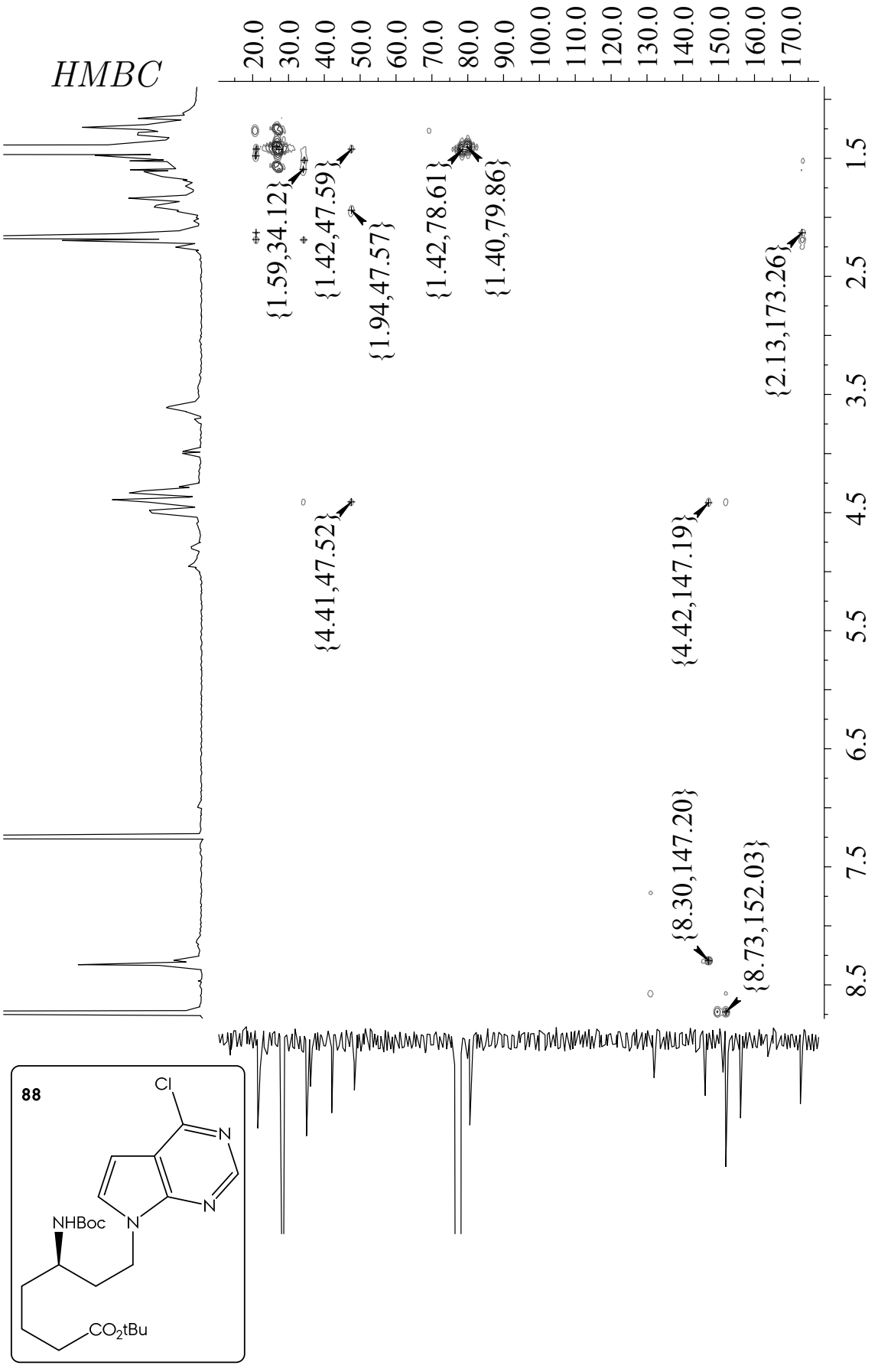
HMBC
20.0
30.0
40.0
50.0
60.0
70.0
80.0
90.0
100.0
110.0
120.0
130.0
140.0
150.0
160.0
170.0
1.5
2.5
3.5
4.5
5.5
6.5
7.5
8.5
{1.59,34.12}
{1.42,47.59}
{1.94,47.57}
{1.42,78.61}
{1.40,79.86}
{2.13,173.26}
{4.41,47.52}
{4.42,147.19}
{8.30,147.20}
{8.73,152.03}
88
Cl
N
N
NHBoc
N
CO2tBu

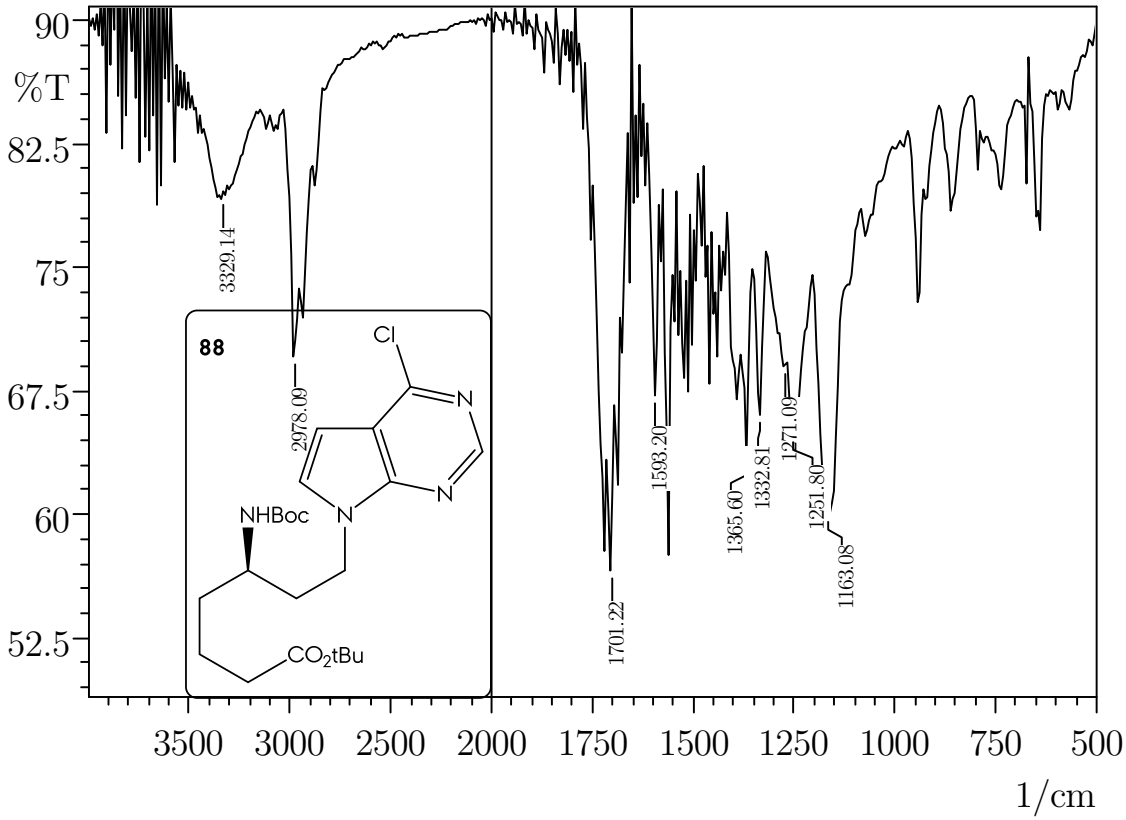
90
%T
82.5
75
67.5
60
52.5
3329.14
2978.09
1701.22
1593.20
1365.60
1332.81
1271.09
1251.80
1163.08
88
Cl
N
N
N
NHBoc
CO2tBu
3500 3000 2500 2000 1750 1500 1250 1000 750 500
1/cm

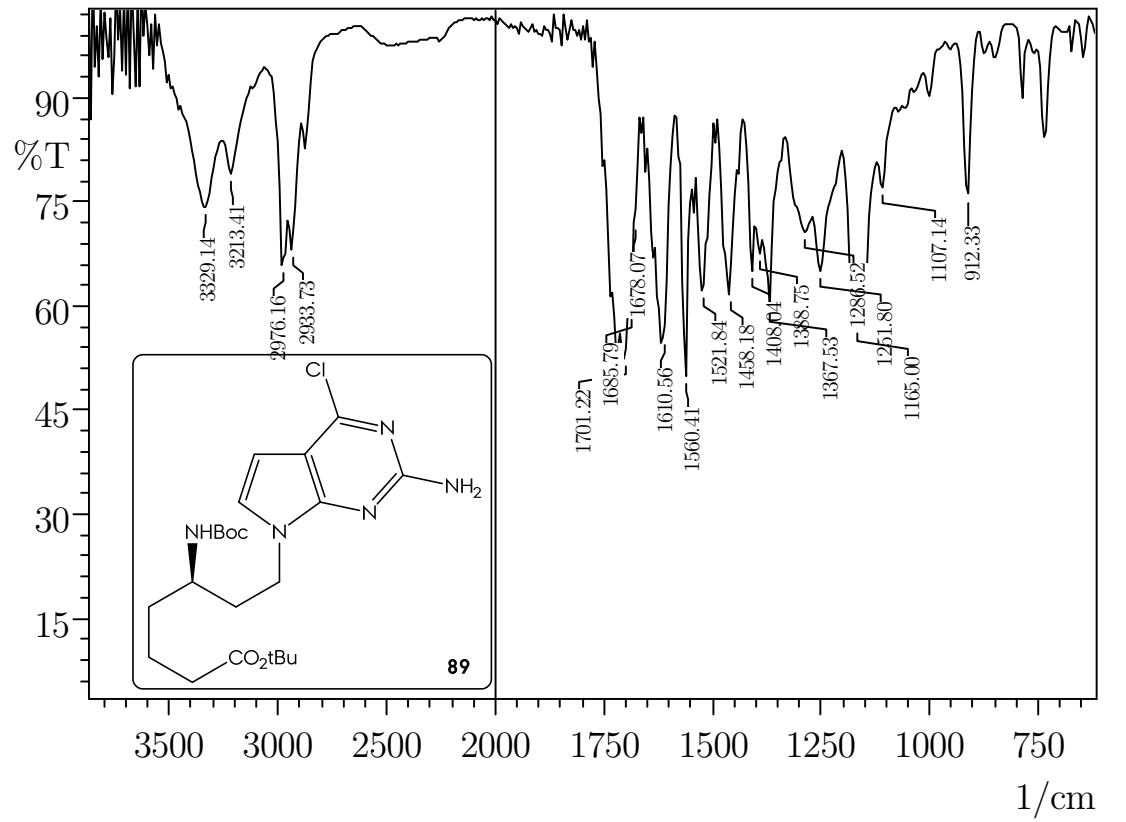
90
%T
75
60
45
30
15
3329.14
3213.41
2976.16
2933.73
1701.22
1685.79
1678.07
1610.56
1560.41
1521.84
1458.18
1408.04
1388.75
1367.53
1286.52
1251.80
1165.00
1107.14
912.33
Cl
N
N
NH2
N
NHBoc
CO2tBu
89
3500 3000 2500 2000 1750 1500 1250 1000 750
1/cm

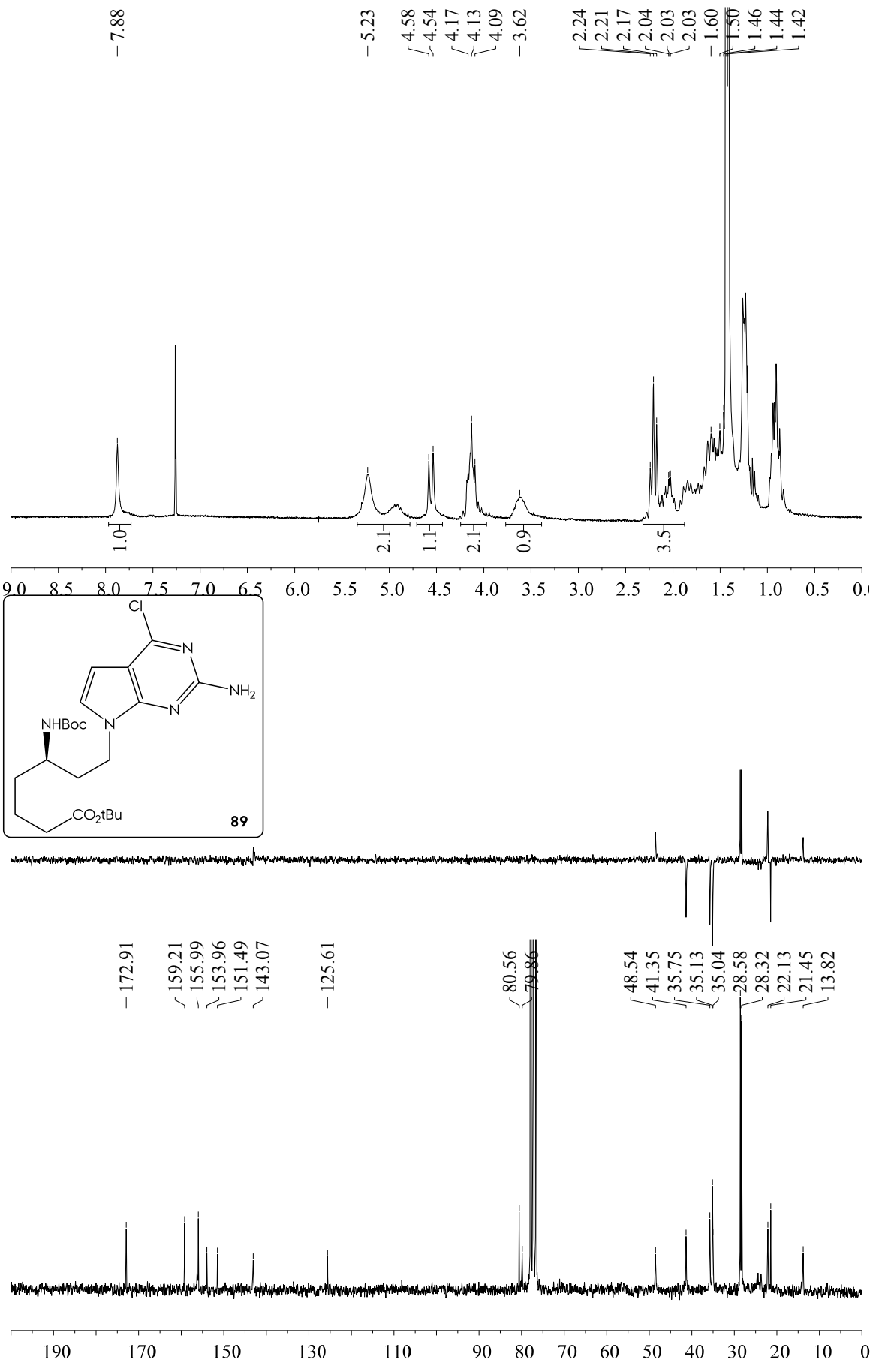
7.88
5.23
4.58
4.54
4.17
4.13
4.09
3.62
2.24
2.21
2.17
2.04
2.03
2.03
1.60
1.50
1.46
1.44
1.42
1.0
2.1
1.1
2.1
0.9
3.5
9.0 8.5 8.0 7.5 7.0 6.5 6.0 5.5 5.0 4.5 4.0 3.5 3.0 2.5 2.0 1.5 1.0 0.5 0.
Cl
N
NH2
N
NHBoc
N
CO2tBu
89
172.91
159.21
155.99
153.96
151.49
143.07
125.61
80.56
79.86
48.54
41.35
35.75
35.13
35.04
28.58
28.32
22.13
21.45
13.82
190 170 150 130 110 90 80 70 60 50 40 30 20 10 0

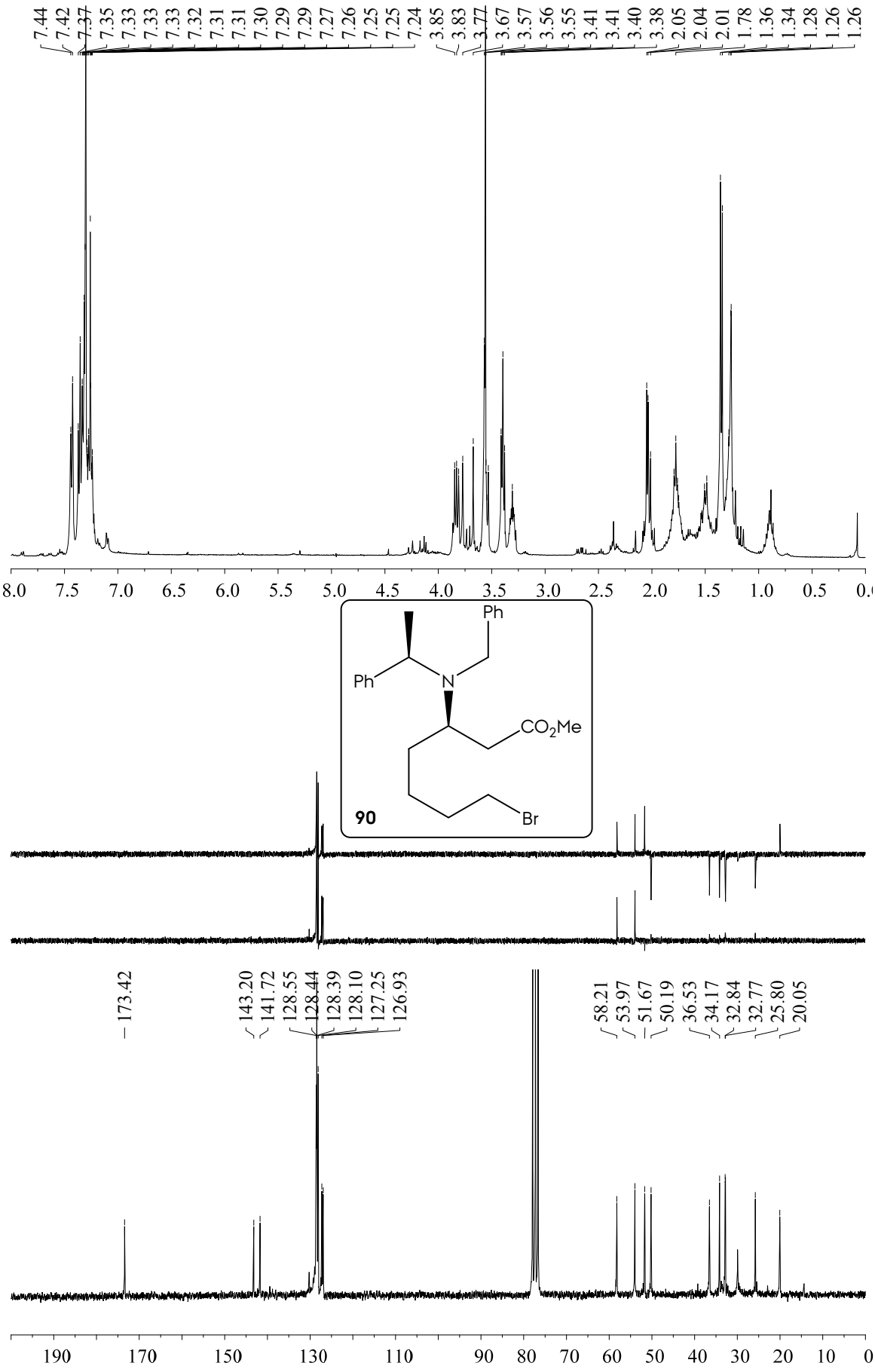
7.44
7.42
7.37
7.35
7.33
7.33
7.33
7.32
7.31
7.31
7.30
7.29
7.29
7.27
7.26
7.25
7.25
7.24
3.85
3.83
3.77
3.67
3.57
3.56
3.55
3.41
3.41
3.40
3.38
2.05
2.04
2.01
1.78
1.36
1.34
1.28
1.26
1.26
8.0 7.5 7.0 6.5 6.0 5.5 5.0 4.5 4.0 3.5 3.0 2.5 2.0 1.5 1.0 0.5
Ph
Ph
N
CO2Me
Br
90
173.42
143.20
141.72
128.55
128.44
128.39
128.10
127.25
126.93
58.21
53.97
51.67
50.19
36.53
34.17
32.84
32.77
25.80
20.05
190 170 150 130 110 90 80 70 60 50 40 30 20 10 0

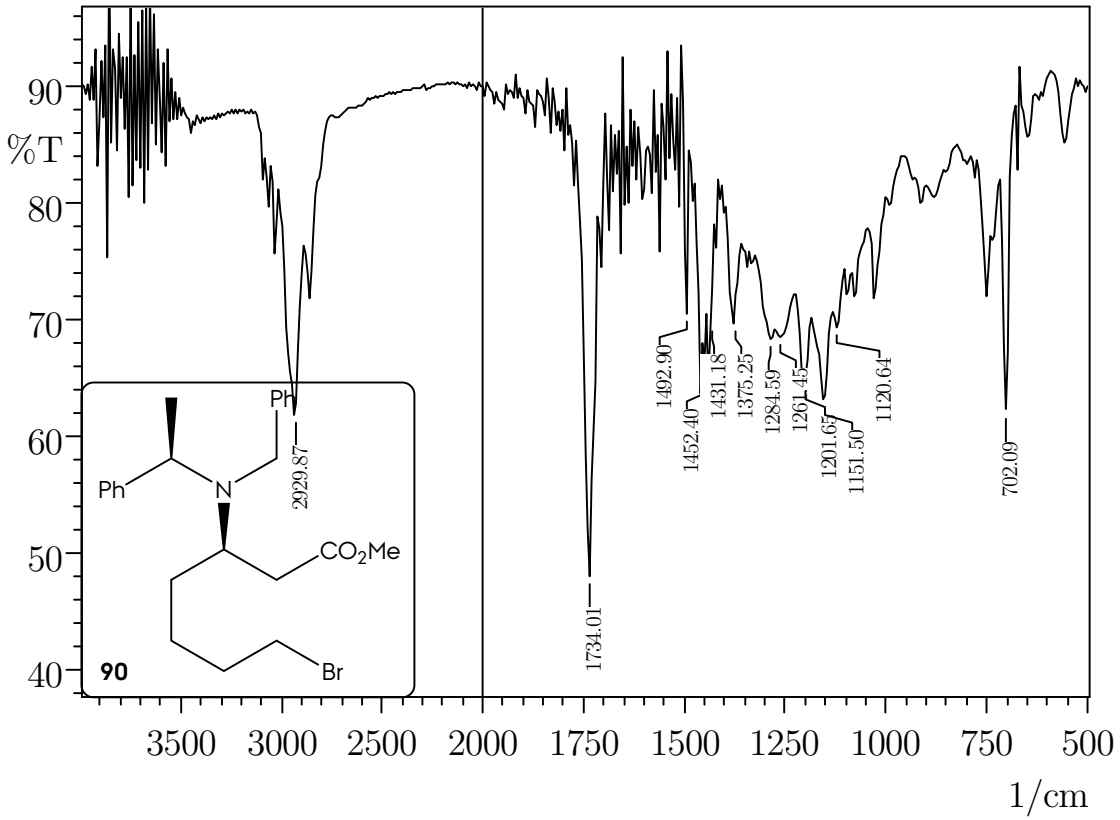
%T
90
80
70
60
50
40
3500
3000
2500
2000
1750
1500
1250
1000
750
500
1/cm
2929.87
1734.01
1492.90
1452.40
1431.18
1375.25
1284.59
1261.45
1201.65
1151.50
1120.64
702.09
Ph
N
Ph
CO2Me
Br
90

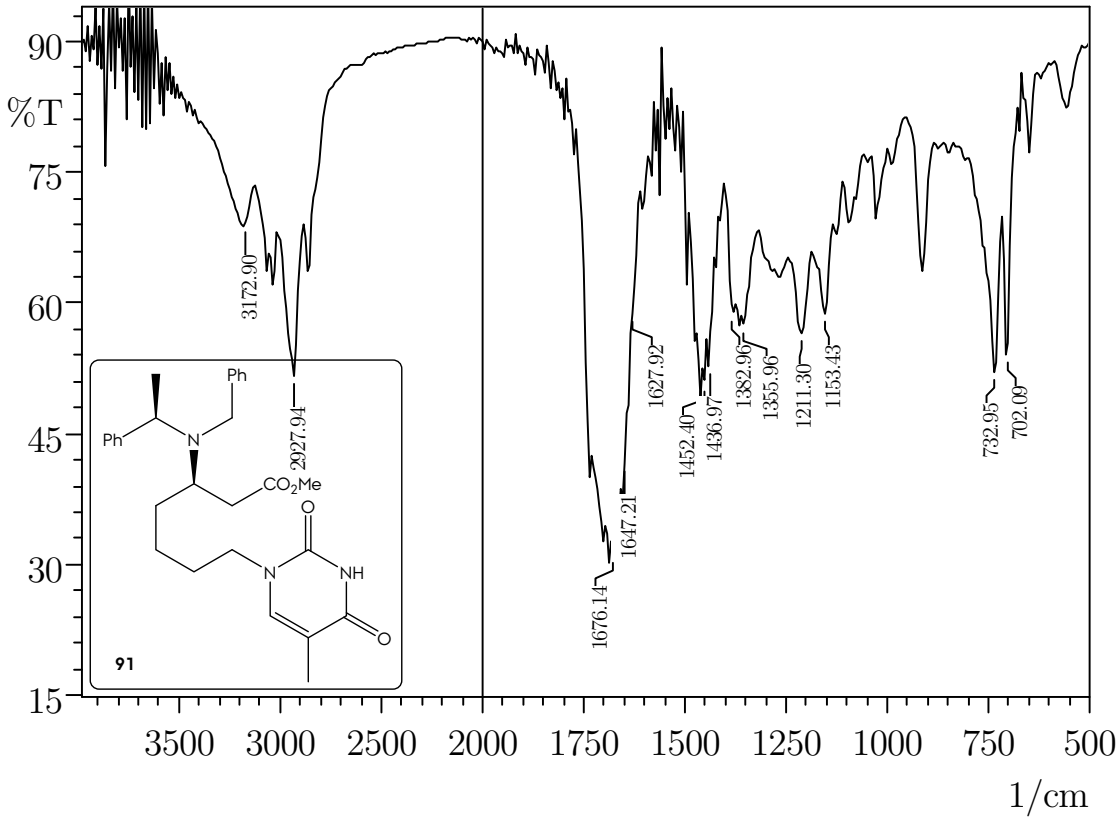
%T
90
75
60
45
30
15
3500
3000
2500
2000
1750
1500
1250
1000
750
500
1/cm
3172.90
2927.94
1676.14
1647.21
1627.92
1452.40
1436.97
1382.96
1355.96
1211.30
1153.43
732.95
702.09
Ph
N
Ph
CO2Me
O
N
NH
O
91

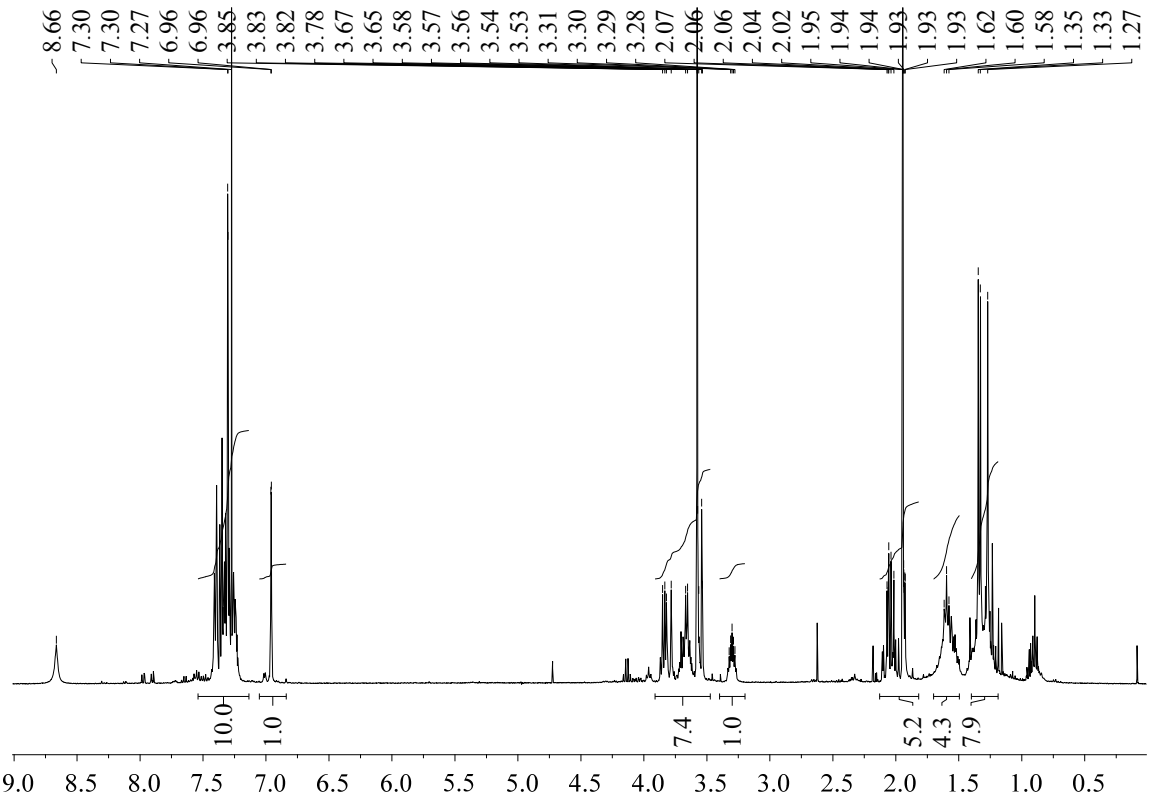
8.66
7.30
7.30
7.27
6.96
6.96
3.85
3.83
3.82
3.78
3.67
3.65
3.58
3.57
3.56
3.54
3.53
3.31
3.30
3.29
3.28
2.07
2.06
2.06
2.04
2.02
1.95
1.94
1.94
1.93
1.93
1.93
1.62
1.60
1.58
1.35
1.33
1.27
10.0
1.0
7.4
1.0
5.2
4.3
7.9
9.0 8.5 8.0 7.5 7.0 6.5 6.0 5.5 5.0 4.5 4.0 3.5 3.0 2.5 2.0 1.5 1.0 0.5

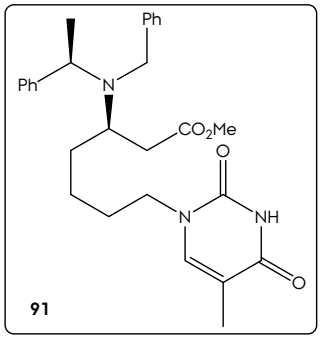
Ph
Ph
N
CO2Me
O
N
NH
O
91

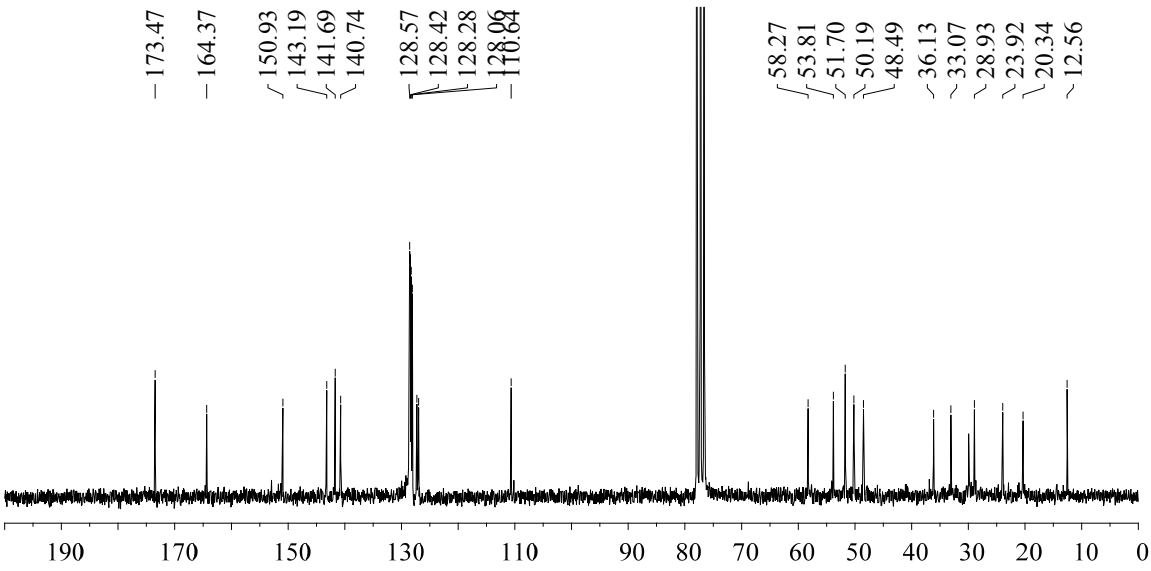
173.47
164.37
150.93
143.19
141.69
140.74
128.57
128.42
128.28
58.27
53.81
51.70
50.19
48.49
36.13
33.07
28.93
23.92
20.34
12.56
190 170 150 130 110 90 80 70 60 50 40 30 20 10 0

Asignación ^{13}C/RMN

(^{13}C NMR Assignation)

When rotameric forms are present, assignations are displayed with different colours.

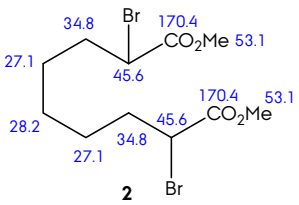

2

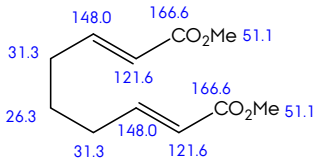

3

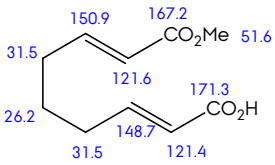

4

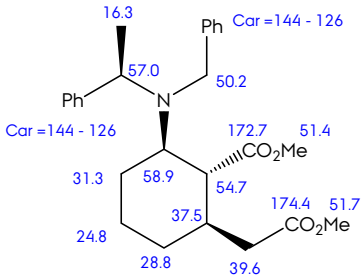

5

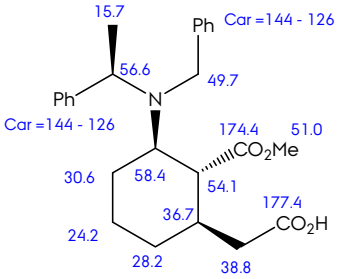

6

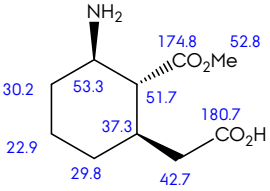

7

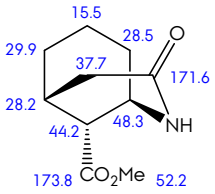

8

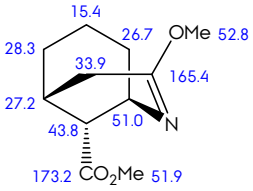

9

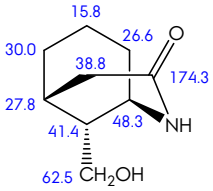

10

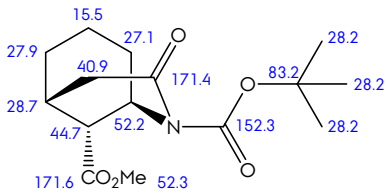

11

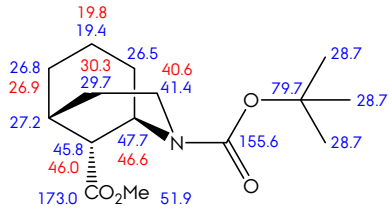

12

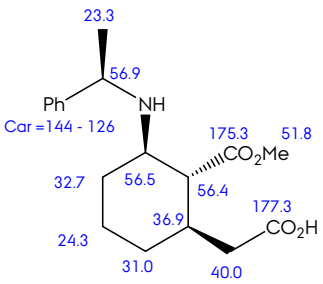

13

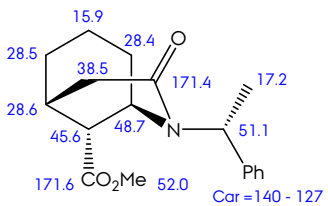

14

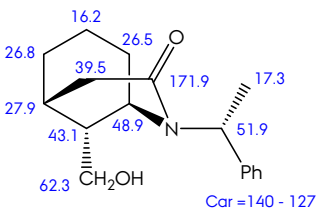

15

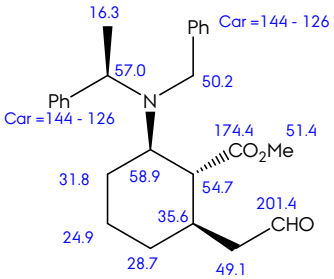

16

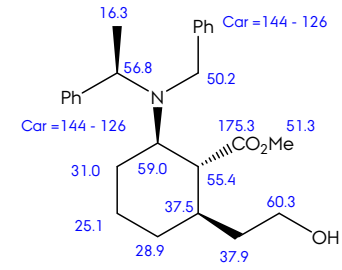

17

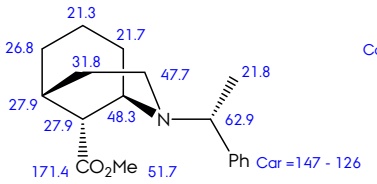

18

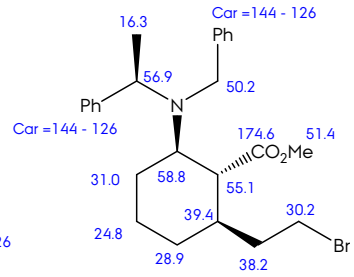

19

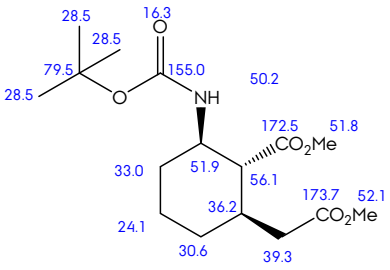

20

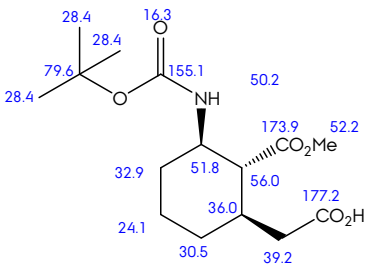

21

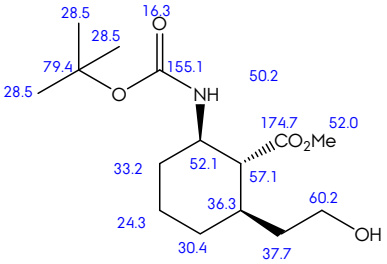

22

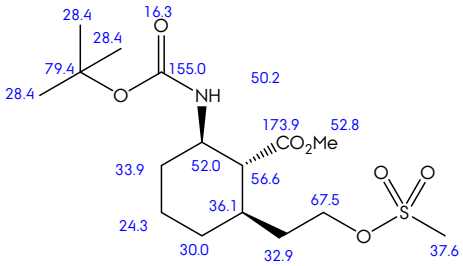

23

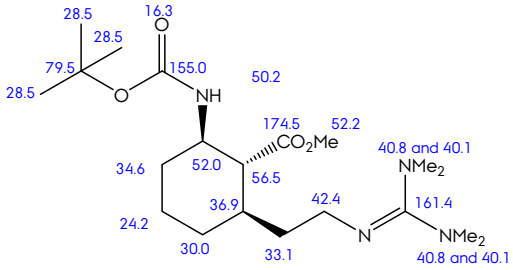

24

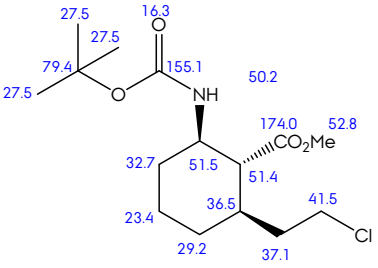

25

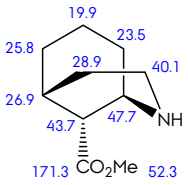

26

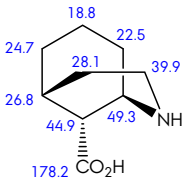

27

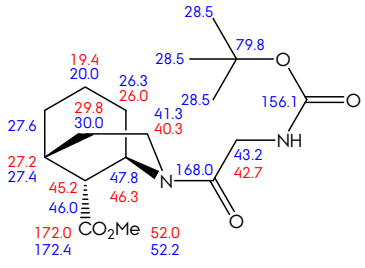

28

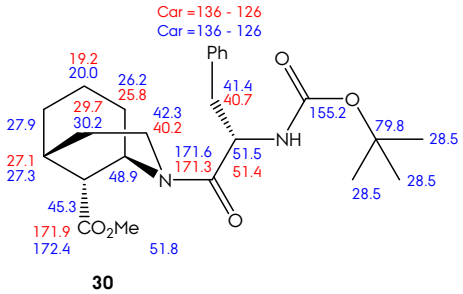

30

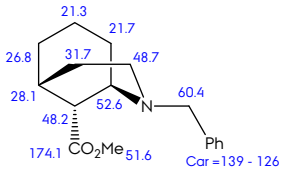

32

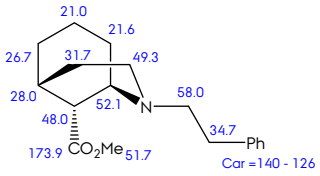

34

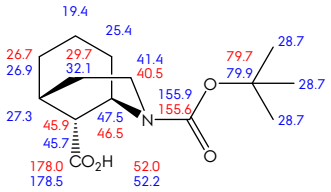

36

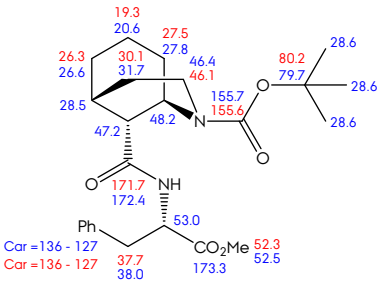

37

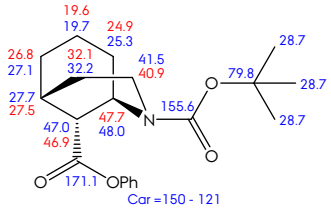

39

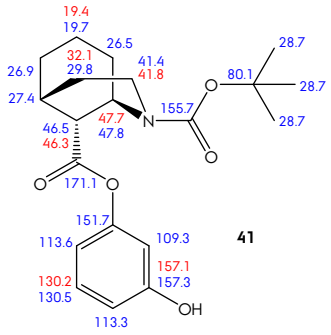

41

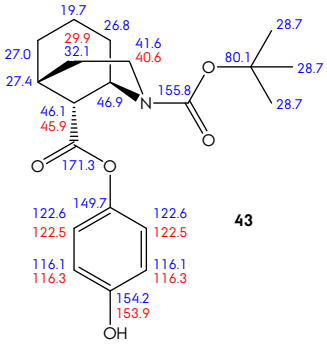

43

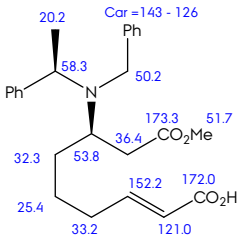

45

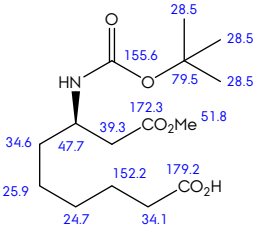

46

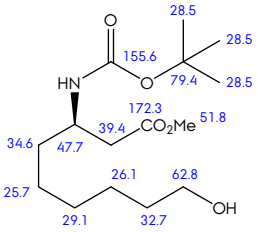

47

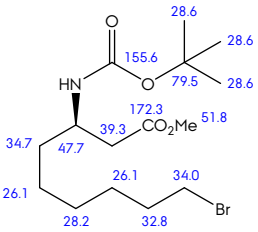

48

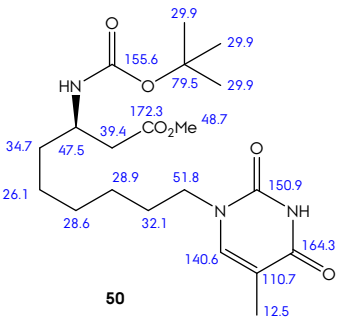

50

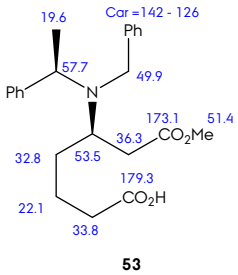

53

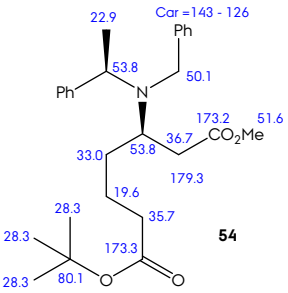

54

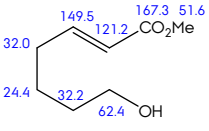

56

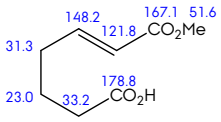

58

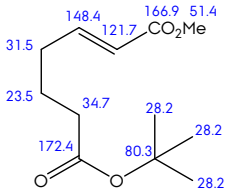

59

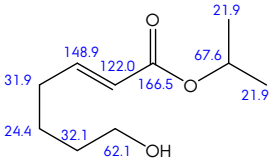

60

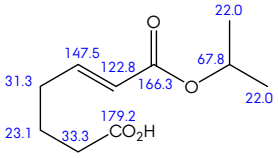

61

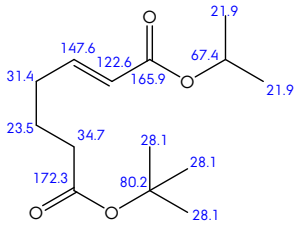

62

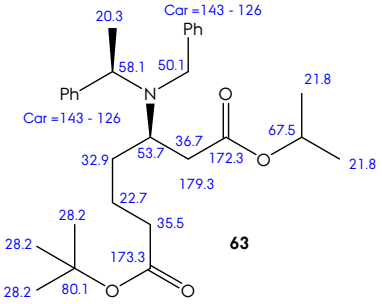

63

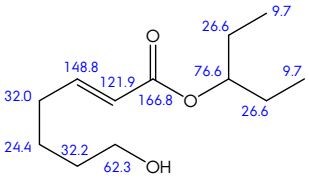

64

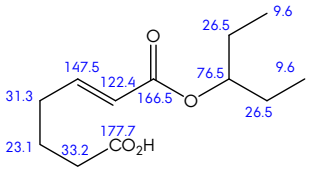

65

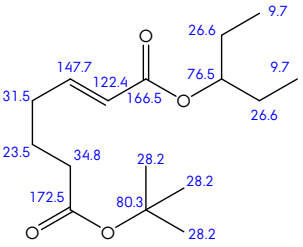

66

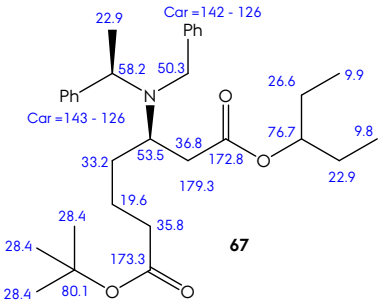

67

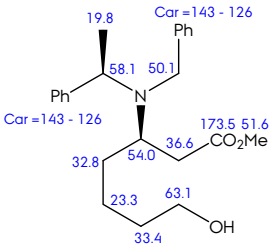

68

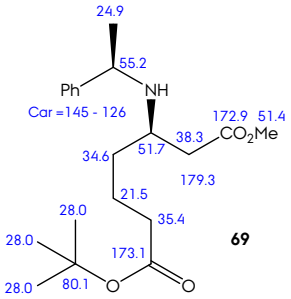

69

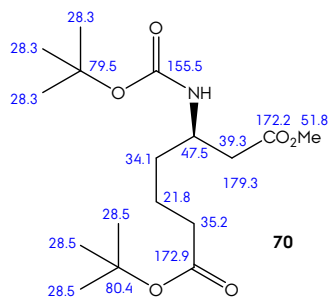

70

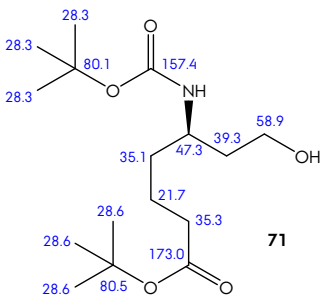

71

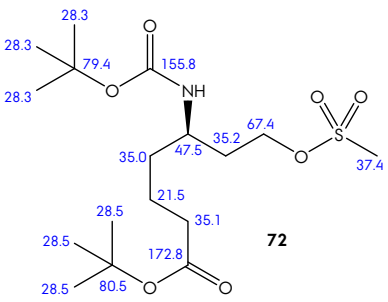

72

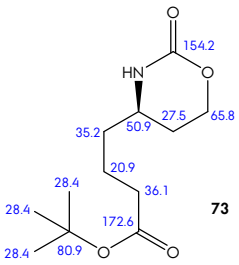

73

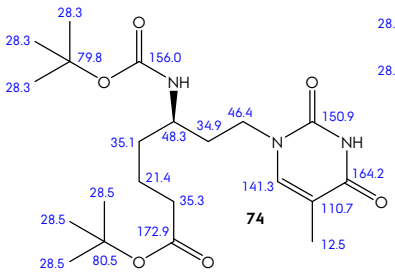

74

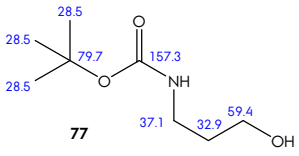

77

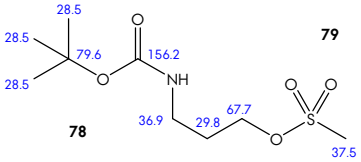

78

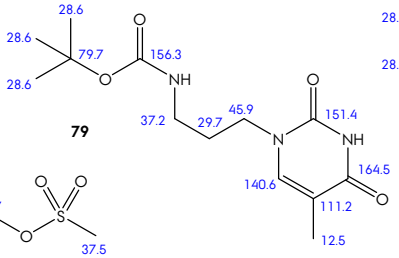

79

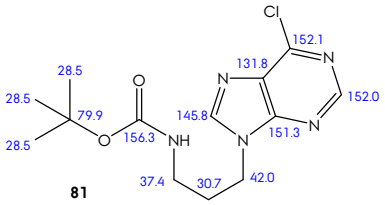

81

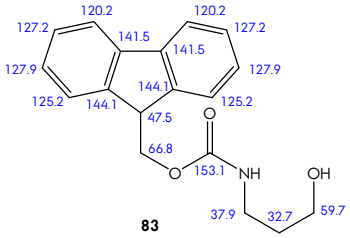

83

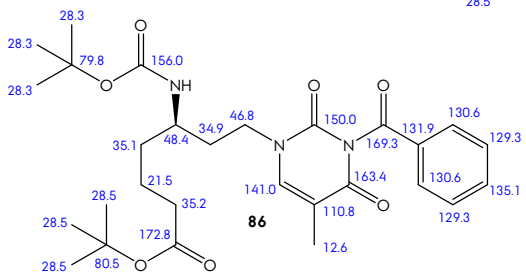

86

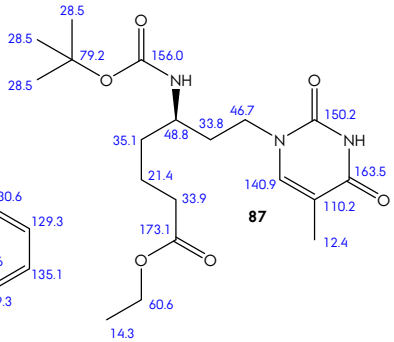

87

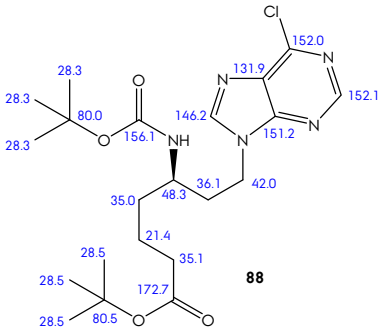

88

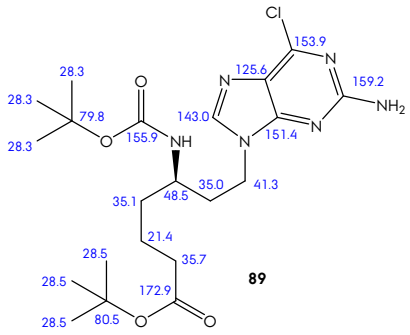

89

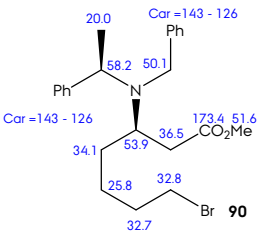

90

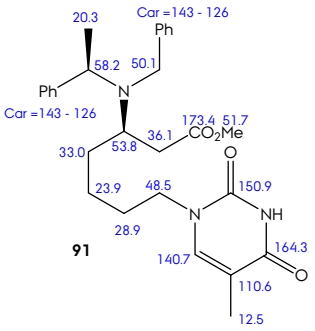

91

Tablas de Correlación Bidimensional

(2D NMR Experiments)

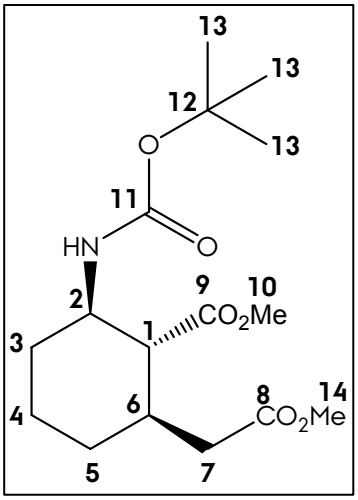

20

C	δ ^{13}C	DEPT	HMQC	HMBC
1	56.1	CH	2.07 (1H)	
2	51.9	CH	3.67 - 3.64 (1H)	
3	33.0	CH_2	2.06 (1H)	
			1.14 (1H, qd, *J* 12.7 3.8)	
4	24.1	CH_2	1.79 (1H)	
			1.41 (1H)	
5	30.6	CH_2	1.77 (1H)	
			0.97 (1H, qd, *J* 12.9 3.6)	
6	36.2	CH_2	2.12 (1H)	H1
7	39.3	CH_2	2.31 (1H, ABX, *J* 14.1 2.8)	
			1.13 (1H, AB, *J* 14.1)	
8	173.7	C		$H14, H7_A$
9	172.5	C		H10, H1
10	51.8	CH_3	3.64 (3H, s)	
11	155.0	C		
12	79.5	C		H13
13	28.5	CH_3	1.40 (9H, s)	
14	52.1	CH_3	3.67 (3H, s)	

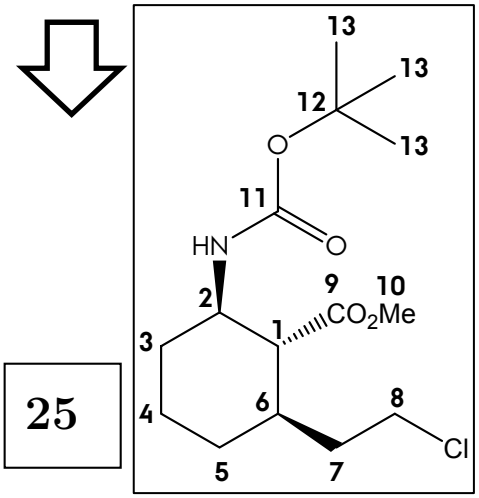

25

C	δ ^{13}C	DEPT	HMQC
1	56.7	CH	2.02 - 1.98 (1H)
2	51.5	CH	3.71 - 3.68 (1H)
3	32.7	CH_2	2.03 (1H)
			1.27 (1H, qd, *J* 12.8 3.8)
4	23.4	CH_2	1.77 (1H)
			1.41 (1H)
5	29.2	CH_2	1.83 (1H)
			0.89 (1H, qd, *J* 12.5 3.0)
6	36.5	CH_2	1.83 (1H)
7	37.1	CH_2	2.02 (1H)
			1.58 (1H)
8	41.5	CH_2	3.57 (1H, ddd, *J* 13.1 8.1 5.0)
			3.48 (1H)
9	174.0	C	
10	51.4	CH_3	3.7 (3H, s)
11	155.1	C	
12	79.4	C	
13	27.5	CH_3	1.42 (9H, s)

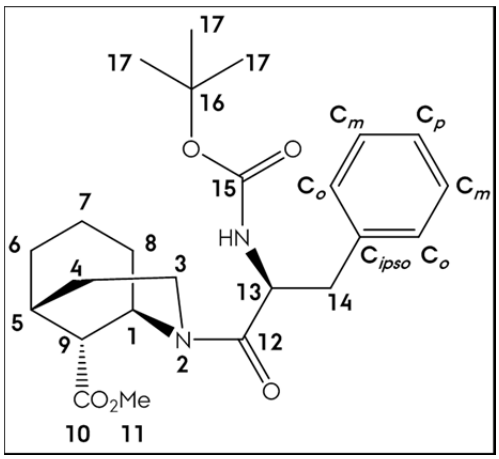

30

C	δ ^{13}C	DEPT	HMQC
1	48.9	CH	4.02 (1H, br s)
3	42.3	CH_2	3.05 (1H, td, *J* 12.8 5.9)
	40.2		3.62 (1H, m, rotamer) and 3.31 (1H, dd, *J* 12.6 6.8)
4	30.2	CH_2	1.54
	29.7		1.61
5	27.3	CH	2.26 (1H, br s, rotamer)
	27.1		2.37 (1H, br s)
6	27.9	CH_2	1.62
7	20.0	CH_2	1.62
	19.2		1.34
8	26.2	CH_2	1.65 (2H)
	25.8		1.74 (2H, rotamer)
9	45.3	CH	2.45 (1H, br s)
10	172.4	C	
	171.9		
11	51.8	CH_3	3.69 (3H, s)
12	171.6	C	
	171.3		
13	51.5	CH	4.90 (1H, m)
	51.4		
14	41.4	CH_2	2.86 (1H, dd, *J* 12.9 9.0)
	40.7		2.98 (1H, dd, *J* 12.9 10.4)
15	155.2	C	

16	79.8	C	
17	28.5	CH_3	1.42 (9H, s)
$\mathbf{C}_{ipso}$	136.6	C	
$\mathbf{C}_o$	129.9	CH	7.27 - 7.18 (2H)
	129.8		
$\mathbf{C}_m$	128.6	CH	7.27 - 7.18 (2H)
	128.5		
$\mathbf{C}_p$	127.1	CH	7.27 - 7.18 (1H)
	126.9		

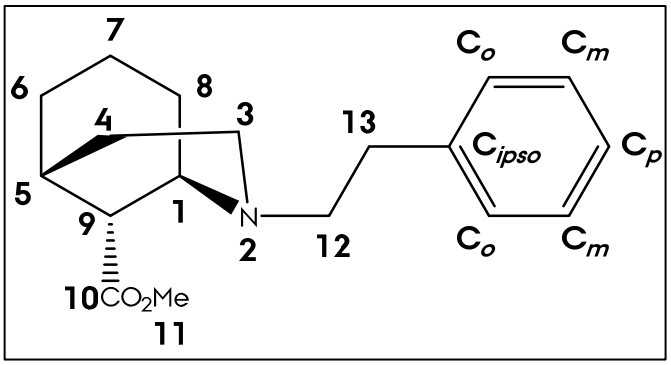

34

C	δ ^{13}C	DEPT	HMQC
1	52.1	CH	3.21 (1H, s)
3	49.3	CH_2	2.82 (2H, dd, *J* 11.5 4.7)
4	31.7	CH_2	1.99 (1H, m)
			1.68 (1H, m)
5	28.0	CH	2.28 (1H, s)
6	26.7	CH_2	1.68 (1H, m)
			1.44 (1H, m)
7	21.0	CH_2	1.84 (1H, m)
			1.44 (1H, m)
8	21.6	CH_2	1.68 (1H, m)
			1.44 (1H, m)
9	48.0	CH	2.60 (1H, s)
10	173.9	C	

11	51.7	CH_3	3.61 (3H, s)
12	58.0	CH_2	2.70 (1H, m)
			2.62 (1H, m)
13	34.7	CH_2	2.69 (2H, m)
$\mathbf{C}_{ipso}$	140.8	C	
$\mathbf{C}_{o,\ m,\ p}$	128.9 - 126.2	CH	7.19 - 7.08 (5H, m)

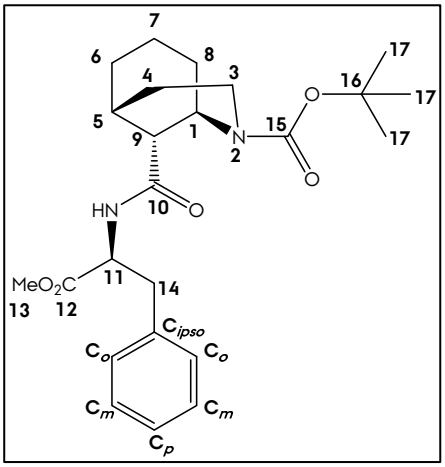

37

C	δ ^{13}C	DEPT	HMQC
1	48.3	CH	4.56 (1H, br s, rotamer)
	47.4		4.46 (1H, br s, rotamer)
	45.4		4.35 (1H, br s)
3	42.0	CH_2	3.48 (1H)
	41.2		3.68 (1H, rotamer)
	40.9		3.74 (1H, rotamer)
4	31.9	CH_2	1.76 (1H, rotamer)
	31.7		1.87 (1H)
	31.6		1.96 (1H)
5	28.5	CH	2.29 and 2.21 (1H, br s, rotamers)
6	27.6	CH_2	-
7	20.6	CH_2	1.60 (1H)
	19.6		1.66 (1H, rotamer)
	19.3		1.46 (1H)
8	26.5	CH_2	1.66 (1H)
	26.0		1.47 (1H)

9	47.2	CH	2.30 (1H, br s)
	46.6		2.41 (1H, rotamer)
	46.1		2.46 (1H, rotamer)
10	173.3	C	
11	54.5	CH	4.93 (1H, br s)
	53.1		4.69 (1H, br s, rotamer)
12	172.4	C	
	171.7		
13	54.2	CH_3	3.76 (3H, rotamer)
	52.6		3.69 (3H)
14	37.9	CH_2	3.21 - 2.88 (2H, rotamers)
	37.8		
15	156.6	C	
	155.6		
16	82.2	C	
	79.7		
17	28.6	CH_3	1.47 (9H, s)
$\mathbf{C}_{ipso}$	136.6	C	
	136.1		
$\mathbf{C}_{o}$	129.3	CH	7.12 (2H)
$\mathbf{C}_{m}$	128.9	CH	7.32 - 7.21 (2H)
	128.8		
$\mathbf{C}_{p}$	127.4	CH	7.32 - 7.21 (1H)
	127.2		

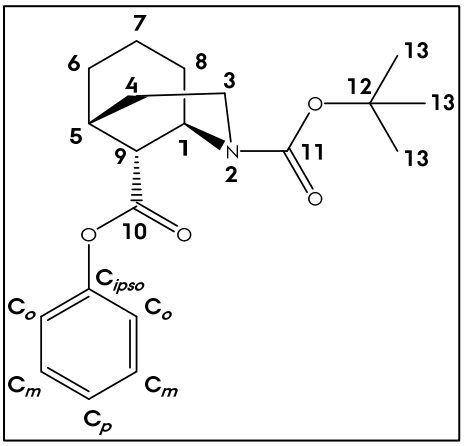

39

C	δ ^{13}C	DEPT	HMQC	HMBC
1	48.0	CH	4.93 (1H, br s, rotamer)	
	47.7		4.82 (1H, br s, rotamer)	
	47.1		4.77 (1H, br s)	H3
	46.6		4.58 (1H, br s, rotamer)	
3	41.5	CH_2	3.77 (1H, m, rotamer)	
	41.3		3.65 (1H, m, rotamer)	
	40.9		3.50 (1H)	
4	32.2	CH_2	2.23 (1H, m)	
	32.1		1.89 (1H)	
	31.7		1.84 (1H, rotamer)	
5	27.3	CH	2.61 (1H)	H3, H1
	26.7		2.56 (1H, rotamer)	
6	27.1	CH_2	1.83 (1H)	
	26.8		1.67 (1H, rotamer)	H7
	26.5		1.62 (1H, rotamer)	
7	19.7	CH_2	2.03 (1H)	H6
	19.7		1.86 (1H)	
	19.6		1.77 (1H, rotamer)	
	19.6		1.64 (1H, rotamer)	
	19.6		1.58 (1H, rotamer)	
8	25.3	CH_2	1.72 (1H, rotamer)	H9
	24.9		1.61 (1H)	H7, H6
9	47.0	CH	2.89 (1H, rotamer)	
	46.9		2.86 (1H, rotamer)	H4

	46.5		2.75 (1H, rotamer)	
	45.9		2.68 (1H)	
10	171.1	C		H9
11	155.6	C		
12	79.8	C		H13
13	28.7	CH_3	1.48 (9H, rotamers)	
			1.44 (9H, rotamers)	
$\mathbf{C}_{ipso}$	150.9	C		m-C_{ar}H, o-C_{ar}H
$\mathbf{C}_{m}$	129.6	CH	7.38 (2H, m)	m-C_{ar}H (transversal)
$\mathbf{C}_{p}$	126.0	CH	7.23 (1H, m)	o-C_{ar}H
$\mathbf{C}_{o}$	121.7	CH	7.06 (2H, m)	p-C_{ar}H, o-C_{ar}H

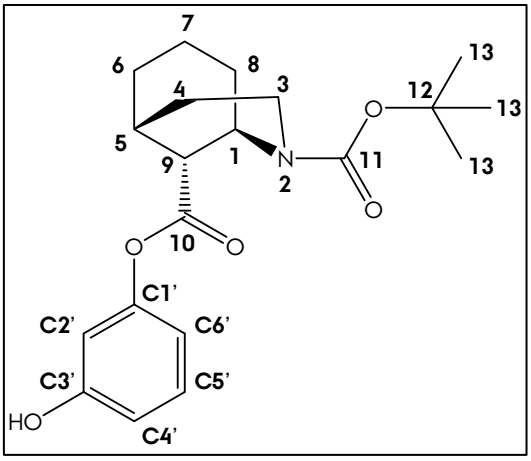

41

C	δ ^{13}C	DEPT	HMQC	HMBC
1	47.8	CH	4.89 (1H)	
	47.7		4.80 (1H, rotamer)	
	46.5		4.76 (1H, rotamer)	
	46.4		4.57 (1H, rotamer)	
3	41.8	CH_2	3.77 and 3.67 (1H, m, rotamers)	
	41.4		3.53 (1H, m)	
4	32.1	CH_2		
	29.8			
5	27.4	CH	2.59 and 2.55 (1H, br s, rotamers)	H3
6	26.9	CH_2		
7	19.7	CH_2		

	19.4			
8	26.5	CH_2		
9	46.5	CH	2.87 (1H, br s)	
	46.3		2.83 (1H, br s, rotamers)	
	46.1		2.73 (1H, br s, rotamers)	
	45.7		2.67 (1H, br s, rotamers)	
10	171.1	C		
11	155.7	C		
12	80.1	C		H13
13	28.7	CH_3	1.49 and 1.44 (9H, s, rotamers)	H13 (transeversal)
C1'	151.7	C		H5'
C2'	109.3	CH	6.62 (1H, m)	H6'
C3'	157.3	C		H5'
	157.1	C		
C4'	113.6	CH	6.72 (1H, t, *J* 7.1)	H6'
C5'	130.5	CH	7.22 (1H, t, *J* 9.1)	
	130.2	CH		
C6'	113.3	CH	6.62 (1H, m)	H2'

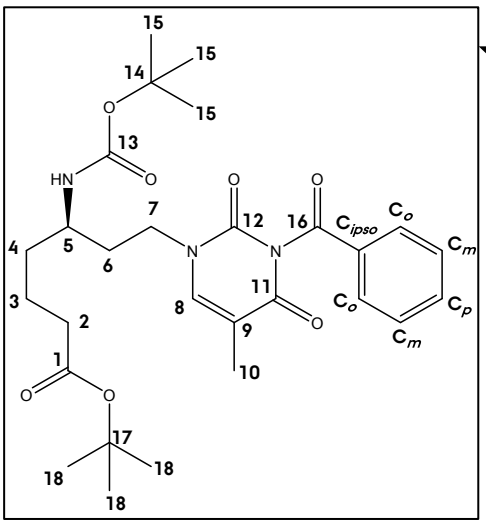

86

C	δ ^{13}C	DEPT	HMQC	HMBC
1	172.8	C		
2	35.2	CH_2	2.21 (2H, q, *J* 6.3)	
3	21.5	CH_2	1.62 (1H)	
			1.51 (1H)	

4	35.1	CH_2	1.91 (1H)	
			1.55 (1H)	
5	48.4	CH	3.62 (1H)	
6	34.9	CH_2	1.66 (2H)	
7	46.8	CH_2	3.93 (1H)	
			3.62 (1H)	
8	141.0	CH	7.23 (1H, br s)	H10
9	110.8	C		
10	12.6	CH_3	1.91 (3H, s)	
11	163.4	C		H8, H10
12	150.0	C		H8
13	156.0	C		
14	79.8	C		H15
15	28.3	CH_3	1.44 (9H, s)	H15
16	169.3	C		o-C_{ar}H
17	80.5	C		H18
18	28.5	CH_3	1.44 (9H, s)	H18
$\mathbf{C}_{ipso}$	131.9	C		m-C_{ar}H
$\mathbf{C}_{o}$	130.6	CH	7.91 (2H, dd, *J* 8.5 1.2)	o-C_{ar}H, p-CarH
$\mathbf{C}_{m}$	129.3	CH	7.63 (1H, t, *J* 7.4)	p-C_{ar}H
$\mathbf{C}_{p}$	135.1	CH	7.63 (1H, tt, *J* 7.4 1.6)	o-C_{ar}H

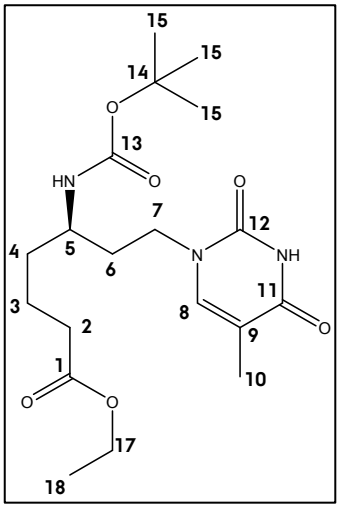

87

C	δ ^{13}C	DEPT	HMQC	HMBC
1	173.1	C		H17
2	33.9	CH_2	2.30 (2H)	H3
3	21.4	CH_2	1.69 (1H)	
			1.55 (1H)	
4		CH_2		
5	48.8	CH	3.60 (1H)	
6	33.8	CH_2	1.66 (2H)	
7	46.7	CH_2	3.82 (1H)	
			3.60 (1H)	
8	140.9	CH	7.12(1H, br s)	H10
9	110.2	C		H10
10	12.4	CH_3	1.92 (3H, s)	
11	163.5	C		H8, H10
12	150.2	C		H8
13		C		
14	79.2	C		H15
15	28.5	CH_3	1.45 (9H, s)	
17	60.6	C	4.12 (2H, q, *J* 7.1)	H18
18	14.3	CH_3	1.25 (3H, t, *J* 7.1)	H17

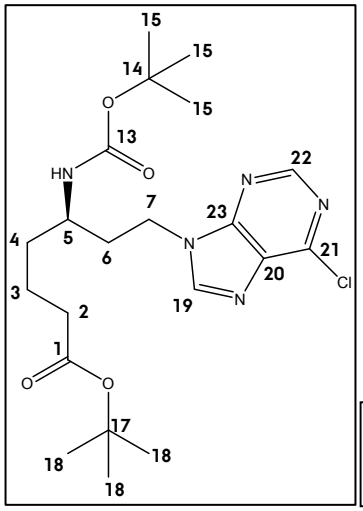

88

C	δ ^{13}C	DEPT	HMQC	HMBC
1	172.7	C		H2
2	35.1	CH_2	2.18 (2H)	H2, H6
3	21.4	CH_2	1.62 (1H)	
			1.49 (1H)	
4	35.0	CH_2	1.91 (2H)	H2, H3
5	48.3	CH	3.61 (1H)	H3, H6, H7
6	36.1	CH_2	1.91 - 1.84 (2H)	
7	42.0	CH_2	4.40 (1H, ABXY, *J* 14.1 7.2 5.2)	
			4.33 (1H, quintet, *J* 7.2)	
13	156.1	C		
14	80.5	C		H14
15	28.3	CH_3	1.40 (9H, s)	H15
17	80.0	C		H18
18	28.5	CH_3	1.44 (9H, s)	H18
19	146.2	CH	8.33 (1H, s)	H7
			8.30 (1H, s, rotamer)	
20	131.9	C		
21	152.0	CH	8.75 (1H, s)	H22
			8.73 (1H, s, rotamer)	
22	152.1	C		
23	151.2	C		H19

Análisis de Difracción de Rayos X

(X-Ray Difraction Analysis)

Datos Cristalográficos de $C_{10}H_{15}NO_3$ (8).

Instrumentación.

Las medidas de las intensidades de las reflexiones de los monocristales presentados en este trabajo, se realizaron a temperatura ambiente con un difactómetro de cuatro círculos SEIFERT XRD 3003 SC, usando radiación CuK (λ =1.54180 Å).

Difracción de RX en monocristal. Compuesto $C_{10}H_{15}NO_3$ (8).

Para la determinación estructural del compuesto $C_{10}H_{15}NO_3$ se seleccionó un monocristal prismático de dimensiones 0.10 x 0.15 x 0.20 mm. Las dimensiones de la celdilla unidad se establecieron por el ajuste de mínimos cuadrados de 25 reflexiones bien centradas en el rango angular $2^o < \theta < 20^o$. Una vez determinada la celda elemental y la simetría del cristal se midieron las intensidades difractadas mediante barridos $\omega/2\theta$ hasta un ángulo máximo de Bragg de 120^o, recogiéndose 5251 reflexiones. Una vez realizadas las correcciones de Lorentz y polarización quedaron 1422 reflexiones observadas [I > 2 (I)] para la resolución y refinamiento de la estructura. Los factores de difusión y corrección de dispersión anómala para los átomos de C N y O, se tomaron de las Tablas Internacionales de Cristalografía[1].

La estructura se resolvió en el grupo espacial monoclínico $P4_12_12$ (N^o = 92) usando métodos directos. Refinamientos por mínimos cuadrados con matriz completa empleando parámetros térmicos anisotrópicos para los átomos de carbono y oxígeno condujeron a los factores de acuerdo R1 = 0.0296, R2 = 0.0691. Las posiciones de los átomos de hidrógeno se calcularon teóricamente.

Todos los cálculos se llevaron a cabo utilizando los programas: CRYSOM[2] para la toma de datos, XRAY80[3] para la reducción de datos y SHELXTLTM[4] para resolver y obtener una representación tridimensional del compuesto.

Datos cristalográficos y refinamiento estructural de $C_{10}H_{15}NO_3$ (8).

Fórmula empírica	C_{10} H_{15} N O_3
Peso molecular	197.23
Temperatura	293(2) K
Longitud de onda	1.54178 A
Sistema cristalográfico, grupo espacial	Tetragonal, $P4_12_12$
Dimensiones de la celda unidad	a = 7.1768(10) A = 90 º
	b = 7.1768(10) A = 90 º
	c = 39.793(8) A = 90 º
Volumen	2049.6(6) A^3
Z, densidad calculada	8, 1.278 Mg/m^3
Coeficiente de absorción	0.778 mm^{-1}
F(000)	848
Tamaño del cristal	0.10 x 0.15 x 0.20 mm
Límites de	de 4.44 a 60.01º
Límites de los indices	$-5 \leq h \leq 7$, $-5 \leq k \leq 7$, $-40 \leq l \leq 43$
Reflexiones adquiridas	5251 / 1422 [R(int) = 0.0178]
Corrección de absorción	No aplicada
Método de refinamiento	Mínimos cuadrados con matriz completa en F2
Datos / restricciones / parametros	1422 / 0 / 145
Bondad de ajuste en F^2	1.079
Índice R final [I > 2 (I)]	R1 = 0.0296, R2 = 0.0691
Índice R (todos los datos)	R1 = 0.0334, R2 = 0.0713
Parámetros de estructura absoluta	-0.06(34)
Coeficiente de extinción	0.0035(3)

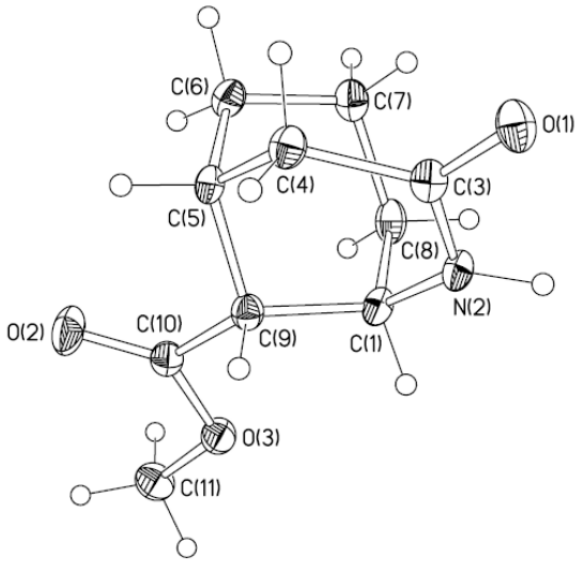

(a)

(b)

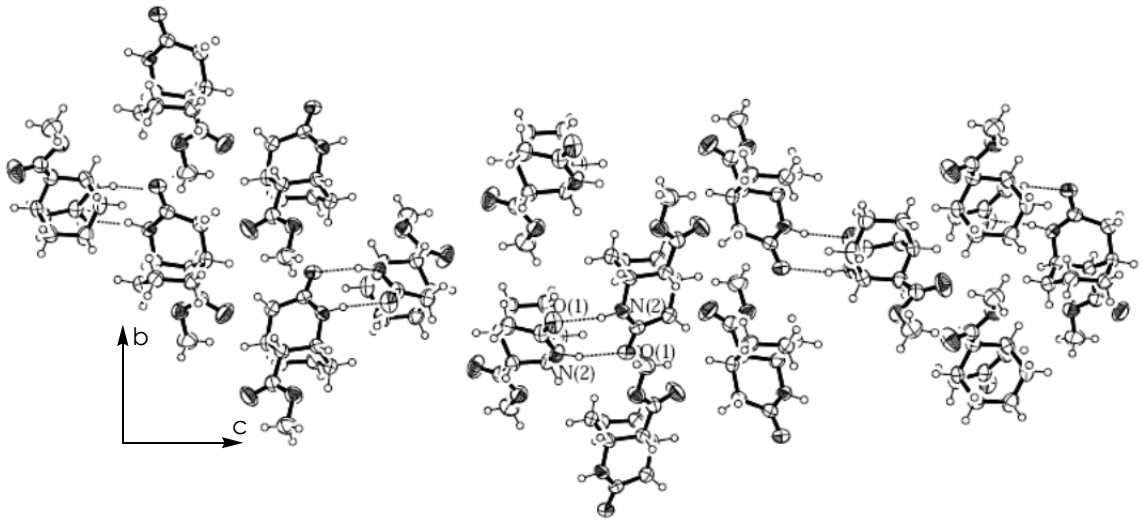

(a) Diagrama ORTEP[5] de $C_{10}H_{15}NO_3$ (50 % de probabilidad). Los átomos de C, O y N se representan con elipsoides, mientras que los átomos de hidrógeno se indican con esferas. (b) Perspectiva de la celda unidad, mostrando los enlaces de hidrógeno intermoleculares como lineas punteadas.

Coordenadas atómicas y parametros equivalentes de desplazamiento isotrópicos para $C_{10}H_{15}NO_3$ (8). U(eq) se define como la tercera parte de la traza del tensor Uij ortogonalizado.

	x	y	z	U(eq)
O(1)	1926(2)	130(2)	406(1)	61(1)
O(2)	-868(2)	7551(2)	1114(1)	81(1)
O(3)	-2546(2)	7417(2)	644(1)	58(1)
C(1)	-441(3)	4556(3)	379(1)	48(1)
N(2)	46(2)	2594(2)	319(1)	48(1)
C(3)	1254(3)	1612(3)	507(1)	48(1)
C(4)	1689(3)	2321(3)	853(1)	51(1)
C(5)	1304(3)	4394(3)	914(1)	45(1)
C(6)	2821(3)	5641(3)	766(1)	53(1)
C(7)	2931(3)	5534(3)	385(1)	58(1)
C(8)	1026(3)	5820(3)	224(1)	57(1)
C(9)	-585(3)	4850(3)	759(1)	45(1)
C(10)	-1299(3)	6758(3)	861(1)	50(1)
C(11)	-3373(3)	9199(3)	720(1)	67(1)

Longitudes de enlace[A] de $C_{10}H_{15}NO_3$ (8).

O(1)-C(3)	1.235(2)	C(4)-H(4A)	0.97
O(2)-C(10)	1.197(2)	C(4)-H(4B)	0.97
O(3)-C(10)	1.330(2)	C(5)-C(9)	1.525(3)
O(3)-C(11)	1.442(2)	C(5)-C(6)	1.526(3)
C(1)-N(2)	1.470(2)	C(5)-H(5)	0.98(2)
C(1)-C(8)	1.521(3)	C(6)-C(7)	1.522(2)
C(1)-C(9)	1.530(2)	C(6)-H(6A)	0.97
C(1)-H(1)	1.00(2)	C(6)-H(6B)	0.97
N(2)-C(3)	1.344(2)	C(7)-C(8)	1.524(3)
N(2)-H(2N)	0.95(2)	C(7)-H(7A)	0.97
C(3)-C(4)	1.501(3)	C(7)-H(7B)	0.97
C(4)-C(5)	1.533(3)	C(8)-H(8A)	0.97

C(8)-H(8B)	0.97	C(11)-H(11A)	0.96
C(9)-C(10)	1.517(3)	C(11)-H(11B)	0.96
C(9)-H(9)	0.92(2)	C(11)-H(11C)	0.96

Ángulos de enlace [º] de $C_{10}H_{15}NO_3$ (8).

C(10)-O(3)-C(11)	117.2(2)	C(5)-C(6)-H(6B)	108.99(10)
N(2)-C(1)-C(8)	109.9(2)	H(6A)-C(6)-H(6B)	107.8
N(2)-C(1)-C(9)	108.00(15)	C(6)-C(7)-C(8)	111.5(2)
C(8)-C(1)-C(9)	111.5(2)	C(6)-C(7)-H(7A)	109.33(11)
N(2)-C(1)-H(1)	106.7(10)	C(8)-C(7)-H(7A)	109.33(11)
C(8)-C(1)-H(1)	109.0(10)	C(6)-C(7)-H(7B)	109.33(11)
C(9)-C(1)-H(1)	111.6(10)	C(8)-C(7)-H(7B)	109.33(10)
C(3)-N(2)-C(1)	124.4(2)	H(7A)-C(7)-H(7B)	108.0
C(3)-N(2)-H(2N)	117.5(11)	C(1)-C(8)-C(7)	111.7(2)
C(1)-N(2)-H(2N)	113.6(11)	C(1)-C(8)-H(8A)	109.28(11)
O(1)-C(3)-N(2)	121.5(2)	C(7)-C(8)-H(8A)	109.28(11)
O(1)-C(3)-C(4)	120.6(2)	C(1)-C(8)-H(8B)	109.28(10)
N(2)-C(3)-C(4)	117.8(2)	C(7)-C(8)-H(8B)	109.28(10)
C(3)-C(4)-C(5)	115.8(2)	H(8A)-C(8)-H(8B)	107.9
C(3)-C(4)-H(4A)	108.32(11)	C(10)-C(9)-C(5)	112.7(2)
C(5)-C(4)-H(4A)	108.32(11)	C(10)-C(9)-C(1)	114.4(2)
C(3)-C(4)-H(4B)	108.32(10)	C(5)-C(9)-C(1)	108.0(2)
C(5)-C(4)-H(4B)	108.32(11)	C(10)-C(9)-H(9)	103.1(11)
H(4A)-C(4)-H(4B)	107.4	C(5)-C(9)-H(9)	109.4(11)
C(9)-C(5)-C(6)	110.7(2)	C(1)-C(9)-H(9)	109.1(10)
C(9)-C(5)-C(4)	107.8(2)	O(2)-C(10)-O(3)	123.4(2)
C(6)-C(5)-C(4)	112.3(2)	O(2)-C(10)-C(9)	124.6(2)
C(9)-C(5)-H(5)	108.7(10)	O(3)-C(10)-C(9)	112.0(2)
C(6)-C(5)-H(5)	108.3(11)	O(3)-C(11)-H(11A)	109.47(11)
C(4)-C(5)-H(5)	109.0(10)	O(3)-C(11)-H(11B)	109.47(11)
C(7)-C(6)-C(5)	113.0(2)	H(11A)-C(11)-H(11B)	109.5
C(7)-C(6)-H(6A)	108.99(11)	O(3)-C(11)-H(11C)	109.47(10)
C(5)-C(6)-H(6A)	108.99(11)	H(11A)-C(11)-H(11C)	109.5
C(7)-C(6)-H(6B)	108.99(11)	H(11B)-C(11)-H(11C)	109.5

Parámetros de desplazamiento anisotrópico (A^2 x 10^3) de $C_{10}H_{15}NO_3$ (23). El exponente del factor de desplazamiento anisotrópico toma la expresión:

$$-2\pi^2[\, h^2\, a^{*2}\, U_{11} + ... + 2\, h\, k\, a^*\, b^*\, U_{12}\,]$$

	U11	U22	U33	U23	U13	U12
O(1)	89(1)	38(1)	56(1)	-1(1)	5(1)	7(1)
O(2)	105(1)	75(1)	62(1)	-30(1)	-24(1)	25(1)
O(3)	59(1)	57(1)	59(1)	-8(1)	-6(1)	12(1)
C(1)	59(1)	42(1)	41(1)	-4(1)	-12(1)	2(1)
N(2)	61(1)	40(1)	42(1)	-8(1)	-9(1)	2(1)
C(3)	61(1)	37(1)	45(1)	4(1)	3(1)	7(1)
C(4)	63(1)	47(1)	43(1)	5(1)	-5(1)	0(1)
C(5)	55(1)	50(1)	30(1)	-2(1)	-4(1)	1(1)
C(6)	58(1)	53(1)	50(1)	-6(1)	-7(1)	8(1)
C(7)	71(2)	53(1)	50(1)	-3(1)	9(1)	13(1)
C(8)	88(2)	45(1)	37(1)	3(1)	2(1)	2(1)
C(9)	51(1)	42(1)	42(1)	-2(1)	2(1)	5(1)
C(10)	51(1)	52(1)	46(1)	-2(1)	-1(1)	1(1)
C(11)	67(2)	57(1)	77(2)	-1(1)	5(1)	12(1)

Coordenadas de los átomos de hidrogeno (x 10^4) y parámetros de desplazamiento isotrópico (A^2 x 10^3) para $C_{10}H_{15}NO_3$ (8).

	x	y	z	U(eq)
H(4A)	2995(3)	2084(3)	899(1)	61
H(4B)	967(3)	1605(3)	1014(1)	61
H(6A)	2581(3)	6921(3)	832(1)	64
H(6B)	4014(3)	5281(3)	860(1)	64
H(7A)	3418(3)	4327(3)	320(1)	69
H(7B)	3783(3)	6481(3)	303(1)	69
H(8A)	650(3)	7109(3)	251(1)	68
H(8B)	1112(3)	5566(3)	-15(1)	68
H(11A)	-4526(10)	9324(9)	600(3)	101
H(11B)	-2538(9)	10177(3)	654(3)	101
H(11C)	-3605(19)	9284(9)	957(1)	101

H(1)	-1658(23)	4778(22)	265(4)	43(5)
H(5)	1240(23)	4622(24)	1156(4)	50(5)
H(9)	-1471(26)	4057(26)	844(4)	44(5)
H(2N)	-131(25)	2212(24)	94(5)	54(5)

Referencias.

[1] *International Tables for Crystallography*, Vol. C, Kluwer Academic Publishers, Dordrecht, New York, **1995**.

[2] M. Martínez-Ripoll, F. H. Cano, *An Interactive Program for Operating Rich. Seifert Single-Cystal Four-Circle Diffractometers*. Institute of Physical Chemistry Rocasolano, C.S.I.C., Serrano 119, Madrid, **1996**.

[3] J. M. Stewart, F. A. Kundell, J. C. Baldwin. *The X-RAY80 System*. Computer Science Center, University of Maryland. Colege Pard, Maryland, USA, **1990**.

[4] Siemens SHELXTLTM Version 5.0, Siemens Analytical X-Ray Instruments Inc., Madison, WI 53719, **1995**.

[5] *Ortep-3* for Windows: L. J. Farrugia, *J. Appl. Cryst.*, 30, **199**), 565.

Conclusiones

(Final Conclusions)

Although more specific conclusions may be found at the final of each section, a summary of the main conclusions are presented here:

- [**Chapter 1**] TS studies of the addition of lithium (*R*)-*N*-benzyl-*N*-(α-methylbenzyl)amide in THF to α,β-unsaturated esters confirmed that the *Si* approach are clearly the most favourable attack at -78 ºC, explaining the observed diastereoselectivity. DFT theories with well-covered medium-range dispersion forces, like the family M05/M06 and the Grimme's D3 corrections are the most appropriate theories to cover the system, even better than MP2. Although coherent with the experimental outcomes, a dimeric amide-substrate TS is required to further study either a trimolecular TS is more favourable.

- [**Chapter 2**] Several routes were explored in order to obtain a morphan β-aminoester structure with three requisites: (1) moderate to good overall yields, (2) good productivity and (3) with the amino and ester functionalities fully armored. The Boc-amine approach accomplished that, yielding a 54 % of **26**, the main molecular goal, from intermediate **5**, obtaining up to 100 mg of production. Other routes failed to accomplished all the three targets, however, a series of morphan structures were obtained and allowed a better understanding of this systems: at reactivity and spectroscopic level.

- [**Chapters 3-4**] A structure-based design was envisaged taking the morphan structure **26** as parent/core compound. Design was carried out taking into account the double nature of our morphan structure: structural simplified morphine motif and β-aminoacid. A total of 9 compounds, the hits of the docking stage, were synthetized in laboratory in few steps and submitted to biological trials. The fourth best candidates were **D8**, **D15**, **D16** and **D20**; which showed good affinities in the competition binding assays. From this feedback, four MD simulations (corresponding to compounds **D8**, **D15**, **D16**, and **D20**) were carried out to refine the docked structure, fit the receptor in a membrane slab, and analyse binding topologies and energies. Analysis of the relative binding energies allowed to rank the ligands from the stronger to the weaker in binding: **D15** > **D16** > **D20** > **D8**. Energy

decomposition in non-bonded contributions of relevant residues showed that the placing of the aromatic ring and polar group introduction were key modifications to explain the differences. Best interactions occur when the aromatic rings are placed in the bottom of the hydrophobic area (**D15**), or 3-hydroxyphenyl ester interacts with Tyr148 through a hydrogen bond (**D16**).

- [**Chapter 5**] A total of 7 PNA monomers have been synthetized: all in common have the same hydrophobic backbones. Key step was the asymmetric Michael addition of (*R*)-*N*-benzyl-*N*-α-methylbenzylamine to afford β-amino esters wit total control of the stereochemistry. The applied methodologies allowed preparing a diversity of PNA's only varying the positions of the functionalized groups in the main backbone. Leumann´s enantiomeric PNA **74** was obtained in a 31 %: a 10-fold yield increase related to Leumann´s approach.

- [**Chapter 6**] 25 ns MD simulated systems revealed conservative double helixes motif, both natural DNA:DNA, as well as antiparallel and parallel PNA:DNA hybrids. Topological analysis based on helical, local and global descriptors confirmed the B-type nature of these systems, with minimal deviations from the canonical structure. DNA natural duplexes are mainly stabilized by means of solvation interaction, dominating the free energy in contrast to the unfavourable enthalpic term, which records the energetic cost of combining to negatively charge moieties. On the other hand, PNA hybrids have a favourable enthalpic interaction, due to the neglecting of the associated charge of the backbone, but with the cost of increasing the free solvation energy value up to the positive region. The dominance of the enthapic terms results in a stronger free binding energy of PNA:DNA hybrids in contrast to DNA:DNA duplexes.

Inventario de Moléculas

(Molecular Inventory)

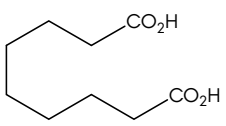

1

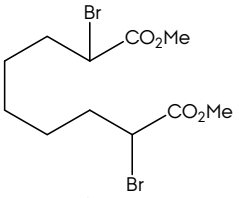

2

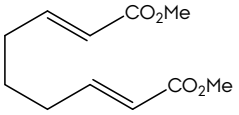

3

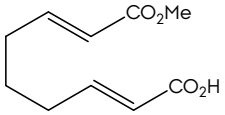

4

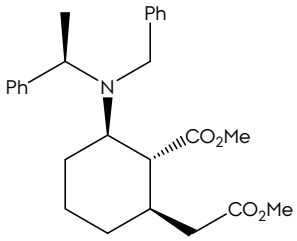

5

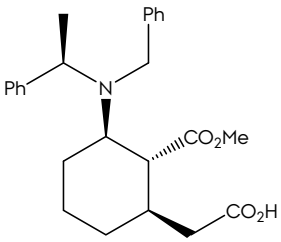

6

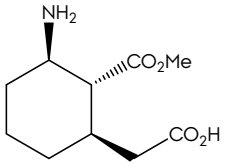

7

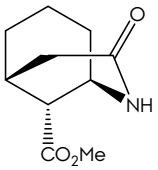

8

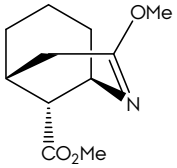

9

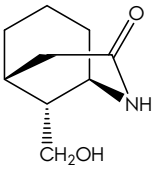

10

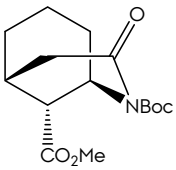

11

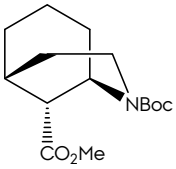

12

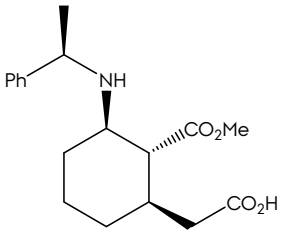

13

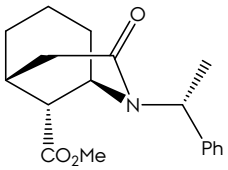

14

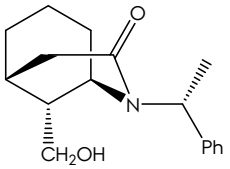

15

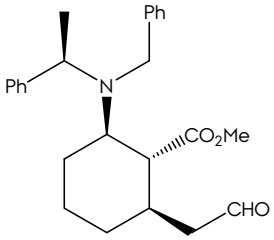

16

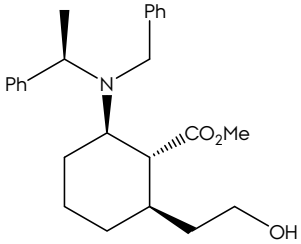

17

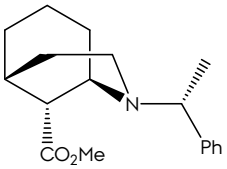

18

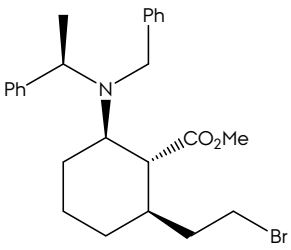

19

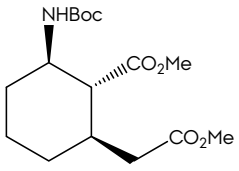

20

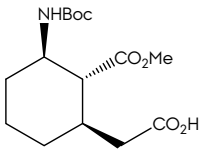

21

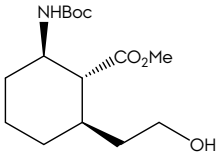

22

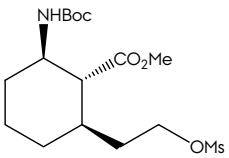

23

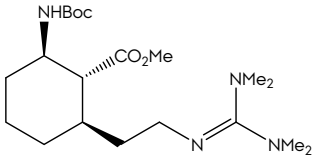

24

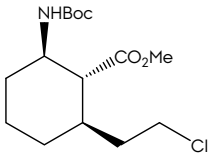

25

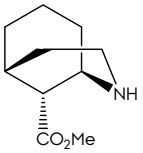

26

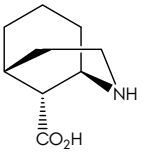

27

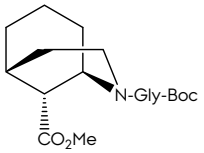

28

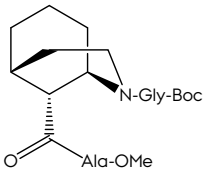

29

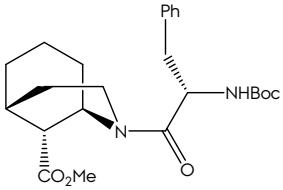

30

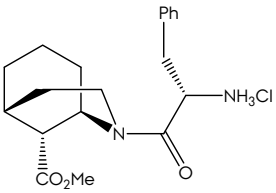

31

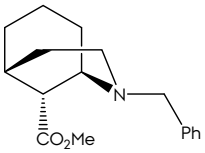

32

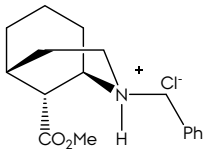

33

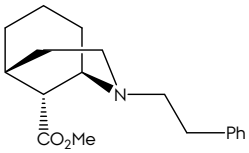

34

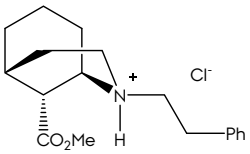

35

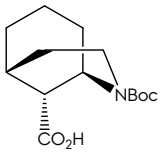

36

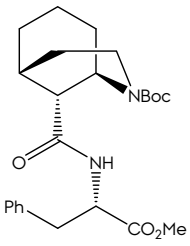

37

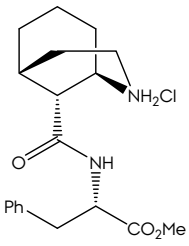

38

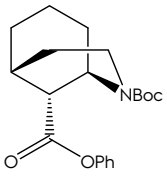

39

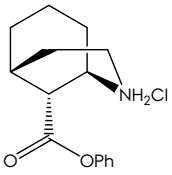

40

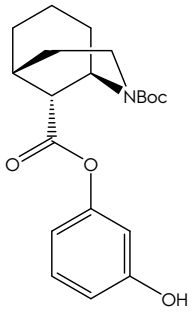

41

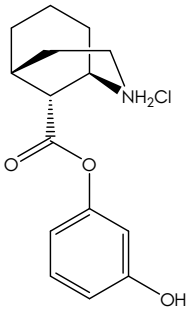

42

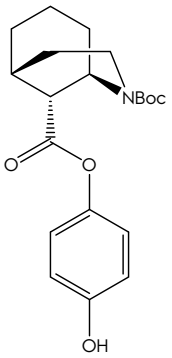

43

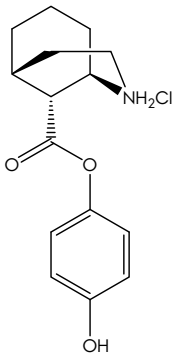

44

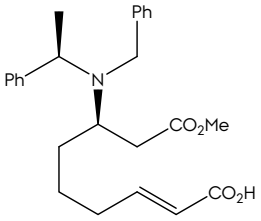

45

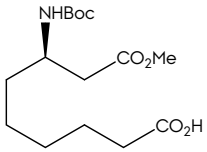

46

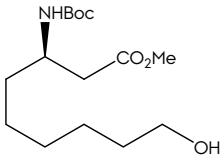

47

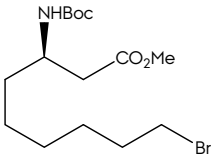

48

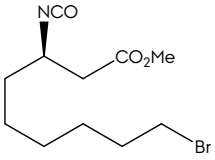

49

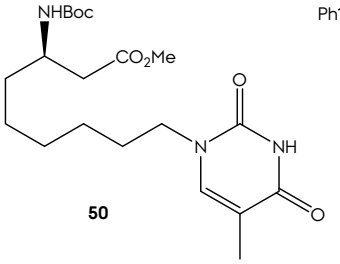

50

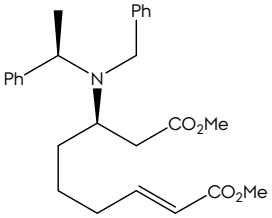

51

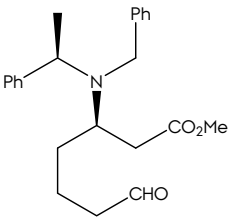

52

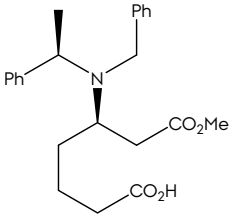

53

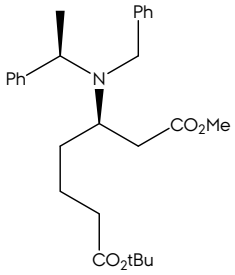

54

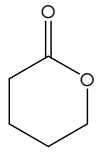

54

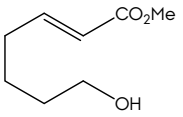

56

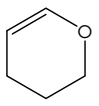

57

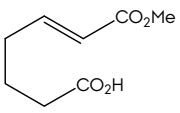

58

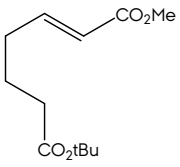

59

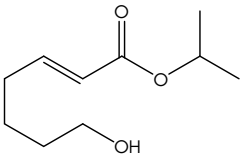

60

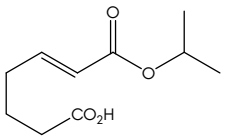

61

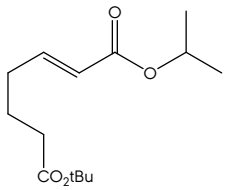

62

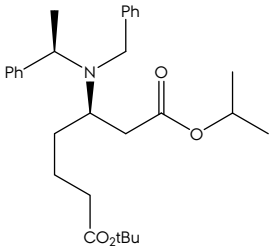

63

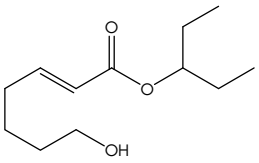

64

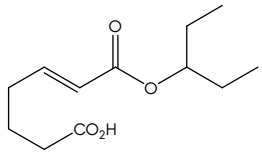

65

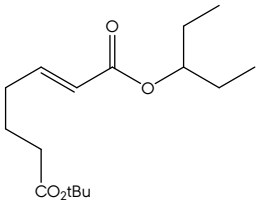

66

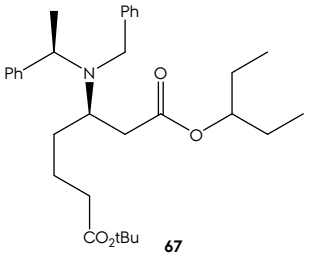

67

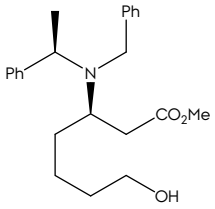

68

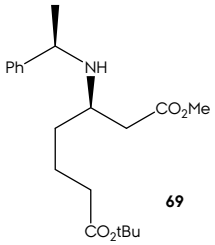

69

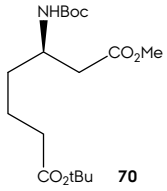

70

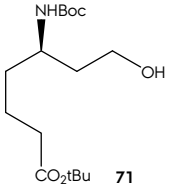

71

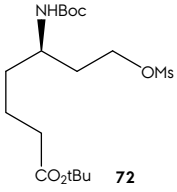

72

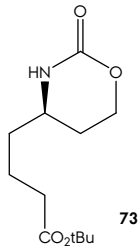

73

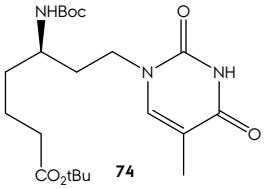

74

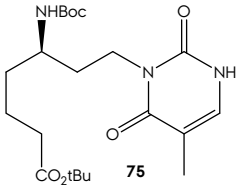

75

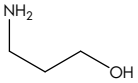

76

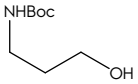

77

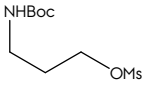

78

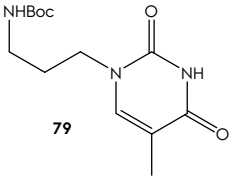

79

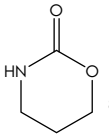

80

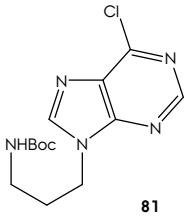

81

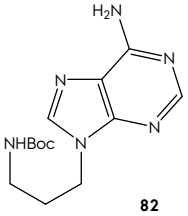

82

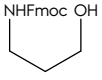

83

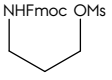

84

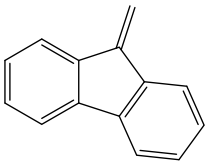

85

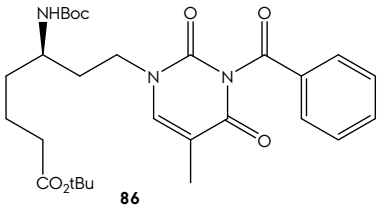

86

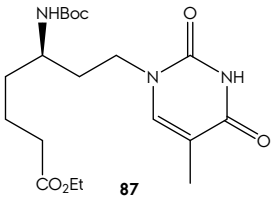

87

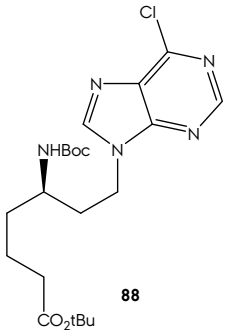

88

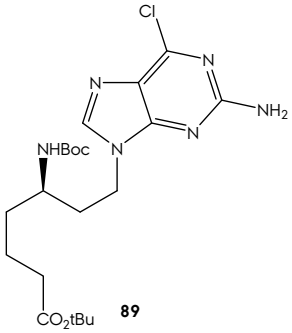

89

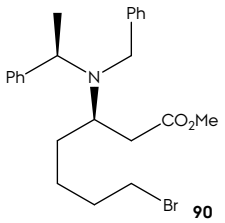

90

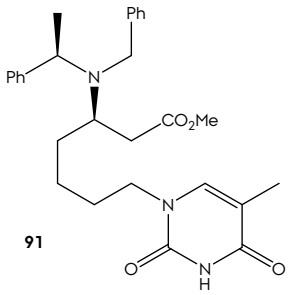

91

"Muchas personas que me conocen bien me han solicitado que les aclare el extraño procedimiento de mi huida, que a muchos pareció en verdad asombrosa, a pesar de que el hecho no era tan sorprendente, si recordamos que desde mi juventud había entrenado mi ingenio para proponer y resolver sutiles enigmas. Y yo sostengo que el estudio de tales intrincados asuntos es provechoso, no solo por el placer que ello proporciona, sino porque un hombre nunca está seguro de si en alguna súbita e imprevista dificultad que pueda sucederle a lo largo de esta vida nuestra, dicho aprendizaje no servirá en gran medida a sus propósitos, y quizás le ayude a superar muchos problemas".

Henry E. Dudeney